Association of Structural Engineers of Serbia - 16. CONGRESS

28 - 30. 09. 2022.
ARANDJELOVAC

ДГКС | ASES

INTERNATIONAL CONGRESS PROCEEDINGS

IN COOPERATION WITH

Република Србија
Министарство
просвете, науке и
технолошког развоја

SUPPORTED BY

Инжењерска
комора
Србије

PLATINUM SPONSORS

GOLD SPONSORS

Izdavač:	**Univerzitet u Beogradu Građevinski fakultet** Beograd, Bulevar kralja Aleksandra 73/I
Suizdvač:	**Društvo građevinskih konstruktera Srbije** Beograd, Bulevar kralja Aleksandra 73
Urednici:	prof. dr Zlatko Marković v.prof. dr Ivan Ignjatović v.prof. dr Jelena Dobrić
Tehnička priprema:	doc. dr Nina Gluhović doc. dr Marija Todorović dr Isidora Jakovljević
Grafički dizajn:	Tijana Stevanović
Dizajn korica:	Luka Pavelka
Štampa:	Grafopak, Aranđelovac
Tiraž:	250 primeraka

Beograd, septembar 2022.

POVODOM TRIDESETOGODIŠNJICE POSTOJANJA
A ZA NAROČITE ZASLUGE I USPEHE POSTIGNUTE
U RAZVIJANJU I UNAPREĐENJU GRAĐEVINSKOG
KONSTRUKTERSTVA I DOPRINOS UZDIZANJU
STRUČNIH KADROVA

ukazom broj 38 od 29. aprila 1983. godine

PREDSEDNIŠTVO SFRJ

ODLIKOVALO JE

SAVEZ DRUŠTAVA GRAĐEVINSKIH
KONSTRUKTERA JUGOSLAVIJE

ORDENOM RADA SA SREBRNIM VENCEM

Organizacioni odbor 16. Kongresa:

prof. dr Zlatko MARKOVIĆ, predsednik
Lazar MARKOVIĆ, potpredsednik,
v.prof. dr Ivan IGNJATOVIĆ, generalni sekretar
prof. dr Boško STEVANOVIĆ, sekretar
prof. dr Đorđe LAĐINOVIĆ, član Predsedništva
prof. dr Dragoslav STOJIĆ, član Predsedništva
v.prof. dr Danijel KUKARAS, član Predsedništva
v.prof. dr Branko MILOSAVLJEVIĆ, član Predsedništva
v.prof. dr Marija NEFOVSKA-DANILOVIĆ, član Predsedništva
v.prof. dr Selimir LELOVIĆ, član Predsedništva
v.prof. dr Jelena DOBRIĆ
v. prof. dr Milan SPREMIĆ
v.prof. dr Vladimir VUKOBRATOVIĆ
doc. dr Vedran CAREVIĆ
doc. dr Jelena DRAGAŠ
doc. dr Nina GLUHOVIĆ
doc. dr Marija TODOROVIĆ
doc. dr Đorđe JOVANOVIĆ
Dimitrije ALEKSIĆ, član Predsedništva
Milan GRČIĆ, član Predsedništva
Branko KNEŽEVIĆ, član Predsedništva
Miroslav MIHAJLOVIĆ, član Predsedništva
Đorđe PAVKOV, član Predsedništva
Darko POPOVIĆ, član Predsedništva
Duško TOMIĆ, član Predsedništva

Naučni odbor 16. Kongresa:

prof. dr Meri CVETKOVSKA (Severna Makedonija)
v.prof. dr Jelena DOBRIĆ (Srbija)
prof. dr Majkl FARDIS (Grčka)
prof. dr Miguel FERNANDEZ RUIZ (Španija)
prof. dr Radomir FOLIĆ (Srbija)
prof. dr Nenad IVANIŠEVIĆ (Srbija)
v.prof. dr Ivan IGNJATOVIĆ (Srbija)
v.prof. dr Vojkan JOVIČIĆ (Slovenija)
prof. dr Miloš KNEŽEVIĆ (Crna Gora)
prof. dr Đorđe LAĐINOVIĆ (Srbija)
v.prof. dr Selimir LELOVIĆ (Srbija)
doc. dr Jože LOPATIČ (Slovenija)
prof. dr Duško LUČIĆ (Crna Gora)
prof. dr Snežana MARINKOVIĆ (Srbija)
doc. Dr Miroslav MARJANOVIĆ (Srbija)
prof. dr Zlatko MARKOVIĆ (Srbija)
prof. dr Goran MARKOVSKI (Severna Makedonija)
v.prof. dr Branko MILOSAVLJEVIĆ (Srbija)
v.prof. dr Primož MOŽE (Slovenija)
v.prof. dr Marija NEFOVSKA-DANILOVIĆ (Srbija)
prof. dr Vlastimir RADONJANIN (Srbija)
prof. dr Marina RAKOČEVIĆ (Crna Gora)
v.prof. dr Andrija RAŠETA (Srbija)
prof. dr Boško STEVANOVIĆ (Srbija)
prof. dr Dragoslav STOJIĆ (Srbija)
prof. dr Nina ŠTIRMER (Hrvatska)
doc. dr Trajana TANKOVA (Portugal)
prof. dr Milan VELJKOVIĆ (Holandija)
v.prof. dr Zlatko ZAFIROVSKI (Severna Makedonija).

16. KONGRES JE ORGANIZOVAN U SARADNJI SA:

GRAĐEVINSKIM FAKULTETOM UNIVERZITETA U BEOGRADU

FAKULTETOM TEHNIČKIH NAUKA UNIVERZITETA U NOVOM SADU.

POKROVITELJ KONGRESA:

INŽENJERSKA KOMORA SRBIJE

ORGANIZACIJU KONGRESA FINANSIJSKI PODRŽALO:

MINISTARSTVO NAUKE, PROSVETE I TEHNOLOŠKOG RAZVOJA
REPUBLIKE SRBIJE

SPONZORI 16. KONGRESA:

Platinasti sponzori:

BECHTEL ENKA Beograd
CRBC Beograd
FOCUS COMPUTERS d.o.o. Beograd
PUT-INŽENJERING d.o.o. Niš
STRABAG d.o.o., Beograd
ŠIRBEGOVIĆ Inženjering, Gračanica, BiH
UTIBER Novi Sad

Zlatni sponzori:

CIP - SAOBRAĆAJNI INSTITUT d.o.o. Beograd
DELTA INŽENJERING d.o.o. Beograd
DELTA REAL ESTATE d.o.o. Beograd
JADRAN d.o.o. Beograd
MORAVACEM d.o.o. Popovac
MOSTOGRADNJA ING d.o.o. Beograd
PEIKKO SLOVAKIA s.r.o. Slovakia
PROCLUB d.o.o. Beograd
TERMOENERGO INŽENJERING d.o.o. Beograd

Srebrni sponzori:

CENROPROJEKT d.o.o. Beograd
DEL ING d.o.o. Beograd
DNEC d.o.o. Beograd
ENERGOPROJEKT ENTEL a.d. Beograd
NEOBIM d.o.o. Beograd
NORTH ENGINEERING d.o.o. Subotica
PERI OPLATE d.o.o. Šimanovci
SIKA SRBIJA d.o.o. Šimanovci
SPREG d.o.o. Aranđelovac

Bronzani sponzori:

BALDINISTUDIO INTERNATIONAL d.o.o. Novi Sad

BETON d.o.o. Gradiška

MAŠINOPROJEKT d.o.o. Beograd

PIRAMIDA d.o.o. Sremska Mitrovica

ŠIDPROJEKT d.o.o. Šid

DOSADAŠNJI KONGRESI, SIMPOZIJUMI I SAVETOVANJA

PRVO SAVETOVANJE
JUGOSLOVENSKIH INŽENJERA KONSTRUKTERA
ZAGREB, decembar 1953. godine

DRUGI KONGRES
JUGOSLOVENSKOG DRUŠTVA GRAĐEVINSKIH KONSTRUKTERA
OPATIJA, maj 1958. godine

Predsednik:	akademik, prof. dr h.c. Đorđe LAZAREVIĆ, dipl.inž.građ, Beograd
Sekretar:	prof. Zvonimir PAVLOVIĆ, dipl.inž.građ. Beograd

TREĆI KONGRES
JUGOSLOVENSKOG DRUŠTVA GRAĐEVINSKIH KONSTRUKTERA
SARAJEVO, septembar 1964. godine

Predsednik:	prof. dr Kruno TONKOVIĆ, dipl.inž.građ. Zagreb
Potpredsednik:	prof. Ljubomir JEVTOVIĆ, dipl.inž.građ. Beograd
Sekretar:	prof. Zvonimir PAVLOVIĆ, dipl.inž.građ. Beograd

ČETVRTI KONGRES
JUGOSLOVENSKOG DRUŠTVA GRAĐEVINSKIH KONSTRUKTERA
PORTOROŽ, jun 1969. godine

Predsednik:	akademik, prof. dr Milan ĐURIĆ, dipl.inž.građ, Beograd
Potpredsednik:	prof. Miloš MARINČEK, dipl.inž.građ, Ljubljana
Sekretar:	Stojan DINIĆ, dipl.inž.građ, Beograd

PETI KONGRES
JUGOSLOVENSKOG DRUŠTVA GRAĐEVINSKIH KONSTRUKTERA
BUDVA, septembar 1974. godine

Predsednik:	akademik, prof. dr Milan ĐURIĆ, dipl.inž.građ, Beograd
Potpredsednik:	prof. Miloš MARINČEK, dipl.inž.građ, Ljubljana
Sekretar:	Stojan DINIĆ, dipl.inž.građ, Beograd

SIMPOZIJUM
JUGOSLOVENSKOG DRUŠTVA GRAĐEVINSKIH KONSTRUKTERA
"GREŠKE, SANACIJE I ISKUSTVA U INVESTIRANJU, PROJEKTOVANJU,
GRAĐENJU I EKSPLOATACIJI GRAĐEVINSKIH OBJEKATA"
CAVTAT, novembar 1976. godine

ŠESTI KONGRES
JUGOSLOVENSKOG DRUŠTVA GRAĐEVINSKIH KONSTRUKTERA
BLED, septembar 1978. godine

Predsednik:	akademik, prof. dr Nikola HAJDIN, dipl.inž.građ, Beograd
Potpredsednik:	prof. Milenko PRŽULJ, dipl.inž.građ, Sarajevo
Sekretar:	Stojan DINIĆ, dipl.inž.građ, Beograd
Sekretar za	
međunarodne veze:	prof. dr Života PERIŠIĆ, dipl.inž.građ, Beograd

SIMPOZIJUM
JUGOSLOVENSKOG DRUŠTVA GRAĐEVINSKIH KONSTRUKTERA I
INSTITUTA ZA MATERIJALE I KONSTRUKCIJE GRAĐEVINSKOG FAKULTETA
UNIVERZITETA U BEOGRADU
"INOVACIJE JUGOSLOVENSKIH PROPISA ZA BETONSKE, METALNE I
SPREGNUTE KONSTRUKCIJE - ISKUSTVA I NOVA SAZNANJA"
TROGIR, maj 1980. godine

Na Skupštini održanoj maja 1980. godine u Trogiru, Jugoslovensko društvo građevinskih konstruktera je promenilo naziv u SAVEZ DRUŠTAVA GRAĐEVINSKIH KONSTRUKTERA JUGOSLAVIJE - SDGKJ. Na Skupštini je odlučeno da Izvršni odbor, izabran na VI Kongresu na Bledu, u istom sastavu obavlja dužnosti Predsedništva SDGKJ do sledećeg kongresa.

Za predsednika i potpredsednika SDGKJ sa jednogodišnjim mandatom izabrani su:

Predsednik:	akademik, prof. dr Nikola HAJDIN, dipl.inž.građ, Beograd
Potpredsednik:	prof. Milenko PRŽULJ, dipl.inž.građ, Sarajevo

Za predsednika i potpredsednika SDGKJ za naredni jednogodišnji mandat izabrani su:

Predsednik:	prof. Milenko PRŽULJ, dipl.inž.građ, Sarajevo
Potpredsednik:	Marijan KOŠČAK, dipl.inž.građ, Zagreb

SEDMI KONGRES
SAVEZA DRUŠTAVA GRAĐEVINSKIH KONSTRUKTERA JUGOSLAVIJE
CAVTAT, april 1983. godine

Predsednik: prof. Milenko PRŽULJ, dipl.inž.građ, Sarajevo
Potpredsednik: prof. dr Stanko ŠRAM, dipl.inž.građ, Zagreb
Sekretar: Stojan DINIĆ, dipl.inž.građ, Beograd
Sekretar za
međunarodne veze: prof. dr Života PERIŠIĆ, dipl.inž.građ, Beograd

SIMPOZIJUM '85
SAVEZA DRUŠTAVA GRAĐEVINSKIH KONSTRUKTERA JUGOSLAVIJE
DUBROVNIK, april 1985. godine

Na sednici Predsedništva SDGKJ, održanoj aprila 1985. u Dubrovniku odlučeno je da se predsedniku, potpredsedniku, sekretaru i sekretaru za međunarodne veze, izabranim na VII Kongresu SDGKJ u Cavtatu, produži mandat do sledećeg kongresa.

OSMI KONGRES
SAVEZA DRUŠTAVA GRAĐEVINSKIH KONSTRUKTERA JUGOSLAVIJE
CAVTAT, april 1987. godine

Predsednik: prof. dr Života PERIŠIĆ, dipl.inž.građ, Beograd
Potpredsednik: prof. dr Franci KRŽIĆ, dipl.inž.građ, Ljubljana
Sekretar: Stojan DINIĆ, dipl.inž.građ, Beograd
Sekretar za
međunarodne veze: doc. dr Jure RADIĆ, dipl.inž.građ, Zagreb

JUGOSLOVENSKO SAVETOVANJE O PRIMENI NOVOG PRAVILNIKA ZA BETON I ARMIRANI BETON BAB 87 ZAJEDNO SA JUDIMK, GRAĐEVINSKIM INSTITUTOM ZAGREB I GRAĐEVINSKIM FAKULTETOM BEOGRAD
DUBROVNIK, april 1989. godine

Na sednici Predsedništva SDGKJ održanoj aprila 1989. u Dubrovniku, ponovo su izabrani za sledeći dvogodišnji period

Predsednik: prof. dr Života PERIŠIĆ, dipl.inž.građ, Beograd
Potpredsednik: prof. dr Franci KRŽIĆ, dipl.inž.građ, Ljubljana
Sekretar: Stojan DINIĆ, dipl.inž.građ, Beograd
Sekretar za
međunarodne veze: doc. dr Jure RADIĆ, dipl.inž.građ, Zagreb

DEVETI KONGRES
SAVEZA DRUŠTAVA GRAĐEVINSKIH KONSTRUKTERA JUGOSLAVIJE
CAVTAT, april 1991. godine

Predsednik:	prof. dr Života PERIŠIĆ, dipl.inž.građ, Beograd
Potpredsednik:	prof. dr Franci KRŽIĆ, dipl.inž.građ, Ljubljana
Sekretar:	Stojan DINIĆ, dipl.inž.građ, Beograd
Sekretar za međunarodne veze:	doc. dr Jure RADIĆ, dipl.inž.građ, Zagreb
Članovi Predsedništva:	prof. Vukašin AČANSKI, dipl.inž.građ, Maribor
	prof. dr Vinko ČANDRLIĆ, dipl.inž.građ, Zagreb
	prof. dr Radomir FOLIĆ, dip.inž.građ, Novi Sad
	akademik, prof. dr Nikola HAJDIN, dipl.inž.građ, Beograd
	prof. Dravan IVANOV, dipl.inž.građ, Skoplje
	prof. Gojko NENADIĆ, dipl.inž.građ, Beograd
	prof. Milenko PRŽULJ, dipl.inž.građ, Sarajevo
	Vladimir STANKOVIĆ, dipl.inž.građ, Titograd
	Vidoje ZELENOVIĆ, dipl.inž.građ, Priština
	prof. dr Stanko ŠRAM, dipl.inž.građ, Zagreb
	mr Cvetan TANEVSKI, dipl.inž.građ, Skoplje
Članovi Nadzornog odbora:	Jovan BOŠKOV, dipl.inž.građ, Novi Sad
	prof. dr Boris KOLJOZOV, dipl.inž.građ, Skoplje
	Zvonimir SABLJAK, dipl.inž.građ, Novi Sad

*Posle raspada SFRJ, Savez društava građevinskih konstruktera Jugoslavije - SDGKJ transformisao se u **Jugoslovensko društvo građevinskih konstruktera - JDGK**, koje je nastavilo delatnost SDGKJ. Na Osnivačkoj skupštini, održanoj 1.12.1994. godine u Beogradu, usvojen je novi statut i imenovano Predsedništvo u sastavu:*

Predsednik:	prof. dr Života PERIŠIĆ, dipl.inž.građ, Beograd
Potpredsednik:	prof. dr Radomir FOLIĆ, dipl.inž.građ, Novi Sad
Generalni sekretar:	Stojan DINIĆ, dipl.inž.građ, Beograd
Članovi Predsedništva:	akademik prof. dr Nikola HAJDIN, dipl.inž.građ, Beograd
	prof. dr Milorad IVKOVIĆ, dipl.inž.građ, Beograd
	Miroslav BAJIĆ, dip.inž.građ, Novi Sad
	Veljko BELADA, dipl.inž.građ, Podgorica
	Vidoje ZELENOVIĆ, dipl.inž.građ, Priština
	prof. dr Mirko AĆIĆ, dipl.inž.građ, Beograd
	prof. dr Aleksandar PAKVOR, dipl.inž.građ, Beograd
	prof. dr Mihailo MURAVLJOV, dipl.inž.građ, Beograd

Jugoslovensko društvo građevinskih konstruktera, zajedno sa Građevinskim fakultetom u Beogradu i Saveznim zavodom za standardizaciju, organizovalo je dva jugoslovenska savetovanja:

PRVO JUGOSLOVENSKO SAVETOVANJE
EVROKODOVI I JUGOSLOVENSKO GRAĐEVINSKO KONSTRUKTERSTVO
BEOGRAD, jun 1995. godine

DRUGO JUGOSLOVENSKO SAVETOVANJE
EVROKODOVI I JUGOSLOVENSKO GRAĐEVINSKO KONSTRUKTERSTVO
BEOGRAD, april 1997. godine

DESETI KONGRES
JUGOSLOVENSKOG DRUŠTVA GRAĐEVINSKIH KONSTRUKTERA
VRNJAČKA BANJA, jun 1998. godine

Na Skupštini JDGK, održanoj juna 1998. godine *u Vrnjačkoj Banji, izabrano je novo Predsedništvo i Nadzorni odbor JDGK, u sledećem sastavu:*

Predsednik:	prof. dr Mirko AĆIĆ, dipl.inž.građ, Beograd
Potpredsednik:	prof. dr Radenko PEJOVIĆ, dipl.inž.građ, Podgorica
Generalni sekretar:	Stojan DINIĆ, dipl.inž.građ, Beograd
Sekretar:	Svetislav SIMOVIĆ, dipl.inž.građ, Beograd
Članovi Predsedništva:	akademik prof. dr Nikola HAJDIN, dipl.inž.građ, Beograd
	prof. dr Milorad IVKOVIĆ , dipl.inž.građ, Beograd
	prof. dr Života PERIŠIĆ, dip.inž.građ, Beograd
	prof. dr Aleksandar PAKVOR, dipl.inž.građ, Beograd
	prof. dr Miodrag SEKULOVIĆ, dipl.inž.građ, Beograd
	prof. dr Arsenije VUJOVIĆ, dipl.inž.građ, Podgorica
	prof. dr Radomir FOLIĆ, dipl.inž.građ, Novi Sad
	prof. dr Živojin PRAŠČEVIĆ, dipl.inž.građ, Beograd
	prof. dr Dragan BUĐEVAC, dipl.inž.građ, Beograd
	prof. dr Milić MILIĆEVIĆ, dipl.inž.građ, Niš
	mr Vidoje ZELENOVIĆ, dipl.inž.građ, Gacko
	Veljko BELADA, dipl.inž.građ, Podgorica
	Ivan MAMUŽIĆ, dipl.inž.građ, Novi Sad
	Dragan VUKADINOVIĆ, dipl.inž.građ, Beograd
	Jožef KERMECI, dipl.inž.građ, Kanjiža
Članovi Nadzornog odbora:	prof. dr Dušan NAJDANOVIĆ, dipl.inž.građ, Beograd - predsednik
	prof. dr Mladen ULIĆEVIĆ, dipl.inž.građ, Podgorica
	Miroslav BAJIĆ, dipl.inž.građ, Novi Sad

Na istoj skupštini izabrani su za počasne članove JDGK:

        akademik prof. dr Nikola HAJDIN, dipl.inž.građ, Beograd

        prof. dr Milorad IVKOVIĆ, dipl.inž.građ, Beograd

        prof. dr Tihomir NIKOLOVSKI, dipl.inž.građ, Skoplje

takođe je izabrano i 14 zaslužnih članova JDGK:

        prof. dr Života PERIŠIĆ, dipl.inž.građ, Beograd

        prof. dr Radomir FOLIĆ, dipl.inž.građ, Novi Sad

        Ivan MAMUŽIĆ, dipl.inž.građ, Novi Sad

        prof. dr Aleksandar PAKVOR, dipl.inž.građ, Beograd

        prof. dr Mirko AĆIĆ, dipl.inž.građ, Beograd

        Stojan DINIĆ, dipl.inž.građ, Beograd

        mr Vidoje ZELENOVIĆ, dipl.inž.građ, Gacko

        prof. dr Boško PETROVIĆ, dipl.inž.građ, Beograd

        prof. dr Miroslav DEBELJKOVIĆ, dipl.inž.građ, Beograd

        mr Branislav VOJINOVIĆ, dipl.inž.građ, Beograd

        prof. dr Milić MILIĆEVIĆ, dipl.inž.građ, Niš

        prof. dr Milan GOJKOVIĆ , dipl.inž.građ, Beograd

        dr Vladimir STANKOVIĆ, dipl.inž.građ, Podgorica

        Veljko BELADA, dipl.inž.građ, Podgorica

SIMPOZIJUM 2000.
JUGOSLOVENSKOG DRUŠTVA GRAĐEVINSKIH KONSTRUKTERA
VRNJAČKA BANJA, 1-3. novembar 2000. godine

Na Skupštini JDGK, održanoj 2. novembra 2000. godine u Vrnjačkoj Banji, Predsedništvo JDGK je prošireno sa dva člana i njegov sastav čine:

Predsednik:	prof. dr Mirko AĆIĆ, dipl.inž.građ, Beograd
Potpredsednik:	prof. dr Radenko PEJOVIĆ, dipl.inž.građ, Podgorica
Generalni sekretar:	Stojan DINIĆ, dipl.inž.građ, Beograd
Sekretar:	Svetislav SIMOVIĆ, dipl.inž.građ, Beograd
Članovi Predsedništva:	akademik, prof. dr Nikola HAJDIN, dipl.inž.građ, Beograd
	prof. dr Milorad IVKOVIĆ, dipl.inž.građ, Beograd
	prof. dr Života PERIŠIĆ, dipl.inž.građ, Beograd
	prof. dr Aleksandar PAKVOR, dipl.inž.građ, Beograd
	prof. dr Miodrag SEKULOVIĆ, dipl.inž.građ, Beograd
	prof. dr Arsenije VUJOVIĆ, dipl.inž.građ, Podgorica
	prof. dr Radomir FOLIĆ, dipl.inž.građ, Novi Sad
	prof. dr Živojin PRAŠČEVIĆ, dipl.inž.građ, Beograd
	prof. dr Dragan BUĐEVAC, dipl.inž.građ, Beograd
	prof. dr Milić MILIĆEVIĆ, dipl.inž.građ, Niš
	mr Vidoje ZELENOVIĆ, dipl.inž.građ, Banja Luka

Veljko BELADA, dipl.inž.građ, Podgorica
Ivan MAMUŽIĆ, dipl.inž.građ, Novi Sad
Dragan VUKADINOVIĆ, dipl.inž.građ, Beograd
Jožef KERMECI, dipl.inž.građ, Kanjiža

Članovi
Nadzornog
odbora: prof. dr Dušan NAJDANOVIĆ, dipl.inž.građ, Beograd - predsednik
prof. dr Mladen ULIĆEVIĆ, dipl.inž.građ, Podgorica
Miroslav BAJIĆ, dipl.inž.građ, Novi Sad

Na istoj skupštini izabrani su za počasne članove JDGK:
prof. dr Sande ATANASOVSKI, dipl.inž.građ, Skoplje
prof. dr Dragan IVANOV, dipl.inž.građ, Skoplje
prof. dr Milenko PRŽULJ, dipl.inž.građ, Ljubljana
prof. dr Vukašin AČANSKI, dipl.inž.građ, Maribor
prof. dr Života PERIŠIĆ, dipl.inž.građ, Beograd
Stojan DINIĆ, dipl.inž.građ, Beograd

Takođe je izabrano i 10 zaslužnih članova JDGK:
prof. Dimitrije ĆERTIĆ, dipl.inž.građ, Beograd
Predrag ŽELALIĆ, dipl.inž.građ, Beograd
prof. Gojko NENADIĆ, dipl.inž.građ, Beograd
Anđelko KOVAČEVIĆ, dipl.inž.građ, Beograd
prof. dr Živojin PRAŠČEVIĆ, dipl.inž.građ, Beograd
Miroslav BAJIĆ, dipl.inž.građ, Beograd
prof. dr Mihailo MURAVLJOV, dipl.inž.građ, Beograd
prof. dr Arsenije VUJOVIĆ, dipl.inž.građ, Podgorica
Lazar PRODANOVIĆ, dipl.inž.građ, Beograd
Johan SKLENA, dipl.inž.građ, Novi Sad

JEDANAESTI KONGRES
JUGOSLOVENSKOG DRUŠTVA GRAĐEVINSKIH KONSTRUKTERA
VRNJAČKA BANJA, 25-27. septembar 2002.

Na Skupštini JDGK, održanoj 24. septembra 2002. godine u Vrnjačkoj Banji, izabrano je novo Predsedništvo i Nadzorni odbor JDGK, u sledećem sastavu:

Predsednik: prof. dr Mirko AĆIĆ, dipl.inž.građ, Beograd
Potpredsednik: prof. dr Radenko PEJOVIĆ, dipl.inž.građ, Podgorica

Generalni sekretar: Stojan DINIĆ, dipl.inž.građ, Beograd
Sekretar: Svetislav SIMOVIĆ, dipl.inž.građ, Beograd
Članovi
Predsedništva: prof. dr Života PERIŠIĆ, dipl.inž.građ, Beograd

prof. dr Radomir FOLIĆ, dipl.inž.građ, Novi Sad
prof. dr Arsenije VUJOVIĆ, dipl.inž.građ, Podgorica
prof. dr Živojin PRAŠČEVIĆ, dipl.inž.građ, Beograd
prof. dr Dragan BUĐEVAC, dipl.inž.građ, Beograd
prof. dr Dušan NAJDANOVIĆ, dipl.inž.građ, Beograd
prof. dr Đorđe VUKSANOVIĆ, dipl.inž.građ, Beograd
prof. dr Mladen ULIĆEVIĆ, dipl.inž.građ, Podgorica
prof. dr Dragoslav STOJIĆ, dipl.inž.građ, Niš
mr Vidoje ZELENOVIĆ, dipl.inž.građ, Gacko
Dragan VUKADINOVIĆ, dipl.inž.građ, Beograd
Ivan MAMUŽIĆ, dipl.inž.građ, Novi Sad
Jožef KERMECI, dipl.inž.građ, Kanjiža

Članovi
Nadzornog
odbora: mr Dragana ČUKIĆ, dipl.inž.građ, Beograd
mr Đorđe LAĐINOVIĆ, dipl.inž.građ, Novi Sad
Igor ĐURANOVIĆ, dipl.inž.građ, Podgorica

Na istoj skupštini izabrani su za počasne članove JDGK:
prof. dr Stanko ŠRAM, dipl.inž.građ. - Hrvatska
prof. dr Miodrag VELKOV, dipl.inž.građ. - Makedonija
prof. dr Aleksandar PAKVOR, dipl.inž.građ, Beograd
prof. dr Miodrag SEKULOVIĆ, dipl.inž.građ, Beograd
Predrag ŽELALIĆ, dipl.inž.građ, Beograd
Veljko BELADA, dipl.inž.građ, Podgorica
mr Vladimir STANKOVIĆ, dipl.inž.građ, Podgorica

Takođe je izabrano i 12 zaslužnih članova JDGK:
prof. dr Dušan NAJDANOVIĆ, dipl.inž.građ, Beograd
prof. dr Radenko PEJOVIĆ, dipl.inž.građ, Podgorica
prof. dr Mladen ULIĆEVIĆ, dipl.inž.građ, Podgorica
prof. dr Petar ČOLIĆ, dipl.inž.građ, Beograd
Dušan SIMOVIĆ, dipl.inž.građ, Beograd
Svetislav SIMOVIĆ, dipl.inž.građ, Beograd
Dragan VUKADINOVIĆ, dipl.inž.građ, Beograd
Boško TRIVIĆ, dipl.inž.građ, Beograd
Jožef KERMECI, dipl.inž.građ, Kanjiža
Vukan NJAGULJ, dipl.inž.građ, Beograd
Dragomir LUKIĆ, dipl.inž.građ, Beograd
Miroslav SUBOTIĆ, dipl.inž.građ, Beograd

SIMPOZIJUM 2004.
JUGOSLOVENSKOG DRUŠTVA GRAĐEVINSKIH KONSTRUKTERA
VRNJAČKA BANJA, 29. septembar - 1. oktobar 2004. godine

Predsednik: prof. dr Mirko AĆIĆ, dipl.inž.građ, Beograd

XI

Potpredsednik:	prof. dr Radenko PEJOVIĆ, dipl.inž.građ, Podgorica
Generalni sekretar:	Stojan DINIĆ, dipl.inž.građ, Beograd
Sekretar:	Svetislav SIMOVIĆ, dipl.inž.građ, Beograd

Članovi
Predsedništva:
    prof. dr Života PERIŠIĆ, dipl.inž.građ, Beograd
    prof. dr Radomir FOLIĆ, dipl.inž.građ, Novi Sad
    prof. dr Arsenije VUJOVIĆ, dipl.inž.građ, Podgorica
    prof. dr Živojin PRAŠČEVIĆ, dipl.inž.građ, Beograd
    prof. dr Dragan BUĐEVAC, dipl.inž.građ, Beograd
    prof. dr Dušan NAJDANOVIĆ, dipl.inž.građ, Beograd
    prof. dr Đorđe VUKSANOVIĆ, dipl.inž.građ, Beograd
    prof. dr Mladen ULIĆEVIĆ, dipl.inž.građ, Podgorica
    prof. dr Dragoslav STOJIĆ, dipl.inž.građ, Niš
    prof. dr Petar ČOLIĆ, dipl.inž.građ, Beograd
    mr Vidoje ZELENOVIĆ, dipl.inž.građ, Gacko
    Dragan VUKADINOVIĆ, dipl.inž.građ, Beograd
    Ivan MAMUŽIĆ, dipl.inž.građ, Novi Sad
    Jožef KERMECI, dipl.inž.građ, Kanjiža

Članovi
Nadzornog
odbora:
    mr Dragana ČUKIĆ, dipl.inž.građ, Beograd
    mr Đorđe LAĐINOVIĆ, dipl.inž.građ, Novi Sad
    Igor ĐURANOVIĆ, dipl.inž.građ, Podgorica

Na istoj skupštini izabrani su za počasne članove JDGK:
    prof. dr Predrag GAVRILOVIĆ, dipl.inž.građ.
    Saško STREZOVSKI, dipl.inž.građ.
    prof. Gojko NENADIĆ, dipl.inž.građ.
    prof. dr Mihajlo TRIFUNAC, dipl.inž.građ.
    prof. dr Milija PAVLOVIĆ, dipl.inž.građ.
    prof. dr David LLOJD SMITH, dipl.inž.građ.
    prof. dr. Arsenije VUJOVIĆ, dipl.inž.građ.
    prof. dr Vlado GOCEVSKI, dipl.inž.građ.
    prof. dr Tomislav RADOJIČIĆ, dipl.inž.građ.
    Ivan MAMUŽIĆ, dipl.inž.građ.

Takođe je izabrano i 12 zaslužnih članova JDGK:
    Jovo SMILJANIĆ, dipl.inž.građ.
    Dragan MAJKIĆ, dipl.inž.građ.
    Lajčo STIPIĆ, dipl.inž.građ.
    prof. dr Milivoje STANKOVIĆ, dipl.inž.građ.
    prof. dr Dragoljub DRENIĆ, dipl.inž.građ.
    prof. dr Dušan PETKOVIĆ, dipl.inž.građ.
    prof. dr Dragan BUĐEVAC, dipl.inž.građ.

mr Dragana ČUKIĆ, dipl.inž.građ.
mr Milan ĐOKOVIĆ, dipl.inž.građ.
prof. dr Božidar S. PAVIĆEVIĆ, dipl.inž.građ.
mr Radivoje MRDAK, dipl.inž.građ.
prof. dr Vojislav MIHAILOVIĆ, dipl.inž.građ.

DVANAESTI KONGRES
JUGOSLOVENSKOG DRUŠTVA GRAĐEVINSKIH KONSTRUKTERA
VRNJAČKA BANJA, 27-29. septembar 2006. godine

Na Skupštini JDGK, održanoj 27. septembra 2006. godine *u Vrnjačkoj Banji, izabrano je novo Predsedništvo i Nadzorni odbor JDGK, u sledećem sastavu:*

Predsednik:	prof. dr Dejan BAJIĆ, dipl.inž.građ, Beograd
Potpredsednik:	Svetislav SIMOVIĆ, dipl.inž.građ, Podgorica
Sekretar:	prof. dr Snežana MARINKOVIĆ, dipl.inž.građ, Beograd
Članovi Predsedništva:	prof. dr Dušan NAJDANOVIĆ, dipl.inž.građ, Beograd
	prof. dr Đorđe VUKSANOVIĆ, dipl.inž.građ, Beograd
	prof. dr Dragoslav STOJIĆ, dipl.inž.građ, Niš
	prof. dr Radomir FOLIĆ, dipl.inž.građ, Novi Sad
	doc. dr Đorđe LAĐINOVIĆ, dipl.inž.građ, Novi Sad
	doc. dr Bratislav STIPANIĆ, dipl.inž.građ, Beograd
	doc. dr Aleksandar RISTOVSKI, dipl.inž.građ, Kosovska Mitrovica
	dr Zoran FLORIĆ, dipl.inž.građ, Novi Sad
	Ivan MAMUŽIĆ, dipl.inž.građ, Novi Sad
	Zoran FILIPOVIĆ, dipl.inž.građ, Beograd
	Branko KNEŽEVIĆ, dipl.inž.građ, Beograd
	Slobodan CVETKOVIĆ, dipl.inž.građ, Beograd
	Slobodan MITROVIĆ, dipl.inž.građ, Beograd
Članovi Nadzornog odbora:	mr Slobodan GRKOVIĆ, dipl.inž.građ, Subotica
	Gojko GRBIĆ, dipl.inž.građ, Loznica
	Miroslav MIHAJLOVIĆ, dipl.inž.građ, Paraćin

Na istoj skupštini izabrani su za počasne članove JDGK:
prof. dr Mirko AĆIĆ, dipl.građ.inž.
prof. dr Radomir FOLIĆ, dipl.građ.inž.
prof. dr Radenko PEJOVIĆ, dipl.građ.inž.
prof. dr Trifun PASKALOV , dipl.građ.inž.
Mr Vidoja ZELENOVIĆ, dipl.građ.inž.

Takođe je izabrano i 5 zaslužnih članova JDGK:
prof. dr Đorđe VUKSANOVIĆ, dipl.građ.inž.
prof. dr Dejan BAJIĆ, dipl.građ.inž.

prof. dr Dragoslav STOJIĆ, dipl.građ.inž.
Jožef BARNA , dipl.građ.inž.
mr Predrag PAVLOVIĆ, dipl.građ.inž.

SIMPOZIJUM 2008.
DRUŠTVA GRAĐEVINSKIH KONSTRUKTERA SRBIJE
ZLATIBOR "ČIGOTA", 24-26. septembar 2008.

Predsednik:	prof. dr Dejan BAJIĆ, dipl.inž.građ, Beograd
Potpredsednik:	Svetislav SIMOVIĆ, dipl.inž.građ, Podgorica
Sekretar:	prof. dr Snežana MARINKOVIĆ, dipl.inž.građ, Beograd

Nije bilo izbora za zaslužne i počasne članove Društva.

TRINAESTI KONGRES
DRUŠTVA GRAĐEVINSKIH KONSTRUKTERA SRBIJE
ZLATIBOR "ČIGOTA", 22-24. septembar 2010. godine

Na Skupštini DGKS, održanoj 22. septembra 2010. godine na Zlatiboru izabrano je novo Predsedništvo i Nadzorni odbor DGKS, u sledećem sastavu:

Predsednik:	prof. dr Miloš LAZOVIĆ, dipl.inž.građ, Beograd
Potpredsednik:	Aleksandar BOJOVIĆ, dipl.inž.građ, Beograd
Sekretar:	prof. dr Boško STEVANOVIĆ, dipl.inž.građ, Beograd
Članovi Predsedništva:	prof. dr Snežana MARINKOVIĆ, dipl.inž.građ, Beograd
	prof. dr Đorđe VUKSANOVIĆ, dipl.inž.građ, Beograd
	prof. dr Mihajlo ĐURĐEVIĆ, dipl.inž.građ, Beograd
	prof. dr Đorđe LAĐINOVIĆ, dipl.inž.građ, Novi Sad
	doc. dr Bratislav STIPANIĆ, dipl.inž.građ, Beograd
	prof. dr Dragoslav STOJIĆ, dipl.inž.građ, Niš
	mr Slobodan GRKOVIĆ, dipl.inž.građ, Subotica
	prof. dr Aleksandar RISTOVSKI, dipl.inž.građ, Kos.Mitrovica
	Gojko GRBIĆ, dipl.inž.građ, Loznica
	dr Zoran FLORIĆ, dipl.inž.građ, Novi Sad
	Đorđe PAVKOV, dipl.inž.građ, Novi Sad
	Svetislav SIMOVIĆ, dipl.inž.građ, Beograd
	Goran VUKOBRATOVIĆ, dipl.inž.građ, Novi Sad
	Branko KNEŽEVIĆ, dipl.inž.građ, Beograd
Članovi Nadzornog odbora:	Miroslav MIHAJLOVIĆ, dipl.inž.građ, Paraćin
	prof. dr Zlatko MARKOVIĆ, dipl.inž.građ, Beograd
	Aleksandar TRAJKOVIĆ, dipl.inž.građ, Beograd

Na istoj skupštini izabran je počasni član DGKS:
Prof. dr Mirko AĆIĆ, dipl.inž.građ.

SIMPOZIJUM 2012.
DRUŠTVA GRAĐEVINSKIH KONSTRUKTERA SRBIJE
VRNJAČKA BANJA, 19-21. septembar 2012. godine

Predsednik:	prof. dr Miloš LAZOVIĆ, dipl.inž.građ, Beograd
Potpredsednik:	Aleksandar BOJOVIĆ, dipl.inž.građ, Beograd
Sekretar:	prof. dr Boško STEVANOVIĆ, dipl.inž.građ, Beograd

Nije bilo izbora za zaslužne i počasne članove Društva.

ČETRNAESTI KONGRES
DRUŠTVA GRAĐEVINSKIH KONSTRUKTERA SRBIJE
NOVI SAD, 24-26. septembar 2014. godine

Na Skupštini DGKS, održanoj 24. septembra 2014. godine u Novom Sadu izabrano je novo Predsedništvo i Nadzorni odbor DGKS, u sledećem sastavu:

Predsednik	prof. dr Đorđe LAĐINOVIĆ, dipl.inž.građ, Novi Sad
Potpredsednik:	Aleksandar BOJOVIĆ, dipl.inž.građ, Beograd
Generalni sekretar:	prof. dr Zlatko MARKOVIĆ, dipl.inž.građ, Beograd
Sekretar:	prof. dr Boško STEVANOVIĆ, dipl.inž.građ, Beograd
Članovi predsedništva:	prof. dr Snežana MARINKOVIĆ, dipl.inž.građ, Beograd
	prof. dr Mira PETRONIJEVIĆ, dipl.inž.građ, Beograd
	doc. dr Selimir LELOVIĆ, dipl.inž.građ, Beograd
	mr Branko MILOSAVLJEVIĆ, dipl.inž.građ, Beograd
	prof. dr Dragoslav STOJIĆ, dipl.inž.građ, Niš
	prof. dr Danijel KUKARAS, dipl.inž.građ, Subotica
	Branko KNEŽEVIĆ, dipl.inž.građ, Beograd
	Đorđe PAVKOV, dipl.inž.građ, Novi Sad
	Goran VUKOBRATOVIĆ, dipl.inž.građ, Novi Sad
	Gojko GRBIĆ, dipl.inž.građ, Loznica
	Lazar MARKOVIĆ, dipl.inž.građ, Subotica
	Aleksandar ŽIVANOVIĆ, dipl.inž.građ, Beograd
	Goran TADIĆ, dipl.inž.građ, Beograd
Članovi Nadzornog odbora:	Ivan IGNJATOVIĆ, dipl.inž.građ, predsednik, Beograd
	prof. dr Dejan DIVAC, dipl.inž.građ, Beograd
	Zoran KOVRLIJA, dipl.inž.građ, Beograd

Nije bilo izbora za zaslužne i počasne članove Društva.

SIMPOZIJUM 2016
DRUŠTVA GRAĐEVINSKIH KONSTRUKTERA SRBIJE
ZLATIBOR, 15-17. septembar 2016. godine

Predsednik:	prof. dr Đorđe LAĐINOVIĆ, dipl.inž.građ, Novi Sad
Potpredsednik:	Aleksandar BOJOVIĆ, dipl.inž.građ, Beograd
Generalni sekretar:	prof. dr Zlatko MARKOVIĆ, dipl.inž.građ, Beograd
Sekretar:	prof. dr Boško STEVANOVIĆ, dipl.inž.građ, Beograd

Nije bilo izbora za zaslužne i počasne članove Društva.

Na Skupštini DGKS, održanoj 02. decembra 2016. godine u Beogradu izmenjen je sastav Predsedništva DGKS. Umesto Aleksandra Živanovića, dipl.inž.građ. izabran je Duško Tomić, dipl.inž.građ. (Energoprojekt Visokogradnja).

Na Skupštini DGKS, održanoj 01. decembra 2017. u Beogradu izmenjen je sastav Nadzornog odbora DGKS. Umesto prof. dr Dejana Divca, dipl.inž.građ. i Zorana Kovrlije, dipl.inž.građ. izabrani su doc. dr Predrag Blagojević, dipl.inž.građ. (Građevinsko-arhitektonski fakultet, Niš) i Vojin Zajić, dipl.inž.građ. (STRABAG, Beograd).

PETNAESTI KONGRES
DRUŠTVA GRAĐEVINSKIH KONSTRUKTERA SRBIJE
ZLATIBOR, 6-8. septembar 2018.

Na Skupštini DGKS, održanoj 07. septembra 2018. na Zlatiboru izabrano je novo Predsedništvo i Nadzorni odbor DGKS, u sledećem sastavu:

Predsednik:	prof. dr Zlatko MARKOVIĆ, dipl.inž.građ, Beograd
Potpredsednik:	Lazar MARKOVIĆ, dipl.građ.inž, Subotica
Generalni sekretar:	doc. dr Ivan IGNJATOVIĆ, dipl.građ.inž, Beograd
Sekretar:	prof. dr Boško STEVANOVIĆ, dipl.inž.građ, Beograd

Članovi predsedništva:	prof. dr Đorđe LAĐINOVIĆ, dipl.građ.inž, Novi Sad
	prof. dr Dragoslav STOJIĆ, dipl.građ.inž, Niš
	prof. dr Danijel KUKARAS, dipl.građ.inž, Subotica
	v. prof. dr Marija NEFOVSKA-DANILOVIĆ, dipl.građ.inž, Beograd
	doc. dr Branko MILOSAVLJEVIĆ, dipl.građ.inž, Beograd
	doc. dr Selimir LELOVIĆ, dipl.građ.inž, Beograd
	Branko KNEŽEVIĆ, dipl.građ.inž, Beograd
	Đorđe PAVKOV, dipl.građ.inž, Novi Sad
	Duško TOMIĆ, dipl.građ.inž, Beograd
	Dimitrije ALEKSIĆ, dipl.građ.inž, Beograd

Milan GRČIĆ, dipl.građ.inž, Šid
Darko POPOVIĆ, dipl.građ.inž, Beograd
Miroslav MIHAJLOVIĆ, dipl.građ.inž, Paraćin

Članovi
Nadzornog
odbora:
doc. dr Predrag BLAGOJEVIĆ, dipl.građ.inž, Niš
doc. dr Jelena DOBRIĆ, dipl.građ.inž, Beograd
Vojin ZAJIĆ, dipl.građ.inž, Beograd

Nije bilo izbora za zaslužne i počasne članove Društva.

SIMPOZIJUM 2020. DRUŠTVA GRAĐEVINSKIH KONSTRUKTERA SRBIJE
ARANĐELOVAC, 13.-15. maj 2021.

Predsednik: prof. dr Zlatko MARKOVIĆ, dipl.građ.inž., Beograd
Potpredsednik: Lazar MARKOVIĆ, dipl.građ.inž., Subotica
Generalni
sekretar: v.prof. dr Ivan IGNJATOVIĆ, dipl.građ.inž., Beograd
Sekretar: prof. dr Boško STEVANOVIĆ, dipl.građ.inž., Beograd
Članovi
predsedništva: prof. dr Đorđe LAĐINOVIĆ, dipl.građ.inž. (FTN Novi Sad)
prof. dr Dragoslav STOJIĆ, dipl.građ.inž. (GAF Niš)
prof. dr Danijel KUKARAS, dipl.građ.inž. (GF Subotica)
v.prof. dr Branko MILOSAVLJEVIĆ, dipl.građ.inž. (GF Beograd)
v.prof. dr Marija NEFOVSKA-DANILOVIĆ, dipl.građ.inž. (GF Beograd)
doc. dr Selimir LELOVIĆ, dipl.građ.inž. (GF Beograd)
Branko KNEŽEVIĆ, dipl.građ.inž. (GP Mostogradnja - Beograd)
Dimitrije ALEKSIĆ, dipl.građ.inž. (DEL ING – Beograd)
Đorđe PAVKOV, dipl.građ.inž. (DNP Inženjering - Novi Sad)
Milan GRČIĆ, dipl.građ.inž. (Šidprojekt Šid - Šid)
Darko POPOVIĆ, dipl.građ.inž. (DNEC - Beograd)
Miroslav MIHAJLOVIĆ, dipl.građ.inž. (Grading – Paraćin)
Danijela MIŠČEVIĆ, dipl.građ.inž. (Energoprojekt Entel - Beograd)
Članovi
Nadzornog
odbora: v.prof. dr Predrag BLAGOJEVIĆ, dipl.građ.inž., (GAF Niš)
v.prof. dr Jelena DOBRIĆ, dipl.građ.inž. (GF Beograd)
Vojin ZAJIĆ, dipl.građ.inž. (STRABAG - Beograd)

Na istoj skupštini izabrana su 2 počasna člana DGKS:

prof. dr Meri CVETKOVSKA, dipl.građ.inž. (GF Skopje)
Predrag POPOVIĆ, dipl.građ.inž. (USA)

PRIZNANJA
SAVEZA DRUŠTAVA GRAĐEVINSKIH KONSTRUKTERA JUGOSLAVIJE

ZA ŽIVOTNO DELO
U GRAĐEVINSKOM KONSTRUKTERSTVU

„Priznanje Saveza društava građevinskih konstruktera Jugoslavije za životno delo u građevinskom konstrukterstvu je najviše priznanje koje Predsedništvo SDGKJ dodeljuje svojim istaknutim članovima za izuzetan doprinos koji su dogogodišnjim radom i rezultatima dali razvoju našeg građevinskog konstrukterstva i napretku Socijalističke Federativne Republike Jugoslavije.“

Priznanje je ustanovljeno 1989. godine.

Dobitnici priznanja SDGKJ za životno delo u građevinskom konstrukterstvu su:

1989.

ĐORĐE LAZAREVIĆ
akademik SANU, profesor dr h.c,
diplomirani građevinski inženjer,
prvi predsednik Jugoslovenskog društva građevinskih konstruktera, od 1958. do 1964. godine

KRUNISLAV TONKOVIĆ
profesor dr,
diplomirani građevinski inženjer,
drugi predsednik Jugoslovenskog društva građevinskih konstruktera, od 1964. do 1969. godine

BRANKO ŽEŽELJ
akademik SANU, profesor,
diplomirani građevinski inženjer

1990.

NIKOLA HAJDIN
akademik SANU, profesor dr,
diplomirani građevinski inženjer,
predsednik Jugoslovenskog društva građevinskih konstruktera, od 1978. do 1981. godine

MILORAD IVKOVIĆ
profesor dr,
diplomirani građevinski inženjer

STANKO ŠRAM
profesor dr,
diplomirani građevinski inženjer

1991.

STOJAN DINIĆ
diplomirani građevinski inženjer,
sekretar i generalni sekretar SDGKJ od 1969. godine -

ZLATKO KOSTRENČIĆ
profesor dr,
diplomirani građevinski inženjer

FRANCI KRŽIĆ
profesor dr,
diplomirani građevinski inženjer,
potpredsednik SDGKJ od 1987. godine -

PETAR SERAFIMOV
akademik MANU, profesor dr,
diplomirani građevinski inženjer

Od 1991. do 1998. godine nisu dodeljivana priznanja za životno delo.

Jugoslovensko društvo građevinskih konstruktera je 1998. godine donelo odluku o nastavljanju dodeljivanja priznanja JDGK za žitovno delo u građevinskom konstrukterstvu.

PRIZNANJA
JUGOSLOVENSKOG DRUŠTVA GRAĐEVINSKIH KONSTRUKTERA

ZA ŽIVOTNO DELO
U GRAĐEVINSKOM KONSTRUKTERSTVU

„Priznanje Jugoslovenskog društva građevinskih konstruktera za životno delo u građevinskom konstrukterstvu je najviše priznanje koje Predsedništvo JDGK dodeljuje svojim istaknutim članovima za izuzetan doprinos koji su dogogodišnjim radom i rezultatima dali razvoju našeg građevinskog konstrukterstva.“

Dobitnici priznanja JDGK za životno delo u građevinskom konstrukterstvu su:

1998.

GOJKO NENADIĆ
profesor,
diplomirani građevinski inženjer

ŽIVOTA PERIŠIĆ
profesor dr,
diplomirani građevinski inženjer,
predsednik SDGKJ/JDGK od 1987. do 1998. godine

2000.

BOŠKO PETROVIĆ
akademik SANU, profesor dr,
diplomirani građevinski inženjer

MILAN GOJKOVIĆ
profesor dr,
diplomirani građevinski inženjer

BOŽIDAR S. PAVIĆEVIĆ
diplomirani građevinski inženjer

2002.

MIRKO AĆIĆ
profesor dr,
diplomirani građevinski inženjer
predsednik JDGK od 1998. godine -

RADOMIR FOLIĆ
profesor dr,
diplomirani građevinski inženjer

ARSENIJE VUJOVIĆ
profesor dr,
diplomirani građevinski inženjer

DIMITRIJE ĆERTIĆ
profesor,
diplomirani građevinski inženjer

2004.

MIROSLAV DEBELJKOVIĆ
profesor,
diplomirani građevinski inženjer

ALEKSANDAR PAKVOR
profesor dr,
diplomirani građevinski inženjer

PREDRAG ŽELALIĆ
diplomirani građevinski inženjer

2006.

MOMIR KRASTAVČEVIĆ
profesor,
diplomirani građevinski inženjer

PRIZNANJA
DRUŠTVA GRAĐEVINSKIH KONSTRUKTERA SRBIJE

ZA ŽIVOTNO DELO
U GRAĐEVINSKOM KONSTRUKTERSTVU

„Priznanje Društva građevinskih konstruktera Srbije za životno delo u građevinskom konstrukterstvu je najviše priznanje koje Predsedništvo DGKS dodeljuje svojim istaknutim članovima za izuzetan doprinos koji su dogogodišnjim radom i rezultatima dali razvoju našeg građevinskog konstrukterstva.“

Dobitnici priznanja DGKS za životno delo u građevinskom konstrukterstvu su:

2008.

MIHAILO MURAVLJOV
profesor dr,
diplomirani građevinski inženjer

2010.

DANILO DRAGOJEVIĆ
diplomirani građevinski inženjer

VUKAN NJAGULJ
diplomirani građevinski inženjer

2012.

LJUBOMIR VLAJIĆ
profesor dr,
diplomirani građevinski inženjer

2014.

ŠERIF DUNICA
profesor dr,
diplomirani građevinski inženjer

2016.

VANJA ALENDAR
diplomirani građevinski inženjer

SLOBODAN CVETKOVIĆ
diplomirani građevinski inženjer

2018.

DEJAN BAJIĆ
profesor dr, Predsednik DGKS od 2006. do 2010. godine,
diplomirani građevinski inženjer

2020.

DUŠAN NAJDANOVIĆ
profesor dr,
diplomirani građevinski inženjer

2022.

ALEKSANDAR BOJOVIĆ
diplomirani građevinski inženjer

DRAGO OSTOJIĆ
diplomirani građevinski inženjer

PRIZNANJA
SAVEZA DRUŠTAVA GRAĐEVINSKIH KONSTRUKTERA JUGOSLAVIJE

ZA NAJBOLJA OSTVARENJA
U GRAĐEVINSKOM KONSTRUKTERSTVU

„U cilju podsticanja stvaralaštva, boljeg vrednovanja postignutih rezultata i najznačajnijih dostignuća našeg građevinskog konstrukterstva, Predsedništvo SDGKJ je početkom 1986. godine ustanovilo posebna godišnja stručna i društvena priznanja za najbolja ostvarenja u građevinskom konstrukterstvu u republikama i pokrajinama i u Jugoslaviji. Republička i pokrajinska društva građevinskih konstruktera dodeljuju svoja priznanja za najbolja ostvarenja u republikama i pokrajinama a Predsedništvo SDGKJ dodeljuje Jugoslovensko priznanje SDGKJ najboljem ostvarenju izabranom u konkurenciji ostvarenja koja su u toj godini dobila republička i pokrajinska priznanja."

Priznanja su prvi put dodeljena za konstrukterska ostvarenja u 1986. godini.

Jugoslovenska priznanja SDGKJ za najbolja ostvarenja u građevinskom konstrukterstvu dobila su sledeća ostvarenja:

1986.

KONSTRUKCIJA NOVOG HANGARA JUGOSLOVENSKOG AEROTRANSPORTA NA AERODROMU BEOGRAD

Odgovorni projektanti konstrukcije:
profesor dr Milorad Ivković, dipl.inž.građ.
profesor dr Života Perišić, dipl.inž.građ.
profesor dr Mirko Aćić, dipl.inž.građ.
profesor dr Aleksandar Pakvor, dipl.inž.građ.

Graditelji konstrukcije:
Živadin Mijailović, dipl.inž.građ.
Višeslav Milosavljević, dipl.inž.građ.

1987.

PROJEKAT KONSTRUKCIJE KOMPLEKSA "CIBONA" U ZAGREBU

profesor dr Milutin Anđelić, dipl.inž.građ.

1988.

Naučnoistraživački rad:

POPREČNA RASPODELA OPTEREĆENJA KOD MOSTOVA SA VEĆIM BROJEM GLAVNIH NOSAČA U POPREČNOM PRESEKKU

asistent dr Zoran Desovski, dipl.inž.građ.

1989.

TEHNIČKO-TEHNOLOŠKO UNAPREĐENJE GRAĐEVINSKOG KONSTRUKTERSTVA NA IZGRADNJI HRAMA SVETOG SAVE NA VRAČARU U BEOGRADU PRIMENOM METODA TEŠKE GRAĐEVINSKE MONTAŽE, SPECIJALNE TEHNOLOŠKE PODIZNE OPREME, KAO I NOVIH KONSTRUKTIVNIH REŠENJA

Vojislav Marisavljević, dipl.inž.građ.
Dušan Arbajter, dipl.inž.građ.
Milutin Marjanović, dipl.inž.građ.
Dragan Kocić, dipl.inž.građ.
mr Milan Matović, dipl.inž.građ.

1990.

HIDROELEKTRANA "VIŠEGRAD"

Mira Pavlica, dipl.inž.građ.
Fevzija Beganović, dipl.inž.građ.
Mirza Pašić, dipl.inž.građ.
Vladimir Vujošević, dipl.inž.građ.

PRIZNANJA
JUGOSLOVENSKOG DRUŠTVA GRAĐEVINSKIH KONSTRUKTERA

ZA NAJBOLJA OSTVARENJA
U GRAĐEVINSKOM KONSTRUKTERSTVU

„U cilju podsticanja stvaralaštva, boljeg vrednovanja postignutih rezultata i najznačajnijih dostignuća našeg građevinskog konstrukterstva, Jugoslovensko društvo građevinskih konstruktera je ustanovilo posebna godišnja priznanja za najbolja ostvarenja u građevinskom konstrukterstvu u SR Jugoslaviji. Priznanja se dodeljuju za oblast projektovanja i/ili građenja konstrukcija objekata i za oblast nauke i tehnologije u građevinskom konstrukterstvu."

Priznanja JDGK za najbolja ostvarenja u građevinskom konstrukterstvu dobila su sledeća ostvarenja:

1994.

Za projektovanje i izvođenje konstrukcije objekta:

PODZEMNO ŽELEZNIČKO STAJALIŠTE "VUKOV SPOMENIK"

SAOBRAĆAJNI INSTITUT - CIP
Odgovorni projektanti konstrukcije:
dr Branislav Popović, dipl.inž.građ.
Miloje Kandić, dipl.inž.građ.
Aleksandar Mojsić, dipl.inž.građ.

ENERGOPROJEKT HOLDING
Graditelji konstrukcije:
mr Dragan Gojgić, dipl.inž.građ.
Stanimir Mandić, dipl.inž.građ.
Vladimir Đurić, dipl.inž.građ.
Boško Grubić, dipl.inž.građ.

1996. i 1997.

Iz oblasti projektovanja i izvođenja konstrukcija:

IZVOĐENJE KONSTRUKCIJE DVORANE ZA MALE SPORTOVE FAKULTETA FIZIČKE KULTURE U BEOGRADU

Živorad Dimitrijević, dipl.inž.građ.

IZGRADNJA KOMPLEKSA ZA PROIZVODNJU LAB/LABS U KIRIŠU U RUSIJI

Svetislav Simović, dipl.inž.građ.
Nikola Lujić, dipl.inž.građ.
Novica Kostić, dipl.inž.građ.

Iz oblasti nauke i tehnologije u građevinskom konstrukterstvu:

STRATEŠKO-TEHNOLOŠKI PROJEKAT „UVOĐENJE EVROKODOVA ZA KONSTRUKCIJE U GRAĐEVINSKO KONSTRUKTERSTVO SRBIJE"

Rukovodilac projekta:
prof. dr Života Perišić, dipl.inž.građ.

Rukovodioci potprojekta:
prof. dr Aleksandar Pakvor, dipl.inž.građ.
v.prof. dr Dragan Buđevac, dipl.inž.građ.
prof. dr Dragoslav Stojić, dipl.inž.građ.
prof. dr Milić Milićević, dipl.inž.građ.
prof. dr Mihailo Muravljov, dipl.inž.građ.
prof. dr Petar Anagnosti, dipl.inž.građ.
prof. dr Radomir Folić, dipl.inž.građ.

1998. i 1999.

Iz oblasti projektovanja i izvođenja konstrukcija:

SPORTSKA DVORANA - BEOGRADSKA ARENA

Autori krovne konstrukcije:
prof. dr Milorad Ivković, dipl.inž.građ.
prof. dr Života Perišić, dipl.inž.građ.

prof. dr Mirko Aćić, dipl.inž.građ.
prof. dr Aleksandar Pakvor, dipl.inž.građ.

Projektanti krovne konstrukcije:
Vanja Alendar, dipl.inž.građ., viši stručni saradnik
asis. mr Snežana Marinković, dipl.inž.građ.
Odgovorni projektant:
Savo Formentunović, dipl.inž.građ.

Saradnik na projektu krovne konstrukcije:
Bojan Tepavčević, dipl.inž.građ.

Graditelji konstrukcije:
Živorad Dimitrijević, dipl.inž.građ.
mr Miilan Đoković, dipl.inž.građ.

MOST NA OBILAZNICI AUTOPUTA U BEOGRADU (OSTRUŽNICA) PREKO REKE SAVE

Projektanti:
Za čeličnu konstrukciju
Slobodan Cvetković, dipl.inž.građ.
Danilo Dragojević, dipl.inž.građ.
Za prilazne konstrukcije
Ivanka Kopčalić, dipl.inž.građ.
Stanislav Mojsilović, dipl.inž.građ.

Izvođači:
Za čeličnu konstrukciju
Stanoje Petković, dipl.inž.građ.
Branko Knežević, dipl.inž.građ.
Siniša Bruski, dipl.inž.građ.
Za betonskku konstrukciju
Miroslav Havram, dipl.inž.građ.
Mihajlo Tadić, dipl.inž.građ.
Ranko Petrović, dipl.inž.građ.

MOST NA BARŽAMA PREKO DUNAVA U NOVOM SADU

Radomir Lukić, dipl.inž.građ.
Vukan Njagulj, dipl.inž.građ.
Đorđe Denčić, dipl.inž.građ.
Miško Gunjača, dipl.inž.građ.
mr Radomir Potić, dipl.inž.građ.

Iz oblasti nauke:

DOKTORSKA DISERTACIJA „PRILOG ANALIZI STABILNOSTI TANKOZIDNIH NOSAČA"

dr Duško Lučić, dipl.inž.građ.

MONOGRAFIJA "METALNE KONSTRUKCIJE"

Autori:
prof. dr Dragan Buđevac, dipl.inž.građ.
asis. mr Zlatko Marković, dipl.inž.građ.
asis. mr Dragana Bogavac, dipl.inž.građ.
asis. mr Dragoslav Tošić, dipl.inž.građ.

2000. i 2001.

Iz oblasti projektovanja i izvođenja konstrukcija:

PROJEKTOVANJE I IZGRADNJA MOSTA PREKO DUNAVA U NOVOM SADU "PETROVARADINSKA DUGA"

Projektanti mosta:
prof. Gojko Nenadić, dipl.inž.građ.
mr Ljiljana Đukić, dipl.inž.građ.

Projektant donjeg stroja:
Vukan Njagulj, dipl.inž.građ.

Projektanti montaže:
Dragomir Lukić, dipl.inž.građ.
Miško Gunjača, dipl.inž.građ.

Šef montaže:
Branko Knežević, dipl.inž.građ.

PROJEKAT KONSTRUKCIJE POSLOVNOG OBJEKTA "ZEPTER" INTERNATIONAL - VARŠAVA

Autori:
doc. dr Miroslav Bešević, dipl.inž.građ.
prof. dr Dejan Bajić, dipl.inž.građ.
prof. dr Dragan Buđevac, dipl.inž.građ.

PROJEKTOVANJE I IZGRADNJA MOSTA PREKO REKE VELIKE MORAVE NA DESNOJ TRACI AUTOPUTA E70 KROZ MESTO MIJATOVAC

Projektant mosta:
Vukan Njagulj, dipl.inž.građ.

Projektant montaže:
Miroslav Havran, dipl.inž.građ.

Rukovodilac radova:
Mihajlo Tadić, dipl.inž.građ.

Iz oblasti nauke:

DOKTORSKA DISERTACIJA „GRANIČNA NOSIVOST PRI PROBIJANJU MONTAŽNIH PRETHODNO NAPREGNUTIH PLOČA U OBLASTI IVIČNIH STUBOVA"

dr Snežana Marinković, dipl.inž.građ.

DOKTORSKA DISERTACIJA „UTICAJ VREMENSKIH DEFORMACIJA NA GRANIČNA STANJA ARMIRANOBETONSKIH PLOČA NAPREGNUTIH U SVOJOJ RAVNI"

dr Pero Vujović, dipl.inž.građ.

2002. i 2003.

Iz oblasti projektovanja i izvođenja konstrukcija:

MOST "UNION BRIDGE" PREKO REKE MORAČE U PODGORICI

Autor idejnog rešenja i odgovorni projektant mosta:
mr Željka Radovanović, dipl.inž.građ.

Odgovorni projektant mosta:
dr Pero Vujović, dipl.inž.građ.

Iz oblasti nauke:

DOKTORSKA DISERTACIJA „IZBOČAVANJE LIMENIH NOSAČA POD DEJSTVOM LOKALNOG OPTEREĆENJA"

dr Nenad Marković, dipl.inž.građ.

XXX

DOKTORSKA DISERTACIJA „PRILOG ANALIZI VITKIH ARMIRANO-BETONSKIH ELEMENATA SA KOSIM SAVIJANJEM“

dr Radomir Zejak, dipl.inž.građ.

DOKTORSKA DISERTACIJA „VIŠEKRITERIJUMSKA ANALIZA SEIZMIČKE OTPORNOSTI KONSTRUKCIJA ARMIRANOBETONSKIH ZGRADA“

dr Đorđe Lađinović, dipl.inž.građ.

2004. i 2005.

Iz oblasti projektovanja i izvođenja konstrukcija:

SANACIJA, REKONSTRUKCIJA, ADAPTACIJA I DOGRADNJA KONSTRUKCIJE P.C. UŠĆE U NOVOM BEOGRADU, NAKON BOMBARDOVANJA 1999. GODINE

Projektanti:
prof. dr Ljubomir Vlajić, dipl.inž.građ.
mr Predrag Blagojević, dipl.inž.građ.
mr Slobodan Grković, dipl.inž.građ.

iz oblasti nauke:

MAGISTARSKA TEZA „PRILOG UTVRĐIVANJU SEIZMIČKE POUZDANOSTI IZVEDENIH ARMIRANO BETONSKIH OBJEKATA“

mr Nataša STOJANOVIĆ, dipl.inž.građ.

2006. i 2007.

Iz oblasti projektovanja i izvođenja konstrukcija:

PROJEKAT DRUMSKOG MOSTA PREKO REKE VISLE U PLOCKU - IZVEDENO STANJE

Projektanti:
akademik prof. dr Nikola Hajdin, dipl.inž.građ.
doc. dr Bratislav Stipanić, dipl.inž.građ.

PUENTE DUARTE REHABILITATION PROJECT IN SANTO DOMINGO

Projektanti:
Slobodan Cvetkovic, dipl.inž.građ.
Stanislav Kolundzija, dipl.inž.građ.
prof. dr Branislav Kolundzija, dipl.inž.građ.

Iz oblasti nauke:

PRILOG REŠENJU PROBLEMA STABILNOSTI DVOPOJASNIH LANČANIČNIH SISTEMA

Dragan Kostić, dipl.inž.građ.

2008. i 2009.

Iz oblasti projektovanja i izvođenja konstrukcija:

NOVI TORANJ NA AVALI. KONSTRUKCIJA TORNJA

prof. dr Šerif Dunica, dipl.inž.građ.
Branislav Životić, dipl.inž.građ.
Aleksandar Bojović, dipl.inž.građ.

SPECIFIČNOSTI IZVOĐENJA OBNOVE TV TORNJA "AVALA"

Goran Milovanović, dipl.inž.građ.
Zoran Mišković, dipl.inž.građ.

Iz oblasti nauke:

PRERASPODELA UTICAJA KOD NAKNADNO KONTINUIRANIH SPREGNUTIH ARMIRANOBETONSKIH NOSAČA TOKOM VREMENA

Snežana Mašović, dipl.inž.građ.

PRORAČUN VITKIH DVOOSNO SAVIJANIH AB STUBOVA

Zoran Brujić, dipl.inž.građ.

2010. i 2011.

Iz oblasti nauke:

DOKTORSKA DISERTACIJA „EKSPERIMENTALNO–TEORIJSKA ANALIZA GRANIĈNIH STANJA ARMIRANOBETONSKIH LINIJSKIH NOSAĈA OJAĈANIH SPREZANJEM SA NSM VLAKNASTIM KOMPOZITIMA“

dr Slobodan Ranković, dipl.inž.građ.

2012. i 2013.

Iz oblasti projektovanja i izvođenja konstrukcija:

NASTAJANJE I RAZRADA IDEJNOG REŠENJA I GRAĐENJE RASKLOPNOG MOSTA „PORT MILENA“

Projektanti:
Goran Tadić, dipl.inž.građ.
Duško Bobera, dipl.inž.građ.
Zoran Luković, dipl.inž.građ.

Iz oblasti nauke:

PONAŠANJE GRUPE ELASTIČNIH MOŽDANIKA KOD SPREGNUTIH NOSAČA OD ČELIKA I BETONA

dr Milan Spremić, dipl.inž.građ.

GRANIČNA NOSIVOST ARMIRANOBETONSKIH GREDNIH NOSAČA OD BETONA SA RECIKLIRANIM AGREGATOM

dr Ivan Ignjatović, dipl.inž.građ.

2014. i 2015.

Iz oblasti projektovanja i izvođenja konstrukcija:

ČELIČNA KONSTRUKCIJA ŽELEZNIČKOG MOSTA PREKO VELIKE MORAVE U ĆUPRIJI

Projektanti:
Siniša Mihajlović, dipl.inž.građ.

Milorad Markovi, dipl.inž.građ.
Biljana Čolić, dipl.inž.građ.
Dejan Srejić, dipl.inž.građ.
prof. dr Šerif Dunica, dipl.inž.građ.
Marina Pešić, dipl.inž.građ.
Branislav Dašić, dipl.inž.građ.

ATLETSKA DVORANA "GENERAL JOVAN MIŠKOVIĆ" U BEOGRADU

Projektanti:
prof dr Zlatko Marković, dipl.inž.građ.
Milomir Živanović, dipl.inž.građ.
doc. dr Jelena Dobrić, dipl.inž.građ.
prof. dr Dragan Buđevac, dipl.inž.građ.

Iz oblasti nauke:

DOKTORSKA DISERTACIJA „PONAŠANJA CENTRIČNO PRITISNUTIH ELEMENATA SLOŽENOG PRESEKA OD NERĐAJUĆEG ČELIKA"

dr Jelena Dobrić, dipl.inž.građ.

DOKTORSKA DISERTACIJA „NELINEARNA STATIČKA I DINAMIČKA ANALIZA OKVIRNIH ZGRADA PREMA PERFORMANSAMA"

dr Mladen Ćosić, dipl.inž.građ.

DOKTORSKA DISERTACIJA „NOSIVOST ZAVRTNJEVA KAO SREDSTVA ZA SPREZANJE U PREFABRIKOVANIM SPREGNUTIM KONSTRUKCIJAMA OD ČELIKA I BETONA"

dr Marko Pavlović, dipl.inž.građ.

2016. i 2017.

Iz oblasti projektovanja i izvođenja konstrukcija:

POSLOVNI KOMPLEKS "SIRIUS" U BLOKU 43 NA NOVOM BEOGRADU

Projektanti:
Vladimir Stefanović, dipl.inž.građ.
Igor Petrović, dipl.inž.građ.

PROJEKAT KONSTRUKCIJE POSLOVNOG OBJEKTA U RAJIĆEVOJ

Projektanti:
Aleksandar Trajković, dipl.inž.građ.
Ivana Leposavić, dipl.inž.građ.
Tanja Karlaš, dipl.inž.građ.
Vladimir Trajković, dipl.inž.građ.
Bojana Žarković, dipl.inž.građ.
Nenad Nedeljić, dipl.inž.građ.

Iz oblasti nauke:

DOKTORSKA DISERTACIJA „PONAŠANJE AKSIJALNO PRITISNUTIH SPREGNUTIH STUBOVA PRI EKSPLOATACIONOM I GRANIČNOM OPTEREĆENJU“

dr Aleksandar Landović, dipl.inž.građ.

DOKTORSKA DISERTACIJA „EKSPERIMENTALNO ISTRAŽIVANJE GRANIČNE NOSIVOSTI OSLONAČKE VEZE OŠUPLJENIH MONTAŽNIH PLOČA“

dr Veljko Koković, dipl.inž.građ, prof dr Dejan Bajić, dipl.inž.građ.

DOKTORSKA DISERTACIJA „NELINEARNA ANALIZA LAMINATNIH KOMPOZITNIH PLOČA I LJUSKI SA DELAMINACIJAMA PRIMENOM MKE“

dr Miroslav Marjanović, dipl.inž.građ.

2018. i 2019.

Iz oblasti projektovanja i izvođenja konstrukcija:

ŽELEZNIČKO-DRUMSKI MOST PREKO DUNAVA U NOVOM SADU

Projektanti:
Aleksandar Bojović, dipl.građ.inž.
prof. dr Zlatko Marković, dipl.građ.inž.
Dimitrije Aleksić, dipl.građ.inž.
dr Marko Pavlović, dipl.građ.inž.
Novak Novaković, dipl.građ.inž.
doc. dr Milan Spremić, dipl.građ.inž.
Uroš Kostić, dipl.građ.inž.
Boško Janjušević, dipl.građ.inž.

Iz oblasti nauke:

DOKTORSKA DISERTACIJA „INOVATIVNI SISTEM ZA SEIZMIČKI OTPORNU ZIDANU ISPUNU U ARMIRANOBETONSKIM RAMOVSKIM KONSTRUKCIJAMA"

dr Marko Marinković, dipl.građ.inž.

DOKTORSKA DISERTACIJA „PONAŠANJE SMIČUĆIH SPOJEVA IZVEDENIH MOŽDANICIMA SA EKSERIMA SA EKSPLOZIVNIM UPUCAVANJEM"

dr Nina Gluhović, dipl.građ.inž.

DOKTORSKA DISERTACIJA „GRANIČNA NOSIVOST ARMIRANOBETONSKIH GREDNIH NOSAČA OD BETONA SA VELIKIM SADRŽAJEM LETEĆEG PEPELA"

dr Jelena Dragaš, dipl.građ.inž.

2020 i 2021

Iz oblasti projektovanja i izvođenja konstrukcija:

MOST MORAČICA NA AUTOPUTU BAR - BOLJARE, DEONICA SMOKOVAC – MATEŠEVO

projektant:
Željko Ličina, dipl.građ.inž.

DRUMSKI MOST PREKO SAVE U OSTRUŽNICI, NA OBILAZNICI OKO BEOGRADA

STRABAG
autori:
Bojan Bizetić, dipl.građ.inž.
Igor Đurđević, dipl.građ.inž.
Branislav Dašić, dipl.građ.inž.
Vukan Njagulj, dipl.građ.inž.
Branko Knežević, dipl.građ.inž.

POSLOVNO-STAMBENI KOMPLEKS BLOKA 65 NA KP 2222/3 U ULICI OMLADINSKIH BRIGADA BR. 86 NA NOVOM BEOGRADU ZA II FAZU – KULA I TRŽNI CENTAR

DEL ING
Projektanti:
Prof. dr Šerif Dunica, dipl.građ.inž.
V.prof. dr Saša Stošić, dipl.građ.inž.

Iz oblasti nauke:

DOKTORSKA DISERTACIJA "NOSIVOST RAZLIČITIH TIPOVA RAVNOKRAKIH UGAONIKA OD NERĐAJUĆEG ČELIKA PRI DEJSTVU CENTRIČNOG PRITISKA"

dr Aljoša Filipović, dipl.inž.građ.

DOKTORSKA DISERTACIJA "UTICAJ PRSLINA NA MEHANIZME DETERIORACIJE I TRAJNOST ARMIRANOBETONSKIH KONSTRUKCIJA"

dr Vedran Carević, dipl.inž.građ.

DOKTORSKA DISERTACIJA "NOVI KONSTITUTIVNI MODEL BETONA FORMULISAN PREMA NAPREGNUTOJ KOMBINACIJI TEORIJA PLASTIČNOSTI – MEHANIKA OŠTEĆENJA"

dr Drago Živković, dipl.inž.građ.

CONTENT

ДГКС ASES

ASES AWARDS
FOR LIFETIME ACHIEVEMENT IN 2022

PRIZNANJE ZA ŽIVOTNO DELO U GRAĐEVINSKOM KONSTRUKTERSTVU ALEKSANDRU BOJOVIĆU, DIPL.INŽ.GRAĐ.

OSNOVNI BIOGRAFSKI PODACI

Aleksandar Bojović rođen je u Beogradu 22. novembra 1948. Osnovnu školu i gimnaziju (VI beogradska gimnazija) završio je u Beogradu. Studirao je na Građevinskom fakultetu Univerziteta u Beogradu, gde je diplomirao januara 1975. na odseku za konstrukcije i smeru metalnih konstrukcija. Govori nemački, engleski i ruski jezik (osnovna znanja). Oženjen je i otac dvoje dece.

Radio je u Mostprojektu (do 1978. pod nazivom Direkcija za izgranju mostova) 1975−1993, u svim zvanjima, počev od inženjera pripravnika do vodećeg projektanta, Mašinoprojektu 1993−1998. kao direktor sektora za konstrukcije, Srpskoj akademiji nauka i umetnosti 1998−2001, kao inženjer-istraživač, i DEL ING-u 2001—2013 (penzionisanje)—danas, kao tehnički direktor.

KARIJERA I REFERENCE

Cela profesionalna karijera Aleksandra Bojovića zasnivala se na tri principa: prvi – inženjer mora da poznaje sve detalje svog posla i – ako je npr. glavni projektant – da može da zameni bilo kog člana svog tima; drugi – obaveza je svakog inženjera da se neprekidno usavršava, već počev od momenta diplomiranja; znanja stečena na studijama su odlična osnova, ali ne i dovoljna u praksi; treći – inženjersko iskustvo, naročito projektanta, mora da bude što raznovrsnije i da uključuje i gradilišno iskustvo; samo na taj način moguće je potpuno sagledavanje objekta i konstrukcije.

Bojović je svoju karijeru gradio postupno, počevši od osnova konstruisanja - kroz stotine ručno izrađenih izvođačkih crteža, zatim godina rada (ukupno sedam) na gradilištima velikih i složenih inženjerskih objekata i konstantnim usavršavanjem preko praćenja i korišćenja inostrane stručne literature i standarda. Ovakva široka osnova znanja i iskustava omogućila je uspešan projektantski rad, između ostalog, i na objektima najveće složenosti i veličine, među kojima su i neki koji spadaju u najistaknutije reference našeg konstrukterstva uopšte.

Bojović je bio projektant čeličnih konstrukcija – mostova, sportskih, telekomunikacionih, industrijskih i javnih objekata, cevovoda, dimnjaka i kao nadzorni inženjer u fabrikama čeličnih konstrukcija i na montažama velikih mostova, konstrukcijama termo elektrana i zgrada. Objekti o kojima je reč su u Srbiji, ex Jugoslaviji, Rusiji, Nemačkoj, Poljskoj, Libiji. Projekti su rađeni prema ugovorima u i saradnji firmi iz Srbije, ex Jugoslavije, Rusije, Nemačke, Italije, Španije i Danske, primenom srpskih, ruskih, nemačkih, britanskih, poljskih ili evropskih standarda. Jezici projekata bili su: srpski, ruski, nemački, engleski i poljski.

Najznačajnije reference kao projektant (najkraći izbor), sa godinama otvaranja:

− Železničko-drumski most preko Dunava, Novi Sad, 2018: Odgovorni projektant. *Svetski rekord raspona* ($L = 219$ m) čeličnih lučnih mostova sa dijagonalnim vešaljkama, železničkih sa dva koloseka.

– Drumski Most slobode u Novom Sadu, 2005. Odgovorni projektant. Ponovna izgradnja mosta srušenog 1999. Most je (prema zahtevu Projektnog zadatka) istog izgleda kao stari, ali sa brojnim izmenama i ojačanjima konstrukcije. Sistema je sa kosim kablovima, L = 351 m.
– Drumski most preko Visle, Plock, Poljska, 2005. Projektant čeličnih i spregnutih konstrukcija. (Glavni projektanti: N. Hajdin i B. Stipanić. Projektanti: A. Bojović, Š. Dunica i M. Lazović). Most sistema sa kosim kablovima, L = 375 m. *Najveći čelični drumski most koji su ikad projektovali srpski inženjeri*. Najveći most u Poljskoj.
– Fudbalski stadion Arena Himki, Himki, Rusija, 2008. Glavni inženjer projekta i odgovorni projektant čeličnih konstrukcija. Stadion za 20.000 gledalaca po standardima UEFA. Prvi veći fudbalski stadion koji su posle više od 50 godina projektovali srpski inženjeri.
– Ledene dvorane za hokej, Podolsk i Čehov, Rusija, 2001. i 2003. Odgovorni projektant čeličnih konstrukcija. Čelične konstrukcije dvorana velikih raspona (L = 62,5 m i 54,0 m).
– Toranj na Avali, Beograd, 2009. Odgovorni projektant čeličnog dela konstrukcije. Toranj identičnog oblika kao stari, srušen 1999, ali potpuno različite konstrukcije. H = 205 m.
– Hangar za remont aviona, Sebha, Libija, 1984. Odgovorni projektant. Čelična konstrukcija, L_{max} = 82,5 m.
– Glavni krst Hrama Svetog Save, Beograd, 1989. Konstrukcija od nerđajućeg čelika, HxB = 11,0x5,5 m.
– Toplovod ispod Mosta Gazela, Beograd, 1992. Odgovorni projektant. Složen sistem cevi, noseće konstrukcije toplovoda i prilaznih mostova i mosta preko reke.

Najznačajnije reference kao nadzorni inženjer:
– Železnički most preko Save, Beograd, 1976-1979. Nadzor na radioničkoj izradi i na montaži konstrukcije.
– Drumski most preko Save u produžetku Brankove ulice, Beograd, 1976-1978. Nadzor na radioničkoj izradi i na montaži konstrukcije.
– Drumski most preko Save, Ostružnica. Nadzor na radioničkoj izradi i montaži čelične konstrukcije i izvođenja betonskih konstrukcija fundamenata i stubova.
– Platforme u dimnjaku H = 280 m TENT B, sanacija čeličnih konstrukcija, 1982.
– Gerist Bloka 1 TENT B, H = 130 m, Obrenovac, sanacija čeličnih konstrukcija, 1985.

PUBLIKACIJE

Aleksandar Bojović je autor 3 knjige, 3 prevoda, 57 radova stručne literature, kao i 5 standarda.

Knjige:
[1] Bojović, A.: Čelični mostovi. Izabrana poglavlja. U pripremama za štampu. Akademska misao, Beograd. Očekivano objavljivanje: jesen 2022.
[2] Bojović, A: Proračun opterećenja vetrom građevinskih konstrukcija. "Građevinska knjiga", Beograd, 1993.
[3] Bojović, A.: Železničko-drumski most preko Dunava u Novon Sadu. Istorijat – Projektovanje – Građenje. Časopis „Izgradnja", Beograd, 2019.
[4] Cvetković, S., Bojović, A., Stipanić, S.: Čelični mostovi, (poglavlje iz knjige-priručnika Tehničar 5). "Građevinska knjiga", Beograd, 1987.

Prevodi:

[5] Bojović,A., Trebinjac,V.: SIA 161/1979 - Švajcarske norme za čelične konstrukcije. Prevod sa nemačkog. Jugoslovenski građevinski centar, Beograd, 1983.

[6] Bojović, A.: Nemački nacionalni dokument za primenu EC 3. Prevod sa nemačkog. ENV 1993-1-1: 1992. EC 3: Proračun čeličnih konstrukcija. Deo 1.1: Opšta pravila za proračun za proračun zgrada. Nacionalni dokumenti za primenu EC 3 Ujedinjenog Kraljevstva, Nemačke, Francuske. Građevinski fakultet Univerziteta u Beogradu, 1995.

[7] Bojović, A.: EN 10025: Vruće valjani proizvodi od nelegiranih konstrukcionih čelika - tehnički uslovi isporuke. Prevod sa nemačkog. ENV 1993-1-1: 1992. EC 3: Proračun čeličnih konstrukcija. Deo 1.1: Opšta pravila za proračun za proračun zgrada. EN 10025: Vruće valjani proizvodi od nelegiranih konstrukcionih čelika - tehnički uslovi isporuke. Nacionalni dokumenti za primenu EC 3 Ujedinjenog Kraljevstva, Nemačke, Francuske. Građevinski fakultet Univerziteta u Beogradu, 1995.

Radovi: 57 radova u domaćim i stranim stručnim časopisima, kao i u zbornicima radova sa domaćih i stranih stručnih i naučnih skupova. Kratak izbor:

[8] Dunica, Š., Bojović, A.: Projekt Drumskog mosta sa kosim kablovima u Plocku, Poljska. Teorija konstrukcija. Monografija posvećena uspomeni na pokojnog akademika Prof. Dr. Milana Đurića, str. 85-92.Građevinski fakultet Univerziteta u Beogradu, Katedra za tehničku mehaniku i teoriju konstrukcija, Beograd, 2008.

[9] Dunica, Š., Bojović, A., Životić, B.: Projekt konstrukcije novog Avalskog Tornja. DGKS Simpozijum 2008. Zbornik radova, str. 231-236. Zlatibor – Čigota, 24-26.09. 2008.

[10] Bojović,A., Velović,N.: Rehabilitation of the Gazelle road bridge in Belgrade. The Eight International Conference „Bridges in Danube Basin". Timisoara – Belgrade, 4-5. 10.2013. Proceedings, p.129-138. Springer Vieweg, Springer Fachmedien Wiesbaden 2013.

[11] Bojović, A., Mora Munoz, A., Marković, Z., Novaković, N.: Network arches over the Danube – Railway Road Bridge in Novi Sad. Bauingenieur 93 (2018), Heft 3.

Standardi:

JUS U.C7.110:1991 do JUS U.C7.113:1991 i JUS U.H2.110:1991, važećih 1991-2013.

PRIZNANJA, NAGRADE

- Povelja za životno delo u oblasti građevinskog konstrukterstva Društva građevinskih konstruktera Srbije (DGKS), 2022.
- Zlatna plaketa IT Saveza inženjera i tehničara Srbije (kao najviše priznanje), 2018.
- Priznanje DGKS za 2018-2019. za najbolje stručno ostvarenje – projekat konstrukcije Železničko-drumskog mosta preko Dunava u Novom Sadu.
- Priznanje DGKS za 2008-2009. za najbolje stručno ostvarenje – projekat konstrukcije Tornja na Avali.
- Priznanje DGKS za 2006-2007. za najbolje stručno ostvarenje – projekat konstrukcije Drumskog mosta preko Visle u Plocku, Poljska.
- Četiri nagrade na međunarodnim konkursima za mostove 1997-2008.
- Tri nagrade na arhitektonskim konkursima 1979-1985, kao član konkursnih timova, kao konstruktor.

FOTOGRAFIJE IZABRANIH REFERENCI KAO ODGOVORNOG PROJEKTANTA

Železničko-drumski most preko Dunava, Novi Sad, 2018. Svetski rekorder raspona u svojoj disciplini lučnih mostova. L_{max} = 219 m.

Drumski most preko Save, Sremska Rača. 2010. L_{max} = 150 m.

Drumski most Most solidarnosti preko Visle, Plock, Poljska. 2005. Najveći čelični drumski most koji su ikad projektovali srpski inženjeri. L_{max}= 375 m. (A.B. = projektant)

Drumski Most slobode preko Dunava, Novi Sad, 2005. Istog izgleda kao srušeni 1999, ali sa obimnim izmenama i ojačanjima u odnosu na prvobitni most (1980). L_{max} = 351 m

Sanacija. Drumski Most Gazela preko Save, Beograd, 2012. L_{max} = 250 m.

Pešački most preko Kanala Budovar, Stari Banovci, 2002.

Fudbalski stadion Arena Himki, Himki, Rusija, 2008. Stadion za 20.000 gledalaca. L_{max} = 48,0 m.

Hala za hokej, Padoljsk, Rusija, 2001. L_{max} = 62,5 m.

Hala za hokej, Čehov, Rusija, 2003. L_{max} = 54,0 m.

Hangar za remont aviona, Sebha, Libija, 1984. L_{max} = 82,5 m.

Toranj na Avali. 2009. H = 205 m.

Belexpo izložbena hala, Beograd, 2005. L_{max} = 38,0 m.

PRIZNANJE ZA ŽIVOTNO DELO U GRAĐEVINSKOM KONSTRUKTERSTVU DRAGU OSTOJIĆU, DIPL.GRAĐ.INŽ.

OSNOVNI BIOGRAFSKI PODACI

Drago Ostojić, dipl. građ. inž., je rođen 1953. godine u Tesliću, Bosna i Hercegovina, gde je završio osnovnu školu i gimnaziju. Na Građevinski fakultet Univerziteta u Beogradu se upisao 1972. godine a diplomirao 1978. godine.

Odmah po diplomiranju se zaposlio na Građevinskom fakultetu kao stručni saradnik u Institutu za materijale i konstrukcije na grupi predmeta Betonske konstrukcije, gde je bio zaposlen do penzionisanja, 2018. godine. Od 1980. godine do penzionisanja učestvovao je u izvođenju nastave na predmetima Betonske konstrukcije, Betonski mostovi, Sanacije betonskih konstrukcija, Tehnologija betona.

NAUČNI, NASTAVNI I STRUČNI RAD

Rad u nastavi, pored održavanja vežbi, učešća na održavanju ispita i predavanja, obeležila je saradnja sa studentima. Kao mentor, asistent i član komisije, učestvovao je u izradi i odbrani preko 200 studentskih diplomskih radova.

Zajedno sa kolegama autor je nekoliko zbirki zadataka i priručnika za studente ali i za inženjere u praksi. U stručnim i naučnim časopisima i na stručnim skupovima do sada je samostalno ili kao koautor objavio oko 30 radova.

U stručnoj praksi se Drago Ostojić, dipl. građ. inž., najviše bavio projektovanjem različitih vrsta objekata. Posebna oblast delatnosti su projekti sanacije ili rekonstrukcije objekata kod kojih su oštećenja nastala usled različitih dejstava (zemljotres, bombardovanje, dotrajalost, promena namene, itd.). Pored toga bavio se i vršenjem stručnog nadzora prilikom izgradnje objekata, vršenjem tehničke kontrole projekata i konsultantskim poslom pri izradi idejnih i glavnih projekta. U dosadašnjem radu Drago Ostojić, dipl. inž. građ., je boravio u Iraku, Alžiru i u Rusiji na različitim stručnim zadacima.

Drago Ostojić poseduje licencu odgovornog projektanta građevinskih konstrukcija objekata visokogradnje, niskogradnje i hidrogradnje, izdatu od strane Inženjerske komore Srbije.

Od 2011. godine je član Komisije za polaganje stručnih ispita i izdavanje licenci za odgovornog projektanta i idgovornog izvođača radova.

Od 2016. godine je Izvestilac Revizione komisije za stručnu kontrolu tehničke dokumentacije za objekte iz člana 133. Zakona o planiranju i izgradnji, za oblast građevinske konstrukcije.

ZNAČAJNIJA KONSTRUKTERSKA OSTVARENJA

Lista značajnijih stručnih stručnih radova u kojim je Drago Ostojić učestvovao, samostalno ili zajedno sa kolegama:
1. Idejni i glavni projekat konstrukcije Hangara 2 JAT na aerodromu Beograd.
2. Idejni i glavni projekat montažne konstrukcije tribina fudbalskog stadiona u Smederevu kapaciteta 40.000 gledalaca, konsultant za konstrukciju i projekat temeljne konstrukcije.

3. Idejni, glavni projekat i projektantski nadzor na izvođenju montažne krovne konstrukcije za kompleks objekata "Utva" u Pančevu
4. Glavni projekti konstrukcije objekata baze 404 u Iraku (devet objekata različite namene).
5. Glavni projekat montažne konstrukcije obloge tunela na obilaznici autoputa oko Beograda.
6. Glavni arhitektonsko - građevinski projekat za kompleks objekata Crpne stanice "Beni Amrane" sistema ISSER-KHEDARA za snabdevanje vodom grada Alžira (27 različitih objekata).
7. Glavni i izvođački projekat konstrukcije i projektantski nadzor za stambeno poslovni objekat u Moskvi, Novopeskovskij pereulok.
8. Glavni projekat konstrukcije hotela "Dom Srpsko Grčkog prijateljstva" u Koštunićima kod Gornjeg Milanovca.
9. Projekat sanacije za dva objekta oštećena bombardovanjem u krugu Vazduhoplovnog zavoda "Moma Stanojlović" u Batajnici.
10. Glavni i izvođački projekat konstrukcije stambeno poslovnog objekta B2 u ulici Balkanska br. 2 u Beogradu. Projektantski nadzor u toku izgradnje objekta.
11. Projekat Železničke stanice Beograd Centar, deo armiranobetonske konstrukcije.
12. Glavni projekti konstrukcije tržnih centara "TEMPO" u Novom Sadu, Nišu i Beogradu.
13. Glavni i izvođački projekat konstrukcije stambenog kompleksa u Moskvi, Zemljedeljčeskij pereulok.
14. Glavni i izvođački projekat konstrukcije sportske dvorane u Tesliću, BiH.
15. Glavni projekat kompletne konstrukcije Gata 4 marine Porto Montenegro u Crnoj Gori.
16. Glavni i izvođački projekat konstrukcije glavnog ispraćajnog objekta (ljuska) na groblju "Orlovača" u Beogradu.
17. Glavni i izvođački projekat konstrukcije tri hotela Roza Hutor, Krasna poljana, Soči, Ruska federacija.
18. Glavni i izvođački projekat konstrukcije stambeno poslovnog objekta B2 u ulici Balkanska br. 2 u Beogradu, površina oko 25 000 m^2. Projektantski nadzor u toku izgradnje objekta.
19. Idejni i glavni projekat konstrukcije sportskog kompleksa u gradu Perm u Rusiji, konsultant za konstrukciju, projekat bazena i tribinskih nosača.
20. Glavni projekat konstrukcije Kula E i F poslovnog centra "Blok 20" u Novom Beogradu.
21. Glavni i izvođački projekat konstrukcije hotelskog kompleksa "Kamelija" u Sočiju, Ruska federacija.
22. Glavni i izvođački projekat konstrukcije poslovnog kompleksa "Olimpijski Univerzitet" u Sočiju, Ruska federacija.
23. Glavni i izvođački projekat konstrukcije tri hotela u kompleksu Roza Hutor, Krasna poljana, Soči, Ruska federacija.
24. Tehnička dokumentacija za sanaciju armitranobetonskog dimnjaka TO Konjarnik u Beogradu sa prethodnom ekspertizom stanja dimnjaka.
25. Ekspertiza i projekat sanacije mosta preko reke Lepenice - kameni most u ulici dr Jovana Rajića u Kragujevcu.
26. Projekat sanacije pešačkog mosta preko reke Lepenice - "Ćiftina ćuprija" u Kragujevcu.

SPISAK OBJAVLJENIH KNJIGA I RADOVA

Knjige:

1. D. Bajić, D. Ostojić: Zbirka rešenih ispitnih zadataka iz betonskih konstrukcija, Naučna knjiga, Beograd, april 1984. godine;

2.   Priručnik za primenu Pravilnika BAB 87 o tehničkim normativima za beton i armirani beton, prilog 4.1. sa prof. Ž. Perišićem, SDGKJ, JUDIMK, Beograd, april 1989. godine;

3.   Beton i armirani beton prema BAB 87, tom 2 - prilozi, prilog 4.1. sa prof . Ž. Perišićem, prilozi 5.1. do 5.8., 6.1. do 6.3., 6.8. do 6.13. i prilog 6.16. sa N. Ojdrovićem, izdanje Građevinska knjiga, Beograd, 1991. godine.

Stručni i naučni radovi:

4.   M. Aćić, D. Ostojić, N. Ojdrović: Prilog proračunu armiranobetonskih ploča prema probijanju, kongres JUDIMK-a, Sarajevo, oktobar 1982. godine;

5.   M. Aćić, Đ. Dinić, N. Ojdrović, D. Ostojić: Prilog proračunu statičkih uticaja u pločama direktno oslonjenim na stubove, kongres SDGKJ, Cavtat, april 1983. godine;

6.   M. Aćić, V. Alendar, D. Ostojić, N. Ojdrović: Analiza faktora koji utiču na duktilitet poprečnih preseka armiranobetonskih elemenata, kongres Društva građevinskih konstruktora Hrvatske, Plitvička jezera, oktobar 1984. godine. Isti rad je objavljen u časopisu "Izgradnja", broj 3/85;

7.   D. Bajić, D. Ostojić: Uticaj poprečne armature na duktilitet armiranobetonskih elemenata, Simpozijum SDGKJ, Dubrovnik, april 1985. godine;

8.   M. Aćić, D. Ostojić: Eksperimentalno ispitivanje armoranobetonskih nosača sa zategom, kongres JUDIMK-a, Portrož, oktobar 1986. godine, 7 strana;

9.   M. Aćić, D. Ostojić, D. Bajić: Glavni stubovi, temelji i elementi fasadne konstrukcije Hangara, Stručni seminar Saveza građevinskih inženjera i tehničara Srbije "Hangar 2 - JAT na aerodromu Beograd", referat po pozivu, Beograd, maj 1986;

10. A. Pakvor, V. ALendar: Konstrukcija krova Hangara 2 JAT-a na beogradskom aerodromu, Stručni seminar Saveza građevinskih inženjera i tehničara Srbije "Hangar 2 - JAT na aerodromu Beograd", referat po pozivu, Beograd, maj 1986;

11. M. Aćić, D. Najdanović, D. Ostojić: Rešenje krove konstrukcije za kompleks objekata "Utva" Pančevo, kongres SDGKJ, Cavtat, april 1987. godine, 5 strana;

12. D. Ostojić: Prilog proračunu armature za prijem transverzalnih sila, Jugoslovensko savetovanje BAB 87, Dubrovnik, april 1988. godine, 4 strane;

13. M. Ivković, Ž. Perišić, M. Aćić, A. Pakvor, D. Ostojić: Eksperimentalno i teorijsko istraživanje olakšanih montažnih armiranobetonskih ploča, jesenja konvencija ACI Filadelfija, novembar 1990. godine, 14 strana;

14. M. Ivković, Ž. Perišić, M. Aćić, A. Pakvor, D. Ostojić: Eksperimentalno i teorijsko istraživanje olakšanih montažnih armiranobetonskih ploča, kongres SDGKJ, Cavtat, april 1991. godine, 10 strana;

15. M. Ivković, Ž. Perišić, M. Aćić, A. Pakvor, D. Ostojić: Experimental and theoretical investigation of the precast holow core slabs, International sympozium on concrete engineering, Nanjing, China, 18.-20. Sept. 1991. godine, 10 strana;

16. A. Pakvor, D. Ostojić, S. Anđelić: Optimizacija konstrukcije tunela "Lipak" i "Železnik" na obilaznici autoputa oko Beograda, rad objavljen u časopisu "Naše građevinarstvo" br 9-10, 1991. godine, 3 strane;

17. A. Pakvor, Lj. Vlajić, N. Ojdrović, D. Ostojić: Ekspreimentalna istraživanja pri projektovanju betonskih konstrukcija, rad u monografiji "Savremene betonske konstrukcije", posvećenoj sedamdesetoj godišnjici prof. dr Milorada Ivkovića, str. 199-203, Beograd 1994. god.;

18. M. Ivković, M. Aćić, D. Ostojić, R. Stopić: Proektiranje i realizacia mnogoetažnog administrativno - žilogo obekta v G. Moskva, publikacija Naučnie raboti yugoslavskih stroiteley, izdanje Saveza građevinskih inženjera i tehničara Srbije, septembar 1997. godine, povodom 850 godina grada Moskve, str. 86-91;

19. M. Ivković, M. Aćić, D. Ostojić: Rešenje konstrukcije višespratnog stambeno - poslovnog objekta u Moskvi, internacionalni simpozijum Društva građevinskih konstruktera Makedonije, knjiga 3, str. 33/1-33/6, Ohrid, oktobar 1997. godine;

20. M. Ivković, M. Aćić, D. Ostojić: Rešenje konstrukcije višespratnog stambeno - poslovnog objekta u Moskvi, 10. Kongres JDGK, Vrnjačka Banja, juni 1998. godine, knjiga K, str. 175-180;

21. M. Ivković, D. Ostojić, S. Ćorić: Fundiranje tribina stadiona fudbalskog kluba "SARTID 1913" u Smederevu, 10. Kongres JDGK, Vrnjačka Banja, juni 1998. godine, knjiga T, str. 331-336;

22. Boris Gligić, Drago Ostojić: Idejni projekat konstrukcije iznad tribina stadiona fudbalskog kluba Sartid u Smederevu, internacionalni simpozijum Društva građevinskih konstruktera Makedonije, knjiga 1, str. ČK4/1-ČK4/6, Ohrid, oktobar 1999. godine;

23. D.Ostojić, V. Matović, M. Stojanović, R.Tošković, M. Jovanović, M. Petrović: Konstrukcija sportske dvorane u Tesliću, Simpozijum JDGK, knjiga 1, str. 321-325, Vrnjačka banja, novembar 2000. godine;

24. T. Kovačević, M. Lazović, D. Ostojić, A. Mufid: Konstrukcijsko rešenje nadogradnje zgrade u Cvijićevoj br. 110 u Beogradu, Simpozijum JUDIMK "Nadogradnja stambenih i javnih zgrada", zbornik radova strana 159-164, Beograd, decembar 2000. godine;

25. Drago Ostojić, Aleksandar Pakvor: Osnovni aspekti nadogradnje stambenih i javnih zgrada, Simpozijum JUDIMK "Nadogradnja stambenih i javnih zgrada", zbornik radova strana 255-260, Beograd, decembar 2000. godine;

26. Drago Ostojić, Branko Milosavljević, Miodrag Stojanović: Konstrukcija krovne ljuske glavnog ispraćajnog objekta na groblju "Orlovača", Simpozijum DGKS, septembar 2008;

27. Boris Gligić, Drago Ostojić, Branko Milosavljević, Miodrag Stojanović, Mirko Jovanović: Projektovanje i izgradnja konstrukcije sportske dvorane u Kazanju u Ruskoj Federaciji, Simpozijum DGKS, septembar 2008.

28. Drago Ostojić¸Mirko Aćić Boško Furtula Radomir Zejak: Primer sanacije krovnih nosača industrijske hale, Simpozijum DGKS, 2006.

29. Aćić, Ostojić: Sanacija kolektora Kriveljske reke u Boru 2007-2008.

30. Ivan Ignjatović, Drago Ostojić, Nikola Muravljov: Procena stanja konstrukcije nakon požara sa merama sanacije i realizacija rešenja, Simpozijum DGKS, 2020.

DRUŠTVENO ANGAŽOVANJE. PRIZNANJA I NAGRADE

Od 2011. godine je član Komisije za polaganje stručnih ispita i izdavanje licenci za odgovornog projektanta i idgovornog izvođača radova.

Od 2016. godine je Izvestilac Revizione komisije za stručnu kontrolu tehničke dokumentacije za objekte iz člana 133. Zakona o planiranju i izgradnji, za oblast građevinske konstrukcije.

Članstvo u profesionalnim organizacijama: Inženjerska komora Srbije, Društvo građevinskih konstruktera Srbije, Srpsko udruženje za seizmičko inženjerstvo (SUZI), Udruženje "Izgradnja".

Za profesionalno angažovanje na otklanjanju posledica zemljotresa u Kraljevu, Drago Ostojić je 2011. godine od Inženjerske komore Srbije dobio Povelju za izuzetno dostignuće u struci.

P1-P6

ASES AWARDS
FOR BEST PROFESSIONAL AND SCIENTIFIC ACHIEVEMENTS IN 2022

Željko Ličina[1], *Liu Huatu*[2], *Vlatko Ćipranić*[3], *Zhang Hong Gang*[4]

GLAVNI PROJEKAT I IZGRADNJA MOSTA MORAČICA NA AUTOPUTU E-763, DEONICA: SMOKOVAC–MATEŠEVO

Rezime:

U radu je prikazan Glavni projekat i izgradnja drumskog mosta preko magistralnog puta Podgorica – Kolašin, reke Morače i platoa Moračica, na autoputu Bar - Boljare, Deonica: Smokovac – Uvač – Mateševo. Most je sistema prethodno napregnutog kontinualnog grednog rama, dužine 960 m, raspona 75+170+3x190+120 m, jedinstvenog sandučastog dvoćelijskog preseka za obe trake autuputa, promenljive visine, širine 22.7 m. Stubovi su armirano betonski, visine do 180 m, sandučastog poprečnog preseka. Konstrukcija mosta je izvedena slobodnom konzolnom gradnjom, a stubovi kliznom skelom i oplatom.

Ključne reči: kontinualni ram, dvoćelijski presek, slobodna konzolna gradnja

MAIN DESIGN AND CONSTRUCTION OF MORAČICA BRIDGE ON HIGHWAY E-763, SECTION: SMOKOVAC - MATEŠEVO

Summary:

The paper presents the main design and construction of the road bridge over the Main road Podgorica - Kolašin, the river Morača and the plateau Moračica, on the highway Bar - Boljare, Section: Smokovac - Uvač - Mateševo. The bridge static system is prestressed continuous girder frame, length 960 m, span 75 + 170 + 3 x 190 + 120 m, unique box two-cell cross section for both lanes of the highway, variable height, width 22.7 m. The piers are reinforced concrete, up to 180 m high, with a box cross-section. The bridge construction is made of free cantilever construction, and the piers with sliding scaffolding and formwork.

Key words: continuous frame, 2-sell cross section, free balanced cantilever construction

---

[1] *Odgovorni projektant, CRBC, Beograd, Srbija, zeljkolicina@gmail.com*

[2] *Projektant, CRBC, Beograd, Srbija, liuhuatu@hpdi.com.cn*

[3] *Glavni inženjer, CRBC, Podgorica, vlatko.cipranic@crbcmontenegro.me*

[4] *Odgovorni inženjer, CRBC, Podgorica*

1. OPŠTE

Most Moračica preko reke Morače projektovan je 2015, izveden 2015-2021. Otvoren je za saobraćaj jula 2022:

Investitor: Vlada Crne Gore, Ministarstvo saobraćaja i pomorstva.

Projektant i Izvođač „China road and bridge corporation, Montenegro branch"

Ugovarač izgradnje celokupne deonice autoputa Bar – Boljare, deonica Smokovac – Mateševo je Kompanija „China Communication and Construction Company" CCCC. „China road and bridge corporation, Montenegro branch" je deo ove kompanije.

Cena izgradnje mosta je oko 100 miliona evra

2. POLOŽAJ MOSTA U OKVIRU MREŽE AUTOPUTEVA EVROPE I CRNE GORE

Most Moračica se nalazi na autoputu označene u u okviru mreže autoputeva Evrope kao autoput E-763 Južni Jadran, deo kroz Crnu Goru je Bar – Boljare, deonica Smokovac – Mateševo. Ova deonica je dugačka oko 41 km. Prolazi kroz težak teren, zbog čega je više od polovine trase deonice u tunelima i na mostovima.

3. PODLOGE ZA PROJEKTOVANJE MOSTA

3.1. ELEMENTI TRASE NA MOSTU I PREPREKE

Na početku mosta, trasa je u prelaznici, a posle je u pravcu. Podužni nagib je +4%, trasa se penje. Poprečni nagib se menja od 4 do 2.5%. Širina kolovoza leve i desne trake je po 7.70 m, pešačke staze su po 2 m, a razdelni pojas na mostu je 4 m.

Most premošćuje, redom, magistralni put Podgorica – Kolašin, reku Moraču i plato Moračica (po kome je most i dobio ime). Na ovom delu, klisura je širine oko 1000 m.

3.2. GEOMORFOLOŠKE I GEOLOŠKE ODLIKE TERENA U ZONI MOSTA

Reka Morača je na ovom delu terena formirala izrazito asimetričnu dolinu. Na desnoj obali, nakojoj je po;etak mosta, padina je podeljena magistralnim putem na dve kosine. Gornja je relativno ujednačenog nagiba oko 30°, mestimično kaskadno oblikovana, u bankovitim jurskim krečnjacima, a donja nagiba u proseku oko 30° u terasnim fluvio-glacijalnim sedimentima(slabo do dobro vezan konglomerat i peskovit šljunak), lokalno promenljivog nagiba sa strmim manjim odsecima i potkapinama.

Korito reke Morače je formirano u terasnim fluvio glacijalnim sedimentima sa savremenim aluvijalnim šljunkovima i peskovitim šljunkovima. Dubina kanjona je 25 do 30 m, a reka se nalazi na nadmorskoj visini oko 70 mnm.

Na levoj obali je fomiran plato Moračica na nivou oko 100 mnm. Plato je formiran od glacio fluvijalnih sedimenata, širine oko 140 m. Dalje, padina je ujednačenog nagiba u proseku oko 30° u trijasko jurskim, slojevitim dolomitima i pri vrhu u krednim slojevitim krečnjacima. Donji delovi padine su pokriveni sa deluvijalno-koluvijalnim materijalom (prašinasto glinovita drobina) koja ublažava nagib i formira blag prelaz ka platou. Nadmorska visina u zoni kraja mosta je oko 285 mnm.

Karakteristike krečnjačkih stena, da se u njima nalaze pukotne, kaverne i pećine, su se potvrdile i tokom izvođenja temelja mosta. One su bile mahom ispunjene crvenicom.

U zoni same mikrolokacije ovog mosta, kao i u neposrednoj okolini, tokom najmanje prethodnih pet vekova, nisu registrovani ili osmotreni zemljotresi sa intenzitetom, odnosno magnitudom iznad nivoa koji je prikazan na prognoznoj karti očekivanih maksimalnih magnituda zemljotresa za povratni reprezentativan period od 100 godina. U konkretnom slučaju mosta "Moračica" to je vrednost koja se može izraziti maksimalnom magnitudom od 5.8 jedinica Rihterove skale, sa maksimalnim dogođenim ubrzanjima na osnovnoj steni predmetne lokacije od 1.05 m/s2, dok očekivana maksimalno horizontalno uzbrzanje za tzv. projektni zemljotres, odnosno povratni period od 95 godina iznosi 0.94 m/s2, odnosno 1.99 m/s2 u slučaju tzv. maksimalnog zemljotresa, odnosno kod povratnog perioda od 475 godina.

4. OPIS DISPOZICIONOG REŠENJA KONSTRUKCIJE SA OBJAŠNJENJEM KONCEPTA

- Polazna osnova za izradu Glavnog projekta je bio Idejni projekat, sa njegovim osnovnim konceptom, statičkim sistemom i usvojenom tehnologijom izvođenja, kao i opštim likovnim izrazom.
- Trasa na delu mosta prelazi preko veoma visoke udoline, pa je visina nivelete iznad terena odredila glavne raspone u estetskom i funkcionalno-tehnološkom smislu;
- Položaj kanjona reke Morače i magistralnog puta, tj. najpre, njihov međusobni položaj i oštra kosina između njih; Naime, kao posledica usvojenih glavnih raspona, pomenutih u prvoj stavci, i predviđene tehnologije izvođenja, date u četvrtoj stavci, a koji diktiraju racionalan odnos glavnih i bočnih raspona, došlo se do položaja stuba 2 u zoni puta i reke. U razmatranju su bile dve varijante, koje su određene, u prvoj varijanti, položajem stuba 2 između puta i reke (Idejni projekat) i, u drugoj varijanti, položajem 2 iznad puta. Na osnovu detaljne prethodne analize, utvreno je da: prvo, postoje teškoće sa dispozicionim rešenjem koje podrazumeva stub sa temeljem između puta i reke, jer bi kosina iskopa bila takva da bi imala za posledicu neophodnost izrade devijacije magistralnog puta za vreme izvođenja radova, česte prekide saobraćaja na tom putu i ugroženu bezbednost učesnika u saobraćaju i izvođača radova. Devijacija (pošto je magistralni put u pitanju) bi morala imati takvu geometriju, koja bi zahtevala veliki obim radova na usecanju njene trase u strmu stenu iznad magistralnog puta. Drugo, sa aspekta obrađenog u ovoj tački, lokacija stuba iznad puta je mnogo povoljnija, zahteva daleko manje iskope, a prekida saobraćaja nije bilo. Treće, stub iznad puta je fundiran u čvrstim krečnjacima, a između puta i reke je bušotinama utvrđen dosta lošiji materijal za fundiranje.
- Predviđene tehnologije izvođenja; Tehnologija slobodne konzolne gradnje određuje da racionalan odnos glavnih i bočnih raspona bude između 0.6 i 0.7, kako je naznačeno u najšire korišćenim francuskim "SETRA" smernicama za projektovanje mostova, koji se izvode konzolnom gradnjom. To je uticalo na raspored raspona i stubova. Ovakav odnos se usvaja radi što većeg umanjenja dela konstrukcije uz krajnje oporce, koji se izvode na skeli. U ovom slučaju je to naročito značajno, jer su nagibi kosina u bočnim rasponima veoma strmi, pa bi postavljanje skele i njihovih temelja bilo otežano. To je posebno naglašeno u poslednjem rasponu. U finalnoj dispoziciji, delovi mostovske konstrukcije, koji se izvode na skeli, su dužine 18.5 m i 28.5 m.

5. OPIS KONSTRUKCIJE MOSTA

- Rasponi .... 95+170+3x190+125 m
- Dužina mosta, osovinski .... 960 m
- Dužina mosta, sa krilnim zidovima .... 988 m
- Ukupna širina mosta .... 23.40 m
- Širina oba kolovoza…2 x (3.50+0.35) .... 7.70 m
- Širina pešačkih staza.. 2x2.00 m

5.1. OPIS TEHNIČKIH KARAKTERISTIKA, SA OBJAŠNJENJEM STATIČKO-KONSTRUKTIVNE KONCEPCIJE

Konstrukcija mosta je kontinualna prethodno napregnuta ramovska, promenljivog poprečnog preseka. Zbog toga što je položaj stuba P2 odabran da bude iznad magistralnog puta, tri glavna središnja raspona su nešto veća nego prvi središnji, P1 - P2. Pri odredjivanju ovog odnosa, vodilo se računa i o odnosima krajnjih i središnjih raspona sa bočnim. Tako se došlo do optimalnog odnosa krajnjih i srednjih raspona, na početku mosta 95/175=0.54 i 125/190=0.66 na kraju mosta i do glavnih raspona od 190 i 170 m. Ovakav odnos raspona je pogodan za kontinualan ramovski konstruktivni sistem, čija se mostovska konstrukcija izvodi metodom slobodne konzolne gradnje.

Stubovi P1 – P5 su kruto vezani za konstrukciju, a krajnji oporci A0 i A1 preko ležišta. Na taj način su horizontalni uticaji raspodeljeni na više stubova i umanjeni u odnosu na rešenje sa svim ležištima. Tako je dobijen sistem sa većom unutrašnjom rezervom nosivosti. Kruta veza je, takodje, povoljna i sa stanovišta tehnologije izvodjenja.
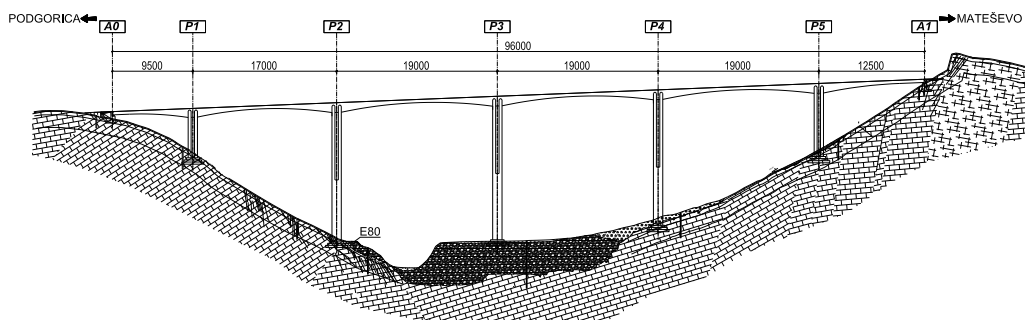
Uzdužni presek mosta
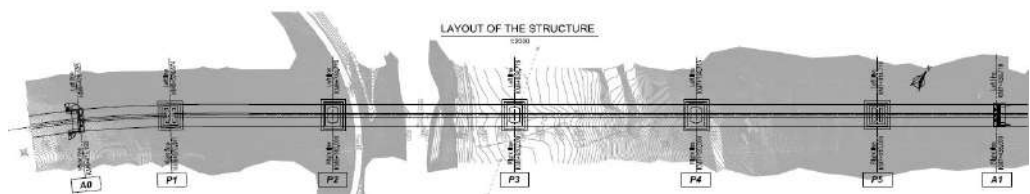
Osnova mosta

5.2. GORNJI STROJ MOSTA

Poprečni presek konstrukcije je dvoćelijski, sandučast, promenljive visine duž raspona. Visina nosača iznad oslonca na stub P1 je 10.5 m, a iznad stubova P2, P3, P4 i P5 je 11.5 m. Visina grede u sredini raspona i iznad oslonaca na krajnje oporce je 3.8 m. Visina glavnog nosača se menja prema paraboli stepena 1.8. Debljina donje ploče varira od 30 – 120 cm, a debljina gornje ploče je konstantna, 30 cm. Debljina rebara baznih segmenata je 85 cm. Postoje tri debljine rebra sandučastog nosača (65 cm, 55 cm i 45 cm). Ova podela odgovara trima dužinama segmenta grede (3.0 m, 3.75 m i 4.50 m). Nad srednjim stubovima su po 4 poprečna nosača, koji se nastavljaju iz zidova stuba. Na mestima oslanjanja konstrukcije na krajnje oporce, na donjoj strani poprečnog nosača iznad stuba, nalaze se kratki elementi za prenos poprečnih horizontalnih sila od vetra (tkzv. shear key) i seizmičkih sila na oporce, preko lončastih bočnih ležišta.

Raspon 170 m   *Raspon 190 m*
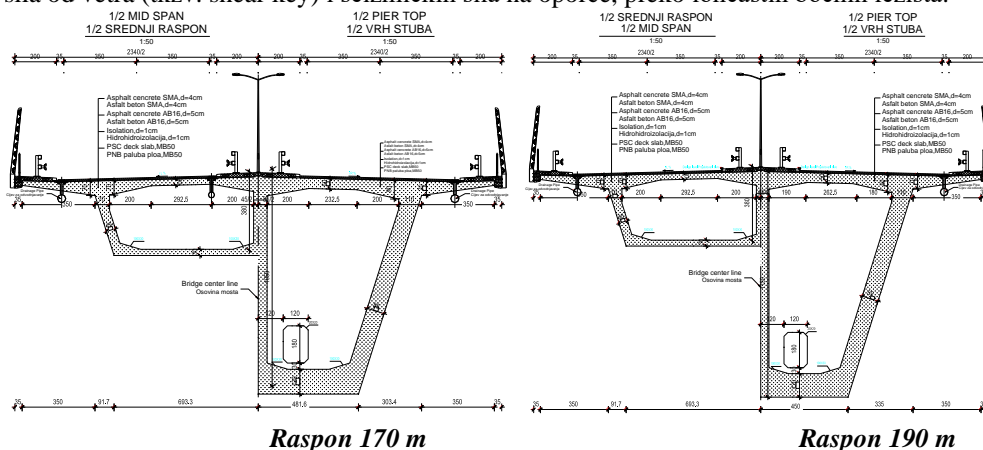
Unutrašnji kablovi su 27Ø15.2 mm, 22 Ø15.2 mm, 19 Ø15.2 mm, 16 Ø15.2 mm i 12 Ø15.2 mm. Kablovi gornje ploče i rebara se postavljaju i utežu tokom izvodjenja radova. Kablovi u gornjoj ploči su u tkzv. kombinovanom rasporedu. U svakom segmentu je predvidjeno sidrenje po 3 kabla, po jedan uz svako rebro, naizmenično sa leve i desne strane rebra, osim u 3 preseka, u kojima se sidri 6 kablova, po 2 uz svako rebro. Svi kablovi u gornjoj ploči se sidre u vutama. Kablovi u rebrima se povijaju na dole i sidre u rebrima. Kablovi u donjoj ploči se utežu nakon spajanja nosača i oni se sidre u ankernim blokovima.

U svim rasponima je ostavljeno ukupno 70 rezervnih cevi kablova, što čini 7.5% ukupnog broja kablova (po 6 u gornjoj i po 4 u donjoj ploči).

U glavnim rasponima su predvidjeni dodatni eksterni kablovi 27Ø15.2 mm, po 4 u svakom polju i po 4 u svakom baznom komadu iznad srednjeg stuba (ukupno 44 kabla na mostu, što čini 4.7% svih kablova). Ovi kablovi su rezervisani za fazu eksploatacije mosta. U toku faze eksploatacije biće prikupljane informacije o naponima i deformacijama kolovozne ploče mosta. Ostavljena je mogućnost da ako naponi i deformacije predju projektovane vrednosti, odredjeni broj spoljašnjih kablova bude utegnut.

Kolovozna ploča je i poprečno prednapregnuta kablovima 3Ø15.2 mm na medjusobnom rastojanju od 75 cm i manje. Ovi kablovi su usvojeni da bi se potpuno eliminisala mogućnost pojave prslina u gornjoj zoni kolovozne ploče, čime je povećana trajnost konstrukcije.

5.3.   DONJI STROJ MOSTA

5.3.1   Stubovi

Velika visina stubova, vetar kao dominantni uticaj i relativno velike razlike u visini stubova su uslovile vrstu, oblik i zakon promene poprečnog preseka po visini. Da bi se ujednačili podužni uticaji na srednje stubove, kraći stubovi P1 i P5, koji bi "navukli" veće uticaje, su manje krutosti, a viši stubovi su veće krutosti do visine ukljештenja kraćih, a dalje, do pune visine, iste krutosti kao i niži. Na taj način se dobija i estetski povoljno rešenje, svi stubovi su bočno transparentni do približno iste visine.

Srednji stubovi P1 i P5 su formirani od 2 sandučasta poprečna preseka, postavljenih paralelno po dužoj strani, poprečno na pravac mosta. Oba preseka su identična, dvoćelijska. Poprečni presek na gornjem delu stubova P2 – P4 je identičan kao i kod stubova P1 i P5. Dva sandučasta preseka gornjeg dela stuba se spajaju u jedinstven poprečni presek donjeg dijela stuba.

Radi sprečavanja pojave turbulencije oko stubova, na bočnim stranama stubova (u odnosu na smer vetra poprečno na most), usvojeni su "žljebovi" dubine 20 cm, radi lakšeg i bržeg "odvajanja" vrtloga od stuba.
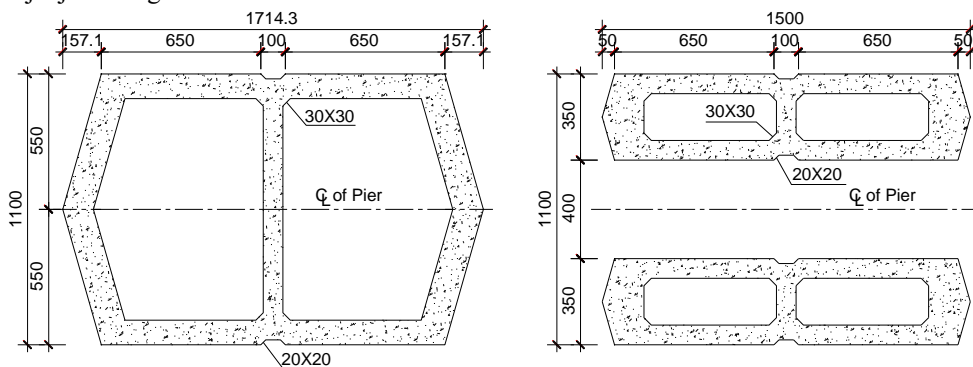
Donji deo stubova P2-P4   *Stubovi P1, P5 I gornji delovi stubova P2-P4*

Glavna armatura srednjih stubova je nastavljana mehaničkim nastavcima - konektorima Nastavci su postavljeni tako da ne bude više od 50% nastavljene armature u jednom preseku.

5.3.2   Temelji

S obzirom na geotehničke uslove odabrano je plitko fundiranje. Svi stubovi su fundirani u krečnjačkoj steni, osim stuba P3, koji je fundiran u terasnim naslagama, konglomeratima. Iako su dozvoljeni naponi izuzetno visoki, čak i za krečnjak, određivanju dimenzija temeljnih stopa se pristupilo sa velikim stepenom sigurnosti, jer je stena ispucala i može biti lokalno nepovoljna, što se i pokazalo tokom izvođenja.

Stepenasti temelji srednjih stubova obezbeđuju siguran i ravnomeran prenos sila iz stuba u tlo. Dimenzije temelja stubova P1 i P5 su 30x26 m, a stubova P2 – P4 33x26 m. Ukupna visina svih temelja je 7.5 m, u obliku trostepene piramide. Visina svih stepenica temelja, kao i odstojanje ivice stuba i ivice temelja, su 2.5 m visine i širine.

6. STATIČKI PRORAČUN

6.1. OPTEREĆENJA

Opterećenja i njihove kombinacije su uzete prema "Pravilniku o tehničkim normativima za odredjivanje veličine opterećenja mostova", prema zahtevima Projektnog zadatka i važećih propisa u Crnoj Gori 2014 godine. Programski paket "Midas" omogućuje nanošenje opterećenja po fazama izvodjenja. Ona obuhvataju sopstvenu težinu, sopstvenu težinu krletke, dodatno stalno opterećenje, prednaprezanje i uticaje tečenja i skupljanja. U toku izvođenja je računato i sa uticajima vetra. Proverene su i dve najgore incidentne situacije, za fazu izvođenja kada su konzole maksimalne, sa zemljotresom EQ1 i sa dvostrukom vrednošću istovremenog uticaja otpadanja „krletke" i segmenta nosača sa jedne strane. Pokretno opterećenje je šema V600+300 za mostove I kategorije.

Opterećenja od zemljotresa su uzeta prema EN 1998-2 što je u saglasnosti sa ProjektnIm zadatkom i Detaljnom seizmičkom studijom. Razmatran je zemljotres T=475 god. i T=95 god. Za zemljotres povratnog perioda od 95 godina za maksimalno ubrzanje se uzima 0.096g. Što se zemljotresa povratnog perioda od 475 godina tiče, za maksimalno ubrzanje je računato sa 0.203g. Faktor ponašanja je zbog značaja mosta usvojen q=1.0. Faktor značaja 1.3 i faktor prigušenja 5%.

Kombinacije opterećenja tokom eksploatacije su odredjene prema Pravilniku za mostove. Kombinacije seizmičkih sila u 3 pravca koordinatnog sistema su usvojene prema EN, sa 100% sile u dominantnom pravcu i po 30% sile u druga 2 pravca. U seizmičkim kombinacijama je uzeto i 20% uticaja od pokretnog opterećenja.

6.2. MODEL

Model konstrukcije je napravljen i sračunat u programskom paketu "Midas". Modelirana je celokupna konstrukcija, bez krajnjih stubova. Korišćena je metoda konačnih elemenata za strukturnu analizu mosta Moračica. Model je linijski, a ovako formirani linijski elementi su modelirani kao 3D elementi u kojima program analizira stanje napona i deformacija u presecima. Model se formira na osnovu redosleda izvodjenja mosta, kako bi se analizirale promene napona i deformacija u različitim fazama. U model su uneti i kablovi kao elementi sistema. Definisani se materijali i njihova svojstva, koja su vremenski promenljiva. Po predvidjenim stvarnim fazama izvodjenja se modelu dodeljuju faze. Svakoj fazi se definiše dužina trajanja i koji elementi i opterećenja se uključuju (ili isključuju) u toj fazi. Uključivanje elemenata od betona je povezano sa vremenski zavisnim efektima tečenja i skupljanja, koji su obuhvaćeni programom.

6.3. REZULTATI PRORAČUNA

U fazi eksploatacije, za merodavne kombinacije opterećenja, ekstremne vrednosti normalnih napona pritiska su 18.50 MPa na donjoj ivici presjeka i 18.31 MPa na gornjoj, što je manje od dopuštenih napona 1.1*18.5 = 20.35 MPa. Čak su i naponi od kombinacije sa EQ2 manji od dozvoljenih. Glavni naponi zatezanja su veći od 0 MPa (potpuno prednaprezanje) za sve kombinacije opterećenja osim za seizmičku, sa EQ2.

Naponi od stalnog opterećenja, koji se kreću od 6 MPa do 13 MPa, pod kojima će konstrukcija biti većinu svog postojanja, su ujednačeni na gornjoj i donjoj ivici, što veoma povoljno utiče na trajnost. Svi naponi smicanja su ispod dopoštenih za beton, nije bila potrebna računska armatura.

Ugibi od pokretnog opterećenja su max. 55.5 mm (na dole) i min. 27.9 mm (na gore). Ugibi (nadvišenja) tokom izvodjenja, su dati po fazama, ali oni su orjentacioni i služe za kontrolu reda veličine stvarnih. Tokom izvodjenja, računati su prema stvarno izmerenim modulima elastičnosti betona.

Za stanje eksploatacije, dimenzionisani su karakteristični preseci na svim srednjim stubovima. Najjače su armirani najkraći stubovi P1(max. 3.51%) i P5(max. 2.96%). Stubovi P2 – P4 su armirarni od 1 do 1.6% i to jače dvodelni preseci na mestu uklještenja u konstrukciju. U modelu je urađena i P-delta analiza, a sekundarni efekti su uzeti u obzir.

Maksimalni naponi na tlo su na stubu P3, središnji oko 0.65 MPa, a ivični 1.39 MPa od maksimalne eksploatacione kombinacije, što je daleko manje od dozvoljenih.

6.4. OSTALI ELEMENTI MOSTA

Ležišta na krajnjim stubovima su po 2 sferna, klizna i po 2 lončasta, koja primaju bočne horizontalne sile preko "Shear key" elemenata, postavljenih na konstrukciju i krajnje stubove.

Zbog velike visine mosta, i samim tim izraženih efekta vetra, postavljene su barijere za zaštitu od vetra - vetrobrani, visine 3 m, obostrano. Barijere su usvojene kao fleksibilne i njihova efikasnost je dokazana posebnom modelskom analizom.

7. IZVOĐENJE

7.1. FUNDIRANJE

Geofizička istraživanja su pokazala da postoji mogućnost pojave pukotina i kaverni u zoni ispod plitkih temelja mosta. Zbog toga je na nekim stubnim mestima, tokom izvođenja, rađeno dodano istražno bušenje, do dubine od 6 m, po celokupnoj površini temeljne spojnice. Na ovaj način je ustanovljeno postojanje kaverni. i pukotina, koje su očišćene i ispunjene nabijenim betonom. Iako je stena dobrih karakteristika, rađena je zaštita kosina armiranim torkret betonom i ankerima. Na slikama ispod se vide temeljna jama sa zaštitom.

Temeljna jama sa zaštitom iskopa stuba P5

Srednji stubovi su izvedeni u kliznoj skeli i oplati, s obzirom na visinu i nepromenljivost spoljašnjih gabarita. Dužine segmenata su bile oko 6 m u svakom potezu betoniranja. U toku izgradnje mosta bila predviđena osmatranja nakon završetka svakog segmenta stuba betoniranja u 12 odnosno 6 tačaka., da bi se održala vertikalnost stubova. Glavne armaturne šipke Ø32, duže od 12 m su nastavljane mehaničkim nastavcima – konektorima.

Glavni nosač mosta je izveden metodom "slobodne konzolne gradnje". Gradnja je počela izgradnjom baznog segmenta, iznad svih srednjih stubova. Bazni segmenti su izvedeni na posebnoj skeli i oplati. Radi postizanja zahtevane geometrije, skela je prednapregnuta pomoćnim kablovima. Nakon očvršćavanja betona baznih elemenata, utegnuti su podužni kablovi, uklonjena skela i oplata baznog komada i postavljena pomična, viseća skela i oplata – tkzv. "krletka", obostrano,.na svih 5 srednjih stubova. Znači, upotrebljeno je 10 rešetki, svaka težine oko 140 t. Dalje, segmenti se izvode obostrano, do završnog segmenta svakog raspona. Za to vreme se izvode delovi glavnog nosača u krajnjim rasponima, koji se liju na skeli, postavljenoj na terenu. Pre betoniranja završnih segmenata, postavljaju se kontrategovi na krajeve konzola. Betoniraju se završni segmenti i istovremeno uklanjaju kontrategovi. Nakon postizanja 90% čvrstoće betona, a da starost betona ne bude manja od 5 dana, utežu se podužni i poprečni kablovi. U rasponima od 190 m je postavljen deo opreme za eksterne kablove za prednaprezanje, koji će biti ubačeni i utegnuti u slučaju potrebe. U toku gradnje je angažovana specijajna grupa za praćenje i preračunavanje nadvišenja, svaka 2-3 izvedena segmenta, na osnovu izmerenih, stvarnih, modula elastičnosti betona. Završno spajanje mosta je bilo 10.10.2019.

Tokom izgradnje

Završen most

8. ZAKLJUČAK

Na početku projekta smatralo se da je most "Moračica" najkritičniji objekat, koji će odrediti vreme izvođenja celokupnog Projekta. Međutim, most je izveden u predviđenom roku, izuzetno kvalitetno, pre nego što je celokupni projekat kompletiran i pušten u saobraćaj

Veliki tim stručnjaka je učestvovao u realizaciji mosta Moračica. Teško bi ih bilo sve nabrojati i ovom prilikom bih želeo svima da im se zahvalim, u moje ime i u ime ostalih autora.

REFERENCE

Knjige Glavnog projekta mosta Moračica

[1]   BBC030MO102GL01 - Opšta i tekstualna dokumentacija

[2]   BBC030MO102GL01 - Numerička dokumentacija

[3]   BBC030MO102GL03 - Grafička dokumentacija: Konstrukcija mosta - Deo 1, 2, 3, 4

[4]   BBC030MO102GL04 - Hidrološko-hidraulički proračun i odvodnjavanje mosta

[5]   BBC030MO102GL05 - Glavni projekat rasvete mosta

[6]   BBC030MO102GL06 - Program probnog opterećenja konstrukcije

[7]   BBC030MO102GL06 - Program održavanja mosta

[8]   BBC030MO102GL07 - Glavni projekat skele

[9]   BBC030MO102GL08 - Glavni projekat osmatranja tla i objekata u toku građenja i eksploatacije

[10] BBC030MO102GL09 - Glavni projekat organizacije i tehnologije građenja

Šerif Dunica[1]*, Saša Stošić*[2]*, Dimirije Aleksić*[3]

KULA I TRŽNI CENTAR – II FAZA POSLOVNO-STAMBENOG KOMPLEKSA BLOKA 65 NA NOVOM BEOGRADU

Rezime:

Kula visine 154,93 m i tržni centar čine drugu fazu poslovno-stambenog kompleksa bloka B65. Podzemni deo objekta je garaža na dva nivoa i sa podzemnim nivoima faze I, koji su osam godna ranije izvedeni, čine celinu. Podzemne etaže tržnog centra i faze I su plitko fundirane u uslovima visokog nivoa podzemne vode i hidroizolacionim spojnicama povezanih sa podžemnim etažama kule koja je duboko fundirana, Prostornu stabilnost kule i otpornost na horizontalne uticaje obezbeđuje armiranobetosko jezgro koje je seizmičkim zidovima povezano sa stubovima i gredama na fasadi.

Ključne reči: kula, armiranobetnoske konstrukcije

THE TOWER AND SHOPING MALL – II PHASE OF THE BUSINESS AND RESIDENTIAL COMPLEX B65 IN NEW BELGRADE

Summary:

The tower and shopping mall are are designed as the second phase of the business and residential complex B65. The underground part of the building consist of a garege on two levels. That part forms a whole with the underground part of phase I that is shalow founded. The tower foundation is deep. A waterproof joints connect the underground part of the tower with the underground part of the rest of the B65 complex. The stability of the tower and resistance to horizontal forces is provided by a reinforced concrete core which is connected to the columns and beams on the facade by seismic walls..

Key words: tower, RC sturcutres

---

[1] *R. prof. u penziji , Građevinski fakultet, Univerzitet u Beogradu, Srbija, dunica49@gmail.com*
[2] *V. prof, Građevinski fakultet, Univerzitet u Beogradu, Srbija, sasa@grf.bg.ac.rs*
[3] *dipl.građ. inž. DELING DOO BEOGRAD, Beograd, Srbija, dimitrije.aleksic@deling.rs*

1. UVOD

Poslovno stambeni komleks u bloku 65 na Novom Beogradu je projektovan i izveden u dve faze. Objekat I faze je projektovan 2010 i izveden do 2012 a obuhvatio je 11 stambenih lamela i pripadajući deo dvoetažnih podzemnih garaža ispod celokupne parcele. Objekat II faze je projektovan u periodu 2016-2020 a izvođenje konstrukcije je završeno u aprilu 2021. Objekat je funkcionalno podeljen na tržni centar spratnosti P+2 i stambenu kulu spratnosti P+ME+40. U podzemnom delu objekat je funkionalno povezan sa prvom fazom kompleksa sa kojima deli dva nivoa podzemnih garaža. Na slici 1 je prikazan ceo kompleks sa tržnim centrom, kulom kao i lamelama prve faze.

Slika 1 – Blok 65 – Tržni centar i kula odnosno lamele izvedene u fazi I iza tržnog centra i kule.

2. KONSTRUKCIJA OBJEKTA

Maksimalna visina tržnog centra je 20,53 m, a kule 154,93 m (sl. 2). Visina prvog podzemnog nivoa je 3,32 m, odnosno, 3,45 m a drugog 2,85 m.

U tržnom centru, osnovni raster stubova je 8,10 m sa 8,10 m. Na nivou ploče prizemlja i na prvom podzemnom nivo, konstrukcija tržnog centra je odvojena od objekta I faze koja je izvedena 2010.

Dilatacionim razdelnicama je konstrukcija kule odvojena od konstrukcije tržnog centra na svim nivoima od drugog podzemnog etaža do krova tržnog centra. Čista širina dilatacionih razdelnica na svim nivoima je 5 cm.
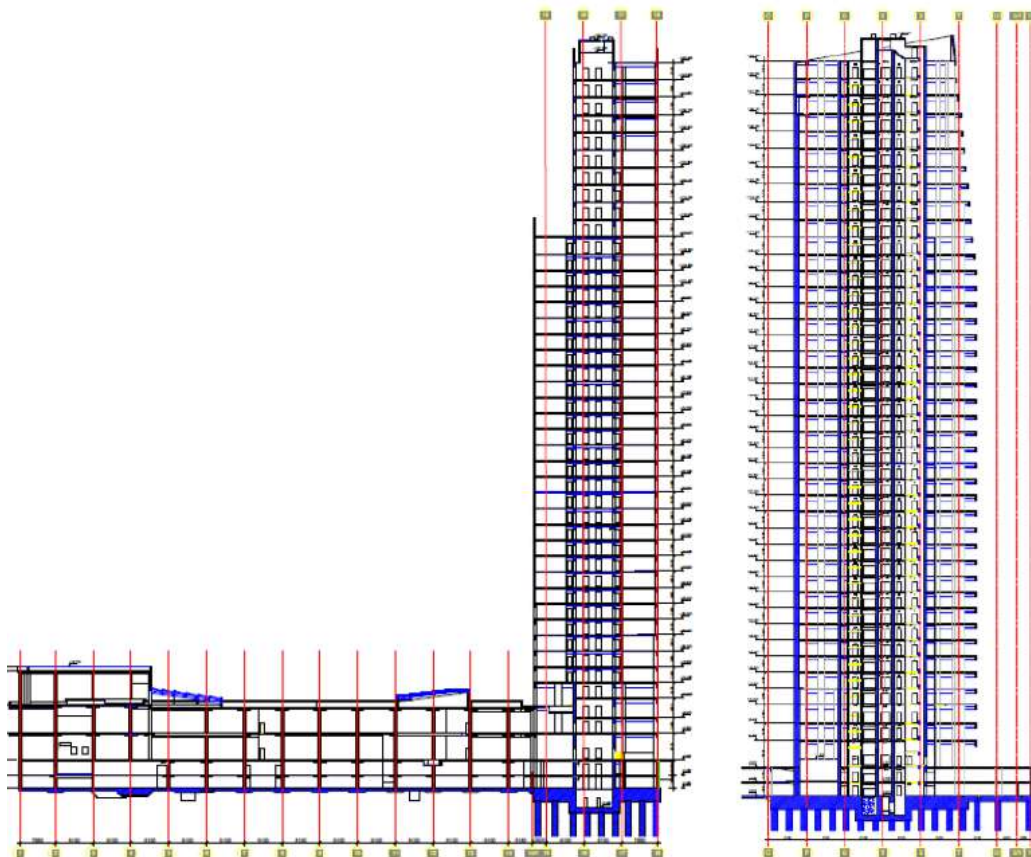
Slika 2 – Podužni presek kroz tržni centar i kulu i poprečni presek kroz kulu

Objekat je koncipiran kao armiranobetonski a projektovane marke betona prikazane su u tabeli 1. Armiranje je vršeno betonskim čelikom B500B i mrežastom armaturom MA 500/560.

Celine koje su projektovane i izvedene kao čelična konstrukcija su: nadstrešnice nad glavnim ulazom i nad ulazom u garažu kule, konstrukcija fasade tržnog centra, dve lanterne na krovu tržnog centra, konstrukcija za nošenje „Media Wall" led ekrana i galerije za potrebe bolničkih usluga u prizemlju tržnog centra.

Tabela 1 – Projektovane marke betona za elemente konstrukcije

Marka betona	Elementi konstrukcije **tržnog centra**	Elementi konstrukcije **kule**
MB 40	Temeljna ploča, elementi iznad kote 1. sprata	Šipovi, temeljna ploča, elementi iznad 31. sprata
MB 50	Između temeljne ploče i kote 1. sprata.	između 20. i 31. sprata
MB 60		između temeljne ploče i 20. sprata

1.1. FUNDIRANJE

Tržni centar je fundiran na armiranobetonskoj ploči debljine 65 cm uz primenu "jet grounding" tehnologije. U zavisnosti od intenziteta normalne sile, ispod određenih stubova, su izvedeni kapiteli sa donje strane temeljne ploče. Kapiteli su predviđeni ispod svih liftova kao i ispod eskalatora. Donja kota temeljne ploče tržnog centra je -6,950 m, ispod liftova -8,200 m, a ispod eskalatora -8,100 m.

Kula je fundirana na bušenim šipovima Ø1200 mm sa temeljnom pločom debljine od 1,20 m do 5,30 m (sl. 3). Dužina šipova ispod najniže kote temeljne ploče je 17,90 m dok su ispod plićih delova temeljne ploče izvedeni duži šipovi od 20,30 m odnosno 22,00 m, tako da su glave svih šipova na istoj koti -29,50 m. Ukupan broj šipova je 131.
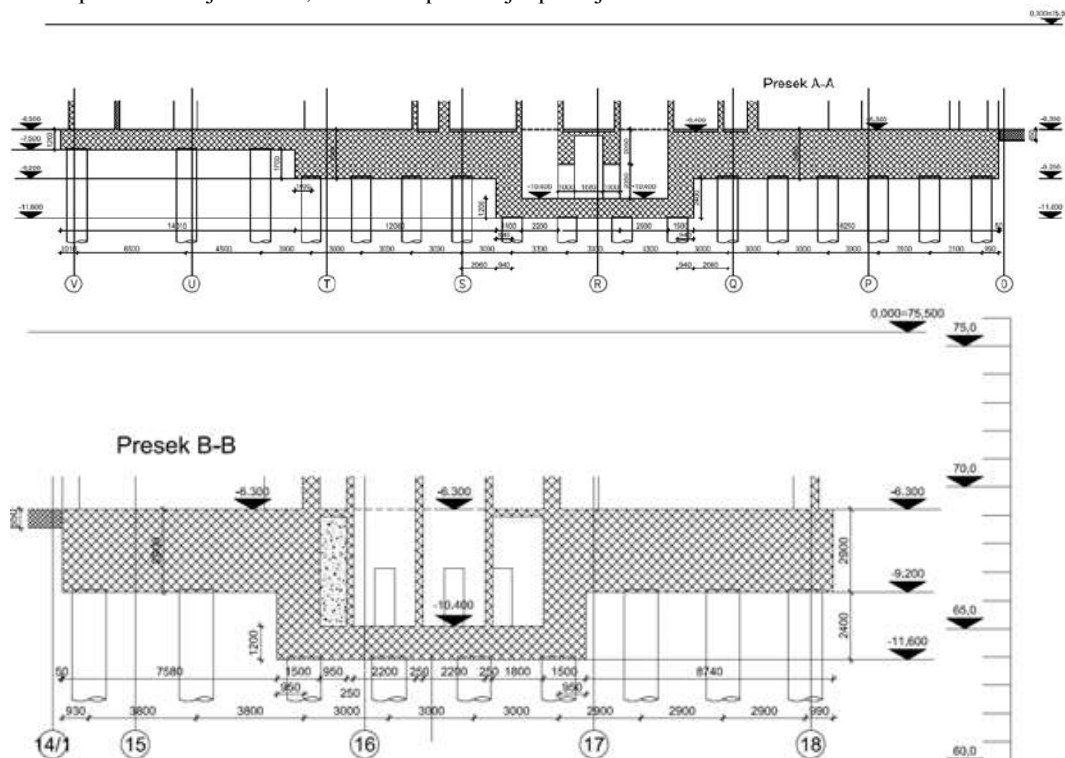
Slika 3 –Poprečni preseci kroz temeljnu ploču kule

Temeljna ploča je armirana u dva ortogonalna pravca rebrastim betonskim čelikom B500B. Za osnovnu armaturu temeljne ploče, u zavisnosti od položaja i debljine ploče, je usvojeno Ø32/150 mm odnosno 2Ø32/150 mm. Za prijem uticaja od temperature, skupljanja betona i sl., na određenim nivoima (na slici 4 označeni brojevima 9, 10, 11, 13 i 14) u srednjim delovima ploča, predviđa se konstriktivna armatura Ø16/400 mm. Na mestima ukrštanja ove armature, predviđena je takođe i vertikalna armatura Ø16/800x400 mm (od armature donje do armature gornje zone). U donjoj zoni temeljne ploče predviđena je takođe i konstriktivna mrežasta armatura Q188 označena kao sloj 0 na slici 4.
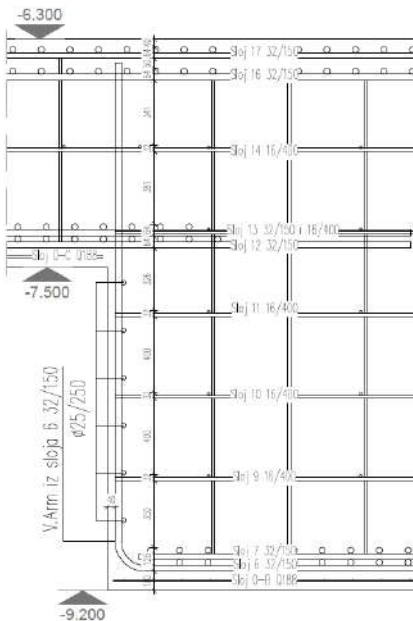
Slika 4 –Fragment armiranja temeljne ploče kule

1.2. MEĐUSPRATNA KONSTRUKCIJA

Tržni centar

Međustpratna konstrukcija tržnog centra je armiranobetoska ploča koja je preko kapitela oslonjena na stubove. Debljina ploče je na prvom podzemnom etažu 20 cm, na prizemlju 25 cm odnosno 22 cm dok je na pločama prvog, drugog i ploči iznad drugog sprata 25 cm. Kapiteli su dimenzija 2,60x2,60 m, dok je visina zavisno od debljine ploče, tako da je ukupna debljina kapitela i ploče 50 cm. Izuzetno, na krovnoj ploči, u delu gde je predviđeno optetećenjem zemljom ukupna debljina je 60 cm.

Kula

Međuspratna konstrukcija kule je armirano betonska monolitna ploča (sl. 5). Na prvom podzemnom nivoa (kota -3,450) debljina ploče je 25 cm, na nivou prizemlja (kota -0,300) debljina ploče je 30 cm, a na svim nivoima iznad prizemlja je debljina ploče 22 cm. Izuzetno, u jednom delu, delu ploča prizemlja ima funkciju transferne konstrukcije i prenosi uticaje dva stuba koji se ukidaju ispod kote prizemlja, te je debljina ploče u tom delu 90 cm.
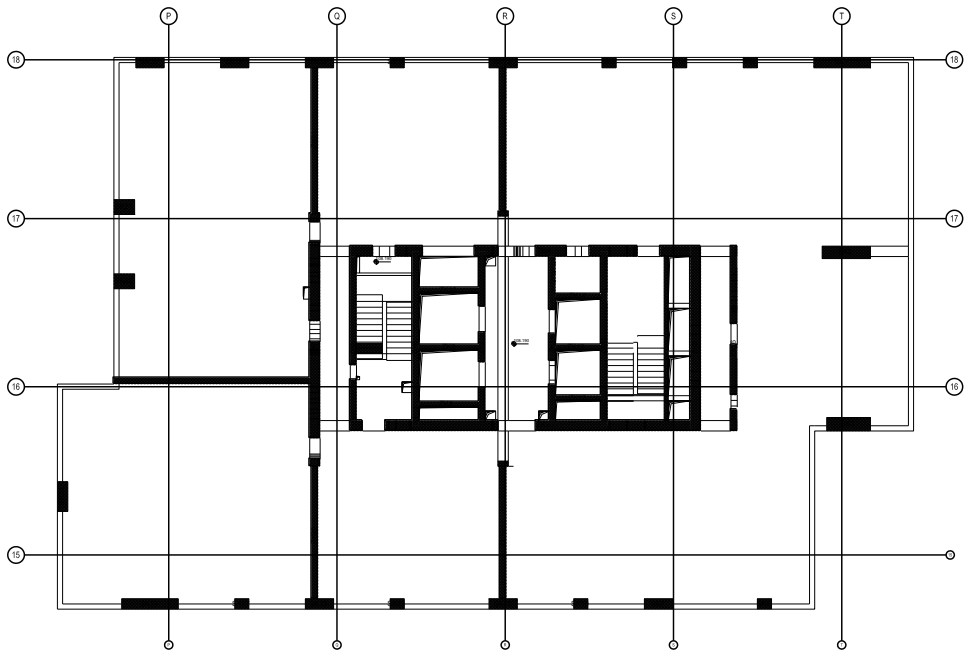
Slika 5 –Osnova 30. sprata-AB jezgro i seizmički zidovi koji povezuju jezgro sa stubovima i gredama na fasadi

1.3. GREDE

Tržni centar

Osim greda koje služe kao oslonac na deo konstrukcije faze I, greda po obodu otvora svetlarnika i oslonaca eskalatora, ističu se grede na koje se oslanja armiranobetonska krovna ploča na nivou drugog sprata.

Kula

Na konturama ploča od prvog sprata do 40. sprata projektovane su AB grede dimezija 25x100 cm. U osi R, na nivoima od trećeg sprata do 31. sprata na delovima hodnika i unutar jezgra predviđene su grede dimenzija 50x60 cm koje spajaju jezgro sa seizmičkim zidom u istoj osi.

1.4. STUBOVI I ZIDNA PLATNA

U **tržnom centru** su stubovi kvadratnog poprečnog preseka dimenzija 60x60 cm s izuzetkom stubova u osi U/1 od ose 2-8 i 11-14 koji su dimenzija 40x60 cm.

Svi stubovi i zidna platna **kule** su armirano-betonski, različitog poprečnog preseka dimenzija od 50x50 cm, 60x60 cm do 272x60 cm, 272x75 cm i 272x90 cm. Poprečni preseci stubova i zidnih platana menjaju se po visini objekta u skladu sa proračunom konstrukcije.

1.5. ZIDOVI

Spoljašnji zidovi podzemnih etaža su debljine 30 cm.
Unutrašnji zidovi tržnog centra su debljine 25 i 30 cm.

U centralnoj zoni kule projektovano je armirano-betonsko jezgro sa debljinama zidova od 25, 30, 50, 60 i 65 cm. Ovo jezgro predstavlja osnovni elemenat konstrukcije koji obezbeđuje opštu stabilnost kule. Iznad ploče trećeg sprata (kota +16,400) između osa P i Q i u osi R projektovani su seizmički zidovi debljine 30 cm. Zid u osi R na delovima hodnika i unutar jezgra je povezan sa jezgrom preko greda dimenzija 50x60 cm.

Tabela 2 –Raspored armature u zidovima jezgra kule

Deo jezgra	Vertikalna Armatura	Horizontalna armatura
Od temeljne ploče do 13. sprata	±Ø32/100 mm	±Ø20/200 mm
Između 13. i 22. sprata	±Ø28/100 mm	±Ø18/200 mm
Između 22. i 31. sprata	±Ø25/100 mm	±Ø16/200 mm
Iznad 31. sprata	±Ø22/100 mm	±Ø14/200 mm
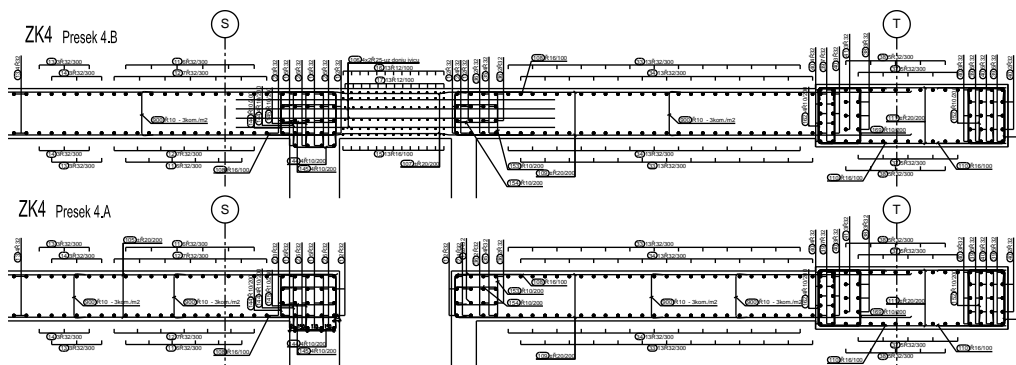
Slika 5 –Fragment armiranja zodova jezgra kule

Da bi se tokom izvođenja zidova jezgra kule mogla koristiti klizna oplata, veze ploča sa zidovima jezgra su projektovane i realizovane primenom "komax" traka. Takođe, nastavljanje armature greda na mestima prodora kroz zidove jezgra kule je izvedeno pomoću mufova.

3. MODELIRANJE I PRORAČUN KONSTRUKCIJE

3.1. OPIS MODELA I ANALIZA

Analiza konstrukcije tržnog centra i kule su vršene na osnovu nezavisnih trodimenzionalnih modela , primenom programskog paketa "Tower 8". Dokaz statičke i dinamičke stabilnosti i dimenzionisanje konstrukcije je sprovedeno korišćenjem Pravilnika za beton i armiranibeton BAB 87. Opterećenje konstrukcije, u zavisnosti od tipa opterećenja je skladu sa standardima *JUS U.C7.0100*, za vertikalna opterećenja odnsno *EN 1991-1-4/NA:2017 - Eurocode 1, Dejstva na konstrukcije-Dejstva vetra*, za dejstvo vetra.

25

Proračun na seizmička dejstva na konstrukciju kule je sproveden prema *Pravilniku o tehničkim normativima za izgradnju objekata visokogradnje u seizmičkim područjima* i prema *SRPS EN 1998-1:2015 Evrokod 8 – Projektovanje seizmički otpornih konstrukcija – Deo 1: Opšta pravila, seizmička dejstva i pravila za zgrade*, primenom proračunskog spektra odgovora Tip 1.

Prema "Pravilniku o tehničkim normativima za izgradnju objekata visokogradnje u seizmičkim područjima" kula se svrstava u objekte van kategorije (visoka zgrada sa više od 25 spratova).

Zbog toga je, pored spekralne analize, sprovedena i takozvana direktna dinamička analiza, korišćenjem akcelerograma kopaoničkog zemljotresa. Za projektno ubrzanje tla je usvojeno $a_g = 1,18$ m/s^2 ($a_g/g=0,12$). Proračun je urađen za dva ortogonalna pravca dejstva zemljoresa.

Pri modeliranju konstrukcije **tržnog centra**, temeljna ploča je tretirana kao ploča na elastičnoj podlozi. Za krutost elastične podloge je usvojena vrednost: $k_{sr} = p_{max}/s_{max} \approx 127$ kN/m^2 / 0,0159 m ≈ 8.000 kN/m^3, gde je $p_{max} \approx 127$ kN/m^2 - maksimalna vrednost napona u tlu ispod temeljne ploče, a $s_{max} \approx 15,9$ mm = 0,0159 m - maksimalna proračunska vrednost sleganja tla na nivou ispod temeljne ploče.

Prema proračunu na osnovu terenskih opita, očekivano sleganje ispod temeljne ploče kule je 65,8 mm. Prema rezultatima probnog opterećenja, očekivano sleganje ispod temeljne ploče kule je 46,2 mm. Usvajanjem srednje vrednosti, za sleganje kule dobijena je vrednost $s_{sr}=(65,8+46,2)/2=56,0$ mm.

U prorčunu kule šipovi se tretiraju kao elastične opruge čije krutosti su određene na osnovu maksimalne sile u šipu N_{max} i očekivanog sleganja objekta smax. Tako se za krutost elastične opruge dobija vrednost $k_{sr} = N_{max}/s_{max} = 7,00$ MN / 0,056 m ≈ 125.0 MN/m.

3.2. REZULTATI PRORAČUNA

Prema rezultatima proračuna, maksimalna vrednost kontaktnog napona u tlu ispod temeljne ploče **tržnog centra** je 132 kPa.

Za maksimalnu vrednost horizontalnog pomeranja **tržnog centra** usled dejstva seizmičkih sila dobija se $v_{max} = 8,1$ mm za pravac y na krovu (kota +18,510), što je znatno manje od dopuštene vrednosti fmax = H/600 = 18510/600 = 30,8 mm .

Horizontalno pomeranje krova **Tržnog centra** usled dejstva seizmičkih sila na nivou krova u pravcu kule (pravac x) je $u_1=3,2$ mm.

Prosečna vrednost sile u jednom šipu ispod **kule**, samo od vertikalnog opterećenja, je N_{sr} = 823,93 MN / 131 šip = 6,29 MN, a maksimalna vrednost sile u jednom šipu samo od vertikalnog opterećenja je $N_{ver} = 6,90$ MN, što je samo za oko 9,7% veća od prosečne vrednosti sile u jednom šipu N_{sr}. Dakle, svi šipovi su skoro ravnomerno opterećeni, što je rezultat pravilnog rasporeda šipova i značajne krutosti temeljne konstrukcije kule.

Prema anvelopama sila u šipovima usled dejstva vertikalnog opterećenja i horizontalnih dejstava (vetra odnosno seizmike) u dva ortogonalna pravca, maksimalna vrednost sile u jednom šipu usled tih uticaja je $N_{max} = 7,39$ MN što je nešto malo veća od dopuštene vrednosti $Q_a=7,36$ MN (prekoračenje je samo 0,4%).

U Tabelama 3 i 4 su prikazane vrednosti horizontalnih pomeranja **ploče krova** kule (kota +149,340) usled dejstva vetra i seizmičkih dejstava u dva ortogonalna pravca, kao i odnosi visine kule i odgovarajućeg horizontalnog pomeranja. Ti odnosi su znatno veći od dopuštenih vrednosti prema članu 16. *Pravilnika o tehničkim normativima za izgradnju objekata visokogradnje u seizmičkim područjima*.

26

Tabela 3 – Pomeranje u x pravcu u zavisnosti od vrste analize

Slucaj opterećenja	Horizonatalno pomeranje u pravcu x u_{max}[mm]	Trenutak vremena [s]	H / u_{max}
Vetar 2 - pravac x	97,0	-	1540
Seimika x - EC8	134,3	-	1112
Dir. din. analiza - x (max vrednost)	41,3	4,78	3608

Tabela 4 – Pomeranje u y pravcu u zavisnosti od vrste analize

Slucaj opterećenja	Horizonatalno pomeranje u pravcu y u_{max}[mm]	Trenutak vremena [s]	H / u_{max}
Vetar 3 - pravac z	29,5	-	5062
Seimika z - EC8	75,7	-	1973
Dir. din. analiza - y (max vrednost)	33,9	4,17	4395

Iz ovih tabela se može jasno zaključiti da su seizmički uticaji prema EC8 (primenom projektnog sepktra) znatno veći od odgovarajućih uticaja od dejstva vetra. Takođe, može se zaključiti da su seizmički uticaji prema EC8 (primenom projektnog sepktra) znatno veći od odgovarajućih uticaja dobijenih direktnom dinamičkom analizom korišćenjem akcelerograma kopaoničkog zemljotresa. Dakle, za dimenzionisanje svih elemenata konstrukcije su usvojeni kao merodavni seizmički uticaji prema EC8 (primenom projektnog sepktra).

U skladu sa "EN 1991-1-4 2005 Eurocode 1 Dejstva na konstrukcije-Vetar, Aneksi B i C", izvršen je i proračun maksimalnih ubrzanja konstrukcije na nekoliko nivoa kule usled dejsva vetra (vetar 2 - pravac x). Tako, za ubrzanje na nivou 30-tog sprata dobija se $a_{x,max}$ = 4,13 mg = 0,00413 g, gde je g - zemljino ubrzanje (g=9,81 m/s^2), a na najvišem, 40-tom spratu dobija se $a_{x,max}$ = 7,44 mg = 0,00744 g.

Treba naglasiti da su dobijene vrednosti vibracija indukovana dejstvom vetra prihvatljiva prema standardu ISO 10137:2008. Takođe, prema standardu *National Building Code of Canada (NBCC 1990) structural design education aid* kao prihvatljiva ubrzanja za kule smatraju se vrednosti od 10 do 30 mg.

4. UČESNICI U PROJEKTOVANJU I IZGRADNJI OBJEKTA

Tabela 5 Učesnici u projektovanju i izgrdnji objekta

Investitor objekta:	**"Agro Development" d.o.o "Farley Investors" d.o.o.,** Omladinskih brigada br 86, Beograd.
Naručilac	**PFB DOO BEOGRAD**, Višnjićeva 8, Beograd
Izvođač za AB konstrukciju	**ZOP inženjering doo**, Karađorđeva 61, Beograd
Stručni nadzor	**BEXEL Consulting d.o.o**. Višnjićeva 8, Beograd
Projekat izradio	Konzorcijum: **PFB design d.o.o Beograd.** Milutina Milankovića 34, Beograd, **DELING d.o.o Beograd**, Omladinskih brigada 43, Beograd
Glavni projektant	Novica Mulidža, dipl. inž. arh., PFB design d.o.o Beograd
Odgovorni projektanti konstrukcije	Prof. dr Šerif Dunica, dipl. inž. građ. V. prof. dr Saša Stošić, dipl. inž. građ. Dimitrije Aleksić, dipl. inž. građ.
Odgovorni izvođači radova	PFB : Rade Risteski, dipl.građ inž. ZOP Inženjering: Miroslav Kopunović, dipl.građ.inž

LITERATURA

[1] SRPS EN 1991-1-1:2012 Evrokod 1 – Dejstva na konstrukcije – Deo 1-1: Opšta dejstva – Zapreminske težine, sopstvena težina, korisna opterećenja za zgrade.

[2] SRPS EN 1991-1-4/NA:2017 Evrokod 1 – Dejstva na konstrukcije, Deo 1-4, Opšta dejstva – Dejstva vetra – Nacionalni prilog.

[3] SRPS EN 1992-1-1:2015 Evrokod 2 – Projektovanje betonskih konstrukcija – Deo 1-1: Opšta pravila i pravila za zgrade.

[4] SRPS EN 1998-1:2015 Evrokod 8 – Projektovanje seizmički otpornih konstrukcija – Deo 1: Opšta pravila, seizmička dejstva i pravila za zgrade.

[5] SRPS EN 10080:2008 Betonski čelik – Zavarivi betonski čelik-Opšti deo.

[6] Report No. 2010/05 Guidelines for Performance-Based Seismic Design of Tall Buildings, Pacific Earthquake Engineering Research Center, College of Engineering, University of California, Berkeley.

[7] Bungale S. Taranath Reinforced Concrete Design of Tall Buildings, CRC Press, Taylor & Francis Group, 2010.

Bojan Bizetić[1], *Igor Đurđević*[2], *Branislav Dašić*[3], *Vukan Njagulj*[4], *Branko Knežević*[5]

IZGRADNJA DRUMSKOG MOSTA PREKO REKE SAVE KOD OSTRUŽNICE

Rezime:

Izgradnja novog mosta preko reke Save kod Ostružnice, za drugu fazu obilaznice Beograda, započeta je u julu 2016. godine, a most je završen i pušten u saobraćaj u junu 2020. godine. Zbog potencijalnog prisustva neeksplodiranih minsko-eksplozivnih sredstava u koritu reke Save u zoni mosta, projektovana konzolna tehnologija montaže, morala je biti izmenjena. Da bi se izbeglo pobijanje privremenih oslonaca - jarmova u rečno dno, kombinovana su tri načina montaže: podužno prevlačenje sa obale, konzolna montaža segmenata nad rečnim stubovima i liftovanje delova konstrukcije koji su prethodno sklopljeni u brodogradilištu.

Ključne reči: drumski most, čelična konstrukcija, podužno prevlačenje, podizanje

CONSTRUCTION OF ROAD BRIDGE OVER THE SAVA RIVER NEAR OSTRUŽNICA

Summary:

Construction of new bridge over the Sava river near Ostružnica began in July 2016 and the bridge was completed and opened to traffic in June 2020. Due to the possible existence of unexploded ordinance (UXO) in the Sava riverbed in the bridge area. designed cantilever installation technology, had to be altered. To avoid setting up of temporary supports in the riverbed, three methods of installation were combined: incremental launching from the riverside, cantilever installation of segments over river piers and lifting of structural segments previously assembled in the shipyard.

Key words: road bridge, steel structure, incremental launching, lifting

---

[1] *dipl.građ.inž, STRABAG, Beograd, Srbija,*

[2] *dipl.građ.inž, STRABAG, Beograd, Srbija,*

[3] *dipl.građ.inž, GP "Mostogradnja" Beograd, Srbija,*

[4] *dipl.građ.inž, GP "Mostogradnja" Beograd, Srbija,s*

[5] *dipl.građ.inž, GP "Mostogradnja" Beograd, Srbija,*

1. OPIS MOSTOVSKE KONSTRUKCIJE

Drumski most preko reke Save kod Ostružnice, ukupne dužine 1.963 m, sastoji se od četiri dela: prednapregnute betonske prilazne konstrukcije na levoj obali (L = 592,30 m), desnoj obali reke (L = 699,13 m), armirano-betonske konstrukcije preko autoputa Beograd–Obrenovac (L = 85,30 m) i čelične konstrukcije preko reke Save (L = 586,00 m). Čelična konstrukcija preko reke Save je kontinualni čelični sandučasti nosač, s pet raspona, promenljive visine, od 3,8 m do 7,9 m i najdužim rasponom od 198 m. Ukupna težina čelične konstrukcije je 4250 tona.
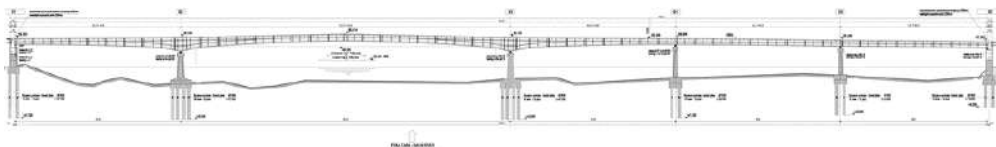
Slika 1 - Dispozicija čelične konstrukcije mosta

2. TEHNOLOGIJA MONTAŽE ČELIČNE KONSTRUKCIJE

Montaža čelične konstrukcije prvobitno je planirana konzolnom ugradnjom 56 sekcija-montažnih polja, dužine 7,5–11,0 m i teških 60–85 tona, korišćenjem plovne dizalice i privremenih oslonaca – čeličnih šipova pobijenih u korito reke. Nakon pregleda rečnog korita magnetometrima visoke rezolucije, ova se metodologija pokazala visokorizičnom zbog mogućeg postojanja neeksplodiranih ubojnih sredstava (NUS), preostalih nakon NATO bombardovanja, koja bi mogla biti aktivirana tokom pobijanja čeličnih šipova u korito reke. Da bi se izbeglo postavljanje privremenih oslonaca u rečnom koritu, projektovana metodologija montaže čelične konstrukcije morala je biti izmenjena. Nakon razmatranja mogućih alternativa uz uslov korišćenja već izrađenih delova konstrukcije mosta, kao optimalna u datim uslovima, usvojena je nova metodologija koja uključuje:
- podužno prevlačenje sekcije mosta S4–S6 ukupne dužine 187 m uz korišćenje pomoćnog plutajućeg oslonca,
- konzolnu montažu delova konstrukcije iznad rečnih stubova S1, S2, S3 i S4,
- podizanje tri sekcije konstrukcije L=77(68) m.

2.1. Podužno prevlačenje

Segment mostovske konstrukcije između stubova S4 i S6 (L=187 m) ugrađen je podužnim prevlačenjem, pošto je presek konstantne visine. Ovaj segment mosta predmontira se na radnoj platformi smeštenoj na obali, a zatim se hidrauličnim presama podužno prevlači na projektovanu poziciju. Ova operacija je podeljena u četiri faze:

- Faza I: podužno prevlačenje 45 m dugačkog segmenta bez pomoćnog oslonca;
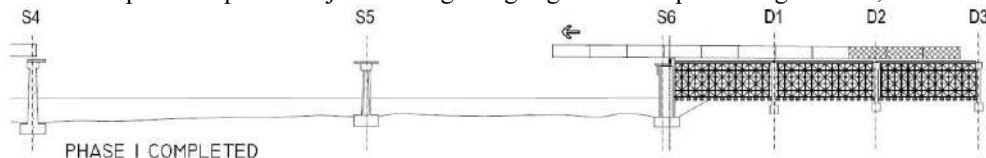
- Faza II: podužno prevlačenje 44 m dugačkog segmenta oslonjenog na pomoćni oslonac, do stuba S5;
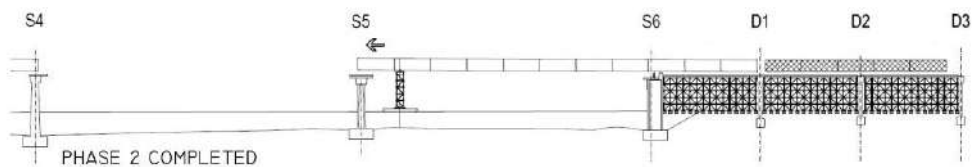
- Faza III: podužno prevlačenje 44 m dugačkog segmenta bez pomoćnog oslonca;
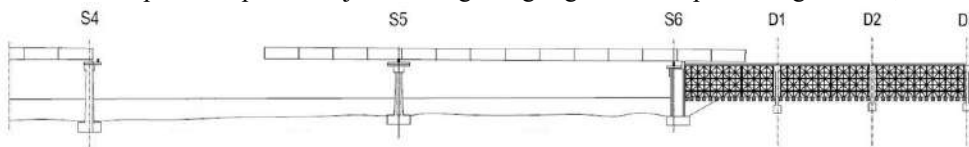
- Faza IV: podužno prevlačenje 55 m dugačkog segmenta oslonjenog na pomoćni oslonac, do stuba S4
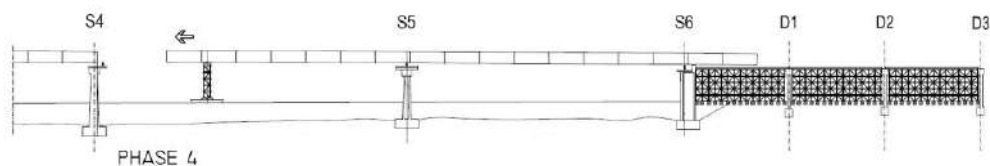
Slika 1 - Prva faza podužnog prevlačenja segmenta S4–S6

Slika 2 - Segment S4–S6 tokom podužnog prevlačenja

2.2. Konzolna montaža delova konstrukcije iznad stubova S1, S2, S3 I S4

Da bi se omogućilo podizanje segmenata konstrukcije koji su predmontirani u brodogradilištu i transportovani na gradilište rekom, potrebno je formirati osnovu sa koje će se raditi podizanje. Zbog toga je izvršena slobodna konzolna montaža najpre baznih (oslonačkih) segmenata iznad stubova S1, S2, S3 i S4, a nakon toga i susednih segmenata. Montaža ovih elemenata izvršena je plovnom dizalicom "Miljacka".
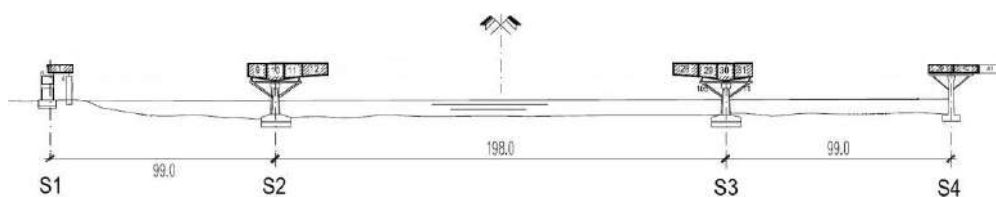
Dispozicija privremenih oslonaca i segmenata konstrukcije koji se koriste pri dizanju sekcija čelične konstrukcije

Kako bi se obezbedila stabilnost elemenata čelične konstrukcije mosta u ovoj fazi montaže, bilo je neophodno konstruisati i montirati pomoćne alate – privremene oslonce na stubovima S2, S3 i S4. Pored obezbeđenja stabilnosti, ovi privremeni oslonci preuzimaju deo uticaja u fazi dizanja i prenose ih na stubove. Pre izrade i montaže privremenih oslonaca izvršena je statička

analiza nosivosti stubova S2, S3 i S4 zbog dodatnih uticaja koji se javljaju u svim fazama podizanja sekcija čelične konstrukcije iz vode. Na ivične segmente čelične konstrukcije montiraju se uređaji za podizanje sekcija čelične konstrukcije - „Derik" kranovi i četiri hidraulične prese kapaciteta po 200 t.
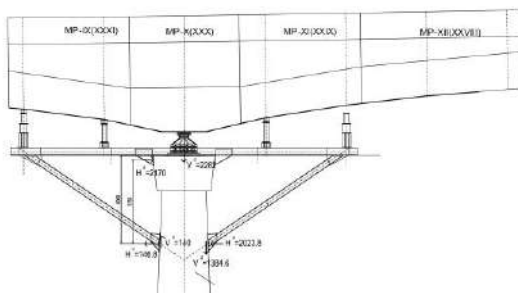
Dispozicija pomoćnog oslonca na stubu S2

2.3. Podizanje tri sekcije čelične konstrukcije

Ostatak čelične konstrukcije montiran je podizanjem tri sekcije (L = 77/68 m, G = 550/450 tona) prethodno montirane u brodogradilištu 10 km od lokacije mosta. Pre porinuća u reku, ugrađeni su dodatni elementi i oprema kojima se obezbeđuje vodonepropusnost i plovnost svake sekcije. Prevoz do mesta ugradnje obavljen je rečnim tegljačima i guračima.

Ovakva tehnologija, koja uključuje proizvodnju elementa u brodogradilištu, njihovo porinuće u reku preko navoza za brodove i transport rekom do mesta ugradnje, je po prvi put primenjena u regionu.

Prednosti ove tehnologije su:
- Brodogradilišta su potpuno opremljena za ovu vrstu radova (dovoljan kapacitet električne energije, portalni kranovi, uređen prostor za proizvodnju, itd.).
- Ukrupnjavanje velikih sekcija mosta se vrši na obali, a ne nad vodom, čime se smanjuje obim radova na reci.
- Tehnički jednostavnije postizanje projektovane nivelete mosta u odnosu na konzolnu montažu.
- Jednostavno porinuće sekcija mosta u vodu putem navoza i kolica.
- Eliminisanje angažovanja barži za prevoz montažnih elemenata mosta, uključujući i neophodna ojačavanja barži.
- Eliminisanje angažovanja plovne dizalice velike nosivosti.
- Paralelizacija rada na više sekcije mosta u brodogradilištu.

Nedostatak ove tehnologije je:
- Neophodnost zadovoljenja propisa za porinuće sekcija mosta u reku i tokom njihovog transporta do mesta ugradnje. Sekcije mosta pri ovakvoj tehnologiji izgradnje se tretiraju kao plovni objekti bez motora (kao barže, šlepovi i sl.).

Slika 3a – Montaža jedne od sekcija mosta u brodogradilištu

Slika 3b – Jedna od sekcija mosta neposredno pred porinuće u reku

Slika 3c - Jedna od sekcija mosta neposredno posle porinuća u reku

Slika 3d - Rečni transport jedne od sekcija mosta

- Faza I: podizanje sekcije MP2–MP8, L=77 m, G~550 t
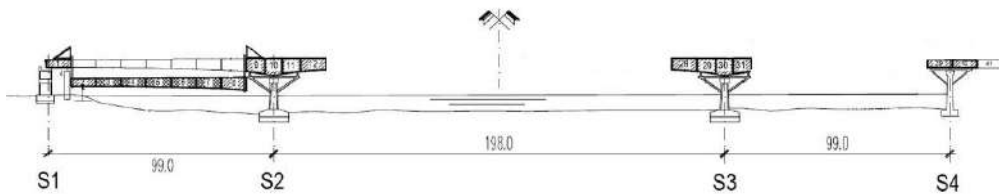
- Faza II: podizanje sekcije MP32–MP38, L=77 m, G~550 t
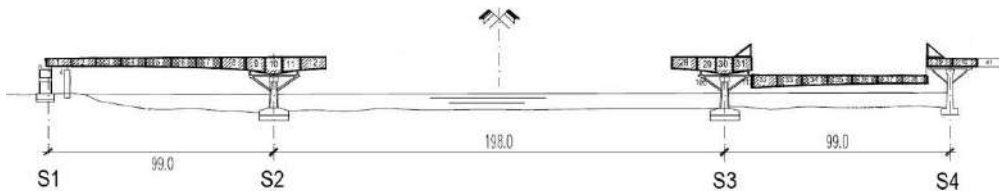
- Faza III: konzolna montaža elemenata MP13–MP16 i MP24–MP27 plovnom dizalicom
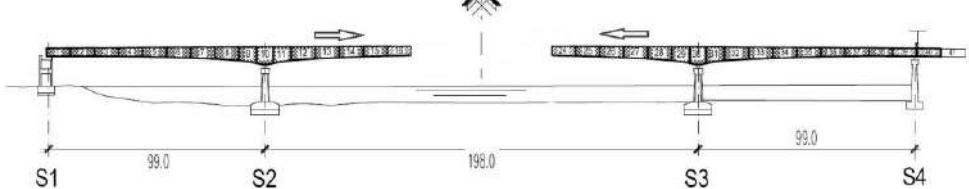
- Faza IV: podizanje sekcije MP17–MP23, L=68 m, G~450 t
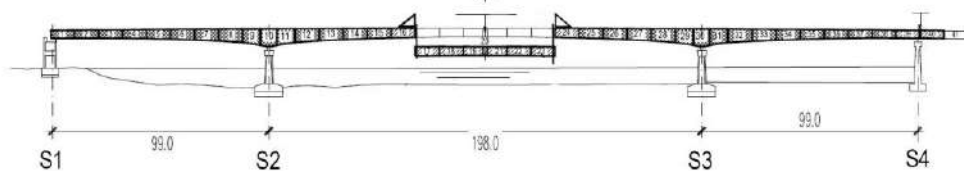
Slika 4 - Podizanje segmenta S1–S2

2.4. ZAKLJUČAK

Ovaj način montaže je prema našim saznanjima prvi put primenjen na rekama u regionu. Usvajanjem izrade konstrukcija na navozima u brodogradilištu postigli smo značajno ubrzanje radova (3 segmenta se istovremeno montiraju), kompletnu montažu izveli uz pomoć lokalnih resursa i postigli visoku preciznost izvedene nivelete mosta.

Vedran Carević[1]

UTICAJ PRSLINA NA MEHANIZME DETERIORACIJE I TRAJNOST ARMIRANOBETONSKIH KONSTRUKCIJA

Rezime:

Na deterioracione mehanizme i koroziju koja nastaje njihovim dejstvom u velikoj meri utiče prisustvo prslina, pa se uloga prslina prouzrokovanih opterećenjem ne sme zanemariti u sagledavanju upotrebnog veka armiranobetonskih (AB) konstrukcija. Za potrebe ispitivanja spravljeni su referentni beton, beton sa 50% letećeg pepela (LP) i beton sa 100% recikliranog agregata (RA). Analizirani su postojeći modeli predikcije dubine karbonatizacije i predložena je njihova modifikacija u slučaju betona sa LP i RA. Nakon što je ustanovljena veza između karbonatizacione otpornosti i čvrstoće pri pritisku, izvršena je analiza upotrebnog veka kroz definisanje potrebne debljine zaštitnog sloja različitih vrsta betona. Pripremljeni su uzorci sa 5 različitih širina prslina (0.05, 0.10, 0.15, 0.20 i 0.30 mm) kao i referentni uzorci bez prslina. Predloženo je ograničenje napona u armaturi koji omogućava da celokupni upotrebni vek (period inicijacije i propagacije) AB elemenata zadovolji propisane zahteve trajnosti.

Ključne reči: trajnost, prsline, karbonatizacija, leteći pepeo, reciklirani agregat, korozija

INFLUENCE OF CRACKS ON THE DETERIORATION MECHANISMS AND DURABILITY OF REINFORCED CONCRETE STRUCTURES

Summary:

The most important factor that affects concrete deterioration is the appearance of cracks on reinforced concrete (RC) structures, so the influence of loading cracks should not be neglected when the service life is analyzed. For the purposes of this research, reference concrete and concretes with 50% fly ash (FA) and with 100% recycled aggregate (RCA) were prepared. The existing carbonation prediction models were analyzed and modification was proposed in the case of FA and RCA concretes. After establishing the relationship between carbonation resistance and compressive strength, the service life analysis was performed by defining the required concrete cover depth for different concrete types. Samples with 5 different crack widths (0.05, 0.10, 0.15, 0.20 and 0.30mm) and samples without cracks were prepared and subjected to accelerated carbonation. For all concrete types steel stress limitation was pro-posed, which allows the entire service life of RC elements to meet the prescribed requirements.

Key words: durability, cracks, carbonation, fly ash, recycled concrete aggregate, corrosion

---

[1] *Docent, Univerzitet u Beogradu, Građevinski fakultet, Beograd, Srbija, vedran@imk.grf.bg.ac.rs*

1. UVOD

Trajnost betona definisana je njegovom otpornošću na dejstvo štetnih agenasa iz spoljašnje sredine koji dovode do različitih vrsta oštećenja (mehanizmi deterioracije). Glavni deterioracioni mehanizmi koji utiču na trajnost betona su karbonatizacija, penetracija hlorida, dejstvo mraza sa ili bez soli za odmrzavanje, alkalno–silikatna reakcija i dejstvo sulfata. Svi ovi mehanizmi dele se u dve grupe u zavisnosti od vrste oštećenja koju proizvode. Mehanizmi deterioracije mogu uticati na strukturu betona (mraz sa ili bez soli za odmrzavanje, alkalno–silikatna reakcija i dejstvo sulfata) ili na pojavu korozije armature unutar betona (karbonatizacija i penetracija hlorida). Deterioracioni mehanizmi zavise od uslova sredine kojima je beton izložen, pa različita geografska područija karakterišu određeni mehanizmi deterioracije. Tri mehanizma deterioracije koji predstavljaju najveću opasnost za objekte u Srbiji su: karbonatizacija, penetracija hlorida i dejstvo mraza i soli za odmrzavanje [1].

Otpornost betona na dejstvo ovih mehanizama deterioracije trenutno se kod cementnih betona sa prirodnim agregatom obezbeđuje adekvatnim zaštitnim slojem betona do armature i propisanim sastavom (minimalna količina cementa i maksimalni vodo-vezivni faktor). Zaštitni sloj betona predstavlja zaštitu armature od ekstremnih uticaja kroz smanjenje transporta štetnih materija koji mogu uzrokovati koroziju. Međutim, u armiranobetonskim (AB) konstrukcijama pojava prslina koje presecaju zaštitni sloj je gotovo neizbežna posledica skupljanja, termičkog širenja, mehaničkih/hemijskih oštećenja ili jednostavno posledica dejstva opterećenja i relativno niske čvrstoće betona na zatezanje. Pojava prslina dovodi do narušavanja strukture zaštitnog sloja betona i do ubrzanja transporta štetnih materija kroz beton do armature, čime utiču na trajnost AB konstrukcija [2]. Održavanje niskog stepena propustljivosti betona (za gasove ili rastvore) od presudne je važnosti za trajnost.

Prsline mogu uticati na deterioracione procese (karbonatizacija, penetracija hlorida i dejstvo mraza i soli za odmrzavanje) i koroziju koja nastaje tim putem. Imajući to u vidu, postavlja se pitanje kakva je uloga zaštitnog sloja betona ispresecanog mrežom prslina u obezbeđivanju upotrebnog veka. Shodno tome, ulogu naponskih prslina ne bi trebalo zanemariti u sagledavanju upotrebnog veka AB konstrukcija. U dosadašnjoj istraživačkoj praksi, deterioracioni procesi i njihovi transportni mehanizmi izučavani su i ispitivani uglavnom na neisprskalim betonskim uzorcima.

Korozija izazvana hloridima bila je predmet mnogih istraživanja proteklih godina, uključujući i uticaj prslina na ovaj deterioracioni mehanizam [3–5]. Za razliku od nje, u literaturi postoji vrlo malo podataka o uticaju prslina na koroziju armature izazvanu karbonatizacijom, pogotovo na razvoj korozije tokom vremena. Došlo se do zaključka da deterioracija AB konstrukcija usled korozije armature izazvane karbonatizacijom predstavlja jedan od glavnih problema trajnosti širom sveta, imajući u vidu da je veliki broj infrastrukturnih objekata izložen okruženju bogatom ugljen–dioksidom (CO_2) čija se koncentracija konstantno povećava. Zbog toga je karbonatizacija postala važno pitanje u analizi trajnosti AB konstrukcija.

Procenjuje se da 7–10% celokupne emisije CO_2 antropogenog porekla nastaje tokom proizvodnje cementa [6]. Ogroman uticaj građevinske industrije na životnu sredinu uglavnom je posledica velike proizvodnje betona, pa je upotreba prirodnih sirovina, potrošnja energije i proizvodnja otpada takođe velika. Jedan od načina da se očuvaju prirodni resursi i beton učini ekološki prihvatljivijim je primena letećeg pepela (LP) i recikliranog agregata (RA) koja je korisna i sa ekonomskog i sa ekološkog aspekta. Međutim, zamena prirodnog agregata (PA) sa

RA ili zamena cementa sa LP uveliko utiče na fizička, mehanička i svojstva trajnosti betona. Uticaj upotrebe RA i LP na graničnu nosivost [7,8] i ponašanje pod dugotrajnim opterećenjem [9] AB elemenata ispitivana su poslednjih godina na Građevinskom fakultetu Univerziteta u Beogradu. Međutim, da bi se osigurala održiva primena ovih zelenih alternativa proizvodnji cementnih betona sa PA, moraju se proveriti njihova svojstva trajnosti.

Da bi se generisalo novo znanje i doprinelo poboljšanju postojećih standarda i inženjerske prakse, razvijena je odgovarajuća eksperimentalna postavka kako bi se ispitao uticaj prslina na dubinu karbonatizacije i trajnost AB elemenata napravljenih od različitih vrsta betona.

2. POSTAVKA EKSPERIMENTA

Eksperimentalno ispitivanje sprovedeno je od 2017. do 2020. godine na Građevinskom fakultetu Univerziteta u Beogradu. Na početku eksperimentalnog programa izvršeno je projektovanje i ispitivanje tri vrste betonskih mešavina. Cilj ovog procesa je bio proizvodnja betona a da se pri tome zadovolji klasa betona potrebna za njegovu konstrukcijsku primenu. Spravljene su tri vrste betonskih mešavina: referentni cementni beton sa PA (NAC), cementni beton sa 100% krupnog RA kao zamena PA (RAC) i beton sa 50% LP kao zamena cementa (HVFAC). Krupni RA korišćen u ovom ispitivanju je dobijen recikliranjem betona 40 godina starog nadvožnjaka. Imao je zapreminsku masu u suvom stanju od 2370 kg/m^3 kao i upijanje vode od 3.9% nakon 24 sata. LP je dobijen iz termoelektrane "Nikola Tesla B" u Obrenovcu i imao je zapreminsku masu od 2300 kg/m^3 kao i srednju veličinu čestica od 8.53 μm. Svi betoni imali su da sličnu čvrstoću pri pritisku (41.0, 41.7 i 42.1 MPa, respektivno) i istu klasu ugradljivosti (klasa S3).

Kako karbonatizacija betona u prirodnim uslovima traje godinama odlučeno je da se ovaj proces ubrza povećavanjem koncentracije CO_2 u specijalizovanim komorama predviđenim za takvo ispitivanje (slika 1).

Slika 1 – Uzorci u komori za karbonatizaciju i izmerene dubine karbonatizacije NAC, RAC i HVFAC betona, respektivno

Zbog toga je pre početka sprovođenja eksperimentalnog ispitivanja uticaja prslina na dubinu karbonatizacije bilo neophodno ispitati uticaj koncentracije CO_2 na sam proces karbonatizacije, kao i mogućnosti primene postojećih modela predikcije na različitim vrstama betona korišćenim u ovom istraživanju. Sprovedeno je komparativno ispitivanje u ubrzanim i prirodnim uslovima. Analiziran je uticaj koncentracije CO_2 (1%, 2%, 4% i 16%) na proces karbonatizacije kod sve tri

vrste ispitivanih betona i pokazalo se da je koncentracija do 2% CO_2 optimalna za ubrzavanje procesa karbonatizacije bez posledica na kinetiku procesa.

U poslednjih dvadeset godina razvijene su razne metode za indukciju prslina u uzorcima nakon standardnog postupka pripreme i nege uzoraka [1]. Na osnovu analize svih dostupnih metoda za indukovanje prslina (metod cepanja klinom, Brazilski opit cepanja, metod ekspanzivnog jezgra, formiranje prslina pomoću umetaka i metod savijanja) uočeno je da metoda savijanja ima najviše prednosti. Prsline indukovane ovom metodom imaju V-oblik i odgovaraju po obliku prslinama nastalim savijanjem u AB konstrukcijama. Prednost u odnosu na ostale metode jeste da nakon formiranja prslina, uzorak se može izložiti ubrzanim testovima deterioracije u opterećenom stanju. U opterećenom stanju, pored uticaja prslina, može se ispitati i uticaj napona pritiska. Još jedna prednost u odnosu na ostale metode je upotreba armature, koja omogućava merenje i praćenje korozije tokom vremena.

Pripremljeni su uzorci sa 5 različitih širina prslina (0.05, 0.10, 0.15, 0.20 i 0.30 mm) kao i referentni uzorci bez prslina. Sve definisane širine prslina bile su manje od dozvoljenih širina definisanih u EN 1992-1-1 [10], – za definisane uslove izloženosti karbonatizaciji maksimalna dozvoljena širina prsline iznosi 0.3 mm. Na slici 2 prikazana je postavka eksperimenta za određivanje uticaja širine prslina na dubinu karbonatizacije i trajnost AB elemenata.
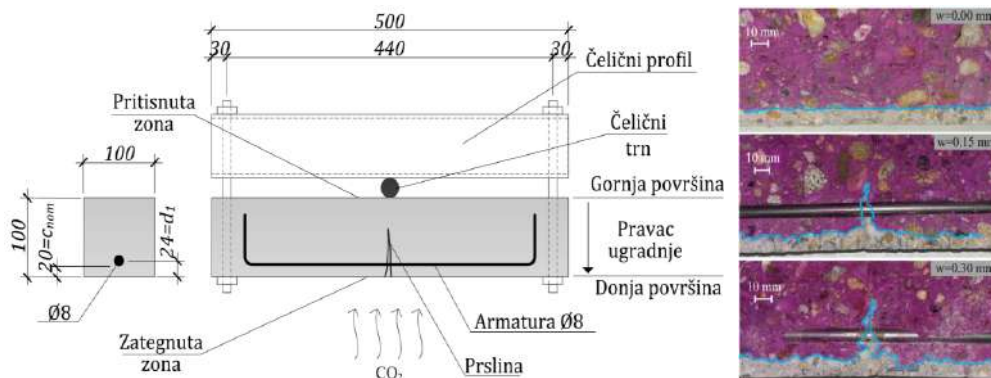
Slika 2 – Postavka eksperimenta za određivanje uticaja širine prslina na dubinu karbonatizacije i trajnost AB elemenata

Uticaj prslina i napona pritiska u betonu na upotrebni vek analiziran je pomoću dostupnog probabilističkog modela predikcije *fib*-Model Code 2010 [11] za određivanje upotrebnog veka.

3. KARBONATIZACIONA OTPORNOST RAZLIČITIH VRSTA BETONA

Kako ubrzavanje karbonatizacije utiče na kinetiku procesa [12] bilo je neophodno ispitati mogućnosti primene postojećih modela predikcije na zelenim betonima korišćenim u ovom istraživanju. Kako bi to bilo moguće uraditi, sprovedeno je komparativno ispitivanje u ubrzanim i prirodnim uslovima na uzorcima bez prslina. Sprovedena je opsežna analiza zasnovana na sopstvenim eksperimentalnim rezultatima i rezultatima objavljenim u literaturi. Vrednosti dubine karbonatizacije u ubrzanim uslovima i odgovarajuća čvrstoća pri pritisku pronađene su u 15 radova za NAC betone, 8 radova za RAC i 17 radova za betone sa LP (*fly ash concrete* – FAC). Ukupno 115, 109 i 138 reultata je prikupljeno za NAC, RAC i FAC betone respktivno.

Na osnovu sprovedene analize zaključeno je da se *fib*-ov [13] model predikcije može primenjivati na sve vrste ispitivanih betona uz modifikacije za betone sa LP [14]. Da bi se omogućila primena ovog modela predikcije, neophodno je sprovesti ubrzani karbonatizacioni test. S obzirom da ovo nije uvek moguće data je veza između karbonatizacione otpornosti i čvrstoće betona pri pritisku nakon 28 dana starosti (f_{cm}), koja se najčešće korsiti kao indikator kvaliteta betona [14,15] (slika 3).

RAC 100% — $R_{ACC}^{-1} = 2.12 \cdot 10^8 \cdot f_{cm}^{-3.013}$, $R^2 = 0.843$

FAC 40-70% — $R_{ACC}^{-1} = 2.80 \cdot 10^7 \cdot f_{cm}^{-2.352}$, $R^2 = 0.679$
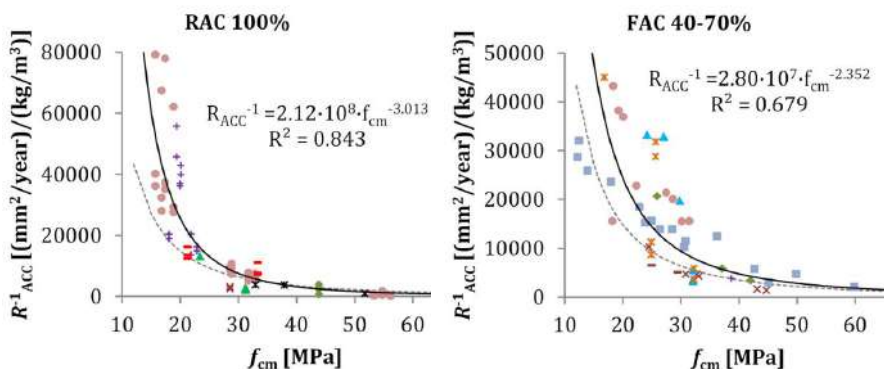
Slika 3 – Odnos između karbonatizacione otpornosti i čvstoće betona pri pritisku (f_{cm}) za betone sa RA i LP

Nakon što je ustanovljena veza između ubrzane inverzne efektivne karbonatizacione otpornosti i čvrstoće pri pritisku na 28 dana (slika 3) primenjen je puni probabilistički pristup za određivanje dužine upotrebnog veka koristeći modifikovani *fib* model predikcije dubine karbonatizacije. Preporučene minimalne debljine zaštitnog sloja za različite vrste betona prikazane su u Tabeli 1.

Tabela 1 – Vrednosti minimalnih debljina zaštitnog sloja za različite vrste betona za upotrebni vek $t_{SL} = 50$ godina [1]

Vrsta betona	$C_{min,dur}$ (mm)			
	XC1	XC2	XC3	XC4
Indikativna klasa betona	C 25/30	C 25/30	C 30/37	C 30/37
Referentni beton	15	25	25	30
RAC (10-50% zamene PA)	15	25	25	30
RAC (100% zamene PA)	16	26	25	30
FAC (10-35% LP)	22	35	40	39
HVFAC (40-70% LP)	35	58	62	61

Iz tabele 1 se vidi da je u slučaju RAC 100% razlika u veličini zaštitnog sloja za klase izloženosti XC1 i XC2 u odnosu na NAC betone bila zanemarljiva (1 mm). Imajući u vidu tačnost probabilističkog modela i posmatranu razliku (6%) može se zaključiti na osnovu dostupnih rezultata i sprovedene analize da se za sve betone sa RA mogu koristiti zaštitni slojevi definisani za NAC u EN 1992-1-1 [10], obezbeđujući pri tome upotrebni vek od 50 godina.

Primena LP kao zamene cementa značajnije je uticala na upotrebni vek. Za betone do 35% LP u ukupnom vezivnom materijalu debljine zaštitnih slojeva potrebnih za obezbeđenje zahtevanog upotrebnog veka veće su prosečno za 1.46 puta u poređenju sa NAC betonima, uzimajući u obzir iste indikativne klase čvrstoće. Kod HVFAC betona (40-70% LP u ukupnom vezivnom materijalu) situacija je bila još drastičnija. Predloženo je povećanje debljine zaštitnih slojeva kod betona sa LP kako bi se omogućio upotrebni vek od 50 godina za predložene indikativne klase čvrstoće. Pored određivanja debljine zaštitnih slojeva za različite klase izloženosti i različite vrste betona, sprovedena je i analiza očekivanih rezultata ubrzane karbonizacione otpornosti betona kako bi se zadovljili različiti uslovi izloženosti sa propisanim debljinama zaštitnih slojeva [16]. Na ovaj način je moguće usvojiti potrebnu debljinu betonskog pokrivača za definisanu klasu izloženosti, na osnovu otpornosti betona na karbonizaciju, kao i dobiti ranu indikaciju kvaliteta betona u pogledu otpornosti na karbonizaciju.

Povećavanje klase betona očekivano dovodi do smanjivanja debljine zaštitnog sloja. Međutim, ovo smanjivanje debljine zaštitnog sloja zbog povećanja klase betona će uticati na povećanje širine prsline na mestu armature što će biti analizirano u nastavku.

4. UTICAJ PRSLINA NA UPOTREBNI VEK AB KONSTRUKCIJA

1.1. UTICAJ PRSLINA NA DUBINU KARBONATIZACIJE

Analiza uticaja prslina na koroziju izazavanu karbonatizacijom sprovedena je na osnovu sopstvenih eksperimentalnih rezultata, kao i primenom dostupnim standarda i modela predikcije. Uticaj prslina na karbonatizacioni front je bio sličan (približno 20 mm) bez obzira na širinu prslina (slika 2). U svim slučajevima, čak i sa najmanjom širinom prsline od 0.05 mm, prslina se ponašala kao dodatna izložena površina kroz koju su molekuli CO_2 prodirali unutar betona upravno na stranicu prsline. Ovaj fenomen je bio prisutan kod svih vrsta ispitivanih betona. Takođe, maksimalna dubina karbonatizacije uzoraka bez prslina je bila i do tri puta manja u poređenju sa uzorcima sa prslinama, pri čemu nije bilo razlike između različitih vrsta betona Ako se uzme u obzir da su RAC i HVFAC betoni imali 40%, odnosno 115%, veću dubinu karbonatizacije neisprskalih uzoraka u poređenju sa NAC betonima, ovo ukazuje da je pojava prslina imala daleko veći uticaj na dubinu karbonatizacije u poređenju sa uticajem vrste betona.

Pored maksimalne dubine karbonatizacije, potrebno je definisati i osrednjenu dubinu karbonatizacije na svim uzorcima. Osrednjena dubina karbonatizacije predstavlja prosečnu dubinu karbonatizacije na određenoj dužini merenja i koristi se pri proračunu upotrebnog veka. Izabrane su tri dužine osrednjavanja: 20 mm (*avg. 2 cm*) što predstavlja uticajnu zonu prsline na karbonatizacioni front, 50 mm (*avg. 5 cm*) što predstavlja uobičajenu dužinu osrednjavanja koja se koristi u standardima za ispitivanje i 140 mm (*avg. 14 cm*) što predstavlja srednje računsko rastojanje između prslina u ovom ekspreimentalnom ispitivanju.

Na slici 4 se može videti da se odnos između sračunatih dubina karbonatizacije uzoraka sa i bez prsline. Ovaj odnos se kretao do vrednosti 2.9 kod NAC i RAC uzoraka, za malu dužinu osrednjavanja (*avg. 2 cm*). Kod HVFAC uzoraka ovaj odnos je bio manji i iznosio je 2.3. To praktično znači da će dubina karbonatizacije uzoraka sa prslinom 0.30 mm u prirodnim uslovima izloženosti biti i do 3 puta veća u poređenju sa neisprskalim uzorcima. Čak i kada se koristi veća dužina osrednjavanja (*avg. 14 cm*), dubina karbonatizacije biće 1.5 puta veća u poređenju sa neisprskalim NAC uzorcima. Na slici 4 se može videti da je za sve vrste betona, pri malim dužinama osrednjavanja (20 i 50 mm) došlo do značajnijeg porasta odnosa dubina

karbonatizacije isprskalih i neisprskalih uzoraka nakon određene širine prsline. U slučaju RAC i HVFAC uzoraka ova promena je nastupila pri širini prsline između 0.20 i 0.30 mm.
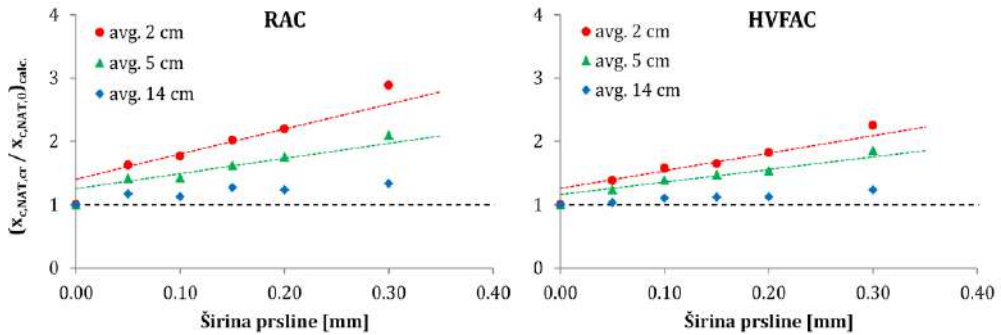
Slika 4 – Odnos između sračunatih dubina karbonatizacije uzoraka sa ($x_{c,NAT,cr}$) i bez ($x_{c,NAT,0}$) prsline za različite dužine osrednjavanja

1.2. UTICAJ NAPONA PRITISKA NA DUBINU KARBONATIZACIJE

Većina istraživanja obavljenih do sada o uticaju napona na dubinu karbonatizacije analizirala su uticaj prslina ili napona zatezanja na karbonatizacionu otpornost, ali samo neka od njih su analizirala uticaj napona pritiska [17–20]. Takođe, napon pritiska u većini tih istraživanja kretao se do nosivosti betona na pritisak, što nije slučaj tokom eksploatacije AB konstrukcija. Vrlo malo pažnje posvećeno je eksplatacionim naponima pritiska (do $0.45 \cdot f_{ck}$), gde je odnos napona i dilatacije u betonu bio linearan. Kako je ovde reč o pritisnutoj strani uzorka umesto širine prsline, koja ne predstavlja faktor za pritisnutu stranu, uveden je pojam dilatacije pritiska na površini betona. Uticaj napona pritiska analiziran je na osnovu merenja dubine karbonatizacije na pritisnutoj strani uzorka i sračunate vrednosti dilatacije pritiska. Dilatacija pritiska na pritisnutoj strani uzorka kretala se do 0.8‰. Na slici 5 je prikazan odnos sračunatih dubina karbonatizacije opterećenih i neopterećenih uzoraka.
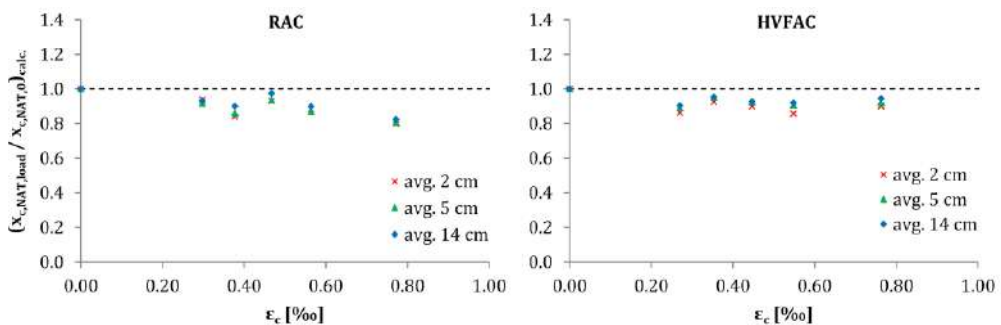
Slika 5 – Odnos između sračunatih dubina karbonatizacije opterećenih ($x_{c,NAT,load}$) i neopterećenih ($x_{c,NAT,0}$) uzoraka

Može se zaključiti da je napon pritiska imao pozitivan efekat na karbonatizacionu otpornost. Pritisak unutar betona zatvara mikro pore i mikro prsline čime smanjuje stepen povezanosti pora, odnosno dovodi do progušćenja cementne matrice. Ovo je posebno bilo izraženo kod RAC

uzoraka koji su imali najveću poroznost zbog prisustva stare cementne paste na zrnima agregata. S obzirom da napon pritiska nije imao značajni efekat na smanjenje dubine karbonatizacije (do 19%), u nastavku se neće razmatrati uticaj napona pritiska na upotrebni vek AB konstrukcija.

1.3. UTICAJ NAPONA U ARMATURI NA UPOTREBNI VEK

Širina prsline na površini betona ne treba da bude izolovani parametar povezan sa korozijom armature. Pokazalo se da je mnogo korisnije koristiti maksimalni napon u armaturi kao moguće ograničenje uticaja prslina izazvanih opterećenjem na razvoj korozije armature. Širina prslina u AB elementima zavisi od nekoliko parametara: debljine zaštitnog sloja, napona prijanjanja. Uspostavljena je analitička veza između napona u armaturi i izmerene širine prsline na površini betona kako bi se napon u armaturi mogao koristiti kao jedan od kriterijuma trajnosti. Ova veza je analizirana za različitie w/c odnose, čvrstoće, debljine zaštitnih slojeva i uslove izloženosti na osnovu sopstvenih eksperimentalnih i rezultata dostupnih u literaturi. U odabranim istraživanjima, čvrstoća pri pritisku je bila u rasponu od 24.0 do 65.2 MPa, w/c odnos se kretao u granicama od 0.40 do 0.65, dok su prsline bile široke od 0.02 mm do 0.64 mm.

Uspostavljanjem linearne relacije moguće je napraviti predikciju dubine karbonatizacije elemenata sa prslinama poznajući napon u armaturi i karbonatizacionu otpornost neisprsklaih uzoraka napravljenih od tog betona. Ovo omogućava da se kod AB elemenata ne definiše minimalni zaštitni sloj i maksimalni w/c odnos kao uslov trajnosti, već napon u armaturi koji zavisi od zaštitnog sloja betona i veličine naprezanja.

S obzirom da se pokazalo da period depasivizacije armature ne znači nužno i kraj upotrebnog veka, analiziran je period propagacije korozije armature u isprskalim AB elementima. Izvršena je analiza rezultata sopstvenih eksperimentalnih ispitivanja primenom polu-probabilističkog modela. Na kraju je na osnovu analitičke verifikacije odnosa napona u armaturi i širine prsline, za različite vrste betona, predloženo ograničenje napona u armaturi koji omogućava da celokupni upotrebni vek (period inicijacije i propagacije) AB elemenata sa prslinama zadovolji propisane zahteve trajnosti (slika 6).
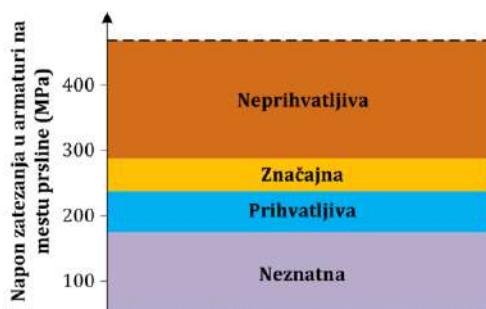
Slika 6 – Veza između napona zatezanja u armaturi na mestu prsline i oštećenja koja nastaju kao posledica korozije za slučaj klasu izloženosti XC2

5. ZAKLJUČAK

Na proces karbonatizacije i koroziju koja nastaje tim putem u velikoj meri utiče prisustvo prslina. Prsline koje nastaju kao posledica savijanja presecaju armaturu i znatno olakšavaju prodor kiseonika i vode. Shodno tome, uloga prslina prouzrokovanih opterećenjem ili

deformacijama ne sme se zanemariti u sagledavanju upotrebnog veka armiranobetonskih konstrukcija.

Da bi ispitala mogućnost primene postojećih modela predikcije na zelenim betonima korišćenim u ovom istraživanju, sprovedeno je komparativno ispitivanje u prirodnim i ubrzanim uslovima. Analizirani su postojeći modeli predikcije dubine karbonatzacije i predložena je njihova modifikacija (parametri k_t i ε_t) u slučaju betona sa RA i LP. Nakon što je ustanovljena veza između ubrzane karbonatizacione otpornosti i čvrstoće pri pritisku, izvršena je analiza upotrebnog veka kroz definisanje debljine zaštitnog sloja različitih vrsta betona.

Drugi deo ovog istraživanja prikazuje rezultate ispitivanja uticaja širine prsline na dubinu karbonatizacije i trajnost AB konstrukcija. Pripremljeni su uzorci sa 5 različitih širina prslina (0.05, 0.10, 0.15, 0.20 i 0.30 mm) kao i referentni uzorci bez prslina. Uticaj prsline na dubinu karbonatizacije postojao na otprilike ±10 mm u odnosu na položaj prsline, bez obzira na vrstu betona i širinu prsline. Takođe, na osnovu izmerenih dubina karbonatizacije duž pritisnute strane uzorka zaključeno je da nije bilo jasnog trenda smanjenja dubine karbonatizacije sa porastom dilatacije pritiska.

Uspostavljena je analitička veza između napona u armaturi i izmerene širine prsline na površini betona. S obzirom da ova veza primarno zavisi od debljine zaštitnog sloja, napon u armaturi analiziran je kao kriterijum trajnosti jer predstavlja prag mikroskopskog oštećenja betona na kontaktu sa armaturom. Analizirani su sopstveni eksperimentalni rezultati i rezultati dostupni u literaturi.

Kako period depasivizacije armature ne znači nužno i kraj upotrebnog veka, analiziran je period propagacije korozije armature u isprskalim AB elementima. Prikazani su rezultati sopstvenih eksperimentalnih ispitivanja i izvršena je analiza tih rezultata primenom polu-probabilističkog modela iz literature. Na kraju je na osnovu analitičke verifikacije odnosa napona u armaturi i širine prsline, za različite vrste betona, predloženo ograničenje napona u armaturi koji omogućava da celokupni upotrebni vek (period inicijacije i propagacije) AB elemenata sa prslinama zadovolji propisane zahteve trajnosti.

LITERATURA

[1] Carević V. Uticaj Prslina na Mehanizme Deterioracije i Trajnost Armiranobetonskih Konstrukcija, PhD Thesis. University of Belgrade, Faculty of Civil Engineering, 2020.

[2] Carević V, Ignjatović I. Influence of loading cracks on the carbonation resistance of RC elements. Constr Build Mater 2019;227:116583. https://doi.org/10.1016/j.conbuildmat.2019.07.309.

[3] Blagojevic A. The Influence of Cracks on the Durability and Service Life of Reinforced Concrete Structures in relation to Chloride - Induced Corrosio A Look from a Different Perspective. Delft University of Technology, 2016.

[4] Pease BJ. Influence of concrete cracking on ingress and reinforcement corrosion. Technical University of Denmark, 2010.

[5] Otieno M, Beushausen H, Alexander M. Chloride-induced corrosion of steel in cracked concrete - Part II: Corrosion rate prediction models. Cem Concr Res 2016;79:386–94. https://doi.org/10.1016/j.cemconres.2015.08.008.

[6] Scrivener KL, John VM, Gartner EM. Eco-efficient cements: Potential, economically viable solutions for a low-CO2, cement-based materials industru. Paris: 2016.

[7] Ignjatović I. Ultimate strength of reinforced recycled concrete beams (in Serbian), PhD Thesis. University of Belgrade, Facuty of Civil Engineering, 2013.

[8] Dragaš J. Ultimate capacity of high volume fly ash reinforced concrete beams, PhD Thesis. University of Belgrade, Faculty of Civil Engineering, 2018.

[9] Tošić N. Behaviour of reinforced concrete beams made with recycled and waste materials under long-term loading, PhD Thesis. University of Belgrade, Faculty of Civil Engineering, 2017.

[10] CEN. EN 1992-1-1. In: CEN, editor. vol. 1. 1st ed., Belgrade: ISS; 2015.

[11] fib-Model Code. Model Code 2010. Volume 2. Lausanne, Switzerland: International Federation for Structural Concrete (fib); 2010.

[12] Carević V, Ignjatović I, Dragaš J. Model for practical carbonation depth prediction for high volume fly ash concrete and recycled aggregate concrete. Constr Build Mater 2019;213:194–208. https://doi.org/10.1016/j.conbuildmat.2019.03.267.

[13] fib-Bulletin 34. Model Code for Service Life Design. 1st ed. Lausanne, Switzerland: International Federation for Structural Concrete (fib); 2006.

[14] Carević V, Ignjatović I. Evaluation of concrete cover depth for green concretes exposed to carbonation. Struct Concr 2020. https://doi.org/10.1002/suco.202000086.

[15] Marinković S, Carević V, Dragaš J. The role of service life in Life Cycle Assessment of concrete structures. J Clean Prod 2021;290:125610. https://doi.org/10.1016/j.jclepro.2020.125610.

[16] Carevic V, Ignjatovic I. Limit values of accelerated carbonation resistance to meet EC2 durability requirements. Build Mater Struct 2022;65:1–6. https://doi.org/10.5937/GRMK2201001C.

[17] Wang XH, Val D V., Zheng L, Jones MR. Influence of loading and cracks on carbonation of RC elements made of different concrete types. Constr Build Mater 2018;164:12–28. https://doi.org/10.1016/j.conbuildmat.2017.12.142.

[18] Ren Y, Huang Q, Liu XL, Tong ZJ. A model of concrete carbonation depth under the coupling effects of load and environment. Mater Res Innov 2015;19:S9-224-S9-228. https://doi.org/10.1179/1432891715Z.0000000001970.

[19] Wan X, Wittmann FH, Zhao T. Influence of mechanical load on service life of reinforced concrete structures under dominant influence of carbonation. Restor Build Monum 2011;17:103–10. https://doi.org/10.1515/rbm-2011-6437.

[20] Tang J, Wu J, Zou Z, Yue A, Mueller A. Influence of axial loading and carbonation age on the carbonation resistance of recycled aggregate concrete. Constr Build Mater 2018;173:707–17. https://doi.org/10.1016/j.conbuildmat.2018.03.269.

Aljoša Filipović[1]

NOSIVOST RAZLIČITIH TIPOVA RAVNOKRAKIH UGAONIKA OD NERĐAJUĆEG ČELIKA PRI DEJSTVU CENTRIČNOG PRITISKA

Rezime:

U važećem evropskom standardu SRPS EN 1993-1-4 nisu eksplicitno definisana pravila za proračun centrično pritisnutih elemenata ravnokrakog L poprečnog preseka od nerđajućeg čelika. Ovaj rad ukratko prikazuje rezultate opsežnog istraživanja sprovedenog na ovom tipu konstruktivnih elemenata sa ciljem definisanja preporuka za njihov proračun. Istraživanje je sprovedeno na Univerzitetu u Beogradu na Građevinskom fakultetu i publikovano u doktorskoj disertaciji „Nosivost različitih tipova ravnokrakih ugaonika od nerđajućeg čelika pri dejstvu centričnog pritiska". Analizirana su tri tipa čeličnih proizvoda, vrućevaljane, laserski zavarene i hladnooblikovane elemente i dve legure nerđajućeg čelika, austenitna i niskolegirana dupleks legura. Na osnovu sistematičnog eksperimentalnog istraživanja i detaljne numeričke analize preporučene su krive izvijanja za kontrolu stabilnosti na fleksiono i fleksiono-torziono izvijanje u skladu sa evropskim proračunskim procedurama.

Ključne reči: Nerđajući čelik, Ugaonik, Fleksiono izvijanje, Torziono-fleksiono izvijanje

RESISTANCE OF DIFFERENT TYPES OF STAINLESS STEEL EQUAL ANGLES UNDER AXIAL COMPRESSION

Summary:

The current European standard SRPS EN 1993-1-4 does not explicitly define the rules for the the design of stainless steel axially compressed equal angle columns. This paper briefly presents the results of extensive research conducted on this type of structural elements with the aim of defining recommendations for their design. The research was carried out at University of Belgrade, Faculty of Civil Engineering and published in PhD thesis "Resistance of different types of stainless steel equal angles under axial compression". Three types of steel products (hot-rolled, laser-welded and cold-formed) and two stainless steel alloys (austenitic and low alloy duplex steel) were analysed. Based on systematic experimental research and detailed numerical analysis, buckling curves were recommended for stability control in flexural and flexural-torsional buckling in accordance with European design procedures.

Key words: Stainless steel, Angle, Flexural buckling, Torsional-flexural buckling

---

[1] *Assistant professor, PhD, University of Belgrade, Faculty of Civil Engineering, afilipovic@grf.bg.ac.rs*

1. INTRODUCTION

In the last decades technological progress has led to wider application of stainless steel in modern structural engineering. Structural behaviour of this material differs significantly from that of carbon steels. There are many benefits of stainless steel which make it desirable for use in offshore platforms, industrial facilities in aggressive environments and bridge structures. Most important properties that make this material superior to carbon steel are: attractive surface appearance that does not require protective coatings, high corrosion resistance, significant plastification capacity, pronounced ductility and high values of yield and tensile strength. Also, stainless steel belongs to a group of clean materials and it is often used for load-bearing structures of tanks and silos for food, liquids and medical remedies storage. Like any structural material, its application is the construction industry is dictated by the technical design regulations. Continuous research of stainless steel elements behaviour is of outmost importance for development of new and improvement of the existing design regulations for stainless steel structures.

Axially loaded elements of trusses, bracings and telecommunication towers are very often made of steel angles. However, existing international standards for the design of stainless steel structures do not provide explicit rules for axially compressed angles, due to insufficient number of relevant studies. Comprehensive research is necessary in order to determine accurate behaviour of stainless steel angles in terms of ultimate bearing capacity and fracture modes.

This paper presents a scientific research on axially compressed pinned angle columns performed at University of Belgrade, Faculty of Civil Engineering. Experimental and numerical analysis were performed to obtain relevant and reliable data that will define guidelines and rules for the design of axially compressed angle columns, considering differences caused by production methods. This research included cold-formed, hot-rolled and laser welded angles in order to determine dependence of initial structural imperfections from production technology. Two stainless steel alloys, low alloy duplex steel EN 1.4162 and austenitic stainless steel EN 1.4301 were considered. The experimental program consisted of determining mechanical properties, bearing capacity, initial geometric imperfections, values and distribution of residual stresses and global forms of instability and flexural and flexural-torsional buckling capacity.

Numerical models based on finite element method were developed in software package Abaqus [1] and calibrated and validated. Developed models were calibrated and validated through comparison with the experimental results. Extensive parametric numerical studies of effects of global slenderness and cross-sectional slenderness on the response of elements in a state of ultimate bearing capacity were performed. Based on these results a comprehensive and reliable database was formed which enabled (1) verification of international standardized methods for the design of axially compressed stainless steel elements and (2) basis for mathematical interpretation of the elements load-bearing capacity and defining appropriate recommendations for their design in accordance with the implemented procedures of European standards for steel load-bearing structures. Furthermore, based on this research development of new buckling curves for each type of angles – cold-formed, hot-rolled and laser-welded for lean-duplex alloy and austenitic stainless steel alloy was made possible.

The analytical background, state of art, experimental procedures, numerical studies and used methodologies are described in detail in recently published papers [2], [3], [4], [5] and [6].

2. EXPERIMENTAL STUDY

A systematic experimental programme was performed to examine the structural behaviour of pin-ended angle columns. The experimental research consisted of a series of tensile material tests, residual stress measurements, compressive stub column tests and global buckling tests. All the tests were performed on hot-rolled and laser-welded equal-angle angles with nominal section dimensions $60 \times 60 \times 6$ mm and $100 \times 100 \times 10$ mm produced from austenitic stainless steel grade EN 1.4301 and press-braked angles from high strength lean-duplex stainless steel grade EN 1.4162 with nominal section dimensions $80 \times 80 \times 4$ mm. All the specimens had a designation AAA $b \times b \times t - L - X$ where the first letters "AAA" indicate acronym of angle hot-rolled (AHR), laser-welded (ALW) or cold-formed (ACF) section, "b" and "t" respectively represent leg width and leg thickness, "L" is the length of the specimens and "X" is a sequential number from 1 to 4, which relates to the repeated specimens within one tested group.

2.1 MATERIAL TESTS

In order to determine material properties of the two considered stainless steel alloys, tensile coupon tests were carried out. The hot-rolled and laser-welded specimens were made of austenitic stainless steel grade EN 1.4301 (X5CrNi18-10), while the cold-formed specimens were press-braked from flat strips of lean-duplex stainless steel EN 1.4162 (X2CrMnNiN21-5-1).

Three flat coupons were cut from both legs of hot-rolled and laser-welded specimens in the longitudinal direction. The material tests on cold-formed angle specimens included two flat coupons longitudinally cut from the legs and two corner coupons used within the boundary of the internal radius of the cross-section's corner region. All coupons were cut by a water jet cutter to decrease heating of the material during preparation. The coupons were tested in accordance with EN ISO 6892-1 [7]. The obtained engineering stress–strain curves for all three types of angle products are provided in Figure 1.
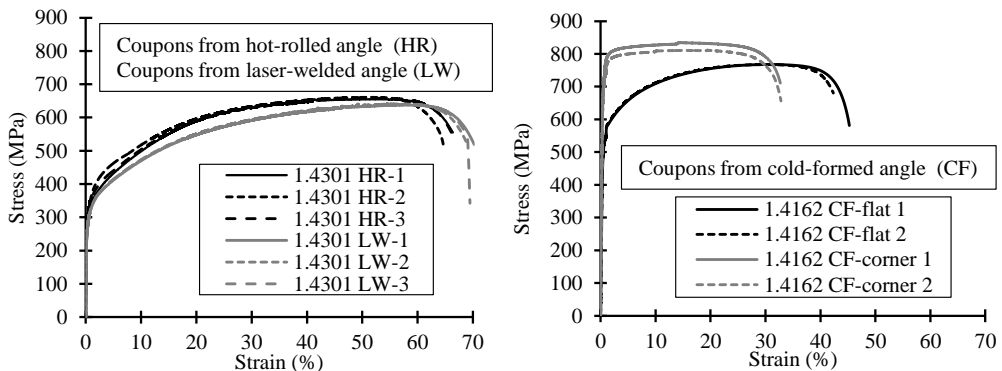
Figure 1 - Engineering stress-strain curves [8]

The measured yield strengths of austenitic stainless steel for hot-rolled and laser-welded angles exceeded the nominal value for stainless steel sections given in EN 1993-1-4 [9] by 52% and 30%, respectively. In case of duplex stainless steel used for cold-formed angles this margin is lower, up to 7% for flat coupons. The enhanced yield strength of the corner regions is approximately 38% higher in comparison with the strength of flat materials.

2.2 MEASUREMENT OF GEOMETRIC IMPERFECTIONS

The very important aspect of the research included accurate determination of specimens' geometry and initial imperfections. A multiplanar laser tracker system was employed for these measurements. To quantify imperfections a commercial laser tracker, the Leica Absolute Tracker AT960 (Hexagon Manufacturing Intelligence, UK) with a spherically mounted retroreflector, was used (see Figure 2a). Geometric data for full field of a target specimen was demonstrated as a point-grid by measuring the outer surface of the specimen at multiplanes of view and recording the individual set of measurements into the same final global coordinate system. The measured segments were entered in the global coordinate system and then coloured based on deviation from nominal specimen geometry (see Figure 2b).

| a) Laser tracker setup with installed specimen | b) 3D reconstructed model of specimen ALW $100 \times 100 \times 10 - 1500 - 3$ |
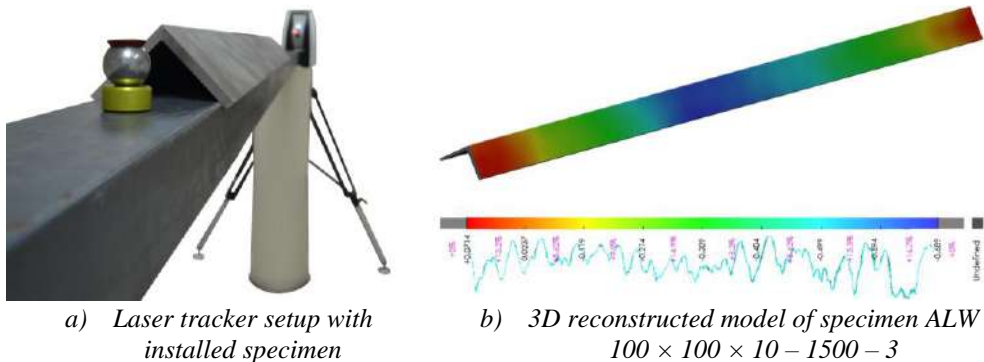
Figure 2 - Measurement of geometric imperfections [5]

Local imperfections related to cross-section distortion and overall imperfections related to bow, camber and twist were identified from the measurement point-grids. All amplitudes of initial imperfections of the specimens were considerably lower than the maximum fabrication tolerances permitted for steel profiles.

2.3 MEASUREMENT OF RESIDUAL STRESS

Equally important measurement for this research was determination of residual stresses. Using the sectioning method at room temperature, the longitudinal residual stress patterns in both hot-rolled and laser-welded stainless steel equal angles with nominal dimensions 100 x 10 mm (austenitic grade EN 1.4301) were measured. The sectioning method consists of abrasive water jet cutting that utilizes a high velocity stream of abrasive particles suspended in a stream of high-pressure water. The test area was at a distance of 3 times the leg width from the specimen ends so as to reduce end effects. Both outer and inner surfaces of legs of each angle specimen were equipped with 40 waterproof strain gauges in total. The strain gauges were attached in pairs on the opposite leg sides except in the angle heel area. The specimens were clamped, and cut transversely in two pieces after which most of the residual stresses were relieved. Afterwards, the subsequent 40 mm long longitudinal cuts were made to relieve the remaining stresses (see Figure 3). To account for any temperature changes, a temperature reference bar was used. Strain measurements were recorded during the entire cutting procedure and approximately 30 min after the cutting was finished. The residual stresses were calculated by multiplying the released strains with modulus of elasticity.
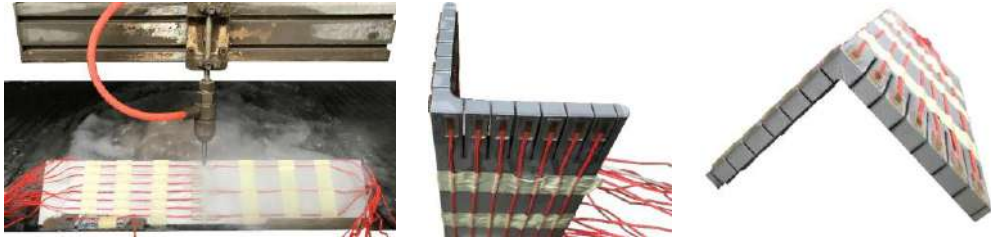
Figure 3 - Measurement of residual stress - sectioning method

Distribution of normalized residual stresses for hot-rolled and laser-welded stainless steel specimens, normalised by the material yield strength, are presented in Figure 4.
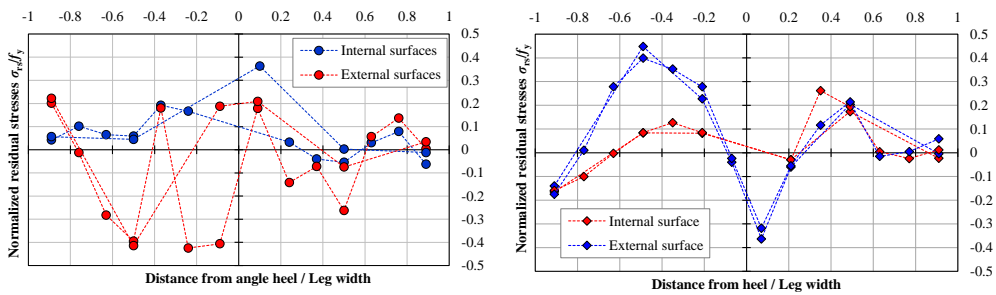
a) *Hot-rolled specimen* b) *Laser-welded specimen*

Figure 4 - Distribution of normalized residual stresses along the angle leg width

2.4 STUB COLUMN TEST

The stub column tests on three specimens of each size of angle products (hot-rolled, laser-welded and cold-formed were performed in accordance with clause A.3.2.1, EN 1993-1-3 [10] to assess their cross-section resistance.
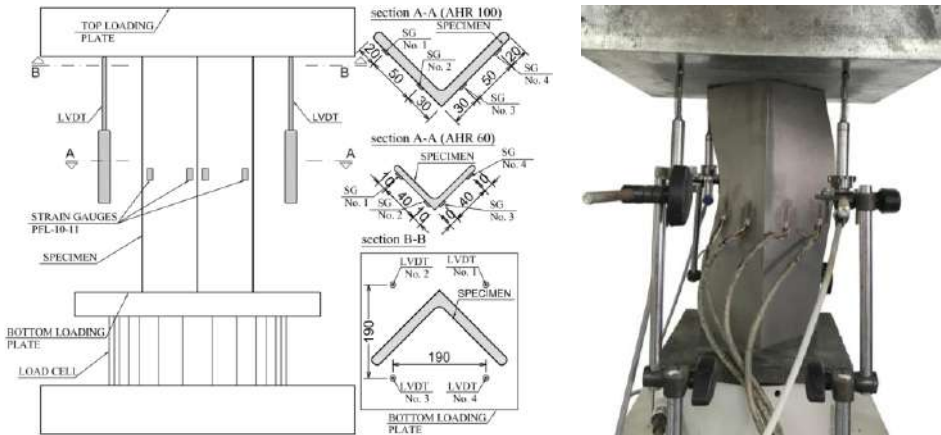
a) *Instrumentation configurations* b) *Test setup*

Figure 5 - Test setup for stub column specimens [4]

The end plates of the testing machine were positioned flat and parallel. Longitudinal displacement transducers (LVDTs) were used to measure end shortening of the specimens and four linear electrical strain gauges (SGs) were used to measure strains at mid-height. Figure 5 depicts the experimental setup and failure mode of hot-rolled specimen.

The failure mode of hot-rolled and laser-welded angle specimens was inelastic local buckling of the legs, while cold-formed angles had an elastic local buckling response at the ultimate limit state. For all specimens, buckling was localised in the middle and characterised by the torsion deformations of angle legs.

2.5 GLOBAL BUCKLING TESTS

Experimental research in order to determine the compressive response of the slender pin-ended angle columns included a total of 48 specimens. The specimens were divided into 12 series varying the type of steel product, cross-sections' dimensions and specimens' lengths. Each series each included four repeated tests. The test setup and mounted instrumentations are all illustrated in Figure 6.
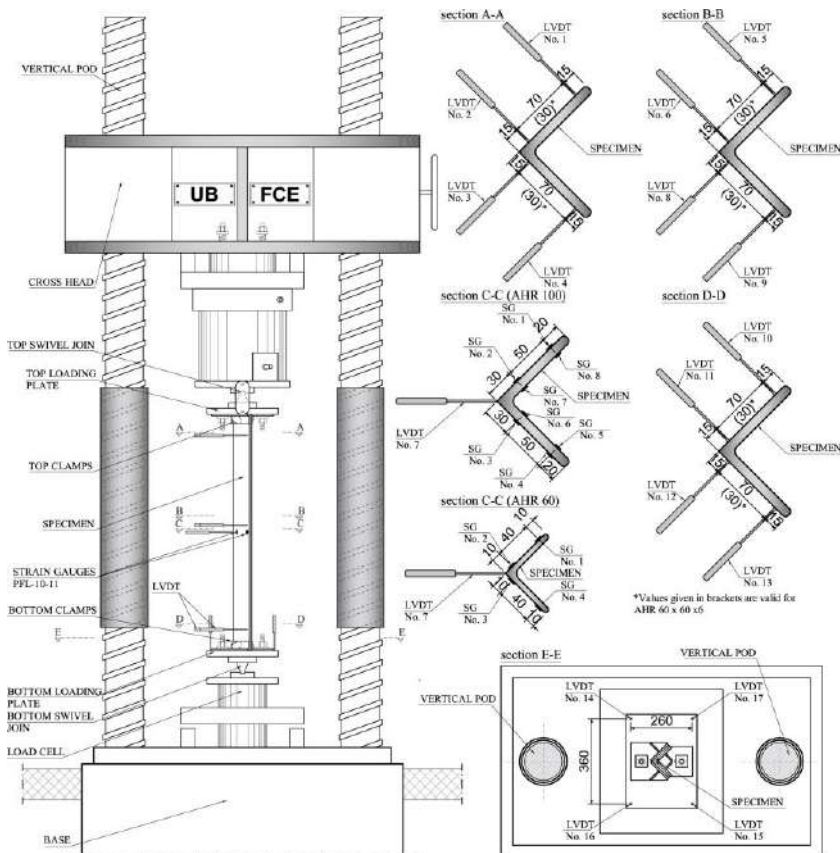
Figure 6 - Test setup for and instrumentation configuration for global buckling tests [4]

The specimens were tested under concentric compression loading using a hydraulic testing machine with a capacity of 5000 kN. The tests were performed monotonically using displacement control to the maximum load capacity and continuing up to approximately 70% of the maximum load before stopping the test. Loading rate did not exceed 0.01 mm/s.

The pin-ended bearings allowed rotations about the minor axis, while restraining major axis rotations as well as twist rotations. The specimens were positioned so that their minor principal axis coincided with the axis of the support rotation, affecting the bending of the specimen about the minor axis. LVDTs were used to record flexural and torsional movements of the specimen cross-sections, the displacement in the expected buckling plane perpendicular to the minor principal axis, bottom bearing plate's rotations and displacements; SGs were used to measure axial strains and a calibrated load cell C6A Force Transducer was used to measure the applied load. Data acquisition system recorded the applied load, LVDTs and SGs readings during the tests.

The specimens failed in flexural, torsional-flexural, and coupled flexural/torsional-flexural modes, depending on the overall slenderness ratios, width-to-thickness leg ratios and initial eccentricity conditions. Typical deformed shapes of selected specimens after buckling are shown in Figures 7–9.
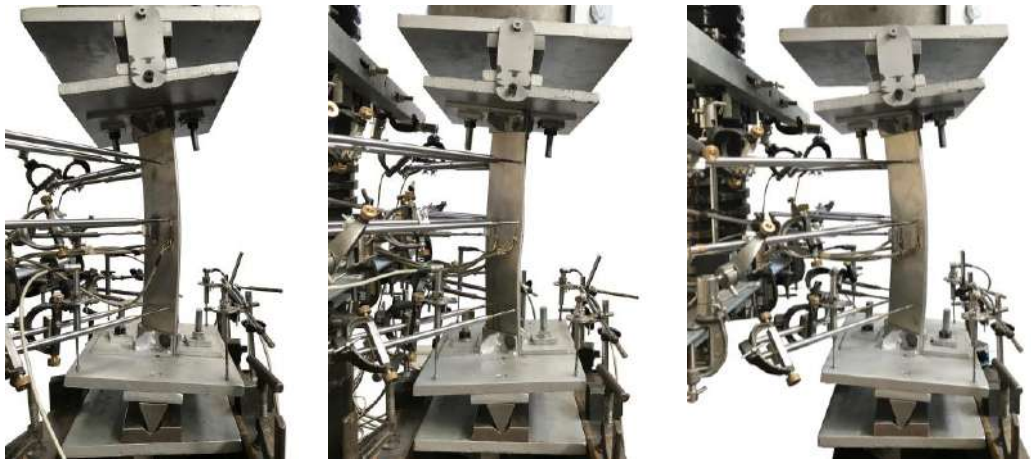
AHR 100 × 100 × 10 – 500 – 2   AHR 100 × 100 × 10 – 500 – 3   ALW 100 × 100 × 10 – 500 – 1

Figure 7 - Typical failure modes of short length specimens
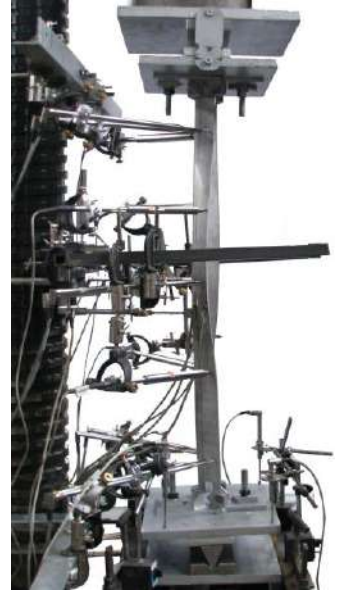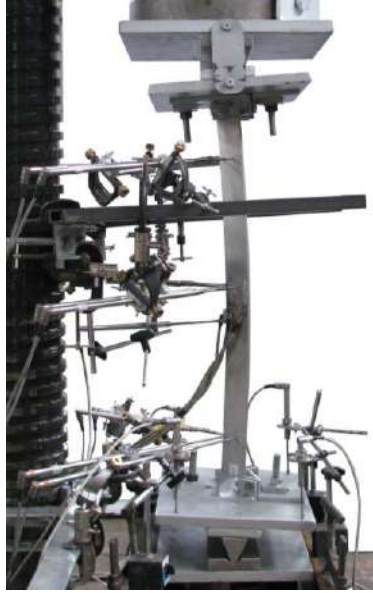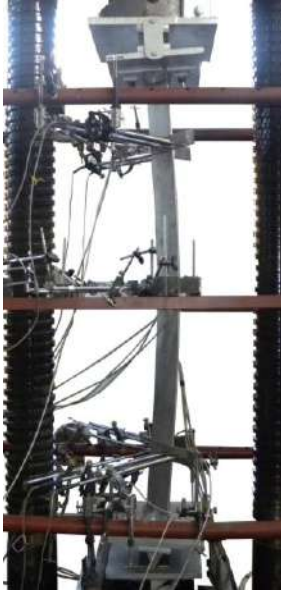
AHR 100 × 100 × 10 – 1500 – 2   *ALW 60 × 60 × 6 – 800 – 3*   *ACF 80 × 80 × 4 – 1000 – 3*

Figure 8 - Typical failure modes of intermediate length specimens

AHR 60 × 60 × 6 – 2000 – 2   *ALW 60 × 60 × 6 – 2000 – 2*   *ACF 80 × 80 × 4 – 2000 – 4*

Figure 9 - Typical failure modes of long length specimens

54

3. FINITE ELEMENT MODELLING AND PARAMETRIC STUDY

Finite element based software package Abaqus [1] was employed for the numerical simulations of the experiments performed on equal angle columns.

(a) FTB mode ACF 80 × 80 × 4 – 1000

(b) Load vs. lateral deflection

(c) Load vs. axial strains
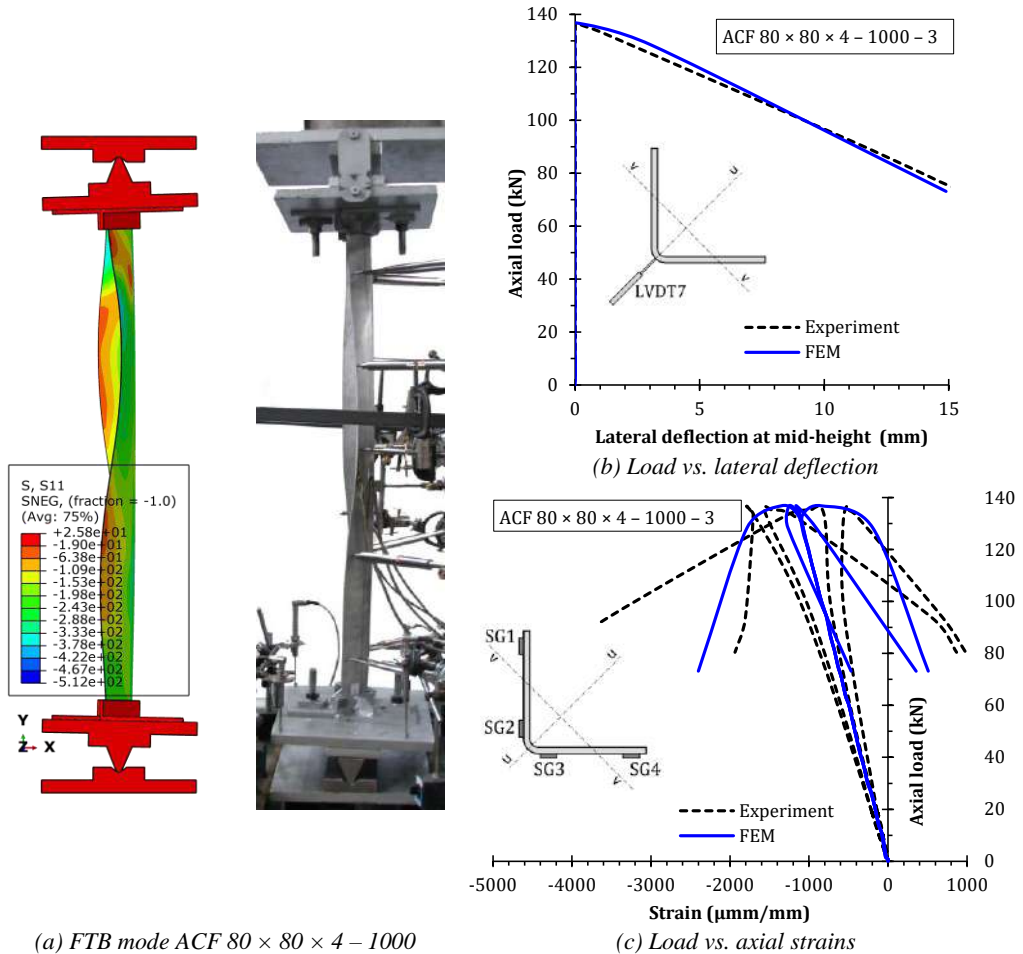
Figure 10 - FE model and experimental buckling mode of intermediate length specimens [3]

The geometrically and materially non-linear analysis (GMNIA) was developed as quasi-static with the dynamic explicit solver and the variable non-uniform mass scaling technique. The S4R shell elements were used for modelling of cold-formed columns and the C3D8R solid elements were adopted to model hot-rolled and laser-welded columns. To accurately simulate the pin-ended supporting conditions in global buckling tests, the hardened steel knife-edge devices attached to steel loading plates, together with top and bottom adjustable clamps were additionally modelled using four solid elements C3D8R. To model material properties of steel end adjustable clamps (S275JR) and the hardened steel knife-edges (S355N), a linear elastic–perfectly plastic material model with a nominal plateau slope was used. Material properties of angles flat legs and corner were imported from the measured stress–strain curves obtained via

55

flat and corner tensile coupon tests. The initial geometric imperfections were explicitly modelled using the lowest local (twist imperfection ─ local/torsional mode) and global (bow imperfection about the minor-principal axis) buckling modes obtained via Linear Buckling Analysis (LBA) performed on equivalent FE models with the same mesh. The imperfection amplitudes matched the measured ones. The 3-point linear model, based on measurements made on hot-rolled and laser-welded equal-leg angle columns was used to define distributions and magnitudes of residual stresses in the FE models in this study.

The qualitative comparisons of the FE model and experimental buckling mode of intermediate length specimens are presented in Figure 10.

Once the developed FE models were verified through the comparison with the experimental results, they were employed to perform an extensive parametric study. The aim of this study was to thoroughly examine the structural responses of cold-formed, hot-rolled and laser-welded equal angle columns. The wide range of columns' global slenderness was considered in the study to investigate LB, major-axis FTB and minor-axis FB resistances. Figure 11 presents a comparison between the results of the FE parametric study and those obtained using EN 1993-1-4 [9] and AISC 27 [11] for minor-axis FB of hot-rolled angle columns, while Figure 12 presents the comparison of the results of the FE parametric study and those obtained using EN 1993-1-4 [9] for FTB of cold-formed angle column.
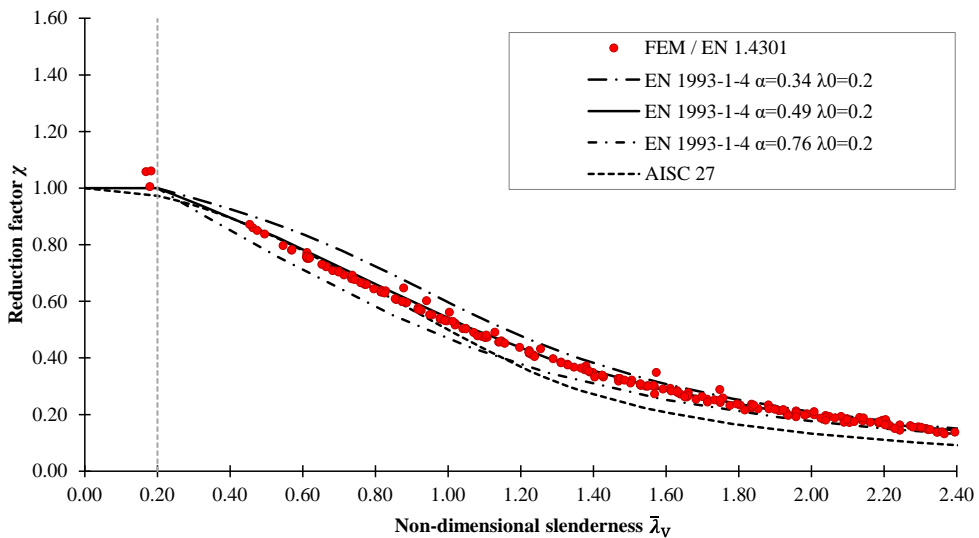
Figure 11 - Comparison of normalised FE data against those obtained using EN 1993 - 1 - 4 and AISC 27 for minor-axis FB of hot-rolled angle columns
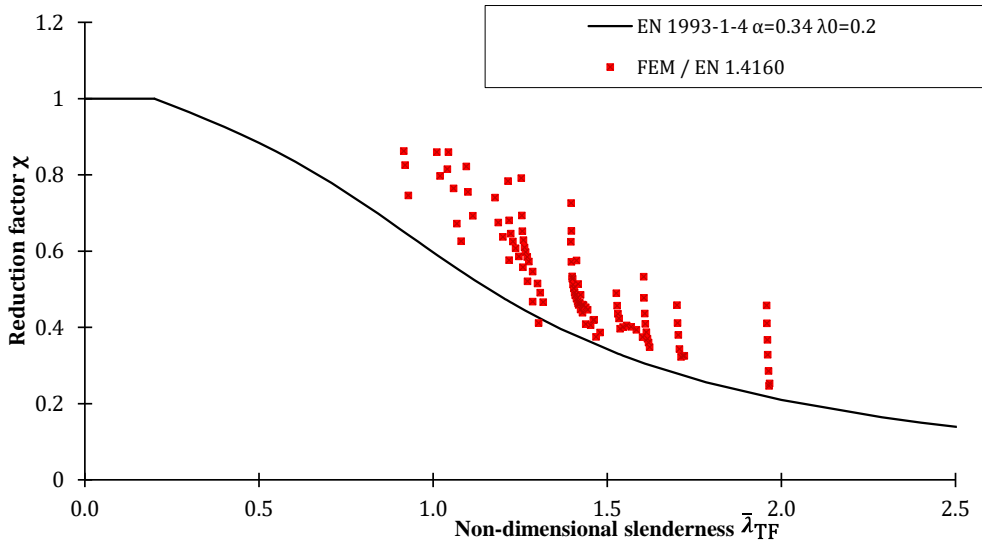
Figure 12 - Comparison of normalised FE data against those obtained using EN 1993 - 1 - 4 for minor-axis FTB of cold-formed angle columns

4. CONCLUSIONS

A comprehensive investigation of the structural behaviour of equal angle columns under pure compression, including experiments (1) and qualitative and quantitative numerical studies (2), was carried out with the aim of acquiring a valuable database that enabled the development of an accurate and reliable design method. The following conclusions were drawn from this investigation:

- For minor-axis flexural buckling, the buckling curve c ($\alpha = 0.49$) in conjunction with the non-dimensional limiting slenderness $\bar{\lambda}_0 = 0.2$ may be used for duplex grades for cold-formed equal-leg angle for all cross-section classes.
- The use of buckling curve b ($\alpha = 0.34$) in conjunction with $\bar{\lambda}_0 = 0.2$ to predict flexural-torsional buckling for duplex grades for cold-formed equal-leg angle leads to safe but quite conservative results characterized by significantly higher scatter.
- For minor-axis flexural buckling, the buckling curve c ($\alpha = 0.49$) in conjunction with the non-dimensional limiting slenderness $\bar{\lambda}_0 = 0.2$ may be safely used for the design of hot-rolled and laser-welded austenitic stainless steel columns both for non-slender and slender cross-sections.
- The use of buckling curve b ($\alpha = 0.34$) in conjunction with $\bar{\lambda}_0 = 0.2$ to predict flexural-torsional buckling for the design of hot-rolled and laser-welded austenitic stainless steel columns leads to safe but quite conservative results characterized by significantly higher scatter.

REFERENCES

[1] ABAQUS User Manual. Version 6.12. Providence, RI, USA: DS SIMULIA Corp; 2012.

[2] Dobrić J, Filipović A, Marković Z, Baddoo N.: Structural response to axial testing of cold-formed stainless steel angle columns, Thin-Walled Structures, 156, 2020, https://doi.org/10.1016/j.tws.2020.106986.

[3] Dobrić J, Filipović A, Baddoo N, Marković Z, Buđevac D.: Design procedures for cold-formed stainless steel equal-leg angle columns, Thin-Walled Structures, 107210, 2020, https://doi.org/10.1016/j.tws.2020.107210.

[4] Filipović A, Dobrić J, Baddoo N, Može P.: Experimental response of hot-rolled stainless steel angle columns, Thin-Walled Structures, 163, 2021, https://doi.org/10.1016/j.tws.2021.107659

[5] Filipović A, Dobrić J, Buđevac D, Fric N, Baddoo N.: Experimental study of laser-welded stainless steel angle columns, Thin-Walled Structures, 164, 2021, https://doi.org/10.1016/j.tws.2021.107777.

[6] Dobrić J, Filipović A, Baddoo N, Buđevac D, Rossi B.: Design criteria for pin-ended hot-rolled and laser-welded stainless steel equal-leg angle columns, Thin-Walled Structures, 167, 2021, https://doi.org/10.1016/j.tws.2021.108175.

[7] EN ISO 6892-1. Metallic materials – Tensile testing. Part 1: Method of test at room temperature. Brussels, Belgium, CEN 2009.

[8] Filipović A, Dobrić J, Marković Z, Spremić M, Fric N, Baddoo N.:Experimental investigation of compressed stainless steel angle columns, *Proc. Int. Colloq. Stab. Ductility Steel Struct. 2019*, pp. 409–416, 2019.

[9] Eurocode 3: Design of steel structures – part 1-4: General rules – supplementary rules for stainless steels, including amendment A1 (2015), EN 1993-1-4:2006+A1:2015, Brussels, Belgium, CEN 2015.

[10] Eurocode 3: Design of steel structures – Part 1-1: General rules and rules for buildings EN 1993-1-1, Brussels, Belgium, CEN 2005

Drago Žarković[1]

P-DELTA ANALIZA POMOĆU MATRIX 3D SOFTVERA ZA NELINEARNU STRUKTURALNU ANALIZU

Rezime:

U ovom radu je prikazan jedan deo tehničke pozadine programa Matrix 3D za strukturalnu, linearnu i nelinearnu analizu, a koji je softver opšte namene. Posebna pažnja u radu je posvećena implementaciji približne procedure pseudo sile za obuhvatanje uticaja drugog reda u softver. Verifikacija implementirane procedure je prikazana kroz P-Delta analize standardizovanih ramovskih konstrukcija iz literature. U radu je pokazano da je procedura pogodna i za nelinearne analize uz korišćenje vlaknastih konačnih elemenata. Takođe, konstrukcija čeličnog regalnog skladišta je modelirana uz pomoć nelinearnih zglobova i rezultati analize su upoređeni sa eksperimentalnim *pushover* testiranjem iz literature, kao i sa rezultatima dobijenim iz komercijalnog softvera SAP2000.

Ključne reči: numeričko modeliranje, P-Delta, analiza drugog reda, metoda pseudo sile

P-DELTA ANALYSIS USING MATRIX 3D NON-LINEAR STRUCTURAL ANALYSIS SOFTWARE

Summary:

In this paper, a part of the technical background of the general-purpose structural linear and non-linear analysis software Matrix 3D is presented. Special consideration is devoted to the implementation of approximate second-order procedure pseudo force in the software. Verification of the implemented procedure is demonstrated on the P-Delta analysis of the proposed benchmark frame structures from the literature. The procedure is proved to be suitable for non-linear analyses using fiber finite elements. Also, the steel storage rack structure is modelled using non-linear hinges and results are compared to the experimental pushover testing from literature, as well as with results obtained by the use of commercial software SAP2000.

Key words: numerical modelling, P-Delta, second-order analysis, pseudo force method

---

[1] Asist. Prof., University of Novi Sad, Faculty of Technical Sciences, Novi Sad, Serbia, dragozarkovic@uns.ac.rs

1.   INTRODUCTION

In structural analysis, an appropriate structural model, as well as analysis procedure, must be employed, so the objective structural response is obtained for the loading scenario. While first-order analysis, in which equilibrium is fulfilled with respect to undeformed geometry, is simple to perform, additional internal forces caused by deflection of structure are neglected. A second-order analysis, with equilibrium taken with respect to deformed geometry, is necessary for stability design. In general second-order effects may be obtained either by including it explicitly, when an iterative procedure is necessary, or they can be approximated by some means in linear analysis. It is essential to note the difference between P-"big" delta (P-Δ) effect, which is a structural effect, taking into account frame deflections, and P-"little" delta (P-δ), which is the individual member effect, within the frame.

There are several approximate procedures for including second-order effects. Two cycles iterative method [1] implies additional analysis of structure, with an updated stiffness matrix, based on the initial analysis. This approach is suitable for linear analysis only. With the pseudo lateral load method [2], fictitious forces are introduced in structure based on the relative drift between the levels. With this approach, only structural P-Δ effects are covered. A pseudo displacement approach implies a re-analysis of structure on deflected geometry, but a solution may not converge in this approach. Finally, the use of a geometric stiffness matrix for linear material analysis is a suitable general-purpose approach.

One of the approximate procedures, the pseudo lateral load method, is implemented in general-purpose structural linear and non-linear analysis software Matrix 3D. In the following chapter, a part of the theoretical background of the software is presented. Special consideration is devoted to second-order analysis within the software, so the following chapter presents verification of the procedure by comparison of results obtained with Matrix 3D with ones recognized from literature. Finally, numerical examples are presented, and results are compared to the ones obtained experimentally or by commercial software on relatively simple two-dimensional frame structures.

2.   MATRIX 3D COMPUTER PROGRAM

Matrix 3D [3–9] is general-purpose finite element method based structural analysis computer program. Linear and non-linear analysis procedures are implemented in the software, as well as modal and buckling analysis also. Modelling is enabled on three dimensional systems modelled with linear, surface or solid finite elements.

2.1. ELEMENTS AND MATERIAL MODELS

Modelling of line structures is enabled by common Euler-Bernoulli beam element, as well as fiber beam-column element. Formulation of flexibility method based fiber beam-column element is presented in detail in previous work [4,9].

Discretization of the system using surface finite elements in Matrix 3D implies the use of triangular elements with 3 nodes, in the vertices of the triangle, or 6 nodes in the vertices and midpoints of the sides of the triangle element, as explained in detail in [9]. For a material non-linear analysis computation with surface elements, layered shell element is defined in software.

Implementation of layered shell element follow the theory presented in [10,11], where the possibility for defining different material models for each separate layer is enabled.

As far as solid finite element modelling is concerned, analogously to surface triangular element types, 4-node and 10-node tetrahedron elements are defined, where for 4-node version nodes in vertices are implied and for 10-node version, apart from nodes in vertices, six nodes are defined at midpoints of sides. The former is recognized as linear in the literature, and the latter as a square tetrahedron, according to the degree of polynomials used as interpolation functions. With introducing of solid finite elements in Matrix 3D, local modelling is enabled, i.e. representation of concrete volume by tetrahedral finite elements and combined with modelling of reinforcing bars with linear elements or fiber non-linear elements, if plastification of reinforcement is expected during analysis [9].

Other than linear, surface and solid elements, modelling of nodal link element, for coupling of degrees of freedom, is also implemented in Matrix 3D. There are global link elements in the software, with the aim of coupling global displacements and/or rotations for two selected nodes in structure, and end-beam link elements (hinges), oriented according to beam local coordinate system. For both type of link elements independent definition of behaviour is provided for all six degrees of freedom. There is possibility of linear finite stiffness coupling of individual DOFs, as well as various non-linear predefined types of force-displacement and moment-rotation relations (multilinear, hysteretic, etc.).

As far as constitutive relations are concerned, apart from common set of linear elastic models, which are basically defined by Young's module of elasticity and Poisson's coefficient, a number of non-linear constitutive relations are implemented in Matrix 3D [9]. These non-linear models can be divided in following groups:

- non-linear link relations
- fiber element models
- solid/surface element models

Non-linear relations, which are applicable to link elements are basically one-on-one relations either force-displacement or moment-rotation and they can be further divided to multi-linear and hysteretic ones. Multi-linear relations do not consider hysteretic behaviour whatsoever, but multi-linear backbone response only (see "M0" in Figure 1). Implemented hysteretic models are pivot point based, which implies that loading/unloading cycles are governed by the directions (REB) defined by two pivot points (P). Since Matrix 3D is, among other, used for non-linear analyses of steel storage racks, in which pivot point behaviour is distinctive for connectors, there are two models implemented: Bernuzzi-Simoncelli model [12] and SRJ model developed by the author and the group [6]. SRJ model schematic behaviour is presented in Figure 1.

Models suitable for fiber finite elements are, similarly to this previously presented link relations, one-dimensional relations applied to single fiber of a cross section, defining stress-strain relation of that single fiber [9]. In this group there are also multi-linear and hysteretic constitutive models. While multi-linear are obviously non-hysteretic relations suitable for monotonic loading conditions, up to some extent, hysteretic relations are suitable for general loading conditions. Among a number of available one-dimensional concrete constitutive relations in literature, model proposed by author Yassin in his PhD thesis, and which is used by group of authors led by Filipou [13] is implemented in Matrix 3D.

For the steel one-dimensional stress-strain representation, the obvious choice is a bi-linear model. In that sense, the most famous among such models is implemented in Matrix 3D, the Menegotto-Pinto model [14]. This model is even more sophisticated than a classical bilinear

model with isotropic hardening since the behaviour of steel is described with, a more realistic, curved line. Other than this model, the classical bi-linear model with isotropic hardening is extended with softening, damage behaviour, in post-peak part.
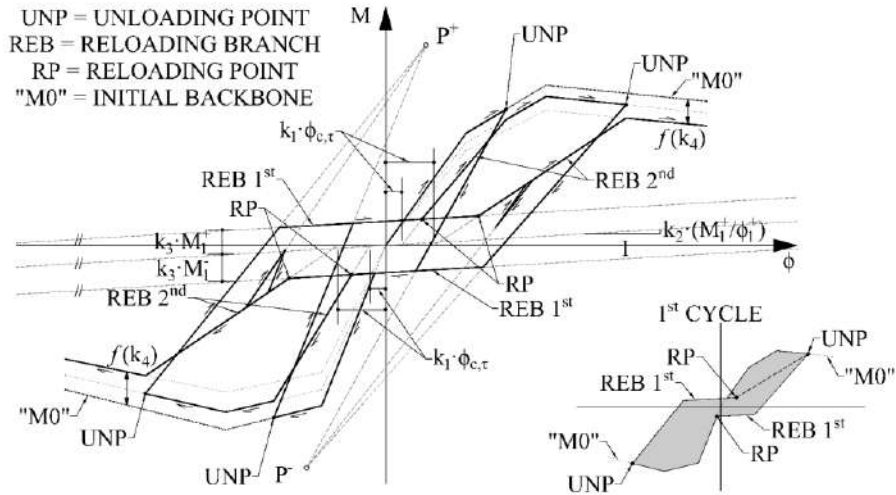
Figure 1 - SRJ pivot type model defined in [4]

For a non-linear analysis with solid elements, two types of constitutive material models are implemented based on the non-linear system solution strategy: secant or tangent-stiffness method. The one implemented in Matrix 3D and suitable for secant approach is Ottosen's concrete model [15,16]. Ottosen's concrete model implementation in Matrix 3D and its capabilities are presented in detail in [3], as well as the advantages and disadvantages of the use of secant-stiffness method. As far as constitutive models suitable with, prevailing tangent-stiffness approach, are concerned, in Matrix 3D, well-known von Mises as well as famous CDPM2 [17,18] models are implemented. Von Mises model is the obvious choice for simulation of the non-linear behaviour of steel [9].

Among a numerous concrete material models in literature, the model formulated in plasticity-damage framework is chosen and implemented in Matrix 3D, since this framework is the most promising for simulation of this type of non-linear behaviour. Non-linear behaviour of concrete is characterized by: crack formation in tension stress states, closing and reopening of existing cracks in cyclic loading, hardening in compression stress states, as well as softening in a post-peak part of the response, both dependent on triaxial stress state, drop of stiffness, plastic deformations in compression stress states, rheological aspects and other. Model of the recent date CDPM2 [17,18], which is proved to be capable for simulation of many aspects of concrete non-linear behaviour, is implemented in Matrix 3D (see Figure 2a). This model is formulated in plasticity-damage framework, and damage is described with two scalar quantities, tension and compression damage state. This exact feature is the main upgrade compared to one scalar damage CDPM1 [19] model, which is the precursor of the CDPM2 model. The difference in behaviour in cyclic loading can be observed in Figure 2b, where the two-scalar damage model advantage is obvious. Figure 2b also shows the behaviour of, maybe the most famous and widespread, CDPM [20,21] model, which is also two-scalar and its advantages in hardening behaviour during

the cyclic loading are evident from the figure. None of this, famous, mentioned models overcome the problem of inadequate modelling of closing and reopening of existing cracks in cycling loading. ECDPM [22] model, as an upgrade of CDPM (E for enhanced), emerged in the literature of the newer date, with its attempt of simulating of closing crack behaviour (see Figure 2b).
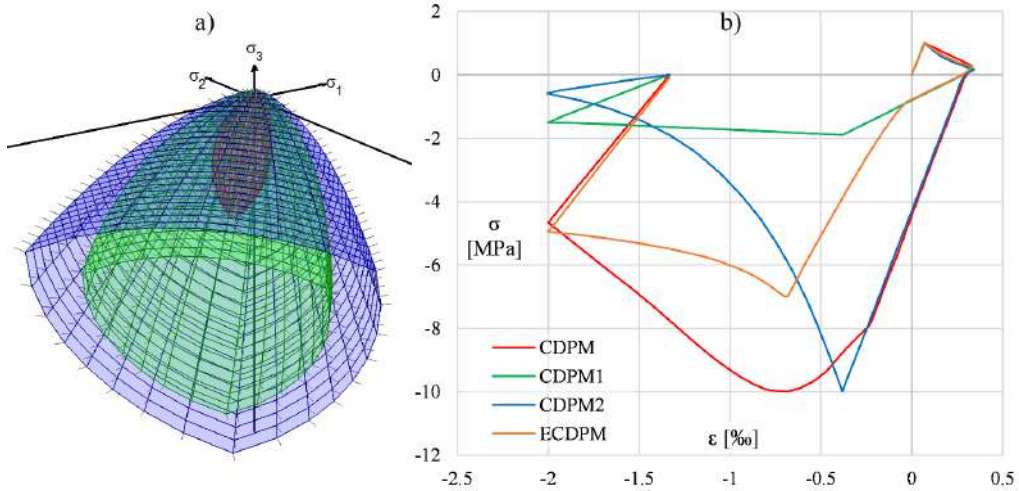
Figure 2 - CDPM2 model yield surface (a) and comparison of concrete damage-plasticity models (b)

Accordingly, a new plasticity-damage model is formulated and presented in the author's PhD thesis [8]. This new model is proved to be superior compared to those previously mentioned, especially when cyclic behaviour is concerned. Successful representation of closing and reopening of cracks is achieved by introducing a secondary yield surface in the formulation. The damage part is represented by two scalars, similar to the previous ones. This model is implemented in Matrix 3D also [9].

2.2. FE SYSTEM SOLVER

As described in earlier paper [9], solution of the finite element system is possible in linear and non-linear analysis in Matrix 3D, and there is an option for static or dynamic analysis, as well as buckling and modal analysis. The solution of the system in terms of a vector of the unknown nodal displacement $\mathbf{q}$, for a given matrix of the stiffness of the system $\mathbf{k}$, and nodal vector of external load $\mathbf{Q}$, is given by the basic equation of the FE method:

$$\mathbf{k} \cdot \mathbf{q} = \mathbf{Q} \tag{1}$$

The system solution in Matrix 3D is found using the specialized Matlab function *mldivide*, which is specially optimized for various types of problems. Afterwards, according to this displacement vector, FE stresses, strains and internal forces are calculated.

As far as non-linear analysis is concerned, the beforementioned secant- and much more common tangent-stiffness methods are implemented in Matrix 3D. Specifics about the secant-stiffness are explained in detail in [3,9]. Tangent-stiffness method implies that the solution is found incrementally for subsequent time steps [7]. Load increment is applied to the FE system, with the stiffness of the elements calculated on the basis of the current state of integration points

(IP). The result is DOF's displacement increment vector $\Delta\mathbf{q}$, rendering IP strain increment in the current step. The strain increment is then used to calculate the current IP's material state on the basis of the stress state from the previous (converged) step. The result of material state determination is either (i) pure elastic increment or (ii) increment with plastic strain with or without the damage change. The former implies the correct assumption of stiffness, i.e. the element stiffness matrix does not need to be changed. The latter implies the need for change of the element stiffness matrix and hence the system stiffness matrix. The new stress state corresponds to internal forces of elements and they are assembled to the system vector of the internal forces $\mathbf{P}$. $\mathbf{P}$ is compared to the external applied load vector $\lambda \cdot \mathbf{Q}$, where λ is load multiplier and $\mathbf{Q}$ is the total external applied load. Subtraction of $\lambda \cdot \mathbf{Q}$ from $\mathbf{P}$ results in the residual (unbalanced) force vector $\mathbf{R}$. The force-based norm ϵ_Q can be set as the measure of the magnitude of error in iterations, defined as the ratio of $\|\mathbf{R}\|$ and $\lambda \cdot \|\mathbf{Q}\|$. Suppose the defined error is larger than the desirable tolerance. In that case, Newton-Raphson (NR) iterations are continued in the current increment with vector -$\mathbf{R}$ as applied load, until the convergence or the maximum number of iterations are achieved [7]. As a tool for finding with global resistance of systems and their post-peak behaviour, the arc-length method of the spherical kind [23], is implemented in Matrix 3D.

2.3. PSEUDO LATERAL LOAD METHOD FOR SECOND-ORDER ANALYSIS

Global geometric non-linearity can be simulated by introduction of pseudo lateral loads [2]. In Matrix 3D this method is implemented by means of introduction of pair of loads on each line finite element, that act perpendicular to element reference axis. Intensity of the lateral V'' forces is equal:

$$V^{II} = N \cdot \Delta / L \tag{2}$$

where N is line element axial force, Δ is relative displacement of element ends, perpendicular to its initial direction and L is element length. Relative displacement Δ is considered in direction of both perpendicular local axes y and z, hence the pseudo forces V'' are applied in both direction, as depicted in Figure 3.
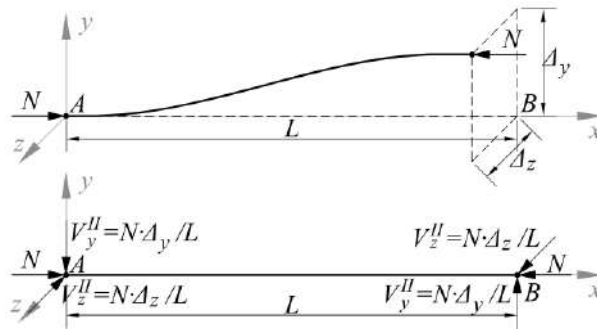
Figure 3 – Lateral pseudo forces of line element for second-order analysis

Pseudo forces V'' are applied in the first iteration of the load increment of Newton-Raphson procedure in Matrix 3D software. Values of element axial force N and relative displacement Δ from the first iteration are utilized for the initial calculation of pseudo forces. Pseudo lateral forces are than applied to the system altogether with the residual forces $\mathbf{R}$ of the increment.

Pseudo forces are recalculated in every iteration, since relative displacements change, and procedure usually converges in 2 or 3 iterations.

3. NUMERICAL EXAMPLES OF P-DELTA ANALYSIS

For the purpose of the verification of the implemented geometrical non-linear second-order analysis (GNA) procedure, several benchmark frames from literature are modelled and analysed in the following section. In next sections possibilities of modelling the material nonlinear behaviour with implemented P-Delta procedure, with imperfections included (GMNIA) is investigated. One of the European calibration frames form literature is modelled using fiber finite elements, and in the following chapter steel storage rack structure is modelled with non-linear hinges.

3.1. MATERIAL LINEAR ANALYSIS OF BENCHMARK FRAMES

Verification of the implemented pseudo force procedure, for the analysis of linear material behaviour of structures (GNA) is executed on several benchmark frames available in the literature [24,25] for this purpose. From the available set of total 22 frames, frames 1, 2, 4 and 11 are chosen in this study. Geometry and loading of frames 1, 2 and 4 is depicted in Figure 4 and frame 11 is shown in Figure 5a. For all frames initial imperfections are included with global sway of H/500 rightwards, which makes this analyses linear with imperfection (GNIA). Modulus of elasticity for all frames is adopted as 159.958 GPa as 80% of nominal value.
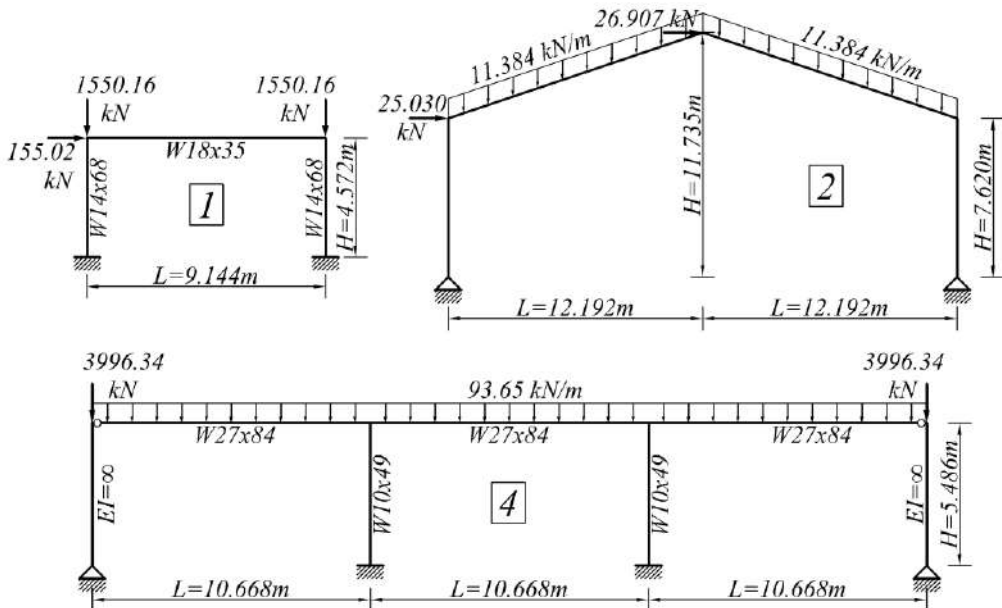
Figure 4 – Geometry and loading of frames 1, 2 and 4 [24,25]

GNIA results are shown in Figure 5b, as well as linear analysis (LA) results for structures. The force-displacement diagram is compared to the one available in the literature [24,25], and it

is labelled with *LIT*. The result obtained in the present study, by the procedure in Matrix 3D, are labelled as *PS*. P-Δ diagram is available only for frame 11, and results for other structures are given tabular. Generally, results are almost perfectly comparable, and some higher discrepancies seem to be present for a higher levels of non-linearity, i.e. higher GNIA to LA displacement ratio.

		LA Δ [mm]		GNIA Δ [mm]		
Struc.	Node	LIT	PS	LIT	PS	Er. [%]
F1	C1L1	26.54	26.55	30.25	30.18	-0.2
	C2L1	25.88	25.88	29.56	29.52	-0.1
F2	C1L1	136.89	135.69	179.59	174.56	-2.8
	C2L1	263.54	265.08	307.54	308.83	0.4
	C0L1	200.33	200.50	244.36	241.82	-1.0
F4	C1L1	8.86	8.86	53.98	49.45	-8.4
	C2L1	8.82	8.82	53.44	49.25	-7.8
	C3L1	8.88	8.88	53.49	49.31	-7.8
	C4L1	8.92	8.92	53.31	49.51	-7.1
F11	C2L1	119.01	119.27	154.37	154.45	0.1
	C2L2	136.17	136.32	174.48	174.35	-0.1
	C2L3	145.13	145.20	184.40	184.08	-0.2
	C2L4	173.09	173.26	214.11	213.68	-0.2

Figure 5 – Geometry and loading of frame 11 [24,25] (a), GNIA results for frames 1, 2, 4 and 11 (b)

3.2. FIBER ELEMENT NON-LINEAR ANALYSIS

Performance of the implemented pseudo force procedure is tested in non-linear material analysis with imperfections included (GMNIA). Geometry, loading and mechanical characteristics of the chosen six-storey two-bay frame are adopted from the European calibration frames for second-order analysis [26]. Initial imperfections are included with global sway of H/450 rightwards and material model is simplified to bilinear, without hardening. Residual stress in HEB and IPE sections are adopted as presented in [26].

In Figure 6a, the force-displacement diagram of the model is presented for 6th and 4th levels of structure. Solid lines are from this study, using pseudo force procedure in Matrix 3D, and dashed lines correspond to available results from literature (Toma-Chen) [26]. Initial stiffness seems to be an almost perfect match to literature results. Likewise, the plastification of sections and non-linear part of the response is acceptably comparable to the literature response. Final displacements are lower, within of 10% margin, for corresponding force.

It is interesting to notice that, aside from beam ends, plastification is also occurring in the mid-spans of upper-level beams. Initial simulation tries, without element subdivision, resulted in stiffer results, with low values of final displacements, since plastification in mid-spans is not captured for beams with a uniformly distributed load. In Figure 6b, it can be noticed that practically complete section IPE240 on the top level is plasticized on mid-span.
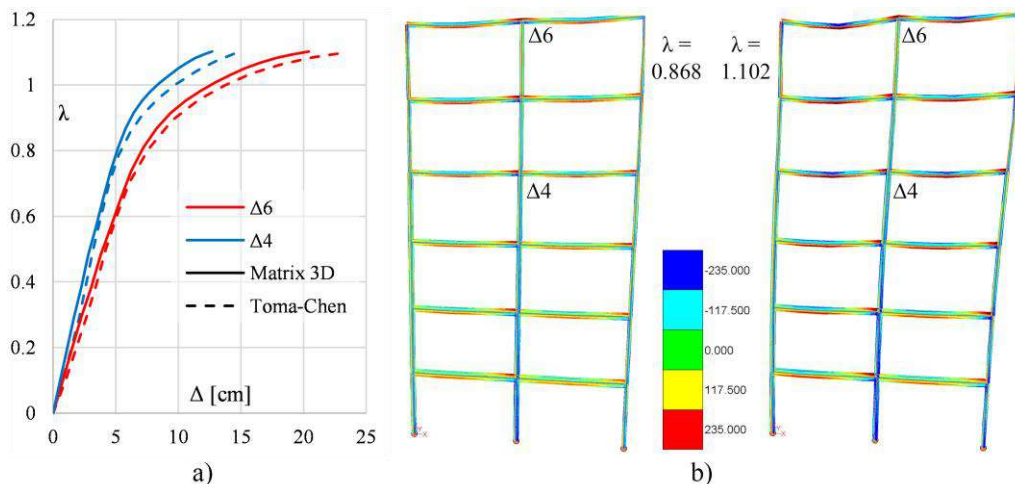
Figure 6 – P-Δ diagram of non-linear fiber frame structure (a), fiber stress states in analysis (b)

3.3. NON-LINEAR HINGE STRUCTURE ANALYSIS

Storage rack structures are one of the typical structures sensitive to P-Delta effects, since the live load they carry is high compared to dead load, cross sections are slender and structure is often considerable high. The beam-to-upright connector, as well as upright base connector are with finite stiffness, and exhibit particular non-linear behaviour, so modelling of this structure is logical to be executed using non-linear hinges [6].

Details of the storage rack structure are taken from SEISRACKS project report [27], where experimental pushover analysis is performed on the structure, and results of the beam-to-upright connector and upright base connector testing are available also. Structure is the three-story two-bay frame, with story height 2.0 m and beam spans of 1.8 m. Details of the section for upright 100/20b and beam TG 130x45x1.5 mm are presented in the report [27] and live load is uniformly distributed 4.72 kN/m. Pushover lateral load is applied in triangular distribution.

The structure is modelled in Matrix 3D and in commercial SAP2000 software. Hinge non-linear behaviour is modelled by the SRJ model from [6], which is implemented in Matrix 3D, and in SAP2000 available Pivot model is used. Pushover diagrams are presented in Figure 7a. Experimental results from the literature are depicted in blue colour, numerical results from commercial software SAP2000 in green colour and results from Matrix 3D in red colour. The importance of consideration of P-Delta effects is evident from the diagram if linear analyses *LA* (dashed line) are compared to geometrical non-linear ones (*P-Δ*, *LD*). Frame resistance is 37 % lower when considering P-Delta effects and acceptable match to experimental results (5.2 %). Numerical results of Matrix 3D and SAP2000 are practically identical in the relevant part of the response. It remains unknown why the P-Delta option in SAP2000 yields identical results as linear analysis, so Matrix 3D results are compared to the large displacement (*LD*) option in SAP2000. Calculation process *CP* of arc-length procedure is labelled in figure.

Moment-rotation diagrams of non-linear hinges are shown in Figure 7b. Middle upright baseplate response is depicted in green colour. The first level left beam-to-upright connector in

red and right one in blue colour. It can be concluded that the baseplate connection has failed the first ($CP = 0.16$), followed by the first level left beam-to-upright connectors and finally the right ones. At $CP = 0.45$ middle upright, below the first level beams, has failed. Non-linear hinges are modelled in all three uprights in this zone because the soft-floor failure is anticipated for the structure.
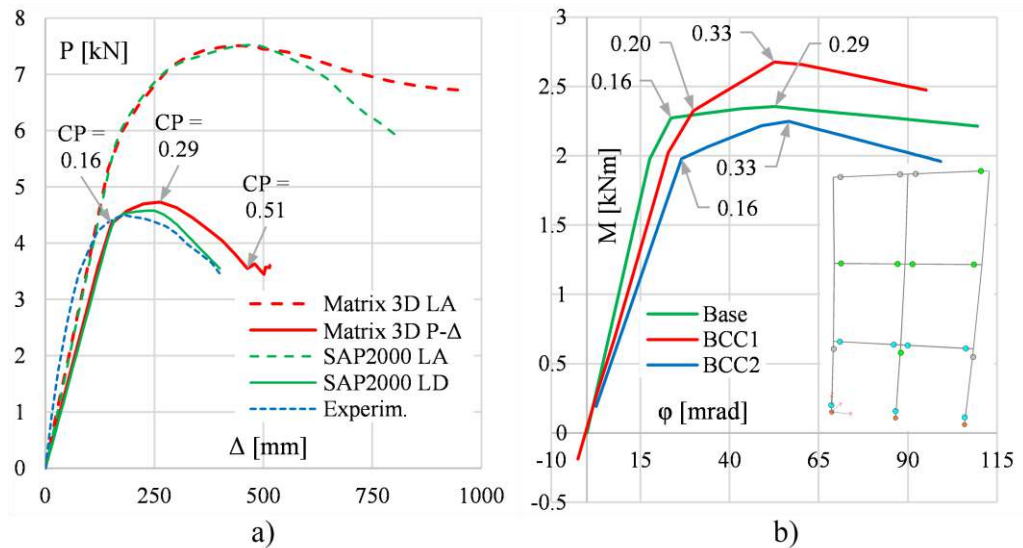
Figure 7 – P-Δ diagram of storage rack structure (a), hinge state of storage rack structure (b)

4. CONSLUSION

In this paper, a part of the technical background of the general-purpose linear and non-linear structural analysis software Matrix 3D is presented. Special consideration in the paper is devoted to the geometrical non-linear analysis, so specifics of the implemented approximate pseudo lateral force method procedure are presented. Several benchmark frames for linear material analysis are modelled, and obtained results are proved to be completely comparable to the results from the literature. Performance of the procedure in the analysis with material non-linear fiber elements is tested on a frame structure, which is also an accepted benchmark frame from literature. Finally, the steel storage rack structure, as especially sensitive to P-Delta effects, is modelled by non-linear hinges and results are compared to available experimental ones, as well as with results in large displacement analysis using commercial software SAP2000. The lateral pseudo force method for accounting of P-Delta effects in structures is proved to be an adequate choice of procedure for linear and non-linear analysis cases.

REFERENCES

[1]   W.F. Chen, E.M. Lui, Stability Desing of Steel Frames, CRC Press, Inc., Boca Raton, 1991.

[2]   E.M. Lui, Practical P-delta analysis method for type FR and PR frames, Eng. J. 25 (1988) 85–98.

[3]   D. Žarković, Z. Brujić, Đ. Lađinović, Application of Ottosen's constitutive model to flexural failure of RC beams, in: E-GTZ Zb. Rad. / Proceedings, Broj 3, 2016: pp. 261–268.

[4]   Đ. Jovanović, D. Žarković, Z. Brujić, Đ. Lađinović, Fiber beam-column element implementation in academic cad software Matrix 3D, Build. Mater. Struct. 60 (2017) 57–77. doi:10.5937/grmk1702057J.

[5]   D. Žarković, Đ. Jovanović, Z. Brujić, Đ. Lađinović, CDPM2 Model betona u formulaciji 3D konačnih elemenata pri cikličnom opterećenju, in: 15. Kongr. Društva Građevinskih Konstr. – DGKS, Zlatibor, 2018: pp. 349–358.

[6]   Jovanović, D. Žarković, V. Vukobratović, Z. Brujić, Hysteresis model for beam-to-column connections of steel storage racks, Thin-Walled Struct. 142 (2019). doi:10.1016/j.tws.2019.04.056.

[7]   D. Žarković, Đ. Jovanović, V. Vukobratović, Z. Brujić, Convergence improvement in computation of strain-softening solids by the arc-length method, Finite Elem. Anal. Des. 164 (2019) 55–68. doi:10.1016/j.finel.2019.06.005.

[8]   D. Žarković, Novi konstitutivni model betona formulisan prema nespregnutoj kombinaciji teorija plastičnosti – mehanika oštećenja, Fakultet tehničkih nauka, Univerzitet u Novom Sadu, 2021.

[9]   D. Žarković, Matrix 3D software for linear and non-linear structural analysis and design, in: Contemp. Civ. Eng. Pract. 2022, 2022: pp. 141–152.

[10]   C.W.S. To, B. Wang, Hybrid strain-based three-node flat triangular laminated composite shell elements for vibration analysis, J. Sound Vib. 211 (1998) 277–291. doi:10.1006/jsvi.1997.1373.

[11]   Y.X. Zhang, M.A. Bradford, R.I. Gilbert, A new triangular layered plate element for the non-linear analysis of reinforced concrete slabs, Commun. Numer. Methods Eng. 22 (2006) 699–709. doi:10.1002/cnm.840.

[12]   C. Bernuzzi, M. Simoncelli, M. Venezia, Performance of mono-symmetric upright pallet racks under slab deflections, J. Constr. Steel Res. 128 (2017) 672–686. doi:10.1016/j.jcsr.2016.10.004.

[13]   E. Spacone, F.C. Filippou, F.F. Taucer, Fibre beam-column model for non-linear analysis of R/C frames: Part I. Formulation, Earthq. Eng. Struct. Dyn. 25 (1996) 711–726.

[14]   M. Menegotto, P.E. Pinto, Method of Analysis for Cyclically Loaded R. C. Plane Frames Including Changes in Geometry and Non-Elastic Behavior of Elements under Combined Normal Force and Bending, Proc. IABSE Symp. Resist. Ultim. Deform. Struct. Acted by Well Defin. Loads. (1973) 15–22.

[15]   N.S. Ottosen, A Failure Criterion for Concrete, ASCE, J. Eng. Mech. 103 (1977) 527–535. doi:10.1017/CBO9781107415324.004.

[16]   N.S. Ottosen, Nonlinear finite element analysis of concrete structures, Risø National Laboratory, Roskilde, 1980.

[17]   P. Grassl, D. Xenos, U. Nyström, R. Rempling, K. Gylltoft, CDPM2: A damage-plasticity approach to modelling the failure of concrete, Int. J. Solids Struct. 50 (2013) 3805–3816. doi:10.1016/j.ijsolstr.2013.07.008.

[18]   D. Xenos, P. Grassl, Modelling the failure of reinforced concrete with nonlocal and crack band approaches using the damage-plasticity model CDPM2, Finite Elem. Anal. Des. 117–118 (2016) 11–20. doi:10.1016/j.finel.2016.04.002.

[19]   P. Grassl, M. Jirásek, Damage-plastic model for concrete failure, Int. J. Solids Struct. 43 (2006) 7166–7196. doi:10.1016/j.ijsolstr.2006.06.032.

[20]   J. Lee, G.L. Fenves, A plastic-damage concrete model for earthquake analysis of dams, Earthq. Eng. Struct. Dyn. 27 (1998) 937–956. doi:10.1002/(SICI)1096-9845(199809)27:9<937::AID-EQE764>3.0.CO;2-5.

[21]   J. Lee, G.L. Fenves, Plastic-Damage Model for Cyclic Loading of Concrete Structures, J. Eng. Mech. 124 (1998) 892–900. doi:10.1061/(ASCE)0733-9399(1998)124:8(892).

[22]   M.R.A. Kakavand, E. Taciroglu, An Enhanced Damage-Plasticity Model for Predicting the Cyclic Behavior of Plain Concrete under Multiaxial Loading Conditions, Front. Struct. Civ. Eng. (2019).

[23]   M.A. Crisfield, Non-Linear Finite Element Analysis of Solids and Structures, John Wiley & sons, Chichester, 1991.

[24]   C.W. Ziemian, R.D. Ziemian, Efficient geometric nonlinear elastic analysis for design of steel structures: Benchmark studies, J. Constr. Steel Res. 186 (2021). doi:10.1016/j.jcsr.2021.106870.

[25]   C.W. Ziemian, R.D. Ziemian, Steel benchmark frames for structural analysis and validation studies: Finite element models and numerical simulation data, Data Br. 39 (2021) 107564. doi:10.1016/j.dib.2021.107564.

[26]   S. Toma, W.-F. Chen, European calibration frames for second-order inelastic analysis, Eng. Struct. 14 (1992) 7–14. doi:10.1016/0141-0296(92)90003-9.

[27]   L. European Commission, Directorate-General for Research and Innovation, Proença, J., Rosin, I., Calado, Storage racks in seismic areas, Publications Office, 2009. doi:https://data.europa.eu/doi/10.2777/60886.

ДГКС ASES

U1-U7

OPENING LECTURES

Jesper Pihl[1]

THE DESIGN OF THE1915 ÇANAKKALE BRIDGE

Extended abstract:

The 1915 Çanakkale Bridge is a world record 2023m main span suspension bridge located at the North-eastern end of the Çanakkale Strait in Turkey where it connects the Gelibolu district to the Northwest with the Lapseki district to the Southeast.
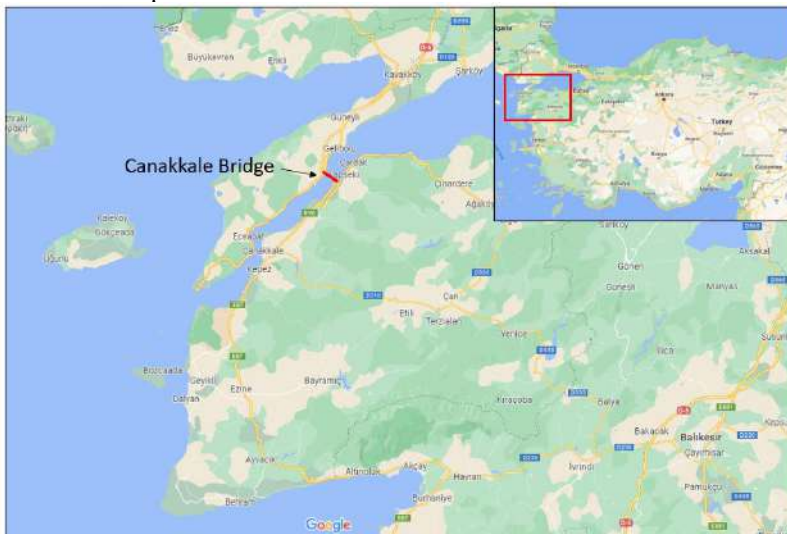
Figure 1 – Location of the Canakkale bridge, Canakkale Strait, Western Turkey

The bridge opened to traffic March 18, 2022, and is expected to increase capacity, improve traffic flow and ease the present and future congestion problems in the region. The only way to travel from Europa to Asia was earlier by crossing the Bosporus strait in the heavy populated region near Istanbul. The Canakkale Bridge allows traffic to cross at the Canakkale strait and will relieve traffic in the Istanbul area.

The 1915 Canakkale bridge has a 2023m main span and two side spans that are each 770m long. Due to poor soil conditions at the crossing, the two anchor blocks have been moved backwards so that they are positioned onshore. To be able to do that, a tie-down arrangement has been

---

[1] *COWI, Lyngby, Denmark, JEPI@COWI.coma*

introduced at the ends of the side spans. The tie-down arrangement consists of four heavy cables anchored to the ground. These cables fix the main cable against vertical movements at the bridge ends. The bridge elevation is shown in the below figure:

Figure 2 – Elevation of the 1915 Canakkale bridge

The main cables have a length of almost 4.4km and a diameter of 0.475m2 and are composed of 144 prefabricated parallel wire strands (PPWS). Each strand is built up from 127 high strength wires with a diameter of 5.75mm. In each side span four extra strands are installed.

The 318m high towers are being constructed out of steel, primarily to allow for fast erection. They comprise tapered box sections with a chamfered corner for better dynamic performance due to wind. These box sections are interconnected by horizontal block joints with welded skin plates and bolted splice connections of the internal longitudinal flat stiffeners.

The bridge deck comprises two stiffened closed steel box girders spaced 9m apart and connected by cross-girders every 24m. The 9m air gap between the two box girders ensures the aerodynamic stability of the bridge deck in strong winds. The overall width of the twin box girder becomes 45m including one maintenance walkway at each outer side. The bridge will carry six lanes, three in each direction. The depth of the twin box girder is 3.5m.
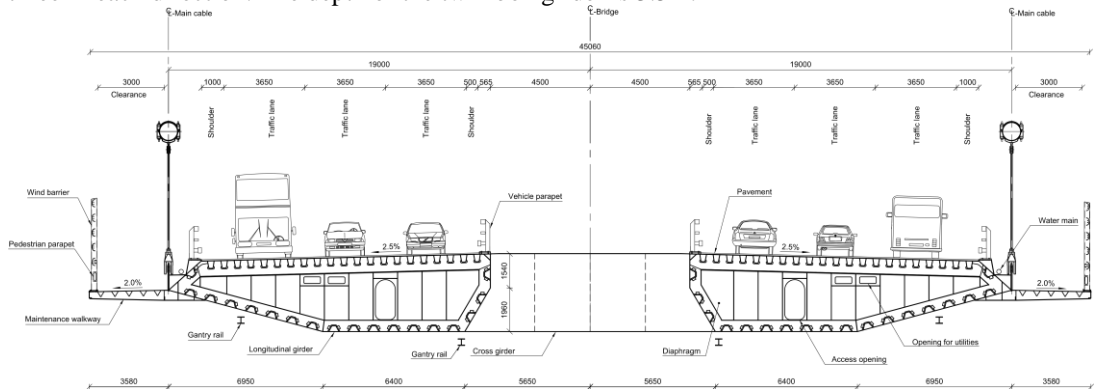
Figure 3 – Deck section – twin box girder with 9m airgap

One of the most important tools in the design of a long-span suspension bridge is the global analysis model. This Finite Element model is built so it represents the bridge reference condition for self-weight and will be used for multiple different analysis in the detailed design:
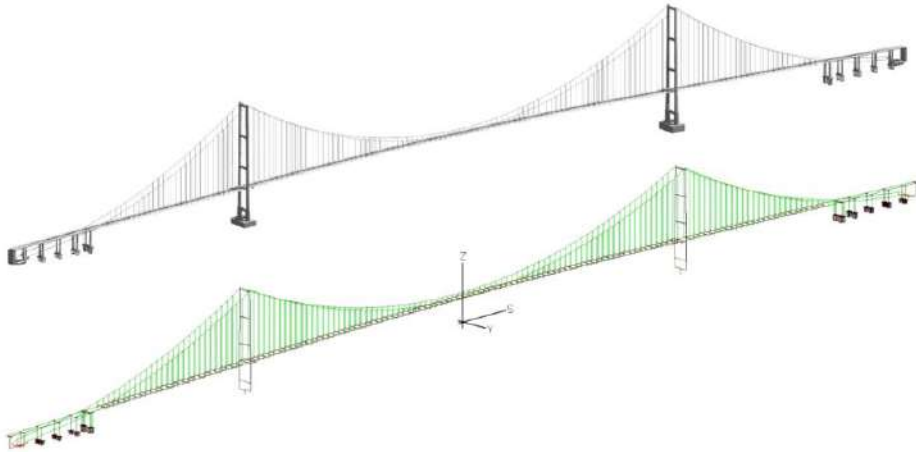
Figure 4 – Global analysis model of the Canakkale bridge: Geometry model and FE-model.

The Global FE-model is built primarily from beam elements. However, Semi-local models of specific areas of the bridge are activated to design these areas directly from the global FE-model. The program used is called IBDAS and is an inhouse developed COWI program. The below figures show semi-local models activated inside the global FE-model.
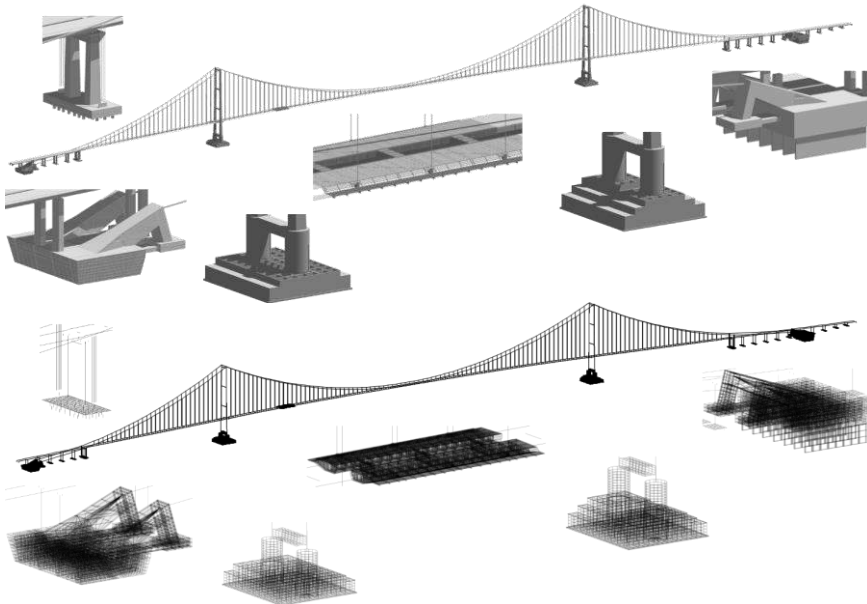
Figure 5 – IBDAS FE-models; Semi-local models activated at anchor blocks, tower foundations and bridge deck.

The Global FE-model is used to determine the loading on different structural elements in the bridge. Based on these loadings multiple local FE-models are used to verify the structures. Below

figure shows an example of the design of a splay saddle at the anchorages and the cable clamps used to connect the suspended hangers to the main cable:
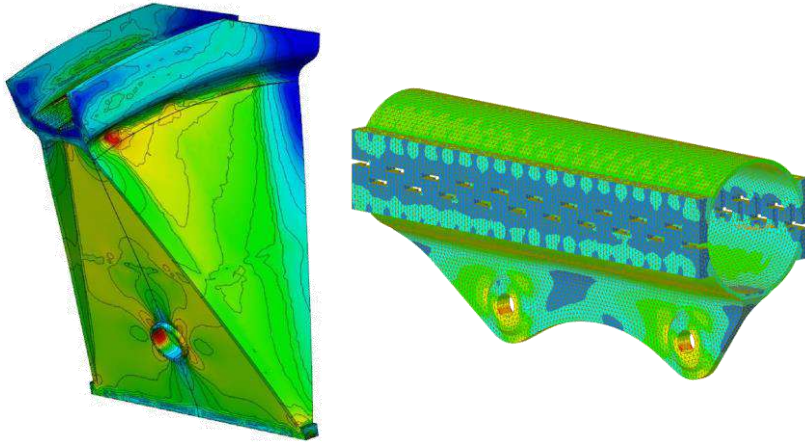
Figure 6 – Von Mises stress plots of splay saddle and cable clamp.

After the finalization of the detailed design, the construction engineering of the erection of the deck segments was performed. A safe erection of the suspended deck is very important. A detailed erection sequence was established and the temporary deck-to-deck connections between the segments were designed.

Figure 7 – Erection of deck segments using lifting gantries operating on top of the main cables.

The design of the Canakkale bridge will be described in detail in the presentation. Special focus will be put to the global analysis model and the design of the major structural elements.

Furthermore, the construction of the bridge including construction engineering of the deck erection will be explained.

The design of the bridge posed a lot of technical challenges. The very long span combined with extreme loadings such as strong winds and possibly earthquake had to be overcome. The challenges that were met during the detailed design and construction engineering will be discussed.

James Pawlikowski[1]

STRATEGIJE PROJEKTOVANJA VISOKIH ZGRADA

Rezime:

Projektovanje visokih zgrada nosi sa sobom specifične faktore i izazove koji ne samo da moraju da se razmotre već pomažu i da se uskladi arhitektura, konstrukcija i izvođenje objekta. Njihovo projektovanje zahteva inkorporiranje različitih faktora, gde je saradnja između arhitekata i inženjera ključna. Ovaj rad istražuje ključne faktore u projektovanju visokih zgrada – vetar, efikasnost, izvodljivost – i razmatra dve studije slučaja: Burdž Kalifa u Dubaiju i Kula Beograd.

Ključne reči: Visoke zgrade, dejstvo vetra, studija slučaja

TALL BUILDING DESIGN STRATEGIES

Summary:

The design of tall buildings has unique drivers and challenges that not only must be considered – they help to inform their architecture, structure, and construction. Their design must incorporate many factors, and as such collaboration between architects and engineers is key for their success. This paper will explore these key drivers in tall building design – wind, efficiency, constructability – and look at two case studies: the Burj Khalifa in Dubai, and the St. Regis in Belgrade.

Key words: Tall buildings, wind design, case study

---

[1] *Principal / Director of Engineering, REX Engineering Group*
Clinical Professor and Fellow, University of Illinois at Urbana, Champaign School of Architecture
Adjunct Instructor, University of Illinois at Urbana, Champaign Deptartment of Civil Engineering

1. DEFINITION

When discussing tall buildings, one must consider the differences between what are considered 'tall' buildings and what are considered 'supertall' buildings. A third and even rarer category are 'megatall' buildings. To be sure, the drivers for their successful design are similar, but there is a greater rigor required to completely satisfy these drivers as the height increases. The Council on Tall Buildings and Urban Habitat (CTBUH) is the official arbiter of building height, based in Chicago. They classify these three height distinctions as follows (Figure 1):

Tall buildings   height < 300m
Supertall buildings   height > 300m
Megatall buildings   height > 600m

Further, consider the following breakdown of Completed Tall buildings by height:

Height	number of buildings
600m+	3
500m+	10
400m+	38
300m+	176
200m+	1627
150m+	5096

Note: all values as per CTBUH January 2022
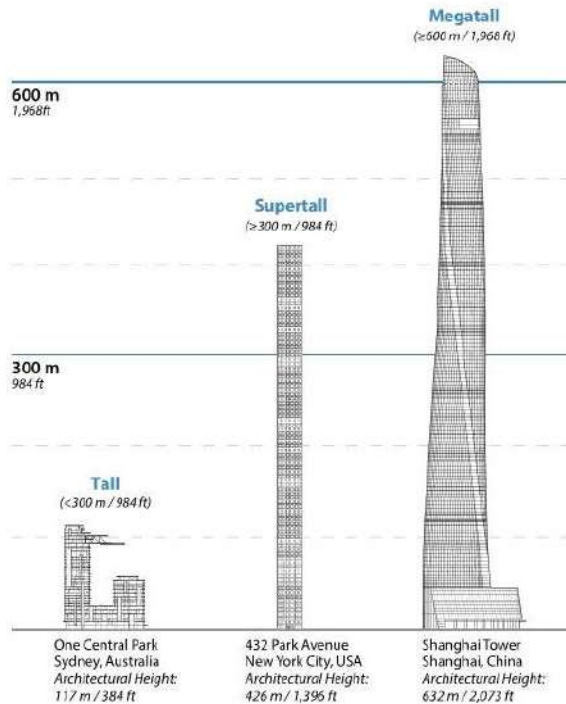
Figure 1 – Tall building definitions (CTBUH)

What this tells us is that Tall buildings are rare – there are only 5000 such examples existing in the world that are over 150m in height – and Supertall buildings are even rarer. There is a substantial basis of knowledge that has been developed regarding their design, but this basis is forever increasing and evolving, especially as heights increase and technologies, materials, and processes continue to advance.

2. SUCCESSFUL TALL BUILDINGS

Successful Tall buildings are those that first and foremost have been realized and developed, and second have done so in a way to satisfy all the drivers influencing their design and performance. There are many tall and supertall buildings that do not become a reality because they do not identify and accommodate all the tall building drivers in their design. These drivers can be divided into the following key characteristics – successful tall buildings are rational, appropriate, fast, efficient, and functional.

2.1. RATIONAL

Tall building structures are rational in that the engineering design takes into account and reflects the underlying physics governing the behavior of tall buildings. For example, when we study the gravity load diagram and the wind overturning diagram for a tall building, it becomes clear where the demand on the structure is greatest; by examining these diagrams, we can start to visualize a potential tall building form, which responds to the loading demands on the structure (Figure 2).

Gravity Load   Wind Overturning   Potential Tall
Diagram   Diagram   Building Form
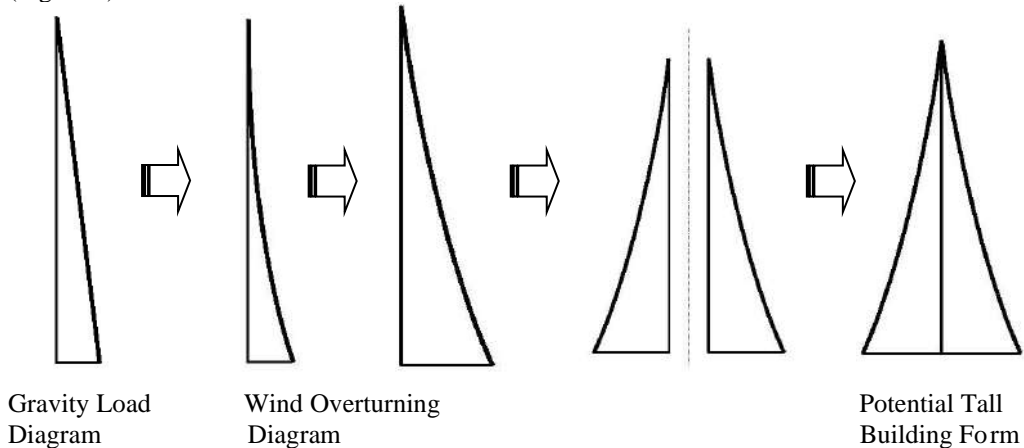
Figure 2 – Evolution of a Potential Tall Building Form (SOM)

This potential form can be seen in tapered buildings, or buildings which simulate a taper through setbacks. In addition to these buildings having a rational form with respect to structural performance, this shaping also has wind performance benefits, which we will explore next.

2.2. APPROPRIATE

Successful tall buildings need to be appropriate responses to their environment. The primary concern in the engineering of tall and especially supertall buildings is the effect of the wind on

the building structure. The shape or massing of a tower is often viewed in architectural terms, but it is the single most important structural design parameter in supertall buildings, because of its ability to influence the effects of wind. As such, appropriate tall building forms can be achieved by choosing a massing that maximizes stiffness, while at the same time provides the key shaping components to reducing wind effects. These shaping components include such measures as changing the building's shape along its height, providing a taper to the building's profile, and providing surface treatments to reduce vibration inducing wind effects (Figure 3).
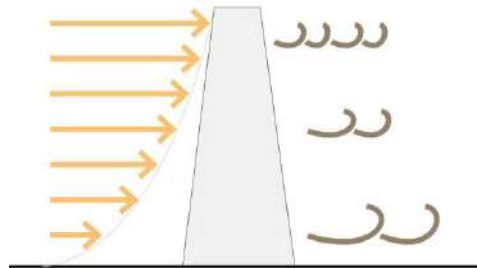
Figure 3 – Wind Behavior (SOM)

2.3. FAST

Tall buildings are significant investments, and require a large amount of time to build simply because of their height. The quicker a building can be built and realized, the quicker a return on the investment. Time requirements relate to the time required to actually construct a given system, as well as the complexity or simplicity of the system's components relating to their constructability.   As such, structural and architectural solutions must take into account constructability, speed of construction, and cost, in order to minimize the construction time. Additionally, construction and technical issues are considered early in the design process, thereby eliminating redesign iterations and construction problems.

2.4. EFFICIENT

Structural designs are optimized for the unique structural demands of tall buildings, thereby maximizing strength and stiffness while minimizing structural quantities.   Of particular importance in designing tall and supertall structures for efficiency is the ability to utilize the gravity load resisting system as part of the lateral load resisting system, while also maximizing the footprint of the lateral system. This provides a resistance to the wind overturning moment that utilizes forces already inherent within the system, thereby providing the opportunity for efficiency by utilizing the vertical structure to resist both gravity and lateral loads.

However, efficiency doesn't stop with just the structural system. The exterior wall system for tall buildings is typically the most costly system of any component of the building – considering efficiencies in its design, as well as the design of all other building systems and components, are also hallmarks of realized tall buildings.

2.5. FUNCTIONAL

The last key characteristic to consider is the function of the building. Tall buildings need to be rational, appropriate, fast, and efficient – but they also need to satisfy the functional aspirations of the program and client. This specifically relates to providing a massing and plan geometry that facilitates the first four key characteristics, but also satisfies the program demands with respect to how the floor plans are used, and what is the final building height. With respect to plan utilization, this relates to several items - the efficiency of the floor plate overall (saleable area vs. non-saleable area); the size, location, and efficiency of the core layout; and the appropriateness of the floor space provided (lease spans provided – distance from core to exterior wall – Figure 4). Depending on the usage of the building, this floor plan efficiency needs to be in the range of 70-85%, and the lease spans need to be in the range of 8-15m. With respect to the final building height – all tall buildings need to justify their building height. That is, what is the minimum reasonable floor-to-floor height that can be realized, considering floor structure thickness, clear height requirements, MEP distribution, and architectural finishes. It is expensive to build tall – every cm that can reduced from each floor has a meaningful impact on the final cost, simply because of the number of floors involved.
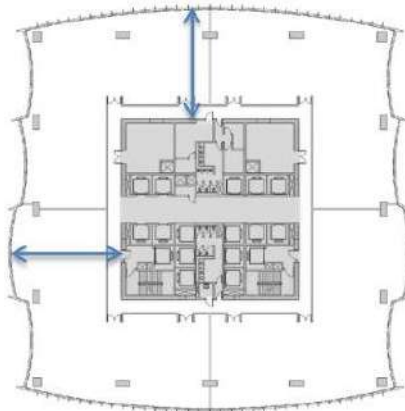
Figure 4 – Lease Spans

Finally, this usability needs to be provided without compromising any of the building systems. For example, the structural system needs to harmonize with the architectural planning, and vice versa. To be sure, there are several examples of built tall buildings which are less successful functionally. However, these are not common, and typically there are other drivers at play which have an influence – for example, perhaps height is a more important driver than floor efficiency for a supertall tower looking to become a showpiece for a larger development, or even a city/nation.

3. CASE STUDY – SUPERTALL BUILDING DESIGN: BURJ KHALIFA, DUBAI

The Burj Khalifa is an excellent example of a supertall building which not only satisfies the key characteristics in tall building design, but expounds upon them (Figure 5). Being the World's Tallest Building (and at the time it was designed it was the World's Tallest Building by a staggering 300m), it was incredibly important to adhere to the key characteristics – not only

conceptually, but to really research them and understand them due to the incredible height. This was only possible by a true collaboration between architects and structural engineers, from the very beginning of the project. Key was determining the shape of the tower, in order to provide an efficient building in terms of its structural system and its response to wind, while still maintaining the integrity of the initial architectural design concept, keeping the structure simple, and fostering constructability.

The overall shape of the tower is an extremely efficient solution to the structural requirements of a supertall residential tower (Figure 5). Starting from a slender top, the building spreads out as the gravity and wind forces accumulate. As such, the tower is a graphical representation of the structural tall building problem – provide structure where load demand is greatest, and extend this structure further away from the building's center to provide increasing stability.

Figure 5 – Burj Khalifa SOM | Nick Merrick © Hedrick Blessing

The tower utilizes a "buttressed" core structural system. Its plan is Y-shaped – a central core with three independent wings extending from it (Figure 6). This is inherently stable as each wing is buttressed by the other two. It is essentially a shear wall structure – a hexagonal central core provides the torsional restraint for the system; walls lining the wing corridors extend from the

core to the wing tips providing the shear resistance; thickened "hammerhead" walls are provided at the end of the corridor walls, increasing flexural stiffness; transverse wing walls and blade-like perimeter columns complete the system. The key to the success of the system is rigidly linking all elements together at each mechanical level through the use of outrigger walls. This allows all vertical concrete to act together in resisting lateral loads – this is an extremely important principle in efficient tall building structural system design. Getting gravity load into your lateral load resisting elements allows you to use the weight of the building to provide a stabilizing force to the overturning moment. Tall building structural systems must both accommodate the direct shear load from the wind, as well as the resulting overturning moment – engaging the entirety of the perimeter structure allows you increase the structural footprint/geometry from a stiffness perspective, as well as to direct load to the perimeter structure – as such you are able to maximize the entire structure to resist lateral loads.
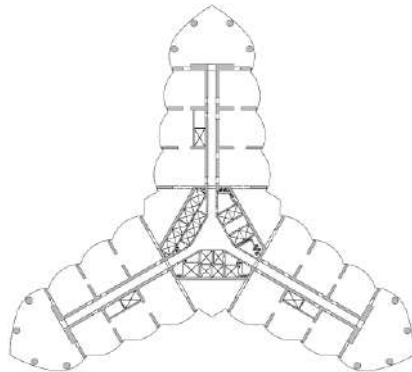
Figure 6 – Burj Khalifa structural plan (SOM)

Linking the structure at several locations throughout the height also has the benefit of being able to redistribute loads / equalize stress in the vertical elements. This is key for consistent behavior in any structure, but particularly in a tall concrete structure, where differential shortening of vertical elements is a key consideration. The concrete vertical elements will shorten because of shrinkage (all elements are wall-like in proportion, which facilitates a uniform behavior), and because of creep (the outriggers allow for unifying stress, which also facilitates a uniform behavior).

3.1. DESIGNING FOR WIND

Wind is a key consideration for tall buildings, and especially so for supertall buildings, as it creates the dominant demand upon their structures. This is not only seen in the amount of lateral load the building needs to be designed to resist, but wind will also induce motions in the structure that need to be kept to a minimum. Key in resisting the impacts due to wind is the ability to manage the vortex shedding behavior of the building. Vortex shedding is the phenomena of how wind behaves as it passes an object. As wind passes a building, a vortex or eddy will be created on the back side of the building. If these vortices organize over the height of the building, they can accumulate in strength such that a strong cross-wind pulsing force is created, which can increase the wind induced loads and motions that the building experiences (Figure 7). Disorganizing these vortices is key to successful tall building design – the desired result is to

"confuse" the wind by encouraging disorganized vortex shedding over the height of the building. This is accomplished through various shaping efforts which are then tested through a rigorous wind tunnel testing program, accompanied by appropriate structural system refinements resulting from the testing.

Key to the wind performance of the Burj Khalifa is its plan shape, and specifically that its plan is constantly changing as it increases in height. Approximately every twelve stories one bay from one of the wings sets back. This is done in a spiraling manner, with this setback occurring at a different adjacent wing each time. This creates 24 different floor plates over the height of the building. This geometry confirms an essential strategy for tall building design – provide differing floor plates to disorganize vortex shedding. The amount of variation of the floor geometries results in the creation of vortices at constantly changing locations over the tower's height, dramatically impairing their ability to organize in strength. This geometry also provided another benefit for the tower – the vertical wind sail kept reducing with height, meaning the magnitude of wind loading experienced at each floor reduced with height.

A rigorous wind tunnel testing program was performed by RWDI in Ontario, Canada (Figure 8). This consisted of over 70 tests to evaluate magnitude, directionality, motions, and comfort levels. This many tests are not typical for a tall building. Typically, the minimum number of tests would be two – one to determine wind loads/overall motions, and one to evaluate occupant comfort. With Burj Khalifa, there were two primary reasons for the number of tests. First, this height of a building had never been built before, so the design team felt it was appropriate to expand the testing to confirm its applicability and results. Second, the wind tunnel was used a design tool, using testing to continually confirm and refine massing and shaping strategies, until the optimum solution was found. This really represents a fundamental evolution in how wind tunnel testing is utilized. With tall buildings and previously with supertall buildings, there is a tendency to use the wind tunnel as more of a confirmation tool – to confirm designs and identify any potential issues. However, more and more the wind tunnel is an active participant in the early design of tall and particularly supertall buildings – using the tunnel as a conceptual tool to help shape tall buildings.
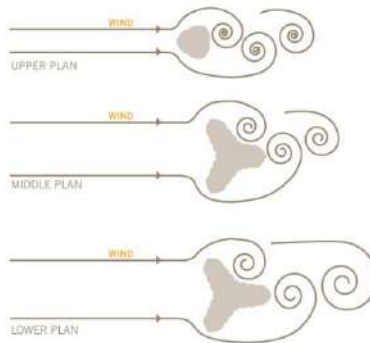
Figure 7–Burj Khalifa Wind Behavior (SOM)

Figure 8 – Burj Khalifa Aeroelastic Wind Tunnel Model (SOM)

3.2. DESIGNING FOR CONSTRUCTABILITY

Material technology and construction means and methods have a significant impact upon the design of supertall building systems. Structural systems must incorporate these elements in order to provide a building that can be built in an efficient and timely manner. Utilizing concrete is a key component of providing an efficient structural system for tall buildings. Concrete offers several advantages – high stiffness, mass, and damping, which assists in controlling motions and accelerations. As such, the systems used to construct concrete structures must be considered during their design.

With tall and supertall buildings, concrete systems are typically constructed utilizing self-climbing automatic formwork systems, with concrete material provided via concrete pumps to great heights (Figure 9). This type of formwork system provides many advantages for the construction of the concrete, primary among them being speed. Speed of construction for a tall building is tied to how the tower cranes are used – the less that tower cranes are used, the quicker the construction can become (due to the pick lengths of the cranes). So the goal is to reduce the amount that the cranes are needed. With an automatic self-climbing formwork system coupled with pumped concrete, the crane is only used to hoist rebar cages into place – and these rebar cages can be pre-fabricated at ground to further reduce the number of picks / increase speed. The formwork system works by attaching itself to the level below that has just been placed. The system can then jack itself up to the next level, without the need of the crane to move it (as in a jump-form type formwork system). The concrete is pumped from ground level, eliminating the need for any bucketing of concrete. It is a very fast system, but it does require a rigor to the design and layout of the structure. Specifically, there are some modifications that can be made to the formwork to accommodate changes – changes in thickness or geometry – but these changes take time to implement, and should be minimized.

Another challenge with this system is the delivery of concrete to height. This requires large pumps at the base of the building, as well as concrete mixes that are fine-tuned to the height at which they are being pumped. With Burj Khalifa, C80 concrete was pumped to over 600m in height – this required several different concrete mixes, with measures incorporated to increase

the fluidity of the concrete as the height it needed to be pumped increased. There was also a pumping test conducted pre-construction, whereby concrete was pumped horizontally through a series of 180-degree bends to simulate the pressure of pumping to 600m (Figure 10).
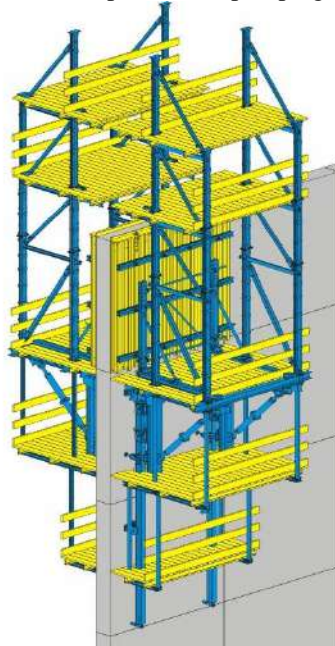
Figure 9 – Automatic Self-Climbing Formwork System (Doka)

Figure 10 – Burj Khalifa Concrete Pumping Test (SOM)

4. CASE STUDY – TALL BUILDING DESIGN: ST. REGIS BELGRADE

The case study of the Burj Khalifa is perhaps an extreme example of tall building design, and the importance of following the key characteristics. However, adhering to these key characteristics is equally important for moderately tall buildings, such as the St. Regis in Belgrade, also known as Kula Belgrade (Figure 11).

Kula is the centerpiece of the new Belgrade Waterfront development. It is 42 stories and 168m in height, and houses a five-star St. Regis hotel, as well as approximately 220 branded apartments. The tower is topped with an observation deck and restaurant. A large conference center facility which houses meeting facilities and hotel back-of-house is immediately adjacent to the tower. Below-grade parking is provided throughout the site.

Key to the design of the tower is that it rotates 90 degrees in plan, approximately 1/3 of the way up the building. This dramatic gesture is done for two reasons – one architectural and one structural. Architecturally, there was the desire to engage multiple contexts, as it is the tallest building in Belgrade and at a featured location. Structurally, rotating the plan is a strategy to enhance the building's performance against wind loading. As such, Kula is an excellent example of architects and engineers collaborating to determine a building shape, and in particular where a structural performance strategy led to the development of the key building aesthetic.

Figure 11 – Kula Belgrade (SOM)

4.1. DESIGNING FOR WIND

The building in plan is a fairly conventional rectangular footprint, with a central core wall system and perimeter columns. The core is strong enough in plan dimension to accommodate all lateral loading, in part because of the 90 degree rotation. The idea to rotate the plan as it progressed in height was borne out of the typical challenge facing rectangular buildings – the short direction of the building is taxed with resisting the largest wind load (the wind load on the broad face of the building – Figure 12). Typically, this results in requiring multiple locations of shear walls or braced frames in the short direction of the building, and often even requires augmenting this with a perimeter frame or engaging the perimeter structure. This can have a detrimental effect on the functional usage of the building in that more structure is needed in plan, as well as on material quantities in that more structure is needed period. By rotating the building 90 degrees, the building has now changed the fundamental equation for a rectangular building – the broad face wind is now accommodated by the long direction of the structure. This allows for a much more efficient resistance of the lateral loads, as now we have almost twice the plan dimension resisting it.
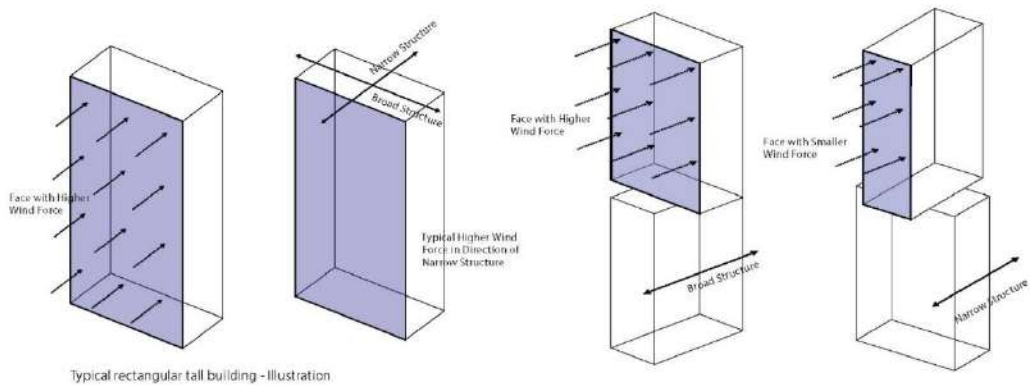
Figure 12 – Benefits of rotating rectangular tower (SOM)

Other strategies were also employed to reduce the wind loading – the building utilizes rounded corners, and also open balconies which create surface roughness. Rounded corners can be a very effective strategy to enhance wind performance for rectangular plan shapes, and it is because of its influence on vortex shedding. The simple yet effective move to soften the corners allows the design to take advantage of the slower vortex shedding associated with rectangular plan shapes, and combine this with the lower energy vortex shedding associated with circular plan shapes.

The tower form resulting from the above strategies is as elegant as it is efficient. Further, targeted hotel and apartment lease spans are maintained throughout, allowing for an efficient planning of the floor plans.

4.2. DESIGNING FOR CONSTRUCTABILITY

The key challenge for the design from a constructability standpoint was how to facilitate the structural transition of the 90 degree rotation in plan. The answer is to align structural workpoints to facilitate load-flow – structural solutions which provide for direct load transfers often are the simplest to understand as well as to construct. The primary challenge is that there are major

building columns which at the upper portion of the tower are located in plan outside of the lower extents of the tower. The solution is that these columns slope from their upper position to their lower position within a multiple-level transfer zone. This sloped zone consists of single-directional sloped columns, aligned with the core wall system – this facilitates the accommodation of any horizontal loading associated with the sloping column. Further, the slope starts and ends at a floor level, and these two levels utilize in-plane bracing elements to create a 'tie floor', allowing for load paths for any unanticipated or non-directional loading. The core wall system at the lower levels consists of a square central core with symmetrical appendages to create a rectangular core wall system – at the beginning of the transition zone these appendages drop off, leaving only the central core to continue vertically (Figure 13). The result is a structural system that can be built efficiently – there are no column transfers as the columns transition from one plan location to another by sloping through the transition zone, and there are minimal complications to the core wall structure in that walls that are no longer required are simply terminated where necessary by the transition geometry.

STRUCTURAL SYSTEM DIAGRAMS
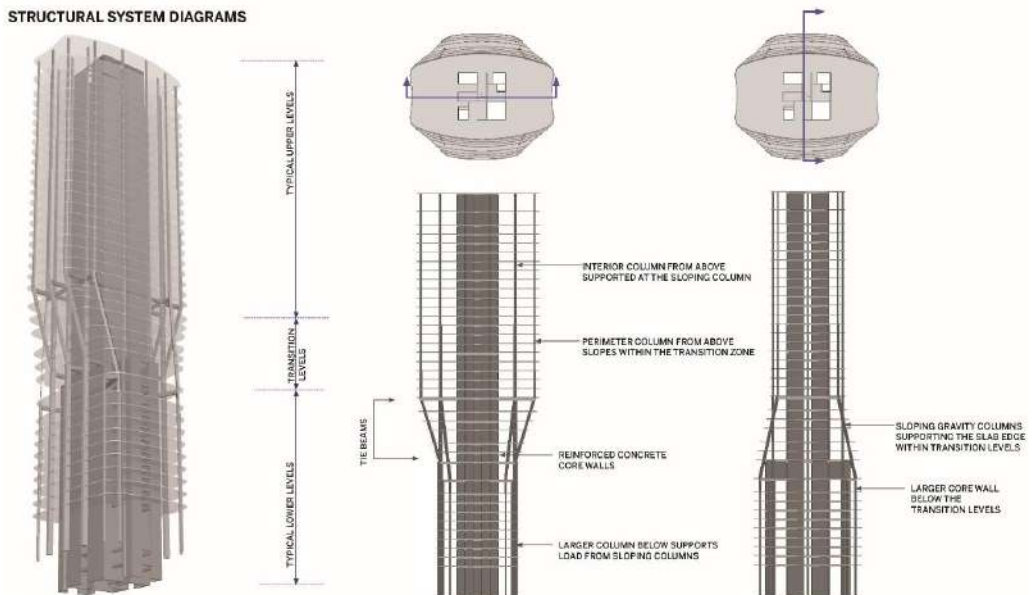
Figure 13 – Plan rotation transition (SOM)

5. CONCLUSION

Successful tall building design requires incorporating many differing strategies, and necessitates full collaboration between the architect and structural engineer, and also the contractor, in order to implement. Solutions must consider all strategies – successful tall buildings are at once designed appropriately with respect to their structure, their function, their aesthetic, their wind performance, and their construction. Successful tall buildings are those whose design is able to not only incorporate these strategies, but to find ways that they compliment and enhance each other, and each discipline

REFERENCES

[1] Baker, W.,F., Korista, D.,S., Novak, L., C., Pawlikowski, J.,J., & Young, B.,S., "Creep & Shrinkage and the Design of Supertall Buildings – A Case Study: The Burj Dubai Tower", ACI SP-246: Structural Implications of Shrinkage and Creep of Concrete, 2007.

[2] [Baker, W.,F., Pawlikowski, J.,J., & Young, B.,S., "The Challenges in Designing the World's Tallest Structure: The Burj Dubai Tower", Proceedings of the SEI/ASCE Structures Congress, 2009.

[3] Baker, W., F., and Pawlikowski, J., J., "Characteristics of supertall building structures." McGraw-Hill Yearbook of Science & Technology (2012): 35-39

[4] Baker, W., F., and Pawlikowski, J., J., "Higher and Higher: The Evolution of the Buttressed Core." Civil Engineering, October 2012: 58-65.

[5] Baker, W., F., and Pawlikowski, J., J., "The World's Tallest Building: The Burj Khalifa." Structure Magazine, June 2011.

Michael N. Fardis[1]

PROJEKTOVANJE AB KONSTRUKCIJA PREMA DRUGOJ GENERACIJI EC8: TEHNIČKA DOSTIGNUĆA I PRIMENA

Rezime:

Prva generacija Evropskih standarda za projektovanje seizmički otpornih konstrukcija razvijana je u periodu od 1998. do 2006. godine. Suprotstavljeni nacionalni standardi morali su biti povučeni do početka 2010. godine. Nakon zvaničnog zahteva Evropske komisije, 2014. godine započet je razvoj druge generacije. Neki delovi Evrokoda su kompletirani i u fazi su finalnog izglasavanja; rad na ostalim delovima (uključujući 6 delova Evrokoda 8) je pri kraju. Rok za povlačenje prve generacije Evrokodova kao nacionalnih standarda i potpunu zamenu drugom generacijom je mart 2028. godine. U drugoj generaciji Evrokoda 8, Deo 1 je podeljen na dva dela: Deo 1-1 koji se odnosi na sve tipove konstrukcija i Deo 1-2 koji se odnosi isključivo na nove zgrade. Odredbe vezane za AB zgrade su pojednostavljenje i prilagođene različitim zahtevima za regione visoke, umerene ili niske seizmičnosti širom Evrope. Broj preporučenih pravila je redukovan i u velikoj meri zamenjen principima projektovanja prema ponašanju. Pri definisanju smičuće nosivosti prizmatičnih elemenata i njihovih veza kao i nosivosti ploča na proboj pri cikličnom opterećenju, primenjena su racionalna uprošćenja koja su u skladu i sa drugom generacijom Evrokoda 2.

Key words: Betonske zgrade, Evrokod 8, Seizmičko projektovanje, Seizmički propisi

DESIGN OF RC BUILDINGS TO THE SECOND GENERATION OF EC8: TECHNICAL DEVELOPMENTS AND IMPLEMENTATION

Summary:

The first-generation European Standard for design of structures for earthquake resistance was developed between 1998 and 2006. Conflicting national standards had to be withdrawn by early 2010. Under Mandate from the European Commission, development of the second generation started in 2014. Some Eurocode parts have been completed and are in the Final Vote stage; technical work on the rest (including the six Parts of Eurocode 8) is near completion. Withdrawal of the first-generation of Eurocodes as national standards and replacement by the full second-generation has to take place by March 2028. The second-generation Eurocode 8 has seen Part 1 split in two: Part 1-1-covers all provisions which apply to all types of structures. Part 1-2 covers exclusively new buildings. The provisions for concrete buildings have been simplified and tuned to the different needs of high, moderate or low seismicity regions across Europe. Prescriptive rules have been reduced and replaced to a very large extent by transparent performance-based provisions. Rational approaches, fully consistent with the second-generation Eurocode 2, were introduced for the cyclic shear resistance of prismatic members and their connections and for cyclic eccentric punching shear.

Key words: Concrete buildings, Eurocode 8, Seismic design, Seismic codes

---

[1] *Professor Emeritus, University of Patras, Patras, fardis@upatras.gr*

1. INTRODUCTION

Sixteen years ago the European Standardisation Committee (CEN) made available to the National Standardisation Bodies (NSBs) the suite of all 58 Structural Eurocodes, including the six parts of Eurocode 8. Since then, NSBs have adopted the Eurocodes as National Standards (normally after translation), developed and published their National Annexes and withdrawn conflicting National Standards (but not necessarily national structural design regulations conflicting with the Eurocodes). A short time after the EN-Eurocodes became the exclusive structural design standard in European Union Member States, the European Commission issued a mandate to CEN for their revision, so that they evolve into the second generation of EN-Eurocodes by the mid-2020s. CEN has responded with a very detailed plan, specifying the needs of each Eurocode part for revision or extension of scope. After the European Commission and CEN converged on the details and terms of the evolution to the second generation, the process started around the end of 2014. The evolution process has now entered its last stage: formal voting of CEN Member States has already taken place for the Eurocode parts which were drafted first and is planned to be completed for all Eurocodes by the end of 2025. The intent is to withdraw all National Standards conflicting with the second generation of the Eurocodes – including those of the first generation – in early 2028.

Figure 1 shows the timeline of the various generations of Eurocode. The development and enforcement process seems to have an apparent period of 18 years. One implication is that the second generation may stay in force as European structural design standards till the mid-2040s.
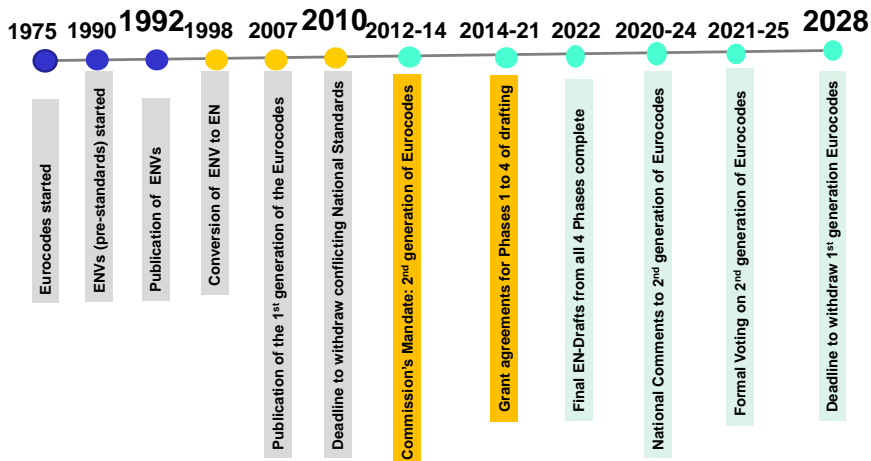
Figure 1 – Timeline of the development of all Eurocode generations

The general objectives of the second generation of Eurocodes are:
- To significantly reduce the number of Nationally Determined Parameters.
- To enhance "Ease of use" by:
    - Improving clarity;
    - Simplifying routes through the Eurocodes;

-   Limiting, where possible, alternative application rules;
-   Avoiding/removing rules of little practical use in design.
- To fill voids and expand the scope.
- To consolidate and produce more succinct text.
- To update the technical content according to recent developments in the State-of-the-Art

Figure 2 depicts the structure, hierarchy and interrelations between Eurocodes in the second generation. Completely new elements, added to those of the first generation, are shown in red.
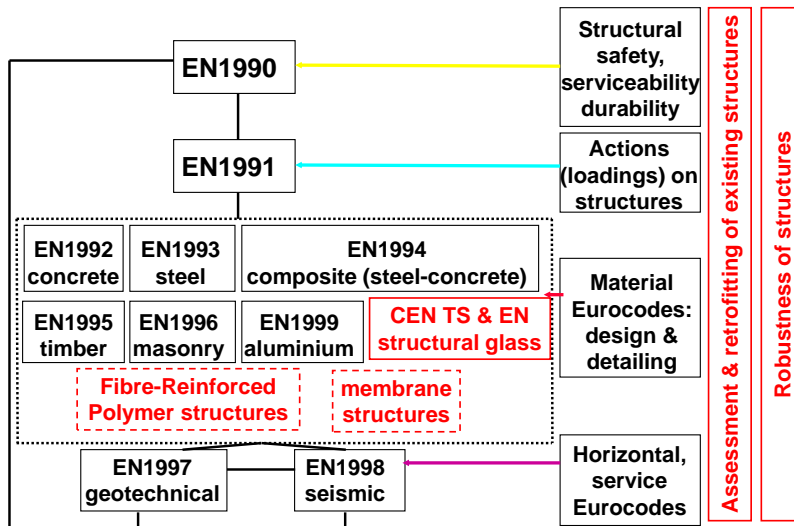
Figure 2 – Structure, hierarchy and interrelations in the second generation of Eurocodes.

2. STRENGTHS AND WEAKNESSES OF FIRST GENERATION EC8

The first-generation European Standard for the design of structures for earthquake resistance comprises six parts (see Table 1): Part 1 covers all general aspects, the seismic action and design of new buildings, Part 2 deals with design of new bridges, Part 3 addresses the seismic assessment and retrofitting of existing buildings, Part 5 covers foundations, retaining structures and geotechnical aspects and Parts 4 and 6 deal with certain types of special structures: tanks, silos, pipelines, towers, masts and chimneys.

Eurocode 8 shares the strengths of the set of Eurocodes: it belongs to a comprehensive, State-of-the-Art portfolio of standards, meant to be seamlessly integrated and internally consistent, as well as user-friendly thanks to sharing the same philosophy, document structure. notation, terminology and methods. Moreover, the Eurocodes enjoy the stature of design standards of the largest and most populous economic entity in the developed world, and indeed the one which leads the world in structural engineering excellence, tradition and achievements. So, they are in the best position to penetrate other parts of present-day's globalized world.

Table 1 – The Parts of the two generations of Eurocode 8

First generation		Second generation	
EN1998-1	General rules, seismic actions, rules for buildings	EN1998-1-1	General rules, seismic action
EN1998-2	Bridges	EN1998-1-2	Rules for new buildings
EN1998-3	Assessment and retrofitting of buildings	EN1998-2	Bridges
EN1998-4	Silos, tanks, pipelines	EN1998-3	Assessment and retrofitting of buildings and bridges
EN1998-5	Foundations, retaining structures, geotechnical aspects	EN1998-4	Silos, tanks and pipelines, towers, masts and chimneys
EN1998-6	Towers, masts, chimneys	EN1998-5	Geotechnical aspects, foundations, retaining and underground structures

It is difficult to list specific strengths of Eurocode 8 without getting into technical details. So, only some general ones are highlighted here:

Eurocode 8 follows the most rational approach among all seismic design codes currently applied around the world. At the time it was drafted it was closer to the State-of-the-Art than any of its contemporaries. Moreover, it provides plenty of flexibility:
- It offers a portfolio of several analysis methods, from simple ones, such as the equivalent static approach, to the most advanced ones, like nonlinear response-history analysis;
- It allows alternative combinations of design strength and ductility (Ductility Classes), without restrictions in their use; even two alternative types of concrete walls (ductile and large lightly reinforced ones) are foreseen within the same Ductility Class;
- In addition to standard force-based design of new buildings or bridges using linear analysis with a reduced response spectrum, Eurocode 8 includes a proto-displacement-based design option, with calculation of deformation demands via nonlinear analysis and their direct verification against deformation capacities;
- Through the system of Nationally Determined Parameters (NDPs), it offers to countries the possibility to choose themselves the levels of protection (i.e., safety) and economy to be provided by Eurocode 8 designs. As a matter of fact, the recommended NDP values give very cost-effective designs, with a good balance of safety and economy.

There are weaknesses too:
- The description of the seismic hazard is behind the State-of-the-Art: two parametrized sets of spectral shapes are provided for each one of the five standard soil types, anchored to a single ground motion parameter (the peak ground acceleration, from national zonation

maps drawn for a single hazard level), allowing countries to choose the values of parameters defining the shape. This results in large discrepancies across borders.

- Certain techniques or technologies are missing from the scope: supplemental energy dissipation in buildings, flat-slab frames, post-tensioning of primary members, etc.

A general drawback of the Eurocodes is noted: being comprehensive, State-of-the-Art standards, they are powerful but demanding tools, more suitable for specialized structural designers and fairly large design offices than for individual practitioners working in a range of areas or types of projects. Pressure from practice, especially from SMEs or individual designers, has led to requests from CEN Member States to improve ease of use in the second generation of Eurocodes. This is understandable: completeness comes at the price of volume and apparent complexity. Besides, the first generation developed mostly from a zero baseline and had not been thoroughly tested before in practice; so, teething problems were expected. So, improvement of "Ease of use" has been a prime objective of the second generation.

3. OVERVIEW OF SECOND GENERATION EUROCODE 8 WITH EMPHASIS ON THE RULES FOR NEW CONCRETE BUILDINGS

In the second-generation Eurocode 8 Part 1 was split in two: Part 1-1 covers all provisions which apply to all types of structures: performance requirements, the seismic action, seismic analysis and member stiffness, resistance and deformation capacity properties for use in all other Parts. It includes a state-of-the-art determination of the elastic spectrum accounting for all relevant topographic and geotechnical conditions and for soil nonlinearity and gives in Annex the first European Maps for 475-year return period spectral values on rock (Figure 3). Part 1-2 covers exclusively new buildings and Part 2 only new bridges. Part 3 has been expanded to include seismic assessment and retrofitting of bridges, in addition to buildings. Parts 4 and 6 have merged into one, covering design of new structures other than buildings or bridges. The scope of Part 5 has expanded very much, to cover underground structures and the use of inelastic deformations in the soil to reduce seismic demands in the superstructure.

ESHM20 Salpha Hazard Values

0 1.2 2.4 3.6 4.8 6.0 7.2 8.4 9.6 10.8 12.0 [m/sec^2]
m/sec/sec

ESHM20 Sbeta Hazard Values

0 0.5 1.0 1.5 2.0 2.5 3.0 3.5 4.0 4.5 5.0 [m/sec^2]
m/sec/sec
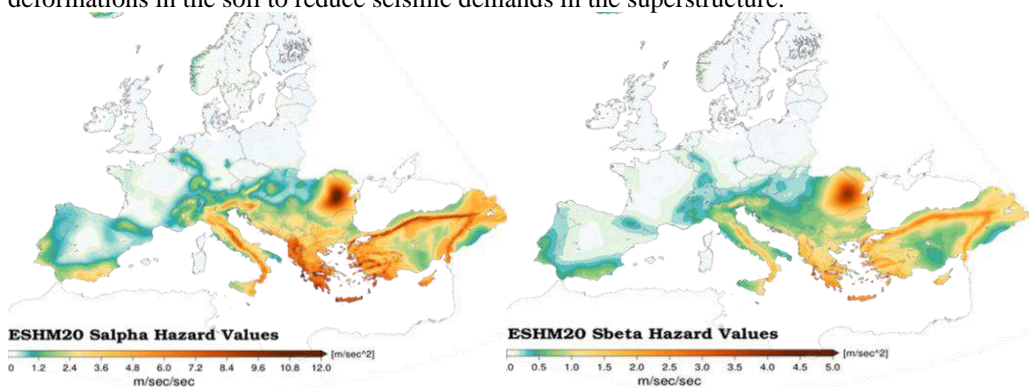
Figure 3 – 475-year return period spectral acceleration on rock at the constant-acceleration plateau of the spectrum, $S_{\alpha,ref}$, and at 1 sec natural period, $S_{\beta,ref}$, in Annex A of Part 1-1.

The displacement-based approach (with nonlinear analysis – pushover or of the response-history type- or, under certain well-defined conditions, linear 5%-damped analysis for estimation

94

of displacements and deformations) is now at an equal footing with the force-based one with reduction of the elastic spectrum by the behaviour factor. Deformation-based criteria for members, common to all types of structures, are given in Part 1-1.

The technical content of the 2022 draft of EN1998-1-1 General rules, seismic action, is concentrated in Chapters 4 to 7 and the Annexes, Normative (N) or Informative (I):

4   Basis of design
    4.1 Performance requirements
    4.2 Consequence classes
    4.3 Limit states and associated seismic actions
    4.4 Primary and Secondary members
    4.5 Compliance criteria for new structures
5   Site conditions and seismic action
    5.1 Site conditions
    5.2 Seismic action
6   Modelling, analysis and verification
    6.2 Modelling
    6.3 Seismic action
    6.4 Force-based approach
    6.5 Non-linear static analysis
    6.6 Response-history analysis
    6.7 Verification to limit states
    6.8 Structures equipped with antiseismic devices
7   Deformation criteria and strength models
    7.2 Reinforced concrete structures
    7.3 Steel and composite-steel structures
    7.4 Timber structures
Annex A (I) European Hazard Maps
Annex B (N) Alternative identification of site categories
Annex C (N) Site-specific elastic response spectra
Annex D (N) Criteria for selection and scaling of input motions
Annex E (N) Determination of target displacement and limit-state spectral acceleration by non-linear response-history analysis of equivalent sdof model
Annex F (I) Simplified reliability-based verification format
Annex G (N) Design of fastenings to concrete in seismic design situation
Annex M (N) Material or product properties in EN 1998-1-1

The technical content of the 2022 draft of EN1998-1-2 Rules for new buildings, can be found in Chapters 4 to 15 and the Annexes.

4. Basis of design
5. Modelling and structural analysis
6. Verification of structural elements to limit states
7. Ancillary elements
8. Base isolated buildings
9. Buildings with energy dissipation systems
10. Specific rules for concrete buildings
11. Specific rules for steel buildings

12. Specific rules for composite steel–concrete buildings
13. Specific rules for timber buildings
14. Specific rules for masonry buildings
15. Specific rules for aluminium buildings
Annex A (I) Characteristics of earthquake resistant buildings and in plan regularity
Annex B (I) Natural eccentricity and torsional radius
Annex C (N) Floor accelerations for ancillary elements
Annex D (N) Buildings with energy dissipation systems
Annex E (N) Seismic design of connections for steel buildings
Annex F (N) Steel lightweight structures
Annex G (N) Design of composite connections in dissipative composite steel-concrete moment resisting frames
Annex H (I) Seismic design of exposed and embedded column base connections
Annex I (N) Design of the slab of steel-concrete composite beams at beam-column joints in moment resisting frames
Annex J (I) Drift limits for eccentrically loaded unreinforced masonry piers
Annex K (I) Simplified evaluation of drift demands on infilled frames
Annex L (N) Load-deformation relationships of dissipative timber components for non-linear analyses

The contents of the Chapters of the 2022 draft of EN1998-1-2 which are relevant to concrete buildings are listed below in more detail :

4. Basis of design
    4.1. Building classification
    4.2. Seismic actions
    4.3. Compliance criteria
    4.4. Characteristics of earthquake resistant buildings
5. Modelling and structural analysis
    5.1. Modelling
    5.2. Minimum design eccentricity in buildings
    5.3. Methods of analysis
6. Verification of structural elements to limit states
    6.2. Verification of Significant Damage (SD) limit state
    6.3. Verification to other limit states
10. Specific rules for concrete buildings
    10.1 Scope
    10.2. Basis of design and design criteria
    10.3. Materials requirements
    10.4. Structural types, behaviour factors, limits of seismic action and limits of drift
    10.5. Beams
    10.6. Columns
    10.7. Beam-column joints
    10.8. Ductile walls
    10.9. Large walls
    10.10. Flat slabs
    10.11. Provisions for anchorages and laps

10.12. Provisions for concrete diaphragms
10.13. Prestressed concrete
10.14. Precast concrete structures
10.15. Design and detailing of foundations

With the behaviour factor q for the reduction of the elastic spectrum in force-based design split in three factors, $q = q_s q_R q_D$, with:

- $q_s = 1.5$ for (member and material) overstrength;
- $q_R \geq 1$ for redundancy of structural system;
- $q_D \geq 1$ for ductility in cyclic loading,

the values of the last two factors, as well as of the composite, total factor, q, for the various types of concrete structural systems of Ductility Classes 1 and 2 are listed in Table 2.

The provisions for concrete buildings have been simplified and tuned better to the different needs of high, moderate or low seismicity regions across Europe. Prescriptive rules have been reduced or replaced by transparent performance-based provisions. Rational approaches, largely based on the Modified Compression Field Theory and fully consistent with the second-generation Eurocode 2, were introduced for the cyclic shear resistance of prismatic members and their connections. Provisions for modelling and verification of flat-slab frames as part of the lateral-load-resisting system have been added and resistance models for cyclic eccentric punching shear proposed, consistent with the new rules in Eurocode 2 for punching shear.

Table 2 – Values of behaviour factor in Part 1-2 for regular in elevation concrete buildings

		q_R	q_D		$q = q_s q_R q_D$	
			DC2	DC3	DC2	DC3
Frame or frame-equivalent dual structures	multi-story. multi-bay frames or frame-equivalent dual structures	1.3	1.3	2.0	2.5	3.9
	multi-story. one-bay frames	1.2			2.3	3.6
	one-story frames	1.1			2.1	3.3
Wall- or wall-equivalent dual structures	wall-equivalent dual structures	1.2	1.3	2.0	2.3	3.6
	coupled walls structures	1.2	1.4		2.5	3.6
	uncoupled walls structures	1.0	1.3		2.0	3.0
	large walls structures	--	--		3.0	
Flat slab structures		1.1	1.2	--	2.0	--
Inverted pendulum system		1.0	1.5	1.5	1.5	1.5

4. COMPUTATIONAL IMPLEMENTATION OF THE FIRST AND SECOND GENERATIONS OF EUROCODE 8 FOR COMPARATIVE APPLICATION

The provisions for concrete buildings in both generations of Eurocodes 2 and 8 have been implemented in a computational platform for fully-automated, cloud-based detailed design of buildings. The scope covers columns of rectangular, circular, L- or T-shaped section, beams and foundation beams with or without flanges at top and/or bottom, walls of rectangular, L-, or U-shaped section, beam-column connections, footings with rectangular plan and the underlying soil, storey- or multi-storey-deep perimeter walls of basements, etc. It covers not only Ultimate Limit State design for resistance and ductility for seismic and non-seismic actions, but also Serviceability Limit State design for quasi-permanent or frequent actions and verification of elements for structural resistance under fire conditions according to Parts -1-2 of Eurocodes 1 and 2 (of both generations). Any layout of elements in plan and elevation can be treated.

Pilot application of the computational capability so far has shown that the second generation is more economic for the majority of cases – especially for walls of the higher ductility class in shear - but, sometimes – e.g., in circular columns or at beam ends – more demanding for the ductility of the compression zone.

Trayana Tankova[1], Filipe Rodrigues[2], Luís Simões da Silva[3]

PROBLEMI STABILNOSTI ELEMENATA IZRAĐENIH OD ČELIKA VISOKIH ČVRSTOĆA

Rezime:

Uvođenjem odgovarajućih standarda za proizvodnju i izvođenje, čelici visokih čvrstoća (HSS) postaju sve popularniji. EN 1993-1-1 daje pravila za proračun stubova, greda i ekscentrično pritisnutih elemenata za čelike klasa čvrstoća do S460, dok EN 1993-1-12 daje dodatne smernice za klase između S500 i S700 (zasnovane uglavnom na numeričkim analizama koje su bile dostupne u vreme pisanja standarda). Nedavne studije koje su se bavile izvijanjem stubova od zavarenih H, I i kutijastih profila čelika S460 do S960, iako relativno limitirane, pokazuju da pri proračunu elemenata od čelika visokih čvrstoća treba primeniti revidovane krive izvijanja. Nedavno je u okviru evropskog projekta STROBE izvršena evaluacija propisa koji pokrivaju oblast stabilnosti stubova, greda i ekscentrično pritisnutih elemenata. Istraživanje se zasnivalo na eksperimentalnom ispitivanju koje je obuhvatilo 20 testova globalne stabilnosti elementa, na merenju zaostalih napona, formiranju naprednih numeričkih modela, predlaganju analitičkih izraza i statističkoj obradi rezultata. Konačno, bilo je moguće predložiti nove, povoljnije krive izvijanja za proračun elemenata od čelika visokih čvrstoća. U ovom radu sumirani su zaključci istraživanja koji se tiču problema stabilnosti elemenata od čelika visokih čvrstoća.

Ključne reči: čelici visoki čvrstoća, proračun elementa, eksperiment, zaostali napon, pouzdanost

STABILITY DESIGN OF HIGH STRENGTH STEEL MEMBERS

Summary:

High strength steel (HSS) is increasingly becoming popular with the introduction of product and execution standards. EN 1993-1-1 gives stability design rules for columns, beams and beam-columns up to S460, whereas EN 1993-1-12 gives additional guidance for S500 up to S700 (based mainly on numerical work available at the time). Recent studies on flexural buckling of welded H, I and box columns in steel grades S460 to S960, even though limited, show that improved curves can be used for members in HSS.

Recently, within the European Project STROBE evaluation of the European stability design rules was carried out covering columns, beams, and beam-columns. The research was based on experimental programme covering 20 full-scale tests, residual stress measurements, advanced numerical models, analytical derivations, and statistical evaluation. Finally, it was possible to provide new, more relaxed recommendations for the buckling curve selection for HSS members. This paper provides a summary of the project conclusions regarding the stability design of steel members in HSS.

Key words: high strength steel, member design, experiments, residual stresses, reliability

[1] *Assistant professor, Delft University of Technology, t.tankova@tudelft.nl*

[2] *PhD student, University of Coimbra, filiperodrigues@uc.pt*

[3] *Full Professor, University of Coimbra, luisss@dec.uc.pt*

1. INTRODUCTION

Nowadays, high strength steels (HSS) are available with excellent weldability and toughness properties due to the advances of the steel production technology such as quenching and thermomechanical rolling. The application of HSS is interesting due to the possibility of material savings and the possibility to go further in the steel design with more challenging structures.

However, HSS lacks wide application due to lack of standards. The steel construction in Europe is highly regulated, whereby the steel product should comply with several standards. Currently, the European steel product standard EN10025 [1] covers steels up to S960, however the fabrication standard EN1090 [2] is currently being extended to accommodate steels up to S960. Following this trend, the revised version of prEN 1993-1-1 [3] will also include steels up to S690 in its main part, whereas rules for steels up to S960 will be given in part 12 [4] with focus on ultra-high strength steels. Even though the new steels will be included, there was a gap between the existing rules and the knowledge acquired since the first publication of Eurocode 3, which was developed in several European research projects.

The most recent contribution was by the European project STROBE (Stronger Steels in the Built Environment) that re-evaluated the design rules for steel members and materials up-to S690.

Concerning the stability design rules, the Eurocode 3 recommendations for members using HSS do not indicate any specific guidelines. However, recent experimental studies have shown that HSS is more accurately represented by more relaxed buckling curves for both columns [5-9] and beams [10-18], this improvement being mostly attributed to more favourable residual stress distributions in HSS welded profiles [19, 20].

This paper presents a summary of the activities performed within the European project STROBE which aimed to providing recommendations for improved buckling curve selection for welded I-sections. The research was based on an extensive parametric study with numerical models validated with experimental tests carried out by the authors. The parametric study covered different buckling modes (flexural buckling and lateral-torsional buckling), bending moment distributions, member lengths, steel grade (S460, S500 and S690) and cross-section dimensions. The numerical results are then compared against the current EC3 design methods. Finally, new design recommendations are proposed for members made of high strength steel, subjected to flexural buckling and lateral-torsional buckling, which were validated with the calculation of partial factors according to EN1990, Annex D [21, 22].

2. EXPERIMENTAL RESISTANCE FOR HSS MEMBERS

2.1. SCOPE

An experimental programme on HSS members covered flexural buckling around major and minor axes and lateral-torsional buckling. The major focus of the experimental programme was on beams in S460 and S690, considering both hot rolled and welded I shaped sections, and the extension of the design rules to hybrid sections.

The experimental programme included 4 columns: two of them tested for flexural buckling about their major axis and the other two about the minor axis. The beam tests consisted of 14 specimens, including welded and rolled HSS uniform I beams, monosymmetric I beams and

hybrid beams. The campaign also includes 2 beam-column tests. The specimen dimensions are given in Table 1. In order to characterize completely the experiments, supplementary tests were performed to characterize the material properties by standard coupon tests, measure the imperfections by laser scan and residual stresses by sectioning method [25].

Table 1 – Experimental programme

Sections	*Steel grades*	*Bucking mode*
$180 \times 100 \times 8 \times 8$ $150 \times 150 \times 8 \times 8$	*S690*	*Flexural buckling y-y*
$220 \times 170 \times 8 \times 16$ $180 \times 180 \times 8 \times 16$	*S690*	*Flexural buckling z-z*
$500 \times 200 \times 8 \times 16$ $310 \times 300 \times 8 \times 16$ $750 \times 200 \times 8 \times 16$ $750 \times 200(400) \times 8 \times 16$ IPE500 HEA320	*S690* *S690 hybrid* *S460* *S460 hybrid*	*Lateral-torsional buckling*

To obtain realistic the residual stresses for the welded members that were used in the buckling tests, the profiles were welded considering an additional length L2 (Figure), which was cut and used for the measurement of the residual stresses. This length L2 was chosen to be longer than two times the section height [25] in order to exclude any possible boundary effects from the measurements.
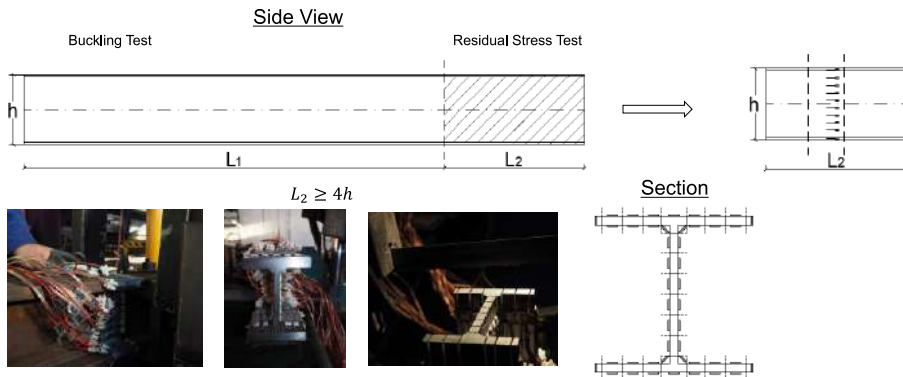
Figure 1 – Residual stresses – sectioning method

2.2. RESULTS

Firstly, the results from the experimental programme were compared to the Eurocode 3 predictions.

The assessment was based on reduction factors calculated using normalized slenderness $\bar{\lambda}$ considering critical forces (or moments) from linear buckling analyses where the same boundary conditions as in the experimental tests were used. The reduction factor $\chi_{\exp}$ from the experimental tests was calculated as the ratio between the experimental resistance (*Nexp* or *Mexp*) and the cross-section resistance using the measured yield stress f_y, where W or A is the plastic, elastic or

effective section modulus for Class 1/2, Class 3 and Class 4, respectively. In general, the results for both columns and beams were much higher than the requirement from the EN 1993 -1-1, Figure 2 This is mainly attributed to the member imperfections. The current design provisions in EN 1993-1-1 do not distinguish between the different steel grades, thus assuming that the residual stresses have the same impact with increasing strength of the steel. Therefore, the trends indicated by the experimental programme need to be addressed in the code by providing adequate design rules for HSS columns and beams.
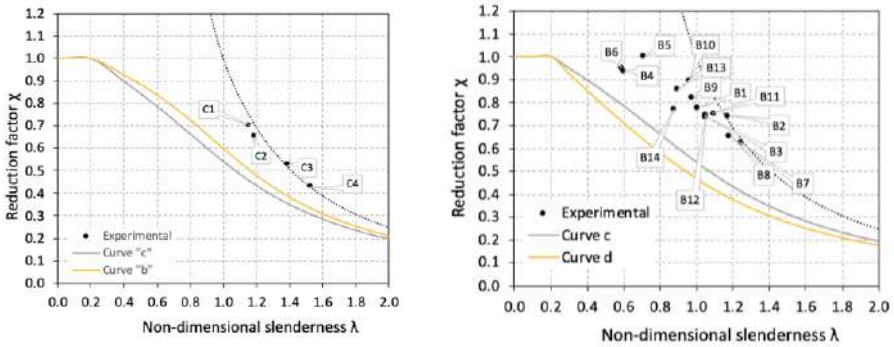
Figure 2 – Experimental results – Column and Beams (General Case)

2.3. NUMERICAL MODEL AND PARAMETRIC STUDY

The experimental results were used for the calibration of numerical model which was then used to enlarge the experimental study by a numerical parametric one. For the validation of the numerical models with experiments a common strategy was adopted for all tests (columns, beams and beam-columns). The models were developed in the software package ABAQUS [26], using shell elements. To reproduce the experimental results, all parameters that were measured were introduced in the model with the as-measured values. For the residual stresses this implied the division of the cross-section in regions which corresponded to the test configuration and apply an average stress according to the performed measurements. The geometrical imperfections were introduced as interpolated values of the measured geometry into the finite element mesh. The material properties were adopted also according to the coupon tests carried out in the scope of the experimental programme.

a) Beam tests   b) Column tests
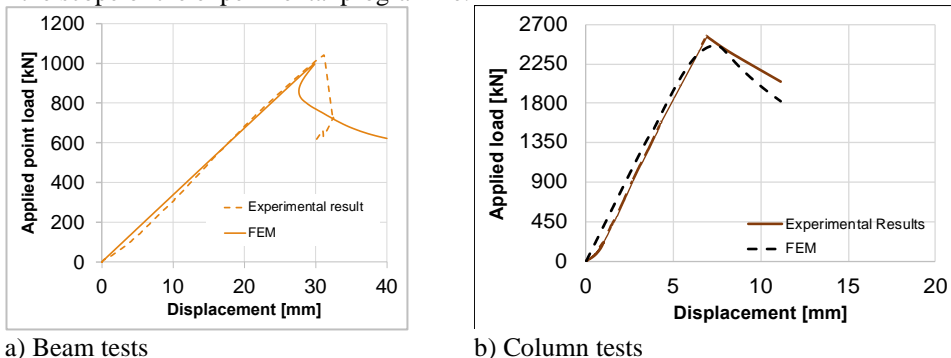
Figure 3 – Comparison of calibrated model for beams and columns assumptions

For exemplification, Figure 3 depicts the good agreement between the experimental results and the numerical model for beams (Fig 3a) and columns (Fig 3b). This calibrated numerical model provided the basis for the extensive parametric study described in the next section.

3. DESIGN RULES FOR HSS MEMBERS

3.1. SCOPE

For the calibration of stability design rules for high strength steel members, a large number (over 11 000) of numerical simulations were performed. The typical modelling assumptions include an idealised material behaviour, initial imperfections according to the lowest global buckling mode and the consideration of residual stresses with f_y = 235 MPa, according to Publication No.33 of ECCS [27]. The parametric study covered a variation in the normalized slenderness from low (0.4) to high (2.5), different steel grades (S460, S500, S690), different cross-sections (47) with flange thicknesses varying from 6 to over 100 mm; and different bending moment distributions for beams and beam-columns. These numerical tests were used to assess the code predictions for the stability resistance and propose improved rules that satisfy the probabilistic safety levels prescribed in the Eurocodes. The new rules were assessed statistically using the EN1990 Annex D procedure. In order to keep consistency with the existing rules in Eurocode 3, the approach was focused on only changing, whenever possible, the current imperfection factors for columns and beams. The proposals are summarized in Table 2.

Table 2 – Proposed buckling curves for HSS

Buckling mode	Limits	Axis	S235 to S420	S460 to S700	γ_{M1}
Flexural buckling	$t_f{\leq}40$ mm	y-y	b	a	1.056
		z-z	c	b	1.036
	$t_f{>}40$ mm	y-y	c	b	0.988
		z-z	d	c	0.977
Lateral-torsional buckling	h/b≤2	-	c	b	0.999
	h/b>2	-	d	c	0.991

Figure 4 shows the scatter plots for major and minor axis flexural buckling using both the current buckling curves and the proposed ones. Table 3 provides statistics of the ratio numerical result over estimated resistance using the current and proposed curves, respectively. It is possible to verify that using the new proposals the design rules are safe-sided, but not unnecessarily over conservative.
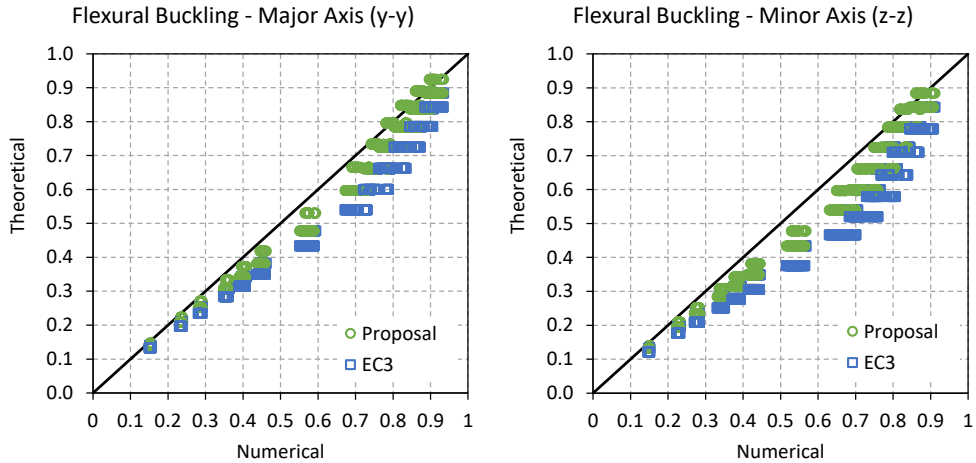
Figure 4 – Scatter plots: flexural buckling

Table 3 – Statistical indicators

Subset	Design rule	n	mean	cov	min	max	>1.1	<0.97
y-y	Proposal	1599	1.090	5.7%	0.965	1.232	674	16
y-y	Current	1599	1.180	6.7%	1.013	1.358	1327	0
z-z	Proposal	1599	1.132	6.4%	0.973	1.303	1086	0
z-z	Current	1599	1.257	8.8%	1.020	1.502	1486	0

For the beams, the same approach was used. In this case it was applied to the General Case and Special Case from the current version of Eurocode 3. For the General case and the newEC3 method it was possible to justify better buckling curves. For the Special Case, the results obtained show that the current curves might be appropriate for the subset of cross-sections with h/b<2, but not for the subsets high ratio higher than 2, where many results were found with higher demand for imperfection. The method has been previously reported as inconsistent [28]-[30] , it will disappear from the revised version of Eurocode 3 and it was not further considered.

Figure 5 shows the scatterplots for the General Case considering the current and proposed imperfection factors. Table 4 summarizes the statistics for the General Case and the newEC3. Similar conclusions to the members in compression can be drawn for members in bending, the new curves provide safe-sided yet not over conservative estimation for the buckling resistance.
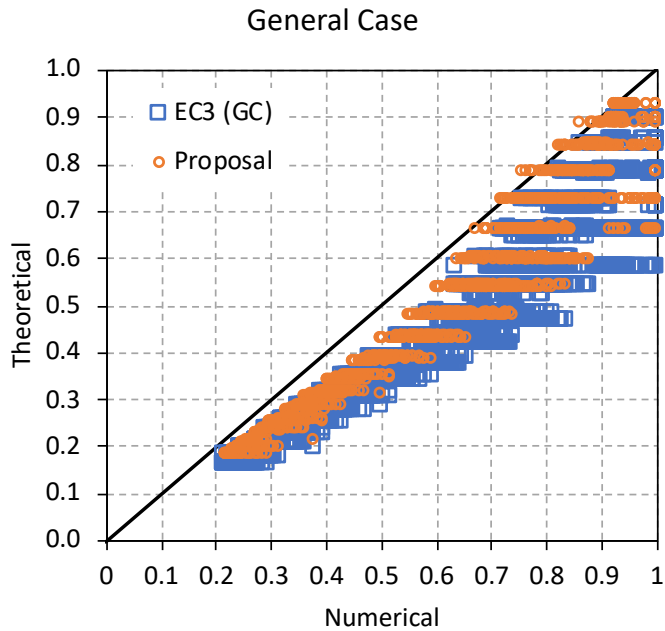
Figure 5 – Scatter plots – lateral-torsional buckling

Table 4 – Statistical parameters (General Case)

Subset	Design rule	n	mean	cov	min	max	>1.1	<0.97
GC	Proposed	4619	1.267	8.3%	0.959	1.811	4251	2
GC	Current	4619	1.405	9.8%	1.024	1.933	4492	0

4. CONCLUSIONS

This paper summarized the assessment of the stability behaviour for HSS members according to Eurocode 3. The research was based on full-scale experimental tests and advanced numerical simulations. The modelling assumptions for the parametric study included residual stresses according to the ECCS recommendations pub. 33.

The parametric study covered different slenderness, steel grade, cross-section dimensions, members under compression and members under bending with different moment distributions.

Based on the results obtained, It was clearly observed that there is increasing safety with the increasing of the steel grade, showing that it is not economical to use the same rules/specifications for high strength steels and normal strength steels. Applying the current rules of Eurocode 3 to high strength steel leads to significant underestimation of the buckling

resistance. On average 20%, in the case of flexural buckling and about 40% in average for lateral-torsional buckling (using the General Case). The special case shows to be inaccurate for some cases and the newEC3 case leads to better results compared to the general case, but still underestimates the buckling resistance.

REFERENCES

[1] EN 10025: 2004 – Hot rolled products of structural steels. CEN, Brussels, 2004.

[2] EN 1090-1, Execution of steel structures and aluminium structures – Part 1: Requirements for conformity assessment of structural components, CEN, Brussels, 2009.

[3] CEN/TC250 (2020), Eurocode 3: Design of steel structures – Part 1-1: General rules and rules for buildings, CEN/TC 250/SC N 2532 – prEN 1993-1-1 – Final draft.

[4] CEN/TC 250/SC 3 N 3080, Report on WG EN 1993-1-12, (2020).

[5] X. Meng, L. Gardner, Flexural buckling of normal and high strength steel CHS columns, Structures 34 (2021) 4364-4375.

[6] L. Schaper, R. Winkler, F. Jörg, U. Kuhlmann, M. Knobloch, Experimental study on LTB behaviour and residual stresses of welded I-section members, Proceedings of the International Colloquia on Stability and Ductility of Steel Structures (2019), September 11-13, Prague, pp. 972-980.

[7] Songzhao Qu, Yonghua Guo, Qing Sun, Resistances of high-strength steel equal-leg-angle section columns eccentrically connected by one leg, Journal of Constructional Steel Research, 191, 2022, 107143.

[8] Songzhao Qu, Bin Zhang, Yonghua Guo, Qing Sun, Yi Wang, Ultimate strength of pinned-end dual-angle cross combined section columns under axial compression, Thin-Walled Structures, 157, 2020, 107062.

[9] Songzhao Qu, Jingyun Wang, Yonghua Guo, Jiping Hao, Xiaochi Yang, Experiment and code-based study on high-strength steel pin-ended angles under axial compression, Thin-Walled Structures, 149, 2020, 106541.

[10] M. Shokouhian, Y. Shi, Flexural strength of hybrid steel I-beams based on slenderness, J. Eng. Struct. 93 (2015) 114-128.

[11] R. Feng, H. Zhan, S. Meng, J. Zhu, Experiments on H-shaped high-strength steel beams with perforated web, J. Eng. Struct. 177 (2018) 374-394.

[12] R. Feng, J. Liu, Z. Chen, K. Roy, B. Chen, J. B. P. Lim, Numerical investigation and design rules for flexural capacities of H-section high-strength steel beams with and without web openings, J. Eng. Struct. 225 (2020) 111278.

[13] Y. Wang, M. A. Brandford, X. Liu, Strength design of welded high-strength steel beams considering coupled local and global buckling, Thin-Walled Struct. 149 (2020) 106391.

[14] T. Le, M. A. Bradford, X. Liu, H. R. Valipour, Buckling of welded high-strength steel I-beams, J. Constr. Steel Res. 168 (2020) 105938.

[15] X. L. Yan, G. Q. Li, Y. B. Wang, J. Jiang, Experimental and numerical investigation on flexural-torsional buckling of Q460 steel beams, J. Constr. Steel Res. 174 (2020) 106276.

[16] K Wang, M. Xiao, K. F. Chung, D. A. Nethercot, Lateral torsional buckling of partially restrained beams of high strength S690 welded I-sections, J. Constr. Steel Res. 184 (2021) 106777.

[17] G. Xiong, Y. Feng, Q. Peng, S. B. Kang, Y. Zhang, Y. L. Fan, Lateral-torsional buckling behaviour of 690 MPa high strength steel beams, Structures 33 (2021) 3999-4010.

[18] T. Tankova, F. Rodrigues, C. Leitão, C. Martins, L. Simões da Silva, Lateral-torsional buckling of high strength steel beams: Experimental resistance, Thin-Walled Struct. 164 (2021) 107913.

[19] Tankova, T., Simões da Silva, L., Rodrigues, D., Balukrishnam, M., Pasternak, H., Launert, B., Tun, T.Y., (2019). "Residual stresses in welded I-section", *Engineering Structures*, **197**, 109398.

[20] Tankova, T., Schaper, L, Knobloch, M, Simões da Silva, L., (2022). "Residual stresses for HSS I-section members", Journal *of Constructional Steel Research*, 188, 107017

[21] EN 1990, Eurocode – Basis of structural design, CEN, Brussels, 2002.

[22] Tankova, T, Simões da Silva, L., Marques, L., Rebelo, C. and Taras, A., (2014). "Towards a standardized procedure for the safety assessment of stability design rules", *Journal of Constructional Steel Research*, **103**, 290-302

[23] Tankova T., Rodrigues F., Simões da Silva L. (2022). *Buckling curve selection for high strength steel members.* Thin-walled structures.

[24] Spoorenberg R.C., Snijder H.H., Hoenderkamp J.C.D. (2010). Experimental investigation of residual stresses in roller bent wide flange steel sections. In: Journal of Constructional Steel Research, Vol. 66, pp. 737-747.

[25] Tebedge N, Alpsten G., Tall L, (1973). Residual-stress Measurement by the sectioning Method. Experimental mechanics, 88-96.

[26] Simulia, ABAQUS 6.21

[27] ECCS (1984). Ultimate Limit State Calculation of Sway Frames with Rigid Joints, Publication No.33 Brussels.

[28] Rebelo C, Lopes N., Simões da Silva L., Nethercot D., Vila Real P.M.M. (2009). Statistical Evaluation of the Lateral-Torsional Buckling Resistance of Steel I-beams, Part 1: Variability of the Eurocode 3 resistance model, In: Journal of Constructional Steel Research., Elsevier, 2009, 65, pp. 818-831.

[29] Snijder H.H., Hoenderkamp J.C.D. (2007). Buckling curves for lateral torsional buckling of unrestrained beams, Rene Maquoi 65th birthday anniversary, 2007, Liège Belguim.

[30] Simões da Silva L., Tankova T., Marques L, Rebelo C., Taras A. (2019). Safety assessment of Eurocode 3 stability design rules for the lateral-torsional buckling of beams, In: Advanced Steel Construction – an International Journal, 14.

Miguel Fernández Ruiz[1]

NAUKA I INŽENJERSTVO – POSMATRANJE I GRAĐENJE

Rezime:

Inženjerstvo je delikatna umetnost na granici između posmatranja i građenja. Neophodno je precizno predvideti odgovor konstrukcije kako bi se moglo opisati ponašanje iste tokom izvođenja građevinskih radova. Sam proces je zasnovan na naučnim osnovama i metodama. Međutim, inženjerstvo nije samo šturo opisivanje ponašanja konstrukcija koje je zasnovano na naučnim principima. U praksi uvek postoji više od jednog rešenja, ali projektant treba da na osnovu svog iskustva i znanja proceni i izabere najbolje moguće rešenje koje će optimizovati konstrukciju. Inženjerstvo je aktivan proces u kome je neophodno donositi odluke i na taj način stvarati i graditi naše okruženje. U okviru ovog rada, prikazan je značaj primene nauke i njenih metoda u toku konceptualnog projektovanja konstrukcija sa osvrtom na niz tema, od projektovanja konstrukcija i procene ponašanja do holističke perspektive koja uključuje i koncept održivosti.

Ključne reči: projektovanje, inženjering, nauka, konstrukcije, održivost

SCIENCE AND ENGINEERING – OBSERVATION AND MAKING

Summary:

Engineering is a delicate art, at the crossing between observation and making. Precise observation and prediction of the response of a system is required to describe the physical reality of civil works. This is performed based on science and following the scientific method. However, engineering is not only a passive description of nature based on science. There is never one single possible solution, but the designer has to actively search and decide for the best solution optimizing the response of a system and reflecting his or her creativity and experience during this process. Engineering is thus an active attitude to decide and to make, changing our built reality. In this paper, the significance of the scientific consistency and its tools in the conceptual design phase is discussed with reference to a number of topics, ranging from structural design and assessment to a holistic perspective incorporating the concepts of sustainability.

Key words: design, engineering, science, structures, sustainability

---
[1] *Professor, Universidad Politécnica de Madrid, Madrid, Spain, miguel.fernandezruiz@upm.es*

1. INTRODUCTION

The culture of engineering has been very much linked to the development and use of tools for decision-making. Such tools are to be used together with engineering judgement and sensitivity as well as clear ethic principles. Ethics, as defined by Larry Churchill [1] refers to:

> "*the capacity to think critically about moral values and direct our actions in terms of such values*".

The ethical dimension of our acts will thus influence our interaction with society and will define our aesthetics. In structural engineering too, the aesthetics (formal appearance of our works) will be dictated by our personal and professional ethics. It is thus instrumental to have clear ethical principles before performing a design and then to have sound tools to develop a project accordingly. As it can be noted, the contrary –the use of sophisticated tools without a clear idea of what do we need– will not necessarily lead to any satisfactory result.

During long time, the ethical principles of engineering have been oriented towards serving to society in an efficient manner, trying to minimise the resources used and to build useful infrastructure and buildings. Such principles, which have been a valid approach and helped improving our society during decades, shall not be forgotten. Moreover, our awareness of environmental issues shall strengthen the ethics of our work, by incorporating the environmental perspective into our guiding principles (together with the social and economic considerations).

In order to develop a project on the basis of clear principles, an engineer also requires sound theories satisfactorily describing the response of systems. In structural engineering in particular, one needs theories that provide freedom to decide on the structural functioning of a system. From most of theories currently used for design, it is notable the introduction of the plastic analysis in structural project. This theory (also known as limit analysis) provides an enhanced freedom to select the load-carrying actions of a structure and has pushed engineers to design and to build in a ductile and robust manner.

In this paper, a review of the significance of the previous concepts is presented, from the capacity of design tools to allow taking decisions, to the evolution of engineering principles towards a sustainability perspective.

2. TOOLS FOR DESIGN AND ANALYSIS

One of the fundamental questions that an engineer has to face to characterize a system is the analysis of its internal forces. Such fundamental step is in many cases performed in a routine manner, following our education and previous experiences and without a critical thought on its implications. It is however, one of the moments of divergence in the project, and the fundamental differences amongst different approaches shall be highlighted.

2.1. LINEAR-ELASTIC RESPONSE

The theory of elasticity was ground on the pioneer works of Hooke (1678) [2], focusing on the uniaxial and bending response of beams. Such works triggered later the development of a school of thought during the XVII-XIX centuries in Europe (Bernoulli, Young, Navier, Poisson, Cauchy, Lamé, Saint-Venant… a detailed review can be consulted in Todhunter and Pearson [3]). Currently, the theory of elasticity is a complete body of knowledge allowing to analyse the

response of structures under multiple situations [4]. Its fundamental assumption refers to the linear relationship between stresses and strains (or between an internal force and its corresponding generalized displacement, see Figures 1a,b).
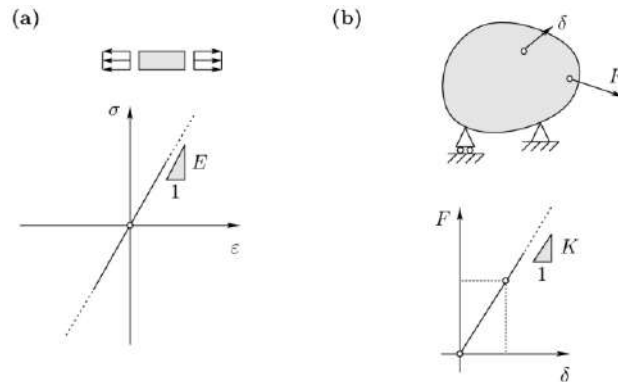
Figure 1 – Elastic response: (a) uniaxial material response; and (b) structural response

The theory of linear elasticity can be formulated by means of equilibrium and compatibility conditions, providing a sufficient number of relationships (equations) to solve the degrees of freedom (unknowns), both in terms of generalized displacements and internal forces. Its main assumption refers to the linear stress-strain relationship adopted for the material response (Figure 1a), as well as to neglecting any potential second-order effect, allowing to assume that superposition of actions is applicable. It can be noted that the elastic solution is unique for a system, which yields to the philosophy that "*every problem has one single solution*". In fact one needs to suitably define the structural system and, if the hypotheses of elasticity apply, the "correct and unique" field of internal forces shall be directly obtained.

In fact, the theory of elasticity is merely providing a solution fulfilling equilibrium and where some conditions associated to compatibility of deformations are satisfied. However, an engineer shall be aware that elastic solutions cannot pretend to be any exact approximation to reality. This is particularly important when one considers the deviation from a linear response of real construction materials (namely near failure) and the inaccuracies of the structural model (stiffness of connections, settlements, internal and external deformations of materials, self-stresses…). This is a key aspect to understand and to value the information obtained. Considered in this way (one possible solution satisfying equilibrium and incorporating conditions on the compatibility of deformations), the elastic solution might be interesting to perform a safe design at failure (as it will later be shown in the plastic response) with a reasonable expected response under serviceability conditions. Also, the theory is particularly useful to estimate deflections, although this may require adopting specific considerations.

Despite the qualities of this theory, it is however to be noted that providing one unique solution for a given case (the main strength of the theory of elasticity), is also its main limitation. This is due to the fact that this approach does not allow the engineer to take decisions on the structural response or to tailor the main load-carrying actions [5].

2.2. PLASTIC RESPONSE

When our predecessors in structural engineering analysed the results of the theory of elasticity, they found that in fact it was significantly differing from the actual behaviour of structures near failure. One of the first to point this was Kazinczy in Hungary in 1914 [6] while testing the influence of the degree of clamping of steel-embedded profiles (as reported in [7], see Figure 2a). Kazinczy observed that, at failure, the bending moments in the beam were not depending on the degree of clamping exhibited at low levels of load, but they were a function of the resistance of the sections, and that three "kinks" or "hinges" were required to develop failure (introducing the concept later named as plastic hinge, see Figure 2a).
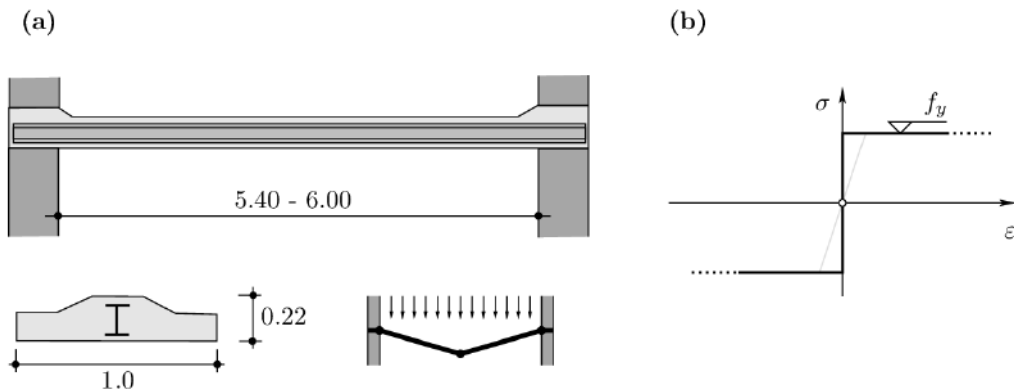
Figure 2 – Plastic response of structures: (a) Kazinczy tests (dimensions in [m] and observed failure mode); and (b) material response (rigid-plastic and elastic-plastic)

In Denmark, works were also performed on the design and verification of slabs in reinforced concrete. This was one of the fields where most difficulties were found to apply elastic design methods to obtain the bending and torsional moments (particularly for non-regular geometries) motivated by the high internal redundancy of the system. In this field, first Ingerslev in 1921 [8] and later K.W. Johansen in 1943 [9] developed an original approach based on the consideration of "failure lines" (later renamed as yield lines). It consisted on the definition of a pattern of yield lines compatible with a failure mechanism, whose failure load could be calculated on the basis of equilibrium considerations. Although at that time the theory was not relying on plasticity (a connection later established in 1964 by M.P. Nielsen [10], a scholar from Johansen) it clearly showed that failure of reinforced concrete plates was attained with a very different condition than the one established by the theory of elasticity.

These two instances, showing the inconsistencies between the well-established elastic theory and the reality at failure, allowed the engineers to question the pertinence of classical design tools as the theory of elasticity. This consideration, connected to a series of previous works on failure mechanisms for geotechnical application (Coulomb [11]) allowed in the first half of the XXth century to develop the theory of plasticity (or limit analysis, see a detailed review on Nielsen and Hoang [12]). In this theory, the materials are assumed to have low or none deformations until a certain stress state is reached (see Figure 2b). At that moment, the material may freely deform. Such response has no unique response in terms of the associated deformation for a given stress state, loosing unicity (formulations are thus normally established in terms of

strain increments). The theory was based on a number of assumptions and theorems, whose three fundamentals are highlighted below:

- Lower-bound theorem: The lower-bound theorem of plasticity establishes that every internal state of stresses equilibrating the external actions and respecting the yield condition of the materials is a lower-bound of the actual failure load.
- Upper-bound theorem: The upper-bound theorem of plasticity establishes that every state of actions leading to an admissible collapse mechanism is an upper-bound of the failure load (which can also be formulated in terms of energetic concepts).
- Theorem of unicity: This theorem states that there is one single stress field in equilibrium with the acting loads and compatible with an admissible failure mechanism (with plastic regions developing where the yield conditions are met). The associated failure load corresponds to the unique and exact solution according to limit analysis, being simultaneously and upper- and a lower-bound (theorem applicable under normality conditions of the strain increments with respect to the yield surface)

These theorems are in fact very important, not only to calculate the failure load of a system, but particularly to understand a suitable approach to design and to assess the resistance of a structure, as it will later be discussed. In particular, the lower-bound theorem is of great relevance for design as the loss of a unique solution allows the engineer to decide on the most suitable load-carrying actions for a structure. The upper-bound theorem will on the contrary be relevant for verification of existing structures, when a failure load is to be determined.

3. BRITTLE AND DUCTILE RESPONSES

An interesting fact of the design based on the theory of plasticity is that it requires having a ductile response of materials (Figure 2b) and of the system. This is in fact an interesting condition, as imposing a structure to behave in a ductile manner has a number of advantages in terms of robustness.

Concerning the material response, steel has a response which is well represented by a plastic resistance (where the elastic regime, Figure 2b can also be accounted for). Concrete has however a more complex response. It is brittle in tension and has a softening response in compression. Thus, for analyses based on the theory of plasticity (such as strut-and-tie-models or even simple analyses of the resistance of columns, refer to FprEN1992-1-1:2022 [13]) the tensile strength is neglected and the peak strength in compression has to be reduced to an equivalent plastic plateau:

$$f_{cp} = f_c \cdot \eta_{fc} \tag{1}$$

Where η_{fc} refers to the brittleness factor ($\eta_{fc} = min\ (1, (30/f_c\ [MPa])^{1/3}$), see for instance Muttoni [14]). In addition, other structural effects such as the influence of transverse cracking on the concrete resistance have to be considered by means of specific strength reduction factors [15,16].
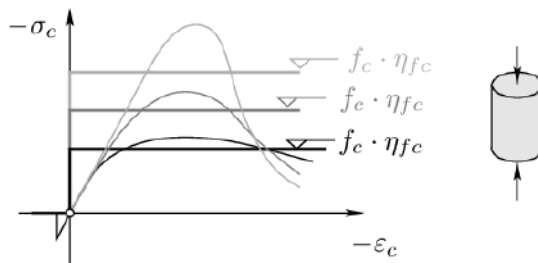
Figure 3 – Idealized plastic response for concrete

As the ductile behaviour allows to maintain the level of stress in the elements for any arbitrary increase of strain, redistributions of stresses can freely occur. This allows dissipating any state of internally self-equilibrated strains present before application of the collapse load. Thus, the resistance of a plastic system becomes independent of such internal self-stresses (only influencing the path to reach to the plastic resistance, but not its value).

With respect to brittle failure modes, they refer to cases where the load-carrying capacity reduces significantly for increasing levels of deformation. This does not allow for redistribution of stresses or to maintain the level of applied load for any arbitrary increase of displacement. Brittle failures are typically those associated to strain localization, as the unstable propagation of cracks in concrete. Also, bifurcation or second order effects are typical cases of brittle failure modes with limited or none ductility. In these cases, the theory of plasticity cannot be applied and the internal forces in the element are governed by the loading history and stiffnesses (with nonlinear or elastic analyses being a reasonable approach). The main difficulty when designing a brittle system is in fact not the accuracy of the model, but the uncertainty on the initial state of stresses and stiffnesses that may lead to premature failure of the system. To avoid this, brittle failure modes shall be prevented if possible (for instance arranging sufficient reinforcement for crack control and to avoid crack localization). Also, for very sensitive and brittle systems, statically-determinate conditions are advised to remove internal (parasitic) forces and to better control thus the resistance. Alternatively, when the brittle response cannot be avoided nor the internal redundancy, detailed analyses of the internal forces shall be performed or at least adopting realistic ratios of the stiffnesses, which might be sufficient to ensure the level of reliability [17,18].

4. DESIGN AND ASSESSMENT

Following the previous concepts, it is quite evident that a plastic response (or at least with sufficient deformation capacity) is desirable to provide the engineer with sufficient freedom to design a structure or to assess the resistance of an existing one without having to know its precise loading history.

4.1. CONSIDERATIONS FOR DESIGN

Design of a new structure requires identifying its main load-carrying actions and defining the amount of load carried by each one. To that aim, the use of lower-bounds is a suitable tool. The engineer has to select one possible state of internal forces in equilibrium with the external actions and then design the resistances accordingly. This is for instance shown in Figure 4 with reference

to the case of a slab. For its design, the strip method is used, neglecting the torsional moment field and allowing thus to define in a simple manner the amounts of load carried in each direction.
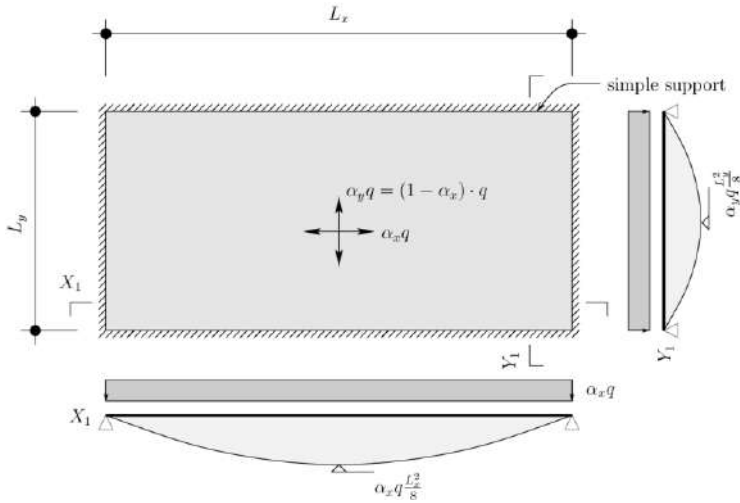
Figure 4 – Design of a new structure using a lower-bound, example of a slab

The engineer has thus complete freedom to select the most suitable transfer of forces, provided that equilibrium is ensured (i.e. $\alpha_x + \alpha_y = 1$) and that at least the minimum amount of reinforcement is arranged in the slab to control cracking. For instance, equalling the maximum bending moment in the two directions (same required thickness of plate or amount of reinforcement), it results:

$$\alpha_x = \frac{1}{1+\left(\frac{L_x}{L_y}\right)^2} \tag{2}$$

Obviously, other criteria may apply and assist in defining the field of internal moments, particularly with respect to the expected response under serviceability conditions (for instance, imposing a comparable maximum deflection for the investigated strips [5]). Also, any estimate based on experience is also admissible. It shall be yet noted that in the strip method, as the torsional field is not accounted for, excessively safe estimates of the strength may result. It can thus be preferred to use more general moment fields [5] to select a more suitable combination of bending and torsional components. Finally, in order to ensure the conditions of a lower-bound, the resistances of the slab shall be designed accordingly to the selected moment field.

As it can be noted, the elastic field of internal forces for a given set of actions is one possible solution to be used as lower-bound, since it satisfies the equilibrium conditions. Such elastic solution considers both flexural and torsional moment fields and can be determined automatically in a unique manner. Once the bending and torsional fields are established on this basis, again, the resistances can be designed accordingly to ensure that the conditions of a lower-bound are respected. This approach has the advantage of being automatic, but has the limitation that the engineer cannot decide on how the structure carries the loads.

4.2. CONSIDERATIONS FOR ASSESSMENT

The assessment of existing structures requires a different sensitivity than the design of structures. In this case, it does not refer to the search for a safe solution, but to the answer to two different questions:

- Is the structure safe enough to carry the design actions?; or
- Is the structure unsafe for the design actions? and, in this case, what could be the maximum admissible load?

With respect to the first question, it can be addressed with the investigation of a suitable lower-bound (Figure 4). As for the cases previously explained, if one can find a state of internal forces in equilibrium with the external actions, such that the yield conditions of the materials are respected, the structure will carry such load or a higher one.

When no lower-bound strength can be found satisfying the actions, one may think that the structure may perhaps not have sufficient resistance for the actions. Demonstration of this fact (proof that the structure needs strengthening or a reduction in the acting loads for instance) requires however to find an upper-bound solution and cannot be theoretically performed only with lower-bounds. I.e. if one can find an admissible collapse mechanism whose strength is lower than the applied actions, the structure will require an intervention or load reduction.

These two aspects, design and assessment, require thus a different approach by the engineer. As shown in Figure 5, for design, lower-bounds open the possibility to actively define the way in which loads are carried. This is closely connected to the engineering philosophy of decision. For assessment, on the contrary, the engineer is acting like a scientist, analysing the maximum load that can be carried by a structure, without taking decisions on it.

$$
\text{verification} \begin{cases} \text{sufficient strength} \implies \begin{array}{l} \text{lower-bound} \\ Q_R \geq Q_E \end{array} \\ \\ \text{insufficient strength} \begin{cases} \begin{array}{l} \text{upper-bound} \\ Q_R \leq Q_E \end{array} \implies \text{strengthening} \\ \\ \begin{array}{l} \text{exact solution} \\ Q_R = Q_E \end{array} \implies \text{failure load} \end{cases} \end{cases}
$$
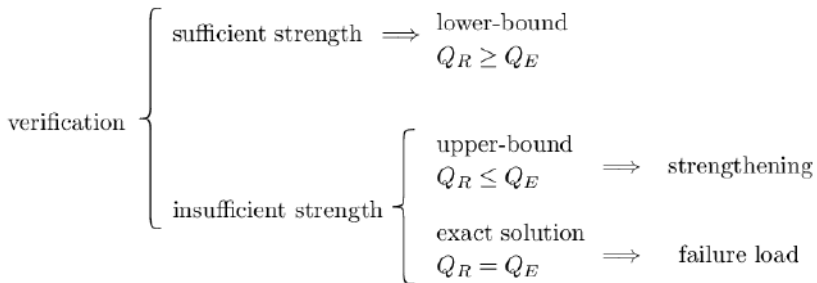
Figure 5 – Strategies for assessment and use of theorems of limit analysis

It can be noted that the information on whether a structure may require strengthening or load-limitation is not always sufficient for the owner, requiring to give accurate levels for it. Such value can be safely estimated by optimization of a lower-bound. In fact, the best lower-bound that can be found refers to the exact solution according to theory of plasticity, whose failure load satisfies both the conditions for an upper- and for a lower-bound (Figure 5). In many cases, the precise assessment of the failure load by means of an exact solution requires an iterative analysis, typically involving a computer-aided analysis.

5. HOLISTIC DESIGN – THE PERSPECTIVE OF SUSTAINABILITY

Following the necessity of engineers to take decisions for a project, it has been shown how the theory of plasticity is an excellent tool that can be consistently used to tailor a structure and

to decide on its basic load-carrying actions. However, not only consistent tools are required for the conceptual design of our structures, but the whole process shall be performed from a broader (holistic) perspective, incorporating the concept of sustainability.

Sustainability shall be a complete sensitivity of the engineer when approaching a project. It is based on the consideration and search for the best solution to preserve as much resources as possible and to help developing the communities within this process. It stands thus on three pillars [19,20]: social, economic and environmental considerations. It is important to state that sustainability is not only a matter of counting and comparing production of CO_2 associated to a given activity, but to look for a solution which globally serves to the community for a specific task, is efficient in terms of cost and helps potentially the development of the community during its production. With this respect, it is interesting to note that there is not a magical formula or weighted criteria leading to "*the*" sustainable solution for a given project. On the contrary, several criteria are to be defined, discussed and, on that basis, the more reasonable solution selected.
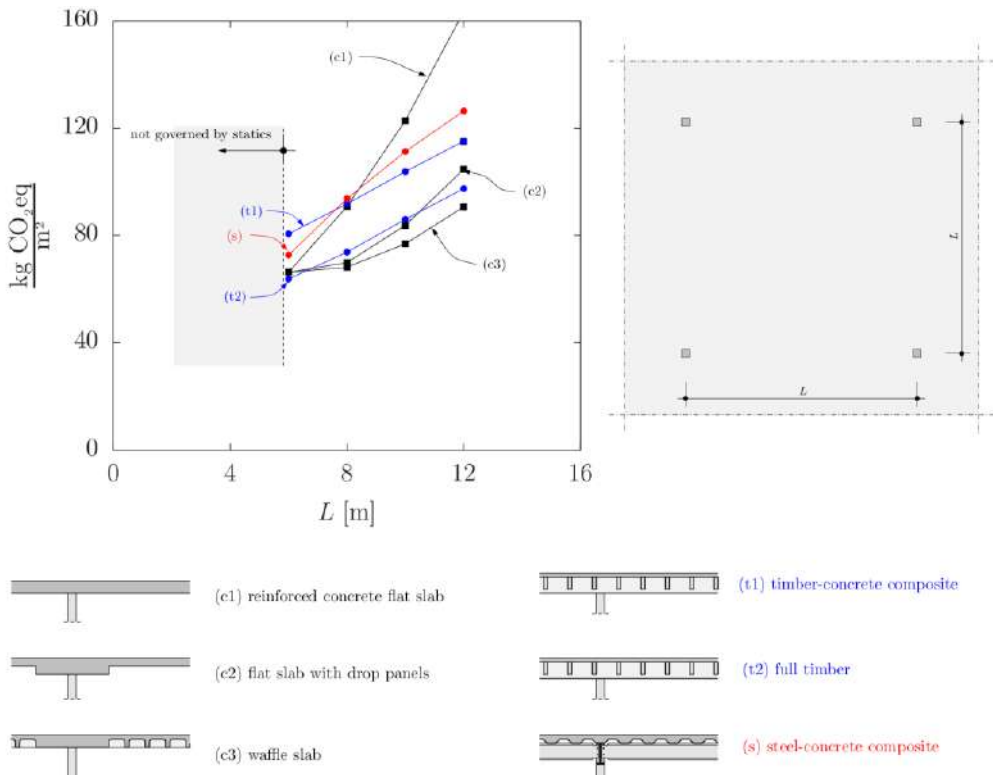
Figure 6 – Analysis of CO2-eq per unit of built surface for different structural solutions (adapted from [21])

The perspective of sustainability is also changing the perception of what is the correct conceptual design of a structure. For instance, Figure 6 shows one of the indicators of sustainability (CO_2-eq production) for the case study of a building [21] where different structural solutions and construction materials are investigated. Small spans might be more representative

of old approaches for construction, while there is a trend in the last decades of increasing span lengths. Although such increase of spans might make sense in terms of potential flexibility and reuse of a building, it is clearly a solution which is not aligned with environmental considerations or cost-efficiency considerations. This is justified by the fact that the associated production of CO_2-eq (sum of all green-house related emissions in terms of equivalent CO_2 gases) severely increases as the span does. This calls for the role of the engineer to communicate such implication during the conceptual design phase.

Another interesting conclusion from the same analysis refers to the fact that one can find various structural solutions in different materials, such as timber, concrete or steel, which may have an equal efficiency in terms of CO_2-eq production. This result, which seems not to be suitably communicated by engineers, has given rise to the perception that concrete solutions are poor approaches for a sustainable development [22]. This is however a superficial conclusion that can be rejected with scientific arguments. Concrete is in itself a material whose environmental footprint is comparable to the others, but whose use is dominant (second most-consumed material on Earth after water [23]).

Every solution might thus be appropriate to satisfy the objectives of sustainability provided that it is structurally efficient and that its materials have been suitably selected. It is thus a question of efficiency and not of materiality, as well as of consideration of local conditions. For instance, as it can be seen in Figure 6, a flat slab in concrete might be highly inefficient for long spans while it can be suitable for small spans.

6. CONCLUSIONS

This paper has presented the importance of decision-making tools for engineers. Such need has been observed by our predecessors and allowed to successfully incorporate tools enhancing our freedom and creativity for design, as the theory of plasticity. Such approach has also generated a culture to build in a ductile and robust manner, allowing for stress redistributions and giving freedom to the designer to establish the basic load-carrying actions for a structure.

Such culture of decision and empowering the engineers during the conceptual design phase shall continue in the coming years. With that respect, not only the concepts related to the structural design itself must be considered, but also sustainability aspects, such as the efficiency of the solutions selected (low consumption of respectful building materials), their competitive cost and the synergies with local communities.

REFERENCES

[1] *Churchill, L.R., Are We Professionals? A Critical Look at the Social Role of Bioethicists. Daedalus, 128(4), 1999. pp. 253–274.*

[2] Hooke, R., Lectures De Potentia Restitutiva or of spring explaining the power of springing bodies, the United Kingdom, John Martyn, printer to the Royal Society at the Bell in St-Paul's Church-Yard. 1678, 24 p.

[3] Todhunter, I. and Pearson. K., A history of the theory of elasticity and of the strength of materials, from Galilei to the present time, Cambridge University Press. 1886, 924 p.

[4] Timoshenko, S. and Goodier, J.N. Theory of elasticity, Mc-Graw Hill, 1951, 506 p.

[5] Fernández Ruiz, M., Estática y rotura de estructuras: Lógica, herramientas y actitudes para el pensamiento resistente, UPM Press, ISBN-10: 8418661151, ISBN-13: 978-8418661150, 1st ed., Madrid, Spain, 2022, 200 p.

[6] Kazinczy, G., Test with clamped beams, Betonszemle, Vol. 2, pp. 68-71, 83-87, 101-104

[7] Kaliszky, S., Sajtos, I., Lógó, B.A., Lógó, J. M., Szabó, Z., Gábor Kazinczy and his legacy in structural engineering, Periodica Polytechnica Civil Engineering, 59(1), 2015, pp. 3–7 (doi: 10.3311/PPci.8016)

[8] Ingerslev, Å., Om en elementær beregningsmetode af krydsarmerede plader. Ingeniøren, 30(69). Denmark, 1921, pp. 507-515.

[9] Johansen, K.W. Brudlinieteorier, Denmark, I kommission hos J. Gjellerup, 1943, 189 p.

[10] Nielsen, M.P., Limit Analysis of Reinforced Concrete Slabs, Acta Polytechnica Scandinavica, Civil Engineering and Building Construction Series, No 26, 1964, 167 p.

[11] Coulomb, C.A., Essai sur une application des règles de maximis et minimis à quelques problèmes de statique, relatifs à l'architecture, Mémoires de Mathématique et de Physique présentés a l'Académie Royale des Sciences, Volume 7, 1776, pp. 343-382

[12] Nielsen, M.P. and Hoang, L.C., Limit analysis and concrete plasticity, 3rd edition, CRC Press, Boca Raton, 2011, 788 p.

[13] CEN, FprEN_1992-1-1_2022-05-29 for Adoption for Formal Vote, Eurocode 2: Design of concrete structures, CEN/TC 250/SC 2, 2022.05.30, 408 p.

[14] Muttoni, A., Die Andwendbarkeit der Plastizitätstheorie in der Bemessung von Stahlbeton, PhD thesis, ETH, Zürich, 1991, 164 p.

[15] Vecchio F. J., Collins M. P., The Modified Compression-Field theory for Reinforced Concrete Elements Subjected to Shear, ACI Journal Proceedings, Vol. 83, No. 2, 1986, pp. 219-231

[16] Kostić N., Topologie des champs de contraintes pour le dimensionnement des structures en béton armé, Thèse EPFL, n°4414, Lausanne, 2009, 235 p.

[17] Valeri, P., Guaita, P., Baur, R., Fernández Ruiz, M., Fernández-Ordóñez Hernández, D.C., Muttoni, A., Textile Reinforced Concrete for sustainable structures: future perspectives and application to a prototype pavilion, Structural Concrete, Wiley, 2020, pp. 1-17 (doi.org/10.1002/suco.201900511)

[18] Yu, Q., Valeri, P., Fernández Ruiz, M., Muttoni, A., A consistent safety format and design approach for brittle systems and application to Textile Reinforced Concrete structures, Engineering Structures, Elsevier, Vol. 249, 113306, 2021, pp. 1-20 (doi.org/10.1016/j.engstruct.2021.113306)

[19] World Commission on Environment and Development. Our Common Future. Oxford University Press; 1987. 383 p.

[20] Fédération internationale du béton, Integrated life cycle assessment of concrete structures, Fédération internationale du béton, Bulletin 71, 2013. 64 p.

[21] Regulez Pérez, B., Faria, D.V., Todisco, L., Fernández Ruiz, M., Corres Peiretti, H., Sustainability in construction: the urgent need for a new ethics, Structural Concrete, Wiley, submited for publication

[22] The Guardian. Concrete: the most destructive material on Earth. 2019 https://www.theguardian.com/cities/2019/feb/25/concrete-the-most-destructive-material-on-earth

[23] United Nations Environment Programme. Eco-efficient cements: Potential economically viable solutions for a low-CO2 cement-based materials industry. UN, 2017, 64 p.

Viktor Markelj[1]

ŽELEZNIČKI VIJADUKT PESNICA – OD IDEJE DO IZGRADNJE

Rezime:

Direkcija za infrastrukturu RS obnavlja železničku prugu Maribor – Šentilj, na kojoj se gradi novi vijadukt Pesnica, koji prelazi preko poplavne doline reke Pesnica. Vijadukt ide paralelno sa postojećim nasipom, koji sadrži ostatke nekadašnjeg najdužeg vijadukta južne pruge Beč - Trst iz 1846. godine.

Dvokolosečni vijadukt sa dužinom od 912,60 m je najduži železnički vijadukt u Sloveniji. Preko njega prolazi kolosek na krutoj podlozi sa beskonačnim zavarenim kolosekom bez dilatacija šina. Pored zanimljive istorije, novi vijadukt ima i inovativan tehnički koncept kao integralna konstrukcija bez ležišta. Koncept se takođe pokazao kao veoma ekonomično rešenje.

Projektant vijadukta je inženjerski biro Ponting d.o.o., a izvođač radova Pomgrad d.d.

Ključne reči: železnica, vijadukt, prednapregnuti beton, integralna konstrukcija, kolosek na krutoj podlozi

THE PESNICA RAILWAY VIADUCT - FROM CONCEPT TO CONSTRUCTION

Summary:

The Slovenian Infrastructure Agency has been renovating the Maribor-Šentilj railway line, which also includes the construction of the new Pesnica viaduct traversing the flood-prone valley of the Pesnica River. The viaduct is being constructed parallel to the existing dyke containing the remnants of the once longest viaduct of the Vienna-Trieste Austrian Southern Railway, dating back to 1846.

The 912.60-metre-long double-track viaduct is the longest railway viaduct in Slovenia. A slab track featuring a continuous welded rail without track dilatation structures is laid across it. In addition to its interesting history, the new viaduct also boasts an innovative technical design, conceived as an integral structure without structural bearings. This concept has also turned out to be a very economical solution.

The viaduct has been designed by the Ponting d.o.o. engineering firm, and the works are being carried out by Pomgrad d.d.

Key words: railway, viaduct, pre-stressed concrete, integral construction, slab track

---

1 PhD, Managing Director at PONTING d.o.o., Maribor, Slovenija, viktor.markelj@ponting.si,
Lecturer at University of Maribor, Faculty of Civil Engineering, Transportation Engineering and Architecture

1. INTRODUCTION

In Slovenia, only smaller bridge structures forming part of grade-separated interchanges, or renovations of existing railway bridges and no larger railway bridge structures, have been constructed thus far. Recently, however, the construction of four larger railway bridges, namely three single-track viaducts on the Divača-Koper second track (the Glinščica, Gabrovica and Vinjan viaducts) and one double-track viaduct (Pesnica on the Maribor-Šentilj railway line – also the longest one), has begun.

Table 1 – Basic project information

Investor/Client	Republic of Slovenia, Slovenian Infrastructure Agency (DRSI)
Project	"The construction of the Maribor-Šentilj-state border from km 595 + 870 to km 599 + 600, central railway station no. 30 Zidani Most- Šentilj-state border"
Consortium	JV Pomgrad d.d., Kolektor Koling d.o.o., SŽ-ŽGP Ljubljana d.d., GH-Holding d.o.o., Gorenjska gradbena družba d.d.
Bridge	PESNICA railway viaduct
Viaduct Contractor	POMGRAD d.d., Murska Sobota
Designer	Inženirski biro PONTING d.o.o., Maribor, design [1]
Engineer	DRI upravljanje investicij d.o.o., Ljubljana

The new railway line section is laid next to the existing Vienna-Trieste railway line, which has a particularly interesting history. The existing single-track line is laid along a dyke on which a 649-metre-long viaduct, the then longest viaduct on the so-called Austrian Southern Railway (Figure 1), was originally constructed in 1846. Constructed under the direction of the Austrian engineer Carl von Ghega, the viaduct included 64 stone and brick vaults and was laid upon wooden pile foundations. The viaduct is said to have begun to decay on account of subsidence and the use of low-quality bricks. After 1860, filling-in began. With the exception of essential spans, it was filled in its entirety [2].

Figure 1 – The former railway viaduct over the Pesnica River Valley dated 1846; left: artistic representation; right: section of the longitudinal profile plan

The dyke, along which the existing single-track line has been laid, is about 15 metres high and has been experiencing stability issues – dyke drifts and rehabilitations – and there have also

been issues with the old tunnel. For this reason, the Client has selected a completely new line layout in this section.

The entire project encompasses 3.73 km of a double-track railway line, out of which 1530 m are in a railway tunnel and 900 m are on the viaduct. The contractual value including the track superstructure (slab track, catenary, signalling and safety devices) at the contractor tender in 2019 amounted to €101m including VAT. Out of this amount, viaduct construction works excluding track systems and the catenary amounted to approximately €12m.

2. DESIGN CONDITIONS

2.1. PURPOSE OF THE VIADUCT AND LOCATION DESCRIPTION

The 18-metre-high railway line bridges the sometimes flood-prone valley and plain, formed by the Pesnica River (Figure 2). Approximately 1 km wide, the entire valley is an agricultural area, used as fields, and located at an altitude of between 250 m and 260 m. The ground has a low bearing capacity and consists of clay silty earth of various kneading levels, from viscous and loose consistency to dense consistency. It also includes fine sand of various compositions, from extremely loose to slightly dense. Groundwater can appear reaching almost to the top. The marlstone bearing layer is located at a depth of 16 m. At the edges of the valley, the bearing base rises to 4 m below the surface.

The viaduct is intended for the electrified double-track railway line to be constructed as a single-track railway line during phase one. The design speed of the train is 120 km/h, and the load-bearing capacity category is D4. In addition to the agricultural valley, the viaduct crosses the A1 Ljubljana-Šentilj highway, the Pesnica-Lenart main road, the Pesnica River, the Cirknica tributary and local roads.

Figure 2 – The existing railway line on the dyke and the new route

2.2. GEOMETRICAL ELEMENTS OF THE RAILWAY LINE AND BRIDGE

The viaduct is just over 900 m long, out of which 380 m of its axis is located in a straight line, 145 m in transition curve and in a R = 850 m radius (380 m long); the elevation of the external track within the radius amounts to 120 mm. The continuously falling gradient of the railway line amounts to i = 9.125‰. On account of the vicinity of the Pesnica railway station, the track spacing on the viaduct varies, from 4.20 m at the beginning to 4.60 m at the end of the viaduct. On technological grounds, the viaduct is of a constant width.

There is a corridor on each side of the viaduct which will be used for any passenger evacuation and auditing purposes. The corridor is 1.73 m wide. At the foundation of the catenary, its local gauge amounts to 1.18 m, allowing installation of an inspection car. The total width of the viaduct amounts to 14.36 m (Table 2 and Figure 3)

Table 2 – Composition of the bridge traffic profile

2x PHO railing installation area	2 x 0.35	0.70 m
2x corridor (including the foundation of the catenary)	2 x 1.73	3.46 m
2x chute (light, open, 30/40cm)	2 x 0.60	1.20 m
Space for a double track	2.20 + 4.60 + 2.20	9.00 m
Total gauge of the viaduct	2.68 + 9.00 + 2.68	**14.36 m**
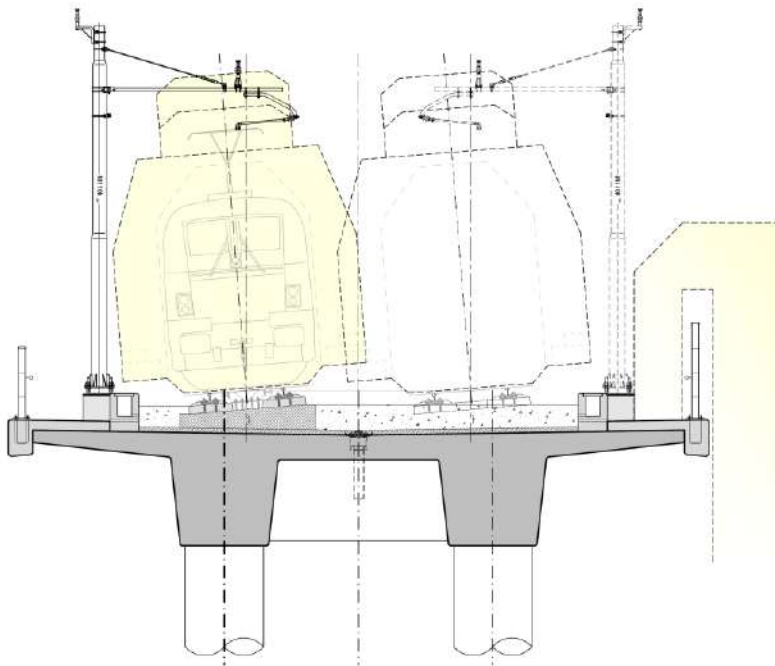
Figure 3 – The characteristic cross section

2.3. TRAFFIC LOAD AND TEHNICAL REGULATIONS

The traffic load of the railway viaduct follows the Eurocodes with a LM 71 load scheme (**4 x 250 kN** axle load and **80 kN/m** uniform load) plus the alpha **α = 1,21** load class factor. In addition to ultimate limit state, the structure shall also have the proper serviceability parameters. As far as railway bridges are concerned, these primarily include deformations, rotations, twists, transverse deformations and vibration of the structure.

The Structural Eurocodes (all parts of EN 1990), TSIs (Technical Specifications for Interoperability) and other Slovenian standards were applied. Where relevant areas were not duly covered, the German railway recommendations (DB Richtlinien) were implemented.

3. CONCEPT DESIGN

During the last decade, a few interesting realisations on new railway connections in Germany have been carried out. It is important to mention two very interesting viaducts: Gänsebachtalbrücke [3] and Stöbnitztalbrücke [4] which have both been laid across low valleys and have been designed as integral viaducts without bearings. The fundamental objectives of such a design are to create a safe and sustainable, but also extremely economical structure, i.e. involving low investment and low maintenance costs. The installation and maintenance of bearings, which can prove rather expensive, is not required for integral bridge structures.

Such long structures are distinguished by their division into short integral segments, facilitating the construction of tracks without special track dilatations, thus the use of a continuously welded track. A track without track dilatations is cheaper to construct and maintain, is more sustainable, results in lower noise emissions, there is a lower train derailment risk and is therefore an overall safer solution [5].

On account of a relatively low position vis-à-vis the valley, we were able to follow the design of the original 19th century viaduct, i.e. by using shorter spans, but in a modern transparent manner (Figure 4).
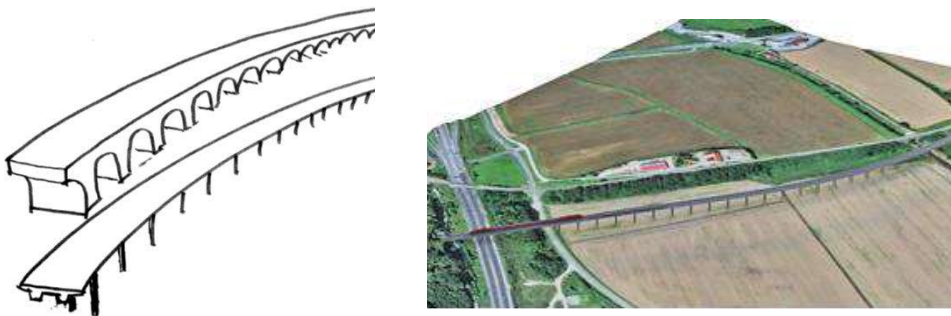
Figure 4 – The design concept following engineering minimalism

4. TEHNICAL DESCRIPTION OF THE SOLUTION

4.1. BRIDGE STRUCTURE

The viaduct is 912.60 m long, its constant width is 14.36 m, and it has 32 spans of 28 m length on average. The 896 m static length between the end axes is divided into nine parts: seven 112 m long intermediary frames and two half-frames of 56 m at each end. length (Figure 5). This leads to the following static spans:

56 m (2 x 28 m) + 7 x 112 m (27 m + 29 m + 29 m + 27 m) + 56 m (2 x 28 m) = 896 m
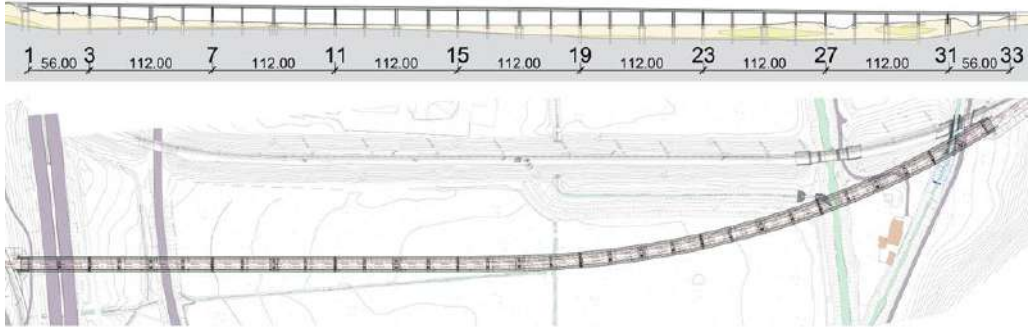
Figure 5 – Longitudinal section and layout - the viaduct is divided into 9 parts

The first and final two spans (2 x 28 m = 56 m) are monolithically connected to both end supports which constitute a fixed-point transitioning to the terrain. The division of the viaduct is illustrated on Figure 6. Each typical intermediary frame of 112 m in length has its own movement centre ("fixed point") in the middle, providing more rigid support (A). All other Type B and C supports are designed in a way that they can adapt the temperature and rheology-related deformations (Figure 7).
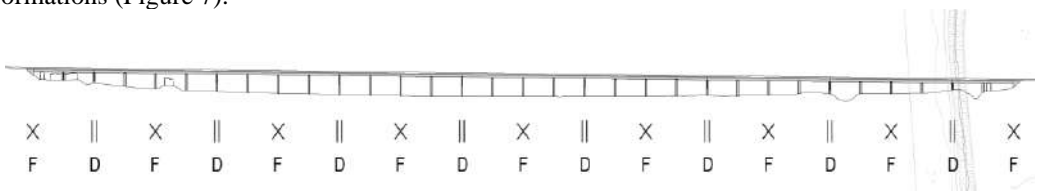
Figure 6 – Division of the viaduct

4.2. SUBSTRUCTURE AND FOUNDATION

All elements of the support structure, all pillars and both supports are integrally connected to the upper structure. The pillars are of a circular ø 160 cm or of an oval cross-section ø 160 / 240 cm and can be divided into three types (Figure 7, Figure 8).

- Type A: central support (support centre), two pillars 160 cm/240 cm, held below into a pilot mat with two types of pilots (2 x 3 = 6 pilots). This type bears the majority of the longitudinal brake force.
- Type B: intermediary support 2 x ø 160, with a load-distributing foundation of one row of 4 pilots ø 150 cm.
- Type C: support on a construction dilatation is in fact a cut round pillar ø 160 cm with a lower rigidity and facilitates heat dilatations in both directions; in terms of shape, it is the same as Type B.

125
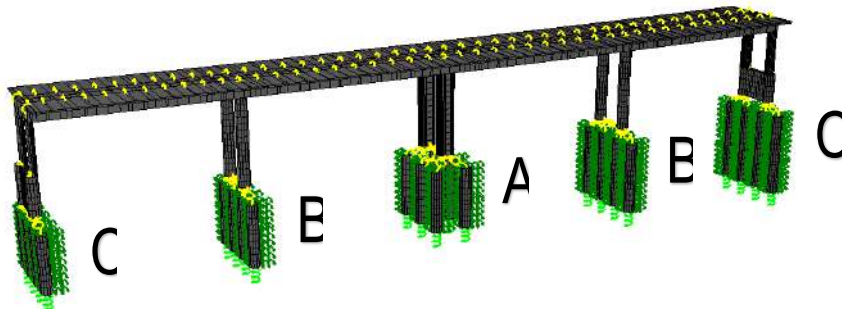
Figure 7 – Model of a typical intermediate segment of 112 m in length
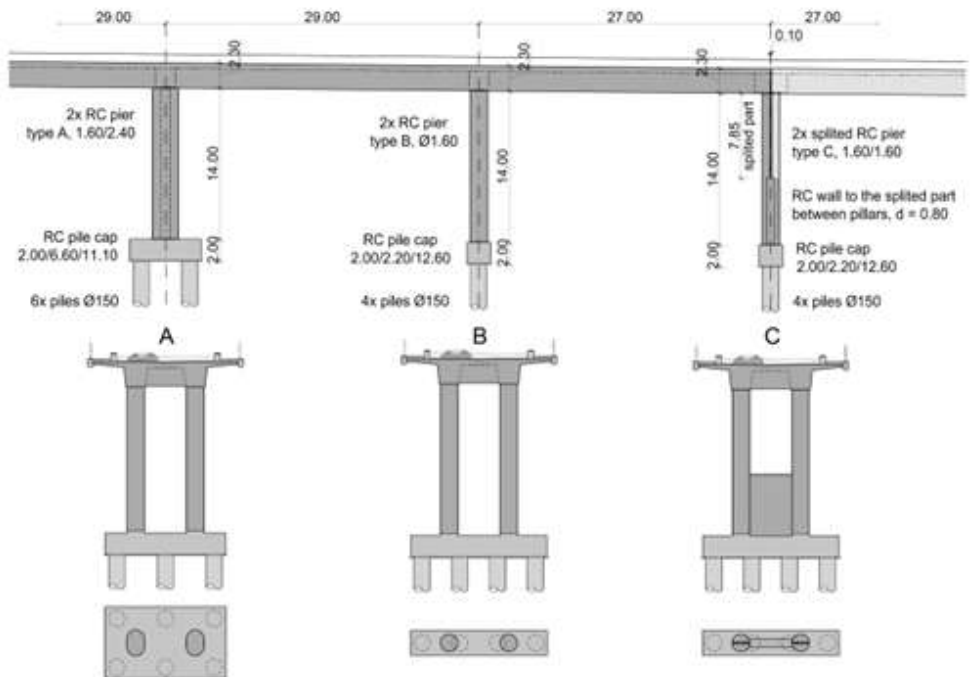
Figure 8 – Three types of supports: Type A provides rigidity to the frame, Type B is intermediary support, Type C is a split pillar for two frames

The entire foundation is deep on concrete piles of 150 cm in diameter. The foundation of Type A supports consists of a group of piles in two rows (2 x 3 pilots) forming a rigid support. The foundation of the remaining Type B and C supports consists of one row of pilots (1 x 4 pilots), forming more flexible support that can adapt to changes in temperature. The supports and foundations are designed in such a way that the average rigidity of the brake force ratio is C + B + A + B + C = 9 % + 18 % + 46 % + 18 % + 9 % = 100 %. This means that the median rigid Type A support take almost one half of the horizontal force (W or N).

126

4.3. PRESTRESSING

It is customary for long viaducts to make use of segmental span by span construction, followed by the pre-stressing of this segment and a repeat of the procedure. The integral frame design is challenging on account of a complex final frame corner, as pre-stressing requires sufficient space and weakens the corner. For this reason, a new frame stressing method from the centre of the frame, has been introduced. Passive prestressing anchorages which do not interfere with the strong reinforcement are installed in the frame corners. Active stressing anchorages are located near the central support, where the cables are switched, matching the bending moment diagram shape (Figure 9). This is innovative solution, compared to the referenced German railway viaducts.

Each of both ribs contains eight cables 19 x 15.7 mm of 62 m in length, stressed to a 3800 kN force. All cables have been installed into plastic PEHD tubes and have been electrically insulated using the Freyssinet system.
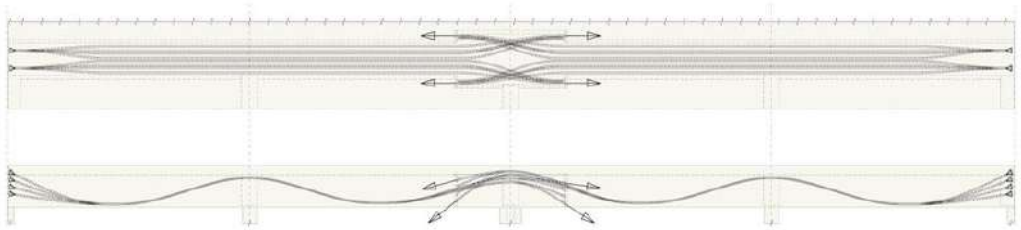
Figure 9 – Prestressing scheme of 112 m long frame structure

4.4. TRACK-STRUCTURE INTERACTION

All strains are thus released in eight construction joints, out of which each receives dilatations for their respective left and right effective lengths (2 x 56 m = 112 m). A continuous track is laid along the construction joint, fixed to the slab track with elastic couplings. The TTP (slab-track system) is used in the ÖBB-PORR Austrian system.

The connection between the tracks and the structure results in an interaction between the strains and stresses (Figure 10). By using elastic couplings properly, the stresses in the ballasted track (dT, Z) remain within acceptable limits. However, as the behaviour of the new integral concept has not been thoroughly investigated and due to lack of long-term experience, shock transmitter units or STUs have been added in-between the divided parts. Two pieces of STU of a 2500 kN load-bearing capacity are foreseen for each braking units, allowing the transfer of seismic and brake forces to more units, whereas temperature and rheological deformations are unrestrained.
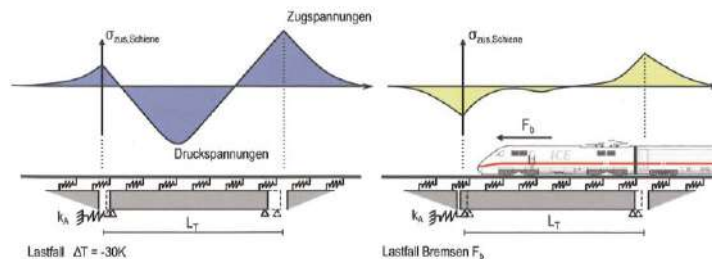
Figure 10 – The track-structure interaction and stresses in a track due to dT and Z [6]

5. DETAILED DESIGN AND CONSTRUCTION

The Pomgrad contractor signed an agreement for design-built project in 2020. The structure is to be constructed between the 2020 and the end of 2022. Railway line will be in service from spring of 2013.

Some special features of the construction:
- Split pillars facilitating the dilatation of the viaduct below the track. These pillars are of a complex shape and contain large quantities of rebars, particularly in the upper corner. For this reason, a full-scale test pillar allowing us to test the feasibility of this complex detail (Figure 11, Figure 12) was implemented.

Figure 11 – Test pillar

Figure 12 – The pillar with 8 m high split part

- Concreting typical 112 m long sections of the superstructure proved to be extremely challenging (1560 m^3 concrete during one phase). The contractor required 14 hours for this concreting using 50 people, 21 concrete mixer trucks with 193 concrete deliveries and three

concrete pumps. To achieve the required C45/55 quality was especially challenging during the hot period of the year (Figure 13).

- Stressing typical 112 m long segments from the centre with 2 x 8 = 16 K19 cables in the cross-section with a 3800 kN force. Switching the cables above the intermediate support means that 32 cables anchorages to be tensioned.

Figure 13 – Concreting of 112 m segment and almost finished structure (spring 2022)

6. CONCLUSION

The concept of integral constructions without bearings can also be applied in long railway installations, which can also prove very advantageous for economical construction purposes. An appropriate viaduct division concept can allow implementation of a continuously welded track without joints which significantly contribute to safe traffic and protection of the environment against noise. Despite considerable technical requirements and restrictions of railway traffic, the result is environmentally friendly and aesthetically pleasing (Figure 13).

REFERENCES

[1]   [Ponting d.o.o.: IDZ (conceptual design), IDP (preliminary design), PGD (final design) and PZI (detailed design) of the Pesnica Viaduct, 2015-2022

[2]   History: https://sl.wikipedia.org/wiki/Pesniški_viadukt, captured on 30/07/2022

[3]   Schenkel M et al.: Die Gänsebachtalbrücke, eine integrale Talbrücke der DB AG auf der Neubaustrecke Erfurt-Leipzig/Halle, Beton- und Stahlbetonbau, Heft 2010/9

[4]   Jung M. et al.: Entwurf und Ausführungsplanung der Stöbnitztalbrücke Eine lagerlose Eisenbahnbrücke im Zuge Erfurt–Leipzig/Halle, Beton-und Stahlbetonbau, Heft 2010/9

[5]   Marx S., Seidl M.: Integral Railway Bridges in Germany, Structural Engineering International 3/2011

[6]   [6] Krontal L.: Zum Entwurf von Eisenbahnbrücken, Structurae Eisenbahnbrücken ISBN:978-3-433-03097-4, Ernst&Sohn 2014

Vojkan Jovičić[1]

GEOTEHNIČKI ASPEKTI GRAĐEVINARSTVA

Rezime:

U radu se naglašava da se geotehničko inženjerstvo ne može jednostavno kategorisati samo kao poddisciplina građevinarstva. Geotehnički inženjerstvo zauzima ključnu ulogu u mnogim drugim savremenim inženjerskim disciplinama koje oblikuju naše izgrađeno okruženje, kao što su ekološki, priobalni, odbrambeni, naftni i geotermalni inženjering. Uloga geotehničkog inženjerstva je istaknuta kroz razvoj kritične infrastrukture, koja omogućava funkcionisanje savremenih društava. U članku je razmatrana regulativa u oblasti geotehnike uključujući različite pristupe projektovanju geotehničkih objekata. Ključni argumenti su ilustrovani na dva primera geotehničkih projekata vezanih za izgradnju tunela.

Ključne reči: Geotehničko inžinjerstvo, kritična infrastruktura, projektovanje, tunelogradnja,

GEOTECHNICAL ASPECTS OF CIVIL ENGINEERING

Summary:

It is accentuated in the paper that Geotechnical engineering cannot be simply categorised only as a sub-discipline of Civil Engineering. Geotechnical Engineering takes pivotal role in many other contemporary engineering disciplines that shape our built environment, such as environmental, offshore, defence, petroleum and geothermal engineering. The role of geotechnical engineering is highlighted through the development of critical infrastructure, which enables functioning of contemporary societies. The regulation in the field of geotechnics is discussed including the different approaches to design of geotechnical structures. The main points are illustrated ton two examples of geotechnical design related to tunnel construction.

Key words: Geotechnical engineering, critical infrastructure, geotechnical design, tunnelling

---

[1] *FGG, Faculty of Civil and Geodetic Engineering, Jamova 2, 1000 Ljubljana, Slovenia*

1. INTRODUCTION

In the last century, the development of critical infrastructure resulted in progressive rise of geotechnical engineering. Critical infrastructure is infrastructure that enables the basic functions of built environment and serves as the backbone of the national economy, safety and health. The critical infrastructure is something that our societies often take for granted: like electricity in our homes, the water we drink, the freedom of movement and the communication networks and tools that enable us to work efficiently. Engineers understand that critical infrastructure is not in any form granted but is the result of the knowledge and efforts of several generations of engineers and technicians from different professions. Critical infrastructure must first be properly positioned in space, then it must be built, maintained, protected and, finally, its impact on nature must be limited. With the development of critical infrastructure, which took place in Europe in the previous century mainly after the second World war, it was gradually becoming obvious that the role of the geotechnical engineering is crucial. This was especially so, following the evolving understanding of the scale and scope of the human impact to nature. The role of geotechnical engineering within the other engineering disciplines is highlighted in the paper in the context of civil engineering. The topics related to geotechnical design are discussed and case examples are given to highlight the main points.

2. THE ROLE OF GEOTECHNICAL ENGINEERING IN CIVIL AND MINING ENGINEERING

The role of geotechnical engineering or geotechnics, with our increasingly deeper understanding of our environment is becoming more and more recognizable as a fundamental technical discipline, which cannot be simply categorized as a subdivision of civil or mining engineering. As indicated in Figure 1, geotechnical engineering is interrelated not only with civil and mining engineering, but also with several other contemporary engineering disciplines, such as environmental, offshore, defense, petroleum and geothermal engineering, etc [1]. Geotechnical engineering emerges as an indispensable discipline in the construction of all infrastructure facilities and includes key elements of natural resource extraction, whether it is a mining or oil industry. Geotechnics is also a key discipline for the exploitation of geothermal resources, with or without the exploitation of groundwater, where exists the sustainable harnessing of the energy accumulated in the ground. Finally, geotechnics is a key technical discipline in the management of natural disasters such as landslides, earthquakes and floods [2].

Geotechnical engineering encompasses terms of rock and soil engineering, although term soil engineering is rarely used and often confused with geotechnical engineering. This artificial confusion is often attributed to the fact that from historical perspective rock mechanics has the origins in mining engineering and soil mechanics in civil engineering. But the absurdness of this confusion easily comes to light when civil engineers need to design underground structure in rock mass or place foundation in soft rock. Also, it easily comes to light when mining engineers need to design tailing embankment along the surface mine, etc.

Geotechnical engineering is firmly based on several technical disciplines: soil mechanics, rock mechanics, fluid mechanics, engineering geology and hydrogeology, and fundamental sciences including the earth science. Geotechnical engineering benefited enormously from

development of numerical methods in applied mathematics and further digitalisation of computational processes.

Figure 1 – The position of geotechnical engineering among the other engineering disciplines, areas of application in civil engineering and underlying technical disciplines and sciences (developed after [1])

In civil engineering, geotechnics is indispensable in the construction of just about every building, regardless of whether the building is built on the ground (foundation of high-rise structures) or in the ground (cuts, underground facilities, such as tunnels or cut and cover structures) or from the ground (low-rise structures - embankments, dams, road infrastructure). Every structure that is built interacts with the ground and affects the state of the environment. There are many examples from practice where this is not understood, and the consequences are often seen as material loss and/or functional inadequacy of the structure itself. European legislation (Eurocode 7 - the European standard for the field of geotechnics SIST EN 1997) [3] is very clear in this regard, as it sets equivalent criteria for both a functional error during the construction of the structure and for a stability error, as both can lead to non-usability of the structure and/or collapse.

As indicated in Figure 2 the role of geotechnics in mining engineering is indispensable for key mining activities such as underground mines, surface mines and tailings, deep extraction boreholes and foundation of utility mining and structures. Geotechnical engineering has a pivotal role in the development of technological procedures such as fracking or geothermal exploration and exploitation.
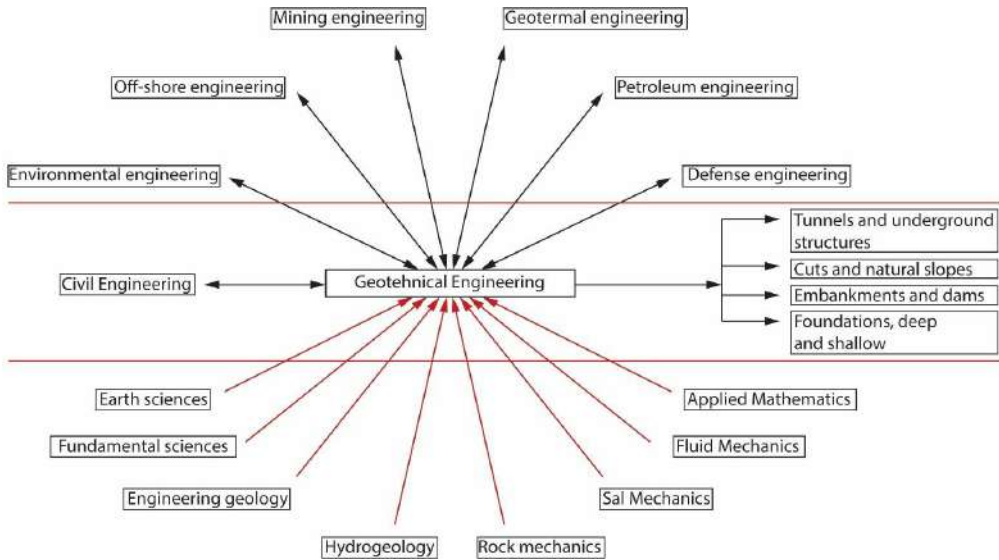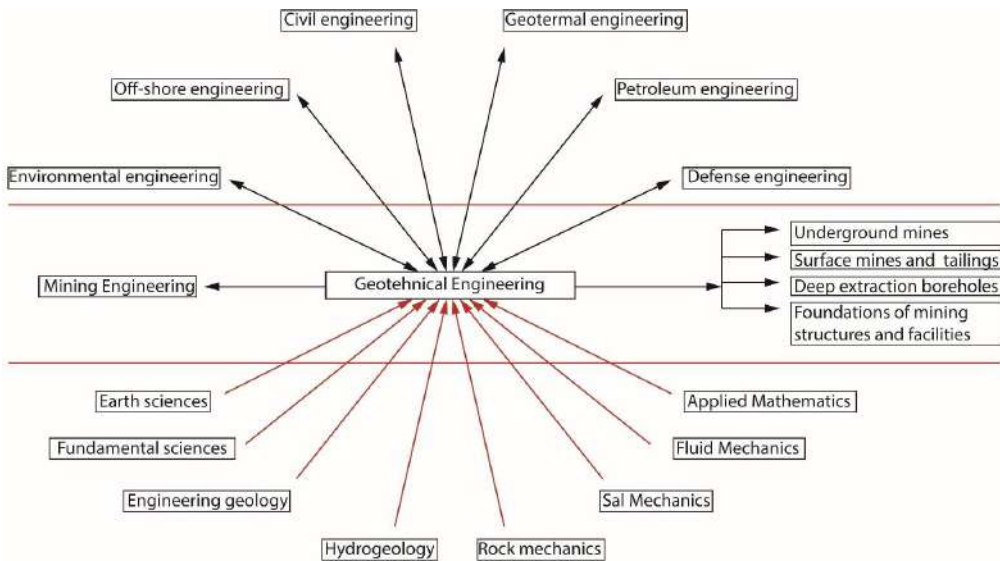
Figure 2 – The position of geotechnical engineering among the other engineering disciplines, areas of application in mining engineering and underlying technical disciplines and sciences (developed after [1])

3. THE STATE OF GEOTECHNICAL PROFESSION IN THE REGION

In the region, geotechnical profession is still insufficiently established in our professional environment. In some Western countries, it is possible to study geotechnical engineering as a special major and graduate as a university graduate in geotechnical engineering. Unfortunately, this is not possible anywhere in eastern Europe. In the chaotic practice, several professions appear in the preparation of geological reports and the planning of geotechnical facilities: from geologists, miners and civil engineers, to foresters, physicists and even chemists. Typically, in the region, with the distinction of North Macedonia, the conditions for registration and issuance of licenses at the Engineering Chambers for the field of geotechnics are not clearly defined. This often causes unprofessional work that is subject to improvisation and poor advice. As a result of this type of deregulation, the geotechnical profession often has an unjustified bad reputation because it does not offer the client a sufficiently high-quality product. In this case, the client, which can also be a public institution, too often chooses services according to the principle of the lowest price and finds himself in high-risk situations that could easily be avoided with a professional approach. It is often found during the supervision of the foundation works that the soil properties in design stage were only assumed and not measured. In practise this means that designers often choose conservative soil properties, which leads to an irrational design of the structure. It is also common the opposite case in which worse soil properties occurs than those foreseen in the project, which leads to construction delays and significant price increases.

The content of project documentation must explicitly contain the information for determining the foundations of the building, the protection of the construction pit and the protection of neighbouring buildings and banks. Obtaining this data is associated with certain costs, and the

rationalization of costs in the process of building the facility should not be on the account of the increased risks due to the omission of soil investigations. Project cost management and risk management on the same project are highly interrelated or interdependent processes, which is unfortunately often overlooked.

Eurocode 7 (SIST EN 1997) [3], which specifies requirements regarding the scope and quality of soil investigations, divides construction into three so-called geotechnical categories. The first category represents constructions bearing small geotechnical risks, the third category is for large risks, and the second category represents most constructions on not overly demanding ground. It should be emphasized that this classification of geotechnical category is not only influenced by the properties of the soil, but by the combination of the complexity of the soil conditions, the design of the structure and the interaction between the structure and the ground. It should be noted that the useful recommendations regarding the extent of soil investigations specified in Eurocode 7 refer only to second geotechnical category. For plans of structures of the third geotechnical category, which is by and large only one adequate for critical infrastructure structures, the recommendations of the Eurocode 7 are not more than scope guidelines, which represent only the smallest acceptable range of investigations.

Several large infrastructure projects are currently under construction in the region, in which the role of the geotechnical profession is indispensable. Currently, it involves mainly the construction of critical highway and railway infrastructure. In Slovenia, for example, these are currently under construction the eastern tube of the Karavanke tunnel, the 3rd development axis and 2nd track of the railway line Divača - Koper. On all three of these large infrastructure projects more than 40 km of tunnels will be built in the next few years, which is more than were built in Slovenia in the last 30 years. During the construction of such facilities, in which geotechnical structures carry up to 90% of the investment value, so-called "geotechnical supervision" takes place. The role of geotechnical supervision is the geotechnical management of the works, whereby the support measures during the construction of the tunnels and geotechnical structures on the route is adapted to the current geological conditions. Geotechnical work management is based on geological-hydrogeological monitoring of excavations, ongoing geophysical research, geodetic monitoring of movements in the tunnels and on the ground surface, and monitoring of the impact of construction on the environment (impact on groundwater, vibrations, damage to neighbouring buildings, impact on plants and animals, etc). In these cases, the public agency clients correctly assessed the decisive role of geotechnics in the planning and construction of critical infrastructure in Slovenia. The regulation in Bosna and Hercegovina also recognises the role of geotechnical engineering through implementation of so called ˝geotechnical missions¨. Geotechnical missions are readily used in the construction of the motorway along the corridor Vc, which is currently ongoing. The role of geotechnical engineering is defined through different types of mission from the early design stages all the way to geotechnical supervision during construction and maintenance.

4. METHODOLOGY OF GEOTECHNICAL DESIGN

As a difference to concrete or steel structures, geotechnical structures are made of or are in interaction with natural materials that are available in-situ. These materials have characteristics that cannot be required or prescribed by the designer, but they must be measured using in situ and laboratory investigation. It is very often the case that material characteristics cannot be devised with high level of accuracy so appropriate risk strategies must be incorporated in design [4]. This is usually performed using the factor of safety approach in which ground material characteristics are reduced by a certain degree and the analyses are performed with reduced parameters. However, this does not work particularly well for deformation analyses in which the ground response can be highly non-linear, and the reduction of parameters can lead to a completely wrong conclusions in terms of deformability or internal forces of structure caused by soil structure interaction.

Generally, a design requirement in Eurocode 7 is that no relevant limit state is exceeded for each geotechnical design situation, which are defined as ultimate and/or serviceability limit states. According to Eurocode 7 one, or a combination of the following design methods, can be applied in design: a) calculations, b) prescriptive measures, c) experimental models and load tests, and d) observational method. Out of four design methods the calculations are used the most, but there are significant restrictions that must be observed. The European regulation standard Eurocode 7 can be safely used for the low-risk structures of second class, that is in some typical cases such as simplified shallow foundation design or simple slope stability cases. For example, in terms of tunnel construction Eurocode 7 approach should not be used as the interaction of ground and tunnel support system cannot be rationally treated by the reduction of material parameters or the use of partial factors of safeties for the load cases. This is a consequence of the interaction between the ground relaxation and the tunnel support system in which ground takes the portion of the relaxation load and the rest of the load is transferred to the tunnel support system. Also, the complex role of underground water in soil and rock mechanics cannot be simplified in such a way that design cases cover both favourable and unfavourable roles, that groundwater might have in interaction with the ground at a given location.

In practise, the combination of calculation and observational methods is the most appropriate for complex structures belonging to third geotechnical category [5]. This methodology, in which the design is reviewed during construction, allows forward and back calculation analyses which can be verified by the observation of the movements and other indicators of deformation state of ground caused by geotechnical works. The method is based on the following requirements, which must be met before construction is started: a) acceptable limits of behaviour are established, b) the range of possible behaviour are assessed, and predictions are made that the actual behaviour will be within the acceptable limits, c) a plan of monitoring is devised to reveal whether the actual behaviour lies within the acceptable limits [6]. Finally, a plan of contingency actions is devised, which may be adopted if the monitoring reveals behaviour outside acceptable limits.
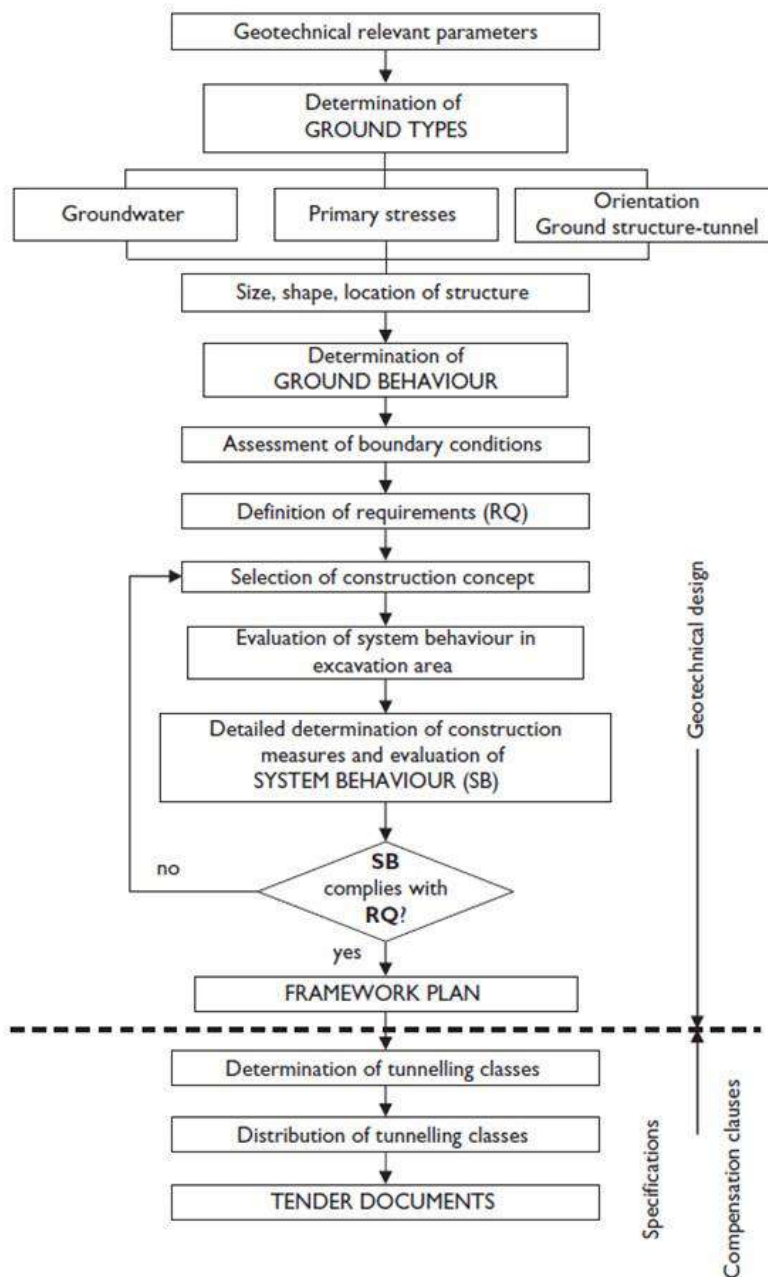
Figure 3 – Schematic procedure of geotechnical design, from Austrian Society for Geomechanics (2010) [7]

Figure 3 shows a schematic of geotechnical design using a form of observational method that was proposed by Austrian geotechnical society as a recommended practise in tunnel construction. This principle is part of New Austrian Tunnelling method (NATM) [8], which is typically used for tunnel construction in the region. After assessment of geotechnical relevant parameters, the ground types are determined, based on geological and hydrogeological site and laboratory investigations. These parameters are presented in geotechnical interpretation report, which also gives information on other relevant boundary conditions such as: presence of groundwater, in-situ stresses, spatial orientation of the tunnel relative to the geo-morphology etc. Following the basic set of information, the prognosis of the determination of ground behaviour is evaluated, which essentially defines possible types of failure during tunnel construction within this geotechnical environment [9]. Through the assessment of behavioural types and selection of the construction concept the definition of requirements is used as the basis for design. The detailed determination of the construction measures is developed for different geological conditions as support systems that are necessary to prevent failure. This is evaluated in such a way that system behaviour must satisfy requirements, usually in terms of limited convergence movements in the tunnel. The observational method is then developed around the condition that system behaviour is within required limits. The support system is corrected during the construction of the tunnel until the condition is not fulfilled (the loop showed in Figure 3).

5. CASE EXAMPLES OF GEOTECHNICAL DESIGN

5.1. PORTAL STRUCTURES AT TUNNEL PEČUJ NORTH

Tunnel Pečuj is a twin motorway tunnel with some 90 m^2 of the excavation clearance profile. The rock massif, through which the tunnel was driven, is made on sediments of the subgroup of Jurassic-Cretaceous age (approx. 70% of the tunnel length) and Oligo-Miocene poly-facial complex. The final position of the tunnel, the layout of the geological strata and the location of pre-existing landslides in the north portal area are shown in Figure 4. At location of the portal the Oligo-Miocene poly-facial complex (clayey, sandy, and marly sediments) is in transition to Jurassic Cretaceous flysch formed of sub-vertical marlstone strata. Both strata are overlain by weathered material overlain by Quaternary deposits, as shown in Figure 4a.
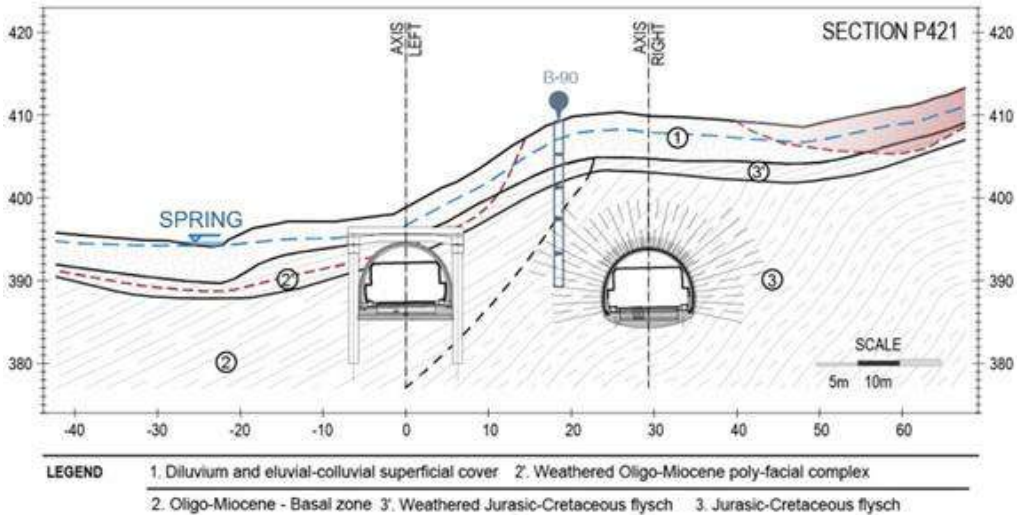
Figure 4a – Cross-section P421 showing stratigraphic features and the locations of pre-existing landslides at the north portal area of tunnel Pečuj [10]
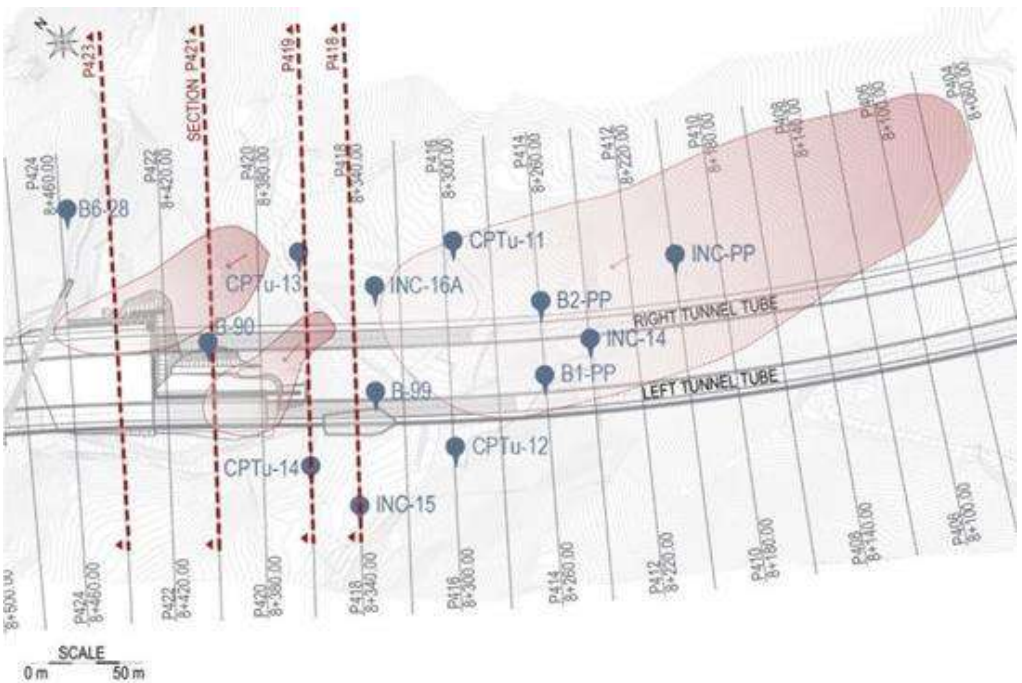
Figure 4b – The plan view indicating the site investigation boreholes (B), CPT tests (CPTu), inclinometers (INC) and the location of landslides at the north portal area of tunnel Pečuj [10]
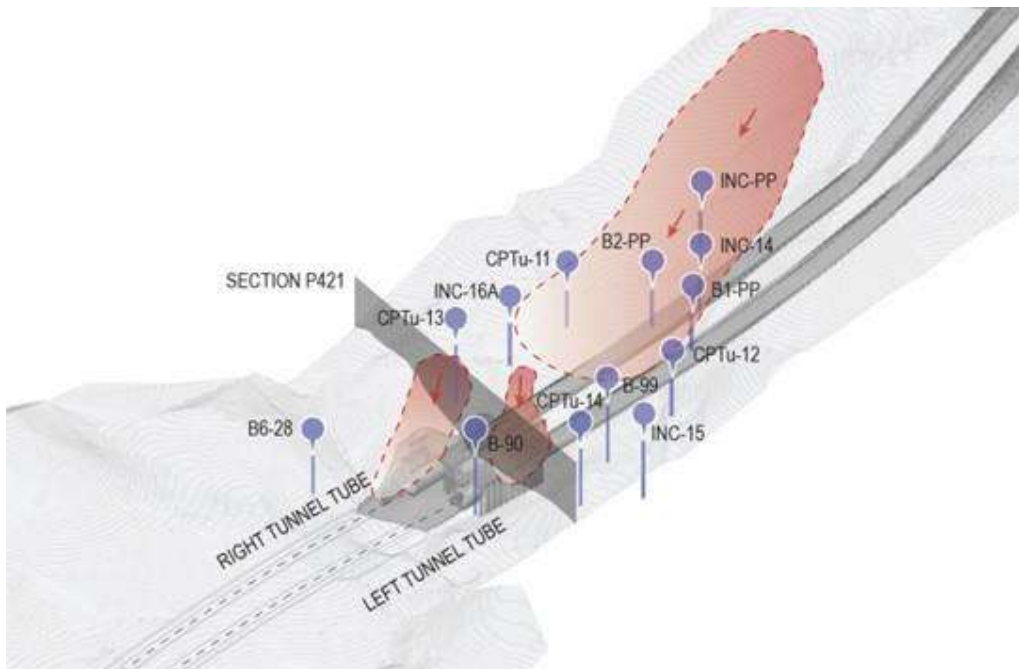
Figure 4c – 3D visualization of the north portal area of tunnel Pečuj [10]

The groundwater table, which varied between surface level and two meters depth, was established using investigation pits. The perched aquifer's flow intersected the surface at a valley wall so that the water had been discharged as a spring, indicated in Figure 4a. For the given geological and hydrogeological boundary conditions at the portal, the Quaternary cover was crisscrossed by the surface and shallow underground waterways, which lead to the abundance of landsliding processes.

The open cut for the northern portal of tunnel Pečuj was initially designed without consideration of the active landslide bodies. The spatial layout of the landsides, the motorway route, and the original portal cuts, up to 50 m high, were placed to clash with the landslides, as shown in Figure 5.
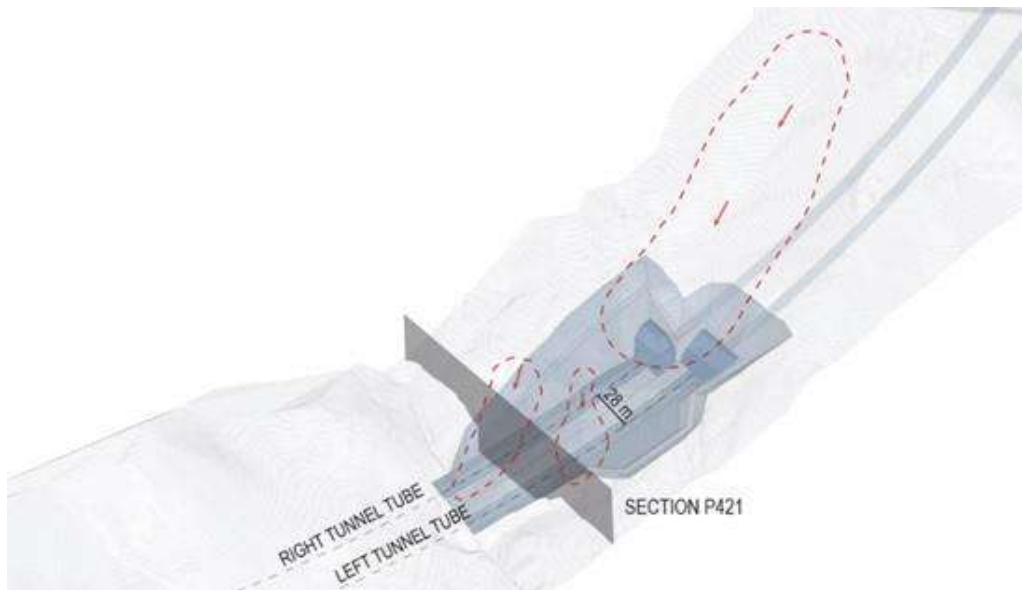
Figure 5 –The spatial layout of the landsides (in red), the motorway route and the original design solution for the portal cuts at the northern portal of tunnel Pečuj [10]

The reactivation of the landslides by the portal cut would be inevitable, bringing detrimental effect on the layout of motorway. Extrapolation of geotechnical model into third dimension was a crucial step to develop a new design solution allowing for the design concepts presented in the previous section. 3D geomorphologic and strati-graphic model was developed to correctly locate the layout of additional geotechnical structures relative to landslide bodies.

The first measure was to lower the height of the pre-cuts, which led to extensions of both tunnel tubes as shown in the plane view in Figure 6 (the right tube was extended 120 meters and the left 90 meters). By elongating the tunnel tubes and thus moving out of the main landslide bodies, it was possible to use corrective structures at their toe and side positions. Corrective structures comprised the six relatively short pile walls shown in Figure 6 (Right side pile wall, Right tube pile wall, Central pile wall, Left tube pile wall, and two parallel pile walls, part of the Cut and Cover structure). Considering 3D geomorphologic and stratigraphic model, each of the pile walls was of different height, at different elevation, constructed at different time to serve different purpose. Their position was chosen relative to: a) the bearing geological strata providing the fixity for the piles, b) the orientation, the depth and the direction of sliding of the two landslides relative to the tunnel layout and c) timing of construction. For example, Right tube pile wall (2) and Left tube pile wall (4) were constructed first to enable working platform for the installation of the piles for all other geotechnical structures.
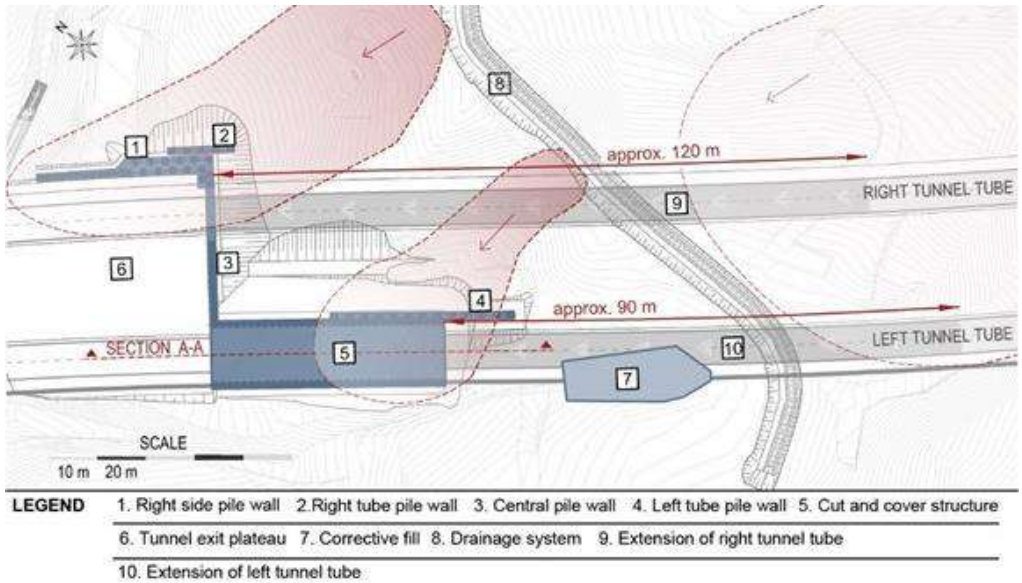
Figure 6 – The plan view showing the structures of the new design solution [10]
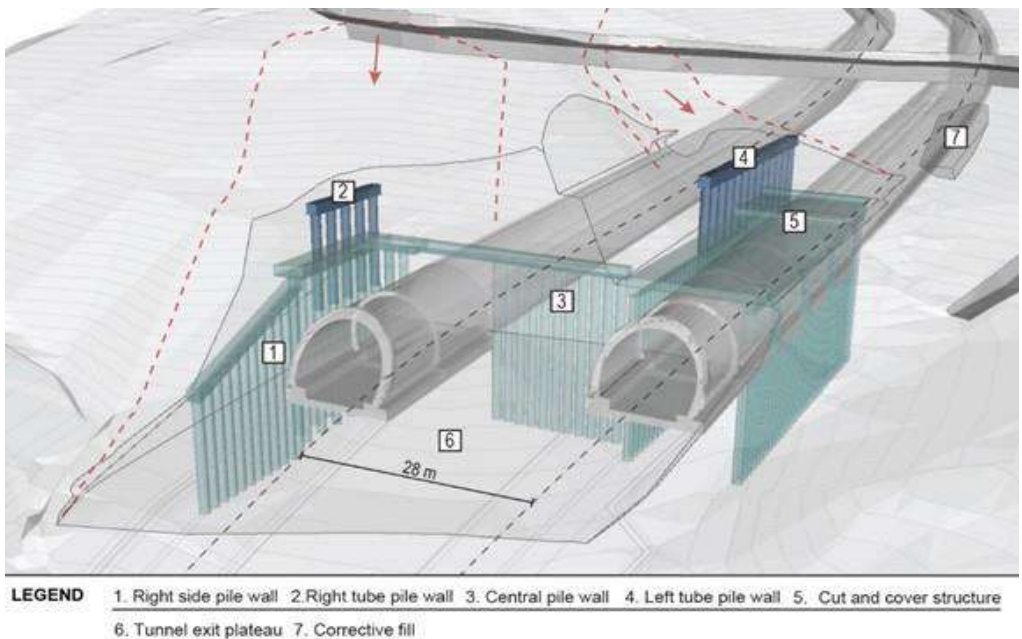
Figure 7 – 3D model of the final layout of support structures at northern portal of tunnel Pečuj (existing landslide bodies are indicated by broken red lines) [10]

The pile walls arrangement was gradually constructed, separately dealing with landslides. Stabilizing of the two landslides indicated in Figure 6 (in red) had to be undertaken first and was achieved by the installation of the right and the left tube pile walls. The deep-seated landslide (only shown in Figure 4) was dealt with by elongating the tunnel tubes completely out of the reach, while considering that the tunnel underground excavation takes place below the landslide failure surface. The pre-cut for the right tube was protected by Right side pile wall (1). The piles were up to 20 meters deep with at least a third of their length embedded in the bedrock. To increase the structural rigidity of the pile wall and avoid the need for the use of geotechnical anchors due to time constrains, the piles in the tallest section of the wall were installed in the zigzag pattern, so that they can work in push-and pull fashion. Both structures were further supported by the Central pile wall (3) located perpendicularly to the aliment of the right tube shown in Figure 6. The purpose of the central pile wall is to protect the frontal slope of the pre-cut and provide the lateral support for the wall on the right side of the left tube. To facilitate the excavation of the left tube, Cut and cover structure (5) was constructed using the top-down procedure. The two parallel pile walls of some 48 m length were installed along the axis of the left tube. The walls were connected by the top and bottom slabs aimed to prop the walls horizontally. This frame structure was needed to provide a secure transition of the left tunnel tube through the unstable saturated diluvium layers and to prevent deconfining of the ground.

The final arrangement of tunnel Pečuj north portal are shown in Figure 8. None of the structures can be seen, except for the Right-side pile wall, since they were covered by the embankment soil. This is in accordance with geotechnical design principle that less is more in terms of visual impact of tunnel portal positioned within natural environment.

Figure 8 – The final arrangement of tunnel Pečuj north portal

142

5.2. CONSTRUCTION OF TUNNEL IVAN IN ANHYDRITE CONTAINING ROCK

Chemical reaction between anhydrite and water results in the formation of gypsum followed by a significant increase in the volume of the rock mass. Tunnel excavation enables increase of water conductivity around the underground opening which, superimposed to the impact of unloading on rock mass, forms sufficient conditions for the transition of anhydrite to gypsum. Suppression of the volume change caused by the primary support results in the build-up of swelling pressure in the rock mass causing damage to the tunnel lining. In the long-term anhydrite reacts to a slow change of moisture of the rock mass, which can affect functionality of the tunnel both due to swelling and sulphate aggression on concrete. Caverns filled with gypsum concentrated solutions were encountered during construction of tunnel Ivan at transgressions between anhydrite rock mass and different geological strata due to abrupt change in rock mass transmissivity and consequent water retention.

This is a twin motorway tunnel situated at European transit Corridor Vc in Bosnia and Herzegovina at the section Tarčin – Mostar. In geological terms tunnel Ivan is located at the transition between Bosnian Flysch unit and Central Bosnian shale Highlands. On the contact with older Triassic and Palaeozoic tectonic unit of Central Bosnian shale highlands there were conditions for the formation of Permian evaporites, which progressed to the surface during orogenesis. The longitudinal geological section of tunnel Ivan is presented in Figure 9, showing a large body of anhydrite rock which was embedded within weathered sandstone and breccia dominated rock.
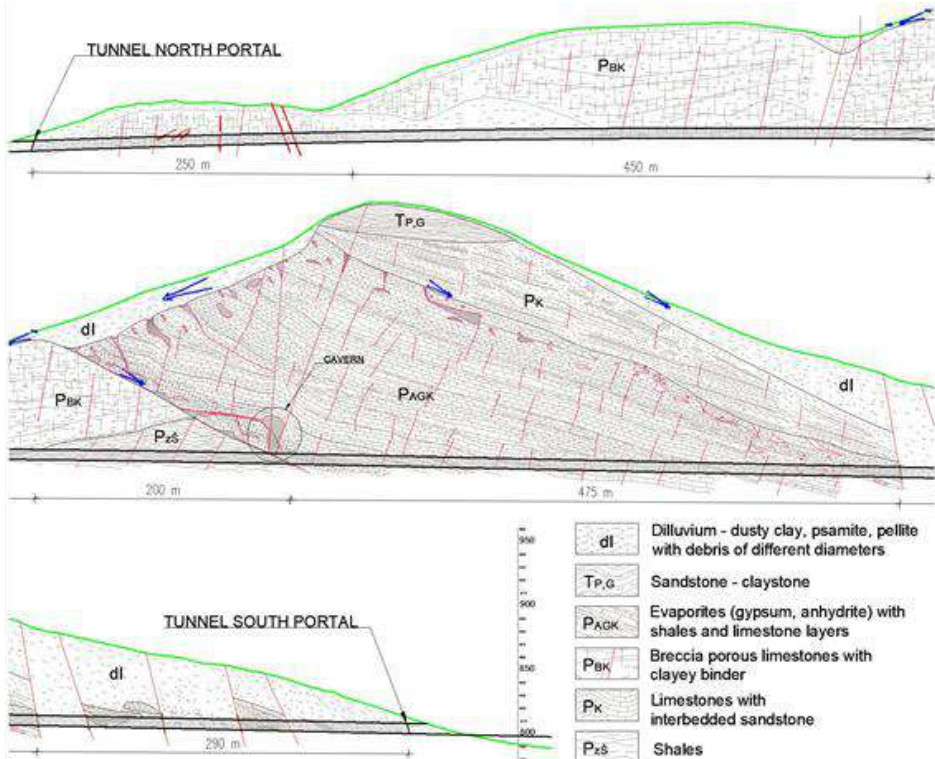
Figure 9 – The longitudinal geological section of tunnel Ivan

The transition zone of approximate length of 200 m occurred between evaporite and shale at the area of contact of two lithological environments was represented by an erosive-tectonic boundary. Palaeozoic clastic rocks here suffered many endogenous processes, due to which the degree of their decay was different. The increased weathering of the slate material was one of the reasons for the local instability at the head of the excavation. Evaporite and shale contact zone was extremely unstable geological environment in which large-diameter caverns with muddy fillings were found resulting in major collapse event. Such processes within the massif constantly affected the change of stress state and degree of disintegration of the rock mass itself. With the further presence of water, there was a further dissolution of anhydrite or gypsum forming caverns filled with (oversaturated) heavy liquid of gypsum solution.

Figure 10 – Loss of stability at the occurrence of cavern in the roof of the right tube of tunnel Ivan

During the excavation of the right tunnel tube, the stability of the material in the roof of the top heading was suddenly lost due to the presence of the cavern. Loss of stability shown in Figure 10 was manifested by the abrupt release of heterogeneous material in heavy fluid state (gypsum solution with lone blocks of anhydrite) at the top of excavation. The cavern was emptied in several minutes. After measuring using a digital laser rangefinder, it was found that the cavern was approximately 30 m high, with variable width in both horizontal directions (6-18 m) comprising the total volume of approximately 5500 m^3. The cavern edge occupied about a third of the ceiling of the right tunnel tube. The layout of the cavern and the tunnel tubes is shown in Figure 11.
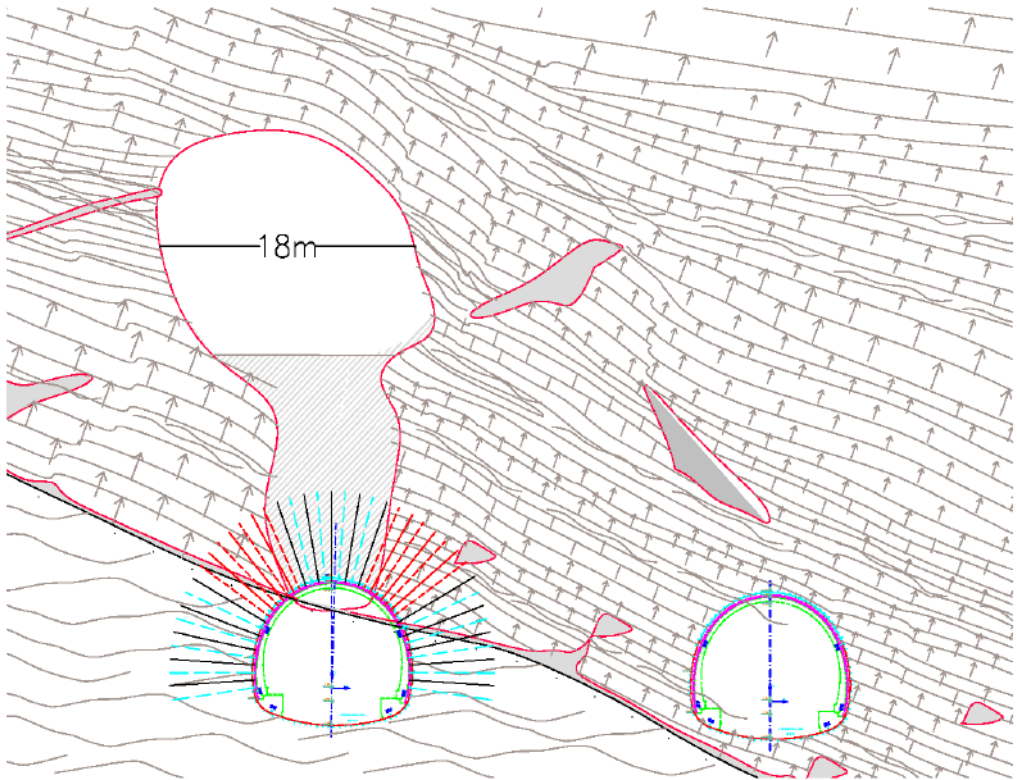
Figure 11 – A schematic showing the layout of the tunnel tubes and the cavern encountered during the excavation of tunnel Ivan.

Rehabilitation works, which ensured global stability of the tunnel excavation, included the use of a heavy support (lattice girder PS 180/10/30 with a horizontal spacing of 50 cm) and the installation of the primary support which comprised of 30 cm thick reinforced shotcrete lining and 9 to 12 meters long IBO anchors at 1.5 m radial spacings. Remediation measures relied heavily on the efficiency of the pipe roof, which was installed prior to the advance beneath the cavern. Pipe roof was also subject to collapse on two occasions as, despite the use of consolidation grouting, there was no firm ground on the opposite side of the cavern to provide the required fixity. After the second failure of the pipe roof, it has been observed that the grouted body above the tunnel was mixed with heavy liquid of gypsum solution and didn't have integrity.

In the third attempt of consolidation grouting, it was decided not to close the cavern completely, but to leave an open part to ensure that the gypsum solution have the possibility to drain into the tunnel. After the installation of the grouting pipes, it was possible to inspect their position in the cavern. Prior to the grouting, once the bottom of the cavern was drained and cleaned of gypsum solution, the cavern was closed. In the next twelve hours, the cavern was filled up to 6-8 m high with lightweight concrete, the level of which was confirmed using inspection pipes. Once the lightweight concrete had hardened, the additional drainage pipes were installed to drain percolating gypsum solution and water from the cavern.

After construction of the primary lining the cavern was further filled up to 18 meters high with lightweight concrete, which was an upper limit for the lining capacity. The remaining empty space of the cavern was about 12 m high and some 12 m to 18 m wide. It was expected that the empty space of the cavern would be soon naturally filled with water, and further on as the chemical process continues, with gypsum solution, which had been the content of the cavern in pre-disturbed state. Before the construction of the secondary lining, the contact injection around the tunnel was carried out to minimize the water inflow into the tunnel.

A final remediation measure that should ensure the long-term stability of the tunnel was the construction of the heavily reinforced secondary lining along the full length of the col-lapse section (some 12 m long). Also, the foundations and the invert were reinforced to improve the durability of the structure.

6. CONCLUSIONS

The role of geotechnical engineering is undervalued and inadequately understood in our region. Although it takes pivotal role in environmental, offshore, defence, petroleum and geothermal engineering it is usually regarded as a subdiscipline of civil or mining engineering. With the evolution of the understanding of the impact of human activity on the environment, the role of geotechnical engineering becomes indispensable in the development of critical infrastructure, which is the backbone of the contemporary societies.

The regulation in the field of geotechnics in the region is based around the European regulations such as Eurocode 7. It is highlighted in the paper that these regulations could be safely used only for less demanding structures, which are not usually found in transport and other critical infrastructure. Deficiencies and pitfalls in the use of standards are underlined and observational method is exposed as the most appropriate method for design of geotechnical structures.

Finally, the main points of the paper are presented on two case examples in tunnel construction. The first example describes the elements of geotechnical design for the construction of portal structures within the active landslide bodies. The second example presents the key aspects of tunnel construction within anhydrite containing rock mass, which is prone to swelling and the presences of collapsible caverns. Both examples demonstrate the complexity of geotechnical design and construction. The examples highlight the necessity of the use of observational method, which is based on the adaptation of the system support to fulfil required conditions in terms of stability and serviceability criteria for a given geotechnical structure.

REFERENCES

[1]   [1]   X.-T. Feng and J. A. Hudson, *Rock Engineering Design*. CRC Press, 2011.

[2]   [2]   C. Jian, P. K. Kwang, and Y. K. Yew, *Geotechnical Engineering for Disaster Mitigation and Rehabilitation*. WORLD SCIENTIFIC, 2005.

[3]   [3]   *European Union (2004). Eurocode 7: Geotechnical Design - Part 1: General rules [Authority: The European Union Per Regulation 305/2011, Directive 98/34/EC, Directive 2004/18/EC] - EN 1997-1 (2004) (English). Luxembourg: Publications Office of the E.*.

[4]   [4]   E. Hoek and E. T. Brown, *Underground excavations in rock*. Institution of Mining and Metallurgy, 1980.

[5]   [5]   A. J. Powderham, "The observational method—learning from projects," *Proc. Inst. Civ. Eng. - Geotech. Eng.*, vol. 155, no. 1, pp. 59–69, Jan. 2002, doi: 10.1680/geng.2002.155.1.59.

[6]   [6]   D. Nicholson and I. of C. Engineers, *The observational method in geotechnical engineering*. Telford, 1996.

[7]   [7]   A. S. for Geomechanics, "Guideline for the Geotechnical Design of Underground Structures with Conventional Excavation.," 2010.

[8]   [8]   L. V Rabcevicz, "The new Austrian Tunelling Method (Part 1 and Part 2)," *Water Power*, vol. November 1, pp. 511-515 and pp. 19–24, 1964.

[9]   [9]   G. Schubert, W., Goricki, A. & Riedmüller, "Guideline for the Geotechnical Design of Underground Structures with Conventional Excavation," *Felsbau 21*, vol. 21, no. 4, pp. 13–18, 2003.

[10]   [10] V. Jovičić, S. Galuf, E. Muhić, "Construction of Tunnel Portal Structures within the Active Landslide Bodies," *Riv. Ital. DI Geotec.*, vol. 56/1, no. January-March 2022, pp. 32–46, 2022, doi: dx.doi.org/10.19199/2022.1.0557-1405.032.

PROCEEDINGS FROM THE INTERNATIONAL
CONGRESS

Emilija Jočić[1], *Miroslav Marjanović*[2]

ANALIZA PROGRESIVNOG LOMA KOMPOZITNIH LAMINATA IZLOŽENIH SILI PRITISKA

Rezime:

U ovom radu sprovedena je analiza progresivnog loma pločastih kompozitnih laminata, opterećenih na pritisak. Hashin-ov kriterijum je korišćen prilikom određivanja inicijacije loma laminata, dok je razvoj oštećenja analiziran primenom modela razmazane pukotine. U cilju poboljšanja efikasnosti proračuna, izabrani model oštećenja je implementiran u numerički model zasnovan na Redijevoj slojevitoj teoriji ploča. Prilikom validacije razvijenog algoritamskog modela, dobijeni rezultati su upoređeni sa numeričkim rezultatima iz literature i dobijena su odlična poklapanja.

Ključne reči: progresivni lom, razmazana pukotina, slojevita teorija, laminat

PROGRESSIVE FAILURE ANALYSIS OF COMPOSITE LAMINATES LOADED IN COMPRESSION

Summary:

This paper deals with the progressive failure analysis (PFA) of plate-like composite laminates loaded in compression. The Hashin failure criterion was used to detect failure initiation, while damage evaluation behaviour was calculated using the smeared crack band (SCB) damage model. SCB damage model have been incorporated into the Full-Layerwise Theory (FLWT) framework to increase the computational efficiency of the PFA. To verify the effectiveness of the FLWT-SCB prediction model, the obtained results were compared against the benchmark data from the literature and excellent agreement has been obtained.

Key words: progressive failure, smeared crack, layerwise theory, laminate

---

[1] *Asistent, student doktorskih studija, Građevinski fakultet, Univerzitet u Beogradu, edamjanovic@grf.bg.ac.rs*

[2] *Dr, Docent, Građevinski fakultet, Univerzitet u Beogradu, mmarjanovic@grf.bg.ac.rs*

1. INTRODUCTION

Due to their outstanding strength and stiffness, low maintenance costs and corrosion resistance, fiber-reinforced composites have been widely used in the construction of aerospace, marine, mechanical and automotive structures which generally require high reliability levels. These materials have a growing use in civil engineering, as well. The low compressive strength of laminar composites is a limiting factor in fully harnessing the capabilities of such structural elements. In real structural elements, holes and notches are often present, which further decreases the compressive strengths due to presence of stress concentration zones. A crucial factor in determining the response of laminar composites in compression is the presence of manufacturing imperfections, such as fiber misalignment and microstructural voids [1]. Such manufacturing imperfections lead to various failure mechanisms in laminar composites under compression, such as fiber buckling and kinking, matrix yielding and cracking, among others. Failure mechanisms often interact with each other, leading to complex crack pathways when modelling fracture problems in laminar composites.

Progressive failure analysis (PFA) of laminar composites has been studied for a long time and used to predict damage progression and post-failure behaviour in composite materials. For the implementation of failure initiation and propagation algorithms within an existing numerical (i.e. finite element) model, damage models are required [2] such as: discrete damage models (DDM) and continuum damage models (CDM). Generally, discrete techniques lead to models that can accurately predict crack propagation with high fidelity, but at the cost of high computational effort. On the other hand, in CDM approaches, intralaminar cracks are smeared out within the finite element domain and the fracture mechanism is then represented through material stiffness degradation, controlled by damage variables.

The earliest CDM approach is instantaneous softening method (ISM), where the material property associated with the failure model degrades instantly to zero (or some small value) of the undamaged material properties [3-5]. A comparison of ISM-based models against the experimental results confirmed that the predicted failure occurs at a substantially lower load than the experimentally determined one, underestimating the laminate strength and neglecting the fact that the damage is indeed localized and a failed lamina still has a solid residual load-carrying capability.

Composite materials generally exhibit quasi-brittle post-failure behaviour resulting in a high fracture energy dissipated and therefore a more gradual propagation of fracture [6, 7]. An alternative approach to ISM is gradual softening method (GSM), where the material property associated with the failure mode is degraded gradually (i.e. linearly or exponentially) until it reaches zero [8-10]. The approaches outlined above suffer from a mesh dependency problem related to strain localization during the PFA, associated with the stress concentration zones in plate-like structures (i.e. notches and holes).

The mesh dependency issue can be overcome via the fracture-mechanics augmented smeared crack-band (SCB) model [11], by scaling the fracture energy using a characteristic element length, as described by the crack-band theory [12]. This approach was originally developed for the macroscopic sub-laminate level modeling of laminar composites [13]. Such model leads to a good compromise between computational cost and solution accuracy, and they are thus used in most of the works dealing with composite failure modelling in conjunction with different plate theories. Most SCB models available in the literature generally focus on

PFA of laminar composites under tension [14-16], and the application of these models for the PFA of compressed laminar composites is relatively rare. Some examples of the use of SCB models for the compressive failure modelling of laminar composites include the failure analysis of open-hole compression (OHC) laminar composites [17], and the axial crush simulation of braided composite tubes [18].

The computational costs associated with PFA of laminar composites can be prohibitive, even considering the relative efficiency of smeared crack-band models, especially for larger structures. This is usually due to the requirement of refined, often 3D meshes, to obtain an accurate stress field.

This paper aims to increase the computational efficiency of the progressive failure analysis of laminar composites and preserve the accuracy of the 3D finite element models, by using a layered FLWT-based finite element model [19] for structural analysis and SCB damage model [11] for material modelling. The proposed FLWT-SCB prediction model was previously developed by authors [20] for the progressive failure modelling of open-hole laminar composites under tension, and here the model applicability for compressed members is highlighted. The developed FLWT-SCB prediction model was implemented into an original FLWTFEM framework [21]. To verify the proposed model implementation for compressive failure within the FLWTFEM framework, a series of single element simulations were carried out. For model validation, the obtained results are compared against the experimental load-displacement curves and strain diagrams by Nagaraj et al. [22].

2. LAYERWISE THEORY FOR 3D STRUCTURAL ANALYSIS OF LAMINAR COMPOSITES

In the paper, a laminated composite plate made of n perfectly bonded orthotropic layers is considered (Figure 1, left). The total plate thickness is denoted as h, while the thickness of the kth lamina is denoted as h_k. The plate is supported along the portion Γ_u of the boundary Γ and loaded with loadings $q_t(x,y)$ and $q_b(x,y)$ acting to either top or the bottom surface of the plate (S_t or S_b). Piece-wise linear variation of all three displacement components through the thickness is imposed, leading to the layer-wise 3D stress field. The displacement field (u, v, w) of an arbitrary point (x,y,z) of the laminate is given as:

$$u(x, y, z) = \sum_{I=1}^{N} U^I(x, y)\Phi^I(z), \quad v(x, y, z) = \sum_{I=1}^{N} V^I(x, y)\Phi^I(z),$$

$$w(x, y, z) = \sum_{I=1}^{N} W^I(x, y)\Phi^I(z)$$

(1)

In Eq. (1), N is the number of numerical layers, $U^I(x,y)$, $V^I(x,y)$ and $W^I(x,y)$ are the displacement components in the Ith numerical layer of the plate in directions x, y and z, respectively, $\Phi^I(z)$ are selected to be linear layerwise continuous functions of the z-coordinate, defined over the considered layer I.

Based on the assumed displacement field, linear strain field can be easily derived and may be found in [19]. To reduce the 3D model to a plate model, the z-coordinate is eliminated by the explicit integration of stresses multiplied with the corresponding functions $\Phi^I(z)$, introducing the constitutive relations of the laminate which can be found in [19].

The finite element discretization is derived by introducing an assumed interpolation of the displacement field into the weak form of the FLWT. All displacement components are interpolated using the same 2-D Lagrange interpolation polynomials. Element stiffness matrix is obtained in a common way, using 2D Gauss-Legendre quadrature for quadrilateral domains. In the paper, quadratic serendipity (Q8) layered quadrilateral elements have been considered (Figure 1, right). To avoid shear locking, reduced integration is used (2×2 points for Q8). After the derivation of the characteristic element matrices, the assembly procedure is performed in a usual manner.
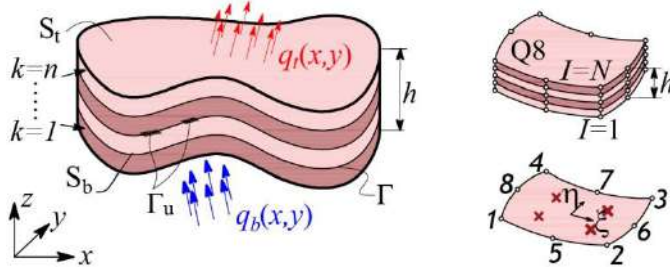
Figure 1 – left: Laminated composite plate with n material layers and N numerical interfaces; right: Quadratic serendipity Q8 layered element with linear layerwise interpolation through the thickness and corresponding Gauss quadrature points for the reduced integration.

Once the nodal displacements are obtained the stresses are evaluated from the well-known lamina 3D constitutive equation in the Gauss points at the top (t) and bottom (b) interfaces of the considered lamina and they are given in [19]. The stresses are calculated both in the laminate (*xyz*) and the local lamina (*123*) coordinate systems. This is crucial in the progressive failure analysis (PFA), since the failure criteria require the stresses in the lamina coordinate system. Since the interlaminar stresses calculated from the constitutive equations are discontinuous at layer interfaces, they are re-computed by assuming quadratic distribution through each layer, using the procedure given in detail in [23].

3. SMEARED CRACK-BAND COMPRESSIVE DAMAGE MODEL

The current work deals with compressive progressive failure of open-hole laminar composites via the fracture-mechanics augmented SCB damage model [11]. The SCB damage model has been previously described in [20] and is briefly recapitulated here for completeness.
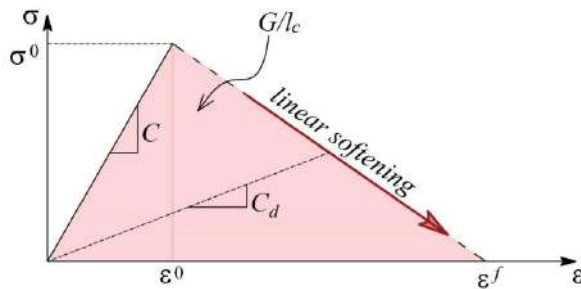
Figure 2 – Stress-strain relationship with linear softening law

In smeared formulations, the fracture energy is distributed (smeared) over the full volume of the element. The response of damaged lamina, in both fiber and matrix direction, was described by distinct bilinear strain-softening curves (see Figure 2), where the peak stress coincides with the fibre and matrix strength, respectively.

This damage law is determined based on the assumption that the total energy needed to fail an element (released strain energy) is equal to the energy needed to create a crack that passes through it. The released strain energy of a failed element is determined as a product of the area under the stress-strain curve, defined in Figure 2, and characteristic element length l_c. In the present work, l_c is defined as the square root of a layered finite element area. This energy is set to be equal to the dissipated fracture energy of the composite material (fracture toughness):

$$\varepsilon^f = \frac{2G}{\sigma_0 l_c} \tag{2}$$

In Eq. (2), ε^f is maximum strain, while σ_0 is the material strength. The fracture toughness G is a material property that must be specified for each failure mode. By including the characteristic element length into the material damage law, the constant dissipated fracture energy is achieved, regardless of the element dimensions.

3.1. DAMAGE INITIATION AND EVOLUTION

Initiation of damage occurs when stresses in the weakest lamina exceed the allowable fiber or matrix strength. In this paper, the Hashin failure criterion [24] is used, a quadratic criterion in a piecewise form based on the material strengths, where each smooth branch represents a failure mode. These criteria consider four different damage initiation modes: fiber tension, fiber compression, matrix tension, and matrix compression. The quadratic Hashin failure criteria are given in [20].

Once the failure has been initiated, the damaged material must be unloaded in a proper manner, so the stresses can be redistributed to the remaining undamaged material. As damage progresses, PFA is performed through the material stiffness degradation, controlled by damage variables. For each failure mode J ($J = $ *fiber tension, fiber compression, matrix tension, matrix compression*) these variables are defined such that they have values between zero (undamaged status) and one (complete damaged status). The evolution of each damage variable is governed by equivalent strain $\varepsilon_{J,eq}$. In this way, each damage mode is represented as a 1D stress-strain problem (Figure 2) instead of the actual 3D stress-strain relation. The equivalent strain and corresponding equivalent stress for each failure mode were defined in detail in [20].

Using the equivalent strain and stress, a damage variable for each failure mode J can be calculated using the following relation:

$$d_J = \frac{\varepsilon_{J,eq}^f \left(\varepsilon_{J,eq} - \varepsilon_{J,eq}^0 \right)}{\varepsilon_{J,eq} \left(\varepsilon_{J,eq}^f - \varepsilon_{J,eq}^0 \right)}, \quad \varepsilon_{J,eq}^0 \leq \varepsilon_{J,eq} \leq \varepsilon_{J,eq}^f \tag{3}$$

In Eq. (3), $\varepsilon_{J,eq}^0$ is the equivalent strain at the initial failure state ($d_J = 0$) and $\varepsilon_{J,eq}^f$ is the equivalent strain at the final failure state ($d_J = 1$). Since damage evolution is an irreversible

process, damage variable is equal to the maximum of its current value and the value obtained from Eq. (3). The equivalent strain at the final failure state $\varepsilon_{\mathrm{J},eq}^{f}$ is computed from Eq. (2).

4. MODEL VALIDATION

This section presents a series of single-element analyses to verify the applicability of the FLWT-SCB prediction model for the progressive failure analysis of laminar composites loaded in compression. Such simulations provide a convenient method to verify the failure initiation and progression of each failure mode independently. In the current verification tests, the structure is a IM7/8552 unidirectional lamina (see Table 1) of thickness $h_i = 0.125$mm, modelled as a single element of size 1 mm × 1 mm and subjected to uniaxial compression. All the material properties are adopted according to reference [22]. The quasi-3D stress analysis was performed using a single Q8 layered quadrilateral element with reduced integration in all numerical simulations. Each lamina is modelled as a single numerical layer, adopting the linear distribution of displacements along the lamina thickness. The use of a single element test is typical for this class of problems, and it is necessary to verify the model reliability. In all simulations, the specimen was clamped on one side and loaded using a 2mm displacement on the opposite side. At the clamped end, all DOFs were constrained.

Table 1 – Material properties of IM7/8552 carbon fibre reinforced polymer

Properties	Values	Properties	Values	Properties	Values
E_1	150 GPa	v_{23}	0.48	$S = T$	90 MPa
$E_2 = E_3$	11 GPa	X_T	2560 MPa	G_{ft}	120 KJ/m^2
$G_{12} = G_{13}$	5.8 GPa	X_C	1690 MPa	G_{fc}	80 KJ/m^2
G_{23}	2.9 GPa	$Y_T = Z_T$	73 MPa	G_{mt}	2.6 KJ/m^2
$v_{12} = v_{13}$	0.34	$Y_C = Z_C$	250 MPa	G_{mc}	4.2 KJ/m^2
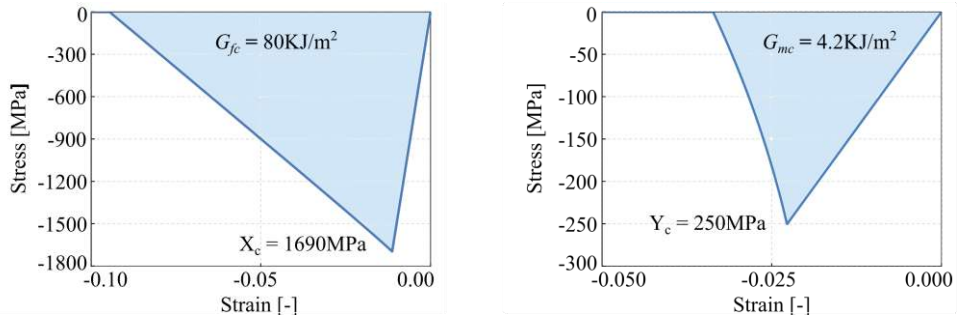
Figure 3 – left: Compressive stress - strain curve of a 1mm×1mm single element lamina loaded in longitudinal (fiber) direction; right: Compressive stress - strain curve of a 1mm×1mm single element lamina loaded in transverse (matrix dominated) direction.

The first simulation involves a specimen made from a single unidirectional layer (0°) under longitudinal compression (in the fiber direction, 0º), which consequently results in a fibre failure mode. The stress-strain curve for this case is plotted in Figure 3a. Next, the same specimen made from a single unidirectional layer (0°) is subjected to transverse compression

(perpendicular to the fiber), resulting in a matrix failure mode. The stress-strain curve for this case has been shown in Figure 3b. The final assessment is the compressive loading of a single element consisting of a quasi-isotropic laminate consists of 16 layers assembled in $[90^o/45^o/0^o/-45^o]_{2s}$ stacking sequence. Since the stacking sequence is symmetric, only half of the laminate through the thickness was modelled to reduce the number of DOFs.

In the symmetry plane, displacements in the thickness direction were set to zero. Figure 4 illustrates the stress-strain response predicted by the developed FLWT-SCB framework, along with reference numerical results [22].
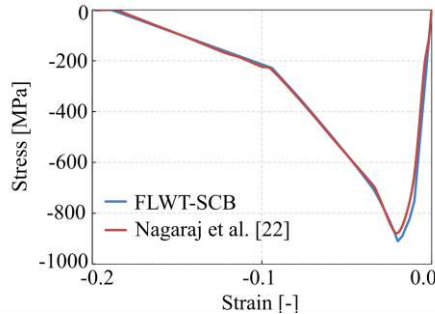
Figure 4 – Compressive stress - strain curve of a 1mm×1mm single element laminate with $[90^o/45^o/0^o/-45^o]_{2s}$ stacking sequence, considering: present FLWT-SCB model (blue lines) and the damage model of Nagaraj et al. [22] (red lines).

The stress-strain response of a specimen made from a single unidirectional layer (0°), loaded in compression parallel and perpendicular to the fiber, follows the bilinear path described by the FLWT-SCB damage model with linear softening, as shown in Figure 3. The peak stress in both cases is equal to the fibre (1690 MPa) and matrix (250 MPa) material strengths. Furthermore the area under the stress-strain curve is equal to the fracture energy in the longitudinal (80 KJ/m^2) and transverse (4.2 KJ/m^2) directions. Finally, the stress-strain response of the single element $[90^o/45^o/0^o/-45^o]_{2s}$ laminate obtained by FLWT-SCB prediction model is in good agreement with reference numerical results [22], as shown in Figure 4.

5. CONCLUSIONS

The present paper aims to increase the computational efficiency of the progressive failure analysis of laminar composites, preserve the accuracy of the 3D finite element models, by using a layered FLWT-based finite element model [19] for structural analysis and SCB damage model [11] for material modelling. The proposed FLWT-SCB prediction model was previously developed by authors [20] for the progressive failure modelling of open-hole laminar composites under tension. The developed FLWT-SCB prediction model was implemented into an original FLWTFEM framework. In SCB approaches, the material stiffness matrix degradation was controlled by damage variables, which evolution are governed by an equivalent strains appropriately defined for each failure mode. The response of damaged lamina, in both fiber and matrix direction, was described by distinct bilinear strain-softening curves, where the peak stress coincides with the fibre and matrix strength, respectively. The mesh dependency problem was reduced by scaling the fracture energy using a characteristic element length, as described by the crack-band theory [12]. The failure initiation and modes of

failure are determined using the Hashin failure criterion. The use of layered quadrilateral elements in the damage modelling of laminar composites is relatively unexplored in the literature, where the standard approach is to use linear solid elements.

To verify the proposed model implementation for compressive failure within the FLWTFEM framework, a series of single elements tests was carried out. The quasi-3D stress analysis was performed using a single Q8 layered quadrilateral element with reduced integration in all tests. For model validation, the obtained results are compared against the experimental load-displacement curves and strain diagrams by Nagaraj et al. [22].

FLWT-SCB demonstrated a bilinear stress-strain response of single element laminas, loaded in compression parallel and perpendicular to the fiber, where the peak stress coincides with the fibre and matrix strength, respectively. Furthermore the area under the stress-strain curve is equal to the fracture energy in the longitudinal and transverse directions. Finally, the stress-strain response of the single element $[90^o/45^o/0^o/-45^o]_{2s}$ laminate obtained by FLWT-SCB prediction model is in good agreement with reference numerical results [22].

The advantages of layered FLWT-based finite element model were demonstrated, in particular the savings in computational costs and the capability to provide the accurate 3D stress field, which is curious for accurate prediction of damage initiation and evolution in problems with highly localized stress peaks. Moreover, the use of layered quadrilateral elements leads to relaxation of element aspect-ratio and size constraints, from which 3D models suffer. These aspects could have significant advantages in improving the computational efficiency during the progressive failure analysis of large-scale composite structures.

Future works includes the extension of the FLWT-SCB framework's capabilities towards PFA of an open-hole fiber-reinforced laminates loaded in compression, the inclusion of cohesive zone modelling to account for delamination, as well as the application of the framework to the prediction of behaviour of cross-laminated timber (CLT) panels.

ACKNOWLEDGEMENTS

REFERENCES

[1]   Sun, Q., Zhou, G., Guo, H., Meng, Z., Chen, Z., Liu, H., Kang, H., Su, X.: Failure mechanisms of cross-ply carbon fiber reinforced polymer laminates under longitudinal compression with experimental and computational analyses, Composites Part B: Engineering, 167, 2019, 147-160.

[2]   Orifici, A. C., Herszberg, I., Thomson, R. S.: Review of methodologies for composite material modelling incorporating failure. Composite Structures, 86(1-3), 2008, 194-210.

[3]   Tan, S. C., Perez, J.: Progressive failure of laminated composites with a hole under compressive loading, Journal of Reinforced Plastics and Composites, 12(10), 1993 1043-1057.

[4]   Camanho, P. P., Matthews, F. L.: A progressive damage model for mechanically fastened joints in composite laminates, Journal of Composite Materials, 33(24), 1999, 2248-2280.

[5]   Chang, F. K., Chang, K. Y.: A progressive damage model for laminated composites containing stress concentrations, Journal of Composite Materials, 21, 1987, 834-855.

[6]   Laffan, M. J., Pinho, S. T., Robinson, P., Iannucci, L.: Measurement of the in situ ply fracture toughness associated with mode I fibre tensile failure in FRP. Part I: Data reduction, Composites Science and Technology, 70, 2010, 606-613.

[7]   Laffan, M. J., Pinho, S. T., Robinson, P., Iannucci, L.: Measurement of the in situ ply fracture toughness associated with mode I fibre tensile failure in FRP. Part II: Size and lay-up effects, Composites Science and Technology, 70, 2010, 614-621.

[8]   Kim, Y. W., Hong, C. S.: Progressive Failure Model for the Analysis of Laminated Composites Based on Finite Element Approach, Journal of Reinforced Plastics and Composites, 11(10), 1992, 1078-1092.

[9]   Lin, W. P., Hu, H. T.: Nonlinear Analysis of Fiber-Reinforced Composite Laminates Subjected to Uniaxial Tensile Load, Journal of Composite Materials, 36(12), 2002, 1429-1450.

[10]   Reddy, Y. S. N., Moorthy, C. M. D., Reddy, J. N.: Non-linear progressive failure analysis of laminated composite plates, International Journal of Non-Linear Mechanics, 30(5), 1995, 629-649.

[11]   Forghani, A., Poursartip, A., Vaziri R.: An orthotropic non-local approach to modeling intra-laminar damage progression in laminated composites, International Journal of Solids and Structures, 180, 2019, 160-175.

[12]   Bazant, Z. P.: Instability, ductility, and size effect in strain-softening concrete. Journal of Engineering Mechanics – Asce, 102(2), 1976, 331-344.

[13]   Williams, K. V., Vaziri, R., Poursartip, A.: A physically based continuum damage mechanics model for thin laminated composite structures, International Journal of Solids and Structurest, 40(9), 2003, 2267-2300.

[14]   Lapczyk, I., Hurtado, J. U.: Progressive damage modeling in fiber reinforced materials, Composites Part A: Applied Science and Manufacturing, 38, 2007, 2333-2341.

[15]   Reiner, J., Feser, T., Schueler, D., Waimer, M., Vaziri, R.: Comparison of two progressive damage models for studying the notched behavior of composite laminates under tension, Composite Structures, 207, 2019, 385-396.

[16]   Nagaraj, M. H., Reiner, J., Vaziri, R., Carrera, E., Petrolo, M.: Progressive damage analysis of composite structures using higher-order layer-wise elements, Composites Part B: Engineering, 190, 2020, 107921.

[17]   Su, Z. C., Tay, T. E., Ridha, M., Chen, B. Y.: Progressive damage modeling of open-hole composite laminates under compression, Composite Structures, 122, 2015, 507-517.

[18]   McGregor, C., Zobeiry, N., Vaziri, R., Poursartip, A., Xiao, X.: Calibration and validation of a continuum damage mechanics model in aid of axial crush simulation of braided composite tubes, Composites Part A: Applied Science and Manufacturing, 95, 2017, 208-219.

[19]   Reddy, J. N.: Mechanics of laminated composite plates and shells: theory and analysis, CRC Press, Boca Raton, Florida, 2004.

[20] Jočić, E., Marjanović, M.: Progressive failure analysis of open-hole composite laminates using FLWT-SCB prediction model, International Journal of Mechanical Sciences, 227, 2022, 107407.

[21] Marjanovic, M., Meschke, G., Damnjanovic, E.: Object-oriented framework for 3D bending and free vibration analysis of multilayer plates: Application to cross-laminated timber and soft-core sandwich panels, Composite Structures, 255, 2021, 112-159

[22] Nagaraj, M. H., Reiner, J., Vaziri, R., Carrera, E., Petrolo, M.: Compressive damage modeling of fiber-reinforced composite laminates using 2D higher-order layer-wise models, Composites Part B: Engineering, 215, 2021, 108753.

[23] Marjanovic, M., Markovic, N., Damnjanovic, E., Cvetkovic, R.: Three-dimensional stress analysis and design of cross-laminated timber panels using full-layerwise-theory-based finite element method, Thin-Walled Structures, 157, 2020, 107-156.

[24] Hashin, Z.: Failure criteria for unidirectional fibre composites, ASME Journal of Applied Mechanics, 47, 1980, 329-334.

R-2

Kongres 2022
Congress 2022

Filip Đorđević[1], *Svetlana M. Kostić*[2]

PROCENA GRANIČNE NOSIVOSTI VITKIH CCFST STUBOVA PRIMENOM VEŠTAČKIH NEURONSKIH MREŽA

Rezime:

U radu je predložena primena algoritama veštačkih neuronskih mreža (ANN) za procenu granične nosivosti pri pritisku vitkih kružnih stubova od čeličnih cevi ispunjenih betonom (CCFST). Skup podataka od 1051 uzorka je primenjen za generisanje odgovarajućeg prognostičkog ANN modela. Empirijske jednačine su takođe razvijene iz najbolje neuronske mreže, a njihovi rezultati su upoređeni sa rezultatima dobijenim standardom Evrokod 4 (EC4). Analize pokazuju da se izlazni rezultati predloženog ANN modela bolje slažu sa eksperimentalnim rezultatima od onih koji su kreirani primenom odredbi EC4 standarda.

Ključne reči: mašinsko učenje, CFST stubovi, empirijske jednačine, predikcija

ESTIMATION OF ULTIMATE STRENGTH OF SLENDER CCFST COLUMNS USING ARTIFICIAL NEURAL NETWORKS

Summary:

This paper proposes the use of artificial neural network (ANN) algorithms to estimate the ultimate compressive strength of slender circular concrete-filled steel tubular (CCFST) columns. A dataset of 1051 samples was applied to generate an appropriate ANN prognostic model. Empirical equations were also developed from the best neural network, and their results were compared with those obtained by Eurocode 4 (EC4) design code. Analyses show that the proposed ANN model has a better agreement with experimental results than those created with provisions of the EC4 design code.

Key words: machine learning, CFST columns, empirical equations, prediction

[1] *Mast.inž.građ, Asistent, Građevinski fakultet Univerziteta u Beogradu, Srbija, fdjordjevic@grf.bg.ac.rs*
[2] *Dr, V.prof, Građevinski fakultet Univerziteta u Beogradu, Srbija, svetlana@grf.bg.ac.rs*

1. INTRODUCTION

Machine learning (ML) is a category of artificial intelligence (AI) that contains a series of algorithms capable of adapting to certain situations and predicting outcomes with high accuracy, based on experience. ML has found applications in many branches including civil engineering.

Concrete-filled steel tubular (CFST) columns play an important role in structural engineering due to their numerous advantages. There are different guidelines for their modelling proposed by several design codes such as Eurocode 4 (EC4). To find better agreement with experimental results than the EC4 design code has, many authors have tried different approaches to predict the axial capacity of CFST columns. The efficient application of the support vector machine (SVM) and artificial neural network algorithms (ANN) for the prediction of the ultimate strength of CFST columns was proposed by Zarringol et al. [1]. Nguyen and Kim [2] recommended a hybrid particle swarm optimization-based artificial neural network (PANN) algorithm on a limited number of specimens (241 experiments). Many accurate surrogate models for a similar problem such as gradient tree boosting (GTB) algorithm [3], adaptive neuro-fuzzy inference system (ANFIS) model [4], and gene expression programming (GEP) method [5] were successfully employed, but without established empirical equations. Đorđević and Kostić [6] found on a small dataset that EC4 design code works better for stub CCFST columns (236 samples) than for slender columns (272 samples), using Decision tree (DT) and Random forest (RF) algorithms. A similar conclusion was provided in [7], using ANN with Levenberg-Marquardt (LM) algorithm for square CFST columns (685 stub columns and 337 slender columns), by the same authors.

This paper proposes an improved LM algorithm with Bayesian Regularization (BRA) for predicting the ultimate compressive strength of slender circular CFST columns (CCFST). Also, this study aims to develop empirical equations. The best ANN model with fine-tuned hyperparameters was developed using a K-fold cross-validation technique. Obtained results show that the ANN model better simulates the behaviour of the axially loaded CCFST columns than the more conservative EC4 design code. Using the regularization method, even with a simpler architecture the results are better than those obtained with the basic LM algorithm [7].

2. EXPERIMENTAL DATASET

In this study, a total of 1051 tests on slender CCFST columns subjected to pure compression were retrieved from various researchers, including Denavit [8] (387 samples), Goode [9] (330 samples), Thai et al. [10] (188 samples), Belete [11] (121 samples), Zeghiche et al. [12] (15 samples), Schneider [13] (8 samples), and Zhichao et al. [14] (2 samples). Table 1 presents major distribution features of the following input and output parameters: outer diameter (D), the thickness of the steel tube (t), length of column (L), steel yield stress (f_y), concrete compressive strength (f_c'), ultimate compressive strength (N_{exp}). It can be seen that wide ranges of all features were considered, even beyond the EC4 design code limitations described in section 3.

CCFST members are categorized as slender columns for $L/D > 4$ [6], [7], [15]. Since in some references, the concrete compressive cube strength (f_{cu}) is reported, these values are converted on the cylinder strength (f_c') according to the following expression proposed by L'Hermite [16]:

$$f_c' = \left[0.76 + 0.21 \cdot log_{10}(f_{cu}/19.6)\right] \cdot f_{cu} \tag{1}$$

Table 1 – Distribution values of the test parameters

Parameter	Unit	Mean	St.Dev.	Min.	Max.
D	mm	135.9	61.08	38.1	500
t	mm	4.27	2.34	0.7	16
L	mm	1562.23	1035.88	350	5000
f_y	MPa	343.5	83.45	178.28	682
f_c'	MPa	38.44	21.18	6.99	186
N_{exp}	kN	1329.88	1577.94	45.2	12838

Since a pre-processing phase is very important for training ANN, to disqualify bias due to different units possessing variables, input and output values were normalized to fall in the interval [-1,1]. The distributions of the database with respect to the steel yield stress, concrete compressive strength, and relative and section slenderness, are graphically presented in Figure 1. It can be seen that a large number of samples have standard geometrical and material properties, but some data exceeds the EC4 limits, marked with dash-dot blue lines.

(a) f_y [MPa]

(b) f_c' [MPa]

(c) $\bar{\lambda}$

(d) $(D/t)(f_y/235)$
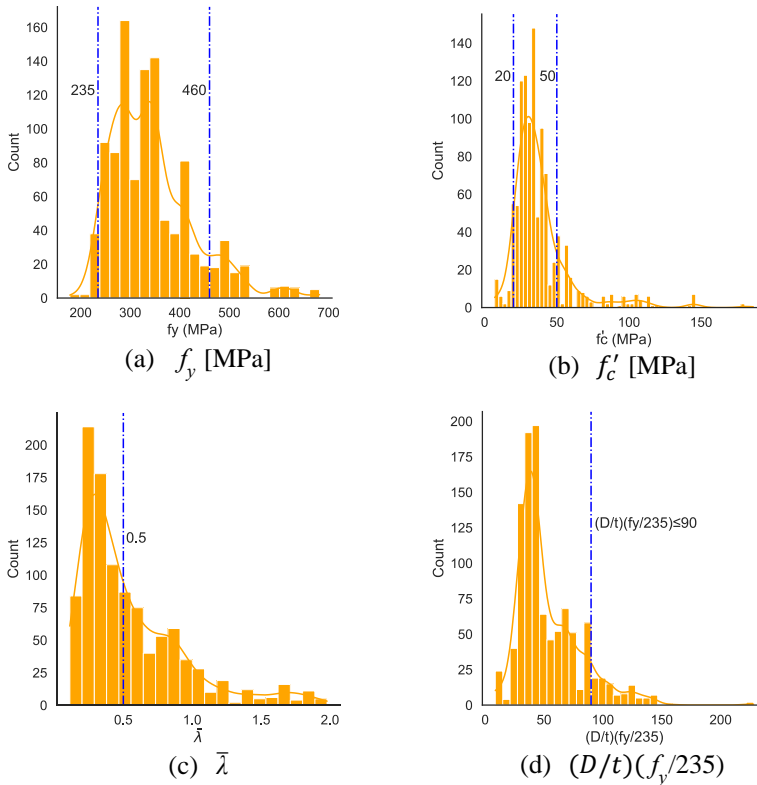
Figure 1 – Distribution of the dataset referred to: (a) steel yield stress, (b) concrete compressive strength, (c) relative slenderness, (d) section slenderness

160

Figure 2 illustrates the heatmap of Pearson correlation coefficients between parameters. It is visible that the highest correlation is obtained between the dimensions of the section and the ultimate compression strength of CCFST columns (0.828 for outer diameter and 0.621 for the thickness of the steel tube). These variables have the strongest relation with each other, and a similar conclusion was derived by Zarringol et al. [1].
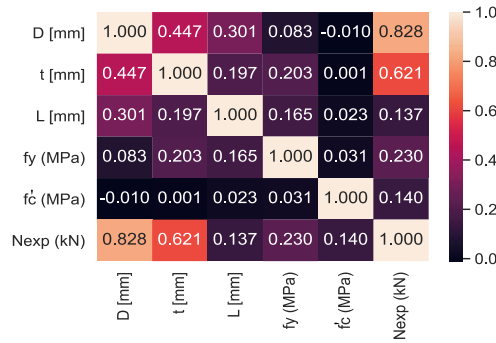
Figure 2 – Heatmap of Pearson correlation coefficients between parameters

3. EUROCODE 4 PROVISIONS

Axial compressive strength of doubly symmetrical CFST columns using a simplified method, with a condition of relative slenderness $\bar{\lambda} \leq 2$, calculates as follows:

$$N_u^{EC4} = \chi \cdot N_{pl,Rd} = \chi \cdot (A_s \cdot f_y + A_c \cdot f_c') \tag{2}$$

For circular CFST columns where relative slenderness does not exceed 0.5 and without eccentricity of the force, the increase in strength caused by the confinement effect can be taken into account:

$$N_u^{EC4} = \chi \cdot N_{pl,Rd} = \chi \cdot \left(A_s \cdot f_y \cdot \eta_s + A_c \cdot f_c' \cdot \left(1 + \eta_c \cdot \frac{t}{D} \cdot \frac{f_y}{f_c'} \right) \right) \tag{3}$$

where $N_{pl,Rd}$ is the plastic resistance to compression, χ is the reduction factor for relevant buckling mode, η_s describes the reduction of the steel yield stress due to expansion of concrete and η_c describes the increase of concrete compressive strength due to the confinement effect

$$\eta_s = \eta_{s0} = 0.25(3 + 2\bar{\lambda}) \leq 1.0 \tag{4}$$

$$\eta_c = \eta_{c0} = 4.9 - 18.5\bar{\lambda} + 17\bar{\lambda}^2 \geq 0 \tag{5}$$

Factor χ and relative slenderness $\bar{\lambda}$ are calculated as follows:

$$\chi = 1 / [\Phi + \sqrt{\Phi^2 - \bar{\lambda}^2}] \leq 1 \tag{6}$$

$$\Phi = 0.5 \cdot [1 + 0.21 \cdot (\bar{\lambda} - 0.2) + \bar{\lambda}^2] \tag{7}$$

$$\bar{\lambda} = \sqrt{N_{pl,Rd} / N_{cr}} \tag{8}$$

161

where N_{cr} is the elastic critical force for relevant buckling mode calculated with effective flexural stiffness EI_{eff} defined as:

$$EI_{eff} = E_s \cdot I_s + 0.6 \cdot E_c \cdot I_c \qquad (9)$$

Limitations of geometrical and material properties shown in Table 2 are prescribed by EC4 and denoted in Figure 1. The first condition in Table 2 refers to the possibility of neglecting the impact of local buckling.

Table 2 – Limitations of geometrical and material properties prescribed in EC4 design code

Design code	Limitations
Eurocode 4	$D/t \leq 90 \cdot 235/f_y$
	$235 \leq f_y \leq 460\ MPa$
	$20 \leq f_c' \leq 50\ MPa$

An additional limitation of the EC4 is the steel contribution ratio δ, which should satisfy the following condition:

$$0.2 \leq \delta = A_s \cdot f_y / N_{pl,Rd} \leq 0.9 \qquad (10)$$

4. ARTIFICIAL NEURAL NETWORKS

In this study, a feedforward neural network with one hidden layer and eight neurons was developed. This network was trained using a backpropagation algorithm based on the modification of the LM algorithm, named BRA. Steps for exploring and creating an ANN model with the best generalization are described in the following sections.

4.1. BAYESIAN REGULARIZATION

Oppose to the basic LM algorithm based on the early-stopping rule, Bayesian improvement of LM belongs to the regularization techniques. The classical LM algorithm modifies the second-order Hessian matrix using the first order Jacobian matrix [7]. Bayesian regularization has proven to make a better generalization less prone to the possible overfitting, even with a simpler ANN architecture. It uses an adapted performance function without the need for the validation subset [17].

The approximation of the Hessian matrix using BRA is described as follows:

$$H = 2 \cdot \beta \cdot J^T \cdot J + 2 \cdot \alpha \cdot I \qquad (11)$$

$$\alpha = \gamma / (2 \cdot E_W(x)) \qquad (12)$$

$$\beta = (n\text{-}\gamma) / (2 \cdot E_D(x)) \qquad (13)$$

where J is the Jacobian matrix, I is the identity matrix, α and β are the regularization parameters, n is the total number of ANN parameters, E_W is the sum of the squared weights and E_D is the selected performance measure. Parameter γ is equal to n in the first iteration, and, in the next iterations, is calculated from Eq.14:

$$\gamma = n - 2 \cdot \alpha \cdot tr(H)^{-1} \qquad (14)$$

The ANN parameters (weights and biases) are determined to minimize the performance function $F(x)$ (Eq.15):

$$F(x) = \beta \cdot E_D(x) + \alpha \cdot E_W(x) \tag{15}$$

$$E_D(x) = MSE = 1 / n_{tot} \cdot \sum_{i=1}^{n_{tot}} (y_i - \bar{y}_i)^2 \tag{16}$$

$$E_W(x) = 1 / n_{tot} \cdot \sum_{i=1}^{n_{tot}} (w_i)^2 \tag{17}$$

where MSE is the mean squared error, y_i is a target value, $\bar{y}_i$ is the predicted value, n_{tot} is the number of samples and w_i are the network weights.

4.2. QUALITY ASSESSMENT

To make a comparison between predicted and experimental results, in addition to the MSE defined in the previous section, other performance indicators as coefficient of determination (R^2) and root mean squared error ($RMSE$) have also been calculated, Eqs.18-19:

$$R^2 = \left(\frac{n_{tot} \cdot \sum_{i=1}^{n_{tot}}(y_i \cdot \bar{y}_i) - \sum_{i=1}^{n_{tot}} y_i \cdot \sum_{i=1}^{n_{tot}} \bar{y}_i}{\sqrt{\left[n_{tot} \cdot (\sum_{i=1}^{n_{tot}} y_i^2) - (\sum_{i=1}^{n_{tot}} y_i)^2 \right] \cdot \left[n_{tot} \cdot (\sum_{i=1}^{n_{tot}} \bar{y}_i^2) - (\sum_{i=1}^{n_{tot}} \bar{y}_i)^2 \right]}} \right)^2 \tag{18}$$

$$RMSE = \sqrt{1 / n_{tot} \cdot \sum_{i=1}^{n_{tot}} (y_i - \bar{y}_i)^2} \tag{19}$$

It is important to note that from the initial dataset, by random selection, 70% of the data are used for the training and 30% for the testing. Outputs from the hidden and output layer are generated through the hyperbolic tangent and simple linear activation functions respectively, which are mathematically defined as (Eqs.20-21):

$$f(x) = (e^x - e^{-x}) / (e^x + e^{-x}) \tag{20}$$

$$f(x) = x \tag{21}$$

4.2.1. Hyperparameters tuning

To evaluate the performance of the ANN model, a 5-fold cross-validation technique is employed. This procedure reduces the chance of overfitting and bias due to the random splitting of the dataset. The experimental dataset is divided into 5 subsets with an equal amount of data, where each time one subset is used for the testing, while others are used for training. After 5 runs of the ANN, the independent performance scores of each fold and average accuracy of each model is reported. Figure 3a illustrates the split of the dataset.
The tested ANN architectures include 5-4-1, 5-5-1, 5-8-1, 5-10-1, 5-12-1, 5-14-1 networks with a different sets of hyperparameters. After analyses is performed, it is concluded that the network 5-8-1 gives the best results on the 5-fold cross-validation with small fluctuations of R^2 (0.985, 0.978, 0.991, 0.979 and 0.984) and with a high mean value (0.983). Figure 3b presents these results. Also, the best set of hyperparameters are μ=0.1, μ_{dec}=0.001, μ_{inc}=10. The role of these hyperparameters is well described in [7]. Figure 4 presents the best-obtained ANN architecture with one hidden layer and eight neurons.

| (a) *5-fold scheme* | (b) R^2 |
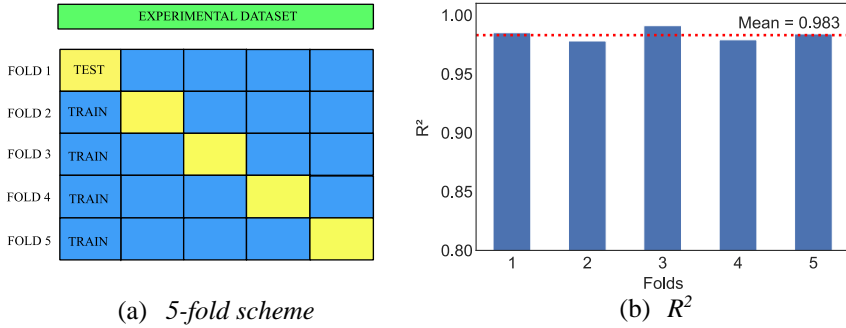
Figure 3 – (a) 5-fold cross-validation scheme and (b) R^2 of the test set per each fold
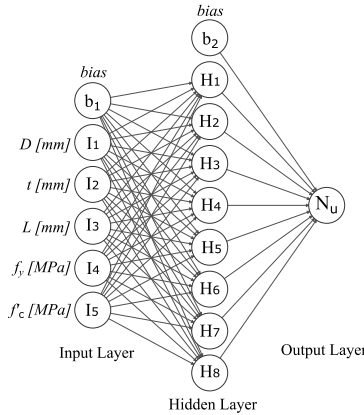
Figure 4 – Proposed ANN model

5. RESULTS

Table 3 compares the computed ultimate compressive strength values of slender CCFST columns with two different approaches: by the presented ANN model and using the EC4 expressions. The recommended ANN model gives more accurate results (R^2=0.992) than EC4 (R^2=0.961) on all samples. It is equally good on the training (R^2=0.992) and test (R^2=0.990) sets. Other performance indicators (*MSE* and *RMSE*) lead to the same conclusion. Figure 5a illustrates that there is no risk of overfitting and the best performance is obtained at the 292nd epoch. Figure 5b shows that a large percentage of errors are close to zero. Several authors have shown similar results for slender columns using various machine learning algorithms as in [6], [7].

Table 3 – ANN and EC4 performance scores

Dataset	R^2		MSE ($\cdot 10^{-4}$)		$RMSE$ ($\cdot 10^{-2}$)	
	ANN	EC4	ANN	EC4	ANN	EC4
Training	0.992	-	4.760	-	2.182	-
Test	0.990	-	5.201	-	2.281	-
All	0.992	0.961	5.069	34.147	2.252	5.844

(a) Training set - ANN (b) Test set - ANN
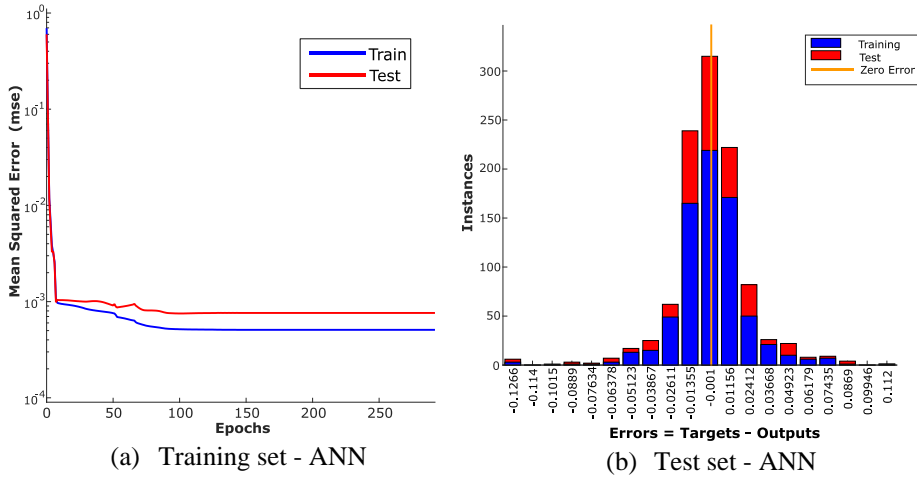
Figure 5 – Train and test results (a) performance functions, (b) error distribution

Figure 6 graphically presents the regression lines for training, test and all data. The ANN results have a good agreement with experimental results for all three subsets. On the other side, EC4 shows a scatter of the results, which is especially pronounced for outputs above 3000 kN. ANN model shows that besides giving more accurate results, the derived expressions can be applied to a wider range of data than the EC4 design code.

(c) Training set - ANN (d) Test set - ANN

(e) All data - ANN (f) All data – EC4
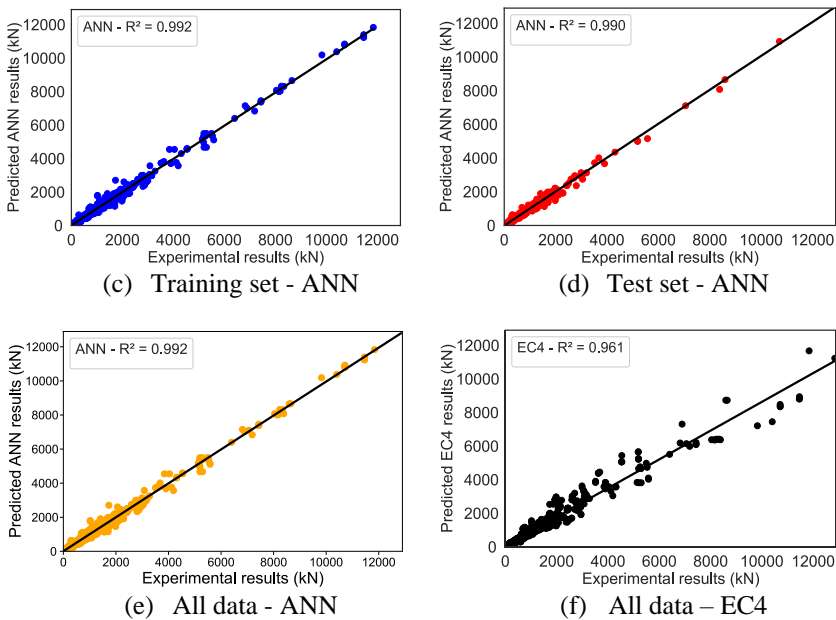
Figure 6 – Comparison of experimental and predicted results (a) Training set, (b) Test set, (c) All data – ANN, (d) All data – EC4

5.1. PROPOSED EQUATIONS

According to the network parameters from the best-trained ANN model, the following empirical equations for calculation of the axial capacity (N_u^{ANN}) of slender CCFST columns are recommended:

$$N_u^{ANN} = N_{u,1-4}^{ANN} + N_{u,5-bias}^{ANN} \tag{22}$$

$$N_{u,1-4}^{ANN} = 2.94144 \cdot H_1' + 0.14098 \cdot H_2' + 0.38613 \cdot H_3' + 1.43560 \cdot H_4' \tag{23}$$

$$N_{u,5-bias}^{ANN} = 1.67761 \cdot H_5' - 2.38619 \cdot H_6' - 0.70682 \cdot H_7' - 1.13363 \cdot H_8' - 1.65957 \tag{24}$$

$$H_1' = Tanh(-1.54932 \cdot D - 0.14438 \cdot t + 0.75599 \cdot L - 0.53019 \cdot f_y - 0.23926 \cdot f_c' + 0.36257) \tag{25}$$

$$H_2' = Tanh(3.0702 \cdot D + 1.10493 \cdot t - 1.22707 \cdot L + 0.88028 \cdot f_y + 0.47573 \cdot f_c' + 3.42817) \tag{26}$$

$$H_3' = Tanh(2.77720 \cdot D - 0.23581 \cdot t + 0.90585 \cdot L - 0.70207 \cdot f_y + 1.17248 \cdot f_c' + 0.02708) \tag{27}$$

$$H_4' = Tanh(3.24453 \cdot D + 1.11523 \cdot t - 2.00113 \cdot L + 1.23696 \cdot f_y + 0.58214 \cdot f_c' - 0.46130) \tag{28}$$

$$H_5' = Tanh(-0.59108 \cdot D - 1.35953 \cdot t - 1.47492 \cdot L + 0.29325 \cdot f_y - 1.17222 \cdot f_c' + 1.44294) \tag{29}$$

$$H_6' = Tanh(-2.94726 \cdot D - 1.24046 \cdot t - 0.19169 \cdot L - 1.57374 \cdot f_y - 1.18168 \cdot f_c' + 1.17002) \tag{30}$$

$$H_7' = Tanh(-3.14082 \cdot D - 0.49002 \cdot t + 1.39387 \cdot L - 1.01158 \cdot f_y - 0.63854 \cdot f_c' - 1.40464) \tag{31}$$

$$H_8' = Tanh(-0.86469 \cdot D + 1.26690 \cdot t - 0.94459 \cdot L + 1.12318 \cdot f_y + 1.00749 \cdot f_c' - 2.04153) \tag{32}$$

6. CONCLUSIONS

The presented ANN model is highly accurate and robust. On the dataset of 1051 samples, the applied LM algorithm with BRA has shown the outstanding prediction performance of the axial capacity of slender CCFST columns. Outputs from the proposed empirical equations have a better agreement with experimental results ($R^2 = 0.992$) than those recommended by the EC4 design code ($R^2 = 0.961$), even for the wider range of test parameters. The proposed ANN model based on one hidden layer and eight neurons can precisely capture the nonlinear behaviour of CFST columns. As opposed to the LM algorithm, there is no need for the validation set of data, which makes the BRA algorithm more efficient with better generalization and with less risk of the possible overfitting. On the other side, analyses also indicate the importance to make a wider dataset for upcoming research. In general, similar surrogate models could be very useful for the engineering practice in the future.

REFERENCES

[1] M. Zarringol, H. T. Thai, and M. Z. Naser, "Application of machine learning models for designing CFCFST columns", *J. Constr. Steel Res.*, vol. 185, June, p. 106856, 2021, doi: 10.1016/j.jcsr.2021.106856.

[2] M. S. T. Nguyen and S. E. Kim, "A hybrid machine learning approach in prediction and

uncertainty quantification of ultimate compressive strength of RCFST columns", *Constr. Build. Mater.*, vol. 302, February, p. 124208, 2021, doi: 10.1016/j.conbuildmat.2021.124208.

[3] Q. V. Vu, V. H. Truong, and H. T. Thai, "Machine learning-based prediction of CFST columns using gradient tree boosting algorithm", *Compos. Struct.*, vol. 259, no. December 2020, p. 113505, 2021, doi: 10.1016/j.compstruct.2020.113505.

[4] H. B. Ly, B. T. Pham, L. M. Le, T. T. Le, V. M. Le, and P. G. Asteris, "Estimation of axial load-carrying capacity of concrete-filled steel tubes using surrogate models", *Neural Comput. Appl.*, vol. 33, no. 8, pp. 3437–3458, 2021, doi: 10.1007/s00521-020-05214-w.

[5] S. Payam, J. Chen, G. A. Panagiotis, J. D. Armaghani, and M. M. Tahir, "Developing GEP tree-based, neuro-swarm, and whale optimization models for evaluation of bearing capacity of concrete-filled steel tube columns", *Eng. Comput.*, p. 19, 2019, doi: https://doi.org/10.1007/s00366-019-00808-y.

[6] F. Đorđević and S. M. Kostić, "Prediction of ultimate compressive strength of CCFT columns using machine learning algorithms", in *The 8th International Conference "Civil engineering – science and practice,"* 2022, March, p. 8.

[7] F. Đorđević and S. M. Kostić, "Axial Strength Prediction of Square CFST Columns Based on The ANN Model", in *First Serbian International Conference on Applied Artificial Intelligence*, 2022, p. 12.

[8] M. D. Denavit, "Steel-concrete composite column database", 2005.

[9] C. D. Goode, "1819 tests on concrete-filled steel tube columns compared with Eurocode 4", *Struct Eng*, vol. 8, no. 33, p. 86, 2008.

[10] S. Thai, H. T. Thai, B. Uy, and T. Ngo, "Concrete-filled steel tubular columns: Test database, design and calibration", *J. Constr. Steel Res.*, vol. 157, pp. 161–181, 2019, doi: 10.1016/j.jcsr.2019.02.024.

[11] D. Belete, "Engineering a Database on Concrete Filled Steel Tube Columns", Addis Abbaba University, 2016.

[12] J. Zeghiche and K. Chaoui, "An experimental behaviour of concrete-filled steel tubular columns", *J. Constr. Steel Res.*, vol. 61, no. 1, pp. 53–66, 2005, doi: 10.1016/j.jcsr.2004.06.006.

[13] P. S. Schneider, "Axially Loaded Concrete-Filled Steel Tubes", *Struct. Concr. Time - Proc. fib Symp.*, vol. 2, October, pp. 777–784, 2005, doi: 10.1061/(asce)0733-9445(1998)124:10(1125).

[14] Z. Lai and A. H. Varma, "Noncompact and slender circular CFT members: Experimental database, analysis, and design", *J. Constr. Steel Res.*, vol. 106, pp. 220–233, 2015, doi: 10.1016/j.jcsr.2014.11.005.

[15] F. Đorđević and S. M. Kostić, "Comparative Study of Two ANN Approaches for Predicting Axial Capacity of Square CFST Columns", in *Learning and Analytics in Intelligent Systems - Applied Artificial Intelligence*, Springer, 2022, Submitted for review.

[16] R. LHermite, "Id´ees actualles sur la technologie du b´eton", Paris, 1955.

[17] D. Foresee and M. Hagan, "Gauss-Newton Approximation to Bayesian Learning", in *Proceedings of the 1997 International Joint Conference on Neural Networks*, 1997, p. 6.

Milica Koprivica[1], *Saša Kovačević*[2], *Aleksandar Ćeranić*[3], *Stanko Ćorić*[4], *Nenad Marković*[5]

ELASTIČNA KRITIČNA SILA PODUŽNO NEUKRUĆENIH I-NOSAČA USLED LOKALIZOVANOG OPTEREĆENJA

Rezime:

U radu se razmatra elastična kritična sila izbočavanja podužno neukrućenih čeličnih I-nosača usled dejstva lokalizovanog opterećenja promenljive dužine, koje deluje u ravni rebra. U aktuelnim propisima, za proračun elastične kritične sile nije uzet doprinos dužine lokalizovanog opterećenja i debljine pojasa. Prikazan je uticaj graničnih uslova na vertikalnim ivicama opterećenog panela na vrednost koeficijenta izbočavanja. Predložen je poboljšan izraz za proračun koeficijenata izbočavanja podužno neukrućenih I-nosača.

Ključne reči: elastična kritična sila, lokalizovano opterećenje, puni limeni nosači

ELASTIC CRITICAL LOAD OF LONGITUDINALLY UNSTIFFENED I-GIRDERS SUBJECTED TO PATCH LOADING

Summary:

The paper considers the elastic critical load of longitudinally unstiffened I-girders subjected to a localized load of variable length in the plane of the web. In the current regulations, the contribution of the patch load length and the flange thickness is not considered for calculating the elastic critical load. The influence of the boundary conditions on the vertical edges of the loaded panel on the value of the buckling coefficient is presented. An improved expression for the calculation of the buckling coefficients of longitudinally unstiffened I-girders is proposed.

Key words: elastic critical load, patch loading, steel plate girders

---

[1] *MSc, teaching assistant, Faculty of Civil Engineering University of Belgrade, Bulevar kralja Aleksandra 73, 11000 Belgrade, Serbia, mbendic@grf.bg.ac.rs*

[2] *Dr, Department of Civil and Environmental Engineering, Imperial College London, London, SW7 2AZ, UK, s.kovacevic@imperial.ac.uk*

[3] *MSc, Spenncon AS, Stabells gate 9, Hønefoss, Norway, ceranicaleksandar@gmail.com*

[4] *Dr, Faculty of Civil Engineering University of Belgrade, Bulevar kralja Aleksandra 73, 11000 Belgrade, Serbia, cstanko@grf.bg.ac.rs*

[5] *Dr, Matice srpske 62/26, 11000 Belgrade, Serbia, markovic.nenad2018@gmail.com*

1. INTRODUCTION

The buckling problem of steel plate girders subjected to patch loading has been a research topic for decades. The subject of research has been isolated web plates and I-girders loaded with a localized load in the plane of the web. Furthermore, the influence of the patch load (or partially distributed load) on the behavior of I-girders without vertical stiffener in the zone of load introduction has been specially investigated. This problem has got importance with a general trend to avoid vertical stiffeners, except at supports and in the case of moving loads, e.g., crane girders loaded by crane wheels and launching phase of multi-span steel plate girder bridges during construction over temporary or permanent supports. In everyday engineering practice, standards for calculating steel plate structures (Eurocode EN1993-1-5 [1]) control the ultimate capacity of structural elements subjected to patch loading. There is a constant tendency to make the standards easy to use while still being accurate enough to describe the problem. Eurocode EN1993-1-5 [1] often leads to conservative values for the patch loading resistance. One of the reasons for that is a simplified expression for buckling coefficient, as indicated in [2-5]. Therefore, an attempt is made in this paper to provide improvements to that procedure and to pay attention to parameters that have been neglected, and their impact is significant.

Critical load for a steel plate girder under localized load acting on one flange and between two vertical stiffeners at a distance a, should be obtained according to EN1993-1-5 [1]:

$$F_{cr} = 0.9 k_F E \frac{t_w^3}{h_w} , \qquad (1)$$

with buckling coefficient

$$k_F = 6 + 2\left(\frac{h_w}{a}\right)^2 . \qquad (2)$$

Equation (2) was obtained by simplifying the expression proposed by Lagerquist [6].

$$k_F = \left(1 + \frac{s_s}{2h_w}\right)\left(5.3 + 1.9\left(\frac{h_w}{a}\right)^2 + 0.4\sqrt[4]{\beta}\right) , \quad \beta = \frac{b_f \cdot t_f^3}{h_w \cdot t_w^3} \qquad (3)$$

As it could be observed, Eq. (2) does not take into account the length of an applied patch load, flange to web stiffness ratio, and ratio between the load length and web depth.

This paper considers the determination of the buckling coefficients for elastic critical loads of unstiffened I-girders using finite element (FE) analysis. The commercial software Abaqus [7] was used in this research as one of the most popular computation tools for application in this field. Numerically obtained elastic critical loads are used to get the buckling coefficient. The aim is to formulate an improved expression for calculation of the critical load for I-girders and make the procedure for determination of patch loading resistance in the current standard EN1993-1-5 [1] more accurate.

The following notations are used in this paper to describe the problem of patch loading, compare the results, and derive conclusions: h_w - web depth, t_w - web thickness, t_f - flange thickness, b_f - flange width, a - distance between vertical stiffeners (web width), s_s - patch load length, ν - Poisson's ratio, E - modulus of elasticity, k_F - buckling coefficient. The influence of the patch load length, aspect ratio (a/h_w), and flange thickness is investigated in this paper.

Recently completed research [8, 9], considered the influence of longitudinal stiffeners on the increase of the carrying capacity of longitudinally unstiffened girders. Numerical parametric analysis provided a large database for longitudinally unstiffened and stiffened girders (162 unstiffened and 486 longitudinally stiffened girders). The main goal of the research was the determination of ultimate loads using nonlinear analysis. Initial imperfections of considered girders were defined as first buckling mode and obtained through elastic numerical analysis. Elastic critical loads for 162 unstiffened girders obtained in that research are used here.

The numerical model is described in Section 2. Details of the parametric analysis are described in Section 3. Detailed analysis of the results and improved expression for buckling coefficient k_F is proposed in Section 4. The statistical analysis of solutions for the ultimate load obtained with the procedure given in EN1993-1-5 by application of the k_F in the current standard, k_F given by Lagerqvist and k_F here proposed, compared with numerically obtained values of ultimate loads is presented in Part 5. Conclusions are given in Section 6.

2. NUMERICAL MODELS

The isolated web steel plate and I-girder with a web panel aspect ratio $a/h_w = 1,2,3$ (schematically presented in Fig. 1), were investigated. Patch load length s_s, flange thickness t_f and web thickness t_w were varied. The boundary conditions for the plate were set according to the clamped plate - that is, degrees of freedom 2 and 5 are only constrained in the vertical edges, degree of freedom 4 in the horizontal edges, while degree of freedom 3 is constrained in all edges. The considered material is homogenous with an elastic modulus of $E = 205$ GPa and Poisson's ratio of $\nu = 0.3$.

For the FE analysis, a general-purpose four-node quadrilateral shell element with reduced integration and six degrees of freedom per node S4R from the Abaqus element library was used. The finite element size is adopted to 5 mm for all numerical runs. The girders are modeled with two rigid vertical stiffeners, preventing rotation. The load is introduced through a rigid block element, which prevents the rotation of the flange around the longitudinal axis in the zone of load application. The finite element model was validated on experimentally tested girders [10, 11], so the selected girders dimensions in the parametric analysis are grounded on that basis.
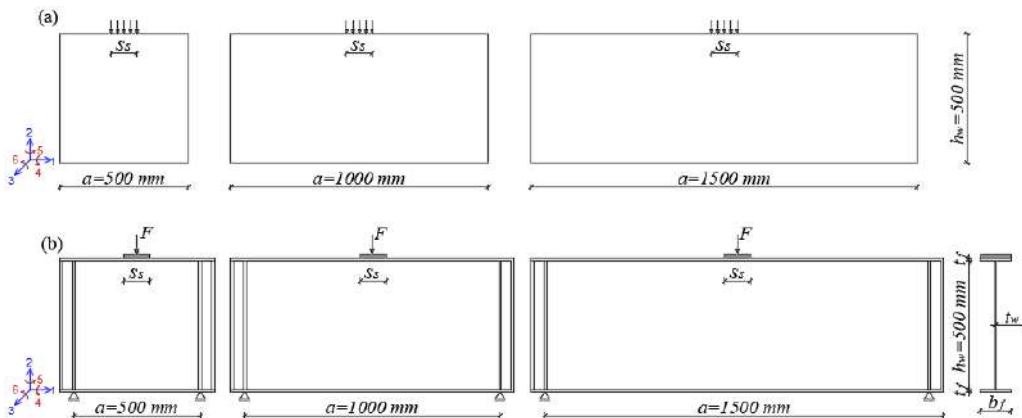

Figure 1 - (a) Plate under patch load; (b) I-girders under patch load

By comparing numerically obtained values of the buckling coefficient of I-girders and using Eq. (3), there were differences in the value of k_F for the aspect ratio a/h_w less than 1.5 that should not be neglected. In order to emphasize the way of modeling the boundary conditions on the vertical edges of the girders, the buckling coefficients for the models with rigid vertical stiffeners (coresponding to analysis in this paper) and simply supported vertical edges (as applied by Laguerqvist) were compared, as shown in Figure 2. For both numerical models, the flange rotation is prevented in the zone of load introduction. The analysis of the obtained results is presented in the paper and commented below.
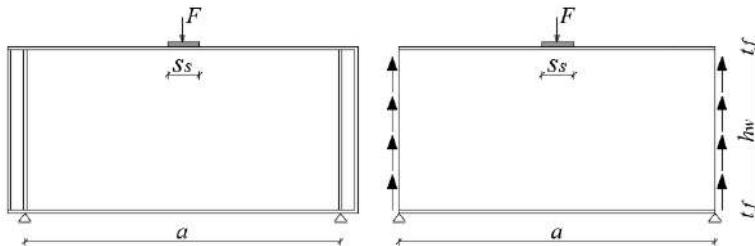

Figure 2 - Boundary conditions on vertical edges

3. PARAMETRIC ANALYSIS

This paper shows how the accuracy of the calculation of the buckling coefficient, obtained from the expression for the elastic critical load, can affect the ultimate load capacity and possibly improve it compared to the procedures in EN1993-1-5 [1]. In order to compare the results of the patch loading resistance obtained using the proposed expression for k_F and the numerically obtained ultimate load, the procedure was carried out on the girders treated in Refs. [8, 9]. The numerical values of the ultimate loads of those girders were given there.

The dimensions of girders employed in the numerical simulations [8, 9] were carefully chosen. They were selected such that characteristic ratios (e.g., a / h_w, h_w / t_w, t_f / t_w) include limiting and average values frequently used in experimental and computational studies. The following geometric parameters were not varied: $b_f = 120$ mm, yield strength of the web $f_{yw} = 323$ MPa and flange $f_{yf} = 323$ MPa. For each parameter that was varied in the numerical simulations, three values were selected such that they give for characteristic ratios (a / h_w, h_w / t_w, t_f / t_w) approximately (i) lower limit, (ii) average value between lower and upper limit, and (iii) upper limit (of those frequently used in experimental and numerical studies).

The following geometric parameters were varied for longitudinally unstiffened girders:

(a) Web panel width $a = 500, 1000, 1500$ mm (i.e., web aspect ratio $\alpha = 1, 2$ and 3).
(b) Three web panel thicknesses $t_w = 1.25, 2, 4$ mm for each web panel width a (web slenderness $h_w / t_w = 400, 250, 125$).
(c) For each of these nine cases, three values of the flange thickness were applied such that
$t_f / t_w = 2, 4$, and 6 (for $t_w = 1.25 \rightarrow t_f = 2.5, 5, 7.5$, for $t_w = 2 \rightarrow t_f = 4, 8, 12$ and for $t_w = 4 \rightarrow t_f = 8, 16, 24$).
(d) For each of these twenty-seven cases, six patch load lengths were applied: $s_s = 0$ (concentrated force), $s_s = 50, 100, 150, 200, 250$ mm ($s_s / h_w = 0 - 0.50$).
Such choice enabled detailed analysis for a much larger range of parameters than applied in Refs. [2-5]. Total number of longitudinally unstiffened models (numerical simulations) was 162.

It was necessary to form additional I-girders models for web aspect ratios $\alpha = 1.25$ and 1.5 and web thickness $t_w = 4$ mm to find the expression for buckling coefficient by correcting Eq. (2). For those models, the elastic critical load was found without performing a nonlinear analysis for calculating ultimate loads. For all girders mentioned in the parametric study, the elastic critical loads of the isolated web plates were also found to obtain the buckling coefficients. Those values are presented in this paper and compared with the buckling coefficients of I-girders.

4. RESULTS AND DISCUSSION

The buckling coefficient k_F of the girder subjected to patch loading affects the value of the elastic critical load and patch loading resistance. Based on the analysis given in this paper, it was shown that the buckling coefficient does not depend significantly on the web thickness. Therefore, additional analyses for the aspect ratio $\alpha = 1.25$ and 1.5 were performed only for the web thickness $t_w = 4$ mm. Table 1 shows the values of k_F for aspect ratio $\alpha = 2$, for different web thicknesses and flange thickness $2t_w$, as a function of patch load length s_s. The buckling coefficients numerically obtained for isolated web plate - k_F^{CC} and I-girder - k_F^{FEA}, and using Eq. (3) – k_F^L are given. The expression proposed by Lagerqvist - Eq. (3) does not take into account the influence of the web thickness on the value of the buckling coefficient, but only the ratio between the flange and web stiffness.

Table 1 - Buckling coefficients of I-girders for different web thicknesses

$t_f = 2t_w$	$\alpha = 2, t_w = 4$ mm			$\alpha = 2, t_w = 2$ mm			$\alpha = 2, t_w = 1.25$ mm		
s_s/h_w	k_F^{CC}	k_F^{FEA}	k_F^L	k_F^{CC}	k_F^{FEA}	k_F^L	k_F^{CC}	k_F^{FEA}	k_F^L
0.00	6.17	6.42	6.25	6.21	6.42	6.25	6.18	6.42	6.25
0.10	6.22	6.57	6.56	6.22	6.56	6.56	6.22	6.56	6.56
0.20	6.34	6.81	6.87	6.34	6.79	6.87	6.36	6.78	6.87
0.30	6.51	7.10	7.18	6.53	7.08	7.18	6.53	7.06	7.18
0.40	6.75	7.45	7.50	6.75	7.41	7.50	6.74	7.39	7.50
0.50	7.02	7.86	7.81	7.00	7.81	7.81	7.01	7.78	7.81

Table 2 - Buckling coefficients of I-girders for different boundary conditions at the vertical edges for $t_w = 4$ mm

$\alpha = 1$	$t_f = 8$ mm		$t_f = 16$ mm		$t_f = 24$ mm	
s_s/h_w	$k_F^{FEA}{}_{SS}$	$k_F^{FEA}{}_{CC}$	$k_F^{FEA}{}_{SS}$	$k_F^{FEA}{}_{CC}$	$k_F^{FEA}{}_{SS}$	$k_F^{FEA}{}_{CC}$
0.00	8.98	7.56	10.10	8.02	11.00	8.48
0.10	9.23	7.72	10.40	8.30	11.34	8.65
0.20	9.70	8.10	11.01	8.74	12.11	9.18
0.30	10.37	8.67	11.86	9.36	13.18	9.87
0.40	11.25	9.41	13.00	10.21	14.65	10.88
0.50	12.37	10.40	14.52	11.35	16.68	12.21

Furthermore, it was shown that the coefficient k_F depends on the boundary conditions on the vertical edges of girder. Table 2 indicates the importance of modeling methods for $\alpha = 1$. The notation *SS* refers to the simply supported edges, and *CC* to the rigid vertical stiffeners at the ends preventing rotation. Significant differences occur for a small aspect ratio - especially for α =1-1.5, for all analyzed models.

In this paper, an expression for the calculation of the buckling coefficient is proposed - Eq. (4), derived from all the analyzed girders described within the parametric analysis, and which have rigid vertical stiffeners on the edges. The expression represents a modified proposal of Lagerqvist, primarily for the aspect ratio smaller than 1.5.

$$k_F = \left(1 + f(\alpha_1) \cdot \frac{s_s}{h_w}\right) \cdot \left[5.30 + f(\alpha_2) \cdot \left(\frac{h_w}{a}\right)^2 + f(\alpha_3) \cdot \sqrt[4]{\bar{\beta}}\right]$$

$$f(\alpha_1) = 1.2\alpha^2 - 3.5\alpha + 3.05$$

$$f(\alpha_2) = 4.6 - 2.4\alpha$$

$$f(\alpha_3) = 1.2\alpha^2 - 3.5\alpha + 3.2$$

For $\alpha > 1.5$ take $\alpha = 1.5$

$$\bar{\beta} = \frac{b_f t_f^3}{\left(\frac{h_w + a}{2}\right) t_w^3} \tag{4}$$

Table 3 shows the values of the buckling coefficient k_F for the considered models of I-girders whose web thickness is set to be $t_w = 4$ mm: obtained numerically - k_F^{FEA}, using Lagerqvist's proposal [6] - k_F^L, and using Eq. (4) proposed in this paper - k_F^F. Results are shown for three flange thicknesses $t_f = 8, 16, 24$ mm and aspect ratio $\alpha = 1, 1.25, 1.5, 2, 3$. Furthermore, Table 3 presents the values of the buckling coefficients calculated using the expressions from EN1993-1-5 [1] - k_F^{EC} and k_F^{CC} - numerically obtained values for isolated web plates.

The buckling coefficient obtained by Eq. (4) corresponds best to the numerical values. However, for an aspect ratio less than 1.5, the improvement achieved using the proposed expression - Eq. (4) compared to Lagerqvist's proposal is more significant. Lagerqvist's expression agrees well with the numerical results for larger aspect ratios, but an improvement is observed for larger flange thicknesses using the expression proposed in this paper - Eq. (4).

Table 3 - Comparison of buckling coefficients of CC plate and I-girders for $t_w = 4$ mm.

$\alpha = 1$			$t_f = 8$ mm			$t_f = 16$ mm			$t_f = 24$ mm		
s_s/h_w	k_F^{CC}	k_F^{EC}	k_F^{FEA}	k_F^F	k_F^L	k_F^{FEA}	k_F^F	k_F^L	k_F^{FEA}	k_F^F	k_F^L
0.00	8.00	8.00	8.98	8.56	7.67	10.10	9.28	7.99	11.00	9.91	8.27
0.10	8.17	8.00	9.23	9.20	8.05	10.40	9.98	8.39	11.34	10.66	8.69
0.20	8.35	8.00	9.70	9.84	8.44	11.01	10.67	8.79	12.11	11.40	9.10
0.30	8.74	8.00	10.37	10.49	8.82	11.86	11.37	9.19	13.18	12.15	9.51
0.40	9.23	8.00	11.25	11.13	9.21	13.00	12.07	9.59	14.65	12.89	9.93
0.50	9.91	8.00	12.37	11.77	9.59	14.52	12.76	9.99	16.68	13.63	10.34

$\alpha = 1.25$			$t_f = 8$ mm			$t_f = 16$ mm			$t_f = 24$ mm		
s_s/h_w	k_F^{CC}	k_F^{EC}	k_F^{FEA}	k_F^F	k_F^L	k_F^{FEA}	k_F^F	k_F^L	k_F^{FEA}	k_F^F	k_F^L
0.00	6.89	7.28	7.46	7.12	6.99	8.06	7.67	7.31	8.40	8.15	7.59
0.10	6.96	7.28	7.57	7.52	7.34	8.20	8.09	7.67	8.55	8.60	7.97
0.20	7.12	7.28	7.88	7.91	7.69	8.56	8.51	8.04	8.98	9.04	8.35
0.30	7.37	7.28	8.30	8.30	8.03	9.04	8.94	8.40	9.55	9.49	8.73
0.40	7.69	7.28	8.82	8.69	8.38	9.67	9.36	8.77	10.28	9.94	9.11
0.50	8.09	7.28	9.49	9.08	8.73	10.46	9.78	9.13	11.22	10.39	9.49

$\alpha = 1.5$			$t_f = 8$ mm			$t_f = 16$ mm			$t_f = 24$ mm		
s_s/h_w	k_F^{CC}	k_F^{EC}	k_F^{FEA}	k_F^F	k_F^L	k_F^{FEA}	k_F^F	k_F^L	k_F^{FEA}	k_F^F	k_F^L
0.00	6.46	6.89	6.83	6.47	6.62	7.40	6.96	6.94	7.64	7.39	7.22
0.10	6.51	6.89	6.92	6.79	6.95	7.50	7.31	7.28	7.75	7.76	7.58
0.20	6.64	6.89	7.18	7.11	7.28	8.37	7.66	7.63	8.07	8.13	7.94
0.30	6.84	6.89	7.51	7.44	7.61	8.13	8.01	7.98	8.47	8.50	8.30
0.40	7.09	6.89	7.91	7.76	7.94	8.58	8.35	8.32	8.98	8.87	8.66
0.50	7.40	6.89	8.41	8.09	8.27	9.13	8.70	8.67	9.60	9.24	9.02

$\alpha = 2$			$t_f = 8$ mm			$t_f = 16$ mm			$t_f = 24$ mm		
s_s/h_w	k_F^{CC}	k_F^{EC}	k_F^{FEA}	k_F^F	k_F^L	k_F^{FEA}	k_F^F	k_F^L	k_F^{FEA}	k_F^F	k_F^L
0.00	6.17	6.50	6.42	6.24	6.25	7.28	6.71	6.57	7.61	7.13	6.85
0.10	6.22	6.50	6.57	6.55	6.56	7.40	7.05	6.90	7.73	7.48	7.19
0.20	6.34	6.50	6.81	6.87	6.87	7.63	7.38	7.22	7.98	7.84	7.53
0.30	6.51	6.50	7.10	7.18	7.18	7.92	7.72	7.55	8.29	8.19	7.88
0.40	6.75	6.50	7.45	7.49	7.50	8.28	8.06	7.88	8.68	8.55	8.22
0.50	7.02	6.50	7.86	7.80	7.81	8.70	8.39	8.21	9.13	8.91	8.56

$\alpha = 3$			$t_f = 8$ mm			$t_f = 16$ mm			$t_f = 24$ mm		
s_s/h_w	k_F^{CC}	k_F^{EC}	k_F^{FEA}	k_F^F	k_F^L	k_F^{FEA}	k_F^F	k_F^L	k_F^{FEA}	k_F^F	k_F^L
0.00	5.62	6.22	6.20	6.05	5.98	7.25	6.49	6.30	7.64	6.88	6.58
0.10	5.67	6.22	6.37	6.36	6.28	7.38	6.82	6.62	7.76	7.22	6.91
0.20	5.78	6.22	6.62	6.66	6.58	7.61	7.14	6.93	8.01	7.57	7.24
0.30	5.95	6.22	6.93	6.96	6.88	7.91	7.47	7.25	8.33	7.91	7.57
0.40	6.15	6.22	7.28	7.27	7.18	8.28	7.79	7.56	8.72	8.25	7.90
0.50	6.41	6.22	7.69	7.57	7.48	8.72	8.12	7.88	9.18	8.60	8.23

Figure 3 shows the diagrams of the buckling coefficient as a function of the patch load length for different aspect ratios. For longer girder widths, i.e., larger aspect ratios, the changes in the values of the buckling coefficient are small. For example, in Figure 3 (a), it can be observed that for the aspect ratio of 1.25, the value of the buckling coefficients drop significantly. Regardless

of the web thickness, for α greater than 1.5, the influence of the girder length, and therefore the boundary conditions on the edges, is significantly reduced. Figure 4 shows the dependence of the buckling coefficient on the patch load length s_s, for different calculation methods: obtained numerically - k_F ^{FEA}, using Lagerqvist's proposal [6] - k_F ^{L}, using Eq. (4) proposed in this paper - k_F ^{F}, obtained by the procedure given in EN1993-1-5 [1] - k_F ^{EC}, and for isolated web plate k_F ^{CC}. For the considered girder and plate models, EN1993-1-5 [1] gives conservative results, while the proposed expression - Eq. (4) best agrees with the numerically obtained values.
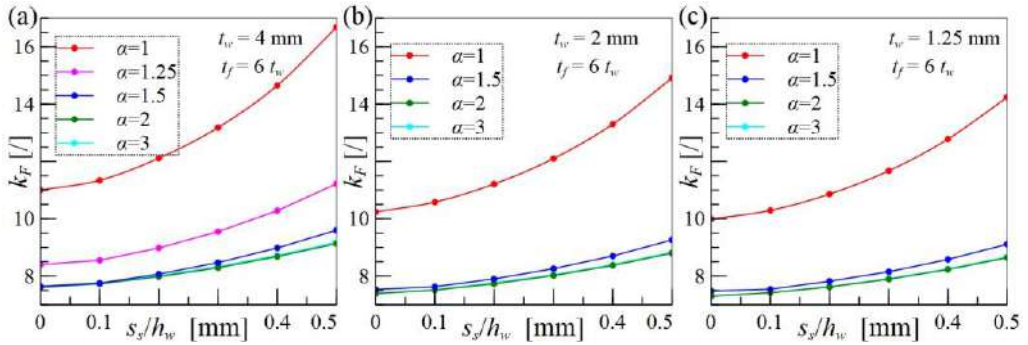

Figure 3 - Comparison of the numerically obtained buckling coefficients for different aspect ratios.
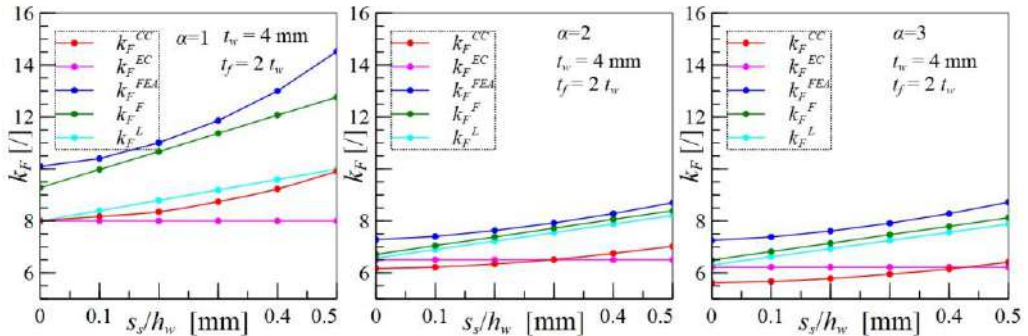

Figure 4 - Comparison of the buckling coefficients for various calculation models.

5. COMPARISON OF THE ULTIMATE LOADS

In the procedure given in EN1993-1-5 [1] for calculating the patch loading resistance, the ultimate load depends on the value of the buckling coefficient k_F. Figure 5 compares the ultimate load values for I-girders described in the parametric analysis, for aspect ratio 1 and web thickness $t_w = 4$ mm and $t_f = 4$ t_w, numerically obtained and using the expression given in EN1993-1-5 [1]. F_{Rd} ^{EC} presents the value of the ultimate load obtained using the buckling coefficient calculated from Eq. (2) - k_F ^{EC}. F_{Rd} ^{L} refers to the patch loading resistance obtained using buckling coefficient calculated from Lagerqvist proposal - k_F ^{L}, Eq. (3). F_{Rd} ^{F} presents the ultimate load calculated using buckling coefficient obtained from the expression proposed in this paper - k_F ^{F},

Eq. (4). The ultimate loads of I-girders obtained using Eq. (4) correspond best to the numerically obtained ultimate loads F_{un}.

		F_{Rd}^{EC}/F_{un}	F_{Rd}^{L}/F_{un}	F_{Rd}^{F}/F_{un}
	$\bar{X}$	0.53	0.56	0.59
all	Sx	0.08	0.08	0.08
	CV	0.15	0.14	0.13
	$\bar{X}$	0.50	0.53	0.58
$\alpha = 1$	Sx	0.09	0.08	0.08
	CV	0.18	0.16	0.14
	$\bar{X}$	0.53	0.56	0.57
$\alpha = 2$	Sx	0.07	0.07	0.07
	CV	0.14	0.12	0.12
	$\bar{X}$	0.56	0.60	0.60
$\alpha = 3$	Sx	0.07	0.07	0.07
	CV	0.13	0.12	0.12

Table 4 - Comparison of the analysed statistical parameters.
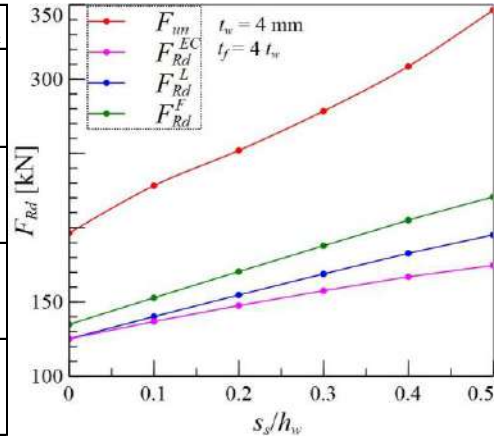

Figure 5 - Comparison of the ultimate loads of I - girders.

Table 4 compares the values for 162 girders of the ultimate loads F_{Rd}^{EC}, F_{Rd}^{L}, F_{Rd}^{F} with the numerically obtained values F_{un} using [7]. The basic statistical quantities were compared for each group of girders (aspect ratio $\alpha = 1, 2, 3$) and ultimate loads obtained through different calculations of buckling coefficients: mean value ($\bar{X}$), standard deviation (S_x) and coefficient of variation (*CV*). It has been shown that statistical parameters are the most favorable in the case of the calculation of the ultimate load obtained by using the buckling coefficient calculated from the expression proposed in this paper - Eq. (4). The greatest improvement in the patch loading resistance was obtained for the small aspect ratio $\alpha = 1$, up to 31%. As the aspect ratio increases, the percentage of ultimate load improvement decreases compared to the ultimate load calculated using the procedures given in EN1993-1-5 [1].

6. CONCLUSIONS

The paper presents the elastic critical load of longitudinally unstiffened I-girders subjected to patch loading. The girders described in the parametric analyses were considered. For those girders, the numerical values of the buckling coefficient were found based on the elastic critical load. The influence of the boundary conditions on the vertical edges of the loaded panel on the value of the elastic critical load is shown. A limit is given in the aspect ratio when these conditions become negligible. It was pointed out that the thickness of the web does not significantly affect the value of the buckling coefficient. The design standard EN1993-1-5 gives conservative results for elastic critical load because the influence of flange stiffness and patch load length is neglected. An improved expression for calculating the buckling coefficient of I-girders that considers the flange thickness, the patch load length and aspect ratio is proposed. The ultimate load depends on the buckling coefficient. The patch loading resistance calculation has improved by applying the expression for calculating the coefficient k_F proposed in this paper. The most significant improvement was obtained for aspect ratio 1 and thicker flange, up to 31%.

More favorable values of statistical quantities were also obtained. The mean value is increased by 10%, and the coefficient of variation is decreased compared to the current standard. All conclusions in the paper refer to precisely defined examples described in Section 2 and Section 3.

REFERENCES

[1] Eurocode 3 (EC3): Design of steel structures. Part 1-5: General rules–Supplementary rules for planar plated structures without transverse loading. EN1993-1-5; 2006

[2] Jakovljević I, Kovačević S, Marković N. Elastic critical load of plates and plate girders subjected to patch load, Building materials and structures, 2018, 55-67

[3] Bendić M, Ćeranić A, Kovačević S, Salatić R, Marković N. Elastic critical load of the web of I-girders subjected to patch loading. Proceedings, Association of Structural Engineers of Serbia, Symposium 2020, Arandjelovac, May 13-15, 2021, S-81, 473-482.

[4] Bendić M, Ćeranić A, Kovačević S, Salatić R, Marković N. Elastic critical load of stiffened I-girders subjected to patch loading. 8th International Conference Contemporary achievements in civil engineering 22-23. April 2021. Subotica, Serbia, 153-161.

[5] Koprivica M, Ceranic A, Kovacevic S, Salatic R, Markovic N. Influence of stiffener and flange on elastic critical load of I-girders subjected to patch loading. Proceedings of the 19th international symposium of MASE (Macedonian Association of Structural Engineers), Ohrid, North Macedonia, 27 – 30 April 2022, SS-5, 858-865.

[6] Lagerqvist O. Patch loading–Resistance of steel girders subjected to concentrated forces, Ph.D. Thesis, Department of Civil and Mining Engineering, Division of Steel Structures, Luleå University of Technology, 1994:159D, Luleå, 1995.

[7] Abaqus Simulia. Dassault Systemes. 2016.

[8] Ceranic A, Bendic M, Kovacevic S, Salatic R, Markovic N. Influence of patch load length on strengthening effect in steel plate girders. Journal of Constructional Steel Research 195 (2022) 107348, 19

[9] Ћеранић А., Утицај подужних укрућења на понашање и граничну носивост лимених носача оптерећеним локалним оптерећењем, Докторска дисертација, Београд, 2022.

[10] Markovic N, Kovacevic S. Influence of patch load length on plate girders. Part I: experimental research, J. Constr. Steel Res. 157 (2019) 207–228.

[11] Kovacevic S, Markovic N. Experimental study on the influence of patch load length on steel plate girders, Thin-Walled Struct. 151 (2020) 106733.

Milica Vidović[1], Marija Nefovska-Danilović[2], Marko Radišić[3]

PROCENA ODGOVORA KONSTRUKCIJE USLED VIBRACIJA OD SAOBRAĆAJA PRIMENOM TRANSFER FUNKCIJA

Rezime:

Kao rezultat ubrzanog razvoja gradova i izgradnje brzih železnica i puteva sve češće se u objektima javljaju vibracije izazvane saobraćajem. Ovaj problem postaje važan jer vibracije mogu negativno uticati na kvalitet života i zdravlje ljudi. U okviru ovog rada izvršena je analiza uticaja krutosti tla na vibracije od saobraćaja koje se javljaju u stambenoj osmospratnoj zgradi, uzimajući u obzir dinamičku interakciju tla i objekta primenom metode podstruktura i metode transfer funkcija. Rezultati su prikazani u vidu transfer funkcija za dve karakteristične tačke unutar zgrade. Pokazano je da se rezonantni odgovor konstrukcije javlja pri nižim frekvencijama za mekše tlo odnosno pri višim za tlo veće krutosti, što ukazuje da interakcija tla i objekta može značajno uticati na nivo vibracija u zgradama.

Ključne reči: Interakcija tla i objekta, Dinamička krutost, Vibracije usled saobraćaja

ASSESSMENT OF TRAFFIC-INDUCED BUILDING VIBRATIONS USING THE TRANSFER FUNCTIONS METHOD

Summary:

As a result of rapid development of cities and construction of high-speed rail/road infrastructure, vibration serviceability of buildings due to traffic-induced vibrations has become a growing issue that affects the comfort of living and health of building occupants. In this paper a numerical study in which the influence of soil stiffness on the traffic-induced vibrations of an eight-story residential building is investigated considering soil-structure interaction and applying the substructuring approach and transfer function method. The results are presented in terms of transfer functions for selected points of interests inside the building. The results show that the resonant response of the structure occurs at lower frequencies for soft soil and at higher frequencies for stiff soil, indicating that soil-structure interaction can significantly affect the vibration response of the building.

Keywords: Soil-structure interaction, Dynamic stiffness, Traffic-induced vibrations

---

[1] *Teaching assistant, Faculty of Civil Engineering, University of Belgrade, Serbia, milica@imk.grf.bg.ac.rs*
[2] *Assoc. Prof., Faculty of Civil Engineering, University of Belgrade, Serbia, marija@grf.bg.ac.rs*
[3] *Assist. Prof., Faculty of Civil Engineering, University of Belgrade, Serbia, mradisic@grf.bg.ac.rs*

1. INTRODUCTION

Rapid development of cities led to the need for high-speed transport and high-rise buildings. The existence of such systems is stricken by the traffic induced ground borne vibrations that affect the comfort of living and the health of the occupants. In order to mitigate the influence of the traffic induced vibrations on buildings, one must predict the response of the building by using a reliable and efficient numerical model that takes into account the soil-structure interaction (SSI).

The SSI is usually performed using the substructuring approach. The system is decomposed into two substructures: the structure and the soil-foundation system. The soil-foundation interaction (SFI) is solved using transform techniques such as Thin Layer Method [1], Boundary Element Method [2] or Integral Transform Method [3] that takes into account the unbounded domain of the soil medium. The aim of the SFI analysis is to provide dynamic stiffnesses of the foundations - impedances, that are assigned to the structure model at the soil-structure interaction joints.

The usage of SSI is still not common in everyday engineering practice. Codes and standards contain limited information and the literature is usually very complex to understand without extensive knowledge. This triggered many researchers to try to simplify the SSI analysis. Analytical solutions of impedances for foundations of regular geometries over homogeneous soil sediments are collected and presented in the literature [4], [5]. The geometry of every structure is unique as well as the dynamic response of the structure. The tendency of researchers is to generalize the response as much as possible and to describe it using geometrical parameters such as bay spans, story heights, number of bays and stories and the characteristics of the structural elements of the system such as soil, column and floor resonances [6], [7]. This is usually done by using transfer functions (TFs) - a frequency dependent functions which output the response of the system for different inputs. In general, input and output could be any parameter. In SSI analysis they are usually displacements, velocities or accelerations.

The aim of this paper is to show the importance of the SSI in the dynamic analysis of structures and to present the methodology of performing a simplified SSI analysis on a dwelling building founded on a homogeneous soil sediment. The analysis is performed by upgrading the FEM model of the building modeled in CSI SAP2000 with impedances obtained using analytical expressions from the literature. The results are presented in terms of transfer functions for selected points of interests inside the building. Since the impact of traffic induced ground borne vibrations on humans is investigated, only vertical vibrations are considered.

2. METHODOLOGY

This paper presents the methodology for problems where the input ground motion at the foundation level of the structure is known. Therefore, only inertial soil-foundation interaction is considered. The methodology for calculation building response including SSI considers:
- creating FEM model of the structure,
- obtaining dynamic stiffnesses of the foundations – impedances,
- implementing impedances in the FEM model of the structure,
- calculation of transfer functions for considered observation points of the structure,

- obtaining the response of the structure by combining transfer functions with the free field vibrations due to an arbitrary excitation.

Dynamic stiffnesses of the foundations - impedances, are obtained using analytical solutions from the literature [5]. Only vertical impedances are calculated, since the impact of vibrations on humans is investigated. In general, the impedance of the foundation is a frequency dependent complex function of the following form:

$$\bar{k} = k + i\omega c \tag{1}$$

where k and c are frequency dependent stiffness and dashpot coefficients and ω is circular frequency of the system.
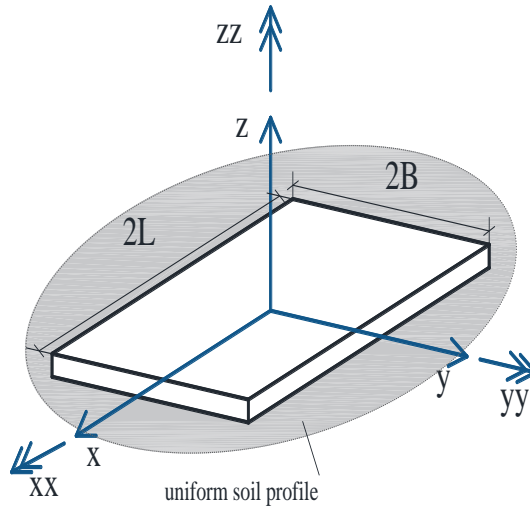

Figure 1 - Disposition of the surface rectangular foundation over uniform soil profile

However, solutions for surface massless rigid rectangular foundations over uniform soil profile, Figure 1, can be given in terms of foundation static stiffness K and dynamic stiffness modifier α [5] as follows:

$$k_z = K_{z,sur}\alpha_z \tag{2}$$

$$K_{z,sur} = \frac{GB}{1-v}\left[3.1\left(\frac{L}{B}\right)^{0.75} + 1.6\right] \tag{3}$$

$$\alpha_z = 1 - \left[\frac{\left(0.4 + \frac{0.2}{L/B}\right)\alpha_0^2}{\left(\frac{10}{1+3(L/B-1)+\alpha_0^2}\right)}\right] \tag{4}$$

$$\alpha_0 = \frac{\omega_1 B}{c_s} \quad , \tag{5}$$

where G is the shear modulus, L and B are foundation dimensions, ν is Poisson's ratio and α_0 is dimensionless frequency. The dashpot coefficient of the foundation c_z accounts for two types of damping: damping ratio of the soil β_s ($\beta_s = 2\%$ in all calculations), and radiation damping ratio β_z:

$$c_z = 2k_z \frac{\beta_z + \beta_s}{\omega} \quad, \tag{6}$$

$$\beta_z = \frac{4\psi \dfrac{L}{B}}{\dfrac{K_{z,sur}}{GB}} \frac{\alpha_0}{2\alpha_z} \quad, \tag{7}$$

$$\psi = \sqrt{2(1-\nu)(1-2\nu)} \quad \text{limited to } \psi \le 2.5$$

where c_s is the shear wave velocity of the soil. The foundation impedances are implemented into the model of the structure as frequency dependent springs, Figure 2.
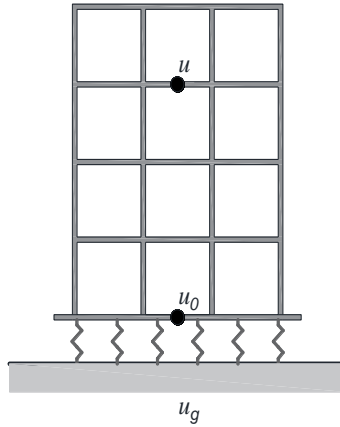

Figure 2 - SSI substructuring approach

In order to easily obtain the response of the structure due to arbitrary loads, frequency dependent TFs are calculated. They represent the structure response spectrum u due to a displacement impulse spectrum applied at the building foundation, u_0, such that:

$$TF = \frac{u}{u_0} \tag{8}$$

The response spectrum of the building at observation point j due to the load spectrum u_g, is obtained as

$$u_j(g) = TF_j u_g \tag{9}$$

The transfer function at observation point j is a set of results of multiple steady state analyses performed for discrete frequencies in a desired frequency range.

3. MODEL

The structure analyzed in this paper is an eight-story dwelling reinforced concrete (RC) building supported by columns and shear walls. The global 3D FEM model of the building is modeled in CSI SAP2000. The structure is founded on rectangular massless rigid surface foundations. The foundations under the building are square footings ($L=B=3$ m) under the columns, and 3 m wide strip footings under the walls ($L=7$ m for walls in the x direction and $L=8$ m for walls in the y direction).

Horizontal elements are slabs 24 cm in thickness, and perimeter beams B1 30x60 cm. Vertical elements are shear walls W1 500x30 cm and W2 600x30 cm. There are three types of column dimensions, the corner ones with dimension C3 30x30 cm, edge ones C2 30x60 cm, and the internal C1 60x60 cm. All beams and columns are modeled as frame elements, walls and slabs as shell elements with material properties of concrete class C30/37. Layout of the building is presented in Figure 3.
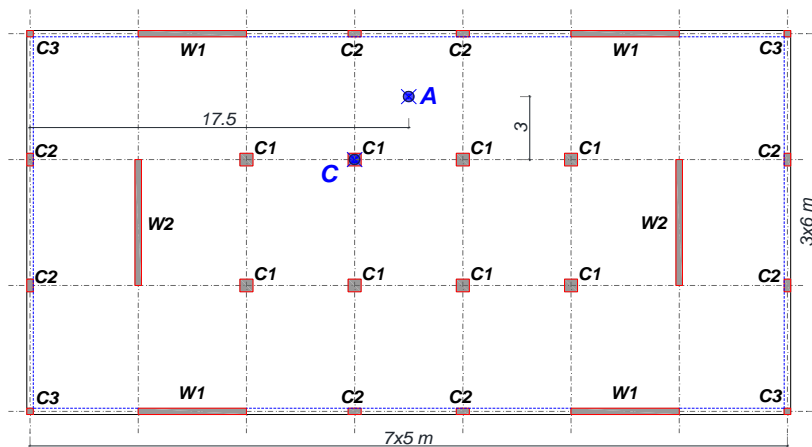

Figure 3 - Plan geometry with observation points A and C

Three different types of soil are considered: soft (S1), medium stiff (S2) and stiff (S3) soil. Soil parameters are given in Table 1. For each soil type, it is adopted Poisson's ratio $v=0.3$ and soil mass density $\rho_0 = 2000$ kg/m³.

Table 1 - Soil types and parameters

Soil type	S1-soft	S2-medium	S3-stiff
c_s [m/s]	100	200	300

The dynamic stiffnesses are obtained using foundation dimensions, soil properties from Table 1 and Equations (2)-(7). The values of dynamic stiffnesses shown in Table 2 are given in terms of k_z and c_z for three soil types at the characteristics frequencies, separately for columns and walls in both directions. Figure 4 shows the real and imaginary part of the vertical impedance of the square foundation below the column C1. The impedances are implemented into the FEM model of the structure using the frequency dependent spring elements.

Values of frequency dependent springs under the columns are taken from Table 2. Under the walls, the spring stiffness given in Table 2 are modeled as series of equivalent frequency

dependent springs attached to the nodes of the wall's finite elements. The stiffness of equivalent frequency dependent springs was calculated as dynamic stiffness from Table 2 divided by the length the of the wall and multiplied by the dimension of the finite element (0.5 m).
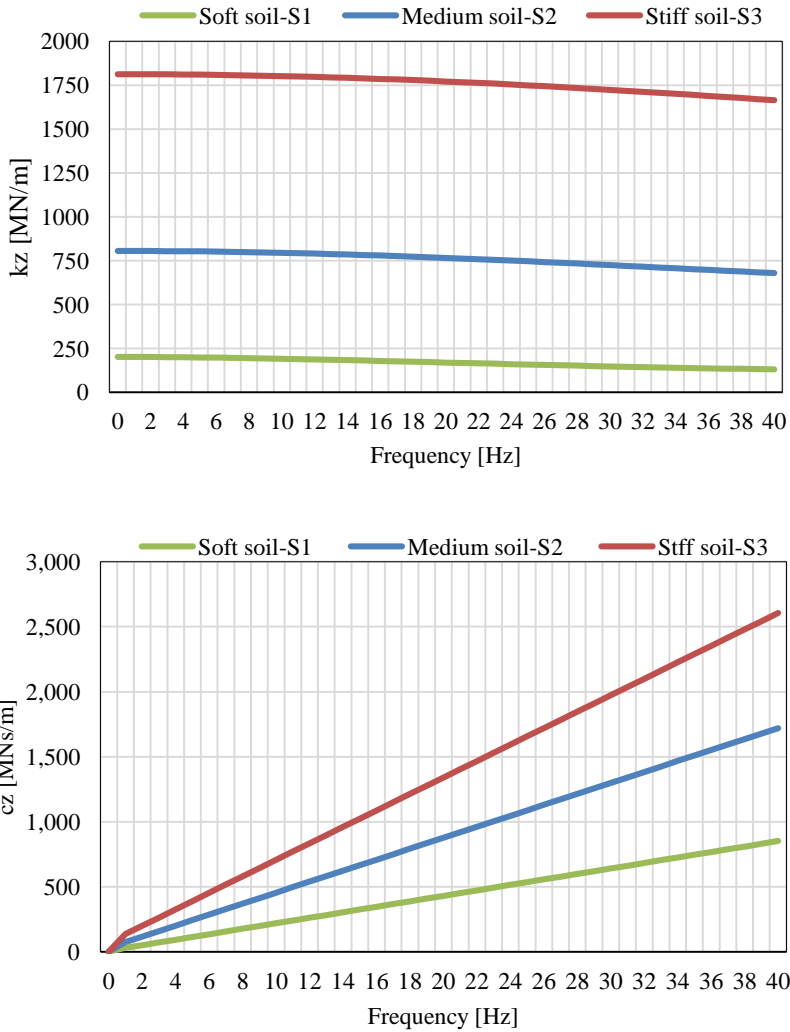

Figure 4 - Real (k_z) and imaginary(c_z) part of the vertical impedance below column C1

Table 2 - Values of kz and cz for three soil types for considered frequency range

	Columns			Walls in X direction			Walls in Y direction			Freq. [Hz]
	S1	S2	S3	S1	S 2	S 3	S 1	S2	S3	
k_z [MN/m]	201	806	1813	319	1278	2875	346	1383	3112	0
	170	766	1772	220	1087	2644	234	1155	2829	20
	130	679	1665	183	881	2259	199	936	2393	40
c_z [MNs/m]	0	0	0	0	0	0	0	0	0	0
	430	877	1340	996	2018	3068	1138	2303	3499	20
	852	1.2	2606	1982	3985	6015	2265	4551	6866	40

A modal analysis of the structure is calculated, in order to observe the modes in which the vertical vibrations of the object occur and to choose the observation points. Vertical mode shapes for three soil types are shown in Figure 5.
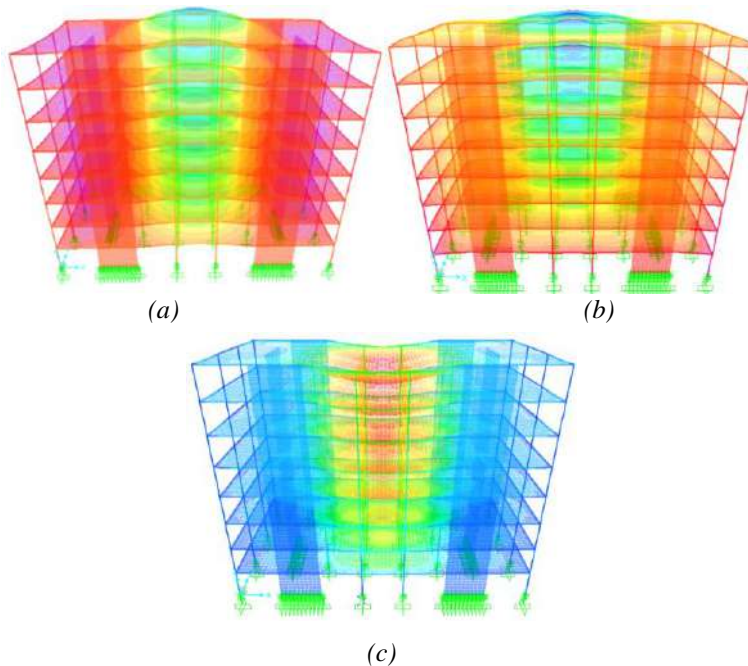

(a)   *(b)*

(c)

Figure 5 - First vertical mode shape: (a) soil S1 (f1v = 5.3 Hz), (b) Soil S2 (f1v = 7.1 Hz) and (c) soil S3(f1v = 8.1 Hz)

The position of two observation points A and C are shown in Figure 3. These points are chosen to describe the behavior of structure as the points with greatest vertical deflections. The TFs at observation points are calculated using the steady state analysis and a unit displacement harmonic excitation $u_0 = 1$ applied to the spring supports. The magnitudes of TFs of observation points are determined on each floor in the frequency range 0-40 Hz, and presented in Figure 6.
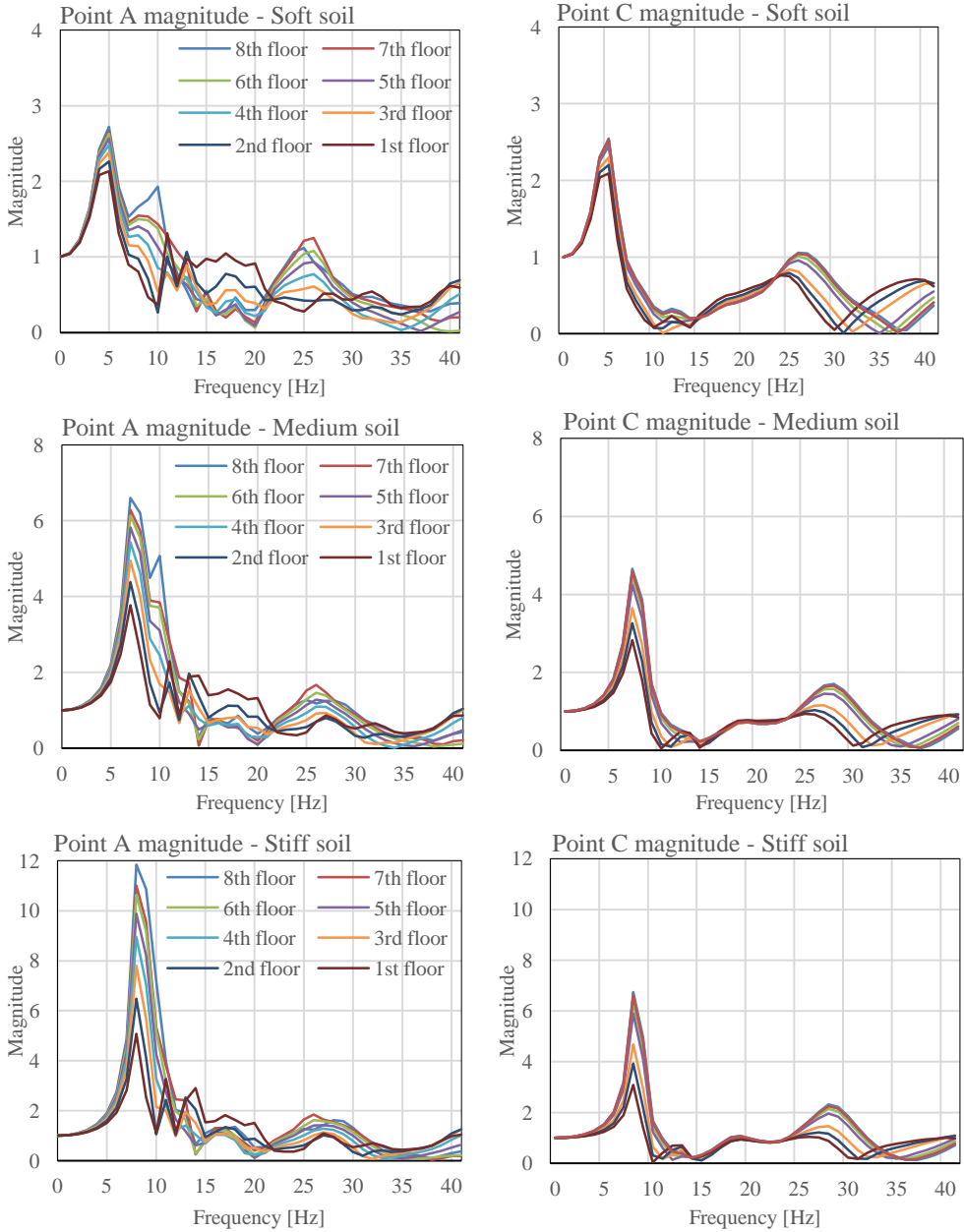
*Figure 6 - TFs for point A and C for soil types S1, S2 and S3*

The free field motion u_g is obtained using in-situ tests performed in Belgrade [11]. Figure 7 shows vertical acceleration time history induced by train and the corresponding frequency spectrum. According to Equation (9), the dynamic response at observation point A due to the measured free-field motion presented in Figure 8 is calculated as the product of the TF at observation point A, TF_A (Figure 6), and the u_g spectrum (Figure 7b):

$$u_A(g) = TF_A u_g$$

(10)

Dynamic response for observation point C is calculated analogously.
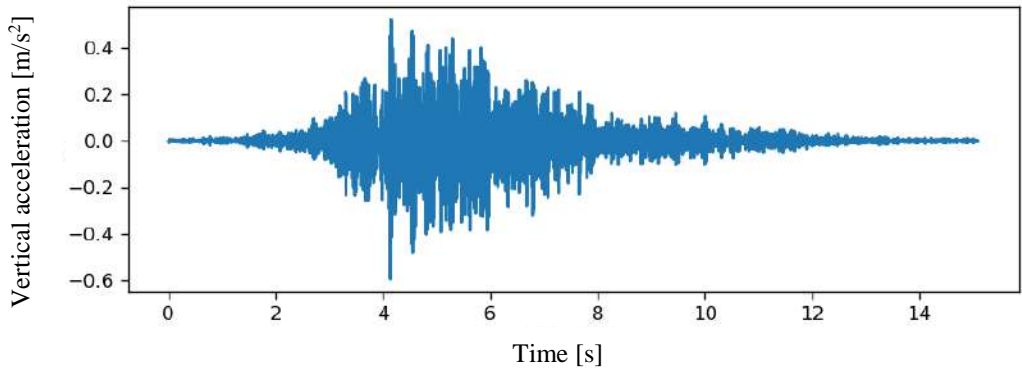
(a)
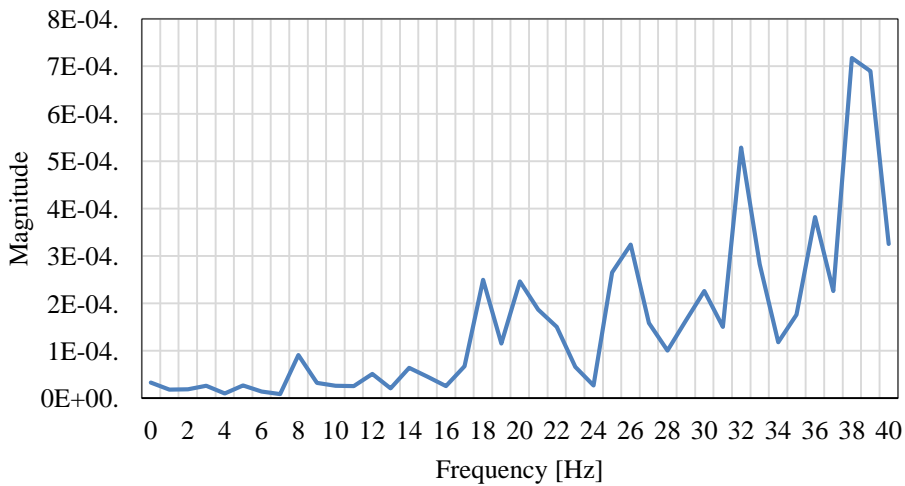
(b)

Figure 7 - (a) vertical acceleration time history induced by train and (b) frequency spectrum for train passage
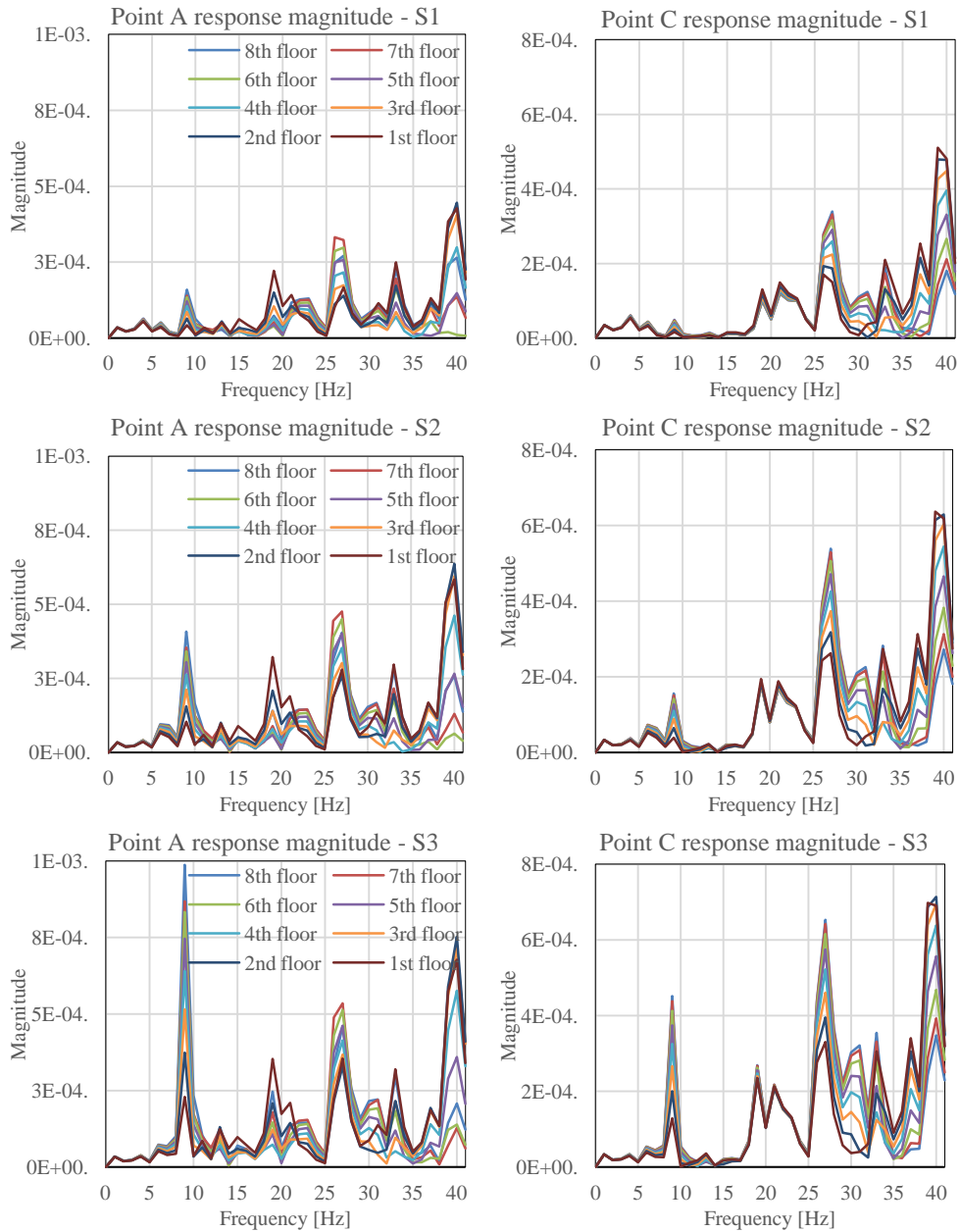
Figure 8 - Dynamic response at points A and C due to measured free field motion

4. DISCUSSION AND CONCLUSIONS

Influence of SSI on the response of an eight story residential building subjected to train-induced free field motion is investigated in this paper. The building is supported by shallow square foundations under the columns, and strip foundations under the walls. The dynamic response of the building due to the measured free-field motion is obtained for three different types of soil: soft (S1), medium (S2), and stiff soil (S3). The response of the building is obtained at two observation points with highest deflections at each story. Based on the performed numerical study, the following conclusions are drawn:

- As expected, for all TFs amplification factor (magnitude in Figure 6) is equal one for zero frequency, while for frequencies larger than 40 Hz it is less than one. This means that free field motion is affected by the building at higher frequencies (i.e. f > 40Hz) [6].

- In the case of soft soil, the building resonance occurs at 5 Hz with highest amplification factors between 2.1 and 2.55 (corresponding to 1st and 8th floor) at observation point C and between 2.1 and 2.7 at observation point A. The building resonance frequency is fully affected by the soil-building resonance frequency [6] determined by the soil stiffness and total mass of the building and is equal 5.7 Hz. In addition, amplification factors between 1 and 1.5 are detected for observation point A for frequencies between 8 and 9 Hz due to the coupling of floor resonance frequency at 10Hz and the soil-building resonance frequency.

- For medium and stiff soil, the building resonance occurs at 7 Hz and 8 Hz, respectively, which is lower than the corresponding soil-building resonance frequencies of 11 Hz and 17 Hz respectively. This means that there is a certain coupling of the soil-building resonance frequencies and the so-called column frequency determined by the wave velocity of the column/wall – floor model and the building height H (for details see ref [6]). The column frequency of the investigated building is 13 Hz, thus building resonance is shifted from 11 Hz to 7 Hz and from 17 Hz to 8 Hz for medium and stiff soil, respectively.

- At the building resonance frequency, drastically higher amplification factors are detected for medium and stiff soil in comparison to the soft soil (up to 6.6 for medium soil and 11.8 for stiff soil). Consequently, soft soil can significantly reduce the response of the structure

- Generally, higher amplification factors are detected at the observation point A than at the observation point C. This is more evident for medium and stiff soil.

- Amplification for both observation points A and C occurs in the range between 25 Hz and 26Hz. This amplification ranges from 1.2 to 2.0 from soft to stiff soil scenario, respectively.

ACKNOWLEDGEMENTS

REFERENCES

[1] J. M. d. O. Barbosa, J. Park, and E. Kausel, "Perfectly matched layers in the thin layer method," Computer methods in applied mechanics and engineering, vol. 217220, pp. 262–274, Apr. 2012, doi: 10.1016/j.cma.2011.12.006.

[2] J. Dominguez, Boundary Elements in Dynamics. WIT Press, 1993.

[3] J. Freisinger, M. Radišić, F. Taddei, and G. Müller, "Dynamic response of three-dimensional rigid and flexible foundations on layered soils with local inhomogeneities,"

Soil dynamics and earthquake engineering, vol. 153, p. 107007, Feb. 2022, doi: 10.1016/j.soildyn.2021.107007.

[4]   J.-G. Sieffert and F. Cevaer, Handbook of Impedance Functions (French Edition). Editions Ouest-France, 1995.

[5]   N. E. H. R. Program, "Soil-Structure Interaction for Building Structures." National Institute of Standards and Technology, 2012.

[6]   L. Auersch and S. Ziemens, "The response of different buildings to free-field excitation – a study using detailed finite element models," 2020, pp. 4560–4576. doi: 10.47964/1120.9371.19375.

[7]   D. López-Mendoza, D. Connolly, A. Romero, G. Kouroussis, and P. Galvín, "A transfer function method to predict building vibration and its application to railway defects," Construction and building materials, vol. 232, p. 117217, Jan. 2020, doi: 10.1016/j.conbuildmat.2019.117217.

[8]   J. E. Luco, A. H. Hadjian, and H. D. Bos, "The dynamic modeling of the half-plane by finite elements," Nuclear engineering and design, vol. 31, no. 2, pp. 184–194, Jan. 1974, doi: 10.1016/0029-5493(75)90140-5.

[9]   G. Schmid and A. Tosecky, "Soil and foundation dynamics, "Lecture for the Master Course *Earthquake Engineering* at IZIIS, University *SS. Cyril and Methodius* Skopje, May 2003

[10]   A. Pals, "Approximate formulas for dynamic stiffnesses of rigid foundations," Soil Dynamics and Earthquake Engineering, vol. 7, no. 4, pp. 213-227, 1988, doi: 10.1016/S0267-7261(88)80005-8

[11]   Z. Mišković, "Elaborat o registrovanim vibracijama na lokaciji Humska 10 u Beogradu tokom perioda od 24h na mestu izgradnje budućeg objekta", Građevinski fakultet Beograd, 2021.

ДГКС
Друштво грађевинских
конструктера Србије

ASES
Association of Structural
Engineers of Serbia

Nevenka Kolarević[1] *,Marija Nefovska-Danilović*[2]

SLOBODNE VIBRACIJE ROTACIONO-SIMETRIČNIH SISTEMA PRIMENOM METODE DINAMIČKE KRUTOSTI

Rezime:

U ovom radu primenjena je metoda dinamičke krutosti za analizu slobodnih vibracija sistema koji se sastoji od kružne cilindrične ljuske i kružnih i/ili prstenastih ploča. Pri formulaciji dinamičkih matrica krutosti korišćena je Flügge-ove teorija ljuski, kao i Kirchoff-ova teorija tankih ploča. Na osnovu razvijenog programa u MATLAB okruženju, urađeno je nekoliko numeričkih primera. Rezultati za sopstvene frekvencije dobijeni primenom metode dinamičke krutosti upoređeni su sa rezultatima dobijenim pomoću komercijalnog programa Abaqus zasnovanog na metodi konačnih elemenata.

Ključne reči: metoda dinamičke krutosti, kružne cilindrične ljuske, kružne ploče

FREE VIBRATION STUDY OF AXISYMMETRIC ASSEMBLIES USING DYNAMIC STIFFNESS METHOD

Summary:

In this paper, the dynamic stiffness method is used for the free vibration analysis of assemblies built up of circular cylindrical shells and circular and/or annular plates. Flügge's shell theory as well as Kirchhoff's theory of thin plates were used in the formulation of dynamic stiffness matrices. Based on the MATLAB code, developed for this particular purpose, several numerical examples were presented. The results for natural frequencies obtained using the dynamic stiffness method are compared with the results obtained using the commercial finite element method - based software Abaqus.

Key words: dynamic stiffness method, circular cylindrical shells, circular plates

[1] *Assistant professor, Faculty of Civil Engineering, University of Belgrade, Serbia, nevenka@grf.bg.ac.rs*
[2] *Associate professor, Faculty of Civil Engineering, University of Belgrade, Serbia, marija@grf.bg.ac.rs*

1. INTRODUCTION

Thin plates and shells play an important role in the variety of engineering fields such as civil, mechanical, aeronautical, naval and ocean engineering. Cylindrical shells are widely used in structural design of water tanks, aerospace fuselages, submarine hulls, to store liquids and gases in a wide variety of applications (pressure vessels), etc. Above-mentioned structures often involve plate/shell coupled structures: aircraft fuselages and submarine hulls are reinforced by ring stiffeners to increase their strength, plates are attached in aircraft fuel tanks to minimize liquid slashing problems and an aircraft fuselage is closed at its end by a circular bulkhead. The vibration behavior of such coupled structures has significant effect on their performance and hence play an important role in analysis and design process. Furthermore, such structures may have natural frequencies in the medium and high frequency range and can be subjected to arbitrary boundary conditions. On the other hand, the dynamic behavior of the combined structure becomes relatively complicated. Therefore, it is of great importance to apply an accurate and reliable method to compute their free vibration characteristics for any combination of boundary conditions and within any frequency range.

The finite element method (FEM) is certainly the most commonly used because of its versatility to handle any structural geometry, load and boundary conditions. However, the FEM may become inadequate and unreliable in the evaluation of the high frequency response, which is essential in many practical problems such as wave propagation and vibro-acoustics. In such cases, analytical methods give a better insight and understanding of the structural dynamic behavior.

In the papers [1-4], free vibrations of cylindrical shells with circular plates at predefined axial position and clamped and simply supported boundary conditions have been studied by using analytical approach. Huang [5] applied receptance method to coupled structure consisting of a simply supported thin circular cylindrical shell and a circular plate which may be joined to the shell at any arbitrary axial position. Yim [6] extended previous work to clamped cylindrical shells. Cheng [7] and Yuan [8] applied Rayleigh-Ritz approach to circular cylindrical shell closed at one end or both ends by circular plates and a wide spectrum of boundary and coupling conditions between the shell and the plate. Ma [9] presented a unified solution for coupled cylindrical shell and annular plate systems with general boundary and coupling conditions by using a modified Fourier-Ritz method. Xie [10] presented an analytical wave-based method to investigate free and forced vibrations of elastically coupled thin annular plate, at any axial locations, and cylindrical shell, based on Flügge shell theory, with arbitrary boundary conditions.

Dynamic stiffness method (DSM) combines the benefits of both analytical and numerical methods. The essential element in the DSM is a continuous element and the corresponding dynamic stiffness matrix. The dynamic stiffness matrix is derived from the strong form solution of the governing differential equations of motion in the frequency domain. It can then be assembled into the global dynamic stiffness matrix, applying similar assembly procedure as in the FEM. Consequently, the DSM can be regarded as highly efficient method used in the vibration analysis of structural assemblies providing the results of high accuracy with minimal structural meshing and with significant saving in computational time.

In the present study, authors applied DSM to the free vibration analysis of plate/shell coupled structures. Dynamic stiffness matrix of a cylindrical shell element, based on the Flügge thin shell theory, is given in [11], while dynamic stiffness matrices of a circular/annular plate element for

transverse vibration based on the thin plate theory and in-plane vibration are given in [12] and [13], respectively. Two numerical examples have been presented to check the accuracy, versatility and efficiency of the DSM. The natural frequencies and mode shapes have been validated against the results obtained by using the finite element software Abaqus [14].

2. DYNAMIC STIFFNESS FORMULATION

DSM is based on the strong solution of the governing differential equations derived for the corresponding elastodynamic problem in the frequency domain. Consequently, for circular/annular plates and circular cylindrical shells closed-form solutions for displacement field is derived. Figure (1) shows components of displacement and force vectors of a circular cylindrical shell element of constant thickness h, radius a and length L, while Figures (2) and (3) show components of displacement and force vectors for transverse and in-plane vibration of a circular and annular plate element of constant thickness h and radius a (inner radius b and outer radius a), respectively. Note that displacements and force vectors are defined along the boundary lines instead at nodes.
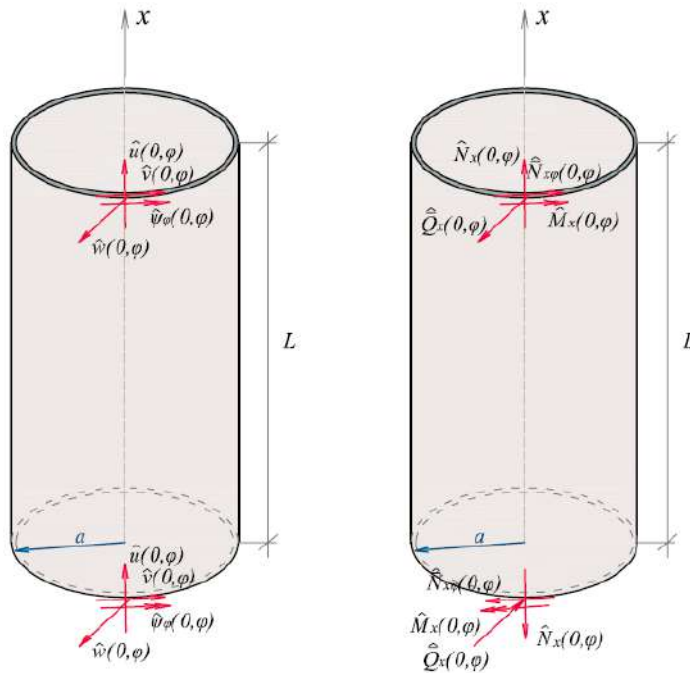

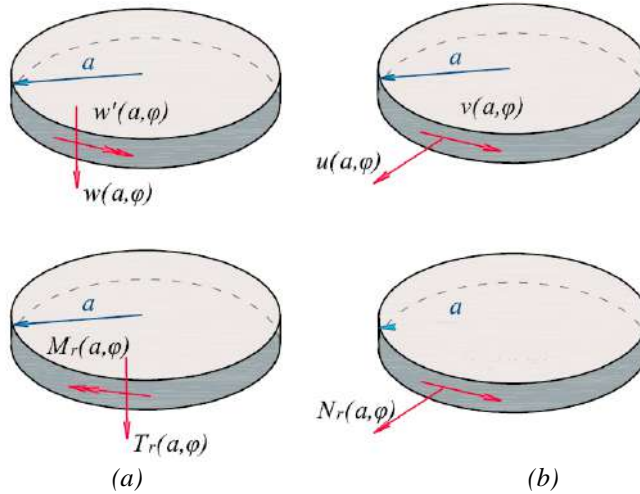*Figure 1 – Components of displacement and force vectors of a circular cylindrical shell*

Figure 2 – Components of displacement and force vectors of a circular plate for transverse (a) and in-plane (b) vibration
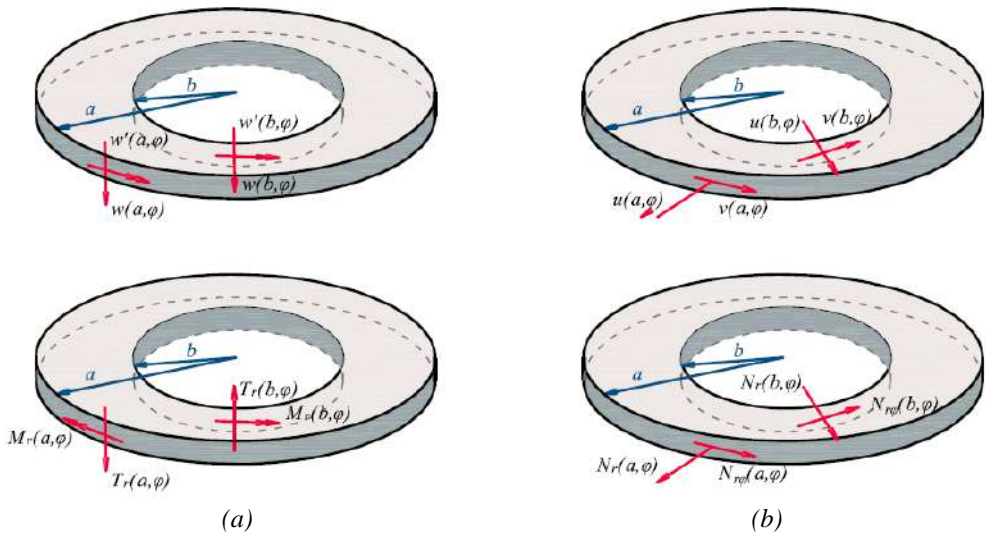

Figure 3 – Components of displacement and force vectors of an annular plate for transverse (a) and in-plane (b) vibration

To relate forces and displacement components along element boundaries and define dynamic stiffness matrix, displacement and force vectors **q** and **Q** can be written in the following manner:

$$\mathbf{q} = [\mathbf{D}] \cdot \mathbf{C} \tag{1}$$

$$\mathbf{Q} = [\mathbf{F}] \cdot \mathbf{C} \tag{2}$$

where **C** is the vector of integration constants in general solution of the displacement field.

By using Eqs. (1) and (2), vectors $\mathbf{Q}$ and $\mathbf{q}$ are related as:

$$\mathbf{Q} = \mathbf{K}_D \cdot \mathbf{q} \,, \tag{3}$$

$$\mathbf{K}_D = \mathbf{F} \cdot \left[\mathbf{D} \right]^{-1}, \tag{4}$$

where $\mathbf{K}_D$ is the dynamic stiffness matrix.

For closed circular cylindrical shell and circular/annular plates, having uniform boundary conditions, solutions for each harmonic m are decoupled. Therefore, $\mathbf{K}_D$ can be written in the following form:

$$\mathbf{K}_D = \begin{bmatrix} \mathbf{K}_{D0} & & & \\ & \mathbf{K}_{D1} & & \\ & & \ddots & \\ & & & \mathbf{K}_{Dm} \end{bmatrix}, m = 0,...,\infty \,, \tag{5}$$

where $\mathbf{K}_{Dm}$ is dynamic stiffness matrix for the mth harmonic, m is the wave number in the circumferential direction.

The dynamic stiffness matrix, based on the Flügge thin shell theory, is given in [11]. For $m \geq 1$ the dimension of the dynamic stiffness matrix $\mathbf{K}_{Dm}$ for each harmonic is 8. The dynamic stiffness matrices for transverse vibration $\mathbf{K}_{Dm}^{CT}$ and $\mathbf{K}_{Dm}^{AT}$, based on the thin plate theory, are given in [12], while the dynamic stiffness matrices for in-plane vibration $\mathbf{K}_{Dm}^{CI}$ and $\mathbf{K}_{Dm}^{AI}$ are given in [13]. The superscripts have the following meaning:

- CT- circular plate transverse vibration,
- AT - annular plate transverse vibration,
- CT- circular plate in-plane vibration,
- AT - annular plate in-plane vibration.

Dimension of both dynamic stiffness matrices for circular plate $\mathbf{K}_{Dm}^{CT}$ and $\mathbf{K}_{Dm}^{CI}$ for each harmonic is 2, while the size of matrices $\mathbf{K}_{Dm}^{AT}$ and $\mathbf{K}_{Dm}^{AI}$ of annular plate is 4 for $m \geq 1$. Consequently, dimension of the dynamic stiffness matrix of a circular plate element $\mathbf{K}_{Dm}^{CP}$ for each harmonic is equal 4, while dimension of the dynamic stiffness matrix of an annular plate element $\mathbf{K}_{Dm}^{AP}$ for each harmonic is equal 8, and they are assembled in the following manner:

$$\mathbf{K}_{Dm}^{CP} = \begin{bmatrix} \mathbf{K}_{Dm}^{CT} & \\ & \mathbf{K}_{Dm}^{CI} \end{bmatrix}_{4 \times 4} \qquad \mathbf{K}_{Dm}^{AP} = \begin{bmatrix} \mathbf{K}_{Dm}^{AT} & \\ & \mathbf{K}_{Dm}^{AI} \end{bmatrix}_{8 \times 8} \tag{6}$$

3. ASSEMBLING PROCEDURE FOR PLATE/SHELL COUPLED STRUCTURE

A procedure for free vibration analysis of plate/shell coupled structure consisting of circular cylindrical shell and circular and annular plates which may be joined to the shell at any arbitrary axial position is given in this section. First, global dynamic stiffness matrix should be formulated. Global coordinate system corresponds to the local coordinate system of cylindrical shell element. Consequently, rotational matrices should be defined for circular and annular plate element only. Displacements in the global coordinate system along circular boundaries are presented in Figure (4).
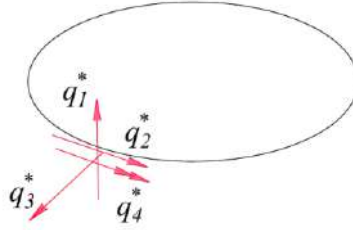

Figure 4 – Displacements components in the global coordinate system

Rotational matrices of circular and annular plate element, for each *m*, are given in the following equation, respectively:

$$
\mathbf{T}_R^{CP} = \begin{bmatrix} -1 & 0 & 0 & 0 \\ 0 & 0 & 0 & -1 \\ 0 & 0 & 1 & 0 \\ 0 & -1 & 0 & 0 \end{bmatrix}, \quad
\mathbf{T}_R^{AP} = \left[\begin{array}{cccc|cccc}
-1 & 0 & 0 & 0 & 0 & 0 & 0 & 0 \\
0 & 0 & 0 & 0 & 0 & -1 & 0 & 0 \\
0 & 0 & 0 & 0 & 1 & 0 & 0 & 0 \\
0 & -1 & 0 & 0 & 0 & 0 & 0 & 0 \\
\hline
0 & 0 & -1 & 0 & 0 & 0 & 0 & 0 \\
0 & 0 & 0 & 0 & 0 & 0 & 0 & -1 \\
0 & 0 & 0 & 0 & 0 & 0 & 1 & 0 \\
0 & 0 & 0 & -1 & 0 & 0 & 0 & 0
\end{array} \right]
\tag{7}
$$

According to the relation between the vectors of displacements/forces in the local, and the corresponding vectors in the global coordinate system, the dynamic stiffness matrix of plate elements in the global coordinate system is derived as:

$$
\mathbf{K}_{Dm}^* = T^T \cdot \mathbf{K}_{Dm} \cdot T
\tag{8}
$$

where $T = T_R^{CP}$ or T_R^{AP}.

Dynamic stiffness matrices of individual elements in the global coordinate system are assembled in the global dynamic stiffness matrix of a coupled structure by applying the similar assembly procedure as in the conventional FEM. Note that the connection is established along circular boundaries, instead at nodes as in the FEM. Afterwards, arbitrary boundary conditions are applied by deleting rows and columns of the global dynamic stiffness matrix corresponding to the constrained displacements and rotations [15].

The natural frequencies are calculated from the expression $\det(\mathbf{K}_{Dm}^{*}) = 0$.

Based on the theoretical considerations given in previous sections, a MATLAB-based software was developed for free vibration analysis of plate/shell coupled structures.

4. NUMERICAL EXAMPLES

The applicability of the presented method for free vibration analysis of a coupled cylinder-plate structure is verified through two numerical examples. Natural frequencies are compared to the results obtained from the finite element-based software Abaqus. The material properties used for the numerical examples are: $E = 210\,\text{GPa}$, $\rho = 7850\,\text{kg/m}^3$ and $\nu = 0.3$, while geometrical properties are given in Figure (5). The thickness of all elements is $h = 0.01$ m. Free – F and clamped - C boundary conditions are assigned along the boundary lines. The first seven natural frequencies of coupled structures (a) and (b) are given in Table 1 and 2, respectively. In the proposed DSM formulation, the discretization of the numerical example (a) has been achieved by using four dynamic stiffness elements, two cylindrical shell and two circular plate elements, while three dynamic stiffness elements, one cylindrical shell and two annular plate elements, are used in the numerical example (b). Circumferential wave number m that corresponds to the natural frequency is also presented in Table 1 and 2. Excellent agreement has been achieved between the proposed method and FEM. Finite element models created in Abaqus consist of 53865 S4R finite elements (total number of variables in the model is 322938) - example (a) and 52776 S4R finite elements (total number of variables in the model is 316872) - example (b). Approximate mash size was 0.05 m. On the other side, DSM models for both examples have only 8 unknowns that have to be determined for each frequency step. In middle and high frequencies range FE mesh should be finer in order to get accurate results. On the other hand, DSM model has the same number of unknowns regardless of the frequency of interest and therefore has a significant advantage in terms of computational time and required computer resources over widely used FEM.
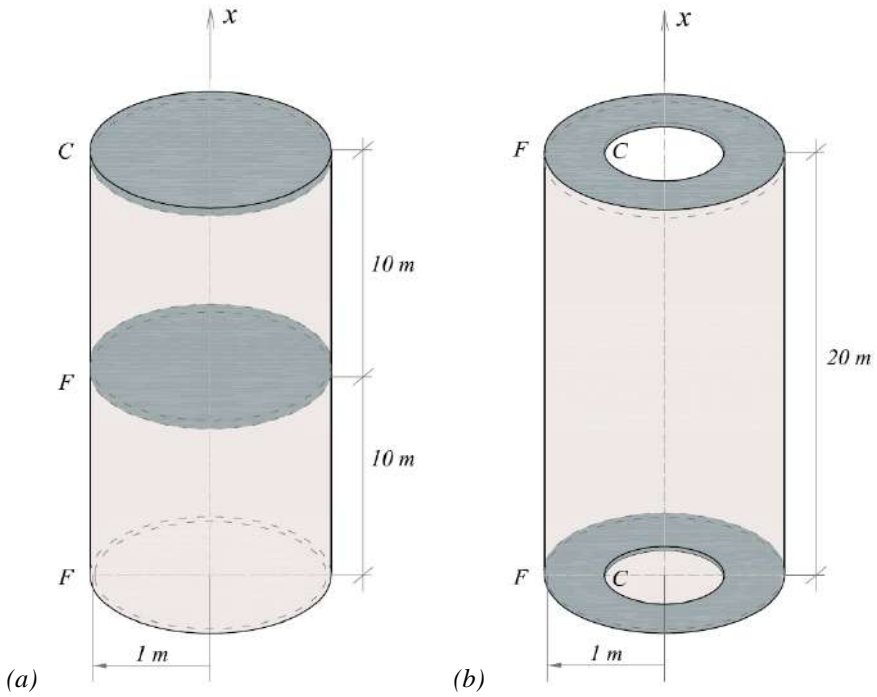
Figure 5 – Geometry of coupled structures for numerical examples

Table 1 – First seven natural frequencies (Hz) of coupled cylindrical shell-circular plate structure (a)

Mode	Proposed model	Abaqus	m
1	5.0	4.9984	1
2	8.0	8.06	2
3	19.0	19.10	3
4	23.2	23.29	3
5	24.5	24.51	0
6	25.4	25.47	0
7	26.6	26.60	3

Table 2 – First seven natural frequencies (Hz) of coupled cylindrical shell-circular plate structure (b)

Mode	Proposed model	Abaqus	m
1	6.1	6.11	0
2	8.1	8.10	2
3	13.8	13.84	1
4	18.9	18.92	2
5	19.1	19.12	3
6	20.9	20.94	3
7	27.0	27.0	3

5. CONCLUSIONS

In this paper, the dynamic stiffness method was extended to the free vibration analysis of plate/shell coupled structure consisting of circular cylindrical shell and circular and annular plates that may be joined to the shell at any arbitrary axial position. Previously developed dynamic stiffness matrices, based on the Flügge thin shell theory and thin plate theory, were transformed to the global coordinate system by the rotational matrices. The presented procedure was implemented in the MATLAB code. Through numerical examples the results obtained using the DSM were validate against the results of the FEM. Study presented in the paper demonstrated high accuracy and efficiency of the proposed method in the free vibration analysis of plate/shell coupled structure having any combination of boundary conditions, regardless on the frequency range.

REFERENCES

[1] Smith B.L, Haft E.E. Vibration of a circular cylindrical shell closed by an elastic plate, AIAA J, 5 (11), 1967, 2080-2082.

[2] Takahashi S, Hirano Y. Vibration of a combination of circular plates and cylindrical shells (1st report, a cylindrical shell with circular plates at ends), Bull Jpn Soc Mech Eng, 13 (56), 1970, 240-247.

[3] Takahashi S, Hirano Y. Vibration of a combination of circular plates and cylindrical shells (2nd report, a cylindrical shell with circular plate in the intermediate section), Bull Jpn Soc Mech Eng, 14 (67), 1971, 20-28.

[4] Yamada G, Irie T, Tamiya T. Free vibration of a circular cylindrical shell double-shell system closed by end plates. J Sound Vib, 108 (2), 1986, 297-304.

[5] Huang D.T, Soedel W. Natural frequencies and modes of a circular plate welded to a circular cylindrical shell at arbitrary axial positions, J Sound Vib, 162 (3), 1993, 403-427.

[6] Yim J.S, Sohn D.S, Lee Y.S. Free vibration of clamped-free circular cylindrical shell with a plate attached at arbitrary axial position, J Sound Vib, 213 (1), 1998, 75-88.

[7] Cheng L, Nicolas J. Free vibration analysis of a cylindrical shell-circular plate system with general coupling and various boundary conditions, J Sound Vib, 155 (2), 1992, 231-247.

[8] Yuan J, Dickinson S.M. The free vibration of circularly cylindrical shell and plate systems, J Sound Vib, 175 (2), 1994, 241-263.

[9] Ma X.L, Jin G.Y, Shi S.X, Ye T.G, Liu Z.G. An analytic method for vibration analysis of cylindrical shells coupled with annular plate under general elastic boundary and coupling conditions, J Vib Control, 23 (2), 2017, 305-328.

[10] Xie K, Chen M, Zhang L, Xie D. Wave based method for vibration analysis of elastically coupled annular plate and cylindrical shell structures, Appl Acoust, 123, 2017, 107-122.

[11] Kolarević N, Nefovska-Danilović M, Petronijević M. Dynamic stiffness method in the vibration analysis of circular cylindrical shell. Gradjevinski materijali i konstrukcije. 59, 2016, 45-61.

[12] Damnjanovic E. Poprečne vibracije kružnih ploča primenom metode spektralnih elemenata, Diploma Thesis, Faculty of Civil Engineering, University of Belgrade, 2014.

[13] Jovanović B. Vibracije u ravni kružnih i prstenastih ploča primenom metode spektralnih elemenata, Diploma Thesis, Faculty of Civil Engineering, University of Belgrade, 2015.

[14] Abaqus, User's manual. Version 6.9, Providence, RI, USA: DS SIMULIA Corp, 2009.

[15] Marjanovic M, Kolarevic N, Nefovska-Danilovic M, Petronijevic M. Shear deformable dynamic stiffness elements for a free vibration analysis of composite plate assemblies-part I: theory. Composite Structures, (159), 2017, 728–744.

Slobodan Ranković[1]*, Todor Vacev*[2]*, Žarko Petrović*[3]*, Darko Živković*[4]

ISPITIVANJE TIPSKIH BETONSKIH KONZOLA ZA ELEKTROENERGETSKE VODOVE PROBNIM OPTEREĆENJEM

Rezime:

In the paper is presented testing of typical reinforced concrete cantilevers for power transmission lines using test load. For applying of the test load, an original mechanism is constructed, by which the forces are simultaneously applied in two perpendicular directions at the points of cable hanging. Results of measuring of the local deformations (dilatations) and global deformations (deflections) under test load are presented, and their analysis is given. Conclusions regarding deformations (deflections) and stresses at work and failure load are drawn, and a defined safety factors.

Ključne reči: ispitivanje, betonske konzole, elektroenergetski vodovi

TESTING OF TYPICAL CONCRETE CANTILEVERS FOR POWER TRANSMISSION LINES USING TEST LOAD

Summary:

U radu je prikazano ispitivanje tipskih armiranobetonskih konzola za elektroenergetske vodove probnim opterećenjem. Za nanošenje probnog opterećenja konstruisan je originalni mehanizam kojim su sile aplicirane istovremeno u dva upravna pravca na mestima zavešenja provodnika. Prikazani su rezultati merenja lokalnih deformacija (dilatacija) i globalnih deformacija (ugiba) pod uticajem probnog opterećenja i data njihova analiza. Izvedeni su zaključci u pogledu deformacija (ugiba) i napona pri eksploatacionom opterećenju i pri ispitivanju do loma i definisani koeficijenti sigurnosti.

Key words: testing, concrete cantilevers, power transmission lines

---

[1] *PhD, assistant prof., Faculty of Civil Eng. and Architecture, Niš, rankovics@gmail.com*
[2] *PhD, associate prof., Faculty of Civil Eng. and Architecture, Niš, todor.vacev@gaf.ni.ac.rs*
[3] *PhD, associate prof., Faculty of Civil Eng. and Architecture, Niš, zarko.petrovic@gaf.ni.ac.rs*
[4] *PhD, assistant, Faculty of Civil Eng. and Architecture, Niš, darko.zivkovic@gaf.ni.ac.rs*

1. INTRODUCTION

Reinforced concrete cantilevers for power transmission lines with nominal voltage of 10kV, 20kV and 35kV are consisted of a concrete column with mounted isolators for carrying of conductors. Their main characteristics are nominal length of the cantilever arm L_{kn} and nominal force F_{kn}. The nominal length of the cantilever arm L_{kn} is the distance between the column shaft axis and the most distant point of hanging for isolator mounting at the end of the cantilever. Nominal forces of the reinforced concrete cantilevers act in the center of gravity of the cross-section of the cantilever at the point of conductor hanging and they are definned depending on the acting direction as: nominal horizontal cantilever force and nominal vertical cantilever force. Regarding the number of cantilever sides, exist single-sided and double-sided cantilevers. Geometry of the cantilever girders resulted from the requirements of the overhead power line designers, technological capabilities of the manufacturers and multiyear experience in production and exploitation. The central void (hole) of the concrete cantilever used for mounting on the column shaft may have different diameters for one single cantilever type, depending on the shaft type and the mounting height of the cantilever. Technical recommendations of the Electric Power Industry of Serbia define standard dimensions and nominal forces (horizontal and vertical), and their correlation with column types In this investigation the requirement of the user related to the so-called "type testing" of the cantilevers, that is, testing of strength, which would represent the exploitation conditions in the most realistic way. It must be remarked that for years these examinations have been conducted partially, that is, by separate action of the vertical and horizontal forces. For the purpose of improvement of the conditions for test load application, an original frame mechanism for simultaneous application of vertical and horizontal forces has been constructed, which corresponds to the real conditions in power transmission lines. Such mechanism for load application, with minimal modifications is in use by the majority of manufacturers in Serbia, and it has been accepted by the user, i.e., the Electric Power Industry of Serbia.

2. EXPERIMENTAL SETUP

In order to simulate the exploitation conditions in the most real way, a facility for testing of the concrete cantilevers has been constructed at the manufacturer's location. For that purpose, a support (column shaft) and a steel frame that enables simultaneous application of vertical and horizontal forces at the points of conductor hanging to the tested cantilevers have been made. The support has been made as a composite steel-concrete column 1 m high, with shape of truncated regular cone, and its behaviour has no influence to the behaviour of the cantilever during its examination with testing load. Using steel cables and a system of winches, simultaneous application of load on both cantilever ends in horizontal and vertical direction is provided. The forces are applied by hydraulic devices (vertical) and by post-tensioning devices (horizontal). The testing procedure has been conducted according to the standard SRPS U.M1.047 and Technical Recommendation No. 10a, Appendix No. 2. Application of the horizontal forces at the cantilever ends was done at the spots of the horizontal voids, and application of the vertical forces at the spots of the outmost vertical voids. Application of the forces in the hanging points is done using an anchor bolt and connection elements.

2.1. EXAMINATION UNDER TEST LOAD

2.1.1. Stages of the test loading

In the 1st stage (stage of stabilization of the fixing) were applied horizontal and vertical force to the level of 50% of the nominal force, in order to eliminate harmful effects of the fixing, which affect the measurement accuracy. After unloading, initial values of displacements, cracks, and dilatations were registered.

In the 2nd stage (stage of control examination) the force was applied to the nominal value, in 4 increments (0,55×F; 0,70×F; 0,85×F i 1,0×F). Sustaining of every load value lasted as long as it took for the instrument reading (reading of displacements in horizontal and vertical direction, tracking of dilatations in characteristic cross-sections, tracking of the support displacement, determining of the width and disposition of cracks. After unloading, values of residual cracks and deformations were registered, as well as the residual dilatations, with analysis of displacements in the fixing point.

In the 3rd stage (stage of type examination) the load was increased in two increments, first, until the needed safety factor has been achieved, i.e., until the 180 % value of the nominal force, and second, until the breaking force. Simultaneously, tracking of deflection, dilatations and cracka has been conducted.
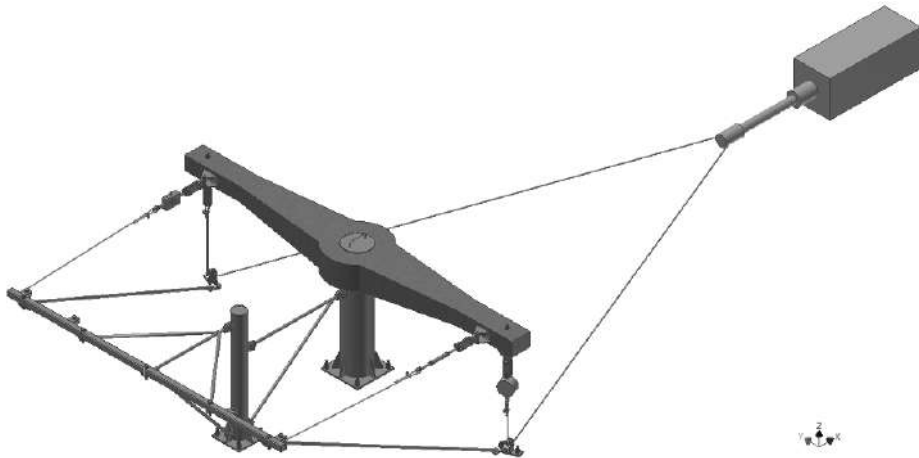

Figure 1 – System (frame) for simultaneous application of load at two orthogonal directions at the point of conductor hanging

2.1.2. Type and disposition of instruments

Deformation of the cantilever under test load has been tracked by measuring of the horizontal and vertical displacement at the cantilever ends using deflectometers. Cracks were measured by crack measuring indicator, with accuracy of 0.05, with use of magnifying glass. Control measuring of the extreme dilatations in the tensioned and compressed zone of the concrete was measured by deformeter, while dilatations and stresses have been calculated using known modulus of elasticity. Considering the ocurrence of biaxial bending, dilatations have been measured in two orthogonal directions. Support displacement in the fixing point has been controlled by deflectometers, too.

3. TEST RESULTS (EXAMPLE)

Results of examination of the mechanical characteristics of the concrete cantilevers under test load are presented on the example of the cantilever type D2Z 100/500/315.
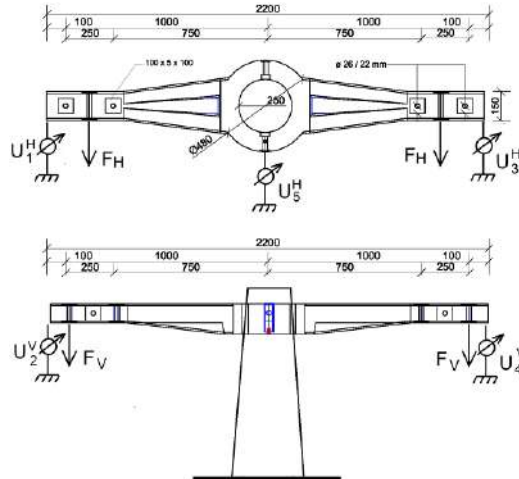

Figure 2 – Disposition of the cantilever during examination: type D2Z 100/500/315 and disposition of instruments
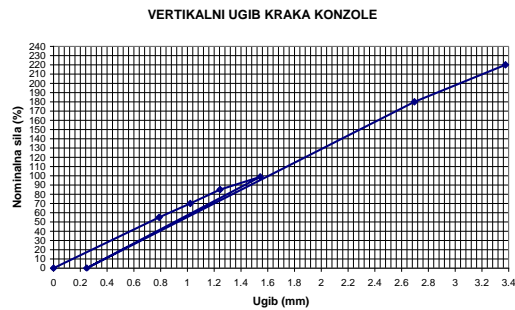

Figure 3 – Vertical deflection of the concrete cantilever arm (type: D2Z 100/500/315)
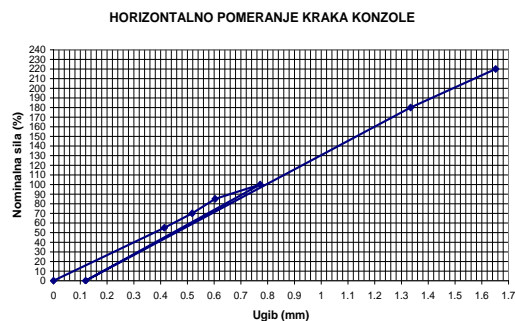

Figure 4 – Horizontal deflection of the concrete cantilever arm (type: D2Z 100/500/315)

Table 1 – Results of deformation examination for cantilever type D2Z 100/500/315

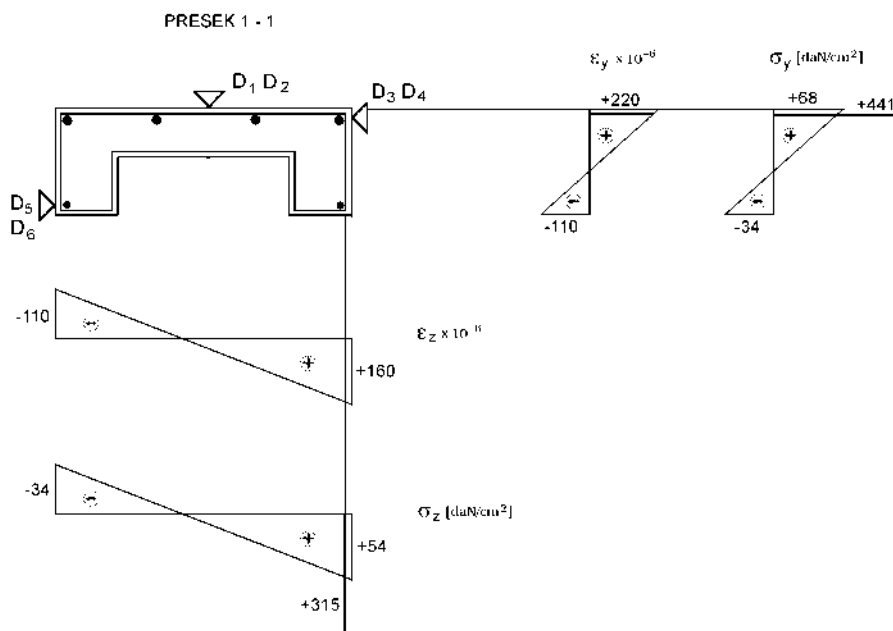| %F	0	0.55·F	0.70·F	0.85·F	**1.0·F**	0	**1.8·F**	2.20·F
Fh/Fv (daN)	0	275/175	350/220	425/270	**500/315**	0	**900/570**	1100/660
U_v/U_H (mm)	0	0.79/0.42	1.02/0.52	1.24/0.60	**1.54/0.77**	0.25/0.12	**2.70/1.33**	3.381.65

Figure 5 – Diagrams of the mean measured dilatations and stresses under nominal forces for the cantilever type D2Z 100/500/315

4. CONCLUSIONS

The frame for applying test load during examination of concrete cantilevers reliably simulates real loading conditions, and represents an original solution, which is, with minimal alterations, recently used at the majority of manufacturers in Serbia. Based on the measured values of the global and local deformations (deflections and dilatations), that is, maximal measured forces (vertical and horizontal), obtained for different types of concrete cantilevers, one may conclude that their strength satisfies required conditions (safety factor higher than $\gamma=1.8$). This also confirms that concrete cantilevers are not "weak points" in the power line conductor, and that failure of the concrete columns arises due to the fracture of the column itself, which proved to be true in many years of exploitation. Values of the failure force at many cantilever types significantly exceed the required safety factor ($\gamma=2.5$-4.2), which leads to the conclusion that they are oversized, and that there is room for savings considering the geometry and the amount of reinforcement, along with fulfilling of the requirements related to their position on the column and disposition of the forces that originate from the conductors.

5. PHOTO DOCUMENTATION FROM THE TESTING

Figure 6 – Experimental setup (testing frame and method of loading of the concrete cantilever)

Figure 7 – Measuring of dilatations and cracks

LITERATURE

[1] Tehničke preporuke br. 10a: "Opšti tehnički uslovi za projektovanje, proizvodnju i korišćenje betonskih stubova za nadzemne vodove nazivnog napona 0,4 kV, 10 kV, 20 kV i 35 kV", 2014.

[2] Dodatak br. 1 Tehničke preporuke br. 10a: "Uslovi i postupak ispitivanja stabala betonskih stubova za nadzemne vodove nazivnog napona 0,4 kV, 10 kV, 20 kV i 35 kV". decembar 2005.

[3] Dodatak br. 2 Tehničke preporuke br. 10a: "Uslovi i postupak ispitivanja kozola od betona stubova za distributivne nadzemne vodove niskog i srednjeg napona", decembar 2005.

[4] Propisi za ispitivanje konstrukcija objekata visokogradnje SRPS U. M1. 047. 1987.

[5] SRPS U.E3.050:1981, Prefabrikovani betonski elementi – Tehnički uslovi za uzradu i ugradnju.

R-7

Kongres 2022
Congress 2022

Tanja Nožica[1], Đorđe Jovanović[2], Drago Žarković[3]

IMPLEMENTACIJA VELIKIH POMERANJA U AKADEMSKOM SOFTVERU MATRIX 3D

Rezime:

U radu su predstavljeni izazovi koji prate softversku implementaciju velikih pomeranja. Komercijalni softveri imaju implementirane u sebi nelinearne analize, među kojima je i analizu velikih pomeranja. Međutim sama nelinearna analiza je vremenski zahtevna za računar, čime se javlja potreba za manje vremenski zahtevnim analizama. Da bi se to postiglo korišćena je korotaciona formulacija koja podrazumeva razdvajanje pomeranja elementa na dva dela: pomeranje krutog tela i deformaciju elementa. U radu je takođe prikazan algoritam implementacije i na primerima su prikazani rezultati

Ključne reči: korotaciona analiza, velika pomeranja, softver, nelinearna analiza

IMPLEMENTATION OF LARGE DISPLACEMENTS IN THE ACADEMIC SOFTWARE MATRIX 3D

Summary:

In this paper, the challenges arising in software implementation of large displacements are presented. Nonlinear analysis, including analysis of large displacement, have been implemented in a number of commercial software. However, the nonlinear analysis itself is time consuming, which initiates the need for less time-consuming analyses. In order to achieve that, the corotational formulation was used, which implies the separation of the element displacement into two parts: the displacement of the rigid body and the element deformation. This paper also presents the implementation algorithm, and some representative results are provided.

Key words: corotational analysis, large displacements, software, nonlinear analysis

[1] *Teach. Asst., University of Novi Sad, Faculty of Technical Sciences, Novi Sad, Serbia, nozica.tanja@uns.ac.rs*

[2] *Asst. Prof., University of Novi Sad, Faculty of Technical Sciences, Novi Sad, Serbia, djordje.jovanovic@uns.ac.rs*

[3] *Asst. Prof., University of Novi Sad, Faculty of Technical Sciences, Novi Sad, Serbia, dragozarkovic@uns.ac.rs*

1. INTRODUCTION

Large displacement analysis of structures is an essential topic due to the development of new materials which enable structures to undergo large deformation; that is why modern structural analysis requires numerical formulations with advanced nonlinear attributes.

At the Faculty of Technical Sciences, the academic software Matrix 3D [1]–[4] is being developed. The Matrix 3D software is primarily designed for nonlinear analysis. The objective of this paper is to improve the aspects that are lacking in the most used software in our country. One of these aspects is the implementation of the theory of large displacements, which is explained in detail in this paper, and the procedure of its implementation is shown. In complex structures, numerical solutions based on the application of the finite element method are used. The nonlinear finite element method is the most popular approach researching the nonlinear behaviour of structures. The development of computers has also led to advances in the nonlinear analysis of structures. Therefore, the theory of large displacements has attracted the attention of various researchers [5]–[12]. Commercial software such as ANSYS, SAP2000 and ABAQUS have implemented nonlinear analysis, including large displacement analysis. However, the nonlinear analysis is time-consuming, creating the need for accurate and computationally inexpensive geometrically nonlinear models. The basics of geometrically nonlinear analysis lie in the theory of kinematics [8]. In kinematics, three basic formulations are given to describe large beam displacements (nonlinear methods):

- **The Total Lagrangian formulation** is the most widespread. It is used by commercial software such as ABAQUS and ANSYS. This formulation uses the Cartesian global coordinate system, which is fixed throughout the analysis; therefore the reference system is the original undeformed configuration. Stresses and strains are calculated relative to the initial configuration

- **The Updated Lagrangian formulation** uses the last calculated configuration as a reference; namely using the previous configuration to calculate the next one. Therefore, the coordinate system is corrected with each computed configuration. Software SAP 2000 uses this formulation. In [9], [11], theoretical explanations of large displacements problems were given, which were solved using the Total Lagrangian formulation and the Updated Lagrangian formulation. It was shown that both formulations provide similar solutions, where the Updated Lagrangian formulation is the less time-consuming analysis.

- **The corotational formulation** is based on the small strain beam theory. It has two coordinate systems: the fixed global coordinate system and the element corotational local coordinate system. The corotational local frame rotates and translates with each element but does not deform with it. As part of the OpenSees software developed at the University of California, Berkeley, De Souza presented in [13] the improvement of software performance by introducing the corotational formulation, thus enabling analysis with large deformations and large rotations

These formulations include large displacements, large rotations, and small deformations. These kinematic formulations are very similar, with the difference in the reference configuration adopted to describe the body motion. Therefore, different solutions are obtained in geometrically nonlinear analysis of structures. It is also possible to use a combination of these formulations.

More attention has been focused on the corotational formulation compared to the Lagrangian formulation when it comes to studying large displacements. Papers [6]–[8], [10], [12], [14], [15] provide insight into two-dimensional elements with geometrically nonlinear behaviour, therefore

with large displacements, while papers [5], [16]–[19] show the problem of large displacements on three-dimensional elements.

2. PROBLEM DEFINITION

In order to analyze beam and frame structures undergoing large displacements by the finite element method, it is necessary to formulate a nonlinear beam model. The large displacement analysis should be used for any structure undergoing significant deformation, and for buckling analysis, particularly for snap-through buckling and post-buckling behaviour. Due to its wide application and efficiency, the corotational formulation was chosen to describe large displacements. The Newton-Raphson method was used at the global level to achieve equilibrium during each incremental load step. However, when problems of snap through or snap back are encountered, the arc length method was used.

3. COROTATIONAL FORMULATION

The corotational theory [[17], [20]] for two-dimensional beam-column elements is summarized in this section. The corotational approach is also a total Lagrangian formulation, but the idea is to decompose element's motion into a rigid body and pure deformational parts. During the rigid body motion, a local coordinate system, fixed to the element, moves and rotates with it. The deformational part is measured in this local system. This method has been extensively applied in nonlinear static analysis.
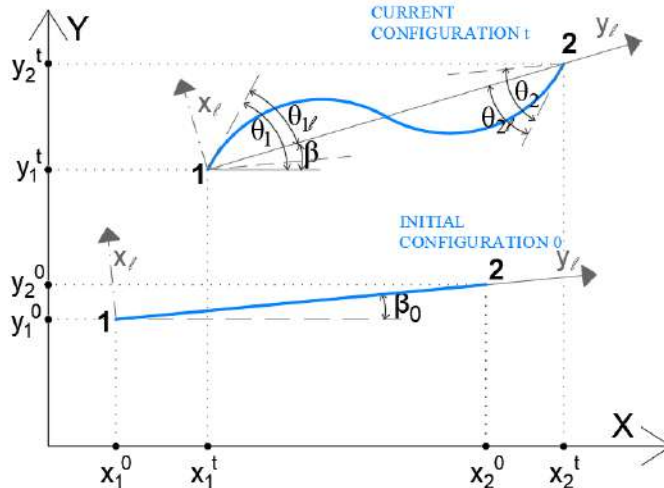

Figure 1 – Initial and current configuration

After the discretization of the beam to finite elements, each element is defined with two nodes and has three degrees of freedom. The rotational local coordinate system is fixed to the beam (Figure 1 – Initial and current configurationFigure 1) and moves like a rigid body relative to the global coordinate system. The following text will mark the local coordinate system with the index l.

From the global coordinates of the initial configuration and global displacements, it is possible further to calculate the global coordinates of the current configuration. Based on the calculated global coordinates, the beam lengths in both configurations are obtained, from which it is further possible to calculate the axial displacement of the element.

$$u_l = \frac{l - l_0^2}{l + l_0}$$

From axial displacement, the connection between global displacements and local deformations is obtained.

Due to the rotation of the corotational coordinate system, it is necessary to find the angle of rotation of the local coordinate system about the global coordinate system. The rotation angle for the current configuration is denoted by β, and for the initial configuration β_0. The sine and cosine of the angles β and β_0 can be obtained from the global coordinates based on which it is possible to calculate the angle β and β_0.

$$\beta = tan^{-1}\left(\frac{(y_2^0 + w_2) - (y_1^0 + w_1)}{(x_2^0 + u_2) - (x_1^0 + u_1)}\right), \qquad \beta_0 = tan^{-1}\left(\frac{y_2^0 - y_1^0}{x_2^0 - x_1^0}\right)$$

Under load, the beam rotates, translates, and has local flexion deformations. Global node rotations are denoted by θ_1 and θ_2. Global rotations are calculated from the global stiffness matrix and measured from a line parallel to the initial configuration (Figure 1). Local node rotations are marked as θ_{1l} and θ_{2l} and are calculated as follows:

$$\theta_{1l} = tan^{-1}\left(\frac{cos\,\beta * sin\,\beta_1 - sin\,\beta * cos\,\beta_1}{cos\,\beta * cos\,\beta_1 + sin\,\beta * sin\,\beta_1}\right), \qquad where \;\; \beta_1 = \theta_1 + \beta_0$$

$$\theta_{2l} = tan^{-1}\left(\frac{cos\,\beta * sin\,\beta_2 - sin\,\beta * cos\,\beta_2}{cos\,\beta * cos\,\beta_2 + sin\,\beta * sin\,\beta_2}\right), \qquad where \;\; \beta_2 = \theta_2 + \beta_0$$

The nonlinear formulation of the tangent stiffness matrix can take the occurrence of large displacements. An accurate stiffness matrix is a key to solving nonlinear structural problems using Newton's method, which requires a calculation of the tangential stiffness matrix for each incremental load step. In the incremental, iterative procedure, the balance of external and internal forces is achieved by the Newton-Raspson iterative procedure. The resultant of the tangent stiffness matrix is obtained by the following expression:

$$K = K_1 + K_2 = B^T * C_l * B + \frac{N}{l}zz^T + \frac{\overline{M_1} + \overline{M_2}}{l^2}(rz^T + zr^T)$$

Where:

$$B = \begin{bmatrix} -cos\,\beta & -sin\,\beta & 0 & cos\,\beta & sin\,\beta & 0 \\ -sin\,\beta/l & cos\,\beta/l & 1 & sin\,\beta/l & -cos\,\beta/l & 0 \\ -sin\,\beta/l & cos\,\beta/l & 0 & sin\,\beta/l & -cos\,\beta/l & 1 \end{bmatrix}$$

$$C_l = \begin{bmatrix} \dfrac{EA}{l_0} & 0 & 0 \\ 0 & \dfrac{4EA}{l_0} & \dfrac{2EA}{l_0} \\ 0 & \dfrac{2EA}{l_0} & \dfrac{4EA}{l_0} \end{bmatrix}, \qquad r = \begin{bmatrix} -\cos\beta \\ -\sin\beta \\ 0 \\ \cos\beta \\ \sin\beta \\ 0 \end{bmatrix}, \qquad z = \begin{bmatrix} \sin\beta \\ -\cos\beta \\ 0 \\ -\sin\beta \\ \cos\beta \\ 0 \end{bmatrix}$$

4. SOFTWARE IMPLEMENTATION

The corotational formulation for large displacement analysis is implemented in the academic software Matrix3D. A detailed implementation algorithm with a theoretical background of the applied Newton Rapson method is presented below.

4.1. NEWTON-RAPHSON METHOD

The Newton-Raphson method is an incremental, iterative method. It performs iterations within a single incremental step to ensure convergence, which is expressed through the equilibrium of external forces with the resisting forces. The equilibrium is achieved by correcting the non-equilibrium of the forces.

When solving a linear system, the solution is simple using the next equation:

$$[K] * \{q\} = \{F\}$$

where:
$[K]$ is the stiffness matrix,
$\{u\}$ is the vector of unknown degrees of freedom,
$\{F\}$ is the vector of applied loads

If the coefficient matrix [K] is itself a function of the unknown degrees of freedom, then the above equation is nonlinear. To solve nonlinear equations, the Newton-Raphson method is commonly employed. In this method, the total load is applied to the structure in each iteration, and the displacement is computed using an approximate but constant stiffness value. Since an approximate value of stiffness is used in each iteration, equilibrium conditions may not be satisfied. Hence at the end of each iteration, the part of the total load that is not balanced is computed and used in the next iteration to calculate the additional displacement increment. The goal is to increase the displacement until the applied force is balanced. The iterative procedure is continued until the equilibrium equations are satisfied to some tolerable degree. The Newton-Raphson method can be written as [21]:

$$[K_i^T] * \{\Delta q_i\} = \{F\} - \{F_i^{nr}\}$$

where:
$\{F_i^{nr}\}$ is the vector of restoring loads corresponding to the element internal load

Both $\{F_i^{nr}\}$ and K_i^T are evaluated based on the values given by $\{q_i\}$. The right-hand side of the equation is the residual or out-of-balance load vector, in other words, the amount of which the system is out of equilibrium.

The solution for one load increment is shown in Figure 2 (left), and for several load increments is shown in Figure 2 (right). Usually more than one Newton-Raphson iteration is needed to obtain a converged solution.
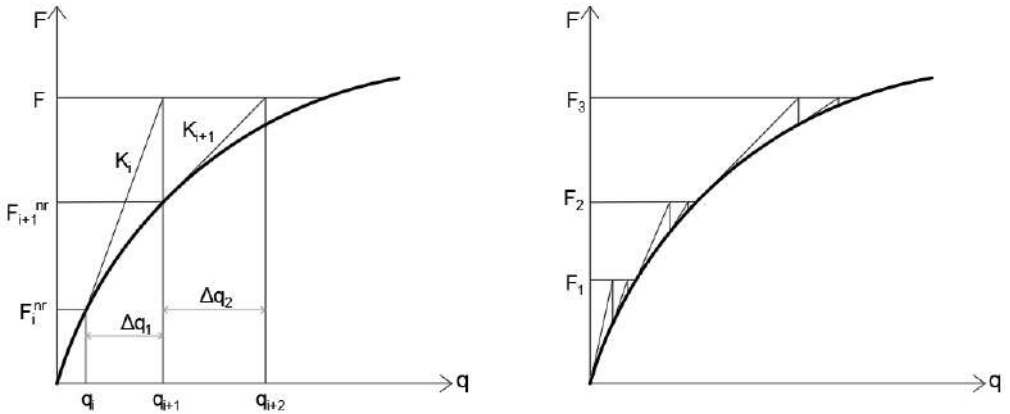

Figure 2 – Newton-Raphson graphic solution

The algorithm of the Newton-Raphson procedure is shown in Figure 3. Where $\{q_0\}$ is usually the converged solution from the previous time step and on the first-time step, $\{q_0\} = \{0\}$.
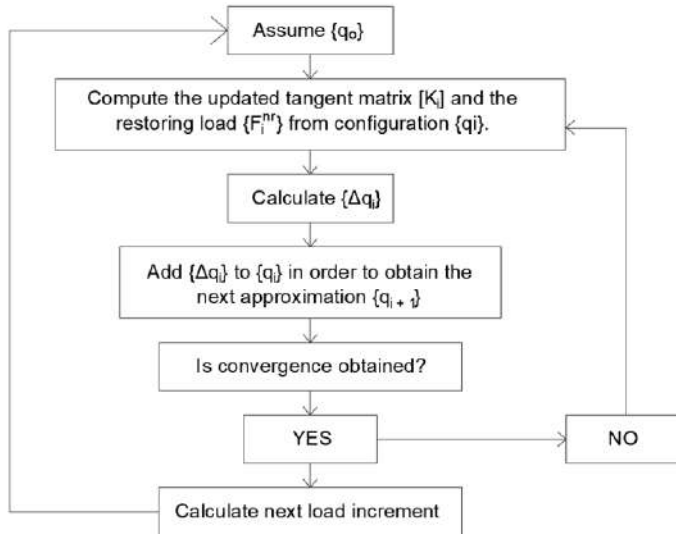

Figure 3 – Newton-Raphson algorithm

The solution obtained at the end of the iteration process would correspond to the load level $\{F\}$. The final converged solution would be in equilibrium, such that the restoring load vector (computed from the current stress state) would equal to the applied load vector $\{F\}$ (or at least to within some tolerance).

4.2. COROTATIONAL ANALYSIS ALGORITHM

The following is an algorithm for performing a 2D corotational beam analysis. The corotational analysis is an implicit formulation which uses Newton-Raphson iterations at the global level to achieve equilibrium during each incremental load step. If there is a snap back or snap through, more sophisticated methods must be used, such as the arc length method. Material nonlinearities are not presently included in the algorithm. A program implementing this algorithm has been written in MATLAB and implemented in the academic software Matrix3D.
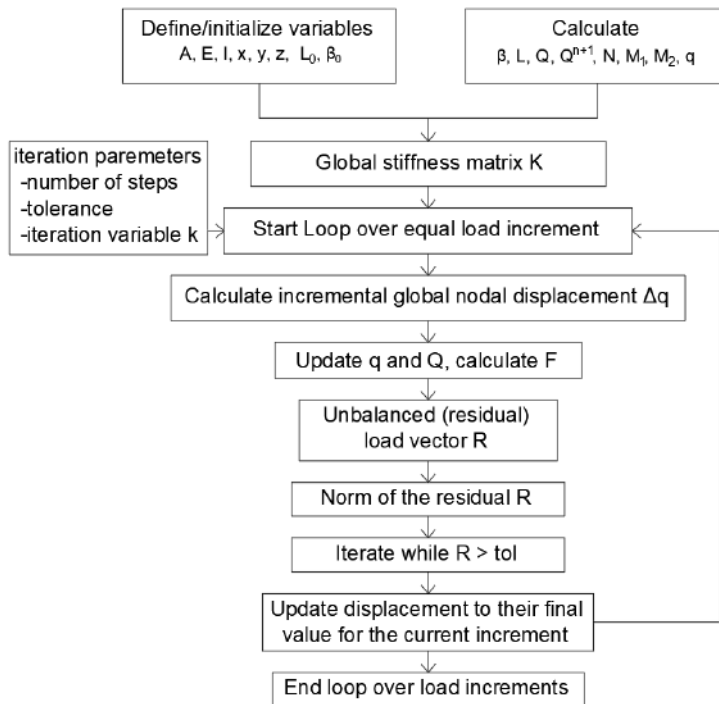

Figure 4 – Corotational analysis algorithm

Figure 4 presents the algorithm of corotational analysis where:
- x, y and z are nodal coordinates in the undeformed configuration,
- Q is the total vector of external global nodal forces,
- Q^{n+1} is the current vector of external global nodal forces,
- F is the storage vector of local forces (N, M_1 and M_2),
- q is the vector of global nodal displacements

5. NUMERICAL EXAMPLES

The corotational formulation is implemented in four examples based on well-documented benchmark problems in the literature, featuring highly nonlinear responses. The software SAP2000 [22] has been selected for validation and comparison purposes. This software uses The

Updated Lagrangian formulation to calculate large displacements. The following table shows the characteristics of the example problems.

Table 1 – Example problems description

Name	Cantilever beam with an end point load	Cantilever beam with an end moment	Toggle frame
Properties	L=0.254m A=26m^2 I=55.49cm^2 E=6.89x10^5 kN/m^2	L=0.254m A=26m^2 I=55.49cm^2 E=6.89x10^5 kN/m^2	L=6m A=900 cm2 b=30cm h=30cm E=200 GPa

5.1. CANTILEVER BEAM WITH AN END POINT LOAD

The first problem to be considered is a cantilever beam subjected to a concentrated load at the free end [7]–[10], [12]–[14], [23], as shown in Figure 5. In this problem, seven elements are used to model the beam. A special feature of this problem is that as the external force increases, the nonlinear solution deviates considerably from the linear branch because extreme rotations of the cross-sections gradually activate increased axial resistance. The results obtained from this study are compared with the solutions obtained by the software SAP2000 [22]. It can be seen from the comparison that a good agreement between the two software is obtained.
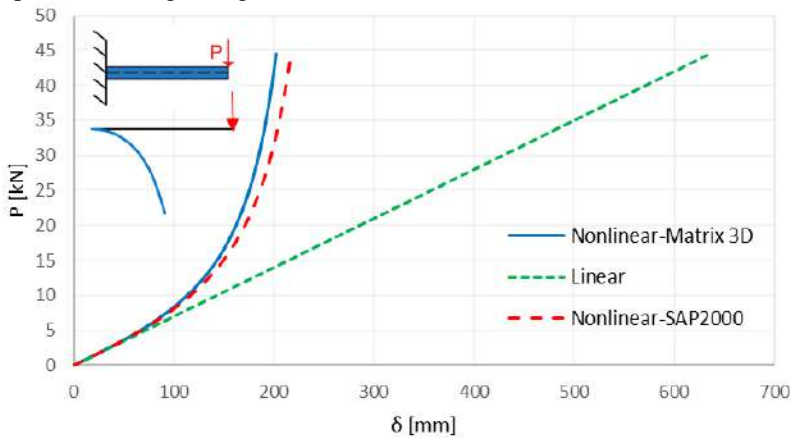

Figure 5 – Cantilever beam with an end point load

5.2. CANTILEVER BEAM WITH AN END POINT LOAD

In this example, the same cantilever as in the previous example is loaded with a concentrated bending moment at the free edge. This structure is also known as the curling beam because of its deformation. Many researchers have used this problem for testing nonlinear beam elements [8], [9], [12]–[14], [19], [23] since the analytical solutions for the problem exist. The results obtained from this study are compared with the solutions obtained by the software SAP2000 [22]. There is a good match of the results for smaller values of the moment, while for larger values, certain deviations are observed.
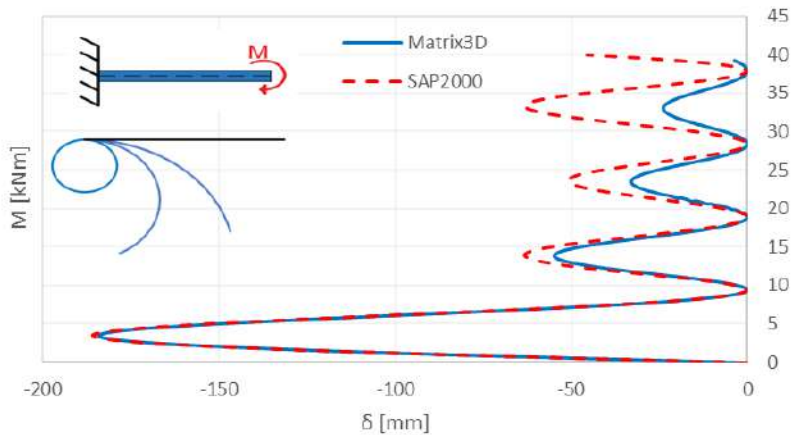
Figure 6 – Cantilever beam with an end moment

5.3. WILLIAMS' TOGGLE FRAME

This problem is considered a good benchmark for testing new nonlinear beam elements, and it has been investigated by many researchers [8], [9], [13], [14], [23]. It is obvious that the load-displacement diagram of this frame includes a snap-through part (Figure 7). The obtained results are compared with the solutions computed by the software SAP2000 [22]. Figure 7 shows a good match between the two software with minor deviations.
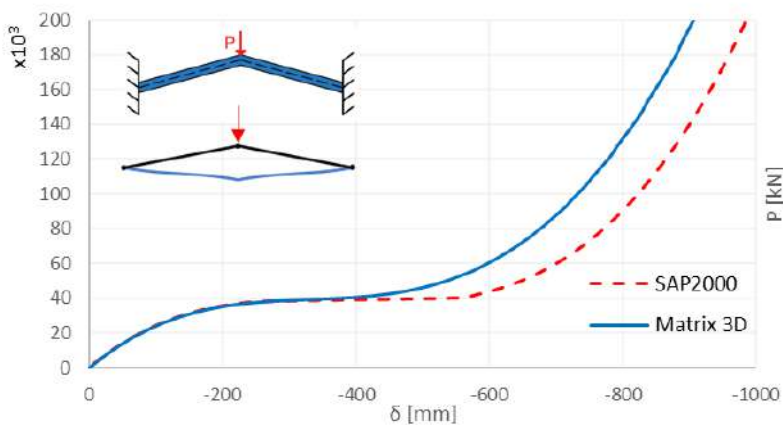

Figure 7 – Williams's toggle frame

5.4. SINGLE-STORY GABLED FRAME

The single-story gabled frame with geometry and loading representative of certain types of industrial structures is shown in **Error! Reference source not found.** [24]. The beams consist of W18x106 profiles and columns of W12x106 profiles. The P-delta analysis and the corotational

analysis of large displacements were performed on this frame to perceive the differences between these two analyses.
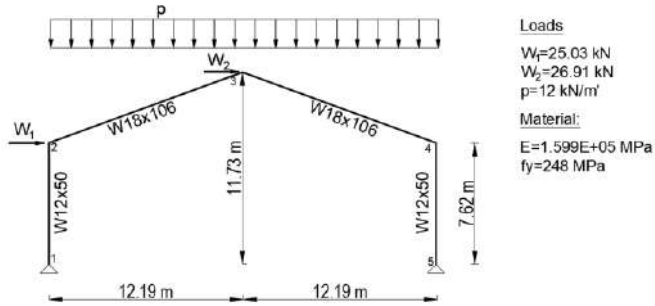

Figure 8 – Description of single-story gabled frame

Four different analyses were performed on this frame, and load-horizontal displacement responses for joint 2 and joint 3 (Figure 8) were compared. In Figure 9, the blue line represents the analysis of large displacement in software SAP2000, and the orange, grey, and yellow lines represent analysis in software Matrix 3D (linear, P-delta and corotational analysis, respectively).
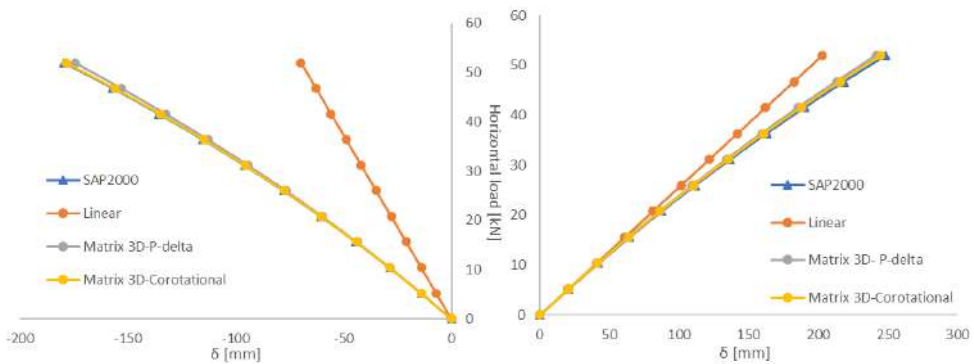

Figure 9 – Load horizontal displacement responses of joint 2 (left) and joint 3 (right)

At both node 2 and node 3, a complete coincidence of the large displacement analysis in the software SAP2000 and the large displacement analysis in the software Matrix 3D is observed. The obtained results also coincide with the benchmark [24]. In [25] it was shown that for low to medium axial load levels, the P-Delta analysis will provide accurate results, because second order effects are minimal, but for high levels the results may be very inaccurate.

6. CONCLUSIONS

The main objective of this research was to provide an efficient finite beam formulation for the nonlinear analysis of flexible beam structures in the software Matrix 3D. The software SAP2000 was used to validate the results, where a good match of the results has been proven.

Though the p-delta and corotational methods both model second-order effects, their scope is different. The p-delta method works best for models where the displaced shape is similar to the

undeformed shape. The corotational method can model large displacements, snap back and snap trought problems, throught it is more computationally intensive. Therefore, the differences in response between the structures incorporating the two methods depend on the performance level considered.

In the stability design, great attention was drawn to the corotational formulation, as it provides the possibility of including warping effects in the analysis. Therefore, the work done in this paper can also be extended to include warping.

REFERENCES

[1] Nožica T, Jovanović Đ, Žarković D Software implementation of section class and resistance calculation for general loading case, Gradjevinski materijali i konstrukcije, 64, (3), 2021, 159–164

[2] Nožica T, Jovanović Đ Žarković D Software implementation of stability design of steel frames, Indis 2021.

[3] Jovanović Đ, Žarković D, Vukobratović V, Brujić Z Hysteresis model for beam-to-column connections of steel storage racks, Thin-Walled Structures, 142, 2019, 189–204

[4] Jovanović Đ, Žarković D, Brujić Z, Lađinović Đ Fiber beam-column element implementation in academic CAD software Matrix 3D, Gradjevinski materijali i konstrukcije, 60, no. 2, 2017, 57–77

[5] Le T. N, Battini J. M, Hjiaj M A consistent 3D corotational beam element for nonlinear dynamic analysis of flexible structures," Computer Methods in Applied Mechanics and Engineering, 269, 2014, 538–565

[6] Le T. N Corotational formulation for nonlinear dynamic analysis of flexible beam structures, Stockholm, 2012.

[7] Le T. N, Battini J. M, Hjiaj M Efficient formulation for dynamics of corotational 2D beams, Computational Mechanics, 48, no. 2, 2011, 153–161

[8] Loui L. Yaw, 2D Corotational Beam Formulation, Walla Walla University, 2009.

[9] Nanakorn P, Vu L. N A 2D field-consistent beam element for large displacement analysis using the total Lagrangian formulation, Finite Elements in Analysis and Design, 42, 2006, 1240–1247, 14–15

[10] Elkaranshawy H. A, H. Elerian A. A, Hussien W. I A Corotational Formulation Based on Hamilton's Principle for Geometrically Nonlinear Thin and Thick Planar Beams and Frames, Mathematical Problems in Engineering, 2018.

[11] Bathet K.J, Bolourchit S Large displacement analysis of three-dimensional beam structures, Department of Mehanical Engineering, Massachussetts Institute of Technology, Massachussetts, U.S.A. 1979.

[12] Aashish A Corotational formulation for beams, University of California, Berkeley, 2015.

[13] Magalhães De Souza R Force-based Finite Element for Large Displacement Inelastic Analysis of Frames, PhD Thesis, University of California, Berkeley 2000.

[14] Steen K Non-linear Modelling and Analysis of Solids and Structures, Cambridge University Press, 2009.

[15] Battini J.M, Pacoste C Co-rotational beam elements with warping effects in instability problems, Computer methods in applied mechanics and engineering, 191, 2002, 1755-1789

[16] Alsafadie R, Hjiaj M, Somja H, Battini J. M A comparative study of displacement and mixed-based corotational finite element formulations for elasto-plastic three-dimensional beam analysis, Engineering Computations (Swansea, Wales), 28, no. 7, 2011, 939–982

[17] Crisfield M. A A consistent co-rotational formulation for non-linear, three-dimensional, beam-elements, Computer methods in applied mechanics and engineering, 81, 1990, 131-150

[18] Felippa C. A, Haugen B A unified formulation of small-strain corotational finite elements: I. Theory, Computer Methods in Applied Mechanics and Engineering, 194, no. 21-24 SPEC. ISS., 2005, 2285–2335

[19] Hsiao K.M, Horng H.J, Chen Y.R A corotational procedure that handles large rotations of spatial beam structures, Computers and Structures, 27, 6, 1987, 769-781

[20] Crisfield M. A, Non-linear Finite Element Analysis of Solids and Structures, 1, 2000.

[21] Bathe K. J, Finite Element Procedures, Prentice-hall Inc., 2006.

[22] SAP2000 Integrated Software for Structural Analysis and Design, Computers and Structures Inc., Berkeley, California.

[23] Limkatanyu S, Prachasaree W, Kaewkulchai G, Spacone V Unification of mixed euler-bernoulli-von karman planar frame model and corotational approach, Mechanics Based Design of Structures and Machines, 42, no. 4, 2014, 419–441

[24] Ziemian C. W, Ziemian R. D Efficient geometric nonlinear elastic analysis for design of steel structures: Benchmark studies, Journal of Constructional Steel Research, 186, 2021,

[25] Hardyniec A An investigation of the behavior of structural system with modeling uncertainties, PhD Thesis, Virginia Polytechnic Institute, 2014

Vladimir Živaljević[1], *Igor Džolev*[2], *Milan Blagojević*[3], *Andrija Rašeta*[4], *Nikola Rajić*[5]

REGISTROVANJE DILATACIJA RAVNIH I UGAONIH EPRUVETA METODOM KORELACIJE DIGITALNIH SLIKA

Rezime:

Proces proizvodnje hladno oblikovanih čeličnih elemenata savijanjem ravnih tabli lima na presi značajno utiče na karakteristike materijala u zonama uglova elementa. U ovom radu je opisano ispitivanje mehaničkih karakteristika čelika na ravnim i ugaonim epruvetama. Merenje deformacije je izvršeno beskontaktnom optičkom metodom korelacije digitalnih slika. Pre postupka merenja, svaki uzorak je bio prekriven prahom bele boje i nasumičnim šablonom crnih tačaka dobijenih prskanjem. Rezultati ispitivanja prikazani su u vidu polja dilatacije epruveta u funkciji opterećenja, kao i u vidu dijagrama napon-deformacija.

Ključne reči: HOP elementi, ispitivanje zatezanjem, korelacija digitalnih slika

STRAIN MEASUREMENT OF FLAT AND CORNER COUPONS USING DIGITAL IMAGE CORRELATION

Summary:

The manufacturing process of cold-formed steel members using the press braking method significantly influences the material properties of the member corner zones. This paper describes the measurement of the steel material properties on flat and corner coupons. The strain measurement was performed by the non-contact optical method of digital image correlation. Prior to the measuring process, each specimen was covered with a white powder and random black dots obtained by spraying. Results of the material testing are presented in form of strain fields of the coupons in relation to the applied load, and in form of stress-strain diagrams.

Key words: cold-formed steel, tensile coupon test, digital image correlation

---

[1] *Teachnig assistant, MSc CE, Faculty of Technical Sciences, University of Novi Sad, Serbia, zivaljevic.vladimir@uns.ac.rs*
[2] *Assistant professor, PhD CE, Faculty of Technical Sciences, University of Novi Sad, Serbia, idzolev@uns.ac.rs*
[3] *Teaching assistant, MSc ME, Faculty of Technical Sciences, University of Priština, Kosovska Mitrovica, Serbia, milan.blagojevic@pr.ac.rs*
[4] *Associate professor, PhD CE, Faculty of Technical Sciences, University of Novi Sad, Serbia, araseta@uns.ac.rs*
[5] *Teachnig assistant, MSc CE, Faculty of Technical Sciences, University of Novi Sad, Serbia, rajic.nikola@uns.ac.rs*

1. INTRODUCTION

Fast manufacturing process is one of the key advantages that induced the increasing trend of utilization of cold-formed steel (CFS) structures in structural engineering. CFS members are moulded from steel material by one of two methods: press-braking or cold rolling. In the cold-rolling method the profile cross-section is obtained by gradual deformation of steel sheet through a series of rollers, while in press-braking method the profile is produced by initiating separate bends along the length of sheet [1]. Either way, induced plastic deformations affect material behaviour of the completed CFS member in terms of development of residual stresses, ductility reduction and yield strength increase [2].

According to both EN 1993-1-3 [3] and AISI S100-2016 [4], the yield strength increase in corner zones of CFS profiles may be taken into account as a uniform increase of yield strength by introducing an average yield strength. In EN 1993-1-3 the average yield strength may be determined from the results of full size tests or, under certain circumstances, calculated based on a number of 90° bends of the cross-section. Similarly, in AISI S100-2016, average yield strength may be determined on the basis of full section tensile tests, stub column tests or the equation given in the design code.

The influence of cold-forming effect in corner zones of CFS elements was in most of the previous research carried out as a part of the great-scale experiments [2,5–7]. More detailed investigation of this effect was addressed in research carried out by A.T. Tran et al. [1] and J. Ma et al. [8]. In these research, the strain was measured in a conventional manner, using an extensometer. During the previous decade, a novel non-contact optical technique – digital image correlation (DIC), found its application in strain measurement [9,10]. The advantage of this method compared to the utilization of an extensometer is that it registers not only the strain at a certain length, but also the entire deformation field of the specimen as well as the field of actual displacement, although only on the surface of the specimen.

In this paper, tensile tests of flat (FC) and corner (CC) coupon specimens with the strain measurement using DIC are presented.

2. EXPERIMENTAL INVESTIGATION

2.1. DESCRIPTION OF SPECIMENS

Material tensile tests were performed on CFS flat and corner coupons that were cut from two different members of the same nominal thickness of the cross-section walls. Water jet technique was used to cut the coupon specimens to avoid disorders in material structure that would otherwise occur in cutting zones due to thermal effects caused by mechanical cutting. Two flat coupons from the web and two coupons from corner zones were cut from each member. Geometry of coupons was defined according to [11]. The nominal geometry of FC and CC coupons is shown in Figure 1, while a list of tested specimens is given in Table 1.
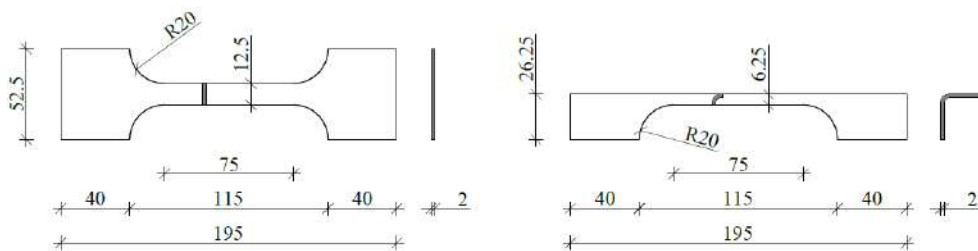
Figure 1 – The nominal geometry of flat (left) and corner (right) coupons

Table 1 – List of tested coupon specimens

Specimen no.	Label	Dimensions [mm]	Cut from member
1.	FC-1	2.10 x 12.70	C100
2.	FC-2	2.01 x 12.60	
3.	CC-1	2.00 x 10.67	
4.	CC-2	2.03 x 11.50	
5.	FC-3	2.00 x 12.76	C150
6.	FC-4	1.97 x 12.77	
7.	CC-3	1.97 x 11.90	
8.	CC-4	1.94 x 11.00	

2.2. DIGITAL IMAGE CORRELATION

DIC is a method based on deformation measurement by overlapping images. Throughout the deformation process of the tested specimen, a series of images is needed to be recorded. The deformation state during load application is determined by observation of the corresponding pixels in successive images. Since this problem does not have a unique solution, it is necessary to observe the close surroundings of the pixel (facet). In order for pixel tracking to be possible, an appropriate preparation of specimens in terms of applying a pattern of white background and randomly arranged black dots is essential. Specimens before and after preparation are shown in Figure 2.

Figure 2 – Coupon specimens before (left) and after (right) preparation

2.3. CONTROL TEST

Since the testing machine records only a change in length between the holding grips, the strain cannot be obtained from these measurements. In order to exclude a deformation of gripped ends and take into consideration only a deformation that occurs at a parallel length of a specimen, it is necessary to use devices for length change measuring (extensometers). Common original gauge lengths for these devices are 25, 50 and 100 mm. The problem which may occur when using extensometers can arise if a necking occurs outside of an original gauge length, therefore, total plastic deformation could remain unknown. This issue could be avoided if DIC method is to be applied, forasmuch as the deformation field of the entire specimen would be determined.

Prior to the experimental testing, control test on one coupon specimen was performed with the aim to examine the reliability of this setup. During the control test, the deformation was measured using both extensometer and DIC method. The extensometer with the original gauge length of 50 mm was centred at the parallel length of the specimen. The deformation change over the same length was later computed using DIC method. Series of images was obtained from a high-definition video recording with a frame rate of 30 frames per second (fps). In subsequent video processing, every thirtieth frame was isolated from the recording. Therefore, the analysis was carried out for a series of images with an interval of exactly 1 s. The control test setup and result comparison are shown in Figure 3.
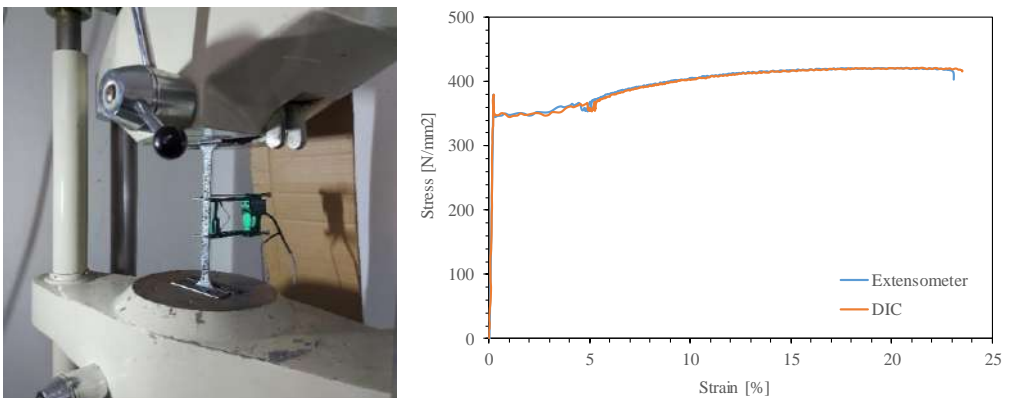

Figure 3 – The test setup of the control specimen (left) and comparison of results (right)

Figure 3 shows a satisfactory matching of the two stress-strain curves, one based on the measurement of extensometer and other on the DIC processing, hence, the DIC method proved to be suitable for this experimental testing.

2.4. TEST SETUP

After the test setup reliability was confirmed, the tensile test of the remaining eight specimens was performed, in which the deformation was registered only by the means of DIC. Test setup of flat and corner coupon specimens is depicted in Figure 4. Before the actual tension of the corner coupons, their grip ends were straightened at the length of 20 mm from the end.
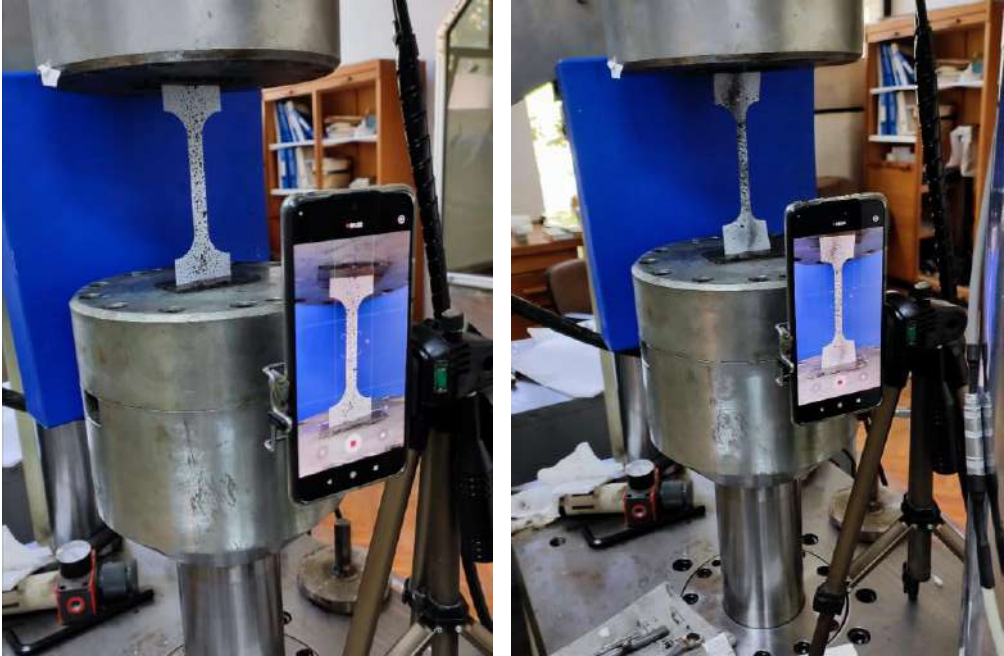
Figure 4 – Test setup of the flat (left) and corner (right) coupons

Test was performed in accordance with [11] on a hydraulic test machine Schenck Hydropuls PSB 250 with a capacity of 250 kN. Recorded output parameters were force, both absolute and normalised displacement of a holding grip, and stress calculated on the basis of defined parameters of coupon specimens.

3. RESULTS OF EXPERIMENTAL TESTING

After the coupon testing was completed, results were analysed. The same method of video processing was employed as with the control test specimen. The DIC processing analysis was carried out using the GOM Correlate software. Several stages of deformation of characteristic flat and corner coupon are shown in Figures 5 and 6.

For all FC specimens, neck forming was characteristic for the zone around the middle of the parallel length. However, necking of CC specimens manifested in a random behaviour. Two CC specimens displayed neck forming at mid-zone, while on the other two, necking appeared at parallel length ends.

The obtained stress-strain curves for both FC and CC specimens are shown in Figures 7 and 8, respectively.

FC specimens demonstrated higher ductile capacity as expected, although their yield strength was lower in comparison to the CC specimens. The yield and ultimate stresses of FC-2, FC-3 and FC-4 were around the values of 300 N/mm^2 and 405 N/mm^2, whereas yield and ultimate stresses of the FC-1 amounted approximately 300 N/mm^2 and 385 N/mm^2, respectively. The highest strain for all four FC specimens was roughly 34%. On the contrary, the values of yield and ultimate stresses were more scattered when it comes to CC specimens. For corner zones of

CFS profiles, it is difficult to estimate the exact value of yield stress, since it is not clearly perceivable, as in cases of FCs. Here, the ultimate stress varied from 405 to 440 N/mm^2, while the highest values of strain were between 10.5 and 14.5%.
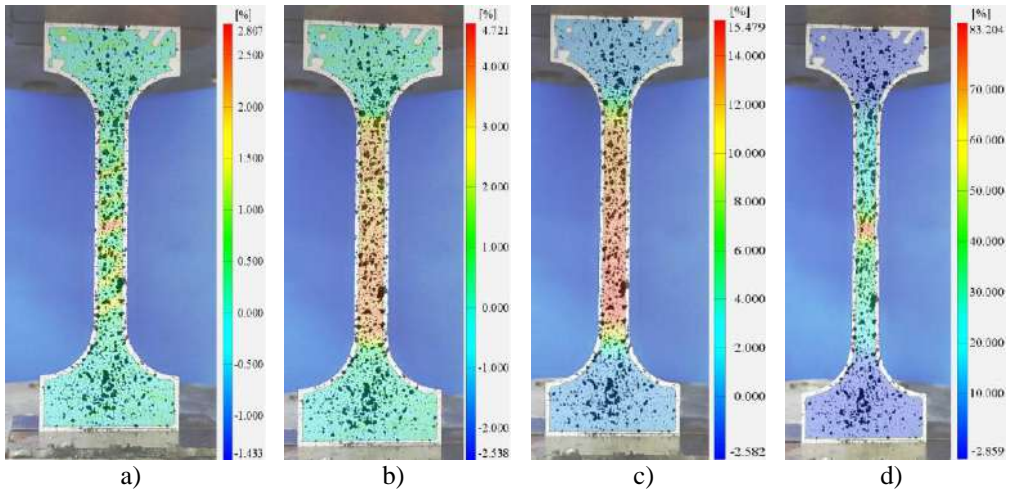

Figure 5 – Strains for flat coupon FC-2 for total displacements of:
a) 0.811 mm, b) 3.332 mm, c) 11.593 mm and d) 23.928 mm
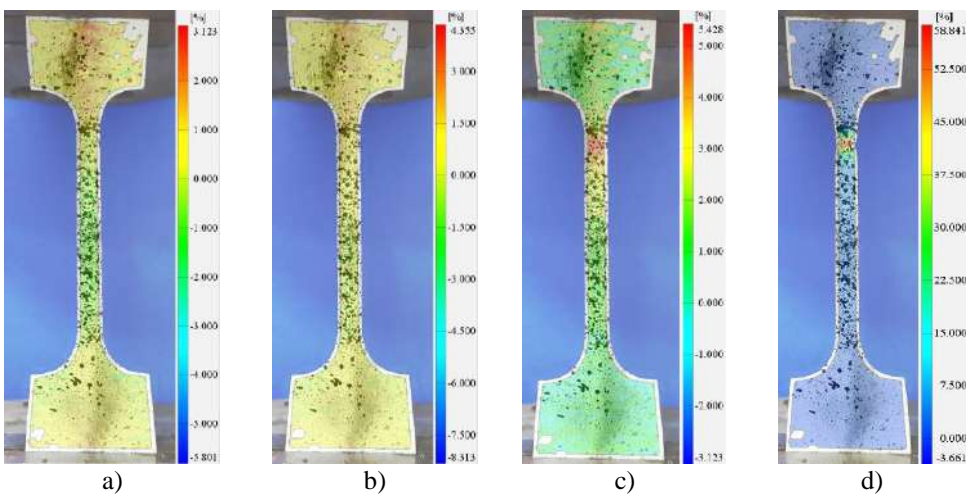

Figure 6 – Strains for corner coupon CC-4 for total displacements of:
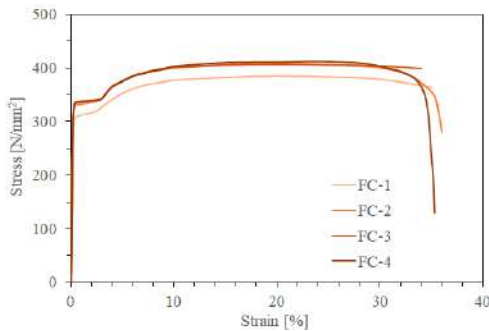*a) 0.789 mm, b) 1.642 mm, c) 3.255 mm and d) 6.078 mm*

Figure 7 – Stress-strain curves for FC
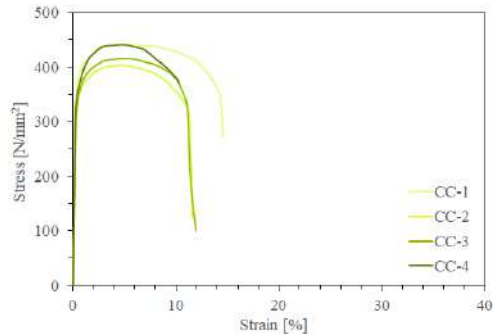specimens

Figure 8 – Stress-strain curves for CC
specimens

4. CONCLUSIONS

The tensile tests of the flat and corner coupon specimens cut from CFS members were performed using the digital image correlation as a method for strain measurement. This non-contact optical technique proved to be convenient for this purpose, since the true strain can be measured directly. Control testing on one control specimen was performed before the actual tests took place, in order to prove the reliability of the DIC method. Afterwards, the stress-strain behaviour of four FCs and four CCs was examined.

Although the DIC method provides a wide range of capabilities in respect of data manipulation, in this research only the length changes between two points from each side of the coupon neck, at a total distance of 50 mm, was controlled. A conclusion may be derived that the DIC method is suitable for deformation measurement, especially in cases of unusual specimen shapes.

REFERENCES

[1] Tran, A.T.; Bernspång, L.; Veljkovic, M.; Rebelo, C.; da Silva, L.S. Influence of Cold-Formed Angle on High Strength Steel Material Properties. *Adv. Steel Constr.* **2019**, *15*, 316–322, doi:10.18057/IJASC.2019.15.4.2.

[2] Afshan, S.; Rossi, B.; Gardner, L. Strength Enhancements in Cold-Formed Structural Sections — Part I: Material Testing. *J. Constr. Steel Res.* **2013**, *83*, 177–188, doi:10.1016/j.jcsr.2012.12.008.

[3] CEN, E.C. for S. *EN 1993-1-3: Eurocode 3: Design of Steel Structures - Part 1-3: General Rules - Supplementary Rules for Cold-Formed Members and Sheeting*; Brussels, Belgium, 2006;

[4] American Iron and Steel Institute *AISI S100-2016: North American Specification for the*

Design of Cold-Formed Steel Structural Members; American Iron and Steel Institute: Washington, DC, USA, 2016;

[5] Tran, A.T.; Veljkovic, M.; Rebelo, C.; Da Silva, L.S. Resistance of Cold-Formed High Strength Steel Circular and Polygonal Sections - Part 1: Experimental Investigations. *J. Constr. Steel Res.* **2016**, *120*, 245–257, doi:10.1016/j.jcsr.2015.10.014.

[6] Chen, M.-T.; Young, B. Tensile Tests of Cold-Formed Stainless Steel Tubes. *J. Struct. Eng.* **2020**, *146*, 1–13, doi:10.1061/(asce)st.1943-541x.0002738.

[7] Chen, B.; Roy, K.; Uzzaman, A.; Raftery, G.M.; Lim, J.B.P. Axial Strength of Back-to-Back Cold-Formed Steel Channels with Edge-Stiffened Holes, Un-Stiffened Holes and Plain Webs. *J. Constr. Steel Res.* **2020**, *174*, 106313, doi:10.1016/j.jcsr.2020.106313.

[8] Ma, J.L.; Chan, T.M.; Young, B. Material Properties and Residual Stresses of Cold-Formed High Strength Steel Hollow Sections. *J. Constr. Steel Res.* **2015**, *109*, 152–165, doi:10.1016/j.jcsr.2015.02.006.

[9] Yang, L.; Smith, L.; Gothekar, A.; Chen, X. *Measure Strain Distribution Using Digital Image Correlation (DIC) for Tensile Tests*; 2010;

[10] Quanjin, M.; Rejab, M.R.M.; Halim, Q.; Merzuki, M.N.M.; Darus, M.A.H. Experimental Investigation of the Tensile Test Using Digital Image Correlation (DIC) Method. *Mater. Today Proc.* **2020**, *27*, 757–763, doi:10.1016/j.matpr.2019.12.072.

[11] British Standards Institution *BS EN ISO 6892-1:2016 - Metallic Materials - Tensile Testing - Part 1 : Method of Test at Room Temperature*; London, UK, 2016;

Marija Docevska[1], *Goran Markovski*[2]

UTICAJ DINAMIKE IZVOĐENJA MOSTOVA NA PONAŠANJE PRETHODNO NAPREGNUTIH KOMPOZITNIH NOSAČA

Rezime:

Kompozitni betonski nosači sastavljeni od prefabrikovanih prethodno napregnutih greda i monolitnu betonsku ploču su često primenjivani kod mostova. Dva kompozitna dela betoniraju se u različito vreme, zbog čega često imaju i nejednake mehaničke i reološke karakteristike. Ovo drugo je odgovorno za redistribuciju napona unutar kompozitnog preseka. Sa ciljem da se istraži ovaj uticaj, izrađena je numerička studija na realnim kompozitnim gredama kontinualnog mosta. Analizirane su četiri razlike u starosti betona kompozitnih delova: 30, 90, 365 i 730 dana. Rezultati ukazuju na to da razlike u skupljanju i tečenju pojedinih delova mogu značajno uticati na redistribuciju napona kao i na konačne deformacije kompozinih betonskih nosača.

Ključne reči: kompozitni nosači, tečenje, skupljanje, faze izvođenja, redistribucija

INFLUENCE OF THE BRIDGE CONSTRUCTION SCHEDULE ON THE COMPOSITE PRESTRESSED GIRDERS BEHAVIOUR

Summary:

Composite concrete beams made of prefabricated prestressed element and cast in place reinforced concrete slab are very popular in bridge engineering. The two composite parts are cast at different time and they often have different mechanical and rheological properties. The latter is responsible for stress redistribution within the composite section. To investigate this influence, a numerical study was performed on a real composite beams as a part of a multi-span continuous bridge. Four age differences between the precast girder and the in-situ slab were considered: 30, 90, 365 and 730 days. The results indicate that different creep and shrinkage properties of the concrete parts can significantly affect the stress redistribution, as well as the final deflections of the composite concrete beams.

Key words: composite beams, creep, shrinkage, construction stages, redistribution

---

[1] *M.Sc., Assistant, PhD student at Ruhr University – Bochum (RUB), Ss. Cyril and Methodius University, Faculty of Civil Engineering – Skopje, Bul. Partizanski Odredi 24, 1000, docevska@gf.ukim.edu.mk*

[2] *PhD, Full Professor, Ss. Cyril and Methodius University, Faculty of Civil Engineering – Skopje, Bul. Partizanski Odredi 24, 1000 markovski@gf.ukim.edu.mk*

1. INTRODUCTION

Composite concrete beams become very popular in present-day bridge construction, especially for short- and medium-span bridges [1]. They are usually made of two concrete elements, a precast pretensioned beam and an in-situ deck slab (Fig.1). These two concrete parts are bonded together and form stiff composite bridge deck. Apart from providing a significant increase to the strength and stiffness of the prestressed girder, the in-situ slab can also provide continuity and lateral stability to the precast elements.

However, there are some specific aspects arising from the construction process that should be carefully considered in the design. The two concrete elements that form the composite section are cast at different time and under different conditions. Inevitably, they have different concrete strengths, different moduli of elasticity and different creep and shrinkage properties (Fig.1).
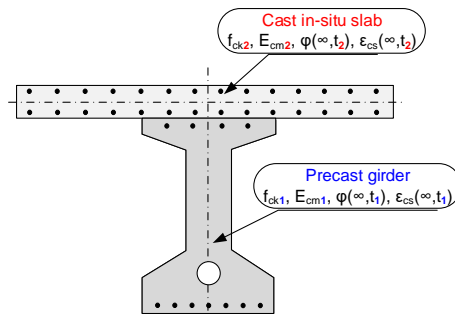

Figure 1 - Typical concrete composite section

The concrete in the precast element is generally of better quality than the concrete in the cast in-situ one. It usually has higher specified target strength and experiences better quality control during construction [2]. Furthermore, the precast part is cast sometime prior the deck slab. With the concrete in the precast element being older and of better quality than the in-situ concrete, a redistribution of stresses within the composite section arises. Certain shrinkage amount of the girder occurs before setting the in-situ slab. Therefore, the subsequent shrinkage of the girder will be less than the shrinkage of the slab. Since the two concrete parts are bonded, the bigger shrinkage in the slab part is restrained by the girder. This internal restrain often results in tensile stresses in the deck slab, redistribution of the girders' stresses and increase in curvature of a section.

At the design stage, the designer has little control over the precast girders' age at which the in-situ slab will be placed. Usually, it is assumed that the age difference between the girder and the slab is within 60 and 90 days. However, there are many cases in practice when this difference is even more pronounced and less cases when it is less pronounced. For instance, in multi-span bridges, the age difference between the slab and the girders placed in the first span sometimes can be significantly large.

2. STRESSES AT STAGES OF LOADING

The history of construction and service stages influences the ultimate and serviceability limit states of composite concrete elements [3]. It is very likely that some intermediate construction

stage can be decisive in the choice of concrete strength class, tendon layout or reinforcement area in the deck slab. Therefore, the construction stages should be carefully treated in the design.

For composite sections, usually the following loading stages need to be considered [2]:

- <u>Transfer of the initial prestress to the precast element</u> – involves calculation of the elastic stresses due to the initial prestress and the self-weight of the precast element (line 1 in Fig.2).
- <u>Period before casting the in-situ slab</u> –requires time analysis to calculate the redistribution of the stresses caused by creep and shrinkage in the precast element (line 2 in Fig.2).
- <u>Casting the in-situ concrete before composite action</u> - requires short-term analysis of the precast element to calculate the instantaneous effects of the superimposed dead load prior to the composite action (line 3 in Fig.2).
- <u>Immediately after the establishment of the composite action</u> - involves short-term analysis of the composite cross section to determine the stresses for all the remaining loads (e.g., superimposed dead loads, live loads etc.) (line 4 in Fig.2).
- <u>Period after the establishment of the composite action:</u> - involves time analysis for the composite cross section until time infinite.
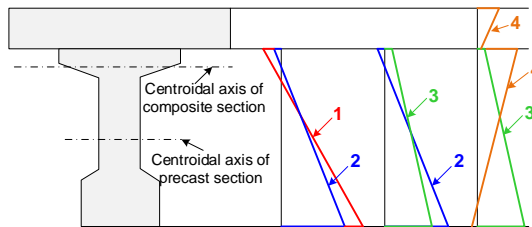

Figure 2 - Concrete stresses at various load stages

3.   ANALYSIS OF COMPOSITE CONCRETE BRIDGE GIRDERS – CASE STUDY

The influence of different age of precast concrete girder and in-situ concrete slab is evaluated through a numerical study on a real example of composite bridge beams. Five-span continuous bridge with composite concrete deck was analysed. This structure is chosen to demonstrate the above-mentioned effect due to the type of its structural system that is sensitive to the effects caused by creep and shrinkage. In addition to this, the age difference between the prestressed girder and the cast in-situ slab was approximately 2 years that is beyond the age difference treated in the design.

In the paper, the analysis was performed for various age differences: 30, 90, 365 and 730 days.

3.1. GENERAL BRIDGE DATA

The subject structure is a five-span continuous bridge (41.89 m + 3 x 42.79 m + 41.89 m) with a composite concrete deck (Fig.3). The superstructure is composed of five precast pretensioned girders (C40/50) continued in a second phase through deck slab reinforcement, cross girders above the piers (C35/45) and cast in-situ concrete slab (C35/45). The characteristic distance between the main girders is 2.20 m (Fig. 3).
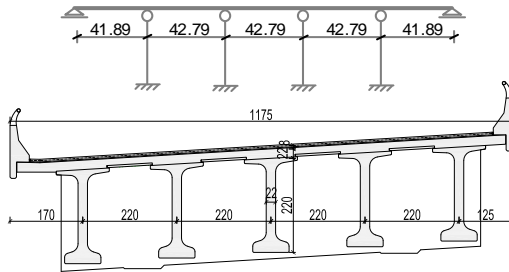
Figure 3 - Structural system and typical cross-section
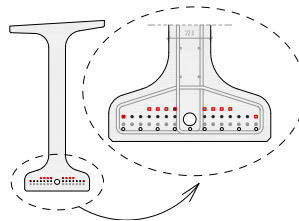
Figure 4 - Prestressing layout

The main girders are pretensioned with 36 straight strands and additionally with one parabolic tendon (1600/1860MPa). The arrangement of the prestressing reinforcement is presented in Fig.4.

3.2. NUMERICAL MODEL

The numerical model, built in FEM software SOFiSTiK, consists of composite girders from two adjacent spans. The model considers the composite action between the precast girder and the in-situ slab, as well as the transformation of the structural system from simple supported to continuous beam. The analysis is done for two phases:
- Phase I: the prestressed girders are acting independently with a structural system simple supported beam (Fig.5 top).
- Phase II: the prestressed girders and the cast in-situ slab are acting compositely with a structural system continuous beam (Fig.5 bottom).

Figure 5 - Phase I (top) and Phase II (bottom)

Construction Stage Manager (CSM) tool in SOFiSTiK was used to simulate the history of construction and service stages of the bridge. The following stages were considered in the analysis (Fig.6):

1. Pretension of 36 strands at $t_1 = 3$ days
2. Self-weight activation of the girders at $t_1 = 3$ days
3. Creep and shrinkage until stressing the parabolic tendon (duration $\Delta t_1 = 11$ days)
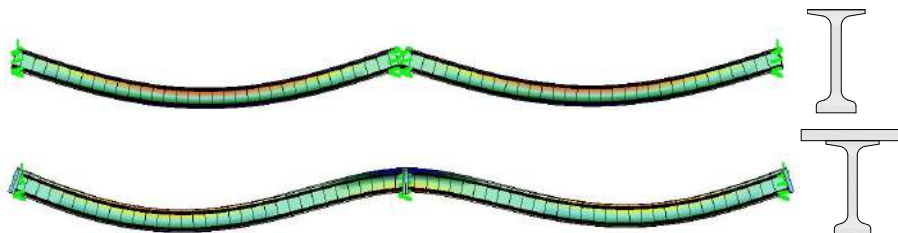4. Prestress of the tendon at $t_2 = 14$ days
5. Creep and shrinkage until casting the in-situ slab (duration $\Delta t_2 = 16/76/351/716$ days)
6. Casting the in-situ slab at $t_3 = 30/90/365/730$ days
7. Hardening of the slab
8. Removing the temporary and placing the final supports
9. Creep and shrinkage until placing the asphalt and other additional loads (duration $\Delta t_3 = 90$ days)
10. Application of additional dead loads at $t_4 = 120/180/455/820$ days
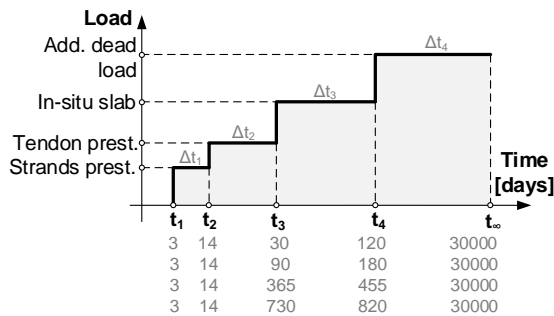11. Creep and shrinkage until the end of service life.

Figure 6 - History of construction stages

In order to calculate the concrete stresses in the stages that require time analysis (stages 3.,5.,9. and 11.), different creep and shrinkage sources were used:
- Real creep and shrinkage strains based on measurements performed on concrete test specimens (provided by the Contractor)
- Available creep and shrinkage models implemented in SOFiSTiK (Eurocode 2 [4], fib Model Code 2010 [5], CEB-FIP Model Code 1990 [6] and Rusch's summation model)

For each concrete age at which immediate change in stresses appeared, different creep curves were developed separately for the girder and the slab:
- Creep coefficient for the precast element when the prestressing of the strands is applied: $\varphi(\infty, t_1) = \boldsymbol{\varphi(\infty, 3)}$;
- Creep coefficient for the precast element when the prestressing of the tendon is applied: $\varphi(\infty, t_2) = \boldsymbol{\varphi(\infty, 14)}$;
- Creep coefficient for the precast element when the in-situ slab is casted: $\varphi(\infty, t_3) = \boldsymbol{\varphi(\infty, 30/90/365/730)}$);
- Creep coefficient for the precast element when superimposed dead loads are applied: $\varphi(\infty, t_4) = \boldsymbol{\varphi(\infty, 120/180/455/820)}$;
- Creep coefficient for the deck slab when the superimposed dead loads are applied: $\varphi(\infty, t_4) = \boldsymbol{\varphi(\infty, 90)}$;

Fig.7 presents the creep and shrinkage curves calculated according to one of the above-mentioned methods and indicates the values necessary for each load step.

On-site measurements of the girders deflections nearly before setting the in-situ slab were on disposal. The measured deflections are result of prestressing forces, self-weight of the girder and creep and shrinkage effects before placing the in-situ slab.

Table 1 contains comparison between the measured and the calculated deflections for the section at the middle of a span.
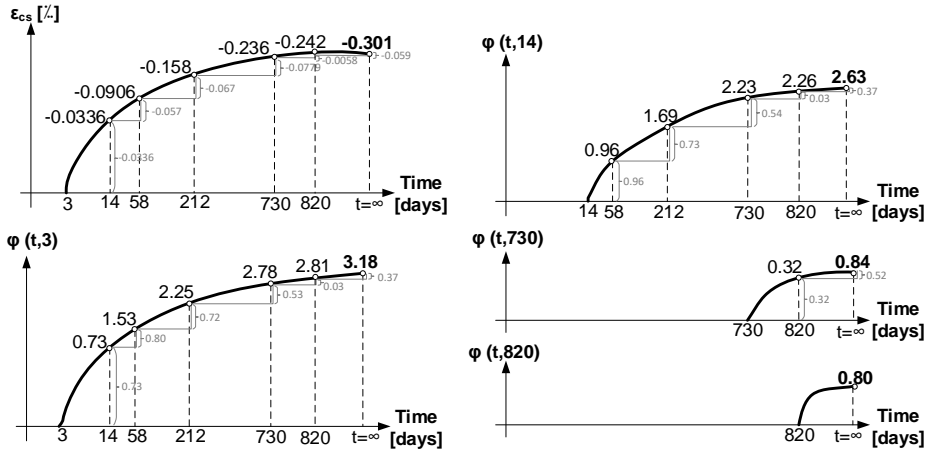
Figure 7 - Creep and shrinkage curves for the prestressed girder (age difference 730 days)

Table 1 - Mid-span deflection of the girders

		Mid-span deflection at t=730 days [mm]
Measured		117.3
Calculated	Real creep and shr.	108.1
	EC2	100.4
	CEB-FIP MC90	107.4
	fib MC10	108.0
	Rusch's method	115.2

The comparison between the measured and the calculated deflections shows relatively good agreement. It suggests that the numerical model is sufficiently accurate to be used for the further analyses.

3.3. RESULTS OF THE ANALYSIS

3.3.1. Stresses

Stresses at different stages of loading were calculated for the varied age differences between the concrete parts (30, 90, 365 and 730 days). An age difference of 90 days was chosen as a reference, since it is usually assumed in the design. Figs. 8 and 9 summarize the calculated stresses in two characteristic cross-sections for the reference age difference. In the presented diagrams, sign"-" corresponds to compression. For the sake of clarity, the stresses are presented

for each subsequent load stage. However, only the results in the stages affected by the considered effect will be discussed.

Right after the establishment of the composite action between the concrete parts (II.2), tensile stresses develop in the in-situ slab. They are more pronounced for the section at the intermediate support (Fig.9). The reason for development of such stresses without any external load effect lies in different creep and shrinkage properties between the concrete parts. Having in mind that approximately 50% of the total shrinkage generally takes place in the first 3 months after casting, it will be clear that at this stage the in-situ slab is shrinking at a faster rate than the precast girder. On the other hand, the precast concrete at the element interface is creeping more than the in-situ slab due to the higher initial compressive stresses. This complex interaction between the concrete parts is responsible for the tensile stresses in the slab and for the redistribution of the stresses in the girder.
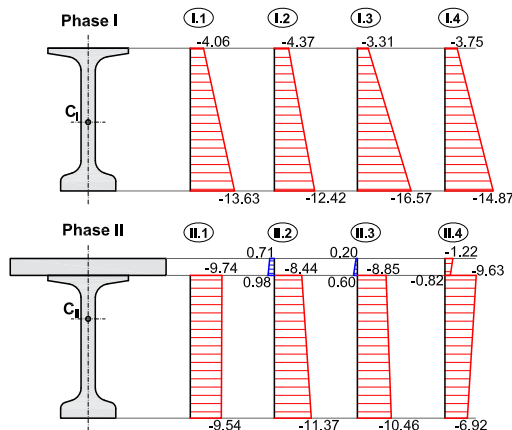
Figure 8 - Concrete stresses for age difference of 90 days at mid-span section

LEGEND:
I.1 - self-weight and prestressing of 36 strands
I.2 - creep and shrinkage until prestressing the tendon
I.3 - prestressing the tendon
I.4 - creep and shrinkage until casting the in-situ slab
II.1 casting the in-situ slab
II.2 - creep and shrinkage until placing the additional dead loads
II.3 - additional dead loads
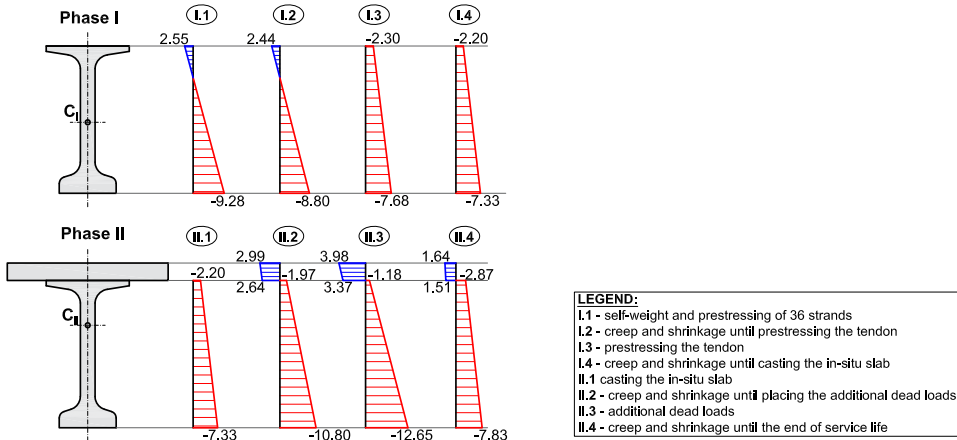II.4 - creep and shrinkage until the end of service life

Figure 9 - Concrete stresses for age difference of 90 days at intermediate support

The comparison between the stresses in the last two stages (II.3 and II.4) indicates that the creep and shrinkage effects increase the compressive stresses at the top fibre of the girder and reduce the stresses at the bottom one.

The influence of various age differences on the redistribution of concrete stresses is presented in Figs. 10-12. The stresses are normalized in terms of the chosen reference age difference. Figs. 10 and 11 show the relation between the age difference in the concrete parts and stresses in the precast girder, while Fig.12 presents the same relation for the stresses in the in-situ slab.

Fig.10 clearly indicates that the compressive stresses at the mid-span section has a tendency to increase with increasing the age difference. However, this tendency is less pronounced for the stresses at the top fibre. For the considered age differences in this study, the maximum increase in the girder stress can reach 25 % in terms of the reference one.
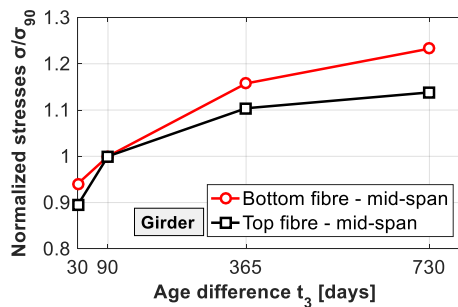
Figure 10 - Relation between age difference and noramalized stresses for mid-span section

The similar trend is observed for the stresses at the bottom fibre of the support section (Fig.11). Unlike the bottom fibre, the stresses at the top fibers are reducing for up to 50% by increasing the age difference. The reduction in concrete compressive stresses means that creep and shrinkage effects induce tensile stresses that increase with age difference.
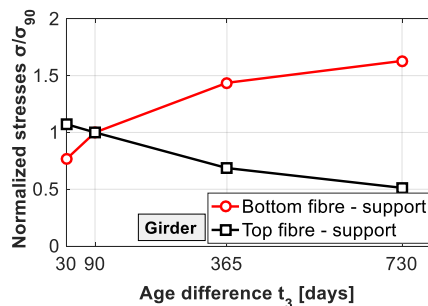
Figure 11 - Relation between age difference and noramalized stresses for support section

Such variation in the prestressed girders' stresses due to different ages of the concrete parts may lead to difficulties in satisfying the serviceability checks for stress limitations.

The age difference has the biggest impact on the development of tensile stresses in the slab part. This is especially pronounced at the intermediate support (Fig.12). The relationship presented in Fig.12 suggests that the deck slab is the most sensitive part of the composite section to the considered effect. For the analysed age differences, the tensile stresses in the slab can be even 3 times bigger than the ones calculated with the reference age difference.
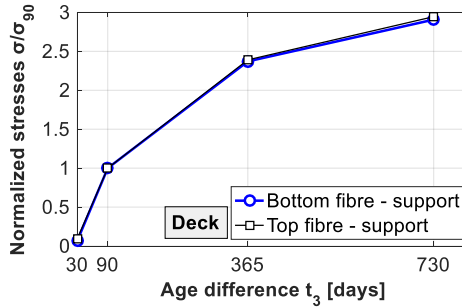
Figure 12 - Relation between age difference and noramalized tensile stresses for concrete deck slab

Usually, these tensile stresses are carried by the reinforcement in the concrete slab. The results here suggest that bigger age difference than considered in the design may result in insufficient amount of reinforcement in the slab, i.e., higher stresses in the reinforcement.

3.3.2. Deflections

Another limit state that has been examined under the effect of different age of concrete parts, was the long-term deflections.

Fig. 13 presents the relationship between the age difference between the concrete parts and the mid-span deflections for some characteristic load stages. The deflections in the diagram are presented as normalized values in terms of the deflections calculated for the reference age difference.

It has to be mentioned that the calculated deflections at the end of service life remained positive values (upwards) for all analysed cases. The relations presented in Fig. 13 show that the deflections increase proportionally to the age difference. It means that if bigger age difference than the one considered in the design occurs, then the structure will suffer bigger upward deflections. For the biggest age difference considered in the study, the increase in deflection is somewhat more than 20% during the construction and around 15% at the end of service life.

Figure 13 - Relation between age difference and noramalized deflections

A misprediction of the positive deflections can be responsible for several serviceability issues. Additionally, it can contribute to many difficulties during the final activities of the bridge construction. Among most common issues arising from over- or underestimation of deflections

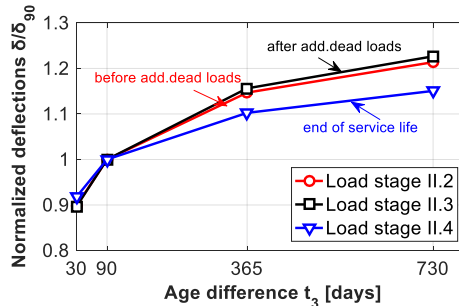at construction stages are: disability of reaching the designed road level, difficulties in providing the designed asphalt depth and consequently providing correct waterproofing details.

4. CONCLUSIONS

Based on the results from the numerical study and the on-site measurements of deflections for the composite concrete bridge girders, the following conclusions are drawn:
- The age difference between the concrete parts has significant effects on the composite girders' behavior.
- Bigger age difference between the girder and the in-situ slab produces higher compressive stresses in the girder. An exception is the top fibre of the intermediate support section.
- In-situ slab at the intermediate support section suffers several times higher tensile stresses for increased age differences between the composite elements.
- The upward deflections at the end of a construction process, as well as, at the end of a service life are bigger as the age difference between the concrete parts is pronouncer.

REFERENCES

[1] Mašović, S., Stošić, S., Pecić, P. (2014) "Research of long-term behaviour of non-prestressed precast concrete beams made continuous" in Engineering Structures 70, pp.11-22.

[2] Gilbert, R.I., Mickleborough, N.C., Ranzi, G. (2017) "Design of Prestressed Concrete to Eurocode 2" in CRC Press, New York.

[3] Gilbert, R.I., Ranzi,G. (2010), "Time-dependent behaviour of concrete structures" CRC Press, London.

[4] EN 1992-1-1 (2004) Eurocode 2: Design of concrete structures. Part 1-1: General rules and rules for buildings.

[5] Model Code 2010 (2013) *fib* model code 2010. Fédération Internationale du Béton.

[6] CEB-FIP Model Code 1990 (1993) Design Code. Thomas Telford, London.

Ivan Nackov[1], Aljoša Filipović[2], Jelena Dobrić[3]

NOVI PRISTUP PRORAČUNA UGAONIKA OD NERĐAJUĆEG ČELIKA – PROCENA ZASNOVANA NA NUMERIČKIM PODACIMA

Rezime:

Stubovi od ugaonika pokazuju složeno strukturno ponašanje koje proizilazi iz specifičnih geometrijskih odlika – ugaonike karakteriše mala torziona krutost i nedostatak otpornosti na savijanje, što dovodi do osetljivosti na fenomene izvijanja koji uključuju torziju. Brojne naučne studije pokazale su da su aktuelni evropski standardi za čelične konstrukcije konzervativni sa velikim rasipanjem podataka u slučaju stubova od ugaonika kod kojih do loma dolazi usled fleksiono-torzionog izvijanja. Nova proračunska procedura je razvijena na Imperijal koledžu u Londonu, koja obuhvata uticaj tranzicije u ponašanju nakon izvijanja i interaktivne efekte između fleksiono-torzionih oblika izvijanja i oblika izvijanja oko slabije ose. Ovaj rad daje procenu tačnosti ove procedure. Poređenje numeričkih podataka i njihovih proračunskih procena pokazuje dobru korelaciju, što ukazuje na bolju tačnost i doslednost u proceni nosivosti u poređenju sa postojećim kodifikovanim pravilima proračuna.

Ključne reči: nerđajući čelik, ugaonik, kritična sila, izvijanje, torziono, fleksiono, proračun.

A NEW DESIGN APPROACH FOR STAINLESS STEEL ANGLES – ACCURACY ASSESSMENT BASED ON NUMERICAL DATA

Summary:

The angle columns exhibit complex structural behaviour that arises from specific geometry features—the angle-section is characterised by low torsional stiffness and lack of primary warping resistance, leading to high sensitivity to buckling phenomena involving torsion. Numerous scientific studies have shown that the current European codes for steel structure are conservative with a high data scatter in cases of angle columns failing in flexural–torsional buckling. A novel design procedure has been developed at Imperial College in London, capturing the transition influence in post-buckling behaviour and the interactive effects between the flexural–torsional and minor-axis flexural buckling modes. This paper provides an accuracy assessment of this procedure. The comparison between the numerical data and their design estimates shows a good correlation, indicating improved accuracy and consistency in resistance predictions compared to the existing codified design rules.

Keywords: stainless steel, angle section, critical force, buckling, torsional, flexural, design.

---

[1] *Teaching assistant, Bulevar kralja Aleksandra 73 Beograd, inackov@grf.bg.ac.rs*
[2] *Assistant professor, Bulevar kralja Aleksandra 73 Beograd, afilipović@grf.bg.ac.rs*
[3] *Associate professor, Bulevar kralja Aleksandra 73 Beograd, jelena@imk.grf.bg.ac.rs*

1. INTRODUCTION

The angle columns exhibit the specific behavioural features, which are responsible for the fact that the current European codes [1], [2] for the design of steel structures do not adequately predict their ultimate responses. The equal-leg angle is singly symmetric cross-section with the shear centre located at the intersection of the leg mid-lines — this implies the lack of primary warping resistance and minute torsional stiffness, thus rendering a high susceptibility to instability phenomena involving torsion effects. The equal-leg angle columns fail in a major-axis flexural–torsional buckling (FTB) mode in the low-to-intermediate slenderness range, and a minor-axis flexural buckling (FB) mode in the high slenderness range. Besides, the clear scientific evidence corroborates that the critical buckling modes of short-to-intermediate lengths columns exhibit a length-dependent interaction between major-axis FTB and minor-axis FB representing a unique interactive instability phenomenon [3]. The short and intermediate length angle columns exhibit the mixed major-axis flexural and torsional deformations — the structural behaviour is featured by single half-wave critical buckling mode with no transverse bending of the cross-section walls (legs). This means that the critical buckling modes with several half-waves (local buckling) never occur in the angle columns. The torsional features of angle sections also depend on the leg width-to-thickness ratio; by increasing the leg widths, the distance between the shear centre and the section centroid is also increase, thus leading to FTB failure in the entire overall column slenderness range.

As an example, the nominal geometric properties of the thin-walled equal-leg angle-section 100×4 mm are shown in Table 1. By using the computer program CUFSM [4] and yield strength f_y=527 N/mm^2, the elastic torsional-flexural buckling stress for a nominal equal-leg angle section under compression was found to be 116.3 N/mm^2, with a corresponding half-wavelength of 2500 mm, see Figure 1.

Table 1 – Nominal geometry properties of an equal-leg angle section 100×4 mm.

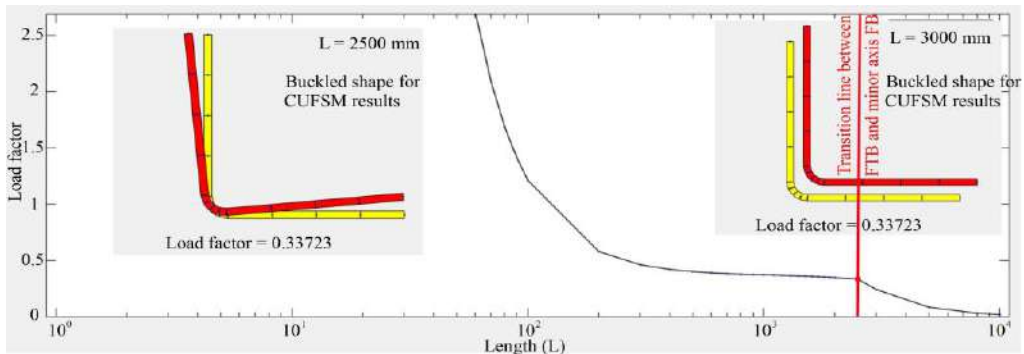| Angle	A (mm^2)	I_y (mm^4)	I_z (mm^4)	I_u (mm^4)	I_v (mm^4)	J (mm^6)	I_w (mm^6)
100×4	766.4	772039.3	772039.3	1254695.9	289382.8	4087.6	81262.1
A − the gross cross-sectional area; I_y, I_z, I_u and I_v – the second moment of area about geometric and principal axes, respectively; J – the St.-Venant torsion constant; I_w – secondary warping constant.							

Figure 1 - Elastic critical buckling load factor versus column length curve for the equal-leg angle 100×4 mm.

In view of what was previously mentioned, the rational structural model for design of equal-leg angle column should be based on the torsional buckling (TB), instead of local buckling (LB) behaviour. The numerous scientific investigations [5], [6], [7], [8] have demonstrated that existing design procedures stated in the European design codes EN 1993-1-1 [1] and EN 1993-1-4 [2] are generally conservative in predicting the ultimate resistances of equal-angle columns. It is worth noting that the EN 1993 design approach is based on a couple of conceptual shortcomings influencing the inaccuracy in predicting the failure loads of these columns failing in FTB — it does not use the interaction between major-axis FTB and minor-axis FB (columns with both slender and non-slender angle-sections) and views LB and FTB as two different phenomena, thus considering in the calculations the same instability effect twice (columns with slender angle-sections). This issue was emphasized in research of Behzadi-Sofiani et al. [8], addressing fixed-ended carbon steel and stainless steel equal-leg angle columns. The authors demonstrate that TB and LB are essentially two names of the same phenomenon, confirming in this way the evidence reported in [9], where it is shown that these instabilities can only occur in longitudinally restrained angle columns.

The paper presents the results of a nonlinear finite element (FE) parametric study covering fixed-ended cold-formed stainless steel (CFSS) equal-leg angle columns failing in major-axis FTB and minor-axis FB. A wide range of cross-section slenderness and column lengths produced from austenitic, duplex and ferritic stainless steel grades were considered. The parametric study was based on the FE models that were calibrated and validated against the experimental results reported in [10]. The FE column ultimate resistances were employed to perform independent accuracy assessment of the novel procedure proposed for design of stainless steel equal-leg angle columns, which was developed and validated in [8]. The statistical indicators concerning the failure loads, are also provided, showing the quality and reliability levels of the proposed method.

2. A NEW DESIGN PROCEDURE [8]

In the low and intermediate slenderness domain, where FTB is the dominant failure mode and $N_{\mathrm{cr,TF}}/N_{\mathrm{cr,F,v}} \leqslant 1.0$, the design buckling resistance $N_{\mathrm{b,Rd}}$ of CFSS equal-leg angle section columns is given as follows:

$$N_{\mathrm{b,Rd}} = \chi_{\mathrm{TF}} A f_{\mathrm{y}}/\gamma_{\mathrm{M1}} \tag{1}$$

In the Eq. (1) the gross cross-sectional area should be used for all classes of angle-sections to avoid double-accounting of local and torsional buckling. The reduction factor χ_{TF} is given by:

$$\chi_{\mathrm{TF}} = \chi_{\mathrm{F}} + \Delta_{\mathrm{F}}(\chi_{\mathrm{T}} - \chi_{\mathrm{F}}) \tag{2}$$

The torsional buckling reduction factor χ_{T} and the flexural buckling reduction factor χ_{F} are respectively given as follow:

$$\chi_{\mathrm{T}} = \bar{\lambda}_{\mathrm{TF}} - 0.188/\bar{\lambda}_{\mathrm{TF}}^2 \text{ but } \chi_{\mathrm{T}} \leqslant 1.0 \tag{3}$$

$$\chi_{\mathrm{F}} = 1/\left(\phi + \sqrt{\phi^2 - \bar{\lambda}_{\mathrm{TF}}^2} \right) \text{ but } \chi_{\mathrm{F}} \leqslant 1.0 \tag{4}$$

and Δ_{F} is given thus:

$$\Delta_{\mathrm{F}} = \left(1 - N_{\mathrm{cr,TF}}/N_{\mathrm{cr,F,v}} \right)^p \tag{5}$$

where:

$$p = \begin{cases} 2.0\bar{\lambda}_{\mathrm{TF}} & \text{for } \bar{\lambda}_{\mathrm{TF}} \leqslant 2.0 \\ 2.93\bar{\lambda}_{\mathrm{TF}}^{0.45} & \text{for } \bar{\lambda}_{\mathrm{TF}} > 2.0 \end{cases} \tag{6}$$

The torsional-flexural slenderness $\bar{\lambda}_{\mathrm{TF}}$ and parameter ϕ are given by:

$$\bar{\lambda}_{\mathrm{TF}} = \sqrt{Af_{\mathrm{y}}/N_{\mathrm{cr,TF}}} \tag{7}$$

$$\phi = 0.5\left[1 + \alpha\beta\left(\bar{\lambda}_{\mathrm{TF}} - \bar{\lambda}_0\right)^{\beta} + \bar{\lambda}_{\mathrm{TF}}^2\right] \tag{8}$$

For CFSS angles, the proposed values for β and the limiting slenderness $\bar{\lambda}_0$ are 1.45 and 0.2, respectively, whereas for the imperfection factor α, value of 0.49 is recommended. In the high slenderness domain where $N_{\mathrm{cr,TF}}/N_{\mathrm{cr,F,v}} > 1.0$, the design buckling resistance $N_{\mathrm{b,Rd}}$ of CFSS equal-leg angle columns should be obtained as follows:

$$N_{\mathrm{b,Rd}} = \chi_{\mathrm{F}}Af_{\mathrm{y}}/\gamma_{\mathrm{M1}} \tag{9}$$

$$\chi_{\mathrm{F}} = 1/(\phi + \sqrt{\phi^2 - \bar{\lambda}^2}) \text{ but } \chi_{\mathrm{F}} \leqslant 1.0 \tag{10}$$

$$\bar{\lambda} = \sqrt{Af_{\mathrm{y}}/N_{\mathrm{cr,F,v}}} \tag{11}$$

$$\phi = 0.5\left[1 + \eta + \bar{\lambda}^2\right] \tag{12}$$

$$\eta = \alpha\beta\left(\bar{\lambda} - \bar{\lambda}_0\right)^{\beta} \tag{13}$$

with β being a factor allowing for the influence of interactive buckling:

$$\beta = 1.9 - 0.45N_{\mathrm{cr,TF}}/N_{\mathrm{cr,F,v}} \text{ but } 1.0 \leq \beta \leq 1.45 \tag{14}$$

When minor-axis FB is critical failure mode, the gross cross-sectional area A in Eq. (9) should be replaced by the effective area A_{eff} for columns with slender Class 4 cross-sections, since the issue of double-counting the torsional effects is no longer relevant. The imperfection factor and limiting slenderness remain as specified above, $\alpha = 0.49$ and $\bar{\lambda}_0 = 0.2$.

3. NUMERICAL PARAMETRIC STUDY

The numerical parametric study was performed on CFSS equal-leg angle columns using the ABAQUS FE software package [11]. The linear bifurcation analysis (LBA), and geometrically and materially non-linear analysis with imperfections (GMNIA) were performed for each FE angle column. The GMNIA was developed as quasi-static with the dynamic explicit solver, and the variable non-uniform mass scaling technique of $5 \times 10^{-6}s$ was used to shorten the computational time. In total, 14 different equal-leg angle section dimensions were considered, as in [5], providing both slender and non-slender cross-sectional behaviour. A 4-noded shell element S4R was employed to model the nominal geometry of the FE columns. A square mesh size of approximately 4 mm was chosen to discretise the flat and corner parts of the modelled cold-formed angle sections. To nonlinear material responses for austenitic, ferritic and duplex grade were replicated using the modified Ramberg-Osgood analytical model [12], as it was described in [5]. Fixed-ended boundary conditions were modelled by restraining the necessary degrees of freedom at the reference points set at the end cross-sections. By employing kinematic

coupling constraints, warping was also prevented at both ends. The failure loading was applied as controlled nodal displacement at one end through a reference point that was free to move longitudinally. Initial geometric imperfections include bow imperfections (out-of-straightness), twist imperfections and cross-section imperfections (out-of-flatness of a section angle legs). A single initial twist imperfection was considered to trigger local and torsional-flexural modes: a sinusoidal half wave mode shape over the column length, reflecting twist eigenmode shape, with an amplitude of $\tan^{-1}(L/1000b)$ at the column mid-height [7], [8]. The amplitude of $L/1000$ was adopted about both principal axes for the initial out-of-straightness. The geometric imperfection pattern reflects the eigenmode displacements obtained via LBA.

4. ACCURACY ASSESSMENT OF THE NEW DESIGN PROCEDURE [8]

A comparison of the generated FE data with the design data obtained according to the proposed design procedure [8] for fixed-ended CFSS equal-leg angle columns is presented in this section. The FE parametric study comprised 156 FE columns (see Table 2), covering the slenderness range from 0.5 to 2.5, made of austenitic, ferritic and duplex grades. The numerical failure mode governed by major-axis FTB or minor-axis FB (see Figure 2) was selected to evaluate the corresponding design failure load. In the predictions of the ultimate column resistances, the safety factor was used equal to 1.0. The elastic critical buckling loads for TB, major-axis FTB and minor-axis FB were analytically determined according to the Theory of elastic stability [13] and via LBA. For analytically determined critical buckling loads, the effective buckling lengths for TB and FTB were taken to be equal to the column length L, whereas the effective buckling length for minor-axis FB was taken as $0.5L$. Figure 3 shows the comparisons between analytically and numerically obtained elastic critical buckling loads.

Table 2 – Cross-section geometries and lengths of CFSS angle columns included in the study.

Equal-leg angle section	Column length L (mm)	Leg width b (mm)	Thickness t (mm)	Internal radius r_i (mm)
50 x 50 x 2	300-2200	50	2	4
50 x 50 x 4	300-2600	50	4	8
50 x 50 x 5	300-2800	50	5	10
60 x 60 x 2	400-2400	60	2	4
60 x 60 x 4	300-3000	60	4	8
60 x 60 x 6	400-3000	60	6	12
80 x 80 x 4	300-3200	80	4	12
80 x 80 x 6	500-3200	80	6	12
150 x 150 x 4	900-3000	150	4	8
150 x 150 x 6	800-3800	150	6	12
150 x 150 x 8	600-4000	150	8	16
200 x 200 x 6	900-3300	200	6	12
200 x 200 x 8	900-3300	200	8	16

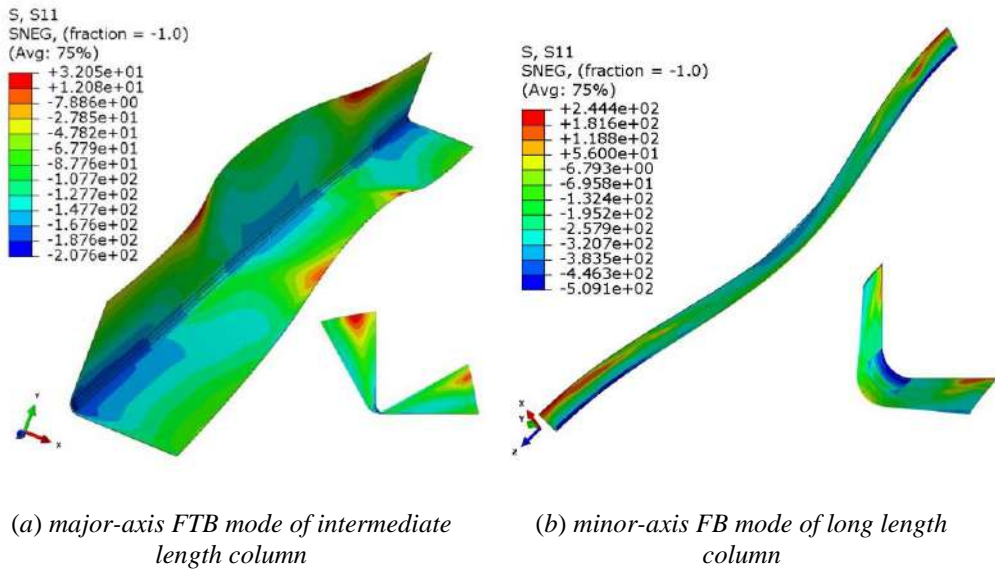(*a*) *major-axis FTB mode of intermediate length column* (*b*) *minor-axis FB mode of long length column*

Figure 2 - The buckling failure modes of FE CFSS equal-leg angle column.

A summary of the comparisons of the FE column compressive capacities against the resistance predictions according to the new proposal is shown in the graphs in Figures 4, 5 and 6 for austenitic, ferritic and duplex CFSS equal-leg columns, respectively, using different colour coding for each stainless steel family. The statistical indicators, mean values, standard deviation, Coefficient of Variations (CoVs) and maximum / minimum values, concerning the failure loads are also provided.

The observation of the buckling results prompts the following remarks:
- The ultimate buckling load decreases monotonically with the column length; the torsional mode almost always plays a key role: it participates in the critical buckling modes of all but the very long columns. In the low and intermediate slenderness range (approximately up to $\bar{\lambda} \approx 1.0$) columns buckle in in mixed major FTB, whereas the long length columns buckle in pure minor-axis FB.
- The well-known theoretical formula for elastic critical FTB loads [13] offers a lower prediction accuracy with a larger scatter, compared to the case of a pure minor-axis FB (see Figure 3), thus causing the prediction inaccuracy for the ultimate column capacities according to design approaches based on separated models for FTB and FB.
- In general, the proposed design approach [8], which captures the transition influence in post-buckling regime and the interactive effects between the TFB and minor-axis FB, yields safe and accurate predictions of the ultimate column strengths, especially in the case of CFSS angle columns that failed dominantly by FB. The assessment of the design methods shows better consistency for ferritic grade, whereas a large margin with highest data scatter was found for duplex stainless steel. Also, there are fewer predictions on the unsafe side for austenitic grade.

- Using the results of previous investigations, collected from literature [5], [6], [8], the comparisons presented herein for FTB modes, indicate an improvement in resistance predictions relative to that currently given in EN 1993. Again, the highest accuracy and consistency of capacity predictions were found for ferritic grade, whereas there is greater scatter in the data with a few uncertain predictions for the austenitic and duplex grades.

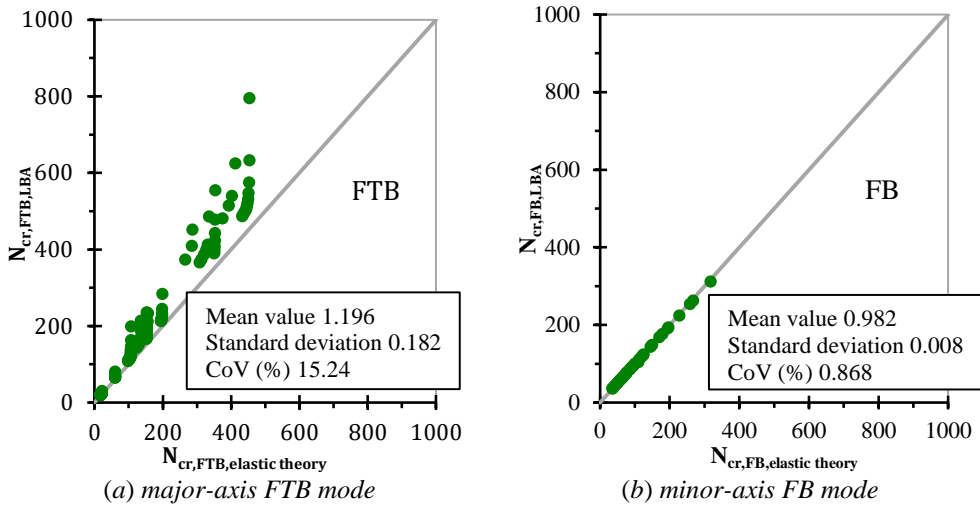(*a*) major-axis FTB mode   (*b*) minor-axis FB mode

Figure 3 - Comparisons between analytically and numerically obtained elastic critical buckling loads.

(*a*) major-axis FTB mode   (*b*) minor-axis FB mode

Figure 4 - FE results against the new design proposal for the austenitic CFSS angle columns.

(*a*) *major-axis FTB mode*   (*b*) *minor-axis FB mode*

Figure 5 - FE results against the new design proposal for the ferritic CFSS angle columns.

(*a*) *major-axis FTB mode*   (*b*) *minor-axis FB mode*

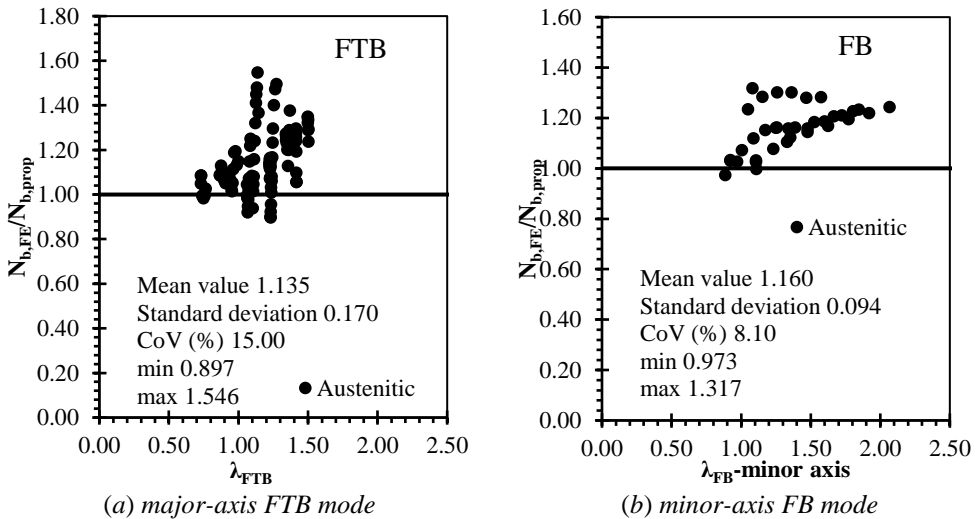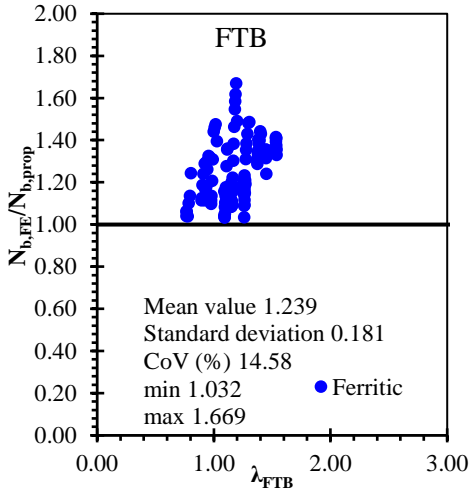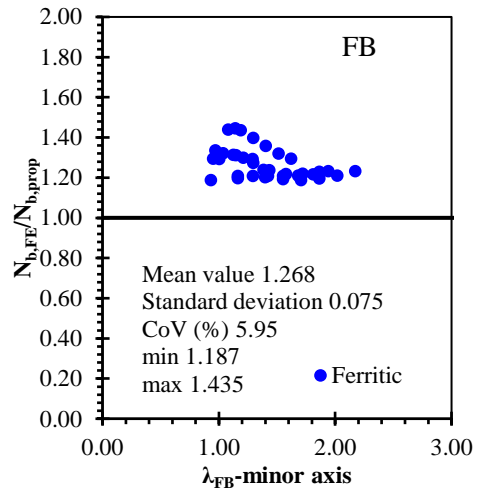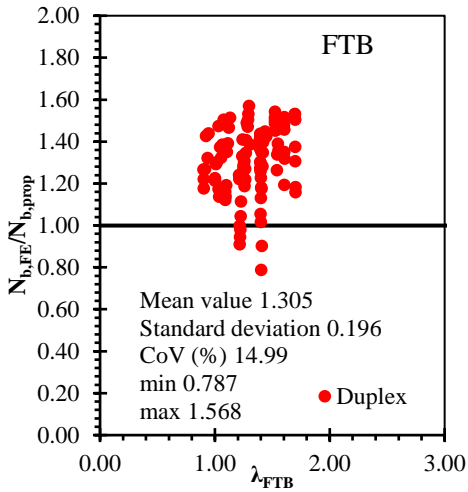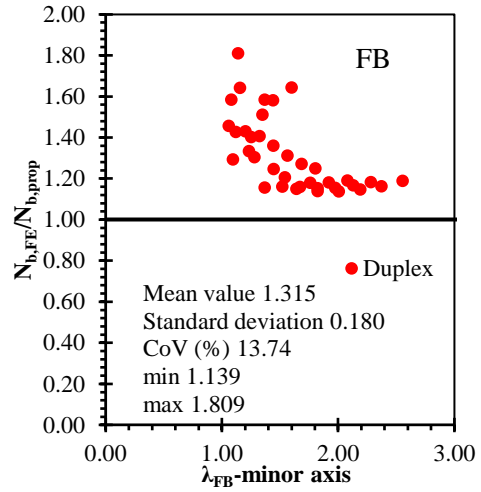*Figure 6 - FE results against the new design proposal for the duplex CFSS angle columns.*

5. CONCLUSIONS

This paper presents the accuracy assessment of the new design proposal for CFSS equal-leg angle columns failing by major-axis FTB and minor-axis FB, using FE database. The FE parametric study covers the slenderness range from 0.5 to 2.5 of 156 FE columns produced from austenitic, ferritic and duplex grades. The results of the comparative study showed that the statistical indicators and data trend lines obtained herein are similar to those acquired in the research of Behzadi-Sofiani et al. [8] — the novel design proposal provides notable improvements in both the accuracy and consistency of column ultimate resistance predictions.

REFERENCES

[1]   Eurocode 3: Design of steel structures – Part 1-1: General rules and rules for buildings EN 1993-1-1, Brussels, Belgium, CEN 2005.

[2]   Eurocode 3: Design of steel structures – part 1-4: General rules – supplementary rules for stainless steels, including amendment A1 (2015), EN 1993-1-4:2006+A1:2015, Brussels, Belgium, CEN 2015.

[3]   A. Landesmann, D. Camotim, P.B. Dinis, R. Cruz, Short-to-intermediate slender pinended cold-formed steel equal-leg angle columns: experimental investigation, numerical simulations and DSM design, Eng. Struct., 132 (2017) 471–93.

[4]   Schafer BW, Ádány S. Buckling analysis of cold-formed steel members using CUFSM: conventional and constrained finite strip methods. In: Proceedings of the eighteenth international speciality conference on cold-formed steel structures. Orlando (USA); 2006.

[5]   Dobrić J, Filipović A, Baddoo N, Marković Z, Buđevac D. Design procedures for cold-formed stainless steel equal-leg angle columns, Thin-Walled Structures, 159 (107210), 2020, pp.19.

[6]   Dobrić J, Filipović A, Baddoo N, Buđevac D, Rossi B. Design criteria for pin-ended hot-rolled and laser-welded stainless steel equal-leg angle columns, Thin-Walled Structures, 167(108175), 2021, pp. 24.

[7]   Behzadi-Sofiani B, Gardner L, Ahmer Wadee M, Dinis P.B, Camotim D. Behaviour and design of fixed-ended steel equal-leg angle section columns, Journal of Constructional Steel Research 182 (2021) 106649, pp 14.

[8]   Behzadi-Sofiani B, Gardner L, Ahmer Wadee M. Stability and design of fixed-ended stainless steel equal-leg angle section compression members, Engineering Structures 249 (2021) 113281, pp 17.

[9]   P.B. Dinis, D. Camotim, N. Silvestre, On the mechanics of thin-walled angle column instability, Thin-Walled Structures 52 (2012) 80-89.

[10] J. Dobrić, A. Filipović, Z. Marković, N. Baddoo, Structural response to experimental axial testing of cold-formed stainless steel equal angle columns, Thin-Walled Struct., 156 (2020) 1-16.

[11] ABAQUS User Manual. Version 6.12. Providence, RI, USA: DS SIMULIA Corp; 2012.

[12] I. Arrayago, E. Real, L. Gardner, Description of stress-strain curves for stainless steel alloys, Materials and Design, 87 (2015) 540-552.

[13] S.P. Timoshenko, J.M. Gere, Theory of Elastic Stability, 2nd ed. McGraw-Hill Book Company, Inc., New York, USA, 1961.

Jelena Nikolić[1], Svetlana M. Kostić[2], Saša Stošić[3]

NUMERIČKO MODELIRANJE AKSIJALNE NOSIVOSTI STUBOVA OD ČELIČNIH CEVI ISPUNJENIH BETONOM

Rezime:

U radu je prikazano numeričko modeliranje aksijalne nosivosti kratkih stubova od čeličnih cevi ispunjenih betonom. Za potrebe analize napravljen je nelinearni 3D model na bazi konačnih elemenata u programu ABAQUS. Modeliranje, granični uslovi, konstitutivni modeli za čelik i beton i interakcija na kontaktu čelične cevi i betona detaljno su razmotreni. Predložena su tri numerička modela koji su validirani pomoću prikupljenih rezultata eksperimenata. Na kraju, aksijalna nosivost spregnutog stuba upoređena je sa nosivošću sračunatom po Evrokodu 4.

Ključne reči: spregnuti stubovi, nelinearna analiza, metod konačnih elemenata

NUMERICAL MODELLING OF CONCRETE-FILLED STEEL TUBE COLUMNS UNDER AXIAL COMPRESSION

Summary:

The paper presents the numerical modelling of concrete-filled steel tube stub columns under axial compression. The nonlinear 3D finite element model for the analysis was developed using ABAQUS software. The modelling, boundary conditions, the constitutive models for steel and concrete and contact interaction between the steel tube and concrete surface are discussed in detail. Three numerical models are proposed and validated using collected experimental data results. Finally, the composite column axial capacity is compared with the Eurocode 4 calculations for composite columns.

Key words: composite columns, nonlinear analysis, finite element analysis

---

[1] *Asistent, Građevinski fakultet Univerziteta u Beogradu, jnikolic@grf.bg.ac.rs*

[2] *V. prof, Građevinski fakultet Univerziteta u Beogradu, svetlana@grf.bg.ac.rs*

[3] *V. prof, Građevinski fakultet Univerziteta u Beogradu, sasa@grf.bg.ac.rs*

1. INTRODUCTION

A concrete-filled steel tube column (CFST) consists of an outer steel tube filled with concrete. The composite action between two materials provides that the concrete stiffens the steel tube and postpones local buckling. In turn, the outer steel tube acts as longitudinal and transverse reinforcement, permanent formwork and provides confinement for the concrete core. CFST columns demonstrated excellent structural behaviour due to their high strength, ductility, and good seismic behaviour.

Due to their overall good performance, CFST columns have been widely used in different types of construction and are still very present in many research fields [1]. Various shapes and types of CFST columns have been constructed in the past [2-5]. Besides, other materials such as fibre-reinforced concrete or fibre-reinforced polymer sheets (FRP) have been used for strengthening the CFST columns [6-7]. In addition, the global tendency to reuse construction waste as alternative aggregate to produce sustainable concrete resulted in hybrid structural members – recycled aggregate concrete-filled steel tubular (RACFST) columns filled with recycled aggregate concrete [8-10].

The numerical model of CFST columns needs to effectively predict structural members' behaviour and provide complex information regarding their structural response [11]. This paper presents a finite element (FE) model of CFST columns under axial loading in ABAQUS [12]. This analysis method has been widely used in the literature to validate experimental results [1-5]. In addition, the FE model in ABAQUS can predict other important information, such as failure modes and deformation patterns, or capture phenomena such as local buckling of the steel tube and confinement of the concrete [8].

The idea was to develop reliable but a simple model, especially in terms of geometry and test setup simulation, boundary conditions and loading. Analysis was performed as displacement controlled and included both material and geometrical nonlinearities.

3D numerical models presented in this paper are validated with the test results available from the literature and previously developed FE models. Because of page limitations, the validation will be presented by comparison with just two specimens from different studies, 3HN [13] and CC-0 [8]. Finally, the ultimate strength results will be compared to the axial capacity of the cross-section calculated by Eurocode 4 (EC4)[14-15].

2. NUMERICAL MODELLING

2.1. MODEL DESCRIPTION

The outer steel tube and the concrete core were modelled using 8-node brick elements (C3D8R) with three translation degrees of freedom at each node. The mesh size was selected following the mesh convergence studies and recommendations provided in [11]. The finite element mesh across the cross-section was chosen as $D/15$ and 2.5 times for the mesh in the longitudinal direction, where D refers to the outer diameter of a circular column.

The steel end plates used in tests are not included in the 3D model to simplify the modelling and shorten the calculation time. Instead, the constraints option available in ABAQUS is applied. It connects all surface nodes to only one reference point (RP) defined in the centre of the column's top and bottom surface. As shown in Figure 1, boundary conditions (BC) are set to RP1 and RP2 only: all displacements are restrained except displacement in the loading direction at the RP1. A displacement-controlled axial loading scheme was applied to the RP1 only.
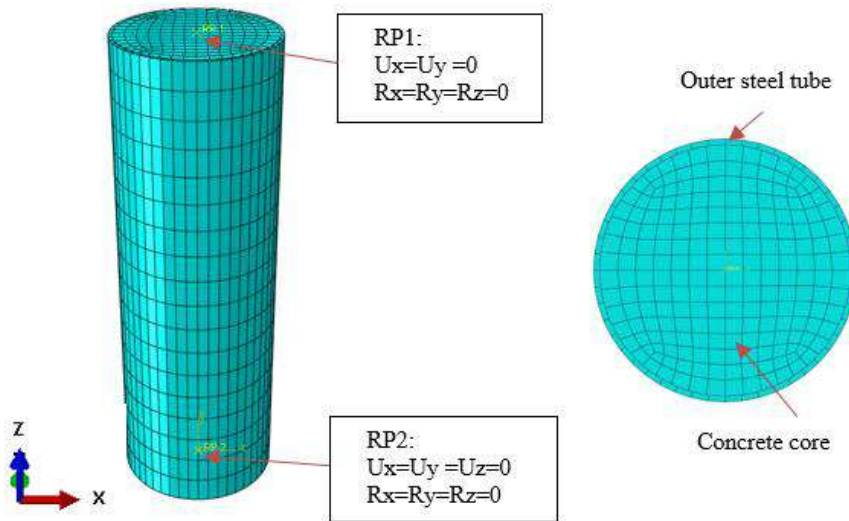
Figure 1 – 3D model of CFST column with RP1 and RP2 with BC; Cross-section and meshing

Interaction between steel tube and concrete core was simulated using the surface-to-surface contact option. The inner tube surface was chosen as the master surface, while the concrete surface was defined as the slave surface. It was essential to allow the separation of the materials in tension and provide no penetration of concrete core into steel tube in compression. The normal behaviour was defined via the "hard" contact option, while tangential behaviour was penalised with a friction coefficient of 0.6, as suggested in [16].

2.2. MATERIAL MODELLING

Numerical modelling of structural steel and concrete constitutive materials followed recommendations by [11] and [16]. This way, two different models were created: Model 1 and Model 2. The third numerical model, denoted as Model 3, investigated material curves proposed by Pre-norm Eurocode 2 (EC2) [17] and Eurocode 3 (EC3) [18] for concrete and steel, respectively. Therefore, three different models have been presented in this paper, as summarized in Table 1.

Table 1 – Numerical models with details of material modelling

	Structural steel	Concrete
Model 1	Tao et al. [11]	Tao et al. [11]
Model 2	Han et al. [16]	Han et al. [16]
Model 3	EC3 [18]	EC2 [17] extended

2.2.1. Material modelling of steel tube

Structural steel properties required for ABAQUS are provided within a uniaxial stress-strain relationship σ-ε. Key input parameres for defining the curve are yield strength f_y, modulus of elasticity E, and the plasticity parameters depending on the chosen curve.

Researchers have investigated stress-strain constitutive models for carbon steel, such as elastic-perfectly plastic, bilinear, and multilinear with hardening [4, 7].

In this paper, three different constitutive models have been considered as illustrated in Figure 2 for specimen 3HN. The first stress-strain curve is proposed in [11] and consists of an elastic branch until the yield strain ε_y, a perfectly plastic branch until $15\varepsilon_y$ and hardening until the ultimate strain ε_u. Hardening is defined by strain-hardening exponent p.

The second is the five-stage elastic-plastic stress-strain model presented in [16]. It consists of elastic, elastic-plastic, plastic, hardening and fracture defined with $\varepsilon_e=0.8f_y/E$, $\varepsilon_{e1}=1.5\varepsilon_e$, $\varepsilon_{e2}=10\varepsilon_{e1}$, $\varepsilon_{e3}=100\varepsilon_{e1}$ respectively, where ε_e is the yield strain and E modulus of elasticity.

The third constitutive model presented is an elastic-perfectly plastic σ-ε relationship for structural steel given in EC3. Material properties for steel used in tests 3HN and CC-0 are provided in Table 2. Poisson's ratio is taken as 0.3.
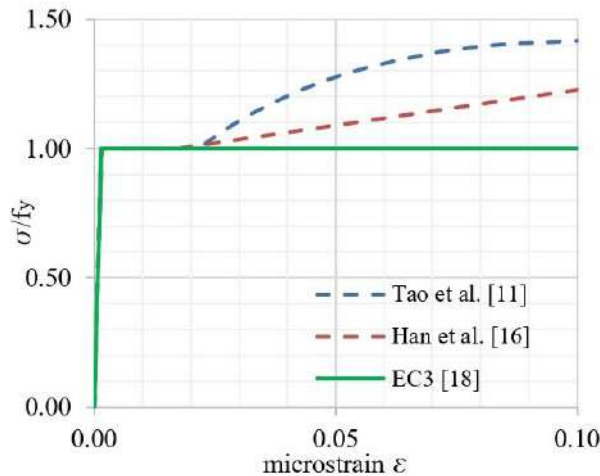

Figure 2 – Constitutive models for the steel tube demonstrated on specimen 3HN [13]

However, this study showed that the choice of the steel stress-strain model did not significantly impact the numerical results. The same observation was previously reported in the literature [4].

2.2.2. Material modelling of concrete core

When the CFST column is subjected to axial compression, concrete reaches a triaxial stress state due to passive confinement provided by the steel tube [11]. This confinement effect is more significant in circular than square columns, as reported in [19].

The concrete Damaged Plasticity (CDP) formulation available in ABAQUS was used to define the nonlinear behaviour of the concrete. Besides, the compressive stress-strain curve of unconfined concrete can be directly defined as the input for the CDP model. However, the model

should include concrete confinement, especially in circular CFST columns. Modelling confined concrete behaviour in CFST columns has been very challenging for many authors. The researchers proved that the passive confinement would increase both the peak strain (ductility) and the strength of the concrete and so the CFST column. One of the possibilities to include the confinement effect in ABAQUS is by modifying the concrete stress-strain curve. This means including softening and hardening behaviour as a result of composite action during the lateral expansion of concrete. This paper has considered three uniaxial models illustrated in Figure 3 for specimen 3HN.
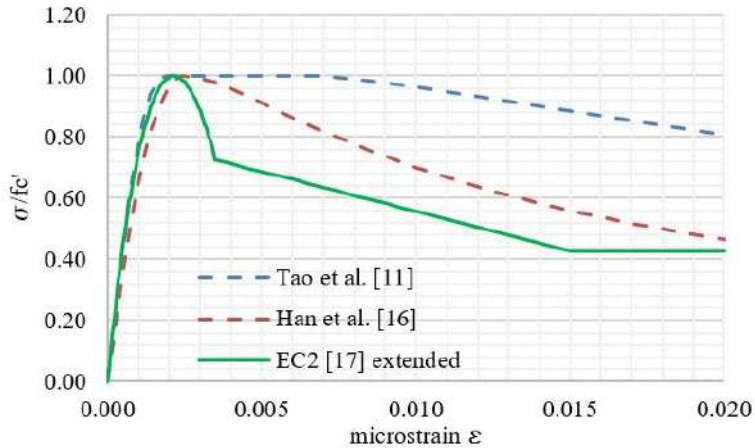

Figure 3 – Constitutive models for the concrete core for specimen 3HN [13]

The first model by Tao et al. suggested that a concrete σ-ε relation considers strain hardening/softening function for confined concrete as the increase in plastic strain (ductility) [11]. The second model by Han et al. is well known for giving good predictions in CDP model in ABAQUS [16]. It defines concrete plastic behaviour depending on the confinement factor ξ. The third model considered is the EC2 stress-strain relation for unconfined concrete in compression with a total strain limit of 3.5‰ [17]. The ascending branch is taken linear elactic until $0.4f_{c'}$ and nonlinear in the plastic region defined by expressions given in Pre-norm EC2 [17]. Beyond strain limit of 3.5‰ , the curve is extended partly following the recommendations for numerical modelling of CFST columns provided in [20]. The residual stress σ_{res} depends on the D/t ratio and concrete compressive strength $f_{c'}$ as given in expression (1). This stress value σ_{res} is reached at the strain of 15‰ and remains constant until the strain of 20‰. For creating Model 3, a simple solution is suggested for defining the stress-strain curve in range 3.5-15‰, with a linear stress-strain branch.

$$\sigma_{res} = \begin{cases} f_c & \frac{D}{t} \leq 24 \\ f_c \left(1.6 - 0.025 \frac{D}{t} \right) & 24 < \frac{D}{t} \leq 64 \\ 0 & 64 < \frac{D}{t} \end{cases} \qquad (1)$$

Furthermore, for application of CDP model several parameters define concrete plasticity: dilation angle (ψ), flow potential eccentricity (e), a ratio of the compressive strength under biaxial loading to uniaxial compressive strength (f_{b0}/f_c'), the ratio of the second stress invariant on the tensile meridian to that on the compressive meridian (K_c) and viscosity parameter. These parameters have been selected as per Tao et al. for Model 1, while Models 2 and 3 have same values as recommended by and Han et al.: 30º, 0.1, 1.16, 2/3 and 0 correspondingly.

Concrete tensile behaviour in the ABAQUS CDP model for Models 1 and 2 was defined following the same recommendations as in their compressive models. Since EC2 does not provide a curve for concrete in tension, Model 3 has the same tension characteristics adopted for Model 2. Damage parameters are not included in modelling as the loading in the test was monotonic.

Material properties for specimens 3HN and CC-0 are provided in Table 2. Poisson's ratio for concrete is taken as 0.2.

Table 2 – Details of specimens 3HN and CC-0 with material properties for concrete and steel

Specimen	Dimensions			Concrete		Steel		
	D [mm]	t [mm]	L [mm]	f_c' [MPa]	E [GPa]	f_y [MPa]	E [GPa]	Poisson ration
3HN	150.0	3.20	450	28.7	-	287.4	200.0	0.300
CC-0	139.1	2.79	420	41.2	23.09	388.5	203.8	0.279

3. VALIDATION OF THE PROPOSED MODELS

Proposed models have been validated against test results and FE modelling results provided in the literature. Here the validation is presented for two circular specimens 3HN [13] and CC-0 [8] test results. Figures 4 and 5 demonstrate axial load–axial strain $(N-\varepsilon)$ diagrams for the column specimens obtained in tests with the results of the proposed FE Models 1-3.

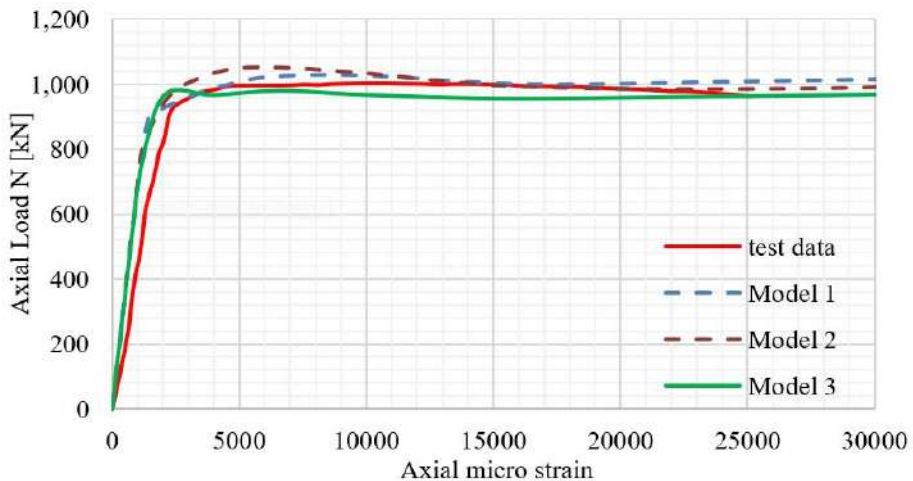*Figure 4 –N-ε diagram for specimen 3HN*

As shown in Figure 4, there is generally good agreement between numerical and test results regarding the shape of the full-range *N-ε* diagram. Still, neither of the three models matches the test results during the initial elastic stage. As assumed, this probably occurred due to change in elastic modulus of concrete obtained from the tests [11]. Besides, Model 3 demonstrates a small peak in total strength and slightly underestimates the total strength. After reaching ultimate strength, all curves match the flattening part of the test curve.

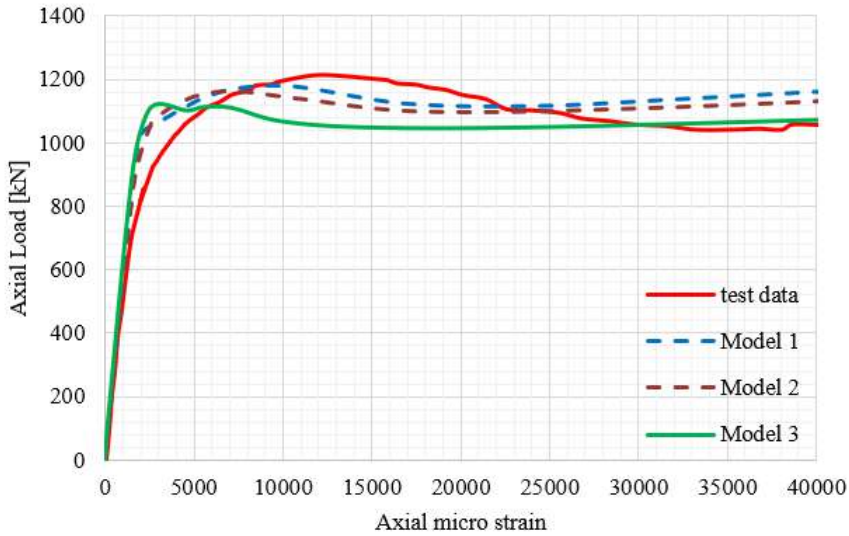Figure 5 shows the *N-ε* diagram for specimen CC-0. The results of all three models have satisfying accuracy.

Figure 5 – N-ε diagram for specimen CC-0

Figure 6 shows the typical failure mode of the stub CFST column under axial load obtained in the analysis, presented for specimen 3HN.
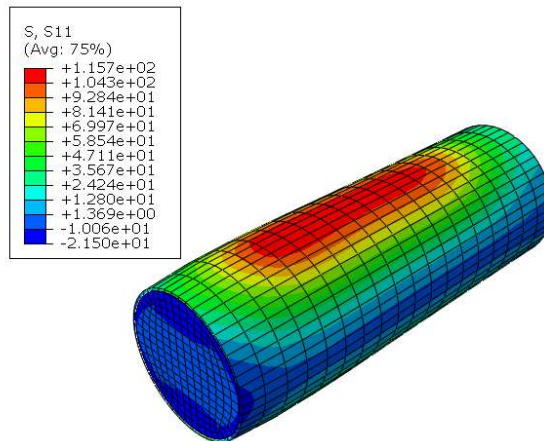

Figure 6 – Typical failure mode of stub circular specimen under axial load

252

The numerical ultimate strength values *Nu* from Figures 4 and 5 for Models 1-3 are compared to the test values $N_{u(test)}$ and well predicted, as presented in Table 3. Differences for both specimens remain within the range of 5%, except for Model 3 of the specimen CC-0, which equals 8,94%.

Table 3 – Summary of ultimate axial strength Nu results

	3HN		CC-0	
	N_u [kN]	$N_u/N_{u(test)}$ [%]	Nu [kN]	$N_u/N_{u(test)}$ [%]
test data	1001.17	100.00	1211.60	100.00
Model 1	1026.80	97.50	1178.42	102.82
Model 2	1052.66	95.11	1163.81	104.11
Model 3	980.35	102.12	1112.16	108.94
EC4	1174.76	85.22	1339.59	90.45

According to EC4, the ultimate plastic resistance to compression of a stub composite column $N_{u,EC4}$ is calculated from Eq. (2). For concrete-filled tubes of circular sections, it considers the decrease in steel strength by factor η_a and increase in strength of concrete caused by confinement factor η_c, Eq. (3-4). The buckling effective length was taken as 0.5 cooresponding to the fixed-ended boundary conditions in tests.

$$N_{u,EC4} = \eta_a A_a f_y + A_c f_c' \left(1 + \eta_c \frac{t}{d} \frac{f_y}{f_{c'}}\right) \tag{2}$$

$$\eta_a = 0.25(3 + 2\bar{\lambda}) \leq 1.0 \tag{3}$$

$$\eta_c = 4.9 - 18.5\bar{\lambda} + 17(\bar{\lambda})^2 \geq 0 \tag{4}$$

where:

A_a and A_c are cross-sectional areas of steel tube and concrete core respectively,

f_y is the nominal value of the yield strength of structural steel,

f_c' is characteristic compressive cylinder strength of concrete,

t is the wall thickness of the steel tube,

d is the external diameter of the column,

$\bar{\lambda}$ is the relative slenderness.

4. CONCLUSION

Numerical modelling in ABAQUS software offers powerfull capabilities for numerical modeling of nonlinear behavior of CFST columns. The presented 3D finite element models successfully simulate the behaviour of circular CFST stub columns under axial compression. The full range response of the columns through $N–\varepsilon$ diagrams and failure modes has been validated against tests with satisfying accuracy. Models 1 and 2, based on previous recommendations, are confirmed to simulate the actual behaviour very well within 5% differences. On the other hand, EC2 proposes stress-strain relation for concrete in compression limited to 3.5‰ strain and no relation for concrete in tension. Even EC4 does not provide instructions regarding modelling of nonlinear behaviour of concrete inside the steel tube. Concrete material curve should include the

confinement strengthening especially beyond the current strain limit in the descending branch of the curve. Therefore, in the paper, a simple proposal was made to extend this curve to consider the effect of confinement. Model 3 showed good agreement with test results regarding the full-range N-ε diagram. The simplified EC4 section strength calculations are moderately conservative but accurate enough for practical applications.

ACKNOWLEDGEMENTS

REFERENCES

[1] M. L. Radovanovic, J. Z. Nikolic, J. R. Radovanovic, and S. M. Kostic, Structural Behaviour of Axially Loaded Concrete-Filled Steel Tube Columns during the Top-Down Construction Method, Applied Sciences, vol. 12, no. 8, Apr. 2022, doi: 10.3390/app12083771.

[2] Y. F. Yang and L. H. Han, Concrete filled steel tube (CFST) columns subjected to concentrically partial compression, Thin-Walled Structures, vol. 50, no. 1, pp. 147–156, Jan. 2012, doi: 10.1016/J.TWS.2011.09.007.

[3] F. xing Ding, W. jun Wang, D. ren Lu, and X. mei Liu, Study on the behavior of concrete-filled square double-skin steel tubular stub columns under axial loading, Structures, vol. 23, pp. 665–676, Feb. 2020, doi: 10.1016/j.istruc.2019.12.008.

[4] Y. Gunawardena and F. Aslani, Finite element modelling of concrete-filled spiral-welded mild-steel tube short and long columns, Structures, vol. 30, pp. 1020–1041, Apr. 2021, doi: 10.1016/j.istruc.2021.01.074.

[5] Z. Bin Wang, Z. Tao, L. H. Han, B. Uy, D. Lam, and W. H. Kang, Strength, stiffness and ductility of concrete-filled steel columns under axial compression, Engineering Structures, vol. 135, pp. 209–221, Mar. 2017, doi: 10.1016/j.engStructures2016.12.049.

[6] N. F. Hany, E. G. Hantouche, and M. H. Harajli, Finite element modeling of FRP-confined concrete using modified concrete damaged plasticity, Engineering Structures, vol. 125, pp. 1–14, Oct. 2016, doi: 10.1016/j.engStructures2016.06.047.

[7] E. Ellobody, Nonlinear behaviour of eccentrically loaded FR concrete-filled stainless steel tubular columns, Journal of Constructional Steel Research, vol. 90, pp. 1–12, 2013, doi: 10.1016/j.jcsr.2013.07.018.

[8] V. W. Y. Tam, Z. Bin Wang, and Z. Tao, Behaviour of recycled aggregate concrete filled stainless steel stub columns, Materials and Structures, vol. 47, no. 1–2, pp. 293–310, Jan. 2014, doi: 10.1617/s11527-013-0061-1.

[9] Y. Tang, S. Fang, J. Chen, L. Ma, L. Li, and X. Wu, Axial compression behavior of recycled-aggregate-concrete-filled GFRP–steel composite tube columns, Engineering Structures, vol. 216, Aug. 2020, doi: 10.1016/j.engStructures2020.110676.

[10] W. H. Zhang, R. Wang, H. Zhao, D. Lam, and P. Chen, Axial-load response of CFST stub columns with external stainless steel and recycled aggregate concrete: Testing, mechanism analysis and design, Engineering Structures, vol. 256, Apr. 2022, doi: 10.1016/j.engStructures2022.113968.

[11] Z. Tao, Z. Bin Wang, and Q. Yu, Finite element modelling of concrete-filled steel stub columns under axial compression, Journal of Constructional Steel Research, vol. 89, pp. 121–131, 2013, doi: 10.1016/j.jcsr.2013.07.001.

[12] R. U. D. S. C. Providence, ABAQUS, User manual. Version 6.9. 2009.

[13] Y. M. M. Tomii, K. Yoshimura, Experimental studies on concrete filled steel tubular stub columns under concentric loading, in Proceedings of the International Colloquium on Stability of Structures under Static and Dynamic Loads, 1977, pp. 718–741.

[14] European committee for standardization, EN 1994-1-1: Eurocode 4: Design of composite steel and concrete structures-Part 1-1: General rules and rules for buildings, 2004.

[15] Deretić-Stojanović Biljana, Kostić Svetlana, and Stošić Saša, Analysis of composite steel and concrete columns, Building materials and structures, vol. 54, no. 1, pp. 62–79, 2011

[16] L. H. Han, G. H. Yao, and Z. Tao, Performance of concrete-filled thin-walled steel tubes under pure torsion, Thin-Walled Structures, vol. 45, no. 1, pp. 24–36, Jan. 2007, doi: 10.1016/j.tws.2007.01.008.

[17] European committee for standardization, prEN 1992-1-1: Design of concrete structures - Part 1-1: General rules - Rules for buildings, bridges and civil engineering structures, 2021.

[18] European committee for standardization, EN 1993-1-1: Eurocode 3: Design of steel structures - Part 1-1: General rules and rules for buildings, 2005.

[19] G. B. Hajjar JF, A cyclic nonlinear model for concrete-filled tubes formulation., Journal of Structural Engineering, ASCE, no. 123(6), pp. 736–44, 1997.

[20] J. M. Portolés, M. L. Romero, F. C. Filippou, and J. L. Bonet, Simulation and design recommendations of eccentrically loaded slender concrete-filled tubular columns, Engineering Structures, vol. 33, no. 5, pp. 1576–1593, May 2011, doi: 10.1016/j.engStructures2011.01.028.

Marija Milojević[1], Strahinja Ljaljević[2], Vitomir Racić[3], Miroslav Marjanović[4], Marija Nefovska-Danilović[5]

SOFTVER ZA PRORAČUN VIBRACIJA MEĐUSPRATNIH KONSTRUKCIJA USLED DINAMIČKE SILE PEŠAKA

Rezime:

Trendovi u savremenoj arhitekturi, koji diktiraju projektovanje komercijalnih i stambenih zgrada sa otvorenim prostorom, prouzrokovali su problem prekomernih vibracija međuspratnih konstrukcija velikih raspona usled aktivnosti ljudi koji se po njima kreću. Saniranje prekomernih vibracija već izgrađenih konstrukcija je skupo i vremenski zahtevno. Zbog toga je najefikasnije i najekonomičnije ovaj problem eliminisati već u fazi projektovanja. U radu je predstavljen softver za procenu vibracija međuspratnih konstrukcija izazvanih pešačkim opterećenjem, jednostavnog grafičkog okruženja i pogodan za svakodnevnu upotrebu u projektovanju.

Ključne reči: vibracije, međuspratna konstrukcija, dinamička sila pešaka

SOFTWARE FOR CALCULATION OF PEDESTRIAN-INDUCED VIBRATION OF FLOORS

Summary:

Trends in contemporary architecture towards open-plan spaces in commercial and residential buildings have created problems with excessive vibrations of large-span floors induced by active people. Solving vibration serviceability problems of as-built structures is costly and time-consuming. Therefore, such a problem is the most efficiently and economically addressed at the design stage. This paper presents software developed by the authors for assessing pedestrian-induced vibrations of floors. The software is designed as a user-friendly graphical interface that could be utilised in everyday design practice.

Key words: vibration, floor, serviceability, pedestrian-induced load

---

[1] *Teaching assistant, PhD student, Faculty of Civil Engineering, University in Belgrade, mmilojevic@grf.bg.ac.rs*
[2] *HP Inc, Hewlett Packard Enterprise, Barcelona, strahinjaljaljevic@gmail.com*
[3] *Associate professor, Faculty of Civil Engineering, University in Belgrade, vracic@grf.bg.ac.rs*
[4] *Assistant professor, Faculty of Civil Engineering, University in Belgrade, mmarjanovic@grf.bg.ac.rs*
[5] *Associate professor, Faculty of Civil Engineering, University in Belgrade, marija@grf.bg.ac.rs*

1. INTRODUCTION

Development of modern, high-strength materials has supported trends in contemporary architecture toward open-plan spaces in commercial and residential buildings. Engineers have been enabled to design long-span and lightweight floors with a tendency towards lower natural frequencies and reduced effective damping. Therefore, floors have become more dynamically responsive, and vibration serviceability (VS) issues have become more prominent [1, 2].

When people walk, they induce dynamic forces that cause structural vibrations. These vibrations are small and rarely cause structural damage. However, excessive vibrations can cause human discomfort and malfunction of vibration-sensitive equipment [3]. Solving VS problems of as-built structures is costly and time-consuming. Only significant changes in structural mass, stiffness or damping can produce a noticeable reduction in vibration. Therefore, such a problem is the most efficiently and economically addressed at the design stage.

Early vibration design criteria were formulated to limit the floor's fundamental frequency or self-weight deflection to prevent excessive vibration. SCI P076 [4], published in 1989, was the first widely recognised design guideline pertinent to the vibration of floors based on the performance-based assessment approach. It described the calculation procedure for predicting the floor vibration response that could arise from a pedestrian walking. In addition, it made an essential distinction between the floors prone to resonant vibrations due to footfall excitation (*low-frequency floors* – LFF) and those whose response is a series of transients due to each footfall (*high-frequency floors* - HFF). Until recently, for floor VS, Eurocode [5] have been providing recommendations for limiting the fundamental frequency of floors. It referred to ISO 10137 [6], which contains only general criteria for vibration perception. To complement the Eurocode in providing a simplified procedure for determining and verifying floor design due to human-induced vibrations, Hivoss guideline [7] was published. It defines the vibration classes depending on floor purpose. Based on the floor's fundamental frequency, modal mass and damping ratio, one can evaluate if the floor can satisfy a defined class. Guidelines popular in the USA(AISC [8]) and the UK(SCI P354 [9]) provide simplified equations for calculating peak or r.m.s. (*root-mean-square*) acceleration values due to walking excitation for both LFFs and HFFs. However, they are mainly focused on steel-concrete composite floors.

The calculation of the human-induced vibration is complicated, even with the floor's most straightforward geometry and material. Floors with complex shapes and those made of non-conventional building materials emphasise the need for a reliable predictive tool to evaluate their vibration performance. Arup's methodology [10], based on the basic principle of structural dynamics, applies to any structure without limits regarding the floor complexity and material. Pavic et al. presented the software VSATs [11] with several procedures for assessing the VS of floors. However, this software was developed in-house and is not made available to the public.

The lack of commercially available software for VS assessment of floor structures that would enable a designer to carry out complex and lengthy hand calculations in a fraction of a second is the key motivation behind the research described in this paper. This paper presents *Hindu,* a prototype of such software that has been developed by the authors for research purposes so far. The *Hindu* is designed as a user-friendly graphical interface (GUI) that provides quick dynamic response calculation and effective visualisation of calculated responses. Thus, it has a great potential to simplify design and make it more user-friendly and reliable.

2. BASIC PRINCIPLES IN ESTIMATING VIBRATION LEVELS

This Section aims to present the fundamental principles and terminology used in VS assessment applied in *Hindu*. According to ISO 10137 [4], every VS problem can be rationalised into vibration *source*, vibration *path*, and vibration *receiver*. Following that framework, the Section is organised to review these three components regarding pedestrian-induced vibration of floors.

2.1. PEDESTRIAN-INDUCED FORCE AS VIBRATION SOURCE

Floors are constantly subjected to excitation induced by human activity. Extensive studies [12] showed that many factors, such as pedestrian height, gender, weight, and walking speed, contribute to the variability of induced dynamic load. Additionally, two types of floor response require different load models: one for resonant response (LFFs) and the other for transient response (HFFs). When assessing the vibration response of LFF, the walking force F_p is assumed to be a perfectly periodic function, represented by a Fourier series:

$$F_p(t) = G + \sum_{h=1}^{N} \alpha_h G \sin(2\pi h f_p t - \varphi_h) \qquad (1)$$

where:
G is the pedestrian weight;
α_h is the Fourier's coefficient, or dynamic load factor (DLF) of the hth walking harmonic;
f_p is the walking frequency;
φ_h is the phase shift of the hth walking harmonic;
N is the total number of contributing harmonics.

Force models proposed by various authors [10, 13-15] differ according to the parameters used in Eq. (1), most commonly in the N and DLF values.

Response of the HFFs is dominated by the impulsive, transient response. In that case, it is appropriate to model a dynamic load as a series of impulses representing each footstep [10, 15].

2.2. FLOOR AS VIBRATION PATH

The floor structure itself is a medium for transmitting vibrations from the source to the receiver. The floor's modal characteristics: natural frequencies, mode shapes, modal masses, and damping define the vibration path. Guidelines usually offer simplified expressions for calculating the floor's modal characteristics. These expressions are limited to floors with simple geometry and boundary conditions. For reliable response estimation, it is necessary to determine floor modal properties as accurately as possible. Nowadays, the Finite element method (FEM) is the most commonly used. Using FEM, natural frequencies, modal masses and mode shapes can be determined. However, damping cannot be calculated numerically. It is usually adopted according to experimental testing (if possible), experience or recommendations.

2.3. VIBRATION RECEIVER

Applying multi-modal analysis, the floor's vibration response is calculated based on the calculated modal properties, assumed damping and a given pedestrian force model. Once the response is calculated, the appropriate vibration criteria for the floor's serviceability should be specified depending on the vibration receiver.

ISO 10137 [6] distinguishes three types of receivers: human occupants, building contents and building structures. Excessive vibration can cause minor damage to structural and non-structural elements if the receiver is the building structure. If the building contents are the receiver, the criteria include a vibration level that assures the sensitive equipment's functioning. Finally, if humans are the receiver, their comfort, life quality, and working efficiency can be reduced.

The acceptable vibration level for people depends on their environment and activity [6]. In BS 6472:1992 guide [16], base curves representing vibration magnitudes for approximately equal human responses in different environments were defined. The vibration level above the base curve increases the probability of adverse comments. The complaints are uncommon if the vibration magnitude is below the base curve.

3. SOFTWARE DEVELOPMENT

Hindu is a Python-based [17] GUI-based software developed by authors for vibration response calculation of floors. Previously developed solver [18] for calculating vibration response based on modal superposition method was upgraded to include pre-and post-processing modules. Fundamental methods incorporated into the software are presented in the first part of this Section (3.1). After that, GUI and its use are illustrated (Section 3.2). It is important to highlight that *Hindu* is fully functional software but still in the developing stage. The main idea is to make the software and GUI expandable and incorporate more features in the future.

3.1. CALCULATION OF VIBRATION RESPONSE

Response calculation process using *Hindu* software consists of several steps, following the framework explained in Section 2. The first step is to define the vibration path. As *Hindu* does not calculate the modal characteristics of the floor, they are imported from the FEM-based software. When the floor's characteristics are loaded, the next step is to define the dynamic force: the user can choose between several so far implemented force models. The user can set the walking path for moving dynamic force, simulating the pedestrian walking. After the receiver point is defined, the vibration response can be finally calculated. The response calculation procedure is based on the modal superposition method [19]. Therefore, it does not contain limitations regarding floor complexity or material. So far, *Hindu* cannot estimate the serviceability of the floor. According to the calculated response and the target vibration level, the user should determine if the floor satisfies the vibration criteria (e.g. proposed in [16]).

3.2. HINDU GRAPHICAL USER INTERFACE

To make *Hindu* user-friendly, a GUI has been developed by using Python's package Tkinter as an application. Running the software opens the start window presented in Figure 1. The *start* button opens the main window (Figure 2).

3.2.1. Main window

Five critical sections of the main window are defined (Figure 2).

The *Menu bar* contains five tabs: File, Floor, Standards, Options and Help (Figure 2a). The tabs were designed to facilitate typical dynamic response analysis in *Hindu*.

The *Mode selection* section (Figure 2b) allows users to select modes to be included in the modal superposition-based dynamic response analysis.
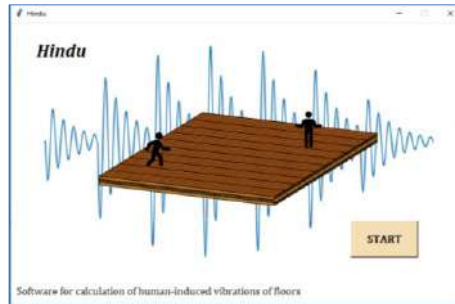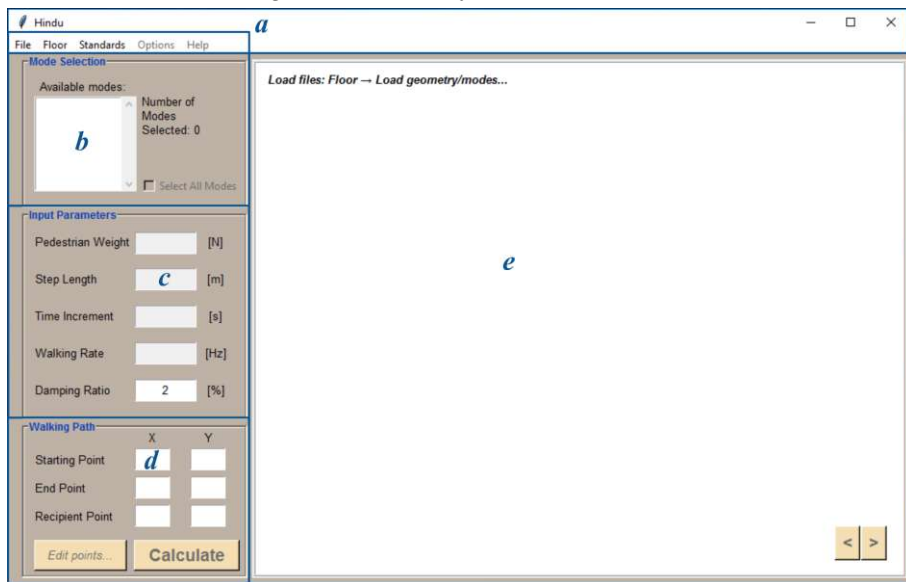
Figure 1 – Hindu software start window

Figure 2 – Hindu software main window and its components: a-Menu bar, b-Mode Selection, c-Input Parameters, d-Walking Path, e-Canvas

Before performing the analysis, several parameters should be defined in the *Input Parameters* section (Figure 2c). Dynamic load represented by the pedestrian weight, step length and walking frequency, as well as the damping ratio and time increment, are input parameters required to solve the SDOF equation of motion for each mode.

In the *Walking Path* section (Figure 2d), the user can define the walking path as a straight line by choosing the start and endpoint. Afterwards, the user can select the receiver point.

Most of the main window is occupied by *Canvas* (Figure 2e), which displays and visualises the loaded floor's modal characteristics and results of the performed modal analysis.

3.2.2. Load FEM model

The *Floor* tab contains two options (Figure 3a): *Load geometry/modes* and *Define walking path*. Users can insert modal characteristics calculated in the FEM software by clicking the *Load geometry/modes*. So far, *Hindu* enables the user to import modal characteristics of the analysed

260

floor from Abaqus CAE [20]. When modal characteristics are loaded, they are graphically presented in *Canvas* (Figure 3b), and available modes are listed in section *Mode Selection*.
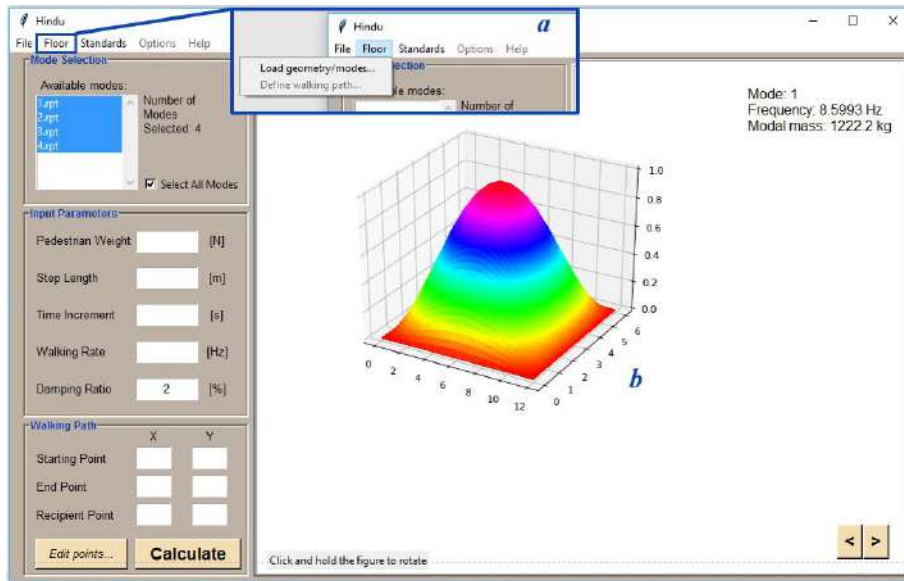

Figure 3 – (a) Floor tab – available options, (b) Displayed loaded modal characteristics

3.2.3. Design guidelines and recommendations

The *Standards* tab enables the user to select the dynamic force model (Figure 4).

Option *ARUP* uses walking force models defined in [10] for both LFFs and HFFs. The methodology distinguishes if the floor is LFF or HFF based on the fundamental frequency and applies an appropriate dynamic force model. Some harmonic force models recommended by various authors are also implemented. Force models proposed by Rainer [13] and Kerr [14] can be applied only to LFFs, while Živanović [15] suggested an advanced force model that can be used for both LFFs and HFFs.
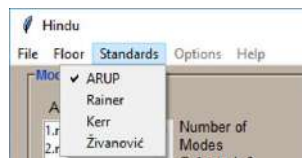
Figure 4 – Standard tab – implemented procedures/dynamic force models

3.2.4. Visualisation & reports

Once all parameters are defined, the software calculates floor response in the receiver point by pressing the button *Calculate*. The time-history acceleration diagram is, by default, presented on *Canvas*, and the maximum value is given as well. In addition, the user can switch between the time-history diagrams for acceleration, velocity, displacement, or calculated so-called running a_{rms} trend (Figure 5).

Finally, the results of the performed analysis can be exported into .pdf and .doc file formats. The file contains the results of the modal analysis, specified input parameters, defined walking path, as well as time-history diagrams. Created reports can be attached to the floor design project.
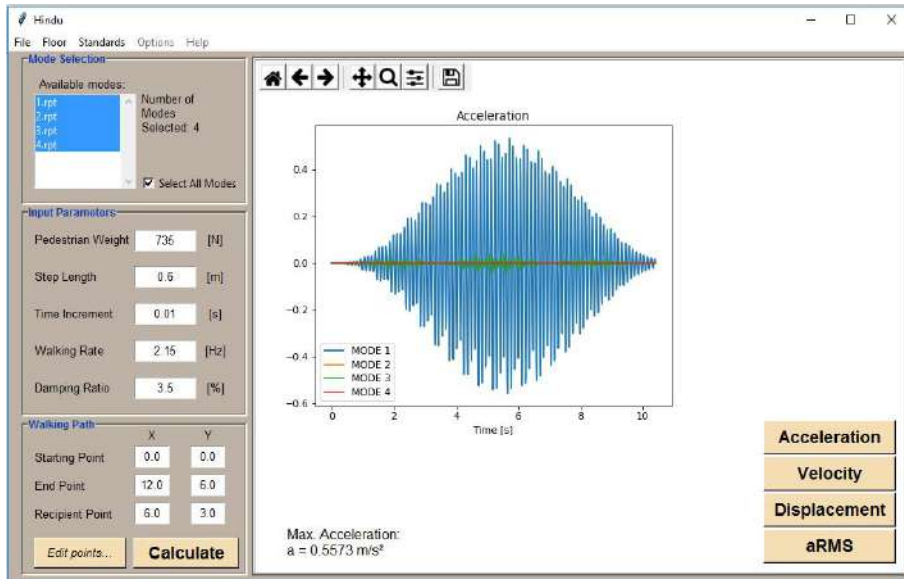

Figure 5 – Displaying results on Canvas

4. NUMERICAL EXAMPLE

Main features and efficiency of *Hindu* are demonstrated through the numerical example of the cross-laminated timber (CLT) floor. Due to the high stiffness-to-weight ratio, CLT structures are flexible and may experience vibration issues. The floor's dimensions are 6x12m, and the cross-section comprises five 3cm thick crosswise layers (Figure 6). The floor is simply supported (S) along all four edges. The outer layers are oriented in the *y*-direction.
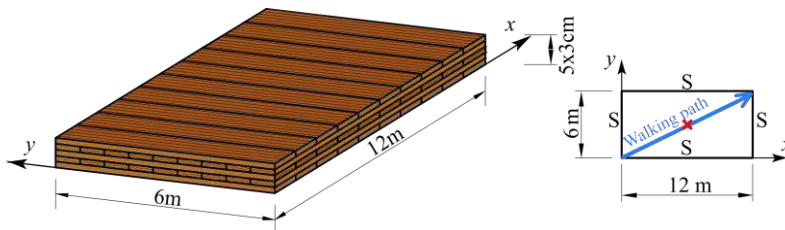
Figure 6 – Numerical example - CLT floor

The CLT floor is modelled in Abaqus CAE using S4R finite elements (4-node linear rectangular shell element with reduced integration) with a composite section. Each lamina is made of a C24 timber class with material properties presented in Table 1. A mesh size of 0.1m is used. Results of the modal analysis are exported from Abaqus CAE, and the first four natural frequencies and modal masses are elaborated in Table 2.

262

Based on Arup's applied methodology, the floor is classified as LFF. Thus, it is prone to a resonant build-up response. The pedestrian walks along the walking path defined according to Figure 6. The walking frequency of 2.15 Hz is adopted, so the fourth harmonic of the dynamic walking force coincides with the floor's fundamental frequency. Additional parameters used in the numerical example are pedestrian weight 735 N, step length 0.6 m, damping ratio 3.5% and time increment 0.01 s.

Table 1 – Material properties for C24 timber class of CLT panel

ρ [kg/m^3]	E_L [MPa]	$E_R=E_T$ [MPa]	$G_{LR}=G_{LT}$ [MPa]	G_{RT} [MPa]	v_{LT}	v_{LR}	v_{RT}
450	11000	370	690	69	0.49	0.39	0.64

Table 2 – Natural frequencies and modal masses of CLT floor

Mode	1	2	3	4
Frequency [Hz]	8.60	10.40	14.57	21.21
Modal mass [kg]	1222.2	1219.5	1219.2	1220.5

Calculated response in the receiver point (marked with a red x in Figure 6), in terms of time-history diagrams for acceleration, velocity, displacement, and running arms trend (moving average), is presented in Figure 7.
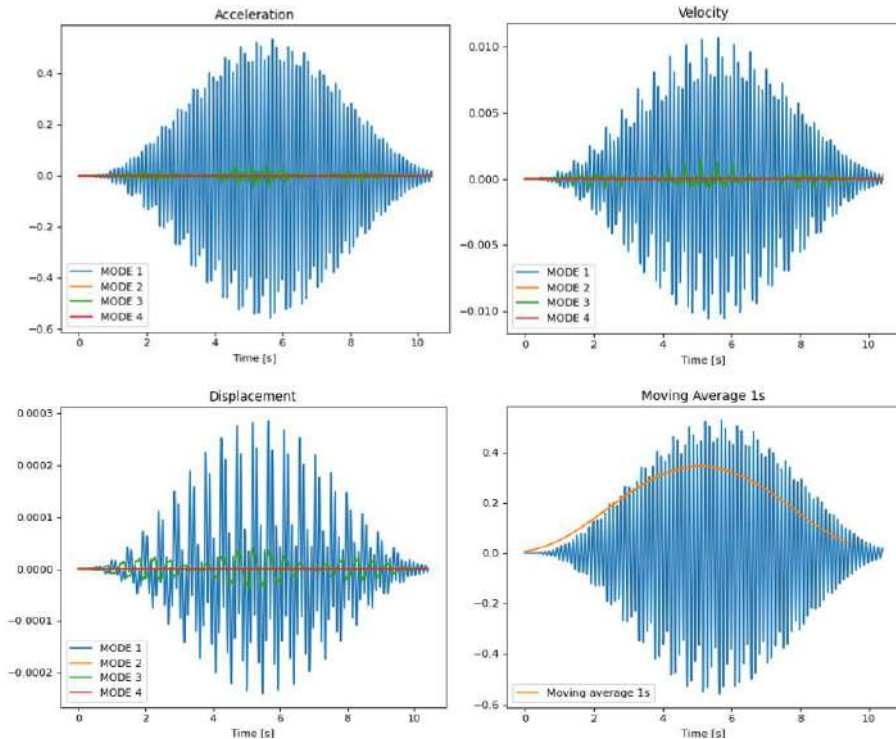

Figure 7 – Calculated response of 6x12 m CLT floor

263

5. CONCLUSION

The era of a rough estimation of the floor vibration is over, and performance-based methods are widely used to assess the floor serviceability under human-induced loading.

Hindu software developed for VS assessment of floors subjected to pedestrian-induced dynamic excitation is a step in the right direction. Basic properties of the developed GUI for pre- and post-processing as well as the calculation procedure were demonstrated through the illustrative example.

The software has several limitations since it is still in its infancy. One of them is compatibility with only one FEM software for modal analysis. Additionally, one guideline and a few recommendations for vibration calculation have been implemented so far. *Menu bar* functions (*Options*, *Help*) that could provide users additional benefits have not been developed.

The software's significant advantage is that Python is open source programming package. It has a simple GUI and is intuitive and straightforward. It can be used for floors of any shape and material. *Hindu* offers the option of calculation reports and has a great potential to be utilised in research and design. One of *Hindu*'s essential features is the potential for further upgrades. The plan for future work will be directed toward creating possibilities to import modal properties from other FEM-based software, to include additional guidelines for calculating the floor's dynamic response and finally, to make *Hindu* an efficient tool for vibration serviceability assessment regarding human-induced vibrations.

ACKNOWLEDGEMENTS

REFERENCES

[1] S. Živanović, A. Pavić and P. Reynolds, "Vibration serviceability of footbridges under human-induced excitation: a literature review," *Journal of Sound and Vibration,* vol. 279, pp. 1-74, 2005.

[2] M. Setareh and M. Lovelace, "Vibration analysis and design of a structure subjected to human walking excitations," *Shock and Vibration,* vol. 17, pp. 631-639, 2010.

[3] A. Pavic and P. Reynolds, "Vibration serviceability of long-span concrete building floors. Part 1: review of background information," *The Shock and Vibration Digest,* vol. 34, 2002.

[4] T. A. Wyatt, "Design Guide on the Vibration of Floors," The Steel Construction Institute, London, 1989.

[5] "Eurocode — Basis of structural design," European Committee of Standardization (CEN), Bruxelles, 2004.

[6] "Bases for design of structures - Serviceability of buildings and walkways against vibrations," International Organization for Standardization, 2006.

[7] M. Feldmann, C. Heinemeyer, M. Lukic, E. De Sa Caetano, A. Cunha, A. Goldack, A. Keil, M. Schlaich, S. J. Hicks, A. Smith, O. Hechler, R. Obiala, F. Galanti and P. Waarts, "Human-induced vibration of steel structures (Hivoss)," Research Fund for Coal and Steel, European Commission, Luxembourg, 2010.

[8] T. Murray, D. Allen, E. Ungar and B. Davis, "Vibrations of Steel-Framed Structural Systems Due to Human Activity," American Institute of Steel Construction, 2016.

[9] A. Smith, S. Hicks and P. Devine, "Design of Floors for Vibration: A New Approach," The Steel Construction Institute, Berkshire, 2009.

[10] M. Willford and P. Young, "A Design Guide for Footfall Induced Vibration of Structures," The Concrete Centre, London, 2006.

[11] A. Pavic, J. M. W. Brownjohn and S. Živanović, "VSATs software for assessing and visualising floor vibration serviceability based on first principles," in *Structures Congress*, Orlando, Florida, 2010.

[12] V. Racic, A. Pavic and J. M. Brownjohn, "Experimental identification and analytical modelling of human walking forces: Literature review," *Journal of Sound and Vibration,* vol. 326, pp. 1-49, 2009.

[13] J. H. Rainer, G. Pernica and D. E. Allen, "Dynamic loading and response of footbridges," *Canadian Journal of Civil Engineering,* vol. 15, pp. 66-71, 1988.

[14] S. Kerr and N. Bishop, "Human induced loading on flexible staircases," *Engineering Structures,* vol. 23, pp. 37-45, 2001.

[15] S. Živanović and A. Pavić, "Probabilistic Modeling of Walking Excitation for Building Floors," *Journal of Performance of Constructed Facilities,* vol. 23, no. 3, pp. 132-143, 2009.

[16] "Guide to Evaluation of human exposure to vibration in buildings (1 Hz to 80 Hz)," British Standard Institution, London, 1992.

[17] G. van Rossum, "Python Tutorial 3.10.4," Python Software Foundation, 2022.

[18] M. Milojević, "https://github.com/mmilojevicgrf/CLT_vibration," Belgrade, 2022.

[19] R. W. Clough and J. Penzien, Dynamics of Structures, Berkeley, CA: Computers & Structures, Inc., 1995.

[20] "Abaqus, User manual, Version 6.9," DS SIMULIA Corp, Providence, RI, USA, 2009.

R-13

Kongres 2022
Congress 2022

Meri Cvetkovska[1], Zlatko Zafirovski[2], Ana Trombeva-Gavriloska [3]

POŽARNA OTPORNOST BETONSKE OBLOGE PUTNOG TUNELA

Rezime:

Požar predstavlja incidentno opterećenje konstrukcija. Iskustvo je pokazalo da se u slučaju požara razvijaju ekstremno visoke temperature, usled čega vrlo često dolazi do urušavanja noseće konstrukcije tunela, najčešće usled eksplozivnog prskanja betona. U okviru ovog rada opisano je nekoliko požarnih krivi, koje se obično koriste u zemljama EU. Razrađena je metodologija za analizu požarne otpornosti putnih tunela na osnovu performansi. Na jednoj studiji slučaja opisan je i primenjen numerički postupak za definisanje ponašanja obloge tunela u slučaju nominalne požarne krive (standardni požar). Analiziran je uticaj požara na naponsko-deformaciono stanje betonske konstrukcije tunela i predložene su mere za pravilno projektovanje tunela u smislu povećanja otpornosti na požar.

Ključne reči: tunel, betonska obloga, požarna kriva, termička analiza, statička analiza

FIRE RESISTANCE OF CONCRETE LINING OF ROAD TUNNEL

Summary:

Fire is an incidental load on structures. Experience has shown that in the event of a fire, extremely high temperatures are developed, as a result of which very often a colapse of the tunnel bearing structure happens, usually caused by spalling of concrete. In the framework of this paper several fire curves, usually used in EU countries, are described. The fire curves characteristics are defined and the most proper fire curve for typical tunnel, as case study, is recomended. A methodology for fire resistance analysis of road tunnels, based on the performance, is elaborated. A numerical procedure for defining the behavior of the tunnel lining in case of nominal fire curve (standard fire) is described and applied on one case study. The impact of the fire on the stress-strain state of the concrete structure of a tunnel is analyzed and measures for proper tunnel design in terms of increasing the fire resistance is proposed.

Key words: tunnel, concrete lining, fire curve, thermal analysis, stress-strain analysis

---

[1] *Prof., PhD, Faculty of Civil Engineering, University "Ss. Cyril and Methodius" (UKIM), Skopje, Republic of North Macedonia, cvetkovska@gf.ukim.edu.mk*
[2] *Prof., PhD, Faculty of Civil Engineering, University "Ss. Cyril and Methodius" (UKIM), Skopje, Republic of North Macedonia, zafirovski@gf.ukim.edu.mk*
[3] *Prof. PhD, Faculty of Architecture, University "Ss. Cyril and Methodius" (UKIM), Skopje, Republic of North Macedonia, agavriloska@arh.ukim.edu.mk*

1. INTRODUCTION

Fires in road tunnels are usually result of ignition of vehicles using the tunnel and are mainly caused by: electrical defects (most common cars); overheating of breaks (about 60% to 70% of fires caused by trucks) and other defects leading to self-ignition of the vehicle [1-3].

Other reasons, which are very rare, but still exist, are: car accidents; technical defects (self-ignition) of equipment in tunnels and improper performance of maintenance work.

Theoretically, the frequency of tunnel fires is related to factors such as: the length of the tunnel, traffic density, speed control and slope. These factors should be taken into account when comparing different tunnels. Therefore, to include the effects of tunnel length and traffic density, the frequency of fires is estimated not only by the number of fires per tunnel, but also by the number of vehicles per kilometer. All these factors define the fire risk.

In general, according to the options given in Eurocodes, a nominal approach for designing fire-safe tunnels has been adopted. Normally, in the past, the rate of increase of fire was adopted in the range up to a maximum value of 30 MW. However, the experience of real large tunnel fires and the tests performed in real dimensions indicated that there could be much larger fires. For this reason, different fire models have been adopted in different countries, ranging from 20 to 300 MW.

Given the large range of fires with a varying intensity, it is evident that the choice of fire intensity for a particular tunnel cannot be precisely defined without including all relevant factors. Several factors need to be considered, such as the type of traffic, the ventilation system, the geometry of the tunnel and the fire-fighting system. Even in the nominal approach, when the fire is defined by a prescribed temperature-time curve, such considerations are taken into account.

In order to provide more guidelines for the selection process, a methodology for a performance-based approach has been developed in this paper and a numerical analysis of the tunnel lining behavior in the case of nominal (standard) fire has been conducted. The influence of the design fire on the stress-strain state of the tunnel was analyzed. Tunnels with and without reinforcement of the secondary lining and with different lining thickness were analyzed. Based on the obtained results, measures for appropriate design of tunnels from the aspect of increasing their fire resistance are proposed.

2. FIRE SAFETY OF ROAD TUNNELS

As a result of more intensive road traffic and the need of fast underground communications, the probability of accidents in tunnels caused by fire has increased. Additional factors that increase the fire risk are: the increased length of modern tunnels; increased vehicle speed; transport of dangerous goods; two-way traffic with physically undivided carriageways; increased fire load as a result of increased vehicle volume and increased transport capacity; mechanical defects in motor vehicles.

There are three reasons for taking protection measures against fire in a tunnel. The first and most important reason is the safety of the passengers. To fulfill this condition, on time evacuation is required, and it depends not only on the stability of the structure, but also on the functionality of the ventilation system, the accessibility of the evacuation exits, etc. The second reason is to enable the tunnel to function and the traffic to run smoothly. Very often, fires in tunnels cause explosive spalling of concrete and collapse of parts of the structure. The third reason are the

economic losses caused not only by the structural damages, but much more by the non-functionality of the tunnel and the interruption of the traffic during the rehabilitation period, which is certainly a long period of time.

In order to ensure adequate fire safety of tunnels, it is necessary to pay attention to the following aspects: fire resistance of the load-bearing structure; air supply system; ventilation and smoke extraction system; construction of evacuation pats protected from smoke and flames; active and passive fire detection systems; fire extinguishing systems; fire doors and alarm systems.

3. FIRE MODELS FOR ROAD TUNNELS

A special feature that makes tunnel fires different from other fires (for example, those that occur in buildings) is the sudden rise in air temperature under the vault, which can reach over 1000 ° C in just a few minutes. This phenomenon negatively affects both the fire extinguishing process (rapid extinguishing is almost impossible) and the structural system.

In order to be able to perform appropriate thermal and static analysis of the tunnel structure and to define its fire resistance, it is first necessary to define the temperature of the fluid (air) inside the tunnel. This is possible by implementing a numerical procedure that solves the differential equations of heat release and transfer based on the laws of fluid dynamics (CFD).

The temperature inside the tunnel is influenced by: the length and geometry of the tunnel, the fire load, the burning time of the primary ignited vehicle, the materials that are built into the structure, etc. The ventilation has an effect on the HRR of the burning items and should be considered when designing the type of fire curve and the period of required fire protection.

Eurocode 1-1-2 [4], which treats fire as an incidental load for the structure, defines the fire load due to the increase in temperature in the fire sector in time. Nominal curves "temperature - time" are defined, but they are valid only for indoor fires (buildings). The European countries, in their national regulations for design of tunnels, define curves "time-temperature" for a nominal fire in a tunnel [1, 2]. They are defined on the basis of results from conducted fire risk analyses, laboratory tests and experiences of fires in tunnels.

The most characteristic and often used "time-temperature" curves are presented in Figure 1. The cellulose or ISO 834 fire curve is typical for fires in buildings. The Hydrocarbon curve is applicable where small petroleum type fires might occur, e.g. car fuel tanks, petrol or oil tankers, certain chemical tankers. The temperature rise in case of Hydrocarbon curve is far more rapid than in case of ISO 834 fire curve, but after the initial 30 min. the temperature follows an almost horizontal line. The RABT-ZTV curve was developed in Germany as a result of a series of tunnel fire tests, such as Eureka project. In RABT curve the temperature rise is very rapid, up to 1200°C within 5 minutes. The duration of this temperature is shorter than for other fire curves and drops after 30 minutes in case of road tunnel, and after 60 minutes in case of railway tunnels.

The RSW curve was developed in Netherlands. This fire curve is based on the assumption that in a worst case scenario, a fuel oil or petrol tanker with a fire load of 300 MW lasting up to 120 minutes could occur. This curve is usable for enclosed area, such as tunnel, where there is little or no chance of heat dissipating into the surrounding atmosphere. The RWS curve simulates the initial rapid growth of a fire in case of petroleum tanker source, and gradual drop in temperatures when the fuel burnt off.

In the Netherlands, this curve lasts 120 minutes, as it is estimated that by then the temperature will have dropped to a level that will allow firefighters to approach the vehicle and put out the

fire. This curve is also used in Switzerland and Austria, but the time is 180 minutes as the tunnels under the mountain massifs are significantly longer. When this curve is applied, the criterion for failure of the structure is taken to be the moment when the temperature of the surface of the primary tunnel lining, which is protected by concrete secondary tunnel lining or by installing insulation materials, reaches 380°C, and the temperature in the reinforcement does not exceed 250°C. If high-strength concrete is used, which is more sensitive to explosive spalling, the surface temperature is limited to 250°C.
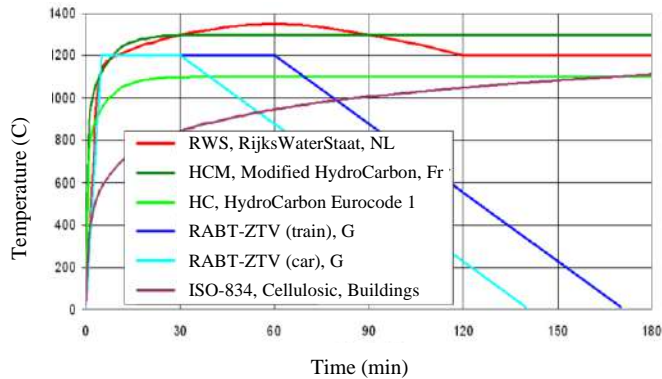

Figure 1 - Standard temperature-time curves used to simulate a fire in a tunnel

4. FIRE RESISTANCE ANALYSIS OF CONCRETE LINING OF ROAD TUNNEL

As it was already mentioned, one of the factors that influence the fire safety of tunnels is the stability of the tunnel structure which is exposed to extremely high temperatures. This problem connects two parallel analyses: thermal analysis for defining the temperature distribution in the cross section of the tunnel linings and the stress-strain analysis for defining the structural response.

This paper presents the analysis results for a road tunnel exposed to RSW fire curve. For the analyses the program FIRE [5], based on Finite Element Method, was used. The tunnel length is about 900 m and belongs to the group of short tunnels. The road width is 3 x 3.50 m, the height of the tunnel is 4.70 m, with a slope of 2.5% to 4.0%.

On one part, the secondary tunnel lining is made of plain concrete, and on the other part as reinforced concrete arch structure. Concrete grade MB30 is applied. The minimum thickness at the top of the dome for section type 1 (plain concrete lining) is d = 30 cm, and for section type 2 (reinforced concrete lining) is d = 45 cm. The two cross-sections are shown in Figure 3.

The calculation of the fire resistance of the tunnel was performed in accordance with Austrian regulations. According to the characteristics of the traffic, the fire load is defined by the nominal fire curve RWS for 3 hours (180 min). The criterion for fire resistance is taken to be the moment when the temperature of the surface of the primary tunnel lining, which is protected by concrete secondary tunnel lining, reaches 380°C, and the temperature in the reinforcement does not exceed 250°C. The moment when one of these two criteria is reached is considered as time of fire resistance. The failure time of the secondary concrete lining is defined as a third criterion. Failure occurs as a result of temperature-induced stresses and in case of failure the primary lining is

directly exposed to fire, so the surface temperature of the concrete is almost equal to the air temperature inside the tunnel.
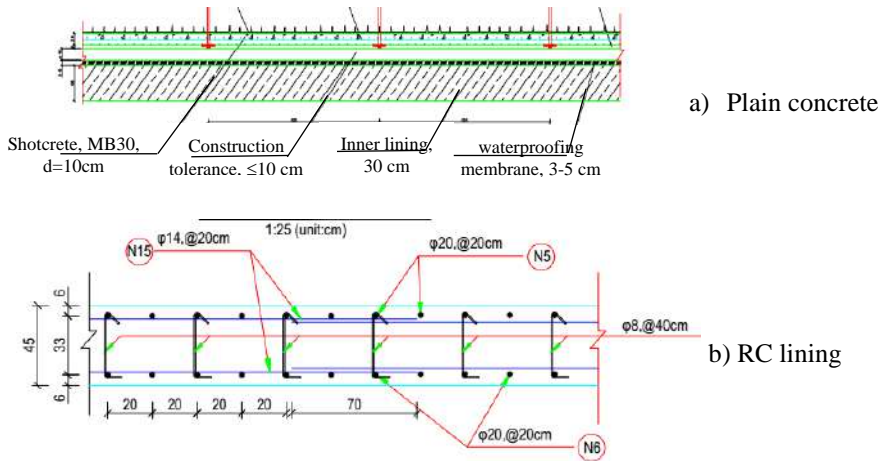

a) Plain concrete

b) RC lining

Figure 2 - Secondary tunnel lining: a) plain concrete d=30 cm, b) RC lining d=45 cm

The thermal analysis was performed for a 1,00 m width strip of the arch structure. Due to the axial symmetry, only one half of the arch structure was analysed. In the thermal analysis, in addition to the concrete lining, the waterproofing layer with a thickness of d = 3 cm, the free air space d = 10 cm and the primary reinforced concrete lining with a thickness of d = 10 cm were included. The discretization of the cross section was performed with 994 finite elements with 4 nodes, of which 680 were used for the secondary lining. The time step was Δt = 0.01 hours = 0.6 minutes = 36 seconds.

The temperature inside the tunnel was defined by the fire curve RWS, Figure 1, as the most appropriate fire load. When discretizing the secondary tunnel lining, the symmetry of the tunnel cross-section and the loads was used. 11 elements with a width of 1 m were used and were placed in such a way to follow the curvature of the tunnel lining (Figure 3a). The first element was fixed in the terrain, while the rotation and the horizontal displacement at the end point of the last element (highest point of the tunnel) were restricted and only vertical displacement was free.

Temperature-dependent physical and mechanical characteristics of concrete and steel (coefficient of thermal conductivity, specific heat capacity, density, compressive strength and tensile strength of concrete, tensile strength of steel and modulus of elasticity) were adopted in accordance with the recommendations given in EN1992-1-2 [4], while the thermal properties for the waterproofing and the air in the cavity were taken in accordance with the data given in the literature.

4.1. THERMAL ANALYSIS OF THE TUNNEL LINING

For the case of tunnel lining type 1 (secondary lining d=30 cm), isotherms in the cross section of the tunnel structure after 180 minutes of fire action are presented in Figure 3b.

According to Figure 3b, it could be concluded that the criterion for fire resistance concerning the temperature at the surface of the primary tunnel lining is not reached after 180 minutes of

fire exposure, as the temperature is lower than 380°C. The temperature in the reinforcement in the primary lining does not exceed 250°C, too.

In case of concrete lining type 2 (d=45 cm), isotherms in the cross section of the tunnel structure after 120 minutes and 180 minutes of fire action are presented in Figure 4. In this case the temperatures are much lower than in case of concrete lining type 1 (d=30 cm).

From aspect of surface temperatures of the primary tunnel lining, the both cross sections satisfy the fire resistance criteria in period longer than 3 hours.

a)   b)
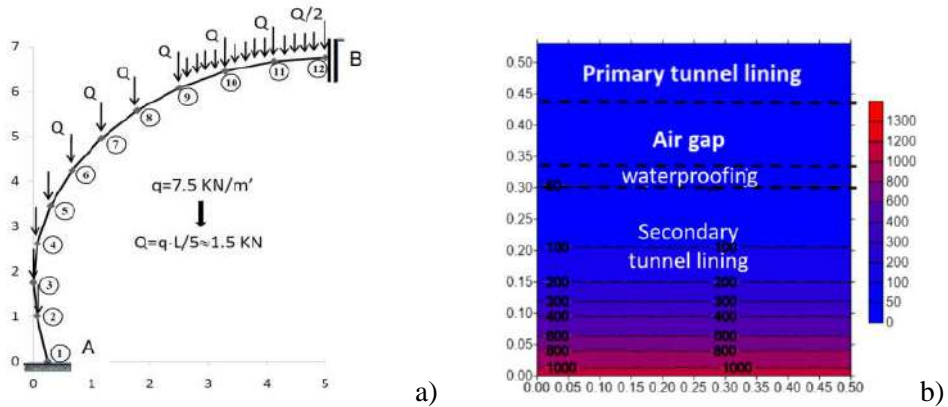
Figure 3 - a) Discretization of the tunnel structure; b) Isotherms in the cross section of tunnel structure in case of lining d=30 cm, after 180 min of fire exposure
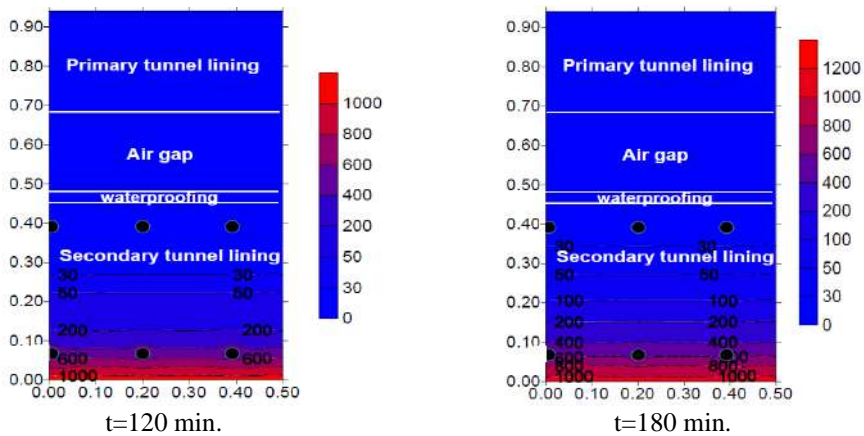
t=120 min.   t=180 min.

Figure 4 – Temperature distribution (isotherms) in the cross section of RC tunnel lining d=45 cm, after a) t=120 min. b) t=180 min. of fire exposure

4.2. STRESS-STRAIN ANALYSIS OF THE TUNNEL LINING

Additionally, the third criterion concerning the collapse of the secondary lining is controlled. The non-uniform temperature field in the initial moments of fire action (only the surface layers of the inner part of the lining are heated to more than 1000°C, while the layers on the opposite

side are at 20ºC) and the inability the thermal dilatation of the cross section to be freely realized, leads to additional bending moments.

If free thermal expansion of the secondary lining is possible, no axial compressive forces will occur and the bending moments caused by temperature difference will result in compression at the hot side of the cross section and tension at the opposite and cold side.

In case when the concrete lining is not reinforced (concrete lining type 1), there is no option for accepting the tensile forces and cracks will appear on the cold side of the lining. At the same time, in the hot inner zone, the compressive stresses reach up to 90% of the concrete strength for the respective temperature. When the cracked zone expands to more than 80% of the lining cross-section, the balance of the internal forces cannot be achieved and the cross-section fails due to crushing of the "hot" concrete. In this case the failure occurs only after t = 0.3 hours= 18 min. (Figure 5a).

In order to solve the problem with the bearing capacity of the secondary lining in the initial moments of fire exposure, there are two solutions: to prevent free dilatation by anchoring the secondary lining to the primary lining, or to install a minimum percentage of reinforcement at the inner cold side of the lining, for accepting the tensile forces. In both cases, the secondary lining achieves fire resistance for more than 6 hours. For the case of secondary concrete lining anchored into the primary concrete lining, the stresses in concrete are all the time in compression and after 3 hours of fire action are shown in Figure 5b.
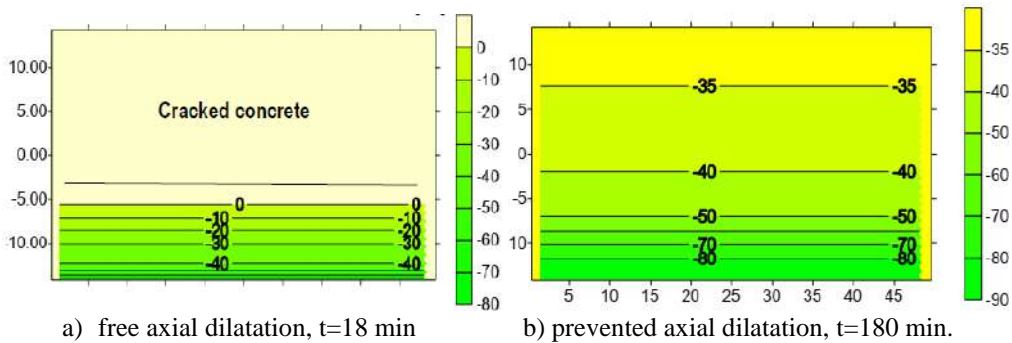

a) free axial dilatation, t=18 min   b) prevented axial dilatation, t=180 min.

Figure 5 – Stresses in secondary concrete lining as a percentage (%) of the concrete compressive strength for corresponding temperature ($\sigma c / fc(T)$),
a) free axial dilatation, (before failure), b) prevented axial dilatation, t=180 min.

Figure 6 presents the time dependent stresses at the top and the bottom edge of the secondary concrete lining, in case of minimal reinforcement ($\mu = 0.1\%$) placed in the tensioned (upper) zone of the cross section, expressed as a percentage of the bearing capacity of the concrete for the actual temperature ($\sigma c/fc(T)$). Due to the large temperature differences in the concrete (hot lower and cold upper part of the cross section) and the impossibility of free thermal expansion, after only 15 minutes of fire action the compression stresses in the lower zone increase significantly, while in the upper zone tensile stress occurs. Over time, as the temperature difference decreases (the temperature penetrates deeper into the cross section), the compressive stresses in the lower zone slowly decrease.

The tensile stresses in the upper zone have to be accepted by the reinforcement, which, even minimal, ensures the balance of the internal forces in the cross section (Figure 7).
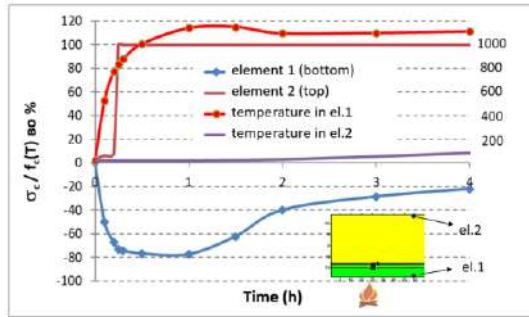
Figure 6 - Stresses at the top and bottom edge of the secondary concrete lining, in case of minimal reinforcement, as a percent of the concrete strength for current temperature ($\sigma_c/f_c(T)$)
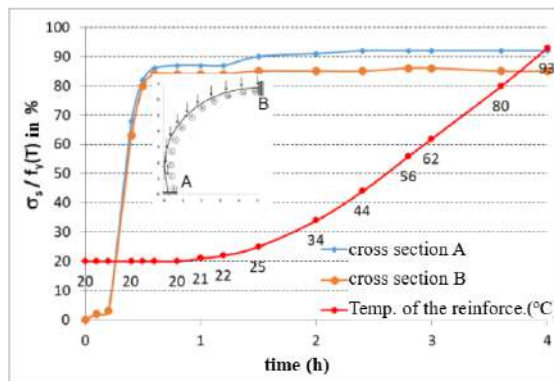

Figure 7 - Time dependent temperatures and stresses of the reinforcement in the top zone, for two typical cross sections

5. CONCLUSION

Based on the numerical analysis, it was determined that in order to ensure stability of the tunnel structure in case of fire, a reinforced concrete secondary lining has to be constructed. Due to the tensile stresses on the cold side of the lining, if there is no reinforcement, the secondary lining will collapse in the first twenty minutes of fire exposure and will not be able to protect the primary tunnel lining during the required period of fire resistance. Reinforcement of the secondary lining, even with a minimum percentage, will delay the moment of failure and will additionally reduce the risk of explosive spalling of concrete, which is a special problem in tunnels and occurs not only in high-strength concrete, but also in normal concrete.

REFERENCES

[1]   ASFP, Tunnel fire protection, www.promat-tunnel.com
[2]   Austrian Guideline Codes for Planning, Construction and Maintenance of Roads (RWS)
[3]   Directive of the European Parliament and of the Council on minimum safety requirements for tunnels in the Trans-European Road Network.

Milan Spremić[1], *Isidora Jakovljević*[2], *Nemanja Dinčić*[3]

POŽARNO OPTEREĆENJE KROVNE I FASADNE ČELIČNE KONSTRUKCIJE – REKONSTRUKCIJA SAVA CENTRA

Rezime:

Rekonstrukcija Sava Centra u Beogradu, kulturnog dobra Republike Srbije, podrazumeva radove na objektu, koji moraju da obezbede da konstrukcija kongresnog centra ispunjava sve savremene zahteve protivpožarne zaštite. U radu su prikazni proračunski požari korišćeni za dokaz otpornosti na dejstvo požara čelične konstrukcije krova i fasade. Primenom analitičkih postupaka definisanih u Evrokodovima za konstrukcije i napredne CFD analize pokazano je da veći deo rožnjača u bloka A Sava Centra zadovoljava nosivost pri dejstvu požara u trajanju od 60 minuta. Sračunavanje požarnih opterećenja pri definisanju proračunskih požara takođe je prikazano u ovom radu.

Ključne reči: otpornost na požar, požarno opterećenje, napredni modeli požara

DESIGN FIRE LOAD OF THE ROOF AND FACADE STEEL STRUCTURE – RECONSTRUCTION OF THE SAVA CENTRE

Summary:

Reconstruction of the Sava Centre in Belgrade, a cultural good of the Republic of Serbia, includes works on the facility, ensuring that the congress centre's construction meets all modern requirements for fire protection. The paper presents the design fires used to conduct fire resistance design of the steel structure of the roof and facade. By applying analytical procedures defined in Eurocodes for structures and performing advanced CFD analysis, it has been shown that most of the purlins in Building A of the Sava Centre satisfy the required 60 minutes of fire resistance. This paper also presents the calculation of the fire loads applied in design fires.

Key words: fire resistance, advance fire models, fire load

---

[1] *Assoc. prof. University of Belgrade Faculty of Civil Engineering, Serbia, spremic@grf.bg.ac.rs*

[2] *Teaching assistant, University of Belgrade Faculty of Civil Engineering, Serbia, isidora@imk.grf.bg.ac.rs*

[3] *TIM Global Engineering, Serbia, nemanja.dincic@timglobaleng.com*

1. INTRODUCTION

The Sava Centre in Belgrade is the largest congress centre in Serbia. It was built in the period between 1976 and 1978 according to the design by the architect Stojan Maksimović and associates. The Sava Centre is one of the most famous structures in Serbia and the region. The Congress Centre is formed of two buildings: Building A - Conference and Commercial Centre and Building B - Congress and Concert Hall. Building A which is the subject of this analysis is parallel to Milentija Popovića Street. The complex was built as a combination of the reinforced concrete structure and steel structure, whereby glass was used as the main material for the facade cladding. The architecture of the building is based on contemporary, mostly sloped forms of glass green-blue facade planes, cascading terraces and gardens with horizontal brise-soleils, as well as concrete facades with small window perforations.

The development of the congress tourism and new regulations and standards in construction, innovative technologies and rapidly developing systems resulted in the need for a thorough reconstruction and rehabilitation of the building. The renovation and adaptation of Building A included: the reconstruction and renovation of the foundations, installation systems, parts of the first and second floors in the areas of new ceilings and parts of the ground floor in the area of new evacuation staircases and panoramic and service elevators.

Due to its characteristics and its importance to society, the Sava Centre was declared a monument of culture, which is why the reconstruction and rehabilitation of the building are very challenging and demanding for all participants in the project. The investor and designers encountered many complex tasks. One of the most complex tasks is the realisation of the structure fire protection. This paper presents the results of the fire resistance analysis study of the steel structure supporting the roof covering and facade cladding of Building A.

The adoption of the new Rulebook for Engineering Structures in the Republic of Serbia paved the way for proving the resistance of building structures to the effects of fire by applying the set of Eurocode standards. Article 5 of the mentioned rulebook defines the requirements that the structure must meet, among which is the requirement that the structure must be safe in case of fire. Article 6 of the rulebook for engineering structures defines the technical properties of structures. The technical properties of the structures must be such that the structure meets all the safety requirements defined by the code. When it comes to resistance to the effects of fire, the technical properties of the building structure must be such that in the event of a fire, the load-bearing capacity and stability of the building structure or its part are preserved during a certain period prescribed by a special regulation. Proof that the structure has the required technical properties is provided by the procedures defined in the standards listed in the Annex of the Code for building structures. Each chapter of the Eurocode in volume 2 of the first book contains a standard covering the issue of fire resistance of building structures (EN 1991-1-2, EN 1992-1-2, EN 1993-1-2, EN 1995-1-2, etc.).

This paper is focused on the fire resistance analysis of the steel structure supporting the roof and facade cladding of the Sava Centre Building A. The design fire loads implemented in order to prove the fire resistance of the structural elements are presented and elaborated. The conducted analyses include different approaches for defining fire load, such as the application of analytical procedures and modelling through advanced CFD simulations.

1.1 THE SUPPORT STRUCTURE FOR THE ROOF AND FACADE CLADDING

The main supporting structure of the Sava Centre is the reinforced concrete prefabricated structure. The roof structure and a part of the sloped facade are formed by reinforced concrete trusses and steel lattice purlins (Figure 1). The spacing between the roof lattice girders is 15 m which is also the span of the simply supported truss purlins. Purlins have been designed as space trusses with three chords. The same type of support has been used for the facade on the glazed surfaces of the sloped facade facing Milentija Popovića street.
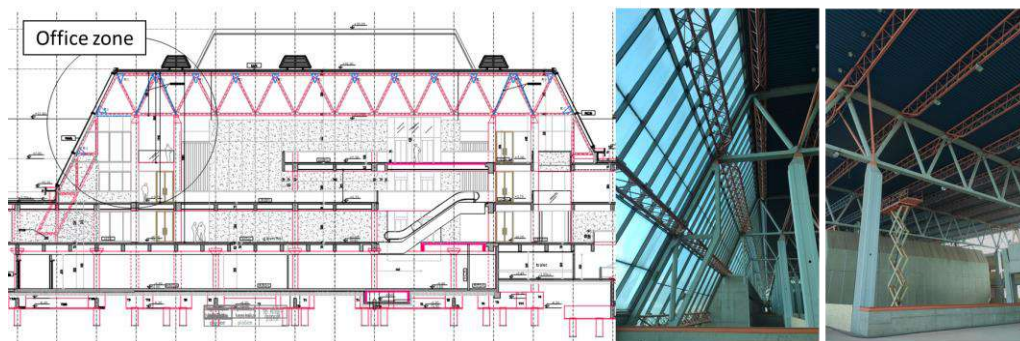

Figure 1 – Cross section: Sava Centre Building A

The compressed chords of the truss girder have been made of hollow tubular sections Ø108x4 mm, whereas the tensioned chord has been made of two tubular sections Ø60.3x6.3 mm. The main elements of the web have been made of solid sections of 30 mm in diameter, while the web for stabilisation of the top chord has been made of a circular cross-section of 18 mm in diameter.

2. FIRE LOAD

The first step in determining the fire load is defining the fire scenarios. It is necessary to define and analyse all possible scenarios of the occurrence of fire, select the critical ones, and for them provide proof of structure resistance to the effects of fire. The analysis of possible fire scenarios was carried out following the recommendations of the ISO 16733-1 Selection of design fire scenarios [1]. The standards EN 1991-1-2 [2] and ISO 16733-2 Design fires [3] were used to define the fire load. These two standards highly overlap and define the same fire load models. It should be noted that the latest revision of the ISO 16733-2 standard [3] is from 2021 and provides significant clarification of fire loads, introducing new types of loads that are not yet included in the Eurocode such as travelling fires.

Eurocode EN 1991-1-2 defines the following models of fire load:
- Standard temperature-time curve,
- Parametric temperature-time curves – Natural fire – Annex A,
- Thermal actions for external members – Simplified calculation method – Annex B,
- Localised fires – Annex C,
- Advanced fire models – Annex D,
- Fire load densities – Annex E.

The complex layout and variety of functions and spaces of the Sava Centre comprised the implementation of multiple different models of fire load. Figure 2 shows the longitudinal cross-section of the Sava Centre building. The walls and the ceiling structure of conference halls in

Building A are formed of reinforced concrete structural elements and they represent a separate fire sector. A fire in the conference hall cannot endanger the facade cladding and roof purlins. Zones of the building where the occurrence of fire may affect the bearing capacity and stability of the steel structure, purlins and facade beams are presented in Figure 2:

- GREEN colour between axes A and G, and axes K and M marks the corridors and hallways of the height of 8 or 12 m;
- YELLOW colour between axes M and P marks the banquet hall of a height of 16 m;
- RED colour between axes G and K, and axes P and R marks the technical room of a height of 4 m;
- BLUE colour between axes A and K marks the office area.

Analysing the areas of the Sava Centre, it was concluded that the application of the standard fire curve is not suitable for any of the mentioned areas. The applied fire loads for each of the zones are presented in the following.
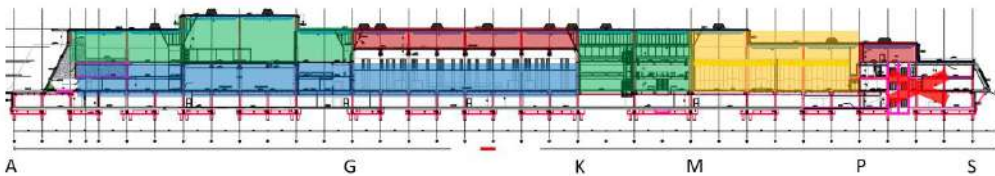

Figure 2 – Fire sectors: Sava Centre Building A

2.1 FIRE LOAD DENSITY

Fire load density is defined in Annex E of EN 1991-1-2 in the following way:

$$q_{f,d} = q_{f,k} \cdot m \cdot \delta_{q1} \cdot \delta_{q2} \cdot \prod_{1}^{10} \delta_{ni}$$

In the previous expression, the following labels are used: m - combustion factor, δ_{q1} – factor considering the danger of fire activation in relation to the area of the fire sector, δ_{q2} – factor considering the danger of fire activation in relation to the type of occupations, $\delta_{n1} - \delta_{n10}$ – factors dependent on active fire fighting measures.

According to the fire protection design, the installation of an automatic fire switchboard and its connection to the fire brigade is provided in the Sava Centre building. In case when there is direct communication of the switchboard with the fire brigade, the value of the coefficient $\delta_{n5} = 0.87$ is disputed by the fire fighting authorities and it is required to use the value of $\delta_{n5} = 1.0$. The authorities corroborated this with the practical issue that the brigade does not spring into action after receiving the signal over the day, but only during the night, between 22.00 and 6.00 o'clock. The other coefficient values were adopted in accordance with the Table E.2 of the standard EN 1991-1-2 [2]. The following value was obtained: $\prod_{1}^{10} \delta_{ni} = 0.57$.

Fire load densities $q_{f,k}$ [MJ/m²] were adopted depending on the area occupancy as defined in Eurocode 1 [2]:

- Corridors and hallways - transport (public space) 122 MJ/m²
- Banquet hall/classroom of a school 347 MJ/m² or theatre 365 MJ/m²
- Office 511 MJ/m²
- Technical room 200 MJ/m²

Fire propagation is defined by the HRR [kW] curve which represents the heat release rate HRR during the fire t [s] (Figure 3a). The integral of the HRR curve is equal to the product of the fire load density and fire sector surface area $[q_{f,k} \cdot A_f]$. The shape of the HRR curve which defines the release of heat during the fire depends on the amount of combustible matter, as well as the ventilation conditions. Two HRR curves are presented in Figure 3b: one which is defined only by the amount of combustible material and the other which is defined by the conditions of ventilation of the fire sector. In case there is no supply of fresh air, the release of heat is longer, but of lower intensity depending on the maximum possible oxygen supply to the fire sector.
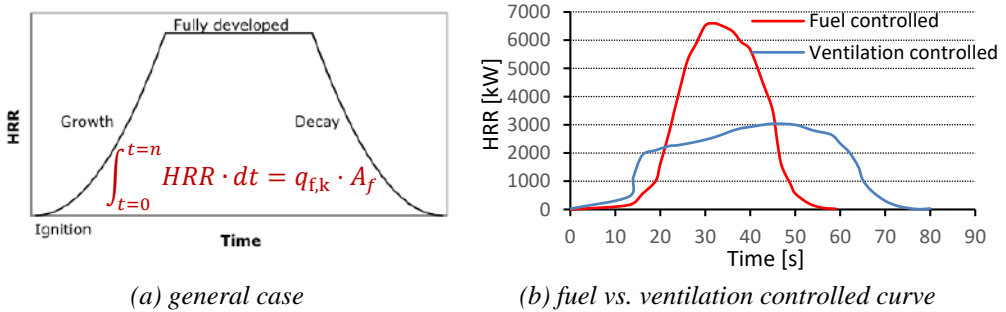

| (a) general case | (b) fuel vs. ventilation controlled curve |

Figure 3 – HRR-time design curves

2.2 CORRIDORS, HALLS AND BANQUET HALL

Due to the large volume of the connected space in the corridors and halls, the occurrence of a fully developed fire is not possible. The combustible material is not present in these areas except for localised pieces of furniture such as the info desk, bar or similar. Instead, according to ISO 16733-2, the development of a local fire or a travelling fire is possible in spaces with large areas and heights [3][4].

The Eurocode defines the fire load density and the algorithm for calculating the flame temperature. There are two possible design situations: the flame is lower than the floor height, and the flame reaches the ceiling and spreads below the surface of the ceiling. The minimum height from floor to ceiling in halls and corridors in the Sava Centre is 8 m. The ceiling height of the banquet hall varies from 12 m to 16 m. In areas of medium size and considerable height, it is possible to have a design situation in which two fire zones are formed; the lower one is colder and the upper one is warmer (two-zone model). However, the formation of two-fire zones in the banquet hall, corridors and halls is not possible due to the small amount of combustible matter compared to the height of the space.

The results of the temperature calculation at a certain height of the flame or above the flame are numerically very sensitive to the value of the diameter of the local fire, which is not defined in the Eurocode. The estimation of the diameter of the local fire was carried out according to the recommendations from Ref. [5]. Table 1 shows the local fire parameters according to Ref. [5]. When calculating the fire load in the banquet hall and the corridors, the parameters of the local fire for the "atrium in the office building" and "hotel reception hall" were adopted, respectively.

The maximum temperature at the height of 7 m in corridors and halls is lower than 250°C. The calculated temperature in the banquet hall at the height of 11 m is 257°C. The calculated temperatures are far below the critical temperatures for the truss purlin elements calculated for the accidental design situation (715°C).

Table 1 – Parameters of the localised fires

	A_{fi}	D	W_{fi}	HRR	q	t_α
	[m^2]	[m]	[m]	[KW/ m^2]	[MJ/m^2]	[s]
Atrium in the office building	9	3.4	12	250	200	300
Hotel reception hall	9	3.4	12	250	200	300
Exhibition hall	36	6.8	24	500	400	150
Church	20	5	18	250	300	150
Office large area	36	6.8	24	500	600	300
Sport hall	9	3.4	12	250	200	300
Supermarket	36	6.8	24	250	400	150
Restaurant room	20	5	18	250	300	150
A_{fi} – Fire area, D – Fire diameter, W_{fi} – Fire perimeter, t_α – Time needed to obtain HRR						

2.3 TECHNICAL ROOM

The fire load in the technical room according to the fire protection design is 200 MJ/m^2. The surface area of the room of 1320 m^2 is 2.5 times larger than the maximum surface area required for the implementation of the fire parametric curve. Considering this, the calculation of the fire load and steel temperature were determined using the software [6]. The machinery hall is the independent fire sector with only one door having dimensions of 1.0 m x 2.2 m. There are smoke domes with a diameter of 1.2 m. The obtained results of the air and steel temperature indicate the ventilation-controlled fire. It was adopted that the doors remain always open and the smoke escapes the area through the roof. The obtained steel temperature change over time is presented in Figure 4.
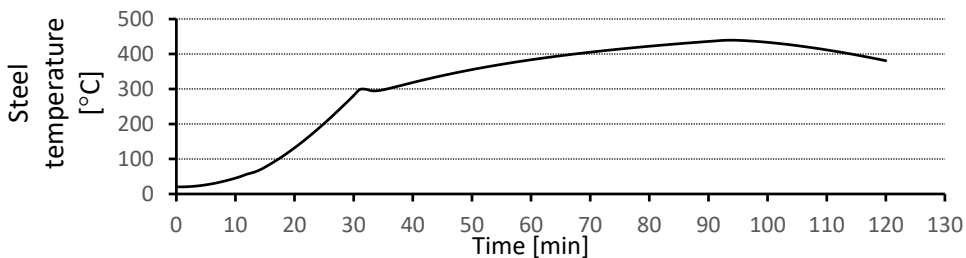

Figure 4 – Steel temperature-time curve

2.4 OFFICES

Office rooms are located along the two longitudinal building facades between axes A and K. The rooms are constructed as reinforced concrete structures with large glass areas, glazed facades and large windows in the wall towards the Sava Centre hall. The ceiling is lined with plasterboards. The investor opted for this combustible ceiling, accepting to fire protect the required number of purlins.

By analysing critical fire situations, it was concluded that the spread of fire from the offices is possible through the ceiling lining or the doors and windows towards the communication corridors in the Sava Centre. It was concluded that the first purlin/facade beam must be protected with fireproof coatings (Figure 5a). To determine if the same applies to the other purlins, the spread of fire outside the office space was analysed using the procedure for calculating the impact of fire on external elements. It was assumed that after a certain duration of the fire, the glass

towards the communication corridors would break and the flames would penetrate the corridor of the Sava Centre. The breakage of the facade glass and the penetration of the flame into outer space are not relevant for the calculation of the fire resistance of the steel purlins. During a fire, the glass starts cracking when the temperature of the heated air exceeds 300°C. The probability of complete glass breakage as a function of temperature could be found in the literature. According to these data, it could be considered that at temperatures higher than 500°C, the glass will be completely broken in one opening. During the analysis, it was assumed that the glass broke on one window or door and that the flame spread into the corridor only through that opening (Figure 5b,c). This assumption is confirmed by the numerical analysis presented in the next section. The calculation was carried out for two typical offices with a smaller area of 75 m² and a larger surface area of around 150 m². A critical fire situation is one when the fire is in a larger office. In this case, the flame reaches the height of approximately 1.0 m under the lower edge of the purlin (Figure 5c). The flame temperature is 538°C which is lower in comparison to the critical temperature of 715°C determined by the bearing capacity of the purlin for the design fire situation. In the case of a smaller office, the flame is far away from the purlins and cannot affect purlins (Figure 5b).

However, the design fire situations with the penetration of flame through the ceiling structure could not be verified using the algorithms provided in Eurocode. In this case, the recommendations provided in Annex D, EN 1991-1-2 [2] for the advanced fire models are used as described in the next section.
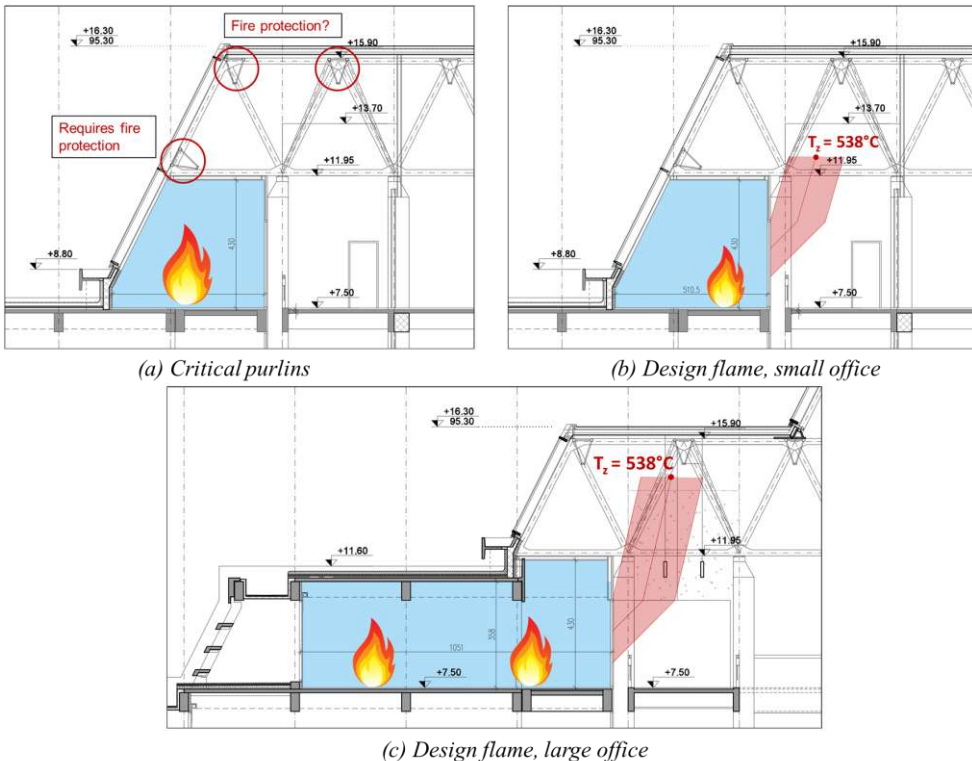

(a) Critical purlins

(b) Design flame, small office

(c) Design flame, large office

Figure 5 – Fire in offices

280

3. CFD FIRE LOAD MODEL

Two different office spaces with four fire load models are analysed through CFD simulations. The two office spaces differ in total surface area and glass surface area (windows). Glass surfaces were modelled assuming cracking at a temperature of 500°C. In three models, the burner was set to the whole floor area, while the fourth model analyses the burn of the workstations. The ceiling was divided into 0.75 x 0.75 m cells to simulate plaster ceiling tiles. Two different approaches to the design of the plaster ceilings were considered. According to the first approach, the temperature was set to 412°C [8,9] at the beginning of combustion, while according to the second approach, the cells of the ceiling disappear without burning when the temperature of 700°C is reached in the thermocouple (a sensor that measures temperature). Thermocouples were also set under the roof, next to steel purlins, to measure the gas temperature required for further steel design.

The first load model represents the office space with a smaller surface area. Using the fire load density value of 511 MJ/m² according to Table E.4 in EN 1991-1-2:2002 [2], the value of heat release rate per area on the burner was calculated to be 250 kW/m². Figure 6a shows the first model with the plaster ceiling burning and eventually disappearing.
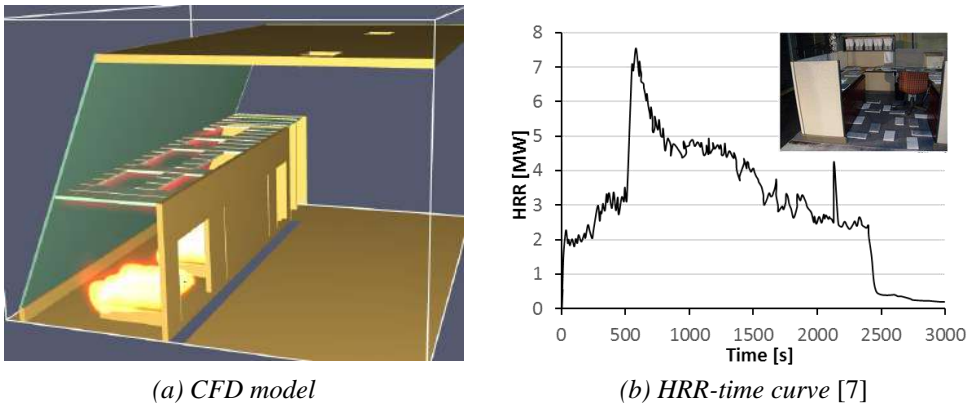

(a) CFD model	*(b) HRR-time curve* [7]

Figure 6 – CFD simulations

The second fire load model has the same parameters as the first one, with the only difference in the approach implemented to the design of the ceiling. The ceiling was divided into 64 cells. A thermocouple was assigned to every cell. The thermocouples were programmed to induce the disappearance of every cell that reaches the temperature of 700°C.

The third fire load model is based on the HRR curves relevant to office workstations taken from previously published research [7]. This model represents a small office space with three workstations with a burning plaster ceiling. Each workstation is a burning surface with the applied HRR-time curve as shown in Figure 6b [7]. The dimensions of the workstations are 2.4 x 2.4 m and the height is 0.5 m.

The fourth fire load model represents the office space with a large surface area. The approach to the design of the fire load is the same as in the first model, with the only difference in the size of the burning surface. The design of the ceiling and the windows is the same as in the first model.

In all analysed models, the temperature of heated air varies in the range of ±15% of the mean value of the obtained results. The model with the combustible ceiling is adopted for further analysis in order to provide safe-sided results. This model is used to explore several fire situations. The first fire situation is the spread of fire through the door or window. The second design situation is the spread of the fire through the ceiling structure.

4. RESULTS OF CFD ANALYSIS

By varying the fire control parameters, several of them were recognised as key parameters affecting the calculation results: the moment of glass breakage, parameters that affect the burning of the ceiling, the opening of the door and the closing of the door. The temperature of flame and air in the first design situation in which the fire spreads through the opening towards the corridor are practically identical to the results obtained using Annex B [2]. At the moment when the glass breaks, the temperature in the room decreases significantly while the heated air leaks through the opening. Heated air continuously leaks, causing the temperature of the air in the room after glass break not reach values above 450°C.
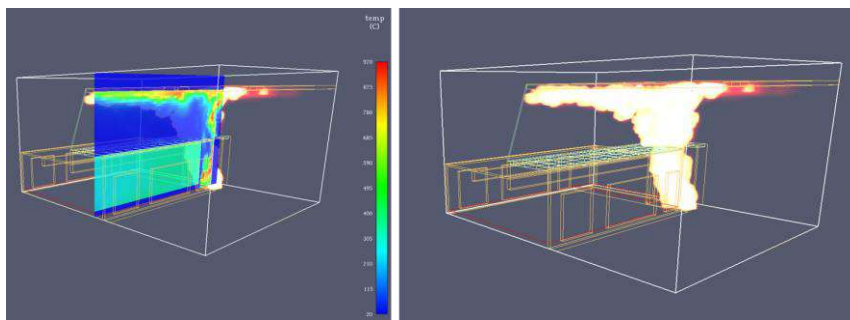

Figure 7 – CFD model visualisation of results

In the second design situation, the glass does not break, instead, a part of the suspended ceiling burns first. This situation is considered the relevant design situation. By opening a part of the ceiling, warm air leaks vertically towards the roof. In this case, a zone of hot air with a temperature of up to 700°C (thermocouple TC8) is formed directly above the office (Figures 7 and 8). At the place of the adjacent purlin next to the thermocouple TC7 (Figure 8), the maximum temperature is about 500°C. Finally, it was concluded that fireproof coatings should be applied to the first two roof purlins in the area next to large offices. Such a decision is on the side of safety because the critical temperature for the purlin is 715°C calculated for the accidental design situation.

5. CONCLUSIONS

The Sava Centre, with its spatial and structural specificities, is a building whose resistance to the effects of fire can be proven only by a comprehensive analysis that includes advanced calculation methods as well as CFD analysis. In the surrounding countries, CFD analysis is obligatory when proving the fire resistance for complex buildings such as congress halls, opera houses and theatres. The calculation of the resistance to fire effects of the structure of the Sava Centre did not include fire protection, but clearly indicated the critical elements of the structure that must be protected against fire.
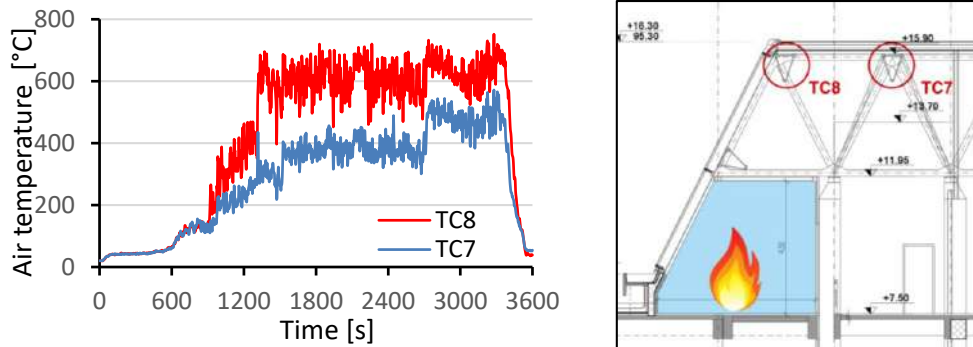
Figure 8 – CFD model results, the temperature of the air

With the adoption of the new Code of Building Structures, the conditions were created for implementing the new approach to solving the fire resistance of a structure. The responsibility is now on the designer of the structure to decide what measures should be implemented to achieve adequate resistance to the effects of fire. In the coming period, it is crucial that the authorities in charge of fire protection closely cooperate with civil engineers in order to create a detailed proving procedure for the safety of the structure against the effects of fire.

REFERENCES

[1] ISO 16733-1:2015 Fire safety engineering — Selection of design fire scenarios and design fires — Part 1: Selection of design fire scenarios

[2] EN 1991-1-2 Eurocode 1: Actions on structures —Part 1-2: General actions — Actions on structures exposed to fire, CEN 2002

[3] ISO 16733-2:2015 Fire safety engineering — Selection of design fire scenarios and design fires — Part 2: Design fires

[4] Egle Rackauskaite, Matthew Bonner, Francesco Restuccia, Nieves Fernandez Anez, Eirik G. Christensen, Nils Roenner, Wojciech Wegrzynski, Piotr Turkowski, Piotr Tofilo, Mohammad Heidari, Panagiotis Kotsovinos, Izabella Vermesi, Franz Richter, Yuqi Hu, Chloe Jeanneret, Rahul Wadhwani, Guillermo Rein, Experiment Inside a Very Large and Open-Plan Compartment: x-ONE, Fire Technology, vol 58, 905–939, 2022

[5] J.M. Franssen, L.G.Cajot, J.B.Schleich, Effects Caused on the Structure by Localized Fires in large compartments, ORBi, the institutional repository of the University of Liège

[6] OZone Documentation 2018.

[7] Thomas Ohlemiller, George Mulholland, Alexander Maranghides, James Filliben, Richard Gann, Federal Building and Fire Safety Investigation of the World Trade Centre Disaster, Fire Test of Single Office Workstations, NIST NCSTAR 1-5C, September 2005.

[8] W.-T. Chung, M.-Y. Lei, Kuang-Chung Tsai, Evaluating Current Fire Test Methods for Determining Flammability Performance of Ceiling Materials, Journal of Marine Science and Technology 22(2):196-203, April 2014

[9] Morgan J. Hurley (editor in chief), SFPE Handbook of Fire Protection Engineering, Society of Fire Protection Engineers 2016, Springer.

Milica Koprivica[1], *Zlatko Marković*[2]

UPOREDNA ANALIZA NOSIVOSTI NA IZBOČAVANJE USLED POPREČNE SILE PREMA POSTOJEĆEM I NOVOM EVROKODU

Summary:

U ovom radu je data uporedna analiza proračuna punih limenih elemenata prema aktuelnom standardu EN1993-1-5:2006 [1] i novoj verziji prEN1993-1-5:2020 [2] koja je u fazi završne izrade. Poseban akcenat je na problemima izbočavanja usled dejstva poprečne sile, interakcija izbočavanja usled normalnih, smičućih napona i poprečne sile i na metodi redukovanog napona. Pored toga, razlike između pravila za proračun datih u postojećem Evrokodu i novom standardu prEN1993-1-5: 2020 [2] su ilustrovane na konkretnim numeričkim primerima.

Key words: Evrokod 3, puni limeni elementi, izbočavanje, izbočavanje usled dejstva poprečne sile, interakcije

COMPARATIVE ANALYSIS OF PATCH LOADING BUCKLING RESISTANCES ACCORDING TO EXISTING AND NEW EUROCODE

Summary:

This paper compares the procedures for calculating steel plate girders according to the current standards EN1993-1-5: 2006 [1] and the new version prEN1993-1-5: 2020, which is in the final stage of development [2]. There is a particular emphasis on problems of resistance to patch loading, the interaction between transverse force, bending moment and shear force, and the reduced stress method. The differences between the current standard and the new version prEN1993-1-5: 2020 [2] are illustrated using specific numerical examples.

Key words: Eurocode 3, plate girders, buckling, resistance to patch loading, interactions

---

[1] *MSc, teaching assistant, Faculty of Civil Engineering, University of Belgrade, Bulevar kralja Aleksandra 73, 11000 Belgrade, Serbia , mbendic@grf.bg.ac.rs*

[2] *Full professor, Faculty of Civil Engineering, University of Belgrade, Bulevar kralja Aleksandra 73, 11000 Belgrade, Serbia , zlatko@imk.grf.bg.ac.rs*

1. INTRODUCTION

The Eurocodes were developed to enable the design of structural construction works, buildings and civil engineering work on the harmonized European level. Long-term confidence in the Eurocodes requires the Eurocodes to be developed appropriately. The new generations of these standards are focused on new methods, materials and market requirements. This paper deal with standard EN 1993-1-5: Design of plated structures. There is a tendency in the new version of Eurocode 3 prEN1993-1-5 [2] for solutions to be harmonized with other parts of Eurocode 3 and easy to use for practical applications. The leading development of additional rules to extend the scope of use of Eurocode 3 EN1993-1-5 [1] include the shear resistance of longitudinal stiffeners, the resistance of longitudinal stiffeners to direct stresses, the resistance of girders subjected to patch loading, rules for corrugated webs, F-M-V interaction, biaxial compression, consideration of torsional stiffness of closed-section stiffeners, flange-induced buckling. The structure in the new version prEN1993-1-5 [2] has vastly been improved by moving the former Annex C "*Finite Element Method of Analysis*" to EN1993-1-14 and by integrating the former Annex D "*Plate girders with corrugated webs*" and former Annex E "*Alternative methods for determining effective cross-section*" into the main text. Specific innovations also exist in the reduced stress method and effective width method whose field of application has been extended to non-rectangular panels. Modifications in new Eurocode 3 prEN 1993-1-5 [2] related to patch loading resistance, the interaction between transverse force, bending moment and axial force, the interaction between transverse force, bending moment and shear force, and reduced stress method are presented and commented on in this paper.

2. PATCH LOADING RESISTANCE

Girders loaded by the localized load in the plane of the web are common cases in engineering practice, for example crane girders or incremental bridge launching design situations. The resistance of steel plate girders subjected to patch loading is very important in the design of steel bridges. This problem has been investigated for decades [3,4], but a solution has not yet been found that includes all parameters important for the influence of patch loading resistance. The modification of Eurocode 3 EN1993-1-5 [1] Chapter 6, which refers to the patch loading resistance of steel plate girders, is a consequence of recent research, which has shown that the current definition of plastic resistance overestimates patch loading capacity in certain cases, as are hybrid girders. However, this capacity is slightly underestimated for very slender girders. This paper provides a brief overview of the modification of the patch loading resistance model in the new Eurocode 3 EN1993-1-5 [2], based on hundreds of experimental and numerical results.

According to the current version of the Eurocode 3 EN1993-1-5 [1], patch loading resistance F_{Rd} is obtained by reducing the plastic load capacity by the reduction coefficient χ_F.

The plastic resistance F_y includes the length l_y, which can be calculated from the geometrical and mechanical properties of the girders using Eqs. (2) and (3).

$$F_{Rd} = \frac{\chi_F F_y}{\gamma_{M1}} = \frac{\chi_F f_{yw} l_y t_w}{\gamma_{M1}} \tag{1}$$

$$l_{\text{y}} = s_s + 2t_{\text{f}} \left(1 + \sqrt{m_1 + m_2}\right) \tag{2}$$

$$m_1 = \frac{f_{\text{yf}} b_{\text{f}}}{f_{\text{yw}} t_{\text{w}}} \quad m_2 = 0.02 \left(\frac{h_{\text{w}}}{t_{\text{w}}}\right)^2$$

if $\overline{\lambda}_{\text{F}} > 0.5$, otherwise $m_2 = 0$ \hfill (3)

$$\overline{\lambda}_{\text{F}} = \sqrt{\frac{l_{\text{y}} t_{\text{w}} f_{\text{yw}}}{F_{\text{cr}}}} \tag{4}$$

$$F_{\text{cr}} = 0.9 k_{\text{F}} E \frac{t_{\text{w}}^3}{h_{\text{w}}} \tag{5}$$

$$\chi_{\text{F}} = \frac{0.5}{\overline{\lambda}_{\text{F}}} \tag{6}$$

In the Eqs. (1) to (6) the following notations are used to describe the problem of patch loading, compare the results, and derive conclusions: h_{w} - the web depth, t_{w} - the web thickness, t_{f} - the flange thickness, b_{f} - the flange width, s_s - the patch load length, f_y - the yield strength, l_{y} - the effective loaded length for resistance to transverse forces, k_{F} buckling coefficient.

Since the publication of the Eurocode 3 EN1993-1-5 [1], significant research has been carried out to improve the existing standard. More significant research was done in France by Davaine [5] and Müller [6], in Sweden and Spain by Chacón [7]. Numerical studies on steel plate girders subjected to patch loading have questioned the validity of the $\chi\text{-}\overline{\lambda}$ approach and the calculation of the effective loaded length l_{y}. Davaine [5] studied the resistance of longitudinally stiffened steel plate girders subjected to patch loading and questioned the physical meaning of the term m_2. Research work by Müller [6] contributed the most to the recalibration of standards EN1993-1-5 [1] and the introduction of the new resistance function. Chacón [7] has presented a research work on patch loading that refers to the effect of the flange yield strength f_{yf} and it was predicted that $f_{\text{yf}} / f_{\text{yw}}$ does not influence the ultimate load capacity of patch loaded girders. According to the current standard EN1993-1-5 [1], the patch loading resistance increases with the flange and web strength ratio through the parameter m_1.

The new proposal for patch loading resistance omitted the value of m_2 when the localized load acts at the mid-span of the vertical stiffeners (types of load application a and b). Also, the influence of the ratio $f_{\text{yf}} / f_{\text{yw}}$, does not affect on the collapse mechanism, so the effective width is calculated according to the expression given in Eq. (7):

$$l_{\text{y}} = s_s + 2t_f \left(1 + \sqrt{m_1}\right)$$

$$m_1 = \frac{b_f}{t_w} \tag{7}$$

In addition to the change in the value of l_{y}, the resistance function for patch loading is improved by new relate of reduction factor χ_{F} and relative slenderness $\overline{\lambda}_{\text{F}}$. Furthemore,

χ-$\overline{\lambda}_F$ function has been changed to harmonize the plastic resistance F_y and the elastic critical buckling load F_{cr}, and to merge both magnitudes in a single formulation. The proposed expression for the value of takes the form of the equation included in Annex B of existing standard EN1993-1-5 [1].

$$\chi_F = \frac{1}{\varphi_F + \sqrt{\varphi_F^2 - \overline{\lambda}_F}} \tag{8}$$

$$\varphi_F = \frac{1}{2}(1 + \alpha_{F0}(\overline{\lambda}_F - \overline{\lambda}_{F0}) + \overline{\lambda}_F) \tag{9}$$

The value of imperfection factor α_{F0} and plateau length $\overline{\lambda}_{F0}$ represents the adaptive magnitudes that can be calibrated to achieve the desired level of safety [8].

The value of the partial safety factor γ_{M1} depends on the combination of the imperfection factor α_{F0} and plateau length $\overline{\lambda}_{F0}$, which was shown by complex statistical studies [8]. Table 1 shows the value of the corrected partial safety factor in function of the α_{F0} and $\overline{\lambda}_{F0}$, which are the result of research work that preceded the changes in the Eurocode standard [8]. The Eurocode 3 prEN1993-1-5 suggest the values of $\alpha_{F0} = 0.5$ and $\overline{\lambda}_{F0} = 0.75$.

Table 1 – Values of the imperfection factor and the plateau length for achieving the desired level of safety [8]

γ_{M1}=1.0		γ_{M1}=1.1	
λ_{F0}	α_{FO}	λ_{F0}	α_{FO}
0.5	1	0.5	0.75

The expression for the buckling coefficient k_F remains the same for both longitudinally stiffened and unstiffened girders. Furthermore, in Eurocode 3 prEN1993-1-5 [2], the value of k_F may be obtained from Annex A and is not given within Chapter 8, which refers to the resistance to patch loading.

The differences in the values of patch loading resistance calculated using EN1993-1-5 [1] and prEN1993-1-5 [2] are illustrated by a numerical example. The example refers to the steel bridge construction, a continuous girder with a span of 3x40 m, and the incremental bridge launching method of construction. The bridge member is a steel plate girder with an open cross-section, as shown in Fig. 1.
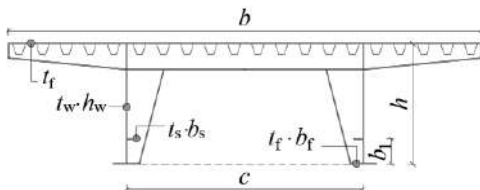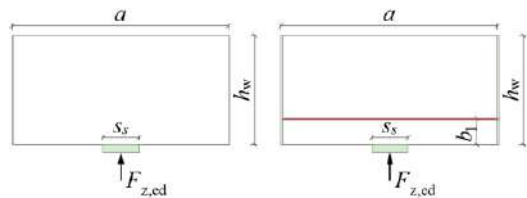

Figure 1 – Cross-section of bridge girder

Figure 2 – Introducing the localized load in the plane of the web

The dimensions of the cross-section are set to be: the top flange width $b = 10000$ mm, the top and bottom flange thickness $t_f = 20$ mm, the web depth $h_w = 2500$ mm, the web thickness $t_w = 14$ mm, the bottom flange width $b_f = 600$ mm, the thickness of the longitudinal stiffener $t_s = 20$ mm, the width of the longitudinal stiffener $b_s = 200$ mm, the distance between vertical stiffeners $a = 2h_w = 5000$ mm.
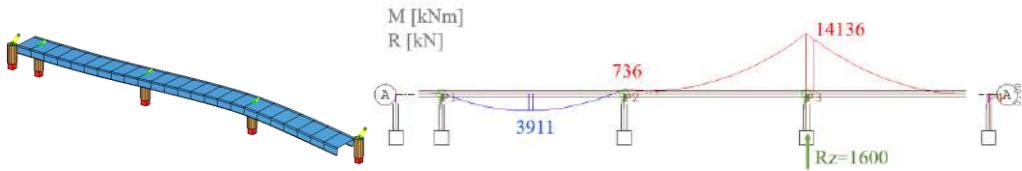

Figure 3 – Critical position of the girder, bending moment diagram and support reaction

The values of the support reactions for the critical position of the girder were calculated - Fig. 3. For the design values of the obtained transverse force, the patch loading resistance was checked for the position of the localized load presented in Fig. 2. The procedure was carried out for the longitudinally unstiffened and stiffened steel plate girder and for two patch load length $s_s = 0.1h_w = 250$ mm and $s_s = 0.3h_w = 750$ mm. In addition to the expression in the Eurocode EN1993-1-5 [1] and prEN1993-1-5 [2], the patch loading resistance was also obtained numerically by Abaqus [9], and using the expression proposed by [10] - Eq. (10-11).

$$F_{rf}^{\text{unstiff}} = 0.75 f(\alpha) f(h_w / t_w) t_w^3 \sqrt{E f_{yw}} \sqrt{t_f / t_w} f^{\text{unstiff}}(s_s) \tag{10}$$

$$F_{rf}^{\text{stiff}} = F_{rf}^{\text{unstiff}} f(b_1) f^{\text{stiff}}(s_s) \tag{11}$$

For the FE analysis [9], a general-purpose four-node quadrilateral shell element with reduced integration and six degrees of freedom per node S4R from the Abaqus element library was used. Finite element size is adopted to 50 mm for all numerical runs. Geometric imperfections correspond to the first buckling shape mode with the magnitude $h_w/200$ according to the proposition of Annex C EN1993-1-5 [1]. The considered material is homogenous with an elastic modulus of $E = 210$ GPa and Poisson's ratio of $v = 0.3$. The stress-strain curve used for material modelling is a simplified bilinear curve.
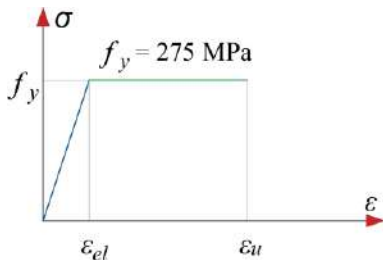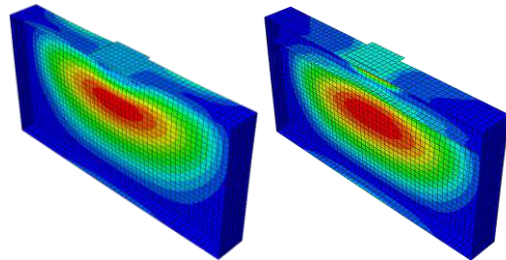

Figure 4 – Material stress-strain curve

Figure 5 – Deformed shape of steel plate girders after local buckling

Table 2 – The ultimate strength of longitudinally stiffened and unstiffened girder, for various patch loading lengths (us-unstiffened, st-stiffened)

	$F_{Rd}^{EC3} / F_{Rd}^{FEA}$	$F_{Rd}^{prEC3} / F_{Rd}^{FEA}$	F_{rf} / F_{Rd}^{FEA}
$s_s=0.1h_w$, us	0.64	0.51	0.72
$s_s=0.1h_w$, st	0.69	0.55	0.71
$s_s=0.3h_w$, us	0.58	0.54	0.81
$s_s=0.3h_w$, st	0.57	0.52	0.75

Table 2 presents the results of the ultimate strengths of longitudinally stiffened and unstiffened steel plate girders subjected to patch loading, analyzed in this paper in the previously described different ways. Patch loading resistances calculated using Eqs. (10,11) and procedures given in the current and new versions of Eurocode are presented and compared to the value of the patch loading resistance obtained numerically. The following notations are used in Table 2 to describe the ultimate strength of steel plate girder subjected to patch loading: F_{Rd}^{EC3} - the ultimate strength obtained by EN1993-1-5 [1], F_{Rd}^{prEC3} - the ultimate strength obtained by prEN1993-1-5 [2], F_{rf} - the ultimate strength obtained using the expression proposed by [10] and F_{Rd}^{FEA} - the numerically obtained ultimate strength [9]. The patch loading resistances F_{Rd}^{EC3}, F_{Rd}^{prEC3} used in the Table 2 and Fig. 6-7 are not divided by the partial safety factor γ_{M1} for steel bridge structures (the partial safety factor was neglected and presented values of ultimate strengths correspond to the characteristic values), so that the results could be compared.
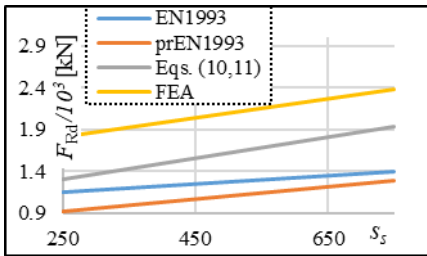

Figure 6 – The ultimate strength of unstiffened steel plate girder-comparison	*Figure 7 – The ultimate strength of stiffened steel plate girder-comparison*
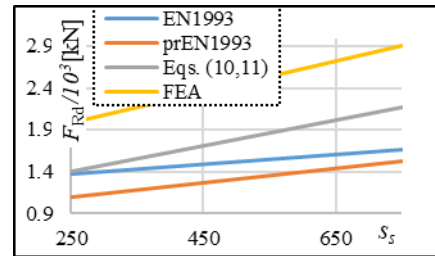
Based on the considered numerical examples, it can be concluded that Eurocode 3 prEN1993-1-5 [2] gives more conservative results than Eurocode 3 EN1993-1-5 [1]. A detailed numerical and statistical analysis should be done to verify whether this is a general trend. Both EN1993-1-5 [1] and prEN1993-1-5 [2] give more conservative results than the numerical results and results obtained by Eqs. (10,11) as shown Fig. 6-7.

3. INTERACTIONS

3.1. INTERACTION BETWEEN DIRECT STRESS AND PATCH LOADING BUCKLINGS

If the girder is subjected to a concentrated transverse force acting on the compression flange in conjunction with bending and axial force, the resistance should be verified using Eq. (12).

$$\eta_2 + 0.8\eta_1 \le 1.4 \tag{12}$$

$$\eta_1 = \frac{N_{Ed}}{f_y A_{eff} / \gamma_{M0}} + \frac{M_{Ed} + N_{Ed} e_N}{f_y W_{eff} / \gamma_{M0}} \tag{13}$$

$$\eta_2 = \frac{F_{Ed}}{F_{Rd}} \tag{14}$$

In the Eq. (12-14) the following notations are used: A_{eff} - the effective cross-sectio area, e_N - the shift in the position of neutral axis of effective cross section, M_{Ed} - the design bending moment, N_{Ed} - the design axial force, W_{eff} - the effective elastic section modulus, γ_{M0} - the partial factor.

The parameter η_2 represents the ratio between the design transverse force F_{Ed} and the design resistance to local buckling under transverse forces F_{Rd}. The interaction formula has not changed in prEN1993-1-5 [2], however the interaction results are different in relation to EN1993-1-5 [1], because of the design value of patch loading resistance F_{Rd}. The interaction formula gives a higher value if the procedure given in prEN1993-1-5 [2] is used, compared to EN1993-1-5 [1]. The difference between the interaction formula results calculated using EN1993-1-5 [1] or prEN1993-1-5 [2] is the same as the difference in the value η_2 obtained by EN1993-1-5 [1] or prEN1993-1-5 [2].

3.2. INTERACTION BETWEEN TRANSVERSE FORCE, BENDING MOMENT AND SHEAR FORCE

In the case of steel structures are subjected to the combination of transverse force, bending moment and shear force the interaction of stability behaviour is an essential aspect of the bridge design and should be taken into consideration. In the current version of the EN1993-1-5 [1] there is no design method for desing resistance of the steel plate girder under the combined loading situation. Therefore, the situation with these three effects simultaneously can often occur in case of bridge girders during launching. The Eurocode 3 prEN1993-1-5 [2] contains the expression for interaction between transverse force, bending moment and shear force. If the girder is subjected to a concentrated transverse force acting on the compression flange in conjunction with bending moment and shear force, the resistance should be verified using Eq. (15-17).

$$\left(\overline{\eta}_1\right)^{3.6} + \left[\overline{\eta}_3 \left(1 - \frac{F_{Ed}}{2V_{Ed}}\right)\right]^{1.6} + \eta_2 \le 1 \tag{15}$$

$$\overline{\eta}_1 = \frac{M_{Ed}}{M_{f,eff,Rd}} \tag{16}$$

$$\overline{\eta_3} = \frac{V_{Ed}}{V_{bw,Rd}}$$

(17)

In the Eq. (15-17) the following notations are used: $M_{f,eff,Rd}$ - the design plastic moment of resistance of the cross-section consisting of the effective area of the flange and the fully effective web irrespective of its section class, $V_{bw,Rd}$ - the contribution of the web to the design resistance to shear.

This interaction should be verified only if $\eta_2 > 0.1$. If $\eta_2 \leq 0.1$ the verification is limited to a bending moment and shear force interaction.

4. REDUCED STRESS METHOD

The current standard Eurocode 3 EN1993-1-5 [1] provides two different calculation methods for a plate buckling assessment: the effective width method and the reduced stress method as an alternative method. The reduced stress method implies a linear stress distribution until the stress limits are reached in the section's weakest part. After that, there is no redistribution of the stress and the stress limits of the weakest part of the cross-section governs the resistance of the full cross-section. This method gives conservative results compared to the effective width method but is suitable for complex stress states and non-uniform geometries. The reduced stress method applies to any geometries and loadings considering the full stress field and its interaction - Fig. 8. It is shown [11] that the interaction verification in its pure format based on the von Mises yield criterion is not able to represent the actual behaviour of biaxially compressed plates. The current formulation of the reduced stress method may lead to unsafe results for the case of the plate under biaxial compression [11], so a modification has been proposed by introducing a ρ_V - factor in the interaction formula in prEN1993-1-5 [2]. This verification - Eq. (18) should be used for each panel and subpanel within the whole cross section.
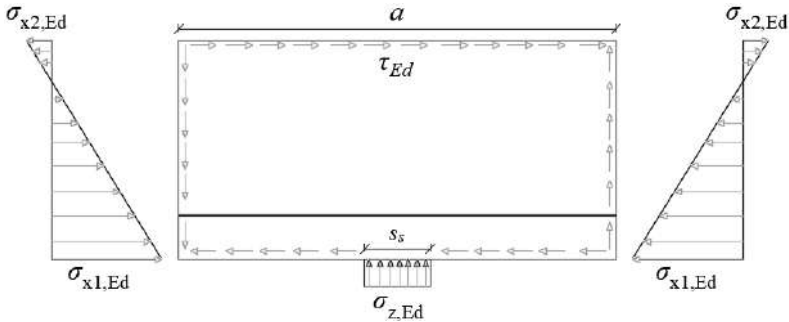

Figure 8 - The plate of girder under the full stress field

$$\sqrt{\left(\frac{\sigma_{x,Ed}}{\rho_{c,x}}\right)^2 + \left(\frac{\sigma_{z,Ed}}{\rho_{c,z}}\right)^2 - \rho_V \cdot \left(\frac{\sigma_{x,Ed}}{\rho_{c,x}}\right) \cdot \left(\frac{\sigma_{z,Ed}}{\rho_{c,z}}\right) + 3 \cdot \left(\frac{\tau_{Ed}}{\chi_w}\right)^2} \leq \frac{f_y}{\gamma_{M1}}$$

(18)

In the interaction formula - Eq. (18), parameter $\rho_V = \rho_{c,x}\rho_{c,z}$ when $\sigma_{x,Ed}$ and $\sigma_{z,Ed}$ are both compression, otherwise $\rho_V = 1/(\rho_{c,x}\rho_{c,z})$. The following notations are used in Eq. (18): $\rho_{c,x}$ - the reduction factor for longitudinal stresses, $\rho_{c,z}$ - the reduction factor for transverse stresses, χ_w - the reduction factor for shear stresses, $\sigma_{x,Ed}$, $\sigma_{z,Ed}$, τ_{Ed} - the components of the stress field in the ultimate limit state.

The Eurocode 3 prEN1993-1-5 [2] provides the formula - Eq (19) to verify the stress limit from the equivalent effective area, for the class 4 plates that are unstiffened and supported out of their plane along all four edges, within Chapter 12 refers to the reduces stress method. The procedure assumes calculating the thickness of each class 4 plates within the cross-section reduced by their individual reduction factor $\rho_n = \min(\rho_{cx}, \rho_{cz}, \chi_w)$.

The effective cross-section properties leads to the values of the stress field in the ultimate limit state $\sigma_{x,eff,Ed}$, $\sigma_{z,eff,Ed}$, $\tau_{eff,Ed}$.

$$\sqrt{\sigma^2_{x,eff,Ed} + \sigma^2_{z,eff,Ed} - \rho_V \sigma_{x,eff,Ed} \cdot \sigma_{z,eff,Ed} + 3\tau^2_{eff,Ed}} \leq \frac{f_y}{\gamma_{M1}} \tag{19}$$

In the interaction formula - Eq. (19), parameter $\rho_V = \rho_n^2$ when $\sigma_{x,eff,Ed}$ and $\sigma_{z,eff,Ed}$ are both compression, otherwise $\rho_V = 1$.

In addition to the EN1995-1-5 [1], the prEN1995-1-5 [2] contains suggestions on sections that plate buckling verification of rectangular stiffened panel should be checked, according to the Fig. 9. The plate buckling verification of a rectangular stiffened internal panel may be carried out with the maximum stress values at a distance $0.4a$ or $0.5b$, section A-A Fig. 9 [2]. For the rectangular subpanel, the maximum stress values may be carried out at a distance $0.4b_{loc}$, section B-B Fig. 9 [2]. In addition, the elastic gross cross-sectional resistance should be checked at the end of the panel, section C-C, according to the Fig 9 [2].

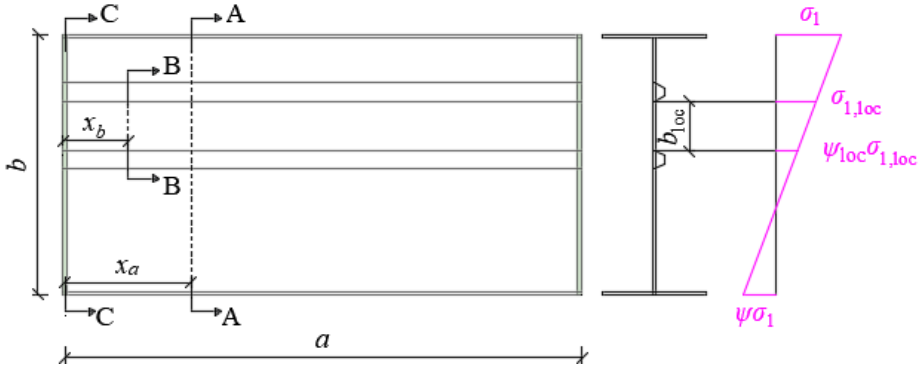*Figure 9 - Application of the reduced stress method for stiffened panels [2]*

In the new Eurocode prEN1993-1-5 [2], the reduced stress method is explained in more detail and a flowchart for the procedure application is given. In addition, the flowchart explains which procedure for calculating the reduction factors must be used for transverse, longitudinal, shear stresses, and column buckling behavior.

5. CONCLUSION

In order to harmonize Eurocode 3 regulations, the new generation of Eurocode 3 prEN1995-1-5 [2] has been modified and improved. The problems of steel plate structures are explained more explicitly and in detail. The modifications are the result of numerious experimental and numerical works. In the field of patch loading resistance, the $\chi\text{-}\overline{\lambda}_F$ approach has been changed. Some modifications have also been made in calculating the effective width l_y. A new interaction equation is introduced that considers the influence of bending moment, shear force and transverse force. The reduced stress method has been expanded, more clearly defined and modified to obtain even more reliable results for biaxially compressed plates. Based on the considered numerical examples, it can be concluded that new version of Eurocode 3 [2] gives more conservative results for patch loading resistance than current Eurocode 3 [1], but a detailed numerical and statistical analysis should be done to verify whether this is a general trend.

REFERENCES

[1]   EN 1993-1-5 (2006) Eurocode 3: Design of steel structures - Part 1-5: Plated structural elements

[2]   prEN 1993-1-5 (2020) Eurocode 3: Design of steel structures - Part 1-5: Plated structural elements

[3]   Lagerqvist, O., Johansson, B.: Resistance of I-girders to concentrated loads. Journal of Constructional Steel Research 39 (1996), No. 2, pp. 87–119.

[4]   Graciano, C: Patch Loading: Resistance of longitudinally stiffened steel girder webs. Doctoral Thesis, No. 2002:18, Lulea University of Technology, Sweden, 2002.

[5]   Davaine, L.: Formulations de la résistance au lancement d'une âme métallique de pont raide longitudinalement. Doctoral Thesis, No. D05-05, INSA de Rennes, France, 2005.

[6]   Müller, C.: Zum Nachweis ebener Tragwerke aus Stahl gegen seitliches Ausweichen. Doctoral Thesis, No. 47, RWTH Aachen, Shaker Verlag, 2003.

[7]   Chacón, R.: Resistance of Transversally Stiffened Hybrid Steel Plate Girders to Concentrated Loads. Doctoral Thesis, Universitat Politècnica de Catalunya, Barcelona Spain, 2008.

[8]   Chacón, R., Braun, B., Kuhlmann, U., Miram, E.: Statistical evaluation of the new resistance model for steel plate girders subjected to patch loading. Steel Construction, Volume 5, Issue 1, p.10-15, 2012.

[9]   Abaqus Simulia. Dassault Systemes. 2016.

[10] Ђеранић А., Утицај подужних укрућења на понашање и граничну носивост лимених носача оптерећеним локалним оптерећењем, Докторска дисертација, Београд, 2022.

[11] Braun, B., Stability of steel plates under combined loading, Dissertation No. 2010-3, Institute of Structural Design, University of Stuttgart, 2010.

Miloš Milić[1], Todor Vacev[2], Predrag Petronijević[3], Andrija Zorić[4], Ivan Nešović[5]

SMANJENJE NOSIVOSTI VEZA U DRVENIM KONSTRUKCIJAMA USLED EFEKTA PRIANJANJA

Summary:

Nosivost veza sa štapastim spojnim sredstvima u drvenim konstrukcijama se određuje kao zbir primarne (Johansenove) i sekundarne nosivosti (efekta prianjanja). Sekundarna nosivost nastaje zbog postojanja sile zatezanja u spojnom sredstvu. Usled sekundarne nosivosti se najčešće javlja poboljšanje karakteristika veze, ali se mogu javiti i slučajevi kod kojih ona deluje nepovoljno. To se događa zbog smanjenja momenta plastifikacije spojnog sredstva pod uticajem normalne sile. U radu je data numerička analiza spojnog spredstva uzimajuću i obzir pomenuti efekat, kao i predlog analitičkog proračuna.

Key words: drvene konstrukcije, veze, efekat prianjanja, nosivost

REDUCTION OF THE LOAD CAPACITY OF CONNECTIONS IN TIMBER STRUCTURES DUE TO THE ROPE EFFECT

Summary:

Load capacity of the dowel-type connections in timber structures is determined as sum of the primary (Johansen's) and secondary load capacity (rope effect). Secondary load capacity arises because of the existence of the tension force in the fastener. Secondary load capacity in most cases causes improvement of the connection characteristics, but cases where it acts adversely may also ocur. It happens because of the reduction of the plasticization moment of the dowel under action of the axial force. In the paper is presented numerical analysis of dowel, taking into account the mentioned effect too. Also, a proposition of an analytical solution is given.

Key words: timber structures, timber connections, rope effect, load capacity

[1] MEng., Junior Researcher, Faculty of Civil Eng. and Architecture, Niš, Serbia, milos.cicevac@gmail.com
[2] PhD, Associate Professor, Faculty of Civil Eng. and Architecture, Niš, todor.vacev@gaf.ni.ac.rs
[3] PhD, Assistant Professor, Faculty of Civil Eng. and Architecture, Niš, predrag.petronijevic@gaf.ni.ac.rs
[4] MEng., Teaching Assistant, Faculty of Civil Eng. and Architecture, Niš, andrija.zoric@gaf.ni.ac.rs
[5] MEng., Research Assistant, Faculty of Civil Eng. and Architecture, Niš, ivan.m.nesovic@gmail.com

1. INTRODUCTION

Acting of shear load in the connections of timber structures generates sliding in the joint plane. Standard EN 26891 [1] proposes that, during testing of timber structure connections realized by mechanical fasteners, load and displacement in the connection are measured until the displacements achieve value of $\delta_{max} = 15$ mm. In the first stage of loading, at sliding $\delta < 5$ mm, only the primary (Johansen's) strength is activated [2]. At higher sliding, and at failure modes that include plastic hinges in the dowel, an extension of the fastener arises, which leads to the occurrence of axial tension force in it. Axial force generates normal stress and friction in the joint plane, that is, a secondary strength called rope effect is activated. Rope effect has mainly favourable action, because increases strength of the connection and safety of the structure.

Standard Eurocode 5 [3], which covers the part related to the calculation connection in timber structures treats primary and secondary strength, and provides relations for determining of strength of different connection types. However, the provided relations do not offer interconnectivity of the primary and secondary strength, but consider them separately. This interconnectivity is reflected in the fact that axial force in the fastener affects on decrease of the yield moment of the fastener, which further leads to the reduced primary strength of the connection, that is, the Johansen's part of it.

Calculation of the yield moment may be done using the Theory of plasticity. According to this, in the older versions of Eurocode 5 [4] the yield moment was calculated based on the plastic section modulus and the yield point of the fastener material. In the contemporary regulations the more precise relation that includes the rotation angle of the fastener is used [5].

In the paper is given a proposition for the calculation of the connection between timber and steel elements made by use of a bolt with nut and washer, applying reduction of the yield moment of the fastener, with presentation of connection calculation on concrete examples. Bolts with different diameters and withdrawal capacity were used as fasteners. Reduction of the yield moment was done based on determining of the part of the cross-section of the bolt that was plasticized by axial force.

2. CONNECTION BEARING CAPACITY ACCORDING TO EUROCODE 5

Two variants of the steel and timber connection, presented in Figure 1, have been considered. Timber part with thickness of $t_1 = 150$ mm is connected to the steel part with thickness of $t_2 = 20$ mm. The timber class is C24, and the bolt is made of steel grade 8.8. In the first variant, a bolt with diameter d = 10 mm and washer with outer diameter Ø30 was used, while in the second variant a bolt with diameter d = 8 mm with washer 50×50 mm was used. The washer and the steel element are on the opposite sides of the timber element. The load acts parallel to the grain.

The connection calculation has been done applying the standard Eurocode 5 [3]. It has been considered that only cases of connection failure that include timber yield occur. According to this, only the deformation of the part of the bolt inside the timber part has been analysed, and the bolt strength at shear and bearing of the steel element has not been considered. The relation of the bolt diameter and the steel element thickness was $t_2/d \geq 1$ in both analysed cases, which implies that the bolt was fixed into the steel element, and there was no rotation of the bolt head.
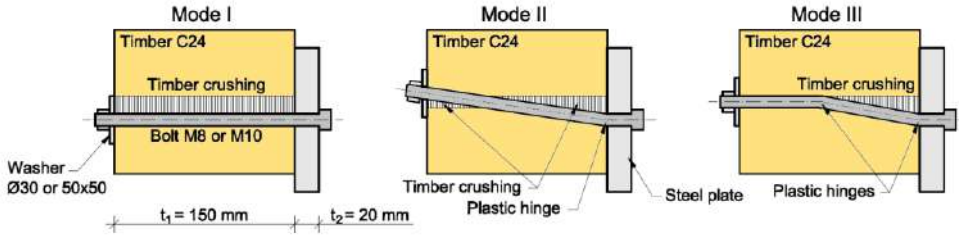
Figure 1 – Possible failure modes of the considered connection

The connection strength is determined according to the formula:

$$F_{v,Rk} = min \begin{cases} f_{h,k} \, d \, t_1 \\ f_{h,k} \, d \, t_1 \left[\sqrt{2 + \frac{4 \, M_{y,Rk}}{f_{h,k} \, d \, t_1^2}} - 1 \right] + \frac{F_{ax,Rk}}{4} \\ 2.3 \sqrt{M_{y,Rk} \, f_{h,k} \, d} + \frac{F_{ax,Rk}}{4} \end{cases}$$ (1)

where:
$f_{h,k}$ is characteristic embedment strength of the timber,
d is bolt diameter,
t_1 is timber element depth,
$M_{y,Rk}$ is characteristic bolt yield moment,
$F_{ax,Rk}$ is characteristic withdrawal capacity of the bolt.

Characteristic embedment strength of the timber may be determined experimentally [6], or using the formula:

$$f_{h,k} = 0.082 \, (1 - 0.01 \, d) \, \rho_k$$ (2)

where:
ρ_k is characteristic mass density of timber in kg/m³.

Characteristic bolt yield moment is determined based on its diameter and steel grade, according to the research [5]:

$$M_{y,Rk} = 0.3 \, f_u \, d^{2.6}$$ (3)

where:
f_u is the ultimate strength in MPa of the steel used for bolt fabrication.

Characteristic withdrawal capacity of the bolt can be determined using the formula:

$$F_{ax,Rk} = 3 \, f_{c,90,k} \, A_w$$ (4)

where:
$f_{c,90,k}$ is the characteristic compressive strength of the timber perpendicular to the grain,
A_w is the area of contact of the washer and timber (perpendicularly to the grain).

Influence of the rope effect at bolt connection can not be greater than of the 25 % Johansen's part. In the Table 1 is presented calculation of the connection for variant 1 and variant 2.

Table 1 – Calculation of the connection timber-steel (variant 1 and 2) according to EC 5

Item	Unit	Variant 1	Variant 2
ρ_k	$[kg/m^3]$	350.0	
$f_{h,k}$	$[N/mm^2]$	25.83	26.40
t_1	$[mm]$	150.0	
f_u	$[N/mm^2]$	800.0	
$M_{y,Rk}$	$[N\ mm]$	95 546	53 487
d	$[mm]$	10.0	8.0
Washer	$[mm]$	Ø 30	50×50
A_w	$[mm^2]$	620	2 413
$f_{c,90,k}$	$[N/mm^2]$	2.50	
$F_{ax,Rk}$	$[N]$	4 650	18 101
$F_{v,Rk,1}$	$[N]$	38 745	31 685
$F_{v,Rk,2}$	$[N]$	18 105	17 032
$F_{v,Rk,3}$	$[N]$	12 588	9 664
$F_{v,Rk}$	$[N]$	12 588	9 664

3. PROPOSITION FOR CALCULATION PROCEDURE OF THE BOLT YIELD MOMENT

Influence of the axial force on the value of the bolt yield moment may be introduced by a non-dimensional coefficient η ($0 \leq \eta \leq 1$), used to multiply the bolt yield moment obtained by relation (3), wherewith one gets the reduced yield moment:

$$M_{y,Rk}{}^{red} = \eta\ M_{y,Rk} \tag{5}$$

Plasticization of the cross-section of the member occurs due to the bending moment and axial force. The axial force plasticizes the cross-section part around the central horizontal axis, while the bending moment plasticizes the parts above and bellow that zone (Figure 2). The zone plasticized by the axial force has an area A_N and height h_N.
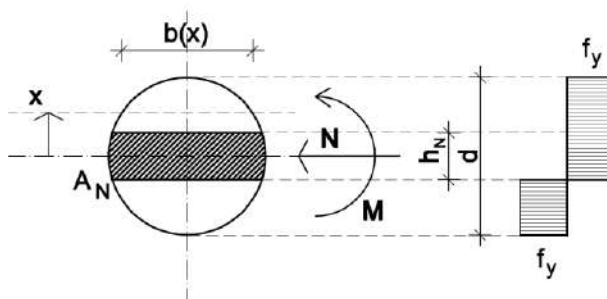

Figure 2 – Zones of plasticization of the bolt cross-section

The function of the cross-section width depending on the distance from the horizontal central axis, which is needed for further derivation:

$$b(x) = \sqrt{d^2 - 4\,x^2} \tag{6}$$

where:
x is the current coordinate.

The area of the zone plasticized by axial force is determined based on the bolt withdrawal capacity and quality of the material used for bolt fabrication. The following relations provide the area A_N, ratio between the area A_N and the total area of the bolt cross-section (A), and ratio of the yield moment with and without the influence of the axial force (η).

$$A_N = \frac{F_{ax,Rk}}{f_y} = \frac{F_{ax,Rk}}{0.8\,f_u} \tag{7}$$

$$A_N/A = \frac{\int_0^{h_N/2} b(x)\,dx}{\int_0^{d/2} b(x)\,dx} \tag{8}$$

$$\eta = M_{y,Rk}{}^{red}/M_{y,Rk} = \frac{\int_{h_N/2}^{d/2} x\,b(x)\,dx}{\int_0^{d/2} x\,b(x)\,dx} \tag{9}$$

where:
f_y is the yield point of the bolt material ($f_y = 0.8\,f_u$) [3].

In the following table are given coefficients of the ratio of the zone height A_N and the bolt diameter, ratio of the areas, and ratio of the reduced yield moment and the yield moment according to Eurocode 5. The figure 3 presents those dependences graphically.

Table 2 – Plasticized/total area and reduced/total moment ratios

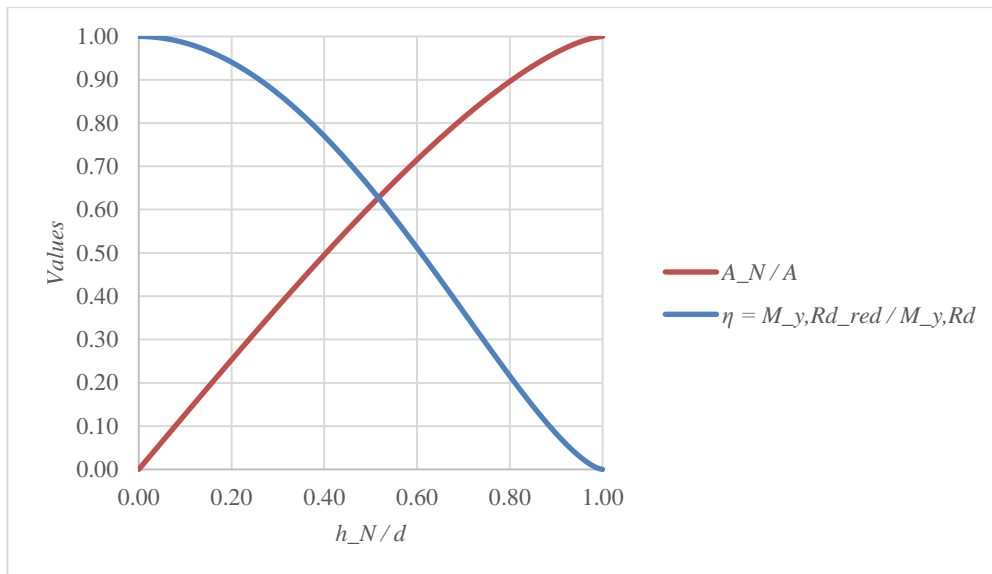| h_N/d	A_N/A	$\eta = M_{y,Rk}{}^{red}/M_{y,Rk}$
0.0	0.000	1.000
0.1	0.127	0.985
0.2	0.253	0.941
0.3	0.376	0.868
0.4	0.495	0.770
0.5	0.609	0.645
0.6	0.715	0.512
0.7	0.812	0.364
0.8	0.896	0.216
0.9	0.963	0.083
1.0	1.000	0.000

Figure 3 – Dependence of the area ratio and yield moment ratio
on the height of the zone plasticized by axial force

4. CONNECTION BEARING CAPACITY ACCORDING TO THE PROPOSED PROCEDURE

For the calculation according to the proposed procedure it is necessary to calculate bolt withdrawal capacity first, and after that the Johansen's part using the reduced bolt yield moment. The connection calculation is presented in Table 3. The values that are identical to the values from the Table 1 are omitted. The values $F_{v,Rk}$ were calculated based on relations (1), except that instead of the bolt yield moment $M_{y,Rk}$, the reduced bolt yield moment $M_{y,Rk}^{red}$ has been taken.

One may see from the table that connection strength of the first variant 12 550 N, and the second 8 090 N. Influence of the axial force on the bolt yield moment is lower at the first variant compared to the second one.

Table 3 – Calculation of the connection timber-steel (variant 1 and 2) according to the proposed procedure

Item	Unit	Variant 1	Variant 2
$F_{ax,Rk}$	$[N]$	4 650	18 101
$A_N = F_{ax,Rk}/(0.8\,f_u)$	$[mm^2]$	7.27	28.28
A_N/A	-	0.09	0.56
h_N/d	-	0.07	0.46
$\eta = M_{y,Rk}{}^{red}/M_{y,Rk}$	-	0.993	0.701
$M_{y,Rk}$	$[N\,mm]$	95 546	53 487
$M_{y,Rk}{}^{red}$	$[N\,mm]$	94 901	37 482
$F_{v,Rk,1}$	$[N]$	38 745	31 685
$F_{v,Rk,2}$	$[N]$	18 099	16 845
$F_{v,Rk,3}$	$[N]$	12 550	8 090
$F_{v,Rk}$	$[N]$	12 550	8 090

5. CONCLUSION

The presented calculation covers two variants of the connection between a timber and a steel element, with different bolt diameters and washer areas. The connections have been calculated according to the Johansen's procedure given in Eurocode 5.

The bolt withdrawal capacity is proportional to the washer area that is in contact with the timber surface. During the calculation it was considered that washers possess sufficient thickness that enables for the whole washer area to press the timber element approximately equally, that is, the maximal possible withdrawal capacity is achieved. The washer area in the variant 2 is greater 289 % compared to the area in the variant 1, which implies that the bolt withdrawal capacity in the variant 2 that higher.

The bolt yield moment is higher in the variant 1 due to the larger bolt diameter. The axial force decrease the bolt yield moment, namely: in variant 1 less than 1 %, while in variant 2 the decrease is 30 %. The significantly higher decrease of the yield moment in variant 2 occurs because of the higher withdrawal capacity and smaller bolt diameter, which contributes that axial force plasticizes considerably larger part of the cross-section.

The connection bearing capacity is 23 % lower in the variant 2 compared to the variant 1, if the influence of the axial force on plasticization is neglected. After the calculation with reduced bolt yield moments, it was deduced that decrease of the connection bearing capacity in variant 1 less than 1 %, while in the variant 2 the strength is reduced 16 %. According to this, one may conclude that the bearing capacity reduction in case of application of bolts with larger diameters and low withdrawal capacity is negligible, while in case of bolts with smaller diameters and high withdrawal capacity it is significant.

The proposed procedure for determining of the reduced yield moment is not complex, so it is recommended to conduct the check of the influence of the axial force in any case.

REFERENCES

[1]   EN 26891: Timber structures – Joints made with mechanical fasteners – General principles for the determination of strength and deformation characteristics, 1991.

[2]   K. W. Johansen. Theory of Timber Connections, Int Assoc Bridge Struct Eng, vol. 9, pp. 249-262, 1949.

[3]   EN 1995-1-1: Eurocode 5: Design of timber structures: Part 1-1: Common rules and rules for buildings, 2004.

[4]   EN 1995-1-1: Eurocode 5: Design of timber structures: Part 1-1: General rules and rules for buildings, 1994.

[5]   H. J. Blass, A. Bienhaus, V. Krämer. Effective bending capacity of dowel-type fasteners, Proceedings PRO, pp. 71-80, 2001.

[6]   EN 383: Timber Structures - Test methods - Determination of embedment strength and foundation values for dowel type fasteners, 2007.

Nađa Simović[1], *Ivan Glišović*[2], *Marija Todorović*[3]

METODE PRORAČUNA VIBRACIJA MEĐUSPRATNIH KONSTRUKCIJA OD UNAKRSNO LAMELIRANOG DRVETA

Rezime:

Unakrsno lamelirano drvo (CLT) je inovativni pločasti proizvod na bazi drveta koji se dobija lepljenjem slojeva ortogonalno postavljenih drvenih lamela (dasaka). CLT paneli predstavljaju efikasno rešenje za međuspratne konstrukcije u jednoetažnim i višeetažnim zgradama. Zbog male težine i velikih raspona, dimenzionisanje ovih međuspratnih konstrukcija najčešće je uslovljeno kriterijumima graničnih stanja upotrebljivosti, tj. ograničenjima za deformacije i vibracije. Vibracije međuspratnih konstrukcija prouzrokovane ljudskim aktivnostima, kao što je hodanje, neće dovesti do loma konstrukcije, ali mogu uticati na komfor korisnika ukoliko nisu adekvatno kontrolisane. U radu je dat pregled nekoliko metoda za proračun vibracija pri proveri graničnih stanja upotrebljivosti CLT međuspratnih konstrukcija stambenih zgrada. Razmatrane su razlike u obuhvaćenim parametrima i graničnim vrednostima ovih metoda.

Ključne reči: CLT međuspratna konstrukcija, vibracije, pobuda hodanjem, proračunska metoda

VIBRATION SERVICEABILITY DESIGN METHODS FOR CROSS LAMINATED TIMBER (CLT) FLOORS

Summary:

Cross laminated timber (CLT) is an innovative engineering wood product made by gluing layers of solid timber boards placed in orthogonally alternating orientation to the neighbouring layers. CLT panels provide an efficient solution for floors in single- and multi- storey buildings. Due to the light-weight and often long-span, design of these floors is generally governed by serviceability limit state criteria, that is deflection or vibration limits. Floor vibrations induced by dynamic actions, such as people walking, do not result in structural failure but may cause discomfort of occupants if the vibrations are not properly controlled. This paper gives an overview of some available methods for vibration serviceability design of residential CLT floors. Differences in considered parameters and limit values of these methods are discussed.

Key words: CLT floor, vibrations, walking excitation, design method

---

[1] *Asst. MSc, Faculty of Civil Engineering, University of Belgrade, Belgrade, Serbia, nsimovic@grf.bg.ac.rs*

[2] *Assoc. Prof., PhD, Faculty of Civil Engineering, University of Belgrade, Belgrade, Serbia, ivang@grf.bg.ac.rs*

[3] *Asst., Prof., PhD, Faculty of Civil Engineering, University of Belgrade, Belgrade, Serbia, todorovicm@grf.bg.ac.rs*

1. INTRODUCTION

Cross laminated timber (CLT) is a massive engineering wood product made by gluing cross-wise layers of solid timber boards to form large-scale panels. CLT products are usually fabricated with an odd number of layers (in general three to seven layers). Due to excellent in-plane and out-of-plane resistance, CLT panels have become very common for walls and floors elements. Advantages such as dimensional stability, good acoustic and thermal properties, and high level of prefabrication make CLT a competitive structural material for many buildings types.

For CLT panels used as floor elements serviceability limit state (deformation, vibration) generally controls the design. Although floor vibrations may result from many sources (e.g. use of machinery, external traffic, explosions), the most common and problematic ones are caused by the occupants themselves from their everyday activities. Such vibrations are particularly problematic because they cannot be easily isolated from the structure and they occur frequently. Human-induced vibrations do not collapse the floors, but can annoy occupants or cause malfunction of vibration sensitive equipment. Consequently, requirement for the design against disturbing vibrational performance is particularly important for light-weight floors built from materials such as timber. In addition, vibration serviceability of timber floors is becoming more relevant due to increased demand for building new floor systems with larger spans.

Vibrational serviceability of timber floor systems has received much attention in recent decades, with different design guidelines being suggested. Proposed design methods range from simple limitations of static deflection to the ones intended to limit fundamental frequency and vibration velocity or acceleration levels at floor surfaces caused by defined excitations [1]. However, vibration serviceability design criterions applied to traditional timber floors are probably not appropriate for CLT floor design.

This paper focuses on the basic principles for vibration design of residential floors made of cross laminated timber. Some available design methods are presented and compared. Due to differences in considered parameters and limit values, application of these methods may lead to significantly divers results.

2. FLOOR DYNAMICS

Annoying vibration of timber floors is commonly associated with walking excitation. Walking frequency (common range 1.5-2.5 Hz) has a direct impact on dynamic load applied. The dynamic force from walking has been found to excite frequencies up to the third or fourth harmonic of walking frequency.

Vibration response of a floor when subjected to dynamic loading depends on its stiffness, mass and damping. Stiffness and mass determine floor's natural frequencies, while damping affects the time it takes for an induced vibration to decay. Depending on the value of fundamental frequency, vibration response of floor due to people walking may differ [2]. So called low-frequency floors have fundamental frequency below 8-10 Hz and can respond to walking excitation with resonant vibrations. The resonance is constantly maintained by continuous walking. On the other hand, high-frequency floors with fundamental frequency above 8-10 Hz show a transient vibration response to individual heel strike from each footstep. Depending on the intervals between successive impacts and damping of vibration, adjacent transient vibration responses may interact with each other.

Response of floors to an impact can be represented by the time history of displacement, velocity or acceleration. Quantities such as peak value or root-mean-square (r.m.s.) value have

been used as a measure of human sensitivity to vibration. The peak value is extracted from the initial part of the response (forced vibration) due to an impact. The r.m.s. value is determined from the entire response, including initial forced and free vibration parts of the response.

3. HUMAN PERCEPTION OF FLOOR VIBRATION

Human body is an incredibly complex and sensitive receiver which is self-adapting and more or less susceptible to almost any type and level of motion, such as periodic, random or transient vibrations, which normally occur in nature [3]. Acceptable vibration levels for human occupancies vary with individual, person's activity, body posture, life environment and expectation of felt vibrations. Presence of visual or audio effects may significantly reduce the acceptable vibration magnitude. Therefore, it is difficult to set the threshold of human perception of vibrations.

Characterization of building vibration with respect to human response is given in ISO 10137 Annex C [4], which includes "base curves" expressed as a function of r.m.s acceleration and frequency. At vibration acceleration magnitudes below values corresponding to the base curves, in general adverse comments, sensations or complaints are very rare. Since the magnitude, which is considered to be satisfactory, depends on the circumstances, multiplying factors are used to increase the acceleration level of these base curves according to intended use of the building. These multiplying factors are referred to as "response factors".
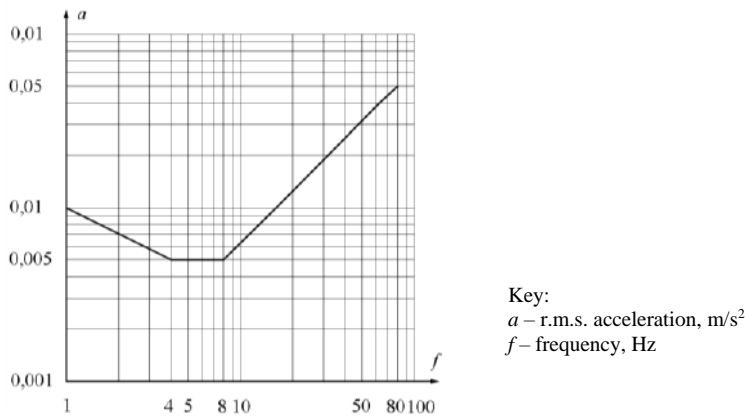

Key:
a – r.m.s. acceleration, m/s^2
f – frequency, Hz

Figure 1 – Building vibration z-axis base curve for acceleration (vertical direction) [4]

The base curve for vertical vibration is presented in Figure 1. The graph shows that the perception threshold for vibrations is lowest for frequency range between 4 to 8 Hz, with constant value of $a_{\text{rms,base}} = 0.005$ m/s^2. Vibrations having a frequency between 4 and 8 Hz are particularly critical because large body organs within the rib cage and abdomen resonate within this frequency range. Above 8 Hz minimum perception level is not constant in terms of acceleration but it increases as the frequency increases. However, when this part of curve is integrated, it can be shown that it is constant in terms of velocity with a value of $v_{\text{rms,base}} = 0.0001$ m/s. Therefore, below floor frequency of 8 Hz acceleration criterion for vibration perception threshold can be applied and above 8 Hz velocity criterion can be applied.

4. DESIGN METHODS FOR CLT FLOOR VIBRATIONS

Vibration serviceability design method in current Eurocode 5 essentially refers to design of timber-joisted floors, where annoying vibration is attributed to isolated floor structure. As CLT floors are solid slabs, their dynamic properties differ from that of traditional timber floors. CLT slabs can have hinge-like joints between adjacent segments that enforce vertical translation continuity but not continuity of curvature at those locations, which makes their behaviour inconsistent with joisted floors. For floor elements supported at four sides, the transverse load-carrying effect should be taken into account. Due to the orthotropic nature of CLT, floor stiffness is not equal in perpendicular directions, but continuous support can be provided to all edges. For multi-span systems, continuous slab effect should be considered.

Multi-storey CLT buildings are generally platform construction, where each successive storey is built from the floor below, hence the floor is clamped in between walls of two storeys. A degree of semi-rigidity is therefore expected in all CLT floor-to-wall connections, which combined with the stiffness of the walls above and below, will influence the dynamic response of the floor. Thus, another highly important aspect of vibrations is seen in the influence of support conditions (e.g. hinged, partly clamped, clamped) and in the influence of upper storey loads transmitted through the walls on the degree of clamping.

4.1. DESIGN METHOD ACCORDING TO HAMM ET AL.

Vibration serviceability design method proposed by Hamm et al. [5] is a result of research project at Technical University of Munich which involved experimental and theoretical investigations of different types of timber floors (timber joisted floors, timber-concrete floors, massive timber floors). Austrian National annex ÖNORM B 1995-1-1 is based on this study. It should be mentioned that this is the only National annex to Eurocode 5 which deals with vibrations of CLT floors.

Rules for design and construction applicable to timber floors are divided in three different classes according to Table 1. First step is to decide whether floors should be with higher or lower demands or without any demands in terms of vibration performance.

In general, fundamental frequency f_1 of floor is used for verification of frequency criterion. Fundamental frequency of simply supported rectangular floor can be calculated as:

- For floors supported on two sides:

$$f_1 = \frac{\pi}{2 \cdot L^2} \sqrt{\frac{(EI)_L}{m}} \quad [\text{Hz}] \tag{1}$$

- For floors supported on all four sides:

$$f_1 = \frac{\pi}{2 \cdot L^2} \sqrt{\frac{(EI)_L}{m}} \sqrt{1 + \left(\frac{L}{B}\right)^4 \frac{(EI)_B}{(EI)_L}} \quad [\text{Hz}] \tag{2}$$

where:
L is floor span, in m;
B is floor width, in m;
m is mass per unit area of floor, in kg/m^2.

($EI)_L$ is effective stiffness in longitudinal direction of the CLT element (with possible final screed, but without composite action, just adding its own moment of inertia), in Nm^2/m;

($EI)_B$ is effective stiffness in transverse direction of the CLT element, where $(EI)_L > (EI)_B$, in Nm^2/m.

Table 1 – Floor classes, constructive requirements and limiting values of criterions [5]

	Floor class I	Floors class II	Floors class III
Vibration demands	Floors with higher demands	Floors with lower demands	Floors without demands
Description of perception of vibrations	- Vibrations are not perceptible or perceptible only when concentrating on them - Vibrations are not annoying	- Vibrations are perceptible - Vibrations are not annoying	- Vibrations are clearly perceptible - Vibrations are sometimes annoying
Type of use	- Corridors with short span - Floors with different occupancies - Floors in offices	- Floors inside occupancies - Floors in single-family houses under normal use	- Floors under non-residential rooms or roof spaces
Constructive requirements	Floating, heavy or light screed on grit fill or not	Floating, heavy or light screed on grit fill or not	-
Frequency criterion	$f_{limit} = 8$ Hz	$f_{limit} = 6$ Hz	-
Stiffness criterion	$w_{limit} = 0.5$ mm	$w_{limit} = 1.0$ mm	-
Acceleration criterion	$a_{limit} = 0.05$ m/s^2	$a_{limit} = 0.1$ m/s^2	-

Since subjective evaluation of vibration behaviour of floors is not in correlation with frequency, it is equally important to check the stiffness criterion. Deflection of floor due to a point load of 2 kN may be determined as:

$$w_{2kN} = \frac{2 \cdot L^3}{48 \cdot (EI)_L \cdot B_{eff}} \quad [\text{mm}] \tag{3}$$

with

$$B_{eff} = \min\left\{ \frac{L}{1.1} \cdot \sqrt[4]{\frac{(EI)_B}{(EI)_L}}; B \right\} \tag{4}$$

where:

B_{eff} is effective floor width for calculating deflection, in m;

L, B, $(EI)_L$ and $(EI)_B$ are as previously defined.

The reason for choosing the load of 2 kN instead of usual 1 kN was good correlation between the values of deflection and subjective evaluation of vibration behaviour.

In verification procedure, vibration serviceability limit state for CLT floors is satisfied if limiting values given in Table 1 are not exceeded. For floors classified as floor classes I and II, fundamental frequency shall be at least $f_{1,min}$ = 4.5 Hz. In the case of floor structure with $f_{1,min} \leq f_1 \leq f_{limit}$, in addition to the stiffness criterion, limiting value of vibration acceleration should be satisfied. Value of vibration acceleration can be calculated as follows:

$$a = \frac{F_{dyn}}{M^* \cdot 2 \cdot \zeta} = \frac{0.4 \cdot F(t)}{0.25 \cdot m \cdot L \cdot B \cdot 2 \cdot \zeta} \quad \left[m/s^2 \right]$$

(5)

where:

F_{dyn} is total dynamic force that includes factor of 0.4 considering that the force on the floor is acting during a limited time and not always in the middle of the span, in N;

$F(t)$ are harmonic parts of the force on the floor (for third harmonic part $F(t)$ = 70 N);

M^* is modal mass of the floor, in kg;

ζ is modal damping ratio of floor construction (for bare CLT floors ζ = 0.01; for CLT floors with floating screed ζ = 0.02);

m, L and B are as previously defined, but for this criterion B should be less than $1.5 \cdot L$.

4.2. DESIGN METHOD ACCORDING TO THIEL ET AL.

Based on in-situ measurements on CLT buildings at different construction phases conducted by the Competence Centre holz.bau forschungs gmbh Austria, Thiel et al. [6] expanded and modified design method suggested by Hamm et al.

As mentioned before, in addition to frequency and stiffness criterion, vibration acceleration if fundamental frequency is below critical value needs to be checked. Without detailed explanation as following equations refer to the previous design method, the focus is on additional parameters that are taken into account.

When floor is supported on all four sides, the transverse load-carrying effect should be considered. That means that both torsional stiffness D_{xy} and effective bending stiffness in transverse direction $(EI)_B$ should be included in calculation of fundamental frequency as follows:

$$f_1 = \frac{\pi}{2 \cdot L^2} \sqrt{\frac{(EI)_L}{m}} \sqrt{1 + \left(\frac{L}{B}\right)^2 \cdot \frac{2 \cdot D_{xy}}{(EI)_L} + \left(\frac{L}{B}\right)^4 \frac{(EI)_B}{(EI)_L}} \quad [Hz]$$

(6)

Furthermore, shear flexibility in CLT element should be taken into account by using the effective apparent bending stiffness $(EI)_L$ (based on bending and shear deformations). Additionally, different support conditions and continuous floor effect for multi-span floors can be considered through modification factors k_m and $k_{f,2}$ that multiply the frequency.

In examination of stiffness criterion, the maximum instantaneous vertical deflection due to a concentrated static force F =1 kN should be determined and compared with the limit value. Load distribution and shear flexibility should be considered when calculating the deflection:

$$w_{1kN} = \frac{F \cdot L^3}{48 \cdot (EI)_L \cdot B_{eff}} + \frac{F \cdot L}{4 \cdot (GA)_L \cdot B_{eff}} \quad [mm]$$

(7)

where:

B_{eff} is floor effective width according to eq. (4);

$(GA)_L$ is effective shear stiffness in longitudinal direction of the CLT element.

Vibration acceleration depends on effective (generalised) floor mass M_{gen}, floor fundamental frequency f_1, excitation frequency f_f (see Table 2), Fourier coefficient of the prevailing harmonic partial oscillation $\alpha_{i,f1}$ (see Table 2), self-weight of excitatory person $F_0 = 700$ N and on modal damping ratio ζ. For single-span floors, it may be determined as:

$$a = \frac{0.4 \cdot \left(\dfrac{F_0 \cdot \alpha_{i,f_1}}{M_{gen}} \right)}{\sqrt{\left(\left(\dfrac{f_1}{f_f} \right)^2 - 1 \right)^2 + \left(2 \cdot \zeta \cdot \dfrac{f_1}{f_f} \right)^2}} \quad \left[\text{m/s}^2 \right]$$ (8)

with effective floor mass:

$$M_{gen} = m \cdot \frac{L}{2} \cdot B_{eff} \quad \left[\text{kg/m}^2 \right]$$ (9)

where B_{eff} is floor effective width according to eq. (4), but with $B_{eff} \leq$ half room width $B/2$.

Table 2 – Fourier coefficients and excitation frequencies based on fundamental frequency [6]

Fundamental frequency f_1 [Hz]	Fourier coefficient $\alpha_{i,f1}$	Excitation frequency f_f [Hz]
$4.5 < f_1 \leq 5.1$	0.20	f_1
$5.1 < f_1 \leq 6.9$	0.06	f_1
$6.9 < f_1 \leq 8.0$	0.06	6.9

The damping ratio ζ for CLT floors was found to be between 2% and 3.5% depending on the type of floor construction and support conditions.

4.3. DESIGN METHOD ACCORDING TO HU AND GAGNON

Hu and Gagnon [7] developed design criterion based on understanding the fundamentals of CLT floor vibrations as well as laboratory tests and subjective evaluation of vibration floor performance conducted in Canada. The CSA O86 Technical Committee included this vibration-controlled design method in the CLT design guidance of CSA Standard.

Based on the laboratory study data analysis, it was found that vibrations induced by normal walking could be effectively controlled by designing a floor with a proper combination of the longitudinal stiffness and mass, expressed by the fundamental frequency f_1 and 1 kN static deflection w of a 1 m wide CLT panel. The design criterion is expressed as:

- For bare CLT floors or CLT floors with light topping:

$$\frac{f_1}{w^{0.7}} \geq 13.0$$ (10)

- For CLT floors with heavy topping (mass per unit area > 100 kg/m^2):

$$\frac{f_1}{w^{0.7}} \geq 20.0$$ (11)

Proposed limit values may be increased for multi-span floors and floors with semi-rigid or rigid support conditions, as these changes of parameters increase the natural frequency.

Fundamental frequency of a simply supported CLT panel may be calculated as:

$$f_1 = \frac{\pi}{2 \cdot L^2} \sqrt{\frac{(EI)_L}{\rho A}} \quad [\text{Hz}] \tag{12}$$

where:
L is floor span, in m;
$(EI)_L$ is effective apparent bending stiffness in span direction for 1 m wide panel, which takes into account shear deformation, in Nm^2;
ρ is density of CLT panel, in kg/m^3;
A is cross section area of 1 m wide CLT panel, in m^2.

Static deflection at mid-span of simply supported CLT panel under 1 kN point load may be calculated as:

$$w = \frac{1000 \cdot F \cdot L^3}{48 \cdot (EI)_L} \quad [\text{mm}] \tag{13}$$

where:
F is vertical concentrated static force of 1000 N applied at mid-span of the floor;
L and $(EI)_L$ are as previously defined.

4.4. DESIGN METHOD ACCORDING TO ABEYSEKERA ET AL.

Abeysekera et al. [8] presented new design rules for vibration serviceability of timber floors, which are currently being drafted in CEN/TC250/SC5/WG3 Sub-group 4 "Vibrations". The revision of the chapter on vibrations in Eurocode 5 is adapted for use in the design of floor structures made from CLT.

The new design method for human induced floor vibrations introduces floor performance levels as given in Table 3. Level I stands for best floor performance level, VI for worst, but still acceptable, and VII for unacceptable floor performance level. Recommendation for selection of floor performance level for residential categories is shown in Table 4. Nevertheless, these floor performance levels should be specified in National annexes of each member country, as it is necessary to consider culture variations between countries, or they should be specified by investors or designers.

Table 3 – Floor performance levels and corresponding criterions [8]

Criterion	Floor performance levels						
	I	II	III	IV	V	VI	VII
Frequency criterion f_1 [Hz] $\geq$	4.5						
Stiffness criterion w [mm] $\leq$	0.25		0.5	0.8	1.2	1.6	no criterion
Response factor $R \leq$	4	8	12	16	20	24	
Acceleration criterion (when $f_1 < 8$ Hz) a_{rms} [m/s^2] $\leq$	$R \times 0.005$						
Velocity criterion (when $f_1 \geq 8$ Hz) v_{rms} [m/s^2] $\leq$	$R \times 0.0001$						

Table 4 – *Recommended selection of floor performance levels for residential use category* [8]

Use category	Quality choice	Base choice	Economy choice
Residential – multi-storey	Level I, II, III	Level IV	Level V
Residential – single house	Level I, II, III, IV	Level V	Level VI

For floor performance levels from I to VI no further investigations are necessary if requirements in respect to fundamental frequency, acceleration or velocity and stiffness from Table 3 are satisfied.

In case of single- or multi-span rectangular floors supported on two or four sides directly onto rigid supports, primarily subjected to uniform loading, fundamental frequency may be determined as:

$$f_1 = k_{e,1} \cdot k_{e,2} \cdot \frac{\pi}{2 \cdot L^2} \sqrt{\frac{(EI)_L}{m}} \quad [\text{Hz}] \tag{14}$$

with

$$k_{e,2} = \sqrt{1 + \left(\frac{L}{B}\right)^4 \frac{(EI)_B}{(EI)_L}} \tag{15}$$

where:

$k_{e,1}$ is frequency multiplier in case of a double-span floor on rigid supports;
$k_{e,2}$ is frequency multiplier in case of a two-way spanning floor;
L is floor span, in m;
B is floor width, in m;
$(EI)_L$ is apparent effective bending stiffness in longitudinal floor direction which should take into account shear deformation where applicable and may take into account bending stiffness of floating floor or screed (without composite action), in Nm^2/m;
$(EI)_B$ is effective bending stiffness in transverse floor direction, in Nm^2/m;
m is mass per unit area of the floor, in kg/m^2.

When calculating vibrations, floor mass should be a unique value including at least the sum of mass caused by permanent loads (self-weight of the floor as well as all supported or suspended horizontal layers). The floor mass may also include mass caused by quasi-permanent value of uniformly distributed imposed loads. It is recommended to consider only additional mass induced by movable equipment (such as furniture) limited to 10% of total imposed loads.

If all factors affecting deflection are considered, for instance when floors are spanning partially or totally on non-rigid supports or when floors are not only subjected to uniform loading, eq. (14) may be replaced with:

$$f_1 = k_{e,1} \cdot k_{e,2} \cdot \frac{18}{\sqrt{\delta_{sys}}} \quad [\text{Hz}] \tag{16}$$

where δ_{sys} is deflection of the floor under self-weight load applied on a single bay in a multi-span case, in mm.

When fundamental frequency of floor is below 8 Hz, floor vibration is assumed resonant. For resonant vibration design situations, root mean square acceleration a_{rms} may be approximated as:

$$a_{\mathrm{rms}} = \frac{0.4 \cdot \alpha \cdot F_0}{\sqrt{2} \cdot 2 \cdot \zeta \cdot M^*} \quad \left[\mathrm{m/s}^2\right] \tag{17}$$

where:

α   is Fourier coefficient according to the fundamental frequency as $\alpha = \mathrm{e}^{-0,4 \cdot f_1}$;
F_0 is vertical load of a walking person, usually taken as 700 N, in N;
ζ   is modal damping ratio;
M^* is modal mass (taken as 50% of $m \cdot L \cdot B$ for floors supported on two sides, and as 25% of $m \cdot L \cdot B$ when floor is supported on all four sides), in kg;

When fundamental frequency of floor is equal to or above 8 Hz, floor vibration is assumed transient. For transient vibration design situations, root mean square velocity v_{rms} may be approximated as:

$$v_{\mathrm{rms}} = \beta \cdot v_{\mathrm{tot,peak}} = \beta \cdot k_{\mathrm{imp}} \cdot v_{1,\mathrm{peak}} = \beta \cdot k_{\mathrm{imp}} \cdot k_{\mathrm{red}} \cdot \frac{I}{M^*} \quad [\mathrm{m/s}] \tag{18}$$

with

$$k_{\mathrm{imp}} = \max \left\{ \begin{array}{c} 0.48 \cdot \left(\dfrac{B}{L}\right) \cdot \left(\dfrac{(EI)_L}{(EI)_B}\right)^{0.25} \\ 1.0 \end{array} \right\} \tag{19}$$

$$I = \frac{42 f_{\mathrm{w}}^{1.43}}{f_1^{1.3}} \tag{20}$$

where:
β $= (0.65 - 0.01 \cdot f_1) \cdot (1.33 - 11.0 \cdot \zeta) \cdot \eta$;
η $= 1.52 - 0.55 \cdot k_{\mathrm{imp}}$ when $1.0 \le k_{\mathrm{imp}} \le 1.5$, else $\eta = 0.69$;
$v_{\mathrm{tot,peak}}$ is total peak velocity response, in m/s;
k_{imp} is impulse multiplier factor;
$v_{1,\mathrm{peak}}$ is peak velocity response for fundamental mode, in m/s;
k_{red} is reduction factor with a value of 0.7 considering that exciting source on floor and sensing person are at a distance from each other;
I is mean modal impulse, in Ns;
f_{w} is walking frequency and is assumed to be 1.5 Hz for residential floors, in Hz;
ζ   is modal damping ratio;
M^*, L, B, $(EI)_L$, $(EI)_B$ and f_1 are as previously defined.

Realistic floor damping values are needed for the design procedure. Unless other values are proven to be more appropriate, modal damping ratio for CLT floors may be assumed between 2.5-6% depending on floor construction, support conditions, presence of non-load bearing partitions and presence of people on the floor.

For all floors, there is a stiffness criterion that checks maximum deflection due to a single point load of 1 kN placed in the most unfavourable position of a single span floor strip having an effective width B_{eff} calculated according to eq. (4). Although this empirical criterion based on historical practice is not very relevant for CLT floors due to the neglecting the floor mass, it allows an approximate comparison of proposed performance levels with existing requirements. Maximum deflection in mid-span of a single span floor may be calculated as:

$$w = \frac{F \cdot L^3}{48 \cdot (EI)_L \cdot B_{\text{eff}}} \quad \text{[mm]} \tag{21}$$

where all of the parameters are as previously defined.

5. DISCUSSION

Overall criterions that should be checked through different design methods are presented in Table 5. All methods have in common verification of frequency and stiffness criterion. Some of them also prove vibration velocity and acceleration.

Table 5 – Overview of considered criterions in different design methods

Method	Frequency	Stiffness criterion	Velocity criterion	Acceleration criterion
Hamm [5]	yes	yes	no	yes
Thiel [6]	yes	yes	no	yes
Hu [7]	yes	yes	no	no
Abeysekera [8]	yes	yes	yes	yes

Although some criterions are common to certain methods, it may happen that same criterions take into account different parameters. This may lead to noticeably different results. An overview of differences in consideration of some parameters is given in Table 6.

Table 6 – Overview of considered parameters in different design methods

Method	Support conditions	Shear flexibility	Transverse load-carrying effect	Effective width B_{eff}	Mass
Hamm [5]	no	no	yes	yes	$g_0 + \Delta g$
Thiel [6]	yes	yes	yes	yes	$g_0 + \Delta g$
Hu [7]	no	yes	no	no	g_0
Abeysekera [8]	yes	no	yes	yes	$g_0 + \Delta g + \psi_2 \cdot p$

Support conditions significantly affect the values of natural frequencies in a way that frequencies are increasing as floor is clamped or partly clamped. Clamping of floor can be achieved when load from upper floor is transferred through walls. This will also have a positive impact on deflections of floor. From the aspect of CLT as a material, shear flexibility is of crucial importance and it is highly advised to take it into account in the context of vibration. Consideration of shear flexibility leads to decrease in fundamental frequency and increase in deflection. Transverse load-carrying effect should be considered when floor is supported on all four sides. This parameter raises floor fundamental frequency depending mostly from the ratio of bending stiffness in longitudinal and transverse direction as well as on the ratio of floor width to span. Effective floor width B_{eff} has an impact on floor deflection in a way that taking into account the effective width reduces floor deflection. As previous parameter, this influence

greatly depends on the ratio of bending stiffnesses. Floor mass affects floor natural frequencies and vibration acceleration. Increase of the mass leads to lower natural frequencies and also vibration acceleration. Taking into account more mass according to vibration sensitivity has more positive than negative effects. Permanent loads should always be considered, but in certain cases it is reasonable to include quasi-permanent part of imposed loads.

When speaking of limit values, it is evident that the limit values for proposed criterions are based on highly subjective opinion of the test person. In order to get a better description of actual behavior of floor structure, a floor classification system based on vibration serviceability performance was developed.

6. CONCLUSION

Vibrational serviceability often governs design of timber floors. Due to its specific dynamic behaviour, the existing design methods for low- and high-frequency floors may not be applicable to CLT floors. For verification of CLT floor vibrations a several methods exist. However, it is currently impossible to define which guidelines would be best suited for prediction of unacceptable vibrations. This is due to differences in consideration of some parameters and limit values. Any reliable design approach should be derived from predictable and measurable parameters and should reflect the type of occupancy for which is it intended. Although simplicity of the procedure in practice is required, it must not be achieved to the detriment of accuracy.

REFERENCES

[1] Weckendorf J, Toratti T, Smith I, Tannert T. Vibration serviceability performance of timber floors, European Journal of Wood and Wood Products, 74, 2016, 353-367.

[2] Järnerö K. Vibrations in timber floors – dynamic properties and human perception. PhD Thesis, Linnaeus University, Sweden, 2014.

[3] Pavić A, Reynolds P. Vibration serviceability of long-span concrete building floors. Part 1: Review of background Information, Shock and Vibration Digest, 34 (3), 2002, 191-211.

[4] ISO 10137: Bases for design of structures – Serviceability of buildings and walkways against vibrations. International Organisation for Standardization, Switzerland, 2007.

[5] Hamm P, Richter A, Winter S. Floor vibrations – new results. World Conference on Timber Engineering – WCTE 2010, Italy, 2010.

[6] Thiel A, Zimmer S, Augustin M, Schickhofer G. CLT and floor vibrations: A comparison of design methods. CIB - W18 Meeting 46, Canada, 2013, paper 46-20-1.

[7] Hu L, Gagnon S. Controlling cross-laminated timber floor vibrations: Fundamentals and method. World Conference on Timber Engineering – WCTE 2012, New Zealand, 2012.

[8] Abeysekera I. K, Hamm P, Toratti T, Lawrence A. Development of a floor vibration design method for Eurocode 5. INTER Meeting 51, Estonia, 2018, paper 51-20-2.

Radomir Folić[1]*, Miloš Čokić*[2]*, Boris Folić*[3]

ANALIZA ROBUSNOSTI AB ZGRADE ZA RAZLIČITE SCENARIJE UKLANJANJA IVIČNIH STUBOVA

Rezime:

Analiza robusnosti konstrukcija je veoma kompleksna sa velikim brojem uticajnih parametara na ponašanje sistema izloženog određenom dejstvu. Robusnost predstavlja mogućnost konstrukcije da se, u slučaju lokalnog/delimičnog loma odupre progresivnom rušwnju. U ovom radu analiziran je uticaj uklanjanja ugaonih stubova na robusnost konstrukcije AB višespratne zgrade. Upoređene su razlika odgovora konstrukcije pri uklanjanju stubova na uglu zgrade i izvorne konstrkcije. Komparativna analiza izražena je sračunatim vrednostima graničnih stanja, krivih povredljivosti i procenjenih gubitka.

Ključne reči: AB zgrada, robusnost, granična stanja oštećenja, povredljivost, gubitak

ROBUSTNESS ANALYSIS OF A RC BUILDING FOR A DIFFERENT CORNER COLUMNS REMOVAL SCENARIOS

Summary:

The robustness of structures is a very complex problem with a large number of parameters that influence the analysis settings and the results that describe the behaviour of the system exposed to a certain action. Robustness represents the ability of a structural system to resist the progressive collapse. In this paper, the effect of the removal of the corner columns on the structural response and robustness of the structure was analysed. The goal of this research was to compare the difference of the structural response of the building, before and after the removal of the corner columns. In this paper, the effect of the removal of the corner columns was described through the limit state values comparison, fragility and vulnerability curves. Based on the analysis, obtained results are compared and final remarks and conclusions were formulated.

Key words: RC building, robustness, damage limit states, fragility, vulnerability

---

[1] *Dr. Ing., Professor Emeritus, University of Novi Sad, Faculty of Technical Sciences, Department of Civil Engineering, Trg Dositeja Obradovića 6, Novi Sad, Serbia, folic@uns.ac.rs , r.folic@gmail.com , (corresponding author)*

[2] *Dr. Ing., Structural Engineer, Termoenergo Inženjering, Bulevar Kralja Aleksandra 298, Belgrade, Serbia, cokicmilos@gmail.com*

[3] *Dr. Ing., University of Belgrade, Innovation Centre, Faculty of Mechanical Engineering, Kraljice Marije 16, Belgrade, Serbia, boris.r.folic@gmail.com*

1. INTRODUCTION

The robustness of the structure is its ability to prevent the complete collapse of the building or of its major part in the event of its partial failure. Robustness analysis is a very complex problem with a large number of parameters that influence the analysis settings and results that describe the behaviour of the system exposed to a certain action. At the same time, damage and collapse of structures cause accidental actions with a low probability of occurrence and often strong effects on the structure. However, in the case of accidental actions, local damage most often occurs, so it is important to assess the extent and location of the damage and their impact on the integrity of the structure, and/or possible loss of the system load bearing capacity.

The progressive collapse of a RC building structures most often occurs when one or more vertical supporting elements lose their load bearing capacity due to accidental actions. These can be terrorist attacks, vehicle impacts, gas explosions, etc. As previously stated, accidental actions occur very rarely, but are often accompanied by major consequences, even progressive collapse of the structure.

The most comprehensive review of numerical and experimental research and technical regulations dedicated to progressive collapse, with comparative analyses is presented in [1]. In the paper [2], a broader review of the literature and regulations for assessing robustness and appropriate recommendations and measures to prevent or mitigate the progressive collapse is presented. Some provisions from international documents related to the robustness of RC building structures were compared.

The paper [3] proposed a definition according to which robustness represents the ability of the structural system to resist progressive collapse. Beside the ones mentioned in the papers [1] and [4], there are several other definitions taken from the DoD UFC Guidelines [5], GSA [6] and corresponding literature. Significantly more precise improvements in the definition and reliability of methods for increasing robustness were proposed in the report COST Action TU-06012 - Robustness of Structures [7].

In the research [8], the results of the analysis of the structural system of buildings were presented, on the basis of which the bearing capacity of new and existing buildings and their influence on progressive collapse would be described. Fragility of RC building structures, which are predominantly present in Europe, is the subject of the paper [9].

The building structure was analyzed using a set of Eurocodes (EC0 to EC8), while the procedure described in [10] was used for the constitutive relations of RC and steel reinforcement.

In this paper, the effect of the removal of the corner columns A1, A2, A3, A4 and A5 on the structural response and robustness of the structure was analysed. A1 is the corner column on the 1st level (ground floor), A2 corresponds to the corner column on the 2nd level, A3 is on the 3rd, A4 is at the 4th and A5 is a corner column at the last floor of the building. The goal of this research was to compare the difference of the structural response of the building, based on the removal of the corner column, but on different level for each column removal scenario. The model of the building that was used in the analysis was used in the paper [11] in which the robustness of the structure was described using fragility curves, for the removal scenarios of all ground columns. In this paper, the effect of the removal of the corner columns was described through limits state values comparison, fragility and vulnerability curves.

Based on the analysis, obtained results are compared and final remarks and conclusions were formulated.

2. METHODOLOGY OF THE ANALYSIS

2.1. PROPERTIES OF THE STRUCTURE, LOADS AND ACTIONS

The subject of the analysis is office-residential building (Fig. 1) with 5 levels (ground floor+4 stories). The structural system exhibits the properties of a frame structural system [4]. The plan view and the 3D model of the structure are shown in Fig. 1. The length of one span in both directions is 4.8 m which makes the total length of the building 19.2 m in both directions. The height of the first story is 3.6 m and the height of the other stories is 3.2 m which makes the total height of the building 16.4 m. In order to simplify the modelling and calculation process, all vertical elements are fixed at the bottom level of the structure, i.e. soil-structure interaction is not included in the calculation and design. [11]
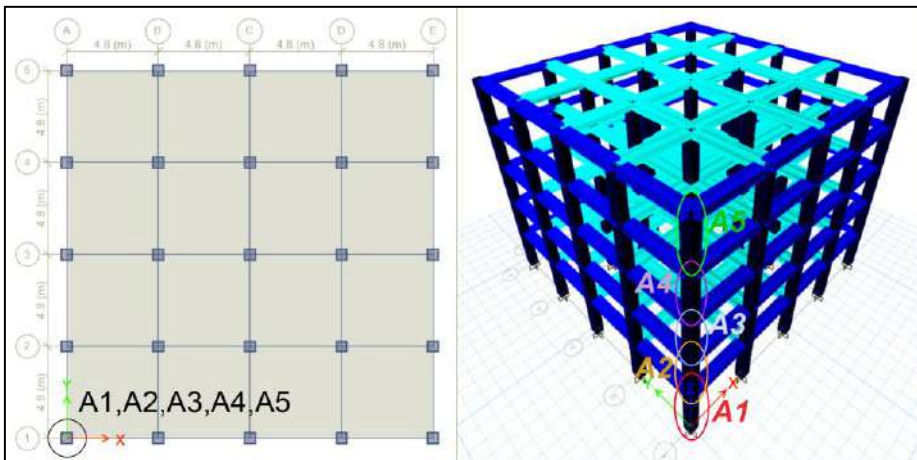
Figure 1 - Building plan with marked removed columns (left) ; Structure model (right)

The design of the structural model is done according to the recommendations given in the set of structural Eurocodes [12], [13], [14], [15]. Structural properties of the model and the loads acting on the structure are described in detail in the paper [11].

Load combinations, for the nonlinear robustness analysis, are used according to [5], [6]:

$$W = 1.2 \cdot G_i + 0.5 \cdot Q_i \qquad (1)$$

$$Q_R = \Omega_R \cdot (1.2 \cdot G_i + 0.5 \cdot Q_i) = \Omega_R \cdot W \qquad (2)$$

where W represents the gravity loads combination and Ω_R represents additional gravity loads parameter or dynamic increase factor (DIF) of the additional gravity load for the analysis of the non-linear behaviour of the structural system. DIF (Ω_R) is incrementally increased for the robustness analysis until the collapse, demanded state or non-convergence of the model is reached. In NDA procedure, loading of the structure and the column removal scenario in the NDA is done according to the [5], [6] provisions.

2.2. MODAL ANALYSIS

Rayleigh viscous (mass – tangent stiffness) proportional damping was used in NDA. Calculation parameters of interest for the robustness analysis are the first and the last period of vibrations $T_{1,i}$ and $T_{2,i}$, which is thoroughly described in [11]. Values of the used periods in seismic and robustness analysis are shown in Table 1.

Table 1 – Relevant vibration periods of models for robustness analysis

Vibration periods	T_1 [s] (Σm_{eff} [%])	T_2 [s] (Σm_{eff} [%])
A1	0.2 s (1.45%)	0.023 s (92.69%)
A2	0.223 s (0.36%)	0.022 s (92.52%)
A3	0.201 s (0.85%)	0.022 s (93.40%)
A4	0.206 s (0.36%)	0.022 s (91.34%)
A5	0.255 s (0.20%)	0.022 s (93.29%)

2.3. NONLINEAR ANALYSIS AND PLASTIC HINGE PROPERTIES

The assumptions, simplifications and plastic hinge properties used in models for post-elastic analysis of structural response to the removal of individual vertical elements are described in the paper [11].
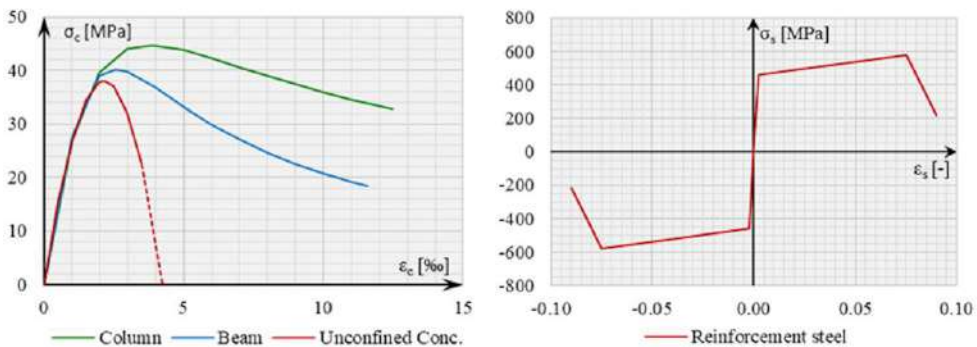
Figure 2 - Material properties of concrete (left) and rebar (right) [11]

3. METHODOLOGY OF THE ANALYSIS

3.1. NONLINEAR DYNAMIC PUSHDOWN ANALYSIS

The results for sudden column removal and its effect on vertical displacement are shown in Fig. 3 and the results of nonlinear dynamic pushdown analyses are shown in Fig. 4.
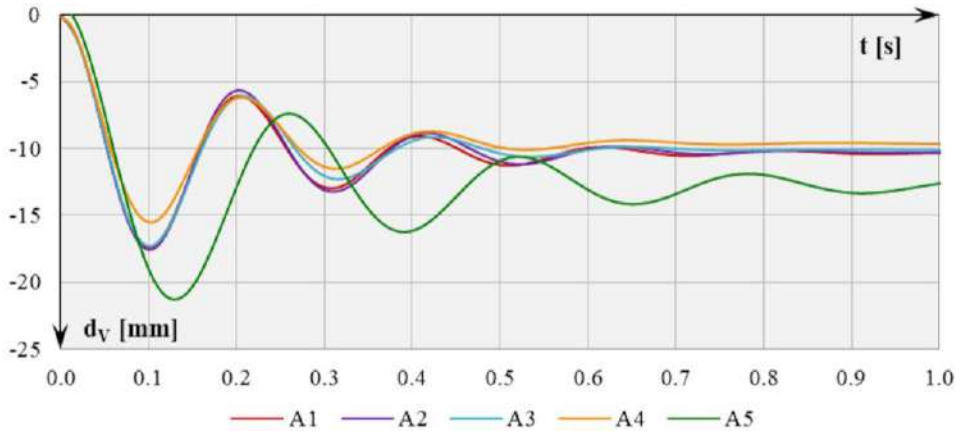
Figure 3 – Vertical displacements after sudden column removal
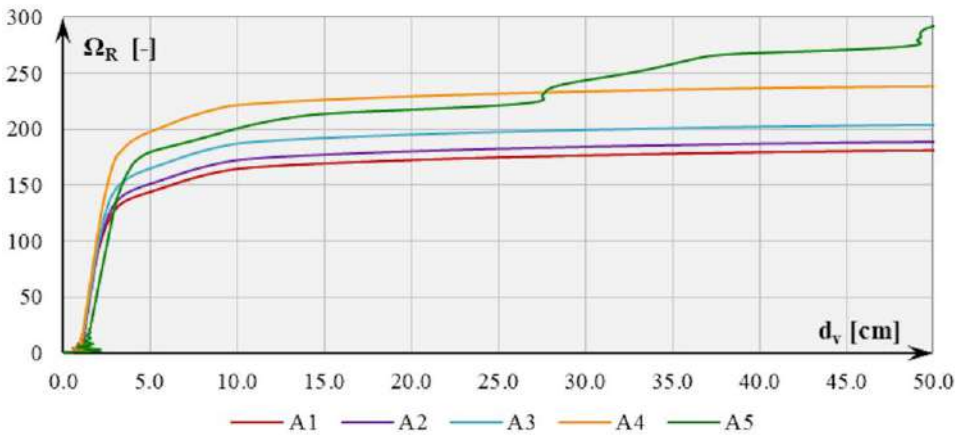
Figure 4 – Nonlinear dynamic analysis pushdown curves

The results show, as expected, that the structural system is more robust and resilient to progressive collapse if the removed corner column is located on the higher level.

3.2. DAMAGE LIMIT STATES

To quantify and compare the results of the corner column removal scenarios, from the perspective of the progressive collapse risk, methods proposed by [8] for the determination of damage LS, based on NDA are used. Limit states in this paper are defined in a following way:

- **LS1** (minor damage): LS1 occurs either in the first step, when reaching the reinforcement creep limit $\left(\varepsilon_{sy} = 0.23\%\right)$ or the stress limit of concrete with maximum strength in the protective layer of concrete $\left(\varepsilon_{c,1} = 2.16\text{‰}\right)$.

- **LS2** (moderate damage): Occurs when the vertical displacement, obtained as the ratio of displacement of the top above the removed column and the length of the beam span, exceeds the determined threshold $d_V = 1.0\%$.

318

- **LS3** (significant damage): This level of damage is assumed to occur when reaching the stress limit in the protective layer of concrete $\left(\varepsilon_{c,u} = 3.5‰\right)$ or the maximum stress of the confined concrete core $\left(\varepsilon_{cc,1} = 2.56‰\right)$.

- **LS4** (severe damage): Occurs in the first step, when the ultimate stress is reached in the confined concrete core $\left(\varepsilon_{cc,u} = 11.56‰\right)$.

- **LS5** (progressive collapse): It is determined as the state at the dilatation value in steel at which tensile fracture in the longitudinal reinforcement bar occurs $\left(\varepsilon_{su} = 7.5\%\right)$.

Damage limit states LS1-LS5 for different column removal scenarios A1-A5 are displayed in Figure 5 as a function of additional load intensity Ω_R.
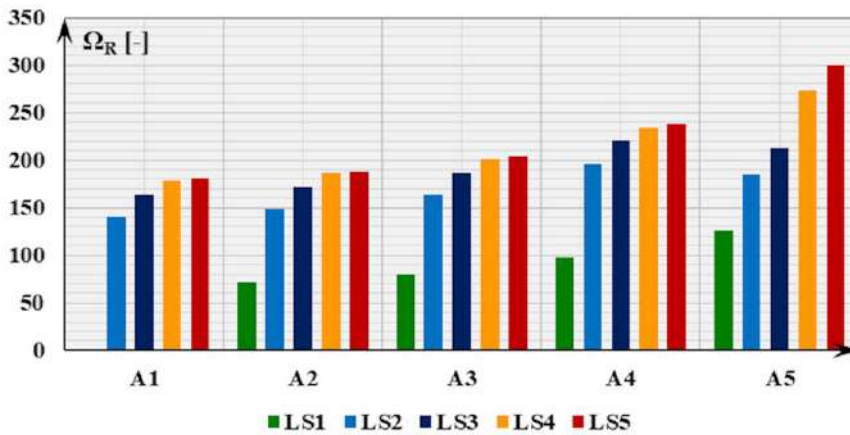
Figure 5 – Damage limit states LS1-LS5 for different corner column removal scenarios

The difference between the referent scenario A1, which is established as the most critical case among the chosen scenarios, and the rest A2-A5, $\Delta\Omega_R$ is displayed in Figure 6.
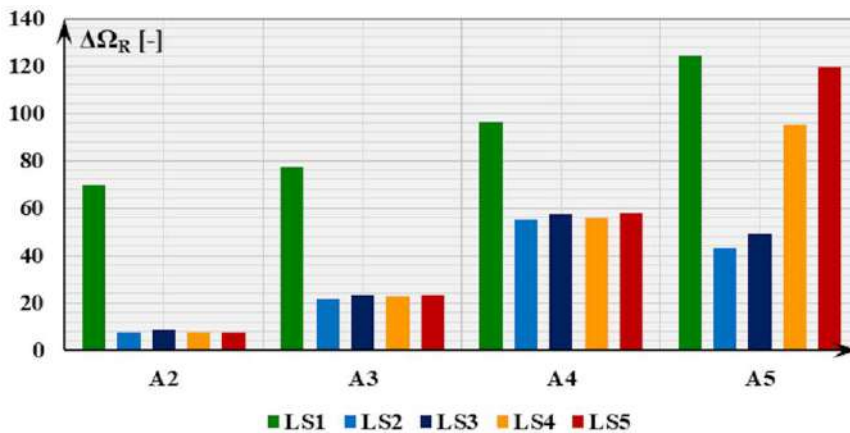
Figure 6 – Difference between damage limit states LS2-LS5 and LS1

Same as NDA, the damage limit state assessment results show, as expected, that the structural system is more robust and resilient to progressive collapse if the removed corner column is located on the higher level and it can be described in general as: $\Omega_R^{A1}(LSi) < \Omega_R^{A2}(LSi) < \Omega_R^{A3}(LSi) < \Omega_R^{A4}(LSi) < \Omega_R^{A5}(LSi)$ with some minor exceptions in case of scenario A5 for damage limit states *LS2* and *LS3*.

3.3. FRAGILITY ANALYSIS

Based on the results obtained through NDA, normal distribution was adopted for the robustness fragility curves calculation. In case of the calculation of robustness fragility curves, using $\Omega_{R,i}$, the fragility function is calculated as analytical cumulative distribution function (CDF) for normal distribution:

$$P_{LS_i|\Omega_{R,i}}\left(\Omega_{R,i}, \mu_{LSi}^{\Omega_R}, \sigma_{LSi}^{\Omega_R}\right) = \Phi\left(\frac{\Omega_{R,i} - \mu_{LSi}^{\Omega_R}}{\sigma_{LSi}^{\Omega_R}}\right) \tag{3}$$

where Φ is the cumulative distribution function of the standard normal distribution, $\mu_{LSi}^{\Omega_R}$ and $\sigma_{LSi}^{\Omega_R}$ are the mean and standard deviation of normal distribution values shown in Fig. 7.
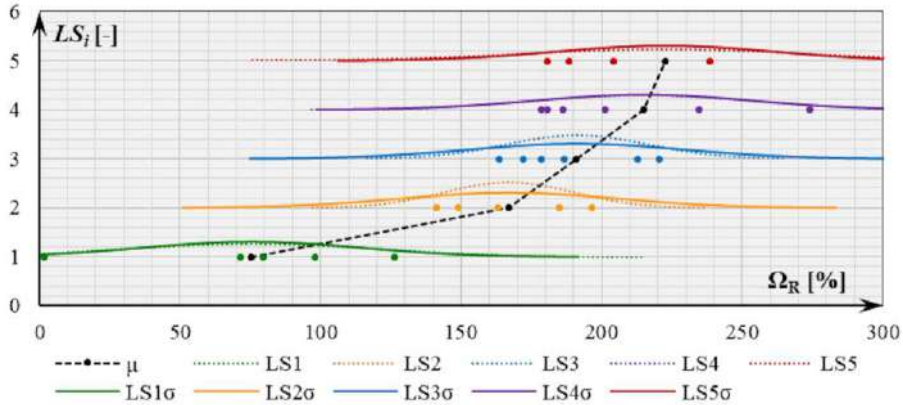
Figure 7 - Calculated (LSᵢ) and corrected (LSᵢσ) normal distribution probability density functions (PDF)

To avoid the overlapping of the fragility functions, their correction is performed by adopting the same standard deviation value for all LS, using the MLE method described in [16], [17]. $\mu_{LSi}^{\Omega_R}$ and $\sigma_{LSi}^{\Omega_R}$ for uncorrected and corrected fragility curves are shown in Table 2 and robustness fragility curves are displayed in Fig. 8.

Table 2 – Robustness fragility parameters

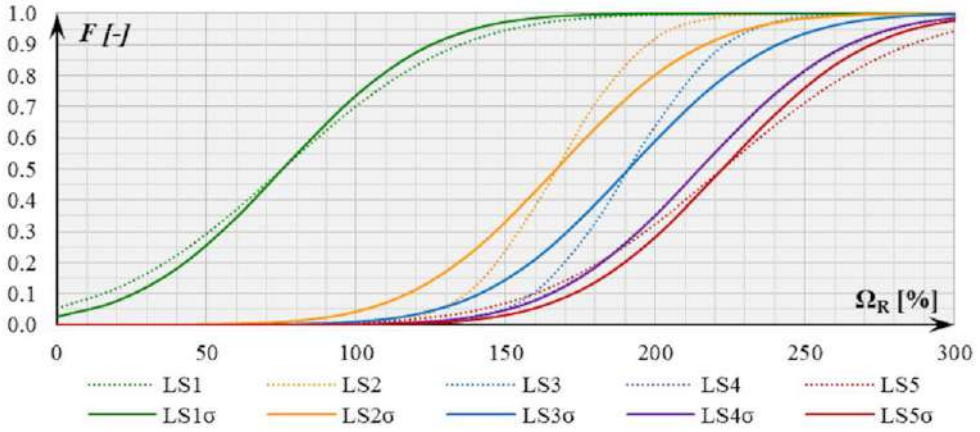| Ω_R [%]	$\mu_{LSi}^{\Omega_R}$	$\sigma_{LSi,unc}^{\Omega_R}$	$\sigma_{LSi,corr}^{\Omega_R}$
LS1	75.44	46.258	
LS2	166.96	23.318	
LS3	191.12	24.959	38.748
LS4	214.88	39.327	
LS5	222.44	48.917	

Figure 8 - Robustness fragility curves for A1-A5 corner column removal scenarios

Calculated fragility functions represent the probability of exceedance of certain damage LS for all different corner column removal scenarios. They can be used to compare the structural response of the building in case of the analogy chosen scenarios for other column positions in the building and give an insight in the fragility of the structure in dependence of the positions of the removed elements.

3.4. VULNERABILITY ANALYSIS

To calculate the vulnerability function for the used scenarios, normal distribution PDFs for mentioned LS_i and no damage limit state ($LS0$) are calculated, according to the equation:

$$
\begin{aligned}
P_{LS_0} &= 1 - P_{LS_1}\left[\Omega_{R,i}, \mu_{LSi}^{\Omega_R}, \sigma_{LSi}^{\Omega_R}\right] \\
P_{DS_i} &= P_{DS_i}\left[\Omega_{R,i}, \mu_{LSi}^{\Omega_R}, \sigma_{LSi}^{\Omega_R}\right] - P_{DS_{i+1}}\left[\Omega_{R,i+1}, \mu_{LSi+1}^{\Omega_R}, \sigma_{LSi+1}^{\Omega_R}\right] \\
P_{DS_n} &= P_{DS_n}\left[\Omega_{R,n}, \mu_{LSn}^{\Omega_R}, \sigma_{LSn}^{\Omega_R}\right]
\end{aligned}
\tag{4}
$$

Vulnerability curve represent the cumulative distribution of the total repair cost of the structure. The transformation of the fragility curves into vulnerability curves can be conducted by using the following total probability relation, according to [18], where: $E(C|LS_0) = 0\%$, $E(C|LS_1) = 1\%$, $E(C|LS_2) = 10\%$, $E(C|LS_3) = 35\%$, $E(C|LS_4) = 75\%$, $E(C|LS_5) = 100\%$.

$$
E(C|\Omega_R) = \sum_{i=0}^{n} E(C|LS_i) \cdot P(LS_i|\Omega_R)
\tag{5}
$$

where n is the number of limit states (LS_i) considered, $P(LS_i|\Omega_R)$ is the probability of a building sustaining LS_i given intensity, Ω; $E(C|LS_i)$ is the complementary cumulative distribution of the cost (loss) given the LS_i; and $E(C|\Omega_R)$ is the complementary cumulative distribution of cost (or loss) given a level of intensity, Ω_R. [18]
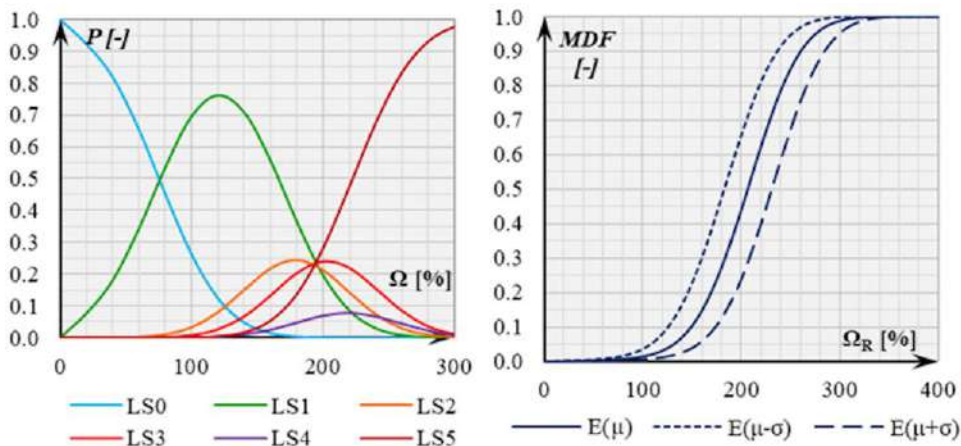
Figure 9 - Normal distribution PDFs (left) and vulnerability curves with ±1 standard deviation value (right)

Calculated vulnerability functions represent the value of the mean damage factor (MDF) of the analysed structures and intensity measure (dynamic increase factor - DIF (Ω_R) in this case). In this way, it is possible to gain insight into the threat to the usability of the structure under accidental actions. They can be used to compare the structural response of the building in case of the analogy chosen scenarios for other column positions in the building and give an insight into vulnerability of the structure in dependence of the positions of the removed elements.

4. CONCLUSIONS

In this paper, the robustness analysis of an RC frame building for the removal of corner columns along all levels is performed. Columns are removed according to the mentioned scenarios and the response of the structure is analysed using nonlinear dynamic pushdown analysis method. Damage limit states are determined and fragility and vulnerability curves were constructed. Based on the obtained results, as expected, it can be concluded that the structural system is more robust and resilient to progressive collapse if the removed corner column is located on the higher level. Through the applied analysis, it was possible to gain the insight into the robustness of the structure. This approach can be used to compare the structural response of each column in the vertical in the building for analogy chosen scenarios for other columns in the building and to gain an insight into the fragility and vulnerability of the structure in dependence of the positions of the removed elements.

REFERENCES

[1] Adam J.M., Parisi, F., Sagaseta, J., Lu, X.: Research and practice on progressive collapse and robustness of building structures in the 21st century, *Engineering Structures*, Vol. 173, 2018, pp. 122-149

[2] Folić, R., Structural Robustness of Monolithic and Precast RC structures, Plenary lecture, Reinforced Concrete and Masonry Structures - Theory and Practice, October 22-23, 2015,

Sofia, Bulgaria, Book of Abstracts, pp. 18, Full paper proceedings pp. 37 – 54. http://www.rc-structures.bg/

[3]   Woliński S. Defining of the structural robustness, Bulletin of the Polish Academy of technical sciences (CE), Vol. 61, No. 1, 2013, pp. 137-134, DOI: 10.2478/bpasts-2013-0012

[4]   Starossek, U., Haberland, M. Measures of Structural Robustness – Requirements & Applications, ASCE SEI 2008 Structures Congress – CB, Vancouver, Canada, April 24-26, 2008, pp. 1/10-10/10

[5]   DoD UFC Guidelines. Design of Buildings to Resist Progressive Collapse, Unified Facilities Criteria (UFC) 4-023-03. Department of Defence (DoD), 2013

[6]   GSA Alternate Path Analysis and Design Guidelines for Progressive Collapse Resistance, October 24, 2013; Revision 1, January 28, 2016

[7]   COST Action TU0601 – Robustness of Structures – Structural robustness design for Practicing engineers, Sept. 2011. http://www.cost-tu0601.ethz.ch

[8]   Parisi, F., Scalvenzi, M., Brunesi, E.: Performance limit states for progressive collapse analysis of reinforced concrete framed buildings, fib STRUCTURAL CONCRETE, 20 (2019) 1; pp. 68–84, Doi: 10.1002/suco.201800039

[9]   Brunesi, E., Parisi, F. Progressive collapse fragility of European RC buildings, 13th International Conference on Applications of Statistics and Probability in Civil Engineering ICASP 13, Seoul, S. Korea, May 26-30. 2019, pp. 1-9

[10] Mander, J., Priestley, M., Park, R.: Theoretical Stress-Strain Model for Confined Concrete, Journal of Structural Engineering, Vol. 114, ISS. 8, 1988, pp. 1804-1825

[11] Čokić, M., Folić, B., Folić, R., Robustness and fragility of the RC building designed according to yu-81 and European Standards, 1st Croatian Conference on Earthquake Engineering, 1CroCEE, 22-24 March 2021, Zagreb, Croatia

[12] EN1998 - Part 1, Eurocode 8: Design of structures for earthquake resistance - Part 1: General rules, seismic actions and rules for buildings, European Committee for Standardization (CEN), 2004/2005

[13] EN1992 - Part 1: Eurocode 2: Design of concrete structures - Part 1-1 : General rules and rules for buildings, CEN, 2004/2005

[14] EN1991: Eurocode 1: Actions on structures - Part 1-1: General actions - Densities, self-weight, imposed loads for buildings, European Committee for Standardization (CEN), 2002

[15] EN1990 - Basis of structural design, European Committee for Standardization (CEN), 2005

[16] Porter, K.: "A Beginner's Guide to Fragility, Vulnerability, and Risk. University of Colorado Boulder", University of Colorado Boulder, 2015, DOI 10.1007/978-3-642-35344-4_256

[17] Baker, J. W. (2015). Efficient analytical fragility function fitting using dynamic structural analysis, Earthquake Spectra, 31(1), 579-599.

[18] D'Ayala, Dina & D'ayala, D. & Meslem, Abdelghani & Vamvatsikos, Dimitrios & Porter, Keith & Rossetto, Tiziana & Crowley, H. & Silva, Vitor. (2014). GEM Guidelines for Analytical Vulnerability Assessment of Low/Mid-rise Buildings.

Žarko Petrović[1], Slobodan Ranković[2], Bojan Milošević[3], Marina Mijalković[4]

NOSIVOST ARMIRANO BETONSKOG PRESEKA OJAČANOG FRP ARMATUROM

Rezime:

Vlaknima armirani polimerni (Fiber reinforced polymer – FRP) materijali su relativno novi kompozitni materijali visoke čvrstoće i male težine koji su napravljeni najčešće od karbonskih ili staklenih vlakana utopljenih u polimernu matricu. Dodavanjem armature od FRP materijala armirano-betonskim (AB) elementima bilo u vidu spolja zalepljenih laminata (Externally bonded – EB metoda) ili ugradnjom u zaštitnom sloju betona (Near surface mounted – NSM metoda) povećava se nosivost AB preseka. U radu je predstavljeno analitičko istraživanje ponašanja poprečnog preseka AB grede, ojačane na savijanje FRP materijalima.

Key words: vlaknima armirani polimeri, armirano-betonske grede, ojačavanje

LOAD BEARING CAPACITY OF RC CROSS SECTION STRENGTHENED WITH FRP REINFORCEMENT

Summary:

Fiber reinforced polymer (FRP) materials are relatively new, high-strength, low-weight composite materials that are most often made of carbon (CFRP) or glass (GFRP) fibers embedded in a polymer matrix. The load-bearing capacity of the RC section is increased by adding reinforcement of FRP material to reinforced concrete (RC) elements, either in the form of externally bonded laminates (Externally bonded - EB method) or by installing in a protective layer of concrete (Near surface mounted - NSM method). The paper presents an analytical study of the cross - sectional behaviour of RC beams, strengthened for flexure with FRP materials.

Key words: fiber reinforced polymer, reinforced concrete beams, strengthening

---

[1] *Assoc. prof, Faculty of civil engineering and archtecture, University of Niš, Serbia, zarko.petrovic@gaf.ni.ac.rs*
[2] *Assis. prof, Faculty of civil engineering and archtecture, University of Niš, Serbia, slobodan.rankovic@gaf.ni.ac.rs*
[3] *Assis. prof, Faculty of mechanical and civil engineering in Kraljevo, University of Kragujevac, Serbia, milosevic.b@mfkv.kg.ac.rs*
[4] *Full prof, Faculty of civil engineering and archtecture, University of Niš, Serbia, marina.mijalkovic@gaf.ni.ac.rs*

1. INTRODUCTION

Interest in the use of FRP materials in building structures is constantly increasing, so nowadays there is a large number of applications of these materials in structures around the world. Some of the most common applications in civil engineering include:

- strengthening and repair of structural elements made of reinforced concrete, steel, aluminium and wood.
- concrete reinforcement with bars and cables made of FRP material,
- production of structures from FRP material,
- production of hybrid constructions.

Strengthening of civil engineering infrastructure has gained significant attention due to deterioration problems of structures and need for meeting up-to-date design requirements [1]. One of the basic factors that causes the unsatisfactory condition of the existing infrastructure is corrosion of reinforced steel in concrete, which causes damage of concrete, loss of reinforcing steel and in some cases failure of construction [2].

The two basic methods most commonly used in strengthening RC beams with FRP material are: strengthening by gluing laminates of FRP material on the surface of concrete beams—EB method; and strengthening by mounting bars or narrow strips of FRP material in grooves made in the cover of concrete—NSM method.

The largest number of researches of RC beams strengthened to bending by FRP reinforcement are experimental or numerical researches. Conclusions of the experimental researches presented in literature, indicate both increases in bearing capacity and reduction of deformations of strengthened beams [3, 4]. In addition to the papers that generally deal with experimental research of strengthened beam girders, there is a significant number of papers in which methods for modelling reinforced RC beams using FEM analysis are proposed [5, 6].

There are many analytical methods for analysing reinforced concrete (RC) beams strengthened with FRP materials [7, 8]. An analytical approach based on cross-sectional analysis can easily determine the ultimate load of a strengthened beam. The approach is based on the principles of strain compatibility, internal force balance and idealized constitutive relations for concrete, steel and FRP reinforcement. These idealized relations, together with the assumption that slip on the contact surface between concrete and FRP systems can be neglected, form the basis for the analysis of the ultimate state of strengthened RC beams [9].

The assumptions introduced in the cross-sectional analysis of RC beams strengthened with FRP reinforcement are as follows [8]:

1. The distribution of strains by section height is linear - Bernoulli's hypothesis of straight sections.
2. No slipping between longitudinal reinforcing steel and concrete;
3. No slipping between FRP system and concrete;
4. Beam failure occurs either due to reaching the ultimate strain of concrete under compression or due to failure of the FRP strengthening system.

The aim of this paper is the development of a mathematical model for the calculation of the load-bearing capacity of the cross section of a RC beam strengthened with fiber FRP materials, subjected to bending.

2. ADOPTED MODELS OF CONSTITUENT MATERIALS

In the analysis of the cross section of the RC beam strengthened with the FRP reinforcement, the parabolic relation between stress and strain for concrete was adopted (Figure 1).
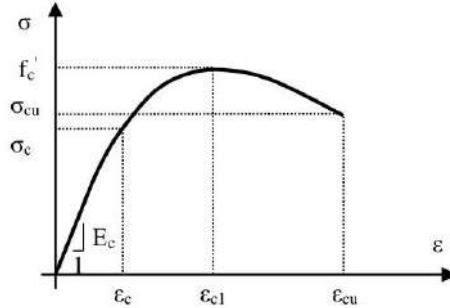

Figure 1 - Idealised stress- strain curve for concrete at axial pressure

The mathematical formulation of this relation can be described by the expressions (1-2) [10]:

$$\sigma_c = f_c' \left[\frac{2\varepsilon_c}{\varepsilon_{c1}} - \left(\frac{\varepsilon_c}{\varepsilon_{c1}} \right)^2 \right] \tag{1}$$

$$\varepsilon_{c1} = \frac{2f_c'}{E_c} \tag{2}$$

where:

σ_c and f_c' are stress in the concrete and compressive strength of concrete, respctively

ε_c is strain in concrete,

E_c is modulus of elasticity of concrete.

Bilinear dependence between stress and strain for reinforcing steel (elastoplastic behavior) with a 1% slope inclination was adopted (Figure 2a).

The mathematical formulation of this dependence can be described by expression (3).

$$\sigma_s = \begin{cases} \varepsilon_s E_s & for & \varepsilon_s \leq \varepsilon_y \\ f_y + E_{sp}(\varepsilon_s - \varepsilon_y) & for & \varepsilon_s \geq \varepsilon_y \end{cases} \tag{3}$$

where:

σ_s and f_y are stress and yield strength of steel reinforcement, respectively

ε_s and ε_y are strain in steel reinforcement and steel strain at the steel yield strength, respectively,

E_s and E_{sp} are modulus of elasticity of steel before and after yielding, respectively.

The linear-elastic relation between stress and strain for FRP reinforcement was adopted, Figure 2b.

The mathematical formulation of this dependence can be described by the expression (4).

$$\sigma_{frp} = \varepsilon_{frp} E_{frp} \tag{4}$$

where:

σ_{frp} is stress in the frp reinforcement,
ε_{frp} is strain in frp reinforcement,
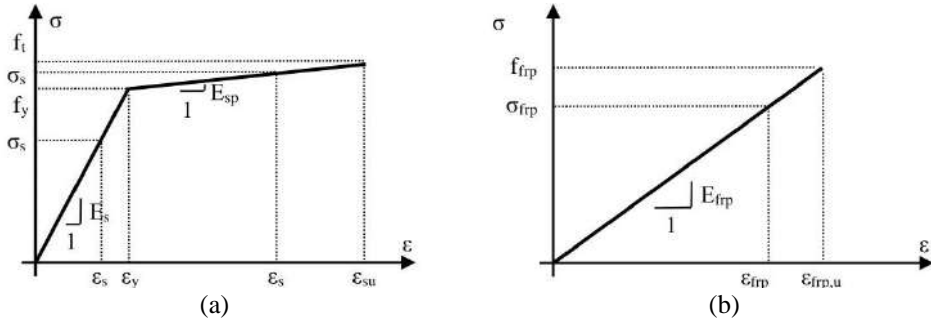E_{frp} is modulus of elasticity of frp reinforcement.

Figure 2 - (a) Idealized stress-strain curve for reinforcing steel (b) Idealized stress-strain curve for FRP reinforcement

3. STRESS-STRAIN STAGES OF THE CROSS SECTION OF THE RC BEAM STRENGTHENED WITH FRP REINFORCEMENT

Figure 3 shows a diagram of the dependence between the bending moment (M) and the curvature (κ) in the cross section of the RC beam strengthened with the FRP reinforcement, which is subjected to bending.
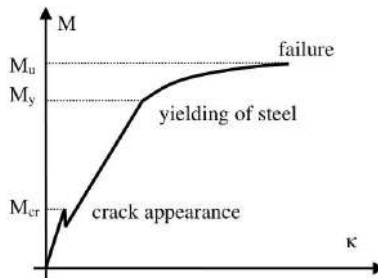
Figure 3 - Diagram of dependence between bending moment (M) and curvature (κ) in the cross-section of RC beam strengthened with FRP reinforcement

The dependence is idealized by a nonlinear curve consisting of three parts:
- zone before cracks appear,
- zone after the appearance of cracks and before the appearance of steel yielding and
- zone after the occurrence of steel yielding to the cross-section failure.

In the cross-sectional analysis of reinforced concrete beams strengthened with the FRP reinforcement, the principles of calculation of complex (composite) cross-sections used in structural theory are applied in this paper [11]. The distribution of strains and stresses by section height is shown in Figure 4 [12]:
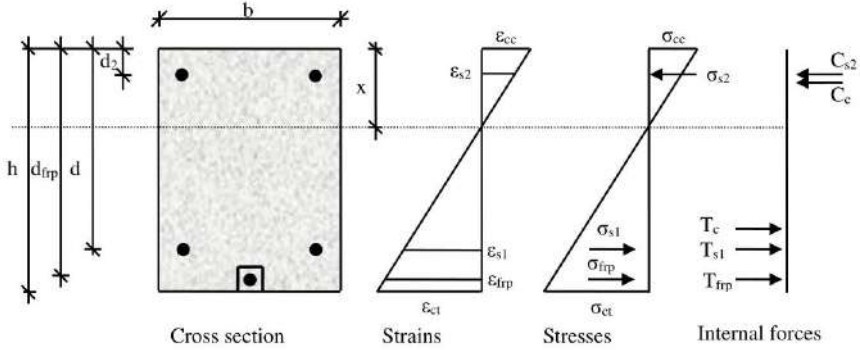
Figure 4 - Assumed distribution of strains, stresses and internal forces in the cross section of RC beams strengthened with FRP reinforcement (with neglection of initial strains)

The corresponding equations of equilibrium of internal forces are based on the assumption that the resultant of internal forces in the cross section is equal to zero ($\Sigma X=0$):

$$\int_{A_{cc}} \sigma_c dA_{cc} + \int_{A_{s2}} \sigma_{s2} dA_{s2} - \int_{A_{ct}} \sigma_c dA_{ct} - \int_{A_{s1}} \sigma_{s1} dA_{s1} - \int_{A_{frp}} \sigma_{frp} dA_{frp} = 0 \qquad (5)$$

as well as that the moment of internal forces is equal to the external bending moment ($\Sigma M = M_{ext}$):

$$\int_{A_{cc}} \sigma_c y dA_{cc} + \int_{A_{s2}} \sigma_{s2} y dA_{s2} - \int_{A_{ct}} \sigma_c y dA_{ct} - \int_{A_{s1}} \sigma_{s1} y dA_{s1} - \int_{A_{frp}} \sigma_{frp} y dA_{frp} = M_{ext} \qquad (6)$$

4. ANALYSIS OF THE MOMENT-CURVATURE RELATIONSHIP IN THE CROSS SECTION OF THE RC BEAM STRENGTHENED WITH FRP REINFORCEMENT

The shape of the moment-curvature diagram is an important characteristic of the cross-section on which the behavior of the RC beam as a whole significantly depends [13]. The relationship between the moment and curvature can be most easily determined by varying the values of edge strains in concrete. Based on the strain on the compressed edge of concrete (ε_{cc}), other characteristic values of strain can be determined according to the following expressions (Figure 4):

$$\varepsilon_{s2} = \varepsilon_{cc} \frac{x - d_2}{x} ; \ \varepsilon_{s1} = \varepsilon_{cc} \frac{d - x}{x} ; \ \varepsilon_{frp} = \varepsilon_{cc} \frac{d_{frp} - x}{x} ; \ \varepsilon_{ct} = \varepsilon_{cc} \frac{h - x}{x} . \qquad (7)$$

By substituting the expressions (7) in the equilibrium condition (5), the distance of the neutral axis from the compressed edge of the concrete (x) can be determined, after which the equilibrium condition (6) can be determined. and the bending moment (M) corresponding to the strain at the compressed edge of the concrete (ε_{cc}).

Using the straight section hypothesis, the magnitude of the curvature in the cross section (κ) can be determined by dividing the strain of the compressed edge of the concrete section (ε_{cc}) by the distance of that edge from the neutral axis (x):

$$\kappa = \frac{\varepsilon_{cc}}{x} \qquad (8)$$

In this way, the relationship between the bending moment and the curvature (M-κ) in the cross section of the RC beam strengthened with FRP reinforcement is obtained. The diagram of dependence between the moment and curvature can be determined by incremental increase of strain of the compressed edge of concrete until one of the following conditions is fulfilled:

1. The value of the strain on the compressed edge of concrete is equal to the strain of concrete crushing,

2. The strain value in the FRP reinforcement is equal to its ultimate strain.

In the paper [14] for the analysis of the cross section of the RC beam strengthened with FRP reinforcement, the program M_k.m in Matlab (MATLAB R2014a) was written.

The program is based on the previously described procedure for determining the dependence between moment and curvature in the cross section of an RC beam strengthened with FRP reinforcement, subjected to bending. Execution of this program determined the curves of dependence between bending moment and curvature. The strain of the compressed edge of the concrete cross section was increased in each step by 10 microstrains (0.00001 mm / mm).

4.1. NUMERICAL EXAMPLE

The focus of the analytical investigation in this paper is on the RC beam with a cross section of 120/200 mm with mechanical characteristics of concrete and steel reinforcement as follows:

- Compressive strength of concrete is fc′ = 40 MPa;
- Beam is reinforced in both compressed and tensioned zones with steel reinforcement 2BØ8 (As = 100 mm2, μs ≈ 0.5%, fy = 400 MPa, Es = 210 GPa).

In order to analyse the influence of the FRP reinforcement on the magnitude of the cracking moment (Mcr), yielding moment (My) and ultimate bending moment (Mu), using the program M_k.m, diagrams of the dependence between the moment and the curvature were obtained for:

1. Cross section without FRP reinforcement;

2. Cross sections strengthened with different amount of CFRP reinforcement (Acfrp=10-100mm2) with tensile strength ffrp,u = 2000 MPa, modulus of elasticity Efrp = 150 GPa and ultimate strain εfrp,u = 0.0133;

3. Cross sections strengthened with different amount of GFRP reinforcement (Agfrp=10-100mm2) with tensile strength ffrp,u = 760 MPa, elastic modulus Efrp = 40.8 GPa and ultimate strain εfrp,u = 0.0186.

In addition to the value of the yielding moment of steel reinforcement and the ultimate bending moment, as it was said, the diagram of the dependence between the moment and the curvature speaks a lot about the behaviour of the RC section. Among other things, the change in the bending stiffness of the cross-section can be clearly seen on it with different amounts of added FRP reinforcement.

A diagram of dependence between bending moment and curvature for cross-sections strengthened with the CFRP and GFRP reinforcement are shown in Figure 5 and Figure 6 respectively.
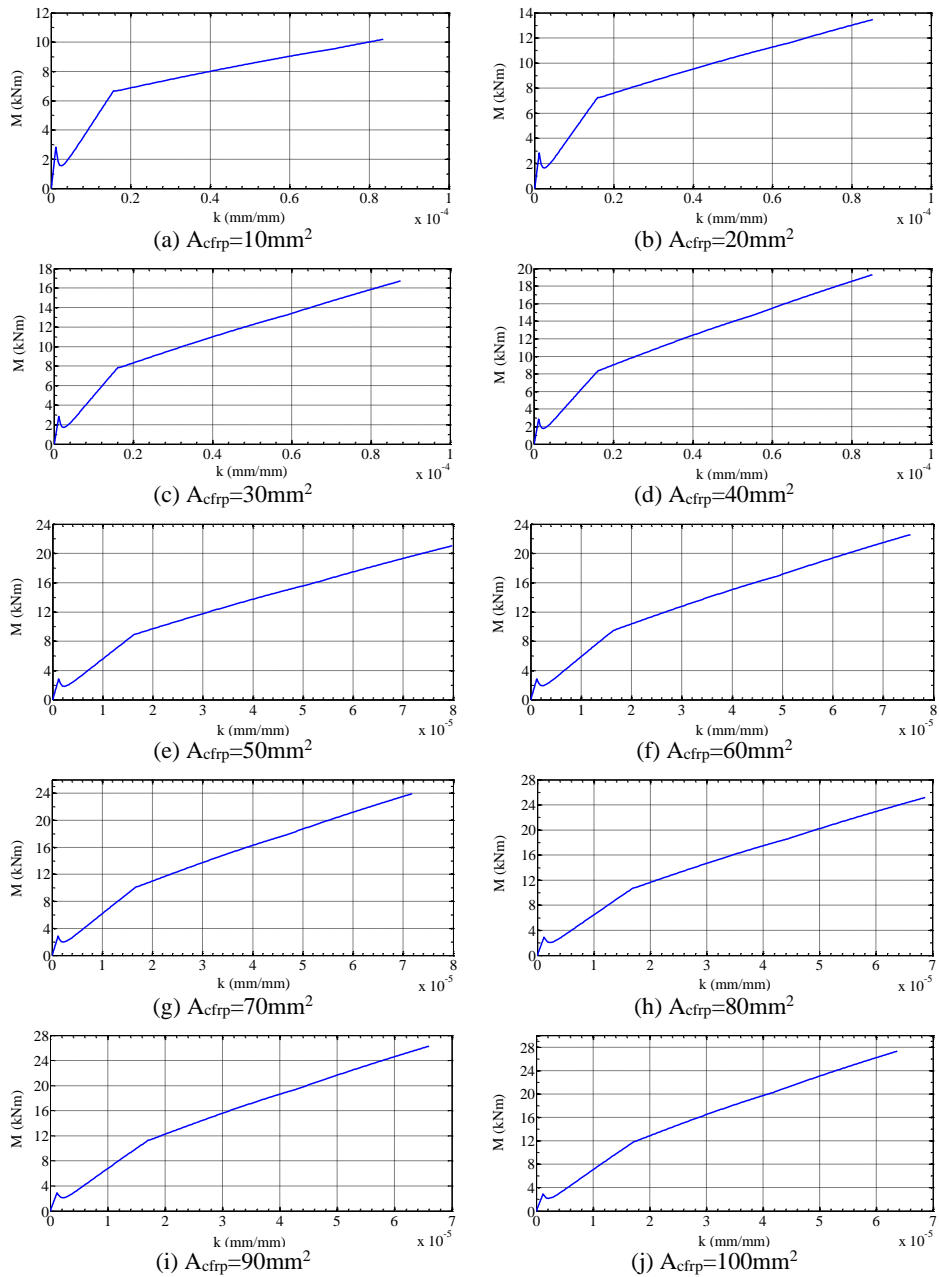
(a) A_{cfrp}=10mm^2

(b) A_{cfrp}=20mm^2

(c) A_{cfrp}=30mm^2

(d) A_{cfrp}=40mm^2

(e) A_{cfrp}=50mm^2

(f) A_{cfrp}=60mm^2

(g) A_{cfrp}=70mm^2

(h) A_{cfrp}=80mm^2

(i) A_{cfrp}=90mm^2

(j) A_{cfrp}=100mm^2

Figure 5 - Diagram of dependence between bending moment and curvature for cross-section strengthened with CFRP reinforcement [14]
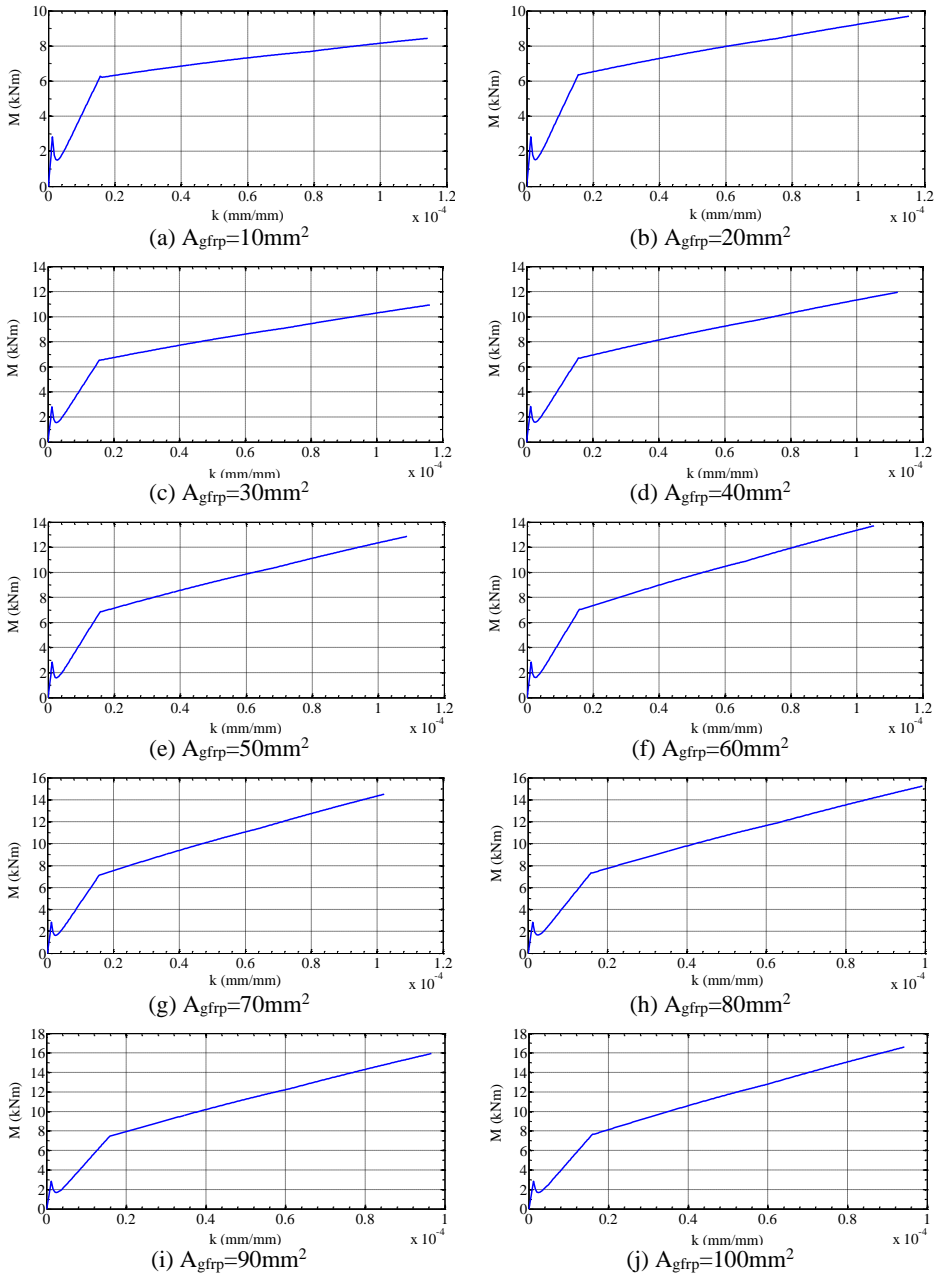
330

(a) A$_{gfrp}$=10mm^2

(b) A$_{gfrp}$=20mm^2

(c) A$_{gfrp}$=30mm^2

(d) A$_{gfrp}$=40mm^2

(e) A$_{gfrp}$=50mm^2

(f) A$_{gfrp}$=60mm^2

(g) A$_{gfrp}$=70mm^2

(h) A$_{gfrp}$=80mm^2

(i) A$_{gfrp}$=90mm^2

(j) A$_{gfrp}$=100mm^2

Figure 6 - Diagram of dependence between bending moment and curvature for cross-section strengthened with GFRP reinforcement [14]

5. CONCLUSION

Based on the obtained diagrams of the dependence between the moment and the curvature (Figure 5 and Figure 6), the following conclusions were drawn:

1. The FRP reinforcement affects the value of the yielding moment, as well as the bending stiffness of the section:

- for beams strengthened with the CFRP reinforcement, the increase in yielding moment (My) is a maximum of 96.33%, while the maximum increase in bending stiffness at the beginning of the yielding of steel reinforcement is 77.56%,

- for beams strengthened with the GFRP reinforcement, the increase in yielding moment (My) is a maximum of 26.17%, while the maximum increase in bending stiffness at the moment of the start of yielding of steel reinforcement is 22.30%.

2. The FRP reinforcement significantly affects the ultimate bending moment, as well as the bending stiffness of the cross section:

- in the case of a beam strengthened with the CFRP reinforcement, the increase in the ultimate bending moment (Mu) is a maximum of 302.8%, while the maximum increase in bending stiffness at the moment of failure is 298.07%,

- in the case of a beam strengthened with the GFRP reinforcement, the increase in the ultimate bending moment (Mu) is a maximum of 144.84%, while the maximum increase in bending stiffness at the moment of failure is 64.70%.

The obtained results indicate a significant influence of FRP reinforcement on the cross - sectional behavior of the strengthened RC beam, considering that even with small amounts of additional reinforcement, the bearing capacity, as well as the bending stiffness, significantly increases.

REFERENCES

[1] Bilotta, A.; Ceroni, F.; di Ludovico, M.; Nigro, E.; Pecce, M.; Manfredi, G. Bond efficiency of EBR and NSM systems for strengthening concrete members. J. Compos. Constr. 2011, 15, 757–772.

[2] ISIS Educational Module 2. An Introduction to FRP Composites for Constructio; A Canadian Network of Centres of Excellence: Ottawa, ON, Canada, 2006.

[3] Ranković, S. Experimental and Theoretical Analysis of Limit State RC Linear Plane Structures Strengthened with NSM FRP Elements; Doctoral Dissertation, Faculty of Civil Engineering and Architecture, University of Niš: Niš, Serbia, 2011; p. 177.

[4] Rahman, M.M.; Jumaat, M.Z. The Effect of CFRP Laminate Length for Strengthening the Tension Zone of the Reinforced Concrete T-Beam. J. Sci. Res. Rep. 2013, 2, 626–640.

[5] Wang, X.; Zhou, C. Numerical investigation for the flexural strengthening of reinforced concrete beams with external pre-stressed HFRP sheets. Constr. Build. Mater. 2018, 804–815, doi:10.1016/j.conbuildmat.2018.08.219.

[6] Zhang, C.; Wang, J. Viscoelastic analysis of FRP strengthened reinforced concrete beams. Compos. Struct. 2011, 93, 3200–3208, doi:10.1016/j.compstruct.2011.06.006.

[7] Vasseur, L., Matthys, S. and Taerwe, L. (2006). Analytical study of a 2-span reinforced concrete beam strengthened with fibre reinforced polymer. IABSE Symposium Report, 92(10), pp.39-46.

[8]   Akbarzadeh, H. and Maghsoudi, A. (2010). Experimental and analytical investigation of reinforced high strength concrete continuous beams strengthened with fiber reinforced polymer. Materials & Design, 31(3), pp.1130- 1147.

[9]   Teng, J. G., Zhang, J. W. and Smith, S. T. (2002). Interfacial Stresses in Reinforced Concrete Beams Bonded with a Soffit Plate: a Finite Element Study. Construction and Building Materials, 16(1), pp. 1-14

[10] Collins, M. P., and Mitchell, D. (1987). Prestressed concrete basics, Canadian Prestressed Concrete Institute (CPCI), Ottawa.

[11] Badawai, M. (2007). Monotonic and Fatigue Flexural Behaviour of RC Beams Strengthened with prestressed NSM CFRP Rods. PhD thesis. University of Waterloo, Waterloo, Ontario, Canada.

[12] ISIS Educational Module 4. An Introduction to FRP Strengthening of Concrete Structures; A Canadian Network of Centres of Excellence: Ottawa, ON, Canada, 2006

[13] Bajić, D. (1985). Prilog nelinearnoj analizi armiranobetonskih elemenata. Doktorska disertacija. Građevinski fakultet, Beograd.

[14] Petrović, Ž. Experimental—Theoretical Analysis of Limit States of Continuous Beams Made of Self-Compacting Concrete Strengthened with Fiber Reinforced Polymer (FRP). Ph.D. Thesis, University of Niš, Niš, Serbia, 2016; p. 247.

Aleksandar Zhurovski[1], Igor Gjorgjiev[2]

DEFINISANJE GRANICA OŠTEĆENJA U PRAĆENJU STANJA KONSTRUKCIJA PRIMENOM NELINEARNE ANALIZE

Rezime:

Istraživanje prikazano u ovom radu je fokusirano na utvrđivanju vrednosti fizičkih parametara koje treba analizirati u procesu praćenja stanja konstrukcija. Istraživanje obuhvata definisanje graničnih vrednosti ovih parametara za različite nivoe oštećenja razmatrane trinaestospratne AB zgrade, koja se zasniva na parametarskoj nelinearnoj dinamičkoj analizi. Nelinearni numerički model je formiran i kalibrisan na osnovu dinamičkih karakteristika konstrukcije koje su dobijene eksperimentalnim putem. Na ovom modelu izvršena je parametarska nelinearna dinamička analiza korišćenjem sintetičkog zapisa zemljotresa. Rezultati istraživanja su pokazali da se ova procedura može koristiti sa visokim nivoom pouzdanosti za definisanje granica oštećenja u praćenju stanja realnih konstrukcija.

Ključne reči: praćenje stanja konstrukcija, granice oštećenja, parametri oštećenja, nelinearni model

NONLINEAR ANALYSIS OF BUILDING STRUCTURES FOR DEFINITION OF ALARM THRESHOLDS FOR SHM

Summary:

This study focuses on establishing values for damage-sensitive physical quantities that should be monitored in the process of SHM of building structures. It covers definition of limit values of these parameters for different damage states of a case study 13-storey RC building based on parametric time-history analysis. Using experimentally defined dynamic characteristics of the structure, a corresponding nonlinear model was fitted and parametric time-history analysis using generated record was done. The results suggest that this procedure can be used for setting up damage alarm thresholds for SHM of full-scale buildings with high knowledge level.

Key words: SHM, alarm thresholds, damage parameters, nonlinear model

[1] *Assist. MSc, Ss. Cyril and Methodius University in Skopje, Institute of Earthquake Engineering and Engineering Seismology (IZIIS), Skopje, North Macedonia, zurovski@iziis.ukim.edu.mk*
[2] *Prof. PhD, Ss. Cyril and Methodius University in Skopje, Institute of Earthquake Engineering and Engineering Seismology (IZIIS), Skopje, North Macedonia, igorg@iziis.ukim.edu.mk*

1. INTRODUCTION

The design life of civil engineering building structures according to all design codes is 50 years to 100 years. During this period, the structures are expected to maintain their structural integrity. Unpredicted and unexpected structure failure due to accumulated damages during design life may cause significant economic losses and even casualties. Therefore, recently, structural health monitoring (SHM) gained much interest and is becoming more and more important. SHM systems provide information about any significant change or damage occurring in a structure. The purpose of structural damage detection is to identify the reason, location, and type of damage, measure the damage severity and predict the structure's remaining service life. This is important from both safety and performance viewpoints (Sivasuriyan et al., 2021).

The assessment of the current structural health of a building can be done once or continuously. Monitoring of certain key parameters provides information on its level of performance and data to judge its state of conservation. When this is done once, the results of the survey can be employed for specific goals (vulnerability and damage assessment, upgrading and retrofitting evaluation, etc.). If this is done continuously, the evolution of its structural health over time can be assessed. In all cases, initial data collection is the necessary step to be performed for interpretation and subsequent analysis to indicate whether intervention is required and the type of intervention to be carried out. In a general perspective, a successful SHM procedure would require a preliminary identification of proper quantities together with the formulation of quantitative criteria for the assessment of the limit states that must not be exceeded during the life cycle of the structure (e.g. safety, durability, serviceability, etc.). Long-term continuous measurements of certain key parameter of the structural response can provide the necessary information about both the global health and the expected performance of the structure.

The Finite Element Method (FEM) is a tool for computing approximate solutions to complex mathematical problems. It is useful for problems with complicated geometries, loadings, and material properties where analytical solutions cannot be obtained, and some degree of error is tolerable. FEM is a powerful numerical technique to solve problems governed by partial differential equations over complex domains. It is usually adopted to solve the so called forward problems in structural engineering. In FEM, a complex numerical model of a structure is developed and for a given or known loading (input), the deformations that the structure undergo (output) can be observed (measured). Opposite to this, SHM requires estimating the state of the structure from the measured output (deformation, velocities, acceleration, etc) for a given defined or undefined force or deformation (input). Such problems are called the inverse problems. Several research have been done in the direction of application of the FEM in SHM for engineering structures (Biliszczuk et al., 2021).

This study focuses on connecting both the inverse problem and forward problem. Practically, for a selected building structure a current structural health was done measuring the dynamic characteristics using ambient and forced vibration techniques. These measurements were then used to develop a numerical FEM model using PERFORM-3D. Finally, parametric time-history analysis of that model was done (with increasing intensity of the ground motion) to define structure's capacity. The parametric analysis and structure's capacity were used to define alarm threshold for Immediate Occupancy limit state according to ASCE-41, 2007. We chose to define this alarm threshold to be monitored for being the most important for the occupants of the building in case of an earthquake event. By using the defined acceptance criteria, we could label

the building as being safe or unsafe for living after any potential earthquake event. Additionally, several "damage" zones of the structure were defined that could be used as help for structural engineers in the after-event on-site inspection. All this procedure is proposed as SHM strategy for continuous monitoring of the damage sensitive parameters for the building.

The paper is organized as follows. In the first chapter following the introduction, the case study building structure is briefly explained. The second chapter summarizes the testing programme along with the results from the measurement of the dynamic characteristics using both forced and ambient vibration. In the third chapter information about the developed numerical model, modelling characteristics, defined rotation capacities, selected time history record and acceptance criteria are given. The fourth chapter contains specific results from the parametric time- history analysis and discussion in terms of decision making. Finally, the last chapter contains conclusions for development of continuous SHM only for this particular structure and recommendations for refinement of the procedure and definition of damage sensitive parameters for future work.

1.2. CASE STUDY

The structure that was chosen for development of strategy for continuous SHM is RC frame structure with central RC shear wall cores for the stairs and elevators. It is 13 storey building consisted of 2 underground floors (used for parking), ground floor and 10 floors. The height of the ground floor and all floors is 2.90m, while the underground floors are 3.70m high. The total height (measured from ground floor) is 31.90m. The characteristic plan dimensions are 45.00m/18.00m (figure 1.). It is an existing structure, located in Skopje, designed according to current seismic standards in 2013, and built in 2014.
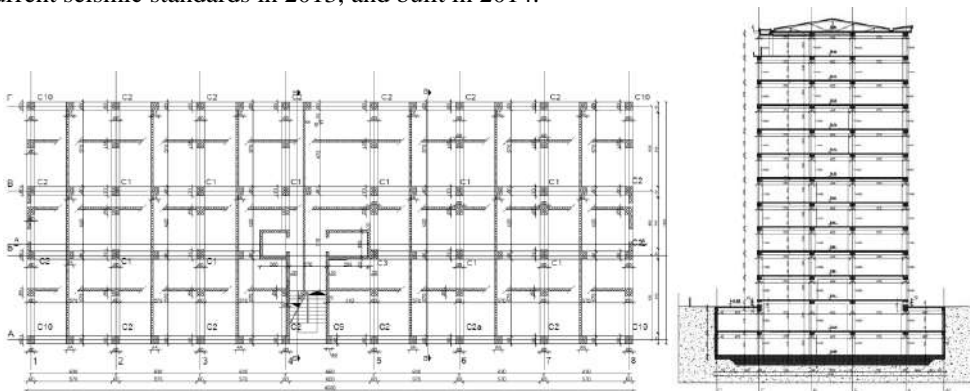
Figure 1 – Characteristic formwork plan and cross- section of the structure

The columns are proportioned 60/90cm and 60/80cm in the first three stories, 60/80cm and 60/70cm in the next four stories, 60/70cm in the next three levels and 60/60 in the last three floors to level +31.90. The central core shear walls are 20cm thick. To avoid torsion, in the outer frames additional shear walls with thickness 20cm are designed. The beams are with the cross-sectional dimension of 60/50cm. The slabs are monolithic with thickness of 16cm and the foundation system is foundation slab with thickness of 120cm. All columns in the underground, ground floor and first floor are designed with grade of concrete MB40 (according to current standards in North Macedonia). All columns on the other levels as well as all the other structural

elements are designed with grade of concrete MB30. All structural elements are designed with reinforcement RA 400/500-2 (yield strength of 400MPa, according to current standards in North Macedonia) The design project containing calculation and all drawings and reinforcement details was available.

2. MONITORING OF CURRENT STRUCTURAL HEALTH

The structure was tested using forced and ambient vibration techniques immediately after the end of the construction. At the time of the testing, the complete structural system was constructed together with all infill walls. Forced vibration testing was carried out for determination of the structure's dynamic characteristics in both horizontal orthogonal directions and torsion. For this purpose, two GSV-101 (Geotronix, USA) vibration generators were used to generate sinusoidal excitation force in the frequency range of 1.0 to 8.0 Hz. Each generator can produce excitation force with an amplitude of up to 2.5 tons. The force was applied at the top of the building. For all tests, the shakers were mounted symmetrically around both orthogonal axes. This configuration allows exciting the structure in both orthogonal directions and simulation of torsional loading without changing shakers position. The measuring instruments were located at the two diagonal corners of the building in two orthogonal directions.

Ambient vibration measurements were carried out along with the forced vibration tests to verify the obtained results and identify the dynamic properties that were unable to be identified by forced vibration testing due physical limitations in the frequency region where the shakers were unable to produce excitation force.

A total of 12 sensors were used (6 in each orthogonal direction). Four sensors were used as referent on the top floor and the remaining 8 were relocated on the lower floors for mode shape determination. Accelerometers PCB Piezotronics Model 393B12 with sensitivity of 10000 mV/g, with a range of up to 4.9 m/sec2 (0.5g) were used for registration of the response. The vibrations were registered with a sampling frequency of 2048 Hz. The data acquisition system consists of module NI cDAQ-9178 and 3 card module NI 9234.

The recorded vibration data were processed in custom-made application developed by the second author for real time data processing, where Enhanced Frequency Domain Decomposition (EFDD) identification method was included. The algorithm is written in C++ language with full support for parallel processing (Gjorgjiev et al. 2018). The graphical visualization of the input and output data is created to present a 3D mode shapes.

2.1. IDENTIFICATION OF THE NATURAL FREQUENCIES, CORRESPONDING MODE SHAPES AND DAMPING RATIOS

The results from ambient vibration tests were used to identify the first three natural frequencies and mode shapes of the structure using the FDD method. On the other hand, the results from the forced vibration tests were used to identify three natural frequencies of the structure as well as the mode shapes using the peak-picking method. In Figure 2a the calculated singular values are presented. In Figure 2b, 2c and 2d, the frequency response curves from the forced vibration tests are also presented. The identified mode shapes obtained from force vibration tests and calculated from FDD analysis are shown in Figures 3, 4 and 5.
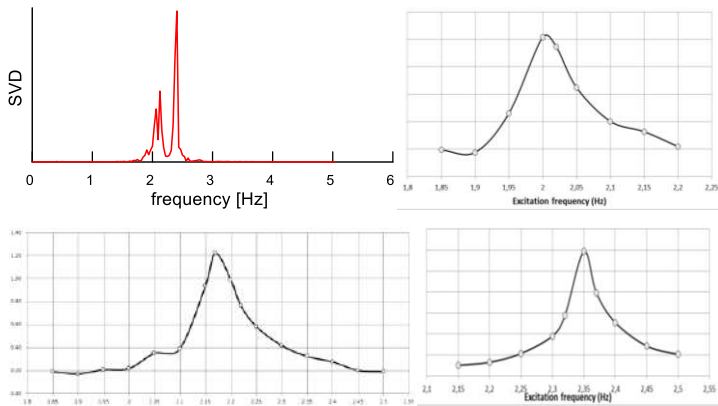
Figure 2 – a) SVD curve- ambient vibration records; b) c) and d) Frequency response curves obtained from the forced vibration tests (Y-Y direction, X-X direction, Torsion)
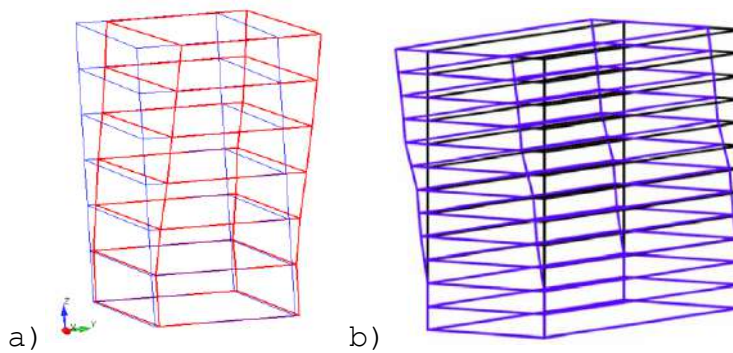

a)   b)

Figure 3 – First mode of vibration in Y-Y direction (identified natural frequency f=2.00Hz), a) analytical FDD method, b) force vibration

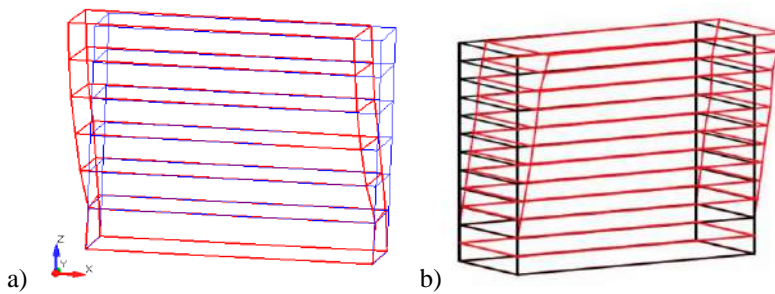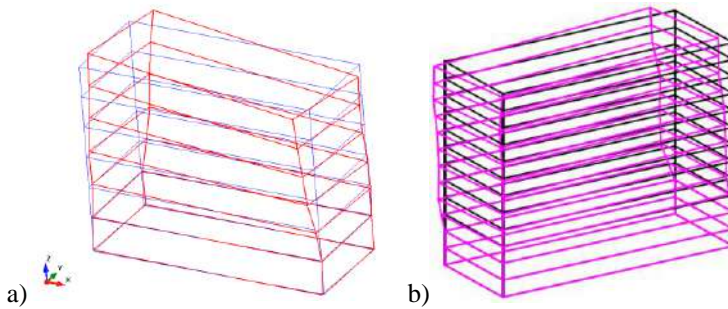a)   b)

Figure 4 – First mode of vibration in X-X direction (identified natural frequency f=2.17Hz), a) analytical FDD method, b) force vibration

*Figure 5 – First mode of vibration in Torsion (identified natural frequency f=2.35Hz), a)
analytical FDD method, b) force vibration*

Damping coefficient ξ of each identified mode in the state of resonance was obtained
applying the half-power method and the logarithmic decrement method. To calculate the
damping coefficient by logarithmic decrement method, the decaying response of the structure
was measured after stopping the excitation force in the resonant state.

Table 1 summarizes all the results from the measurements. The resonant frequencies of the
structure's first three modes of vibration obtained from forced vibration and ambient records are
listed, together with damping ratios from forced vibration testing by using half- power bandwidth
and logarithmic decrement methods. From the presented results, it is concluded that the
experimentally and analytically identified natural frequencies and mode shapes are matched.
Modal damping estimation using different methods fits quite well and all methods give
approximate modal damping values.

*Table 1 – Natural frequencies (forced and ambient vibration) and damping ratios from forced
vibration testing (Half- power Bandwidth and Logarithmic decrement methods)*

Mode Shape	FV- resonant frequency (Hz)	AV- EFDD- Resonant frequency (Hz)	FV- Damping coefficient (%)- Half-power Bandwidth	FV- Damping coefficient (%)- Logarithmic decrement
I mode, Y-Y	2.00	2.04	1.75	1.60
I mode, X-X	2.17	2.13	1.57	1.7
I mode, torsion	2.35	2.37	1.02	1.00

3. FINITE ELEMENT MODELING OF THE STRUCTURE

CSI PERFORM-3D was used to model the structure. The program offers several different
types of elements to be used depending on the modelling requirements. Each element is
consistent of basic components and numerous different basic components are available to be
used to simulate the nonlinear behaviour of all type of structural elements. For this case study,
the basic components used for the modelling are as follows:

Inelastic non-buckling steel material was defined for the reinforcement according to the
provisions given in the national standard (reinforcement with yield strength of 400MPa). The

stress-strain relationship of the reinforcement was modelled as trilinear, with strength loss (at point L), without cyclic stiffness degradation. The model curve is shown in fig. 6a.

A macro model with Mander stress-strain relationship is most frequently used to describe working condition of confined concrete in uniaxial compression (Mander, J.B. et al. 1984), which is related with section shape and the configuration condition of stirrup. In PERFORM-3D, the model is transferred in the standard force-deformation (F-D) relationship. Hence, for the design quality of concrete, two concrete model curves were computed according to the Mander model, mean value of concrete's strength and elastic modulus (fig. 6b).

As known that energy can be dissipated by nonlinear component under cyclic loading and the dissipated energy can be represented by the area of hysteretic loop. Hence, to a great extent, the structural response is governed by the area and shape of hysteretic loop. PERFORM-3D gives the required energy degradation through adjusting the unloading-load stiffness, and the coefficient of energy degradation is taken as the ratio of the area of degraded and non-degraded hysteretic loop (Xuewei, C et al. 2011). In this paper, parameters of energy degradation were defined according to the degradation rule of unloading-load stiffness in Mander model and on the base of previous research done by the authors (Zhurovski et a. 2018), as shown in Figure 6c.

a)   b)   c)
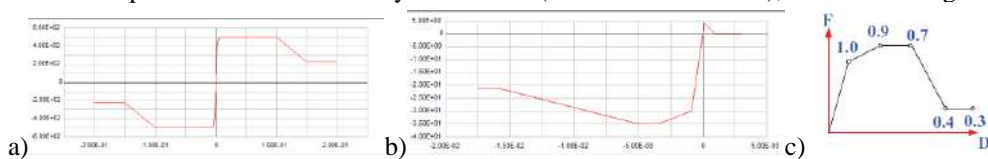
Figure 6 – Material models, a) Reinforcement, b) Confined concrete, c) degradation coefficients of concrete

The columns were modelled using inelastic fiber sections that were assigned at the corresponding lengths of the elements to simulate the plastic hinge region, with the rest of the element remaining elastic. The shear walls were modelled inelastic fiber sections while concentrated (lumped) plasticity approach was used for the beams using inelastic moment hinges, rotation type. Beam-column joints were taken as rigid elements.

The deformation capacities for the components or the so-called performance acceptance criteria corresponding to different building performance levels are generally defined in terms of plastic rotation capacities. In the present study, plastic rotation capacities for Immediate Occupancy (IO), Life Safety (LS) and Collapse Prevention (CP) levels given in ASCE-41, 2007 were used for the column, shear wall and beam elements. These values are shown in table 2. It also includes the defined inelastic strain capacities of both materials (reinforcement and concrete) for the three performance levels.

Table 2 – Rotation Capacities for the materials and structural elements used in the analysis

Rotation Capacities					
Level	Fiber Sect-Column Rot Capacities (rad)	Moment Hinge-Beam Rot Capacities (rad)	SW- Rot Capacities (rad)	Reinforcement-Inelastic Strain Capacities	Concrete-Inelastic Strain Capacities
IO	0.005	0.005	0.003	0.01	0.002
LS	0.025	0.01	0.006	0.02	0.0035
CP	0.035	0.02	0.009	0.06	0.06

To perform the parametric time- history analysis on the base of which different alarm threshold levels should be defined, we generated an artificial ground motion. The time- history record was generated so that its response spectra matched the design spectra according to Eurocode- 8 for the location of the building- Skopje (type 1 design spectra, PGA=0.25g, soil type B, damping 5%)- figure 7. Only this record was scaled, with acceleration scaling factor of 0.1 to 2.6 (with a step of 0.1) and applied on the model in both orthogonal directions separately (not acting simultaneously) since the aim of the study was not to perform assessment but to define parameters for SHM independent in both orthogonal directions.
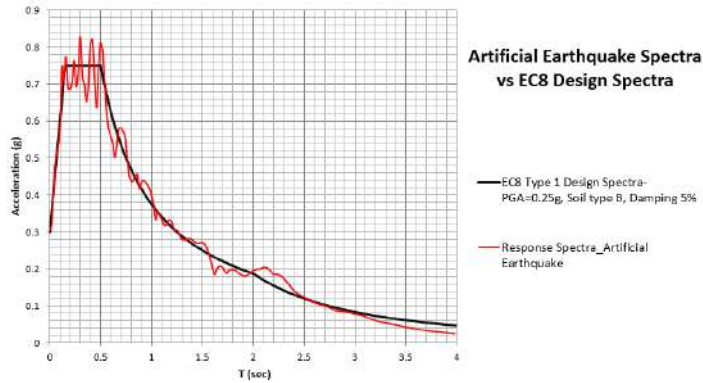
Figure 7 – Response spectra of the record matched to EC-8 design spectra

4. RESULTS

Since the measurements were done in the phase where all interior and exterior infill elements were constructed, modeling only the structural system gave significant error in the obtained dynamic characteristics (table 3). This error was present in the order of the mode shapes as well as the values of the natural frequencies. To account for the "lost" stiffness due to the interaction effect between walls and frame elements, we modeled all infill walls that we considered significant for stiffness increase (all walls connected to columns on both sides). These elements were included in the model as Linear Elastic Infill Panel elements (available in PERFORM-3D). In this way, we almost perfectly matched the results obtained by signal processing of the measurements in the shapes of the modes of vibration as well as the values of natural frequencies (table 3).

Table 3 – Natural frequencies - comparison

Natural frequencies- comparison			
Mode	Forced Vibration measurement in Hz	Numerical Model (without infills) in Hz	Numerical Model (with infills) in Hz
I mode, Y- Y- direction	2.00	1.21	1.98
I mode, X- X- direction	2.17	0.94	2.17
I mode, torsion	2.35	1.16	2.45

After fitting the numerical model, the parametric time- history analysis was done on the model without the infill walls, as it is common engineering practice. Figure 8 shows the results from the parametric time- history analysis in terms of Base Shear vs Top Displacement diagrams for both orthogonal directions. This is commonly accepted way of interpretation of structures' capacity. We chose the roof level displacement to be the parameter to be monitored for the purpose of SHM and decision making in case of event, although due to the characteristics of the structure and for cost-efficiency reasons. Other parameters such as ground storey and top story interstory drift may be indicative too.

On the diagrams several top displacement levels are marked, having important meaning. These lines were set by following the response of the structure under the increasing seismic events and the nonlinear response of the structure elements, mainly columns and shear walls, as we consider them essential for the stability of the building structure.
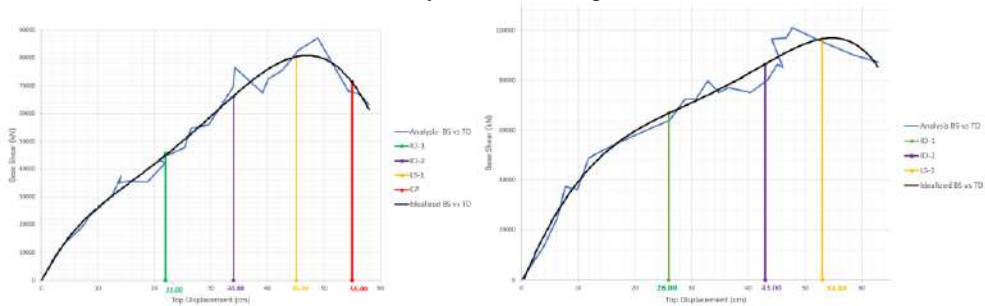
Figure 8 – Base shear vs Top Displacement- X-X direction (left), Y-Y direction (right).
Definition of alarm thresholds

When setting up these top displacement levels, we followed the definition for acceptance criteria for deformation- controlled actions used in nonlinear procedures given in the update to ASCE/SEI 41 Concrete Provisions (Elwood et al. 2007). Based on the defined rotation capacities for columns, given in table 2, and the abovementioned acceptance criteria we defined five levels of rotation capacities for columns (table 4).

Table 4 – Acceptance criteria used for definition of alarm thresholds

Acceptance criteria- rotation Limits (in terms % of Column CP rotation capacity from table 2)		
Name of acceptance criteria	% of Column CP rotation capacity	Description
IO-1	15%	Original IO rotation capacitiy- defined in table 2
IO-2	35%	Acceptance criteria for IO (67% of 75% of original LS point)
LS-1	52%	Acceptance criteria for LS (75% of original LS point)
LS-2 = CP-1	70%	Original LS rotation capacity & Acceptance criteria for CP (75% of original CP point)
CP-2	100%	Original CP rotation capacity

We assumed the first line (green line) on the diagrams as the alarm level that is important for the users of the building. This is the evacuation level e.g. level marking that the inhabitants

should not get back inside the building until corresponding authorities (structural engineer) visually check its state after an earthquake event. This corresponds to the IO-1 level. The other lines correspond to different "damage" levels. We defined them to be helpful for the structural engineers making an after-event visual inspection on what type of damage to expect and where to look it for. So, the second line (purple) corresponds to the state where first columns on the ground level reach IO-2 state. Third line (orange) is the state where more columns reach LS-1 state and the last line (red) means that some of the columns have reached LS-2=CP-1 state. For the Y-Y direction we were not able to define the last limit state due to numerical instability at the higher levels of excitation. The decision making- process is sublimated in figure 9 and structure's performance level when reaching the alarm level is given in figure 10 (for both orthogonal directions). Figure 9 does not contain information for the first 5 levels of excitation (0.1 to 0.5) since no structural element reached the rotation level corresponding to the defined acceptance criteria.

EQ Level	Excitation in X-X direction			Excitation in Y-Y direction		
	Top Displ. (cm)	Alarm thresholds, acceptance Criteria and "damage" description		Top Displ. (cm)	Alarm thresholds, acceptance criteria and "damage" description	
0.6	14.15	IO-1	No observed damage	16.50	IO-1	No observed damage
0.7	13.79		No observed damage	22.58		First top floor Column IO-1
0.8	15.45		First top floor Column IO-1	26.12		First ground level Column IO-1
0.9	18.85		Four top floor Columns IO-1	28.81		More ground level Columns IO-1
1.0	21.90		First ground level Column IO-1	30.75		----
1.1	20.83	IO-2	More ground level Columns IO-1	32.87	IO-2	Four top floor Columns IO-2
1.2	25.39		All ground level Columns IO-1	34.77		----
1.3	26.49		Four top floor Columns IO-2	36.57		More Columns IO-2
1.4	29.59		More Columns IO-2	40.37		----
1.5	33.87		Two top Columns LS-1	43.40		Four ground floor Columns IO-2
1.6	34.26		First ground floor Column IO-2	45.13		----
1.7	39.13	LS-1	More Columns LS-1	46.15	LS-1	----
1.8	40.15		----	44.13		First two top Columns LS-1
1.9	42.64		More ground floor Columns IO-2	46.76		----
2.0	45.51		First ground floor Columns LS-1	47.74		More Columns LS-1
2.2	48.89	CP	----	52.53		First ground floor Columns LS-1
2.4	54.36		Almost all Columns LS-1	58.43		No Columns CP
2.5	56.25		First Columns CP-1	62.87		
2.6	57.96		More Columns CP-1	N/A		

Figure 9 – Definition of Alarm Thresholds- "Observed" damage and acceptance criteria limits
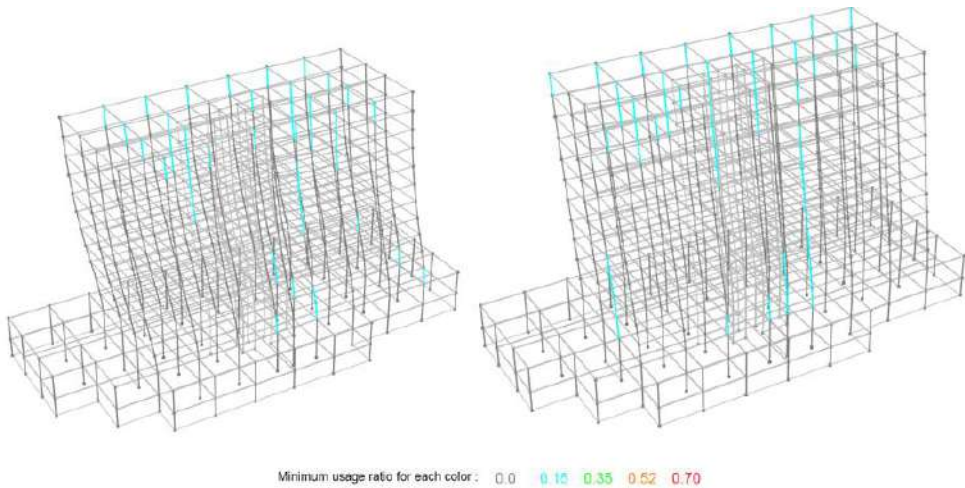
Figure 10 – Performance of RC columns for IO alarm threshold, X-X direction (left), Y-Y direction (right)

5. CONCLUSIONS

The presented paper is an attempt to merge the results and obtained knowledge from experimental testing, SHM and FEM modeling with the aim of definition of alarm thresholds for continuous SHM of a selected building structure. Initially, experimental testing was realized, and the conclusions led to fitting a corresponding finite element model. A parametric time- history analysis using generated accelerogram and scaling of the amplitude (from 0.1 to 2.6) was performed. Structure's performance evaluation and alarm threshold definition was done on the base of ASCE 41 acceptance criteria for deformation- controlled actions and the correspondent column rotation capacities. For this case study, we chose the top floor displacement to be the monitoring parameter from the cost-efficiency point of view. The next step is to mount a corresponding, sensitive sensor at the top floor that could measure structure's top displacement in real- time. Some of the conclusions are:

- The results from the experimental testing indicate that there have been no temporary or local imperfections in the construction process of the building and that the structural stiffness distribution is favorable and it follows the structural design recommendations.
- Being designed according to national standards, the structure does not reach damage pattern that would make the structure unstable up to greater acceleration levels (scaling factor of more than 2.5).
- The top displacement is good indicator for structural behavior and should be continuously monitored. The structure has the IO alarm threshold for the X-X direction should be set at a top displacement of 22cm, and for the Y-Y direction at a top displacement of 26cm.
- Several other levels of top displacement were defined that could be helpful to on-site engineers in the after- event inspections.

The paper shows that this procedure is useful for definition of alarm thresholds for SHM of building structure. Future work should include several sets of bi-directional ground motions and

taking average values for the observed response quantities (similarly to the assessment procedures). The role of infill walls should be reassessed and included in the analysis (especially for definition of the IO performance level). Other damage- sensitive parameters can be monitored such as the top and/or bottom story interstory drift. The acceptance criteria for other structural elements (shear walls and/or beams) can play important role as well and should be included in the definition of alarm thresholds.

REFERENCES

[1] Biliszczuk, J., Hawryszków, P., Teichgraeber, M. (2021). SHM System and a FEM Model-Based Force Analysis Assessment in Stay Cables. Sensors 2021, 21, 1927. https://doi.org/10.3390/s21061927.

[2] Elwood, K.J,, Matamoros, A.B., Wallace, J.W., et al. (2007) Update to ASCE/SEI 41 Concrete Provisions. Earthquake Spectra. 2007;23(3):493-523. doi:10.1193/1.2757714

[3] Gjorgjiev I., Jekikj, G., Zhurovski, A. (2018). Analytical verification of results from forced vibration tests by enhanced frequency domain decomposition method. X Jubilee International Scientific Conference "Civil Engineering Design and Construction (Science and Practice), Sept. 20-22, 2018, Varna, Bulgaria

[4] Mander, J.B., Priestley, M.J.N., Park, R. (1984). Theoretical Stress-Strain Model For Confined Concrete. ACI Journal, 1984.

[5] Sivasuriyan, A., Vijayan, D.S., Górski,W., Wodzy´nski, Ł., Vaverková, M.D., Koda, E. (2021). Practical Implementation of Structural Health Monitoring in Multi-Story Buildings. Buildings 2021, 11, 263. https://doi.org/10.3390/buildings11060263

[6] Xuewei, C., Xiaolei, H., Fan, L., Shuang, W. (2011). Fiber Element Based Elastic-Plastic Analysis Procedure and Engineering Application. Procedia Engineering, Volume 14, 2011, Pages 1807-1815, https://doi.org/10.1016/j.proeng.2011.07.227

[7] Zhurovski, A., Nechevska- Cvetanovska, G., Garevski, M. (2018). Nonlinear Dynamic Analysis as Seismic Assessment Tool for RC Frame Structures. 16th European Conference on Earthquake Engineering, June 18-21, 2018, Thessaloniki, Greece.

[8] Computers and Structures, Inc. – CSI PEFRORM-3D- Components and Elements. Version 7, January 2018.

Bojan Milošević[1], *Žarko Petrović*[2], *Marina Mijalković*[3], *Andrija Zorić*[4]

UTICAJ ZIDANE ISPUNE NA NOSIVOST RAMOVSKIH KONSTRUKCIJA

Rezime:

Kod objekata visokogradnje, velika je primena ramovskih konstrukcija, kod kojih je prostor između stubova i greda u potpunosti ili delimično ispunjen nearmiranim zidovima. U procesu modeliranja i projektovanja ramovskih konstrukcija uticaj zidova ispune, kao i njihova krutost su se uglavnom ignorisali tokom analize konstrukcije. Cilj ovog rada je da se prikažu neke od metoda modeliranja koje su danas dostupne za opisivanje odziva ramovskih konstrukcija ispunjenih zidovima, kao i njihova interakcija sa elementima ramovske konstrukcije kada su podvrgnute opterećenju u svojoj ravni.

Ključne reči: ramovski nosači, zidana ispuna, zamenjujući dijagonalni štap

EFFECT OF WALL INFILL ON THE CAPACITY OF THE FRAME STRUCTURES

Summary:

In building construction, frame structures are widely used, in which the space between columns and beams is completely or partially filled with unreinforced walls. In the process of modelling and design of frame structures, the impact of the walls, as well as their rigidity, were largely ignored during the structural analysis. The aim of this paper is to present some of the modelling methods available today to describe the response of frame structures filled with walls and their interactions with frame structures when subjected to load in their plane.

Key words: frame structures, wall infill, equivalent diagonal strut

---

[1] *Assis. prof, Faculty of mechanical and civil engineering in Kraljevo, University of Kragujevac, Serbia, milosevic.b@mfkv.kg.ac.rs*

[2] *Assoc. prof, Faculty of civil engineering and archtecture, University of Niš, Serbia, zarko.petrovic@gaf.ni.ac.rs*

[3] *Full prof, Faculty of civil engineering and archtecture, University of Niš, Serbia, marina.mijalkovic@gaf.ni.ac.rs*

[4] *Assitant, Faculty of civil engineering and archtecture, University of Niš, Serbia, andrija.zoric@gaf.ni.ac.rs*

1. INTRODUCTION

The use of frame structures that are filled with walls made of masonry elements in the building structure, industrial and commercial buildings, is wide. The role of the wall infill between the structural elements of the reinforced concrete frame is related to the architectural demands such as protection of the interior of the building from the environment and to separate the interior spaces.

During the process of designing new structures and assessing the load-bearing capacity of the existing ones, the wall infill located between the elements of the frame structure is usually considered as a non-structural element. In general, the role of masonry infill in the analysis of frame structures is neglected and it is assumed that it will not participate in the transmission of any load both axial and lateral, and its influence on the frame structure is ignored due to ignorance of their composite behaviour [1, 2]. The filling walls not only increase the mass of the building but on the one hand increase the stiffness while on the other hand reduce the ductility of the structure, which leads to a change in the period of oscillation of the frame structure [3, 4]. The wall infill can significantly increase the load-bearing capacity of the frame structure and thus serves as an important reserve of strength in case of unpredictable extreme events (local impact, explosion or earthquake).

If the building meets the conditions of regularity both in the base and in the height of the building, i.e., if the wall infill is properly distributed in the design phase, it usually has a positive impact on the static and dynamic characteristics of the structure. On the other hand, the negative effects caused by improper positioning of the infill walls can lead to the formation of short elements, the appearance of a flexible floor or the appearance of torsion of the building [2]. These phenomena cannot be avoided, but they can be significantly prevented by proper design. Therefore, it is necessary for civil engineers in the design phase of structures to consider all the necessary factors, including the infill walls, which play an important role in the load-bearing capacity of the structure and its deformation characteristics [5].

The reason for neglecting the walls of the infill in the design process is partly the result of incomplete knowledge of the behaviour of quasi-brittle materials from which the infill is made and the lack of conclusions of experimental and analytical results that support the reliability of procedures for adequate and safe design of these structures [3]. The lack of realistic and simple analytical models for filling modelling as well as the ignorance of the interaction between the infill walls and the frame structure is another obstacle for its consideration in the analysis and constructive modelling of structures [6].

The aim of this paper is to consider the proposed analytical macromodels for the analysis of a frame structure filled with a wall whose width is not related to the stiffness of the material from which the wall is made, as well as to point out special challenges imposed by the presence and complex action of filling. The paper presents simplified analytical expressions for modelling a wall infill using the macro method, namely simplified simple single models and their application through concrete examples.

2. MODELLING OF FRAMES FILLED WITH MASONRY WALLS

In the phase of analysis and design of frame structures that are filled with walls, due to the large number of different parameters, the behavior of the frame structure is difficult to determine, especially due to the large number of possible forms of failure that must be considered [7]. Analytical modeling of a frame structure filled with a wall contains various parameters that define the elements for masonry, mortar, as well as the connection between the frame and the wall infill. As the wall infill is made of masonry elements of different strengths and stiffnesses in the modeling phase of the frame structure filled with walls, special attention should be paid to the adequate modeling of the wall infill. The mechanical characteristics of the masonry infill depend on both the masonry elements and the applied mortar.

Since the first attempt to model the response of a frame structure filled with walls as a composite, several methods have been developed, which are grouped into two main categories: micro-models, i.e., detailed models, based on the finite element method and macro-models or simplified models, based on the diagonal bar equivalent method [8].

Micro-modeling is a complex method that can be used to simulate the behavior of a structure in detail, using appropriate constitutive models, and is based on the division of the wall infill and the frame structure into an appropriate number of finite elements. The main advantage of micro modeling is reflected in the fact that it takes into account local effects related to stress distribution, cracking, crushing and interaction of masonry infill and frame structure [1]. Although micro modeling can provide an accurate computational representation of material and geometric aspects, it is rarely used because the calculation itself is computer-intensive and too time-consuming to be used in the practical analysis of large structures [9].

Wall modeling using macro elements can be defined as the use of different types of diagonal bars. It is generally accepted that under horizontal loading, the infill wall acts as an equivalent diagonal bar that can be modeled as an element connecting the nodes between the beams and columns, and is applicable only when the wall infill is without openings [7]. Since the first attempts to model the behavior of frame structures filled with walls, indicated that a diagonal bar with appropriate geometric and mechanical characteristics can solve the problem, the single diagonal bar model is the most commonly used macro model. The geometric property of the diagonal rod required in the analysis is the cross-sectional area of the rod, which is defined as the product of the wall thickness of the infill and the width of the equivalent diagonal bar - w. The length of the diagonal bar, d, is determined by the length of the diagonal of the wall infill (Figure 1).

(a)   (b)
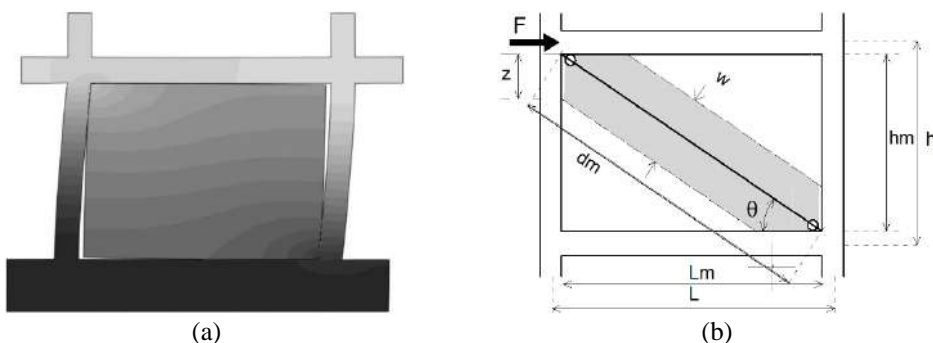
Figure 1 – Models of the masonry infill walls in RC frames: a) micro-model b) macro-model

In recent decades, a large number of experimental and numerical studies have been conducted to define an acceptable model for structural analysis that would take into account the interaction between the wall infill and the frame structure [6]. In the modeling of masonry infill using a diagonally pressed bar, a large number of methods have been presented in the literature that have been defined by various researchers or presented in regulations for the calculation of structures. Each method defines a simplified analytical model for reproducing the main aspects of the interaction mechanism, which defines the width of the diagonal rod w depending on the length of the pressed diagonal. Some of the macro models take into account the relative stiffness between the infill and the frame structure when defining the equivalent width of the diagonal bar, while other models determine the width of the diagonal bar indirectly based on the length of the diagonal relative to the wall geometry.

In the early 1960s, Polyakov was the first to notice that an infill wall could be represented by a diagonal element [11]. Based on Polyakov's research, Holmes conducted experimental research on steel frames filled with brick walls and concrete masonry elements [12]. He developed a semi-empirical method for designing frames that are exposed to lateral loads. Holmes states that the width of the diagonal bar should be one third of the length of the diagonal of the wall infill.

Based on experimental data obtained by examining steel frames filled with walls, Stafford Smith [13], defines that the *w/d* ratio is in the range of 0,10 to 0,25.

Syrmakezis and Vratsanou [14] model the pressed diagonal of a wall infill using five bars, proposing an empirical equation for determining the total width of the pressed diagonal:

$$\frac{w}{h} = 0,64\frac{l}{h} + 3\left(\frac{d_c}{l} - 0,1\right),$$

where h and l are the length of the column and the beam respectively and d_c is the thickness of the column

Priestley and Cavali [15] respectively pointed out that the large width of the diagonal rod results in a stiffer structure and thus a potentially larger seismic response. They proposed that the *w/d* ratio is 0,25 when the frame structure is filled with a wall and exposed to seismic forces.

In the Romanian regulations [16] for the design of structures in seismically active areas, the width of the diagonal bar with which the infill wall can be replaced is one tenth of the diagonal bar length (*w*=0,10*d*)

Hamburger and Chakradeo studied steel-frame buildings with masonry infill, and gave special attention to the beam-column joint [17]. They proposed the use of equivalent diagonal struts placed next to the openings (i.e., one infill wall with one opening, thus two struts are used). The struts should be tangent to the corner of the window opening. Looking at the results of the numerical model they recommended that the width of each equivalent strut should not exceed twice the infill thickness.

3. NUMERICAL ANALYSIS

In order to analyze the influence of the wall infill on the behavior of the RC frame structure exposed to horizontal force, a numerical analysis was performed. The frame is made of C25/30 concrete, filled with Porotherm 38 N+F clay masonry elements, connected with M 10 mortar. The geometry of the examined masonry-infilled RC frame is shown in Figure 2.
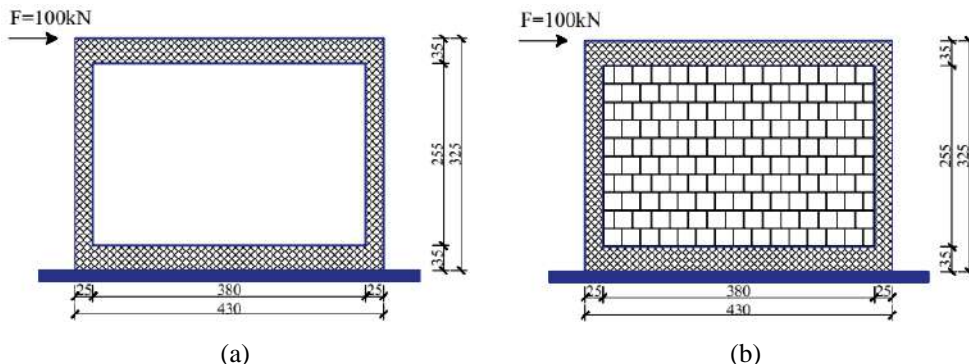
(a)   (b)

Figure 2 – The geometry of examined structure: a) bare frame b) infilled frame

Table 1 – Mechanical characteristics of the masonry according to EC6 [18]

Compressive strength of masonry mortar	f_m [MPa]	10,00
Normalized mean compressive strength of a masonry unit	f_b [MPa]	8,53
Characteristic compressive strength of masonry	f_k [MPa]	4,03
Modulus of elasticity of masonry	E [MPa]	4027,68

Based on the dimensions of the framed structure (Figure 2), as well as on the mechanical characteristics of the masonry infill (Table 1) numerical models were developed in the Tower and Abaqus software packages. The analysis was performed using bare frame model and infilled frame macro-models. Macro-models with beam and shell elements were examined. Standard bar and shell elements built-in in Tower software package were used, and in case of Abaqus software package the beam elements B32 and shell quadrilateral elements S8R with quadratic shape functions were used. The translational degrees of freedom were constrained at the adjacent nodes of beam and shell elements in the case of macro-models with shell elements for infill wall. Therefore, the connection between RC frame and infill wall was modelled as ideal without slipping. The values of the width of the diagonal strut in model with beam element was determined based on the recommendations in the literature [11-17] (Table 2).

Table 2 – Diagonal strut width

	Holms	Smiths	Paulay and Pristley	Symakezis	Hamburger
w [cm]	156,00	46,90	117,25	225,90	50,00

3.1 RESULTS AND DISSCUSION

A comparative analysis of the obtained displacements of the top of the frame structure under the action of a horizontal test load is performed.

Figures 3 a-f show the displacements obtained using the Tower software [19], while Figures 4 a-f show the displacements obtained using the Abaqus software [20].
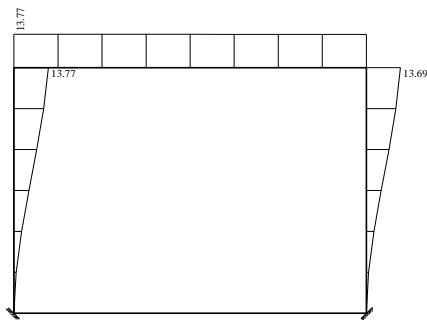
Uticaji u gredi: max Xp= 13.77 / min Xp= 0.00 m / 1000
(a)
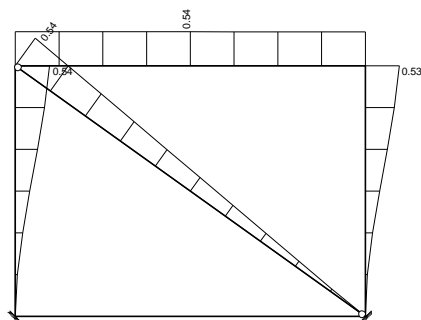
Uticaji u gredi: max Xp= 0.54 / min Xp= 0.00 m / 1000
(b)
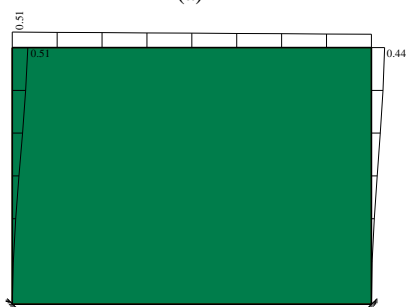
Uticaji u gredi: max Xp= 0.51 / min Xp= 0.00 m / 1000
(c)
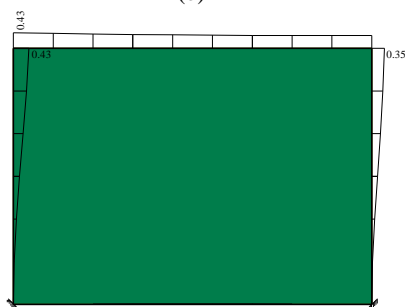
Uticaji u gredi: max Xp= 0.43 / min Xp= 0.00 m / 1000
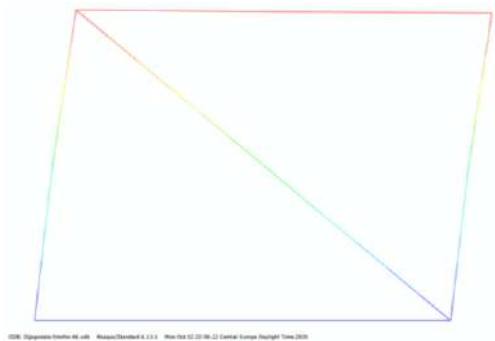(d)
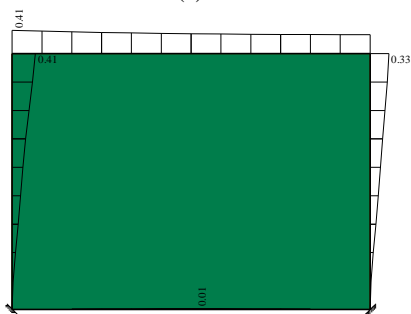
Uticaji u gredi: max Xp= 0.41 / min Xp= 0.00 m / 1000
(e)
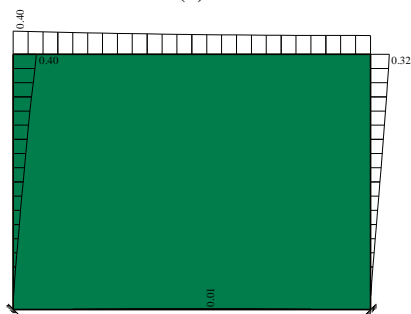
Uticaji u gredi: max Xp= 0.40 / min Xp= 0.00 m / 1000
(f)

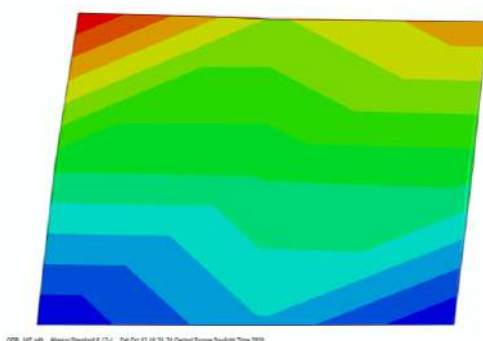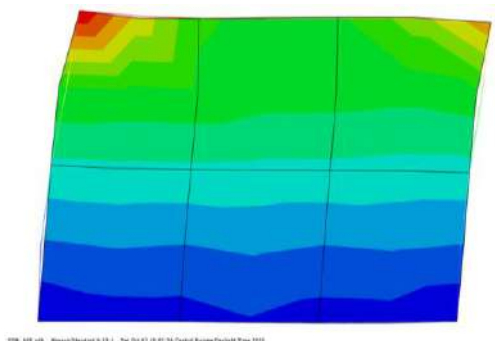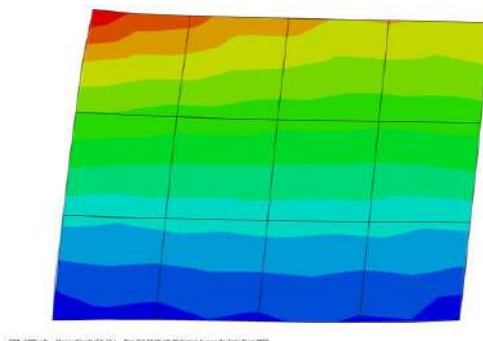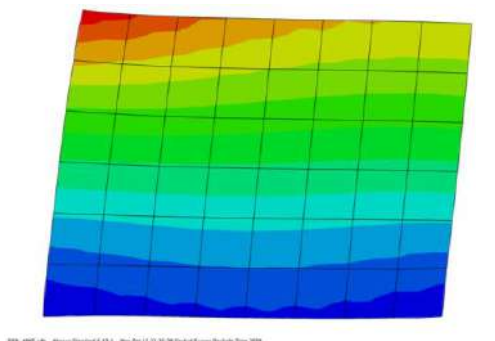*Figure 3 – Displacements for the examined masonry frame RC structure modelled in Tower: a) bare frame model, b) model with diagonal strut, c) model with 1 shell element, d) model with 6 shell elements, e) model with 12 shell elements, f) model with 48 shell elements*

351
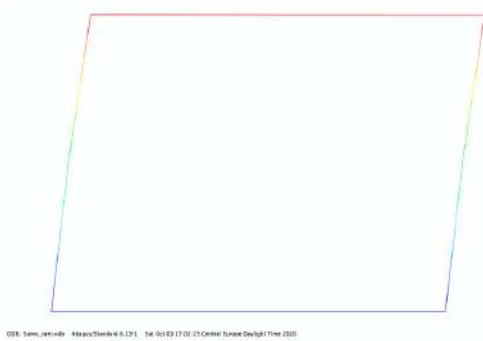
Figure 4 – Displacements for the examined masonry frame RC structure modelled in Abaqus: a) bare frame model, b) model with diagonal strut, c) model with 1 shell element, d) model with 6 shell elements, e) model with 12 shell elements, f) model with 48 shell elements

Comparative representation of the obtained displacements of the top of the examined frame is shown in Table 3.

Table 3 – Presentation of obtained results

		w [cm]	Displacement of the top of the frame structure [mm]	
			Tower	Abaqus
	Bare frame structure	/	13,77	13,77
Models with diagonal strut	Holms	156,00	0,54	0,54
	Smiths, Rumunski propis	46,90	1,49	1,50
	Smiths, Paulay i Pristley	117,25	0,68	0,68
	Symakezis	225,90	0,39	0,39
	Hamburger	50,00	1,41	1,42
Models with shell elements	1 finite element	/	0,51	0,37
	6 finite elements	/	0,43	0,39
	12 finite elements	/	0,41	0,29
	48 finite elements	/	0,40	0,27

The results show good agreement between models developed in the commercial software package Tower and highly sophisticated software package Abaqus. There is slight deviation of the results in the cases of the models with shell elements, which arises from the different finite element formulations in two software packages. There are significant differences in the displacement of the top of the frame in cases of the models with diagonal strut protracted due to different width of the diagonal strut.

4. CONCLUSION

The paper presents the modelling of reinforced concrete frame girders with infill walls. The existing literature points out the importance of the analysis of such girders with regard to their frequent use in building structures. One of the basic methods for analysing the impact of infill walls: the macro method has its advantages and disadvantages which are reflected in the accuracy but also the practicality of their application.

The results obtained by numerical analysis of the frame girder examined in the paper can be seen the influence of the infill walls on the behaviour of reinforced concrete frame girders. The parameter that was analysed is the displacement of the top of the object as one of the basic parameters in the seismic analysis of structures. The difference between the displacement of the top of the frame girder with and without the infill is large, considering the significantly stiffer structure of the frame with the infill. The application of the diagonal rod is very simple from the aspect of numerical analysis, but the results depend directly on the adopted width of the rod, which varies significantly from author to author. Based on the analysis of the obtained results of displacement of the top of the frame structure without masonry infill, as well as the frame

structure when it is filled with wall, it is concluded that the use of replacement diagonal bar is limited.

REFERENCES

[1] Furtado, H. Rodrigues, A. Aresde; Modelling of masonry infill walls participation in the seismic behaviour of RC buildings using OpenSees; International Journal of Advanced Structural Engineering, Vol.7, No.2, pp:117–127, ISSN: 2008-3556, (2015) DOI 10.1007/s40091-015-0086-5

[2] S.S. Sankhla, D. Bhati, A; Comparative Study on the Effect of Infill Walls on RCC Frame Structures; IOSR Journal of Mechanical and Civil Engineering, Vol 13, No. 6, Ver. VI, pp: 01-08, ISSN 2278-1684, (2016), DOI:10.9790/1684-1306060108

[3] P. G. Asteris, S. T. Antoniou, D. S. Sophianopoulos, C. Z. Chrysostomou; Mathematical macromodeling of Infilled Frames: State of the Art: Journal of Structural Engineering, Vol. 137, No. 12, (2011), pp: 1508-1517, ISSN 0733-9445, DOI:10.1061/(ASCE)ST.1943-541X.0000384

[4] U. Albayrak, E. Ünlüoğl, M. Doğan; An Overview of the Modelling of Infill Walls in Framed Structures; International Journal of Structural and Civil Engineering Research, Vol. 6, No. 1, pp: 24-29, (2017), doi:10.18178/ijscer.6.1.24-29

[5] B. Singh, K. V. Ramesh, G. Sudheer, C. R. Ramesh; Comparison of reinforced concrete frames modelled with and without infill walls; International Journal of Civil Engineering and Technology, Vol. 8, Issue 8, pp. 1636–1644, (2017), ISSN: 0976-6308,

[6] R. K. Mazumder, R. Dey, M. S. Uddin, A. R. Bhuiyan; Structural Response Analysis of Reinforced Concrete Frame with Unreinforced Masonry Infill Walls; International Conference on Recent Innovation in Civil Engineering for Sustainable Development, (2015), pp:564-569

[7] P. G. Asteris, I. P. Giannopoulos, C. Z. Chrysostomou; Modeling of Infilled Frames with Openings; The Open Construction and Building Technology Journal, Vol. 6, pp: 81-91, (2012)

[8] D. M. Samoilă; Analytical Modelling of Masonry Infills; Acta Technica Napocensis: Civil Engineering & Architecture Vol. 55, No. 2, pp: 127-136, (2012)

[9] E. Smyrou, C. Blandon, S. Antoniou, R. Pinho, F. Crisafulli; Implementation and verification of a masonry panel model for nonlinear dynamic analysis of infilled RC frames; Bulletin of Earthquake Engineering, Vol. 9, Issue 5, pp:1519–1534, (2011), https://doi.org/10.1007/s10518-011-9262-6

[10] N. Tarque, L. Candido, G. Camata, E. Spacone; Masonry infilled frame structures: state-of-the-art review of numerical modelling; Earthquakes and Structures, Vol. 8, No. 1, pp:733-759, (2015), ISSN: 1225-4568, http://dx.doi.org/10.12989/eas.2015.8.1.895

[11] S.V. Polyakov; On the interaction between masonry filler walls and enclosing frame when loading in the plane of the wall; Translation in earthquake engineering, Earthquake Engineering Research Institute (EERI), San Francisco, Calif, USA, pp. 36-42, (1960).

[12] M. Holmes; Steel frames with brickwork and concrete infilling; Proceedings of the Institution of Civil Engineers, London, Part 2, vol. 19, pp. 473-478, (1961).

[13] B.S. Smith; Lateral stiffness of infilled frames; Journal of the Structural Division, ASCE, Vol. 88, No. 6, pp. 183-199, (1962).

[14] Syrmakezis, C. A., and Vratsanou, V. Y. (1986), "Influence of Infill Walls to R.C. Frames Response", Proceedings of 8th ECEE, 3, 47-53. Lisbon, Portugal.

[15] M. J. N. Priestley, G. M. Calvi; Towards a capacity-design assessment procedure for reinforced concrete frames; Earthquake Spectra, vol. 7, no. 3, pp. 413-437, (1991)

[16] P 100-1/2006. Cod de proiectare seismică – Prevederi de proiectare pentru clădiri. România.

[17] Hamburger, R.O. and Chakradeo, A.S. (1993), Methodology for seismic-Capacity Evaluation of Steel-Frame Buildings with Infill Unreinforced Masonry, Proceedings of the National Earthquake Engineering Conference, II, 173-191. Memphis, Tennessee.

[18] EN 1996-1-1 (2005) (English): Eurocode 6: Design of masonry structures – Part 1-1: General rules for reinfoced and unreinforced masonry structures. European Committee for Standardization, Brussels.

[19] Radimpex, Tower 8, Program za statičku i dinamičku analizu, Uputstvo za rad sa programom.

[20] Dassault Systèmes Simulia Corporation, Abaqus Theory Manual, Providence, RI, USA, 2014.

Duško Bobera[1], *Predrag Bakić*[1], *Goran Milutinović*[1]

SEIZMIČKA IZOLACIJA MOSTOVA NA MORAVSKOM KORIDORU

Rezime:

Moravski Koridor je novi autoput dugačak 112km trenutno u izgradnji u Srbiji sa ukupno 117 mostova. Osam najdužih mostova na koridoru (ukupne dužine više od 3.3 km) su seizmički izolovani i njihova analiza i dimenzionisanje su prezentovani u ovom radu. Njihovo konstruktivno ponašanje, kao i odgovarajući zahtevi Evrokoda za seizmičku izolaciju su izloženi.

Ključne reči: Moravski Koridor, seizmička izolacija

SEISMIC ISOLATION OF BRIDGES ON MORAVA CORRIDOR

Summary:

The Morava Corridor is a new 112-km-long motorway currently under construction in Serbia, with total of 117 bridges. The eight longest bridges, with a total length of more than 3.3 km, are seismically isolated and their analysis and design are presented in this paper. Their behaviour as well as the applicable Eurocode requirements for seismic isolation are discussed.

Key words: Morava Corridor, seismic isolation

---

[1] *DB Inženjering, Golsvordijeva 36, Belgrade, Serbia, db_inzenjering@yahoo.com*

1. OVERVIEW OF THE PROJECT

The Morava corridor is a new 112-km-long motorway currently under construction in Serbia. *Figure 1* shows a map of all bridges along the corridor, with each arrow representing one bridge, for a total of 117 bridges. The eight longest bridges, located at stations km 1+347, 8+519, 9+933, 15+857, 29+910, 48+115, 74+655, and 109+411 (together over 3.3 km long), have been built or are currently under construction using the construction technology brought by the contractor, Bechtel Enka Joint Venture. These eight bridges are seismically isolated structures and their seismic analysis and design are discussed and presented in this paper. This is one of the first uses of seismic isolation in Serbia. Another aspect of these bridges unique for Serbia is the use of pretensioning of the beams (as posttensioning is usually used).
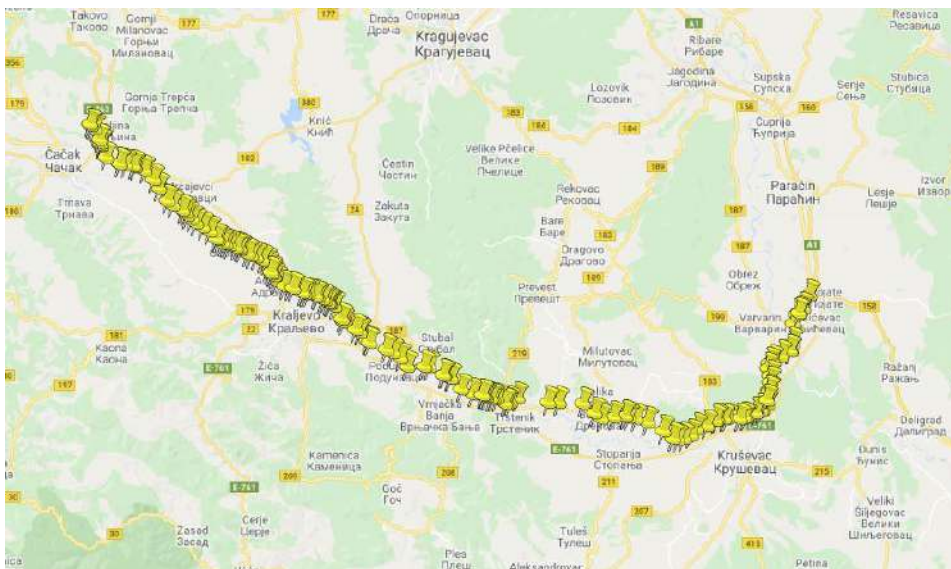
Figure 1 – Morava corridor (each arrow is a bridge structure)

2. DESCRIPTION OF SEISMICALLY ISOLATED BRIDGES

The typical superstructure of the seismically isolated bridge on the Morava Corridor as described in this paper consists of a series of simply-supported spans, each up to 40 m in length. The simple spans are connected between each other by means of 25-cm-thick link slabs over the piers. The flexural stiffness of the link slab is several orders of magnitude smaller than the mid-span flexural stiffness. The typical cross section of the superstructure consists of three precast pre-tensioned U beams (or five I beams for the other subtype of the seismically isolated bridge on this project) composite with the cast-in-place reinforced concrete deck (*Figure 2*).

The substructure consists of either hollow box column sections or solid circular columns as shown in *Figure 3*. Due to its superior hydraulic shape compared to the hollow box sections, and in accordance with the hydraulic design, the circular piers were specified in the riverbed. The

columns are supported by pile caps, which in turn are supported by cast-in-place reinforced concrete bored piles (drilled shafts). The clear height between the pile cap and pier cap varied from 5 m to 11 m. Pile lengths varied from 5 m to 20 m.
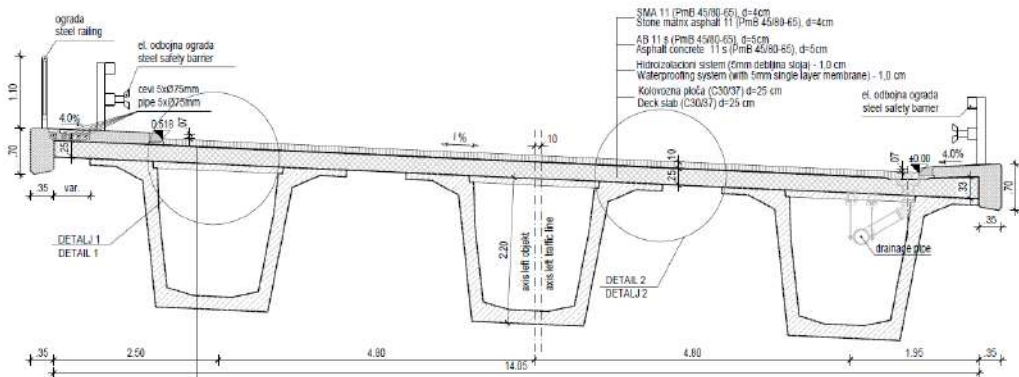

Figure 2 – Typical cross sections (U-beam bridges)

Soil types were either type A (sound rock at not more than 5 m below ground level), or type B (very stiff clay or very dense sand with average SPT values larger than 50 in the first 30 m), or type C (stiff clay or medium dense sand with average SPT values in the range of 15 to 50, in the first 30 m), with respect to the soil amplification of the seismic ground motion (as per EN 1998-1). Peak ground acceleration varied from 0.15g near Kruševac to 0.2g near Kraljevo, as provided by the map in the Serbian National Annex to EN 1998-1, for the return period of 475 years. Behaviour factor equal to 1.0 was used in order to have completely elastic behaviour.
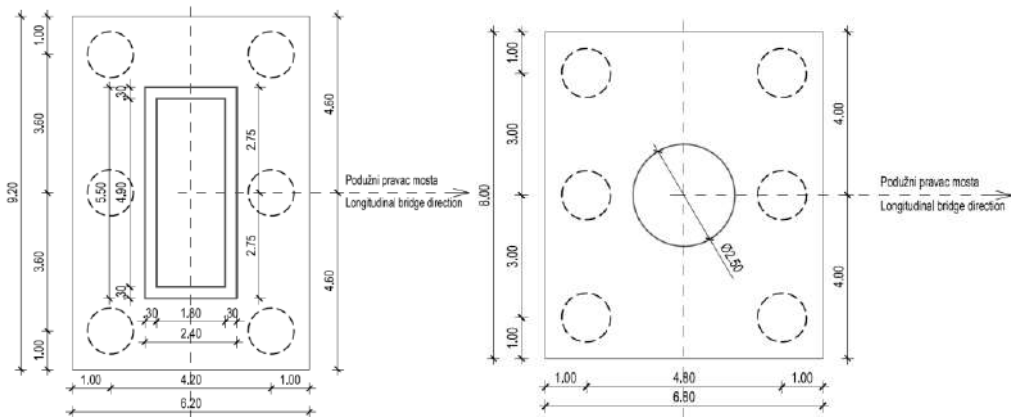
Figure 3 – Typical hollow-box pier (left) and circular pier (right)

Longitudinal view of the built bridge at km 8+519 is shown in *Figure 4*. The superstructure is supported on the substructure by laminated elastomeric bearings, which is otherwise completely separated from the substructure. The detail at the supports is shown in *Figure 5*. The purpose of the upper part of the pier head is to support the launcher during beam installation. A polystyrene layer separates the link slab from the pier cap at the interface between the two

components. Expansion segments (total length between expansion joints) are limited to a maximum of approximately 200 m, in order to satisfy all design checks for elastomeric bearings. The number of expansion segments per bridge varied from one to four.

Figure 4 – Longitudinal view of the bridge at km8+519 (under construction)

Elastomeric bearing dimensions were 400x500x101, 350x450x77 and 350x450x65, where first two numbers are its plan dimensions, while the last number is the elastomer thickness. The bearing size depends not only on the seismic design combination, but also on the non-seismic ultimate limit state (ULS) combination, which includes temperature and shrinkage. It should be noted that rapid set, type R cement has almost exclusively been used as of late in Serbia, as found in practice and literature [1], significantly increasing the shrinkage strain when compared with normal, type N cement.
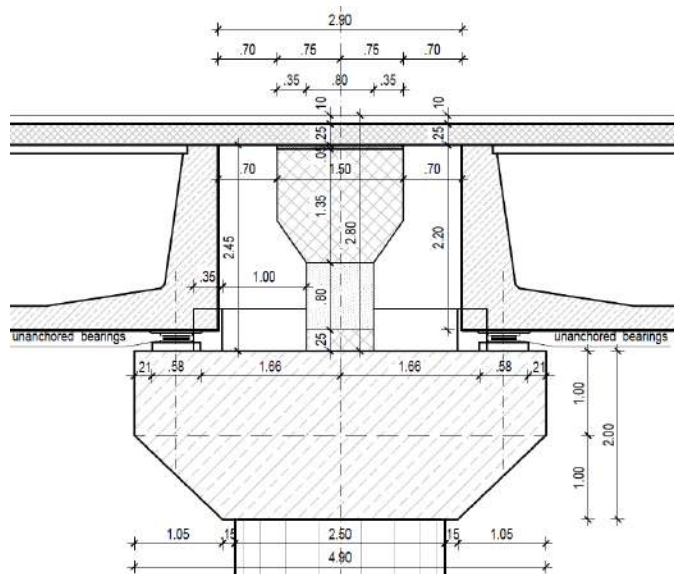
Figure 5 – Link slab detail

Typical reinforcement ratios for the columns ranged from 0.6% to 1.3% for longitudinal reinforcement. The stirrup arrangement with link bars for columns was necessary to satisfy Eurocode requirement EN 1992-1 9.2.2 (8) for the transverse spacing of stirrup legs. Reinforcement ratios from 0.8% to 1.7% were typically used for the longitudinal reinforcement of the piles. The completed detail at the pier support is shown in *Figure 6*.

Figure 6 – Built pier support detail

3. BEHAVIOUR DURING EARTHQUAKE (CONCEPT OF SEISMIC ISOLATION)

The concept of the seismic isolation involves softening the structure by providing an additional flexible element (elastomeric bearings) to support the relatively large percentage of the total structure mass. The effective stiffness of the structure is then the combined stiffness of the conventional structure (e.g. the bridge pier) and that of the flexible isolation device. Such a reduced stiffness increases the period, which in turns results in decreased acceleration (and therefore reduced seismic forces), but also increases displacements obtained from the response spectra. The effect of period shift and reduced seismic acceleration (and therefore forces) for a more flexible structure is illustrated in *Figure 7*.

The concept of isolation is often used in bridge structures throughout the world, primarily for the following two reasons: (1) elastomeric bearings are routinely used in bridges for non-seismic purposes (supporting the superstructure, which is a large percentage of the total mass of the bridge), and (2) bridges are often classified as "important" structures, designed to remain functional even after major earthquakes.

Laminated elastomeric bearings consist of alternating layers of rubber reinforced with steel shims. Apart from their inherent purpose as vertical supports, elastomeric bearings can effectively perform the period shift when used as an isolation device, but without increased

energy dissipation. This gives way to reduced seismic acceleration, but with increased seismic displacement. Their hysteretic loop is narrow, providing around 5% damping, which is the value typically used as part of conventional design. Therefore, the usual response spectrum curve for 5% damping should be used in the case of elastomeric bearings.

If the displacement were to become unacceptably large (which was not the case in this project), one solution would be the use of lead-rubber bearings instead of conventional elastomeric bearings. This would provide additional damping, reducing the entire displacement response spectrum, and therefore reducing the displacement due to increased damping. An analysis of lead-rubber bearings is presented in [2] and [3].
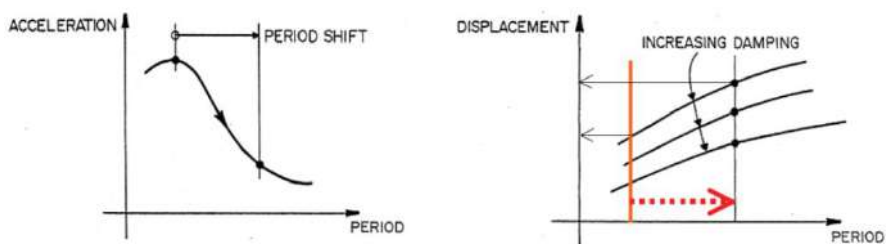
Figure 7 – Response spectrum showing the effect of period shift and increased damping [4]

The above-described behavior (period shift, but not increased damping) occurs in the bridges discussed in this paper. The elastomeric bearings dominantly control the stiffness of the entire substructure system – the global structural stiffness is almost insensitive to the change of the column height or column cross section dimensions. The superstructure is free to "float" completely independent of the substructure.

Seismic blocks, however, are used as "the last line of defense" to prevent the unseating of the superstructure in the case of catastrophic earthquake or unforeseen structural behaviour of the bridge. The necessary gap between the girders and seismic blocks were calculated as a maximum of 10 cm for both seismic and ULS combinations, which included both, temperature and shrinkage (see *Figure 5* for the locations of seismic blocks). If the superstructure "floats" and the deflection relative to the substructure is greater than the calculated gap, the superstructure would collide with the substructure (seismic block). The resulting global behaviour would be completely different – there would no longer be any seismic isolation. Expansion joints are designed for the seismic design situation to provide both free longitudinal and lateral movement, since the seismic isolation concept, or "floating superstructure," refers to free oscillation in any direction during an earthquake.

4. EUROCODE APPROACH – LOW-DAMPING ELASTOMERIC BEARING AS SEISMIC ISOLATOR

Conventional laminated elastomeric bearings are used in this project and they play a dominant role in the seismic response of the structure. According to EN 1998-2, such bearings are referred to as "simple low-damping elastomeric bearings" and are used as seismic isolators. They must be in compliance with EN1337-3 (European norm for elastomeric bearings), but need not be in compliance with EN15129 (European norm for anti-seismic devices). Bearing deformations were checked against two load cases:

1. Conventional ULS non-seismic check:
   Temperature (±20°C) + 1.0 × Shrinkage
   - An additional temperature of ±20°C was added to the previously calculated temperature range in accordance with EN1991-5 6.1.3.3 Note 2, given that the temperature of the "locking" of the structure was not defined.
   - For this combination, the permissible elastomer shear strain is less than 1.0, equivalent to a bearing deformation angle of arctan(1) = 45°.
2. The only additional check for seismic isolator of this type:
   0.5 × Temperature + 1.5 × Seismic + 1.0 × Shrinkage
   - For this combination the permissible shear strain is less than 2, which is equivalent to an angle of arctan(2) = 63°. Seismic effects are amplified by an additional 50% for increased reliability, given that the bearing is the key seismic element.

According to EN1337-3, the target mean value (G_g) for the elastomer shear modulus is 0.9 MPa, which corresponds to a shear strain range smaller than 1 (as in the case of the non-seismic ULS combination). For larger shear strain ranges (e.g. larger than 1.0 and smaller than 2.0, as permitted for seismic combinations), the secant shear modulus is increased according to EN 1998-2 7.5.2.4(5). It is usually in the range of 1.1 to 1.4 of G_g, and is best determined by tests. In this project, $G_b = (1.1 + 1.4)/2 \times G_g = 1.25 \times G_g = 1.1$ MPa was used. Furthermore, according to EN1998-2 7.5.2.4(6), the creation of two independent models is necessary for seismic loads; one with lower bound design properties (LBDP; $G_b = 1.1$ Mpa) of the elastomer, and one with upper bound design properties (UBDP; $1.2 \times G_b = 1.3$ MPa). The reason behind the upper and lower bounds is the fact that the elastomer properties change over time due to aging and variations in temperature. As a result, three models were generated:

- For non-seismic checks with $G_b = 0.9$ MPa
- For seismic LBDP checks with $G_b = 1.1$ MPa
- For seismic UBDP checks with $G_b = 1.3$ MPa

Bearing stiffness is calculated according to the following expression:

$$K_{brg} := \frac{G_{brg} \cdot A_{brg}}{t_{brg}}$$

where A_{brg} is area of the bearing in plan, t_{brg} is the elastomer thickness, and G_{brg} is the elastomer shear modulus, G_b.

It is expected that the model with the lower bearing stiffness (more flexible structure) will govern for checks involving displacement, while the model with the upper bearing stiffness (stiffer structure) will govern for column design and for minimum compression of the bearing (bearing anchorage requirement).

The longer side of the elastomeric bearing is normally in the transverse direction of the bridge, to minimise the rotational restraint in the longitudinal direction and – if used under a precast girder – to stabilise it laterally during erection [5]. Among the various types of elastomeric bearings specified in EN 1337-3, two in particular deserve to be acknowledged: type C, with top and bottom steel plates provided (either profiled or anchored to the parts of the bridge on either side of the bearing), and type B, without steel or any other type of plate attached to the top or bottom surfaces of the elastomer. Type B was used on the entire project. The minimum pressure requirements for this type of bearing were checked and found to be acceptable.

The provided type of expansion joint is the modular expansion joint, which enables the appropriate free transverse movement. This was the consequence of the suggestion made by the Technical Control, thus allowing the free transverse seismic movement of the bridge, necessary for the designed behaviour of the entire structure during an earthquake, even for the maximum considered earthquake level. For the maximum considered earthquake (475 year return period), the expansion joint can be damaged according to the European norms, but shall not change the global behaviour of the entire structure; the expansion joints must remain undamaged for the "frequent" level of the earthquake (EN1998-2 2.3.6.3 (5)). Therefore, two load combinations were checked when designing the expansion joints:

1. Leading temperature
   $1.0 \times$ Shrinkage (with type R cement) + $1.0 \times$ Temperature (with additional $\pm 20°C$)
2. Frequent earthquake
   $1.0 \times$ Shrinkage (with type R cement) + $0.4 \times$ Seismic + $0.5 \times$ Temperature
   - In accordance with EN1998-2 2.3.6.3 (5), for frequent earthquakes it is necessary to save the integrity of the non-critical structural components.

Besides these two load combinations, a third combination was also checked against the full design seismic load: whether there is enough of a provided gap or clearance, such that the superstructure (expansion segment) does not collide with the abutment or adjacent expansion segment through the expansion joint, and therefore changes the global behavior of the structure and its structural system. This free movement in both directions is enabled with the use of modular expansion joints, both laterally and transversely.

5. FEM MODEL AND SIMPLE HAND CALCULATIONS FOR VERIFYING THE FEM MODEL

The 3D finite element method (FEM) model was generated to perform the analysis of the bridges described in this paper. The model is shown in *Figure 8*. Three models were made with different elastomer characteristics as shown in
Table 1. For column, pile cap and pile design, the controlling model was the one with the upper bound of the elastomer shear modulus. For bearing design, primarily involving displacement, the controlling model was with the lower bound of the modulus. The corresponding first modes for different models are also shown for one of the bridges from the corridor in *Figure 9*. Elastomeric bearings are modeled with link elements having an appropriate shear stiffness, K_{brg}. Fifty modes are considered in the analysis in order to result in a participating modal mass larger than 90% of the total mass of the bridge, as required by Eurocode (EN 1998-2 4.2.1.2 (2)). The first and second mode shapes clearly illustrate the concept of the "floating superstructure" – the superstructure displacement is much larger than that of the substructure. Most of the structural displacement is concentrated in the bearings (see *Figure 9*).

Since the finite element method, in general, is easily "used and abused"[6], simple hand calculations were performed to verify the full 3D model. The simple hand calculations consist of single-degree-of-freedom (SDOF) analyses representing a single column and tributary superstructure mass, also known as the fundamental mode method in EN 1998-2. The SDOF system is shown in *Figure 10*. Since the column height, in general, is different in each bay, an averaged column height in one expansion segment should be used for this SDOF system.

Location of the point of fixity of the SDOF system is questionable, but in this case it is irrelevant, since the stiffness of the entire bridge system is dominated by the elastomeric bearing stiffness.
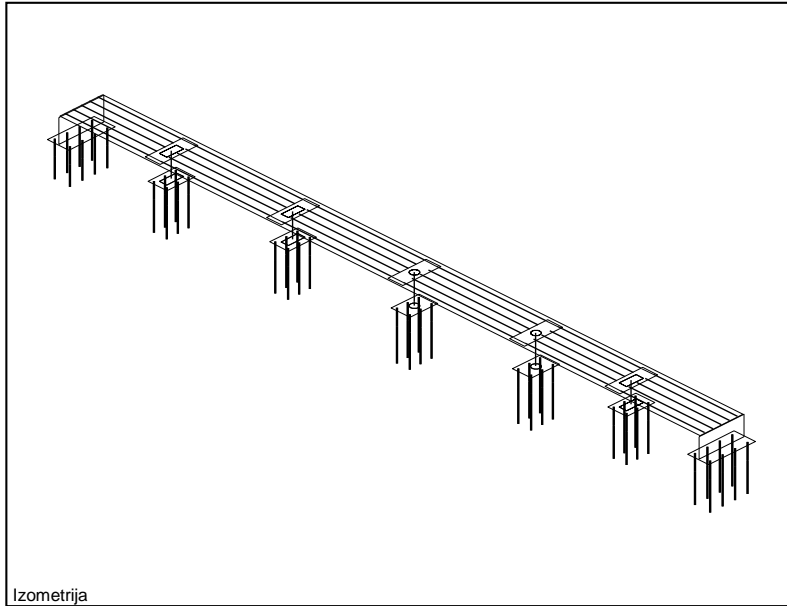

Izometrija

Figure 8 – FEA model of the bridge for seismic analysis

The effective mass of the SDOF system (M_{eff}) is equal to the tributary mass of the superstructure (equal to one span), and entire pier cap weight and half of the column weight. The stiffness of the column (K_{pier}) is calculated as for the usual cantilever:

$$K_{pier} := \frac{3 \cdot E_{cm} \cdot I_c}{\left(col_{height} + 2m\right)^3}$$

where E_{cm} is equal to the concrete modulus of elasticity, col_{height} is equal to clear height of the column (clearance between pile cap and pier cap), 2 m is the pier cap height, and I_c is the column section moment of inertia.

The stiffness of the elastomeric bearing (K_{brg}) is calculated as previously described:

$$K_{brg} := \frac{G_{brg} \cdot A_{brg}}{t_{brg}}$$

The effective stiffness of the entire substructure is equal to serial connection between column stiffness and bearing stiffness:

$$K_{eff} := \frac{K_{pier} \cdot K_{brg}}{K_{pier} + K_{brg}}$$

Table 1 – First modes for different models

Model	Shear modulus of elastomer stiffness	First mode (sample bridge)
Non-seismic load	0.9 MPa	1.43 s
Seismic load, lower bound	1.1 MPa	1.30 s
Seismic load, upper bound	1.3 MPa	1.22 s

Izometrija
Forma oscilovanja: 1/50 [T=1.2162sec / f=0.82Hz]

Izometrija
Forma oscilovanja: 2/50 [T=1.2104sec / f=0.83Hz]
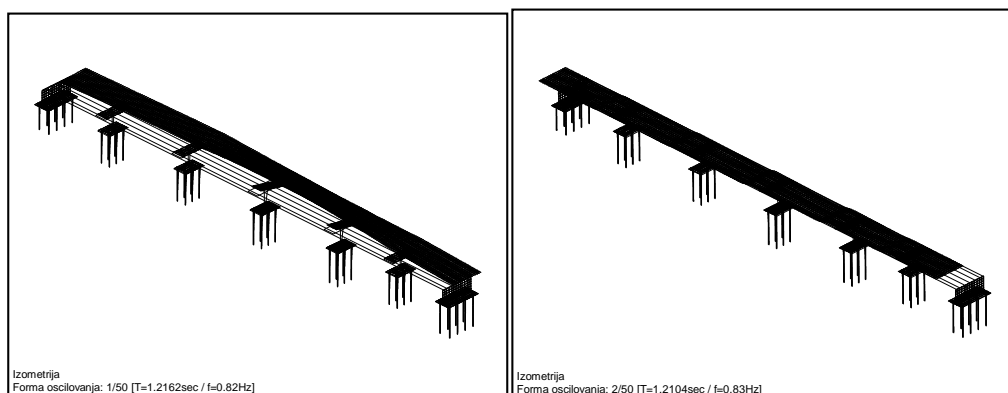
Figure 9 – First and second oscillation mode

The first fundamental period of the bridge can be calculated as:

$$T_{fund} := 2 \cdot \pi \cdot \sqrt{\frac{M_{eff}}{K_{eff}}}$$

Spectral acceleration can be calculated according to the response spectrum equations of the EN 1998-1, which for the period range in question is equal to the following expression:

$$S_d := a_g \cdot S_{soil} \cdot \frac{2.5}{q} \cdot \frac{T_c}{T_{fund}}$$

where S_{soil} and T_c are the parameter from EN 1998-1 describing the response spectrum.

The equivalent static seismic force (F_{eq}) acting at the superstructure centre of mass and the corresponding moment at the base of the column ($Moment_{eq}$) are the following:

$$F_{eq} := M_{eff} \cdot S_d \qquad \text{and} \qquad Moment_{eq} := F_{eq} \cdot arm_{eq}$$

As expected, the hand calculation results were within 10% of the refined analysis with the FEM model (for which, of course, a significant amount of more time is spent). This is in accordance with the principle that Westergaard described in his book on the theory of plasticity many years ago – "A simple device can yield perhaps 80% of the truth, whereas the next 10% would be difficult to obtain and the last 10% impossible…"[7].

To illustrate the effectiveness of seismic isolation, approximate design was performed for comparison – if longitudinal reinforcement demand in one circular column for seismically-isolated structure is 300cm^2, then for equivalent non-seismically-isolated structure the reinforcement demand would be 1400cm^2 (having the behaviour factor as 1.0 in both cases).
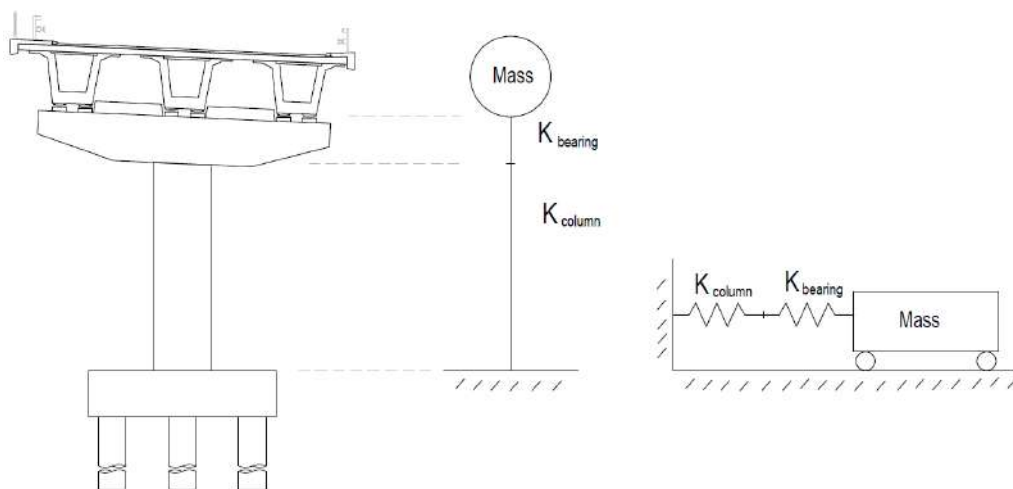
Figure 10 – SDOF system of the bridge with serial stiffness connection

6. CONCLUSION

This paper discusses the analysis and design of eight seismically isolated bridges along the Morava Corridor, together having a length of more than 3.3 km. It can be concluded that seismic isolation can be effectively done on road bridges (especially since the elastomeric bearings are often used for nonseismic purposes anyway), saving a large amount of the reinforcement in the substructure. However, one shortcoming of the use of seismic isolation in this case was the necessity of having expansion joint at maximum distance of about only 200m – these expansion joints must also have movement allowed in both longitudinal and transverse direction. It should be noted that expansion joints allowing simultaneous movements in both directions (longitudinal and transverse) are much more expensive (multiple times), than usual expansion joints allowing movements only in longitudinal direction.

ACKNOWLEDGMENTS

LITERATURE

[1]   Dragojević M, Savatović S, Jevtić D, Zakić D, Savić A, Radević A, et al. Statistical analysis of results of testing of concrete cubes. Tehnika 2019;74:191–7.

[2]   Šumarac D, Đorđević F, Matić D, Milutinović G V. A PREISACH MODEL FOR THE LEAD-RUBBER BEARING HYSTERESIS LOOP. 8th Int. Conf. Contemp. Achiev.

Civ. Eng. 22-23. April 2021. Subotica, SERBIA, vol. 37, 2021, p. 263–74.

[3]   Salatic R, Mandic R, Tosic N. EFFECT OF BASE ISOLATION ON SEISMIC RESPONSE OF MULTI-STORY BUILDINGS – A CASE STUDY. 5TH Int. Conf. Civ. Eng. - Sci. Pract., 2014, p. 17–21.

[4]   Constantinou MC, Kalpakidis I, Filiatrault A, Lay RAE. LRFD-Based Analysis and Design Procedures for Bridge Bearings and Seismic Isolators. 2011.

[5]   Fardis MN, Pecker A. Designers' Guide to Eurocode 8: Design of bridges for earthquake resistance. 2012. https://doi.org/10.1680/dber.57357.

[6]   Barker RM, Puckett JA. Design of Highway Bridges. 2013.

[7]   Sozen M. The simplicity of the complexity 1999.

Jelena Ristić[1], *Venera Hajdari*[2], *Labeat Misini*[3], *Danilo Ristić*[4]

TESTIRANJE MODELA ODBOJNIKA OD GUME KAO ZAŠTITE MOSTOVA OD ZEMLJOTRESA I POPLAVA

Rezime:

Eksperimentalnim kvazi-statičkim cikličnim testovima realizovanim putem simulacije rastujućih amplituda pomeranja potvrđeno je veoma stabilno histerezisno ponašanje kreiranih prototipskih modela uređaja odbojnika od gume primenljivih za efikasnu zaštitu standardnih i seizmički izolovanih mostova izloženih jakim zemljotresima ili katastrofalnim poplavama. Posle izvršenog unapređenja izolovanog (USI) sistema mosta sa uređajima za disipaciju energije, adaptiran je i originalan uređaj odbojnika od gume koji predstavlja veoma važnu liniju odbrane od iznenadno nastalih maksimalnih opterećenja.

Ključne reči: most, test-model, zemljotres, poplava, odbojnik od gume, sigurnost

TESTING OF RUBBER BUFFER MODELS PROTECTING BRIDGES UNDER EARTHQUAKES AND FLOODS

Summary:

With the extensive experimental quasi-static cyclic tests conducted with simulated gradually increasing displacement amplitudes, confirmed were very stable hysteretic responses of created prototype models of rubber buffer (RB) devices applicable for efficient protection of common and isolated bridges exposed to either strong earthquake or flood disasters. Following upgrading of seismically isolated (USI) bridge system with energy dissipation devices, the adopted original rubber buffer (RB) devices represent important line of defense against abrupt loadings.

Key words: bridge, model testing, earthquake, flood, rubber buffer, safety

[1] *Assoc. Prof., Dr., Faculty of Engineering, Department of Civil Engineering, International Balkan University (IBU), Skopje, Republic of N. Macedonia, jelena.ristic@ibu.edu.mk*
[2] *PhD student, Institute of Earthquake Engineering and Engineering Seismology (IZIIS), Ss. Cyril and Methodius University in Skopje, N. Macedonia, venerahajdari95@gmail.com*
[3] *PhD student, Institute of Earthquake Engineering and Engineering Seismology (IZIIS), Ss. Cyril and Methodius University in Skopje, N. Macedonia, labeat.misini@gmail.com*
[4] *Full Prof. Dr., Institute of Earthquake Engineering and Engineering Seismology (IZIIS), Ss. Cyril and Methodius University in Skopje, Republic of N. Macedonia, danilo.ristic@gmail.com*

1. CONCEPT OF EARTHQUAKE AND FLOOD PROTECTIVE BRIDGE SYSTEM

Extensive experimental and analytical study was performed devoted to development of integrated earthquake and flood protective (EFP) bridge system. It represents extension of the conducted integral research project led by the fourth author during three and a half years, in the Institute of Earthquake Engineering and Engineering Seismology (IZIIS), Ss. Cyril and Methodius University (Skopje), realized in the frames of the innovative NATO Science for Peace and Security Project "Seismic Upgrading of Bridges in South-East Europe by Innovative Technologies (SFP: 983828)", involving five European countries, Fig. 1.
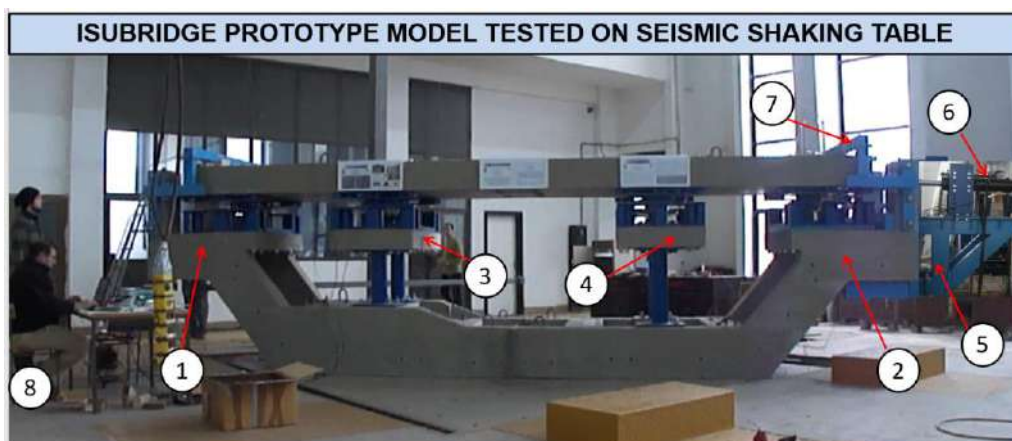
Figure 1 – EFP bridge prototype model on the IZIIS shaking table: left end support (1); right end support (2); support above shorter piers (3); support above longer piers (4); actuator supporting structure (5); actuator (6); support of DL devices (7); computer controlling the cyclic tests (8), (Commonly re-used prototype: Ristic, J., 2016); Ristic, J.,et all., 2021).

The presently introduced EFP bridge system represents a specific extended segment of the integral research. The upgraded seismically isolated (USI) system with integrated space flange (SF) energy dissipation (ED) devices is developed as a mechanical passive concept to provide harmonized response of bridge structures to earthquakes. It was formulated as an adaptive system, which follows the adopted concept of global optimization of seismic energy balance, through utilization of newly designed dissipation devices as a supplementary damping level to bridge isolation. The new EPF-bridge system is based on obligatory incorporation of the following four integrated complementary systems: *(1) Seismic isolation (SI) system:* The seismic isolation system (SI) provides low stiffness in horizontal direction while being capable of safely carrying the weight of the super-structure. Adequately designed seismic isolators may be installed at each supporting point of the bridge super-structure, transferring the weight to the middle piers and/or to the rigid abutments. Hence, there is a variety of adequate seismic isolation systems to be selected, including the technical solutions used here; *(2) Seismic energy dissipation (ED) system:* The seismic energy dissipation system (ED), unlike seismic isolators, provides sufficient damping for dissipation of seismic energy. In general, these devices provide a large capacity of energy dissipation through non-linear behavior and development of

hysteretic properties. They have to be designed in an optimal manner and in relation to the seismic performances of the selected seismic isolators. These requirements address the optimal stiffness in order to prevent transfers of inertial impulse forces and the optimal bearing capacity set to a design limit to prevent generation and transfer of large inertial forces to the piers. Finally, the ED system needs to be designed to have sufficiently large available ductility and to sustain a large deformation prior to its damage. Significant advances in respect to these requirements have been achieved by the formulation of the proposed new SF energy dissipation devices;
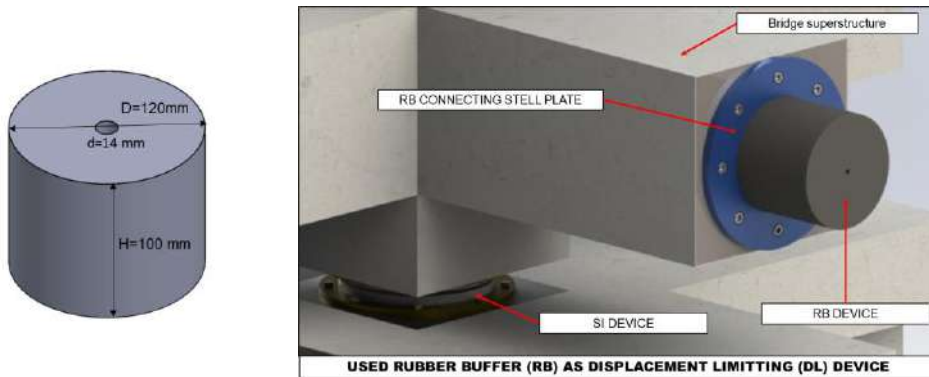
Figure 2 – Tested model geometry and installation of RB as displacement limiting device

(3) Displacement limiting system (DL): During strong earthquake vibrations, a limited number of very strong impulses may occur, followed by large displacement amplitudes, which are not controlled in a reliable engineering mode. Thus, the introduced specific DL devices, presently implemented in the form of specific rubber buffer (RB) devices, may reduce or eliminate a strong impact effect, Fig. 2. In addition, the implemented RB devices will efficiently protect large uncontrolled side displacements and total collapse of bridge superstructure under generated increasing very strong flood pushing forces, and *(4) Uplift protection system (UP):* The implemented-UP devices will efficiently protect uncontrolled vertical uplift displacements and total collapse of bridge superstructure under generated strong vertical flood uplift forces. Actually, the integrated DL and UP devices will act as specific interactive protection systems, efficiently protecting uncontrolled failure of bridge superstructure under generated uncontrolled combined horizontal and vertical forces during extreme earthquakes and floods.

The conducted extensive experimental research included two main parts. The first part involved quasi-static tests of constructed models of *(1) seismic isolation (SI) devices and (2) seismic energy dissipation (ED) devices*, which were mounted in the constructed large-scale ISUBRIDGE prototype bridge model. In this way, the seismic isolation devices, the components of the energy dissipation devices and the assembled devices were tested separately. In the second part, seismic testing of the USI-SF bridge model was performed under simulated effect of strong earthquakes by the use of the shaking table equipment. The physical bridge model was designed and constructed after special design considerations to be compatible for successful performance during both quasi-static testing of components and devices and seismic shaking table testing.

In this paper briefly are presented selected original results obtained from the conducted extensive experimental tests of created and constructed rubber buffer (RB) prototype models with different hardness, directly applicable for protection of isolated bridge superstructures exposed to generated large horizontal forces, either during severe earthquakes or flood disasters.

2. MODEL PROTOTYPES OF DISPLACEMENT LIMITING RB DEVICES

2.1. DESIGN OF MODELS OF RB DEVICES:

In the case of very strong earthquake excitations that could be sometimes unexpected and surprising, very large relative deformations can be produced in the base of the isolated bridge superstructure. In that case, due to the extremely large displacements, the structure could possibly fallout from the seismic isolators, or more precisely, heavy damage or total failure of the seismic isolators could take place. This type of damage is very unfavorable and may lead to intolerable damage to the structure and big economic losses. Such severe damages to seismically isolated structures have already been observed in practice. The most characteristic example is the heavily damaged Bolu viaduct in Turkey that, although being seismically isolated, suffered heavy damages during the surprisingly strong Koceli earthquake that took place in 1999. It is characteristic that the damages were the most extensive at the seismic isolation devices and seismic energy dissipation devices themselves.

Table 1 – Testing program & tests of elements (specimens) of prototype models of RB devices

Test No.	RB Model	RB Element	Test type	D (mm)	H (mm)
1		M1-RB-40SH-E1	*Original*	120	100
2	M1	M1-RB-40SH-E1	*Repeated*	120	100
3		M1-RB-40SH-E2	*Original*	120	100
4		M1-RB-40SH-E2	*Repeated*	120	100
5		M2-RB-50SH-E1	*Original*	120	100
6	M2	M2-RB-50SH-E1	*Repeated*	120	100
7		M2-RB-50SH-E2	*Original*	120	100
8		M2-RB-50SH-E2	*Repeated*	120	100
9		M3-RB-60SH-E1	*Original*	120	100
10	M3	M3-RB-60SH-E1	*Repeated*	120	100
11		M3-RB-60SH-E2	*Original*	120	100
12		M3-RB-60SH-E2	*Repeated*	120	100
13		M4-RB-70SH-E1	*Original*	120	100
14	M4	M4-RB-70SH-E1	*Repeated*	120	100
15		M4-RB-70SH-E2	*Original*	120	100
16		M4-RB-70SH-E2	*Repeated*	120	100

Due to these heavy damages, the entire seismic isolation bridge system had to be replaced completely by a new one, which represented a considerably big impact from the aspect of economic losses. Similarly, heavy damages to seismically isolated bridge structures can be

expected due to induced large superstructure displacements by large horizontal forces generated during severe flood disasters.

To assure required protection of isolated bridges from large uncontrolled superstructure displacements caused by generated large forces during severe floods or strong earthquakes, created was new innovative USI-SF-DL bridge system, representing advanced technological upgrading of common seismically isolated bridges. The newly incorporated displacement limiting DL system consist of designed and optimally distributed rubber buffers (RB). The actual hysteretic response of the created individual rubber buffers (RB) under increasing and repeated compressive loads, extensive experimental tests have been performed on constructed prototype models of RB devices.

In this paper briefly are presented representative results obtained from realized extensive experimental tests of rubber buffer prototype models in the frame of related specific innovation sub-project. The key functioning targets of displacement limiting (DL) devices are: (1) To enable physical limitation of maximum relative displacements of seismic isolation devices; (2) To achieve predefined physical limitation of relative displacements by properly avoided the so called "hard" structural impact; and, (3) To provide efficient protection of seismic isolation (SI) and energy dissipation (ED) devices by assured limitation of relative displacements. To achieve the stated goals, prototype models of DL devices are designed and manufactured in the form of cylindrical rubber (pads) buffers cast by use of rubber with four different hardness measured in shores, H40, H50, H60 and H70. To obtain comparative experimental results, two experimental test specimens (elements) of each type of RB devices have been constructed, amounting to eight specimens in total. To investigate the effect of repeated loading, two tests (original and repeated) have been performed on each test specimen. Therefore, the integral experimental program was extended, amounting to completed 16 experimental quasi-static tests in total, Table 1.

The present experimental RB sample specimens have been designed in the form of cylinders with a diameter of D=120mm and height H=100mm. In the middle of the cylinder, designed is one central opening with a diameter d=14mm to be used for successful positioning of the experimental device prototype for its experimental testing, Fig. 2.

2.2. RUBBER PROPERTIES OF TESTED RB MODELS

To define the characteristics of the rubber material to be used for the manufacturing of the experimental sample specimens, several initial requirements have been taken into consideration:

(1) The used rubber material should not be very "hard" in order to avoid problems referring to strong "hard" impact;

(2) The used rubber material should not be very soft in order to avoid effect of unfavorable strong "hard" impact resulting from its high compressibility;

(3) The optimal lower and the upper limit of hardness of the rubber material should be predefined since these parameters should meet real practical interest.

In the concrete case, the lower limit of hardness of the rubber has been defined as being in the range of 40 shores, while the upper limit of hardness is in the range of 70 shores. A rubber material with hardness between these two ultimate values, i.e., rubber with hardness of 50 and 60 shores has been used in production of experimental laboratory tests samples. In this way, proper conditions have been created for the obtaining the representative experimental results on rubber samples of different hardness which is very important for their use in practice.

2.3. PROTOTYPES OF RB DEVICES

For the needs of casting of the experimental model prototypes of RB devices, it was at first necessary to manufacture an adequate strong formwork in which casting was performed. The formwork for the casting of the experimental model prototypes has been made of metal in the form of strong structure in order that it could sustain the created high pressure during the casting of the rubber elements. By the performed previous sample hardness measurement, it has been confirmed that the proportions of the cast rubber prototype models correspond with the designed quantities.

For each designed prototype model of RB devices, two experimental test specimens were cast. Following their manufacturing process, with final checking of the dimensions and actual hardness, correctness of the designed parameters of the manufactured specimens was confirmed. With this checking, the following hardness per experimental model types has been defined:

1) Model M1: Hardness 39 shores (considered as designed 40);
2) Model M2: Hardness 40 shores (considered as designed 50);
3) Model M3: Hardness 63 shores (considered as designed 60);
4) Model M4: Hardness 72 shores (considered as designed 70).

With these measurements, it has been defined that the produced experimental prototype models of RB devices satisfy the design conditions and parameters and they were applied in the realization of the experimental study according to the original testing program. Following completed manufacturing of eight designed model prototype specimens, the planned laboratory tests were successfully completed in compliance with the original experimental test program.

3. EXPERIMENTAL TESTING OF PROTOTYPE MODELS

3.1. EXPERIMENTAL TESTING PROCEDURE

The experimental program for evaluation of the seismic performances of the innovative RB devices included testing of four models of RB devices produced of rubber of four different hardness in shores (SH): 40SH; 50SH; 60SH and 70SH. For each RB model, two experimental specimens were constructed.
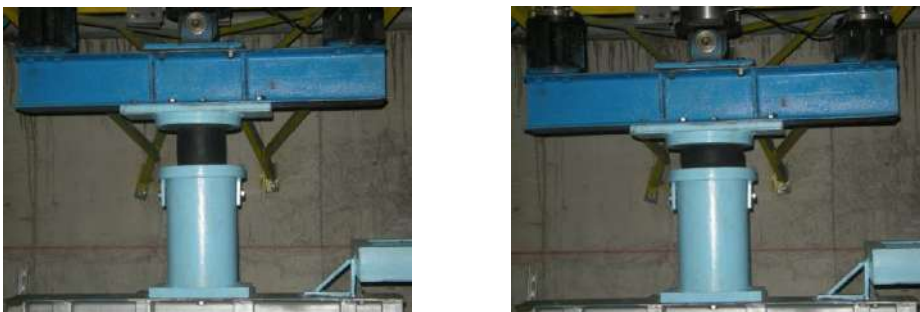

Figure 3 – Experimental test set-up used for testing of model prototypes of RB displacement control devices under simulated cyclic loads with increasing displacement amplitudes

These were indicated as Element-E1 and Element-E2. The other details of the produced original experimental models are shown in Table 1. More specifically, the table shows that, for each of the four model of devices, two experimental elements (E1 & E2) were produced, meaning that the experimental program included testing of eight different specimens, in total.

However, due to the need for getting an insight into the behavior of the innovative RB devices under repeated compressive loading effects, all 8 specimens were tested twice. The first (virgin) test was marked as original, while the second one was named as repeated, Table 1. Then, the entire experimental program resulted in realization of 16 experimental tests in total.

The role of the RB devices is to be effective only under generated compression forces during dynamic response of structures under strong earthquakes. The presented experimental tests were realized by application of repeated compressive forces, which were increased in each successive cycle until reaching of the maximum "allowed" working level. Due to such defined specific experimental conditions, an adequate experimental platform was created, Figure 3. This platform enabled all the necessary conditions for the realization of the specified experimental tests. Testing was carried out by activation of an actuator in vertical direction in order to produce compressive force upon the experimental element since it was fixed, on the upper side, to the constructed rigid steel frame. The experimental element (model) was completely made of rubber and on the lower side, it was placed on a very rigid base that did not suffer any deformations, Figure 3. For "zero" point of deformation and "zero" point of force, there was selected a position indicating only an direct contact between the actuator plate and the experimental rubber element, without transfer of any force (contact without force or zero contact). From that position, compressive forces were further simulated up to a certain initial level of deformation and then the deformation was returned to the zero point that represented a cycle. More concretely, a compression cycle was defined by loading up to a certain level of deformation and unloading down to zero deformation.

The analogous cycles of loading and unloading were repeated a number of times, but in each successive cycle, the amplitude of the reached deformation was increased. In that way, there were created favorable conditions for identification of the real hysteretic behavior of all the tested experimental models up to the phase of deformations representing the optimal working level. In Fig. 3 left, shown is experimental model at the defined zero level of deformations prior to the beginning of the realization of the experimental test, while Fig. 3 (right) shows the model at realized considerable amount of total deformation (being within working deformation), being lower than the allowed working deformation, (D $_{allowed}$).

3.2. ORIGINAL EXPERIMENTAL TEST RESULTS

In accordance with the provided conditions, it is clear that the realized experimental program provided original and highly valuable experimental results that enable getting a realistic insight into the nonlinear-hysteretic behavior of the tested RB models and respective elements. First series of four recorded hysteretic responses of tested model M1, from original and repeated tests of specimens M1-RB-40SH-E1 and M1-RB-40SH-E2, under simulated cyclic loads are shown in Figure 4. Second series of four recorded hysteretic responses of tested model M2, from original and repeated tests of specimens M2-RB-50SH-E1 and M2-RB-50SH-E2, under simulated cyclic loads are shown in Figure 5. Third series of four recorded hysteretic responses of tested model M3, from original and repeated tests of specimens M3-RB-60SH-E1 and M3-RB-60SH-E2, under simulated cyclic loads, are shown in Figure 6. Finally, fourth series of the four recorded hysteretic responses of tested model M4, from

original and repeated tests of specimens M4-RB-70SH-E1 and M4-RB-70SH-E2, under simulated cyclic loads, are shown in Figure 7.
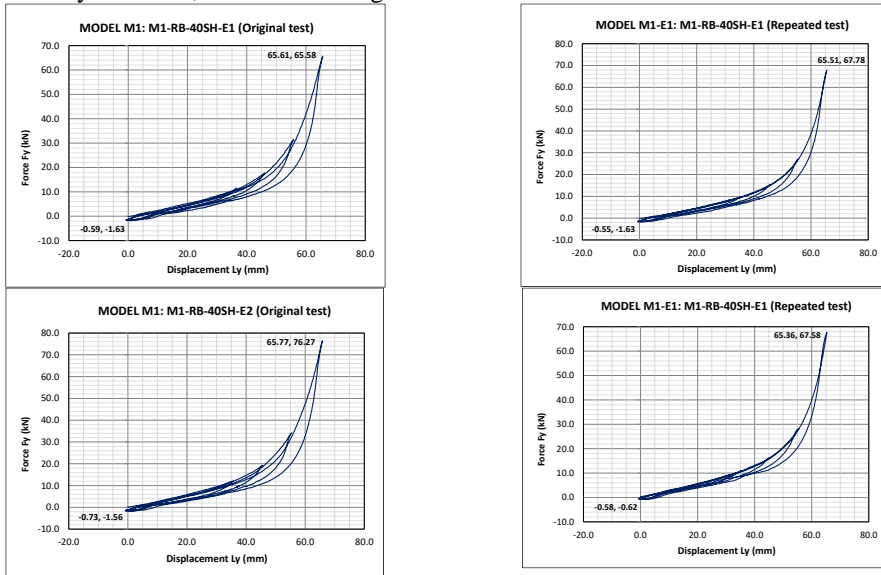

Figure 4 – Recorded hysteretic response of model M1 from original and repeated tests of specimens M1-RB-40SH-E1 and M1-RB-40SH-E2 under simulated cyclic loads
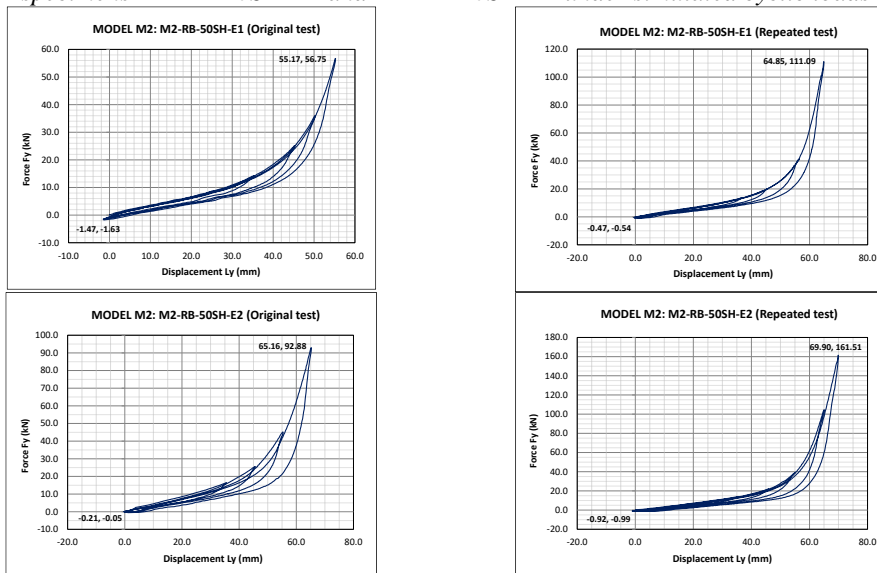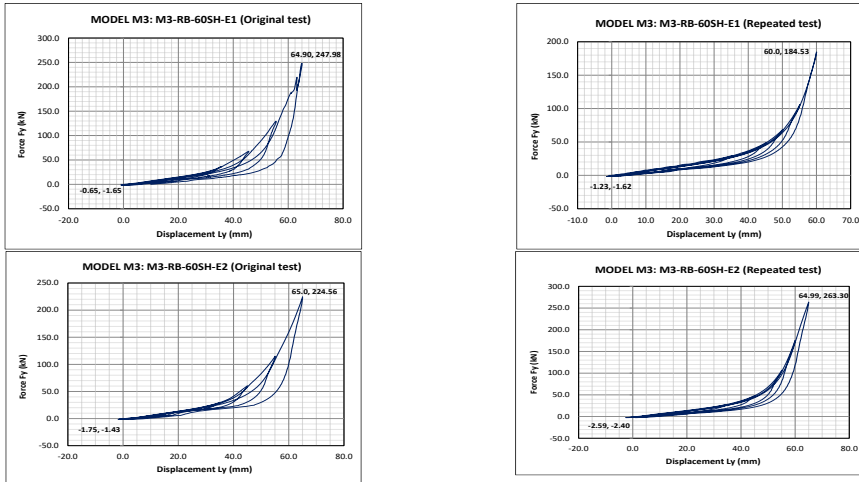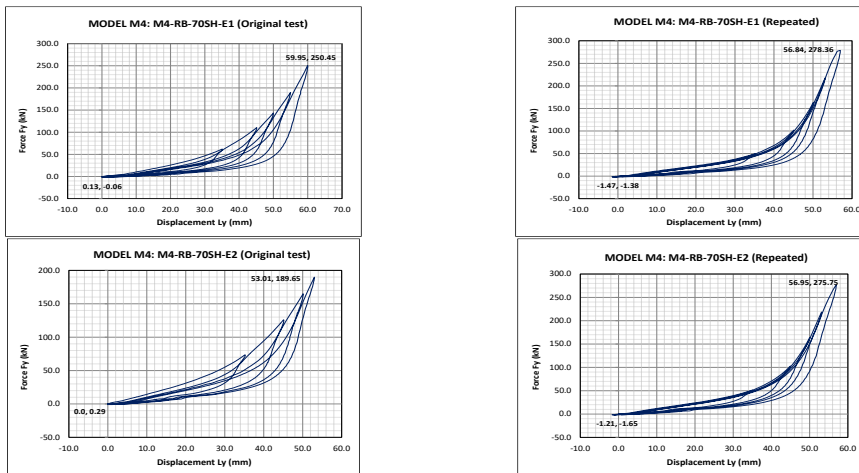

Figure 5 – Recorded hysteretic response of model M2 from original and repeated tests of specimens M2-RB-50SH-E1 and M2-RB-50SH-E2 under simulated cyclic loads

Figure 6 – Recorded hysteretic response of model M3 from original and repeated tests of specimens M3-RB-60SH-E1 and M3-RB-60SH-E2 under simulated cyclic loads

Figure 7 – Recorded hysteretic response of model M4 from original and repeated tests of specimens M4-RB-70SH-E1 and M4-RB-70SH-E2 under simulated cyclic loads

The presented experimental results from all the performed experimental tests are fully consistent, provide conditions for detailed analyses and represent reliable data for defining characteristics and conditions for realistic practical needs. If obtained experimental results for different models are simply compared, the following resulting differences are obtained:

(1) RB model M1 with rubber hardness of 40 shores: A total of four tests were conducted, two tests (original and repeated) for element E1 and two tests (original and repeated) for element E2. For these two tested models, an very good consistency of experimental results was observed. For example, for induced deformation of D=50mm (representing 50% of the element height H), recorded are the corresponding response forces, Table 2. *(2) RB model M2 with*

rubber hardness of 50 shores: From realized four experimental tests, the recorded representative values are presented in Table 3. *(3) RB model M3 with rubber hardness of 60 shores:* From realized four experimental tests, the recorded representative values are presented in Table 4. *(4) RB model M4 with rubber hardness of 70 shores:* From realized four experimental tests, the recorded representative values are presented in Table 5.

Table 2 – Characteristic points from recorded hysteretic response of RB model M1

Test No.	RB Model	RB Element	Test type	D (mm)	F (kN)
1	M1	M1-RB-40SH-E1	*Original*	50	22.00
2		M1-RB-40SH-E1	*Repeated*	50	21.62
3		M1-RB-40SH-E2	*Original*	50	24.00
4		M1-RB-40SH-E2	*Repeated*	50	20.50
Average stress for specified displacement: 1911.7 kN/m²				**50**	**21.62**
Stress for actual maximum displacement: 5815.7 kN/m²				**65.77**	**76.27**

Table 3 – Characteristic points from recorded hysteretic response of RB model M2

Test No.	RB Model	RB Element	Test type	D (mm)	F (kN)
5	M2	M2-RB-50SH-E1	*Original*	50	36.00
6		M2-RB-50SH-E1	*Repeated*	50	26.00
7		M2-RB-50SH-E2	*Original*	50	32.50
8		M2-RB-50SH-E2	*Repeated*	50	30.00
Average stress for specified displacement: 2751.8 kN/m²				**50**	**31.12**
Stress for actual maximum displacement: 14281.5 kN/m²				**69.90**	**161.51**

Table 4 – Characteristic points from recorded hysteretic response of RB model M3

Test No.	RB Model	RB Element	Test type	D (mm)	F (kN)
9	M3	M3-RB-60SH-E1	*Original*	50	90.00
10		M3-RB-60SH-E1	*Repeated*	50	70.00
11		M3-RB-60SH-E2	*Original*	50	85.00
12		M3-RB-60SH-E2	*Repeated*	50	70.00
Average stress for specified displacement: 6963.4 kN/m²				**50**	**78.75**
Stress for actual maximum displacement: 23282.3 kN/m²				**64.99**	**263.30**

Table 5 – Characteristic points from recorded hysteretic response of RB model M4

Test No.	RB Model	RB Element	Test type	D (mm)	F (kN)
13	M4	M4-RB-70SH-E1	*Original*	50	149.00
14		M4-RB-70SH-E1	*Repeated*	50	152.00
15		M4-RB-70SH-E2	*Original*	50	153.00
16		M4-RB-70SH-E2	*Repeated*	50	152.00
Average stress for specified displacement: 13396.4 kN/m²				**50**	**151.50**
Stress for actual maximum displacement: 24616.2 kN/m²				**56.84**	**278.36**

Based on the obtained experimental results and the complete hysteretic relationships plotted for all realized experimental tests, an highly valuable data base was created to enable

formulation of optimal characteristics of RB displacement limiting devices for practical purposes.

4. CONCLUSIONS

From the presented integral experimental results, the following observations are confirmed:

(1) The proposed innovative RB displacement limiting devices show preferable characteristics and are convenient for the specific role given to them to represent the last line of defense against extremely large lateral displacements.

(2) Although only cyclic compressive loads were applied, occurrence of open hysteresis and variable energy dissipation capacity was observed.

(3) After the first loading of the experimental models, although the tested specimens suffered very large total deformations and large distortions of their shape, they were able to return to their initial shape (so, they possess a shape-memory ability). The only permanent consequence, which is relatively minor is manifested by very small permanent deformations of the specimen height. The height of the specimen H=100.0mm is reduced for 2.0 ~ 2.5 mm, which is an amount within the frames of $\Delta D=2\% \sim 2.5\%$.

(4) The difference in the restoring force is very large among rubbers of different hardness. This fact points out that selection of the rubber hardness is a very important step. Therefore, by adequate selection of rubbers of different hardness, it is possible to create different structural displacement limiting options in compliance with the specific requirements.

(5) As far as rubber is concerned, the initial geometrical form of the experimental specimen extensively affects its global behavior under the effect of cyclic compression. Therefore, the shape of the rubber is also to be considered in fitting the optimal options for different structural solutions.

REFERENCES

[1] Kelly, J. M. (1986): Aseismic Base Isolation: A Review and Bibliography, *Soil Dynamics and Earthquake Engineering* 5, 202-216. [DOI]

[2] Kunde, M. C., Jangid, R. S. (2003): Seismic Behavior of Isolated Bridges: A-State-of-the-art Review, *Electronic Journal of Structural Engineering* 3, 140-170.

[3] Iemura, H., Taghikhany, T., Jain, S. K. (2007): Optimum Design of Resilient Sliding Isolation System for Seismic Protection of Equipment, *Bulletin of Earthquake Engineering* 5, 85–103. [DOI]

[4] Zayas, V. A., Low, S. S., Mahin, S. A. (1990): A Simple Pendulum Technique for Achieving Seismic Isolation, *Earthquake Spectra* 6, 317-334. [DOI]

[5] Mokha, A., Constantinou, M. C., Reinhorn, A. M. (1990): Teflon Bearings in Seismic Base Isolation I: Testing, *Journal of Structural Engineering* 116, 438-454. [DOI]

[6] Constantinou, M. C., Kartoum, A., Reinhorn, A. M., Bradford, P. (1992): Sliding Isolation System for Bridges: Experimental study, *Earthquake Spectra* 8, 321-344. [DOI]

[7] UNCRD (1995): Comprehensive Study of the Great Hanshin Earthquake, UNCRD Research Report Series No. 12, United Nations Centre for Regional Development (UNCRD), Nagoya, Japan.

[8] NIST (1996): The January 17, 1995 Hyogoken-Nanbu (Kobe) Earthquake: Performance of Structures, Lifelines, and Fire Protection Systems, NIST SP 901, U.S. Department of Commerce, Technology Administration, Washington, USA.

[9] Fujino Y., Siringoringo D. M., Kikuchi M., Kasai K., Kashima T. [2019]: Seismic Monitoring of Seismically Isolated Bridges and Buildings in Japan—Case Studies and Lessons Learned; In: Limongelli M., Çelebi M. (eds) Seismic Structural Health Monitoring, Springer Tracts in Civil Engineering, Springer, Cham. [DOI]

[10] Li, X., Shi, Y. [2019] Seismic Design of Bridges against Near-Fault Ground Motions Using Combined Seismic Isolation and Restraining Systems of LRBs and CDRs, *Shock and Vibration*, vol. 2019, Article ID 4067915, 11 pages, 2019. [DOI]

[11] Ristic, J., Misini, M., Ristic, D., Guri, Z., Pllana, N. (2017): Seismic Upgrading of Isolated Bridges with SF-ED Devices: Shaking Table Tests of Large-Scale Model, *Gradjevinar*, 2147-2017. [DOI]

[12] Candeias, P., Costa, A. C., Coelho, E. (2004): Shaking Table Tests of 1:3 Reduced Scale Models of Four-Story Unreinforced Masonry Buildings, 13th World Conference on Earthquake Engineering, Vancouver, Paper: 2199.

[13] Ristic, D. (1988): Nonlinear Behavior and Stress-Strain Based Modeling of Reinforced Concrete Structures Under Earthquake Induced Bending and Varying Axial Loads, Doctoral Dissertation, School of Civil Engineering, Kyoto University, Japan.

[14] Ristic, D., Ristic J. (2012): Advanced Integrated 2G3 Response Modification Method for Seismic Upgrading of Advanced and Existing Bridges, 15th World Conf. on Earthquake Engineering, (WCEE), Lisbon.

[15] Ristic, J. (2016): Modern Technology for Seismic Protection of Bridge Structures Applying Advanced System for Modification of Earthquake Response, PhD Thesis, Institute of Earthquake Engineering and Engineering Seismology (IZIIS), "SS Cyril and Methodius" University, Skopje, Macedonia.

[16] Ristic, J., Brujic, Z., Ristic, D., Folic, R., Boskovic, M. (2021): Upgrading of isolated bridges with space-bar energy-dissipation devices: Shaking table test, Advances in Structural Engineering, June 23, 2021; pp. 2948–2965.

Labeat Misini[1], *Jelena Ristić*[2], *Viktor Hristovski*[3], *Danilo Ristić*[4]

SEIZMIČKI ODGOVOR PREFABRIKOVANOG SISTEMA HALE SA TESTIRANIM UNAPREĐENIM VEZAMA

Rezime:

U radu su prikazani originalni rezultati izvršenih nelinearnih analiza seizmičkog odgovora odabrane reprezentativne industrijske prototipske hale transformisane preko re-projektovanja u seizmički unapređen i siguran sistem (USS-sistem) putem primene unapređenih konstruktivnih veza. Sa primenom adekvatno formuliranog 3D nelinearnog analitičkog modela demonstrirana je visoka seizmička sigurnost unapređenog sistema preko stabilnog histerezisnog odgovora unapređenih veza i preko povoljnih karakteristika seizmičkog odgovora integralnog sistema pri dejstvu simuliranih realnih jakih zemljotresa.

Ključne reči: prefabrikovan sistem, veze, nelinearan odgovor, seizmočka sigurnost

SEISMIC RESPONSE OF PREFABRICATED HALL SYSTEM WITH TESTED UPGRADED CONNECTIONS

Summary:

This paper shows the original results from the conducted nonlinear seismic response analysis of a selected representative industrial hall prototype structure that was transformed, through re-design, into a qualitatively upgraded seismically safe system (USS-system) with implemented upgraded connections. The formulated advanced 3D nonlinear analytical model was applied to demonstrate the high seismic safety of the upgraded system confirmed by the stable hysteretic responses of the upgraded connections and favorable nonlinear response characteristics of the integral structure under simulated real strong earthquakes.

Key words: prefabricated system, connections, nonlinear response, seismic safety

---

[1] *PhD student, Institute of Earthquake Engineering and Engineering Seismology (IZIIS), Ss. Cyril and Methodius University in Skopje, N. Macedonia, labeat.misini@gmail.com*

[2] *Assoc. Prof., Dr., Faculty of Engineering, Department of Civil Engineering, International Balkan University (IBU), Skopje, Republic of N. Macedonia, jelena.ristic@ibu.edu.mk*

[3] *Full Prof. Dr., Institute of Earthquake Engineering and Engineering Seismology (IZIIS), Ss. Cyril and Methodius University in Skopje, Republic of N. Macedonia, viktor@iziis.ukim.edu.mk*

[4] *Full Prof. Dr., Institute of Earthquake Engineering and Engineering Seismology (IZIIS), Ss. Cyril and Methodius University in Skopje, Republic of N. Macedonia, danilo.ristic@gmail.com*

1. PROTOTYPE OF PREFABRICATED STRUCTURE

The selected *common prototype* structure represents a precast frame system formed by installed fourteen (14) three-span frames in transverse direction (span Lt=20.00m), Figure 1, and four (4) frames in longitudinal direction, with 13 spans (span Ll=12.00m), Figure 2. Having 4 columns in transverse direction and 14 columns in longitudinal direction, the hall structure integrates a total of 56 columns supported by 56 individual precast foundations of variable dimensions 400x400cm and 300x300cm, depending on the actual vertical load acting on the column.
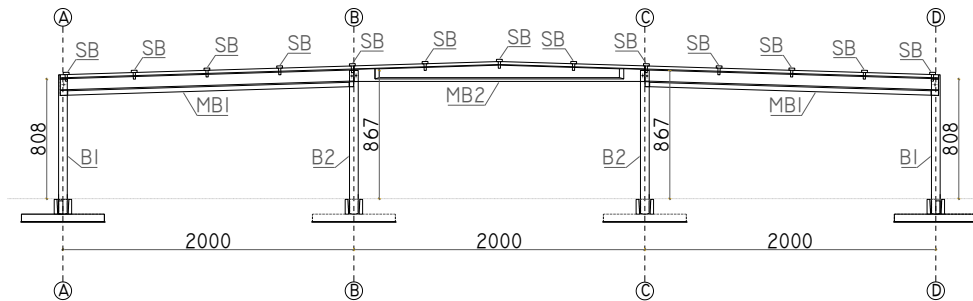
Figure 1 – Transversal cross-section of the industrial hall prototype structure.

In x and y direction, the dimensions of the structure at plan are L_x=13x12.00=156.00m and L_y=3x20.00=60.00m, Figure 1 and Figure 2. The columns are designed with the same cross-sections 60x60cm (cast with concrete C40) and two different types of reinforcement.
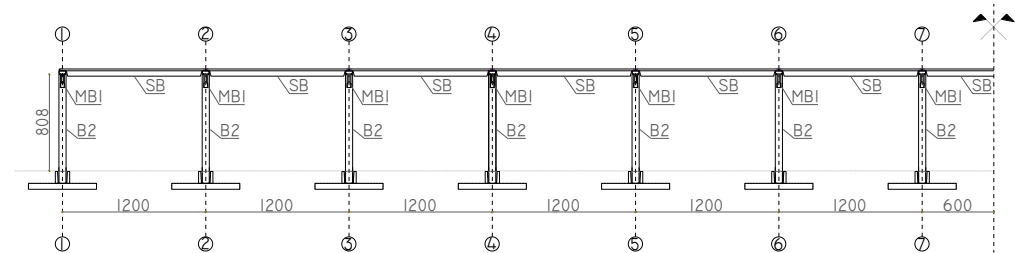
Figure 2 – Longitudinal cross-section of the industrial hall prototype structure.

Column B1, Figure 1 and Figure 2 and column B2 are reinforced with longitudinal bars 12ϕ20mm (ties ϕ8/15cm+ϕ10/15cm) and 12ϕ25mm (ties ϕ8/15cm+ϕ10/15cm), respectively. The height of the central and side columns is H_c=8.67m and H_s=8.08m, respectively. The roof structure is formed of precast roof I-beams with h=140cm and span L=20.17m, and roof beams with h=134.35m and L=20.00m. The other roof members represent secondary elements.

The structure is founded in soil class C, taking into account Eurocode 8 (CEN2004), namely, a design spectrum corresponding to peak ground motion of 0.2 g and behaviour factor of *q=1.5*. The dowel connections are designed in accordance with the capacity design approach used in Eurocode 8 (CEN 2004) and the modifications given by Zoubek et al. 2014.

2. MODELING AND SEISMIC RESPONSE ANALYSIS OF PROROTYPE HALL SYSTEM WITH UPGRADED CONNECTIONS (System: M2-UCON)

2.1. FORMULATED ADVANCED NONLINEAR 3D ANALYTICAL MODEL

The formulation of an advanced nonlinear 3D analytical model is based on structural geometry, material properties and characteristics of prefabricated members and their connections. The selected hall prototype structure consists of prefabricated concrete elements such as columns, main beams and secondary beams, which together form a 3D structure. The main frames are designed at every 12m, forming a total of 13 spans. A main frame consists of three equal spans of 20m each.

Nonlinearmodel of connections
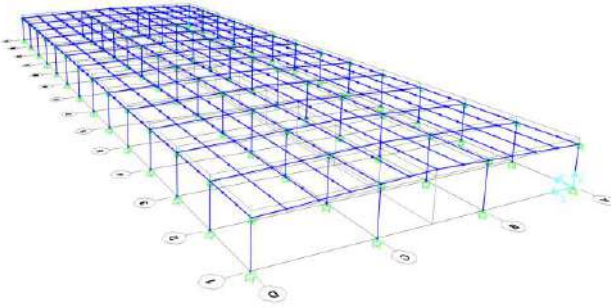
Link-L7 & Link-L-10

Figure 3 – Formulated nonlinear 3D model of prototype structure.
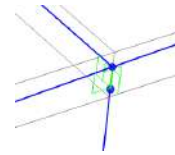
Figure 4 – Link models

All concrete structural prefabricated elements (columns, main beams, and secondary beams) are made of C30/37 concrete. Columns (56 in total, 28 side and 28 inner columns) and main beams (56 in total) as well as secondary beams (169 in total) are connected on the top of the columns with hinge connections. In structure model, columns are considered as fixed to the prefabricated foundation, using fixation point at distance of dh=0.1m of the actual height of the columns.

a) Nonlinear model of "strong" connections: The constructed large-scale (1:2) prototype model of "strong" conventional roof beam-column (CRBC) connection was experimentally tested, Figure 5 (middle), and quite specific capacity "envelope curve" was recorded, Figure 5 (right),
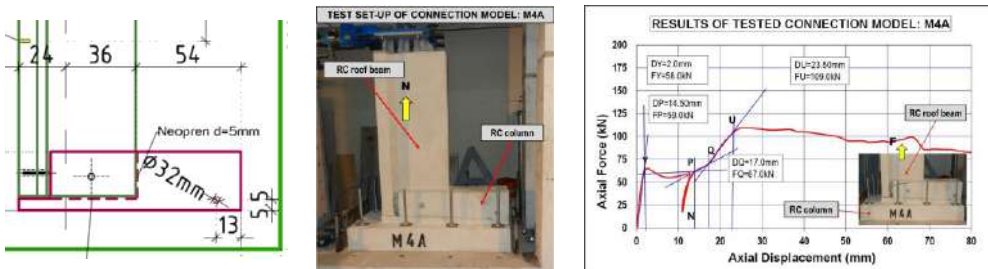

Figure 5 – Experimental test of prototype model M4A representing CRBC-connection

The connection was created by installing two anchored "pin" connectors (dowels) with diameter 16mm, and was improved by other column confining reinforcement, Fig 5 (left). Based

on model similarity rules, original bi-linear CRBC connection model for single roof-beam column connection of prototype structure was defined and used in conducted analytical studies, Figure 16 (right). The nonlinear response of CRBC connection was simulated considering two-node nonlinear link elements with respective parameters in x and y direction, Figure 4.

b) Nonlinear model of "week" connections: The nonlinear bi-linear model parameters of used "week" CRBC connection of prototype structure was intentionally considered to be 50% of the "strong" connection, Figure 16 (left), providing realization of comparative analytical study.

c) Advanced nonlinear modeling of columns: Advanced fiber modeling concept was use for nonlinear behavior modelling of all prefabricated columns, [SAP2000]. All adopted cross-sections of the columns were modeled considering a total of 488 fibers, involving types of confined concrete fibers, unconfined concrete fibers and steel fibers, respectively. Using fiber models, a highly advanced simulation of plastic hinges of columns was provided. Side columns are designed with height $H1=6.5m$, while the height of inner columns is $H2=7.15m$.

Using the realistic nonlinear behaviour characteristics of the implemented structural members and connections, a nonlinear analytical model of the integral full-scale precast prototype industrial hall structure was formulated in SAP2000, Figure 3, Figure 4. The formulated model consisted of 632 effective joints and 56 fixed boundary joints, and was used to study the seismic response performances of the structure under the effect of strong earthquakes.

2.2. DYNAMIC CHARACTERISTICS OF THE M2-UCON SYSTEM

From the analysis of the dynamic characteristics of the initial state of the **M2-UCON system**, the first twelve vibration modes and periods (frequencies) were defined.

Table 1a – Computed dynamic characteristics of the structure (System: M1-WCON)

Mode	Period (sec)	Frequency (cyc/sec)	Mode	Period (sec)	Frequency (cyc/sec)
1	1.276431	0.783434	7	0.582971	1.715351
2	1.211326	0.825541	8	0.577706	1.730983
3	1.167516	0.856519	9	0.574829	1.739648
4	0.592302	1.688328	10	0.565856	1.767234
5	0.587990	1.700709	11	0.565785	1.767455
6	0.586765	1.704260	12	0.563391	1.774964

Table 1b – Computed dynamic characteristics of the structure (model- M2-UCON). (Presented to confirm that the initial dynamic properties are identical)

Mode	Period (sec)	Frequency (cyc/sec)	Mode	Period (sec)	Frequency (cyc/sec)
1	1.276431	0.783434	7	0.582971	1.715351
2	1.211326	0.825541	8	0.577706	1.730983
3	1.167516	0.856519	9	0.574829	1.739648
4	0.592302	1.688328	10	0.565856	1.767234
5	0.587990	1.700709	11	0.565785	1.767455
6	0.586765	1.704260	12	0.563391	1.774964

Detected as dominant were vibration periods of the first three modes with periods: $T_1=1.276431$s, $T_2=1.211326$s and $T_3=1.167516$s, exposed dominantly in x-direction, y-direction and in torsion mode direction, respectively. The next higher modes were with closed period values and mainly expressed the global-local characteristics of the structure, Table 1b. The obtained initial vibration periods and mode shapes for the system with upgraded connections (System M2-UCON) were the same as the obtained initial vibration periods and mode shapes for the analysed system with weak connections (M1-WCON system), Tab. 1b and Tab. 1a, respectively. The results from the analysis were correct because the initial stiffness (only) of both systems was considered the same.

2.3. DISPLACEMENT TIME-HISTORY RESPONSE UNDER EARTHQUAKE ACTION IN DIRECTION-X

The seismic response of the M2-UCON structure was analysed for the case of simulated two selected representative strong earthquake effects acting in x and y direction, separately. The considered seismic ground motions in this study actually represented the El-Centro earthquake record and the Ulcinj-Albatros earthquake record, and both were scaled to the very high intensity represented by peak ground acceleration PGA=0.50g. The seismic response of the structure resulted in computed time-response characteristics of all related physical parameters. The most important results are processed and presented in the subsequent sections.
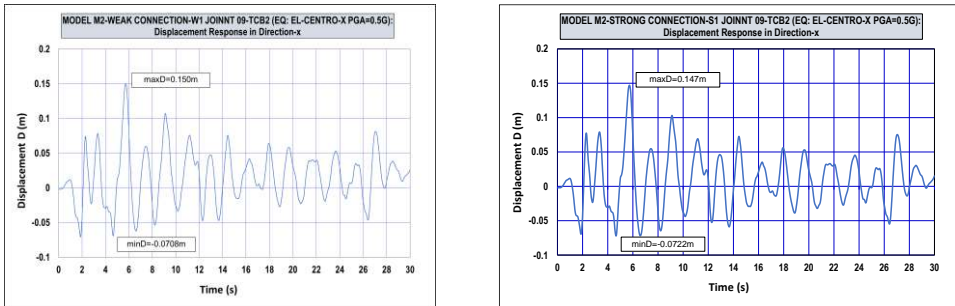

Figure 6 – Compared seismic responses of the system with weak (l) and strong connections (r): Displacement history of J-09; EQ: El-Centro-x (PGA=0.50G).
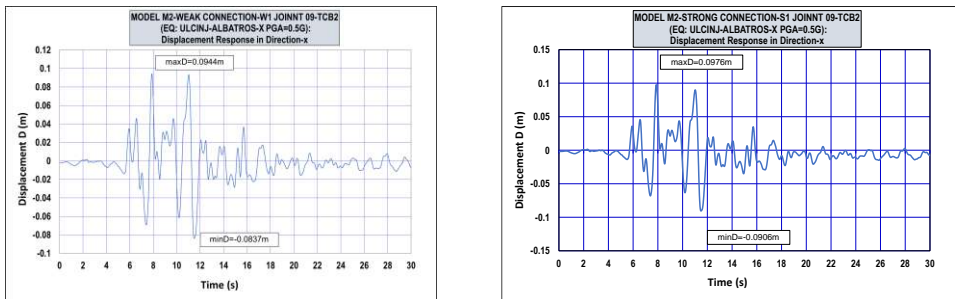

Figure 7 – Compared seismic responses of the system with weak (l) and strong connections (r): Displacement history of J-09; EQ: Ulcinj-Albatros-x (PGA=0.50G).

The computed displacement time-history responses of the M1-WCON system and the M2-UCON system under the action of two earthquakes in direction-x with PGA=0.50g are comparatively shown in two representative figures. Figure 6 comparatively shows the computed displacement responses of node J-09 (top of column) under the simulated El-Centro earthquake, while Figure 7 comparatively presents the computed displacement response of the same node J-09 (top of column) in the case of the simulated Ulcinj-Albatros earthquake.

2.4. DISPLACEMENT TIME-HISTORY RESPONSE UNDER EARTHQUAKE ACTION IN DIRECTION-Y

The computed displacement time-history responses of the M1-WCON and M2-UCON systems under the action of two earthquakes in direction-y, with PGA=0.50g, are of similar magnitudes. Such tendency was observed from the computed displacement responses of node J-09 (top of column) under the simulated El-Centro earthquake, and the computed displacement response of the same node J-09 (top of column) in the case of the simulated Ulcinj-Albatros earthquake.

2.5. VELOCITY TIME-HISTORY RESPONSE UNDER EARTHQUAKE ACTION IN DIRECTION-X

The computed velocity time-history responses of the M1-WCON and M2-UCON systems under the action of two earthquakes in direction-x, with PGA=0.50g, are comparatively shown in two representative figures. Figure 8 comparatively shows the computed velocity responses of node J-09 (top of column) under the simulated El-Centro earthquake, while Figure 9 comparatively displays the computed velocity response of the same node J-09 (top of column) in the case of the simulated Ulcinj-Albatros earthquake.
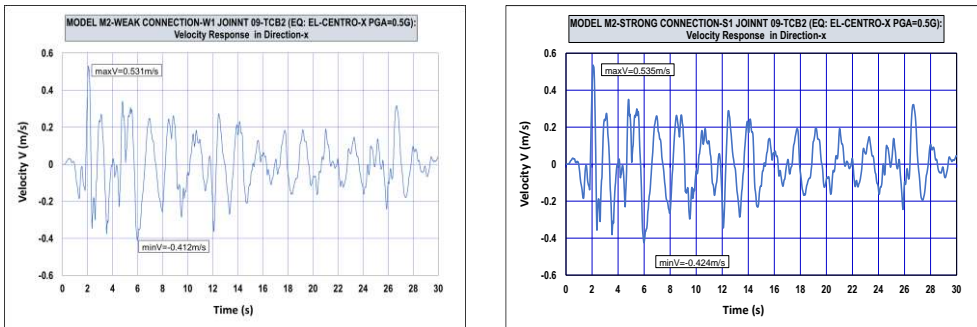

Figure 8 – Compared seismic responses of the system with weak (l) and strong connections (r): Velocity history of J-09; EQ: El-Centro-x (PGA=0.50G).

2.6. ACCELERATION TIME-HISTORY RESPONSE UNDER EARTHQUAKE ACTION IN DIRECTION-X

The computed acceleration time-history responses of the M1-WCON and M2-UCON systems under the action of two earthquakes in direction-x, with PGA=0.50g, are comparatively shown in two representative figures. Figure 10 comparatively shows the computed acceleration responses of node J-09 (top of column) under the simulated El-Centro earthquake, while Figure

11 comparatively presents the computed acceleration responses of the same node J-09 (top of column) in the case of the simulated Ulcinj-Albatros earthquake.
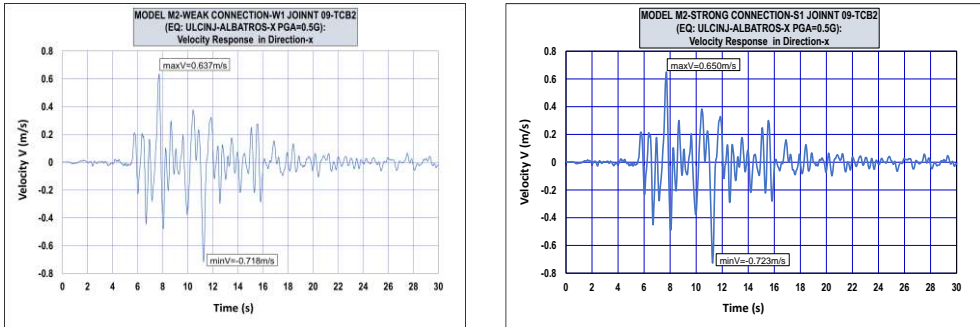

Figure 9 – Compared seismic responses of the system with weak (l) and strong connections (r): Velocity history of J-09; EQ: Ulcinj-Albatros-x (PGA=0.50G).
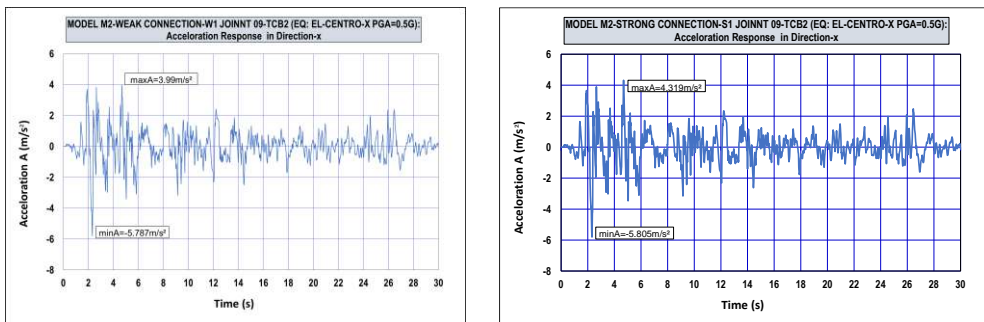

Figure 10 – Compared seismic responses of the system with weak (l) and strong connections (r): Acceleration history of J-09; EQ: El-Centro-x (PGA=0.50G)
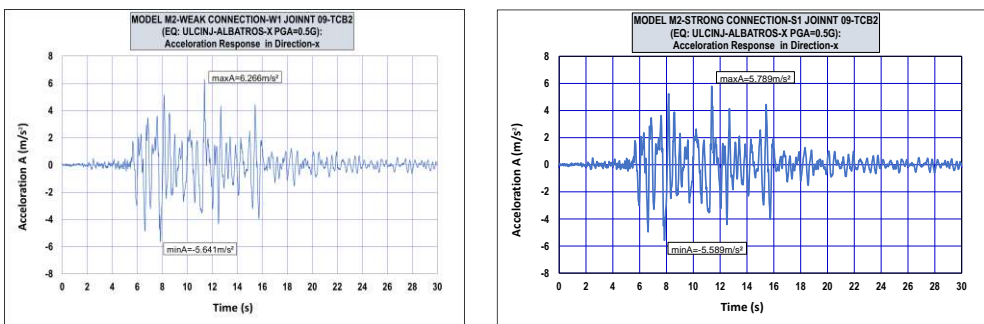

Figure 11 – Compared seismic responses of the system with weak (l) and strong connections (r): Acceleration history of J-09; EQ: Ulcinj-Albatros-x (PGA=0.50G).

3. NONLINEAR HYSTERETIC RESPONSE OF CRITICAL CONNECTIONS

From the computed time-history seismic response of the integral structure for the case of the simulated two representative strong earthquake effects acting in x and y direction, separately, scaled to PGA=0.50g, the two main critical connections were identified at Axis 2-A and 2-B: (1) Fixed section of columns showing hysteretic response and (2) Connections created to connect the main beams and columns exposed to critical nonlinear response. Some selected representative results are shown in the subsequent sections.

3.1. HYSTERETIC RESPONSE OF COLUMNS UNDER EARTHQUAKE ACTION IN DIRECTION-X

A representative figure shows comparatively the computed characteristic hysteretic responses of the M1-WCON system and the M2-UCON system. The hysteretic responses are comparatively presented by an initially computed envelope (capacity) curve, showing actually the relation between the base shear force and the displacement at the top of the column B1, under the action of the first earthquake (El-Centro) in direction-x, with PGA=0.50g. Figure 12 shows comparatively the computed hysteretic responses of column B1 under the simulated El-Centro earthquake. Similar results were observed when the hysteretic response of column B1 and column B2 was computed in the case of the simulated Ulcinj-Albatros earthquake.
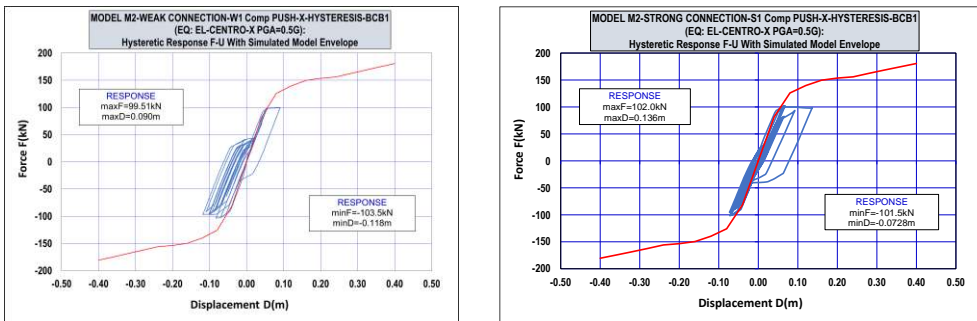

Figure 12 – Compared seismic responses of the system with weak (l) and strong connections (r): Hysteretic response with simulated model envelope of column B1; EQ: El-Centro-x (PGA=0.50G).

3.2. HYSTERETIC RESPONSE OF COLUMNS UNDER EARTHQUAKE ACTION IN DIRECTION-Y

Four representative figures show comparatively the computed characteristic hysteretic responses of the M1-WCON system and the M2-UCON system. The hysteretic responses are comparatively presented by an initially computed envelope (capacity) curve, showing actually the relation between the base shear force and the displacement at the top of the columns, column B1 and column B2, under the action of two earthquakes in direction-y, with PGA=0.50g. Observed also from the four representative figures are the computed hysteretic responses of column B1 and column B2 under the simulated El-Centro earthquake and the computed hysteretic response of column B1 and column B2 in the case of the simulated Ulcinj-Albatros earthquake.

3.3. HYSTERETIC RESPONSE OF CONNECTIONS UNDER EARTHQUAKE ACTION IN DIRECTION-X

For an earthquake action in direction-x, the four representative figures show comparatively the computed characteristic hysteretic responses of the connections resulting from the M1-WCON system and the M2-UCON system. The hysteretic responses of connection L7 and connection L10 are comparatively shown by initially computed capacity envelope curves. Figure 13 and Figure 14 show the computed hysteretic responses of connections L7 and L10 under the simulated El-Centro earthquake, while Figure 15 and Figure 16 display the computed hysteretic response of connection L7 and L10 in the case of the simulated Ulcinj-Albatros earthquake.
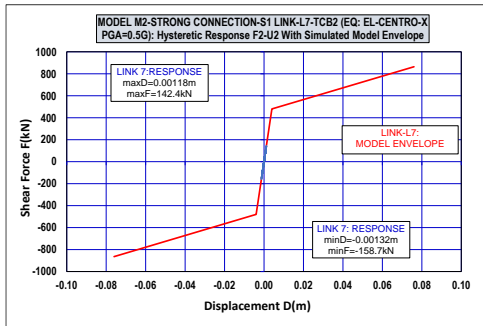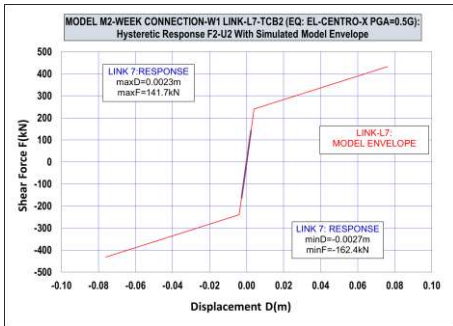

Figure 13 – Compared seismic responses of the system with weak (left) and strong connections (right): Hysteretic response of link-L7; EQ: El-Centro-x (PGA=0.50G).
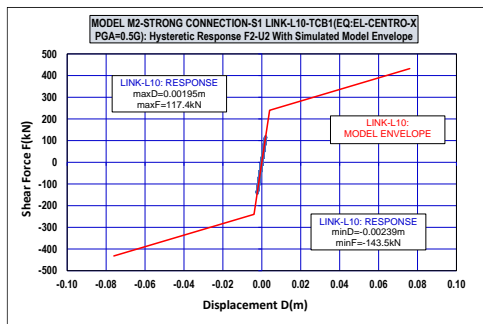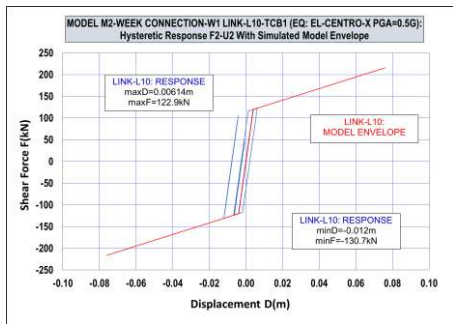

Figure 14 – Compared seismic responses of the system with weak (left) and strong connections (right): Hysteretic response of link-L10; EQ: El-Centro-x (PGA=0.50G).

3.4. HYSTERETIC RESPONSE OF CONNECTIONS UNDER EARTHQUAKE ACTION IN DIRECTION-Y

For an earthquake action in direction-y, characteristic hysteretic responses of connections (including capacity envelope curves) resulting from analysis of the M1-WCON system and the M2-UCON system were comparatively computed and analyzed. The computed hysteretic responses of connections L7 and L10 under the simulated El-Centro earthquake and the computed hysteretic responses of connection L7 and L10 in the case of the simulated Ulcinj-Albatros earthquake showed similar comparative relations.
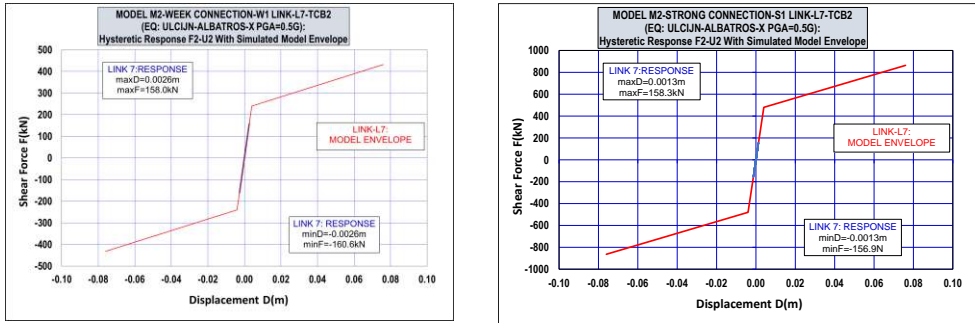
Figure 15 – Compared seismic responses of the system with week (left) and strong connections (right): Hysteretic response of link-L7; EQ: Ulcinj-Albatros-x (PGA=0.50G).
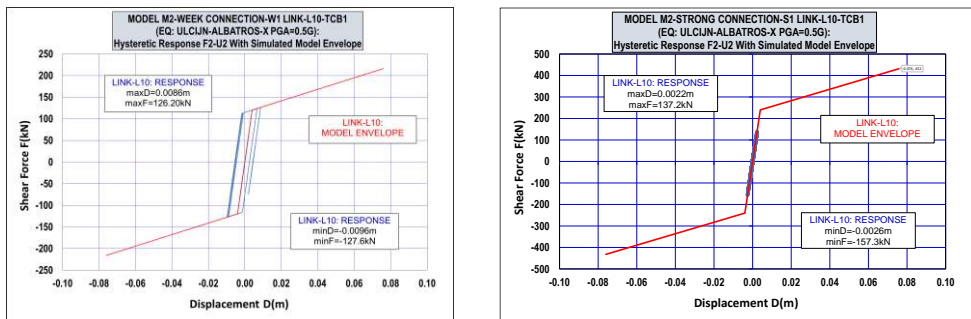

Figure 16 – Compared seismic responses of the system with weak (left) and strong connections (right): Hysteretic response of link-L10; EQ: Ulcinj-Albatros-x (PGA=0.50G).

5. CONCLUSIONS

From the presented extensive analytical research conducted by consideration of different behavior characteristics and strength-deformation capacity of weak and strong connections, (having the integral experimental results from tested various types of connections needed for development of a novel, seismically resistant prefabricated system), the following conclusions are summarized:

(1) Based on the full set of obtained and presented original analytical research results and provided evidence of sound, global nonlinear response of the analyzed upgraded prototype structure, it was confirmed that the analyzed system with upgraded connections (System M2-UCON) showed a high level of seismic safety under strong earthquakes. This is clear because the maximum response force of the connection under critical earthquakes will be always smaller than the related actual bearing capacity of strong connections at yielding point;

(2) With the comparatively presented corresponding set of analytical results and provided evidence of global nonlinear response of the structure with weak connections, it is shown that the system with "weak" connections or with RBC connections having reduced bearing capacity, (System M1-WCON) is exposed to possible total failure under strong earthquakes. This is clear because the response force of the connection under critical earthquakes can become larger than the related actual bearing capacity of weak connections at yielding point;

(3) The obtained initial vibration periods and mode shapes for the system with upgraded connections (System M2-UCON) are the same as the obtained initial vibration periods and mode shapes for the system with weak connections (System M1-WCON) due to existence of hinged connections in both cases, Table 1a and Table 1b;

(4) The conducted and completed experimental research (not comprehensively discussed here) contributed essentially to derive modeling parameters for the upgraded connections. Their stable and favorable behavior properties are clearly proved. The introduced new upgraded connections will open a wide possibility for their future successful application for the purpose of increasing the safety level of structures in regions of the highest seismicity;

(5) The performed supplemented experimental tests and analytical research confirmed that standard footing-column connection possessed the required safety for seismic loads and could be used in practice. However, correct design is needed in order to assure application of columns with optimal cross-sections and reinforcement (ductile column and designed stronger footing).

REFERENCES

[1]   Arslan MH, Korkmaz HH, Gulay DG (2006) Damage and Failure Pattern of Prefabricated Structures after Major Earthquakes in Turkey and Shortfalls of the Turkish Earthquake Code. Eng Fail Anal 13(4):537–557

[2]   ATC-08 (1981) Proceedings of a workshop on design of prefabricated concrete buildings for earthquake loads. ATC, NSF, Redwood City, California, USA

[3]   Apostolska R, Necevska-Cvetanovska G & Bojadziev J, Fischinger M, Isakovic T& Kramar M (2012) Analytical Investigations of Beam-Column Connections in Precast Buildings under Seismic Loads, 15 WCEE Lisbon 2012

[4]   Bournas A, Negro P, Taucer FT (2013a) Performance of Industrial Buildings during the Emilia Earthquakes in Nort Italy and Recommendations for their Strengthening. Bull Earthq Eng, published on-line, June 2013

[5]   Bournas A, Negro P, Molina FJ (2013b) Pseudodynamic Tests on a Full-scale 3-Storey Precast Concrete Building: Behavior of the Mechanical Connections and Floor Diaphragms. Eng Struct 57:609–627

[6]   CEN (2004) Eurocode 8: Design of Structures for Earthquake Resistance-Part 1: General Rules, Seismic Actions and Rules for Buildings, EN 1998–1. European Committee for Standardization, Brussels

[7]   EERI (1979) Friuli, Italy Earthquakes of 1976. Earthquake Engineering Research Institute, Oakland, California, USA

[8]   EERI (2000) Kocaeli, Turkey, Earthquake of August 17, 1999. Earthq Spectra Supplement, Oakland, California, USA

[9]   Engström B (1990) Combined Effects of Dowel Action and Friction in Bolted Connections. Nordic Concrete Research, The Nordic Concrete Federation, Publication no. 9, Oslo 1990, pp 14–33

[10]   Fajfar P, Banovec J, Saje F (1978) Behaviour of Prefabricated Industrial Building in Breginj during the Friuli Earthquake. In: 6th ECEE, Dubrovnik, vol 2. pp 493–500

[11] Fajfar P, Duhovnik J, Reflak J, Fischinger M, Breška Z (1981) The Behaviour of Buildings and other Structures during the Earthquakes of 1979 in Montenegro, IKPIR publication 19A, University of Ljubljana, Ljubljana

[12] Fischinger M, Kramar M, Isaković T, Kante P (2007) Seismic Behaviour of Precast Concrete Structures with Respect to EC8, final report on the contribution of the University of Ljublajana,

[13] Fischinger M, Zoubek B, Isaković T (2014): Seismic Response of Precast Industrial Buildings, Editors Ansal A Perspectives on European Earthquake Engineering and Seismology, Volume 1, pp 131-177

[14] Isaković T, Zoubek B, Lopatoč J, Urbas M, Fischinger M (2013) Report and Card Files on the Tests Performed on Existing Connections. Deliverable 1.2, SAFECLADDING, University of Ljubljana, Ljubljana

[15] Kramar M (2008) Seismic Vulnerability of the Precast Reinforced Concrete Structures. Ph.D. thesis (in Slovenian) University of Ljubljana, Ljubljana

[16] Kramar M, Isaković T, Fischinger M (2010a) Seismic Collapse Risk of Precast Industrial Buildings with Strong Connections. Earthq Eng Struct Dyn 39(8):847–868, http://onlinelibrary.wiley. com/doi/10.1002/eqe.970/pdf

[17] Ristic J., Pavlov S., Pavlov P., Misini L., Ristic D.: Laboratory Testing of Constructed Prototype Models of Typical Connections Used in Prefabricated RC Construction System of Industrial Halls Implemented by PUT Inzenering, Serbia: Experimental Laboratory Testing of Prototype Model-M1 Representing Connection Between Prefabricated Column and Prefabricated Footing, RESIN Lab. of Industrial Sciences and Technology, Report: RESIN-011-2017.

[18] Tzenov L, Sotirov L, Boncheva P (1978) Study of Some Damaged Industrial Buildings due to Vrancea Earthquake. In: 6th ECEE Dubrovnik, vol 6. pp 59–65

[19] UNDP/UNIDO (1985) Building Construction under Seismic Conditions in the Balkan Region. UNDP/UNIDO Project RER/79/015, vol 2: Design and Construction of Prefabricated Reinforced Concrete Building Systems, Vienna Austria; Skopje Macedonia

[20] Zoubek B, Fischinger M, Isakovic´ T (2014a) Estimation of the Cyclic Capacity of Beam-to-Column Dowel Connections in Precast Industrial Buildings. Bulletin of Earthquake Engineering, Springer, Netherlands. *DOI 10.1007/s10518-014-9711-0.*

[21] Zoubek B, Fischinger M, Isaković T (2014b) Seismic Response of Dowel Connections in Precast Industrial Buildings, Second European Conference on Earthquake Engineering and Seismology, Istanbul, 25–29 August 2014

[22] Wilson E.L., Habibullah A.: SAP2000, Structural and Earthquake Engineering Software, Computers and Structures Inc., Berkeley, California, USA.

Marko Marinković[1], *Svetlana Brzev*[2], *Nemanja Krtinić*[3], *Željko Žugić*[4]

PONAŠANJE ŠKOLSKIH OBJEKATA U SKORAŠNJIM ZEMLJOTRESIMA: LEKCIJE ZA SRBIJU

Rezime:

Bezbednost škola pri dejstvu zemljotresa treba da bude jedan od najviših prioriteta svakog društva. Osim što je važno da se školski objekti projektuju i izvedu tako da se ne oštete i ne sruše, treba omogućiti da budu funkcionalni i bezbedni kako bi služili kao mesto za evakuaciju nakon zemljotresa. Stoga je cilj ovog rada da se podigne svest o važnosti izučavanja i procene seizmičkog rizika postojećih škola, kao i da se naglasi potreba za adekvatnom pažnjom pri projektovanju novih školskih zgrada. Primeri oštećenja školskih zgrada u nedavnim zemljotresima u regionu su predstavljeni, jer su relevantni za Srbiju. Zapažanja iz pregleda školskih zgrada u Srbiji korišćena su za poređenje sa reprezentativnim slučajevima oštećenih školskih objekata u Hrvatskoj i Albaniji, na osnovu čega su izvedeni zaključci šta se može očekivati u Srbiji u slučaju zemljotresa umerene jačine.

Ključne reči: školske ustanove, zemljotres, ponašanje pri zemljotresu, oštećenja, seizmički rizik

SEISMIC PERFORMANCE OF SCHOOL BUILDINGS IN RECENT EARTHQUAKES: LESSONS FOR SERBIA

Summary:

Seismic safety of schools should be one of the highest priorities for each community. Besides being important to design the school buildings such as to avoid damage or collapse in earthquakes, they should also remain safe and functional as a shelter for evacuation after an earthquake. The aim of this paper is to raise awareness of the importance to study and assess the seismic risk of existing schools, as well as to emphasize a need for adequate seismic design of new school buildings. Examples of damage in school buildings due to recent earthquakes in the region were presented since they are relevant for Serbia. Observations from the survey of school buildings in Serbia have been used for a comparison with the representative examples of damaged school buildings in Croatia and Albania, thus deriving the conclusions of what could be expected in Serbia in a case of moderate earthquake.

Key words: educational facilities, earthquake, seismic performance, damage, seismic risk

[1] *Ass. Prof, Faculty of Civil Engineering, University of Belgrade, Serbia, mmarinkovic@grf.bg.ac.rs*
[2] *Adjunct.Prof, University of British Columbia, Vancouver, Canada, svetlana.brzev@gmail.com*
[3] *PhD student,Faculty of Civil and Geodetic Engineering, University of Ljubljana, Slovenia, nkrtinic@fgg.uni-lj.si*
[4] *Project Coordinator, Goverment of Serbia, Public Investment Managment Office,Serbia, zeljko.zugic@obnova.gov.rs*

1. INTRODUCTION

Seismic safety of educational facilities, especially schools and kindergartens, is of utmost importance because children are among the most vulnerable sections of each community. Several international initiatives related to school safety have been launched, such as the "Comprehensive school safety" framework, with an objective to protect school children and teachers from injuries and fatalities in schools, and to ensure educational continuity. The framework was adopted by the United Nations agencies and international non-governmental organizations [1]. It rests on three pillars: 1) Safe Learning Facilities, 2) School Disaster Management, and 3) Risk Reduction and Resilience Education. In 2014 the World Bank has launched the Global Program for Safer Schools [2], which aims to improve the safety and resilience of school infrastructure at risk from natural hazards and enhance the quality of learning environments for children.

A motivation for these initiatives is significant vulnerability of school buildings in past earthquakes. In Nepal, the April 25, 2015 Gorkha earthquake (M 7.6) and the May 12, 2015 Central Nepal earthquake (M6.8) caused collapse of more than 27,000 classrooms and damage of additional 26,000 classrooms [3]. The September 2017 Mexico earthquakes (M8.2 Tehuantepec and M7.1 Puebla) caused widespread damage to the schools in the affected areas. It was estimated that more than 19,000 schools, accounting to approximately 27.6% of the total school inventory in the affected areas, experienced damage or collapse in these earthquakes [4]. A comprehensive initiative focused on seismic assessment and retrofitting of school buildings was launched in Mexico after these earthquakes [5].

In many cases, school buildings are older buildings and were not designed according to the latest seismic design codes and are prone to damage even in moderate earthquakes. Recent earthquakes in the Balkan region, including the November 26, 2019 Albania earthquake and the December 29, 2020 Petrinja, Croatia earthquake caused significant damage of educational buildings. Serbian Association for Earthquake Engineering (SUZI-SAEE) organized visits of the teams of experts to the affected areas after these earthquakes. This paper presents findings of reconnaissance studies from Albania and Croatia which are focused on the performance of school buildings, as well as results of a survey of school buildings in Serbia and proposed classification of school building typologies.

2. THE NOVEMBER 26, 2019 ALBANIA EARTHQUAKE

An Mw 6.4 earthquake occurred on Tuesday, November 26, 2019, with the epicentre at 16 km north of Durrës, and 33 km northwest of Tirana, the largest city and capital of Albania. It caused 51 fatalities, while 913 people were injured. More than 95,000 housing units in 11 affected municipalities were damaged (corresponding to 18% of all housing units in those municipalities), and the total economic loss was estimated at 985.1 million EUR [6]. Fortunately, the earthquake occurred in the early morning hours (at 3:54 local time), hence educational buildings were not occupied.

Based on a briefing by the Minister of Education of Albania, two months after the earthquake 56 primary and secondary school buildings were severely damaged and were assigned damage state (DS) 4 and 5 on the scale of 1 to 5, where DS5 denotes collapse), thus rendering them unsafe for use [1]. According to the same source, 66 school buildings

experienced moderate damage and were assigned DS2 and DS3, whereas additional 151 buildings experienced light damage (DS1). Several reports documented the performance of buildings after this earthquake [6]-[12]. The following text presents observations related to damage of selected school buildings due to this earthquake.

A two-storey unreinforced masonry (URM) school in the Thumanë village (Figure 1) was severely damaged (note that in the same village two low-rise URM apartment buildings collapsed). The school was built in the 1970s and it was recently refurbished. Building damage at the exterior was not visible, however a heavy damage was observed in the interior, with diagonal cracks and failure of loadbearing URM walls and masonry piers in walls with opening. The building was determined to be unsafe and had to be demolished. Several other URM school buildings experienced damage at the slab-wall connections, indicating risk of potential out-of-plane wall collapse. Other damage patterns, such as light cracking of masonry walls and plaster, damage of parapets and other non-structural elements, were also widespread in schools in Albania.
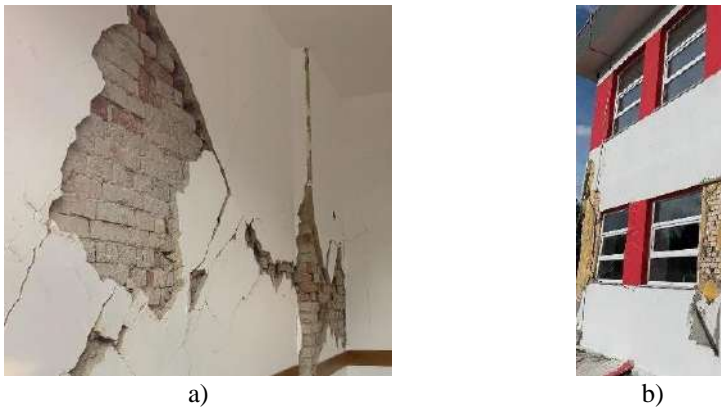

a)   b)

Figure 1 – Damage of a school building in Thumanë, Albania: a) failure of the loadbearing URM wall and b) damaged masonry piers [6]

a)   b)

Figure 2 – Damage of a school building in Maminas, Albania: a) failure of the RC column and b) damaged masonry infill walls [6]

Damage of reinforced concrete (RC) school buildings was similar as damage observed in residential buildings of the same typology. These buildings experienced mostly non-structural damage to masonry infills and partition walls. For example, excessive lateral deformations occurred at the ground floor level in the school building in Maminas, causing extensive damage of exterior RC columns (Figure 2a). These columns were subjected to a high displacement demand, but the detailing was inadequate: the ties had 90 degree hooks and failed to provide required confinement. Furthermore, infill-frame interaction contributed to higher seismic demand in the columns as well as infill walls and caused failure and heavy non-structural damage in these elements (Figure 2b). Another school, Neim Babameto in Durrës, had a RC moment frame system consisting of columns and beams with a "strong beam-weak column" configuration, which was one of the causes of severe structural damage as well as infill failures.

3.   THE DECEMBER 29, 2020 PETRINJA EARTHQUAKE

On December 29, 2020 a magnitude M_w 6.4 earthquake occurred in the Sisak-Moslavina county of Croatia, with the epicentre located 3 km west-southwest of the city Petrinja. The earthquake caused 7 deaths while other 26 people were injured [13]. The physical damage was estimated at approximately 4.8 billion EUR [14]. The earthquake occurred in the early afternoon, but the schools were not in session due to the COVID-19 restrictions.

Out of 53 schools in the Sisak-Moslavina County, 5 required complete reconstruction, 9 schools were significantly damaged, while 13 schools experienced non-structural damage and needed minor repairs. As a result, more than 5,000 students had to be relocated to other schools. Performance of buildings in this earthquake is presented elsewhere [13], [15]-[17], whereas this section presents observations related to the damage of selected school buildings.

a)   b)

Figure 3 – Damage of URM schools in Petrinja, Croatia: a) exterior damage of the First school building and b) inclined shear cracks in the walls of the Petrinja High School

Structural system of the First Primary School in Petrinja, which was built at the beginning of 20th century, consisted of URM walls and jack arch floor slabs (known as *Pruski svod* in Serbian). The building had a timber roof with clay tile roofing, which partially collapsed (Figure 3a). The building also experienced significant non-structural damage, especially in the interior partition walls between the classrooms which were severely damaged due to

inadequate slab-wall connection. Another school in Petrinja, Petrinja High School, was a massive URM building constructed in 1860, and experienced extensive damage in the form of inclined shear cracks in the loadbearing walls (Figure 3b). It could be observed that cracking in exterior walls above the windows was less pronounced, but the reported interior damage was so severe that the building was classified as unsafe for entry.

Majority of RC school buildings in Petrinja experienced minor structural damage, however non-structural damage was severe. Elementary school Dragutin Tadijanović, built in 1974, is a masonry-infilled RC moment frame structure with an irregular plan shape. The building did not experience structural damage, but several infill walls experienced long cracks along the infill-frame interface (Figure 4a). Another educational building, Faculty of Education, was built in 1962 as an RC frame building with masonry infills. The infill walls were severely damaged due to in-plane seismic effects, with diagonal cracks in the walls (Figure 4b) and along the infill-frame connection. Out-of-plane displacements were observed in several infill walls. Furthermore, a ceiling collapsed in one of the classrooms.

a)   b)

Figure 4 – Damage of RC schools in Petrinja, Croatia: a) cracks at the infill-frame interface, school Dragutin Tadijanović and b) damage of infill walls and plaster spalling, the Faculty of Education
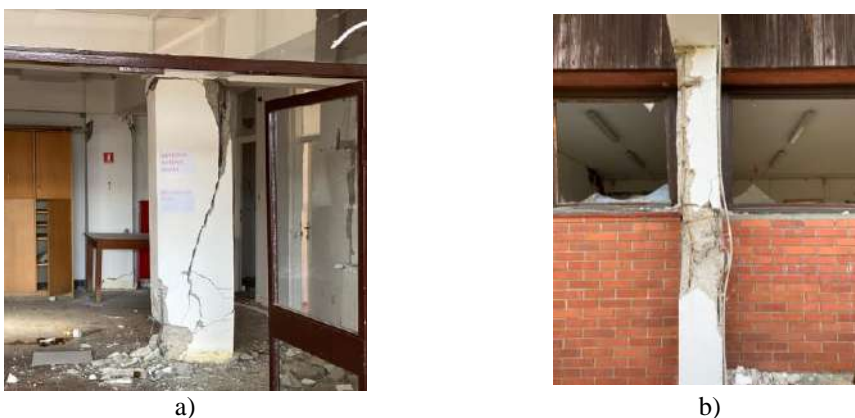

a)   b)

Figure 5 – Damage in the former elementary school in Donja Bačuga: a) shear failure of an interior column and b) a "short column" failure of an exterior column

Former elementary school in Donja Bačuga is currently the Centre for Plum and Chestnut, an educational institution for agriculture, has an RC moment frame system with masonry infill walls, and experienced severe structural damage in the earthquake. Interior columns had 55x30cm cross-sectional dimensions (longer dimension was aligned in transverse direction) and experienced shear failure, as shown in Figure 5a. The building survey showed that ties were provided at 20 cm spacing in interior columns and at 30 cm for exterior columns. Excessively large tie spacing and interaction between partial-height infill and the frame in exterior columns caused a "short column" effect (Figure 5b). Almost all infill walls in the building experienced severe cracking in the walls and horizontal cracks at the infill-to-top beam interface.

4. SURVEY OF SCHOOL BUILDINGS IN SERBIA: PRELIMINARY RESULTS

The territory of the Republic of Serbia is located in a seismically active area characterized by moderate seismicity. More than 10 earthquakes with magnitude of 5.0 or higher occurred in the 20th century. The strongest earthquake in the 21st century hit Kraljevo in November 2010 (M 5.4), causing 2 fatalities and significant damage and material losses. At least 12 school buildings in Kraljevo experienced damage and had to be repaired after the earthquake [18], which indicated vulnerability of school buildings in Serbia due to even moderate earthquakes.

This section presents preliminary results of a detailed study on 212 elementary and secondary schools in Serbia which are located in seismic zone VIII according to the national seismic hazard map. This study was part of the Serbia National Disaster Risk Management Program: Scaling Up Resilient Infrastructure Project, funded by World Bank, implemented by Public Investment Management Office Government of Republic of Serbia. It included a field survey and the assessment of building condition, and the results were presented in the form of detailed reports. A database containing relevant information for each school was created, and selected results are presented here.

Although the scope of the project included 212 schools, additional buildings were constructed in some schools due to a need to increase school capacity (number of students) over time. As a result, the database includes information on 366 buildings, including the original school buildings, additional (new) school buildings, and gymnasiums.
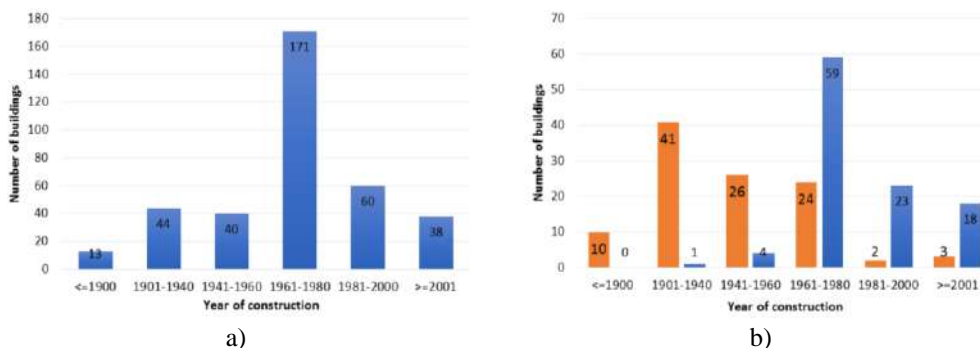

Figure 6 – Year of construction: a) all surveyed school buildings and b) RC (blue) and URM (orange) buildings

One of the most relevant indicators of level of seismic safety is the year of construction, which is shown in Figure 6a. It can be seen that approximately 50% of all school buildings were built in the period 1961-1980, when the 1964 Yugoslav seismic design code was in place.

One of the most important criteria is the type of structure, i.e., material of loadbearing (vertical) system, which is the same as the material of Lateral Load Resisting System (LLRS). Vertical system was classified into RC, URM, confined masonry, wood, steel, prefabricated, and combined (e.g. URM and RC, masonry and wood). Horizontal structure has been classified into vaults, flexible floors (e.g. wooden floors), semi-rigid floors (e.g. steel beams), rigid floors (RC slabs), and others. Figure 7 illustrates types of vertical and horizontal structures for the surveyed buildings. It can be observed that most schools (211 out of 366 buildings) have either masonry or RC vertical loadbearing structure. In terms of the horizontal structure, majority of schools (approximately 60%) have rigid floors. Figure 6b shows that most URM school buildings were constructed in the first half of 20th century, whereas majority of RC school buildings were constructed in the second half of the 20th century, mostly from 1961 to 1980.
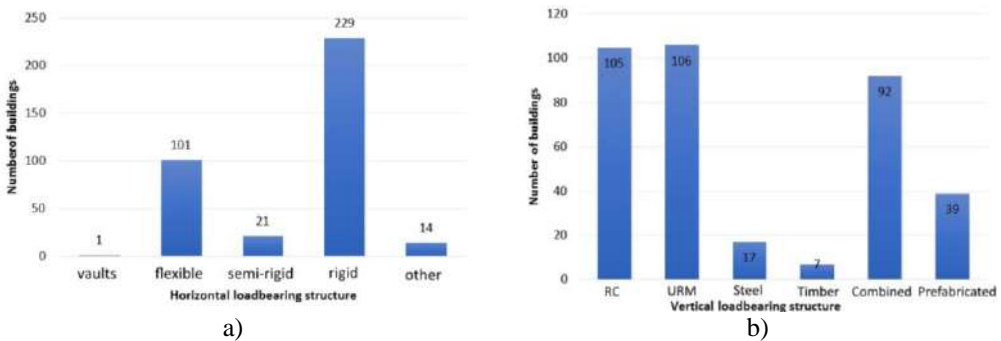

Figure 7 – Loadbearing structure: a) horizontal and b) vertical

Figure 8 – URM schools in Serbia: a) Primary School Milisav Nikolić in Malo Crniće and b) High School in Valjevo

If we take a look at the building type and year of construction of schools damaged in earthquakes in Albania and Petrinja (Croatia), it can be seen that exactly the most dominant structural types and year of construction of schools in Serbia match to them. Most of the schools are RC frame buildings and URM. Significant number of surveyed URM school buildings in Serbia is the same as the two-storey URM school in Thumanë (Figure 1) that was severely damaged. Most URM school buildings are built at the beginning of the 20th century

(Figure 6b), as it was the case with the highly damaged First Primary School in Petrinja (Figure 3a). One example is Primary School Milisav Nikolić in Malo Crniće (Figure 8a), built at the same time and in the same structural type (URM walls and jack arch floor slabs, known as *Pruski svod* in Serbian). Petrinja earthquake also showed what could be expected with the massive URM building of High School in Valjevo (Figure 8b) and similar, since it was built at the same time and with an identical structural type as Petrinja High School (Figure 3b).

The results of the survey showed that the most common structural type of schools in Serbia is RC frame (Figure 6b and 7b). Frames are always filled with masonry infill walls. Furthermore, the biggest number of the RC framed schools is built between 1960 and 1970. In exactly the same period as damaged school buildings in Petrinja, (Figure 4 and 5). Since at that period Serbia and Croatia were part of the same country (Yugoslavia), it is for sure that the same materials and construction practice were used in building these schools both in Serbia and Petrinja. Therefore, the performance of the damaged schools in Petrinja can serve as an example what can be expected in Serbia. Some representative examples of the schools from Serbia matching the damaged ones from Petrinja are Primary School Sveti Sava in Mladenovac (Figure 9a), Primary School Slavko Rodić in Sečanj (Figure 9b) and others.

a)   b)

Figure 9 – Infilled RC frame schools in Serbia: a) Primary School Sveti Sava in Mladenovac and b) Primary School Slavko Rodić in Sečanj

5. PROPOSED CLASSIFICATION OF EDUCATIONAL BUILDINGS IN SERBIA

A classification of school building typologies in Serbia has been proposed by the authors, based on the survey of school buildings in Serbia presented in this paper, and also similarity between school building typologies in Serbia and neighbouring countries which experienced recent earthquakes, especially Croatia [19]. The authors have also reviewed more comprehensive classifications/taxonomies, such as the GEM taxonomy [20], as well as recently developed global taxonomy for school buildings (GLoSI) with 12 attributes [21]. The proposed classification was developed by considering the most important attributes which are believed to influence the seismic performance of schools, such as i) LLRS, e.g. moment frame, wall, dual frame-wall system; ii) material of LLRS (e.g. masonry, RC), and iii) type of floor/roof diaphragm (flexible or rigid). The survey of school buildings in Serbia showed that majority of buildings were constructed using masonry and RC, hence the proposed classification is focused on these materials, while steel and wood can be classified as "Other" systems. The classification is intended to be simple and easy for application in field surveys. It is important

to note that other relevant attributes, such as building height and year of construction, also need to be considered in the classification.

Table 1 – Classification of school buildings in Serbia

Material of construction	Typology ID	Description
Masonry	M1	Earthen buildings (rammed earth or adobe)
	M2	Unreinforced masonry buildings with flexible floors
	M3	Unreinforced masonry buildings with rigid floors
	M4	Confined masonry buildings
Reinforced concrete	RC1	RC frames (cast in-situ) with masonry infills
	RC2	RC structural walls (cast in-situ) or dual RC frame-wall system
	RC3	Prefabricated (precast) RC buildings
Other	O	Steel or wood structures

6. SUMMARY

The aim of this paper was to raise awareness of the seismic vulnerability of school buildings in Serbia, through examples of damage caused by recent earthquakes in the region. Damage of school buildings due to recent earthquakes in Albania and Croatia can be attributed to design flaws and interventions (building extensions, removal of structural walls etc.) which did not consider seismic safety. The damage of infills and partitions may cause a need for repair/reconstruction, thereby reducing building functionality, interrupting the business etc.

Observations from the survey of school buildings in Serbia showed that majority of school buildings are similar to the ones damaged during the earthquakes in Croatia and Albania. The most dominant structural types, construction practices, and year of construction are very similar for schools in Serbia and Croatia, hence earthquake damage patterns in Croatian schools are very useful to predict damage in school in Serbia due to future earthquakes.

REFERENCES

[1] UNDRR (2014). Comprehensive School Safety. United Nations Office for Disaster Risk Reduction and the Global Alliance for Disaster Risk Reduction and Resilience in the Education Sector.

[2] GFDRR (2014). Global Program for Safer Schools. Global Facility for Disaster Reduction and Recovery, World Bank (https://gpss.worldbank.org/)

[3] UNAM (2018). Advisory services to support the recovery of school infrastructure in Mexico affected by the September 2017 earthquakes - Executive Summary. Instituto de ingenieria, UNAM, Mexico (in English) (https://www.resilienciasismica.unam.mx/normas_guias.html)

[4] Alcocer, S. et al. (2021). Rehabilitación sísmica de la infraestructura física educativa de México. Guía técnica. INIFED and BANOPBRAS, Mexico, 283 p. (in Spanish)

[5] Petrašković, Z. and Petrašković, Ž. (2015). Škole i zemljotres Kraljevo (Schools and Kraljevo Earthquake). Copy Studio, Belgrade, 90 p.

[6] Andonov, A. et al. (2022) EERI earthquake reconnaissance team report: M6.4 Albania Earthquake on November 26, 2019.

[7] Marinković, M. et al. (2022) Performance of RC cast-in-place buildings during the November 26, 2019 Albania earthquake. Bulletin of Earthquake Engineering, 1-54.

[8] Freddi, F. et al. (2021) Observations from the 26th November 2019 Albania earthquake: the earthquake engineering field investigation team (EEFIT) mission. Bulletin of Earthquake Engineering, 19(5), 2013-2044.

[9] Verzivolli A, Baballëku M, Luka (2020) Analysis of data collected from damaged building, International Symposium on Durrës Earthquakes and Eurocodes, Polytechnic University of Tirana, Tirana.

[10] Nikolić-Brzev S, et al. (2020) Consequences of the 26.11.2019 Albania earthquake on buildings and infrastructure (in Serbian). Serbian Association for Earthquake Engineering (SUZI-SAEE), Belgrade.

[11] Milićević I, et al. (2021) Performance of RC frames in 26.11.2019. Albania earthquake: effects of irregularities and detailing, Building Materials and Structures, vol. 64, p.p. 207-213.

[12] Lekkas E, et al. (2019) The November 26, 2019 Mw 6.4 Durrës (Albania) earthquake. Newsletter of Environmental, Disaster and Crises Management Strategies, No. 15, ISSN 2653-9454.

[13] Miranda, E., et al. (2021) StEER-EERI: Petrinja, Croatia December 29, 2020, Mw 6.4 Earthquake Joint Reconnaissance Report (JRR).

[14] World Bank (2021) Croatia December 2020 Earthquake, Rapid Damage and Needs Assessment, Government of the Republic of Croatia, The World Bank, USA.

[15] Marinković, M. et al. (2022). Performance of masonry buildings during the November 26, 2019 Albania earthquake (Mw 6.4) and December 29, 2020 Petrinja earthquake (Mw 6.4), 19th MASE Symposium, Ohrid, North Macedonia.

[16] M.Marinković, et al. (2021), Out-of-plane behaviour of loadbearing and non-structural masonry walls during recent earthquakes, 1st Croatian Conference on Earthquake Engineering, Zagreb, Croatia, 22-24 March, 2021.

[17] Markušić, S., et al. (2021). Destructive M6. 2 petrinja earthquake (Croatia) in 2020—Preliminary multidisciplinary research. Remote Sensing, 13(6), 1095.

[18] Green, R., Pandey, B., and Friedman, R. (2015). Safer Schools, Resilient Communities: A Comparative Assessment of School Safety after the 2015 Nepal Earthquake. Risk RED, USA

[19] Hadzima-Nyarko, M. and Kalman Šipoš, T. (2017) Insights from existing earthquake loss assessment research in Croatia. Earthquakes and Structures, 13:4, 365-375.

[20] Silva, V., et al. (2021). A Building Classification System for Multi-hazard Risk Assessment. Int J Disaster Risk Sci (2022) 13:161–177

[21] World Bank (2022). Catalog of Building Types. Global Program for Safe Schools, World Bank, Washington, D.C. (https://gpss.worldbank.org/en/glosi/building-catalogue-types)

Milan Kovarbašić[1], Diego Pizarro Pohl[2], Božidar Stojadinović[3]

EKSPERIMENTALNA STUDIJA SEIZMIČKOG PONAŠANJA ARMIRANO-BETONSKIH ZIDOVA

Rezime:

Kratki (niski) armirano-betonski (AB) zidovi predstavljaju često rešenja za obezbeđivanje horizontalne krutosti u konstrukcijama kao što su na primer vijadukti ili nuklearne elektrane. Međutim, nedoumice vezane za formiranje mogućih mehanizama loma u ovakvim elementima, usled različitih nivoa seizmičkih hazarda, i dalje su prisutne. Nerazumevanje potencijalnih oblika loma i tranzicije među njima za rezultat može imati lošu procenu u pogledu zahtevanih pomeranja konstrukcije. U ovom radu su prikazani najvažniji rezultati eksperimentalnih istraživanja na uzorku od šest AB zidova sa odnosom visine i dužine od 1.85.

Ključne reči: AB zid, seizmičko ponašanje, mehanizmi loma, zahtevana pomeranja

EXPERIMENTAL STUDY ON THE SEISMIC BEHAVIOR OF REINFORCED CONCRETE SHEAR WALLS

Summary:

Reinforced concrete (RC) shear walls with low to moderate aspect ratios are frequently seen as a solution to provide the lateral strength to structures such as viaducts or nuclear power plants. However, there is still a significant uncertainty regarding failure mechanisms that may occur in these elements under different seismic hazard levels. Misinterpretation of potential failure modes and transitions between them may result in a wrong estimate of displacement demands of the structure. This paper presents most important findings from experimental campaign conducted on six large-scale RC shear wall specimens with aspect ratio of 1.85.

Key words: RC shear wall, seismic behavior, failure modes, displacement demand

---

[1] *PhD Candidate, ETH Zürich, Zürich, Switzerland, kovarbasic@ibk.baug.ethz.ch*
[2] *PhD Candidate, ETH Zürich, Zürich, Switzerland, pizarro@ibk.baug.ethz.ch*
[3] *Professor, ETH Zürich, Zürich, Switzerland, stojadinovic@ibk.baug.ethz.ch*

1. INTRODUCTION

Reinforced concrete (RC) shear walls are frequently used as the lateral force-resisting structural elements in zones of moderate to high seismicity. Generally, the construction process of shear walls, as in all RC members, requires splicing of rebars, favouring in many cases their location to be in zones where plastic deformations can occur. Typical examples can be found in bridges, where the reinforcement is commonly spliced just above the construction joints between bridge piers and foundations. Field observations after recent earthquakes have shown that the failure of lap splices can increase the vulnerability of RC structures [1], [2], [3]. Although current design codes [4], [5] recommends to avoid splicing of reinforcement in zones of potential plastic hinges, the detail is not strictly forbidden and can be found in many existing structures as well. Code provisions for design and detailing of lap splices in shear walls originate mainly from experimental investigation performed on RC beams [6]. Moreover, primary focus of these studies was on the characterization of strength of lap splices [7], [8] and little attention was given to their load-deformation behaviour. Recently, the load-deformation behaviour of lap splices under uniaxial cyclic loading was addressed in work of Tarquini et al. [9]. Experimental data on the seismic performance of RC shear walls with lap splices is scarce and elaborated in the literature review by Almeida et al. [10]. Even scarcer is the research on the shear walls with lap splices that have lower aspect ratios (H/B < 2), according to authors knowledge there is only a single test conducted by Almeida et al. [11]. The behaviour of these walls up to the failure of lap splices can be well predicted [12]. But the failure of lap splices or its combination with rebar ruptures may lead in the transition from dominant flexural-shear response to the rocking motion of the wall. Neglecting this transition can result in selection of inappropriate numerical model. The consequence can be a methodologically erroneous estimation of the displacement demand of structure. The scarcity of experimental data requires further investigations. The first phase of our research project includes laboratory tests on RC shear walls with lap splices. The goal of this investigations was to produce data to understand the response of these walls to earthquake-induced lateral loads. A selection of the obtained experimental results is presented in this paper.

2. EXPERIMENTAL PROGRAM

The experimental campaign consists of six RC shear walls. The geometry and reinforcement configuration of the reference test-wall (SW01) were selected to resemble the wall-type piers, common for bridges built in Switzerland in 1970s and 1980s [13] in the scale 1:2. Other specimens have variations in terms of transverse reinforcement and lap splice length, and were subjected to different loading protocols. The length and the height of the specimens were chosen to produce an aspect ratio less than two, as well as to facilitate their transport and manipulation in the laboratory. In this paper the results from series of four quasi-static cyclic tests are presented. Each specimen consists of a footing, a wall and a top beam. Specimens were cast in the vertical position in three steps, starting with the casting of footing, followed by casting of the wall itself and finally casting of the top beam. The construction sequence for preparing test specimen as well as concrete casting reflects the actual field conditions. The geometry of all specimens was the same. The footing was 2.9 m long, 1.65 m wide and 0.4 m tall. The wall was 2.75 m tall, 1.8 m long and 0.4 m thick. The top beam was 1.8 m long, 1.65m wide and 0.4 m tall. The longitudinal reinforcement ratio of 1 % provided by 14 mm bars was kept in all

specimens. The transverse reinforcement consisted of 8 mm diameters stirrups with 135° hooks, with reinforcement ratios varying from 0.25 % in the test unit SW01, SW03, SW04 to 0.34 % in the test unit SW02. Confinement of boundary zones was provided in the test unit SW04 following the provisions of the current American building code for structural concrete [5]. In all test units the longitudinal reinforcement was spliced at the base of the wall with the splice length of approximately 43 bar diameters (600 mm), except the specimen SW03 where the splice length was approximately 64 bar diameters (900 mm). All the rebars composing the longitudinal and transverse reinforcement were obtained from the same production batch. All reinforcement was grade B500B, cold-formed steel without any yield plateau, common on the Swiss construction market. The average yield stress of longitudinal and transverse reinforcement derived from uniaxial tension tests were 460 MPa and 475 MPa respectively. Concrete strength and modulus of elasticity were assessed for each casting step by testing three 150 x 300 mm cylinders according to SIA 162/1 [14]. The average concrete cylinder strengths at the day of the test varied between 38 MPa and 42 MPa.

3. TEST FACILITY, INSTRUMENTATION AND PROCEDURE

The tests were conducted using the ETH Multi-axial Subassemblage Testing (MAST) facility. ETH MAST, shown in Figure 1, comprises 10 servo-hydraulic actuators reacting against the strong floor (1) and reaction walls and one modular steel cross-head (2). Six horizontal actuators (3) with strokes of +/- 600 mm provide lateral loads up to +/- 4 MN in one and +/- 2 MN in another direction. Additionally, four +/- 2.5 MN vertical actuators (4) are capable of applying a total force of +/- 10 MN and strokes of +/- 600 mm. This allows the system to apply six degrees of freedom (DOF) (tri-axial control, roll, pitch and yaw) in mixed force/displacement control. The movement of the crosshead is controlled by combined movement of all 10 actuators. Since the system is over-constrained, INOVA control system is utilized to simultaneously control six DOF of the crosshead at its control point (5). Kinematic transformations are used to transform each actuator displacements from its local coordinate system to the global coordinate system of the crosshead control point. In addition, the control system compensates the flexibility of the crosshead and gaps in clevises. The specimens (6) were placed on 850 mm high RC blocks (7) and post-tensioned to the strong floor and to the steel cross-head. On the lower surface of the crosshead, two 90 mm thick steel plates (8) were installed and a thin layer of mortar (9) was used to ensure uniform displacement and load transfer to the specimen.
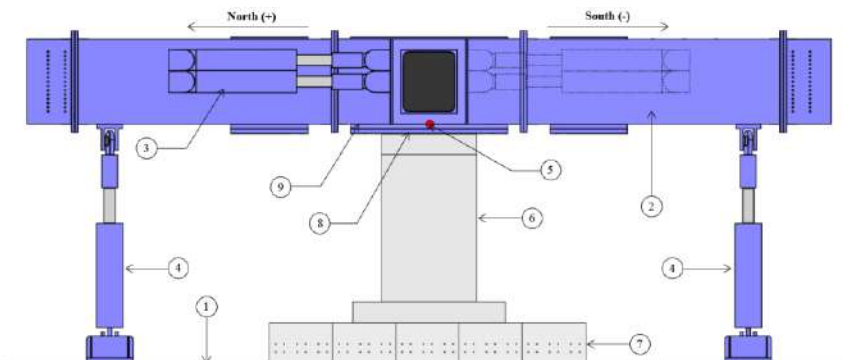

Figure 1 – ETH Zürich MAST Facility: Longitudinal section

The control point in all tests was set to be on the lower surface of the crosshead. Therefore, the effective height (vertical distance from the control point to the wall base) and aspect ratio of tested specimens were 3.33 m and 1.85 respectively. The walls were tested as cantilever walls and the same test procedure was followed in the quasi-static cyclic series of tests. In the first step, the vertical force of 2 MN was applied. The applied axial load corresponds to approximately 10 % of the compressive strength of the specimen, the value that are typically found in bridge piers. Subsequently, the wall was subjected to the lateral force and displacement reversals around its stronger axis. The loading history was defined in accordance with the guideline of American Concrete Institute [15]. Two cycles were applied at each deformation level. First, in order to capture performance of the wall within the elastic range of deformations, test was conducted in force control with target load levels that correspond approximately to one third and two thirds of yield force. Afterwards, the test was continued in displacement control with subsequent increase of displacements in increments of yield displacement. The loading history is given in Table 1.

Table 1 – Loading history

Force Control							
Target Force [kN]	300				600		
Loading speed [kN/s]	2				2		
Cycles [-]	1,2				3,4		
Displacement Control							
Target Displacement [mm]	8	16	24	32	40	48	56	64
Loading speed [mm/s]	0.1	0.1	0.1	0.1	0.1	0.2	0.2	0.2
Target Drift [%]	0.24	0.48	0.72	0.96	1.20	1.44	1.68	1.92
Ductility [-]	1	2	3	4	5	6	7	8
Cycles [-]	5,6	7,8	9,10	11,12	13,14	15,16	17,18	19,20

An INDEL GIN-SAM4 real-time computer was connected to the INOVA control system via EtherCAT and used to send force and displacement commands. Moreover, the INDEL GIN-SAM4 real-time computer was used to collect external linear variable differential transformers (LVDTs) measurement data and to trigger the digital image correlation (DIC) system at the pre-defined forces/displacements in each load history cycle applied. LVDTs were mounted in such a way to measure relative sliding and uplifting of the specimen with respect to the crosshead and to the RC blocks at multiple positions. The 2D-DIC system was used to obtain the full-field in-plane deformations of the Western wall face. For that purpose, a random speckle pattern with dot size of approximately 2 mm was applied on the wall surface. On the lower half of the Eastern wall face, 96 light emitting diodes (LED) were glued and their position were tracked during the test using the optical measurement system NDI Optotrak Certus. In addition to the measurement

surface strains, a pair of spliced bars in wall ends were instrumented with optical fibers connected to an optic reflectometer device to measure strains along their length.

4. TEST OBSERVATIONS

The following section summarizes the observed response of the test specimens. The values of the peak horizontal forces (H_{max} and H_{min}), recorded during testing, are summarized in Table 2. Further, displacements ($d_{t,max}$ and $d_{t,min}$) corresponding to the initial transition from flexure to rocking motion, as well as the values of specimen initial (tangent) stiffness K_0 are also reported. The horizontal force-displacement hysteresis curves of four test units are shown in Figure 2. Note that positive force and displacement values correspond to loading towards the North side of the specimen and negative values corresponds to loading towards the South side. For each cycle, the wall was loaded first towards the North and then towards the South.

Table 2 – Measured response characteristics. No transition from flexure/shear to rocking was observed during the test of specimen SW03.

Specimen	Peak Load [kN]				Transition Displacement [mm]				K_0 [kN/mm]
	North		South		North		South		
	H_{max}	Cycle	H_{min}	Cycle	$d_{t,max}$	Cycle	$d_{t,min}$	Cycle	
SW01	1405	11	-1422	11	31.4	14	-33.5	13	193
SW02	1409	11	-1449	11	26.7	16	-36.5	15	194
SW03	1363	11	-1443	11	-	-	-	-	192
SW04	1422	11	-1422	13	40.4	17	-50.2	17	190

During the first load cycles the test specimens remained nearly without cracks. The first cracks developed in all walls during load cycle 3, when the horizontal force was approaching to 600 kN, mainly at the height of the second stirrup above the wall base. By applying the target displacement corresponding to displacement ductility $\mu_\Delta = 1$, flexure-shear cracks formed up to approximately the half of the height in all walls, with the main crack distance equal to the stirrup spacing. With the increase of the applied target displacement, new cracks developed to the top of the walls and some of previous grew longer and almost reached the opposite edge of the wall. From load cycles 9 and 10 (target displacements of $\mu_\Delta = 3$) onwards, deformations started to concentrate in the cracks at the wall bases and just above the splices. On the other hand, pre-existing cracks within the lap-splices progressively reduced their width. In almost all tested walls, the peak horizontal forces were reached in load cycle 11 (target displacement of $\mu_\Delta = 4$), with measured values of around 1.4 MN. All specimens showed quite similar response (dominant flexural response) and crack development (see Figure 3) in the displacement control testing phase up to the target displacement of $\mu_\Delta = 4$. While the top displacement in the SW01 was increased to $\mu_\Delta = 5$ South, vertical splitting cracks started to form at the North edge of the wall and the first lap splice failure occurred when the top displacement of 33.5 mm was reached. Following load cycles led to extensive spalling of concrete cover with combination of further splice failures and rebar fractures. The horizontal force rapidly dropped to the residual value of approximately 500 kN and the wall continue to respond in stable rocking motion. Similar failure modes were observed in the specimens SW02 and SW04. However, the transitions from the flexural to

rocking response in these cases were initiated by applying target displacement of $\mu_\Delta = 6$ and $\mu_\Delta = 7$ respectively. In the SW03, the transition was not observed. The crushing of the concrete core, preceded by the extensive concrete cover spalling and buckling of the rebars, was the failure mode in this case.
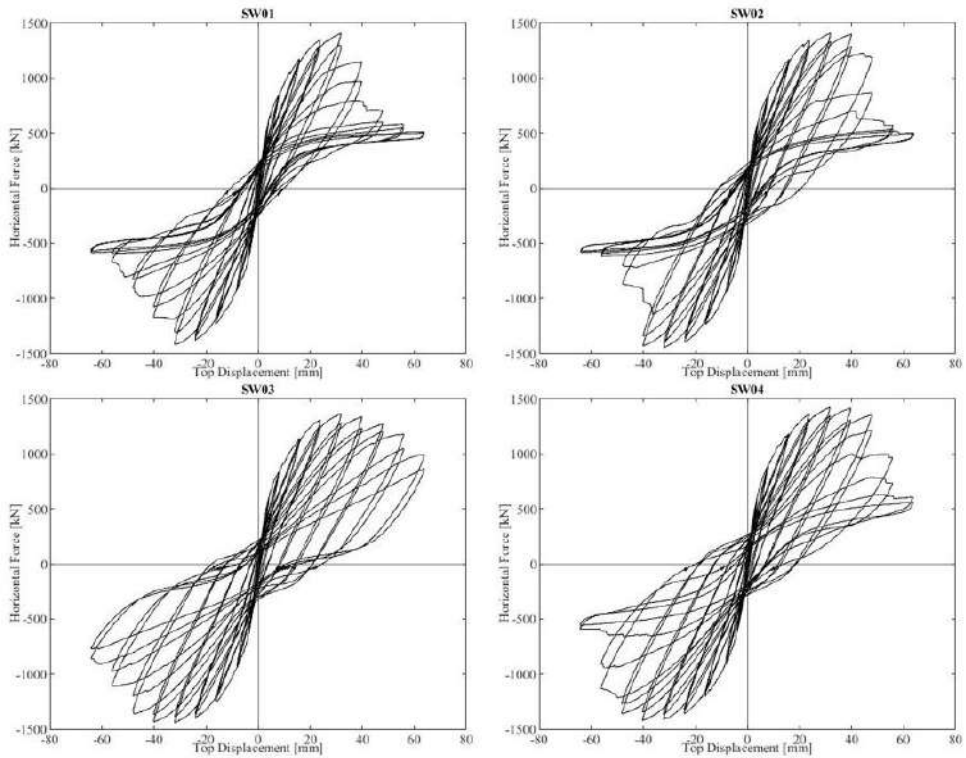

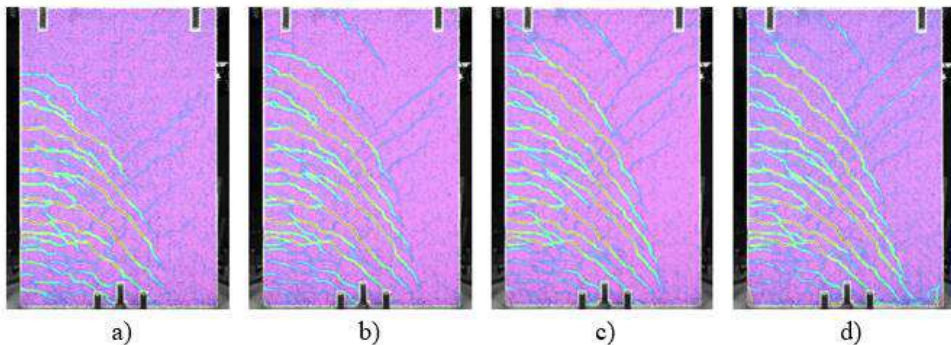*Figure 2 – Horizontal force-displacement response hysteresis curves*

*Figure 3 – Crack development in the specimen SW01; a) $\mu_\Delta = 2$, b) $\mu_\Delta = 3$, c) $\mu_\Delta = 4$,
d) first lap splice failure*

5. DISCUSSION OF RESULTS

The response of the shear walls was monitored using multiple types of instrumentation, mentioned in Section 3. Data from these instruments were used to get better understanding of response mechanisms. Some of results are presented in next sections.

5.1 CURVATURE DISTRIBUTION

Curvatures are parameter that is frequently used in the design and assessment of RC shear walls. Therefore, experimentally determined variation of curvatures along the wall height of tested specimens are presented in Figure 4. Curvatures were computed from the average vertical strains measured at the same elevations at the two wall ends assuming plane section remaining plane. The average vertical strains were obtained from DIC measurements. Each point in the curve represents the mean of two estimates at a given drift ratio. All specimens experienced the largest curvatures near the wall base. Another (smaller) concentration of curvatures was observed just above the end of lap splices in all tested specimens. It is also observed that curvatures reduce at a higher rate along the height compared to results of tests on walls with continuous longitudinal reinforcement.
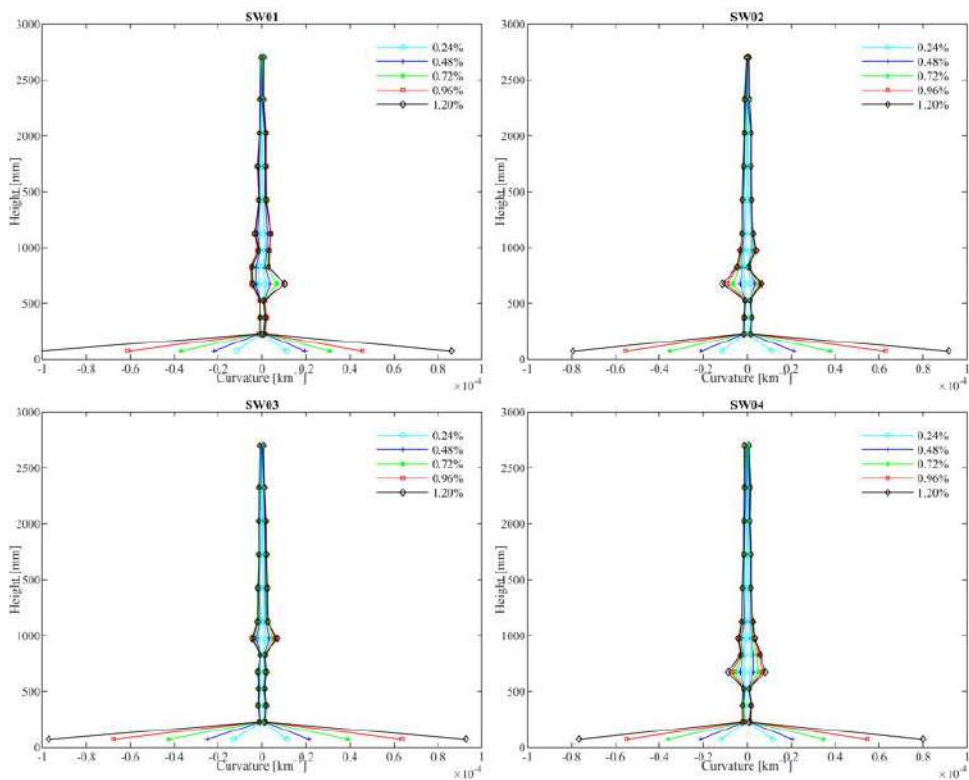

Figure 4 – Contribution of deformation components with the increase of applied displacements

5.2 DEFORMATION COMPONENTS

The extensive instrumentation of the walls allowed to determine the contribution of each deformation component to the total displacements. Deformation components (flexure, uplift, shear, sliding) were calculated by means of DIC measurement data. The flexural displacements were calculated by integrating the curvature over the height twice. The total flexural deformations were further decomposed into the actual flexural deformations and uplift deformations caused by opening of the crack at the wall base and slipping between the spliced bars. The uplift deformations were estimated by multiplying the base rotation (difference of two vertical displacements) with the height. The shear displacements were calculated from the diagonal measurements following the method by Hiraishi [16]. The mean horizontal displacement located above the wall base was assumed to represent the sliding deformation. The summation of deformation components yields total displacements that agrees very well with the measured displacements. The maximum error of all tests equals around 3 % and the average error is less than 1 %. Figure 5 shows the deformation components of tested specimens for the second load cycle of applied target displacements.
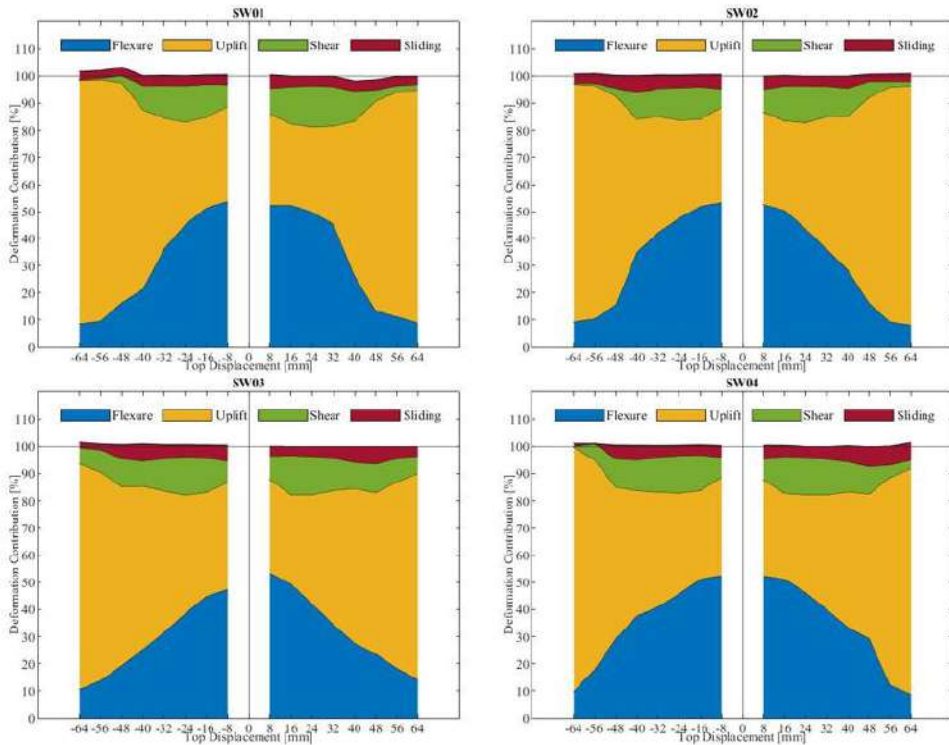

Figure 5 – Contribution of deformation components with the increase of applied target displacements shown for $\mu_\Delta \geq 1$

All shear walls behaved similarly and deformation contributions remain mostly unchanged up to target displacements of $\mu_\Delta = 2$. At that moment, total flexural deformations contributed around 80 % of the total displacements. Within the flexural contribution, around 40 % was due

to uplift. With the further increase of target displacements, the contribution of the uplift to the total flexural displacement continue to increase, but the ratio of the total shear to total flexural deformations remained constant (around 15-20 %). Past tests on RC shear walls with continuous reinforcement showed that shear to flexure displacements ratio remains more or less constant over the entire ductility range [17]. However, the failure of lap splices and rupture of rebars, resulted in decrease of both, flexural and shear deformation contributions. The final response in the SW01, SW02 and SW04 specimens was nearly 90 % of uplift which had as consequence stable rocking motion of these specimens. On the other hand, concrete core crushing and bar buckling led to slight decrease of shear deformations in the SW03 but their contribution to the total displacements was still around 10 % at the end of the test.

5. CONCLUSIONS

Four large-scale RC shear walls were tested using the advanced capabilities of the ETH MAST facility. The walls were designed to simulate wall-type piers with the spliced longitudinal reinforcement at the base. The tests investigated the impact of confining reinforcement and lap splice length on earthquake performance of RC shear walls with low aspect ratio (H/B < 2). Global load-deformation data, high-resolution local deformation measurements and observed damages were used to get better understanding of their seismic behaviour and performance. Lap splices caused a concentration of curvatures near the wall base. With the increase of target displacement, deformations were concentrated in the cracks at both splice ends. The plastic hinge with distributed plasticity and cracking (typically seen in RC shear wall tests) was not observed in this case. The presence of lap splices of medium length ($\sim40d_b$) in the plastic hinge zone triggered transition from flexural behaviour to rocking motion. Further, it is shown that in the case of medium lap splice length ($\sim40d_b$), walls with the higher amount of transverse reinforcement or confined boundary zones exhibited transitions for larger ductility demands. For the case of long lap splice length ($\sim60d_b$), neither failure of lap splices nor transition between response modes were observed. Although, the failure of lap splice caused rapid drop of lateral strength, significantly below 80 % of the respective maximum capacity, walls showed stable rocking response with not much additional damage.

REFERENCES

[1] Kilic S., Sozen M.A. Evaluation of effect of August 17, Marmara Earthquake on two tall reinforced concrete chimneys, ACI Struct J, 100 2003, 357-364.

[2] Kim S., Shiohara, H. Dynamic response analysis of a tall RC Chimney damaged during 2007 Niigata-ken Chuetsu-Oki Earthquake, Proceedings of the fifteenth world conference on earthquake engineering, Portugal, 2012.

[3] Song C., Pujol S., Lepage A. The collapse of the Alto Rio building during the 27 February 2010 Maule, Chile, earthquake, Earthq Spectra, 28, 2012, 301-334.

[4] CEN Eurocode 8. Design of structures for earthquake resistance, Part 1: General rules, seismic actions and rules for buildings. EN 1998-1. The European Union per Regulation, 2004.

[5] ACI Building code requirements for structural concrete (ACI 318-14) and commentary, American Concrete Institute, 2012.

[6] ACI Bond and development of straight reinforcing bars in tension (ACI 408R-03). American Concrete Institute, 2003.

[7] Zuo J., Darwin D. Splice strength of conventional and high relative rib area bars in normal and high strength concrete, ACI Struct J, 97, 2000, 630-641.

[8] Canbay E., Frosch R.J. Bond strength of lap-spliced bars, ACI Struct J, 102, 2005, 605-614.

[9] Tarquini D., Almeida J.P., Beyer K. Experimental investigation on deformation capacity of lap splices under cyclic loading, Bull Earthquake Eng, 17, 2019, 6645-6670.

[10] Almeida J.P., Prodan O., Tarquini D., Beyer K. Influence of lap-splices on the cyclic inelastic response of reinforced concrete walls. I: Database assembly, recent experimental data, and findings for model development, J Struct Eng, 143, 2017.

[11] Almeida J.P., Prodan O., Rosso A., Beyer K. Tests on thin reinforced concrete walls subjected to in-plane and out-of-plane, Earthq Spectra, 33, 2016, 323-345.

[12] Kolozvari K., Tran T.A., Orakcal K., Wallace J.W. Modeling of Cyclic Shear-Flexure Interaction in Reinforced Concrete Structural Walls. II: Experimental Validation, J Struct Eng, 141, 2015.

[13] Bimschas M. Displacement based seismic assessment of existing bridges in regions of moderate seismicity, PhD Thesis, ETH Zurich, 2010.

[14] SIA SIA 162/1, Betonbauten-Materialprüfung, Swiss Society of Engineers and Architects, 1989.

[15] ACI Guide for testing reinforced concrete structural elements under slowly applied simulated seismic loads (ACI 3742R-13), American Concrete Institute, 2013.

[16] Hiraishi H. Evaluation of shear and flexural deformations of flexural type shear walls, Bulletin of the New Zealand Society for Earthquake Engineering, 17, 1984, 135-144.

[17] Beyer K., Dazio A., Priestley M.J.N. Shear deformations of slender reinforced concrete walls under seismic loading, ACI Struct J, 108, 2011, 167-177.

Ivica Živanović [1], *Matthieu Guesdon*[2]

SEDLA ZA MOSTOVE SA KABLOVIMA: RAZVOJ I KVALIFIKACIJA TEHNOLOGIJE KOSIH KABLOVA

Rezime:

Sedla za prevoj kablova su redovno korišćena na projektima mostova sa kosim kablovima, visećim mostovima ili extrados mostovima. Najbitnija karakteristika sedla su zaštita od korozije i zamor kablova. Savremeni razvoj sistema sedla omogućava prolaz užadi kroz sedlo. Užad prolaze direktno kroz otvore u kalupu od Ultra High Performance Fibre Concrete (UHPFC). Zahvaljujući optimizovanom poprečnom preseku pojedinačne rupe omogućavaju maksimalno trenje između betona i specijalno obložene užadi sa lokalnom primenom kohezivne obloge (Cohestrand®), omogućavajući tako užadima značajne asimetrične sile u sedlu bez proklizavanja. U isto vreme kontinuirana zaštita od korozije je obezbeđena neprekinutom oblogom užadi od ankernog bloka na jednoj strani mosta do ankernog bloka na drugoj strani. Ovakvo rešenje sedla mosta je danas jasno definisan u poslednjim PTI i fib bulletin 89 preporukama, kojih definišu proces kvalifikacije tehnologije sedla, naročito u pogledu minimalnog koeficijenta trenja i otpornosti na zamor.

Key words: fiber beton, kablovi, sedla, paralelna užad, extrados mostovi, Cohestrand

DEVIATION SADDLES FOR CABLES BRIDGES: DEVELOPMENT AND QUALIFICATION OF STAY CABLE TECHNOLOGY

Summary:

Deviation saddles for cables are regularly used in projects such as cable stayed bridges, suspended bridges or extradosed bridges. The key issues for saddles are corrosion protection and fatigue regarding the cable behaviour. The most recent saddle system developed consists in allowing the passage of the strands through the saddle. Strands go directly through concrete recesses within the Ultra High Performance Fibre Concrete (UHPFC) matrix. Thanks to an optimized cross section of the recesses, individual holes maximize the friction between the concrete and specially sheathed strands (cohesive sheathing - Cohestrand®), which allow strands to transfer important asymmetrical loads to the saddle without sliding. Meanwhile, a continuous corrosion protection is ensured by the strand sheathing from one deck anchorage to the other. Such saddle design is nowadays clearly described in the last edition of the PTI and fib bulletin 89 recommendations, that specify the qualification process of saddle technologies, particularly in regard to the minimum friction coefficient and fatigue resistance.

Key words: fibre concrete, cable, saddle, parallel strands, extradossed bridge, Cohestrand

---

[1] *Deputy Technical Director, Freyssinet International, Paris, France, ivica.zivanovic@freyssinet.com*

[2] *Head of Project Systems, Technical Dpt,Freyssinet International, Paris, France, matthieu.guesdon@freyssinet.com*

1. INTRODUCTION

1.1. FIELD OF APPLICATION

Three categories of cables supported bridges can require deviation saddles to deviate a cable or a bundle of parallel strands from one side of a pylon to the other.

Cable stayed bridge: the choice of a deviation saddle may be imposed to improve the bridge aesthetics with a slender pylon and to simplify the construction with a solid pylon without anchorage chambers and routine maintenance plan associated.

Suspended bridges: the suspension cables are usually continuous between either anchorages at ground level, and deviated over the pylon by a deviation saddle. Historically most of the main suspension cables are built with full locked coil cable or parallel wire strands (PWS) cable but parallel strands are also a viable alternative as developed by Freyssinet using the Cohestrand® technology and specific hanger collars.

Extradosed bridges: They are intermediate between conventional post-tensioned cantilever bridges and cable stayed bridges. The deck has a significant bending inertia and the pylon is very short. Thus, extradosed cables and anchorages are derived from stay cable technology. They cross the pylon through a deviation saddle derived initially from the deviator of external post-tensioning *tendons.*

1.2. SADDLE DESIGN SPECIFICATION

Saddle conception shall offer a fixed anchor point of the cable to ensure a safe transfer of forces and of differential tangential forces of stay cables due to differential live loads coming from each side of the pylon and transferred into the pylon structure without cable slippage. The limit force before slippage can be defined based on the saddle geometry as well as the minimum friction coefficient deriving from the technology used. This latter and highly critical value can be defined as per the test protocol referred to in paragraph 3. As a fixed point for the cables, angular deviations must be filtered at each extremity of the saddle. Moreover, deviated cables are subject to bending stresses and fretting fatigue (small relative movements due to fatigue loading between individual tensile elements combined with transverse pressure), hence saddles design must also limit this effect to ensure the required cable system performances.

1.3. SADDLE STATE OF THE ART FOR MULTI-STRAND SADDLE

For parallel strand cables, two design of saddle exist. First design mainly used to deviate strand bundle is made of a steel curved pipe where all tensile elements (strands) are contained in and grouted after stressing. Transfer of differential forces from curved pipe to the pylon is achieved by mechanical connections such as bonded strands in the cement grout. However grouted stay cable saddles since long time ago tends to be withdrawn from conception disposition due to fatigue performance and corrosion protection that they are no more used. Second existing design of saddle is called Multitube saddle. Multitube saddle are made of individual tubes, one for each strand, placed inside an outer steel curved guide pipe poured by concrete. Friction ensures in such case the transfer of differential forces.
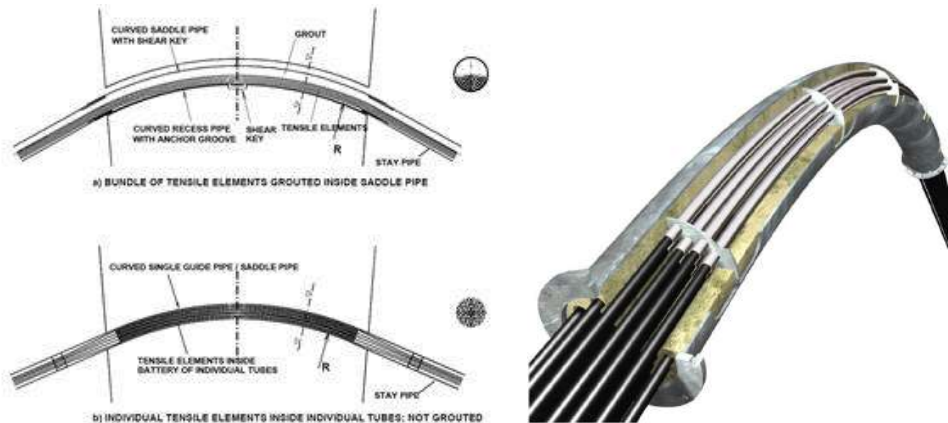
Figure 1 - Typical saddle conceptions a) and b) / Typical mutlitube saddles of previous generation with individual metallic tubes

2. FREYSSINET SADDLE DEVELOPMENTS

Freyssinet recently paved the way of a new design for saddle using a concept of multi slots saddle where Cohestrand® is directly in contact with Ultra High Performance Fibre Concrete (UHPFC). No more individual metallic tubes are necessary which enables a life expectancy and completely avoids the metal-to-metal contact that seriously enhance fretting corrosion (in comparison with strand bundle in the saddle tube cement grouted after stressing).

This new saddle has been successfully implemented in several extradosed, stay cable or even suspended bridges.

2.1. SADDLE CONCEPT

The new saddle system developed by Freyssinet consists in allowing the passage of the strands through the saddle without individual tubes. The strands (Cohestrand®) go directly through concrete recesses within the Ultra High Performance Fibre Concrete (UHPFC) of the saddle. The recesses are made thanks to reusable rubber bars removed after poured concrete is hardened. An optimized cross section and surface of the recesses has been developed under intensive Research and Development program by Freyssinet in order to ensure the friction between concrete and individually sheathed strands (Cohestrand®) which allow strands to transfer important asymmetrical loads to the saddle (pylon) without slippage. This allows also to ensure a continuity of the strand corrosion protection at the production stage in factory without any operation on site.
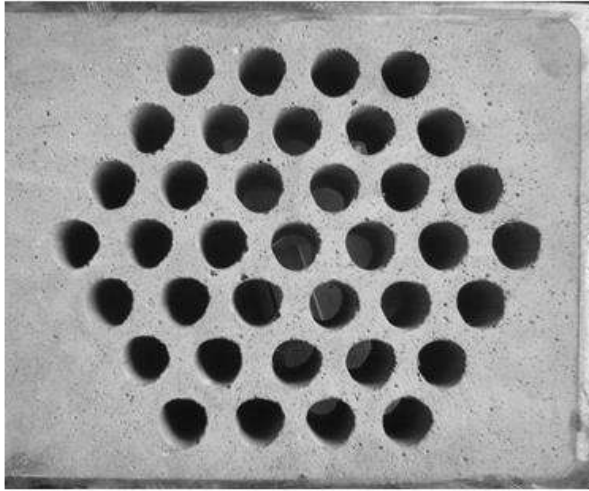
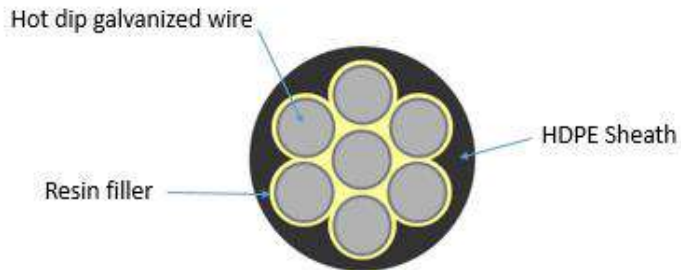*Figure 2 – Typical cross-section of Freyssinet UHPFC Saddle*

Figure 3 – Cohestrand® cross section

As previously evoked, a bending filter similar to the one located at the exit of anchorage is integrated at each extremity of the saddle. This feature can handle an angular deviation of 50 milliradians, while keeping the bending stresses in the strands at a low level.
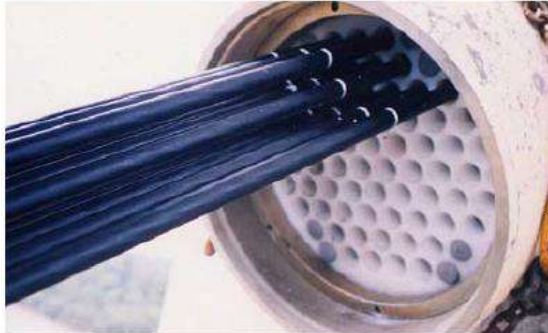
Figure 4 – Bending filter at saddle exit

2.2. MANUFACTURING AND INSTALLATION

Steel formwork (saddle) is prepared in workshop. Formwork plates and outer tube are bend to the exact radius expected by the project. Every steel parts are hot dip galvanized as per applicable international standard. Positioning plates are tack welded inside the steel formwork steadily along the curved length every 200 mm approx. These positioning plates are drilled as per the pattern of the cable bundle arrangement and aim to guide the rubber bars between the two extremities of the saddle.

When saddle steel formwork is fully assembled, the bars are threaded one by one through each holes of the positioning plates which guarantee the relative position of the strands inside the bundle all along the saddle curved length. Choice of the rubber bars for the strand recesses in the saddle was made for several reasons:

- flexibility needed to ensure the final individual holes in order to follow an exact circular arc without any risk of straight segment lines.
- rubber component is very easy to remove after the concrete is hardened. Thanks to his very high elongation properties, bars are withdrawn from the saddle just by pulling them from one side.
- bars are enough resistant to be re-usable several times.

After threading of all the rubber bars, saddle is ready to be poured with UHPFC.

Figure 5 – Saddle steel formwork with recesses bars installed

UHPFC is prepared from premix batch mechanically mixed with water, additives for workability and steel fibres. Accelerator may be used to speed up production rate.

When UHPFC mix procedure is finished, saddle pouring can start with a level of precautions needed to fill the saddle without any voids.

Figure 6 – Saddle UHPFRC pouring

When concrete is hardened, the recesses bars are removed from the saddle by pulling them from one extremity. Saddle is then ready to be delivered on site. Depending on the pylon type (steel or reinforced concrete), saddle can be placed in the pylon before casting of concrete, using a template to ensure a precise geometric positioning, or bolted onto the pylon in case of metallic structure.

3. PERFORMANCES WITH PTI AND FIB QUALIFICATION

The transmission of horizontal differential loading to the pylon is obtained by bonding between the Cohestrand® and its sheath, and friction between the HDPE sheath and the surrounding concrete. Individual holes ensure friction between HDPE sheath and concrete thanks to an appropriate shape of individual holes with notched pattern along the curved length of the saddle.

The blocking of unsymmetrical forces can be checked with the following formula:

$$F_{max} = F_{min}.exp^{\mu\alpha} \tag{1}$$

Where:
Fmax and *Fmin* are the simultaneous tension of the cable on either side of the saddle
μ is the friction coefficient
α is the deviation angle of the saddle

Conventionally metallic tubes were used in Multitube saddles as a casting for individual holes and to improve distribution of strand radial forces into the concrete. Freyssinet overcome this thanks to the development of an adequate formulation of Ultra High Performance Fibre Reinforced Concrete (UHPFC) with steel fibres and workability adapted to the individual holes

proximity imposed by the cable strand bundle arrangement. Hence, this formulation ensures a good pouring of saddle and gives enough compression and yield strength to sustain compression load from cable up to strand numbers that constitute the cable as for example192 strands.

It is now clear that among the various parameters used in the justification of saddle anchorage, the friction coefficient is the only item related one, and probably the most discussed one.

To ease and clarify for all cable suppliers and designers the saddle system qualification, the PTI and fib recommendations have introduced in their last edition a clear process for saddle system qualification.

3.1. QUALIFICATION TESTS

The new PTI saddle qualification process is based on several qualification steps that aim at ensuring that all fundamental functions of a saddle system are fulfilled:
- Ultimate resistance
- Fatigue resistance
- Durability
- Constant friction behaviour for all load cases.

The process is divided into two main parts: multi-strand tests to qualify the fatigue, ultimate and leak tightness of the saddle system, and monostrand tests to qualify the minimum friction coefficient at different load levels.

Table 1 – Qualification tests as per PTI DC45.1-18

Type of test	Saddle with isolated MTE elements
Fatigue	3 (min, average and large size, min 19 strands)
Fatigue and tensile strength	1 (any size, min 19 strands)
Fatigue and friction T2=30% MUTS	1 (any size, min 19 strands)
Fatigue and leak tightness	1 (any size, min 19 strands)
Initial load T2=10% MUTS	12 x single strand
Initial load T2=30% MUTS	12 x single strand
Initial load T2=50% MUTS	12 x single strand
Initial load T2=70% MUTS	12 x single strand

It is straightforward that the leak tightness test does not apply to a saddle concept that it does not rely on the use of an injected filler to reinstate the strand external barrier, and the durability against corrosion is instead to be demonstrated by proving that the factory applied strand sheathing remains undamaged after fatigue cycles.

Aside the full-scale qualification test, that covers both the fatigue, multi-strand friction and ultimate test, the biggest part of the qualification lies in the multiple monostrand tests to be performed to assess the declared friction coefficient.

3.2. FOCUS ON THE FRICTION DETERMINATION AND FREYSSINET SADDLE SYSTEM QUALIFICATION

A thorough test campaign was hence organized to perform the several tests required to assess the effective friction coefficient at all loads levels. Test were duplicated to assess the fiction coefficient under increasing load variations and decreasing load variations, and with angular deviation of strand and with the maximum angular deviation of strand at the saddle extremity.

All these tests evidenced the following results:
- Declared friction coefficient is 0,65,
- The achieved friction coefficient is generally higher when measured with a decrease in load,
- The maximum achieved coefficient at the minimum load (10% GUTS) is much lower than the maximum coefficient measure at all other loads levels (0.73 to be compared to values higher than 0.81),
- Values achieved at 50% and 70% GUTS are very similar, pleading for a similar behaviour for both usual service load and ultimate or strength load envelope.

Freyssinet saddle ensures friction coefficient of at least 0,65 (under all load levels).

Finally, a monostrand fatigue test bench was designed to assess the impact of fatigue cycles on the measured friction coefficient. Such assessment confirmed that the achieved friction coefficient after fatigue cycles at a load of 30% remains 15% higher than the minimum friction coefficient recorded throughout the whole campaign, close to the overall average.

Figure 7 – Fatigue and subsequent friction with ultimate resistance testing

The dismantling of samples after subsequent ultimate tensile test also confirmed the resistance of the strand HDPE sheathing to up to the cable breaking load.

Saddle system shall satisfy the same bending fatigue and tensile performance requirements as anchorage systems as defined in fib bulletin 89. An additional testing procedure is required to verify fatigue resistance of saddle systems under transverse cyclic deformations. The procedure is intended to simulate cable angular deviations observed frequently on cable stayed structures. Such test does not apply to saddle systems with extradosed applications as a main use. This test consists to apply 100 000 cycles as first fatigue loading phase with an angular deviation of $\alpha = \pm 25$ mrad. Then, second fatigue loading phase of 2 million bending fatigue cycles with an angular deviation of $\alpha = \pm 10$ mrad. After all fatigue phases a subsequent tensile test is performed.

The others test parameters and requirements are as for axial fatigue including the tensile test performance after fatigue.

The Freyssinet saddle system is fully compliant including this test to fib bulletin 89 and PTI recommendations.

3.3. LOCALLY COHESTRAND WITH RECENTS PROJECTS

To provide a cost-effective solution Freyssinet developed with the saddle system an equipment able to manufacture strand with Cohestrand part only in the area required as at deviation saddle location, the strand part outside (each part not in the saddle area) being produced with wax between wires and HDPE sheath of the strand itself. Such strand called hereafter LCS. The production tool allows to produce strand with wax or resin between the 7-wire steel and HDPE sheath alternatively providing a mechanical resistance to transfer the force in the saddle area as needed which is not the case in the free length. This is done without interruption of the production of the individually sheathed strand by switching along the length from wax to resin under HDPE sheath extrusion. The part locally cohestrand is marked along the length on the sheath allowing to identify the length including extra corresponding to the saddle location.

The following table shows the project references with this new saddle system and using Cohestrand or Locally cohestrand.

Table 2 – Saddle project references with Cohestrand or Locally Cohestrand

Project	Country	Year	Structure	Strand type
Vam Co Tay	Vietnam	U.C.	Extradosed	LCS
Vinh Phu	Vietnam			LCS
Song Hieu	Vietnam			Cohestrand
Seolwoon	Korea			Cohestrand
M44 Tisza	Hungary	U.C.	Stays	LCS
Sam Cheon	Korea	2022	Extradosed	Cohestrand
GoSam	Korea	U.C.	Extradosed	Cohestrand
GeunHo	Korea	2022	Extradosed	Cohestrand
Nano	Korea	2021	Extradosed	Cohestrand
SeolWoon	Korea	U.C.	Extradosed	Cohestrand
Podgorica	Montenegro	2021	Extradosed	LCS
Nkrumah Railway	Tanzania	2021	Stays	Cohestrand
CTW 130	KSA	U.C.	Extradosed	LCS
Cua Dai	Vietnam	2018	Extradosed	Cohestrand
Dim Cayi	Turkey	2018	Extradosed	Cohestrand
Perene Suspension	Peru	2018	Suspension cable	Cohestrand

4. CONCLUSION

The saddle system developed by Freyssinet ensures a safe transfer of vertical forces and of differential horizontal forces of stay cables due to load variation coming from each side of the pylon into the pylon structure thanks to a friction mechanism between Cohestrand® individual HDPE sheathing and Ultra High-Performance Fibre Reinforced Concrete (UHPFC).

This new design allows to install deviation saddles on bridges with main span up to 350m such as recently done in Binh Khanh Bridge (Vietnam) or Podgorica Bridge (Montenegro).

Combined with Cohestrand®, this saddle offers an un-interrupted individual steel corrosion protection applied on factory at production stage of each strand from anchorage to anchorage which enables to achieve a 100-year design lifetime, alike on parallel strand stay cable with anchorages in pylon. Moreover, individual strand can be easily replaced if necessary, with no access to the saddle area, as no protective filler need to be injected inside the individual holes after strand tensioning, nor a complicated unsheathing is required. The declared friction coefficient of 0,65 as per the PTI or fib bulletin 89 recommendations makes it a high-performance saddle system from both a structural and durability against corrosion points of view.

REFERENCES

[1] PTI recommendations for Stay Cable Design, Testing and Installation, 7th Edition, DC45.1-18

[2] fib Bulletin 89 Acceptance of cable systems using prestressing steels recommendation

Ksenija Janković[1], Marko Stojanović[2], Anja Terzić[3], Dragan Bojović[4], Srboljub Stanković[5]

UTICAJ VELIČINE ČESTICA I MORFOLOGIJE SITNOG AGREGATA NA RANE ČVRSTOĆE SCC-A

Rezime:

Sprovedena je uporedna studija performansi samougrađujućeg betona (SCC) sa letećim pepelom i krečnjačkim filerom. Eksperimentalni program obuhvatao je proizvodnju referentnog SCC-a projektovanog od portland cementa, rečnog peska i krečnjačkog filera i četiri eksperimentalna samozbijajuća betona sa različitim vrstama sitnih agregata, filera i specijalnog dodatka za povećanje otpornosti na smrzavanje i odmrzavanje. Ispitivani su i diskutovani efekti koje različite sitne frakcije i dodaci imaju na svojstva svežeg SCC-a (sleganje rasprostiranjem, test V-levka i test L-kutije) i čvrstoće na pritisak u ranoj starosti (3 i 7 dana).

Ključne reči: leteći pepe, krečnjčki filer, SCC, čvrstoća pri pritisku

IMPACT OF FINE AGGREGATE PARTICLE SIZE AND MORPHOLOGY ON THE EARLY STRENGTHS OF SCC

Summary:

A comparative study of performances of self compacting concrete (SCC) with fly ash and limestone filler was conducted. The experimental program included the production of reference SCC designed with Portland cement, river sand and limestone filler and four experimental self compacting concretes with different types of fine aggregates, fillers and special additive to increase freeze-thaw resistance. The effects that different sand and additions have on the properties of fresh SCC (slump-flow test, V-funnel test, and L-box test) and compressive strengths in early ages (3 and 7 days) were investigated and discussed.

Key words: fly ash, limestone filler, SCC, compressive strength

---

[1] *Principal research fellow, IMS Institute, Belgrade, Serbia, ksenija.jankovic@institutims.rs*
[2] *Professional adviser, PhD candidate, IMS Institute, Belgrade, Serbia, marko.stojanovic@institutims.rs*
[3] *Principal research fellow, IMS Institute, Belgrade, Serbia, anja.terzic@institutims.rs*
[4] *Research associate IMS Institute, Belgrade, Serbia, dragan.bojovic@institutims.rs*
[5] *Senior research associate, Intitute of Nuclear Sciences „Vinča", Univ. of Belgrade,* srbas@vin.bg.ac.rs

1. INTRODUCTION

Coal combustion residues (fly ash and bottom ash) as coal ash, are formed during ignition of coal in power plants. Fly ash is a fine powdery raw material (collected from a filter) consisting mainly of spherical hollow particles. The bottom ash is a coarse-grained incombustible by-product collected from the bottom of the furnace. Fly ash particles range in size from 0.5 - 300 μm. 50 - 90% of ash mass passes through a 4.75 mm sieve, while the upper particle size usually ranges from 19 - 38.1 mm). Coal ash can be found in different colors and characteristics depending on the type of coal, geolocation of the deposit, as well as the construction of the furnace and the combustion process used in the thermal power plant [1-4]. The average composition of the coal ash is: 60 - 85% of amorphous solids, 10 - 30% of crystalline components and up to 5% of unburned carbon. There are two types of fly ash: class C ash with up to 10% CaO and class F ash with 15 - 40% CaO. Class F fly ash is highly pozzolanic. Bottom ash contains approximately 2 - 18% CaO and is significantly less pozzolanic.

Self-compacting concrete (SCC) has a higher flow rate compared to conventional vibrated concrete. This flowability is achieved by including large amounts of extra fine particles (mineral fillers) in its composition [5]. This is achieved by including large amounts of extra fine particles (mineral fillers) in its composition [5].

The aim is to limit the proportion of cement while reaching the required high paste content. Among the fillers used in SCC, fly ash is one of the most common due to its availability and low cost. Components and their ratios, as well as the type and particle size of the filler, the conditions of casting, production and curing of SCC significantly affect the fresh and hardened properties of concrete. The influence of fly ash on the properties of cementitious materials is described as a combination of plasticizing effect (due to spherical shape in small part sizes), microaggregate effect (due to the ability to refill) and active effect (because of his pozzolanic ability). The combination of these effects causes noticeable changes in the maintenance of fresh concrete, and affects the microstructure of solid concrete and its characteristics. This means that it changes the rate of hydration to form a microstructure (both solid and porous phases). This leads to a change in the properties of hardened SCC (strength, Young modulus, water absorption, permeability, etc) [6-8].

The problem of industrial waste disposal is conventionally being solved by making planned landfills. However, landfills occupy large territorial areas and waste disposal is always complicated and expensive. The use of industrial by-products and waste materials such as fly ash solves the problem of their disposal in the design of concrete, so instead of creating new landfills, new ecological materials are created [9]. The paper presents the technology and fresh properties of self-compacting concretes, the design of which is based on alternating water / cement ratios and the amount of fly ash as filler. The aim of this research is to increase the content of fly ash in SCC, as a means of following the principles of the circular economy regarding the production of concrete and the use of man-made and waste resources in their composition.

2. EXPERIMENTAL RESEARCH

2.1. MATERIALS USED IN THE EXPERIMENT

Self-compacting concrete was prepared using Portland cement CEM I 42.5R. Chemical composition of cement is provided in Table 1. A large amount of fine particles is necessary for production of a self-compacting concrete mixture. In this case, two mineral additives were used as fillers. Namely, limestone was used in the mix-design of the referent concrete, while fly ash was employed in experimental SCC samples. Chemical analyses of aggregates and mineral fillers are given in Table 1, while the rest of determined properties are shown in Table 2.

The chemical analyses were conducted by means of EDXRF method on a Spectro Xepos system (Spectro XRF Analyzer Pro, Xepos C Software) equipped with a 50 W and 60 V X-ray tube with a binary Co/Pd alloy thick target anode. The excitation mode of the X-ray tube was combined polarized/direct excitation. The characteristic radiation emitted by the elements present in the sample was detected by a silicon drift detector with Peltier cooler system.

Table 1 - Chemical compositions of cement, aggregates and mineral additives (fillers)

Oxide	Content, %				
	Cement	Fly ash	Limestone	Natural, river aggregate 1	Natural, river aggregate 2
SiO2	18.92	55.60	1.07	77.2	65.03
Al2O3	4.46	25.51	0.39	8.64	3.13
Fe2O3	2.36	5.38	0.06	2.01	0.76
CaO	63.40	4.83	54.54	3.07	18.89
MgO	1.78	2.86	0.77	1.98	0.40
Na2O	0.24	0.43	0.01	2.98	0.51
K2O	0.70	1.50	0.06	1.09	1.46
SO3	3.23	0.80	0.02	0.04	0.05
P2O5	0.11	0.05	0.01	0.08	0.06
Mn2O3	0.07	0.06	0.003	0.04	0.03
TiO2	0.18	0.8	0.009	0.23	0.05
Cl	0.029	<0.0002	0.001	0.004	17.20
Cr2O3	0.02	0.03	0.001	0.02	0.00
LoI at 1000°C	4.16	1.99	42.88	2.35	9.55

Table 2 - Physical and mechanical properties of mineral fillers

Properties	Fly ash (milled sample)	Fly ash	Limestone
Sieve residue, %			
0.2 mm	0.8	12.1	6.3
0.09 mm	3.5	45.3	25.1
0.063 mm	8.6	54.8	29.3
0.043 mm	16.6	66.4	39.7
Bulk density, kg/m3	2310		
Specific surface, cm2/g	7990		
Pozzolanic activity, MPa			
-flexural strength	4.9		
-compressive strength	14.1		

Natural, separated aggregate with 0/4 (two kinds), 4/8, and 8/16 mm fractions was used in the mix-design of SCC-s. The percentage share of aggregate per fraction was 0/4 mm – 45 %, 4/8 mm – 20 %, and 8/16 mm – 35 %, respectively. Grain-size analysis of the aggregate mixtures is illustrated in Figure 1.
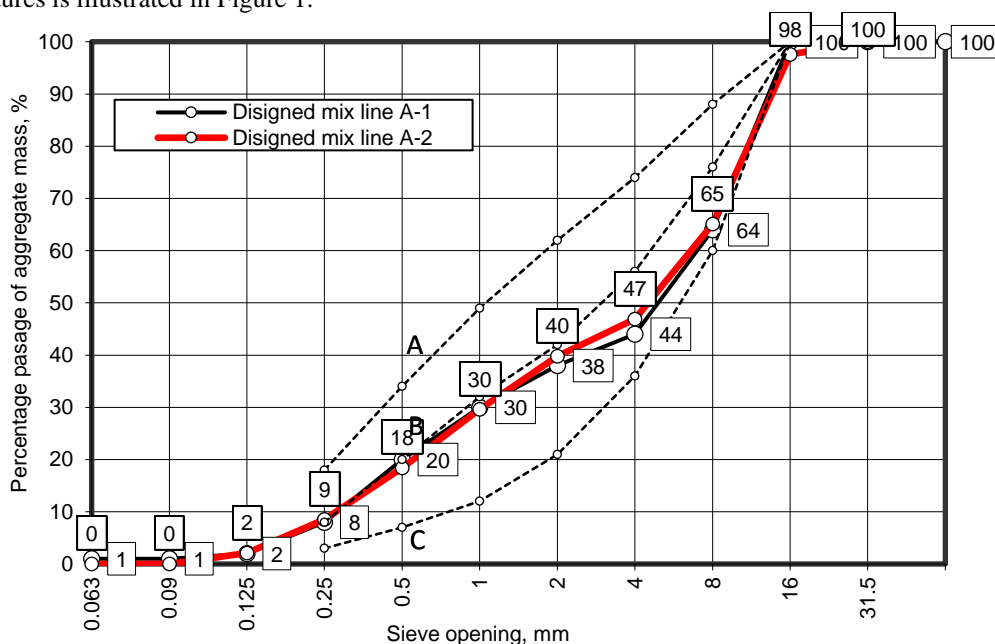
Figure 1 – Grading curves of aggregate mixtures for SCC samples

2.2. CONCRETE MIXTURE

Five mixtures of three-fraction self compacting concretes were prepared for this experiment (Table 3).

Table 3 - Self compacting concretes compositions

Sample No.	Share of the componential material, kg/m³				
	P10	P11	P12	P13	P14
Cement	400	400	400	400	400
Water	200	200	200	200	200
Limestone	100	-	-	100	-
Fly Ash	-	80	80	-	80
River 1 0/4	756	756	756	-	-
River 1 4/8	336	336	336	336	336
River 1 8/16	588	588	588	588	588
River 2 0/4	-	-	-	756	756
Admixture Sika Viscocrete 35 Techno	4	8	8	6	8
Sika Aer Solid	-	-	3.6	-	3.6
Bulk density	2384	2366	2370	2388	2370

Besides previously mentioned cement (CEM I 42.5R), mineral additives - limestone and fly ash, and natural separated aggregate (two kinds of fine aggregate 0/4, 4/8, and 8/16mm fractions), superplasticizer (Sika Viscocrete 35 Techno) was employed as admixture, as well as tap water. Special additive (Sika Aer Solid) to increase freeze-thaw resistance is also added in two mixtures. Fresh concrete was designed to meet the minimum of required properties of self-compacting concrete, according to EN 206 standard. Referent concrete (P10) was prepared using limestone as filler and natural aggregate – River 1.

The mixtures are designed to meet the following criteria: Slump-flow 650±50 mm, t500≥2s, V –funnel 9-25 s, L-box with 3 bars H2/H1≥08. All types of concrete were made with w/c=0.50. The superplasticizer was added in an amount to meet the required SCC properties in the fresh state.

3. RESULTS AND DISCUSSION

3.1. PROPERTIES OF FRESH CONCRETE

The fresh concrete tests were conveyed for following properties: density, fluidity - slump flow test according to EN 12350-8, viscosity – T500 test according to EN 12350-8, V funnel test according to EN 12350-9, and the ability of the passage between the reinforcement – L box test according to EN 12350-10.

The test results for concrete in the fresh state are shown in Table 4.

Table 4. Test results for concrete in the fresh state

Concrete mixture	Density, kg/m^3	Slump-flow, mm	t500, s	L – box, H1/H2	V-funnel, s
P10	2363	620	3	0.800	9
P11	2325	660	8.5	0.900	12
P12	2326	660	7	0.830	13
P13	2348	670	4	0.833	9
P14	2332	700	6	0.833	10

Slump-flow test, which is considered as the initial key characteristics of SCC, was used for controlling of the mixture's flowability. The spreading measures of the referent P10 was 620 mm and meet the criteria for SF1 class. Mixtures P11-P14 achieve SF2 class, varied from 660 to 700 mm.

V–funnel is an experimental test used in determination of viscosity of a mixture. All concrete samples corresponded to the VF2 class. Measured passing time being from 9 to 13 s. Segregation and accumulation of water at the surface were not noticed in any of the observed concrete fresh mixtures.

T500 property is defined as time-interval in which fresh concrete slump spreads to the limit diameter of 500 mm. This fresh concrete's characteristic is usually measured during slump-flow test. It represents a specific approbation of the mixture's viscosity. Namely, the recommended t500 interval for class SF2 is accounted from 3.5 to 6.0 s. The t500 values for concrete mixtures varied from 3 to 8.5 s. Measured intervals which were longer than 2 s, placed all tested mixtures in the VS2 viscosity class.

L-box test is employed in determination of the third key property of SCC, i.e. the ability of mixture to pass between reinforcing bars without blocking them. All mixtures met the criterion for the height ratio of the concrete mixture at the ends of L-box, which has to be at least 0.8. Mentioned mixtures also conformed to regulations of testing performances regarding their flow through three reinforcing bars, which is an important requirement for densely reinforced structures. Thereby, P10-P14 concretes belong to the same class - PL2. The test results were in the range from 0.83 to 0.90. Blocking of the passage between reinforcement bars by aggregate grains was not recorded in any of the conducted experiments.

For the same class of consistency, higher amount of superplasticizer was needed for preparation of SCC mixture with fly ash.

3.2. COMPRESSIVE STRENGTH

Concrete was compacted without vibration in metal cube-shaped molds with an edge length of d = 100 mm, and the samples were cured in water at a temperature of + 20 ° C until they were tested according to SRPS EN 12390-2 standard.

Testing compressive strength of concrete at the age of 3 and 7 days was carried out according to SRPS EN 12390-3 standard. Bulk density of hardened concrete was tested according to SRPS EN 12390-7 standard and ranged from 2300 to 2350 kg/m^3. The test results are shown in Figure 2.
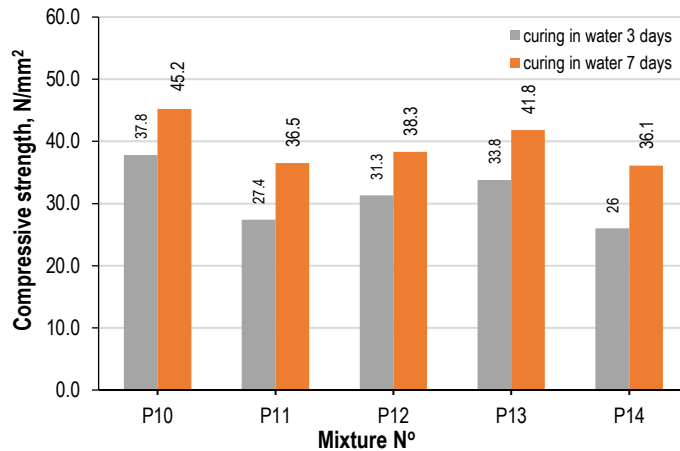
Figure 2 – Test results for concrete compressive strength

Comparing concretes made with the same aggregate, it can be concluded that samples using fly ash and Sika Aer Solid have 20 ± 3% less strength at 3 days and 15% at 7 days compared to concretes made with limestone filler.

If we look at concretes made with the same aggregate and filler (River 1, Fly Ash) using Sika Aer Solid, we get 14% higher strength at 3 days, and 5% at 7 days.

Concrete made with River 1 and Fly Ash aggregate will have 28% less strength in 3 days and 19% less in 7 days compared to concrete made with lime filler.

For concretes made with the same additives, concretes with fine fraction River 2 have 14 ± 3% less strength in 3 days, or 7 ± 1% compared to concretes made with River 1.

For mixtures made with the same additives (limestone or fly ash, with or without Sika Aer Solid), SCC with fine fraction River 2 have less strength compared to concrete made with River 1. Also, the same trend was observed at 3 and 7 days, but the difference in strength decreases with age. This can be explained by the difference in chemical composition. River sand 1 has high content of silicon dioxide, while calcium oxide is relatively low – characterizing this type of aggregate as siliceous. River sand 2 showed a very high CaO content placing this sand into calcite group. Due to its hardness, siliceous sand contributed to the high early strengths. CaO from calcite sand participated in hydration reactions creating additional C-S-H gel, the part of the paste responsible for later concrete strength.

4. CONCLUSIONS

Fly ash has been successfully applied in the design of three self-compacting concretes. The following conclusions were made:

- The spreading measures of referent P10 concrete achieve SF1 class. For other mixtures slump-flow varied from 660 to 700 mm and were categorized in SF2 flowability class.
- All concrete samples corresponded to the viscosity VF2 class.
- According to t500 values, all concrete mixtures were into VS2 class.

- All concrete types belong to the same class - PL2, since all mixtures met the criterion regarding height ratio of the mixture at the ends of L-box.

- For the same class of consistency, higher amount of superplasticizer was needed for preparation of SCC mixture with fly ash.

- Applying fly ash instead of lime filler will reduce the strength of the concrete, but the drop is smaller if Sika Aer Solid is added to the concrete. The same trend was observed at 3 and 7 days, but the difference in strength decreases with age. Sika Aero Solid additionally influenced flowability and 'packing' of particles within concrete microstructure due its "ball bearing effect".

ACKNOWLEDGMENTS

REFERENCES

[1] P. Chindaprasirt et al, *Comparative study on the characteristics of fly ash and bottom ash geopolymers,* Waste Manage. 29 (2009) 539-54;

[2] X. Zhou et al., *Micromorphology and microstructure of coal fly ash and furnace bottom slag based light-weight geopolymer*, Const. Build. Mater. doi: 10.1016/j.conbuildmat.2020.118168;

[3] B. Lee et al., Evaluation of time to shrinkage-induced crack initiation in OPC and slag cement matrices incorporating circulating fluidized bed combustion bottom ash, Constr. Build Mater. 25 (2020) doi: 10.1016/j.conbuildmat.2020.119507;

[4] S. Lee et al., Effect of particle size distribution of fly ash-cement system on the fluidity of cement pastes, Cem Concr Res 33 (2003) 763-768.

[5] H. Nguyen et al., Effects of sulfate rich solid waste activator on engineering properties and durability of modified high volume fly ash cement based SCC, J Build. Eng. 20 (2018) 123-129;

[6] G. Barluenga et al. Effect of full scale pumping at early age and on hardened microstructure and properties of SCC with fly ash in hot-dry curing conditions, Constr. Build. Mater. 191 (2018) 128-1138.

[7] C. Shi et al., A review on mixture design methods for self-compacting concrete, Constr. Build. Mater. 84 (2015) 387–398; P.L. Domone, A review of the hardened mechanical properties of self-compacting concrete, Cem. Concr. Compos. 29 (2007) 1–12.

[8] Zhang, Z., Qian, S., Ma, H., Investigating mechanical properties and self-healing behavior of micro-cracked ECC with different volume of fly ash, Construction and Building Materials 52 (2014), pp. 17-23

[9] EFNARC, ERMCO, EFCA, CEMBUREAU, bibm: The European Guidelines for SCC:Specification, Production and Use; May 2005.

Marko Stojanović[1], *Lana Antić-Aranđelović*[2], *Ksenija Janković*[3], *Dragan Bojović*[4], *Ljiljana Lončar*[5]

UTICAJ RAZLIČITIH VRSTA VLAKANA NA ČVRSTOĆU PRI ZATEZANJU SAVIJANJEM

Rezime:

U radu je prikazan uticaj primene različitih vrsta vlakana u betonskim gredama na čvrstoću pri zatezanju savijanjem. Sve betonske grede su izrađene od istih komponentnih materijala i sastava, osim količine vlakana koja je varirana. Nakon očvršćavanja, betonskim gredama je sečenjem u središnjem delu smanjena visina na 125 mm. Merenje čvrstoće pri zatezanju savijanjem izvršeno je prema SRPS EN 14651. Na osnovu rezultata ispitivanja, u zavisnosti od vrste, oblika, količine i rasporeda vlakana, analizirane su vrednosti granične i preostale čvrstoće.

Ključne reči: mikroarmirani betoni, rezidualna čvrstoća pri zatezanju savijanjem

INFLUENCE OF DIFFERENT TYPES OF FIBERS ON FLEXURAL TENSILE STRENGTH

Summary:

The paper presents the influence of the application of different types of fibers in concrete beams on the flexural tensile strength. All concrete beams were made of the same component materials and composition, except for the amount of fiber, which is varied. After hardening, the height of the concrete beams in the central part was reduced to 125 mm by cutting. The measurement of flexural tensile strength by was performed according to SRPS EN 14651. Based on the test results, depending on the type, shape, quantity and distribution of fibers, the values of ultimate and residual strengths were analyzed.

Key words: fiber concrete, residual flexural tensile strength

---

[1] *Professional adviser, PhD candidate, IMS Institute, Belgrade, Serbia, marko.stojanovic@institutims.rs*
[2] *Senior technical associate,* MSCE, *IMS Institute, Belgrade, Serbia, lana.antic@institutims.rs*
[3] *Principal research fellow, IMS Institute, Belgrade, Serbia, ksenija.jankovic@institutims.rs*
[4] *Research associate IMS Institute, Belgrade, Serbia, dragan.bojovic@institutims.rs*
[5] *Professional adviser IMS Institute, Belgrade, Serbia, ljiljana.loncar@institutims.rs*

1. INTRODUCTION

Fiber reinforced concrete is a technique that has been investigated for several decades, mainly to reduce the cracking problem in certain special reinforced concrete structures such as tunnels, floors of industrial buildings, etc. [1], [2], [3], [4], [5], [6].

Concrete is typically brittle in nature and the rapid propagation of cracks under applied stress is responsible for its low tensile strength. One of the solutions to enhance its tensile strength and achieve ductile behaviour is to introduce steel and polypropylene fibres, resulting in fibre reinforced concrete (FRC) [7]. The tensile and flexural strengths of concrete can be substantially increased by fibre reinforcement which can effectively prevent the brittle propagation of cracks [8].

The idea driving FRC is that on the deformation of the matrix under stress, load is transferred to the fibres. Since the early 1960 s, there has been an increased interest in FRC. At that time, there were only a few research studies that described the basic concept of adding fibres to the concrete mix; however, its application was not discussed. Research on glass fibre was carried out in the UK, USA and Russia in the early 1950 s. However, glass fibre was found to be prone to alkaline attacks. The Portland Cement Association began their investigation on fibre reinforcement at the end of the 1950 s. The development of FRC gained momentum at this time and more advances were made in parallel with increasing applications. This led to the addition of a wide variety of fibres such as glass, carbon, steel, organic and polypropylene fibres to the concrete mix. During the 1950 s and 1960 s, the modern concept of addition of steel fibres was proposed from the first studies of Romualdi and Batson [9], [10] whose investigation was based on composite materials prepared from a cementitious material. The impact of this research was quite significant for the construction industry and prompted new research. Though the benefits conferred by the FRC had not been investigated, at that time steel fibre-reinforced concrete (SFRC) was used for the construction of pavements, which needed a high resistance to abrasion.

Model Code 2010 [11] permits the use of fiber-reinforced concrete in structural components. Its equations yield the values of residual flexural tensile strength ($f_{R,i}$), provided by fibers, particularly, those with crack openings of 0.5 mm ($f_{R,1}$) and 2.5 mm ($f_{R,3}$). Those values are obtained from a tensile stress curve – CMOD, on an empirical basis, as they are specific to each concrete.

The values of residual flexural tensile strength are strongly conditioned by the amount of fibers and by their orientation. In the case of orientation, it has been noted that the fibers work more efficiently when they are aligned in parallel to the tensile stress direction, and, in consequence, the greater the residual tensile strength of the concrete [12], [13].

This research aims to determine the limit of proportionality of LOP, as well as the residual flexure tensile strength ($f_{R,i}$) of samples reinforced with steel and polypropylene fibers.

Fiber-reinforced concrete has been used in our construction for years. The most common application is in the production of industrial floors where the use of steel fibers is established. However, the use of polypropylene fibers as a substitute for steel fibers is increasing. In this work, a three-point flexural strength test was performed on fiber-reinforced concrete beams. Concrete beams were made with Sika Fiber Force polypropylene fibers and steel fibers produced by Dramik and Spajić.

2. EXPERIMENTAL RESEARCH

2.1. MATERIALS USED IN THE EXPERIMENT

Fiber Reinforsed Concrete was made with ordinary Portland cement with added slag CEM II/A-S 42.5 R Našicecement. The limestone filler as a filler "Agro Hemik" was used as a mineral supplement. Natural fractionated stone aggregate of fractions 0/4, 4/8, 8/16, 16/32 mm from the Drina River was used. Polypropylene fibers with a length of 60 mm and a diameter of 0.84 mm manufactured by "SikaFiber Force" in the amount of 2, 3 and 4 kg/m3 were used in this research. Steel fibers with hooks at the ends in quantities of 20 kg/m3, manufactured by "Dramix 3D" with a length of 60 mm and a diameter of 0.75 mm and manufactured by "Spajić" with a length of 50 mm and a diameter of 1.05 mm, were used.

Chemical composition of cement and limstone is provided in Table 1.

Table 1 - Chemical compositions of cement,

Oxide	Content, %	
	Cement	Limestone
SiO_2	21.85	1.07
Al_2O_3	5.73	0.39
Fe_2O_3	2.26	0.06
CaO	60.13	54.54
MgO	3.11	0.77
$Na2O$	0.30	0.01
K_2O	0.79	0.06
SO_3	3.18	0.02
P_2O_5	0.14	0.01
Mn_2O_3	0.34	0.003
TiO_2	0.27	0.009
Cl	0.060	0.001
Cr_2O_3	0.02	0.001
LoI at 1000°C	1.62	42.88

The appearance and type of the fibers are shown in Figure 1.

a) polypropylene fiber　　*b) steel fiber*　　*c) steel fiber*
"SikaFiber Force"　　　*"Dramix 3D"*　　　*"Spajić"*
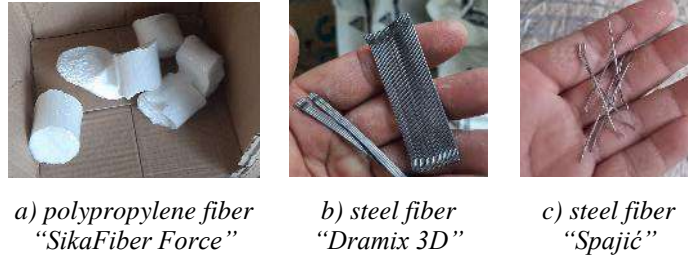
Figure 1 – The appearance and type of the fibers

Basic characteristics of fibers are showed in Table 2.

Table 1 - Basic characteristics of fibers

Material properties	SikaFiber Force	3D Dramix 80x60 BG	Spajic ZS/N 1,05x50
Fiber Type	Polypropylene	Steel	Steel
Fiber shape	Straight embossed fibres	Straight hooked ends	Straight hooked ends
Bundling	Bundled	Glued	Loose
Length l [mm]	60	60	50
Diameter d [mm]	0.84	0.80	1.05
Aspect ratio (l/d)	0.71	0.75	0.47
Tensile strength [N/mm^2]	465	1225	1250
Modulus of elasticity [GPa]	7.5	200	200

2.2. CONCRETE MIXTURE

Six mixtures of three-fraction concretes were prepared for this experiment.

Fresh concrete was designed to meet the minimum of required properties of concrete, according to EN 206 standard [12]. The appearance of fresh concrete with polypropylene fibers is shown in Figure 2.

Figure 2 – The appearance of fresh concrete with polypropylene fibers

The mixtures are designed to meet the following criteria: Slump 160-210 mm and Air content 1-3%. All types of concrete were made with w/c=0.524. Fiber reinforced concrete compositions are showen in Table 3.

Table 3 – Fiber reinforced concretes compositions

Sample No.	Share of the componential material, kg/m³					
	MIX 0	MIX 1	MIX 2	MIX 3	MIX 4	MIX 5
Cement	315	315	315	315	315	315
River 0/4 mm	843	843	843	843	843	843
River 4/8mm	367	367	367	367	367	367
River 8/16mm	623	623	623	623	623	623
Mineral supplement	61	61	61	61	61	61
Admixture Sika Viscocrete 4077x	1.8	1.8	1.8	1.8	1.8	1.8
Water	168	168	168	168	168	168
Polypropilene SikaForce Fiber	-	2	3	4	-	-
Steel fiber Dramix	-	-	-	-	20	-
Steel fiber Spajić	-	-	-	-	-	20
Bulk density	2379	2381	2382	2383	2399	2399

3. RESULTS AND DISCUSSION

3.1. FLEXURE TENSILE STRENGTH

For the purposes of testing the flexure tensile strength of fiber-reinforced concrete, samples were made in the form of beams with dimensions of 150x150x600 mm³. Concrete with fibers was compacted with a vibrating needle in metal molds that hardened in water at a temperature of +20°C until the moment of testing according to the SRPS EN 12390-2 standard. The flexural tensile strength of concrete was tested at the age of 28 days according to SRPS EN 14651:2009 [15]. Before testing, the beams were cut with a diamond saw to a depth of 25 mm and a width of 5 mm from the underside of the beam.

The rate of loading CMOD (crack opening displacement) was 0.05 mm/min until CMOD=0.1 mm, then CMOD=0.2 mm/min until CMOD=4 mm, when the test ended.

After the test, force values were obtained on the basis of which we calculate the Limit of Proportionality (LOP) and residual tensile strength at the crack opening of CMOD=0.05; 0.5; 1.5; 2.5; 3.5 mm according to the following equation:

$$f_{ct,L}^{f} = \frac{3F_L L}{2bh_{sp}^2} \qquad (1)$$

where:

$f_{ct,L}^{f}$ is the LOP, in Newton per square millimetre;

F_L is the span length, in millimetres;

b is the width of the specimen, in millimetres;

h_{sp} is the distance between the tip of the notch and the top of the specimen, in millimetres.

The position of the beam before the test is shown in Figure 3.

Figure 3 – The position of the beam before the Flexure Tensile Strength according SRPS EN 14651

After testing the concrete beams for flexure, the values of the limit of proportionality LOP - $f_{ct,L}$ and residual tensile strength for bending from $f_{R,1}$ to $f_{R,4}$ are shown in Table 4.

Table 4 – The results of Flexure strength of concrete beams

Sample No.	Limit of proportionality - LOP (N/mm^2) $f_{ct,L}$	Residual flexural tensile strength (N/mm^2) $f_{R,1}$	Residual flexural tensile strength (N/mm^2) $f_{R,2}$	Residual flexural tensile strength (N/mm^2) $f_{R,3}$	Residual flexural tensile strength (N/mm^2) $f_{R,4}$
MIX 0 - without fibers	3.833	0.819	0.208	0.089	0.000
MIX 1 - SFF - 2kg	4.301	1.482	1.299	1.102	0.994
MIX 2 - SFF - 3kg	4.887	1.767	1.553	1.414	1.261
MIX 3 - SFF - 4kg	6.140	2.805	2.696	2.572	2.320
MIX 4 - 3D DMX - 20 kg	5.404	5.864	5.833	5.714	5.410
MIX 5 - SPJ - 20 kg	5.284	5.503	2.347	2.435	2.256

The resulting diagram of flexural tensile strength - crack mouth opening displacement is shown in Figure 4.
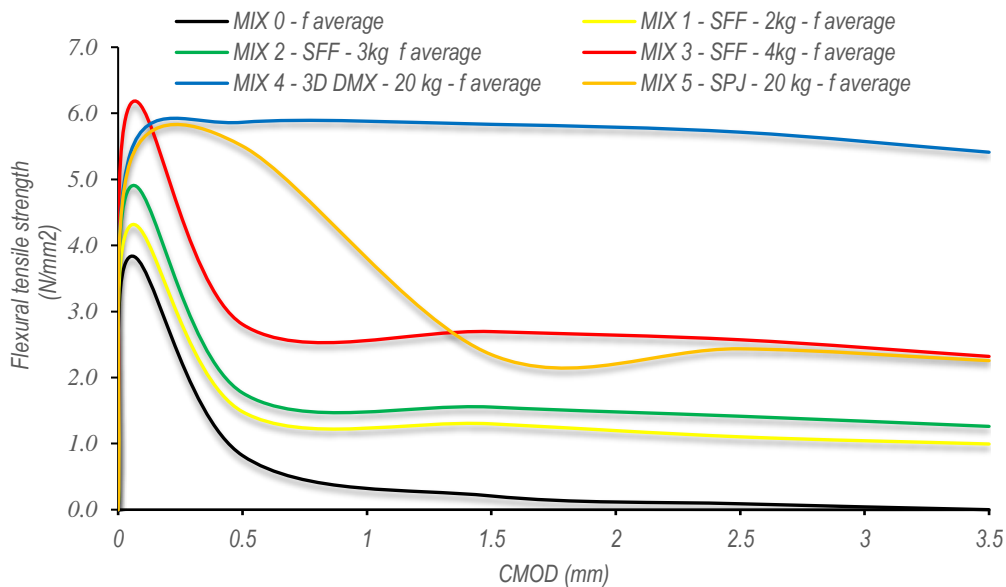
Figure 4 – Diagram of flexural tensile strength - crack mouth opening displacement

After the first peak or burst occurred, the stress suddenly dropped for the fiberless MIX - 0 samples (Figure 4).

Concrete beams MIX 1, MIX 2, MIX 3, which are made with concrete reinforced with polypropylene fibers with a content of 2, 3 and 4 kg/m3, the appearance of all three curves shown in the diagram have the same shape, Figure 4.

The obtained flexural tensile strength values $f_{ct,L}$ for concrete reinforced with polypropylene fibers are higher by 14% MIX 2 - SFF-3kg and by 43% MIX 3 - SFF - 4kg compared to MIX 1 - SFF - 2kg shown in Figure 4. With increasing the amount of polypropylene fibers, higher flexural tensile strength results were obtained.

3D Dramix steel fibers have a aspect ratio of 0.75, while this ratio for Spajic ZS/N steel fibers is 0.47.

Concrete beams with steel fibers reinforced MIX 4 - 3D DMX - 20 kg, achieved higher flexural tensile strength values $f_{ct,L}, f_{R,1}, f_{R,2}, f_{R,3}$, and $f_{R,4}$ by 2%, 7%, 149%, 135% and 140% compared to MIX 5 - SPJ - 20 kg respectively.

Based on the test results of fiber-reinforced concrete beams, the highest flexural tensile strength values were obtained for beams marked MIX 3 - SFF - 4kg, MIX 4 - 3D DMX - 20 kg and MIX 5 - SPJ - 20 kg.

By comparing the results of the flexural tensile strength test fct,L, we found that the concrete reinforced with polypropylene fibers a aspect ratio of 0.71 MIX 3 - SFF - 4kg achieved higher results by 14% and 16% compared to steel fibers reinforced concrete beams MIX 4 - 3D DMX - 20 kg and MIX 5 - SPJ - 20 kg.

However, higher residual flexural tensile strengths $f_{ct,L}$, $f_{R,1}$, $f_{R,2}$, $f_{R,3}$, and $f_{R,4}$ were obtained for concrete beams reinforced with steel fibers aspect ratio of 0.75 MIX 4 – 3D DMX - 20 kg by 109%, 116%, 122% and 133% compared to MIX 3 - SFF - 4kg, respectively.

After testing, the best fiber arrangement on the fractured side was obtained with 3D Dramix and SikaFiber Force fibers. The appearance and arrangement of fibers on the broken cross-section of the beam is shown in Figure 5.

a)   b)
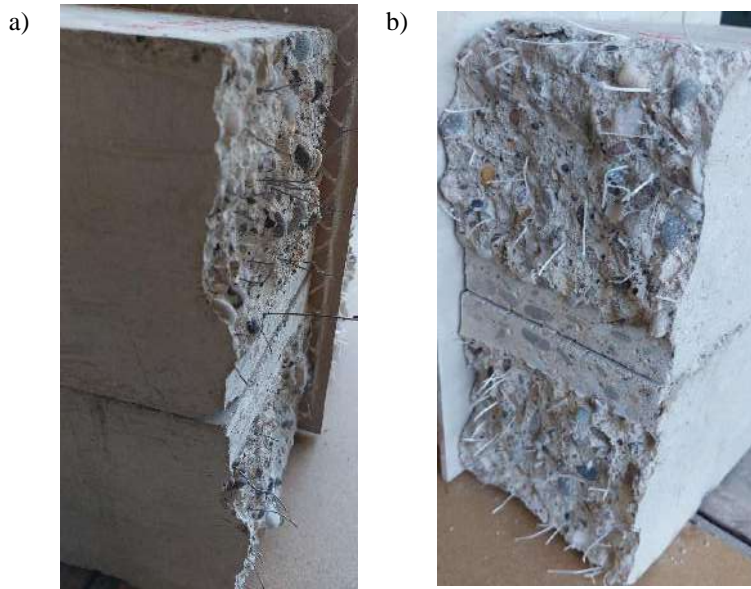
Figure 5 – The appearance and arrangement of fibers on the broken cross-section of the beam: a) 3D Dramix-20kg/m³, b) SikaFiber Force – 4kg/m³

4. CONCLUSIONS

By determining the content of polypropylene and steel fibers, which achieves an average residual flexural tensile strength of at least 1.5 MPa at a CMOD of 0.5 mm and an average residual flexural tensile strength of at least 1 MPa at a CMOD of 3.5 mm, fiber-reinforced concrete is considered to meet the requirements of SRPS EN 14845 -2 .

Fiber-reinforced concrete beams MIX 2 to MIX 5 meet the requirements of SRPS EN 14845-2.

Based on the testing of fiber-reinforced concrete beam MIX 1 SikaFiber Force - 2 kg/m3 achieved lower values than the required average residual flexural tensile strength of 1.482 MPa < 1.5 MPa at CMOD of 0.5 mm, and average residual flexural tensile strength of 0.994 MPa < 1.0 MPa.

The highest value of the LOP proportionality limit was obtained with concrete beams MIX 3 - SikaFiber Force of 4kg/m3, $f_{ct,L}$ = 6,140 N/mm2.

The highest residual strength values were obtained with concrete beams MIX 4 - 3D DMX - 20 kg/m3, that too: $f_{R,1}=5.864$ N/mm^2, $f_{R,2}=5.833$ N/mm^2 , $f_{R,3}=5.714$ N/mm^2 and $f_{R,1}=5.410$ N/mm^2.

We can conclude that all fiber-reinforced concrete beams meet the requirements of SRPS EN 14651 and have achieved a residual flexural tensile strength of at least 1.5 MPa at a CMOD of 0.5 mm and an average residual flexural tensile strength of at least 1 MPa at a CMOD of 3.5 mm, except for the beams MIX 1 – SikaFiber Force – 2kg/m^3, which does not meet the stated requirements of the standard.

ACKNOWLEDGMENTS

REFERENCES

[1] J. Tejchman, J. Kozicki, Experimental and Theoretical Investigations of Steel-Fibrous Concrete, Springer, 2010, p. 293. ISBN 978-3-642-14602-2.;

[2] S.A. Ahmed, Properties and mesostructural characteristics of linen fiber reinforced self-compacting concrete in slender columns, Ain Shams Eng. J. 4 (2013) 155–161.;

[3] W. Abbass, M.I. Khan, S. Mourad, Evaluation of mechanical properties of steel fiber reinforced concrete with different strengths of concrete, Constr. Build. Mater. 168 (2018) 556–569.;

[4] E. Ayan, ¨O. Saatçiog˘lu, L. Turanli, Parameter optimization on compressive strength of steel fiber reinforced high strength concrete, Constr. Build. Mater. 25 (2011) 2837–2844.;

[5] M.A. Alhassan, R.Z. Al Rousan, E.A. Al Shuqari, Bond-slip behavior between fiber reinforced concrete and CFRP composites, Ain Shams Eng. J. (2019);

[6] A. Sofi, B.R. Phanikumar, An experimental investigation on flexural behaviour of fibre-reinforced pond ash-modified concrete, Ain Shams Eng. J. 6 (2015) 1133–1142;

[7] Harvinder S. Steel fiber reinforced concrete: behavior, modelling and design. Springer Singapore. 2017. Google Scholar;

[8] P.K. Mehta, P.J.M. Monteiro Concrete: microstructure, properties, and materials (3d ed.), McGraw Hill Professional, New York (2005) Google Scholar;

[9] J.P. Romualdi, G.B. Batson, Behavior of reinforced concrete beams with closely spaced reinforcement, ACI Journal Proceedings, Vol. 60 (No. 6) (1963), pp. 775-790,

[10] J.P. Romualdi, J.A. Mandel, Tensile strength of concrete affected by uniformly distributed and closely spaced short lengths of wire reinforcement, ACI Journal Proceedings, Vol. 61 (No. 6) (1964), pp. 657-672,

[11] International Federation for Structural Concrete, Model code for concrete structures, FIB Bulletin 65, Lausanne, Switzerland, 2010. Google Scholar

[12]   A. Orbe, J. Cuadrado, R. Losada, E. Rojí: Framework for the design and analysis of steel reinforced self-compacting concrete structures, Constr. Build. Mater., 35 (2012), pp. 676-686

[13]   T. Plagué, C. Desmettre, J.P. Charron, Influence of fibre type and fiber orientation on cracking and permeability of reinforced concrete under tensile loading, Cem. Concr. Res., 94 (2017), pp. 59-70

[14]   EN 206: 2013 + A2:2021 – Concrete. Specification, performance, production and conformity

[15]   SRPS EN 14651:2009 - Test method for metallic fibre concrete - Measuring the flexural tensile strength (limit of proportionality (LOP), residual)

Tiana Milović[1], Mirjana Malešev[2], Vlastimir Radonjanin[3]

UTICAJ LETEĆEG PEPELA KAO SCM NA OGRANIČENO SKUPLJANJE REPARATURNOG CEMENTNOG MALTERA

Rezime:

U ovom radu su prikazani rezultati sopstvenog eksperimentalnog istraživanja ograničenog skupljanja reparaturnih maltera koji sadrže leteći pepeo kao SCM. Reparaturni malteri su spravljeni sa dva različita vodovezivna faktora. Portland cement je zamenjen sa 0%, 10% i 20% letećeg pepela. Pri starosti od 28 dana, „sanirani" uzorci su stavljeni na kondicioniranje u skladu sa EN 12617-4, a potom je određena čvrstoća prianjanja reparaturnih maltera putem pull-off metode. Na osnovu dobijenih rezultata utvrđeno je da su svi malteri ispunili uslov za konstrukcijske reparaturne maltere klase R4 prema EN 1504-3 sa aspekta ograničenog skupljanja.

Ključne reči: leteći pepeo, reparaturni malter, ograničeno skupljanje, prionljivost

EFFECT OF FLY ASH AS SCM ON RESTRAINED SHRINKAGE OF REPAIR CEMENT MORTAR

Summary:

This paper presents the results of an own experimental study of the restrained shrinkage of repair mortars containing fly ash as SCM. Repair mortars were prepared with two different water-to-binder ratios. Portland cement was substituted with 0%, 10% and 20% fly ash. At the age of 28 days, the "repaired" specimens were conditioned in accordance with EN 12617-4 and, afterwards, the bond strengths of repair mortars were determined by pull-off test. Based on the obtained results, it was concluded that all mortars met the requirement for structural repair mortar class R4 according to EN 1504-3 in a term of restrained shrinkage.

Key words: fly ash, repair mortar, restrained shrinkage, bond strength

---

[1] *PhD, Research Associate, Faculty of Technical Sciences, University of Novi Sad, Serbia, tiana.milovic@uns.ac.rs*

[2] *dr, Full Professor, Faculty of Technical Sciences, University of Novi Sad, Serbia, miram@uns.ac.rs*

[3] *dr, Full Professor, Faculty of Technical Sciences, University of Novi Sad, Serbia, radonv@uns.ac.rs*

1. INTRODUCTION

The bond between the old concrete and the new-repair mortar/concrete usually presents a weak link in the repaired structure. Cracking due to restrained shrinkage represents one of the major durability problems for repaired concrete structures. Besides the fact that cracking may cause excessive deflections which may limit the serviceability of structures, cracks also allow ingress of water and aggressive chemicals into concrete which leads to accelerated corrosion of reinforcing steel [1]. Therefore, the bond strength between repair material and concrete substrate represents the primary condition for a successfully performed repair. In the standard EN 1504-3 [2] are given the requirements that repair mortars have to satisfy to be detected under one of the four classes of repair mortars. One requirement relates to the restrained shrinkage of repair mortar tested in accordance with EN 12617-4 [3]. Based on the published results, only one paper has been found dealing with restrained shrinkage of repair mortar in accordance with EN 12617-4 [3]. Schuab et al. [4] evaluated the performance of metakaolin/blast furnace slag alkali-activated materials as repair mortars under free shrinkage test according to EN 12617-4 [3], but also the restrained shrinkage test according to: (i) EN 12617-4 [3] - some changes were made to the standard procedure, and (ii) ASTM C 1579 [5] - ring test.

As it is known, repair mortars may contain supplementary cementitious materials (SCMs). The advantages of using fly ash (FA) as an artificial/waste pozzolanic material for the aforementioned purposes, are certainly sustainable development, easy availability (200 million tons of FA is deposited in landfills in Serbia [6] and the existence of harmonized European standards for its application. A very few studies have been performed dealing with the effects of FA as SCM on performances of repair mortars [7-10] while the restrained shrinkage of repair cement mortars containing FA as SCM and applied on concrete substrate, in accordance with standard EN 12617-4 [3] has not been studied yet. Just few authors investigated the effect of FA as SCM on restrained shrinkage, but only in the case of the concretes (not as repair material) by ring tests. Altoubat et al. [11] examined the effectiveness of FA on the restrained shrinkage cracking resistance of self-compacting concrete in accordance with AASHTO PP34 [12] and ASTM C 1581 [13], and founded that the cracking potential for the self-compacting concrete mixes was affected significantly by the type and proportion of SCMs, curing regime and degree of restraint. Lee et al. [14] investigated the effect of dune sand on drying shrinkage cracking of FA concrete in accordance with ring test ASTM C 1581 [13]. Based on the results of restrained drying shrinkage cracking, the mixtures with a dune sand/FA ratio of 20% showed the highest crack resistance, which was 24% higher than the lowest crack resistance.

In order to determine the effect of FA as SCM on restrained shrinkage of repair cement mortars applied on reference concrete substrate, in accordance with EN 12617-4 [3], an own experimental research was realized. This paper deals with the adhesive bond strength between repair cement mortars containing 0%, 10% and 20% FA (made with two different water-to-binder ratios) and concrete substrate, after 28 days of adequate "repaired" specimens' curing and 56 days of additional storing.

2. MATERIALS AND METHODS

2.1. MORTAR AND REFERENCE CONCRETE CONSTITUENTS

In order to examine the effect of FA as SCM on restrained shrinkage of the repair blended cement mortars previously applied on reference concrete substrate, by pull-off method, the following component materials were used for the repair mortars preparation:
- Ordinary Portland cement CEM I 42.5R (Lafarge-BFC Serbia),
- FA from thermal power plant Nikola Tesla B,
- CEN standard sand, in accordance with EN 196-1 [15],
- Superplasticizer (HRWRA) (SikaViscoCrete 3070, Sika Switzerland),
- Deionized water.

For the preparation of the reference concrete substrates, the following component materials were used:
- Ordinary Portland cement CEM I 42.5R (Lafarge-BFC Serbia),
- Natural fractionated aggregate of river origin (fractions: 0-4 mm and 4-8 mm),
- Superplasticizer (HRWRA) (SikaViscoCrete 4000BP, Sika Switzerland),
- Tap water.

The rapid hardening two component epoxy adhesive (Sikadur 31 EF) was used for the gluing the dollies to the previously adequately prepared surface of "repaired" specimen.

True densities of PC (3.126 g/cm^3) and FA (2.313 g/cm^3) were determined in accordance with SRPS B.B8.032 [16], while the specific surface of PC (4188.6 cm^2/g) and FA (10212.5 cm^2/g) were determined in accordance with the procedure specified in standard SRPS B.C8.024 [17]. The FA activity index was determined in accordance with the standard EN 450-1 [18], and after 28 and 90 days FA activity indexes were 125 % and 131 %, respectively.

The chemical composition of FA was determined by X-ray fluorescence (XRF) spectroscopy. The instrument used for the XRF analysis is an ED-XRF spectrometer, manufacturer Spectro Xepos from Germany. The system uses a Silicon Drift Detector (SDD), band-pass filter and focuses the X-rays from a binary Co/Pd alloy thicktarget anode (50 W/60 kV) combining polarized/direct excitation. Sample tray used for these measurements was with rotating positions for pellets. Measurements were carried out in vacuum atmosphere and Spectro XRF Analyzer Pro software was used. The sample for ED-XRF analysis was prepared in accordance with the pressed powder method. Tested materials (5 g) and binding agent (Cereox wax, Fluxana) were mixed (1 g) and the 32 mm diameter pellet was formed. The pellet was formed under 10 tones load applied via a laboratory hydraulic press. The loss on ignition (LOI) of FA was determined after exposing the sample in the amount of 2 g, to a temperature of 950 °C for 1 h. The obtained results are shown in Table 1.

Table 1 – Chemical composition of FA

Chemical composition of FA (%)								
Na$_2$O	MgO	Al$_2$O$_3$	SiO$_2$	P$_2$O$_5$	SO$_3$	Cl	K$_2$O	LOI
0.329	2.941	22.256	45.255	0.084	3.113	0.000	1.130	
CaO	TiO$_2$	Cr$_2$O$_3$	Mn$_2$O$_3$	Fe$_2$O$_3$	ZnO	SrO	BaO	2.3
10.464	1.442	0.080	0.234	10.073	0.116	0.087	0.140	

Since the sum of SiO_2, Al_2O_3, and Fe_2O_3 oxides of the tested sample is higher than 70% (77.584 %), FA belongs to the type II addition in accordance with EN 206 [19] and EN 450-1 [18]. Based on the obtained value of the LOI, FA belongs to category A prescribed by standard EN 450-1 [18].

Mineralogical analysis of FA was performed by XRD analysis (Philips PW1710 device) under the following experimental conditions: monochromatic Cu Kα radiation with 1.5418 Å wavelength in the 5–55° of 2θ range, scan rate 0.02° and 0.5s per step, at a voltage of 40 kV and a current of 30 mA.

According to the XRD analysis results (Fig. 1) the following minerals are presented in FA sample: quartz, mullite, feldspar, melilite, magnesite, magnetite and ankerite.
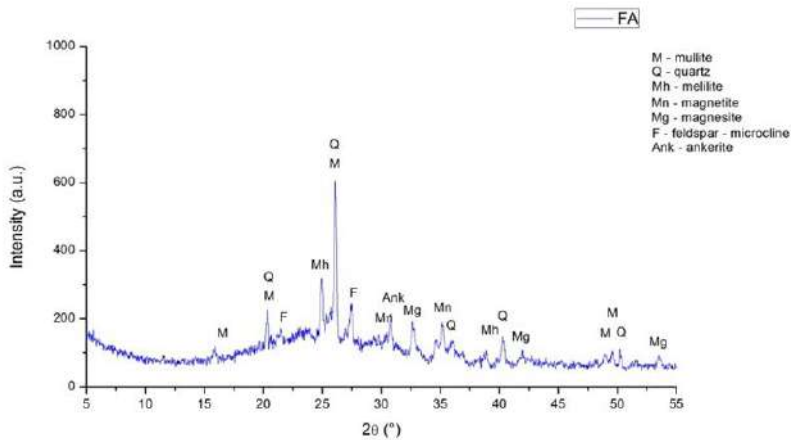
Figure 1 - XRD diffractogram of FA

2.2. REFERENCE CONCRETE SUBSTRATE

For the purpose of evaluation the restrained shrinkage of the potential repair mortar, at first, the concrete substrates with reproducible surface texture and appropriate strength had to be made and properly cured in accordance with EN 1766 [20]. In this case, standard EN 1504-3 [2] prescribes the usage of concrete substrate, type MC (0.40). Recommendations for concrete mix composition, type MC (0.40) and required properties for hardened concrete, in accordance with EN 1766 [20], as well as adopted concrete mix proportion are given in Table 2.

Total of 7 concrete substrates (350x350x50mm) and three standard cubes (150x150x150mm) were prepared and cured in moulds under polyethylene sheeting for 24 h after casting, at (20 ± 2)°C. After that, they were demoulded (Fig. 2) and cured for 27 days underwater at (20 ± 2)°C, in accordance with standard EN 1766 [20].

After 28 days, the cubes were used for determination of concrete compressive strength. The obtained mean value of 67.95 MPa satisfied required class C 50/60 according to EN 206 [19].

At the age of 28 days, the bottom face of concrete specimens were, at first, prepared by sand-blasting, and then the specimens were stored under normal laboratory conditions, at (21 ± 2)°C and (60 ± 10)% relative humidity, until the age of 3 months. One concrete substrate was used for the determination of surface tensile strength by pull-of test according to EN 1542 [21], immediately before application of mortars on the remaining substrates. The achieved mean

value of 5.87 MPa, met the requirement for minimum surface tensile strength of 3.0 MPa. The remaining 6 concrete substrates were used for application of six different types of repair mortars (one type of mortar per concrete substrate - 10 measuring places per "repaired" substrate).

Table 2 – Recommendations for concrete type MC (0.40) composition with required properties and adopted concrete mix proportion

Required properties in accordance with EN 1766		Adopted concrete mix proportion	
Concrete type	MC(0.40)	Mix proportion for 1 m^3 of concrete	
Maximum aggregate size (mm)	8	Aggregate (kg) Fractions 0-4mm & 4-8mm	1650
Water/cement ratio	0.40	Tap water (kg)	179
Cement content (kg/m^3)	455	Cement (kg)	455
28 day mean compressive strength	to satisfy class C50/60	Superplasticizer (HRWRA+SRA) SikaViscoCrete 4000BP (g)	4.55
Minimum required surface tensile strength (MPa)	3.0		

Figure 2 - Reference concrete substrates after demoulding

2.3. REPAIR MORTARS

Six different cement/cement-based potential repair mortars were made with 0%, 10% and 20% of FA as SCM, by mass, to determine the restrained shrinkage by pull-off method. Mortar mixtures were prepared with two water-to-binder ratios, 0.4 and 0.5 according to EN 12190 [22]. Composition of mortar mixtures is shown in Table 3. Superplasticizer (HRWRA) SikaViscoCrete 3070 was added just in mortar mixtures with a lower water-to-binder ratio.

Mortar mixtures were applied on adequately prepared concrete substrates, in a layer with thickness of 25 mm, Figure 3. These six specially prepared ("repaired") specimens were cured in accordance with recommendations given in EN 12617-4 [3]: 24 h in moulds and 27 days underwater at $(21 \pm 2)°C$.

Table 3 – Composition of repair mortar mixtures

Repair mortar mix proportions						
	PCa	FA10a	FA20a	PCb	FA10b	FA20b
CEM I 42.5 R (g)	450	405	360	450	405	360
FA (g)	-	45	90	-	45	90
Standard sand (g)	1350	1350	1350	1350	1350	1350
Deionized water (g)	225	225	225	180	180	180
Superplasticizer (g)	-	-	-	5.4	5.4	5.4
w/b ratio	0.5	0.5	0.5	0.4	0.4	0.4

Figure 3 - Repair mortars placed on concrete substrates

2.4. METHODS

After 28 days of recommended curing regime, six "repaired" specimens were stored in the standard laboratory climate at $(21 \pm 2)°C$ and $(60 \pm 10)\%$ relative humidity for next 56 days (the storage period) in accordance with EN 12617-4 [3], and then the adhesive bond strengths between repair mortars and concrete substrate were examined in accordance with EN 1542 [21]. As pull-off test equipment, Dyna Z16 pull-off tester (Proceq SA Switzerland) was used. Based on the obtained results, the classes of repair mortars were determined according to the criteria given in the standard EN 1504-3 [2], in term of the restrained shrinkage.

In accordance with EN 12617-4 [3] "repaired" specimen (mortar applied on the half of the substrate) per repair mortar type was tested to determine the control values for pull-off strength after 28 days in accordance with EN 1542 [21], and the obtained results were presented by Milović et al. [10].

3. RESULTS AND DISCUSSION

3.1. VISUAL INSPECTION OF THE TEST SURFACE

Upon completion of the storage period (56 days), the "repaired" specimens were inspected for evidence of cracking (maximum permissible average crack width ≤ 0.05 mm with no crack ≥ 0.1 mm) or delamination. Based on the visual inspection results, Figures 4 and 5, the delamination of mortar layer from concrete substrate or/and delamination/cracking in mortar layer were not noticed, therefore all mortars met the requirement for repair mortars in a term of restrained shrinkage according to EN 1504-3 [2].

Figure 4 - "Repaired" specimens look after the storage period (mortars prepared with w/b=0.5): left – PCa, middle – FA10a, right – FA20a

Figure 5 - "Repaired" specimens look after the storage period (mortars prepared with w/b=0.4): left – PCb, middle – FA10b, right – FA20b

3.2. BOND STRENGTH AFTER THE STORAGE PERIOD IN ACCORDANCE WITH EN 12617-4

Mean bond strength values (f_{hm}) for the dominant type of failure of "repaired" specimens, as well as photos of representative dollies after pull-off tests, are shown in Table 4. During the visual inspection, it was noticed that failures had occurred through the mortar layer (type B – cohesion failure in mortar layer). Just in one case failure had partly occurred between the dolly and the adhesion layer (type Y/Z), therefore the result did not take into account. The loads at failure type B were accepted as valid, according to EN 1542 [21].

All types of applied mortars had mean bond strength higher than 2.00 MPa, Figure 6, and for that reason they fulfilled the requirement for structural repair mortars of class R4 in a term of restrained shrinkage in accordance with standard EN 1504-3 [2]. The range of the bond strength was from 4.50-4.70 MPa for mortars made with w/b=0.5 and from 5.22-5.47 MPa in the case of mortars made with w/b=0.4.

Table 4 – Mean bond strength values of "repaired" specimens for the dominant type of failure after the storage period

Mortars prepared with w/b=0.5			Mortars prepared with w/b=0.4		
Type of mortar	Photo of representative dolly	f_{hm} (MPa)	Type of mortar	Photo of representative dolly	f_{hm} (MPa)
PCa		4.70	PCb		5.42
FA10a		4.67	FA10b		5.22
FA20a		4.50	FA20b		5.47
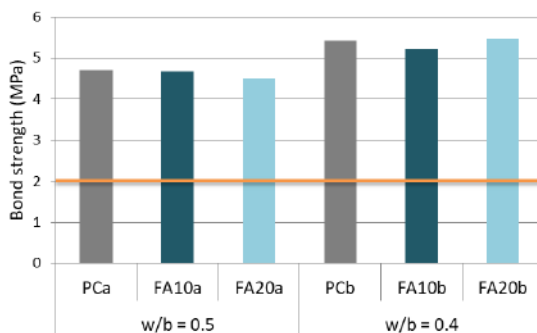
Figure 6 - Repair mortars' adhesive bond strength

The relative bond strengths of the mortars are presented in Figures 7.
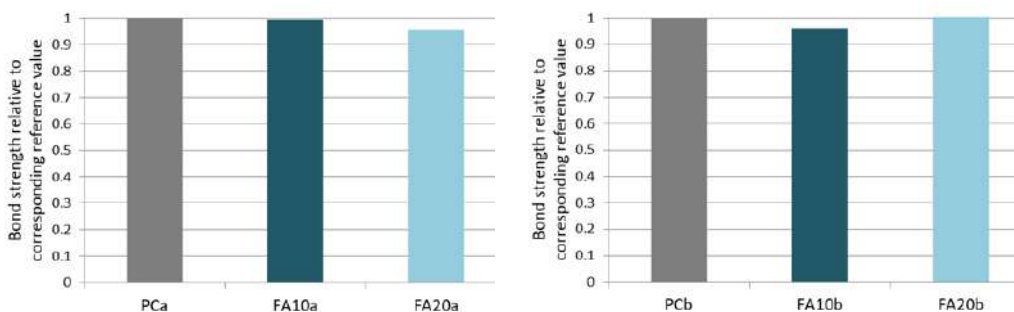
Figure 7 - Bond strength of repair mortars (left - w/b=0.5; right - w/b=0.4) relative to corresponding reference value

447

With the applied water-to-binder ratio of 0.5 (Fig. 7 - left), repair mortars containing 10% and 20% FA as SCM had lower bond strength by 0.6% and 4.3% compared to the reference value, respectively.

In the case of the mortars made with a water-to-binder ratio of 0.4 (Fig. 7 - right), the bond strength of mortar containing 10% FA was lower by 3.7% compared to the reference value, while the bond strength of mortar containing 20% FA was higher by 0.9%. Since the changes in the bond strength were less than 5%, it can be concluded that the level of substitution of PC with FA (up to 20%) did not affect the restrained shrinkage, but the value of the applied water-to-binder ratio. With the reduction of the water-binder ratio, the bond strength of reference mortar increased by 15%, while in the case of mortars with 10% and 20% FA the bond strengths increased by 12% and 22%, respectively.

4. CONCLUSION

Based on the analysis of the obtained experimental results, in a term of the restrained shrinkage of the repair mortars according to EN 12617-4 [3], the following can be concluded:

- According to the visual inspection results, the delamination of mortar layer from concrete substrate or/and delamination/cracking in mortar layer were not noticed, therefore all mortars met the requirement prescribed in EN 1504-3 [2] for repair mortars in a term of restrained shrinkage;
- With mean bond strength values higher than 2.00 MPa, all tested mortars (containing 0%, 10% and 20% fly ash as SCM, and made with water-to-binder ratio of 0.5 or 0.4) fulfilled the requirement for structural repair mortar of class R4 in a term of the restrained shrinkage, in accordance with EN 1504-3 [2];
- The level of Portland cement substitution with fly ash (up to 20%) did not affect the restrained shrinkage, but the value of the applied water-to-binder ratio;
- With the reduction of the water-binder ratio, there was an increase in the adhesion bond strength, i.e. the bond strength of reference mortar increased by 15%, while in the case of mortars with 10% and 20% fly ash by 12% and 22%, respectively.

REFERENCES

[1] Tongaroonsri S, Tangtermsirikul S. Effect of mineral admixtures and curing periods on shrinkage and cracking age under restrained condition, Construction and Building Materials, 23, 2009, 1050–1056.

[2] BS EN 1504-3:2005 - Products and systems for the protection and repair of concrete structures - Definitions, requirements, quality control and evaluation of conformity - Part 3: Structural and non-structural repair.

[3] BS EN 12617-4:2002 - Products and systems for the protection and repair of concrete structures - Test methods - Part 4: Determination of shrinkage and expansion.

[4] Schuab M.R, dos Santos W.J, Borges P.H.R. On the development of MK/BFS alkali-activated materials as repair mortars: Performance under free and restrained shrinkage tests, Construction and Building Materials, 275, 2021, 122109, 1-14.

[5] ASTM C 1579 - Standard Test Method for Evaluating Plastic Shrinkage Cracking of Restrained Fiber Reinforced Concrete, 2006.

[6] Dragaš J, Marinković S, Ignjatović I, Tošić N. Properties of high-volume fly ash concrete and its role in sustainable development, in Conference: Contemporary achievements in civil engineering, Subotica, 2014, 849-858.

[7] Saraswathy V, Song H.-W. Evaluation of Cementitious Repair Mortars for Corrosion Resistance, Portugaliae Electrochimica Acta, 26, 2008, 417-432.

[8] Shi J, Liu B, Qin J, Jiang J, Wu X, Tan J. Experimental study of performance of repair mortar: Evaluation of in-situ tests and correlation analysis, Journal of Building Engineering, 31, 2020, 101325.

[9] Milović T, Malešev M, Radeka M, Radonjanin V. Thermal compatibility of repair mortars based on fly ash as SCM according to EN 13687-1, in Conference: Construction Materials for a Sustainable Future-COMS, Bled, Slovenia, 2021, 235-243.

[10] Milović T, Malešev M, Radeka M, Radonjanin V. Effect of fly ash as SCM on repair mortars' bond strength in accordance with EN 1542, in Conference: Planning, design, construction and Building Renewal - INDIS 2021, Novi Sad, 2021, 717-724.

[11] Altoubat S, Junaid M.T, Leblouba M, Badran D. Effectiveness of fly ash on the restrained shrinkage cracking resistance of self-compacting concrete, Cement and Concrete Composites, 79, 2017, 9-20.

[12] Standard Practice for Estimating the Crack Tendency of Concrete. AASHTO Designation PP 34-89.

[13] ASTM C 1581, Standard Test Method for Determining Age at Cracking and Induced Tensile Stress Characteristics of Mortar and Concrete under Restrained Shrinkage, 2004.

[14] Lee E, Ko J, Yoo J, Park S, Nam J. Effect of Dune Sand on Drying Shrinkage Cracking of Fly Ash Concrete, Applied Sciences, 12, 2022, 3128.

[15] SRPS EN 196-1:2008 - Methods of testing cement - Part 1: Determination of strength.

[16] SRPS B.B8.032:1980 - Testing of natural stone - Determination of bulk density, density, coefficient of density and porosity.

[17] SRPS B.C8.024:1964 - Determination of specific surface of Portland cements.

[18] BS EN 450-1:2012 - Fly ash for concrete Definition, specifications and conformity criteria.

[19] SRPS EN 206:2021 - Concrete - Specification, performance, production and conformity.

[20] BS EN 1766:2000 - Products and systems for the protection and repair of concrete structures - Test methods - Reference concretes for testing.

[21] SRPS EN 1542:2010 - Products and systems for the protection and repair of concrete structures - Test methods - Measurement of bond strength by pull-off.

[22] BS EN 12190:1999 - Products and systems for the protection and repair of concrete structures - Test methods - Determination of compressive strength of repair mortar.

Vesna Bulatović[1], Tiana Milović[2], Slobodan Šupić[3]

PROCENA OTPORNOSTI CEMENTNE PASTE SA ZEOLITOM NA VISOKE TEMPERATURE PUTEM TGA/DTA

Rezime:

Kada su betonske konstrukcije izložene dejstvu meke vode tokom dužeg vremenskog perioda, dolazi do narušavanja njihove trajnosti usled ispiranja kalcijuma i povećane osetljivosti na visoke temperature. U ovom radu su prikazani eksperimentalni rezultati otpornosti cementnih pasta koje sadrže prirodni zeolit kao SCM u količini od 0%, 10%, 20% i 30% na dejstvo visoke temperature nakon delovanja meke vode. Kako bi se simuliralo dejstvo meke vode u laboratorijskim uslovima, uzorci pasta su bili izloženi ispiranju u dejonizovanoj vodi tokom 365 dana. Nakon toga je urađena karakterizacija pasta primenom TGA/DTA.

Ključne reči: prirodni zeolit, pasta, TGA/DTA, dejstvo meke vode

EVALUATION OF HIGH TEMPERATURE RESISTANCE OF CEMENT PASTE CONTAINING ZEOLITE USING TGA/DTA

Summary:

When concrete structures are exposed to soft water attack for an extended period of time, they become significantly less durable due to calcium leaching and more sensitive to high temperatures. This paper presents the experimental results of high temperature resistance of cement paste containing 0%, 10%, 20% and 30% natural zeolite as SCM after soft water attack. In order to simulate soft water attack in laboratory conditions, paste specimens were exposed to leaching in deionized water up to 365 days. Afterward, the characterization of pastes was performed by TGA/DTA

Key words: natural zeolite, paste, TGA/DTA, soft water attack

---

[1] *PhD, Assistant Professor, Faculty of Technical Sciences, University of Novi Sad, Serbia, vesnam@uns.ac.rs*

[2] *PhD, Research Associate, Faculty of Technical Sciences, University of Novi Sad, Serbia, tiana.milovic@uns.ac.rs*

[3] *PhD, Assistant Professor, Faculty of Technical Sciences, University of Novi Sad, Serbia, ssupic@uns.ac.rs*

1. INTRODUCTION

Leaching caused by the exposure to pure or natural water with pH value close to neutral (salt free-distilled or deionized, rainwater, snow-melt water, water from the river, etc.) has been identified as very important for the structures exposed to external applications like concretes used in hydro structures (dams, water tanks, and other allied structures [1]), tunnels [2], tanks, retaining walls, etc.

Exposure to high temperature as a result of the exposure to e.g. fire, lava or nuclear meltdown, is well known to negatively impact the physical and mechanical properties of concrete [3], especially when it was previously exposed to soft water attack on long-term. Properties of cement matrix have a great impact on the overall properties of mortar or concrete. Therefore, in order to examine the behavior of concrete at elevated temperatures, it is necessary first of all to understand the behavior of mortar or paste. Some studies have shown that with the increasing temperature, the strength and some other properties are decreasing. However, the selection of suitable materials can minimize the adverse effects of high temperature. The thermal analysis methods are useful for evaluating the high temperature behavior of material.

Commonly used natural pozzolans are metakaolin and some bio ash, but recently, natural zeolites (NZ) are also used in the mortar and concrete due to having good pozzolanic properties. NZs are crystalline aluminosilicate minerals with an open three-dimensional structured framework of SiO_4 and AlO_4 tetrahedra that are linked by oxygen atoms situated in the structural intersections [4]. NZ can absorb and desorb water due to high porosity of up to 30% and has cation exchange capability depending on the types of species, silica/alumina ratio, pH of pore solution, etc. The most common types of NZs used in cement composites are clinoptilolite, heulandite, and faujasite. Clinoptilolite exhibits satisfactory pozzolanic activity i.e., the superior contents of silica present in this NZ can react with $Ca(OH)_2$ from the portland cement system and produce an additional phase of calcium silicate hydrate (C–S–H) [5]. As a result of the pozzolanic reaction in the presence of NZ the amount of C-S-H increases, the microstructure of hardened paste is significantly improved and the performance of the mortar and concrete is positively affected.

Recently, considerable effort has been spent investigating the effectiveness of using NZ as a supplementary cementitious material (SCM) and/or aggregate, most of which show that the addition of NZs leads to an improvement of the mechanical strength, durability properties, and/or weather resistance of cement and concrete. In cases in which improvements to concrete performance were not observed, or performance was diminished, it was concluded that NZs still offer an economically and environmentally friendly substitute for cement [3].

Many physical and chemical changes such as volatilization of water vapor from the system and de-alumination of zeolitic structure could occur simultaneously during heating of NZs. Collapse of the microporous structure of NZ, melting of product and entrapment of gaseous products are some of these phenomena [6].

The primary objective of this study is to investigate the resistance of the cement paste containing 0%, 10%, 20% and 30% NZ as SCM to the high temperatures after 365 days of exposure to soft water.

2. MATERIALS AND METHODS

2.1. COMPONENT MATERIALS

In order to examine the effect of NZ as SCM on high temperature resistance of the blended cement pastes, by TGA/DTA method, the following component materials were used for the pastes preparation:

- Ordinary Portland cement (PC) CEM I 42.5R (Lafarge-BFC Serbia),
- NZ from a quarry in Igroš (Brus, Serbia) with particle size less than 125 µm,
- Deionized water.

True densities of PC (3.13 g/cm^3) and NZ (2.31 g/cm^3) were determined in accordance with SRPS B.B8.032 [7], while the specific surface of PC (4189 cm^2/g) and NZ (5393 cm^2/g) were determined in accordance with the procedure specified in standard SRPS B.C8.024 [8]. The NZ activity index was determined in accordance with the standard EN 450-1 [9], and after 28 and 90 days NZ activity index was 86 % and 90 %, respectively.

The chemical composition of NZ was determined by X-ray fluorescence (XRF) spectroscopy. The instrument used for the XRF analysis is an ED-XRF spectrometer, manufacturer Spectro Xepos from Germany. The system uses a Silicon Drift Detector (SDD), band-pass filter and focuses the X-rays from a binary Co/Pd alloy thicktarget anode (50 W/60 kV) combining polarized/direct excitation. Sample tray used for these measurements was with rotating positions for pellets. Measurements were carried out in vacuum atmosphere and Spectro XRF Analyzer Pro software was used. The sample for ED-XRF analysis was prepared in accordance with the pressed powder method. Tested materials (5 g) and binding agent (Cereox wax, Fluxana) were mixed (1 g) and the 32 mm diameter pellet was formed. The pellet was formed under 10 tones load applied via a laboratory hydraulic press. The loss on ignition (LOI) of NZ was determined after exposing the sample in the amount of 2 g, to a temperature of 950 °C for 1 h. The obtained results are shown in Table 1.

Table 1 – Chemical composition of NZ

Chemical composition of NZ (%)					
SiO_2	Al_2O_3	Fe_2O_3	CaO	MgO	LOI
62.78	12.20	2.37	5.09	2.65	
Na_2O	K_2O	P_2O_5	SO_3	Cl	12.36
0.42	0.74	0.05	0.01	0.05	

Since the sum of SiO_2, Al_2O_3, and Fe_2O_3 oxides of the tested sample is higher than 70% (77.35 %), NZ belongs to the type II addition in accordance with EN 206-1 [10] and EN 450-1 [9]. Based on the loss on ignition result, NZ could not be classified into any category proposed by the standard EN 450-1 [9].

The mineralogical characterization of NZ was performed by XRD analysis (Philips PW1710 device) under the following experimental conditions: monochromatic Cu Kα radiation with 1.5418 Å wavelength in the 5–60° of 2θ range, scan rate 0.02° and 0.5 s per step. The diffraction pattern of the NZ is presented in Figure 1.
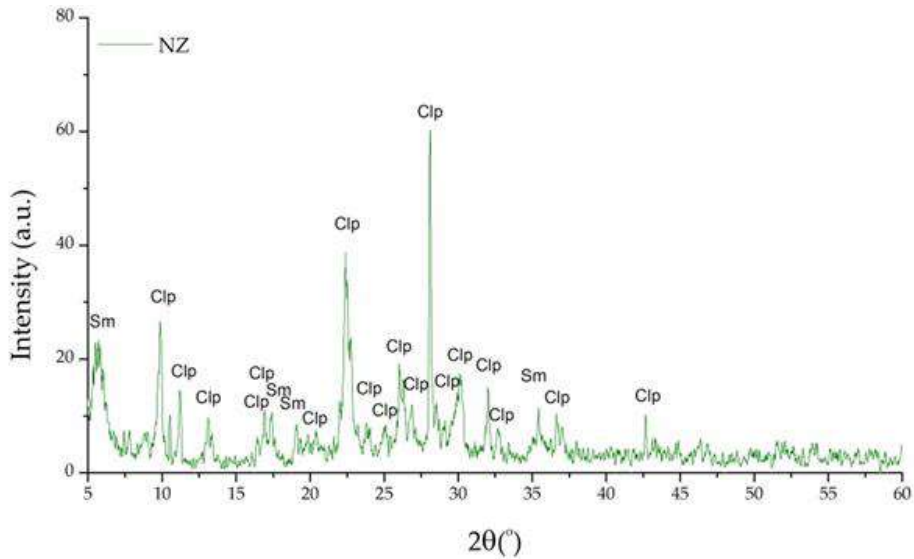
Figure 1 - XRD diffractogram of NZ

According to the XRD analysis results, NZ consists mainly of clinoptilolite (type of NZ mineral) and smectite (known as "swelling" or "expandable" clay mineral). The presence of smectite in zeolite tuff, as a secondary component, can affect the properties of fresh and hardened NZ blended cement composites [11].

2.2. MIXTURE COMPOSITIONS

Mixture proportions of the reference and three blended cement pastes, containing 10%, 20% and 30% NZ as SCM per cement mass, are provided in Table 2.

The prism specimens with the dimensions of 10 mm×10 mm×60 mm were prepared and kept in moulds for 1 day and then submerged in deionised water up to the age of 365 days. Reference and each type of blended cement pastes were immersed in separate sealed containers filled with deionised water.

Table 2 – Composition of paste mixtures

	C	CZ 10	CZ 20	CZ 30
CEM I 42.5 R (g)	450	405	360	315
NZ (g)	-	45	90	135
Deionized water (g)	225	225	225	225

2.3. METHODS

After 365 days of the previously described curing regime, samples were taken from deionized water, crushed and sieved through a 125 μm sieve and then dried at 35°C to constant mass. The behavior of the paste with NZ under high temperatures was investigated experimentally by means of Labsys Evo (Setaram) thermal analyzer using TGA/DTA (Thermogravimetric

453

analysis/Differential thermal analysis). TGA analysis was carried out to obtain the weight loss. Differentiation of the thermogravimetric data (mass loss rate) allows a better resolution and identification of weight losses (DTA). During the experiment, the sample was placed in an alumina crucible whereas an empty one was used as a reference. The output information from each test was a change of sample mass (TGA) and mass loss rate (DTA), as a function of temperature. The TGA/DTA measurements were performed in the temperature range 25–1090°C which simulated the ISO 834 standard fire curve in the argon atmosphere. The sample mass was about 30 mg.

3. TGA/DTA RESULTS OF NZ BLENDED CEMENT PASTES AND DISCUSSION

The TGA test was used to provide information about the chemical reactions due to the heating process. Thermal behavior of paste containing NZ was investigated by using TGA and DTA. The masses loss for the observed pastes in the most important temperature ranges and total are presented in Table 3. The curves are given in Figure 2.
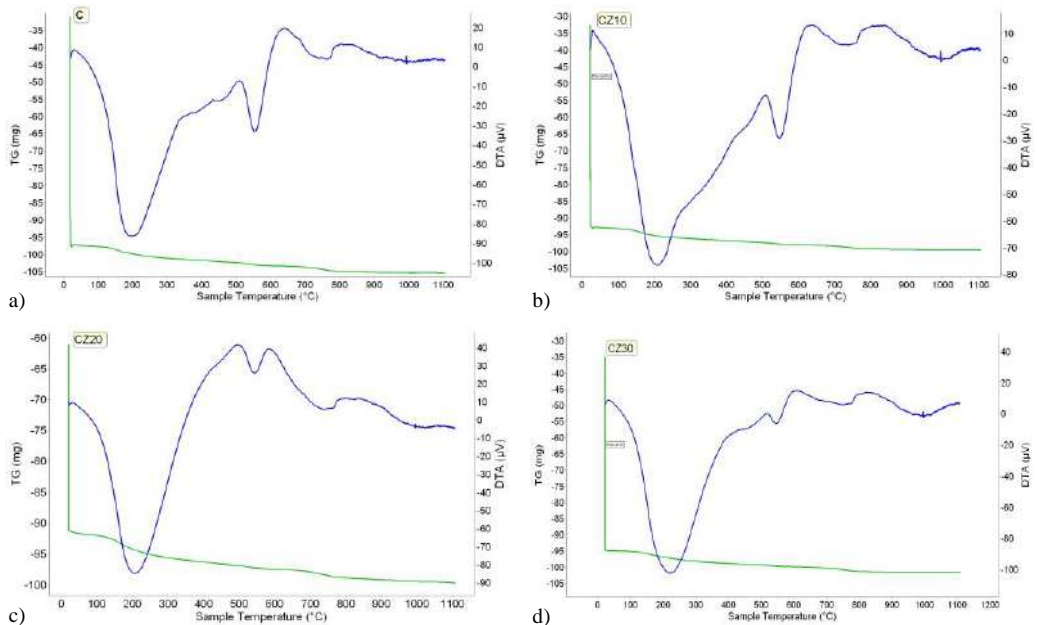
Figure 2 - Results of TGA-DTA a) C; b) CZ10; c) CZ20; d) CZ30

According to this figure, the first endothermic peak occurs in the temperature range 25-350°C, which represents the evaporation of the free water and dehydration of some hydration products (the temperature of dehydration and disappearance of ettringite and C-S-H) [12]. The weight loss of the sample at this range increases with increasing NZ content (14.12% for CZ10, 15.37 for CZ20), except for CZ30 (12.62%), and is larger than the reference sample (11.89% for C). Higher content of NZ in the samples makes the peak more pronounced. This may indicate that clinoptilolite participated in the pozzolanic reactions by forming C-S-H. Peaks corresponding to temperature at this range have shifted to higher values for samples containing

NZ. It may be attributed to the strengthening the bonding of paste components relative to the reference sample. The TGA results show that the maximum rate of weight loss occurs at this temperature range.

The second major endothermic peak appears around 520°C (temperature range 450-650°C) and represents the $Ca(OH)_2$ decomposition. The weight loss in this region may indicate the pozzolanic activity of NZ or due to calcium ion leaching. The mass loss due to the decomposition of $Ca(OH)_2$ was decreased as the amount of NZ increases within the cement paste. The mass loss of samples C, CZ10, CZ20 and CZ30 were measured 3.93%, 3.74%, 3.21% and 2.88%, respectively. This decrease of $Ca(OH)_2$ (portlandite) phenomena may represents the formation of C–S–H [3] or leaching of calcium ion.

The shallow endothermic peak and corresponding weight loss about 700°C is probably due to the decomposition of calcium carbonate ($CaCO_3$) [12]. The carbonation of the paste is an accidental event that may take place during the preparation of the paste or during the grinding of the paste previous to the TGA measurement. The mass loss of samples in the temperature range 650-850°C are given in Table 3. As can be seen, the largest amounts of carbonate are in the reference sample.

The TGA/DTA curves show a continuous mass loss during heating up to 850°C, due to the removal of free water, dehydration and dehydroxylation of the pastes. An exothermic peak at approximately 1000°C may indicate the formation of new phases in the structure.

The obtained data on the mass losses in the temperature range 25-1090 °C indicate that the total amount of products in samples CZ10 and CZ20 are higher in regard to reference sample C5. The CZ30 sample deviates from this conclusion.

Table 3– Mass loss of pastes (%) at different temperature ranges

	25-350°C	350-450°C	450-650°C	650-850°C	850-1090°C	Total
C	11.89	1.90	3.93	4.85	0.74	23.31
CZ10	14.12	2.10	3.74	4.07	0.53	24.56
CZ20	15.37	2.02	3.21	4.56	1.76	26.92
CZ30	12.62	1.87	2.88	4.60	0.39	22.34

4. CONCLUSION

Based on the analysis of the obtained experimental results, in a term of the reference and NZ blended pastes resistance to high temperature via TGA/DTA analyses, the following can be concluded:
- The maximum weight loss of the sample is at the first temperature range (25-350°C). It may indicate on participated of NZ in the pozzolanic reaction because these are the temperatures at which certain hydration products are degraded and values at blended cement are larger than at reference sample.
- The effect of soft water on observed samples perhaps may be best analyzed across the temperature range corresponding to the decomposition of portlandite (450-650°C) where it is seen that the weight loss in samples with NZ is less than that of the reference one which may indicate on pozzolanic reactions but also on leaching of calcium ion.

- The mass loss of samples with NZ at temperature range 650-850°C, related to reference sample, may indicate on less tendency blended samples towards carbonization, but in this test the difference is insignificant.
- The change in mass for extremely high temperatures is small and for most samples (except CZ20) can be considered negligible.
- Total mass losses are higher in samples containing NZ compared to the reference sample, which in the initial part of the TGA curve indicates on higher content of bound water or a higher proportion of hydration products.

For a better understanding of the high temperature behavior of NZ blended cement paste, in addition to thermal analysis, some other analyzes of the microstructure should be done, such as XRD, FTIR etc.

ACKNOWLEDGMENTS

REFERENCES

[1] Anand B, Sharma S.N. Leaching corrosion of concrete due to soft water attack, Recent Advancements in Mineral and Water Resources, 2016, 155-161.

[2] Otieno M, Alexander M, du Plessis J. Soft water attack on concrete tunnel linings in the Ingula pumped storage hydro-power scheme: Assessment of concrete resistance and protection, J. S. Afr. Inst. Civ. Eng., 59(3), 2017, 57-67.

[3] Kushnir A. R. L, Heap M. J, Griffiths L, Wadsworth F. B, Langella A., Baud P, Reuschle T, Kendrick J. E, Utley J. E. P. The fire resistance of high-strength concrete containing natural zeolites. Cement and Concrete Composites, 116, 2021, 103897.

[4] Colella C, Wise W. The IZA handbook of natural zeolites: a tool of knowledge on the most important family of porous minerals, Micropor. Mesopor. Mater., 189, 2014, 4–10.

[5] Islam M. S, Mohr B.J, Berge D. V. Performance of natural clinoptilolite zeolite in the cementitious materials: A comparative study with metakaolin, fly ash, and blast furnace slag, Journal of Building Engineering, 53, 2022, 104535.

[6] Duvarcı Ö. Ç, Akdeniz Y, Özmıhcı F, Ülkü S, Balköse D, Çiftçioğlu M. C. Thermal behaviour of a zeolitic tuff, Ceramics International, 33, 2007, 795–801.

[7] SRPS B.B8.032:1980 - Testing of natural stone - Determination of bulk density, density, coefficient of density and porosity.

[8] SRPS B.C8.024:1964 - Determination of specific surface of Portland cements.

[9] BS EN 450-1:2012 - Fly ash for concrete Definition, specifications and conformity criteria.

[10] SRPS EN 206-1:2011 - Concrete - Part 1: Specification performance, production and conformity.

[11] Milović T, Rudić O, Furgan S.O, Radeka M, Malešev M, Radonjanin V, Baloš S, Laban M. Effects of soft water attack on Portland and natural zeolite blended cements, Chem. Ind. Chem. Eng. Q., 27, 2021, 403–415.

[12] Perraki Th, Kakali G, Kontori E. Characterization and pozzolanic activity of thermally treated zeolite, Journal of Thermal Analysis and Calorimetry, Vol. 82, 2005, 109–113.

Ivan Ignjatović[1], Stefan Ž. Mitrović[2], Jelena Dragaš[3], Vedran Carević[4]

PRIMENA TEHNOLOGIJE 3D ŠTAMPANOG BETONA U KONSTRUKCIJAMA

Rezime:

Tehnologija 3D štampanja betona omogućila je prostor za napredak u industrijalizaciji, optimizaciji i automatizaciji procesa u savremenom konstrukterstvu. U ovom radu dat je prikaz najčešće korišćenih metoda za 3D štampu betonskih konstrukcija, naglašene su prednosti i mane ove tehnologije, kao i pravaca daljeg razvoja. Prikazani su primeri dosadašnje primene u vidu izvedenih građevinskih objekata i sumirani zaključci u vezi svojstava u očvrslom stanju. Izvršena je analiza postojećih znanja u vezi uticaja deterioracionih mehanizama na 3D štampane betone. Takođe, izvršena je ocena ove tehnologije sa različitih aspekta održivosti.

Ključne reči: beton, 3D štampa, tehnologija, konstrukcija, trajnost, održivost

STRUCTURAL APPLICATION OF 3D CONCRETE PRINTING TECHNOLOGY

Summary:

3D concrete printing technology enabled a new progress in industrialization, optimization and automatization of processes in contemporary construction works. This paper shows the commonly used methods of concrete 3D printing. Advantages, disadvantages and perspectives for further development of this technology are emphasized. Conclusions with regard to hardened properties testing are summarized and examples of structural applications are shown. The analysis of existing knowledge about the influence of deterioration mechanisms on printed concrete was made. Evaluation of 3D concrete printing technology in terms of different aspect of sustainability has been done.

Key words: concrete, 3D printing, technology, structure, durability, sustainability

[1] V. prof, Građevinski fakultet Univerziteta u Beogradu, Bul. Kralja Aleksandra 73, ivani@imk.grf.bg.ac.rs
[2] Asistent, Građevinski fakultet Univerziteta u Beogradu, Bul. Kralja Aleksandra 73, smitrovic@imk.grf.bg.ac.rs
[3] Dr, Docent, Građevinski fakultet Univerziteta u Beogradu, Bul. Kralja Aleksandra 73, jelenad@imk.grf.bg.ac.rs
[4] Dr, Docent, Građevinski fakultet Univerziteta u Beogradu, Bul. Kralja Aleksandra 73, vedran@imk.grf.bg.ac.rs

1. INTRODUCTION – BASIC PRINCIPLES OF 3D CONCRETE PRINTING TECHNOLOGY (3DCP)

3D printing technology appeared in the 1980s, as an innovative technology for the production of various elements based on the idea of Charles Hull [1]. The main motivation can be found in the idea of making elements of various complex shapes by gradually applying the material in layers with high manufacturing precision without using casting molds, complex tools, and machines. In relevant literature, this process is often called *Additive manufacturing* (AM-gradual production). 3D printing was initially applied for metal, polymers, ceramics, textiles, and other composite materials. Elements and parts obtained by this technique quickly found their application in various branches of the economy such as mechanical engineering, automotive industry, aero industry, and medicine [1].

The main device of this system is a special type of a printer. There are numerous types of printers different in size and degrees of freedom. Some of the most famous manufacturers of 3D printers for concrete are COBOD BOD2, Apis Cor, Contour Crafting, and XtreeE [2]. The most important part of the printer is the head or a tail. There are different nozzles with a rectangular or circular cross-section, as well as nozzles that lay the material forward or backward or at an angle. The computer system in the background is also an important part. The movement of the head is defined by the G-code generated from the CAD drawing. Therefore, it can be said that 3D printers are similar to CNC machines that are being commonly used in last decade, mostly in the production of steel structures.

Generally, basic methods of 3D printing are: Stereolithography (SLA), method of fusion deposition (Fused Deposition Modeling, FDM), Ink printing (inkjet printing), and production of contours (Contour Crafting CC, [3,4]), [5]. For the purpose of 3D printing of concrete, several of the above-mentioned 3D printing techniques have been used so far. The FDM method (Fused Deposition Modelling), is the most common method for making concrete structures with 3D printing technology. The principle of operation is based on the extruding of layers by pushing them out through a nozzle that moves along a precisely determined path defined according to the G code that was created according to the CAD drawing [3,4],Figure 1.
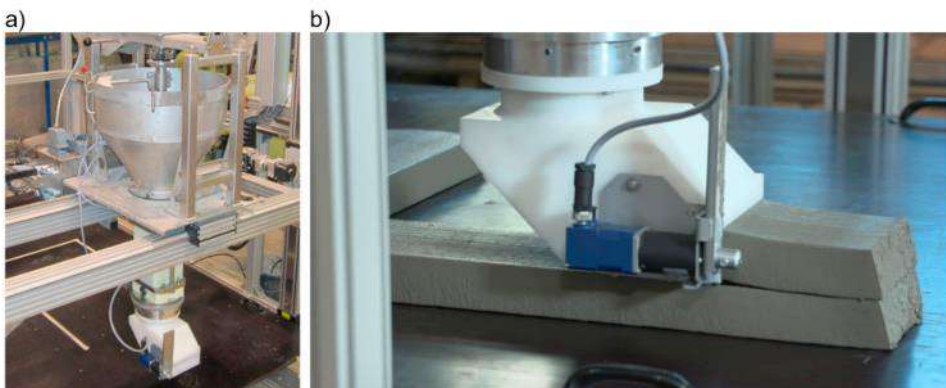
Figure 1 - FDM technology for 3D printing with extrusion of filaments (TU Dresden): a) the printhead of CONPrint3D printer, b) view of the nozzle with extruded filaments [6]

In addition to the extrusion of fresh concrete mix, a concept of material spraying is also used. The method called Shotcrete 3D Printing (SC3DP) has been successfully developed by a research group from the TU Braunschweig, Figure 2a. In the context of traditional construction, SC3DP is similar to pumped concrete, which has been successfully used for years in the construction of tunnels [7]. So, in this particular case, the material is not laid down, but is scattered and thus forms a layer [7,8]. This method can be particularly effective in the context of placing reinforcement in 3D printed concrete structures.

The ink printing method has been successfully used during the past 20 years by company D-Shape [9]. During this process which is similar to the inkjet powder bed technology, binder is sprayed on the printing material placing it layer by layer [9]. What makes D-Shape stand out on market is its special visual impression. The elements and objects obtained with this technology are particularly notable for their artistic value and represent architecturally important works. So far, numerous objects and elements have been successfully executed, Figure 2b. It should be noted that D-Shape has been actively working on the project of 3D printing of objects on Mars and Moon since 2007. [10].

a)   b)
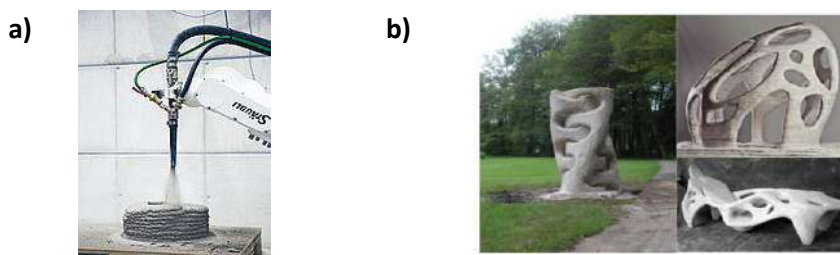
Figure 2 - a) 3D printing technology with concrete spraying (SC3DP) - example of a concrete column [8]*, b) D-Shape technology - example of concrete sculptures.* [9]

Regardless the method of printing, the material that passes through the system is actually mortar because the maximum grain size is not usually larger than 3 mm. In addition to fine aggregate, different cement types (CEM I or CEM II) have been used so far. Also, a large number of chemical additives (setting accelerators, setting retarders, hydration controllers, superplasticizers, viscosity modifiers) and other components such as silicate fume, granulated glass blast, and limestone filler are added to the mixtures [10]–[19]. Specific properties of fresh mixture are buildability, extrudability, flowability, i.e. printability [18] and should be carefully studied in order to ensure adequate quality, i.e. good hardened properties of printed concrete.

2. ADVANTAGES AND OBSTACLES IN STRUCTURAL APPLICATION

There numerous advantages of using 3D printing technology in the field of structural engineering: avoiding formwork, higher precision of construction, material saving, reduction in labor needs, speeding up construction time, the possibility of application in difficult environmental conditions, reducing costs, better working condition on the site and protection of the environment. However, several disadvantages have also been noted: needs for sophisticated equipment, higher initial costs, need for qualified labor, insufficient knowledge of printed material quality, insufficiently developed connections, lack of standards [19–23]. Nevertheless, there is a significant increase in number of companies and research groups dealing with this

topic, Figure 3. In addition, the active participation of RILEM organization with two technical committees (TC PFC and TC ADC) will certainly contribute to developing of standards and regulations for the production and application of 3D printed concrete structures shortly.
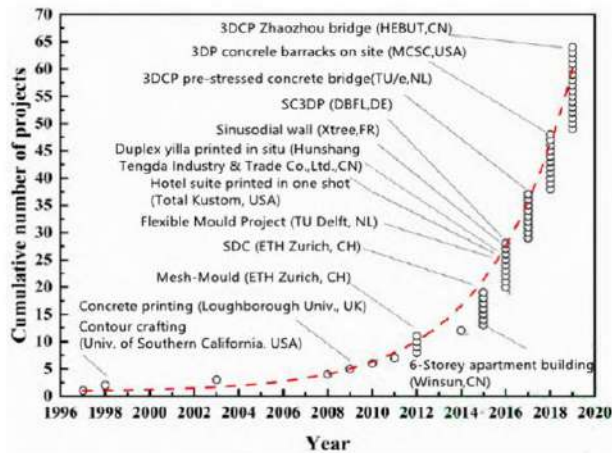

Figure 3 - An increasing number of scientific organizations and projects for 3D printing in concrete [19,21]

3D concrete printing (3DCP) has been applied for different purposes, from panels, facade elements, benches, furniture, columns and walls to pedestrian bridges and residential buildings, Figure 4 [3,10,19,20,24–26].

a)

b)
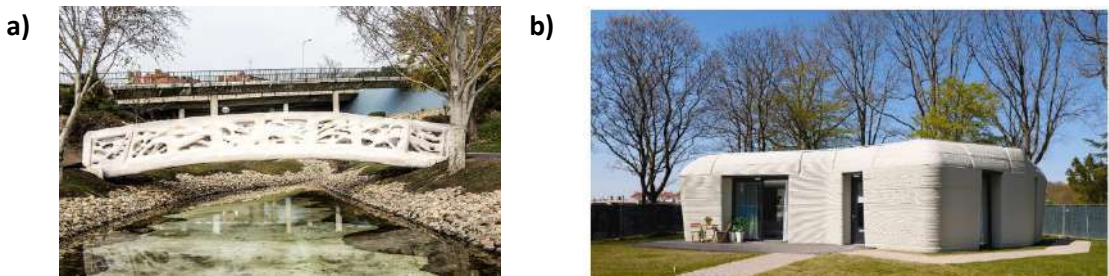
Figure 4 - Representative example of using 3D printing technology in concrete structures: a) bridge in Madrid, Spain, b) Milestione House

3DPC has also been used in the Republic of Serbia since last year. Company Natura Eco successfully printed the first-ever 3D printed concrete house on Western Balkan (ProtoDOM, Figure 5a). At the same time, at the University of Belgrade, Novi Sad and Nis a scientific research groups oriented to this technology were formed. First-ever university 3D printer for concrete in this region was installed at Faculty of the Civil Engineering University of Belgrade, Figure 5b.
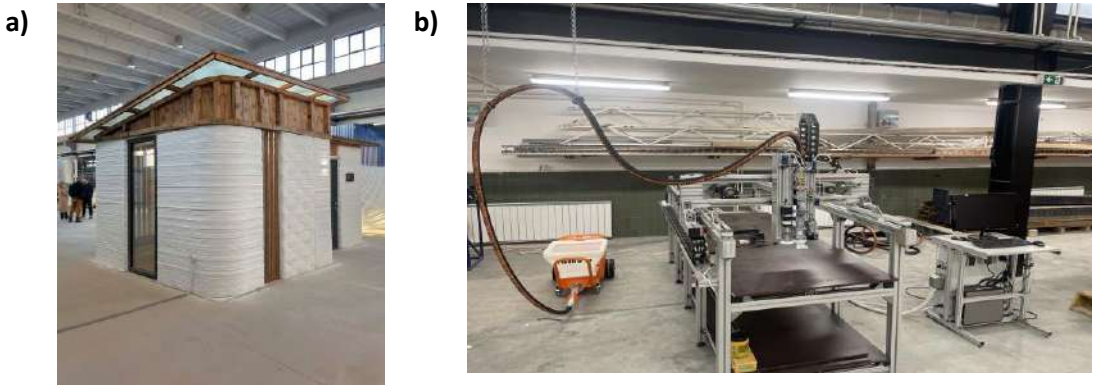
Figure 5 - Application of 3D concrete printing in Serbia: a)ProtoDOM NaturaECO, b)3D concrete printer at Faculty of Civil Engineering University of Belgrade

Significant obstacle for wider application of 3DCP technology is the incorporation of reinforcement into the printing process, i.e. positioning of reinforcement at the proper place into printed structural element [27]. Currently, there are three basic concepts for placing of reinforcement in printed concrete structure (Figure 6):
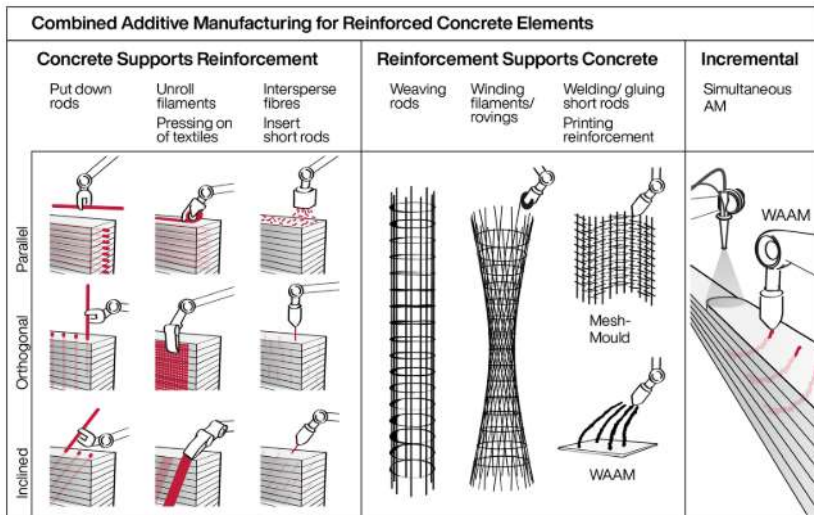
Figure 6. Examples of possible approaches to combining reinforcement and concrete during 3D printing within the new classification [28]

1) the concept where the reinforcement is a support for the concrete – there is a formed reinforcement cage, mainly made of steel and carbon around which the concrete is printed by laying or spraying,

2) the concept where the concrete is the support for the reinforcement - first the concrete part of the structure is printed, after which the reinforcement is placed. There are different

possibilities: a) reinforcement is placed inside the printed contour (the layers form the formwork), b) reinforcement is placed as bars on the layers or through the layers, c) insertion of short rods and fibers into the fresh or hardened mixture. It should be noted that the reinforcement is inserted through the layers (vertically or obliquely at an angle) in a fresh or hardened state,

3) the simultaneous concept that actually represents the WAAM technique - simultaneous printing of both concrete and reinforcement.

The goal to only use a machine for reinforced concrete elements production is not reached, as the additional labor for placing of reinforcement is needed. The most efficient and easy-to-use method is the application of fibers in the concrete mixture instead of reinforcement. Nevertheless, that causes a problem on the other side – a concern whether the printed elements with fibers have sufficient robustness and ductility. This method certainly includes the WAAM, which, at the moment, has the highest chance of achieving the mentioned goal. However, this method currently requires great technological preparation and precision, which certainly results in increased costs.

Assembling of printed concrete segments into a reliable structural system is still an important issue for 3DPC community. General concept that is used during the construction is to print a concrete „formwork„ and fill it with concrete and reinforcement in the form of vertical columns at the corners of the object. There is also a „truss" system in which printed diagonals connect the outer and inner walls made of 3D printed concrete, Figure 7a. That method can contribute to increased stability both during and after printing (in the hardened state). Vertical connections betwen printed elements are provided by concrete columns on the ends. Horizontal joints between printed elements are filled with concrete, Figure 7c. The foundation of 3DPC buildings is usualy cast in-situ reinforced concrete base plate. Anchors are embedded in the base plate and provide connections between foundation and segments obtained by digital fabrication Figure 7b. Connection of printed segments with the roof plate is ensured in a similar way.
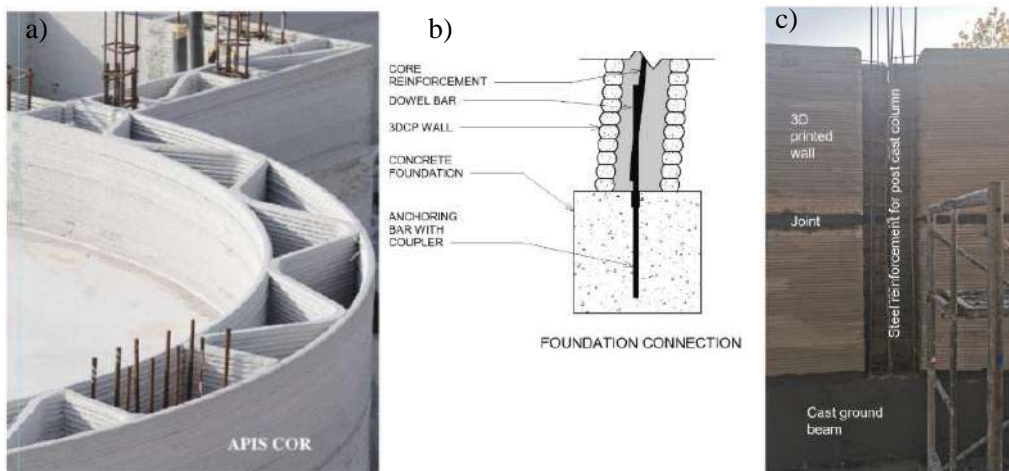
Figure 7 – Connections in 3D printed concrete structures: a) Dubai Office, b)-d) B-Hut [24]

3. HARDENED PROPERTIES OF 3D PRINTED CONCRETE

Based on the analysis of relevant articles and technical reports [6,13,26,29–31], usual experimental testing of hardened properties of 3DCP are the following one:

1) Compressive strength – tested on printed specimens or specimens made in molds. The shape of specimens in both cases is a cube, usually 10x10x10 cm. In this way the effect of layers on mechanical properties can be determined. In the test, the force can be applied perpendicular, longitudinal or lateral to the layer orientation.
2) Flexural strength – determined in the same way as compressive strength.
3) Bond strength between layers is the critical point in the analysis of ultimate strenght of 3DCP structures. Lost capacity of bond as a failure mode should be avoided. At the moment, dominant method for testing interlayer bond strength is the axial (directly) tension test.

Experimental investigation on individual printed columns and walls under the axial load are not rare. Typical setup of experimental testing of 3DCP wall (in this case: 1.3 m x 0.9 m x 0.125 m) is shown at Figure 8.

(a) at breaking of 3DP concrete shell   (b) right after breaking of 3DP concrete shell

Figure 8 - Example of 3DCP wall under axial load [31]

4. DURABILITY

Durability of concrete is defined by its ability to resist harmful environmental agents that damage the concrete - deterioration mechanisms. These mechanisms affect inner concrete structure (sulphate attack, freeze/thaw with or without de-icing salt) or induced reinforcement corrosion (carbonation and chloride penetration). The durability properties of 3DPC are different from traditionally casted concrete due to the use of different mixing proportions, high dosage of chemical admixtures, and layer-by-layer production methods [32]. Researchers have so far focused more on improving mechanical than the durability properties of printed concrete. Only a few researchers have studied the durability of 3DCP, and these results are presented below.

Chloride ion resistance depend on the connectivity of the pores at the layers interface [32,33]. Compared to casted concrete, 3DCP had higher chloride ion ingress [33–35], i.e. lower chloride resistance. As the time gap between printed layers increased, the depth of chloride ingress also increased [34,36]. Although the 3DPC resistance was lower, the value of D_{RCM} was $4x10^{-12}$ [35], which classifies it as high-resistance concrete [37]. On the other hand, 3DPC showed higher carbonation resistance compared to conventional concrete [33]. Certainly, the 3DPC carbonation resistance mainly depends on layer orientation in relation to the CO_2 diffusion direction.

Zhang et al [33] investigated the influence of the freeze/thaw cycle on the concrete dynamic modulus of elasticity and weight loss for 3DPC. 3DPC had a larger decrease in dynamic modulus compared to casted concrete. In contrast to the change in dynamic modulus of elasticity, 3DPC showed smaller weight loss compared to casted concrete [33]. Obviously, the dynamic modulus of elasticity was more sensitive to freeze-thaw cycles than weight loss for the 3DPC, contrary to casted concrete. A useful way to improve 3DPC resistance is to add air-entraining admixture or styrene-butadiene rubber which increase the flexibility of 3DPC, leading to improvement in bond properties [38].

It is well known that concrete with ordinary Portland cement has low acid resistance due to high alkalinity. Sulfuric acid (H_2SO_4) reacts with the calcium hydroxide (CH) of the hydrated cement paste, and produces gypsum. Since 3DPC usually contain larger amounts of cement, it is necessary to examine their sulphate acid resistance. The results available in the literature show that 3DPC have slightly better resistance compared to casted concrete [33,39]. Unlike casted concrete, the cracking of 3DPC propagates along the layer interface [33]. As the sulphate attack progresses, the matrix failure mode is interlayer cracking rather than aggregate peeling.

5. SUSTAINALBILITY

The term sustainability generally refers to three main pillars: societal, economic and environmental. The positive societal impact of using 3DCP is expected to be significant. The reduction of manual labour for preparing and lifting of formwork, pouring and compaction of concrete will enable the employment of skilled workers for handling the printer and controlling the printing process [40]. This could efficiently mitigate the shortage of skilled labour and open a possibility to improve the gender balance among construction workers, by employing more woman. Automation will also help reduce errors and improve safety at the construction site.

When we think about the economical aspect, productivity and cost of materials and labour are first to look at. Stagnating, recently even decreased, productivity in construction industry is a significant concern. The main causes for this are the resistance to introduce changes in a highly traditional sector, low industrialization and low investments in research and development. 3DCP introduces a new paradigm in the construction sector with decreasing the time of construction and liberation of the need for moulds in component manufacturing [41]. With current technology level and future developments in the robotic field, productivity of the construction sector can be significantly increased. By eliminating the formwork, the costs can also be reduced. In total concrete structure cost, formwork costs are around 28%, or up to 50% for complicated geometry [42]. If we include the decrease in time, it is evident that cost reduction can be achieved. However, 3DCP has greater amount of binder in its mixture, and

that binder usually has greater amounts of cement. Also, in order to achieve specific requirements associated with 3D printing technology, different additives (both chemical and mineralogical) are needed. These aspects increase the price of concrete when compared with the traditional one, but the possibility to reduce them with further research development are significant.

Environmental aspect of concrete is usually analysed by looking at the cement amount, natural resource consumption, waste generation, water and energy usage. Environmental benefits of using 3DCP can be obtained through several aspects: the reduction of concrete waste, less water and energy compared with the traditional technology, possibility for structural optimisation due to flexibility of obtained shapes, higher productivity and less formwork material. Also, electricity needed for concrete pumps and 3D printers can easily be obtained from sustainable energy sources, like the energy of sun. However, due to its specific requirement, 3DCP currently incorporates only fine aggregate. As a consequence, it has greater amounts of binder paste, and lower amount of water needed for adequate strength development. Fine aggregate is usually of a natural origin and obtained from quarries. This presents a great influence on the environment, and it consumes significant amount of energy for extraction. The use of recycled concrete aggregate in 3DCP is still restricted due to the fact that fine recycled concrete aggregate has great water absorption and it is still not suitable for construction grade concrete [43]. Different alternatives for natural sand are being explored, but incorporation of coarse aggregate is one of the most important directions in the future research, especially for large-scale 3D printing [41]. Another negative environmental effect of 3DCP is higher amount of cement needed for required concrete properties. Having in mind that cement is the main CO_2 source in concrete, great part of current research is oriented toward lowering its amount, or using alternative binders. The most promising solutions so far are cement replacement with waste materials like slag and fly ash, alkali-activated materials (like geopolimers), particle packaging method and composite cementitious systems including limestone-calcined clay cement. Maybe the most promising alternative at the moment is the application of geopolymer concrete that has a rapid hardening nature, which can significantly improve the buildability without the need of any additional chemical accelerators [44].

6. CONCLUSIONS

Based on the considered reviews and own research, the following conclusions in the field of additive manufacturing technology in concrete structures can be drawn:

1) Application of 3DCP technology for structural purposes are numerous, proving its general feasibility.
2) Currently, methods of printed concrete specimens testing are the same as for casted concrete specimens. The influence of layers on strengths, particularly on bond strength is significant. New methods for testing of printed concrete are under devolopment.
3) Societal and economic aspects of 3DCP sustainability are expected to be significant, while environmental aspect have to be improved by partial substitution of cement with green alternatives.
4) The further directions of research are development and possible improvements in the field of technology, i.e incorporating of reinforcement in the process of 3D printing of concrete, as well as design of connections and joints between printed elements.

5) Technical requirements for structural 3DCP and elements are necessary to be defined in the form of technical sheets and standards.

REFERENCES

[1] Shahrubudin N, Lee TC, Ramlan R. An overview on 3D printing technology: Technological, materials, and applications. Procedia Manuf 2019;35:1286–96. https://doi.org/10.1016/j.promfg.2019.06.089.

[2] MB & ton 2021.

[3] Bos F, Wolfs R, Ahmed Z, Salet T. Additive manufacturing of concrete in construction: potentials and challenges of 3D concrete printing. Virtual Phys Prototyp 2016;11:209–25. https://doi.org/10.1080/17452759.2016.1209867.

[4] Khoshnevis B. Automated construction by contour crafting - Related robotics and information technologies. Autom Constr 2004;13:5–19. https://doi.org/10.1016/j.autcon.2003.08.012.

[5] Ngo TD, Kashani A, Imbalzano G, Nguyen KTQ, Hui D. Additive manufacturing (3D printing): A review of materials, methods, applications and challenges. Compos Part B Eng 2018;143:172–96. https://doi.org/10.1016/j.compositesb.2018.02.012.

[6] Mechtcherine V, Nerella VN, Will F, Näther M, Otto J, Krause M. Large-scale digital concrete construction – CONPrint3D concept for on-site, monolithic 3D-printing. Autom Constr 2019;107:102933. https://doi.org/10.1016/j.autcon.2019.102933.

[7] Heidarnezhad F, Zhang Q. Shotcrete based 3D concrete printing: State of art, challenges, and opportunities. Constr Build Mater 2022;323:126545. https://doi.org/10.1016/j.conbuildmat.2022.126545.

[8] TU Braunschweig. Force flow optimised Design through SC3DP 2022.

[9] Dini E, Colla V. Large Scale 3D Printing: from Deep Sea to the Moon. Low--cost 3D Print Sci Educ Sustain Dev 2013:127–32.

[10] Cesaretti G, Dini E, De Kestelier X, Colla V, Pambaguian L. Building components for an outpost on the Lunar soil by means of a novel 3D printing technology. Acta Astronaut 2014;93:430–50. https://doi.org/10.1016/j.actaastro.2013.07.034.

[11] Chen Y, He S, Gan Y, Çopuroğlu O, Veer F, Schlangen E. A review of printing strategies, sustainable cementitious materials and characterization methods in the context of extrusion-based 3D concrete printing. J Build Eng 2022;45. https://doi.org/10.1016/j.jobe.2021.103599.

[12] Chen Y, Chaves Figueiredo S, Li Z, Chang Z, Jansen K, Çopuroğlu O, et al. Improving printability of limestone-calcined clay-based cementitious materials by using viscosity-modifying admixture. Cem Concr Res 2020;132. https://doi.org/10.1016/j.cemconres.2020.106040.

[13] Yu S, Xia M, Sanjayan J, Yang L, Xiao J, Du H. Microstructural characterization of 3D printed concrete. J Build Eng 2021;44:102948. https://doi.org/10.1016/j.jobe.2021.102948.

[14] Dressler I, Freund N, Lowke D. The effect of accelerator dosage on fresh concrete properties and on interlayer strength in shotcrete 3D printing. Materials (Basel) 2020;13. https://doi.org/10.3390/ma13020374.

[15] Malaeb Z, Hachem H, Tourbah A, Maalouf T, El Zarwi N, Hamzeh F. 3D Concrete Printing: Machine and Mix Design. Int J Civ Eng Technol 2015;6:14–22.

[16] Rahul A V., Santhanam M, Meena H, Ghani Z. 3D printable concrete: Mixture design and test methods. Cem Concr Compos 2019;97:13–23. https://doi.org/10.1016/j.cemconcomp.2018.12.014.

[17] Le TT, Austin SA, Lim S, Buswell RA, Gibb AGF, Thorpe T. Mix design and fresh properties for high-performance printing concrete. Mater Struct Constr 2012;45:1221–32. https://doi.org/10.1617/s11527-012-9828-z.

[18] Bukvić O, Radonjanin V, Malesev M, Laban M. Basic fresh-state properties of extrusion-based 3D printed concrete. Build Mater Struct 2020;4:99–118.

[19] Buswell RA, Leal de Silva WR, Jones SZ, Dirrenberger J. 3D printing using concrete extrusion: A roadmap for research. Cem Concr Res 2018;112:37–49. https://doi.org/10.1016/j.cemconres.2018.05.006.

[20] Sanjayan JG, Nematollahi B. 3D Concrete Printing for Construction Applications. Elsevier Inc.; 2019. https://doi.org/10.1016/b978-0-12-815481-6.00001-4.

[21] Lyu F, Zhao D, Hou X, Sun L, Zhang Q. Overview of the Development of 3D-Printing Concrete: A Review. Appl Sci 2021;11:9822. https://doi.org/10.3390/app11219822.

[22] Avrutis D, Nazari A, Sanjayan JG. Industrial Adoption of 3D Concrete Printing in the Australian Market. Elsevier Inc.; 2019. https://doi.org/10.1016/b978-0-12-815481-6.00019-1.

[23] Holt C, Edwards L, Keyte L, Moghaddam F, Townsend B. Construction 3D Printing. vol. 42. Elsevier Inc.; 2019. https://doi.org/10.1016/b978-0-12-815481-6.00017-8.

[24] Bos FP, Menna C, Pradena M, Kreiger E, da Silva WRL, Rehman AU, et al. The realities of additively manufactured concrete structures in practice. Cem Concr Res 2022;156:106746. https://doi.org/10.1016/j.cemconres.2022.106746.

[25] Lowke D, Dini E, Perrot A, Weger D, Gehlen C, Dillenburger B. Particle-bed 3D printing in concrete construction – Possibilities and challenges. Cem Concr Res 2018;112:50–65. https://doi.org/10.1016/j.cemconres.2018.05.018.

[26] Zhang J, Wang J, Dong S, Yu X, Han B. A review of the current progress and application of 3D printed concrete. Compos Part A Appl Sci Manuf 2019;125:105533. https://doi.org/10.1016/j.compositesa.2019.105533.

[27] Mechtcherine V, Buswell R, Kloft H, Bos FP, Hack N, Wolfs R, et al. Integrating reinforcement in digital fabrication with concrete: A review and classification framework. Cem Concr Compos 2021;119:103964. https://doi.org/10.1016/j.cemconcomp.2021.103964.

[28] Kloft H, Empelmann M, Hack N, Herrmann E, Lowke D. Reinforcement strategies for 3D-concrete-printing . Civ Eng Des 2020;2:131–9. https://doi.org/10.1002/cend.202000022.

[29] Rehman AU, Kim J-H. 3D Concrete Printing: A Systematic Review of Rheology. vol. 14. 2021.

[30] Li Z, Hojati M, Wu Z, Piasente J, Ashrafi N, Duarte JP, et al. Fresh and hardened properties of extrusion-based 3D-printed cementitious materials: A review. Sustain 2020;12:1–33. https://doi.org/10.3390/su12145628.

[31] Patiphat Jiramarootapong LP, Chalermwut Snguanyat GT, Tangtermsirikul S. Load Carrying Capacity and Failure Mode of 3D Printing Mortar Wall Panel Under Axial Compression Loading. vol. 28. 2020. https://doi.org/10.1007/978-3-030-49916-7_4.

[32] Rehman AU, Kim J-H. 3D Concrete Printing: A Systematic Review of Rheology. vol. 14. mdpi; 2021.

[33] Zhang Y, Zhang Y, Yang L, Liu G, Chen Y, Yu S, et al. Hardened properties and durability of large-scale 3D printed cement-based materials. Mater Struct Constr 2021;54. https://doi.org/10.1617/s11527-021-01632-x.

[34] Van Der Putten J, De Volder M, Van den Heede P, De Schutter G, Van Tittelboom K. 3D Printing of Concrete: The Influence on Chloride Penetration. Second RILEM Int. Conf. Concr. Digit. Fabr., Eindhoven, The Netherlands: Springer: Cham, Switzerland; 2020, p. 500–7.

[35] Blaakmeer J, Lobo B. A Robust Mortar and Printing System. Second RILEM Int. Conf. Concr. Digit. Fabr., Eindhoven, The Netherlands: Springer: Cham, Switzerland; 2020, p. 1091–103.

[36] Weger D, Kim H, Talke D, Henke K, Kränkel T, Gehlen C. Lightweight Concrete 3D Printing by Selective Cement Activation – Investigation of Thermal Conductivity, Strength and Water Distribution. Second RILEM Int. Conf. Concr. Digit. Fabr., Eindhoven, The Netherlands: Springer: Cham, Switzerland; 2020, p. 162–71.

[37] fib-Bulletin 34. Model Code for Service Life Design. 1st ed. Lausanne, Switzerland: International Federation for Structural Concrete (fib); 2006.

[38] Assaad JJ, Hamzeh F, Hamad B. Qualitative assessment of interfacial bonding in 3D printing concrete exposed to frost attack. Case Stud Constr Mater 2020;13:e00357. https://doi.org/10.1016/j.cscm.2020.e00357.

[39] Baz B, Aouad G, Kleib J, Bulteel D, Remond S. Durability assessment and microstructural analysis of 3D printed concrete exposed to sulfuric acid environments. Constr Build Mater 2021;290:123220. https://doi.org/10.1016/j.conbuildmat.2021.123220.

[40] Bhattacherjee S, Basavaraj AS, Rahul AV, Santhanam M, Gettu R, Panda B, et al. Sustainable materials for 3D concrete printing. Cem Concr Compos 2021;122. https://doi.org/10.1016/j.cemconcomp.2021.104156.

[41] Ma G, Buswell R, Leal da Silva WR, Wang L, Xu J, Jones SZ. Technology readiness: A global snapshot of 3D concrete printing and the frontiers for development. Cem Concr Res 2022;156:106774. https://doi.org/10.1016/j.cemconres.2022.106774.

[42] De Schutter G, Lesage K, Mechtcherine V, Nerella VN, Habert G, Agusti-Juan I. Vision of 3D printing with concrete — Technical, economic and environmental potentials. Cem Concr Res 2018;112:25–36. https://doi.org/10.1016/j.cemconres.2018.06.001.

[43] Khan SA, Koç M, Al-Ghamdi SG. Sustainability assessment, potentials and challenges of 3D printed concrete structures: A systematic review for built environmental applications. J Clean Prod 2021;303. https://doi.org/10.1016/j.jclepro.2021.127027.

[44] Dey D, Srinivas D, Panda B, Suraneni P, Sitharam TG. Use of industrial waste materials for 3D printing of sustainable concrete: A review. J Clean Prod 2022;340. https://doi.org/10.1016/j.jclepro.2022.130749.

Duško Lučić[1]*, Tome Trombev*[2]*, Mladen Muhadinović*[3]

ČELIČNA KROVNA KONSTRUKCIJA FUDBALSKOG STADIONA NA CETINJU

Rezime:

Predstavljen je projekat, proizvodnja i montaža čelične krovne konstrukcije Gradskog stadiona na Cetinju. Krovna konstrukcija je oslonjena na armirano betonske stubove i grede. Izrađene su dvije konstrukcije u ogledalu koje pokrivaju zapadnu i istočnu tribinu. Jedna krovna konstrukcija se sastoji od 16 radijalno postavljenih lučnih nosača. Krovni nosači su projektovani kao dvostruki konzolni rešetkasti nosači. Glavni rešetkasti nosači izrađeni su od CHS profila. Projekat objekta uradio je Institut za građevinarstvo iz Podgorice, dok je izgradnju, proizvodnju i montažu objekta uradio Monting inženjering iz Bitolja u dogovorenom roku od 150 dana.

Ključne reči: čelična krovna konstrukcija, stadion, veze, montaža čelične konstrukcije

STEEL ROOF STRUCTURE OF THE FOOTBALL STADIUM IN CETINJE

Summary:

The design, production and erection of the steel roof structure of the City Stadium in Cetinje, Montenegro were presented. The roof structure is supported by reinforced concrete pillars and beams. Two mirror-like constructions covering the west and east grandstands were made. One roof structure consists of 16 radially placed arch girders. Roof girders are designed as double cantilever lattice girders. The main lattice girders were made with CHS. The design of the structure was done by the Civil Engineering Institute, Podgorica, while the construction, production and erection of the structure were done by Monting Engineering, Bitola, within the agreed period of 150 days.

Key words: steel roof structure, stadium, connections, steel structure erection

---

[1] *Full professor, Civil engineering faculty, University of Montenegro, Podgorica, Montenegro, dlucic@ucg.ac.me*
[2] *MSc, Civil Engineer, General manager, Monting Engineering, Republic of North Macedonia, tome.trombev@monting.mk*
[3] *MSc, Teaching assistant, Civil engineering faculty, University of Montenegro, Podgorica, Montenegro, mladen.m@ucg.ac.me*

1. INTRODUCTION

Cetinje is the old capital of the Kingdom of Montenegro. In today's state of Montenegro, Cetinje is not the capital, but it has retained the title of capital and the old splendor of the cultural and historical center. Recently, this city is adorned with a new city stadium, the construction of which was jointly financed by the Football Association of Montenegro, the Public Works Administration and the Capital City of Cetinje.

Figure 1 - Aerial view of the new stadium

2. LOADS AND DESIGN CONDITIONS

In Montenegro, European regulations for structural design have been successfully translated and national annexes have been made for all 58 parts of the EN standard for structural design. Also, the law on the mandatory application of these standards was passed. Until August 1, 2022, the parallel application of old standards and new European standards is possible. After this date, only EN standards will be binding in Montenegro, which is called MEST EN standards in Montenegro. The construction of this stadium was designed according to old Montenegrin standards.

In February 2012, the heaviest snowfall in a century occurred in Montenegro and several steel roof structures collapsed. This phenomenon has caused a change in snow load regulations in 2018. In the continental part of Montenegro, a significantly higher load of snow is prescribed than the previously valid load. This change has been implemented in the Montenegrin national snow load annex by the appropriate methodology MEST EN 1991-1-3 NA.

The steel roof structure design of the stadium was done before the snow regulations were changed. To start the construction, it was necessary to check and harmonize the project documentation with the new conditions of the snow load. A higher snow load also causes higher seismic forces, since the mass of the object should be calculated together with the load from snow. It turned out that most of the previously adopted structural elements do not have sufficient bearing capacity and need to be changed. A practically new project of the roof construction of the stadium was done.

471

Climatic conditions of the location of the facility require that a snow load of 2.65 kN/m^2 should be taken into account. The wind load was calculated based on an average wind speed of 26.0 m/s, averaged over 60 minutes, with a return period of 50 years. Based on the geometry of the object and the elastic properties of the structure, dynamic coefficients and coefficients of force or pressure were adopted. The seismic load was modeled by the ESL (Equivalent Static Load) method concerning the IX degree of seismicity, a return period of 475 years with a seismic coefficient for the horizontal direction calculated in the geotechnical study for the stadium location. According to Montenegrin standards, the building is classified in the II category.

3. DESCRIPTION OF THE STRUCTURE

The roof structure of the stadium is made of steel, supported by reinforced concrete pillars and beams. Two mirror-like roof structures for the west and east stands of the stadium have been designed.

One roof structure consists of 16 radially placed arch girders. Roof girders are designed as double cantilever lattice girders. Due to their length, the six middle girders are additionally supported by V supports.

Arched girders are formed as lattice girders which are polygonal, with a grid node spacing of 1500 mm.
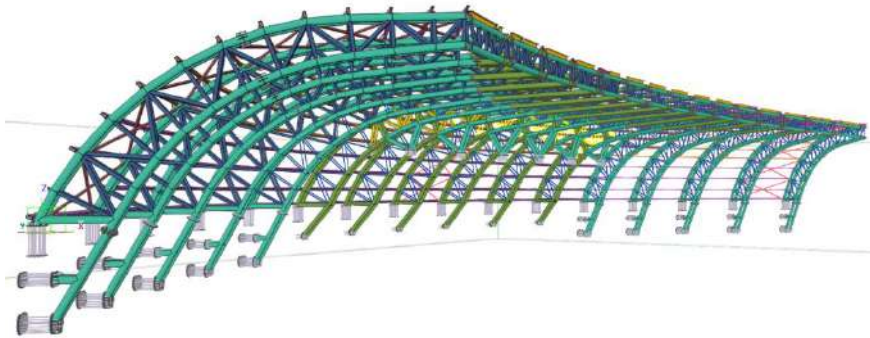
Figure 2 - 3D structural model
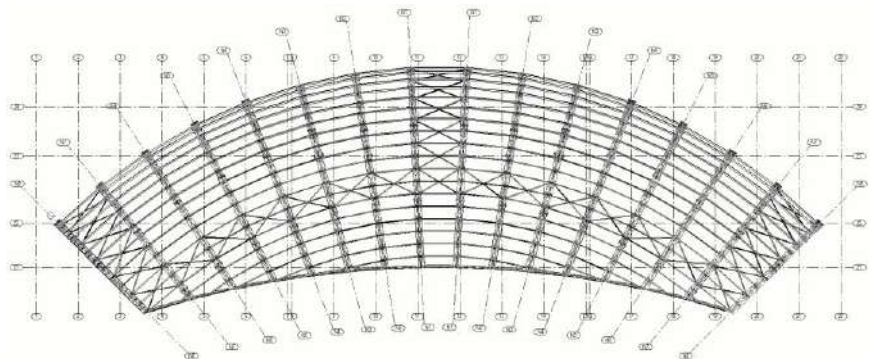
Figure 3 - Plan view of structural members

472
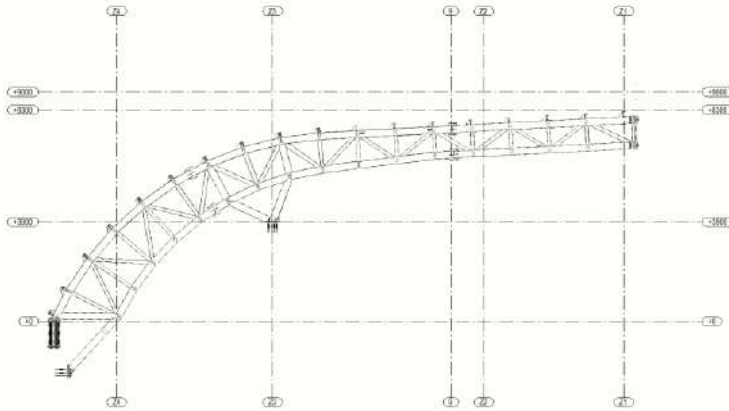
Figure 4 - Main arch lattice girder with V support
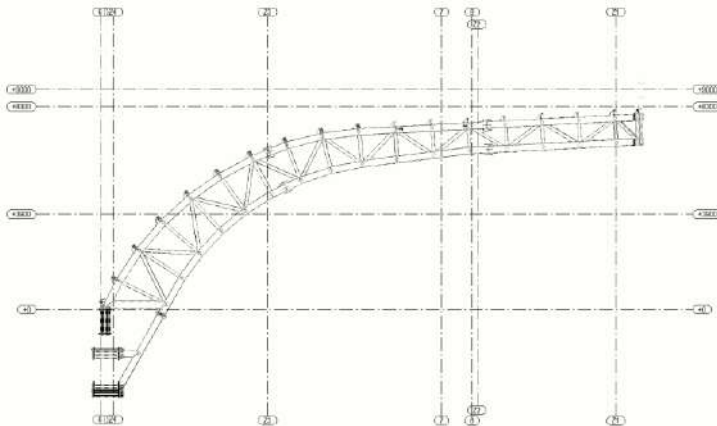
Figure 5 - Console main arch lattice girder

The roof structure is single-pitched with a slope of approximately 2.70˚ (4.71%), after which it passes into the arched part to the support. The roof covering is an arched trapezoidal panel, 40 mm thick, with 0.7 mm thick galvanized upper and lower sheets. The roof panel rests on the purlins. The connection between the panel and the purlins is made with self-tapping screws.

The roof is base arched with measures approximately 115 x 25.2 m. The height elevation of the roof structure on the pillars (± 0.00 m) corresponds to an elevation of +11.40 meters, or an absolute elevation of +659.90 m.

The main supporting system is a structure consisting of double lattice main girders interconnected by a linear lattice structure at their ends. The construction is additionally stiffened by a system of roof bracings in the plane of the upper chord of the main girder, to achieve precise geometry on the assembly.

The main roof arch girders N1, N2 and N3 are of the static beam system with overhang, supported on the concrete structure in axes R1 and 13. They are designed as lattice girders with double chords made from cold-formed circular cross-section CHS Ø273x8 and CHS Ø273x5

and with diagonal and vertical bars made from CHS Ø133x5 and CHS Ø159x5. They have been supported on axis 13 via the V supports which are made from CHS Ø273x8.

The main roof arch girders N4, N5, N6, N7 and N8 are of the static console system, supported on the concrete structure in the R1 axis. They are designed as lattice girders with double chords made from cold-formed circular cross-section CHS Ø273x8 and CHS Ø273x5 with diagonal and vertical bars made from CHS Ø133x5. The lower chords of these girders are lowered diagonally to the level of the POS 200 plate, to achieve a better fixed end.

The splices of the main girders are made by welding. To achieve precise assembly, spacers were designed, which were removed after welding.
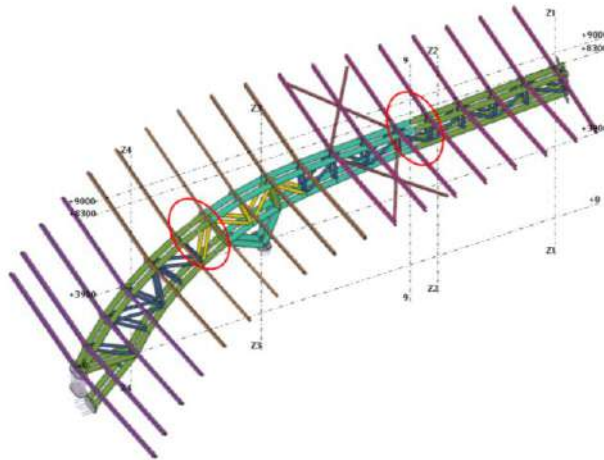
Figure 6 - Position of splices on the main girder
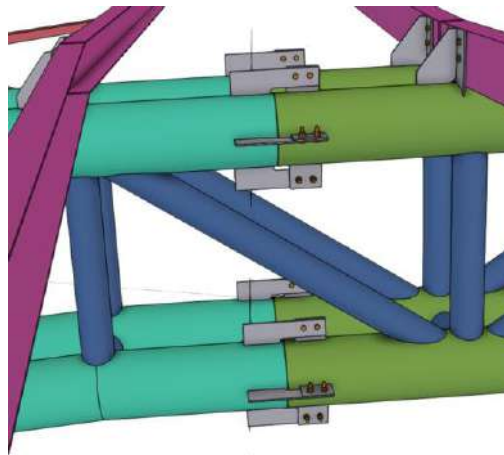
Figure 7 - Chord member splices – welded splices with spacers

The connection between the main girder and the concrete pillar is made via base and backing plates 25 mm thick and with untreated bolts M24, 10.9. A 15 mm thick anchor template was concreted into the pillar.
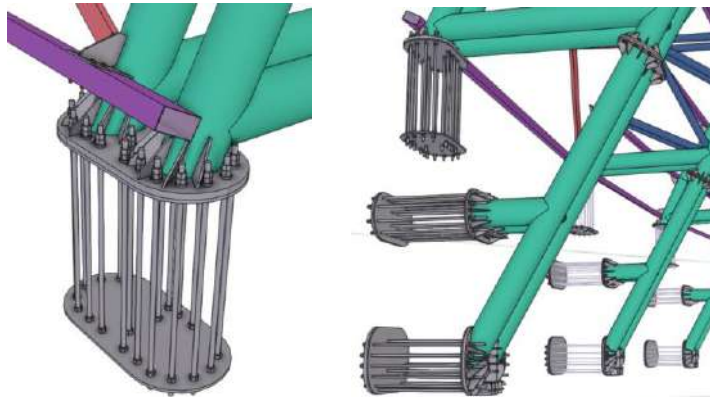
Figure 8 - Base plates, backing plates, concrete anchor templates and anchors

The purlins of the building are designed as cold-formed U profiles 200x100x5, RHS 200x100x5 and RHS 200x120x5. The purlins of the static system are simply supported beams with spans from 6.70 m to 4.50 at a distance of 1.50 m. The connection of the purlins with the main support is made by 8 mm thick plates and untreated M12 bolts, strength class 8.8. The purlins are interconnected by Ø12 roof bracings.
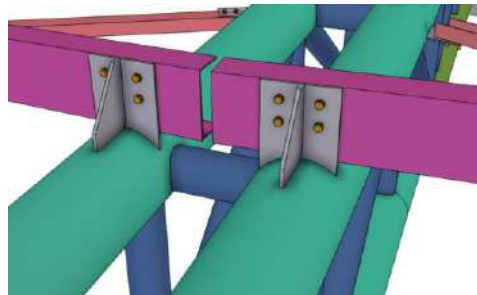
Figure 9 - Purlins and connection to chord members of the main truss

The roof bracings of the upper chord are designed as cold-formed U profiles 100x60x4. The connection between bracings and main girders is made with 8 mm thick plates and untreated M16 bolts, strength class 8.8.

4. STRUCTURAL SYSTEM AND STATIC-DYNAMIC ANALYSIS

In the global analysis, the structure is spatially modeled with real support conditions. TOWER 7 software package was used for construction analysis, while control was performed in SAP 2000 software package.

The adopted dimensions of steel elements and connections are determined by applicable regulations and ensure the prescribed safety, stability, usability and durability of the structure.

According to the old Montenegrin regulations, wind load and seismic force load are not combined at the same time, so it has been shown that the relevant combinations are load when combining own weight, permanent loads, snow and in some cases wind. To define the seismic load according to the old Montenegrin regulations, the ESL method (Equivalent static load

method) was used, according to which seismic load is defined as equivalent static load and directly depends on the mass of the structure and inertial excitation.

5. STRUCTURE MATERIAL

The steel construction is entirely made of S235J0 steel. Untreated bolts are strength class 8.8. Anchors are strength classes 10.9. All welds, considering the performance class, are with quality B.

6. PRODUCTION OF THE STEEL STRUCTURE

Components of the structure are classified in the consequence class CC3. Construction components are classified in the SC2 maintenance category. Construction components are classified in the PC1 construction category. The construction as a whole, with all its components, is classified in execution class EXC3.

To realize such a demanding project, a BIM model was made in the TEKLA software package. With the help of the BIM model, workshop documentation was made, for the production of elements and assemblies of steel structure in the workshop, specification of all materials, as well as the necessary graphic documentation for the assembly of the structure.

Elements for the structure were purchased from Makstil, Skopje, N. Macedonia (plates of various thicknesses) and IGM, Kavadarci, N. Macedonia (circular pipes with different wall thicknesses).

The construction was produced in the production plant of the company Monting Engineering, Bitola, N. Macedonia, in all respects meeting the requirements prescribed by standards EN ISO 3834-2 and EN 1090-2, EXC3. The company Monting Engineering, Bitola, N. Macedonia is certified for EXC4 quality of work by TUV SUD. Monting Engineering has complete traceability for every process of the production of the elements of the steel structure. At any given time, it is known from which material the element is made, which welder welded that element, what NDT is made, deviations from the design measurements, the thickness of the anti-corrosion layers, etc.

Quality Assurance was satisfied by submitting the certification documentation and measurement reports to the investor's representatives after the steel structure is completed.

Figure 10 - Assemblies production

7. ANTI-CORROSION PROTECTION

According to the classification of the environment and the category of atmospheric corrosivity, the level of protection C3 (medium) is required for the construction. Corrosion protection is made with two layers of primer EPOKSAL R EPO (manufacturer Pitura, Zemun, Serbia) with a thickness of each layer of 80 μm (minimum thickness of both layers of 160 μm) and with one final polyurethane layer TOP PUR-AY RAL 9010 (manufacturer Pitura, Zemun, Serbia) with a layer thickness of 80 μm, so that the total thickness of corrosion protection is not less than 240 μm.

Figure 11 - Application of anti-corrosion protection

8. TRANSPORT OF THE STEEL STRUCTURE

The transport of the steel structure was a rather complex operation considering that the steel segments were oversized to transport and that the structure had to be transported 400 km, through three countries, crossing two borders. The problem of oversized steel segments was solved by using a low-load platform, which corrected the transport of steel segments outside the allowed dimensions to normal transport. The entire steel structure was transported with 42 vehicles, over 3 months.

Figure 12 - Assemblies of steel structure prepared for transport

Figure 13 - Transport of steel structure assemblies

9. ERECTION OF THE STEEL STRUCTURE

The erection of the structure is organized through several phases. The first phase involved the enlargement of the structure on the construction site - welding of the segments of the main roof girders and the formation of the final shape of the main grating lattice girders, together with base and backing plates and V supports. Welding was performed according to premade WPS. After welding of all assemblies, the control of geometric deviation from the allowed values was done. The second phase involved the erection of the main roof girders and assembling them in the design position. The erection started from the N1 girder and all the other girders are erected and interconnected with the front lattice girder and horizontal roof bracings. The third phase involved the assembly of the purlins.

Figure 14 - Preparation of main girders on construction site

| *Figure 15 - Lifting of main girder N1* | *Figure 16 - Lifting of main girders* |

Each girder was lifted with a car crane, and then the upper and lower chords of the roof girder were welded to the base plates at the level of + 11.40m and + 9.43m. After 50% of the seam was welded, the car crane released the girder and proceeded to lift the next girder. After the geodetic check that the first girder N1 was erected to the designed position, further erection of the structure

was continued. When the second girder N1 was erected, the interconnection with the front lattice girder and horizontal roof bracings started, to form a geometrically accurate and stable field.

Figure 17 - Erected steel structure

10.   CONCLUDING REMARKS

The total mass of the installed steel structure is 380,000 kg. The works were completed on November 4, 2020. The deadline for the construction of the steel structure was 150 days and the construction was completed within the set deadline.

General designer: Studio K, Podgorica, Montenegro
Designer of steel structure: Civil Engineering Institute, Podgorica, Montenegro
General constructor: Erlang, Podgorica, Montenegro
The constructor of
steel structure: Monting Engineering, Bitola, Republic of North Macedonia

REFERENCES

[1] Rule book on technical requirements for steel structures, Official gazette of Montenegro, No. 025/18, 20.04.2018, No. 040/19, 19.07.2019, No. 045/20, 19.05.2020, No. 071/21, 29.06.2021;

[2] Main design of roof steel structures of City Stadium, Cetinje, Montenegro - Civil Engineering Institute, Podgorica, Montenegro;

[3] Method statement for production of roof steel structures of City Stadium, Cetinje, Montenegro - Monting Engineering, Bitola, Republic of North Macedonia;

[4] Method statement for application of the anticorrosive protection of roof steel structures of City Stadium, Cetinje, Montenegro - Monting Engineering, Bitola, Republic of North Macedonia.

Goran Milutinovic[1], Rade Hajdin[2], Duško Bobera[3]

RAZLIKE U PROJEKTOVANJU I IZGRADNJI MOSTOVA IZMEĐU SAD I SRBIJE

Rezime:

Razlike u projektovanju i izgradnji putnih mostova malih i srednjih raspona između SAD i Srbije su predstavljene, bazirane na iskustvima autora u radu u obe zemlje. Nekoliko aspekata putnih mostova je pregledno, analizirano i upoređeno. Razmatrane su teme kao što su karakterističan poprečni presek mosta, tip dubokog temeljenja, upotreba naknadnog ili athezionog prednaprezanja, upotreba hidroizolacije i zaštitnih ograda, karakteristike normi za projektovanje i pristup u analizi mosta.

Ključne reči: putni mostovi, SAD, Srbija, projektovanje, izgradnja

DIFFERENCES IN BRIDGE ENGINEERING BETWEEN USA AND SERBIA

Summary:

Differences in design and construction of short-span and middle-span road bridges in the U.S.A. and Serbia are discussed in this paper. It is based on the authors' perspective and experience in both countries. Several aspects of road bridges are listed and compared, one by one. Issues such as typical bridge cross section, foundation type, use of pretensioning or posttensioning, typical waterproofing and barrier use, design code characteristics and bridge analysis approach are discussed.

Key words: road bridges, USA, Serbia, design, construction

[1] *Bridge Designer at DB Inženjering, Belgrade, Serbia, and PhD Student at University of Belgrade, Faculty of Civil Engineering, Serbia, email: gormilutin@gmail.com*
[2] *Full Professor at University of Belgrade, Faculty of Civil Engineering, Serbia, and President of Infrastructure Management Consultants (IMC) GmbH, Signaustrasse 14, 8008 Zurich, Switzerland, email: rade.hajdin@grf.bg.ac.rs*
[3] *President of DB Inženjering, Belgrade, Serbia, email: dusko_bobera@yahoo.com*

1. INTRODUCTION

In this paper, differences in design and construction of short-span and middle-span road bridges in the U.S.A. and Serbia are discussed based on the authors' perspective and experience in these countries. The first and third authors are licensed civil engineers in both countries. The paper uses the Serbian practice as the representative of the entire region (which is traditionally leaned on the German practice), and compares it with the U.S.A. practice. Each chapter is intended to cover one specific topic where there is a difference in the U.S.A. and Serbian practice regarding the bridge engineering. An upper limit for short-span and middle-span bridges in Serbia is usually taken as 50m – for example, special design license is needed for the company to design bridges above 50m span. On the other hand, in the U.S.A. this span limit is often taken as 61 meter (200 feet) – for instance, this is the span length for which the AASHTO live load model had been statistically calibrated. This paper focus on concrete bridges, but a lot of aspects are also applicable for bridges with steel beams acting compositely with the concrete slab (a type often encountered in the U.S.A). In the U.S.A, AASHTO LRFD Bridge Design Specification is the main design standard, while each of the fifty states and its Department of Transportation (DOT) has its own manual to represent the state unique practice environment. DOTs are responsible for bridge management in their states. There are more than 600,000 bridges in the National Bridge Inventory (NBI), which is the database containing the most important information for every bridge in the U.S.A. (bridge is considered every structure carrying road traffic with span larger than 6m, i.e. 20ft). In Serbia, the main design standard currently is the Eurocode, and as each country using the Eurocode, Serbia has defined its own National Annexes, where Nationally Determined Parameters from the Eurocode are specified (until recently, the Yugoslav codes have been used). In Serbia, the number of bridges is estimated to approximately 7,000, and they are managed by JP Putevi Srbije, Koridori Srbije, and local communities (bridge is considered every structure carrying road traffic with span larger than 5m). It can be easily calculated that there are around two times more bridges per person in the U.S.A. then in Serbia. Further, the U.S.A. 'bridge market' is a large and relatively homogenous market – this fact strongly influences the bridge engineering practice in the country. It is worth noting at the beginning, that in the U.S.A. imperial units are used, while in Serbia metric system is used.

2. PROJECT TYPE

The U.S.A is a developed country, which among other things means that its infrastructure is mostly already built. The U.S. Interstate is the main motorway system in the U.S.A. consisting of over 75,440 km of roadway. It is mostly built in the late 1950s and in 1960s. Its rapid construction in these approximately 15 years, in an almost assembly-line fashion, and lessons learned during this mass construction, shaped the today's U.S.A. bridge engineering approach [1]. According to U.S. standards, the bridge design life is 75 years (while the Eurocode set the bridge design life to 100 years). The U.S.A. infrastructure is currently an aging infrastructure, with large funds dedicated each year for its rehabilitation. Currently, 46,154, or 7.5% of the U.S.A bridges, are considered 'structurally deficient' (having one of the key structural elements rated 'poor' or worse). Also, there are more than 94,000 'functionally obsolete' bridges (with inadequate vertical or horizontal clearances or approach roadway geometry). Nearly 231,000

bridges in the U.S.A., need some kind of repair and preservation work [1]. Consequently, most bridge projects in the U.S.A. are rehabilitation projects of existing bridges of the following types:

- Bridge widening for newly added traffic lanes (due to traffic growth),
- Bridge replacement (new bridge at the place of heavily deteriorated existing bridge), and
- Bridge condition upgrading (without changing the bridge original geometry).

Serbia is a developing country, which among other things means that its infrastructure is currently being built. Consequently, most of the bridge projects in Serbia are new construction on a new motorways, highways or railways.

3. SUPERSTRUCTURE TYPE

In the U.S.A, most of the short and middle span bridges, with spans up to 61m (200ft), are prefabricated beam bridges with concrete cast-in-place slab. Prefabricated beams are either (a) pretensioned precast concrete beams or (b) steel rolled beam or plate girder (Figure 1). For shortest spans, simple cast-in-place integral concrete constant-thickness slab bridges are often designed. On contrary, the large portion of the bridges in Serbia are cast-in-place concrete slab structure, with various typical cross sections, shown in Figure 2 (larger span upper left, smaller span upper right, and in between spans for lower left cross section type). These types of bridges, completely built on the falsework, are posttensioned for longer spans and are without prestressing for shortest spans. Also, concrete precast posttensioned beam bridges are becoming more popular in recent years (Figure 2, lower right). The precast beam bridges seem to be more cost-effective than cast-in-place slab structures, although probably less durable. For bridges on curved alignments in Serbia, the typical cast-in-place concrete cross sections on Figure 2 are used; in the U.S.A., in these situations, curved steel plate girders acting compositely with concrete deck are often used.
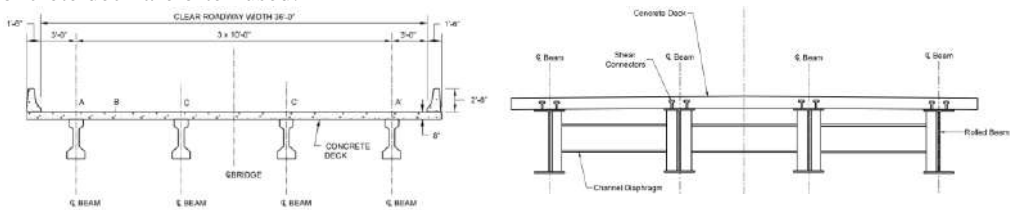
Figure 1 – Left: typical U.S.A. precast pretensioned concrete beam bridge cross section; right: typical U.S.A. steel rolled beam bridge cross section [2]
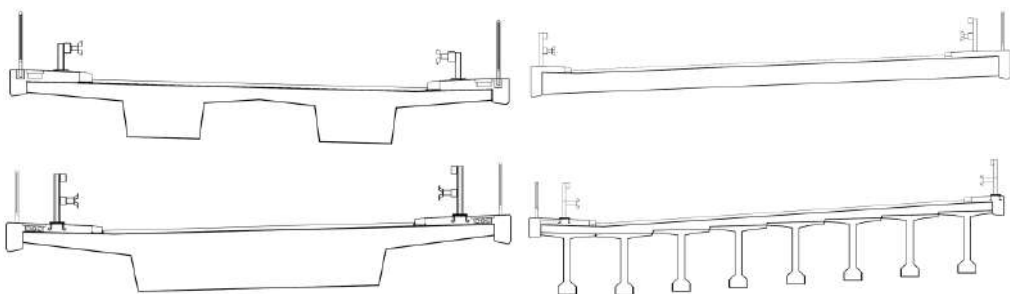
Figure 2 -Typical Serbian cast-in-place concrete bridge superstructure (left upper, left lower, and right upper) and precast posttensioned beam bridge cross section (right lower)

4. DEEP FOUNDATIONS – PILES

In the U.S.A, steel H piles are constructed very often as bridge foundations. These are displacement piles – structural steel H-shape sections are driven into ground by blows of an impact hammer, without any soil removal. In general, during installation of the displacement piles, soil elements originally located where the pile will be installed, or near it, undergo large displacements. Consequently, displacement piles may be seen as having preloaded the soil during the installation process, which affect the pile behavior significantly. The advantages of steel H piles include their high resistance to driving and handling, as well as their large flexural stiffness. An additional advantage is the ease by which these piles are cut off or extended. Extension is usually done by welding. Further, corrosion of steel piles is rarely a problem. The reason appears to be the absence in soils of sufficient supply of oxygen for corrosion to develop substantially, even in fairly aggressive soils [3]. In Serbia, the cast-in-place concrete bored piles (sometimes also called drilled shafts) are very often used for bridge foundations. Bored piles are installed by first removing a volume of soil from the ground by drilling, then placing the rebar cage, and finally filling the resulting cylindrical void left in the ground with concrete. For soil stabilization during excavation, either steel caissons or bentonite slurry is used. Therefore, these are non-displacement piles which do not preload the soil during its installation, as the soil elements around the pile are not pushed away or displaced from the original position. The behavior of the displacement piles and non-displacement piles are significantly different.

5. PRESTRESING

In the U.S.A., the pretensioning of the beams is much more frequently used than the posttensioning. The posttensioning is applied in special cases, when pretensioning cannot offer the solution to the considered problem. In general, in the U.S.A., labor is more expensive than material, so the main design philosophy is that the design should be such that the construction is fast and simple. This is probably the main reason for popularity of the pretensioning, since it is effectively done in precast plants – beams are set for installation after just a few days after casting. It is very descriptive to watch the following YouTube video as an illustration of the pretensioning process in a typical U.S.A. precast plant [4]. In Serbia, the situation is opposite – the post-tensioning is almost always applied. Nevertheless, pretensioning had been used recently on Morava Corridor bridges [5].

6. BARRIERS

In the U.S.A., the dominant type of the barrier is the cast-in-place concrete barrier integrated with the slab (shown in Figure 3). This barrier is routinely checked for vehicle collision force (denoted as F_t in upper right part of the Figure 3) – the barrier flexural capacity check as well as check of the rebar connection between barrier and slab is performed. The yield line analysis, schematically described in lower right part of the Figure 3, is performed for the ultimate moment capacity check of the concrete barrier due to vehicle collision forces. The slab overhang (part of the slab outside of the exterior girder) is often thickened to resist the vehicle collision force. The intent is to make the deck overhang overdesigned, and to sacrifice the barrier itself, if needed, in the case of the collision force. The barrier is not considered as the primary structural component of the bridge, and the bridge would not be closed for traffic in the case of the barrier damage, as it would be in the case of the slab damage. In Serbia, the typical barrier detail is shown in Figure

4. The only rebar connection between slab overhang and the walkway with steel railing usually used is the reinforcement Ø14mm at the distance smaller than 30cm crossing the vertical connection between two elements. This reinforcement is usually not directly obtained by calculation – it is a standard detail widely used.
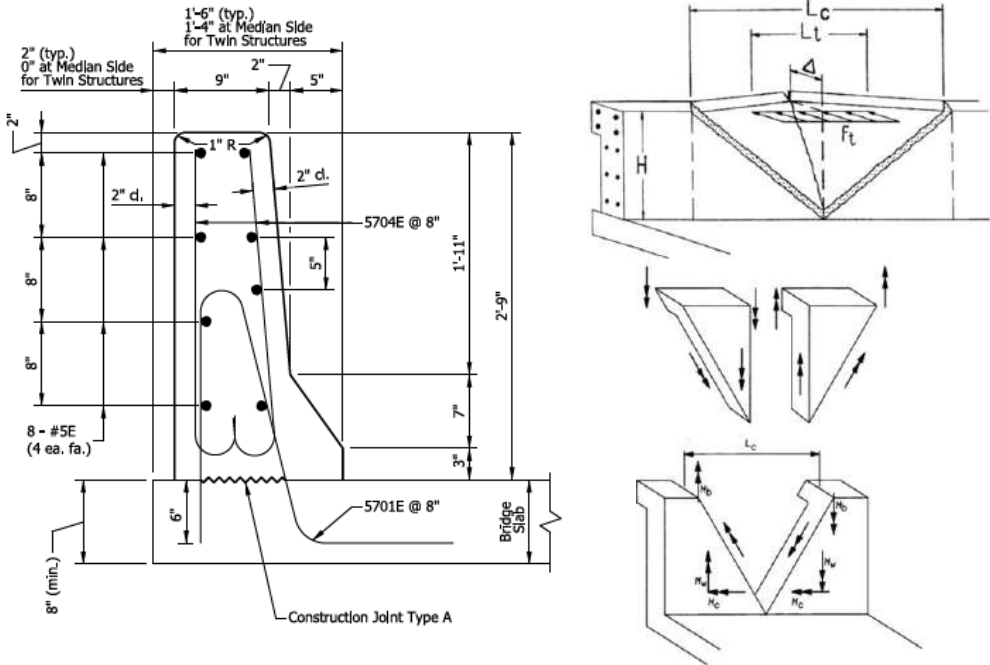

Figure 3 – Left: INDOT concrete barrier detail; right: yield line analysis of the barrier
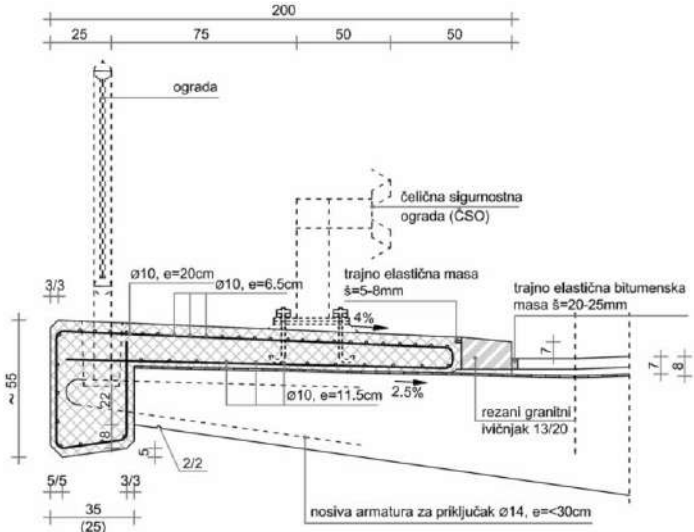

Figure 4 - Typical barrier detail in Serbia

7.   WEARING SURFACE AND WATERPROOFING OF THE SLAB

The wearing surface for a bridge structure is designed to resist traffic wear, and with periodic maintenance, to provide a smooth riding surface. In the U.S.A., the wearing surface can take one of the following forms[6]:

1. Asphalt concrete overlay resting on the top of the deck. To protect the slab from moisture and chemical agents, a waterproofing membrane should be installed between the asphaltic wearing surface and the slab;
2. Polymer modified concrete, composed of cement, aggregate, and a synthetic organic polymer which replace 10%-15% of cement binder in the concrete mix. When latex is used, the concrete may also be called latex modified concrete. The compressive strength of polymer modified concrete can reach as high as 140MPa by adding special additives. With regard to wearing surface, polymer modified concrete provides for a surface that is less porous, thereby limiting the intrusion of water and chlorides;
3. Integrated wearing surface – monolithic part of the slab itself. Therefore, top portion of the concrete slab is taken as the wearing surface. From design standpoint, this means that a portion of the top of the slab is neglected for section properties resisting loads, but it is still included as the dead load.

Please note that in the last two types, there is no waterproofing membrane between the wearing surface and the concrete slab. European agencies consistently reported success incorporating waterproofing membranes into concrete bridge deck construction to both extend service life and delay the need to rehabilitate or replace bridge decks. In contrast, their general use in the United States remains limited [4]. NCHRP Synthesis 425 [7] found that only 60% of U.S. state agencies (DOTs) reported the use of waterproofing membranes. The reasons reported by DOTs for not using waterproofing membranes include nonuse of deicing salts, poor performance of membranes in the past, the use of alternative deck protection strategies (such as use of the polymer modified concrete for an overlay), and the preference for having an exposed concrete deck to observe any deterioration. Although several types of defects have been observed with waterproofing systems, the three predominant ones according to U.S. practice are: (a) lack of adhesion between the waterproofing membrane and the concrete deck, (b) lack of adhesion between the waterproofing membrane and the asphalt surface, and (c) moisture penetration through the membrane. The usage of waterproofing membrane by state in 2011 is shown in Figure 5 [7]. NCHRP Synthesis 425 further states that usage of waterproofing membrane declined from 1974 to 1994, and remained on the same level in 2011[8]. According to [9], in the U.S.A., bridges typically undergo major deck replacement after about 40 years of service life. This fact actually reflects the quality of bridge engineering practice decades ago, and not quality of the current practice. Regardless of the type of the wearing surface, DOTs usually have strict requirement for detailing of the concrete slab. For example, these are some of the Indiana DOT (INDOT) requirements, typical for most of the U.S.A.:

- The bottom-reinforcement cover should be 25mm (1 in). The top-reinforcement cover should be 64mm (2½ in).
- The top 13mm (½ in.) of the bridge deck should be considered sacrificial and should not be included in the structural design, as part of the composite section. This sacrificial wearing surface is to account for (a) future resurfacing of the slab and thereby milling of the top portion of the concrete slab, and for (b) possibility that the slab has integrated wearing surface.
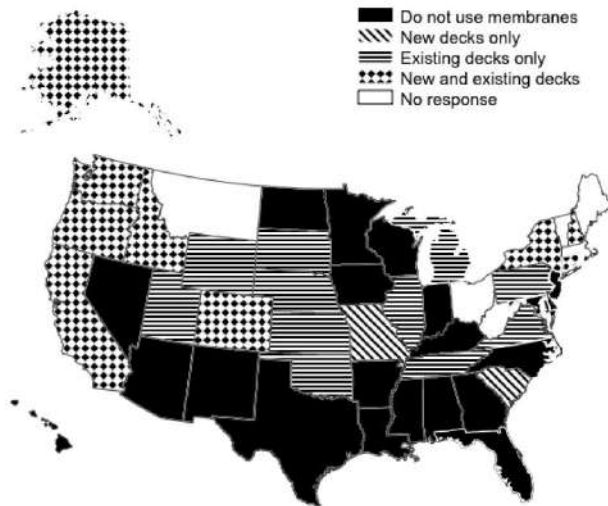- All reinforcing steel for a bridge slab supported on beams shall be epoxy coated.

Figure 5 - Usage of waterproofing membrane in USA by state in 2011[7]

Since the early 1980s, most reinforcing steel used in bridge slab has been coated with epoxy to inhibit corrosion by limiting the effects of moisture and chlorides [6]. An epoxy-coated rebar is a standard deformed bar that has been blast-cleaned, heated, and then subjected to an electrostatic spray of dry powder. The epoxy-coated bars are being criticized as non-efficient in Europe. Recently, to limit the extent of corrosion, galvanized and stainless steel reinforcement has been widely used in the northeast U.S.A. where deicing chemicals are extensively used in winter seasons.

In Serbia, asphalt concrete is almost always a wearing surface on the bridge, and consequently, waterproofing membrane is very often used. In case of precast concrete beams, clear covers calculated according to EN 1992 are 40 mm, same for top rebar and for bottom rebar, due to the same concrete exposure class XC3 – external concrete sheltered from rain. Top deck surface is sheltered due to waterproofing membrane, and bottom surface is sheltered by the precast girders. Alternative waterproofing, below the asphalt wearing, sometimes used in Serbia is a liquid waterproofing system called Methyl Methacrylate (MMA) which is applied to deck by spraying. Consequently, MMA has the advantage that it cannot be teared off at the location of the anchors extended from the deck (and start losing its function), in contrary to waterproofing membrane which is vulnerable and sensitive to tearing off. From [10], it can be concluded that the average time when the deck should be replaced in Serbia is 45 years (time from opening to traffic to the condition 'very bad' in the inspection report). This conclusion is based on the statistical study of the historical inspection reports from the Serbian bridge inventory database.

8. DECK FORMS BETWEEN PRECAST GIRDERS

In the U.S.A, flanges from adjacent beams are usually separated from each other (see Figure 1, on the left). Between flanges of adjacent beams, temporary or permanent forms are provided for casting the slab. The permanent-type formwork is also called stay-in-place (SIP) formwork (see Figure 6). In some states like Indiana or Virginia, it is often used, while in some states, such as Illinois, it is actually forbidden. Construction of SIP forms is fast, safe and easy and can be

performed in a fraction of the time needed to install conventional forms. On the other hand, the reasons for not using the SIP forms are: (a) lower side of the deck is not possible to inspect during the life of the bridge, and (b) moisture may be collected above the SIP forms in the deck. When the adjacent beam flanges are not touching each other, the transverse slab analysis should be done for the wheel loads (using a load model for local analysis – the LM2 if the Eurocode is applicable).

Figure 6 – Left: Stay-in-place forms – view from underneath the bridge (catalog New Millennium Building Systems); right: stay-in-place forms connection detail (catalog LB Foster)

In Serbia, the flanges of adjacent beams often touch each other - there is no need for formwork for the slab in that case (Figure 2). The slab (being on large distance from section centroid) is then not effectively contributing to the composite section moment of inertia.

9. EARTH-RETAINING STRUCTURES AND ABUTMENTS

In Serbia, for earth retaining structures and bridge approach embankments, usually conventional cast-in-place reinforced concrete retaining walls are used. Contraction joints are placed usually at 6m segments and expansion joints at 12m segments. Reinforced earth is offered on the Serbian market, but it is not widely used. In contrast, in last few decades in the U.S.A, MSE (mechanically stabilized earth) walls are dominantly used for the retaining structures and bridge approach embankments. When used as part of the bridge abutment and wing walls (see Figure 7), MSE walls are used for earth retaining purposes, while reinforced concrete abutment is located behind the MSE walls and represent a fixed point for the bridge superstructure support. MSE walls are commonly built of a suitable soil (traditionally sandy soil with less than 15% fines) reinforced typically using strips, sheets, or grids made of extensible (polymer) or inextensible (mild steel or aluminum) materials. The general idea behind the reinforced soil is to alternate layers of reinforcement and soil – the interaction between the reinforcing element and the backfill is the key to the design of the MSE walls. Reinforced soil walls typically have a facing, but this facing is not assumed to contribute to the wall stability. The facing can be made of precast concrete panels, cast-in-place concrete, shotcrete, metal, gabion, or fabric. The reinforcing elements are typically linked to the facing by suitable connections [3]. Advantages of the MSE walls are rapid, predictable, and repetitive construction, allowing for nearly any geometry. It is used in the U.S.A. since 1970s and has been performing satisfactorily. With regards to the use of conventional reinforced concrete retaining walls in the U.S.A., it is interesting to note that AASHTO is specifying the maximum segment length – contraction joint must be placed at maximum of 9m, and expansion joints at maximum of 27m. This type of earth-retaining structure are used in the U.S.A., but not to a greater extent.
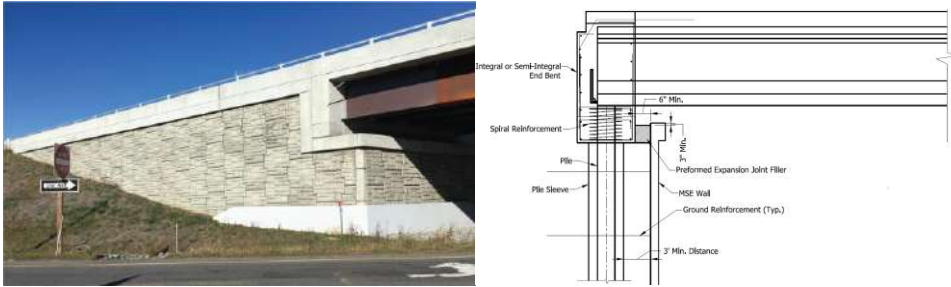
Figure 7 – Left: an abutment with MSE walls – RECo website (a design company and material supplier, recognized as the inventor of modern MSE walls); right: standard INDOT detail

10. CULVERTS

Culvert is defined as a short-span structure through which water runoff flows. In the U.S.A., the most frequent culvert type is the corrugated steel pipe (shown in Figure 8) with the standard spans up to 7 to 8m. There is a minimum cover requirement above the corrugated steel culvert, depending on the highway or railway load. This minimum fill is measured from the top of the pipe to the bottom of the asphalt pavement course and it is typically greater then span/8 or 30cm. By this minimum fill above the culvert, the soil is providing lateral support to the steel pipe, maintaining its shape, so the pipe wall acts as a compression ring. The design checks are made to ensure that the pipe wall has the required resistance to compression crushing and instability. Bending moments are generally disregarded. The corrugated steel culvert design is covered in detail by the AASHTO LRFD Bridge Design Specification. These structures are relatively light in weight and can be handled with simple, light equipment. Installation is very quick. Since there are large number of steel corrugated structures in the U.S.A. bridge inventory for a long time (over 100 years), a lot of research about them has been performed and their performance showed generally well in practice (e.g. the same experience is also made in Switzerland). Excellent reference on this topic is [11]. In Serbia, these short-span bridges (less than 7m) are almost always done as cast-in-place reinforced concrete closed box.

Figure 8 – Upper: steel corrugated pipe installation (Contech catalogue); lower: typical steel corrugated pipe culverts in the U.S.A

11. DESIGN CODE CHARACTERISTICS

The bridge design standard in the U.S.A., the AASHTO LRFD Bridge Specification, is a mostly practice-oriented design code, enabling the designer fast and accurate use of its provisions. On the other hand, the Eurocode is often more research-oriented, providing principles of analysis and showing a lot of code development background, often without providing practical implementation details (although corresponding guidelines are published in most countries). It should be noted that both codes provide the similar level of refinement of analysis and design. As stated by Michael Fardis, who led the development of the seismic part of the Eurocode, the process of drafting the design codes in Europe is dominated by academics; in the United States, the process is controlled by practitioners. Academics, especially in continental Europe, appreciate grand unifying theories as the background of practical engineering. Practitioners, especially in the United States, value the effectiveness and practicality of design rules [12].

Table 1 - AASHTO load factors and load combinations

Load Combination Limit State	DC DD DW EH EV ES EL PS CR SH	LL IM CE BR PL LS	WA	WS	WL	FR	TU	TG	SE	Use One of These at a Time			
										EQ	IC	CT	CV
Strength I (unless noted)	γ_p	1.75	1.00	—	—	1.00	0.50/1.20	γ_{TG}	γ_{SE}	—	—	—	—
Strength II	γ_p	1.35	1.00	—	—	1.00	0.50/1.20	γ_{TG}	γ_{SE}	—	—	—	—
Strength III	γ_p	—	1.00	1.40	—	1.00	0.50/1.20	γ_{TG}	γ_{SE}	—	—	—	—
Strength IV	γ_p	—	1.00	—	—	1.00	0.50/1.20	—	—	—	—	—	—
Strength V	γ_p	1.35	1.00	0.40	1.0	1.00	0.50/1.20	γ_{TG}	γ_{SE}	—	—	—	—
Extreme Event I	γ_p	γEQ	1.00	—	—	1.00	—	—	—	1.00	—	—	—
Extreme Event II	γ_p	0.50	1.00	—	—	1.00	—	—	—	—	1.00	1.00	1.00
Service I	1.00	1.00	1.00	0.30	1.0	1.00	1.00/1.20	γ_{TG}	γ_{SE}	—	—	—	—
Service II	1.00	1.30	1.00	—	—	1.00	1.00/1.20	—	—	—	—	—	—
Service III	1.00	0.80	1.00	—	—	1.00	1.00/1.20	γ_{TG}	γ_{SE}	—	—	—	—
Service IV	1.00	—	1.00	0.70	—	1.00	1.00/1.20	—	1.0	—	—	—	—
Fatigue I—LL, IM & CE only	—	1.50	—	—	—	—	—	—	—	—	—	—	—
Fatigue I II—LL, IM & CE only	—	0.75	—	—	—	—	—	—	—	—	—	—	—

The difference between practice-oriented AASHTO approach and principles-oriented Eurocode approach is best illustrated by showing how the load factors and load combinations are provided in each code. In Table 1, the AASHTO approach is shown for all ultimate, service, and fatigue limit states – each row represent one load combination and each column is the load factors for specific load (self-weight, live load, wind etc.). These load factors are then very straightforward to apply in everyday routine practice. In contrary, the Eurocode approach consists of a thorough study of several tables needed for such a simple task as applying the load factors for different load combination. General principles for complex probabilistic and reliability study behind the load factors should be recognized and understood by the practicing engineer, but load factor application should be fast and straightforward. By making the code

more practice-oriented, more time is left to the designer, in an often relatively hectic environment, to more important things such as the understanding the behavior of the structure and its durability. Without providing final practical implementation details, the potential for design errors due to misinterpretation of the code is enlarged.

12. TRAFFIC LOAD ANALYSIS

In the U.S.A., non-finite-element-method softwares (e.g. Bentley's Conspan) are usually used for traffic load analysis, superstructure design checks and proportioning of the routine steel and concrete beam bridges (which are majority of the U.S. bridge inventory). This type of analysis is based on 1D line analysis of continuous or simple beam and application of the so called distribution factors (DF) on the results of 1D analysis. Therefore, this type of calculation is very easy to perform and to automate – no finite element modelling is needed. Finite-element modelling is done in the U.S.A. only for non-routine short-span and middle span bridge structures, and of course for long-span bridge structures. Distribution factor is a percentage of the lane load carried by a beam bridge that will be resisted by one beam. These factors, proposed by AASHTO Specification, are based on extensive research project where large number of beam bridge types and beam bridge configuration were analyzed by finite-element-analysis (FEA) software, and parametric studies were made to establish the distribution factor equations [13]. The AASHTO live load model HL-93 was applied on these bridges and a percentage of the total load resisted by one beam was determined. Different AASHTO distribution factor are provided for different bridge types (e.g. cast-in-place concrete slab on precast concrete I sections), for moment and for shear, for interior and for exterior beam. Parameters in distribution factor equations are the span length, beam and slab stiffness, beam spacing and skew. Creation of AASHTO distribution factors was possible due to large and homogenous U.S. bridge market.

Lever rule is another method proposed by AASHTO for lateral distribution of traffic load on beam bridge. It is a simple and slightly conservative approach, very easy to use in practice. The bridge cross section is approximated as series of simple beams spanning from beam centerline to beam centerline - a hinge is assumed at every beam location and support is provided at every beam location (see Figure 9 for a three-girder bridge). The live load is then applied transversely in several arrangements. Reaction at every support represents the fraction of the lane load carried by the bridge (computed by 1D analysis) that goes to that beam (i.e. reaction at each support is the distribution factor for that beam). The lever rule is an easy and fast way to check the results of refined time-consuming FEA modeling. In contrast to AASHTO distribution factors originally created with the AASHTO load model (different when compared with the Eurocode LM1), the lever rule can be applied with the Eurocode Load Model 1. In addition to the lever rule, another hand calculation for transverse load distribution mentioned in AASHTO is the rigid method (analogous to conventional rigid pile cap formula for pile force distribution), where the deck is assumed perfectly rigid – this method is also used in Serbia. Based on the authors' experience, the lever will provide results within 10% of the refined FEA modelling for wider spacing of the precast beams; for narrow beam spacing (e.g. beam flanges touching each other), the rigid method gives more accurate results than the lever rule.

In Serbia, on the other hand, refined finite-element analysis are done for all types of bridges, routine and non-routine. This requires significantly more time for calculation for routine bridge structures, when compared with the use of non-FEA software described above. The accuracy of two approaches (FEA and with distribution factors) is comparable – although the use of DF

introduce some (small) level of approximation, the finite-element analysis always carry a risk to make a significant human error, since the FEA in general are 'easy to use and abuse' [14]. For this reason, obligatory extensive courses on the topic of continuum mechanics and theoretical finite element analysis are present in most USA structural engineering university curriculum.
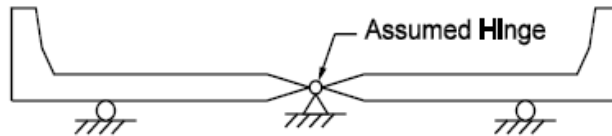

Figure 9 - Notional model for applying lever rule to three-girder bridge from AASHTO

13. CONCLUSION

Several differences in design and construction of short-span and middle-span road bridges in the U.S.A. and Serbia are discussed and compared. By comparing practices from different perceptions and from different parts of the world, one should be able to widen perspective and improve engineering judgment.

REFERENCES

[1]   "ASCE Infrastructure Report Card, 2021."
[2]   "Indiana Design Manual." Indiana Department of Transporation, 2020.
[3]   S. Rodrigo, *The Engineering of Foundations*. Mc Graw Hill, 2011.
[4]   *Prestressed/Precast Plant Tour (www.youtube.com/watch?v=HLnV-fdf9kQ&t=66s)*.
[5]   D. Bobera, P. Bakic, G. Milutinovic, "Seismic isolation of bridges on Morava Corriror," presented at the DGKS, Arandjelovac, Serbia, in review 2022.
[6]   J. Zhao and D. Tonias, *Bridge Engineering: Design, rehabilitation, and maintenance of modern highway bridges*, Third Edition. 2012.
[7]   NHCRP Synthesis 425, *Waterproofing Membranes for Concrete Bridge Decks*. Washington, D.C.: Transportation Research Board, 2012.
[8]   "INDOT Bridge Inspection Manual." Indiana Department of Transporation, 2020.
[9]   B. Phares, J. Shane, J. Dahlberg, and H. Dang, "Methods for Removing Concrete Decks from Bridge Girders final report," FHWA, Iowa State University, 2014.
[10] S. Masovic and R. Hajdin, "Assesment of the bridge deck slab deterioration according to the Serbian bridge information database," presented at the DGKS Simpozijum, 2012.
[11] NCSPA, "Corrugated Steel Pipe Design Manual," 2008.
[12] M. Fardis, "Capacity design: Early history," *Earthquake Engng Struct Dyn.*, 2018, doi: 47:2887–2896. https://doi.org/10.1002/eqe.3110.
[13] T. Zokaie, T. Osterkamp, and R. Imbsen, "NCHRP 12-26 - Distribution of wheel loads on highway bridges," 1991.
[14] R. Barker and J. Puckett, "Design of Highway Bridges: An LRFD Approach," 2013.

Miroslav Marjanović[1]*, Marija Milojević*[2]*, Miloš Jočković*[3]

SPECIFIČNOSTI PROJEKTOVANJA ANEMOMETARSKIH ČELIČNIH JARBOLA U REPUBLICI SRBIJI

Rezime:

Projektovanje i izgradnja velikih vetroparkova zahteva prethodno merenje vetroenergetskog potencijala na predmetnoj lokaciji. Za ove potrebe, koriste se anemometarski čelični stubovi (jarboli) koji nose opremu za merenje brzine i pravca vetra na različitim visinskim novoima. U ovom radu biće prikazane neke specifičnosti u analizi, konstrukcijskom oblikovanju, fundiranju i montaži čeličnih jarbola, uočene tokom projektovanja (od strane autora) i izgradnje više ovakvih konstrukcija u Republici Srbiji u poslednje tri godine.

Ključne reči: čelični jarbol, Evrokod, nelinearna analiza, segmentno opterećenje

IMPORTANT ASPECTS IN DESIGN OF ANEMOMETRIC STEEL MASTS IN THE REPUBLIC OF SERBIA

Summary:

Design and construction of large wind farms requires preliminary measurement of wind energy potential at the future wind farm location. For these purposes, anemometer steel guyed masts are used, which carry equipment for measuring wind speed and direction at different altitudes. This paper will present some important aspects in the analysis, structural design, foundation and assembly of steel masts, identified during the design (by the authors) and construction of several such structures in the Republic of Serbia in the last three years.

Key words: steel mast, Eurocode, nonlinear analysis, wind patch loads

---

[1] *Assistant professor, Faculty of Civil Engineering, University of Belgrade, Serbia, mmarjanovic@grf.bg.ac.rs*
[2] *Assistant, Faculty of Civil Engineering, University of Belgrade, Serbia, mmilojevic@grf.bg.ac.rs*
[3] *Assistant professor, Faculty of Civil Engineering, University of Belgrade, Serbia, mjockovic@grf.bg.ac.rs*

1. INTRODUCTION

Due to the increasing demands of modern industry concerning communication and energy, the design and construction of large wind farms have been conducted in Serbia in the last 15 years. This required a preliminary measurement of wind energy potential at the future wind farm location. For carrying equipment for measuring wind speed and direction at different altitudes, guyed lattice steel masts are usually used. They are very slender and tall structures, consisting of a vertical central mast laterally supported at several levels along its height by sets of inclined pre-tensioned guy ropes. Due to the required lifespan, the number of collapses of masts is relatively far greater than for other types of structures [1].

The optimal design of a guyed mast requires a series of iterations between the conceptual design and the structural analysis. It is relatively hard to give a precise height above which the guyed mast is an optimal structural solution. This depends on factors such as land cost for the specific location, but quite often the guyed masts are used for heights above 60-80m.

The central mast usually consists of:
- the base segment, forming a fixed or pinned connection with the foundation,
- the main part, consisting of a number of standard segments, each usually 3.00m long, and
- the last segment, usually carrying a measuring device and lightning rod.

The standard segment is a spatial lattice structure, usually of triangular leg layout and side length varying between 0.45-0.90m. It comprises leg members and horizontal and diagonal elements welded to the leg members. The connection between the segments is made through the bearing plates. Due to the dynamic nature of wind loading, prestressed bolts with full prestressing forces are used (see Figure 6d).

Figure 1 - Installed guyed masts of 120.78m, 160.00m and 126.30m height, respectively (source: NETInvest Engineering and Consulting Solutions)

The anemometric masts do not require big and heavy frame sections due to the very small dimensions and weight of the attached equipment. Consequently, these structures are lighter

than other mast types (i.e. for telecommunication purposes), and the standard segments can be easily manipulated, lifted and connected to one another [2-4].

This paper presents some important aspects of structural analysis, design, foundation and execution of temporary steel anemometric masts, identified during the design (by the Institute of Numerical Analysis and Design of Structures - INP) and construction of four such structures in the Republic of Serbia in the last three years (see Figure 1).

2. CONSIDERED GUYED MAST STRUCTURES

In the last three years, four guyed mast structures have been designed or validated by the INP. The main properties of the considered structures are given in Table 1, while the schematic layout of the structures and their cross sections of the mast shaft are illustrated in Figure 2.

Table 1 - Properties of the considered guyed mast structures

#	Height	$v_{b,0}$	Ice class	Steel	Leg members	$N_{b,Rd}$	m
1	120.78 m	21 m/s	ICG-3	S275	∅50×4mm	159 kN	26 kg/m
2	141.30 m	25 m/s	ICG-2	S355	∅40mm (full)	300 kN	54 kg/m
3	126.30 m	25 m/s	ICG-2	S355	∅40mm (full)	300 kN	54 kg/m
4	160.00 m	32 m/s	ICG-2	S355	∅88.9×6.3mm	571 kN	62 kg/m
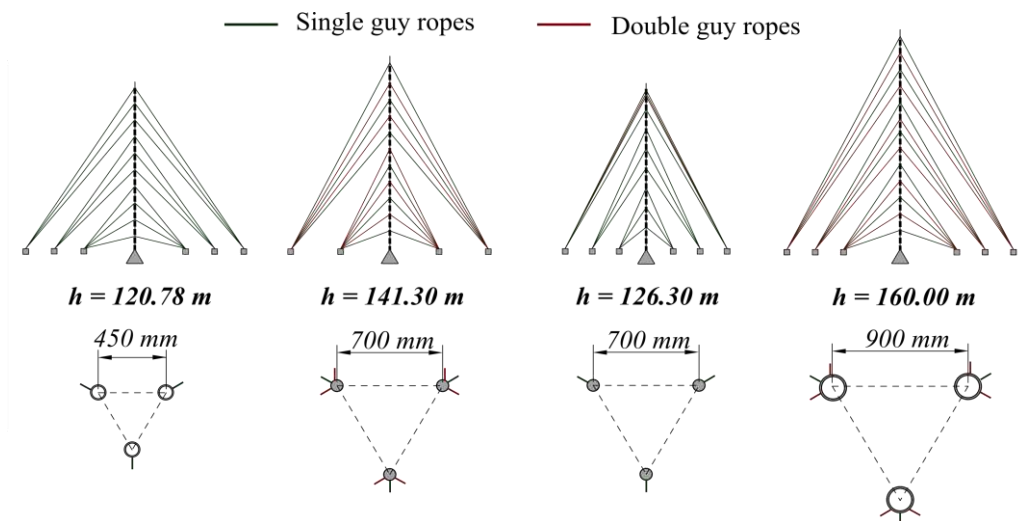
Figure 2 - Schematic layout and cross-sections of the considered mast structures

It should be pointed out that structures 1-3 have been designed (validated) based on the existing structural solution of the mast shaft. In these cases, the layout of the cables, foundation solution and complete structural validation according to SRPS standards was done by the INP, but without the possibility to change the steel grade, members and detailing of the mast shaft. In structures 2-3 illustrated in Figure 2, the leg members are full circular sections, which generate lower wind load on the mast shaft, but have lower flexural buckling resistance $N_{b,Rd}$ in comparison against CHS, according to SRPS EN 1993-1 [5].

Based on the experience gained through design validation of structures 1-3, a 160.00m guyed mast was entirely designed by the INP, including the layout, complete structural detailing and foundations in 2020.

Obviously, all considered structures had a triangular layout of leg members of the mast shaft. This layout has an advantage against the square layout by means of lower wind incidence factor K_θ and lower wind force coefficients $c_{f,s,0}$, according to Section B.2.2. of SRPS EN 1993-3-1 [6]. Consequently, it induces lower wind forces on the the mast structure.

All members of the mast shaft are circular (full or hollow section). The flat members should be avoided because their drag (pressure) coefficients are more than twice higher when compared against the circular members. Finally, the discrete ancillary items on the structure are almost negligible, and their area A_A was adopted as 10-20% of the structural area A_s.

In all cases, guy ropes were made of galvanized steel with a tensile strength of 1770 N/mm^2, type 6×19+FC, with a minimum breaking force extracted from [7]. When selecting the guy layout, several important aspects should be taken into account: (i) number of guy levels, (ii) number of guys per guy level, (iii) distance between the adjacent guys, (iv) guy lengths and (v) guy diameter and material properties. These factors influence the decision whether the equivalent static analysis may be performed, which is quantified through the factor β_s, according to [6]. In all considered structures, the dominant selected guy distance was 12m.

The number of guys per guy level is also important for preventing the torsion of the mast shaft. The preferred solution by the authors is to use alternately the guy levels with 3 and 6 guys per level, respectively. The cables are attached to concrete blocks, radially distributed around the mast shaft in several concentric circles (where the diameter of the outer circle is approximate to the mast height). This solution requires 6 concrete blocks per circle (Figure 2), and more guys to be attached to the mast shaft, when compared with the classical solution of 3 guys per level along the entire mast shaft and thus 3 concrete blocks per circle (3×120º layout).

The proposed solution, successfully applied in the 160.00m mast, prevents the mast's torsion and provides a more uniform distribution of the forces in the guys. The maximum forces in the guys are proportionally lower, leading to the easier anchorage of the guys to both the mast shaft and the concrete blocks. Anchoring details are given in Section 5.

The mast is supported by a central RC foundation, which is usually square, due to the simple solution for the reinforcement and formwork. Of course, the symmetry of the structure implies that a circular central foundation may be used.

3. STRUCTURAL ANALYSIS

Steel lattice masts are slender and vulnerable structures. Structural analysis of a guyed mast is thus complex due to the geometrically nonlinear behaviour of the structural system and the random nature of the wind loads. Geometrically nonlinear analysis was performed with P-Δ effects, and all load combinations were constructed as independent load cases without the superposition principle.

The masts were modeled in SAP2000 [8], based on the finite element method, as an equivalent spatial beam structure, supported by guys at different altitudes. The initial prestressing forces were assigned to the cable elements. According to EN1993-1-11 [9], the catenary effect was taken into account by applying an effective modulus of elasticity for guys, E_t=130GPa (combinations without ice load) and E_t=121GPa (combinations with ice loads), according to the following formula:

$$E_t = E / \left(1 + \frac{w^2 \cdot l^2 \cdot E}{12\sigma^3}\right) \qquad (1)$$

where: $E = 165$ GPa is the elasticity modulus of the guy; w is the guy unit weight; l is the guy length σ is the stress in the guy.

Based on the obtained member forces, the ultimate limit state (ULS) and stability checks of all structural members were performed according to [6, 7], while the joints calculation was performed according to [10].

The serviceability limit state (SLS) was checked according to SRPS EN1993-1-11 [9] to provide the elastic service conditions by limiting strains in cables. In that manner, corrosion control measures were not affected and the fatigue design was catered to uncertainty. The stress in cables was limited to $f_{SLS} = 0.50 \, \sigma_{uk}$, where $\sigma_{uk} = F_{uk}/A_m$, and A_m is the area of the metallic cross-section and F_{uk} is the minimum rope braking force.

Finally, leg members were controlled against the fatigue effects according to [11].

4. ACTIONS ON THE STRUCTURE

The characteristic values of the actions were calculated in accordance with a set of Eurocode-based SRPS standards [5-7, 9-15] and the relevant ISO standard [16] for determining ice loading. The design values of the actions were determined according to the load combinations defined in [6, 12]. The following loads were considered: (i) self-weight and additional dead load, (ii) cable pretension forces, (iii) ice load, (iv) wind action and (v) seismic actions. The snow and temperature effects were neglected.

Few computer programs are available for a complete dynamic stochastic analysis of guyed masts. Therefore, considerable efforts were spent in producing simplifications for the design rules for codes and standards. Relatively reliable simplified procedure was developed and adopted SRPS EN1993-3-1 [6]. The procedure is based on simplified static patch wind models. According to [6], 3 criteria must be satisfied to ensure that the equivalent static analysis of the guyed mast can be performed. A check of these conditions showed that equivalent static analysis might be applied for all considered mast structures.

4.1. VERTICAL ACTIONS AND CABLE PRESTRESSING

The self-weight was assigned automatically. The additional dead load originates from the equipment on the mast according to the manufacturer's specification. Initial prestressing forces were assigned in cable elements using SAP2000. They were adopted in the range 10-20% of the minimum rope braking force, according to [7].

The effect of ice on the structure has been investigated by many authors [17]. It was calculated according to [16], for considered glaze ice-class (ICG), and assigned as equally distributed vertical loading to the mast and guys.

4.2. WIND ACTION

The lattice masts are sensitive to the dynamic action of the wind. Ice on a mast will by its weight change the dynamic behaviour, as well as it may increase the wind drag of a lattice mast dramatically. Therefore, it is essential that masts are analyzed for the dynamic response to the

wind [1]. Therefore, the wind resistance of the structure must be accurately determined, including its ancillaries such as ladders and cables.

Wind loads on the mast structure should be calculated according to the fundamental wind velocity $v_{b,0}$, and the appropriate terrain type and orography factor c_o according to [13]. The design value of wind load on a mast with a triangular layout of leg members should be calculated for three characteristic wind directions: +Y, -Y and X, see Figure 3.
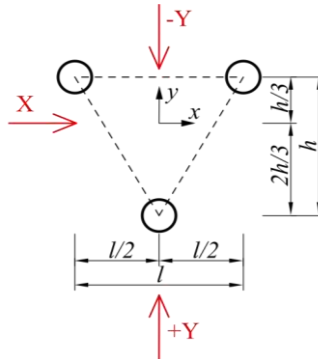
Figure 3 - Considered wind directions

The total wind effect on the structure should be calculated as a sum of equivalent static action of the *mean wind* load, corresponding to a 10-minute mean wind velocity in the direction of wind action, and fluctuating load due to wind gusts (*patch wind load*). For the sake of simplicity, a mean wind can be modelled as a uniformly distributed load along the considered mast segment, where the reference height z is the height of the top of the segment. Mean wind load to the guys lies in the plane defined by the considered guy and the considered wind direction. For the sake of simplicity, a uniform load distribution along the guy may be used, with $q_p(z)$ determined for $z=2H/3$ (H is the height of the guy attachment to the mast).

Successive patch wind loads should be assigned to the mast sections as follows: (i) on each span of the mast between adjacent guy levels, including the span from the base of the mast to the first level of the guy and the cantilever, (ii) from mid-point to mid-point of adjacent spans, (iii) from the base of the column to the mid-height of the first level of guys, and (iv) from the middle of the height of the span between the penultimate and the top guy level, if there is no cantilever present, or including the cantilever if relevant. The patch load on the guys should be applied within the same boundaries, perpendicular to each guy, in the plane containing the guy and the wind direction. For simplification, the patch loading may be smeared over the whole height of the relevant guy by multiplying the wind load with the ratio z_p/z_G, where z_p is the height of the patch on the guy and z_G is the height to the attachment of the guy to the mast.

As the superposition principle is not valid, forces due to the patch loads $S_{p,Li}$ should be obtained as the difference of: (1) forces due to the sum of the mean wean load and i^{th} patch wind load, and (2) forces due to the mean wind load only. The total effect of wind fluctuation (patch load), S_p, should be obtained by combining the individual effects of all patch loads as:

$$S_P = \sqrt{\sum_{i=1}^{N} S_{pLi}^2} \tag{2}$$

where N is the total number of patch load cases. The overall effect on the structure, which introduces the effect of wind fluctuation, is equal to the envelope of the following loads:

$$S_T = S_M \pm S_P, \qquad (3)$$

where S_M is the effect of mean wind load, while S_P is the effect of patch load.

4.2.1. The effect of atmospheric icing combined with the effect of wind

The icing of the mast significantly increases the structure's weight, while the thickness of the ice increases the surface of the structural elements exposed to the wind. Therefore the wind force on the structure increases, which may have a very adverse effect on the mast. The calculation of the wind effect is the same as for the ice-free structure, with the changes in the thickness of the structural elements and appropriate drag coefficients. The ice may completely block the structure if masts are located in areas where severe atmospheric icing occurs.

The effects of ice and wind are combined in two ways:
- Dominant wind (high probability of occurrence) + associated ice (low probability),
- Dominant ice (high probability of occurrence) + associated wind (low probability).

Due to the low probability that a 50-year wind and high ice will occur simultaneously, a coefficient k, which reduces the wind pressure on the iced structure, is introduced in [16].

4.3. LOAD COMBINATIONS

According to SRPS EN1990 [12] and SRPS EN1993-3-1 [6], taking into account the reliability class 1 (towers and masts built on unmanned sites in open countryside; towers and masts, the failure of which would not be likely to cause injury to people) and partial safety factors for actions (γ_G, γ_P, $\gamma_{Q,w}$, $\gamma_{Q,ice}$), coefficients for the combinations of variable actions (ψ_w, ψ_{ice}) and coefficient for the reduction of wind action in the combination with ice (k), the following design situations are adopted for the ultimate limit state (ULS):

$$
\begin{aligned}
&\gamma_G \cdot G_k \; + \gamma_P \cdot P_k \; + \gamma_{Q,w} \cdot Q_{k,w} \\
&\gamma_G \cdot G_k \; + \gamma_P \cdot P_k \qquad\qquad\qquad\qquad + \gamma_{Q,ice} \cdot Q_{k,ice} \\
&\gamma_G \cdot G_k \; + \gamma_P \cdot P_k \; + \gamma_{Q,w} \cdot k \cdot Q_{k,w,ice} \quad + \gamma_{Q,ice} \cdot \psi_{ice} \cdot Q_{k,ice} \qquad\qquad (4)\\
&\gamma_G \cdot G_k \; + \gamma_P \cdot P_k \; + \gamma_{Q,w} \cdot k \cdot \psi_w \cdot Q_{k,w,ice} \quad + \gamma_{Q,ice} \cdot Q_{k,ice}
\end{aligned}
$$

In (4), G is the self-weight + additional dead load; P is the prestressing force; W is the wind on the ice-free structure; Qice is the ice loading and Qw,ice is the wind action on the iced structure. Based on the obtained results, extreme force values in structural members were determined, and their envelopes were drawn, as shown in Figure 4.

4.4. SEISMIC ACTION

Seismic action was determined using the equivalent lateral force method and multimodal analysis for the considered soil category, depending on the mast location. Elastic spectrum type, structural damping, design ground acceleration a_g and behavior factor $q=1.0$ are adopted according to [15]. In all cases, it was shown that the seismic action was not relevant because the maximum seismic force S_{max} is several times lower than the force due to the effect of mean wind loading $F_{m,w}$.

5. RESULTS AND GOVERNING LOAD CASES

This section briefly illustrates the envelopes of compression force $N_{c,Ed}$ distribution along the mast shaft leg members, for all considered structures. The forces are plotted in Figure 4 for the following load scenarios: maximum self-weight + prestressing of cables, maximum ice, and maximum wind load (with or without the ice effects). For all considered structures, +Y or –Y directions were the critical ones, because in these cases the greater area is subjected to wind load when compared to the X direction.

As shown in Figure 4, for the first structure validated against the ICG-3 ice class, as expected, dominant ice + associated wind was the governing load scenario. For all other structures, dominant wind + associated ice was the critical load scenario. Therefore, for the guyed masts subjected to the average ice conditions, this load scenario should be considered first in the conceptual design phase.
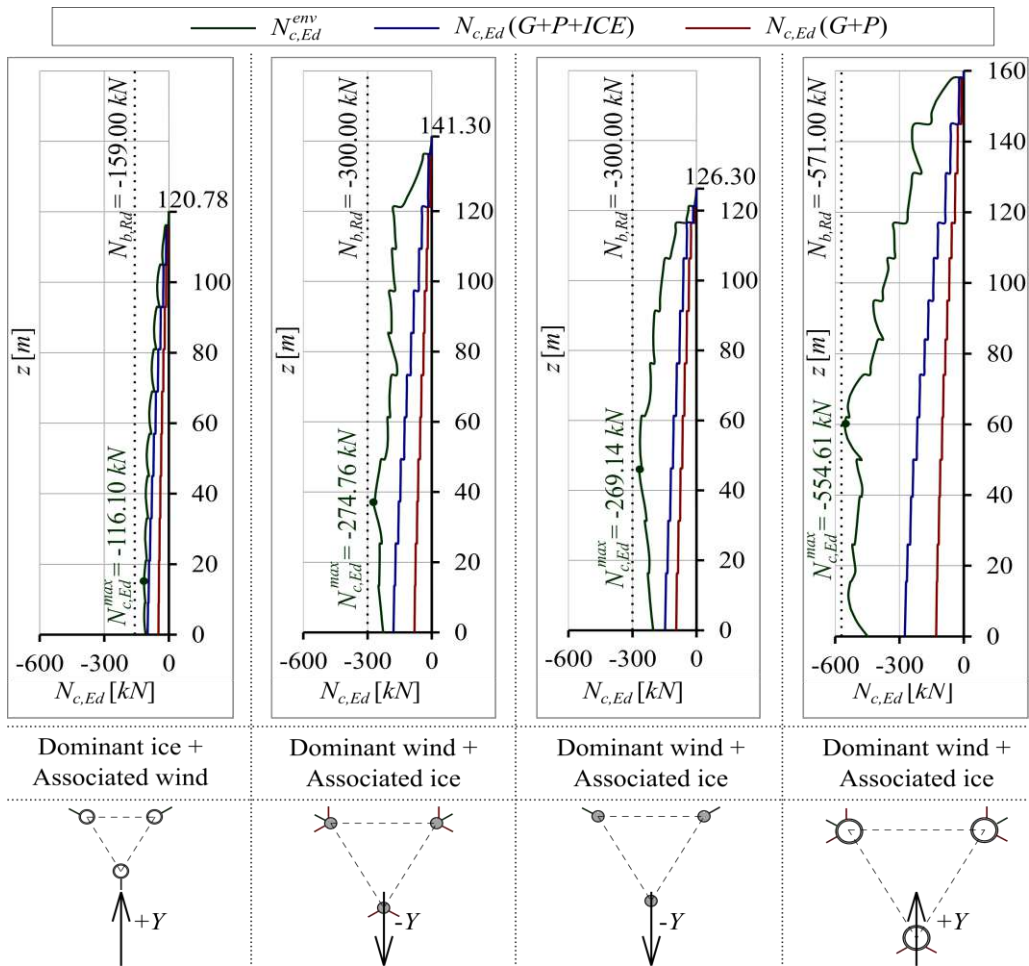
Figure 4 - Compression force $N_{c,Ed}$ distributions in leg members of the considered mast structures, with governing load scenarios and critical wind directions

6. FOUNDATIONS AND STRUCTURAL DETAILING

The important choice to be taken in the conceptual design phase is whether the mast base should be fixed or pinned to the mast foundation [1]. The authors suggest that pinned connection should nearly always be adopted for the following reasons: (i) the fixed mast base is susceptible to foundation settlement, (ii) the fixed mast base requires relatively large foundation dimensions, and (iii) the pinned connection leads to the axially loaded foundation.

There are several ways to design and execute the pinned connection between the mast shaft and the foundation. The pivoted tower base with a M30 8.8 bolt was used for the mast of 120.78m height (Figure 5a), while the tapered tower base, which is the most common solution, was used for both masts of 160.00m and 126.30m (Figure 5b-c).
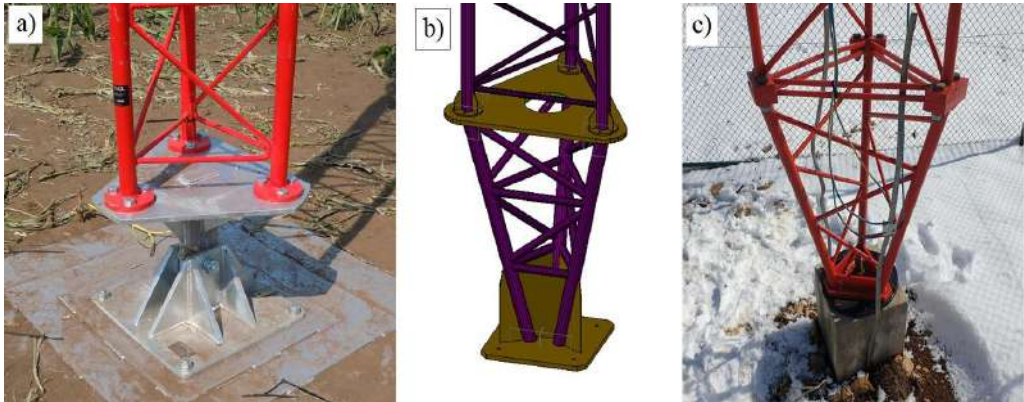
Figure 5 - First segments of installed guyed masts of 120.78m, 160.00m and 126.30m height, respectively (source: NETInvest Engineering and Consulting Solutions)

The detailing of the guy attachment to the mast (Figure 6b-c) and especially to the guy foundation (Figure 6a) is of the outmost importance, because of the relatively high forces in guys and their dynamic nature. It is essential that the guys can pivot as freely as possible under dynamic loading. In the considered mast structures, the guys were attached both to the foundation and the mast shaft using the steel bow shackles, according to SRPS EN13889 [18].
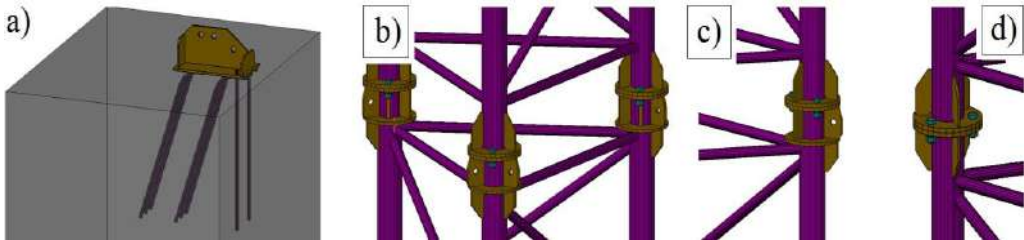
Figure 6 - a) guy anchoring system; b) segment-to-segment connection with double guy rope anchoring detail; c) single guy rope anchoring; d) standard segment-to-segment connection

According to SRPS EN1993-1-11 [9], the characteristic value of the breaking strength F_{uk} for guy ropes should be determined based on the selection of the terminations of steel wire

ropes. The ropes are equipped with thimbles [19] and U-bolt grips [20], which govern the loss factor k_e to be appropriately selected when determining F_{uk}.

At the attachment of the guys to the guy foundations, an adjustable tension system should be installed to apply initial tension to the guys. Mast shaft foundations are very simple unless unusual soil conditions are encountered. The guy foundation design is governed by several limit states: sliding, overturning and uplift. In the considered structures, solid concrete blocks were used for the guy foundation, with the appropriate steel reinforcement anchorage system, shown in Figure 6a.
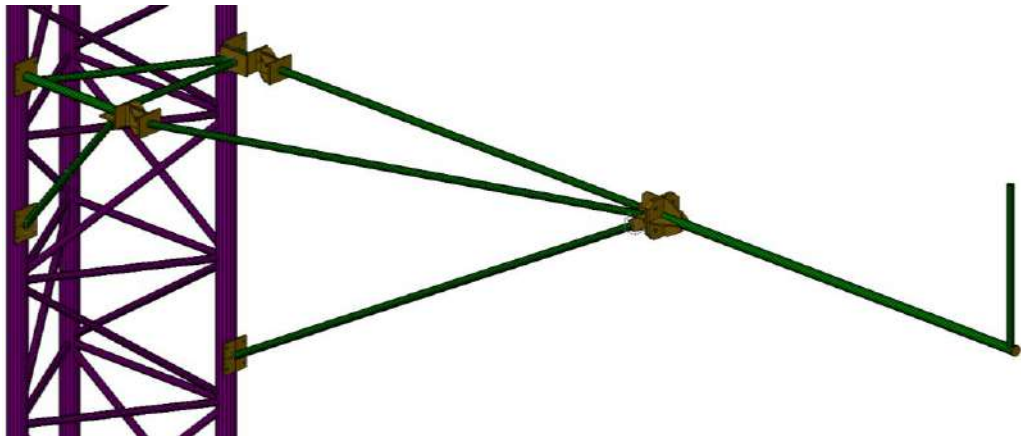
Figure 7 - Anemometer boom (green color) attached to the 160.00m mast shaft leg members

The side anemometers and wind-vanes were attached to the mast shaft on different altitudes, using the special steel booms (green color in Figure 7), constructed to be easily lifted with the mast segment and then attached to the mast in three points.

7.   CONCLUSIONS

In the paper, some important aspects of structural analysis, design, foundation and execution of temporary steel anemometric masts, identified during the design and construction of several such structures in the Republic of Serbia in the last three years, have been presented. These structures are slender and vulnerable, thus requiring relatively complex geometrically nonlinear analysis with P-Δ effects. The complexity of the structural analysis is governed by the fact that all load combinations must be constructed as independent load cases without the superposition principle. For this purpose, SAP2000 was used.

Some important aspects in structural modeling and analysis were discussed, and several notes on the actions on these structures according to SRPS standards were presented. The discussion has been made on the criteria for using the equivalent static analysis instead of the dynamic analysis of the wind load influence on guyed masts.

Based on the previous experience, some important aspects in defining the proper structural layout of guyed masts were highlighted, along with the remarks of structural detailing of such structures. The importance of preventing the mast shaft torsion has been pointed out, along with the proposed solution for guy layout.

Finally, based on the results of structural calculation of several guyed masts with different guy layouts, the conclusions have been derived on the governing wind directions and load scenarios to be considered in the conceptual design phase. It was shawn that for ICG-2 ice class, dominant wind and the associated ice loading will be critical for design of leg members, while for ICG-3 the dominant ice and the associated wind will be critical.

ACKNOWLEDGMENTS

REFERENCES

[1] Nielsen M. G., Støttrup-Andersen U. Design of guyed masts, http://www.latensored.org/wp-content/uploads/2019/05/p_02_nielsen_andersen.pdf

[2] Jiang W. Q, Wang Z. Q, McClure G, Wang G. L, Geng J. D. Accurate modeling of joint effects in lattice transmission towers, Engineering Structures, 33 (5), 2011, 1817-1827.

[3] Zhuge Y, Mills J. E, Ma X. Modelling of steel lattice tower angle legs reinforced for increased load capacity, Engineering Structures, 43, 2012, 160-168.

[4] Erdem R. T. Analysis of guyed steel lattice mast subjected to environmental loads, Gradjevinar, 67 (7), 2015, 681-689.

[5] SRPS EN 1993-1-1: Eurocode 3: Design of steel structures - Part 1-1: General rules and rules for buildings, Belgrade, Serbia, Institute for Standardization of Serbia, 2012.

[6] SRPS EN 1993-3-1: Eurocode 3 - Design of steel structures - Part 3-1: Towers, masts and chimneys - Towers and masts, Belgrade, Serbia, Institute for Standardization of Serbia, 2012.

[7] SRPS EN 12385-4: Steel wire ropes - Safety - Part 4: Stranded ropes for general lifting applications, Belgrade, Serbia, Institute for Standardization of Serbia, 2009.

[8] SAP2000, Integrated Finite Element Analysis and Design of Structures Basic Analysis Reference Manual, Computers and Structures Inc. Berkeley, 1995.

[9] SRPS EN 1993-1-11: Eurocode 3 - Design of steel structures - Part 1-11: Design of structures with tension components, Belgrade, Serbia, Institute for Standardization of Serbia, 2012.

[10] SRPS EN 1993-1-8: Eurocode 3: Design of steel structures - Part 1-8: Design of joints, Belgrade, Serbia, Institute for Standardization of Serbia, 2012.

[11] SRPS EN 1993-1-9: Eurocode 3 - Design of steel structures - Part 1-9: Fatigue, Belgrade, Serbia, Institute for Standardization of Serbia, 2012.

[12] SRPS EN 1990: Eurocode – Basis of structural design, Belgrade, Serbia, Institute for Standardization of Serbia, 2012.

[13] SRPS EN 1991-1-4: Eurocode 1: Actions on structures - Part 1-4: General actions - Wind actions, Belgrade, Serbia, Institute for Standardization of Serbia, 2012.

[14] SRPS EN 1997-1: Eurocode 7: Geotechnical design - Part 1: General rule, Belgrade, Serbia, Institute for Standardization of Serbia, 2017.

[15] SRPS EN 1998-1: Eurocode 8: Design of structures for earthquake resistance - Part 1: General rules, seismic actions and rules for buildings, Belgrade, Serbia, Institute for Standardization of Serbia, 2015.

[16] ISO 12494:2017. Atmospheric icing of structures. International Organization for Standardization, 2017.

[17] Makkonen L., Lehtonen P., Hirviniemi M. Determining ice loads for tower structure design, Engineering Structures, 74, 2014, 229-232.

[18] SRPS EN 13889: Forged steel shackles for general lifting purposes - Dee shackles and bow shackles - Grade 6 - Safety, Belgrade, Serbia, Institute for Standardization of Serbia, 2009.

[19] SRPS EN 13411-1: Terminations for steel wire ropes - Safety - Part 1: Thimbles for steel wire rope slings, Belgrade, Serbia, Institute for Standardization of Serbia, 2009.

[20] SRPS EN 13411-5: Terminations for steel wire ropes - Safety - Part 5: U-bolt wire rope grips, Belgrade, Serbia, Institute for Standardization of Serbia, 2012.

R-36

Kongres 2022
Congress 2022

Novak Novaković[1], Nemanja Kozarac[2], Serkan Kaplan[3]

PROJEKAT MONTAŽE MOSTA PREKO REKE SAVE KOD SREMSKE RAČE

Rezime:

Most koji nije projektovan da se izgradi, montira, postupnim navlačenjem je preprojektovan. Izabrano je najekonomičnije rešenje, konstrukcija je ojačana i most postupno lansiran u konačni položaj. Širina profila za autoput pokrivena je sa dve paralelne konstrukcije, svaka širine 14,75 m. Glavni most čini kontinualna čelična sandučasta greda preko tri raspona 90+150+90 m. Čisto rastojanje između paralelnih konstrukcija je 1,50 m. Visina poprečnog preseka je konstantna. Niveleta na mostu je nesimetrična, sa leve obale penje se nagibom od 1,7%, prelazi kružnom krivinom prečnika 24 km i pada ka desnoj obali nagibom od 2,3%.

Ključne reči: montaža, čelični, mostovi, Sava, postupno navlačenje

LAUNCHING OF BRIDGE OVER RIVER SAVA NEAR SREMSKA RAČA

Summary:

The Bridge originally not designed to be incrementally launched is redesigned. Best solution was chosen, according to results superstructure is strengthened and launched across the Sava river. Highway width is covered with two parallel bridges with three spans of 90+150+90 m. The deck width of each is 14,75 m. Clear distance between parallel structures is 1,50 m. Cross section is steel box girder of constant height. The vertical alignment follows the alignment of the road, from the left river bank bridge rising at a strait gradient of 1,7% and falling to the right river bank at a grade of 2,3%, curved in the middle at a radius of 24 km.

Key words: incremental launching, bridge, Sava, steel superstructure

---

[1] *Glavni inženjer, DEL ING DOO, Beograd, Srbija, novak.novakovic@deling.rs*
[2] *Inženjer, DEL ING DOO, Beograd, Srbija, nemanja.kozarac@deling.rs*
[3] *Inženjer, Metal Yapi Eng & Const, Istanbul, Turska, serkan.kaplan@metalyapi.com*

1. INTRODUCTION

The Sava Bridge is composed of two parallel bridges, one for each carriageway. The north bridge (right highway lane) has a total length of 1311,5 m and the south bridge (left highway lane) 1320,5 m. Each bridge crosses the Sava River with three spans of 90+150+90 m – main bridge structure. The deck width in both cases is 14,75 m. Separate bridge structures, spaced at 15.50 m (axis to axis), are planned for each highway direction. Clear distance between parallel structures is 1,50 m.

The vertical alignment of the main spans follows the vertical alignment of the road. From the left river bank bridge rising at a strait gradient of 1,7% and falling to the right river bank at a grade of 2,3%, curved in the middle at a radius of 24.000 m. The steel girders are continuous over 3 spans with expansion joints only at end piers. Uniform cross fall of the bridge deck of 2.5% towards outer curbs is in conformity with drainage requirements.

Erection method was a Contractor condition. Designer of bridge structure (CIP Beograd [1]) did not take into account any constriction phase of loads during construction. Bridge was originally designed as on full scaffold build at once, even there was some kind of requirement from Main Contractor.

At the beginning of construction, we have received bridge structure documentation [1], [3] and Method Statement [2] from Subcontractor in charge for launching. The Main Contractor required complete verification before starting the operation.

2. SITE CONDITIONS

Main bridge steel structure has a total length of 330 m and weight of around 2700 t. It consists of 21 prefabricated pieces length of 15 m and two 8,25 m (first and last segment)
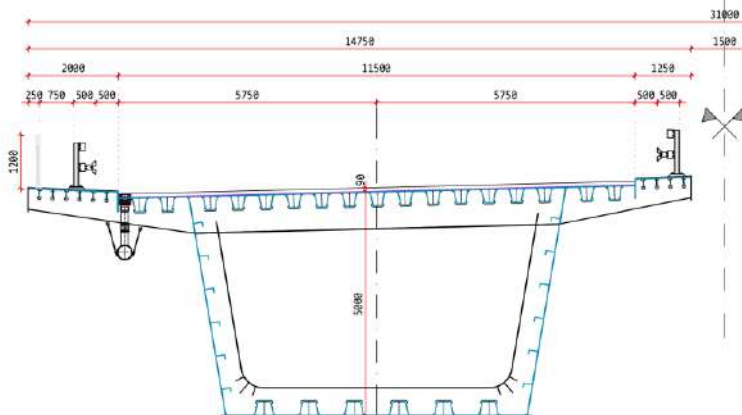
Figure 1 - Cross section of one bridge

The steelwork was prefabricated and transported to the site in sections of up to 15 m long weighing up to 170 t. There are five different sections of box girder (Figure 2). The difference is in web, bottom and top plate thickness and some part with different material.

The depth of the steel box girder is constant height of 5000 mm measured on bridge centerline (Figure 1). Webs of the box section are inclined at 80 degrees so the web spacing at the top is

8377 mm, while at the bottom is spaced at 6707 mm. Longitudinal stiffeners of the bridge deck are shaped as of closed trapezoidal cross section, 300 mm high, 320 mm wide and 8 mm thick. They are situated at center-to-center spacing of 620 mm. Cross girders are spaced at 3,0 m apart and together with vertical stiffeners on vertical webs and transverse stiffeners on bottom slab (sole slab), they form a rigid frame system.
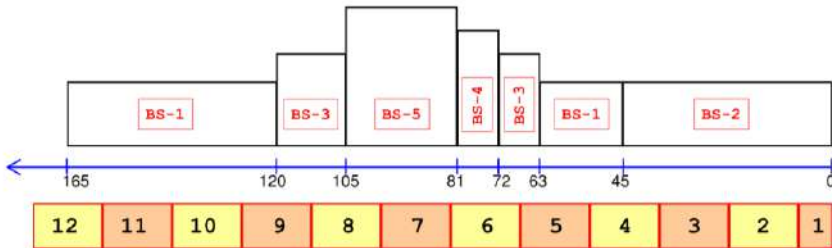
Figure 2 - Half bridge sections and segments arrangement (Box size represents I_y approx.)

Solid diaphragms together with adequate stiffeners will be placed above supports, in a box. The box bottom plate, 6910 mm wide, is formed of sheet metal of variable thickness (from 20 mm to 45 mm). Stability of the plate is ensured by means of six longitudinal stiffeners of trapezoidal shape, 300 mm high and 420 mm wide. These trapezoidal stiffeners are 8 mm thick except in the area of the intermediate support over 18,0 m length where thickness is increased to 10 mm. Webs at the box are of variable thickness (from 14 mm to 20 mm), i.e., they are 30 mm thick in the area of intermediate support. Stability of vertical web is ensured using longitudinal stiffeners, formed of angles L200x100x12, spaced at 760 mm apart.

3. INCREMENTAL LAUNCHING METHOD

Initial version of launching stages we received from Subcontractor. This version includes three main temporary structures for installation of Bridge: launching nose, sliding bearings and steel tower with cables (Figure 3).
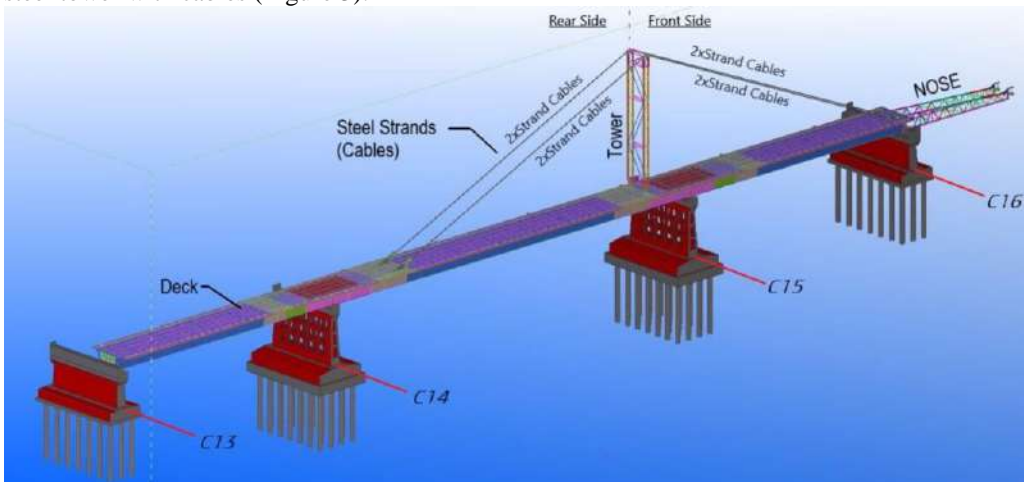
Figure 3 - Initial version of launching

According to this solution steel tower should be pin connected to bridge structure with cable stays from the top of the tower to front of the structure to keep deflection in acceptable range during launching. So, the tower transfers vertical forces from front and back to one point that is not fixed but rather movable together with deck – bridge superstructure.

We begin the verification of this idea (Contractor desire) of launching method. Shortly after first results of critical stages analysis we established that bridge structure as designed would not withstand internal stresses from selfweight. Also, capacity of vertically adjustable sliding supports was limiting factor. Our proposal was to introduce temporary piers, enough to launch structure without strengthening. As Sava is navigable river so that clear width of "channel" should be at least 80 m, there was an option for only one temporary pier.

So, with side spans 90 m and after costs analysis, we decided to use only one temporary pier and "lightly" strengthen the bridge structure. The main problems were stability during first steps of launching (short back structure), web buckling stability and deformations of structure. This big launching span required strong "nose" so it can take reaction as soon as it reaches next sliding support.
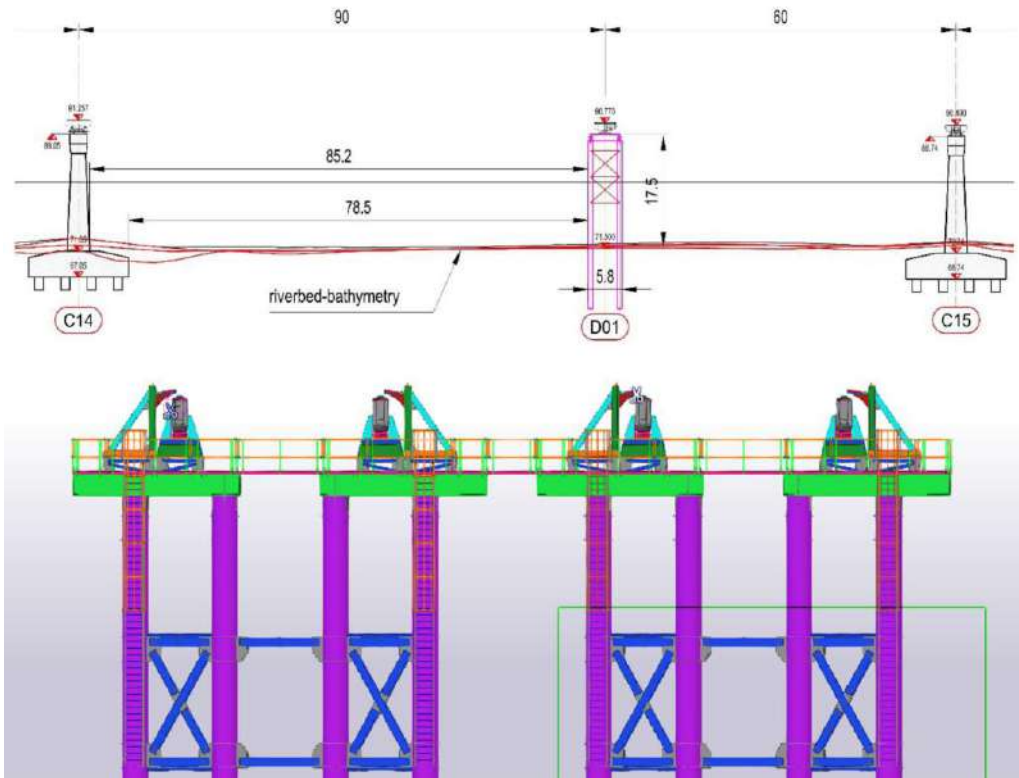
Figure 4 - Temporary pier location and cross section with sliding bearings and guiding devices on top

Another problem was size of launching sliding bearings and vertical curvature of the bridge. Levels of all sliding supports are carefully studied so that vertical alignment (including pre-camber) of bridge and deflection do not capture temporary support. There were two types of

sliding supports: fixed and vertically adjustable. We used vertically adjustable supports also to control the reaction forces, by some percent, in continuous beam system some force could be transferred from one to another by rising the bearing.

Temporary support position is chosen to maintain navigable channel width. Design of temporary pier was our resposnability. Vertically adjustable sliding bearing (Figure 5) was positioned on top of the temporary pier. Top level was chosen so that bearing could be removed after launching is finished.
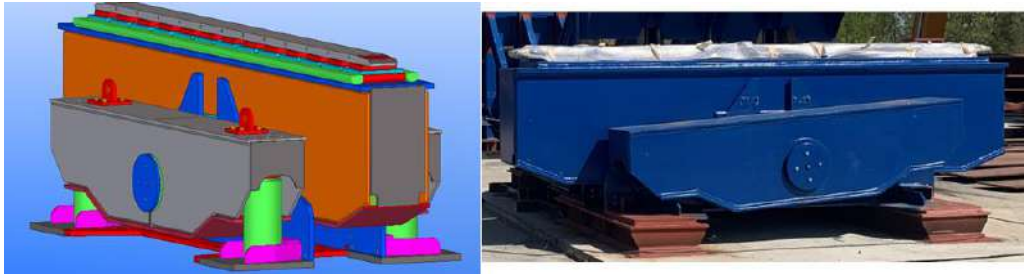
Figure 5 - Vertically adjustable bearing

4. CONSTRUCTION STAGES VERIFICATION

During bridge launching, the system changes continually. Therefore, each bridge position has to be verified. Box section flanges and webs have to resist the varying internal forces and support reactions. Verifying bending, shear and torsion, special attention is paid to local buckling of compression flange and to the problem of patch loading of web at the supports.

Patch loading is related to the stability of thin webs under high in-plane compression forces. As the bridge moves over the supports (including temporary one), the reaction force is transferred through the web panels between transversal stiffeners (diaphragms).

Patch loading resistance is calculated according to Eurocode. Method to determine the critical force is numerical using FEM of a panel including horizontal and added vertical stiffeners.

Loading during launching is determined by stage construction analysis using SOFiSTiK module CSM. Firstly, all stages at every 3 m were studied to choose most relevant positions which are then analyzed in detail (regarding reaction forces, internal forces and deflections). As sliding bearings cannot withstand negative reaction, complete calculation was nonlinear. But also we adjusted bearings levels if necessary to activate inactive bearing and to relax adjacent.

Following diagrams (Figure 6) shows one of most critical stages regarding stress in bottom flanges and webs. Other critical stage with maximum bending moment at structure-nose connection was used for verification of nose structure and connections.

In one stage 30 m of structure is to be assembled on assembly area. Next step is launching for 30 m in one day.

As steel for main bridge structure were already reserved or purchased, increasing the thickness of webs was not an option. Most economical solution was to add additional vertical or horizontal stiffeners (Figure 7), which are not required for the final in-service states.

Global stability is verified for most critical stages i.e., CS 108. Safety factor for overturning the structure is 1,55 (relative to the ULS – already factored loads).

Critical force of buckling for unstiffened and stiffened web is 11100 kN and 17700 kN, respectively, which gives 22% higher load bearing capacity. Also that was the maximum capacity of jacks that are used for adjustable bearings.
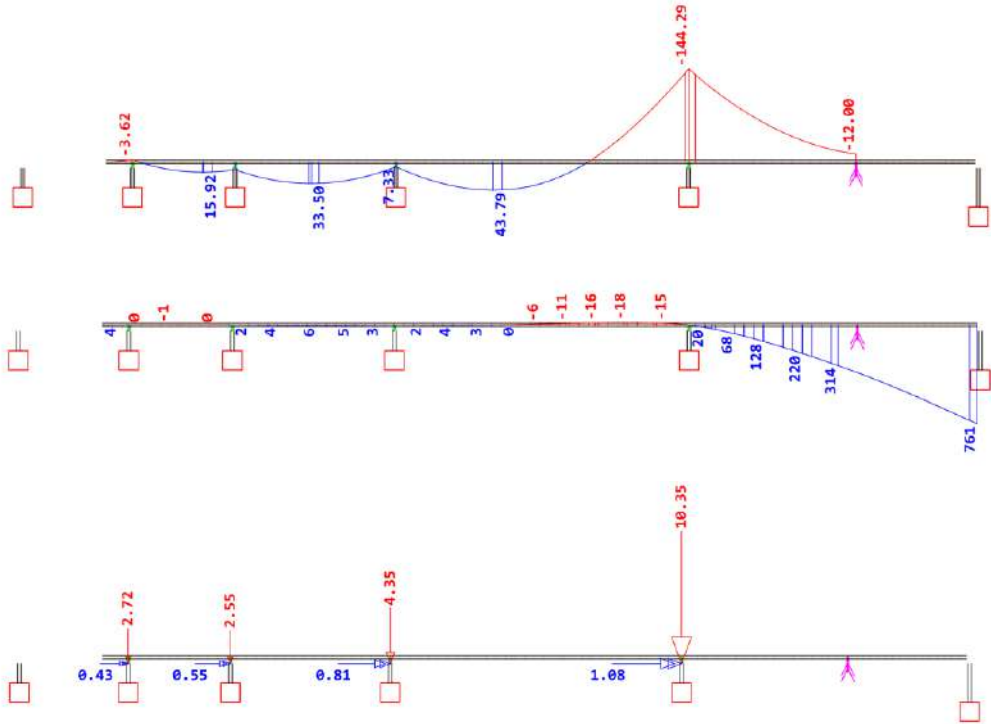
Figure 6 - One of relevant stages (CS 123): bend. moment (MNm), z deflection (mm), reaction (MN)

Table 1 - Patch load bearing capacity per web (stiffened vs unstiffened)

	$F_{cr} =$	17700	11100	kN
	$t_w =$	14	14	mm
	$l_y =$	3000	3000	mm
	$f_{yw} =$	355	355	N/mm^2
$F_{y,Rk} = l_y t_w f_{yw}$	$F_{y,Rk} =$	14910	14910	kN
$\lambda_F = (F_{y,Rk}/F_{cr})^{0,5}$	$\lambda_F =$	0,9178	1,159	
$\chi_F = 0,06 + 0,47/\lambda_F$	$\chi_F =$	0,572	0,466	
$F_{Rd} = \chi_F F_{y,Rk}/\gamma_{M2}$	$F_{Rd} =$	7754	6310	kN
	$l_{supp} =$	3300	3300	mm
$F_{Rd,supp} = l_{supp} F_{Rd}/l_y$	$F_{Rd,supp} =$	8530	6941	kN
	$F_{Ed,max} =$	8300	8300	kN
	$\alpha_{web} =$	80,5	80,5	deg
$F_{Ed,web} = (F_{Ed,full}/2)/sin(\alpha_{web})$	$F_{Ed,web} =$	8415	8415	kN
	$F_{Ed,web}/F_{Rd} =$	0,99	1,21	
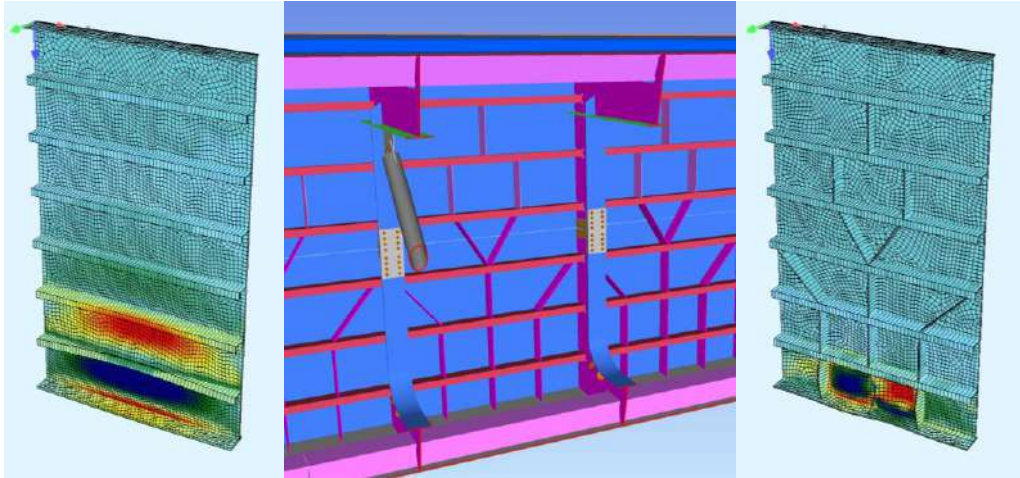
Figure 7 - Additional stiffeners, buckling modes for unstiffened and stiffened web

5. EXECUTION

Each segment is consisting of seven assemblies, which will be joined on precast-yard area by welding and/or bolting. Temporary structures used for launching are temporary pier D01, nose truss and sliding bearings. Other used equipment are: pulling lugs, anchor blocks, steel strands and guiding devices.

Nose is steel truss structure, length around 42 m and weight around 65 t. It was assembled in front of the deck, to shorten the cantilever length. On nose tip cylindrical hydraulic jacks, vertically adjustable are mounted to be able to overcome deflection of cantilever and control the reaction.
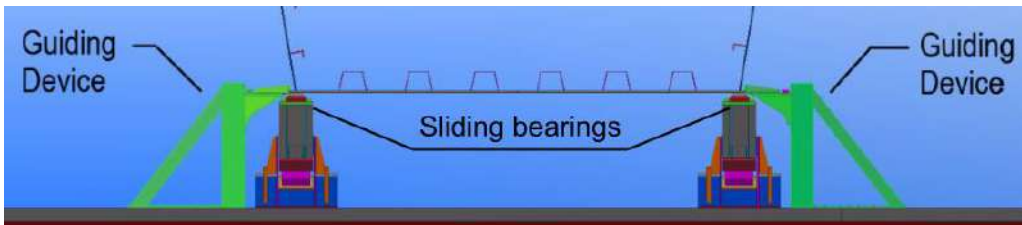
Figure 8 - Position of sliding bearings and guiding devices on piers

Guiding devices are placed on every pier to keep the structure in line during launching. Strand lugs are designed to pull the bridge over the launching bearings. Pulling lugs are fixed on pier C13 and on the other side under the bottom plate of box section. Every launching step puling lugs were dismantled and installed on another position 30 m away. They were connected by prestressing bolts on bottom side of the box section. The maximum cantilever during launching is 91 m, with 42 m long launching nose used to reduce the cantilever of bridge itself to 49 m.

Figure 9 - Beginning of the launching, one bridge launched 30 m
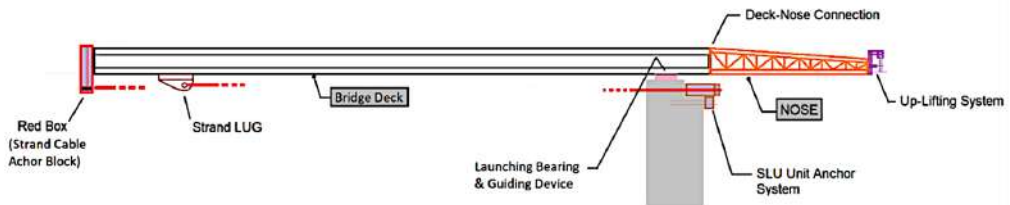
Figure 10 - Launching system, naming of structural parts and equipment

Due to pre-cambered shaped production of steel bridge structure, the distribution of the weight of the structure to the supports was affected by temperature differences on the top and bottom parts of the deck. That is why most of the launching (especially the most critical stages) was tried to completed in the early of the morning. Just to be safe, loads of the bearings were checked on every 3 m. If need, after close coordination with the design team, vertically adjustable support levels were re-arranged to work within the prescribed load-bearing ranges.

The bridge geometry of vertical curvature and pre-chamber had to be considered for launching. To solve the problem, vertically adjustable support is provided at second permanent pier C14 and two at launching pad TS-1 and TS-2. Other supports, including on temporary pier are fixed (on last pier C16 is adjustable as it is transported from TS-1). This arrangement of supports allows full control of reactions. The supports are adjusting in order to avoid lift-off or unacceptably high support reactions. Maximum vertical displacement of adjustable supports is 800 mm using hydraulic jacks.

Figure 11 - First bridge reaching the temporary pier in the river

Basic installation schedule:

- preparation of launching location;
- connecting first 6 segments of bridge structure on assembly area – 83,3 m;
- installation of nose structure which is supported on pier C13 and temporary supports;
- control of geometry and monitoring equipment before launching;
- incremental launching across pier C13 in the direction of pier C14 for 30 m;
- assembling of next 2 segments (30 m) at assembly area;
- control of geometry and launching for another 30 m.

Last two steps repeat until the whole bridge structure is launched.

Jacking on TS-1, TS-2 and C14 is every 15 m during launching. Changing the levels on these supports control the reactions and geometry flow of bridge.

Monitoring during launching included measurement of reaction forces on adjustable supports, flange and web stresses are measured on several places with conventional strain gauges.

LITERATURA

[1] Čelična konstrukcija glavnog mosta, Glavna konstrukcija mosta preko reke Save, PZI Projekat za izvođenje, Deo 2/1.1.2.1, Saobraćajni institut CIP d.o.o. Avgust 2020.

[2] Method Statement for ILM, Main Bridge over the Sava River, Metal Yapi Eng&Const, Septembar, 2020.

[3] Geotehnički elaborat, Sveska E1/1, Geotehnički uslovi izgradnje mosta preko reke Save u Sremskoj Rači, Saobraćajni institut CIP d.o.o. Jul 2020.

[4] Izgradnja drumskog mosta preko reke Save kod Sremske Rače na putu M18 Sremska Rače – Bijeljina; DGKS Zlatibor 2010, Dragomir Lukić, Zoran Luković, Slavica Bjelica, Vladimir Novaković

Dalibor Gelo[1], *Šime Serdarević*[2], *Eduard Fot*[3], *Željko Lebo*[4]

PROCENA OTPORNOSTI NA ZEMLJOTRESE ZGRADE OZONA KOJA JE DEO VODOSNABDEVANJA

Rezime:

Zemljotres jačine 6,2 stepena Rihterove skale potresao je 29. decembra 2020. godine područje Petrinje u Republici Hrvatskoj. Posledice zemljotresa su značajna oštećenja na velikom broju objekata. Kako bi se moglo pristupiti što efikasnijem renoviranju, zakon predviđa izradu analize seizmičke otpornosti postojećeg objekta. U radu će biti prikazana procena seizmičke otpornosti objekta ozona koji je deo postrojenja za zahvatanje i preradu vode za piće u Novom Selištu. Analiza obuhvata istražne radove, predloge hitnih mera i numeričku procenu seizmičke otpornosti.

Ključne reči: zemljotres, seizmička otpornost, numerička analiza

SEISMIC RESISTANCE EVALUATION OF OZONE BUILDING AS PART OF THE WATER SUPPLY SYSTEM

Summary:

On December 29, 2020, an earthquake of 6.2 Richter hit the area of Petrinja in the Republic of Croatia. The consequence of an earthquake is a significant damage to many buildings. As a part of building reconstruction, the Croatian law predicts the evaluation of seismic resistance of the existing buildings. This paper presents a seismic resistance evaluation of ozone building as a part of the water supply in city of Novo Selišće. Evaluation includes experimental research, proposals for emergency measures and numerical analysis.

Key words: earthquake, seismic resistance, numerical analysis

---

[1] *senior lecturer, Zagreb University of Applied Sciences, Zagreb, Croatia, dalibor.gelo@tvz.hr*
[2] *lecturer, Zagreb University of Applied Sciences, Zagreb, Croatia, sime.serdarevic@tvz.hr*
[3] *engineer, Filedo d.o.o., Sveti Ivan Zelina, Croatia, eduard.fot@gmail.com*
[4] *senior lecturer, Zagreb University of Applied Sciences, Zagreb, Croatia, zeljko.lebo@tvz.hr*

1. BUILDING DATA

The building was built in the early 1980s and is a part of the Petrinja water purification plant near the right bank of the Kupa river. Its rough dimensions are 24 m by 22 m and height is 8 m, and the structural system was achieved by combining monolithic and prefabricated elements – it combines reinforced concrete frames (columns and beams), plates and walls. The epicenter of the devastating 6.2 magnitude earthquake is less than 5 kilometers away from the building and the damages following the earthquake were clearly visible, leading to an urgent seismic inspection of the building. Inspection of the building revealed significant damage, leading to its closure. The figures below show a floorplan and a section of the building. The north is on the upper side in the floorplan and on the left in the section.
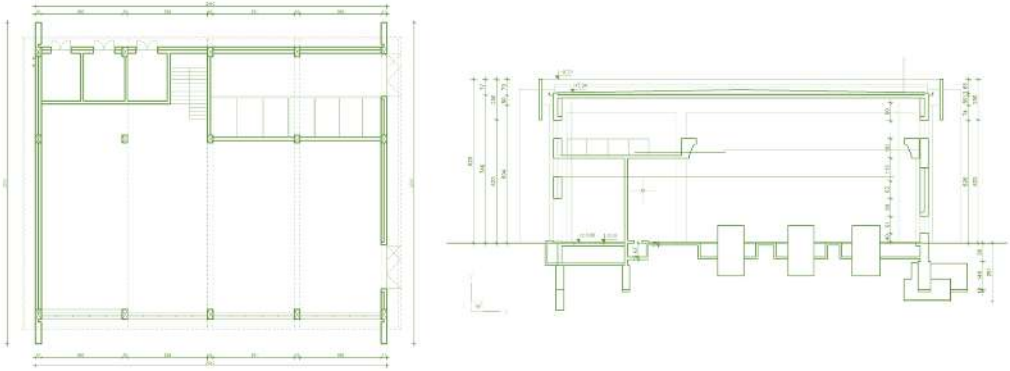
Figure 1 – Ground floor plan and north-south section
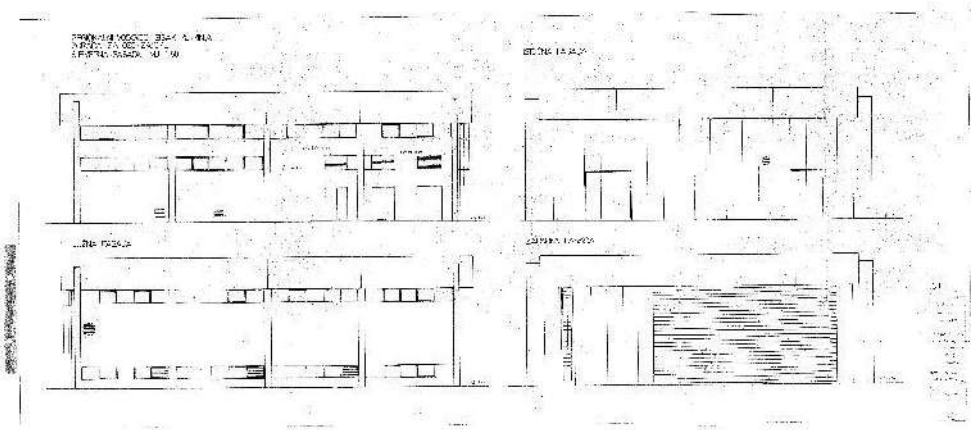
Figure 2 – Building elevations (clockwise from the upper left elevation: north, east, west, south)

Figure 3 – View of the building from the south-east corner

Figure 4 – View of the building from the south-west corner

Figure 5 – Interior of the building, looking to the south

2. DAMAGES OVERVIEW

Out of all the damages, the diagonal cracks in the load-bearing reinforced concrete columns were recognized as critical. They appeared on all columns on the south side of the frames, at window level, due to excessive shear forces at that point during the earthquake. This is obviously the structure's weak point and was poorly designed, so these damages had to be fixed as soon as possible in case of further aftershocks.

Figure 6 – View of one diagonal crack

517

Furthermore, the westward wall placed between the reinforced concrete columns and beams is a masonry wall, unlike the eastward reinforced concrete wall. This westward wall has suffered a large out-of-plane displacement due to the lateral forces of the earthquake, and it was noticed that it could fall to the exterior. This was promptly secured by removing the masonry wall and placing a "sandwich" panel in its place.

Figure 7 – Out of plane displacement of the westward masonry wall

3. URGENT STRENGTHENING OF THE COLUMN DIAGONAL CRACKS

In order to proceed with any further work or assessments, it was crucial to secure the columns' diagonal cracks. This was done by removing the first windows on both sides of the columns and pouring a reinforced concrete wall segment in their place. These walls were additionally reinforced by embedding steel HEB200 profile columns in the concrete near the reinforced concrete columns. The new concrete segments were anchored to the walls above and below, and also to the existing columns using 16 mm dowels at 15 cm spacing. The used steel mesh is Q503, and the concrete itself is C30/37. This secured the columns at their most exposed point. This urgent securing was proven as sufficient at this point after the numerical analysis.

Figure 8 – Added steel columns by the concrete columns
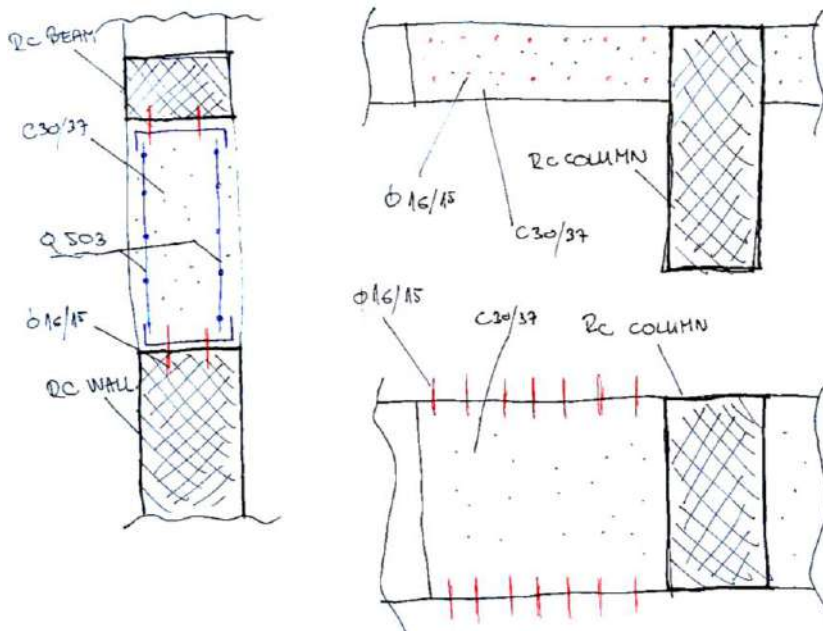
Figure 9 – reinforcement sketches (clockwise from the left: section, floorplan, elevation)

Figure 10 – RC segment after pouring of concrete

4. FIELD TESTS

The field tests determined the actual quality of the used materials (concrete and reinforcement) after over 30 years of use. The concrete compressive strength and density were determined at different positions in the building using 21 cylindrical samples taken from the structure. The actual positions of the reinforcement were determined at 6 points, along with a check of the thickness of the protective layer and the size of reinforcement bars using electromagnetic induction. Additionally, the intensity of corrosion was determined by measuring

half-cell potentials. All field and laboratory tests led to the expected conclusion – the quality of the concrete has fallen off during the years, or the designed quality concrete was never achieved. What came as a surprise was that one group of samples from a column showed that the designed quality was MB30, and the evaluated compressive strength was 16,2 MPa, which is a 46% drop. Regarding the reinforcement, the position and sizes matched the original designs retrieved from the building's archives. The probability of corrosion was estimated as less than 10%, and the carbonatization depth reached the reinforcement at only a few spots, which leads to the conclusion that the existing reinforcement is in good condition.

5. NUMERICAL ANALYSIS

With these field tests and preserved original design documentation, it was possible to create a reasonably accurate building model. The concrete quality for the whole building was modelled as either MB30 reduced by 70%, or as an exact value according to the field test results. The reinforcement was inputted as GA 240/360 (smooth reinforcement), in the exact sizes and positions as tested or as drawn in the original plans.
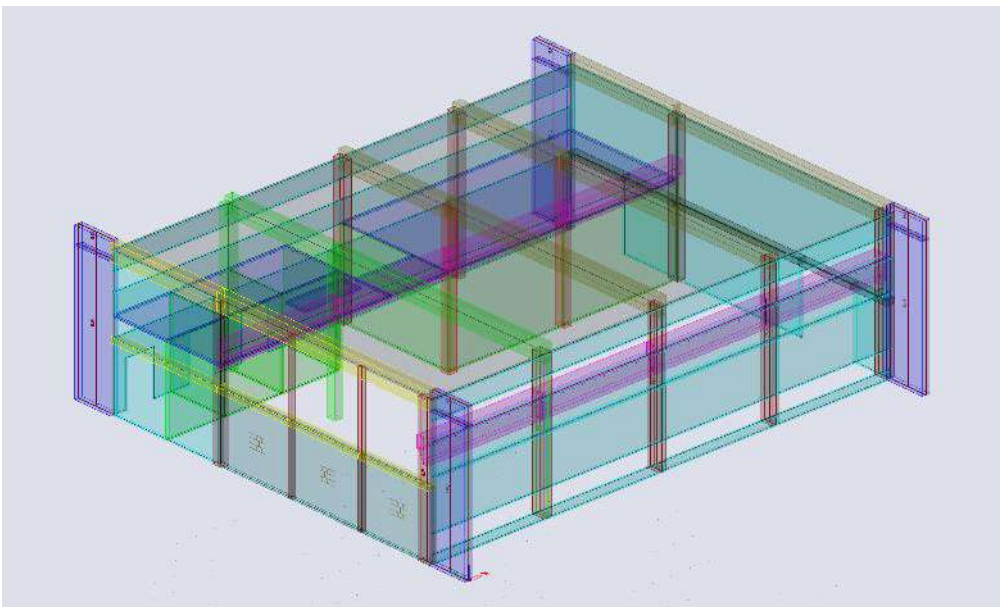
Figure 11 – View of the analytical model from the south-west side

The considered loads were as follows: building self-weight, imposed loads, additional snow loads, and lateral earthquake loads. The earthquake loads were created by using a spectrum response analysis. All loads were defined according to the currently valid Eurocodes. According to the Croatian seismic map, the peak ground acceleration is 0.16g for the 475-year return period. The soil type is C, and the spectrum type is 1 because we expect an earthquake's magnitude to be higher than 5.5. The behavior factor is 1.5 to consider a design spectrum for the worst-case scenario. Over 90% of building mass activation was achieved when taking into account the first 100 vibration modes.
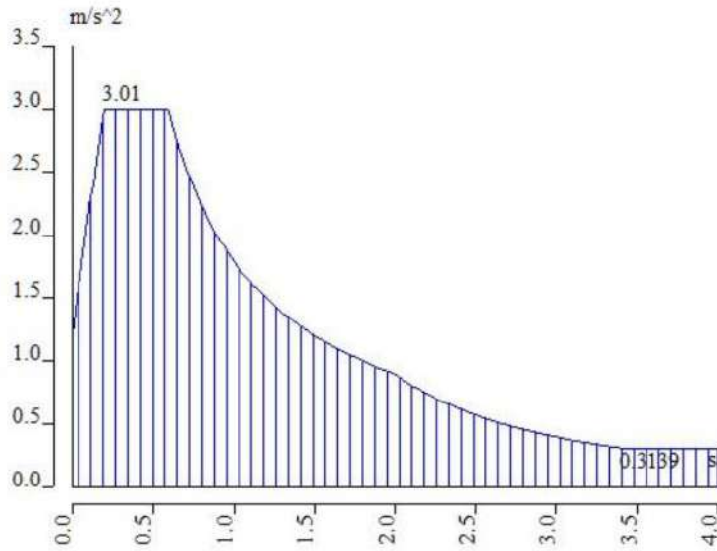
Figure 12 – Used design response spectrum
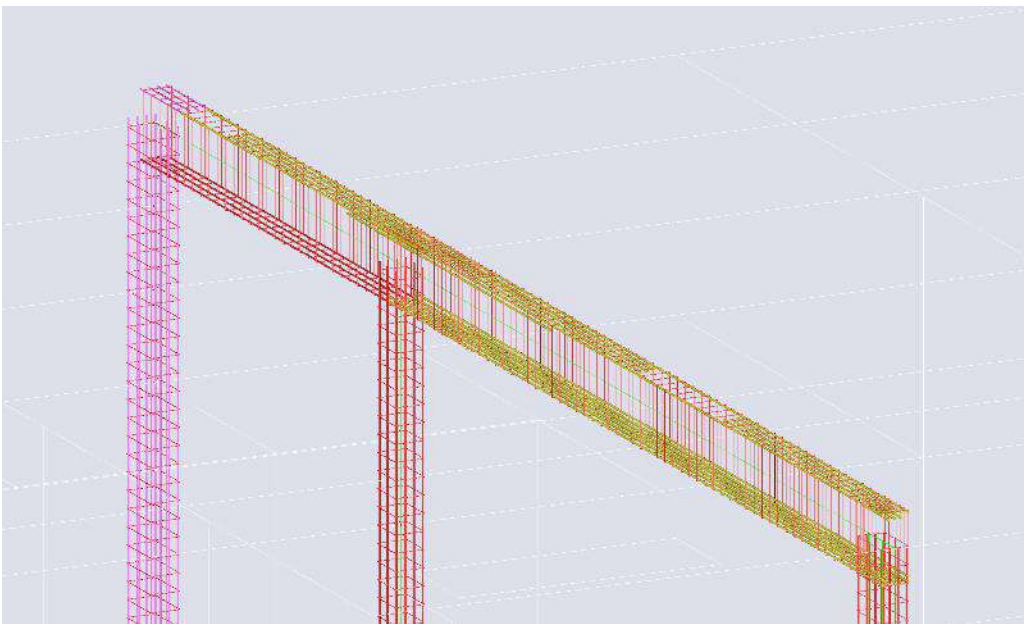
Figure 13 – Actually used reinforcement of the second frame

The results were reviewed and checked for any inconsistencies, and the model was iteratively perfected to gain a more real overview. The structure's elements were checked for the applied forces, and all elements' resistance checks were performed.

Figure 14 – 2nd frame south façade column unity checks before and after the urgent strengthening

The figures show the action/resistance (E_d/R_d) ratios for the 2nd frame south facade column before and after the undertaken urgent measures described earlier. The critical ratios all over the column come from the column's resistance to the lateral earthquake forces. This confirms the starting assumption: the columns failed at these points because of the underestimated earthquake lateral forces. After the columns' securing the internal forces of the structure were redistributed, and now the critical point is also on these columns, but by the upper row of windows. Based on all other analysis results it was determined that the plate elements (plates and walls) mostly satisfy today's criteria, except for several specific points which need reinforcement. The columns and beams often fail today's criteria, especially because of significant shear forces.

6. CONCLUSION AND FURTHER RECCOMENDATIONS

Following all the field tests, strengthening, and numerical analyses, it was concluded that the first and urgent securing was valuable and indispensable to the continued safety of the structure. However, work mustn't stop here. To secure the structure and raise it up to today's standards, a wholly encompassing strengthening proposal is needed which will include all elements that need reinforcement at all necessary positions. After finishing all works and owing to the structure's value and infrastructural meaning, further monitoring and maintenance are paramount.

LITERATURE

[1]   HZN, 2012. HRN EN 1991-1-1. s.l.:s.n.

[2]   HZN, 2011. HRN EN 1998-1. s.l.:s.n.

[3]   HZN, n.d. Karte potresnih područja Republike Hrvatske. [Web], Available at: http://seizkarta.gfz.hr/hazmap/karta.php

[4]   SCIA, n.d. Scia Help. [Na mreži], Available at: https://help.scia.net/webhelplatest/en/

Dragan Manojlović[1], *Vladimir Vukobratović*[2], *Andrija Rašeta*[3], *Anka Starčev-Ćurčin*[4], *Tanja Nožica*[5]

OJAČANJE DRVENIH TAVANICA PRIMENOM NORMALNOG I LAKOAGREGATNOG BETONA

Rezime:

Sprezanje drveta i betona je jedna od najčešće primenjivanih tehnika koje se koriste za ojačanje postojećih drvenih tavanica. Upotreba lakoagregatnog betona umesto normalnog betona omogućava optimizaciju u pogledu smanjenja sopstvene težine tavanice i racionalnog izbora spojnih sredstava, kao i povoljnije ponašanje spregnute tavanice sa aspekta preraspodele unutrašnjih sila. Sprovedena komparativna analiza ukazuje na razlike u mehaničkom ponašanju spregnutih tavanica kada se primene dva različita konstrukcijska betona. Cilj rada je da ukaže na prednosti i nedostatke primene lakoagregatnog betona za potrebe ojačanja postojećih drvenih tavanica.

Ključne reči: drvene tavanice, sprezanje drvo-beton, lakoagregatni beton, ojačanje

STRENGTHENING OF TIMBER FLOORS USING NORMAL AND LIGHTWEIGHT AGGREGATE CONCRETE

Summary:

Coupling of timber and concrete is one of the most commonly used techniques for strengthening of existing timber floors. The application of lightweight aggregate concrete, instead of normal concrete, allows optimization in terms of the floor weight reduction and rational choice of fasteners, as well as a more favourable behaviour of the composite floor in terms of redistribution of internal forces. A conducted comparative analysis indicates differences in mechanical behaviour of composite floors, when two different structural concretes are used. The aim of this paper is to present advantages and disadvantages of lightweight aggregate concrete utilization for the strengthening of existing timber floors.

Key words: timber floors, timber-concrete composite, lightweight aggregate concrete, strengthening

---

[1] *Teach. Asst., University of Novi Sad, Faculty of Technical Sciences, Novi Sad, Serbia, manojlovic.dragan@uns.ac.rs*
[2] *Assoc. Prof., University of Novi Sad, Faculty of Technical Sciences, Novi Sad, Serbia, vladavuk@uns.ac.rs*
[3] *Assoc. Prof., University of Novi Sad, Faculty of Technical Sciences, Novi Sad, Serbia, araseta@uns.ac.rs*
[4] *Asst. Prof., University of Novi Sad, Faculty of Technical Sciences, Novi Sad, Serbia, astarcev@uns.ac.rs*
[5] *Teach. Asst., University of Novi Sad, Faculty of Technical Sciences, Novi Sad, Serbia, nozica.tanja@uns.ac.rs*

1. INTRODUCTION

Everyday construction practice is accompanied by increasingly complex requirements imposed on today's engineers when demands need to expand the capacity of residential and commercial spaces. In addition to the design of new buildings, while the planning documents make their construction impossible in certain situations, there is an increasingly widespread view of the possibility of using existing buildings for the abovementioned purposes. This requirement leads to the need to increase and/or repurpose the spatial capacities of existing buildings in the case of upgrading or adaptations.

In these situations, engineering practice followed by scientific achievements in the construction field found answers to the set requirements in composite structures. Constructive systems created by the combination and application of appropriate materials in construction, in terms of the best use of material and mechanical characteristics, are one of the basic requirements of the optimal design of modern structures. Due to this idea, composite constructions have found their wide application in construction engineering. Various composite structures have been developed, and the most common coupled systems are steel-concrete and timber-concrete. Along with "classic" steel-concrete composite structures, the use of timber-concrete composite structures has found its broader application in the design of new constructions (bridges, residential, commercial, industrial and other buildings), as well as in the reconstruction and rehabilitation of old timber floor structures. Coupling timber and concrete are one of the most commonly applied techniques to strengthen existing timber floors [1].

With the development of new, but also with the application of traditional materials, modern timber constructions' constructive and economic advantages come to the express when timber-concrete systems are applied. By coupling timber and concrete, where timber is placed in a tensioned zone due to its relatively high tensile strength, while concrete is entrusted with the compressed zone of the coupled section [2], a more rational construction is obtained, where a high degree of utilization of both materials can be achieved.

Applying such hybrid systems in floor structures increases stiffness, fire resistance, reduction of the floor vibrations, and better thermal and acoustic properties. A justified floor structure was obtained, with an increased bearing capacity (about two times) and stiffness (from three to four times) compared to pure timber floors. It also increased the entire building's overall stability and seismic resistance because it obtained a rigid diaphragm [3]. Compared to classic floor structures made of different materials (concrete, steel, etc.), the listed advantages have shown their economic justification, not only because of their lower price but also because of the simplicity of construction and significantly less weight.

In modern construction, from the use of normal concrete, lightweight aggregate concrete has found its application when it comes to rehabilitating and strengthening old timber floor structures. Using lightweight aggregate concrete can increase the advantages of composite timber-concrete structures in terms of improving structural performance, energy efficiency and sound, temperature and fire insulation, with an additional reduction in the structure's weight [4]. Concrete in the timber-concrete composite beam is reduced to a minimum, especially the thickness of the RC slab, which ranges from 5-10 cm in the case of floor structures.

In composite timber-concrete structures, apart from the connection as one of the main factors affecting the mechanical behaviour of the composite beams, the characteristics of hardened concrete are of particular interest: modulus of elasticity, compressive strength, tensile

strength and density. Apart from the advantages mentioned earlier, constructive lightweight aggregate concrete has a compressive strength comparable to normal weight concrete, but a much lower modulus of elasticity (even comparable to timber), which can significantly affect the redistribution of internal forces and the deformation of the composite beam.

In this paper, a comparative analysis was conducted, which indicates the differences in the mechanical behaviour of timber-concrete composite floors using two different structural concretes. The paper aims to point out the advantages and disadvantages of using lightweight aggregate concrete to strengthen existing timber floors.

2. STRUCTURAL LIGHTWEIGHT AGGREGATE CONCRETE

According to EN 1992-1 [5] and EN 206-1 [6], structural concrete made of lightweight aggregate is classified as concrete with a closed structure and an oven-dry density of 800-2000 kg/m^3 and is produced using lightweight aggregate in whole or in part in relation to the total amount of applied aggregate. Lightweight aggregate concrete can be made from artificial or natural lightweight aggregate whose oven-dry density must be less than 2000 kg/m^3.

In EN 206-1, light aggregate is classified according to its oven-dry density (ρ) into density classes (D1,0-D2,0), Table 1. Also, the table shows the corresponding densities for plain and reinforced concrete with the usual percentage of reinforcement, which can be used for calculation purposes when determining self-weight or other permanent loads.

Table 1 – Density classes and corresponding design density of lightweight aggregate concrete according to EN 206-1 [6]

Density class		D1,0	D1,2	D1,4	D1,6	D1,8	D2,0
Oven-dry density of lightweight aggregate (kg/m^3)		801-1000	1001-1200	1201-1400	1401-1600	1601-1800	1801-2000
Density (kg/m^3)	unreinforced concrete	1050	1250	1450	1650	1850	2050
	reinforced concrete	1150	1350	1550	1750	1950	2150

According to EN 1992-1, provisions are given for normal weight concrete (NWC) apply, with many characteristics of lightweight aggregate concrete (LWAC) being related to its oven-dry density ρ (corresponding to the upper limit of the oven-dry density for the relevant class, Table 1). To determine the relevant characteristics of lightweight aggregate concrete, and based on the values for normal weight concrete (given in table 3.1, EN 1992-1), conversion coefficients η are used to determine the modulus of elasticity ($\eta_E=(\rho/2200)^2$) and tensile strength of concrete ($\eta_1=0,4+0,6\cdot(\rho/2200)$). When accurate data is needed, for example, when deflections are of great importance, it is necessary to conduct experimental tests to determine the value of the modulus of elasticity of lightweight aggregate concrete.

For composite timber-concrete structures, the technical specification (CEN/TS 19103) for timber-concrete composite structures [7] covers the use of normal weight concrete (strength classes from C12/15 to C60/75) and lightweight aggregate concrete (strength classes from LC12/13 to LC60/66). Table 2 shows the compressive strength, tensile strength and modulus of elasticity of lightweight aggregate concrete for some characteristic strength classes (LC16/18, LC25/28 and LC40/44) and density classes (D1,0; D1,4 and D1,8) for comparison with normal weight concrete.

Table 2 – Relevant characteristics of lightweight aggregate concrete

Strength class	D	ρ [kg/m^3]	$f_{lck,cube}$ [MPa]	η_1	f_{lctm} [MPa]	η_E	E_{lcm} [GPa]
LC16/18	1,0	1000	18	0.673	1.3	0.207	6.0
	1,4	1400		0.782	1.5	0.405	11.7
	1,8	1800		0.891	1.7	0.669	19.4
LC25/28	1,0	1000	28	0.673	1.7	0.207	6.4
	1,4	1400		0.782	2.0	0.405	12.6
	1,8	1800		0.891	2.3	0.669	20.8
LC40/44	1,0	1000	44	0.673	2.4	0.207	7.2
	1,4	1400		0.782	2.7	0.405	14.2
	1,8	1800		0.891	3.1	0.669	23.4

Based on the values given in Table 2, it can be seen that the density class of lightweight aggregate has a significant influence on the modulus of elasticity of lightweight aggregate concrete, which can significantly affect the stiffness and deformations of the timber-concrete composite beam. Also, the modulus of elasticity of lightweight aggregate concrete, for smaller density classes, has similar values to the modulus of elasticity of timber. Regarding compressive and tensile strength, lightweight aggregate concrete has comparable values to normal weight concrete, which is advantageous in terms of the load-bearing capacity of concrete in a composite beam.

From the aspect of reducing the self-weight of the composite structure, the use of lightweight aggregate concrete in relation to normal weight concrete is more than obvious, which can be seen based on the specific weight of plain and reinforced concrete shown in Table 1. This reduction has a favourable effect on the reduction of the self-weight of the concrete slabs in the amount of 14.6-56.3%, Figure 1 right, where the dependence of self-weight is also shown in relation to the usual thicknesses of concrete slabs in composite timber-concrete composite beam [8], Figure 1 left.
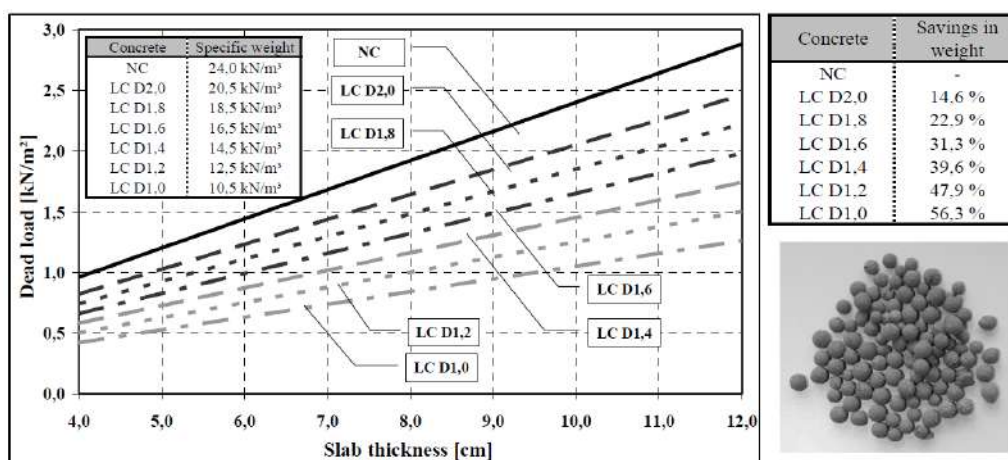
Figure 1 – The influence of using lightweight aggregate concrete by the savings of weight [8]

Based on the previous considerations, the use of lightweight aggregate concrete is desirable from the point of reducing the self-weight of the composite structure. From the point of the mechanical characteristics of hardened concrete, compressive and tensile strength, it has sufficient bearing capacity as well as normal-weight concrete.

The question arises of the mechanical behaviour of the composite member when using lightweight aggregate concrete, i.e. the redistribution of forces within the composite beam, as well as the deformation of the member at a lower modulus of elasticity. In the continuation of this paper, a comparative analysis will be conducted to determine the mechanical behaviour of the composite beams when using LWAC in relation to NWC.

3. COMPARATIVE ANALYSIS

For the purposes of the analysis, the real timber-concrete composite floor structure is adopted, and the geometric and mechanical characteristics of the elements of the composite beam are given in Figure 2. The load of the self-weight acts on the construction of the composite floor $g=g_{el}+\Delta g$ (gel - by the adopted materials and dimensions of the elements, $\Delta g=0,5kN/m^2$ – additionally permanent load) and imposed load $q=2,5kN/m^2$. The calculation was conducted according to the proposed simplified "gamma" method (EN 1995-1 [9], Annexe B). The stiffness of the connection, described by the slip modulus K, in this analysis will be considered as a function of the efficiency of the fasteners, represented by the shear connector reduction factor γ1 (dependent on the shear behaviour of the transverse layer).
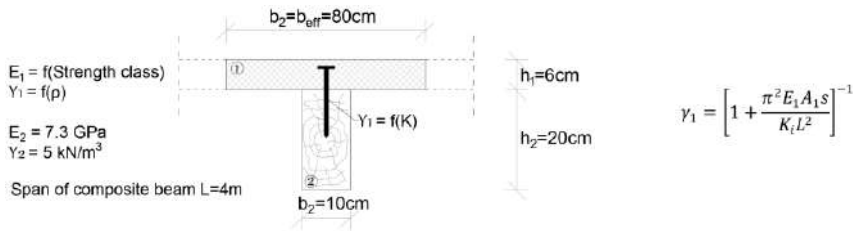
Figure 2 – Geometry and mechanical characteristics of the composite beam

NWC and corresponding LWAC were considered: NWC strength classes - C16/20, C25/30 and C40/50, LWAC strength classes - LC16/18, LC25/28 and LC40/44. Also, with LWAC, different density classes of lightweight aggregate were considered D1,0 ($\rho_{1,0}=1000kg/m^3$), D1,4 ($\rho_{1,4}=1400kg/m^3$) and D1,8 ($\rho_{1,8}=1800kg/m^3$). The corresponding specific weights of reinforced concrete used to calculate self-weight are adopted from Table 1, while the values of modulus of elasticity for LWAC are taken from Table 2.

3.1. ANALYSIS OF DESIGN PARAMETERS

Figure 3 (left) shows the effect of increasing the modulus of elasticity (E) and the thickness of the concrete slab (d_p) on the effective stiffness (EI_{eff}) of the composite beam. According to the diagram, the composite beam effective stiffness can be increased by using concrete with a higher modulus of elasticity or by increasing the thickness of the concrete slab. It can be seen that the thickness of the slab (exponential growth) dramatically influences the increase in effective stiffness in relation to the modulus of elasticity (~ linear growth). The use of stronger concrete, with a much higher modulus of elasticity, in composite floors in buildings is not

justified from the aspect of significantly increasing the effective stiffness of the composite beam due to a slight linear increase. For NWC, this solution can increase the composite structure's self-weight, and in this case, it is essential to reduce the specific weight of concrete by using LWAC. In Figure 3 (right), it is shown that, for an increase in slab thickness of only 1-2 cm and using LWAC, approximately the same effective stiffness of the composite beam can be achieved as in the case of NWC, while the self-weight remains unchanged or is reduced (by 10-30%).
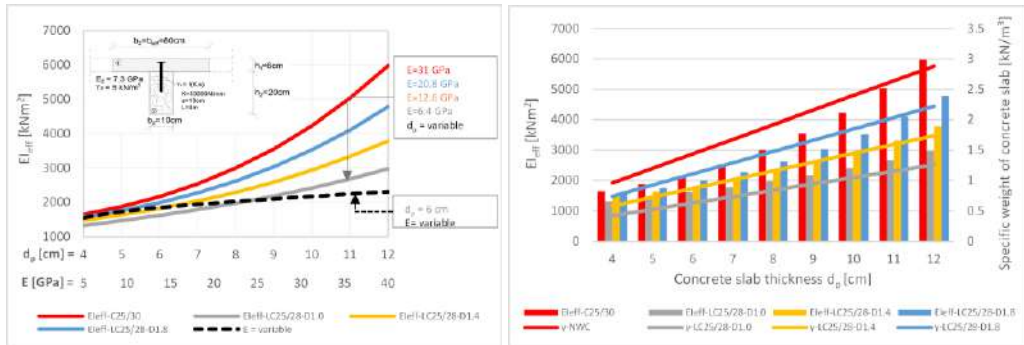
Figure 3 – Influence of modulus of elasticity and slab thickness on the effective stiffness [10] (left), and influence of slab thickness to specific weight of the concrete slab (right)

In the paper, slip modulus K is considered so that the value of the efficiency of the fasteners means (γ_1 coefficient) varied from 0.1-0.4, Figure 4. These limits usual correspond to the zone of efficiency of the fasteners, for the case of the application of traditional fasteners for coupling (placed at a distance of 10-50 cm) [11].

For the condition to be fulfilled and the analysis results to be comparable (for a certain γ_1), the value of the slip modulus K is variable for varying modulus of elasticity E. At the same time, the other parameters (A, s and L) are constant. The consequence of this condition is a smaller slip modulus since the ratio E_1/K must be the same for all conducted analyses, Table 3. Suppose the proposed limits (0.1 and 0.4) for the coefficient γ_1 are adopted, and the slip modules' K are calculated for different modules' elasticity of the considered concretes. In that case, the required diameters of the fasteners can be determined (using the expression $K=2 \cdot \rho_d^{1,5} \cdot (d/23)$, EN1995). The values shown in Table 3 indicate the favourable influence of the smaller modulus of elasticity of LWAC on the size of the required slip modulus and the diameter of the fasteners. A smaller diameter of the fasteners (more flexible fasteners) is needed to achieve the exact value of the efficiency of the fasteners in relation to NWC. Although the efficiency of the fasteners is the same in this case, the reduction of the elastic modulus results in a reduction of the effective stiffness (EI_{eff}) of the composite beam, which affects the increase of the composite beam deflection in the mid-span (f), Table 3.

It should be noted that the effective stiffness of the composite beam, viewing the coefficient γ_1 (expression given in Figure 2), apart from the slip modulus **K**, the distance of the fasteners **s** and the span of the composite beam **L**, is also affected by the characteristics of the concrete section (E and A). Regarding the change of modulus of elasticity and cross-sectional area of concrete (slab thickness dp or effective width b_{eff}), if the modulus of elasticity E increases, the coefficient γ_1 decreases, which is also true for the increase of the concrete section (considering the increase of slab thickness). The analysis of parameters E and A(d_p) indicates

that concretes with a higher modulus of elasticity and a larger cross-sectional area (thickness of the slab) can reduce the efficiency of the fasteners and the composite's efficiency action and increase the self-weight of the structure, with a slight increase in the effective stiffness of the composite beam.

Table 3 – The slip modulus and the diameter of the fastener depending on the efficiency coefficient of the fasteners and the modulus of elasticity of the concrete

Strength class		$\gamma=0.1$					$\gamma=0.4$				
		K [N/mm]	d [mm]	EI_{eff} [kNm²]	$\dfrac{EI_{eff}}{EI_{min}}$	f [mm]	K [N/mm]	d [mm]	EI_{eff} [kNm²]	$\dfrac{EI_{eff}}{EI_{min}}$	f [mm]
C16/20		9541	9.8	2109	2.33	5.9	38162	39.3	2859	3.16	4.3
LC16/18	D1,0	1974	2.0	980	1.71	10.4	7896	8.1	1661	2.90	6.1
	D1,4	3849	4.0	1341	2.05	8.1	15397	15.8	2151	3.28	5.0
	D1,8	6382	6.6	1727	2.25	6.6	25529	26.3	2539	3.31	4.5
C25/30		10199	10.5	2179	2.33	5.7	40794	42.0	2914	3.12	4.2
LC25/28	D1,0	2106	2.2	1008	1.74	10.1	8422	8.7	1706	2.95	6.0
	D1,4	4145	4.3	1391	2.08	7.8	16581	17.1	2207	3.30	4.9
	D1,8	6843	7.0	1788	2.27	6.4	27372	28.2	2593	3.30	4.4
C40/50		11515	11.8	2311	2.33	5.3	46058	47.4	3018	3.05	4.1
LC40/44	D1,0	2369	2.4	1063	1.80	9.6	9475	9.7	1790	3.03	5.7
	D1,4	4672	4.8	1476	2.14	7.3	18686	19.2	2298	3.33	4.7
	D1,8	7698	7.9	1897	2.30	6.0	30793	31.7	2686	3.26	4.3
Note: adopted distance of fasteners s=0.1m to determine the slip modulus K.											

According to Linden [12], the strength and stiffness of a composite beam are not only defined by the stiffness of the connection (K). However, they are also a function of dimensions of cross-sections of the elements of the composite beam (i.e. their mutual relationship), which can be concluded based on the expression for γ_1. Consequently, the efficiency of the composite action (i.e. coupling efficiency), expressed through the ratio (EI_{eff}/EI_{min}), besides being achieved by the rational choice of dimensions of the cross-sections of the composite beam [12], can also be achieved by changing the modulus of elasticity of concrete. This indicates another possibility of increasing the effective stiffness of the composite beam (to a certain extent) if it is impossible to change the dimensions of the cross-sections of the elements. In Table 3, it can be seen that this ratio is approximate for LWAC with a modulus of elasticity of 19.4-23.4 GPa (class D1,8), where the difference in effective stiffness is about 18%, while for LWAC with a modulus elasticity of 11.7-14.2 GPa (class D1,4), this difference is up to 36%, compared to NWC. Accordingly, the influence of effective stiffness on mid-span deflections at smaller modules has a similar trend as for EI_{eff}, i.e. 12% (class D1,8) and 38% (class D1,4).

3.2. ANALYSIS OF INTERNAL FORCES IN THE COMPOSITE BEAM

The following figures, Figures 5-7, show diagrams with values of internal forces (bending moments in concrete M_1 and timber M_2, normal force $N = - N_1 = N_2$), stresses in concrete (σ_{1t} - top and σ_{1b} - bottom fibers) and timber (σ_{2t} - top and σ_{2b} - bottom fibers), shear force in the

fasteners F_v and mid-span deflection f of the composite beam, for the variation of the modulus of elasticity (considered concrete) and the efficiency of the fasteners γ_1, in the range of 0.1-0.4.
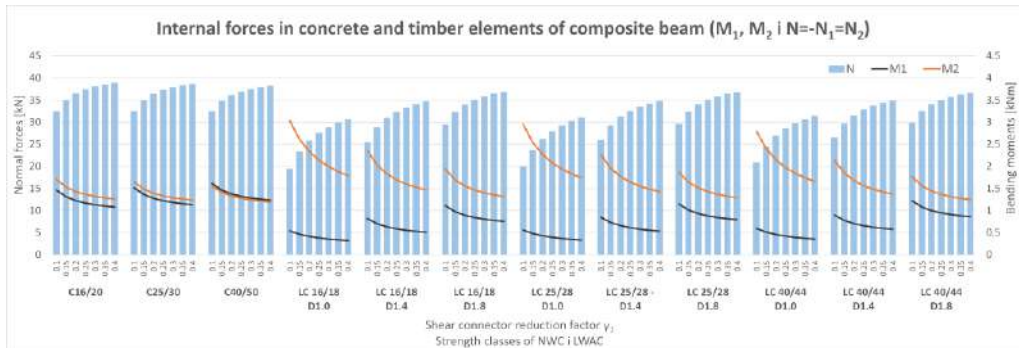
Figure 5 – Internal forces in the composite beam
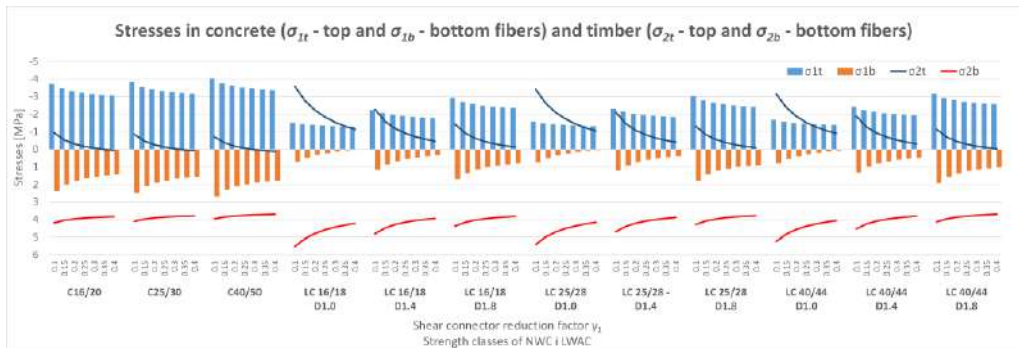
Figure 6 – Stresses in concrete and timber

Figure 7 – Shear forces and mid-span deflections

From the shown diagrams (Figures 5-6), the favourable influence of the change in modulus of elasticity (when reducing the modulus of elasticity of concrete) on the distribution of internal forces and stresses can be seen. This is reflected in the reduction of the bending moments in the concrete and thus stresses, which is favourable in lower tensile stresses and is

the result of the displacement of the neutral axis of the composite cross-section (i.e. centre of gravity of composite cross-section towards concrete part). Contrary to effects in concrete, there is an increase in bending moments in timber and thus stresses, which is expected due to the redistribution of forces in the composite beam.

In this paper, with the idea of using concrete with a lower modulus of elasticity, it was shown that the coupling concept was maintained. A concrete slab takes the majority of compression stresses (or with the appearance of more minor tensile stresses in the bottom zone), whereas reinforcing steel mesh takes over the potential tensile stresses in the concrete and reduces the widths of the cracks. At the same time, timber, placed in the tensioned zone, has the main role in tension stress-bearing capacity due to its relatively high tensile strength.

Observing the values of the shear forces in the fasteners (at the shear plane between concrete and timber), Figure 7 shows their favourable reduction with the use of LWAC, which is also the result of the redistribution of forces in the composite beam. It is also important from the side of the load-carrying capacity of the fasteners.

When it comes to the deformations of the composite beam (Figure 7) with the use of LWAC, there is an increase in mid-span deflection, resulting from less effective stiffness of the composite beam, i.e. a smaller modulus of elasticity of the concrete. In that case, attention should be paid when choosing an adequate LWAC, that is, choosing an appropriate density class of aggregates that will give a modulus of elasticity of concrete with a higher value than the modulus of elasticity of timber. It is recommended to use LWAC with aggregate density classes D1,4 and higher.

Considering the effectiveness of the composite action, as previously stated, it can be shown that if these ratios are similar (the same) for different types of LWAC, the effects and the mechanical behaviour of the composite beams will be more favourable compared to NWC. With the dependence of the ratio (EI_{eff}/EI_{min}) and the efficiency of the fastener γ_1, shown in Figure 8 (left), it can be seen that LWAC of density classes D1.4 and D1.8 for a specific value of γ_1 have a similar ratio (EI_{eff}/EI_{min}). Figure 8 (right) shows the effects in the members of the composite beam for comparison with NWC.
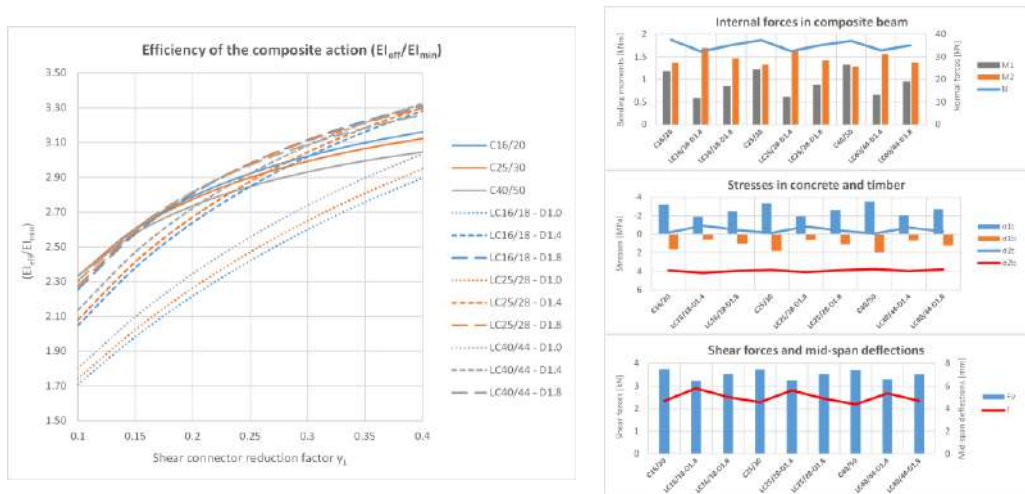
Figure 8 – Efficiency of the composite action depending on concrete modulus of elasticity and efficiency of fasteners (left); the effects in the members of composite beam for $\gamma_1=0.25$ (right)

4. CONCLUSION

In this paper, the favourable influence of LWAC on the mechanical behaviour of composite beams is explained through a comparative analysis and the presented interpretations. Based on their physical and mechanical properties, lightweight aggregate concrete have adequate performance that is necessary and suitable for use in composite timber-concrete structures when it comes to repairing and strengthening old and designing new floor structures.

REFERENCES

[1] Stevanovic B. Jedan način ojačanja drvenih međuspratnih konstrukcija kod nadgradnje zgrada, Materijali i konstrukcije, 44 (1-2), 2001, 41-45.

[2] Stevanović B. Eksperimentalna i teorijska analiza spregnutih nosača drvo-beton izvedenih mehaničkim spojnim sredstvima, Materijali i konstrukcije, 47(1–2), 2004.

[3] Ž. Unuk, M. Premrov, V. Žegarac Leskovar, "Timber floors and strengthening techniques (illustrated with a numerical example)," Teknik Dergi/Technical Journal of Turkish Chamber of Civil Engineers, 30(4), 2019, 9261-9288

[4] Kozarić Lj. Vibracije izazvane ljudskim delovanjem kod spregnutih međuspratnih konstrukcija tipa drvo-laki beton, Doktorska disertacija, Građevinski fakultet Subotica, Univerzitet u Novom Sadu, 2016.

[5] EN 1992-1-1: Eurocode 2: Design of concrete structures - Part 1-1: General - Common rules and rules for buildings, , 2004

[6] SRPS U.M1.206: Concrete- Specification, performance, production and conformity – Rules for the implementation of SRPS EN 206-1, 2013

[7] EN 1995-1-1: Eurocode 5: Design of timber structures –Part 1-1: General –Common rules and rules for buildings, Brussels, Belgium, 2004.

[8] Kieslich H., Holschemacher K. Composite constructions of timber and high-performance concrete, Advanced Materials Research, 133-134, 2010, 1171–1176.

[9] CEN/TS 19103: Eurocode 5: Design of Timber Structures. Structural design of timber-concrete composite structures. Common rules and rules for buildings, 2021.

[10] Holschemacher K., Kieslich H. Recent developments in timber-concrete composite, Il Congreso Latinoamericano de Estructuras de Madera, 2017.

[11] Clouston P., Schreyer A. C. Wood-Concrete Composites: A Structurally Efficient Material Option, Civil engineering practice, Boston Society of Civil Engineers BSCE Section/American Society of Civil Engineers ASCE, 5–22, 2006.

[12] van der Linden M. Timber-Concrete Composite Floor Systems, Ph.D. Delft University Press, Technische Universiteit Delft. The Netherlands, 1999.

Goran Jekic[1], *Veronika Shendova*[2], *Roberta Apostolska*[3], *Aleksandar Zlateski*[4], *Aleksandar Zhurovski*[5], *Elena Delova*[6], *Julijana Bojadjieva*[7]

IZIIS PROTOKOL ZA PROCENU SEIZMIČKE SIGURNOSTI POSTOJEĆIH ZGRADA

Rezime:

Cilj prezentovanog rada je definisanje Protokola za procenu seizmičke sigurnosti za postojeće objekte, primenjivog u regionima sa sličnom konstruktivnom tipologijom i građevinskom praksom. Protokol je namenjen da bude praktičan alat za pouzdanu kvantitativnu i kvalitativnu procenu sigurnosti zgrada u regionima sa različitim seizmičkim hazardom. Takva procena bi pružila dragoceno znanje o seizmičkoj otpornosti postojećeg građevinskog fonda.

Ključne reči: seizmički proračun, konstruktivna praksa, ocena seizmičke sigurnosti

IZIIS' SEISMIC ASSESSMENT PROTOCOL FOR EXISTING BUILDING STRUCTURES

Summary:

The goal of the presented work was defining a seismic safety assessment Protocol for existing buildings, applicable in regions with similar structural typology and construction practice. The Protocol is meant to be a practical tool for a reliable quantitative and qualitative assessment of the buildings' safety in regions with various seismic hazard levels. Such evaluation would provide valuable knowledge on the seismic resistance of the existing building stock.

Key words: seismic design, construction practice, seismic safety score

---

[1] *Assist. Prof. PhD, Ss. Cyril and Methodius University in Skopje, Institute of Earthquake Engineering and Engineering Seismology (IZIIS), Skopje, North Macedonia, jekic@iziis.ukim.edu.mk*

[2] *Prof. PhD, Ss. Cyril and Methodius University in Skopje, Institute of Earthquake Engineering and Engineering Seismology (IZIIS), Skopje, North Macedonia, veronika@iziis.ukim.edu.mk*

[3] *Prof. PhD, Ss. Cyril and Methodius University in Skopje, Institute of Earthquake Engineering and Engineering Seismology (IZIIS), Skopje, North Macedonia, beti@iziis.ukim.edu.mk*

[4] *Assist. MSc, Ss. Cyril and Methodius University in Skopje, Institute of Earthquake Engineering and Engineering Seismology (IZIIS), Skopje, North Macedonia, azlate@iziis.ukim.edu.mk*

[5] *Assist. MSc, Ss. Cyril and Methodius University in Skopje, Institute of Earthquake Engineering and Engineering Seismology (IZIIS), Skopje, North Macedonia, zurovski@iziis.ukim.edu.mk*

[6] *MSc, Ss. Cyril and Methodius University in Skopje, Institute of Earthquake Engineering and Engineering Seismology (IZIIS), Skopje, North Macedonia, delova@iziis.ukim.edu.mk*

[7] *Assoc. Prof. PhD, Ss. Cyril and Methodius University in Skopje, Institute of Earthquake Engineering and Engineering Seismology (IZIIS), Skopje, North Macedonia, jule@iziis.ukim.edu.mk*

1. INTRODUCTION

The latest inventories of buildings conducted every ten years in the European Union show that 80% of the total construction fund were built before 1990, while 40% were built before 1960. A significant percentage of the older buildings is classified as a cultural heritage. Due to the unexpected misbehavior of the buildings while exposed to the recent earthquakes (Italy, Greece, Albania) which resulted in significant economic losses, serious injuries and loss of human lives, as well as due to high energy consumption, the need for reconsidering and improving the seismic safety and energy efficiency of existing facilities in the EU is becoming a priority [1].

As there is no regular building inventory in the country, official data can be obtained from the population and dwellings censuses, (the last one was carried out in 2021 but still without official data). With cross-analysis of the statistical data from the last censuses from 1991 and 2002 and the available data from the State Statistical Office, it can be summarized that in 2002 the percentage of buildings built before 1970, out of the total number of particular type of facilities, is 35% for residential, 82% for school, 81% for tourist and 39% for health facilities [2, 3]. Based on the trend of newly built residential buildings in the last two decades, it can be estimated that nowadays the percentage of residential buildings, built before 1970, is certainly reduced, but the percentage of school and health facilities is still high. Thus, for a significant percentage of the construction stock in the country, the level of seismic protection is unknown. In such conditions, with the adoption of the first national regulation for energy performance of buildings from 2013, the first initiatives at national and local level to improve the energy efficiency of buildings begun, but without regulating a review of their seismic safety.

The current European Disaster Management Strategy calls for increased resilience in urban areas - a qualitative response of the state and the community to disasters from the current emergency response to a more proactive prevention and preparedness. Three components are essential for seismic resistance of urban environments: defining the seismic hazard, inventory of the exposed facilities and finally their vulnerability assessment.

Until September 2020, when Eurocodes were adopted as parallel code, the regulation in the field of construction in North Macedonia does not prescribe a fully defined and standardized approach on when it is necessary to evaluate the seismic resistance of existing buildings and how the procedure should be performed. This was an indirect reason for the ignorant attitude towards the existing building structures while designing interventions for the increasingly popular purpose conversions, reconstructions, extensions, upgrades, energy efficiency improvements, renovations, etc. It results in a vast number of buildings which are decades old, but with new, often expensive interiors.

2. GOAL, ACTIVITIES AND STRUCTURE OF THE PROTOCOL

The goal of the presented work is defining a seismic safety assessment Protocol for existing buildings, meant to be a practical tool for a reliable quantitative and qualitative assessment of the buildings' vulnerability in regions with various seismic hazard levels [4]. The Protocol was designed to serve as a practically applicable procedure for each of the necessary phases of reliable quantitative and qualitative assessment of whether and how much the buildings in seismically prone regions are potentially risky for exploitation, and hence suitable for other types

of future interventions. The Protocol's structure follows the modern methodological approaches worldwide [5, 6, 7, 8, 9], including pre-defined conditions and step procedures for identification of vulnerable buildings. It contains three levels of assessment:
- Rapid Visual Screening (RVS) procedure,
- Simplified Structural Analysis (SSA) and
- Rigorous (in-depth) Seismic Analysis (RSA) of buildings.

The assessment procedure is meant to take a major role in establishing a seismic safety rating system in North Macedonia - a "Seismic Certificate" for a specific building. The algorithm for each phase of the Protocol depends on the knowledge level of the relevant parameters: site seismicity, local soil conditions, type and regularity of the structural system, importance class, construction period, design and construction regulations at the time, control of the construction process, history of purpose conversion and changes in the structural system, previous exposure to other hazards etc. Such evaluation, if made for a significant number of buildings, would provide a clearer picture of the seismic resistance of the existing building stock in the country. The flow chart of the activities is demonstrated in Fig. 1.
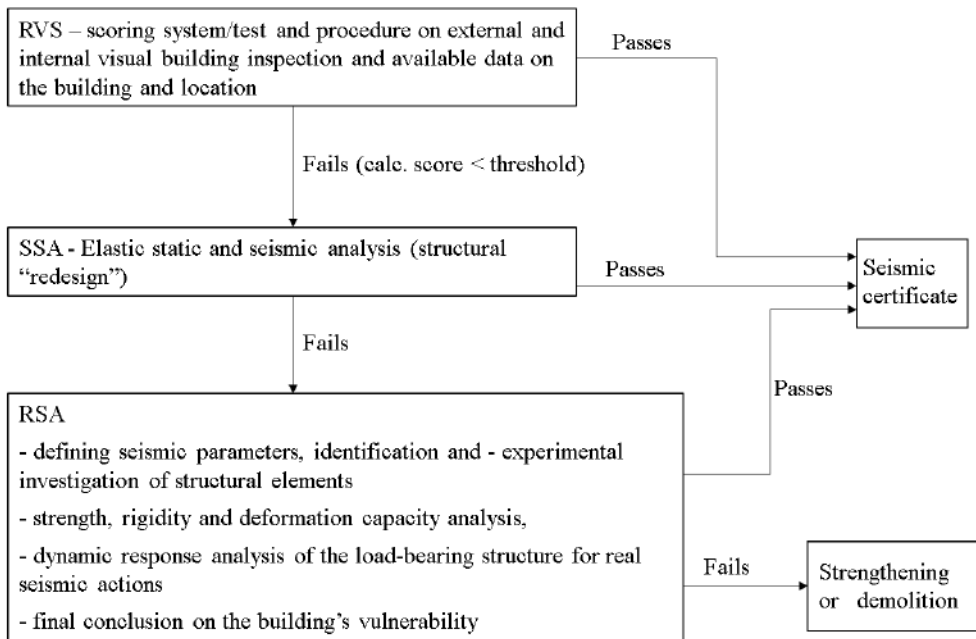
Figure 1 - Flow chart of the Protocol's activities

The RVS procedure for buildings' seismic safety estimation is applicable for screening a larger number of buildings in a short period of time. The accomplishing RVS process involves filling out a form for the basic relevant building attributes, based on external and internal visual inspection, conducted by structural engineers with an expertise in earthquake engineering and the available data on the seismicity of the location and the building itself. Providing a specific information from the initial review significantly affects the need for the second and the third step for seismic safety estimation for as many buildings as possible. That way, it is possible for the

seismically safe buildings to obtain a seismic certificate with a procedure that is relatively fast and easily applicable and without significant financial costs for the users, the local government unit, or any other person, company or institution that needs it.

If the building does not meet the criteria of RVS, the following is a recommendation for moving to the second step - numerical analysis of the building's stability (SSA), which should be performed by professionally trained structural engineers with practical structural design experience.

The final (RSA) consists of a strength capacity analysis, stiffness and deformability, as well as a non-linear dynamic response analysis of the load-bearing structure to real seismic effects on the site. RSA will result in a final conclusion on the building stability and vulnerability. This type of analysis involves control technical measurements and on-site investigations to define the seismic potential of the site, identifying the geometry and ascertaining the condition of the load-bearing elements and the built-in material quality and quantity. Within this activity, identification of the structure's weak points is enabled, i.e. whether is there a lack of global structural stability or local stability of individual structural elements, as well as guidelines for necessary interventions for the safety and stability improvement.

2.1. RAPID VISUAL SCREENING PROCEDURE (RVS)

The RVS procedure for specific buildings has been developed to assess the seismic risk to which they are exposed. The risk is assessed considering the seismic hazard on the location, the building's structural integrity and the specific structural and non-structural parameters that affect their vulnerability. The purpose of RVS is that the buildings can be assessed as with a sufficient seismic safety (acceptable seismic risk), without being subject to numerical analysis where it is not necessary.

Within this project, for the first time in North Macedonia, a form for visual inspection of buildings for assessment of their seismic safety is defined and proposed. If a building does not meet the established criteria through this assessment as seismically safe, or is identified as potentially hazardous, it should undergo additional analysis, conducted by qualified personnel to determine whether, in fact, they really pose a threat to the safety of users and the stored material values. The RVS procedure applies a methodology based on external and internal inspection and a data collection form. They include a space for documenting the identification information - photography, purpose, structural system and features that might reduce or increase the seismic safety. Based on the data, collected during the screening, a numerical result is calculated, indicating the expected building's seismic safety. Once a decision has been made to conduct RVS for a group of buildings, the screening effort can be accelerated by on-site planning, including evaluators' training and careful overall process management.

The RVS procedure applies basic scores and their modifiers for two the most present structural systems in the region (reinforced concrete and masonry structures), and their subclasses. Filling in the field data collection form begins with identifying the primary structural system and built-in materials. Basic ratings for the different types of construction systems are given in the form. The evaluators begin the basic assessment for the appropriate structural system by initial scoring and further modify it by appropriate score modifiers. The score modifiers relate to a specific structural property and are then added to or subtracted from the basic score to obtain the final score. Addition to or subtraction from the basic score depends on whether the specific property is favorable or unfavorable for the structure's seismic performance. The final score reflects the probability of damage or collapse in case of a design earthquake intensity scenario.

Higher final score corresponds to higher seismic safety, thus to lower probability for severe damage or collapse.

The entity that decides to implement a RVS program may be a state legislature, local authority, private company, school district or other organization and is referred to as the RVS Authority. The application of community based RVS allows the RVS Authority to classify the buildings into two categories: those that are expected to behave favorably during design seismic impacts and those that need to be processed with the next procedure (SSA) to assess their seismic resistance level. The value 2.0 is adopted as a threshold value of the final score for acceptable seismic risk. The threshold value is based on the thresholds in similar methodologies [5] and verified by IZIIS' experience in numerous seismic safety analyses. If the building receives a passing score (2.0 or higher), it is considered that the data collected during RVS are sufficient for the building to be assessed as seismically resistant. According to the threshold value, the buildings with a final score of less than 2.0 should pass to the next (SSA) stage of seismic safety assessment. The buildings with a lower final score should have priority over the buildings with a higher final score.

2.1.1. Parameters defining the initial score

Two parameters define the initial score:
- location in accordance with one of the actual seismic hazard maps (Fig. 2), used for defining seismic actions in the structural design process,
- the structural type.
- The initial scores for various types of structural system are shown in Table 1.

Table 1 – Initial building score values

Seismic zone	Structural type			
	C1	C2	C3	URM
7	2.5	2.7	2.9	2.5
8	2.2	2.4	2.6	2.2
9	2.0	2.2	2.4	2.0

The building types are the following: C1 (Concrete moment-resisting frame buildings), C2 (Concrete moment-resisting frame buildings with presence of shear walls), C3 (Concrete shear wall buildings) and URM (Unreinforced masonry bearing wall buildings).
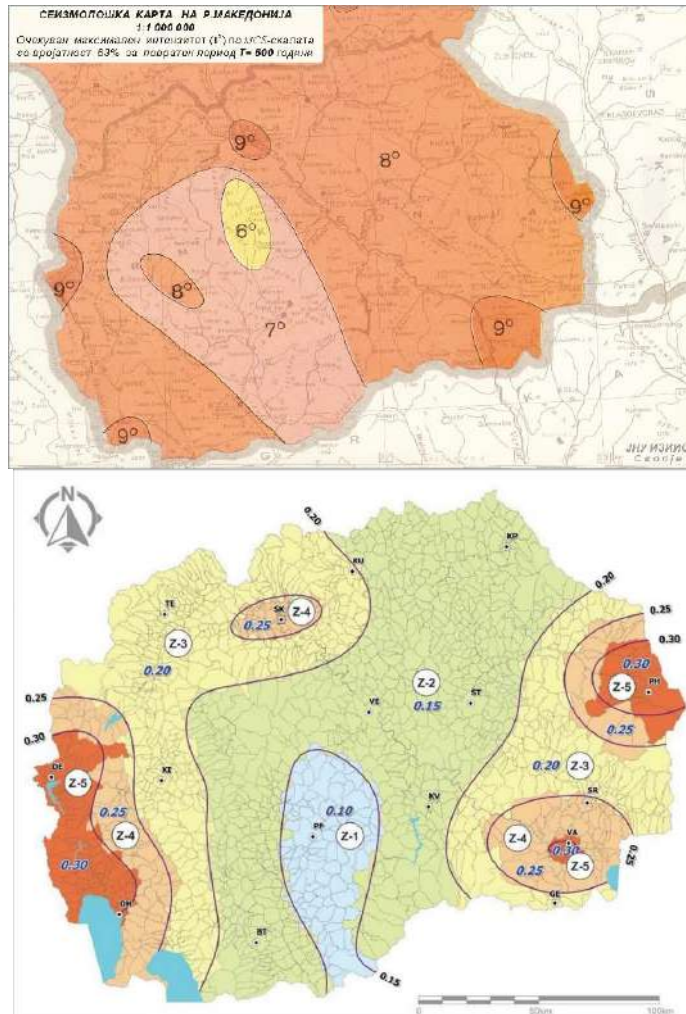
Figure 2 - Actual seismic hazard maps of North Macedonia, seismic intensity map from 1990 (top), PGA map from 2020 (MKS EN 1998-1:2012/NA:2020) (bottom)

2.1.2. Parameters defining the score modifiers

The specific features that modify the initial score and thus determining the final score of buildings' seismic safety assessment, are based on several aspects considering the construction period, available technical documentation, structural irregularities, local soil conditions, foundation, structural redundancy, post-construction modifications, repairs and strengthening, later modifications with no structural design process and visible structure deformations or damages. The score modifiers referring to the construction period are based on the design and seismic codes, as so as the construction control and other legal regulations and practice at the time of the structural design and construction of the building of interest.

The features, shown in Table 2, are selected based on IZIIS' knowledge on seismic design and construction practice in North Macedonia. The score modifier for each of the listed feature is different for each seismic zone (Fig. 2).

Table 2 – Required building score modifiers information by structural system

Score modifiers	Reinforced concrete structures	Masonry structures
Construction period	Before 1964 1964-1981 1982-1990 1991-2008 2009-2013 After 2013 Bearing capacity knowledge level	
Vertical irregularity	Sloping site Moderately weaker storey than above Highly weaker storey than above Column setback Short columns Split level Any other obvious irregularity	Soft story Vertical openings misalignment Abrupt wall thickness change Number of stories Lower neighboring buildings No basement levels Any other obvious irregularity
Plan irregularity	Flat slabs above ground level Torsional irregularity Out-of-plane offsets of beams Discontinued lateral bearing systems Non-orthogonal bearing systems Large diaphragm openings Flat slab cantilevers (3.0 m or longer) Any other obvious irregularity	High length/width ratio (3 or higher) "L" shaped in plan Low lat. bearing capacity in one dir. Large openings No horizontal belt courses Flexible floor and roof diaphragms Horizontal misalignment of openings Any other obvious irregularity
Foundation issues	Soil type C or weaker (according to Table 3.1, clause 3.1.2, EN 1998-1) Unfavorable foundation conditions	
Redundancy	3 or more bays in both directions	2 or more bays in both directions Nearly equal plan length and width Only one story above ground Wall thickness greater than 50 cm
Post-construction modifications	Repaired and strengthened Additional stories (without structural design project)	
Other score modifiers	Visible deformations or damages Structural brick wall infills	Visible deformations or damages Vertical belt courses on critical joints

2.2. SIMPLIFIED STRUCTURAL ANALYSIS (SSA)

If the building does not receive a passing score of 2.0 during the RVS, the next step is required, which is essentially an elastic structural analysis of the building to static and seismic impacts, based on the actual codes considering the seismic hazard for the location, built-in materials' quality and quantity and the existing structural elements' dimensions. The structure is then "redesigned". As a result, obtained from SSA, it is assessed whether the structure meets the current regulations in the country.

2.3. RIGOROUS SEISMIC ANALYSIS (RSA)

If SSA determines that the building doesn't meet the current regulations, an additional structural analysis is necessary to define the real load capacity and deformability for the real quality and quantity of built-in materials, followed by time history dynamic analysis for defined seismic parameters.

The load bearing and deformability capacity analysis for gravitational and seismic loads has to be made first and then applied as an input parameter in the time history dynamic response analysis. At the end of RSA the seismic safety and reliability of the existing structure are quantitatively determined. This methodology has been applied by IZIIS for seismic safety analysis of existing buildings for more than fifty years.

3. IMPLEMENTATION OF THE PROTOCOL

Based on the defined RVS methodology, 161 residential buildings in Karposh municipality (located in 9th seismic zone) were evaluated and scored using data obtained from a previously conducted visual inspection [10, 11]. The buildings were evaluated individually according to the RVS approach and a comparison with the previous assessments was made (methodology prescribed in FEMA-154) (Fig. 3). Differences between the two methodologies appear because the IZIIS' RVS approach contains score modifiers that are specific to the region and to the history of the design and construction practice in the Balkans.
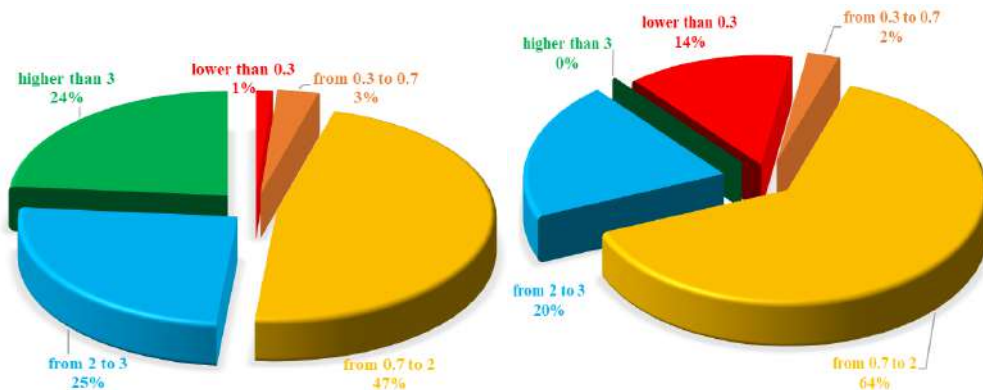
Figure 3 - Review of the final scores of 161 residential buildings in Karposh municipality
FEMA-154 (left), IZIIS' RVS (right)

Most of the buildings that received a final score lower than 0.3, applying IZIIS' RVS, are masonry structures that contain more than 3 storey levels. According to the actual seismic code, these structures are not permitted for construction in the 9th seismic zone, thus they automatically receive final score value of 0.0.

4. CONCLUSIONS

Within this project a system for a seismic safety evaluation of existing buildings is proposed in the form of a Seismic Certificate with specific numerical parameters. Procedures for three levels of seismic safety evaluation in the form of a Protocol are defined:
- form for rapid visual screening of buildings;
- required documentation and procedure for simplified seismic safety analysis and
- necessary investigations and technical controls of the building's location and necessary rigorous structural and seismic analyses for defining the seismic safety of existing buildings.

A scientific approach is applied in solving a problem that is becoming important and relevant, especially in the Balkan region due to existence of vast number of old buildings and a lack of building inventory. The development of the presented methodology and its transposition into an applicable Protocol provides opportunity for collecting information and relevant knowledge for many buildings in a short time. It gives a possibility for their prioritizing in future intervention plans such as purpose conversion, reconstruction, structural expansion, energy efficiency upgrades etc. It also contributes to decision making in implementation of the national earthquake disaster mitigation policies.

REFERENCES

[1] Gkournelos, P., Bournas, D., Triantafillou, T. (2019). Combined seismic and energy upgrading of existing buildings using advanced materials. EUR 29172 EN, Publications Office of the European Union, Luxembourg, ISBN 978-92-79-81825-7, doi:10.2760/278999, JRC111303.

[2] Shendova V., Apostolska R., Vitanova M. (2019). Structural Classification of Building and Bridge Assets in R.N. Macedonia. SERA Balkans Seismic Risk Workshop, EU Horizon 2020, ID 730900, Belgrade, Serbia.

[3] Shendova, V. (2011). Building Inventory Data for Republic of Macedonia. NERA - European Building Inventory Workshop, EU FP7-infrastructures, ID 262330. Pavia, Italy.

[4] Jekic G. et al. (2021). Defining a Protocol for Evaluation of Seismic Resistance of Existing Buildings - Seismic Certificate. IZIIS Internal Project. IZIIS Report 2021-64. Skopje, North Macedonia.

[5] Applied Technology Council (www.ATCouncil.org). (2015). Rapid Visual Screening of Buildings for Potential Seismic Hazards: A Handbook, Third Edition, FEMA P-154. Redwood City, California, USA.

[6] Pinto P.E., Franchin P. (2014). Existing Buildings: The New Italian Provisions for Probabilistic Seismic Assessment. In: Ansal A. (eds) Perspectives on European Earthquake Engineering and Seismology. Geotechnical, Geological and Earthquake Engineering, vol 34. Springer, Cham. https://doi.org/10.1007/978-3-319-07118-3_3.

[7] Ozdemir, P., Boduroglu, M.H., Ilki, A. (2005). Seismic Safety Screening Method. Proceedings of the International Workshop SPEAR (Seismic Performance Assessment and Rehabilitation of Existing Buildings) - an event to honour the memory of Prof. Jean Donea, Ispra, Italy.

[8] Rai D.C. (2005). Seismic Evaluation and Strengthening of Existing Buildings. Document: IITK-GSDMA-EQ06-V4.0, IITK-GSDMA-EQ18-V2.0, IITK-GSDMA-EQ24-V2.0, Draft Final Report: A - Earthquake Codes IITK-GSDMA, Project on Building Codes. Department of Civil Engineering Indian Institute of Technology Kanpur. Kanpur, India.

[9] Boğaziçi University, Istanbul Technical University, Middle East Technical University, Yildiz Technical University. (2003). Earthquake Master Plan for Istanbul.

[10] Necevska-Cvetanovska G. et al. (2013). Upgrading the Information System of the Municipality of Karposh with New Attributes for Recording and Monitoring of Seismic Stability and Safety of The Existing Facilities on the Territory of the Municipality of Karposh GIS Environment IZIIS Report 2013-47, Vol. 1 (Visual Inspection and Opinion on the Current Condition of the Facilities on the Location of the Municipality of Karpos and Recording in a Defined Form). Skopje, North Macedonia.

[11] Apostolska R. et al. (2018). Seismic performance assessment of "hybrid" structures using two-level multy group GIS oriented approach: case studies, Bull Earthquake Eng 16, 4797–4824, https://doi.org/10.1007/s10518-018-0366-0.

Predrag L. Popović[1]

REHABILITACIJA ELEMENATA DONJEG STROJA MOSTOVA

Rezime:

Elementi donjeg stroja mosta ukučuju obalne i rečne stubove, ležišta i ostale elemente mosta ispod kolovozne ploče. Ovi elementi su isloženi uticajima temperature, korozije, pomeranjima, požaru, udarima vozila i sleganju temelja. Tipična oštecenja su opisana i efectivne metode rehabilitacija su prikazane.

Ključne reči: mostovi, stubovi, ležišta, temelji, opravke, sanacije, požar, korozija

EFFECTIVE REPAIRS OF BRIDGE SUBSTRUCTURE

Summary:

Bridge substructure consists of bridge piers and abutments, bridge bearings and bearing seats, and other elements below slabs with driving surfaces. They are exposed to temperature movements, chemical and corrosion attacks, displacements, impact and fire damage and settlement of foundations. Typical causes of the damage are described and effective methods for repairs are presented.

Key words: piers, abutments, bearings, foundations, repairs, fire damage, impact

---

[1] *Vice President, Wiss, Janney, Elstner Associatges, Inc., Northbrook, Illinois, USA, ppopovic@wje.com*

1. INTRODUCTION

The bridge substructure generally consists of bridge piers, abutments, bearings, foundations including piles, concrete arches, and beams and slabs that are integral elements of other parts of the substructure. Generally, all bridge elements that are below driving surfaces could be considered part of the bridge substructure. While they are not exposed directly to the driving vehicles and chemicals placed on the driving surfaces, they are subject to temperature changes, longitudinal and transverse forces, wind loads and corrosion.

Typical distress includes bearing movement and rotation, spalling of bearing seats, settlement of foundations, cracking and displacement of bridge elements, corrosion of prestressed and regular steel, chemical attack, fire damage, impact and damage to the steel, concrete or wood piles.

2. CORROSION DAMAGE REPAIR

Due to water and salt leakage through the expansion joints, the top of piers and abutments are exposed to corrosive environment which results in corrosion of reinforcing bars and spalling of concrete (Figure 1). The repairs will include removal of deteriorated concrete, cleaning of corroded reinforcing bars and casting the new concrete (Figure 2). The new concrete can be applied by casting it in place, applying shotcrete, or pumping the concrete. Figure 3 shows the cast-in-place concrete repair of a deteriorated concrete pier.

Figure 1 - Pier corrosion under expansion joint

Figure 2 - Removal of deteriorated concrete

Sometimes it is appropriate to repair the structure using the form and pump procedure. It includes the usual removal of deteriorated concrete and surface preparation and flowable concrete is being pumped between the concrete surface and forms. An example of repair of a soffit of a concrete arch bridge is shown in Figures 4 and 5.

Figure 3 - Forms in place and completed repair

Figure 4 - Preparation of reinforcing steel and concrete formwork
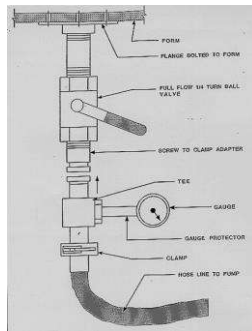
Figure 5 - Form and pump equipment and completed repair

546

Another method to repair corrosion damage is the use of shotcrete. This is a pneumatically applied concrete under pressure to a prepared concrete surface. Figure 6 shows shotcrete repair of a bridge pier and Figure 7 is repair of an abutment.

Figure 6 - Shotcrete repair of bridge pier

Figure 7 - Shotcrete repair of bridge abutment

A special case presents the repairs of corrosion damaged piles. Piles are the load-bearing elements of the structure and special procedures may be required during their repairs. Concrete piles in the water are subject to corrosion at the level of the water table and timber piles can also be damaged at that water level. Figure 8 shows the damaged piles. Damaged portions of the piles can be replaced but more often the repairs include installation of pile jackets. The jackets are made of fiberglass or steel liners filled with concrete, grout or epoxy. Figure 9 shows concrete pile jackets.

Figure 8 - Damaged concrete and wood piles

Figure 9 - Concrete pile jackets

3. BEARING REPAIRS

Bridge bearings are subject to movement, rotation and deterioration. Due to different factors, sometimes they do not perform as intended. Warning signs of bearing distress include cracks in abutment or pier, spalled concrete, bump in bridge joint, deflection in bridge railing at joint, tipped pier or abutment, rust streaking on face of substructure, expansion joint closed, hanger links out of plumb, and rockers tipped more than expected for temperature condition or skewed to line of movement.

Bearing distress includes freezing, unequal bearing action, out of position/missing, damaged supports, damaged bearing, wear on pins and elastomeric pad failures.

Frozen bearings are the result of steel corrosion, as shown in Figure 10. The repair includes cleaning the corrosion and resetting or replacing steel bearing with either new steel or neoprene bearing. Rocker bearing rehabilitation includes lifting the girder and resetting the bearing in its proper position (Figure 11).

Figure 10 - Frozen bearings

Figure 11 - Damaged support condition

Bearing seat can spall due to corrosion of reinforcing bars or concentrated load on the unreinforced concrete edge (Figure 11). The repair can include rebuilding of the edges of the concrete seat and/or adding a supplemental steel support (Figure 12).

Figure 12 – Bearing seat retrofit

Wear, fatigue or corrosion of the steel pin/hanger can result in their cracking or displacement (Figure 13). An example of pin-hanger retrofit is shown in Figure 14.
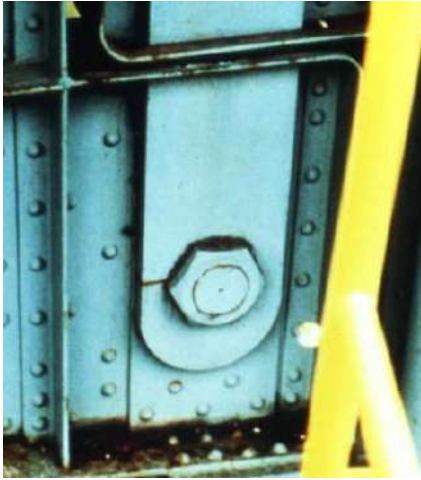
Figure 13 - Wear, fatigue, corrosion of pin/hanger
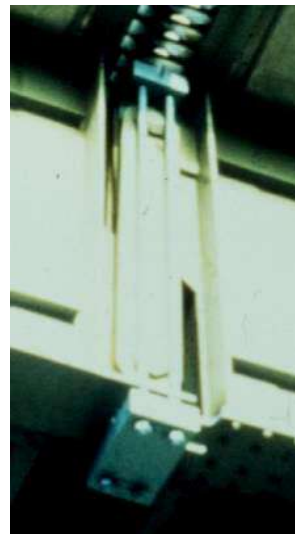
Figure 14 - Pin-hanger retrofit

4. IMPACT AND FIRE DAMAGE

There are instances when the fuel truck may hit a bridge, pier or abutment and cause a high intensity fire which will damage the pier and abutment. The damage should be investigated and based on the results of the investigation, the appropriate repairs should be performed (Figure 15).

There are many instances that vehicles with excessive heights impact concrete or steel girders. It is important to perform a proper evaluation in order to assess the extent of damage and decide about proper repair approach. If the steel girder is bent due to the impact, sometimes it could be heat-straightened rather than replaced. Concrete prestressed girder repair may involve the retensioning and splicing of prestressed cables in addition to concrete repairs.

Figure 15 - Fire damaged concrete pier

5. FOUNDATIONS

There are instances when the bridge foundations move or settle due to changes in bearing soil conditions. An example is a steel arch bridge whose foundations moved outward due to the horizontal component of arch reaction. That resulted in deflection of the arch at its crown. The repair included stabilizing the foundations by installing diagonal tiebacks to keep the abutments from spreading out (Figure 16). Bridge foundations which settled may have to be stabilized and repaired by installing the underpinning under and around settled footing.
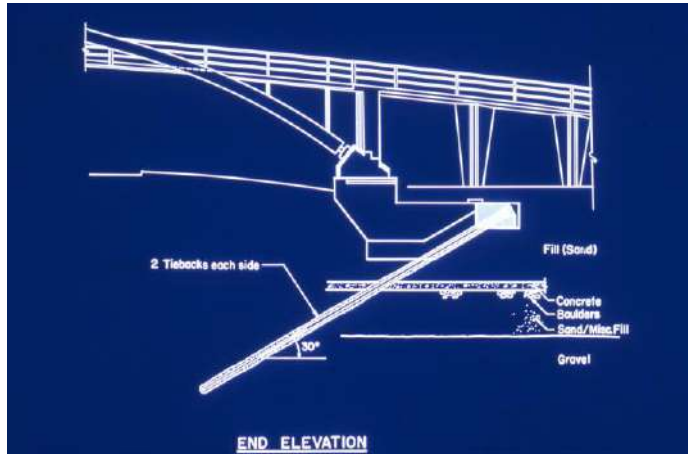
Figure 16 - Stabilizing arch bridge foundation

6. CONCLUSIONS

The substructure elements of a bridge may be subject to deterioration, corrosion and chemical attacks, displacements, impact, fire, cracking, foundation settlement and bearing damage. Proper investigation and analysis is required in order to design appropriate repairs. Various approaches are available and some commonly used are presented here.

The author wishes to thank engineers from his company who participated in bridge repair projects shown here.

Isidora Jakovljević[1], *Milan Spremić*[2], *Nina Gluhović*[3], *Zlatko Marković*[4]

MOŽDANICI SA GLAVOM U PROFILISANOM LIMU: PREGLED I KOMENTARI

Rezime:

Moždanici sa glavom su najčešće primenjivana mehanička spojna sredstava u spregnutim gredama od čelika i betona. Ponašanje moždanika razlikuje se u zavisnosti od toga da li se primenjuju u punim betonskim pločama ili u spregnutim pločama na profilisanom limu. Iako su proračunski modeli za nosivost moždanika u profilisanom limu dati u standardima za projektovanje, važećim proračunskim procedurama datim u EN 1994-1-1 pripisuju se izvesni nedostaci. Iz tog razloga nekoliko istraživača je predložilo alternativne proračunske modele. U radu su prikazani predloženi modeli proračuna i data je uporedna analiza nosivosti moždanika sa glavom u različitim tipovima profilisanog lima.

Ključne reči: spregnuta greda od čelika i betona, elastični moždanik, profilisani lim, nosivost na smicanje

HEADED STUDS IN PROFILED STEEL SHEETING: OVERVIEW AND COMMENTS

Summary:

Headed studs are the most commonly used mechanical shear connectors in composite steel-concrete beams. The behaviour of headed studs differs whether they are applied in solid concrete slabs or composite steel-concrete slabs with profiled steel sheeting. Although design codes provide calculation models for shear resistance of headed studs in profiled steel sheeting, certain weaknesses are attributed to design procedures given in EN 1994-1-1. Alternative design models have been proposed by several researchers. In this paper, novel models are presented and compared through the example of headed studs in different types of profiled steel sheeting.

Key words: steel-concrete composite beam, headed stud, profiled steel sheeting, shear resistance

---

[1] *Teaching assistant, Faculty of Civil Engineering, University of Belgrade, Serbia, isidora@imk.grf.bg.ac.rs*

[2] *Assoc. prof, Faculty of Civil Engineering, University of Belgrade, Serbia, spremic@imk.grf.bg.ac.rs*

[3] *Asst. prof, Faculty of Civil Engineering, University of Belgrade, Serbia, nina@imk.grf.bg.ac.rs*

[4] *Professor, Faculty of Civil Engineering, University of Belgrade, Serbia, zlatko@imk.grf.bg.ac.rs*

1. INTRODUCTION

For developing shear action between the concrete slab and steel profile in steel-concrete composite beams, headed studs are commonly used as shear connectors. They feature good mechanical performance, sufficient slip capacity and adequate shear resistance.

The behaviour of headed studs differs whether they are applied in solid concrete slabs or composite steel-concrete slabs with profiled steel sheeting. When applied in solid concrete slabs, the resistance of headed studs is mainly dependent on their geometry, material properties of the stud material and the concrete. However, in the case of the application in profiled steel sheeting, several additional factors may affect the shear resistance of headed studs, such as profiled sheeting geometry, the number of connectors and their position within the concrete rib, installation technique – whether studs are installed in pre-punched holes or they are welded through profiled sheeting. For this reason, analytical interpretation of the shear resistance of headed studs in profiled sheeting is more complex than in solid concrete slabs.

Design codes such as EN 1994-1-1 [1] and ANSI/AISC 360-16 [2] provide calculation models for shear resistance of headed studs both in solid slabs and composite slabs on profiled steel sheeting. The design procedure for studs in solid slabs given in EN 1994-1-1 is based on two possible failure modes: stud shear failure and concrete failure, which are analytically interpreted. However, the expressions for shear resistance of headed studs in profiled sheeting are not based on the possible failure modes – instead, they are statistically developed according to the experimental results, and defined through reduction factors that establish the relation between the shear resistance of studs in solid slabs and composite steel-concrete slabs. This statistically-based approach and the application of reduction factors have been criticised by some researchers [3], which pointed out the fact that failure modes significantly differ in the case of solid and composite slabs, and therefore making the correlation between resistances in those two cases is found inadequate. However, the main shortcoming of the current design rules given in EN 1994-1-1 is attributed to the underestimation of the stud shear resistance for some types of profiled steel sheeting which are present in the European construction market, in the case when ribs are transverse to the supporting beam. This is not surprising knowing that the geometry of profiled sheeting used a few decades ago in the time when the expressions for resistance of headed studs were developed, differs from the profiled sheeting used nowadays. A significant underestimation of the resistance has been observed for profiled sheeting with narrow ribs, such as Cofraplus 60 (ArcelorMittal). In addition, the fact that EN 1994-1-1 does not cover cases for alternative positions of headed studs within the rib, except the central position, is found another weakness of the current codified rules.

In order to improve the existing expressions for stud shear resistance and solve the weaknesses of the current design procedures for headed studs in profiled steel sheeting with ribs transverse to the beam, several design models have been proposed recently. Suggested models with their scope of application are listed in Table 1, together with EN 1994-1-1 model and its limits. Models with the widest range of applications are those proposed by Konrad [4] and Nellinger [3], covering both re-entrant and open trough profiled sheeting, and considering different stud positions inside the rib. The model suggested by Nellinger was later on simplified by Odenbreit and Nellinger [5] into a model more convenient for engineering practice. This model was the base for the design procedure suggested by the working group CEN/

TC250/SC4.PT3 [6], made in particular for open through profiled sheeting with small anchorage depths ($h_{sc} - h_p \leq 2.7d$) or a short distance between the headed stud and the rib wall ($e \leq 60$ mm).

Table 1 – Design models for the resistance of headed studs in profiled sheeting with ribs transverse to the beam

Model	Applicable for open trough profiled sheeting	Applicable for re-entrant trough profiled sheeting	Max. number of studs per rib	Considers stud position inside the rib	Max. profiled sheeting depth [mm]	Other limits
EN 1994-1-1 [1]	yes	yes	2	no	85	$d \leq 22$ mm $b_0 \geq \max\{h_p, 50\text{ mm}\}$ $h_{sc} - h_p \geq 2d$ $h - h_p \geq 50$ mm $h \geq 90$ mm
Lungershausen [7]	yes	yes	3	no	140	$h_{sc}/d \geq 4$ $h_{sc} - h_p \geq 2d$
Johnson and Yuan [8]	yes	no	2	yes	not specified	$16\text{ mm} \leq d \leq 20\text{ mm}$ $0.8 \leq b_0/h_p \leq 3.2$ $h_{sc} - h_p \geq 35$ mm
Rambo-Roddenberry [9]	yes	no	2	yes	76	$h_p = \{25; 38; 51; 76\}$ mm
Ernst [10]	yes	no	2	no	not specified	not specified
Konrad [4]	yes	yes	2	yes	not specified	$16\text{ mm} \leq d \leq 22\text{ mm}$ $h_{sc}/d \geq 4$ $h_{sc}/h_p \geq 1.56$
Nellinger [3]	yes	yes	3	yes	155	$16\text{ mm} \leq d \leq 22\text{ mm}$ $h_{sc} - h_p \geq d$
Vigneri [11]	yes	yes	2	no	136	$19\text{ mm} \leq d \leq 22\text{ mm}$ $h_{sc} - h_p \geq 2d$

Notation: d – diameter of the headed stud; b_0 – mean width of the profiled steel sheeting rib; h_p - overall depth of the profiled steel sheeting; h_{sc} – overall height of the headed stud; h – overall depth of a concrete slab.

In this paper, two models proposed by Konrad [4] and Odenbreit and Nellinger [5] are presented. Design predictions given by EN 1994-1-1 and two newly proposed models are compared through the example of headed studs in different types of profiled steel sheeting. Differences in the obtained resistances of headed studs are analysed and discussed, giving a

useful overview of the applicability of the codified and proposed design procedures to the engineering audience.

2. DESIGN PROCEDURES FOR HEADED STUD SHEAR RESISTANCE

2.1. MODEL PROPOSED BY KONRAD

The model proposed by Konrad [4] for ribs transverse to the supporting beam, suggests the calculation of headed stud resistance through a similar algorithm as prescribed in EN 1994-1-1, i.e. the headed stud resistance in solid slabs should be multiplied by a specific reduction factor, $k_\perp$. Konrad also defined new expressions for the headed stud resistance inside a solid slab, intending to improve the current EN 1994-1-1 predictions. New expressions include parameters of headed stud diameter and material properties of concrete slab and headed stud, which are also included by EN 1994-1-1. However, unlike the current design procedures, Konrad incorporated the effective area of the weld collar, $A_{\text{Wulst,eff}}$, into the proposed expressions for design resistance.

The design resistance of a headed stud in a solid concrete slab is obtained as the minimum between Eqs. (1) and (2), where Eq. (1) refers to the stud shear failure and Eq. (2) refers to the failure of concrete:

$$P_{\text{Rd,s}} = \left[313\, A_{\text{Wulst,eff}} \left(\frac{f_{\text{ck}}}{30}\right)^{2/3} + 240\, d^2 \left(\frac{f_{\text{u}}}{500}\right) \right] \frac{1}{\gamma_{\text{V}}} \qquad [\text{N}] \qquad (1)$$

$$P_{\text{Rd,c}} = \left[326\, A_{\text{Wulst,eff}} \left(\frac{f_{\text{ck}}}{30}\right)^{2/3} + 220\, d^2 \left(\frac{f_{\text{ck}}}{30}\right)^{1/3} \left(\frac{f_{\text{u}}}{500}\right)^{1/2} \right] \frac{1}{\gamma_{\text{V}}} \qquad [\text{N}] \qquad (2)$$

where:

$A_{\text{Wulst,eff}}$ is the effective area of the weld collar of a headed stud,

$A_{\text{Wulst,eff}} = 0.5\, h_{\text{Wulst}}\, d_{\text{Wulst}}$ [mm^2];

d is the headed stud shank diameter in mm;

h_{Wulst} is the height of the weld collar in mm;

d_{Wulst} is the diameter of the weld collar in mm;

f_{u} is the characteristic stud tensile strength in MPa, $f_{\text{u}} \leq 740$ MPa;

f_{ck} is the characteristic cylinder compressive strength of the concrete in MPa, 20 MPa $\leq f_{\text{ck}} \leq 100$ MPa;

γ_{v} is the partial safety factor, 1.25.

The scope of application of Eqs. (1) and (2) is limited to headed studs of diameter 16 mm $\leq d \leq 25$ mm. Unlike EN 1994-1-1 which prescribes the reduction factor α when the ratio between headed stud height and diameter is in the range $3 \geq h_{\text{sc}}/d \geq 4$, the model proposed by Konrad explicitly requires that $h_{\text{sc}}/d \geq 4$.

Although expressions for resistance of headed studs in solid slabs might seem as statistically obtained, they were developed assuming certain failure mechanisms. Three load components are considered: pressure on the weld collar, bending of the stud shank and the horizontal component of the tensile force in the stud.

According to Konrad, the design resistance of a headed stud in profiled steel sheeting with ribs transverse to the beam should be obtained as:

$$P_{\text{Rd}} = k_\perp\, P_{\text{Rd,c}} \leq P_{\text{Rd,s}} \qquad (3)$$

The reduction factor $k_\perp$ is defined as:
- for pre-holed steel sheeting:

$$k_\perp = k_n \left[k_e \; 0.038 \; \frac{b_m}{h_p} + 0.597 \right] \leq 1 \qquad (4)$$

- for welded-through headed studs, with sheeting thickness $t \geq 0.75$ mm:

$$k_\perp = k_n \; k_{Tr} \left[k_e \; 0.042 \; \frac{b_m}{h_p} + 0.663 \right] \leq 1 \qquad (5)$$

where:

$$k_n = \begin{cases} 1.0, & n_r = 1 \\ 0.8, & n_r = 2 \end{cases}$$

$$k_e = \begin{cases} 1.0, & 55 \text{ mm} \leq e \leq 100 \text{ mm} \\ 2.0, & e > 100 \text{ mm} \end{cases}$$

$$k_{Tr} = \begin{cases} 1.25, & \text{re-entrant trough profile} \\ 1.00, & \text{open trough profile} \end{cases}$$

n_r is the number of headed studs in the rib;
b_m, h_p and e are defined in Figure 1.

open trough profile   re-entrant trough profile
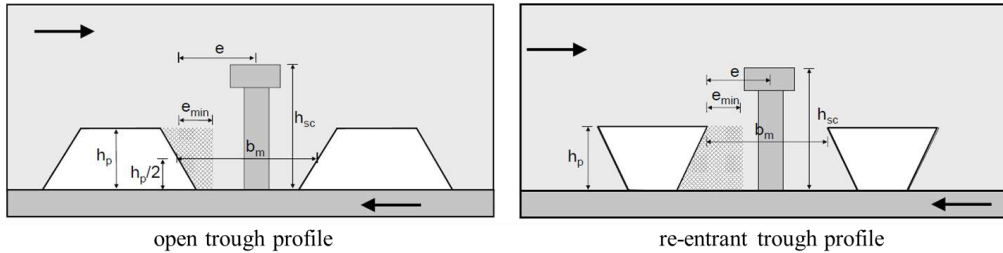
Figure 1 – Geometric parameters according to Konrad [4]

As well as the current design standard EN 1994-1-1, Konrad's model is limited to the maximum of two headed studs per rib and connectors with a diameter between 16 mm and 20 mm for through deck welding, i.e. from 16 mm to 22 mm in the case of the pre-holed steel sheeting. The minimum anchorage depth of connectors is required to comply with the following condition $h_{sc}/h_p > 1.56$.

However, Eq. (3) is not applicable when the distance e is smaller than 55 mm, which is labelled as the unfavourable position of headed studs. Even though Konrad proposed another equation for connections with $e < 55$ mm, he suggested avoiding such stud placing as the high coefficient of variation had been observed between design predictions and experimental results. However, for some commonly applied profiled steel sheeting, for example, Cofraplus 60 or Cofraplus 77 (Figure 3), the criteria $e > 55$ mm cannot be matched even when a headed stud is placed centrally inside the rib. For that reason, further experimental testing was conducted through the DISCCO project funded by Research Fund for Coal and Steel [12] and analysed by Eggert [13], who tested the following equation given by Konrad:

$$k_\perp = k_n \left[0.317 \; \frac{b_m}{h_p} + 0.06 \right] \leq 0.8 \qquad (6)$$

Eggert reported that Eq. (6) provides mostly safe-sided predictions when compared with experimental push-out test results for two types of profiled steel sheeting: Cofraplus 60 and Cofrastra 56 (ArcelorMittal).

It could be concluded that expressions for the reduction factor $k_\perp$ are more complex in comparison to the reduction factor k_t, which is defined in EN 1994-1-1, including different parameters such as the number of headed studs, the distance between the stud and the rib wall, profiled sheeting type (re-entrant or open trough), rib width and depth. The reduction factor k_t defined in EN 1994-1-1 is limited to values in the range of 0.60–1.0, which are commonly decisive in the determination of this factor. On the contrary, the reduction factor $k_\perp$ does not have limits smaller than 1.0, except in the special case when $e < 55$ mm, when the upper limit is 0.8.

2.2. MODEL PROPOSED BY ODENBREIT AND NELLINGER

Unlike the model suggested by Konrad, the model proposed by Odenbreit and Nellinger [5] provides directly two equations for obtaining the shear resistance of headed studs in profiled steel sheeting without the requirement for obtaining the reduction factor and shear resistance of a headed stud in a solid concrete slab previously. Proposed expressions are based on the load-bearing components observed in headed studs in profiled steel sheeting: failure of concrete in tension during concrete cone failure, stud resistance to bending and shear failure of a stud. Load-bearing components are described through simplified static schemes, assuming the possible development of one or two plastic hinges along the headed stud height due to stud bending. Except for the material properties, expressions for headed stud resistance include parameters such as the section modulus of the concrete cone surface, number of studs per rib and profiled sheeting depth, as well as the number of plastic hinges, the position of the upper plastic hinge, headed stud bending resistance and stud diameter. Expressions got their final form by applying adequate calibration factors C_1 and C_2 in order to match the experimental push-out test results.

The resistance of a headed stud applied in a steel-concrete slab with profiled sheeting ribs transverse to the beam is defined as the minimum between Eqs. (7) and (8), where Eq. (7) incorporates possible failure of concrete, and Eq. (8) considers the failure of a headed stud:

$$P_{\mathrm{Rd},1} = C_2 \left[\frac{\alpha_{\mathrm{ct}} f_{\mathrm{ctm}} W}{h_{\mathrm{p}}\, n_{\mathrm{r}}} + \frac{n_{\mathrm{y}}\, M_{\mathrm{pl}}}{h_{\mathrm{s}} - d/2} \right] \frac{1}{\gamma_{\mathrm{V}}} \tag{7}$$

$$P_{\mathrm{Rd},2} = C_1 f_{\mathrm{u}} \pi \frac{d^2}{4} \frac{1}{\gamma_{\mathrm{V}}} \tag{8}$$

where:
C_1 is the calibration factor, suggested value is 0.6;
C_2 is the calibration factor, suggested value is 0.9;
α_{ct} is the factor that accounts for the relaxation of concrete strength, proposed as $\alpha_{\mathrm{ct}} = 0.85$;
f_{ctm} is the concrete tensile strength, $f_{\mathrm{ctm}} \geq 20$ MPa;
W is the section modulus of the concrete cone surface, $W = 0.4\, h_{\mathrm{sc}}\, b_{\mathrm{max}}^3 / b_{\mathrm{top}}$;
h_{sc} is the overall shear connector height;
b_{max} is the maximum width of the rib;
b_{top}, h_{p} and h_{A} are defined in Figure 2;
n_{r} is the number of headed studs in the rib;
n_{y} is the number of plastic hinges,

$$n_y = \begin{cases} 1, & h_A \le 2d\sqrt{n_r} \\ 2, & h_A > 2d\sqrt{n_r} \end{cases}$$

M_{pl} is the bending resistance of a stud, $M_{pl} = f_u d^3/6$;

f_u is the characteristic stud tensile strength, $f_u \ge 400$ MPa;

d is the stud shank diameter;

h_s is the position of the upper plastic hinge, $h_s = \beta h_{sc} \le h_p$;

$$\beta = \begin{cases} 0.41, & \text{re-entrant trough profile} \\ 0.45, & \text{open trough profile} \end{cases}$$

γ_v is the partial safety factor, 1.25.
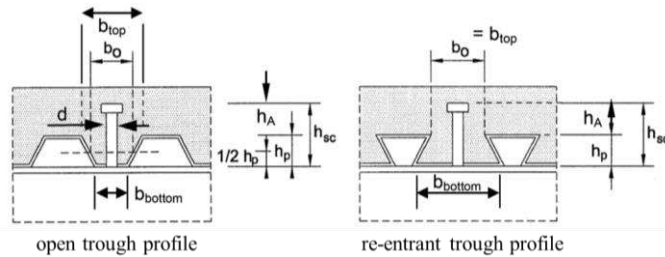
Figure 2 – Geometric parameters according to Nellinger [3]

It is noted that unlike the original model suggested by Nellinger [3], the simplified model proposed by Odenbreit and Nellinger [5] does not incorporate the influence of different stud positions inside the rib.

3. COMPARATIVE ANALYSIS

A comparison between design rules given in EN 1994-1-1 [1] and presented models proposed by Konrad [4] and Odenbreit and Nellinger [5] is shown in the example of several different types of commercially available profiled steel sheeting. Six different open trough profiled steel sheeting and three re-entrant profiled steel sheeting are analysed, all presented in Figure 3. In each case, one headed stud of a diameter of 19 mm is assumed to be centrally placed inside the rib, which is the common solution applied in steel-concrete composite building design. Headed stud height is varied in the range from 100 mm to 150 mm depending on the profiled sheeting depth (Table 2), making the detailing requirements given in EN 1994-1-1 satisfied. Characteristic stud tensile strength is adopted as 500 MPa, while the concrete class is C30/37. Profiled steel sheeting has pre-punched holes.

Shear resistance calculated according to EN 1994-1-1 [1], Konrad [4] and Odenbreit and Nellinger [5] is presented and compared in Table 2. The graphical presentation of the results is shown in Figure 4.

According to EN 1994-1-1, the design resistance of a headed stud with 19 mm in diameter is the same for almost all of the considered profiled steel sheeting types. In each case, the reduction factor k_t is 0.75, which is the upper limit value. Therefore, it may be concluded that EN 1994-1-1 is not sensitive to the variations in profiled steel sheeting geometry. On the contrary, the other two models predict values in the wide range from 31.79 kN to 68.05 kN.
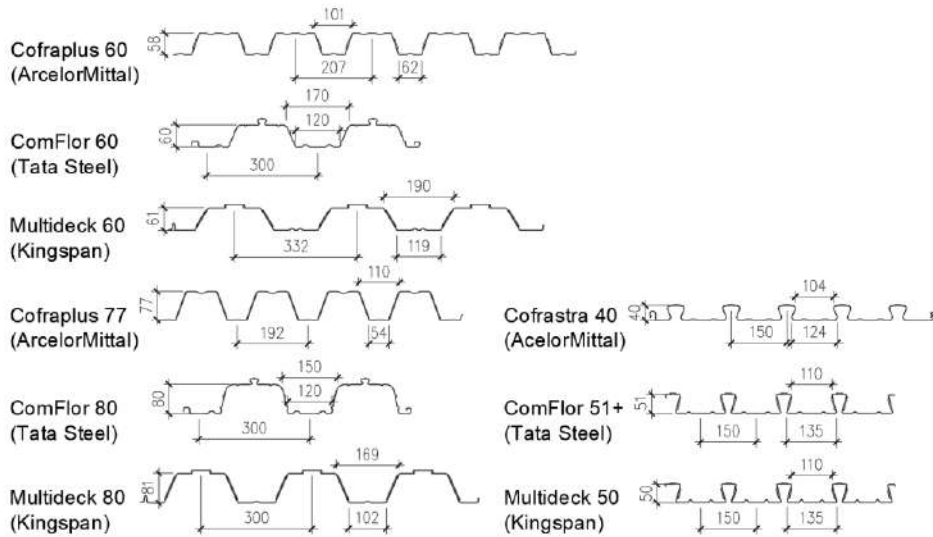
Figure 3 – Geometry of considered profiled steel sheeting

Table 2 – Comparison between design resistance for headed studs
in ribs transverse to the beam

Profiled steel sheeting		Headed stud height	Design resistance			Ratio		
			EN1994-1-1	Konrad	Odenbreit, Nellinger	$P_{Rd,K}$ /$P_{Rd,EN}$	$P_{Rd,O}$ /$P_{Rd,EN}$	$P_{Rd,O}$ /$P_{Rd,K}$
		h_{sc} [mm]	$P_{Rd,EN}$ [kN]	$P_{Rd,K}$ [kN]	$P_{Rd,O}$ [kN]			
Open trough	Cofraplus 60	125	62.34	40.42	33.19	0.65	0.53	0.82
	ComFlor 60	125	62.34	55.08	60.30	0.88	0.97	1.09
	Multideck 60	125	62.34	55.44	68.05	0.89	1.09	1.23
	Cofraplus 77	150	58.75	31.79	30.90	0.54	0.53	0.97
	ComFlor 80	150	62.34	52.87	44.10	0.85	0.71	0.83
	Multideck 80	150	62.34	52.87	51.93	0.85	0.83	0.98
Re-entrant	Cofrastra 40	100	62.34	63.97	59.64	1.03	0.96	0.93
	ComFlor 51+	100	62.34	59.47	57.23	0.95	0.92	0.96
	Multideck 50	100	62.34	60.57	57.85	0.97	0.93	0.96
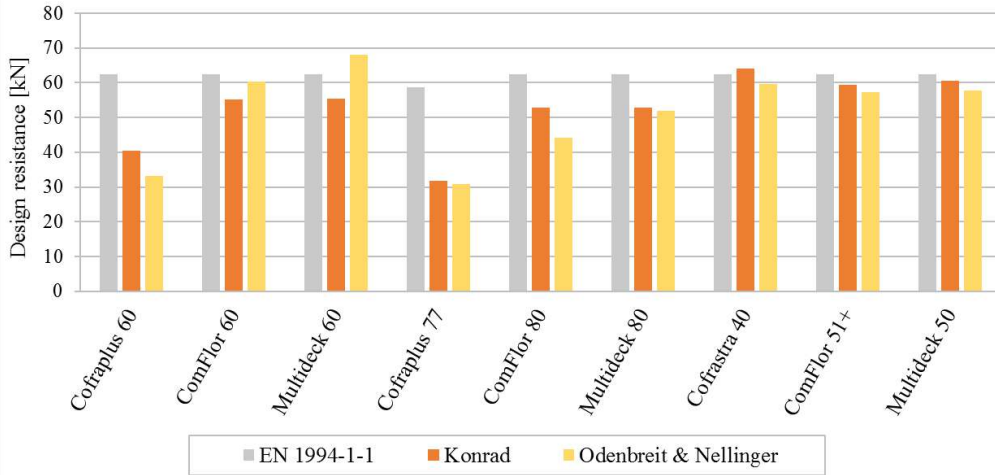
Figure 4 – Design resistance of a headed stud connector (d = 19 mm)

For re-entrant profiled sheeting Cofrastra 40, ComFlor 51+ and Multideck 50, design values according to all three analysed models do not considerably vary. However, differences in predictions obtained for open trough profiled steel sheeting are significant. The largest variations of up to 50% of the design resistance according to EN 1994-1-1 are present for profiled steel sheeting Cofraplus 60 and Cofraplus 77, which have narrow ribs of the mean width of 81.5 mm and 82.0 mm, respectively. This is not surprising considering that the experimental results proved underestimation of the shear resistance by EN 1994-1-1 predictions for these types of profiled steel sheeting [12]. Therefore, the design of a composite steel-concrete beam with profiled steel sheeting with narrow ribs should be carefully accessed in practice, considering the possible application of alternative design models.

The trend in design resistance values for models proposed by Konrad and Odenbreit and Nellinger cannot be easily determined, meaning that for some of the considered profiled sheeting types, design resistance according to Konrad is larger than according to Odenbreit et al, whereas in other cases, it is otherwise. The values of the headed stud resistance in open trough profiled sheeting predicted by Konrad are smaller than the ones calculated according to EN 1994-1-1. However, it is not the case for all resistance values according to the model proposed by Odenbreit and Nellinger, which for example assumes somewhat larger resistance than EN 1994-1-1 for profiled sheeting Multideck 60.

4. CONCLUSIONS

In this paper, a brief overview of the recently proposed design models for headed studs in profiled steel sheeting with ribs transverse to the beam is given. Although different models have been proposed in the past years, the focus of this paper is put on two models with a relatively wide scope of application proposed by Konrad and by Odenbreit and Nellinger. Both models were developed with the intention to solve some weaknesses observed in the codified design procedures of EN 1994-1-1.

Comparative analysis including various types of re-entrant and open trough profiled steel sheeting showed that novel design models are more sensitive to variations in profiled sheeting geometry than EN 1994-1-1. The most significant dissimilarities between design predictions are present for open trough profiled sheeting with narrow ribs. In this case, the design resistance according to novel models is nearly 50% smaller than according to EN 1994-1-1.

In order to solve Eurocode overestimations in headed stud resistance, the working group CEN/TC250/SC4.PT3 proposed analytical expressions for obtaining resistance of headed studs when placed in narrow ribs or near the rib wall in an unfavourable position, or when insufficient anchorage depth is applied. These expressions are expected to be available in the next generation of Eurocodes. Until then, the calculation of headed stud shear resistance should be carefully approached particularly in these special cases when the application of alternative design procedures is suggested to get safe-sided results.

REFERENCES

[1]   EN1994-1-1: Eurocode 4: Design of composite steel and concrete structures. Part 1-1: General rules and rules for buildings, CEN, Brussels, 2004.

[2]   ANSI/AISC360-16: Specification for Structural Steel Buildings, American Institute of Steel Construction, Chicago, 2016.

[3]   Nellinger S.: On the Behaviour of Shear Stud Connections in Composite Beams with Deep Decking. University of Luxembourg, 2015.

[4]   Konrad M.: Tragverhalten von Kopfbolzen in Verbundträgern Bei Senkrecht Spannenden Trapezprofilblechen. Universität Stuttgart, 2011.

[5]   Odenbreit C., Nellinger S.: Mechanical model to predict the resistance of the shear connection in composite beams with deep steel decking, Steel Construction, 10, 2017, 248–253.

[6]   Odenbreit C., Vigneri V.: Headed studs in profiled steel sheeting transverse to the beam - Investigations on design resistance of headed stud shear connectors on the basis of the Final Draft of SC4.PT3, Rev. B, Luxembourg, 2021.

[7]   Lungershausen H.: Zur Schubtragfähigkeit von Kopfbolzendübeln. Ruhr-Universität Bochum, 1988.

[8]   Johnson R.P., Yuan H.: Models and design rules for stud shear connectors in troughs of profiled sheeting, Proceedings of the Institution of Civil Engineers - Structures and Buildings, 128, 1998, 252–263.

[9]   Rambo-Roddenberry M.: Behavior and Strength of Welded Stud Shear Connectors. Virginia Polytechnic Institute and State University, 2002.

[10] Ernst S.: Factors Affecting the Behaviour of the Shear Connection of Steel-Concrete Composite Beams. University of Western Sydney, 2006.

[11] Vigneri V.: Load Bearing Mechanisms of Headed Stud Shear Connections in Profiled Steel Sheeting Transverse to the Beam. University of Luxembourg, 2021.

[12] Lawson R.M., Aggelopoulos E.S., Obiala R., Nellinger S., et al.: Development of Improved Shear Connection Rules in Composite Beams (DISCCO), Luxembourg, 2017.

[13] Eggert F.: Einfluss Der Verdübelung Auf Das Trag- Und Verformungsverhalten von Verbundträgern Mit Und Ohne Profilblech. Universität Stuttgart, 2019.

Šemso Kalač[1], *Naja Zejnelagić*[2], *Mladen Muhadinović*[3], *Duško Lučić*[4]

PREGLED NACIONALNO ODREĐENIH PARAMETARA U EN 1993-1-6

Rezime:

Cilj ovog rada je prikazati pregled nacionalno određenih parametara u EN 1993-1-6. Ukupno je 18 NOP-a. Za potrebe njihove analize podijeljeni su u sedam grupa: materijali i geometrija (1 NOP); granična stanja nosivosti kod čeličnih ljuski (1 NOP); rezultante napona i naponi u ljuskama (1 NOP); granično stanje plastičnog loma (1 NOP); granično stanje ciklične plastičnosti (2 NOP-a); granično stanje izbočavanja (11 NOP-a); granično stanje zamora (1 NOP). Komparativna analiza je sporevedena kako bi se predstavile vrijednosti za NOP usvojene u različitim evropskim državama.

Ključne reči: čelična ljuska, Eurokod, EN 1993-1-6, komparativna analiza

OVERVIEW OF NATIONAL DETERMINED PARAMETERS IN EN 1993-1-6

Summary:

The aim of this paper is to present an overview of national determined parameters in EN 1993-1-6. There is a total of 18 NDPs. For the purpose of their analysis they were divided into seven groups: materials and geometry (1 NDP); ultimate limit states in steel shells (1 NDP); stress resultants and stresses in shells (1 NDP); plastic limit state (1 NDP); cyclic plasticity limit state (2 NDPs); buckling limit state (11 NDPs); fatigue limit state (1 NDP). The comparative analysis was carried out in order to present the values for NDPs adopted in different European countries.

Key words: steel shell, Eurocode, EN 1993-1-6, comparative analysis

---

[1] *PhD student, Civil engineering faculty, University of Montenegro, Podgorica, Montenegro*
kalac.semso91@edu.ucg.ac.me,

TA, Faculty of polytechnics, University Donja Gorica, Podgorica, Montenegro, semso.kalac@udg.edu.me
[2] *Msc student, Civil engineering faculty, University of Montenegro, Podgorica, Montenegro,*
zejnelagicnaja_94@hotmail.com
[3] *PhD student, Civil engineering faculty, University of Montenegro, Podgorica, Montenegro, mladen.m@ucg.ac.me*
[4] *Full professor, Civil engineering faculty, University of Montenegro, Podgorica, Montenegro, dlucic@ucg.ac.me*

1. INTRODUCTION

The EN Eurocodes are the reference design codes from which are expected to contribute to the greater transparency in design methods and lead to a more uniform level of construction safety in different European regions. This will increase competitiveness of the European civil engineering firms, contractors, designers and product manufacturers as among them and worldwide [1].

It is mandatory for the Member States of EU to accept designs to the Eurocodes. It is up to Member States, National Authorities and National Standardization Bodies to design and set-up an appropriate Implementation Plan for the Eurocodes in their country. Implementation Plan should include translation of the Eurocode Part in authorized national language, setting the Nationally Determined Parameters to be applied on their territory, publishing the National Standard transposing the EN Eurocode and the National Annex, containing the national choice on the NDPs and reference to non-contradictory complementary information [1].

As the EN Eurocodes are the result of bringing together and harmonizing the different design traditions, the differences in the environmental conditions and in the ways of life among the Member States require flexibility in the National Application of the EN Eurocodes. Therefore, is up to Member states to define Nationally Determined Parameters (NDPs) [1].

2. NDPS IN EN 1993-1-6

Eurocode EN 1993-1-6 provides basic rules for the design of shell-shaped steel structures. Like other European standards in the field of construction, this standard is an integral part of the application standards that are related to the purpose of construction and that define the initial parameter and guidelines for shell design. This Eurocode is based on the principle of limit states [2].

This standard gives alternative procedures [3], values and recommendations with notes indicating where national choices may have to be made. Therefore, the National Standard implementing EN 1993-1-6 should have a National Annex containing all Nationally Determined Parameters to be used for the design of steel structures to be constructed in the relevant country. In EN 1993-1-6 there are a total of 18 NDPs. For the purpose of their analysis they will be divided into seven groups:
- Group 1 – Materials and geometry (1 NDP)
- Group 2 – Ultimate limit states in steel shells (1 NDP)
- Group 3 – Stress resultants and stresses in shells (1 NDP)
- Group 4 – Plastic limit state (LS1) (1 NDP)
- Group 5 – Cyclic plasticity limit state (LS2) (2 NDPs)
- Group 6 – Buckling limit state (LS3) (11 NDPs)
- Group 7 – Fatigue limit state (LS4) (1 NDP)
  In the following subsections NDPs belonging to each group will be reviewed.

2.1. MATERIALS AND GEOMETRY

In section materials and geometry are defined material criteria of steel as material and geometry criteria of shell which are relevant for application of EN 1993 part 1-6. In this part

there is one NDP thru which could be made national choice regarding basis of design and material properties. This national determined parameter should give more information about material properties at temperatures exceeding 150°C thru national annex [3], [9].

2.2. ULTIMATE LIMIT STATES IN STEEL SHELLS

Following ultimate limit states are defined in EN 1993 part 1-6 [3] and have to be taken in consideration during design:
- plastic limit state LS1;
- cyclic plasticity state LS2;
- buckling state LS3;
- fatigue state LS4.

Plastic limit LS1 is defined thru clause 4.1.1 (1) as the limit state in which the capacity of the structure to resist actions on it is exhausted by yielding of the material. Criteria for LS1 limit state is defined as the plastic collapse load obtained from a mechanism based on small displacement theory [3].

The limit state of cyclic plasticity LS2, on the other side, is defined by energy absorption capacity of the material, clause 4.1.2 (1) [3]. This limit state is defined thru condition in which repeated cycles of loading and unloading produce yielding in tension and in compression at the same point, thus causing plastic work to be repeatedly done on the structure leading to local cracking. All variable actions which might be applied with more than three cycles in the life of the structure should be taken in consideration for LS2.

The limit state of buckling LS3 is caused by loss of stability under compressive membrane or shear membrane stresses in the shell wall, leading to inability to sustain any increase in the stress resultants, possibly causing total collapse of the structure. This limit state is defined thru clause 4.1.3(1) [3].

Fatigue LS4 as limit state is caused by cyclic load with N_f cycles of increasing and decreasing stress lead to the development of a fatigue crack, clause 4.1.4 (1). N_f is Nationally Determined Parameter. The proposed is $N_f = 10\ 000$ [3].

2.3. STRESS RESULTANTS AND STRESSES IN SHELLS

There are the eight stress resultants in the shell wall that at any point should be calculated. But, the shear stresses τ_{xn}, $\tau_{\theta n}$ due to the transverse shear forces q_{xn}, $q_{\theta n}$ are insignificant compared with the other components of stress in almost all practical cases, so they may usually be neglected in design, clause 5.1 (1). Therefore, the evaluation of the limit states may be made using only the six stress resultants in the shell wall n_x, n_θ, $n_{x\theta}$, m_x, m_θ, $m_{x\theta}$ [3].

In this section there is only one NDP to define and it is concerning to the radius to thickness ratio. This ratio represents criteria when the curvature of the shell may be ignored when calculating the stress resultants from the stresses in the shell wall, clause 5.2.4 (1). Proposed value is 25 [3].

2.4. PLASTIC LIMIT STATE (LS1)

In this section there is only one NDP to define and it is concerning of defining plastic limit state with GMNA (global material nonlinear analysis) analysis. In an MNA or GMNA analysis based on the design yield strength f_{yd}, the shell should be subject to the design values of the load cases, progressively increased by the load ratio r_R until the plastic limit condition is reached [3].

"6.3 (5) Where a GMNA analysis is used, if the analysis predicts a maximum load followed by a descending path, the maximum value should be used to determine the load ratio $r_{R,GMNA}$. Where a GMNA analysis does not predict a maximum load, but produces a progressively rising action-displacement relationship without strain hardening of the material, the load ratio $r_{R,GMNA}$ should be taken as no larger than the value at which the maximum von Mises equivalent plastic strain in the structure attains the value $\varepsilon_{mps} = n_{mps} (f_{yd} / E)$." Recommended value of $n_{mps}=50$ (6.3 (5)) [3].

2.5. CYCLIC PLASTICITY LIMIT STATE (LS2)

For the cyclic plasticity limit state (LS2) there are two NDPs which have to be defined. First NDP is about the type of numerical analysis which should be used for determination of the design values of total accumulated plastic strain when the design is done by global numerical MNA or GMNA analysis. Recommendation is to use an MNA analysis for this purpose 7.3.1 (1) NOTE 1. But according to 7.3.1 (1) NOTE 2: The National Annex may give recommendations for a more refined analysis [3].

The second NDP is also corelated to design by global numerical MNA or GMNA analysis and it refers to the total accumulated von Mises equivalent plastic strain $\varepsilon_{p,eq.Ed}$ at the end of the design life. According to 7.3.2 (1): "Unless a more sophisticated low cycle fatigue assessment is undertaken, the design value of the total accumulated von Mises equivalent plastic strain $\varepsilon_{p,eq,Ed}$ should satisfy the condition":

$$\varepsilon_{p,eq,Ed} \leq n_{p,eq} (f_{yd} / E) \tag{1}$$

Recommended value of $n_{p,eq}$ is 25. The National Annex may choose the value of $n_{p,eq}$.

2.6. BUCKLING LIMIT STATE (LS3)

For checking buckling limit state, all relevant combinations of actions causing compressive membrane stresses or shear membrane stresses in the shell wall shall be taken into account [3]. For this limit state there are 11 NDPs that have to be defined. Six of eleven NDPS are concerning to values of tolerances: Out of roundness tolerance (1 NDP), accidental eccentricity tolerance (3 NDPs), dimple tolerances (1 NDP), interface flatness tolerance (1 NDP). The rest, five NDPs are concerning to stress design: buckling strength (3 NDPs) and design value of resistance (2 NDPs).

$U_{r,max\ max}$ is the out-of-roundness tolerance parameter for the relevant fabrication tolerance quality class and may be obtained from the National Annex, recommended values are given in following Table 1 [3].

Table 1 – Recommended values for out-of-roundness tolerance parameter $U_{r,max}$ [3]

	Diameter range	d [m] ≤ 0,50m	0,50m < d [m] < 1,25m	1,25m ≤ d [m]
Fabrication tolerance quality class	Description	Recommended value of $U_{r,max}$		
Class A	Excellent	0,014	0,007 + 0,0093(1,25−d)	0,007
Class B	High	0,020	0,010 + 0,0133(1,25−d)	0,010
Class C	Normal	0,030	0,015 + 0,0200(1,25−d)	0,015

e_a is the accidental eccentricity between the middle surfaces of the joined plates [EN 1993 part 1-6], and it should be evaluated from the measurable total eccentricity e_{tot} and the intended offset $e_{int.}$ The accidental eccentricity should be less than the maximum permitted accidental eccentricity $e_{a,max}$ for the relevant fabrication tolerance quality class. The recommended values of $e_{a,max}$ are given in Table 2. The maximum permitted accidental eccentricity may be obtained by National annex [3].

Table 2 – Recommended values for the maximum permitted accidental eccentricity $e_{a,max}$ [3]

Fabrication tolerance quality class	Description	Recommended values for maximum permitted accidental eccentricity $e_{a,max}$
Class A	Excellent	2 mm
Class B	High	3 mm
Class C	Normal	4 mm

The accidental eccentricity e_a should also be assessed in terms of the accidental eccentricity parameter U_e given by 8.4.3 (3) [3]:

$$U_e = \frac{e_a}{t_{av}} \ or \ U_e = \frac{e_a}{t}$$
$$(2)$$

where:

t_{av} is the mean thickness of the thinner and thicker plates at the joint.
The accidental eccentricity parameter Ue should satisfy the condition:

$$U_e \leq U_{e,max} \qquad\qquad (3)$$

Values for the accidental eccentricity tolerance parameter $U_{e,max}$ may be obtained from the National Annex. The recommended values are given in Table 3 [3].

Table 3 – Recommended values for the accidental eccentricity tolerance parameter $U_{e,max}$ [3]

Fabrication tolerance quality class	Description	Recommended values for maximum permitted accidental eccentricity $e_{a,max}$
Class A	Excellent	2 mm
Class B	High	3 mm
Class C	Normal	4 mm

8.4.4 (4) The value of the dimple parameters U_{0x}, $U_{0\theta}$, U_{0w} should satisfy the conditions [3]:

$$U_{0x} \leq U_{0,max} \qquad\qquad U_{0\theta} \leq U_{0,max} \qquad\qquad U_{0w} \leq U_{0,max} \qquad (4)$$

where: $U_{0,max}$ is the dimple tolerance parameter for the relevant fabrication tolerance quality class [3].

Recommended values for the dimple tolerance parameter $U_{0,max}$ are given in Table 4.

8.4.5 (1) Interface flatness tolerance: Where another structure continuously supports a shell (such as a foundation), its deviation from flatness at the interface should not include a local slope in the circumferential direction greater than β_θ. The National Annex may choose the value of β_θ. The value $\beta_\theta = 0,1\% = 0,001$ radians is recommended [3].

Table 4 – Recommended values for dimple tolerance parameter $U_{0,max}$ [3]

Fabrication tolerance quality class	Description	Recommended value of $U_{0,max}$
Class A	Excellent	0,006
Class B	High	0,010
Class C	Normal	0,016

The five NDPs are concerning to stress design: buckling strength (3 NDPs) and design value of resistance (2 NDPs) [3].

The design buckling resistance is defined by the buckling stresses which depend on value of the partial factor for resistance to buckling γ_{M1} should be taken from the relevant application standard or National Annex, recommended value is 1.1 [3].

The buckling reduction factors χ_x, χ_θ and χ_τ should be determined as a function of the relative slenderness of the shell λ which depends on following parameters: α (the elastic imperfection reduction factor), β (the plastic range factor), η (the interaction exponent), λ_0 (the squash limit relative slenderness). The values of these parameters should be taken from Annex D. Where Annex D does not define the values of these parameters, they may be given by the National Annex [3].

Following expression (5) describes the elastic buckling stress, accounting for geometric imperfections [3].

$$\chi = \frac{\alpha}{\lambda} \tag{5}$$

Where the behavior is entirely elastic, the characteristic buckling stresses may alternatively be determined directly from $\sigma_{x,Rk} = \alpha_x\, \sigma_{x,Rcr}$, $\sigma_{\theta,Rk} = \alpha_\theta\, \sigma_{\theta,Rcr}$, and $\tau_{x\theta,Rk} = \alpha_\tau\, \tau_{x\theta,Rcr}$ [3].

The design buckling resistance is determined as a load factor r_R applied to the design values F_{Ed} of the combination of actions for the relevant load case. The largest tolerable deformation should be assessed relative to the conditions of the individual structure. If no other value is available, the largest tolerable deformation may be deemed to have been reached when the greatest local rotation of the shell surface (slope of the surface relative to its original geometry) attains the value β [3]. Recommended value for β is 0,1 radians. The National Annex may choose the value of β.

Modification of the adopted mode of geometric imperfections to include realistic structural details (such as axisymmetric weld depressions) should be explored. The National Annex may define additional requirements for the assessment of appropriate patterns of imperfections [3].

2.7. FATIGUE LIMIT STATE (LS4)

The fatigue assessment presented in EN 1993-1-9 should be used. The partial factor for resistance to fatigue γ_{Mf} shall be taken from the relevant application standard. Recommended value of γ_{Mf} should not be taken as smaller than $\gamma_{Mf} = 1,1$ (8.8.2(20)) [3].

3. COMPARATIVE ANALYSIS OF ADOPTED NDPS IN DIFFERENT EUROPEAN COUNTRIES

In this section of the paper National Annexes of different European countries are going to be compared. The countries that are analyzed are: Croatia (nHRN EN 1993-1-6 -2008/NA [4]), Cyprus (CYS National Annex to CYS EN 1993-1-6:2007 [5]), Romania (SR EN 1993-1-6/NA-

2011: [6]), Denmark (EN 1993-1-6 DK NA, 2007-11-14, [7]), Bulgaria (EN 1993-1-6/NA-2012 [8]) and Montenegro (rnMEST EN 1993-1-6_NA [9]).

Table 5 – Comparative analysis of adopted NDPs in different European countries

Parameter	Country					
	Croatia [4]	Cyprus [5]	Romania [6]	Denmark [7]	Bulgaria [8]	Montenegro [9]
3.1(4) The material properties above 150°C	No further information	No further information	In accordance to SR EN 1993-1-2	No further information	In accordance BDS EN 1993-1-2	No further information
4.1.4(3) N_f cycles	Recommended value	Recommended value	Recommended value	Recommended value	Recommended value	Recommended value
5.2.4(1) Minimum the radius to thickness ratio (r/t) min	Recommended value	Recommended value	Recommended value	Recommended value	Recommended value	Recommended value
6.3(5) The value n_{mps}	Recommended value	Recommended value	Recommended value	Recommended value	Recommended value	Recommended value
7.3.1(1) NOTE 2 Design by global numerical MNA or GMNA analysis	No further information	No further information	No further information	No further information	No further information	No further information
7.3.2(1) Value $n_{p,eq}$	Recommended value	Recommended value	Recommended value	Recommended value	Recommended value	Recommended value
8.4.2(3) Values for the out-of-roundness tolerance parameter $U_{r,max}$	Recommended values	Recommended values	Recommended values	Recommended values	Recommended values	Recommended values
8.4.3(2) Values for the maximum permitted accidental eccentricity $e_{a,max}$	Recommended values	Recommended values	Recommended values	Recommended values	Recommended values	Recommended values
8.4.3(4) Values for the accidental eccentricity tolerance parameter $U_{e,max}$	Recommended values	Recommended values	Recommended values	Recommended values	Recommended values	Recommended values
8.4.4(4) Values for the dimple tolerance parameter $U_{0,max}$	Recommended values	Recommended values	Recommended values	Recommended values	Recommended values	Recommended values
8.4.5(1) Value for local slope in the circumferential direction	Recommended values	Recommended values	Recommended values	Recommended values	Recommended values	Recommended values
8.5.2(2) The partial factor for resistance to buckling γ_M	1,2	Recommended value	Recommended value	National standard	Recommended value	Recommended value
8.6.3(5) NOTE 1 The values of these parameters α, β, η, λ	No further information	No further information	No further information	No further information	No further information	No further information
8.8.2(9) the greatest local rotation of the shell surface β	Recommended value	Recommended value	Recommended value	National standard	Recommended value	Recommended value
8.8.2(18) requirements for the assessment of appropriate patterns of imperfections	No further information	No further information	No further information	No further information	No further information	No further information
8.8.2(20) Value of n_i	Recommended value	Recommended value	Recommended value	Recommended value	Recommended value	Recommended value
8.8.2(20) Values for the dimple tolerance parameter U_{n1} and U_{n2}	Recommended values	Recommended values	Recommended values	Recommended values	Recommended values	Recommended values
9.2.1(2)P The partial factor for resistance to fatigue γ_{Mf}	HRN EN 1993-1-9:2008/NA:2013	Recommended values	Recommended values	NA EN 1993-1-9	BDS EN 1993-1-9	Recommended values

4. CONCLUSION

In this paper an overview of national determined parameters in EN 1993-1-6 is presented. NDPs are analysed separately and briefly discussed.

For all NDPs comparative analysis was carried out in order to present the values for NDPs adopted in different European countries.

From this analysis clearly, it could be seen that observed countries tend to adopt recommended values and procedures. At points where it is possible to add another approach or more precise information or procedure, observed countries didn't use this possibility and there was no further information.

REFERENCES

[1] https://eurocodes.jrc.ec.europa.eu/

[2] S. Kalac, N. Zejnelagic and D. Lucic, "THE ALGORITHM OF ANALYSIS AND DESIGN OF STEEL WATER TANK ACCORDING TO EUROCODES", in MASE 19, Ohrid, 2022;

[3] MEST EN 1993-1-6:2019 Eurokod 3 - Projektovanje čeličnih konstrukcija - Dio 1-6: Čvrstoća i stabilnost ljuski, Institut za standardizaciju Crne Gore, Podgorica,2019;

[4] nHRN EN 1993-1-6 -2008/NA – Eurokod 3 „ Projektiranje čeličnih konstrukcija- Dio 1-6: Čvrstoća i stabilnost ljuskastih konstrukcija- Nacionalni dodatak ", Hrvatski zavod za norme, veljača 2013;

[5] EN 1993-1-6/NA-2009: EUROCODE 3 „CYS National Annex to CYS EN 1993-1-6:2007", Eurocodes Committee, Scientific and Technical Chamber of Cyprus, Nicosia 2009;

[6] SR EN 1993-1-6/NA-2011: Eurocode 3: STANDARD ROMÂN, "Design of steel structures. Part 1-6: Strength and Stability of Shell Structures National Annex", ROMANIAN STANDARDS ASSOCIATION (ASRO), 2011;

[7] EN 1993-1-6 DK NA, 2007-11-14, 2. Udgave "Stålkonstruktioner –Del 1-6: Styrke og stabilitet af skalkonstruktioner"

[8] EN 1993-1-6/NA-2012: ЕВРОКОД 3 "ПРОЕКТИРАНЕ НА СТОМАНЕНИ КОНСТРУКЦИИ; Част 1-6: Якост и устойчивост на черупкови конструкции Национално приложение", БЪЛГАРСКИ ИНСТИТУТ ЗА СТАНДАРТИЗАЦИЯ, София 2012;

[9] MEST EN 1993-1-6:2019/NA: 2019: Eurokod 3: Projektovanje čeličnih konstrukcija - Dio 1-6: Čvrstoća i stabilnost ljuski - Nacionalni aneks, Institut za standardizaciju Crne Gore, Podgorica,2019.

Tatjana Kočetov Mišulić[1]*, Aleksandra Radujković*[2]

TRADICIONALNO VIZUELNO GRADIRANJE DRVETA I EFEKTI NA SISTEM KLASA ČVRSTOĆE

Rezime:

Vizuelno ocenjivanje se uobičajeno koristi u brojnim zemljama EU, sa različitim nacionalno optimizovanim standardima za ocenjivanje lokalno dostupnog drveta. Srpski standard za vizuelnu klasifikaciju drveta (1983) nije usklađen sa Direktivom o građevinskim proizvodima i EN 14081-1, te zahteva novi pristup klasifikaciji zbog koncepta projektovanja prema graničnim stanjima koji je usvojen u EC5 za drvene konstrukcije. Jedan od glavnih izazova je evaluacija rezane građe za konstrukcijsku primenu i njeno svrstavanje u sistem klasa čvrstoće koji se zasniva na tri relevantna svojstva drveta: gustini, čvrstoći i krutosti pri savijanju.

Ključne reči: vizuelno ocenjivanje, čvrstoća i krutost pri savijanju, korelacija

EFFECTS OF TRADITIONAL APPROACH IN VISUAL GRADING OF TIMBER ON STRENGTH-CLASS SYSTEM

Summary:

Visual grading is commonly used in a number of EU countries, with different grading national standards optimized for locally available wood. Serbian standard for visual classification of timber (1983) is not compliant with Construction Product Directive and EN 14081-1 and requires new classification approach due to limit state design concept adopted in EC5 for timber structures. One of the mayor challenges is assessment and evaluation of sawn timber for structural application and its classification into strength-class system that is based on three relevant timber properties: density, bending strength and bending stiffness.

Key words: visual grading rules, bending strength, bending stiffness, correlation

---

[1] *Assist.Prof. Faculty of Technical Sciences, University of Novi Sad, Serbia, tanya@uns.ac.rs*
[2] *Assist.Prof. Faculty of Technical Sciences, University of Novi Sad, Serbia, leksa@uns.ac.rs*

1. IMPORTANCE AND TYPES OF TIMBER GRADING

Classification of timber for various commercial purposes is essential for its proper application. It is known that the physical and mechanical properties of wood as an organic material vary within a single tree, between the same tree species in the same location, among the same species in different geographical locations, as well as between botanically similar species in the same and different locations. In order to ensure the safe and economic commercial use of wood material for various purposes, different types of sorting and classification of timber have been introduced into national standards around the world.

Sawn timber could be used for non-structural and structural purposes, so different grading procedures are applied due to the final use of the material. Generally, the grading process is always based on **visual sorting**, but opposite to grading of non-structural elements that is exclusively based on (surface) appearance, grading of structural elements also considers determination of relevant strength & stiffness properties i.e. it is visual grading followed by strength classification [1], [2].

Appearance grading is assessing of the prescribed number and size of parameters by visual sorting and it is not designed to take into account the final use of timber (for example: linings, joinery, packaging or construction). Acceptable timber for structural engineer in bearing sense could be completely unacceptable for an architect in appearance.

Structural grading is assessing the timber grades for construction purposes by adequate appearance requirements (particularly related to size and position of knots and their perceived effects on bending strength and stiffness) as useful indication, but followed by experience and additional (destructive) testing of load-bearing properties on relevant samples or by non-destructive mechanical (machines) strength grading using mechanical bending, X-rays, acoustic resonance...

Although the basic principles of timber grading remain the same for decades, the expected results in a form of stress i.e. "quality" grades (used in allowable stress design concept) or strength-class system (used in limit-state design concept) are not easy comparable. The idea and goal of the paper is to clarify the "new" rules for appearance and visual strength grading of structural timber in order to make easier the use of strength-class system for designers of modern timber structures in country and SEE region.

2. KEY EN STANDARDS RELATED TO GRADING OF STRUCTURAL TIMBER

Each timber grading process commence with the preliminary sorting of ungraded timber, where well established visually based grading methods (mostly commercial) are used for the preliminary sort. When dealing with structural timber, there are two parallel systems for grading: visual and machine, that both follow the non-destructive and predictive assessment of bearing grade properties. In structural grading of timber, our country and SEE region are still based on visual grading, while it is expected that the new generation of portable and lower cost grading machines will assist visual grading process in the future, in improving the assignment of timber into strength classes (for example - Slovenia has introduced the simple grading tool called "STIG" based on tablet computer and measurement of timber frequencies provoked by hammer). Despite advances in machine grading, much structural timber in Europe continues to be graded visually and based on national standards.

The change in the design concept of timber structures from allowable stresses with global safety factors (SRPS) into the concept of limit states with partial safety coefficients (EC5) imposed a more detailed classification of wood, i.e. the transition from small number of "quality" grades to strength classes system with a number of structural timber classes.

The new adopted concept implies a change in the entire infrastructure of accompanying standards on wood as a material and its classification (visual or mechanical). Basic principles of timber classification remains the same and are based on national traditional rules, but have to be correlated with new demands that follow the new challenges of modern timber industry. Consequently, this considers adjustment of visual grading rules for structural timber in national standards (that differs around the world as more or less prescriptive) to general requirements in EN standards (EN 14081-1). Besides, the main task for each country is to assign and link the archive data about own species and growth origin into strength classes, in order to provide the input data for structural design within the country borders.

In Table 1 some key codes related to visual and strength classification of structural timber are listed and referenced. Besides EN standards, the correspondent SRPS standards (in Serbian) are given, although the strict link could not be established because of different structures in standards nomenclature. The visually grading and allotting strength classes is in reality more complex procedure, so the related standards about laboratory testing and statistical calculation of obtained data are included in order to ensure the practical remainder and background [1].

Table 1 –Key EN standards related to visual grading and strength classification

(SRPS) EN standards	SRPS (JUS) withdrawn	Comments
Visual grading		
EN14081-1 (2016): Timber structures - Strength graded structural timber with rectangular cross section - Part 1: General requirements	JUS U.D0.001 (1983): Projektovanje i izvođenje drvenih konstrukcija - Materijali za izradu drvenih konstrukcija i tehnički uslovi	Minimum EN requirements for visually grading timber, as framework document that requires national standard in accordance.
Appearance grading		
EN 1611-1 (2007): Sawn timber - Appearance grading of softwoods - Part 1 : European spruces, firs, pines, Douglas fir and larches	JUS D.C1.040 (1955): Borova rezana građa JUS D.C1.041 (1982): Rezana građa jele - smrče	Appearance grading is the category that in such form doesn't exist in SRPS, the link is indirect. Standards for selection of non-structural (commercial) purposes
Visible defects, terminology, measurements		
SRPS ISO 24294 (2015): Timber - Round and sawn timber - Vocabulary EN 1309- 1, 3 (2018): Round and sawn timber. Methods of measurements & Sawn timber, Features and biological degradations EN 844 (2019): Round and sawn timber — Terminology	JUS D.A0.101 (1969): Greške drveta-Terminologija, definicije i merenje JUS D.A1.041 (1957): Ispitivanje drveta - Greške drveta - Merenje JUS D.B0.022 (1984): Proizvodi eksploatacije šuma - Razvrstavanje i merenje neobrađenog i obrađenog drv	Terminology, description and limits of visible defects and their measurements. Thickness classes of sawn timber. Basis for appearance and visual grading. Partially present in withdrawn SRPS, in EN adjusted to demands of modern construction industry

Laboratory testing		
EN 408 (2012): Timber structures - Structural timber and glued laminated timber - Determination of some mechanical and physical properties	JUS D.A1.035 (1975): Ispitivanje drveta - Određivanje modula elastičnosti pri statičkom savijanju JUS D.A1.046 (1979): Ispitivanje drveta - Određivanje statičke savojne čvrstoće JUS D.A1.044 (1979): Ispitivanje drveta - Određivanje zapr. mase	Test methods for determining the mechanical and physical properties (and dimensions, moisture content and density) of structural timber. Withdrown SRPS testing methods differ comparing to EN (three and four point bending tests, small clear vs full size specimens)
Sample size and number of samples, Calculation of characteristic values of properties		
EN14358 (2016): Timber structures - Calculation and verification of characteristic values	JUS D.A1.040 (1979): Ispitivanje drveta - Uzimanje uzoraka	Calculation methods for representative values, significantly different statistical methods EN- SRPS
EN384 (2018): Structural timber - Determination of characteristic values of mechanical and physical properties and density	JUS D.A1.040 (1979): Ispitivanje drveta - Uzimanje uzoraka	Assessment methods, number of samples and compliance criteria. Includes adjustment factors for characteristic values in EN
Strength classes		
EN338 (2016): Structural timber - Strength classes	- (JUS U.C9.200 / 300*)	EN Strength class system instead SRPS stress grades
EN 1912 (2013) : Structural Timber - Strength classes - Assignment of visual grades and species	- (JUS D.A0.021 - 1970: Komercijalne vrste drveta četinara - domaće i strane)	EN links visual grading classifications with strength classes for species and growth areas, SRPS gives only the list of species
Design concepts for timber structures		
EN1990 Eurocode 0: - Basis of structural design EN1995-1-1 Eurocode 5: Design of timber structures - Part 1-1: General - Common rules and rules for buildings	JUS U.C9.200 / 300 (1984)*: Projektovanje i izvođenje drvenih konstrukcija - Konstrukcije od monolitnog drveta i ploča / Lamelirane lepljene konstrukcije - tehnički uslovi	EN: Reliability basis of the Eurocodes and design of timber structures using strength classes and characteristic values vs. SRPS: allowable stress design using "quality" grades and mean values

During the transition of the SRPS timber structure regulation to the EN standards, with a huge number of standards that were worked on by various commissions, an oversight occurred: the domestic standard SRPS U.D0.001 was withdrawn without an adequate, modernized replacement compliant with EN 14081-1 framework.

3. GRADING RULES FOR NON-STRUCTURAL AND STRUCTURAL TIMBER

Traditional grading of sawn timber is primary based on manual ocular inspection of wood surfaces that leads to sorting of timber for non-structural or structural purposes.

Although sorting according to appearance is not decisive for the classification of structural timber, the basic (and innovative) postulates in EN standards may be indicative for structural timber selection.

Appearance grading (EN 1611-1) may be performed on the faces and the edge (G4 - four sided visual sorting), or only on the faces (G2 - two sided). The grading designations are followed by number 0-4, stating the quality of wood (0 is the highest quality). Grade is determined by the number and size of different parameters, and generally takes into account wider spectra of defects than it is relevant for strength grading. The principle of appearance grading is that each side is judged separately and assigned to its own class, while the grading of the whole peace of timber is shown on Fig 1. Construction timber of spruce and pine usually lays in a appearance grade's range of G4-0 to G4-2, while G4-2 is the most common [2].
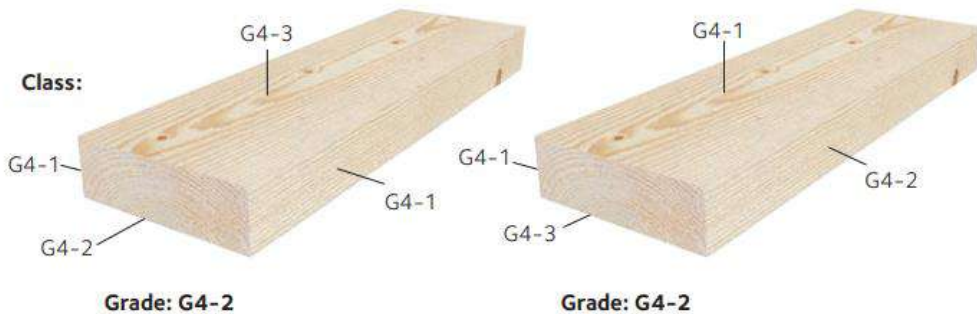
Figure 1 – Assessment of grade by appearance grading - example [2]

Besides sorting parameters like fissures, wane, warp, rot and insect damages, that are common for appearance and strength grading (with different limits due to final use of sawn timber) the most important parameters determining the structural use of timber are knots, slope of grains and rate of growth [1]. Construction timber is used for load-bearing structures and hence has to be subjected to specific requirements concerning strength and stiffness. Therefore, standards for visual classification are the precondition for strength grading of structural timber.

Regional standard for visual classification of timber JUS U.D0.001 from 1983 was based on the second version of DIN 4074 standard from 1958. According to this JUS standard, which is still in use in most parts of the region, timber is classified into stress classes I, II and III. DIN 4074 underwent new changes in 1989, and stress classes were transferred to the "quality" grades with designations S13, S10 and S7. With later amendments (2002, 2008 and 2012) and harmonization with the Construction Product Directive, DIN 4074 became compliant with EN 14081-1, while JUS standard remained unchanged.

Due to new demands of timber industry, the crucial novelties introduced in DIN 4074-1 are the four kinds of cross-section with different specifications and possibilities of flatwise and edgewise orientation of planks and boards, Table 2. That imposes that different orientation of the same slender element could lead to different "quality" grade because of different criteria due to final position of timber element in the structure. In parallel, Table 2 contains dimensions of corresponding JUS coniferous elements, spruce-fir (earlier version of DIN).

Table 2 – Classification of sawn timber elements by dimensions [3]

Coniferous sawn timber	JUS D.C1.041	DIN 4074-1
Battens	24/24 - 28/48 mm	$d \leq 40$mm, $b < 80$mm
Boards	$d \leq 48$mm, $b \geq 5d$	$d \leq 40$mm, $b \geq 80$mm
Planks	$d \geq 49$ mm, $b > 3d$	$d > 40$mm, $b > 3d$
"Squared" timber (joists) (beams)	$b \geq 49$ mm, $b \leq h \leq 2b$ - lath 80/80mm $\leq b/h \leq$ 220/300mm flatwise orientation	$b \leq h \leq 3b$, $b > 40$mm $h \geq 200$mm flatwise or edgewise orientation

Differences between JUS U.D0.001/1983 and DIN 4074-1/2012 in 3 selected requirements for visual grading (knots, slope of grain and rate of growth) are given in Table 3, in parallel with actual EN 14081-1 general strength reducing requirements. Labels given in parenthesis (like S7K) are referred to the so called "squared" timber - "kantholz" or joists i.e. slender elements of dimension of planks that are positioned edgewise. The knot limits vary significantly between compared visual grading codes for the same quality classes, in relation of type of knot (single or group), position (flatwise / edgewise) and specific limits. DIN 4074-1/2012 as an improved version of JUS, has a more detailed classification of knots and thus better prerequisites for more accurate further classification into strength classes. Requests for slope of the grain are more stringent in JUS, except for edgewise orientation for lowest quality grade. Rate of growth i.e. thickness of annual rings is specify in JUS only for I "quality" grade, while DIN has specified limits for all coniferous grades with additional note for Daglas fir.

According to EN infrastructure, besides visual grading, it is necessary to test (destructively or non-destructively) observed batch of sawn timber, by species and region, in order to establish the strength class system with strength and stiffness properties as the basis for structural design. Timber from national territory, of a certain grade, species, and source, could be assigned to strength classes by national authorities as well, using long experience history and archive data. The EN 1912 standard specifies how the national strength grades of different countries correspond to the C (coniferous) strength grades binding for the entire European Union. In Table 4 are given representatives for North and Central Europe, Gradewood project [4]. South Eastern Europe and Balkan countries didn't participate in the project and still not made an official assignment of timber "quality" (stress) grades into strength class system.

Due to economic constraints, visual classification of timber is effective with small number of "quality" grades (2-4), what is opposite to strength class system with a number of classes.

575

Table 3 – Comparison of JUS (1983) and DIN (2012) relevant parameters for visual grading
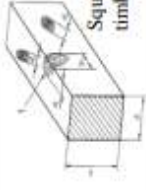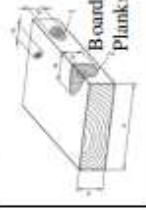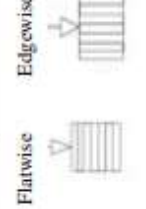
Sorting of coniferous timber	JUS U.D.0.001:1983 (SRPS)			DIN 4074-1:2008 (2012)						EN 14081-1: 2016
				Boards / Planks flatwise			Squared timber and board/planks - edgewise			
Timber grades	I	II	III	S13	S10	S7	S13(K)	S10(K)	S7(K)	Requirements
Knots										Max knots specified in relation to width, cross-section or as absolute values
Single	≤ 1/4	-	-	≤ 1/5	≤ 1/3	≤ 1/2	≤ 1/5	≤ 2/5	≤ 3/5	
Groups	≤ 1/3	≤ 1/3	≤ 1/2	≤ 1/3	≤ 1/2	≤ 2/3	-	-	-	
Narrow side	-	-	-	≤ 1/3	≤ 2/3	-	-	-	-	
Slope of grain	≤ 5%	≤ 10%	≤ 15%	≤ 7%	≤ 12%	≤ 16%	≤ 7%	≤ 12%	≤ 12%	Slope of grain's limitation for each grade has to be specified
Rate of growth	≤ 4mm	-	-	≤ 4mm *≤ 6mm	≤ 6mm *≤ 8mm	≤ 6mm *≤ 8mm	≤ 4mm *≤ 6mm	≤ 6mm *≤ 8mm	≤ 6mm *≤ 8mm	If rate of growth is specified, it shall include limits.
Note							* for Daglas fir			
Explanations				Squared timber			Boards & Planks			Flatwise Edgewise

Table 4 – Assignment of visual graded timber of same species and different geographical areas of growth into strength classes (EN 1912)

EN 1912	source	Spruce *Picea abies*	Fir *Abies alba*
Germany DIN 4074-1:2012	CNE Europe	S13(K) → C30 S10(K) → C24 S7(K) → C18	S13(K) → C30 S10(K) → C24 S7(K) → C16
Slovenia SIST DIN 4074-1:2009	Slovenia	S10 → C24 S7 → C18	S10 → C24 S7 → C16
Nordic countries INSTA 142:2009	NNE Europe	T3 → C30 T2 → C24 T1 → C18 T0 → C14	T3 → C30 T2 → C24 T1 → C18 T0 → C14
Balkan countries JUS	SEE Europe	I → ? II → ? III → ?	I → ? II → ? III → ?

Table 4 shows that strength classes C30, C24, C18 and C14 are the most represented in CNE and NNE Europe. General description of these strength classes are the following [2]:
- C30 is a strength class where factors that affect the strength and deformation of structural timber are permitted to a very low extent and is intended to load bearing structures that require high strength. It is a homogenous but not widespread and cannot be found easily and in large dimension.
- C24 is used in load-bearing structures that require relatively high strength, where factors that affect the strength and deformation are permitted to a low extent. It is widespread and considered as common construction timber, with variety in dimensions.
- C18 is used for load-bearing structures that do not require high strength, with strength affecting factors in a moderate extent. It is suitable for use in constructions of minor importance and where large dimensions are needed.
- C14 is used for load-bearing structures that have not too stringent demands, where factors that affect the strength and deformation are permitted to a large extent. It is suitable for use in construction of walls and could be found in relatively small dimensions.
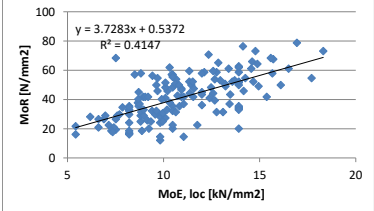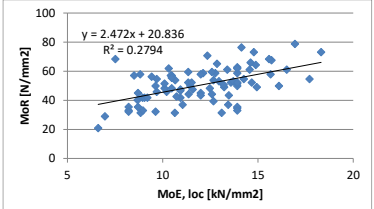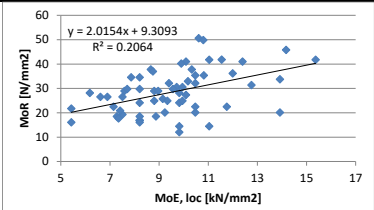
4. EFFECTS OF VISUAL GRADING ON STRENGTH CLASS ESTIMATION: RESULTS AND DISCUSSION

The method of visual classification in SRB and the region did not change for many years, while in EU countries it was updated to the regulations that follow modern trends in the wood construction industry (use of smaller cross-sections). In order to establish the effects and applicability of the traditional classification on the assessment of stress grades in terms of strength classes according to EN 338, a preliminary analysis was carried out on an archive data sample of 150 specimens (spruce/fir timber visually graded planks in SRPS II stress grade) [5]. The archive sample was analyzed as a whole and divided into two subsamples (Good and Low), using adjustment factors for adaptation of EN testing methods and by following the statistical procedures given in EN standards, that was discussed in details in [6], [7], [8].

The results of the analysis are shown in Table 5, where the division of all data on two new samples was made afterwards on the basis of documentation and description of each specimen (e.g. zone and size of knots, slope of grains, annual rings were not considered because are not limited by SRPS for II grade), because of new requirements in visual grading rules in EU.

Table 5 – Estimation of strength class for coniferous timber classified into stress grade II

Stress grade vs. Strength class	JUS	Eurocode
All data		
	σ_{md}=10.33 MPa $\rightarrow$ II stress grade E_{IIm}=10.08 GPa (II stress grade)	$f_{m,k}$=15.16 N/mm^2 $\rightarrow$ C14 $E_{0,mean}$ =10.8 kN/mm^2 $\rightarrow$ C22
Good Lot		
	σ_{md}=12.6 MPa $\rightarrow$ II / I stress grade E_{IIm}=10.81 GPa (II stress grade)	$f_{m,k}$=25.6 N/mm^2 $\rightarrow$ C24 $E_{0,mean}$ =11.8 kN/mm^2 $\rightarrow$ C27
Low Tail		
	σ_{md}=7.11 MPa $\rightarrow$ III stress grade E_{IIm}=9.03 GPa (II stress grade)	$f_{m,k}$=12.18 N/mm^2 $\rightarrow$ – $E_{0,mean}$ =9.3 kN/mm^2 $\rightarrow$ C18

It is obvious from obtained results that all specimens, visually graded as SRPS (JUS) II stress grade, have a good match with allowable stress (mean value of bending stress), that confirms that visual grading procedure was adequate for design procedure when global safety factors is 4. Moderate correlation between MoR and MoE (r=0.64) shows that prescribed value for MoE (10GPa) was quite adequately established. Recalculation procedure according to EN leads to C14 for characteristic bending strength (5% fractile) that is quite low strength class comparing with predictive assignment of construction timber in EU countries (Table 4). This could be explained by the use of tested timber (wall studs, C14) [2], but it is not correct to use this result like evaluation factor for the timber population. Therefore, more strict grading rules were applied in sorting of all data to Good and Low samples, what leads to new stress and strength class estimation: Good lot shows bending stress results near to I stress grade (moderate correlation r=0.53), while strength class prediction leads to C24 (commonly used construction timber in EU); Low tail shows results as III stress grade (also moderate correlation r=0.45), while it can't be classified into strength class.

Results of MoE in all 3 samples show better strength class prediction in EN procedure: C22, C27 and C18 respectively, The fact that MoE values are higher comparing to strength, so that strength is the crucial parameter for assignment of visual grades, is noticed in numerous extensive investigation projects of wood grading [3], [4]. Results of MoE in SRPS are given as single value for all grades of coniferous solid timber, so they are not the parameter for stress grade evaluation, as well as density that is given in general range.

5. CONCLUSION

Visual classification is traditional method which dominantly depends on species and source of timber on certain growth area and has to be aligned with. In modern timber construction industry the use of large cross-section dimensions is reduced, so the visual grading criteria have to be adjusted on small cross-section sizes (oriented flatwise and edgewise) and to perform precisely. Although the visual classification seeks for additional testing (of bending strength & stiffness properties) and supplementary statistical procedures in order to establish strength class system over certain growth region, it is very useful and necessary precondition. The Balkan region needs a united interstate effort of forestry and civil engineers to put construction wood on the map of Europe and facilitate the design process of timber structures.

ACKNOWLEDGEMENT

REFERENCES

[1] Bather M. Technical note on the use of visual grading codes for the appraisal of individual in situ structural timber elements. University of Liverpool, 2021.

[2] https://www.swedishwood.com/wood-facts/about-wood/wood-grades, accessed Jun 2022.

[3] Stapel P. Strength grading of timber with regard to different grading methods, PhD thesis, TU München, 2014.

[4] Ranta-Manus A, Denzler J, Stapel P. Strength of European Timber, Part 2- Gradewood project. VTT 179, Finland, 2011.

[5] YU-USA research project. Damage and collapse in Low-Rise Wood Frame Buildings produced in Yugoslavia. Part 1, Serbia, 1985-1988.

[6] Kočetov Mišulić T, Radujković A. Proposal for Assignment of Visually Graded Timber into Strength Classes in Existing Structures. The 15th International Scientific Conference iNDIS 2021, Serbia, 2021, 707-716.

[7] Kočetov Mišulić T, Radujković A. Differences in Statistical Evaluation of Timber Bending Strength according EN 384 and EN 14358. The 8th International Conference GNP 2022, Montenegro, 2022, 517-524.

[8] Kočetov Mišulić T, Radujković A. Evaluation of Bending Modulus of Elasticity in Timber according to EN 384 and EN 14358. The 19th International Symposium, MASE - 2022, North Macedonia 2022, 320-327.

Todor Vacev[1], Miloš Milić[2], Andrija Zorić[3], Ivan Nešović[4], Slobodan Ranković[5]

PROJEKTOVANJE ČELIČNOG RAMA ZA ISPITIVANJE PREMA STANDARDU EN 1993-1-14 – STUDIJA SLUČAJA

Rezime:

Predmet studije je čelični ram za ispitivanje ferocementnih panela. Ram je projektovan prema novom predloženom standardu EN 1993-1-14, Projektovanje čeličnih konstrukcija pomoću MKE, i predviđen je kao praktični primer u Tehničkom Izveštaju uz Standard. Proces projektovanja se sastojao od modeliranja i statičke analize primenom elemenata grede i ploče, kao i zavrtanjskih i zavarenih veza. Verifikacija projektovanja je obavljena nizom analiza konstrukcije, linearnim i nelinearnim, sa i bez imperfekcija. Konvergencija mreže i opterećenja je takođe sprovedena. Studija može poslužiti kao vodič za buduću primenu Standarda.

Ključne reči: čelične konstrukcije, MKE, Standard EN 1993-1-14, Tehnički izveštaj

DESIGN OF A TEST FRAME STRUCTURE ACCORDING TO STANDARD EN 1993-1-14 – CASE STUDY

Summary:

The subject of study is a steel frame for ferrocement panel testing. The frame was designed according to the newly proposed standard EN 1993-1-14, Design assisted by FEA, and it was intended to be a worked example in the Technical Report of the standard. The design process consisted of modelling and static analysis using both beam and plate finite elements, and bolted and welded connections. Verification of the design process was done by subduing the structure to a series of linear and non-linear analyses, with and without imperfections. Mesh and load convergence were done, too. The study may serve as a guide for future use of the Standard.

Key words: steel structures, FEA, Standard EN 1993-1-14, Technical Report

---

[1] *PhD, Associate Professor, University of Niš, Faculty of Civil Eng. and Architecture, A. Medvedeva 14, Niš, Serbia, todor.vacev@gaf.ni.ac.rs*
[2] *MEng, Junior Researcher, Faculty of Civil Eng. and Architecture, Niš, milos.cicevac@gmail.com*
[3] *MEng, Teaching Assistant, Faculty of Civil Eng. and Architecture, Niš, andrija.zoric@gaf.ni.ac.rs*
[4] *MEng, Research Assistant, Faculty of Civil Eng. and Architecture, Niš, ivan.m.nesovic@gmail.com*
[5] *PhD, Assistent Professor, Faculty of Civil Eng. and Architecture, Niš, rankovics@gmail.com*

1. INTRODUCTION

The aim of this study is to demonstrate the procedure for application of the new proposed standard [1], and to present verification methodology recommended in its use, on one concrete steel structure.

The subject of design is a steel frame intended for testing of ferrocement panels. The panels can take different dimensions, and the maximal are: length L = 6000 mm, width: B = 4000 mm, and depth: H = 300 mm. The panel sample and the frame lie in horizontal plane. Panels are supposed to be tested under pressure acting in their midplane (panels act as a diaphragm). Pressure is provided by a series of hydraulic jacks. Max. testing force is P = 3000 kN, and deformation of the cross beams is limited to 5 mm. The frame is consisted of two cross beams (one fixed, one adjustable) and two longitudinal beams which serve as a support for the cross beams and guide rails for the inserted beam, used as a pad between the presses and the panel sample (Fig. 1). The whole frame is supported on special supports fixed in RC foundation.

Connections between the cross beams and longitudinal beams are bolted, as well as the connections betweeen the longitudinal beams and the support stuctures. Support structures are mounted to the foundation using anchor bolts and base plates.

The design process consists of the following stages:
1. Modelling and static analysis of the structure using BEAM finite elements (FE);
2. Modelling and static analysis of the structure using PLATE FE);
3. Modelling and static analysis of the bolt connections using BEAM FE;
4. Modelling and static analysis of the bolt connections using SOLID FE and contact analysis;
5. Modelling and static analysis of the welded connections using PLATE FE;
6. Comparative analysis of th results and conclusions.

2. MATERIAL, ACTIONS, AND PARTIAL SAFETY FACTORS

The steel material data for the structure and the connecting bolts are given in Table 1.

Table 1 – Steel material data

Item	Symbol	Value	Unit	Note
Base material	**S355**			
Yield strength	f_y	355	MPa	
Ultimate strength	f_u	510	MPa	
Modulus of elasticity	E	2.1E11	MPa	
Tangent modulus (E/10000)	E_t	2.1E7	MPa	Material NL analysis
Bolts				
Grade	10.9	-	-	
Yield strength	f_y	900	MPa	
Ultimate strength	f_u	1000	MPa	
Modulus of elasticity	E	2.1E5	MPa	
Tangent modulus (E/10000)	E_t	2.1E1	MPa	Material NL analysis

The structure is exposed to the following actions:

1. Self-weight of the structure.
2. Imposed load (from the action of hydraulic presses).

The structure does not fall into any of the common categories covered by EN standards. For load analysis and partial safety factor use, the standard [2] was applied.

The imposed load from the action of hydraulic presses is taken as static, due to the slow rate of pressure increase. Since the self-weight of the structure and the imposed load are sole actions on the structure, both loads are taken as permanent, which is on the safe side. According to this, the partial safety factor is: $\gamma_{G,sup} = 1.35$. For the ultimate limit state (ULS) analysis the imposed load is factored by the adopted partial safety factor: $P_u = P * \gamma_{G,sup} = 3000 * 1.35 = 4050$ kN.
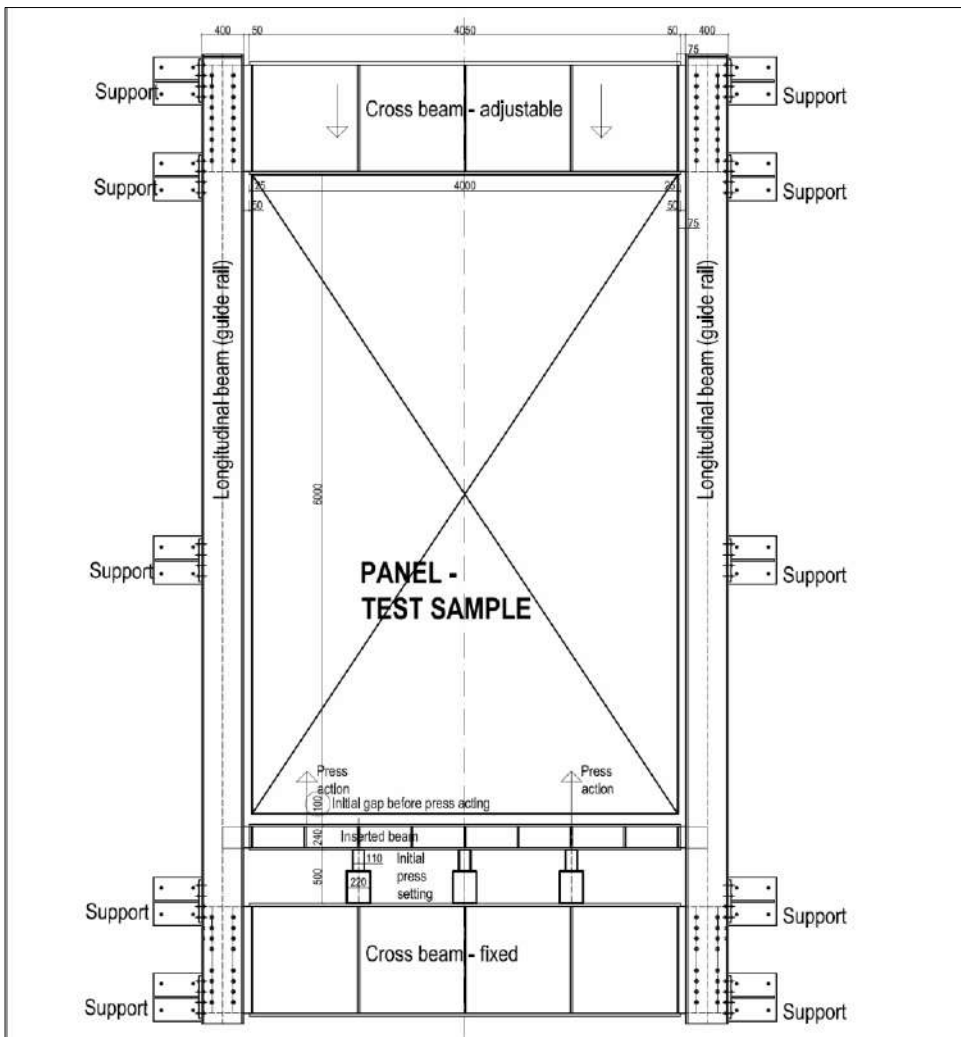
Figure 1 – Functional scheme of the test frame structure, floor plan; dimensions in [mm]

3. MODELLING AND STATIC ANALYSIS USING BEAM FE

After preliminary calculations, the following profiles were adopted for the frame structure:
- Cross beams: welded I-profile with web ‖1000x20 mm, and flanges ═350x30 mm;
- Longitudinal beams: double standard hot rolled profile][400 mm;
- Inserted beam: welded I-profile with web ‖200x20 mm, and flanges ═350x20 mm.

The flanges of the cross beams are cut at the ends in order to enable insertion between the][profiles and provide connection surface for the longitudinal beams. The][400 profiles are provided with certain number of bolt holes to enable adjustment of one cross beam, depending on the test sample dimensions. Modelling is done using BEAM FE (Fig. 2). The frame is loaded with self-weight and imposed distributed load from the press action on the cross beams (action and reaction). The imposed load is as follows: $q = P_u / L = 4050000 \text{ N} / 4.000 \text{ m} = 1012500 \text{ N/m}$.
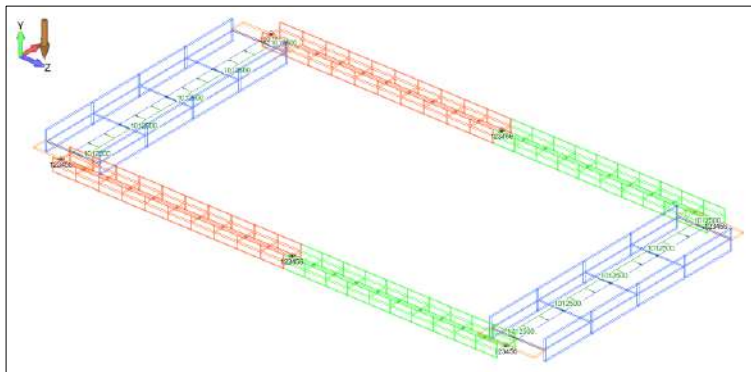
Figure 2 – BEAM FE model, supports, load; isometric view

The analyzed structure has been subdued to a series of analysis stages, which encompassed different analysis levels regarding the linearity of the analysis, and convergence checking as a part of the FE model verification. The analysis stages, and their main features were as follows:

1. Linear analysis (LA), as the simplest analysis level for starting.
2. Mesh convergence check; mesh density of the critical parts is doubled.
3. Load convergence check, by doubling the load intensity.
4. Linear buckling analysis (LBA), for preliminary check of stability and as a base for further calculation of imperfections.
5. Geometric non-linear analysis (GNA), for checking of eventual influence of geometric nonlinearity on strength and behavior of the structure; the load was applied incrementally.
6. Geometric non-linear analysis with imperfections (GNIA), for checking of eventual influence of the structural imperfections on strength and behavior of the structure.
7. Geometric and material non-linear analysis with imperfections (GMNIA), as the most comprehensive, for checking of all structural factors on strength and behavior of the structure.

The first verification step was to remesh the critical parts of the frame, the cross beams, splitting the elements into two FE. The mesh statistics for both meshes is shown in Table 2. This model was analyzed on LA level; after that, the load was doubled in order to conduct the load convergence verification. All further analysis steps were performed on the model with MESH2.

Table 2 – Mesh statistics (MESH1 / MESH2)

Structural element	FE length [mm]	Number of FE	Total nodes	Total FE
Cross beam	1000 / 500	12 / 20	52 / 60	52 / 60
Longitudinal beam	385 / 385	40 / 40		

The next step was the LBA analysis, which produces the critical load factor (LF) needed to multiply the imposed load to cause instability. This factor is used only for preliminary assessment of the stability of the structure. The more important role of this analysis is to supply buckled shape displacement values (Fig. 3), so the imperfections could be calculated.

The allowed geometrical imperfection for the structural elements was taken from [2], p. 120, Table D.1.3: $\Delta = \pm L / 750$. The characteristic length of the most deformed structural part (the cross beam) is $L = 4.50$ m. According to this, the allowed imperfection for the cross beam is: $\Delta_{allowed} = L / 750 = 4.50 / 750 = 0.006$ m.

The maximal relative total displacement of the structure, taken from the LBA (Fig. 3) is $\Delta_{max} = 0.28$ m. Using this value, the scaling factor for imperfections is: $k = 0.006 / 0.28 = 0.0214$. The scaling factor k is then applied to move all nodes of the FE model and to obtain an imperfect structure for further analysis.
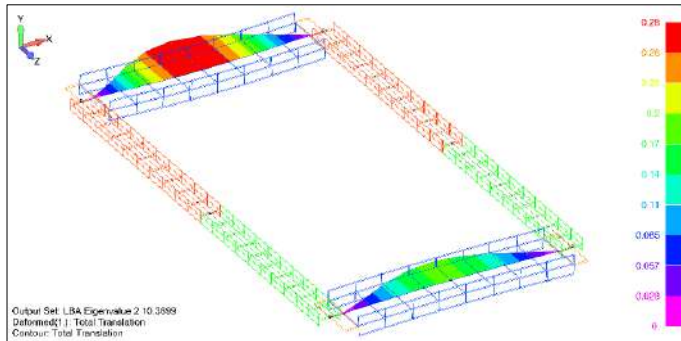
Figure 3 – Analysis level: LBA, 2nd buckling mode; max. total displacement: δ = 280 mm

Output results of the final analysis (GNIA), displacements in the direction of load (Z) and combined stresses in the BEAM elements, are presented in Fig. 4.
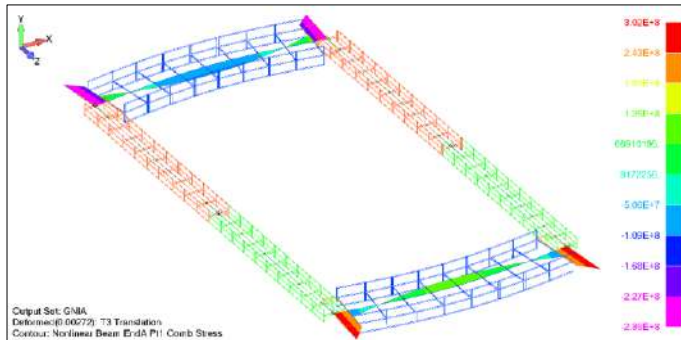
Figure 4 – Analysis level: GNIA; Z_{max} = 2.72 mm; $σ_{max}$ = 302 MPa

584

Table 3 – Analysis stages and result review

Analysis level	Load [%]	σ_{max} [MPa]	σ [%]	Z_{max} [mm]	Z [%]	Comment
LA (MESH1)	100%	302	100	2.72	100	Initial analysis - referent
LA (MESH2)	100%	302	100	2.72	100	Mesh convergence OK
LA (MESH2)	200%	596	197	5.43	200	Load convergence OK
LBA (MESH2)	100%	LF=10.37	-	280.00	-	Stability OK
GNA (MESH2)	100%	302	100	2.72	100	Output stable
GNIA (MESH2)	100%	302	100	2.72	100	Output stable
GMNIA (MESH2)	-	-	-	-	-	Not done

Comment: all levels showed stable output, and the structure is under stress limits.

4. MODELLING AND STATIC ANALYSIS USING PLATE FE

The procedure of analysis was analogous to the BEAM model (see Section 3). The PLATE model comprises of cross and longitudinal beams as the BEAM model, but also includes support structures and some stiffening ribs. The mesh statistics is given in Table 5. Again, the first analysis stage was the LA. Next, the mesh convergence was conducted by splitting every FE in the model into four FE. Mesh statistics for both meshes is given in Table 4, and the FE model with MESH2 is presented in Fig. 5. After analysis using LA, here too the load was doubled in order to conduct the load convergence verification. All further analysis steps were performed on the model with MESH2.

Table 4 – Mesh statistics (MESH1 / MESH2)

MESH	Avg. FE size [mm]	Nodes total	FE total
MESH1 / MESH2	75 / 37	9002 / 34636	8576 / 33638

The imposed load for this model was surface load on internal flanges of the cross beams.
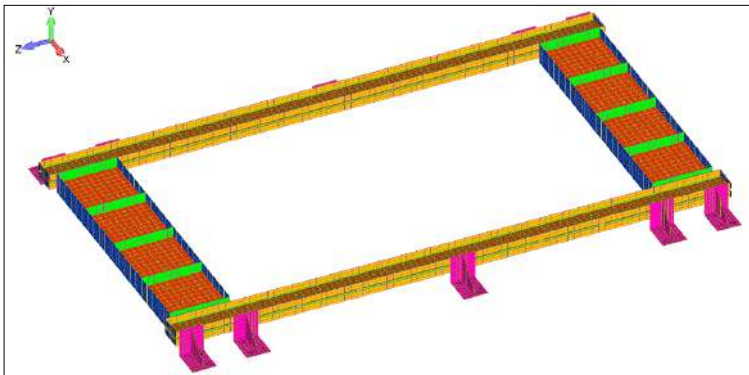
Figure 5 – FE model, supports; isometric view

The LBA analysis was done next, and the deformed shape of the frame is shown in Fig. 6.

The imperfection calculation was done similarly as for the BEAM model (see Section 3). Here, the characteristic length of the most deformed structural part was: $L = 4.50$ m (cross beam). Allowed imperfection for the cross beam is: $\Delta_{allowed} = L / 750 = 4.50 / 750 = 0.006$ m

The maximal relative total displacement of the structure taken from the LBA (Fig. 6) is $\Delta_{max} = 0.635$ m, and the scaling factor for imperfections is: $k = 0.006 / 0.635 = 0.0094$. Again, scaling factor k is applied to move all nodes of the FE model in order to obtain an imperfect structure.

After that, the GNA, GNIA, and GMNIA analyses were conducted. Characteristic output results for the final analysis (GMNIA) are presented in Fig. 7.
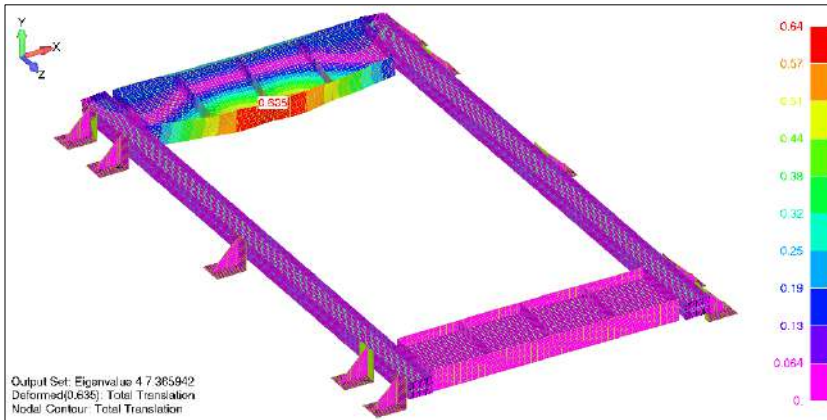
Figure 6 – Analysis level*: LBA, 4th buckling mode; max. total displacement: $\delta = 635$ mm*
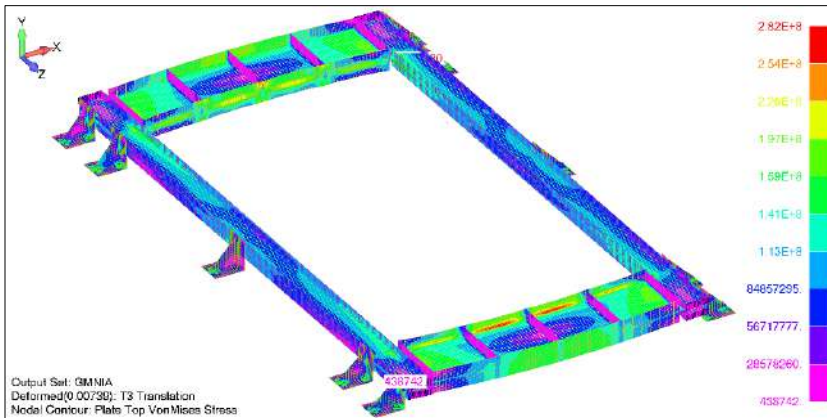
Figure 7 – Analysis level: GMNIA; $Z_{max} = 7.39$ mm; max. von Mises stress $\sigma_{max} = 282$ MPa

In the Table 5 is given the overall review of all analysis stages and accompanied output data. The comments refer to the status of the verification steps.

Table 5 – Analysis levels and result review

Analysis level	Load [%]	σ_{max} [MPa]	σ [%]	Z_{max} [mm]	Z [%]	Comment
LA (MESH1)	100%	299	100	7.03	100	Initial analysis - referent
LA (MESH2)	100%	**447 (+26%)**	149	7.10	101	Mesh convergence failed
LA (MESH2)	200%	903	302	14.20	202	Load convergence OK
LBA (MESH2)	100%	LF = 7.37	-	635.00	-	Stability OK
GNA (MESH2)	100%	284	95	7.06	100	Output stable
GNIA (MESH2)	100%	282	94	7.39	105	Output stable
GMNIA (MESH2)	100%	254	85	6.65	95	Output stable

Comment: all levels showed stable output, except the LA (MESH2) level; however, non-linear analyses confirmed that the structure is under stress limits.

5. MODELLING AND STATIC ANALYSIS OF THE CONNECTIONS

The connections between the cross beam and the longitudinal beam, and between the longitudinal beam and the support structure are assumed as bolted. The bolt shafts are modelled as short BEAM FE (Fig. 8, dark blue). The bolts are assumed as clamped into the connected base elements (profiles, plates). Partial safety factor for the bolt connection is $\gamma_{M2} = 1.25$, which is lower than the overall partial safety factor for the structure ($\gamma_{G,sup} = 1.35$). In order to check the strength of the integral structure (the base material and the bolted connections) on one FE model, the common safety factor of 1.35 is adopted, which is on the safe side.
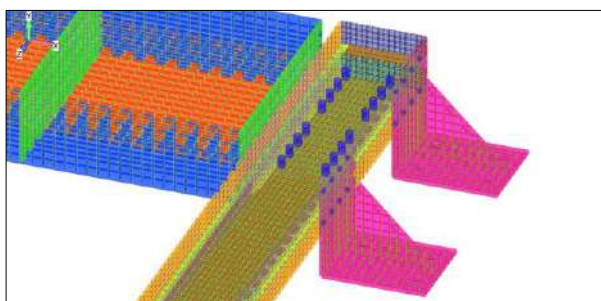
Figure 8 – FE model, detail of the bolted connections, isometric view

5.1 BOLT CONNECTION CROSS BEAM-LONGITUDINAL BEAM

This connection passed the complete verification procedure like the frame structure itself, and the results review is presented in Table 6. Stress distribution for one typical bolt group is shown in Fig. 9. The bolts are stressed unevenly, opposing the classic assumptions.

Table 6 – Bolt connection cross beam-longitudinal beam - Analysis levels and result review

Analysis level	Load [%]	σ_{max} [MPa]	σ [%]	Comment
LA (MESH1)	100%	757	100	Initial analysis - referent
LA (MESH2)	100%	837	111	Mesh convergence failed
LA (MESH2)	200%	1770	223	Load convergence OK
LBA (MESH2)	100%	-	-	-
GNA (MESH2)	100%	865	114	Output increase
GNIA (MESH2)	100%	865	114	Output increase
GMNIA (MESH2)	100%	**925**	122	Output increase

Comment: levels showed stress increase with the increase of the level of non-linearity; however, the final level, GMNIA, showed that bolt stresses surpass the limits only 2.8 %. The review proves the significance of the non-linear approach to connection analysis.

This bolt connection between the longitudinal beam - and the support structure was analyzed analogously as the previous one.
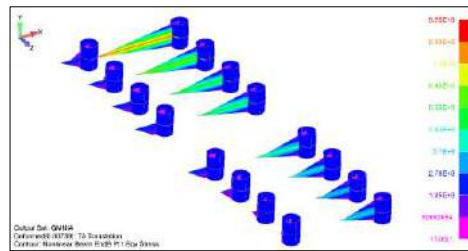
Figure 9 – Analysis level: GMNIA; bolt connection detail; $\sigma_{max} = 925$ MPa

5.2 WELDED CONNECTION FLANGE-WEB OF THE CROSS BEAM

The welded connections between the flange and the web of the cross beam, and between the support structure elements were not modelled in particular. Strength check of those connections was done by comparing the von Mises stresses in the zones of weld connections with proposed thickness. The detailed procedure for this checking is given in further text.

The strength calculation of the weld is as following:

Flange thickness: $t_f = 30$ mm

Web thickness: $t_w = 20$ mm

Max. single weld throat thickness: $a_{w1} = 0.7 * 20 = 14$ mm

Correctional factor for steel S355: $\beta_w = 0.90$

Strength condition: $\sigma_{eq} \leq f_{uw,d} = f_u / (\beta_w * \gamma_{M2}) = 510 / (0.90 * 1.25) = 453$ MPa

Max. double weld throat thickness: $a_w = 2 * a_{w1} = 2 * 14 = 28$ mm $> t_w = 20$ mm

Max. von Mises stress in the weld zone: $\sigma_{max} = 279$ MPa (Fig. 10)

Strength check: $\sigma_{calc} = 279$ MPa $< f_{uw,d} = 453$ MPa **(SATISFYING)**

Under given assumptions, total weld throat thickness is greater than the base material thickness, and the stresses in the model are lower than those given by strength condition.

The strength calculation of the welded connection between the support parts is conducted analogously as for the previous weld.
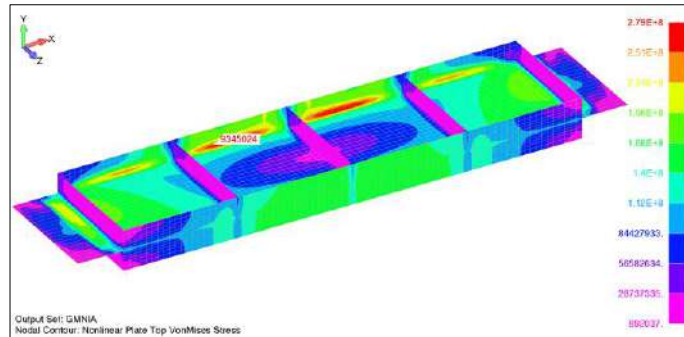
Figure 10 – Analysis level: GMNIA; cross beam, detail; von Mises stress σ_{max} = 279 MPa

5.3 BOLT CONNECTION CROSS BEAM-LONGITUDINAL BEAM USING CONTACT ANALYSIS

For the purpose of verification of the bolt connection modelling, a sophisticated model with contact FE was analyzed. It was done for the connection between the cross beam and longitudinal beam only, and due to the symmetry, only 1/8 of the structure was modelled, with appropriate boundary conditions. The structure was modelled using SOLID FE with 8 nodes. The material model for the beams was adopted as linear, except for the immediate vicinity of the bolt holes, and the bolts were entirely modelled using non-linear material. The load from the presses is applied via the fictive elements that act on the cross beam.

In Fig. 11 are presented stress results for the frame elements which excess the yield point of the base material. One may note that only couple of elements surpass the given yield point (stress exceeding is 36 %). All critical elements are in the bolt holes, as expected, and extend only 10-15 mm from the hole perimeter. Again, all critical elements are in the internal bolt column of the connection, as it was in the simplified bolt connection analysis (see Section 5.1).
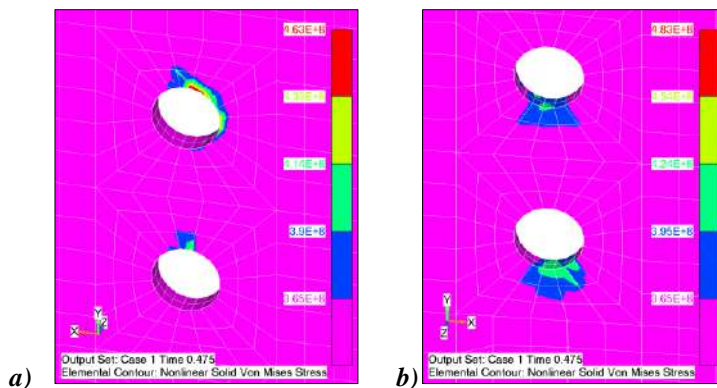
Figure 11 – Analysis level: GMNA; von Mises stress σ_{max} = 483 MPa;
a) detail of the longitudinal beam bolt holes; b) detail of the cross beam bolt holes

In Fig. 12 are presented contact pressures for the bolt elements. This type of structural output is not a regular part of steel structure calculation, but it is presented here to illustrate the

589

complexity of the bolted connections, impossible to perceive by EN procedures. High stress values obtained here can be only be compared to the contact calculations, well-known as Hertz's formulas. However, those high pressures readily decrease at distance of 5-10 mm of the bolt hole, taking values close to the von Mises stresses, used for strength proof.
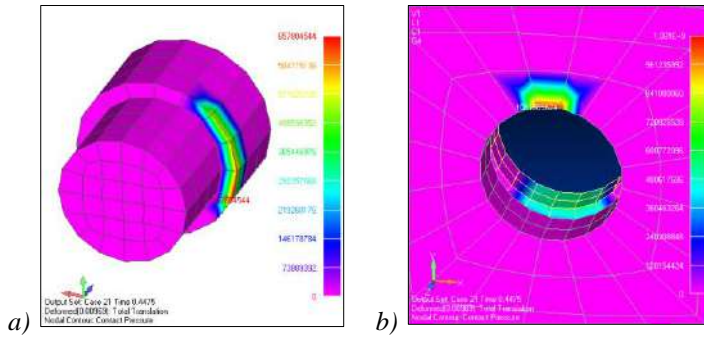
Figure 12 – Analysis level: GMNA; contact pressure;
a) bolt detail, $\sigma_{c,max}$ = 658 MPa; b) bolt hole detail, $\sigma_{c,max}$ = 1081 MPa;

In Fig. 13 are presented stress results for the bolt elements. One may note that all bolt elements are below the yield point for the adopted bolt material (σ_y = 900 MPa), and, again, that all critical elements are in the internal bolt column of the connection.
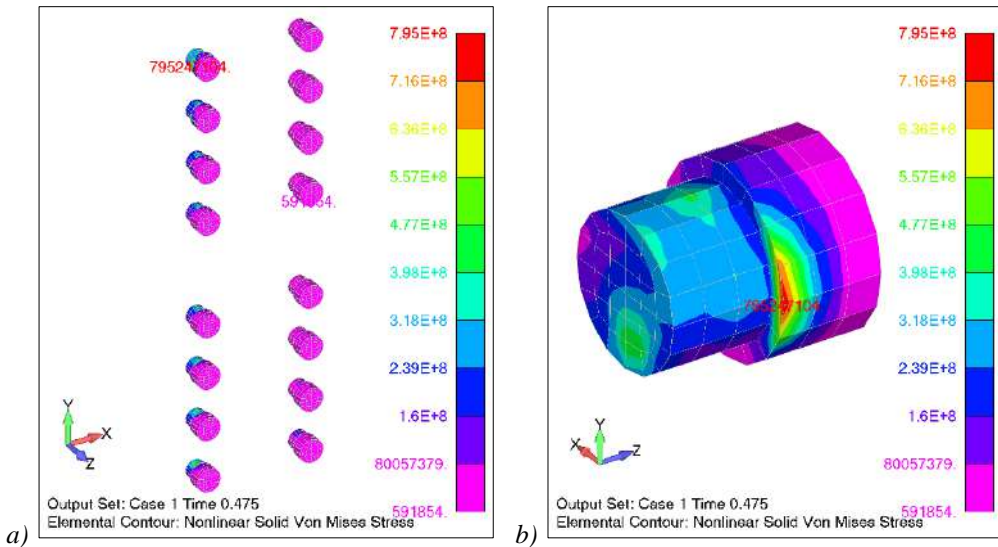
Figure 13 – Analysis level: GMNA; von Mises stress for bolts, σ_{max} = 795 MPa;
a) bolt group detail, internal bolt column on the left; b) the most stressed bolt (top left bolt)

6. CONCLUSIONS

In this case study are combined data from existing EN standards, guidelines from the proposed EN 1993-1-14 standard, FEM and engineering judgment, in attempt to present a practical design procedure for one real structure, which may serve as a benchmark case and a possible contribution to the Technical Report that will accompany EN 1993-1-14 standard.

The structure is subdued to two FE modelling approaches: using BEAM FE and PLATE FE. Both approaches passed a series of analysis levels, from the simplest to the most complex: LA, LBA, GNA, GNIA, and GMNIA, in order to verify the FE model. Also, mesh and load convergence has been conducted. The structure strength was checked for the ULS. The stress comparison between different analysis levels showed stable output production, and thus verified the proposed model. The only exemption is the LA for the MESH2, when the stresses surpassed the yield point limit. However, the following non-linear analyses showed good results.

It is shown that the PLATE FE allowed a much more detailed modelling, and enabled inclusion of the fastenings into the analysis. Within the PLATE model, the bolt connections were first modelled simply, as BEAM FE clamped into the fastened parts of the structure. Secondly, the whole structure, including the bolt bodies were modelled using SOLID FE, and sophisticated contact analysis was applied. Comparison of results did not show any significant deviation between the two modelling approaches, meaning that the simple method was satisfying enough to calculate and prove the connection strength. We also remark that such arbitrary connection could not be calculated using the existing standard [4]. Moreover, both presented methods showed the inaccuracy of the classic assumption of equal share of all bolts in load transfer.

The welded connections were not modelled in detail (i.e., the weld volume), but the weld strength was proved indirectly, by assessing the stresses in the weld zones. A more detailed modelling would imply using solid FE, both for the structure and for the weld.

The study was finalized with the most complex analysis level (GMNIA). Taking into account the application of *sensitivity check of input parameters, engineering judgment, discretization error check,* and *imperfection sensitivity analysis,* this analysis should fall into the *numerical simulation* category [1], and the safety factor γ_{FE} for this study was adopted as: $\gamma_{FE} = 1.0$ [1].

The whole presented procedure may be used as a design pattern for a variety of structures for practicing engineers. As it is shown, the BEAM FE modelling may serve as a preliminary one, while the PLATE FE model may give an insight into critical points of the structure, and an opportunity to optimize it. The ultimate solution could be a SOLID FE model, although not convenient for everyday practice.

The structure should be checked and the analysis procedure verified for the serviceability limit state (SLS), too, but the available space of this paper does not facilitate it. Generally, such check would include all the steps applied for the ULS.

REFERENCES

[1] EN 1993-1-14 Design of steel structures - Part 1-14: Design assisted by finite element analysis (in preparation)

[2] EN 1090-2 Execution of steel structures and aluminium structures - Part 2: Technical requirements for steel structures

[3] EN 1991-3 - Actions induced by cranes and machinery

[4] EN 1993-1-8 Design of joints

Jovana Topalić Marković[1]*, Mirjana Terzić*[2]*, Vladimir Mučenski*[3]

UČEŠĆE JAVNOSTI U PROCENAMA UTICAJA NA ŽIVOTNU SREDINU KAO PREVENCIJA NEGATIVNIH UTICAJA GRAĐENJA

Rezime:

Učešće javnosti u odlučivanju u procenama uticaja projekata na životnu sredinu definisano je zakonskom regulativom Republike Srpske. Neophodno je da javnost bude upućena, u svoja zakonski regulisana prava, i da učestvuje aktivno u donošenju odluka vezanih za životnu sredinu i ekosistem u kome žive. Podizanjem i jačanjem svesti javnosti kroz sistem obrazovanja i vaspitanja, naučnoistraživačkog i tehnološkog razvoja, javnog informisanja i popularizacije zaštite životne sredine podstaći će se aktivno učešće javnosti u odlučivanju u procenama uticaja na životnu sredinu. Na taj način mogu se smanjiti negativni uticaji građenja na životnu sredinu.

Ključne reči: učešće javnosti, životna sredina, uticaj

PUBLIC PARTICIPATION IN ENVIRONMENTAL IMPACT ASSESSMENT AS PREVENTION OF NEGATIVE CONSTRUCTION IMPACTS

Summary:

Public participation in the decision-making of a project's environmental impact assessment is defined by the legislation of the Republic of Srpska. The public must know about their legally defined rights and actively participate in decision-making about the environment and the ecosystem in which they live. By raising and strengthening public awareness through the education system, scientific and technological development, communication with the public, and environmental protection popularisation, active public participation in the assessment of environmental impacts will be encouraged. This way, it's possible to decrease the negative impacts of construction projects on the environment.

Key words: public participation, environmental protection, impact

---

[1] *Research Associate, Faculty of Technical Sciences, Novi Sad, Serbia, e-mail: jovanatopalic90@uns.ac.rs*
[2] *Assistant, Faculty of Technical Sciences, Novi Sad, Serbia, e-mail: terzic.mirjana@uns.ac.rs*
[3] *Associate Professor, Faculty of Technical Sciences, Novi Sad, e-mail: mucenskiv@uns.ac.rs*

1.   INTRODUCTION

Construction projects generally generate a significant share of environmental pollution. Usually, the investors and managers of construction projects pay attention to the project implementation with the shortest duration and the lowest cost, whereas less attention is paid to the environmental effects of the implementation of projects [1]. This could represent a big problem because of the project's negative impact on the environment.

With the rapid growth of infrastructure development, the ecological impact of these works has caused higher stress levels in the surrounding environment [2]. There are negative impacts on land and all segments of the environment. In general, construction of infrastructure generates environmental issues associated with land, ecology, water resources, materials, energy, GHG, and other emissions into the atmosphere [3]. Also, in the publication under reference [3] is said that when determining environmental pollution generated by infrastructure, the construction phase can exhibit significant ecological impacts from a normalised temporal and spatial perspective in comparison to other steps, such as the operation phase [4] [5].

In Bosnia and Herzegovina, there have been a lot of construction projects after the pandemic. Considering the increasing number of ongoing construction projects, the negative impact is something that has to be dealt with. The construction industry is one sector with significant adverse effects on the environment [6]. For the concerned companies, different options are available for them to become "greener". For example, there is a need for innovative and environmentally friendly products and organisational improvements.

Greener solutions are a massive challenge for companies, and not only for them but also for stakeholders. Designers and construction planners are also responsible for new solutions and their impact on the environment while the construction process is ongoing.

One of the unusual ways to increase the negative impact on the environment is by including public opinion in decision-making for phases of planning and design of construction projects. According to Law, public participation is a principle in the arrangement and use of space and environmental protection [7]. Public participation could reduce the costs of monitoring violations and take responsibility for prosecuting violators [8]. Citizen involvement is intended to produce better decisions, and thus generate more efficient benefits for the rest of society [9]. Public participation has not only improved environmental policies, but also played an important educational role and helped resolve the conflict and mistrust that often plague environmental issues [10].

It is very important to involve people in decision-making, because of the importance of their opinion on specific subjects of environmental protection. Decision-making is represented as the public participation. The public participation in environmental impact assessment is the way to approach to the public and make their opinion important. Also, this is mandatory because of the legal regulations of the Republic of Srpska country.

The only problem with including public opinion is insufficient information about projects and lack of knowledge about the topic and public rights in decision-making. Active public participation can be encouraged by raising and strengthening public awareness through the education system, scientific and technological development, communication with the public, and environmental protection popularisation. By including public opinion, some decisions dangerous to the environment can be prevented. This is the way to decrease the negative impacts of construction projects.

2. REGULATORY FRAMEWORKS FOR PUBLIC PARTICIPATION

The environmental impact assessment procedure is defined pursuant to Articles 60 to 79 of the Environmental Protection Law of the Republic of Srpska [8]. In accordance with Article 14 of the Environmental Protection Law of the Republic of Srpska, the environmental impact assessment is defined as identification, description and adequate assessment in every specific case. The impact of the project on elements or factors of population, flora and fauna, land, water, air, climate, material goods, historical heritage and interaction of all factors is defined by the provisions of this Law. [8]. Environmental impact assessment is the process of grading the acceptability of a project that impacts the environment and choosing adequate measures for environmental protection to minimise negative impacts and maximize protection [9]. Competent authorities will assure public participation in processes of environmental impact assessment.

This topic is very important because of various projects, which have an impact on the environment, such as the Wastewater treatment plants projects. The construction of a wastewater treatment plant is a complex and extensive project, which sometimes takes several years. Plants represent multi-million investments due to their complexity, equipment and a large number of people involved in all parts of the project.

The Republic of Srpska will have several projects like these and those projects can have an impact not only on the environment, but also on the ecosystem and the health of the population. So, there is a need to introduce the population to the importance of participation in the environmental impact assessment procedure. The population interested in impact assessment is a population which can be affected by these projects, like citizen's associations and environmental protection agencies. Because of this, it is very important to involve the affected population in decision-making in order to prevent the negative impact of construction projects.

As defined in the Article 35 [8], all citizens regardless of statehood, nationality or place of residence, and legal entities, are to have public access to information and a right to participation in ensuring the protection of rights in the field of environmental protection.

The Ministry should act independently or in cooperation with associations and foundations, and should promote environmental protection and provide information in a transparent manner about the environment using publications in a printed and online form, which are easily accessible, as well as using the media. All this information must be public. If there is an imminent threat to human health or the environment, the Ministry independently or in cooperation with associations and foundations shall provide all available data in time to the interested public of endangered area with the goal of taking measures to prevent or mitigate damage arising from said threat.

One of the main problems with including the public in the decision-making is the lack of data. For example, with big projects like the wastewater treatment plants, the whole group of risks arise. And that risks must be collected and presented to the public. Especially, the environmental risks are specific for this type of projects. The public in general has problem with the terminology and explanation of risks in order to understand the impact on the environment for the specific project. That impact of specific project is the most important thing for the public participation. When these data is collected, explained and presented the public can conclude why it is important to take the participation in the decision-making. In order to prevent negative impact, the public needs to be aware of the availability of this data.

Speaking of public participation in the decision-making processes of environmental impact assessment, an entire range of problems arise. These problems are primarily: insufficient information presented to the citizens, minimal interest for community problems as well as lack of knowledge about specific fields. In all formerly socialist territories such as the Republic of Srpska, the citizens are distant from formal and informal forms of citizen participation in public affairs. The reason for this is the inherited political culture which does not look kindly upon this kind of civic engagement in public life [10].

As there is a lack of attention to the problem of public participation, the issue itself is underrepresented and unaddressed. Thus, it happens that individual decisions, within environmental impact assessment, pass without the active participation of the interested public. This represents a significant problem because, in all democratic societies, population decision-making is encouraged. In the Republic of Srpska, but also in adjacent territories, there is potential for this practice to be implemented with the scope of decreasing negative impacts of construction. Decreasing of the negative impacts of construction will be easier with the active public participation in the decision-making.

3. PUBLIC PARTICIPATION IN ENVIRONMENTAL IMPACT ASSESSMENT

Republic of Srpska municipalities conducted a research through local ecological action plans (LEAP) about the importance of public participation in active governance in the field of environmental protection. In the process of establishing environmental protection, the principle of access to information and public participation is of particular importance for several reasons. First, these processes require radical changes in the citizen's habits concerning their treatment of the environment, raising their awareness about specific issues. To gain the trust of citizens and willingness to cooperate, it is necessary to educate the population by including it directly in the process of establishing environmental standards [11].

Local ecological action plans include processes of sustainable development, public participation in associations of citizens, and social organizations in the general process of democratization and decentralization. In this way, it contributes to increasing transparency and efficiency, as well as the quality of the process of decision-making in the area of environmental protection [12].

Authorities and NGOs can create strong and effective coalitions which support the capability of each to solve problems or raise funds. For example, local authority seeking funds for the improvement of living environment, has a better chance to succeed if it cooperates with NGOs. Such a cooperation can show the commitment of local authorities to public participation and democratic decision-making [13].

As part of the preparation of local environmental action plans, authors made SWOT analyses defining the advantages and disadvantages. The identified problems are:
1. Low level of environmental awareness of the population, insufficient education, and inadequate participation of the population in decision-making
2. Public disinterest in participation in decision-making processes and the assessment of environmental impact of programs and projects on the environment

When it comes to projects for which an application is made for environmental impact assessment, the project holder submits the impact study in two written copies and four online copies to the Ministry, with a request for a decision approving the study from an authorised Legal entity within 30 days of receiving the study. Within 15 days from the date of submission for approval of the

study, the project holder must inform the public and stakeholders about the submitted application in one of the daily newspapers in the Republic of Srpska, available in the territory of the local community where the project is planned. Such notice shall contain the following information:

a) Basic information about the request
b) Summary of the content and conclusions of the impact study
c) The place and time where free public access to the request is provided
d) Estimated place and time of the public hearing about the impact assessment study
e) Deadline for submitting written opinions about the application and the impact study
f) Address to which opinions may be submitted
g) The fact that it is a project with a possible impact on the environment of the other entity or Brčko district

The Ministry announce a notice of public hearing and the impact study on its website, after the publication of the notice in one of the daily newspapers until the deadline for submitting remarks and opinions expires.

Public participation in the impact assessment procedures is defined in Article 55 of the Law [9]. The process begins with preparing responsible authority for the Plan and Program ensuring public participation in the process of reviewing the report on the strategic assessment before submitting the Report to the Ministry. The public considers the report as a part of the presentation of the Plan and Program to the public and a public hearing is held, unless directed otherwise by the Law. The Responsible Authority for preparing the Plan and Program shall prepare a report within 30 days on the participation of interested sides (authorities, organisations and the public).

The Ministry shall give the opinion, within 30 days pursuant to Articles 54 and 56 of the Law [9] considering environmental aspects, conservation, and improvement of the environment, especially:

a) the degree of impact of plan implementation on the environment, considering the impact of individual segments, as well as the cumulative impact on the area covered by the Plan and Program

b) measures and activities planned to be undertaken in order to reduce and avoid the negative impact of the implementation

v) the Report on the conducted consultations with responsible authorities and organizations and public

g) the Report on the conducted consultations with responsible authorities and organizations and the public of the other entity, district of Brčko or another country

d) the manner in which the monitoring of the impact on the environment and the implementation of the Plan and Program are envisaged, as well as the measures that will be taken if a negative impact on the environment is anticipated.

The project holder organizes a public hearing on impact assessment in the local community in which the project is located. At the public hearing, a representative of the Ministry must participate, and he/she presides the hearing. Experts and representatives of the affected local community attend the public hearing and give opinions, and all other persons attending the public hearing give remarks, as defined by Law. The resources of modern environmental policy are regulatory measures, prohibiting restrictions, environmental impact assessment, economic measures, licenses and permits, public participation in public hearings etc. [14].

The project holder prepares and submits to the Ministry the public hearing report within 8 days from the day of the event. The interested public may within 30 days, from the day of the

public hearing, submit remarks and opinions to the project holder regarding the written request and impact assessment. So, public decision-making is defined in the legislation of the Republic of Srpska. But these activities are not promoted or announced enough for easy access by the interested public.

The importance of involving citizens was shown by the city of Bijeljina, which was the first municipality in the Republic of Srpska involving citizens and civil organizations in decision-making processes at the local level. One of the approaches they used is a strategic approach with broad public participation, to meet the needs of people and companies in cities, in their environment, in order to improve the quality of life [15]. In that case, the public can easily decrease the negative impact on the environment by active participation in decision-making.

It is very important to say that there is a need to measure the impact or effect of public participation. Results from measuring can be presented as examples of good practices for the interested public. Measuring the implementation effect of public participation and reaching high effectiveness in public participation has consistently drawn the attention of researchers [16]. Shanghai and Hong Kong [17] for example, adopted qualitative methods to measure the implementation effect of public participation, and suggested that key stakeholders should be involved in improving the level of public participation. They also [18] established a framework to evaluate the effectiveness of public participation methods, mainly from the acceptance criteria and process criteria, but the research remains at the level of qualitative discussion.

Based on conducted analyses, there is a conclusion that public authorities do not promote, during their actions, the basic principles of good governance as a base for building an open state. It means that they do not provide the minimum standard of transparency, responsibility, and participation in creating and implementing of public policies and regulations. By resolving this usual practice, the involved public can be pushed to active participation in environmental impact assessment. This can lead to a decrease in the negative impact of construction processes.

4. CONCLUSION

In the Republic of Srpska, the legal framework clearly defines the postulates of public participation in environmental impact assessment processes. It is necessary to underline that the public must have access to information for projects, plans and changes before adoption. The availability and understanding the data is very important for the public participation.

The main problem is insufficient awareness that they can influence with their remarks on environmental projects, as well as the fact that they are not introduced to many projects or decisions they can influence. Therefore, they can't know whether a project will affect their environment or ecosystem because they lack knowledge and information. It is essential to raise citizens' awareness and refer them to NGOs that are up to date with potential problems and decisions that are being submitted to public hearings. By including public opinion, some decisions dangerous to the environment can be prevented. That is the way to decrease the negative impacts of construction projects.

REFERENCES

[1] Banihashemi Sayyid Ali, Khalilzadeh M., Kazimieras Zavadskas E., Antucheviciene J. Investigating the Environmental Impacts of Construction Projects in Time-Cost Trade-Off

Project Scheduling Problems with CoCoSo Multi-Criteria Decision-Making Method, *Sustainability* **2021**, 13, https://doi.org/10.3390/su131910922

[2] Chao L., Zhang J., Philbin S.P., Yang X., Zhangeng D., Hong J., Ballesteros-Perez P. Evaluating the impact of highway construction projects on landscape ecological risks in high altitude plateaus, *Scientific reports* **12**(1), 2022, https://doi.org/10.1038/s41598-022-08788-8

[3] Martinez S., del Mar Delgado, Martinez Marin R., Marchmalo M., Alvarez S. Pre-construction quantification of embodied environmental impacts to promote sustainable construction projects: The case study of a diversion dam, *Journal of Environmental Management* 314, 2022

[4] Melissa, B., Robert, R., Scott, M.H., L, S.A., Example of a hybrid life-cycle assessment of construction processes. *J. Infrastruct. Syst.* 12, 2006, 207–215. https://doi.org/10.1061/(ASCE)1076-0342(2006)12:4(207)

Li, X., Zhu, Y., Zhang, Z., An LCA-based environmental impact assessment model for construction processes. *Build. Environ.* 45, 766–775, 2010 https://doi.org/10.1016/j.buildenv.2009.08.010

[5] Ding, Z., Zhu, M., Tam, V.W.Y., Yi, G., Tran, C.N.N. A system dynamics-based environmental benefit assessment model of construction waste reduction management at the design and construction stages. *J. Clean. Prod.* 176, 676–692. https://doi.org/10.1016/j.jclepro.2017.12.101., 2018.

[6] *Official Gazette of Republic of Srpska*: Law on spatial planning and construction 40/2013, 2/2015, 106/2015 and 3/2016., 104/2018 and 84/2019)

[7] *Official Gazette of Republic of Srpska*: Law on environmental protection (71/2012, 79/2015)

[8] Public scientific institution for protection and ecology of Republic of Srpska: Procedure of environmental impact assessment, Banja Luka, 2016

[9] Conference of cities and municipalities: Direct participation of citizens in public life at the local level, Belgrade, 2006

[10] Municipality of Bratunac: *Official Gazzete of Bratunac Municipality*, 2017

[11] Institute for Civil Engineering IG Banja Luka: The local ecological action plan for city of Banja Luka 2016-2021, Banja Luka, 2015

[12] Municipality of Doboj: The local ecological action plan, 2005

[13] Pajtić B.: Sustainable development and environmental impact assessment, Faculty of Law Novi Sad 46(1):409-425, 2012, doi:10.5937/zrpfns46-2034

[14] Municipality of Bijeljina: Bijeljina City Sustainable Urban Mobility Plan, 2020

[15] Zhao H., Yuanyuan G., Zhang J.: Evaluation on the implementation effect of public participation in the decision-making of NIMBY facilities, *PloS ONE* **17**(2), https://doi.org/10.1371/ journal.pone.0263842, 2022

[16] Sun L, Zhu D, Chan EHW. Public participation impact on environment NIMBY conflict and environmental conflict management: Comparative analysis in Shanghai and Hong Kong. *Land Use Policy*. 2016;58:208–17.

[17] Rowe G, Frewer LJ. Public Participation Methods: A Framework for Evaluation. *Science, Technology, & Human Values*. 2000; 25(1):3–29. https://doi.org/10.1179/2046905514Y.0000000146 PMID:25309997

Zoran Perović[1]*, Stanko Ćorić*[2]*, Snežana Isaković*[3]*, Saša Stošić*[4]

PREDNOSTI UGRADNJE ZELENIH KROVOVA NA ZGRADAMA SA RAVNIM KROVOVIMA

Rezime:

U ovom radu se analiziraju različiti aspekti postavljanja zelenog krova na nekoliko tipskih zgrada u Beogradu. Razmatrani su ekstenzivni i intezivni tipovi takvih krovova. Cilj rada je bio određivanje njihovog uticaja na promenu termičkih karakteristika i nosivosti konstrukcije postojećih objekata. Na osnovu promena energetskih performansi i efekata na samu konstrukciju objekta, određena je opravdanost postavljanja zelenih krovova.

Ključne reči: zeleni krov, nosivost konstrukcije, energetska efikasnost, benefit

BENEFITS OF GREEN ROOF INSTALLATION ON BUILDINGS WITH FLAT ROOF

Summary:

In this paper, different aspects of a green roof installation are analyzed on several typical buildings in Belgrade. The analysis is performed for buildings with extensive and intensive green roofs. The goal was to determine their influence on existing buildings' structural capacity and thermal characteristics. According to the impact on the structure and its energy performance, the overall effect and justification of the installation of the green roof are determined.

Key words: green roof, structural capacity, energy efficiency, benefit

---

[1] *Assistant professor, Faculty of Civil Engineering, University of Belgrade, Serbia, zperovic@grf.bg.ac.rs*
[2] *Assistant professor, Faculty of Civil Engineering, University of Belgrade, Serbia*
[3] *MSc civil eng., Senior Advisor, Municipality of Stari Grad, Serbia*
[4] *Associate professor, Faculty of Civil Engineering, University of Belgrade, Serbia*

1. INTRODUCTION

Archetypes of green roof implementation are identified through various periods in human history, and its importance for urban areas has been recognized since the middle of the 20th century [1]. In the last decades of the 20th century, green roof technology improved, and its application in the building industry has substantially increased. It was seen as a practical tool with valuable features for urban areas.

Establishing its impact and benefit in different climate zones is crucial for developing implementation strategies and appropriate city policies. In Belgrade, a new concept of the development of the city includes the installation of the green roof and greenery systems on public buildings and the development of an adequate approach for education and subsidy system for citizens. The strategic goals of the city of Belgrade can also be indirectly linked to the green roof concept through goals of preserving and increase of green areas, air quality, quality of life, green solutions, and biodiversity.

Green roofs could be classified as extensive, semi-intensive and intensive based on the vegetation, construction, and maintenance factors. An extensive green roof (EGR) represents a structure with lower substrate thickness (8-15 cm), while the intensive green roof (IGR) is usually with a growing medium layer from 20 to 40cm or even higher. According to the type of the usage, they can be inaccessible or accessible, in the form of a garden or spaces for recreation.

The impact of the application of green roofs is reflected through individual and public (social and environmental) benefits. Green roofs can mitigate the urban heat island effect up to 3 °C at large-scale implementation [2]. Relative reduction of energy needed for heating and cooling depends on the climate and thermal properties of the thermal envelope, but it can reach 20-40% [3], [4]. In these calculations, the part of the building affected by the green roof is limited to adjacent and areas relatively close to the green roof [5]. Annual water retention is also a very significant aspect from an ecological and economic point of view, as it can delay the discharge of excess water (40%-90%) [6].

The estimated life of the green roof varies from 40-55 years [7], which can be considered as a membrane longevity benefit since the usual replacement or reconstruction of the conventional roof is considered to be performed every 20 years.

Other benefits include an increase in biodiversity, positive aspects on mental health, reduced air pollution and improved acoustic insulation. All of the benefits mentioned above could be monetized in life cycle cost (LCC) analysis as presented in [7][8].
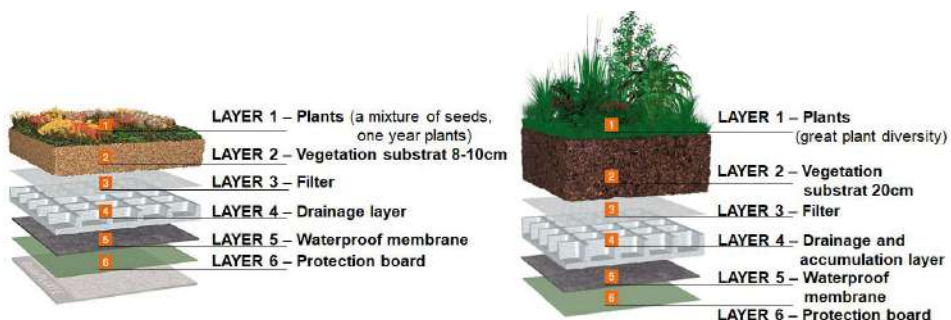
Figure 1 – Layers in extensive and intensive construction [10]

601

Standard layers for green roof structure include, besides substrate layer, thermal insulation, root barrier, irrigation system (inside or above), drainage layer and additional filters [9]. It is very important to provide permanent and sometimes load-distributing protection of the waterproofing layer against mechanical, thermal and chemical reactions.

The most common barriers to green roof implementation are related to the maintenance cost and structural implications. However, by taking into account the net present value (NPV) of life cycle cost analysis, from both public and individual perspectives, the payback period is estimated from 5-14 years [11], [12], depending on the type of the green roof.

2. EFFECTS OF GREEN ROOF ON THE STRUCTURE

Comprehensive green roof guidelines for planning, construction and maintenance of the green roof are presented in [6], which is based on DIN and DIN EN standards. The waterproofing layer is critical to the successful performance of the roof as a whole, but the technical properties of all materials and layers of the green roof must comply with corresponding standards.

The main concern in the global structural response of the building with a green roof represents an increase in weight on the roof of the building. The rise of vertical loading due to the implementation of the green roof must be determined in the saturated condition (including the retained and captured water). The difference in weight between that condition and the case where the rainfall or irrigation is actively occurring, approximated by the weight of transient water in the drainage layer, is considered a live load [13]. According to [14], the saturated density of the substrate is calculated as $\gamma_s = \gamma_d + n \cdot \gamma_w$, where γ_w is the density of water and n porosity of the substrate.

Estimated permanent loading of the EGR layers above the structure (substrate layer 10cm and drainage layer 6cm) in saturated substrate conditions can vary from 1.25 to 2.43 kN/m^2 for various substrate types. [14]. The permanent loading on the flat roof without vegetation (above the structure) can be in a similar range or even higher, from 1.5 to 3 kN/m^2.

Paving slabs weigh approximately 1.6–2.2kN/m^2, and gravel 0.9–1.5kN/m^2, which in each case could be replaced with an extensive green roof with a decent thickness of substrate according to [15]. There is also a light sedum system of EGR that weighs only 0.5-0.96 kN/m^2 in the saturated state [16]. On the other hand, for the IGR, the weight of the substrate and drainage layer can have a wider range.

Green roofs are usually required to have a vegetation-free zone near the electrical and HVAC systems. They can have higher or lower percentage areas covered with vegetation, depending on design, safe access and maintenance purpose. Hence the imposed loads (people, vehicles, point loads for items) scheme can differ. The difference between EGR and IGR can be significant even in live load increase, especially for accessible green roofs for recreational purposes. The standard from the USA [17] identifies that accessible roof gardens must have minimal capacity to support 4.79 kN/m^2 live loading. In contrast, non-occupied vegetated roof decks should be designed for live loads of 0.958 kN/m^2 under saturated conditions. According to [18], the minimum imposed load for an inaccessible green roof, predicted for maintenance purposes, is 0.5kN/m^2, and for IGR (accessible), this loading is assumed to be 1.46kN/m^2.

Wind loads in roof areas can cause damage during construction (erosion problems) and after the green roof is finished. The primary consideration in wind design for green roofs [19] is the

determination of wind coefficient, the height of the building, the influence of parapet walls and the security and stability of wooden plants, which must be ensured.

3. CASE STUDY FOR FOUR RESIDENTIAL BUILDINGS IN BELGRADE

In this paper, the thermal performance of residential buildings is determined for different scenarios of green roof implementation, and by investigating other implications, a corresponding LCC analysis is performed.

In table 1, information about the analyzed residential buildings is presented. Description of thermal envelope is not given, but the calculated energy needed for heating/cooling for those buildings indicates satisfactory thermal characteristics of opaque and transparent parts of the thermal envelope. Designed structures of flat roofs with no vegetation were analyzed in scenarios with EGR and IGR implementation, and the increase of loading at roof level was determined.

Table 1 – Buildings' energy need for heating/cooling and type of the flat roof

	Number of floors	Total Area [m^2]	Energy needed for heating [kWh/m^2 a]	Energy needed for cooling [kWh/m^2 a]	Flat roof type and top layer
1	Po+P+3	500	49.1	22.9	Gravel - inaccessible
2	Po+P+3	1800	36.11	10.85	Gravel - inaccessible
3	Po+P+7	5400	35.8	9.9	Paving - accessible
4	P+4	890	48.6	15.8	Paving - accessible

The layers representing concrete laid to fall or cement screed are present in all scenarios with similar thickness. Also, the waterproofing and thermal insulation layers are insignificant for estimating the difference in weight between flat roof layers without vegetation and green roofs. The main relative difference in the presented analysis can be observed in the top layers of the roof, where the substrate for a green roof is used in comparative analysis against gravel or paving slab as the top covering layer of the designed (existing) flat roof.

Table 2 presents the difference in loading for the green roof compared to the designed flat roof. EGR is assumed with variable substrate thickness from 8 (inaccessible) to 15cm (accessible), where the density of the substrate also ranges from 550 to 1200kg/m^3 in dry conditions and 1300 to 2000kg/m^3 in saturated conditions, respectively. For IGR, the thickness is assumed to be between 20 and 40 cm and with the same substrate density as EGR. In Table 2, the weight of the concrete layers, insulation (and filter layers) and covering layers are taken into calculation separately and with a different range as well, accounting for all buildings in the analysis.

Table 2 – Relative increase of permanent loading for different types and thickness of the green roof

	Top layers		Total permanent loading		Relative increase		Relative increase	
	min [kN/m²]	max [kN/m²]	min [kN/m²]	max [kN/m²]	min [kN/m²]	max [kN/m²]	min [%]	max [%]
Existing	1	1.5	2.05	3.65				
EGR-dry	0.6	1.68	1.65	3.83	-0.4	0.18	-19.5	4.9
IGR-dry	2.64	5.28	3.91	7.48	1.86	3.83	90.7	104.9
EGR-sat.	1.2	2.4	2.27	4.6	**0.22**	**0.95**	10.7	26.0
IGR-sat.	3.84	7.68	5.11	9.88	**3.06**	**6.23**	149.3	170.7

As it was proposed in [18], not all roof areas could be covered with green roofs, so it is assumed that only 80% of the roof area is covered with vegetation. Distributed live loading difference is only significant for IGR (4.8kN/m²) in comparing to EGR and existing flat roof structure (inaccessible type has 1kN/m² and accessible type 2kN/m²).

Following the local difference in loading on the roof, global structural implications can be assumed. It can be seen from Table 2 that no significant difference in loading level is observed in the comparison between EGR and existing designed flat roof construction if the maximum and minimum values are compared. The relative maximum increase of permanent weight at the roof level could be up to 8%, 14%, 20% and 21% in the scenarios with EGR for building 1, 2, 3 and 4, respectively. If IGR is constructed instead of the adopted structure of a flat roof, the maximum permanent weight at the roof level could be increased to 112%. 120%, 138 and 140%, in the scenarios for building 1, 2, 3 and 4, respectively.

The difference in NPV in LCC analysis is calculated based on the cost and individual benefits of such projects. Since the flat roof structure of the analyzed buildings has adequate thermal properties, as it is the requirement for all parts of the thermal envelope according to the Rulebook on Energy Efficiency of Buildings from 2011, no significant difference in calculated energy needs is observed in the conventional procedure for determination of thermal properties of green roof. For the existing buildings, besides concrete structure and exterior top layers of gravel, the most contributing part for thermal resistance is provided for buildings 1, 2,3 and 4 as 20-30 cm thickness layer expanded polystyrene. Calculating heat transfer coefficient U[W/m²K] for a green roof system requires modelling in software [20] that will take into account special features provided by vegetation. Therefore, the Ecoroof model (EnergyPlus) is used to simulate and evaluate the thermal and energy performance of a building which leads to a more realistic reduction in energy consumption, especially for cooling.

The profitability of proposed IGR and EGR installation projects is based on the probabilistic approach for the life cycle profit analysis. The total cost in the LCC analysis represents the difference in installation cost between the existing flat roof structure and green roof structure with additional maintenance costs. On the other hand, the benefits include savings obtained by reduction of the annual energy need for heating and cooling of the building and membrane longevity in the case of green roof installation.

The results of the economic analysis are determined for three different scenarios: installation of inaccessible EGR, accessible semi-intensive green roof (SIGR) and IGR. As is expected, energy saving varies in a small range (similar for all buildings) depending mainly on the type of the green roof. Saving from reduced energy need for cooling is estimated in the range of 0.04-0.20 EUR/m^2 of roof area for all buildings in analysis. On the other, a reduction in the energy need for heating can lead to savings in the range of $0.1 - 0.4$ EUR/m^2 of roof area.

Based on the presented input data, computed life cycle NPV for all IGR and SIGR is negative, and for EGR, the value can be positive for buildings 3 and 4. Minimum and maximum NPV at the end of life cycle of EGR installation is calculated as -26 EUR/m^2 and -4 EUR/m^2, -33 EUR/m^2 and -1 EUR/m^2, -26 EUR/m^2 and +4 EUR/m^2, -42 EUR/m^2 and +10 EUR/m^2 for buildings 1,2,3 and 4 respectively. On the other hand, minimum and maximum NPV at the end of life cycle of SIGR installation is calculated as -92 EUR/m^2 and -16 EUR/m^2, -90 EUR/m^2 and -20 EUR/m^2, -90 EUR/m^2 and -13 EUR/m^2, -88 EUR/m^2 and -6 EUR/m^2 for buildings 1,2,3 and 4 respectively. Minimum and maximum NPV at the end of life cycle of IGR installation is calculated as -227 EUR/m^2 and -98 EUR/m^2, -234 EUR/m^2 and -107EUR/m^2 , -230 EUR/m^2 and -101 EUR/m^2, -225 EUR/m^{2}and -95 EUR/m^2 for buildings 1,2,3 and 4 respectively. In sensitivity analysis, it is concluded that the most influential parameters for the outcome of the analysis are maintenance and installation costs. A usual individual benefit that can be accounted for is a property value increase that can be in the range relatively close to the installation cost. For example, it is estimated that installation of EGR and IGR will lead to an increase of property value 2-5% and 10-20%, respectively [11], or in the range from 20-80EUR/m^2 for EGR and 45-180EUR/m^2 for IGR [21]. In this case of accounting the property value increase as a benefit, and especially energy savings, a distinction must be made between residential units below the roof and other residential units.

Furthermore, the public (social and environmental) benefits predicted in [11] include aesthetics benefit, reduction of infrastructure improvement and flood risk, mitigation of urban heat island effect, habitat creation, improvement of air quality and carbon reduction. However, the cost of air pollution (during the production of material) and landfill costs must also be taken into account. It is estimated in [11] that at the end of the lifecycle, the most probable NPV, accounting for the social benefit only, would be 20EUR/m^2 and 60EUR/m^2 for EGR and IGR, respectively.

In a study performed in the USA [22], a comparison between economic preferences between white, black and green roofs concluded in favour of white roofs, but if the local environment is a primary interest, green roofs would be preferred option.

4. CONCLUSION

In the presented paper, two general aspects of a green roof installation are discussed. Evaluation of their influence on the increase of loading in roof level and benefits for existing buildings is aimed to provide the basis of profitability analysis of the proposed projects. It is important to indicate that the presented analysis was associated with the potential modification of flat roofs in new buildings in Belgrade, where the limit of the loading is not the restricted (analysis could be performed in design stage), and with the existing flat roof configuration that have satisfactory thermal properties.

Various benefits of a green roof installation on a flat roof are indicated, but the realistic economic analysis included only individual (private) benefits. Although a diverse green roof

system can be designed, in the presented analysis, it is estimated that 80% of the roof is under vegetation of EGR or IGR. Based on the design of four typical residential buildings in Belgrade, the difference in permanent loading is estimated in the cases of green roof installation. The increase of weight on the roof level can be generally associated with corresponding scenarios in LCC analysis.

Current private benefits from the installation of a green roof are limited to energy savings and membrane longevity benefits. This resulted in negative NPV for nearly all scenarios of EGR, SIGR and IGR models of flat roofs. It is also important to indicate that significant individual benefit – property value increase is not taken into account in the analysis, and the presented literature review indicated its substantial influence on project profitability. Since its wider implementation could have various public benefits, evaluated results could therefore be used to estimate the level of the potential subsidy or tax reduction for the green roof implementation to be more affordable for investors.

REFERENCES

[1]   I. D. Stewart, "Why should urban heat island researchers study history?," *Urban Clim.*, vol. 30, Dec. 2019, doi: 10.1016/j.uclim.2019.100484.

[2]   M. D. Lalošević, M. S. Komatina, M. V. Miloš, and N. R. Rudonja, "Green roofs and cool materials as retrofitting strategies for urban heat Island mitigation - Case study in Belgrade, Serbia," *Therm. Sci.*, vol. 2018, 2018, doi: 10.2298/TSCI171120086L.

[3]   Z. Tian, Y. Lei, and X. Gu, "Building Energy Impacts of Simple Green Roofs in the Hot Summer and Cold Winter Climate Zone: Suzhou as a Study Case," *Procedia Eng.*, vol. 205, pp. 2918–2924, Jan. 2017, doi: 10.1016/J.PROENG.2017.10.095.

[4]   B. Raji, M. J. Tenpierik, and A. Van Den Dobbelsteen, "The impact of greening systems on building energy performance: A literature review," *Renewable and Sustainable Energy Reviews*, vol. 45. Elsevier Ltd, pp. 610–623, 2015, doi: 10.1016/j.rser.2015.02.011.

[5]   S. Saiz, C. Kennedy, B. Bass, and K. Pressnail, "Comparative life cycle assessment of standard and green roofs," *Environ. Sci. Technol.*, vol. 40, no. 13, pp. 4312–4316, Jul. 2006, doi: 10.1021/es0517522.

[6]   A. Sachverständige Gartenbau -Landschaftsbau-Sportplatzbau eV and Z. Gartenbau, "Guidelines for planning, construction and maintenance of green roofs," Bonn, 2018.

[7]   F. Bianchini and K. Hewage, "How 'green' are the green roofs? Lifecycle analysis of green roof materials," *Build. Environ.*, vol. 48, no. 1, pp. 57–65, Feb. 2012, doi: 10.1016/j.buildenv.2011.08.019.

[8]   H. Feng and K. N. Hewage, "Economic Benefits and Costs of Green Roofs," in *Nature Based Strategies for Urban and Building Sustainability*, Elsevier Inc., 2018, pp. 307–318.

[9]   N. Shishegar, "Enhancing energy and environmental performance of buildings," 2012.

[10]   "https://www.bauder.rs/sr/gruendach-eu/." .

[11]   F. Bianchini and K. Hewage, "Probabilistic social cost-benefit analysis for green roofs: A lifecycle approach," *Build. Environ.*, vol. 58, pp. 152–162, Dec. 2012, doi: 10.1016/j.buildenv.2012.07.005.

[12]   B. Kotzen, "Economic benefits and costs of green streets," in *Nature Based Strategies for Urban and Building Sustainability*, Elsevier Inc., 2018, pp. 319–331.

[13]   ASTM, "Standard Practice for Determination of Dead Loads and Live Loads associated with Green Roof Systems," 2019. [Online]. Available: www.astm.org,.

[14]   S. Cascone, F. Catania, A. Gagliano, and G. Sciuto, "A comprehensive study on green roof performance for retrofitting existing buildings," *Build. Environ.*, vol. 136, pp. 227–239, May 2018, doi: 10.1016/j.buildenv.2018.03.052.

[15]   H. F. Castleton, V. Stovin, S. B. M. Beck, and J. B. Davison, "Green roofs; Building energy savings and the potential for retrofit," *Energy and Buildings*, vol. 42, no. 10. Elsevier Ltd, pp. 1582–1591, 2010, doi: 10.1016/j.enbuild.2010.05.004.

[16]   B. Munby, "Feasibility study for the retrofitting of green roofs," in *Civil and Structural Engineering*, Sheffield: University of Sheffield, 2005.

[17]   B. Dvorak, "Comparative analysis of green roof guidelines and standards in Europe and North America," *J. Green Build.*, vol. 6, no. 2, pp. 170–191, 2011, doi: 10.3992/jgb.6.2.170.

[18]   P. Van Der Walt, "Retrofitting South Africa's cities with green roofs: Cost benefit analyses for large scale green roof implementation," 2018. [Online]. Available: https://scholar.sun.ac.za.

[19]   SPRI, "Wind Design Standard For Vegetative Roofing Systems," Waltham, MA, 2016. [Online]. Available: www.spri.org.

[20]   D. J. Sailor, "A green roof model for building energy simulation programs," *Energy Build.*, vol. 40, no. 8, pp. 1466–1478, 2008, doi: 10.1016/j.enbuild.2008.02.001.

[21]   A. Mahdiyar, S. Tabatabaee, A. N. Sadeghifam, S. R. Mohandes, A. Abdullah, and M. M. Meynagh, "Probabilistic private cost-benefit analysis for green roof installation: A Monte Carlo simulation approach," *Urban For. Urban Green.*, vol. 20, pp. 317–327, Dec. 2016, doi: 10.1016/j.ufug.2016.10.001.

[22]   J. Sproul, M. P. Wan, B. H. Mandel, and A. H. Rosenfeld, "Economic comparison of white, green, and black flat roofs in the United States," *Energy Build.*, vol. 71, pp. 20–27, Mar. 2014, doi: 10.1016/j.enbuild.2013.11.058.

CONGRESS SPONSORS

BECHTEL ENKA

Bechtel-Enka UK Limited is a consortium of two major construction companies that have been working together on projects since 1986.

Founded in 1898, Bechtel is a global engineering, construction and project management company. Bechtel helps its customer deliver projects of purpose that create a lasting positive legacy. These are projects that create jobs and grow economies; tackle critical environmental challenges to protect people and the planet. Since 1898, Bechtel has helped customers complete more than 25,000 projects in 160 countries on all seven continents.

Founded in 1957, ENKA is a global engineering, procurement and construction company that designs and builds some of the world's most complex projects with a focus on the protection of the human life and environment. The company creates and delivers innovative and integrated solutions for its clients with engineering, procurement, fabrication, construction, maintenance and project management services. Since 1957, more than 550 engineering and construction projects in 47 countries were successfully completed by ENKA.

BECHTEL ENKA

Bechtel ENKA has been in the Balkan region for more than 30 years and have built over 700 km of motorways and currently undertaking Morava Corridor Motorway Project.

Morava Corridor Motorway Project is a 112 km dual-carriageway motorway from Pojate and the A1 (the North-South motorway in central Serbia) through Kruševac and up into Preljina in the north of Čačak.

The Project runs from east to west in the West Morava River valley and will connect central Serbia and Pan-European Corridors 10 and 11.
To perform this important infrastructure project, Bechtel-ENKA will rely on its top-level engineering, production, quality, environment, health and safety, and sustainability standards.

Contact details:

Bechtel ENKA
UK Limited Branch Belgrade
Address: Resavska 23, Belgrade

Offices in Kruševac:
Jasicki put 52 dj, 37000 Krusevac / Serbia
e-mail: bejvdcc@besmp.rs
mob: +381 069 8068300

中国路桥工程有限责任公司
CHINA ROAD AND BRIDGE CORPORATION

塞尔维亚泽蒙博尔蔡大桥及附属连接线工程
Zemun-Borca Bridge with the Accompanying Roads Project, Serbia

Bridge Projects

桥梁工程
BRIDGE PROJECTS

Bar-Boljare Highway (Section: Smokovac-Matesevo) Project, Montenegro

The first highway in Montenegro, and also an important cooperative project between China and Central-Eastern European countries. The 41km-long section Smokovac-Matesevo constructed by CRBC is the most demanding section of technology and construction, bridges and tunnels make up to about 60% of the entire route.

黑山公路Moracica大桥效果图
Effect picture of Moracica bridge on highway

STRABAG
TEAMS WORK.

KO SMO MI?

STRABAG je evropski tehnološki koncern za građevinske radove, vodeći po inovaciji i jačini kapitala.Vršimo sve vrste građevinskih usluga i time stvaramo dodatnu vrednost za investitore.

Pravi ljudi na pravom mestu u pravo vreme, sa pravim materijalima i mehanizacijom – tako se realizuju i najsloženiji projekti, i to uvek visokog kvaliteta, u roku i po optimalnoj ceni.

DELATNOST

Niskogradnja i razvoj infrastrukture
Visokogradnja i inženjerske konstrukcije
Ekološka tehnika-prečišćavanje voda,deponije

NAŠE VREDNOSTI

Poverenje
Angažman
Pouzdanost
Poštovanje
Partnerstvo
Solidarnost
Dugoročnost
Skromnost
Radost inovacije

STRABAG
TEAMS WORK.

STRABAG SRBIJA
Milutina Milankovića 3b
11 070 Beograd / Srbija
Tel.: +381 (0)11 2221-700
office.rs@strabag.com

STRABAG SEVERNA MAKEDONIJA
Mirce Acev 2, Skoplje-Centar
1 000 Skoplje / Severna Makedonija
Tel.:+389 (2) 510-1800
macedonia@strabag.com

STRABAG CRNA GORA
Zetskih Vladara 5
81000 Podgorica / Crna Gora
Tel.:+382 (20) 448-300
office@crnagoraput.me

www.strabag.com

ŠIRBEGOVIĆ ®

150 000 m² - Ukupna površina
35 000 m² - Proizvodni pogoni

1	PREDNAPREGNUTE AB KONSTRUKCIJE
2	METALNI POGON I AKZ
3	POGON ZA IZRADU I SKLADIŠTENJE ARMATURE
4	POGON ZA VEZIVANJE ARMATURE
5	MAGACIN
6	UPRAVA
7	SERVIS
8	DUPLI ZIDOVI, FASADE I TEMELJI
9	FABRIKA OLAKŠANIH PLOČA
10	POGON ZA MLIJEVENJE AGREGATA
11	POGON ZA SEPARACIJU
12	OTVORENO SKLADIŠTE GOTOVIH PROIZVODA

FIRMA KOJA GRADI FIRME

COVID BOLNICA - NOVI SAD

Izgrađenih preko 6.000 objekata i preko 11 miliona m² prostora.
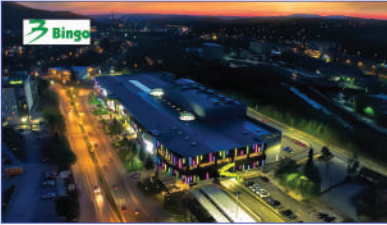
UTIBER
PROJECT BIRO

Contract: Consultancy services for supervision of Detailed Regulation Plan, Design and implementation of Sremska Rača – Kuzmin highway and bridge over Sava river
Client: Ministry of Construction, Transport and Infrastructure   **Investor:** Public Enterprise "Roads of Serbia", Republic of Serbia

Contract: Consultancy services for supervision of Hungarian-Serbian railway project on the territory of the Republic Serbia:
Sector 1 – Belgrade Centar – Stara Pazova; Sector 2 – Stara Pazova – Novi Sad
Client: Ministry of Construction, Transport and Infrastructure   **Investor:** JSC for public railway infrastructure management "Serbian Railways Infrastructure"

Project Biro Utiber (PBU) is established in June 2014 by renowned Hungarian company Utiber Közúti Beruhazo Ltd. With support and knowhow of its mother company and by acquiring wide pool of experts, PBU strongly established itself on the market, participating in various domestic and internationally funded projects. Among our Clients are: Ministry of Construction, Transport and Infrastructure, Public Enterprise "Roads of Serbia", Koridori Srbije, EU delegation, IBRD, EIB...

Main activities performed by UTIBER are providing all kinds of consulting engineering services in the field of transport and infrastructure systems (roads, railways, airports, water systems), especially under FIDIC contracts conditions, and production of technical documentation in the field of civil engineering including related infrastructure, with all the accompanying studies.

PROJECT BIRO **UTIBER d.o.o.**
Temerinska 76 21138 Novi Sad Srbija Tel: +381 21 537 341 www.utiber.rs

INSTITUTE OF TRANSPORTATION

CIP

With over a century of tradition, Institute of Transportation CIP is today a leading research, design and consulting company in Serbia and south-east Europe.

Institute of Transportation CIP successfully carries out all design activities, such as geodetic works, geological research, laboratory tests in the field of environmental protection, preparation of study, planning and technical documentation, professional and technical checking of technical documentation, testing of structures, professional supervision during construction, technical inspection of buildings, engineering consulting services.

With a staff of over 500 and over 300 experts licensed by the Serbian Chamber of Engineers and the Republic Geodetic Authority, Institute of Transportation CIP is a reliable partner to state institutions, faculties, local and foreign companies. It has modern equipment and software for design, geodetic surveys and geotechnical research.

In more than 140 years of business, CIP has remained synonymous with a high concentration of technical knowledge and a team of top experts who are ready to find the most rational solutions to the most complex projects.

The result of decades of successful work by CIP in the country and abroad is more than 8,000 kilometres of designed, built and reconstructed railways, 25 major railway junctions, more than 2,000 kilometres of roads and motorways, 1,200 bridges, 550 tunnels and underground facilities for various purposes and more than a million square metres of health, cultural, business, residential, sports and industrial facilities.

The CIP is designing modern high-speed railways, a major leap in the history of the design and construction of railways with train speeds of 200 km/h and with which Serbia will connect to most European countries.

An optimal combination of many years of tradition and experience, following global achievements and trends, Institute of Transportation CIP has become a formula for business, quality, speed and trust, and has remained at the top of the list of the world's engineering design companies.

INSTITUTE OF TRANSPORTATION

CIP

Managing Director
Milutin Ignjatović, dipl. inž.
Nemanjina 6/IV, 11000 Beograd,
Republic of Serbia
Tel. 011/361-69-29, 361-82-87;
Fax: 011/361-67-57
E-mail: office@sicip.co.rs;
www.sicip.co.rs

Gradimo bolji svet

Biznis ne zna za granice. Investiramo od Alpa do Crnog mora.
U novim gradovima podižemo prestižne objekte i otvaramo nova radna mesta.
Stvaramo biznis, stvaramo bolji svet.

▼

CROWNE PLAZA BELGRADE • INTERCONTINENTAL HOTEL LJUBLJANA
DELTA PLANET BANJALUKA • DELTA PLANET VARNA • DELTA PLANET NIŠ
SAVA CENTAR • INDIGO HOTEL • DELTA HOUSE

DELTA HOLDING
Creating Business

deltaholding.rs

DELTA REAL ESTATE
Building Business

deltarealestate.rs

GENERALNI
IZVOĐAČ

JADRAN

GRADIMO BUDUĆNOST
ČUVAMO TRADICIJU

www.jadran-bg.rs

GRADIMO ČVRSTE VEZE

Stvari o kojima sanjate pretvaramo u objekte koje gradite.
Zato je naša veza čvrsta.

MORAVACEM
A CRH COMPANY

MOSTOGRADNJA ING

Kompanija **Mostogradnja ING** specijalizovana je za projektovanje i izgradnju infrastrukturnih projekata niskogradnje: mostova, tunela i puteva.

Nastojimo da budemo prepoznatljiva kompanija u realizaciji internacionalnih projekata, zasnovana na načelima poslovne izvrsnosti, a zahvaljujući posebnim znanjima i veštinama naših zaposlenih – postati i opstati strateški partner od poverenja.

Gradilište Makiš

Projekat: Izgradnja infrastrukture i nasipanja platoa za depo metroa u Makiškom polju u Beogradu

Gradilište Kraljevo (Gledićka reka)

Projekat: Izgradnja mosta preko Gledićke reke u Turici, MZ Čukojevac

Gradilište Fruška gora

Projekat: Podizvođački ugovor za izvođenje potporne konstrikcije na šipovima na ulaznom portalu tunela Fruška gora

Gradilište Beograd na vodi

Projekat: Izrada i montaža terase trapeznog oblika, Faza III, Globalnog gradilišta Beograd na vodi u Beogradu

Mostogradnja ING

TERMOENERGO INŽENJERING je osnovan 1989. godine kao specijalizovana organizacija za projektovanje, konsalting i inženjering.
Najznačajniji objekti iz nomenklature posla su iz oblasti petrohemijskih kompleksa, proizvodnje toplotne i električne energije, kao i objekti hemijske industrije, papirne i drugi objekti bazne industrije.

INVESTITORI